



HAL
open science

Exploiting boron-fluorine bonds for fluorination and synthesis of potential bi-modal imaging agents

Omar Sadek

► **To cite this version:**

Omar Sadek. Exploiting boron-fluorine bonds for fluorination and synthesis of potential bi-modal imaging agents. Coordination chemistry. Université Paul Sabatier - Toulouse III; University of British Columbia. Library, 2018. English. NNT: 2018TOU30141 . tel-02146608

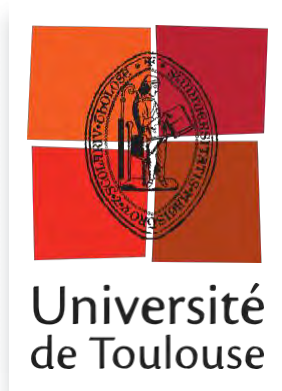
HAL Id: tel-02146608

<https://theses.hal.science/tel-02146608>

Submitted on 4 Jun 2019

HAL is a multi-disciplinary open access archive for the deposit and dissemination of scientific research documents, whether they are published or not. The documents may come from teaching and research institutions in France or abroad, or from public or private research centers.

L'archive ouverte pluridisciplinaire **HAL**, est destinée au dépôt et à la diffusion de documents scientifiques de niveau recherche, publiés ou non, émanant des établissements d'enseignement et de recherche français ou étrangers, des laboratoires publics ou privés.



THÈSE



En vue de l'obtention du

DOCTORAT DE L'UNIVERSITÉ DE TOULOUSE et DE L'UNIVERSITÉ DE COLOMBIE BRITANNIQUE

Délivré par :

Université Toulouse 3 Paul Sabatier (UT3 Paul Sabatier)
et l'Université de Colombie Britannique (UBC) à Vancouver

Présentée et soutenue par :

OMAR SADEK

Le 4 Octobre 2018

Titre :

Exploiting Boron-Fluorine Bonds for Fluorination and Synthesis of Potential Bi-modal Imaging Agents

École doctorale et discipline ou spécialité :
ED SDM : Chimie Moléculaire – CO 046

Unité de recherche :

Laboratoire de Chimie de Coordination (LCC, UPR 8241)

Directeurs de Thèse :

Dr. Emmanuel GRAS, CR CNRS, LCC, UPR 8241
Pr. David M. PERRIN, Professeur, University of British Columbia

Rapporteurs :

Dr. Gilles ULRICH, DR CNRS, ICPEES, UMR 7515, Rapporteur
Pr. Andy WHITING, Professeur, Durham University, Rapporteur

Autre(s) membre(s) du jury :

Pr. Philippe BELMONT, Professeur, Université Paris Descartes, Examinateur
Pr. Montserrat GOMEZ, Professeur, Université Toulouse III Paul Sabatier, Examinatrice
Pr. Chris ORVIG, Professeur, University of British Columbia, Examinateur
Dr. Yan Alexander WANG, Professeur, University of British Columbia, Examinateur
Pr. Laurel SCHAFER, Professeur, University of British Columbia, Invité

Abstract

The B-F bond has an expansive and rich history in chemical transformations and the versatility of the B-F bond has also shown immense utility in fields as far reaching as PET and NIRF imaging. The application of B-F bonds for nucleophilic C-F bond formation and the development of novel fluorophores with potential applications in PET/NIRF bi-modal imaging are investigated in this work.

Organotrifluoroborates are well known as indispensable synthetic tools for the elaboration of organic molecules. However, the trifluoroborate functionality is generally regarded as an auxiliary group, and its potential as a nucleophilic F^- source has remained untested. In this context, the ability of organotrifluoroborates to serve as competent sources of F^- was investigated. In an update to the historic Balz-Schiemann reaction, that traditionally uses BF_4^- as a source of F^- , organotrifluoroborates were shown to mediate the fluorodediazotiation of *in situ* generated aryl diazonium salts under mild reaction conditions (chapter 2). In reactions with an analogous substrate class, unsymmetrical diaryliodonium salts could also be fluorinated using phenyltrifluoroborate via thermal decomposition of the ion pair (chapter 3). Finally, the ability of the trifluoroborate moiety to mediate intramolecular fluorination reactions was investigated through the synthesis of various trifluoroborate-containing molecular scaffolds (chapter 4).

We also investigated novel fluoroborate ($B-F_n$) complexes of the 2-aryl-benzothiazole scaffold, known for its interaction with $A\beta$ aggregates, as fluorophores. Three complexes were isolated, characterised and their photophysical properties are reported. A 2,4-diaryl-benzothiazole monofluoroborate complex displaying the most promising photophysical

properties, was shown to be stable to aqueous conditions. Fluoride abstraction from this complex was also demonstrated, providing promising preliminary results towards the viability of radiolabelling via ^{19}F - ^{18}F isotope exchange. The monofluoroborate complex also showed interesting structural properties given the asymmetric boron centre. Enantiomers of the complex were successfully chirally resolved from the racemic mixture, characterised by Circular Dichroism and their stability to racemization via inversion investigated (chapter 5).

Lay Summary

This work focuses on new uses and applications of the Boron-Fluorine chemical bond; organic compounds containing this bond are called 'organofluoroborates'. Our work has focused on investigating the use of organofluoroborates as a source of fluorine for chemical reactions in which a substrate is fluorinated, which is a departure from the classical use of organofluoroborates. We have also investigated the synthesis and characterisation of new organofluoroborates as potential tools in medical imaging.

Preface

This thesis is submitted as part of the requirements for the degree of Doctor of Philosophy in Chemistry as part of a joint PhD agreement between the University of British Columbia and Université Toulouse III Paul Sabatier. All experiments in this thesis were designed by Pr. David M. Perrin, Dr. Emmanuel Gras and myself unless otherwise indicated.

Chapter 2. Research work was performed by myself and Dr. Tharwat Mohy El Dine in the groups of Pr. David M. Perrin and Dr. Emmanuel Gras. The project was conceived by both Pr. David M. Perrin and Dr. Emmanuel Gras, initial reactions, parameter optimisation and protocol design were conducted by myself. Final reaction conditions were developed by Dr. Tharwat Mohy El Dine. The results reported in this chapter are of equal contribution by both Dr. Tharwat Mohy El Dine and myself. This work was published in 2018: Mohy El Dine, T.; Sadek, O.; Gras, E.; Perrin, D. *Chem. - A Eur. J.* **2018** (DOI: 10.1002/chem.201803575). The manuscript was written by myself and edited by Dr. Tharwat Mohy El Dine, Dr. Emmanuel Gras and Pr. David M. Perrin. This chapter was written by myself.

Chapter 3. Research work was performed by myself in the groups of Pr. David M. Perrin and Dr. Emmanuel Gras. The project was conceived by myself, Dr. Emmanuel Gras and Pr. David M. Perrin. All syntheses, characterization, protocol development and experimental work were performed by myself. This chapter was written by myself.

Chapter 4. Research work was performed by myself in the groups of Pr. David M. Perrin and Dr. Emmanuel Gras. The project was conceived by myself, Dr. Emmanuel Gras and Pr. David M. Perrin. Samson Lai, an undergraduate student under my supervision,

performed the experimental work reported in section **4.2.1.3** with substrate **4.22** using NBS. All other syntheses, characterization, protocol development and experimental work were performed by myself. This chapter was written by myself.

Chapter 5. Research work was performed by myself in the groups of Pr. David M. Perrin and Dr. Emmanuel Gras. The project was conceived by myself, Pr. David M. Perrin and Dr. Emmanuel Gras. All syntheses, characterization, experimental work and theoretical calculations were performed by myself. This chapter was written by myself.

Table of Contents

Abstract.....	ii
Lay Summary.....	iv
Preface	v
Table of Contents.....	vii
List of Tables.....	xi
List of Schemes.....	xiii
List of Figures	xxii
List of Abbreviations and Symbols	xxiv
Acknowledgements.....	xxix
1 Introduction.....	1
1.1 Sources of fluorine in organic synthesis.....	1
1.1.1 Electrophilic and radical sources of fluorine.....	2
1.1.2 Nucleophilic sources of fluorine	3
1.1.2.1 The B-F bond as a F- source	6
1.1.2.2 BF ₄ ⁻ and BF ₃ ·OEt ₂ as F- sources.....	6
1.1.3 Organofluoroborates as F- sources	12
1.1.3.1 Fluorination of organotrifluoroborates	16
1.2 Molecular Imaging.....	18
1.2.1 PET imaging	18
1.2.1.1 B-F in PET Imaging.....	20
1.2.2 NIRF Imaging	26
1.2.2.1 B-F in NIRF Imaging	28
1.3 Objectives of this Work	33
2 Organotrifluoroborates as nucleophilic fluorine sources in the Balz-Schiemann reaction	35
2.1 Introduction	35
2.1.1 The Balz-Schiemann Reaction	36
2.1.1.1 Mechanism.....	36
2.1.1.2 Decomposition in the solid state	38

2.1.1.3	Decomposition in inert solvents	39
2.1.1.4	Development of one-pot and continuous flow processes	40
2.1.1.5	Importance of the fluoro-ate anion	41
2.1.1.6	Organotrifluoroborates as anions in Balz-Schiemann reaction	42
2.2	Results and Discussion	44
2.2.1	Initial optimization	44
2.2.2	Extension to one-pot Balz-Schiemann reaction	46
2.2.3	Mechanism	57
2.3	Conclusion and Perspectives	59
2.4	Experimental	61
2.4.1	Characterization Data of the Synthesized Aryltrifluoroborates.....	65
3	Organotrifluoroborates as nucleophilic fluorine sources in the fluorination of diaryliodonium salts	91
3.1	Introduction	91
3.1.1	Diaryliodonium salt reactivity and selectivity.....	92
3.1.2	Fluorination of diaryliodonium salts	94
3.1.2.1	Metal-free fluorination of diaryliodonium salts	94
3.1.2.2	Metal-mediated fluorination of diaryliodonium salts.....	100
3.1.3	Organotrifluoroborates as an alternate source of fluorine.....	101
3.2	Results and Discussion	102
3.2.1	Synthesis of Unsymmetrical Diaryliodonium Phenyltrifluoroborates	102
3.2.2	Fluorination studies of unsymmetrical diaryliodonium phenyltrifluoroborates	108
3.2.2.1	Solvent optimisation	108
3.2.2.2	Reaction scope and selectivity	110
3.2.2.3	Mechanism.....	112
3.3	Conclusion and Perspectives	116
3.4	Experimental	118
3.4.1	Synthetic procedures and characterization data for 3.11 – 3.26.....	119
4	Organotrifluoroborates applied towards intramolecular fluorination.....	132
4.1	Introduction	132

4.1.1	Intramolecular fluorination	133
4.1.1.1	Intramolecular fluorine transfer to reaction intermediates	133
4.1.1.2	Formal intramolecular fluorination	136
4.1.2	Applying organotrifluoroborates as intramolecular sources of fluoride	137
4.2	Results and Discussion	139
4.2.1	Synthesis and fluorination studies of substrates for intramolecular Balz-Schiemann type reaction	139
4.2.1.1	Synthesis of zwitterionic 2-diazonio-2-trifluoroboratebiphenyl 4.20...	139
4.2.1.2	Synthesis and fluorination studies of zwitterionic (2-diazoniophenoxy)methyltrifluoroborate 4.21	147
4.2.1.2.1	Synthesis of 4.21	147
4.2.1.2.2	Fluorination studies of 4.21	157
4.2.1.2.3	Discussion of results with 4.21	159
4.2.1.3	Synthesis and fluorination studies of styrene derivative 4.22	160
4.2.1.3.1	Discussion of results with styrene derivative 4.22	164
4.2.1.4	Synthesis and fluorination studies of styrene oxide derivative 4.23 ..	165
4.2.1.4.1	Discussion of results with styrene oxide derivative 4.23	168
4.3	Conclusion and Perspectives	168
4.4	Experimental	172
4.4.1	Synthetic procedures and characterization data for 4.21 – 4.44	173
5	Benzothiazole B-F_n Complexes as Potential Bi-modal Imaging Agents for Alzheimer's Disease.....	188
5.1	Introduction	188
5.1.1	PET Imaging for AD	192
5.1.1.1	PET Ligands Derived from ThT/ThS	192
5.1.1.2	PET Ligands Derived from CR	194
5.1.2	NIRF Imaging for AD	195
5.1.3	Bi-modal Imaging Probes for AD	201
5.1.4	Benzothiazole-based B-F _n Complexes as Potential Bi-modal probes for A β 204	
5.2	Results and Discussion	206
5.2.1	Synthesis of Benzothiazolyl B-F _n Complexes	206

5.2.1.1	Summary of Ligand and B-F _n Complex Syntheses	217
5.2.2	Structure of B-F _n Complexes	218
5.2.2.1	Asymmetry of B-F complex 5.19	220
5.2.3	Photophysical Studies of B-F _n Complexes	223
5.2.3.1	Theoretical Calculations	228
5.2.4	Stability Studies of B-F _n Complexes	230
5.2.4.1	Fluorine exchange studies of 5.19	234
5.3	Conclusion and Perspectives	238
5.4	Experimental	241
5.4.1	Synthetic procedures and characterization data for 5.1 – 5.31	242
6	Conclusion	275
7	Résumé Français	279
7.1	Introduction	279
7.2	Résumé Chapitre 2	280
7.3	Résumé Chapitre 3	285
7.4	Résumé Chapitre 4	288
7.5	Résumé Chapitre 5	291
7.6	Conclusion	295
	References	300
	Annex A: Chapter 2	319
	NMR Spectra of selected compounds.....	319
	Annex B: Chapter 3	381
	NMR Spectra of selected compounds.....	381
	X-ray Data Tables	414
	Annex C: Chapter 4	420
	NMR Spectra of selected compounds.....	420
	Annex D: Chapter 5	451
	NMR Spectra of selected compounds.....	451
	X-ray Data Tables	487

List of Tables

Table 1.1 Bond Dissociation Energies of O-F or N-F bond from selected electrophilic fluorine reagents ^{14,15}	3
Table 1.2 Fluorination of various substrates using fluoroborate 1.17	14
Table 2.1 Selected yields of aryl fluorides using different “fluoro-ate” anions.....	41
Table 2.2 Effect of perfluoroorganotrifluoroborates on the yield of 1,4-difluorobenzene	43
Table 2.3 Initial optimization of Balz-Schiemann reaction using organotrifluoroborates	45
Table 2.4 Optimization of one-pot Balz-Schiemann reaction solvent	47
Table 2.5 Effect of diazotizing agent on reaction yields.....	48
Table 2.6 Acid optimization for the one-pot reaction	50
Table 2.7 Effect of temperature on reaction yields	51
Table 2.8 Effect of organotrifluoroborate on reaction yields	52
Table 2.9 Control fluorination experiments with various 'fluoride' salts.....	54
Table 3.1 Fluorination of diaryliodonium salts in solution and in the melt.....	96
Table 3.2 Radiofluorination of diaryliodonium salts	97
Table 3.3 Solvent optimisation for the decomposition of 3.20	109
Table 3.4 Product distribution from the decomposition of salts 3.21-3.26	111
Table 3.5 Product distribution from the decomposition of salts 3.14-3.16	116
Table 4.1 Borylation reaction conditions for the formation of 4.26 and 4.25.....	141
Table 4.2 Attempted Pd-catalysed borylation of <i>N</i> -protected substrates 4.27 and 4.28. Isolated yield of 4.30	143
Table 4.3 Cross-coupling conditions for synthesis of biphenyl fragment using 4.33 ...	146
Table 4.4 Conditions tested for the alkylation of 2-aminophenol	148

Table 4.5 Attempted alkylation of N-protected aminophenols 4.41 and 4.42	151
Table 4.6 Optimisation of parameters for the reduction of 4.43.....	153
Table 4.7 Optimisation of parameters for the diazotization of 4.39	155
Table 4.8 Decomposition conditions for intramolecular fluorination of 4.21.....	158
Table 4.9 Effect of <i>N</i> -bromine reagents on bromofluorination of 4.22	162
Table 4.10 Effect of bromodimethylsulphonium bromide on bromofluorination of 4.22	164
Table 4.11 Conditions tested for activator-free intramolecular fluorination of 4.23.....	166
Table 4.12 Effect of epoxide activators on the intramolecular fluorination of 4.23.....	167
Table 5.1 Photophysical properties of 5.11, 5.12, 5.15 and 5.17-5.19	227
Tableau 7.1 Distribution du produit à partir de la décomposition des sels 3.20-3.26. .	287

List of Schemes

Scheme 1.1 Examples of F ⁺ /F ⁻ reagents.	2
Scheme 1.2 Selected nucleophilic fluorinating agents.	4
Scheme 1.3 Deoxyfluorination reagents developed by Ritter <i>et al.</i> (top) and postulated leaving group formed by reagents (bottom).....	5
Scheme 1.4 Oxidative fluorination pathways with F ⁻	6
Scheme 1.5 The Balz-Schiemann reaction.	7
Scheme 1.6 Fluorination of aryllead(IV) acetates.....	7
Scheme 1.7 Fluorination of simple arenes BF ₃ ·OEt ₂	8
Scheme 1.8 Fluorination of 3-phenylpropyl ethers.	9
Scheme 1.9 Fluorination of <i>gem</i> -dichlorides/iodides and trichlorotoluene with AgBF ₄ . .	10
Scheme 1.10 Modified Mitsunobu reaction for the synthesis of glycosyl fluoride 1.13. .	11
Scheme 1.11 Selected examples of oxa- and aza-Prins cyclization-fluorination reactions.	12
Scheme 1.12 Synthesis of zwitterionic sulfonium fluoroborate 1.16.....	13
Scheme 1.13 ¹⁸ F ⁻ capture/release using phosphonium boranes for radiofluorination. ..	15
Scheme 1.14 Cartridge-based ¹⁸ F ⁻ capture/release in the production of [¹⁸ F]-Setoperone (adapted with permission from Perrio <i>et al. Chem. Commun.</i> 2017, 53, 340-333, copyright Royal Society of Chemistry).	16
Scheme 1.15 Fluorodediazotiation of aryl diazonium perfluoroorganotrifluoroborates. 16	
Scheme 1.16 Metal-free fluorination of alkenyl (a) and aryl or benzylic (b) trifluoroborates. c, metal-mediated/catalysed fluorination of aryl trifluoroborates.....	17
Scheme 1.17 Synthesis of [¹⁸ F]-FDG.	20

Scheme 1.18 Aqueous radiofluorination of boronic ester 1.21 to [¹⁸ F]-trifluoroborate 1.22.	21
Scheme 1.19 a, hydrolytically stable [¹⁸ F]-trifluoroborate 1.23. b, radiolabelling of marimastat-boronic ester 1.24 to marimastat-[¹⁸ F]-trifluoroborate 1.25.....	22
Scheme 1.20 Radiolabelling trifluoroborates by IEX.	23
Scheme 1.21 "Clickable" [¹⁸ F]-trifluoroborate synthon 1.27.....	24
Scheme 1.22 Zwitterionic trifluoroborates as bioconjugatable radioprosthetic synthons.	25
Scheme 1.23 a, Synthesis of PPCy-4a for <i>in vivo</i> imaging. b, PPCy-Arg ₉ -8 used as a HeLa cell label.....	29
Scheme 1.24 pH activated <i>in vivo</i> probe for osteoclasts.	30
Scheme 1.25 Synthesis of 1-BODIPY as an <i>in vivo</i> drug biodistribution probe. Antiparasitic motif highlighted in blue.	31
Scheme 1.26 a, lysosome pH activated Off/On fluorescence for tumour imaging. b, BODIPY-RGD conjugate for <i>in vivo</i> tumour imaging.	32
Scheme 1.27 Molecular structures of NIR B-F ₂ complexes MCY-BF ₂ and PEB.....	33
Scheme 2.1 Balz-Schiemann reaction.	36
Scheme 2.2 Substrate scope of the one-pot Balz-Schiemann reaction with potassium phenyltrifluoroborate. Reaction conditions: aniline (0.25 mmol), 85% aq. H ₃ PO ₄ (0.5 eq.), potassium phenyltrifluoroborate (0.38 mmol), <i>t</i> -BuOH (1.3 mL) in pressure vial with Teflon lined cap, Ar purge, then <i>t</i> -BuONO (0.38 mmol), rt for 20 min, then heated at 45-50 °C for 2 h. Yield determined by ¹⁹ F NMR spectroscopy using 2,4-dinitrofluorobenzene as an	

internal standard. Isolated yield in parentheses. ^a 98% H ₂ SO ₄ used instead of 85% aq. H ₃ PO ₄ in <i>t</i> -BuOH at 95 °C.	56
Scheme 2.3 Proposed reaction mechanism.....	59
Scheme 3.1 Fluorination of diaryliodonium salt 3.1.....	95
Scheme 3.2 Auxiliaries used for the selective fluorination of unsymmetrical diaryliodonium salts.....	98
Scheme 3.3 Effect of solvent and salt removal on diaryliodonium fluorination.	99
Scheme 3.4 Cu-catalysed fluorination of diaryliodonium salts. Values in brackets are the ratio of fluorinated product to 3.3.....	101
Scheme 3.5 Iodonium trifluoroborate zwitterion bifunctional reagents.	102
Scheme 3.6 Stuart <i>et al.</i> one-pot diaryliodonium salt synthesis conditions.	103
Scheme 3.7 Olofsson <i>et al.</i> one-pot diaryliodonium salt synthesis conditions. Isolated yields.	104
Scheme 3.8 Synthesis of iodomesitylene diacetate.	104
Scheme 3.9 Scope of unsymmetrical diaryliodonium tetrafluoroborate salts synthesized. Isolated yields.	105
Scheme 3.10 Attempts at anion exchange (isolated yields in parentheses). a, anion exchange in acetone or MeCN. b, anion exchange in biphasic CH ₂ Cl ₂ /saturated aqueous KHF ₂	106
Scheme 3.11 Scope of unsymmetrical diaryliodonium phenyltrifluoroborates synthesized. Isolated yields.	107
Scheme 3.12 Accepted mechanism for the fluorination of unsymmetrical diaryliodonium salts.....	113

Scheme 3.13 Product distribution and selectivity from the (radio)fluorination of a: 3.30, b: 3.11 and c: 3.14.	114
Scheme 3.14 Proposed mechanism for the fluorination of diaryliodonium salts with phenyltrifluoroborates.....	115
Scheme 4.1 Proposed intramolecular fluorination for the formation of fluorinated derivatives.	133
Scheme 4.2 Intramolecular fluorine transfer in the synthesis of <i>syn</i> -fluorohydrins and fluoroamines.....	134
Scheme 4.3 Proposed mechanism for deoxyfluorination of phenols by PhenoFluor™.	135
Scheme 4.4 a, proposed intramolecular fluorination mechanism. b, experimental evidence for absence of an intermolecular process.	137
Scheme 4.5 Proposed substrates for intramolecular fluorination with trifluoroborates. [B] = BF ₃ ⁻ , B(OR) ₂ (R = H, alkyl).	138
Scheme 4.6 Planned synthesis for substrate 4.20.	139
Scheme 4.7 Synthesis of 4.24 via Suzuki-Miyaura cross-coupling. Isolated yield.....	140
Scheme 4.8 Attempted borylation of 4.24 via a, lithium-halogen exchange. b, photolysis.	142
Scheme 4.9 Protection of 4.24 as carbamate 4.27 or phthalimide 4.28. Isolated yields.	142
Scheme 4.10 Attempted borylation of 4.28 (a) and 4.29 (b) via lithium-halogen exchange.	144
Scheme 4.11 Proposed synthesis of biphenyl scaffold using 4.33.....	145

Scheme 4.12 Proposed synthesis of 4.21.....	147
Scheme 4.13 Failed alkylation using boronic ester.	149
Scheme 4.14 Possible 2-aminophenol alkylation pathways. a, multiple <i>N</i> - and <i>O</i> -alkylation. b, EAS alkylation of aromatic ring.....	150
Scheme 4.15 <i>N</i> -protection of 2-aminophenol as phthalimide 4.41 and carbamate 4.42. Isolated yields.	151
Scheme 4.16 Synthesis of 4.43 and 4.44 by alkylation of 2-nitrophenol. Isolated yields.	152
Scheme 4.17 Attempted one-pot two step fluorination of 4.39.	159
Scheme 4.18 Resonance stabilization of 4.21.	160
Scheme 4.19 Synthesis of styrene derivative 4.22.....	160
Scheme 4.20 Over-brominated products observed during attempted bromofluorination of 4.22 using Br ₂	161
Scheme 4.21 Possible intramolecular fluorination via 4.45.	163
Scheme 4.22 Epoxidation of 4.22 to 4.23 using DMDO.	165
Scheme 4.23 Trifluoroborate-containing scaffolds for intramolecular fluorination.	169
Scheme 4.24 Further functionalization of aryl fluoride via boronic acid.....	170
Scheme 4.25 Conformationally flexible alkene and epoxide containing trifluoroborate scaffolds.....	171
Scheme 5.1 Chemical structures of Thioflavin T (ThT), Thioflavin S (ThS) and Congo Red (CR).....	191
Scheme 5.2 Chemical structures of the most widely used ThT derived tracers selective for A β	192

Scheme 5.3 Chemical structures of stilbene derivatives [¹⁸ F]-Florbetapir and [¹⁸ F]-Florbetaben	195
Scheme 5.4 D-π-A design of NIR fluorescent probes. Acceptor (A) in red, Donor (D) in blue	196
Scheme 5.5 Selected structures and properties (Stokes shift = Δ _{ss} , Quantum Yield (QY) = Φ _F) of NIRF probes for Aβ. Acceptor motif in red, Donor motif in blue	197
Scheme 5.6 Chemical structure of the natural compound curcumin	200
Scheme 5.7 Chemical structures of BODIPY7 and [¹²⁵ I]-BODIPY7	202
Scheme 5.8 Chemical structures of radiotracers [¹²⁵ I]-FIAR and [¹⁸ F]-FIAR	203
Scheme 5.9 Chemical structure of [¹⁸ F]-FDANIR-4c	204
Scheme 5.10 Chemical structure of proposed benzothiazole B-F _n complexes and potential synthesis of PET probes by IEX	205
Scheme 5.11 Modular synthetic strategy towards functionalized 2-arylbenzothiazoles and 2,4-diarylbenzothiazoles.....	207
Scheme 5.12 a, Synthesis of 6-substituted-2-aminobenzothiazoles from anilines. b, Synthesis of 4-substituted-2aminobenzothiazoles via arylthioureas. Isolated yields...	208
Scheme 5.13 Sandmeyer bromination and iodination of 2-aminobenzothiazoles. Isolated yields.	209
Scheme 5.14 2-arylbenzothiazole synthesis via Suzuki-Miyaura cross-coupling. Isolated yields.	210
Scheme 5.15 Isolated benzothiazole B-F _n complexes. Isolated yields.....	211
Scheme 5.16 Possible degradation pathway of 2-(benzo[d]thiazol-2-yl)aniline B-F _n complexes via HF elimination and hydrolysis	212

Scheme 5.17 Reported <i>N,N</i> -benzothiazole and <i>N,N</i> -benzoxazole B-F ₂ complexes ...	212
Scheme 5.18 mono <i>N</i> -methylation of 5.14 and 5.16 to 5.20 and 5.21, respectively. Isolated yields.	213
Scheme 5.19 Attempted formation of B-F _n complexes with 5.20 and 5.21.....	213
Scheme 5.20 Selective mono-arylation of 5.10 via Suzuki-Miyaura cross-coupling. Isolated yields.	214
Scheme 5.21 Synthesis of 5.25. Isolated yields.	215
Scheme 5.22 Synthesis of 2,4-diarylbenzothiazoles. Isolated yields.	216
Scheme 5.23 Isolated B-F _n complexes	217
Scheme 5.24 Selected examples of chiral boron complexes	220
Scheme 5.25 Synthesis of racemic 5.32	221
Scheme 5.26 Selected examples of highly conjugated (top) and enhanced D-π-A (bottom) 2-arylbenzothiazole B-F ₂ complexes.....	227
Scheme 5.27 BODIPY radiolabelling strategies via hydroxide (a) or triflate pre-activation (b) and Brønsted or Lewis acid-assisted IEX (c)	235
Scheme 5.28 Fluoride abstraction from 5.19 to form 5.33 and proposed regeneration of 5.19 by addition of [F ⁻] source	236
Scheme 5.29 Isolated and characterised B-F _n complexes	239
Scheme 5.30 Prospective theranostic platform based on benzothiazole ligand.....	240
Scheme 6.1 Reaction summary for one-pot two-step Balz-Schiemann reaction with organotrifluoroborates.	275
Scheme 6.2 Reaction summary for thermolysis of unsymmetrical diaryliodonium phenyltrifluoroborate salts.	276

Scheme 6.3 Molecular scaffolds for intramolecular fluorination using trifluoroborate moiety.....	277
Scheme 6.4 Isolated and characterised B-F _n complexes.....	278
Scheme 6.5 Fluoride abstraction from 5.19.....	278
Schéma 7.1 La réaction Balz-Schiemann.	281
Schéma 7.2 Fluoration du sel d'aryle diazonium avec du phényltrifluoroborate.....	281
Schéma 7.3 Substrat de la réaction de Balz-Schiemann en un pot avec le phényltrifluoroborate de potassium. Conditions de réaction : aniline (0,25 mmol), 85% H ₃ PO ₄ aq. (0,5 éq.), Phényltrifluoroborate de potassium (0,38 mmol), <i>t</i> -BuOH (1,3 ml) dans un flacon de pression avec capuchon doublé de téflon, purge Ar, puis <i>t</i> -BuONO (0,38 mmol), t.a. pendant 20 min, puis chauffé à 45-50 °C pendant 2h. Rendement déterminé par RMN ¹⁹ F en utilisant le 2,4-dinitrofluorobenzène comme étalon interne. Rendement isolé entre parenthèses. ^a 98% H ₂ SO ₄ utilisé comme acide dans du <i>t</i> -BuOH à 95 ° C.....	284
Schéma 7.4 Sels de tétrafluoroborate de diaryliodonium dissymétriques synthétisés.	286
Schéma 7.5 Sels de phényltrifluoroborate de diaryliodonium dissymétriques synthétisés.	286
Schéma 7.6 Substrats proposés pour la fluoration intramoléculaire avec des trifluoroborates. [B] = BF ₃ ⁻ , B(OR) ₂ (R = H, alkyle).....	289
Schéma 7.7 Synthèse du diazoniotrifluoroborate 4.21.....	290
Schéma 7.8 Complexes B-F _n isolés et caractérisés.....	292
Schéma 7.9 Abstraction du fluorure de 5.19 à la forme 5.33.	295

Schéma 7.10 Résumé de la réaction de Balz-Schiemann en deux étapes en un pot avec des organotrifluoroborates.	296
Schéma 7.11 Résumé de la réaction pour la thermolyse de sels de phényltrifluoroborate de diaryliodonium dissymétriques.	297
Schéma 7.12 Motifs moléculaires pour la fluoration intramoléculaire utilisant un groupement trifluoroborate.	298
Schéma 7.13 Complexes B-F _n isolés et caractérisés.	298
Schéma 7.14 Abstraction du fluorure de 5.19.	299

List of Figures

Figure 1.1 Basic schematic of PET imaging.....	19
Figure 1.2 Basic schematic of NIRF imaging.	28
Figure 2.1 a, implicated mechanisms in the dediazonation of aryl diazonium tetrafluoroborates. b, isotopic rearrangement of ¹⁵ N-labelled aryl diazonium salts.....	38
Figure 3.1 a, scope of nucleophiles arylated by diaryliodonium salts. b, intermediates implicated in the metal-free and metal-mediated arylation of nucleophiles with diaryliodonium salts.....	92
Figure 3.2 λ ³ -iodane equilibrium. a, electronic effect on equilibrium. b, steric "ortho" effect on equilibrium.....	94
Figure 3.3 X-ray crystal structures of 3.20, diphenyliodonium tetrafluoroborate (3.27), ²⁰⁹ (2-methylphenyl)(phenyl)iodonium fluoride (3.28). ²⁰⁹ Solvent molecules omitted for clarity. Hydrogen in white, carbon in grey, iodine in purple, boron in pink, fluorine in green/yellow.	108
Figure 4.1 Selected fluorinating agents: anhydrous TBAF for nucleophilic fluorination, PhenoFluor™ for deoxyfluorination, Selectfluor® for electrophilic fluorination.	133
Figure 4.2 ¹ H- ¹⁹ F HMBC NMR spectroscopy showing the correlation between methylene protons and fluorine atoms in 4.39.	154
Figure 4.3 ATR IR spectrum of 4.21.....	156
Figure 5.1 The amyloid cascade hypothesis (adapted with permission from Noël <i>et al.</i> , <i>Chem. Soc. Rev.</i> , 2013, 42, 7747-7762, copyright Royal Society of Chemistry).....	190

Figure 5.2 [¹¹ C]-PiB standardized uptake value (SUV) in healthy (left) and AD (right) patients (adapted with permission from Klunk <i>et al.</i> , <i>Ann. Neurol.</i> , 2004, 55, 306-319, copyright John Wiley and Sons).....	193
Figure 5.3 Enantiomers of 5.19 in the X-ray crystal structure. Hydrogen atoms omitted for clarity.....	221
Figure 5.4 HPLC chromatogram of racemic 5.19 (left), 5.19a (right, top) and 5.19b (right, bottom) after 1 week.....	222
Figure 5.5 CD spectra of 5.19 _{rac} , 5.19a and 5.19b in CH ₂ Cl ₂ at 25 °C	223
Figure 5.6 Calculated FMOs, excitation energies and corresponding oscillator strengths (f) for 5.17 (left), 5.18 (middle) and 5.19 (right)	230
Figure 5.7 ¹⁹ F and ¹¹ B NMR spectra evolution for 5.17 (top two spectra) and 5.19 (bottom two spectra) in CD ₃ CN/D ₂ O.....	233
Figure 5.8 Evolution of ¹⁹ F (top), ¹¹ B (middle) and ¹ H (bottom) NMR spectra of 5.19 with TMS-OTf	238
Figure 7.1 Chromatogramme HPLC de racémique 5.19 (à gauche), 5.19a (à droite, en haut) et 5.19b (à droite, en bas) après 1 semaine.....	294

List of Abbreviations and Symbols

(p,n)	(proton,neutron)
β^+	positron
Δ	heat
ΔG	change in Gibbs free energy
Δ_{ss}	Stokes shift
λ^3	oxidation state +3, (III)
λ_{abs}	absorbance wavelength
λ_{em}	emission wavelength
λ_{exc}	excitation wavelength
λ_{max}	absorption maximum
σ^*	antibonding orbital of sigma symmetry
Φ_F	fluorescence quantum yield
$^{\circ}C$	degrees Celsius
AcOH	acetic acid
AD	Alzheimer's disease
A β	amyloid-beta
AlkylFluor	1,3-bis(2,6-diisopropylphenyl)-2-fluoro-1 <i>H</i> -imidazol-3-ium tetrafluoroborate
BBB	blood-brain barrier
B ₂ pin ₂	bis(pinacolato)diboron
B-F	Boron-Fluorine
BF ₃ ·OEt ₂	boron trifluoride diethyl etherate complex
BF ₄ ⁻	tetrafluoroborate anion
Boc	<i>tert</i> -butyl carbamate
Boc ₂ O	di- <i>tert</i> -butyl dicarbonate
BODIPY	boron-dipyrromethene
CD	circular dichroism
C-F	Carbon-Fluorine
CN	cyano

C-Pb	Carbon-Lead
CR	Congo red
CS _N Ar	concerted nucleophilic aromatic substitution
CT	computed tomography
CuAAC	copper(I)-catalysed alkyne-azide cycloaddition
DAST	diethylaminosulphur trifluoride
dba	dibenzylideneacetone
DBH	1,3-dibromo-5,5-dimethylhydantoin
DDQ	2,3-dichloro-5,6-dicyano- <i>p</i> -benzoquinone
DEAD	diethyl azodicarboxylate
Deoxo-Fluor	bis(2-methoxyethyl)aminosulphur trifluoride
DIPEA	<i>N,N</i> -diisopropylethylamine
DMA	<i>N,N</i> -dimethylacetamide
1,2-DME	1,2-dimethoxyethane
DMDO	dimethyldioxirane
DMF	<i>N,N</i> -dimethylformamide
DMSO	dimethyl sulfoxide
dppf	1,1'-ferrocenediyl-bis(diphenylphosphine)
D-π-A	Donor-π-Acceptor
EAS	electrophilic aromatic substitution
EMA	European Medicines Agency
Et ₂ O	diethyl ether
Et ₃ O ⁺	triethyloxonium
EtOH	ethanol
f	oscillator strength
FDA	Food and Drug Administration
FDG	fluoro-2-deoxy-D-glucose
FMO	frontier molecular orbital
<i>gem</i>	geminal
HBpin	pinacolborane
HFIP	hexafluoroisopropanol

HMBC	heteronuclear multiple bond correlation
HOMO	highest occupied molecular orbital
HPLC	high-performance liquid chromatography
IEX	isotopic exchange
<i>i</i> OPr	isopropyl
LA	Lewis acid
LUMO	lowest unoccupied molecular orbital
<i>m</i>	<i>meta</i>
<i>m</i> CPBA	<i>meta</i> -chloroperoxybenzoic acid
MeCN	acetonitrile
MeOH	Methanol
MesI(OAc) ₂	iodomesitylene diacetate
MIDA	methyliminodiacetic acid
MRI	magnetic resonance imaging
MS	mass spectrometry
MTBE	methyl <i>tert</i> -butyl ether
NBS	<i>N</i> -bromosuccinimide
NFSI	<i>N</i> -fluorobenzenesulphonimide
NEt ₃	triethylamine
NIR	near-infrared
NIRF	NIR fluorescence
NMR	nuclear magnetic resonance
<i>o</i>	<i>ortho</i>
OAc	acetate anion
OMe	methoxy
OTf	trifluoromethanesulfonate, triflate
<i>p</i>	<i>para</i>
PCM	polarizable continuum model
PEG	polyethylene glycol
PET	Positron Emission Tomography
PhBF ₃ K	potassium phenyltrifluoroborate

PhenoFluor	1,3-bis(2,6-diisopropylphenyl)-2,2-difluoro-2,3-dihydro-1 <i>H</i> -imidazole
PIDA	phenyliodine(III) diacetate
pK _a	acid dissociation constant
PPh ₃	triphenylphosphine
ppm	parts-per-million
<i>p</i> -TsOH	<i>para</i> -toluenesulfonic acid
RCC	radiochemical conversion
ROS	reactive oxygen species
S ₀	ground state
S ₁	first excited state
SA	specific activity
S-C	Sulphur-Carbon
Selectfluor	1-chloromethyl-4-fluoro-1,4-diazoniabicyclo[2.2.2]octane bis(tetrafluoroborate)
S _N 1	unimolecular nucleophilic substitution
S _N Ar	nucleophilic aromatic substitution
S _n <i>i</i>	internal nucleophilic substitution
SPECT	single photon-emission CT
SPhos	2-dicyclohexylphosphino-2',6'-dimethoxybiphenyl
S ₂	second excited state
t _{1/2}	half-life
TBACN	tetra- <i>n</i> -butylammonium cyanide
TBAF	tetra- <i>n</i> -butylammonium fluoride
TBAI	tetra- <i>n</i> -butylammonium iodide
TBASPh	tetra- <i>n</i> -butylammonium phenylthiolate
<i>t</i> -BuLi	<i>tert</i> -butyllithium
<i>t</i> -BuOH	<i>tert</i> -butanol
<i>t</i> -BuOK	potassium <i>tert</i> -butoxide
<i>t</i> -BuONO	<i>tert</i> -butylnitrite
<i>t</i> -Butyl	<i>tert</i> -butyl

TD-DFT	time-dependent density functional theory
TEMPO	2,2,6,6-tetramethyl-1-piperidinyloxy
Tf ₂ O	trifluoromethanesulfonic anhydride
TFA	trifluoroacetic acid
THF	tetrahydrofuran
ThS	Thioflavin S
ThT	Thioflavin T
TLC	thin-layer chromatography
TMAF	tetramethylammonium fluoride
TMS	trimethylsilyl
US	ultrasound
XantPhos	4,5-bis(diphenylphosphino)-9,9-dimethylxanthene

Acknowledgements

I would firstly like to express my sincere gratitude to my supervisors Prof. David M. Perrin and Dr. Emmanuel Gras. I would like to thank them for taking a chance on me and accepting me into their research groups. Their dedication towards their research programs and students is admirable and it has been a real privilege to observe and participate in. They have allowed me to freely explore chemistry, to make mistakes and most importantly to learn. They have been exceptional mentors, who have been supportive throughout this experience. It has been my pleasure to experience their creativity, enthusiasm and passion for chemistry and research.

I would also like to sincerely thank my supervisory committee, Prof. Ed Grant, Prof. Jason Hein and Prof. Laurel Schafer. I am particularly grateful to Prof. Hein and Prof. Schafer for their time in reviewing this thesis and their useful comments. Their support throughout is greatly appreciated.

None of this work would have been possible without the excellent support of exceptional people in the offices, shops and services of both institutions. I would particularly like to thank Isabelle Fabing for help with preparative chiral HPLC and Dr. Charles-Louis Serpentine for help with CD spectroscopy. Sincere thanks to our secretary at UBC Sheri Harbour for her tireless and amazing work. Sincere thanks to Catherine Stasiulis and Sandra Geminiano at our Human Resources and International Relations offices at UPS for all their help with cotutelle PhD contracts, visas and residency permits.

I would have not been able to finish this work without the financial support of the French Canada Research Fund (FCRF), they are gratefully acknowledged. Financial support from the Arnold By fellowship is also gratefully acknowledged.

I am very grateful to Samson Lai and Nicolas Jean-Bart, two exceptional students who worked with me. Their dedication, passion, work ethic and humour has been a pleasure.

Thanks to the joint PhD I have had the honour and privilege of becoming part of two research groups, the Perrin lab and Equipe F. I would really like to thank all members of these groups, past and present, for the years we have shared together, through the anxiety, frustration and more importantly the laughter and good times. It has been a real pleasure to interact with individuals of such a high calibre, resilience, character and humour. It has been my honour to know all of you.

Surviving these past few years would have been impossible if it were not for the unwavering support of great friends. From housing me while homeless in my transition between two countries, to always being there for a game of basketball, squash or a run, to being there for a drink, laugh and holding a pan. I am deeply grateful to all of you for your company, support and encouragement.

Most importantly, I thank my family. To my parents, this work is yours, this is your achievement more than it is mine, this is a testament to how you educated me and the values you instilled in me. To my parents, brother, aunts and the rest of the family: your support has been invaluable and encouragement lifting.

1 Introduction

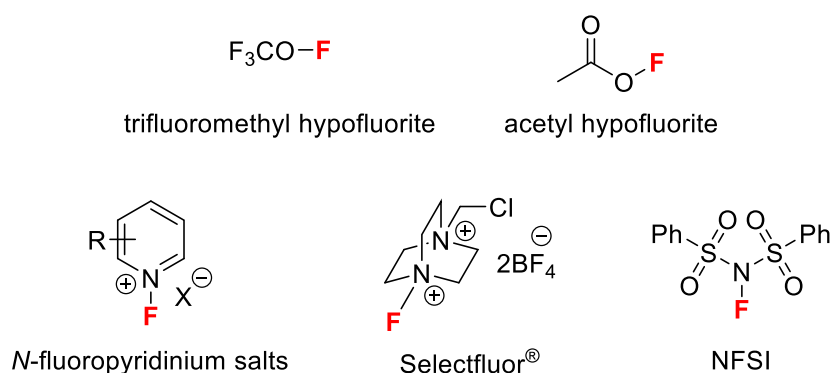
This thesis is built around one central theme, the Boron-Fluorine (B-F) bond. The B-F bond has an expansive and rich history in chemical transformations as well as materials and fundamental bonding studies, while finding valuable applications in organic structure elaboration by contributing to the domains of cross-coupling reactions,¹ fluoride ion capture and sensing,² and fluorination in both chemical and radiochemical contexts³ among countless others. The versatility of the B-F bond has also shown immense utility in fields as far reaching as Positron Emission Tomography (PET)⁴ and fluorescence imaging⁵. We are especially interested in the use of the B-F for nucleophilic Carbon-Fluorine (C-F) bond formation and the development of novel fluorophores with potential applications as bi-modal PET/fluorescence imaging agents. A general bibliographic presentation of the B-F bond in C-F bond formation and its use in PET and fluorescence imaging probes will be detailed in this chapter.

1.1 Sources of fluorine in organic synthesis

The fluorine atom is a versatile tool in the chemist's tool box. Its incorporation in a molecule can have dramatic effects on pK_a , conformation, lipophilicity, bioavailability and metabolic stability.⁶⁻¹¹ The remarkable ability of fluorine to induce such favourable properties has underscored the need for and driven the development of practical and efficient fluorination methodologies. To this end, various nucleophilic, electrophilic and radical fluorination strategies have been reported.¹²

1.1.1 Electrophilic and radical sources of fluorine

Generally, the sources of fluorine described below can function as sources of both electrophilic (F^+) and radical ($F\cdot$) fluorine, expression of either form of reactivity is highly dependent on reaction conditions. The main source of F^+ and $F\cdot$ is F_2 , this gas is highly reactive and as such reactions can often be unselective; diluting F_2 in inert gases (N_2) has been used as a strategy to control reactivity.¹³ Xenon difluoride (XeF_2) has been found as an easier to handle alternative. F^+ itself does not exist as an independent species, however several strategies have been developed to allow nucleophilic attack at fluorine effectively allowing F^+ transfer. The use of electron-withdrawing or good leaving groups adjacent to fluorine have been successful in the generation of numerous F^+ reagents (Scheme 1.1).



Scheme 1.1 Examples of $F^+/F\cdot$ reagents.

Fluoroxy reagents, such as trifluoro and acetyl hypofluorite, can serve as both F^+ and $F\cdot$ sources, however their toxicity and latent explosivity has limited their use.¹³ Through the stronger N-F bond (see Table 1.1), N-F reagents are more stable and have the added advantage of usually being solid and crystalline facilitating their handling.¹³ Given these favourable properties a vast number of N-F reagents have been developed the most

notable of which are SelectfluorTM and *N*-fluorobenzenesulphonimide (NFSI). The use of these reagents has greatly facilitated the advancement of electrophilic fluorination reactions.¹³

Table 1.1 Bond Dissociation Energies of O-F or N-F bond from selected electrophilic fluorine reagents^{14,15}

Reagent	Bond Dissociation Energy (kcal/mol)
trifluoromethyl hypofluorite (O-F)	44 ^a
NFSI (N-F)	63 ^b
Selectfluor [®] (N-F)	64 ^b
<i>N</i> -fluoropyridinium (N-F)	76 ^b

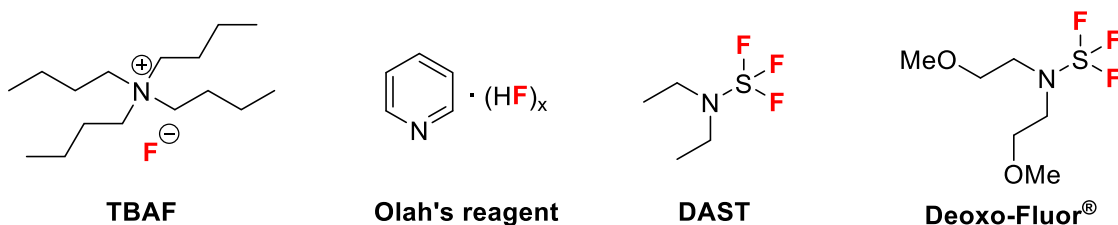
^a experimental value. ^b calculated values.

1.1.2 Nucleophilic sources of fluorine

Typical sources of nucleophilic “naked” fluoride (F⁻) are inorganic alkali metal fluoride (MF) salts such as NaF, KF, CsF and KHF₂. However, these salts are generally insoluble in organic solvents due to tight ion-pair formation. While soluble in water, F⁻ displays low nucleophilicity due to its high hydration energy (-104 kcal/mol).¹⁶ Common strategies for improving the solubility and reactivity of MF salts include increasing reaction temperatures and the use of chelating agents (crown ethers or cryptands) or solvents (glymes and glycols).¹³

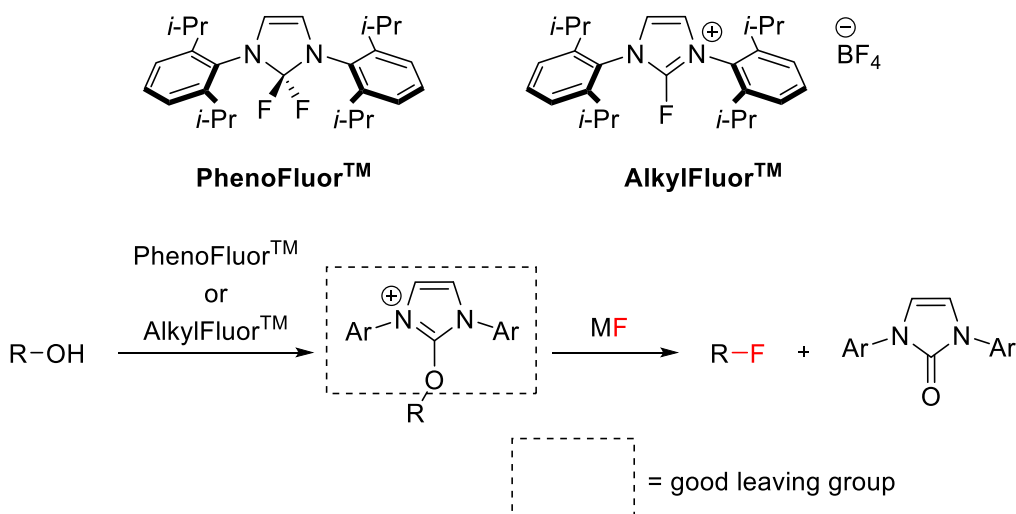
Efforts to overcome inherent drawbacks of MF salts led to development of various nucleophilic fluorinating agents (Scheme 1.2). Tetra-*n*-butylammonium (TBAF) has become a widely used fluorinating agent, and further advancements by DiMagno *et al.* in the production of anhydrous TBAF demonstrate the effectiveness of this reagent in the fluorination of various substrates.^{17,18} Polypyridinium hydrogen fluoride, more commonly

known as “Olah’s reagent”, and other alkyl amine hydrogen fluorides were developed to “tame” the corrosive nature of anhydrous hydrogen fluoride, and have found widespread applications in the fluorination of alkene and epoxide functionalities.^{13,19,20} Sulphur-based reagents such as diethylaminosulphur trifluoride (DAST) and Deoxo-Fluor[®] have been successfully used in deoxofluorination reactions.



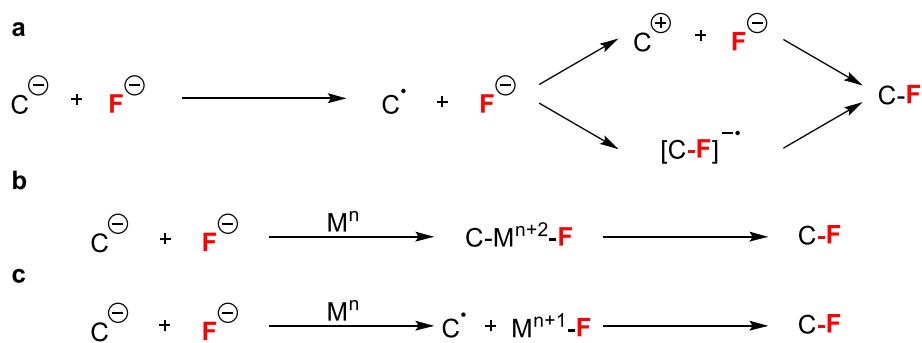
Scheme 1.2 Selected nucleophilic fluorinating agents.

Ritter *et al.* have also developed a suite of deoxyfluorination reagents that use simple MF salts (CsF and KF) as sources of F⁻ (Scheme 1.3). These reagents activate the alcohol or phenol into a leaving group which then allows facile fluorination by F⁻. Using these reagents, a wide substrate scope of phenols and alcohols can be fluorinated with good functional group tolerance.²¹ PhenoFluor[™] will be discussed in further detail in chapter 4.



Scheme 1.3 Deoxyfluorination reagents developed by Ritter *et al.* (top) and postulated leaving group formed by reagents (bottom).

Finally, oxidative fluorination strategies have been developed as alternatives to electrophilic fluorination methodologies. These methods allow access to electron-rich fluorinated systems via reactivity umpolung of the substrates. Oxidative fluorination using F^- can proceed in 3 ways: a) oxidation of the substrate to form an electrophilic carbon centre which is fluorinated by F^- , b) oxidation of the substrate to form a high-valent metal fluoride intermediate from which reductive elimination occurs to produce the fluorinated substrate and c) oxidation of the substrate to form a carbon-centred radical or radical cation species followed by radical fluorination (Scheme 1.4).²² Examples of these pathways will be discussed in the next section.

Scheme 1.4 Oxidative fluorination pathways with F⁻.

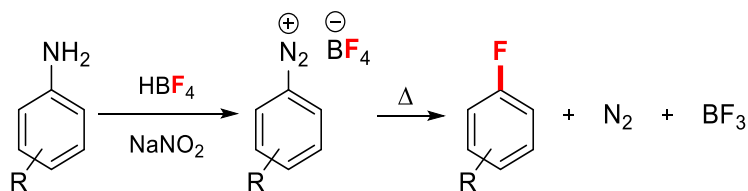
1.1.2.1 The B-F bond as a F⁻ source

The use of the B-F bond as a F⁻ source for various organic transformations is well documented. Historical applications and new paradigms using B-F bonds for fluorination will be outlined in the following sections.

1.1.2.2 BF₄⁻ and BF₃·OEt₂ as F⁻ sources

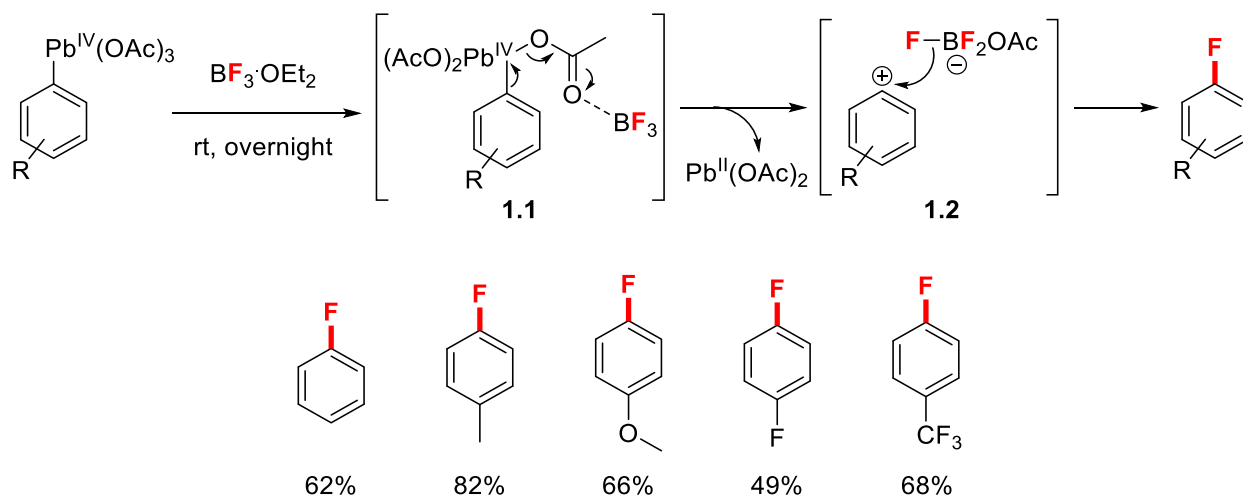
The use of the tetrafluoroborate ion (BF₄⁻) and boron trifluoride diethyl etherate (BF₃·OEt₂) as sources of F⁻ remain attractive as they are inexpensive, easy to use, soluble in organic solvents and are of low molecular weight and high F⁻ content.³ BF₄⁻ and BF₃·OEt₂ have been employed in a multitude of reactions including the ring-opening fluorination of strained ring systems, and addition to unsaturated systems such as alkenes and alkynes (examples of these reactions will be detailed in chapter 4). The following section will present selected examples of the application of BF₄⁻ and BF₃·OEt₂ as F⁻ sources in C-F bond formation.

The earliest and most representative example of BF₄⁻ as a F⁻ source is the Balz-Schiemann reaction, first reported in 1927 (Scheme 1.5).²³ While this reaction will be the focus of chapter 2, it is an important milestone to mention in the use of the B-F bond for fluorination.



Scheme 1.5 The Balz-Schiemann reaction.

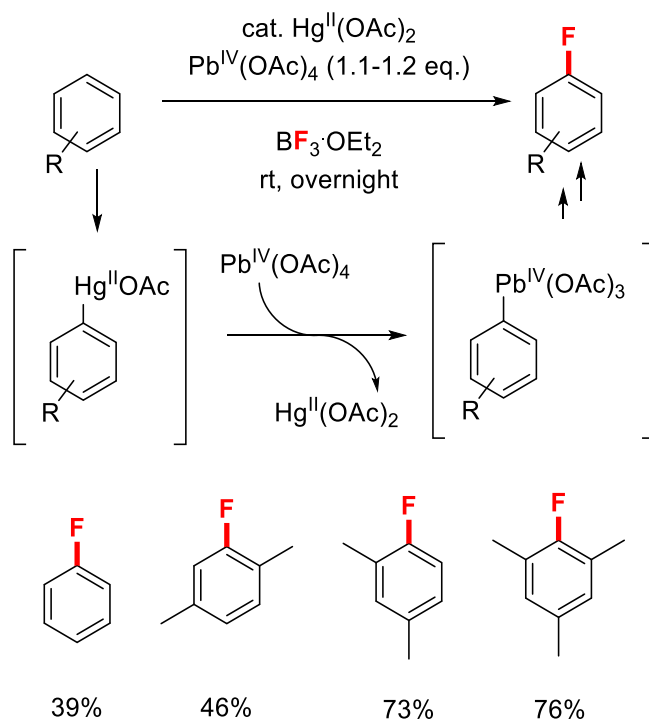
An alternative approach to the synthesis of aryl fluorides, reported by Pinhey *et al.*, is the fluorodeplumbation of aryllead(IV) acetates by excess $\text{BF}_3 \cdot \text{OEt}_2$ (Scheme 1.6). This methodology allowed the synthesis of a range of electron-rich and electron-poor aryl fluorides in low to good yields.^{24,25} Fluorination was proposed to occur via BF_3 -assisted heterolytic cleavage of the C-Pb bond (Scheme 1.6, intermediate 1.1) to generate aryl cation intermediate 1.2, which is fluorinated by the OAcBF_3^- ion. This methodology could also be extended to the fluorination of aryltrimethylsilanes and triarylboroxines using stoichiometric $\text{Pb}(\text{OAc})_4$ and $\text{BF}_3 \cdot \text{OEt}_2$ as the solvent, avoiding the isolation of aryllead(IV) triacetates.



Scheme 1.6 Fluorination of aryllead(IV) acetates.

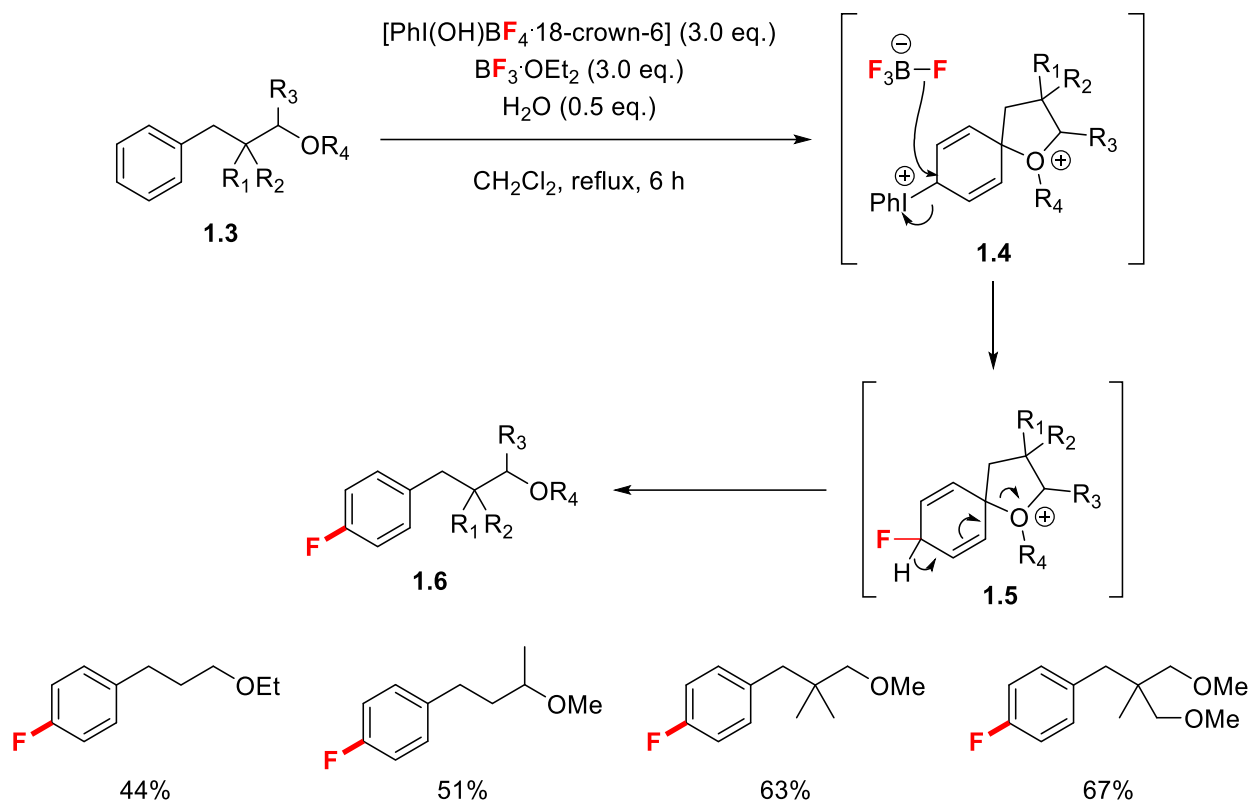
The authors also reported that simple arenes could be fluorinated in good yields in the presence of catalytic amounts of $\text{Hg}(\text{OAc})_2$ and stoichiometric amounts of $\text{Pb}(\text{OAc})_4$ in

$\text{BF}_3 \cdot \text{OEt}_2$ (Scheme 1.7).²⁴ The transformation is proposed to occur via initial electrophilic aromatic mercuration, followed by transmetalation from mercury to lead, after which fluorination occurs through similar intermediates proposed in scheme 1.6.



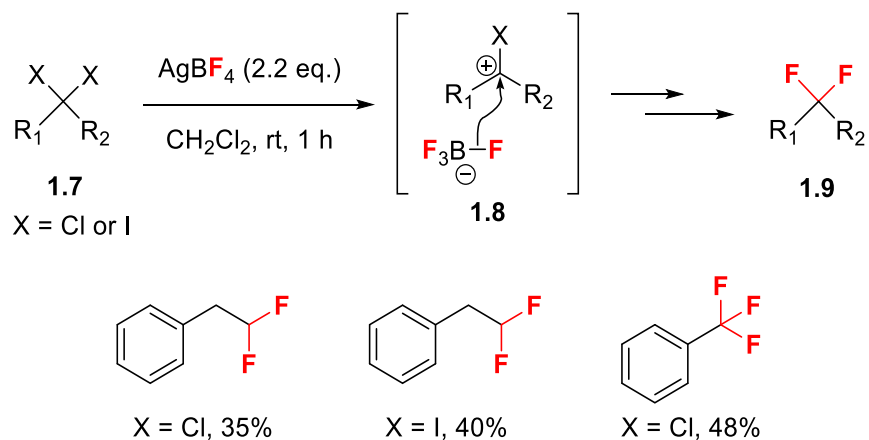
Scheme 1.7 Fluorination of simple arenes $\text{BF}_3 \cdot \text{OEt}_2$.

Miyamoto *et al.*, reported access to aryl fluorides via selective *para*-fluorination of 3-phenylpropyl ethers in low to good yields (Scheme 1.8).²⁶ The hypervalent phenyl- λ^3 -iodane mediated reaction is proposed to occur via initial electrophilic iodination of **1.3** at the *para* position, followed by intramolecular ether oxygen attack to furnish intermediate **1.4**. Nucleophilic fluorine substitution of the phenyl- λ^3 -iodanyl group by BF_4^- generates intermediate **1.5**, which upon subsequent re-aromatization provides fluorinated products **1.6**.



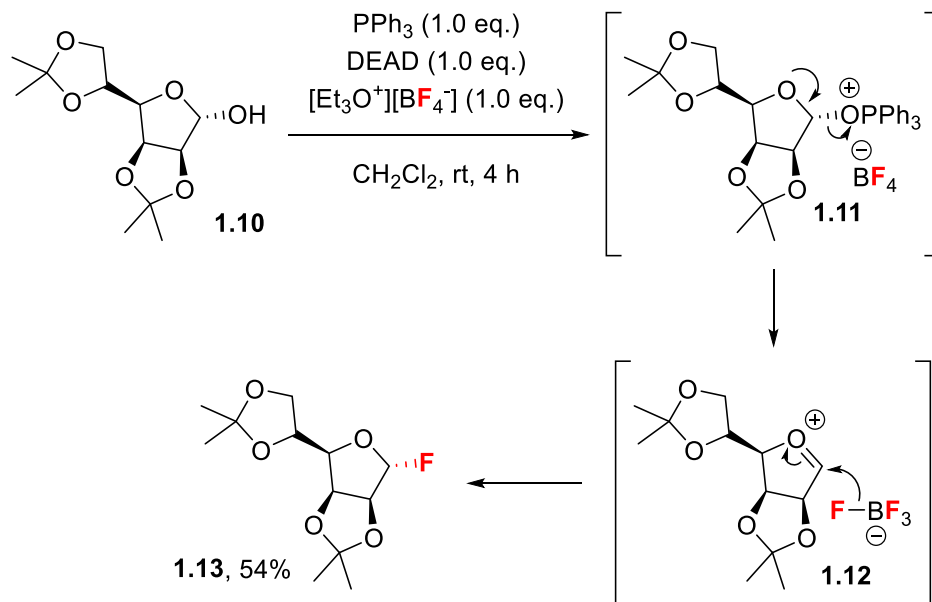
Scheme 1.8 Fluorination of 3-phenylpropyl ethers.

Bloodworth and Mitchell *et al.* demonstrated the fluorination of halocarbenium ions in the presence of BF₄⁻ that afforded convenient access to *gem*-difluorides under mild conditions (Scheme 1.9).²⁷ Silver-induced dehalogenation of *gem*-dichlorides and iodides **1.7**, generates halocarbenium ion **1.8**, which is consequently fluorinated by BF₄⁻ to provide a series of *gem*-difluorides **1.9** in moderate yields. Under these same conditions, α,α,α-trifluorotoluene could be obtained from α,α,α-trichlorotoluene in 48% yield.



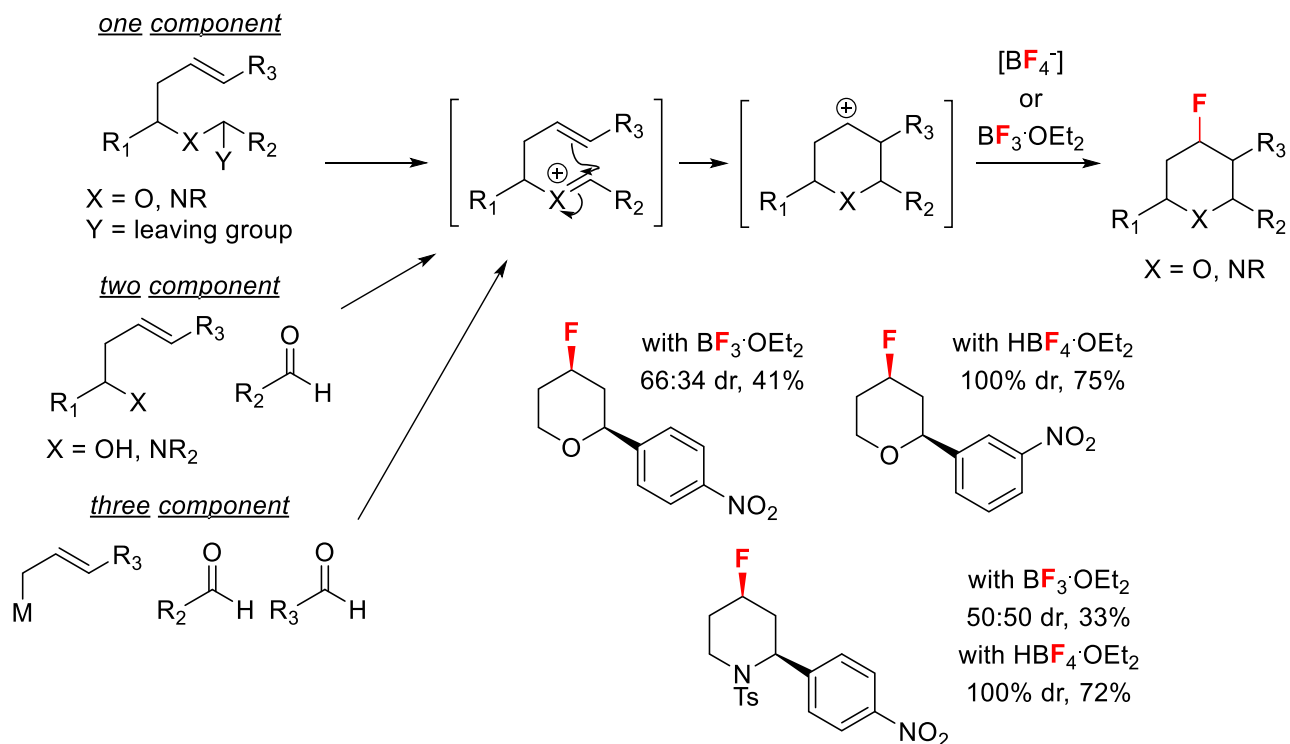
Scheme 1.9 Fluorination of *gem*-dichlorides/iodides and trichlorotoluene with AgBF_4 .

A novel modification of the Mitsunobu reaction was reported by Kunz and Swager, where diisopropylidene-mannofuranose **1.10** is converted into the corresponding glycosyl fluoride **1.13**, in 54% yield, by treatment with diethyl azodicarboxylate (DEAD), PPh_3 and triethyloxonium tetrafluoroborate ($[\text{Et}_3\text{O}^+][\text{BF}_4^-]$). The reaction is proposed to occur via formation of alkoxytriphenylphosphonium intermediate **1.11**, which collapses to the glycosyl cation **1.12** and undergoes consequent fluorination by BF_4^- to produce the glycosyl fluoride **1.13** (Scheme **1.10**).²⁸



Scheme 1.10 Modified Mitsunobu reaction for the synthesis of glycosyl fluoride **1.13**.

An important reaction class in which BF_4^- and $\text{BF}_3 \cdot \text{OEt}_2$ have found notable applications is the Prins cyclization-fluorination (Scheme **1.11**). One-, two- and three-component oxa-Prins cyclization-fluorination reactions allow access to a variety of substituted 4-fluorotetrahydropyrans.^{29–31} Similarly, substituted 4-fluoropiperidenes can be synthesized through one and two component aza-Prins cyclization-fluorination.^{30,32} When $\text{BF}_3 \cdot \text{OEt}_2$ is used as the F^- source, diastereoselectivities of oxa- and aza-Prins cyclization-fluorination products were generally found to be low as reported by O'Hagan *et al.*³⁰ Interestingly, Yadav *et al.* showed that switching to $\text{HBF}_4 \cdot \text{OEt}_2$ improved yields and allowed the formation of 4-fluorotetrahydropyran and 4-fluoropiperidene products as single diastereomers.^{33,34}

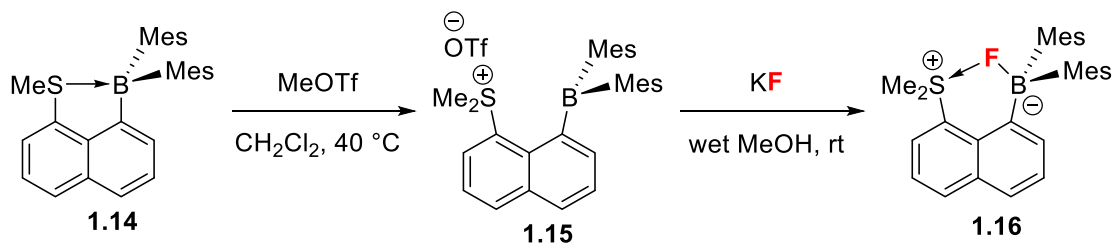


Scheme 1.11 Selected examples of oxa- and aza-Prins cyclization-fluorination reactions.

1.1.3 Organofluoroborates as F- sources

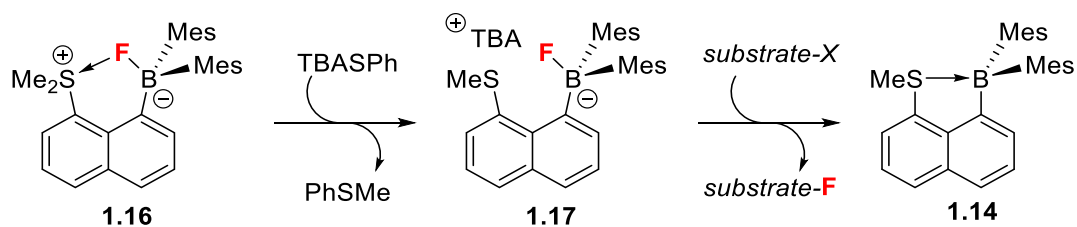
In contrast to the abundant use of BF_4^- and $BF_3 \cdot OEt_2$, there are few reports describing the use of organofluoroborates as nucleophilic F^- sources. Building on their expertise in the design and synthesis of cationic borane systems for F^- sensing,^{2,35,36} Gabbaï and Zhao reported the application of sulfonium boranes in the capture of F^- from aqueous solutions, followed by nucleophilic fluorination of organic substrates via a triggered release of F^- in organic solutions (Scheme 1.12).³⁷ Sulfonium borane **1.15**, obtained from the methylation of **1.14**, could be efficiently converted to the corresponding zwitterionic sulfonium fluoroborate **1.16** using KF in wet MeOH, highlighting the fluorophilicity of boron and the ability of cationic borane species to sequester F^- from aqueous solutions. Characterization of zwitterion **1.16** led the authors to conclude that the ability of **1.15** to

sequester F^- from aqueous solutions was due to favourable Coulombic effects and additional stabilization provided by donor-acceptor interaction between a lone pair on F and the Sulphur-Carbon (S-C) σ^* orbital. They further rationalized that if these stabilizing factors could be removed, then the lability of the B-F bond would greatly increase and F^- release could be triggered.



Scheme 1.12 Synthesis of zwitterionic sulfonium fluoroborate **1.16**.

Using tetra-*n*-butylammonium phenylthiolate (TBASPh), sulfonium fluoroborate **1.16** could be demethylated to furnish fluoroborate **1.17**. Addition of various organic substrates to solutions of **1.17** resulted in rapid and efficient fluorination of most substrates (Table **1.2**, entries 1, 2 and 3), whereas fluorination of benzylchloride and 1-bromooctane required heating of reaction mixtures (entries 4 and 5). The authors concluded that at ambient temperatures F^- transfer occurs directly from **1.17**, however at elevated reaction temperatures **1.17** dissociates to produce anhydrous TBAF.

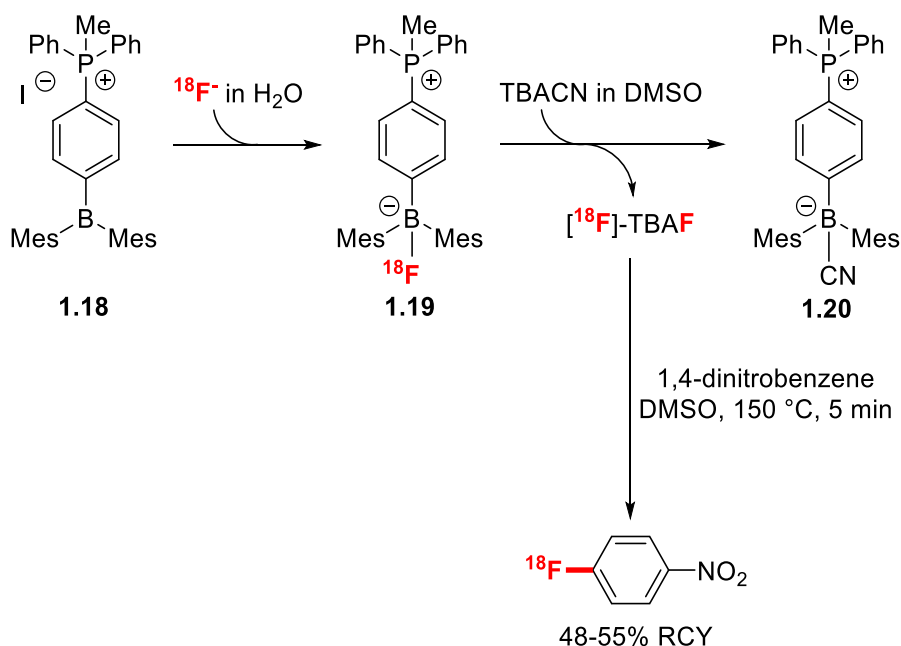
Table 1.2 Fluorination of various substrates using fluoroborate **1.17**

Entry	<i>substrate-X</i>	reaction conditions	<i>substrate-F</i>	Yield (%) ^a
1		1.17 (1.4 eq.) CD ₃ CN, rt, 5 min		>95
2		1.17 (1.4 eq.) CD ₃ CN, rt, 5 min		>95
3		1.17 (1.2 eq.) CD ₃ CN, rt, 2h		>95
4		1.17 (2.0 eq.) CD ₃ CN, 70 °C, 1 h		80
5		1.17 (2.0 eq.) CD ₃ CN, 70 °C, 1 h		45

^a Yield determined by integration of ¹H NMR spectra

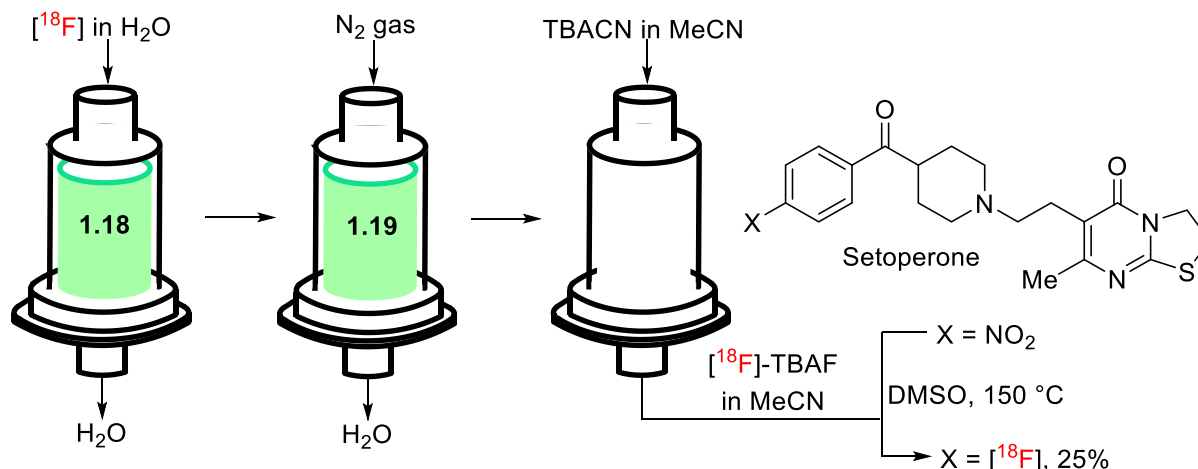
Inspired by this work, Gras and Perrio *et al.* demonstrated the extension of F⁻ capture/release by cationic boranes to radiofluorination (Scheme **1.13**).³⁸ Using phosphonium borane **1.18**, known to sequester F⁻ from aqueous solutions, the authors demonstrated the successful and quantitative trapping of ¹⁸F⁻ in water by **1.18** to generate

the zwitterionic phosphonium fluoroborate **1.19**. Zwitterion **1.19** was dried under a flow of N_2 and heating to remove all traces of water. $^{18}F^-$ release was triggered by anion exchange with tetra-*n*-butylammonium cyanide (TBACN), to produce anhydrous [^{18}F]-TBAF and phosphonium cyanoborate **1.20**. The authors then demonstrated that the anhydrous [^{18}F]-TBAF could be used in the nucleophilic aromatic fluorination of 1,4-dinitrobenzene to produce 4- ^{18}F -fluoronitrobenzene in 48-55% radiochemical yield.



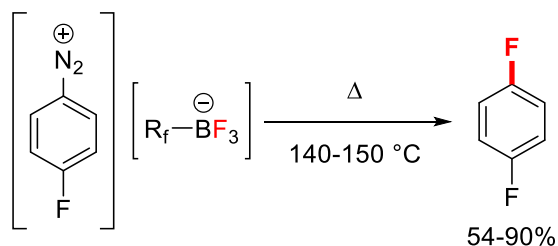
Scheme 1.13 $^{18}F^-$ capture/release using phosphonium boranes for radiofluorination.

The authors further demonstrated that the capture and release of $^{18}F^-$ could be adapted to a solid-supported adsorption strategy (Scheme **1.14**). A reverse-phase C18 cartridge was pre-loaded with **1.18** into which $^{18}F^-$ in water/MeCN was eluted to quantitatively produce **1.19** in the cartridge. Quantitative elution of $^{18}F^-$ was achieved using a MeCN/TBACN solution. The efficiency of this cartridge-based method was showcased by the synthesis of [^{18}F]-Setoperone, a 5-HT_{2A} antagonist.



Scheme 1.14 Cartridge-based ^{18}F - capture/release in the production of $[^{18}\text{F}]$ -Setoperone (adapted with permission from Perrio *et al.* *Chem. Commun.* **2017**, 53, 340-333, copyright Royal Society of Chemistry).

Frohn *et al.* reported the only example of employing organotrifluoroborates as F^- sources, describing the neat fluorodediazotiation of aryl diazonium perfluoroorganotrifluoroborates (Scheme 1.15).³⁹ This will be further detailed in chapter 2.

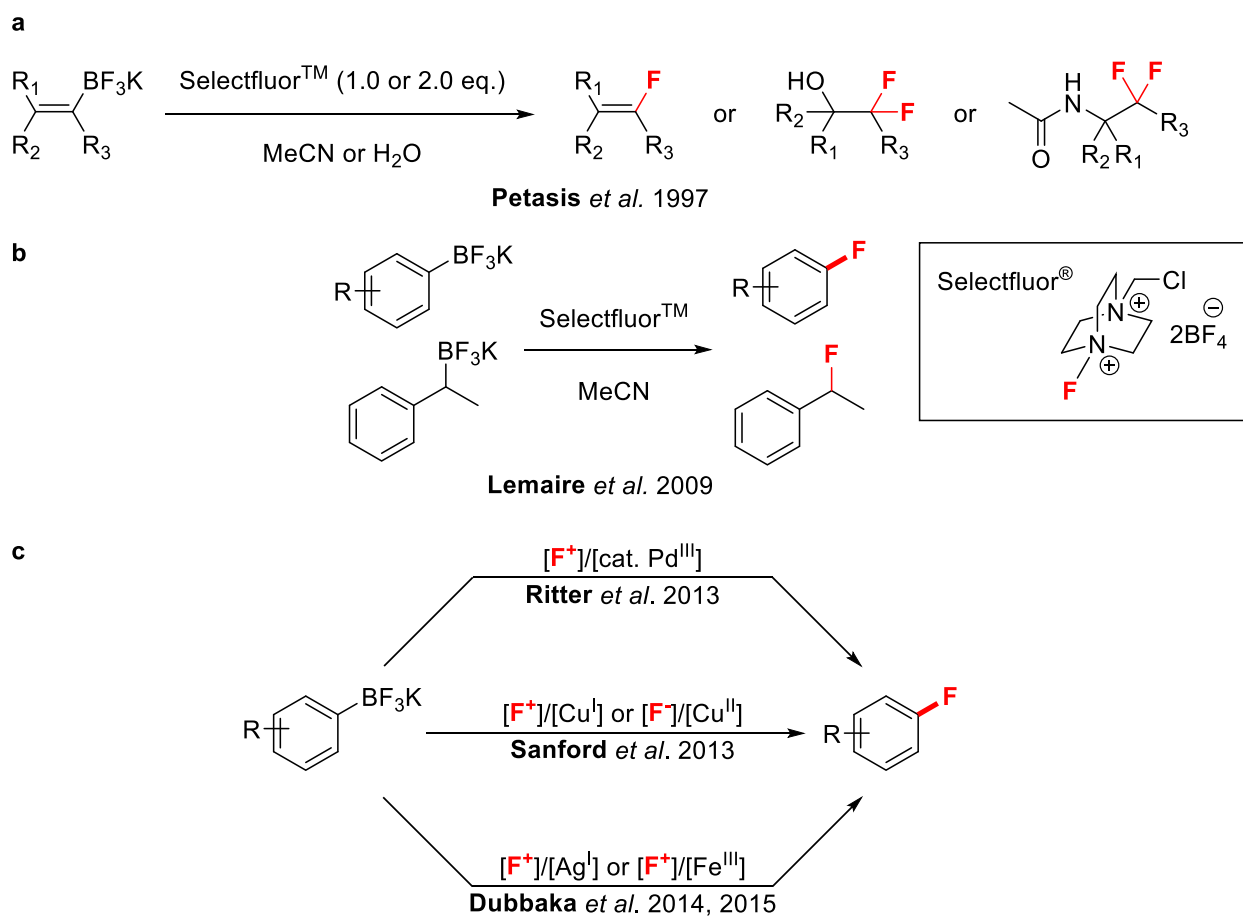


Scheme 1.15 Fluorodediazotiation of aryl diazonium perfluoroorganotrifluoroborates.

1.1.3.1 Fluorination of organotrifluoroborates

At this point it is important to note that organotrifluoroborates have been previously used in fluorination reactions, not as sources of F^- but as substrates. Petasis, Olah and Prakash *et al.* were the first to describe the electrophilic fluorination of alkenyl trifluoroborates using Selectfluor[®] to the corresponding alkenyl fluorides or difluoromethylated alcohols or amides (Scheme 1.16, a).⁴⁰ Over a decade later, Lemaire *et al.* extended this

methodology towards the fluorination of aryl and benzylic trifluoroborates (Scheme 1.16, **b**).⁴¹ The substrate scope of these transformations was expanded through metal-mediated processes (Scheme 1.16, **c**). Sanford *et al.* reported a Cu^I-mediated electrophilic fluorination of aryl trifluoroborates using *N*-fluoro-2,4,6-trimethylpyridinium triflate as an electrophilic fluorine (F⁺) source.⁴² The same authors then reported the Cu^{II}-mediated nucleophilic fluorination of aryl trifluoroborates using KF.⁴³ In the same year Ritter *et al.* described the Pd^{III}-catalysed fluorination of aryl trifluoroborates with Selectfluor[®].⁴⁴ Finally, Dubakka *et al.* described the Ag^I or Fe^{III}-mediated electrophilic fluorination of aryl trifluoroborates using Selectfluor[®].^{45,46}



Scheme 1.16 Metal-free fluorination of alkenyl (**a**) and aryl or benzylic (**b**) trifluoroborates. **c**, metal-mediated/catalysed fluorination of aryl trifluoroborates.

The works discussed above are the only examples of the use of organofluoroborates as sources of F^- for fluorination. Additionally, with only one report using organotrifluoroborates as a F^- source, the application of organotrifluoroborates in this context has been overlooked and merits further investigation.

1.2 Molecular Imaging

Molecular imaging is a rapidly evolving and expanding field that plays increasingly important roles in drug development, early disease diagnosis and therapeutic evaluation.^{47,48} Generally, molecular imaging is defined as the non-invasive “ability to visualize and quantitatively measure the function of biological and cellular processes *in vivo*”.⁴⁷ Molecular imaging requires two important aspects: 1) the probe/ligand used to detect a specific biological process must display a change in concentration or spectral properties and 2) an appropriate method is available to monitor these probes.⁴⁸ Typically, *in vivo* molecular imaging probes are Near-Infrared (NIR) emitting molecules or compounds that have been labelled with radioisotopes.^{47,48} Currently there are various molecular imaging modalities available, the choice of which is dependent on the desired application, these include: Computed Tomography (CT), PET, Single Photon-Emission CT (SPECT), Magnetic Resonance Imaging (MRI), Ultrasound (US) and Optical (near-infrared fluorescence (NIRF)) imaging. The following sections will focus on the use of B-F bonds in probes designed for use in PET and NIRF imaging.

1.2.1 PET imaging

PET imaging is based on the emission of a positron (β^+) resulting from the decay of a radionuclide. The emitted β^+ travels a mean free path, dependent on its kinetic energy

(determined by the nature of the radionuclide), before colliding with an electron (e^-) in the surrounding tissue and undergoing an annihilation event. The annihilation event results in the simultaneous emission of two γ -rays of equal energy (511 keV) and opposite direction. The γ -rays are detected on opposite sides of a circular array of detectors, from which the position of the annihilation event can be determined. Reconstruction of the location of these annihilation events produces a 3D image of regions in which the positron-emitting probe has accumulated (Figure 1.1).

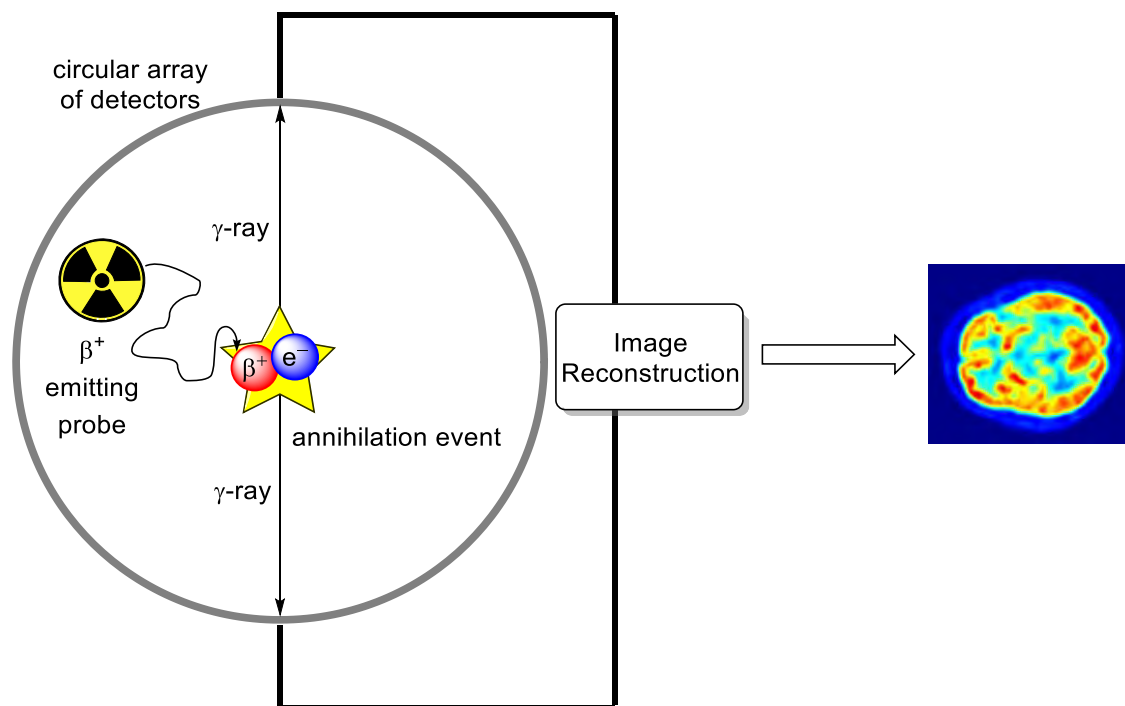
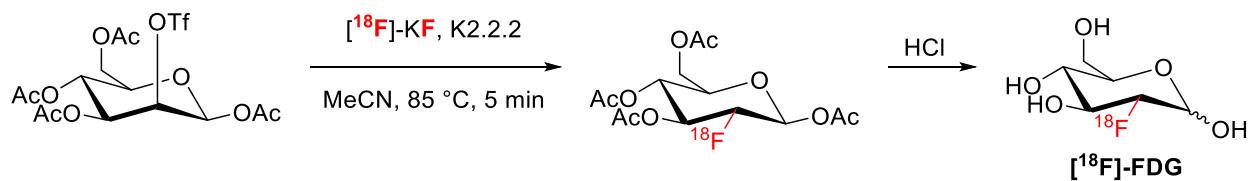


Figure 1.1 Basic schematic of PET imaging.

A range of β^+ radionuclides are commonly used in PET imaging including ^{11}C , ^{15}O , ^{18}F , ^{64}Cu , ^{68}Ga and ^{89}Zr . Among these ^{18}F has emerged as a radionuclide of particular utility in the radiolabelling of small molecules due to its small size, sufficient half-life ($t_{1/2} = 110$ min), weak β^+ energy (shorter mean free path) and clean decay (97% β^+ decay).

Most ^{18}F -labelled radiopharmaceuticals are synthesized using nucleophilic $^{18}\text{F}^-$ for C- ^{18}F bond formation, which is produced by the nuclear reaction of $^{18}\text{O}(p,n)^{18}\text{F}$ through the proton bombardment of $[^{18}\text{O}]\text{-H}_2\text{O}$ in a cyclotron.^{49,50} A consequence of the high hydration energy of the fluoride anion, radiotracer syntheses typically require the stringent “drying” of generated $^{18}\text{F}^-$. In most cases $^{18}\text{F}^-$ is trapped on an anion exchange column, then eluted in a mixture of water and acetonitrile with a base and a cryptand (usually K.2.2.2). Water is ultimately removed by repeated cycles of azeotropic drying under heating, reduced pressure and inert gas flow. Finally, radiofluorination can occur in anhydrous solvent (routinely MeCN, DMSO or DMF) at elevated temperatures.⁴⁹ This process has been extensively used for the production of many ^{18}F -PET imaging probes,^{49,50} most notably 2- $[^{18}\text{F}]$ -fluoro-2-deoxy-D-glucose ($[^{18}\text{F}]\text{-FDG}$) which has found extensive diagnostic applications in oncology among other domains (Scheme 1.17).^{51,52}

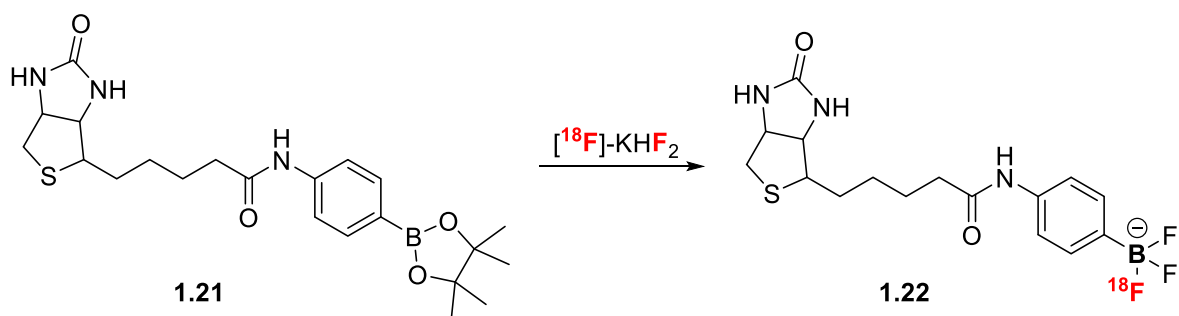


Scheme 1.17 Synthesis of $[^{18}\text{F}]\text{-FDG}$.

1.2.1.1 B-F in PET Imaging

To circumvent some of the limitations associated with traditional C- ^{18}F bond formation, other groups have looked towards harnessing the fluorophilicity of main group elements as a way to introduce ^{18}F into molecules of interest. To this end, ^{18}F -labelling has been reported with the formation of P- ^{18}F ,^{53,54} Si- ^{18}F ,^{55–58} B- ^{18}F bonds, and Al- ^{18}F ^{59–61} and Ga- ^{18}F ^{62,63} complexes.

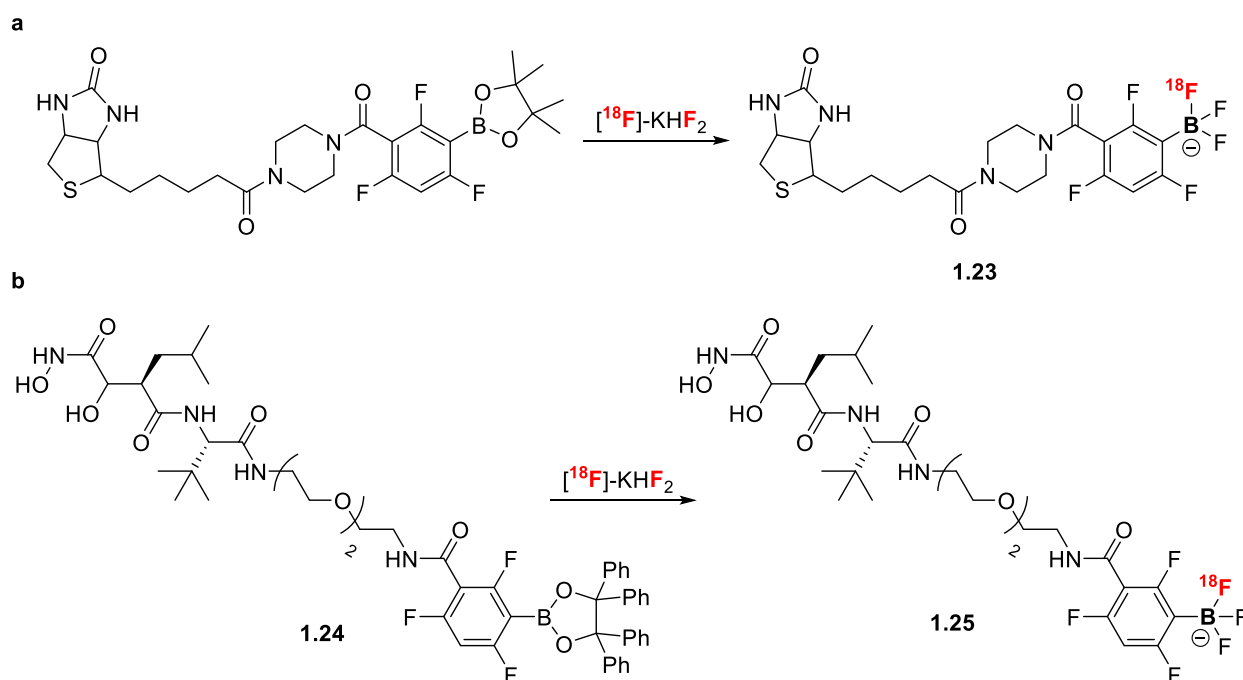
The use of the B-F bond in this context is particularly interesting given boron's high affinity for fluoride, demonstrated by the plethora of organotrifluoroborates used in synthesis¹ and the application of triarylboranes as fluoride sensors.² The first example of B-¹⁸F formation was reported by Perrin *et al.* in 2005, where the authors showed that a biotinylated aryl boronic ester **1.21** could be easily converted into the corresponding radiolabelled [¹⁸F]-trifluoroborate **1.22** (Scheme 1.18).⁶⁴ They also observed that the specific activity (SA) of **1.22** was three times that of the source ¹⁸F, highlighting that boron can be used to effectively concentrate radioactivity and triple SA.



Scheme 1.18 Aqueous radiofluorination of boronic ester **1.21** to [¹⁸F]-trifluoroborate **1.22**.

With intended applications *in vivo*, the hydrolytic stability of the trifluoroborate moiety is important to ensure stability in physiological conditions avoiding solvolysis of the radionuclide from the probe. Through a thorough and systematic study on *in vitro* stability of a series of aryl trifluoroborates Perrin *et al.* demonstrated that electron-withdrawing groups dramatically increased the solvolytic stability of aryl trifluoroborates.⁶⁵ To validate these findings Perrin *et al.* synthesized a biotinylated aryl trifluoroborate **1.23**, bearing three fluorine atoms on the phenyl ring (Scheme 1.19, a). The probe was injected into a mouse and PET images showed the accumulation of the probe in the liver, bladder and salivary glands, but most importantly no accumulation in the skeleton of the mouse could

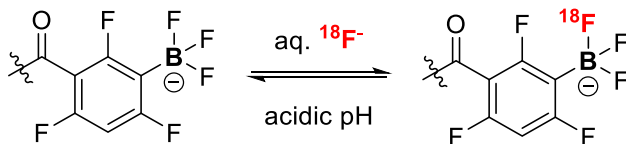
be observed (free $^{18}\text{F}^-$ is deposited in bone due to the presence of high concentrations of calcium).⁶⁶ Further validation was provided by the conjugation of the same phenylboronic ester to marimastat, a noncovalent matrix metalloproteinase inhibitor, for tumour targeting. Conjugate **1.24** was radiolabelled under aqueous conditions in one-step to [^{18}F]-trifluoroborate **1.25** and injected into tumour-bearing mice, PET images showed detectable and specific tumour uptake demonstrating the clinical applicability of these probes (Scheme **1.19**, **b**).^{67,68}



Scheme 1.19 **a**, hydrolytically stable [^{18}F]-trifluoroborate **1.23**. **b**, radiolabelling of marimastat-boronic ester **1.24** to marimastat- ^{18}F -trifluoroborate **1.25**.

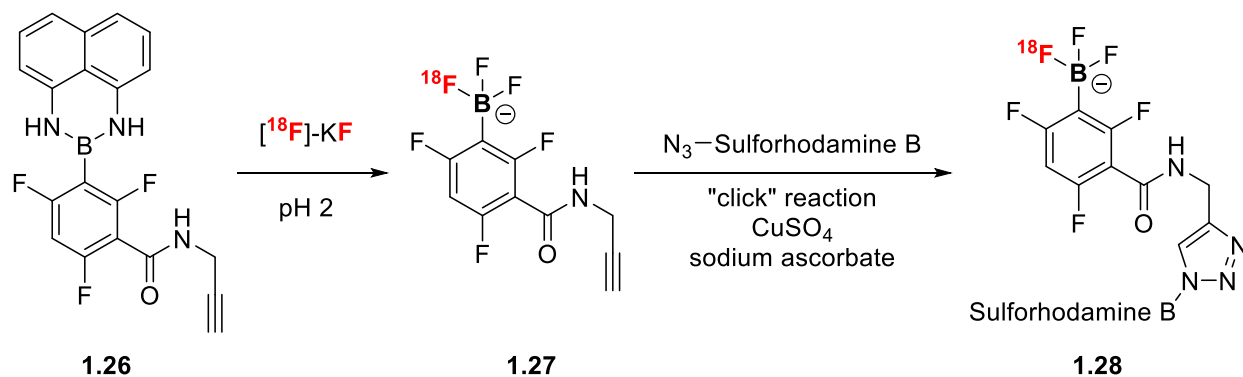
Building on the seminal work reported by Shirrmacher *et al.* on the ^{18}F radiolabelling of organosilyl fluorides by isotope exchange (IEX)⁶⁹, Perrin *et al.* reported that this procedure could be extended to a kit-like approach using trifluoroborate-labelled precursors (Scheme **1.20**).^{70,71} IEX is an attractive radiolabelling method as the stable precursor can

be synthesized and stored beforehand, also the precursor is the product so time consuming purification methods can be avoided.



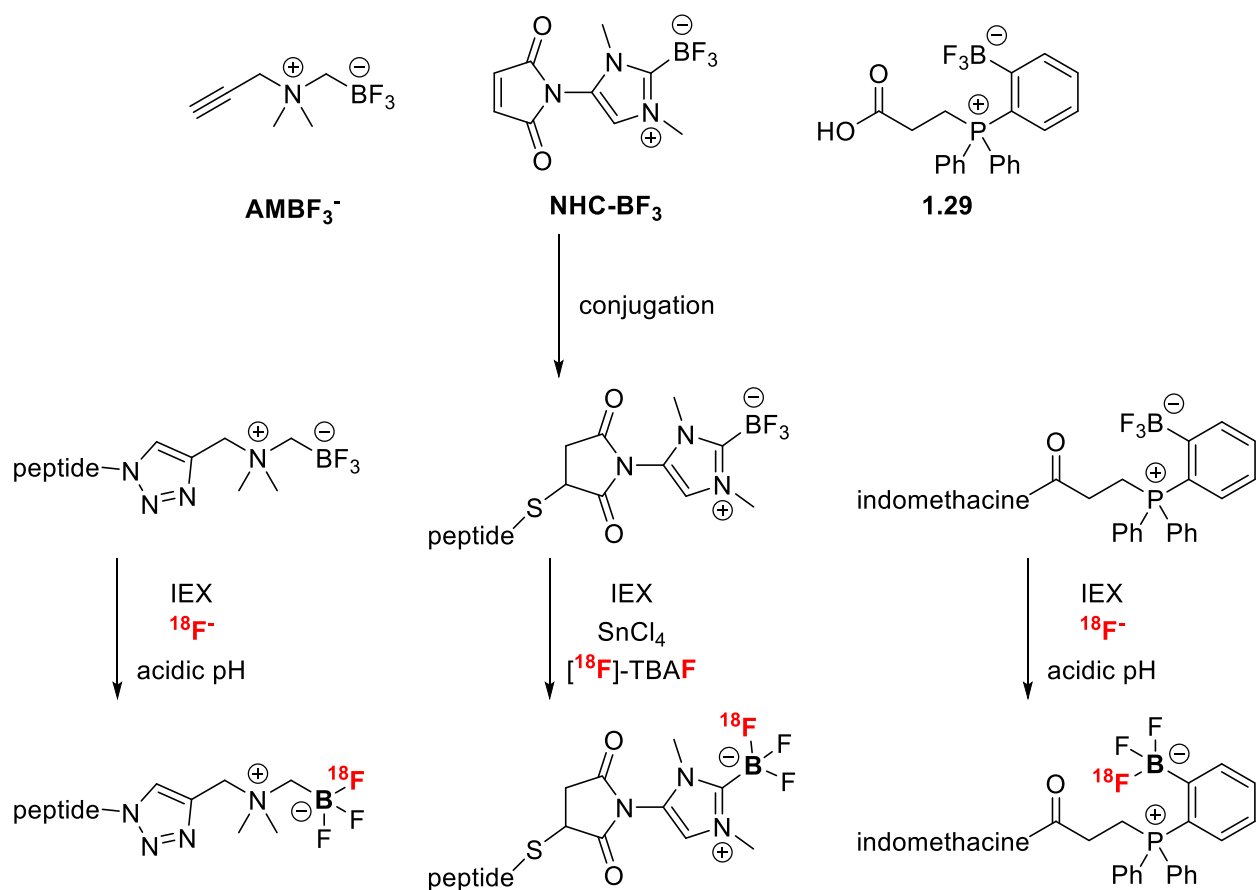
Scheme 1.20 Radiolabelling trifluoroborates by IEX.

With the aim of providing a generally applicable labelling methodology Perrin *et al.* reported the synthesis of various prosthetic precursors with a pendent alkyne motif for copper(I)-catalysed alkyne-azide cycloaddition (CuAAC or “click”) reactions; click reactions are an appealing approach for prosthetic group conjugation to molecules of biological interest (Scheme **1.21**). The authors demonstrated that precursor **1.26** could be readily converted to [¹⁸F]-trifluoroborate **1.27** using [¹⁸F]-KF in acidic pH. Then in a one-pot two-step reaction they could click **1.27** to azide-derivatized Sulforhodamine B, using copper(II) sulphate and sodium ascorbate, to produce rhodamine- [¹⁸F]-trifluoroborate conjugate **1.28**. This fluorescent conjugate was used to further validate the tripling of SA.⁷² This one-pot two-step method, using radiosynthon **1.27**, could also be applied to the radiolabelling of biological molecules of interest and used in *in vivo* animal models.^{72–74}



Scheme 1.21 "Clickable" [^{18}F]-trifluoroborate synthon **1.27**.

With the demonstrated fluorophilicity and hydrolytic stability of cationic boranes, as demonstrated by Gabbaï *et al.*,^{35,36,75–78} both Perrin and Gabbaï extended this technology to the synthesis of potential radioprosthetic groups. A cationic group, ammonium, phosphonium or sulfonium for example, greatly increases the fluorophilicity of a nearby boron atom, and once the fluoroborate is formed it is stabilized by favourable Coulombic forces and donor-acceptor interactions.³⁵ Within this context both groups developed a range of bioconjugatable zwitterionic trifluoroborates that display favourable radiolabelling and hydrolytic stability properties (Scheme **1.22**).



Scheme 1.22 Zwitterionic trifluoroborates as bioconjugatable radioprosthetic synthons.

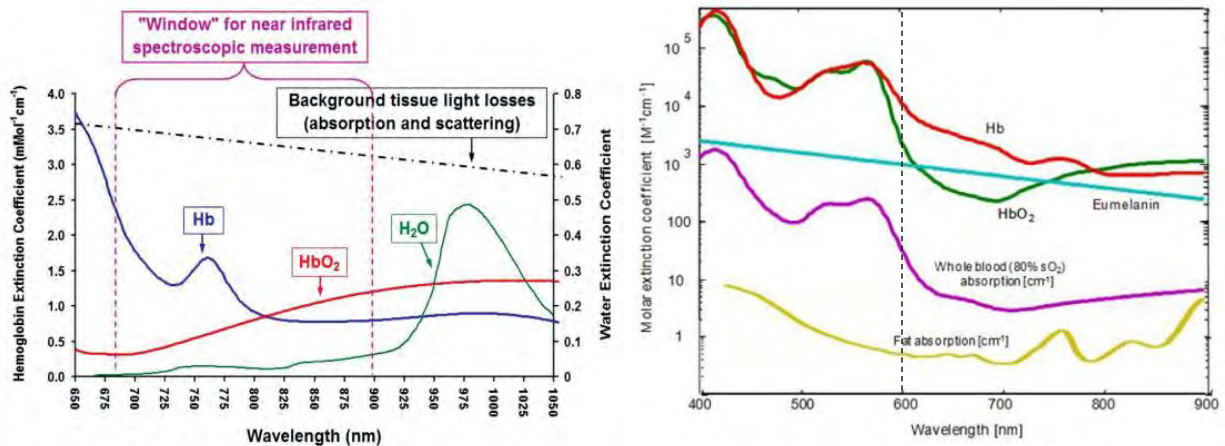
Ammoniomethyltrifluoroborate (AMBF_3^-), reported by Perrin *et al.*,⁷⁹ is readily prepared from the preceding tertiary amine followed by treatment with KHF_2 (Scheme 1.22). AMBF_3^- was demonstrated to be hydrolytically stable and could be “clicked”, via the alkyne moiety, to a variety of tumour targeting peptides including octreotate, bombesin and bradykinin and successfully employed in *in vivo* animal models.^{80–82} *N*-heterocyclic carbene- BF_3 (NHC-BF_3) was developed by Gabbaï *et al.* and was observed to hydrolyse extremely slowly ($t_{1/2} > 10\,000$ min), given this hydrolytic stability IEX had to be mediated by using SnCl_4 as a Lewis acid (Scheme 1.22). NHC-BF_3 could be “click” conjugated to a series of tumour peptides (cyclic RGD and neurotensin) using thiol-Michael addition to the maleimide group.^{83,84} Gabbaï *et al.* also showed that phosphonium trifluoroborate **1.29**

was suitably stable and easily radiolabelled. Zwitterionic **1.29** was conjugated to indomethacine and successfully radiolabelled via IEX and shown to be stable *in vivo* (Scheme **1.22**).⁸⁵

The radiolabelling of boron-dipyrromethene (BODIPY) dyes also represents an emerging application due to their popularity as fluorescent tags in biology and their potential as bi-modal imaging agents (PET and NIRF).⁸⁶ However, given the stability of B-F bonds in these compounds, radiolabelling via IEX usually requires Brønsted or Lewis acid activation; these conditions will be further detailed in chapter 5. Radiolabelled BODIPY dyes have been successfully conjugated to the Trastuzumab antibody,⁸⁷ cyclic RGD peptide^{88,89} and a biologically relevant PARP inhibitor small molecule.⁹⁰

1.2.2 NIRF Imaging

In vivo NIRF is of particular interest, as the absorption coefficient of biological tissue and its constituents is minimal in the NIR window, from 600-900 nm (Figure **1.2**).⁹¹⁻⁹⁵ Additionally, both light scattering and autofluorescence from endogenous fluorophores (e.g. elastin, collagen, mitochondria, lysosomes) are decreased in the NIR. These two factors allow deeper penetration of NIR, compared to visible, light into tissue which enables the investigation and assessment of biological processes from deeper structures.⁹³ Low endogenous absorption and emission are conducive to high signal-to-background ratios, which contribute to improved determination of specific or unspecific binding of a probe to its designated target. The low cost of equipment (light sources and detectors) and non-radiative nature of NIRF imaging make this modality an attractive and promising technology for research and potential clinical applications.



NIRF imaging relies on the detection of light emitted by the excitation of a fluorophore (Figure 1.3). Light of an appropriate energy ($h\nu_1$), based on the absorption properties of the probe, is generated by a light source, this light is absorbed by the probe in its ground state. Absorption of light causes the excitation of electrons from the vibrational ground state (S_0) into a vibrational excited state (S_1 , S_2 etc.). Relaxation of these excited electrons back down to S_0 , without a change in electron spin, with the release of light of a longer wavelength ($h\nu_2 > h\nu_1$) is termed fluorescence. The emitted photons can then be detected by a digital camera and then processed to generate an image. Like PET, NIRF imaging relies on the accumulation of probes in regions of interest.^{91–93} Generally, other than endogenous NIR peptides, NIRF imaging probes are divided into two groups: 1) nanoparticle probes and 2) organic small molecule fluorophores.

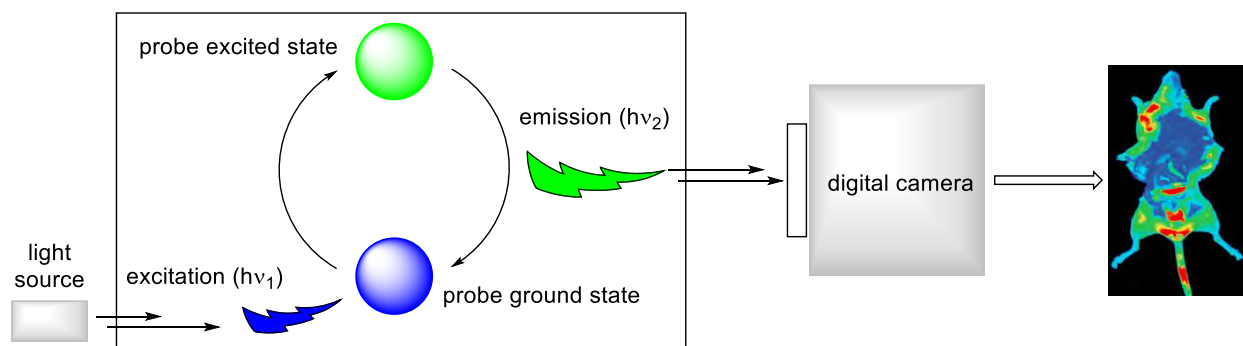


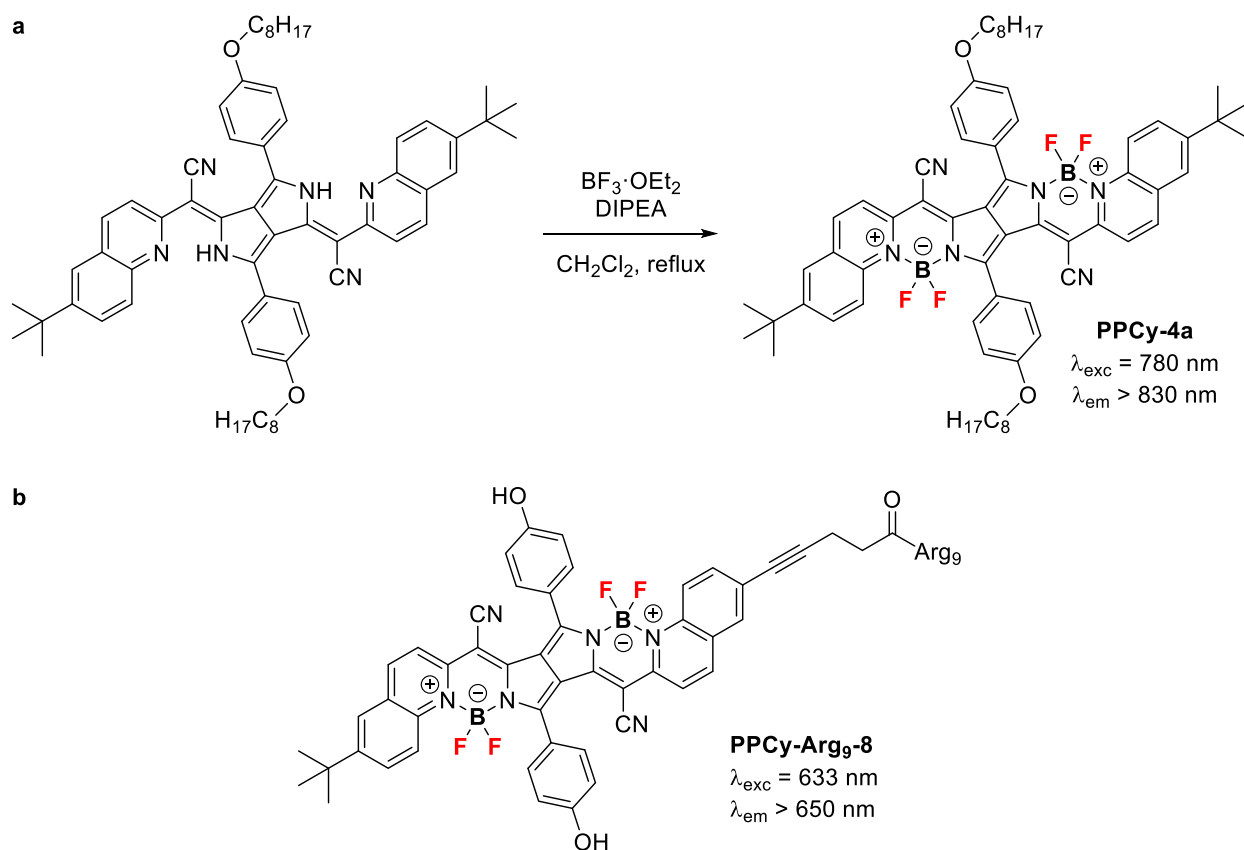
Figure 1.2 Basic schematic of NIRF imaging.

1.2.2.1 B-F in NIRF Imaging

While fluorescent probes have been routinely employed in biology as selective stains, translation of these probes to *in vivo* applications has required the development of NIR emitting probes.⁹³ Emission wavelengths can be shifted towards the NIR by increasing the degree of π -conjugation within the molecular structure of the probe. Another successful strategy involves the rigidification of molecular scaffolds by B-F₂ complexation, this renders the entire structure increasingly planar and increases the extent of π -conjugation. Increased structural stiffness and π -conjugation usually induce sharp absorption and emission profiles, high quantum yields and increase fluorescence lifetimes.⁹⁶ Additionally, the B-F₂ ring complex can function as an acceptor in Donor- π -Acceptor electronic architectures (see chapter 5).

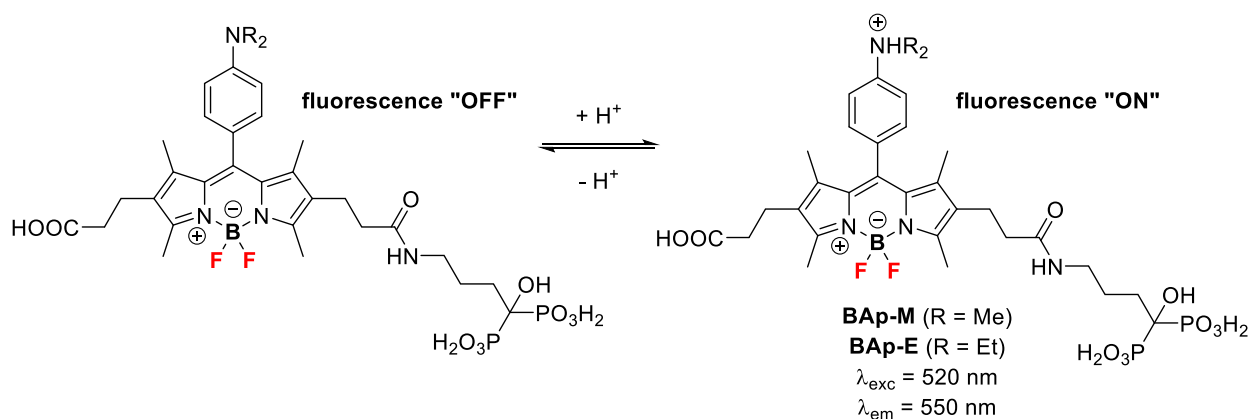
These rigidification effects were exemplified by Zumbusch and Achilefu *et al.* who demonstrated that complexation of pyrrolopyrrole cyanine dyes (**PPCy**), similar in structure to BODIPY dyes, with B-F₂ resulted in favourable spectroscopic properties including a bathochromic shift in absorption and emission into the NIR, accompanied by high quantum yields and long fluorescence lifetimes.^{97,98} Achilefu *et al.* reported that **PPCy-4a** could be used *in vivo* by injection into mice; they found that the injected dye

was stable for several hours post-injection and that the mice displayed no adverse effects several days after administration of the dye (Scheme 1.23, a).⁹⁷ Zumbusch *et al.* further elaborated the synthesis of these dyes to produce a series of C_2 symmetric and asymmetric **PPCy**s. They described the synthesis of a derivative of **PPCy-4a** with a carboxylic acid functionality for conjugation to the *N*-terminus of an Arg₉ peptide for cell internalization (Scheme 1.23, b). The conjugate **PPCy-Arg₉-8** was incubated with live HeLa cells, and after washing confocal microscopy revealed internalization of **PPCy-Arg₉-8**.



Scheme 1.23 a, Synthesis of **PPCy-4a** for *in vivo* imaging. **b**, **PPCy-Arg₉-8** used as a HeLa cell label. As previously mentioned the BODIPY family of dyes has been extensively used as a biological fluorescent tag and therefore it is not surprising to find that several NIRF probes

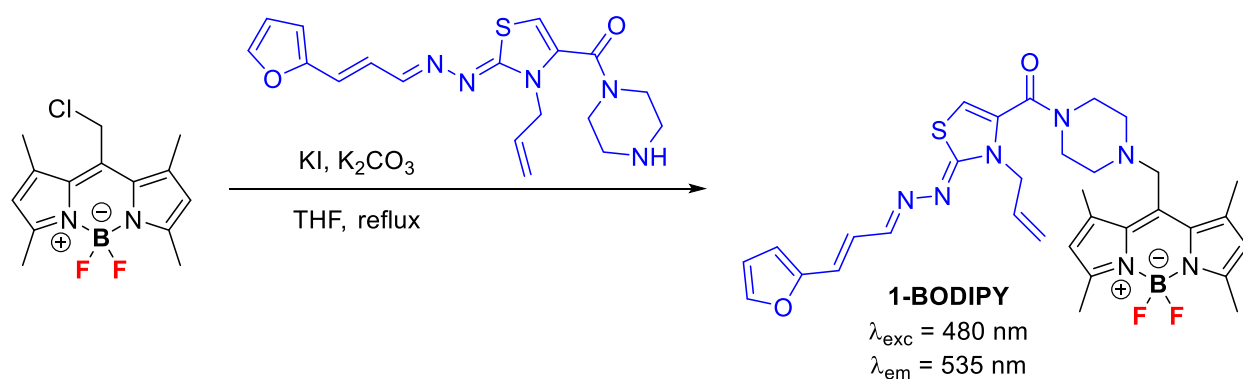
incorporate a BODIPY motif as the fluorophore.⁹⁹ The BODIPY core is attractive due to its facile synthesis and further functionalization as well as its stability towards physiological conditions.^{100,101} Kikuchi *et al.* reported the synthesis of a BODIPY analogue sensitive to the pH of its environment that could be used for the *in vivo* imaging of bone-resorbing osteoclasts (Scheme 1.24).¹⁰² They designed the probe to incorporate a *N,N*-alkyl aniline at the meso position of the BODIPY core which functions as a pH probe to detect acidified bone regions due to osteoclast activity (pH ~4.5); fluorescence is quenched when the aniline is deprotonated and turned on when protonated in acidic environments. The BODIPY core was also functionalized with bisphosphonate for bone targeting. Both **Bap-M** and **Bap-E** were demonstrated to bind to hydroxyapatite (a main constituent of bone) *in vitro*, additionally their pH responsiveness was validated by increasingly high fluorescence intensities observed with decreasing pH. These findings were further validated *in vivo* in mice, where osteoclasts were detected and real-time imaged using two-photon microscopy.



Scheme 1.24 pH activated *in vivo* probe for osteoclasts.

BODIPY dyes could also be used to investigate the biodistribution of an antiparasitic (*Trypanosoma cruzi*, Chagas disease) drug candidate as described by González and

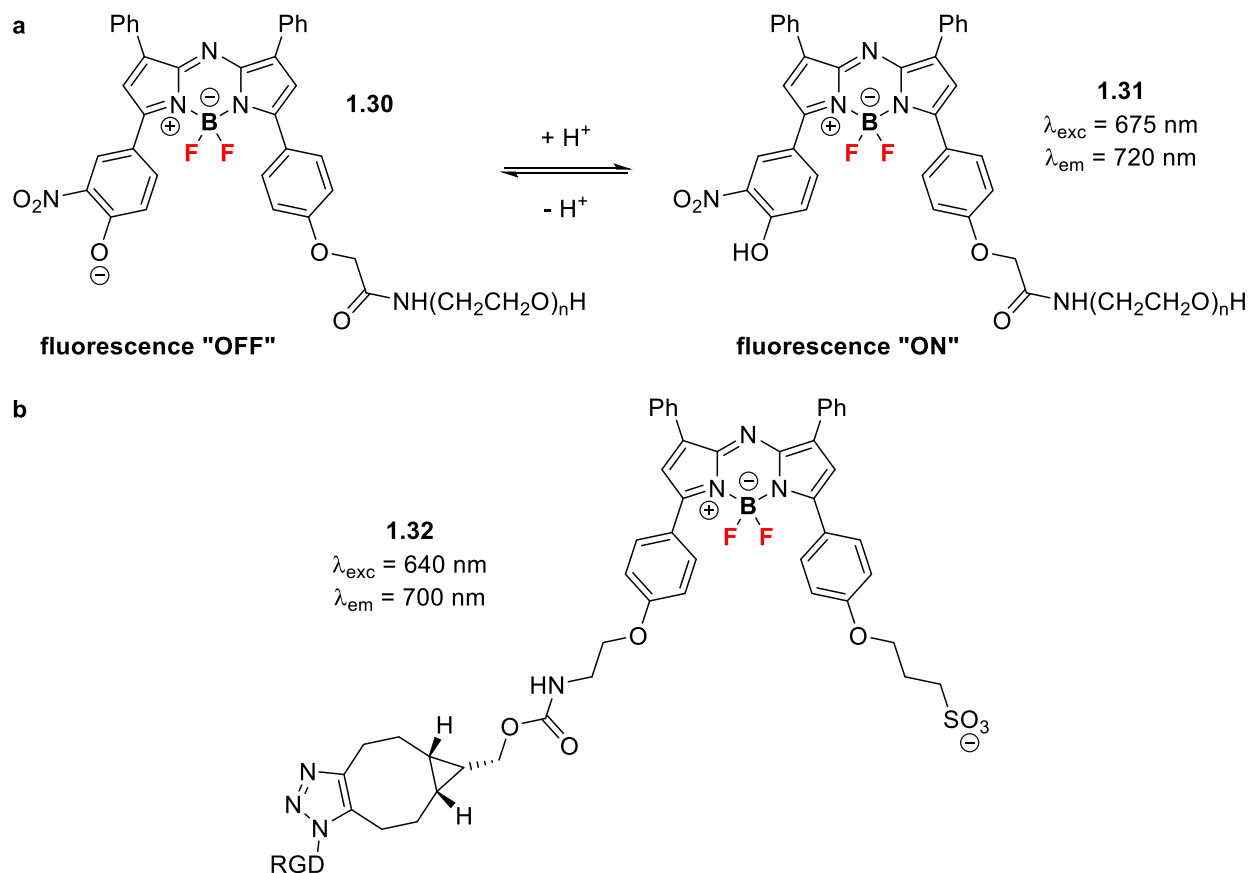
Cerectto *et al.*¹⁰³ The BODIPY-drug conjugate **1-BODIPY** was synthesized using a conjugatable form of a known antiparasitic agent with a piperidinyll handle and 1,3,5,7-tetramethyl-BODIPY (Scheme 1.25). While possessing appropriate photophysical properties, **1-BODIPY** was also determined to display similar *in vitro* bioactivity to the unmodified antiparasitic agent. **1-BODIPY** was then administered to mice and the biodistribution imaged *in vivo* over 24 hours. Accumulation of the probe was observed in the bladder, liver, lungs and Chagas disease relevant organs such as the heart and intestines; this was confirmed by *ex vivo* organ fluorescence studies.



Scheme 1.25 Synthesis of **1-BODIPY** as an *in vivo* drug biodistribution probe. Antiparasitic motif highlighted in blue.

O'Shea *et al.* developed functionalized aza-BODIPYs (nitrogen instead of carbon at meso position of BODIPY) as potential *in vivo* tumour imaging agents (Scheme 1.26). Aza-BODIPY **1.31** was designed as a highly selective lysosome (organelles implicated in cancer proliferation and cell death) probe (Scheme 1.26, a).¹⁰⁴ Fluorescence is triggered by the acidic environment of lysosomes (pH ~4.5) through protonation of phenolate **1.30** which would be the predominating species in extracellular and cytosol environments (pH ~7.2-7.4). *In vitro* assays showed **1.31** to undergo endocytosis by HeLa cells and to selectively stain lysosomes. *In vivo* imaging of subcutaneous tumours in mice was

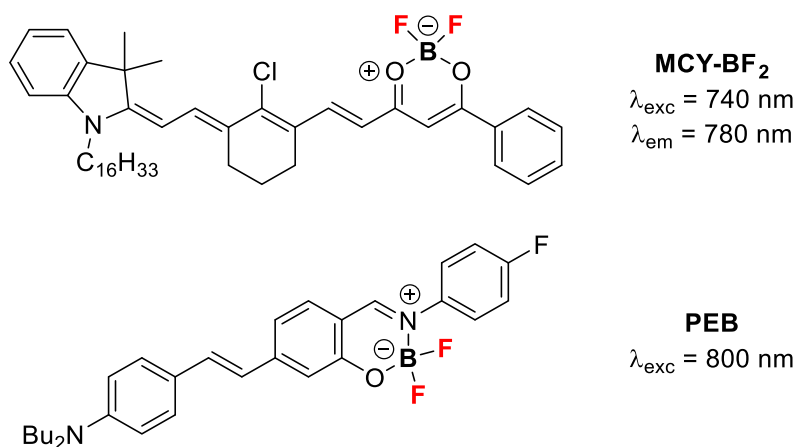
possible with **1.31** as the tumour was clearly distinguished compared to background signals. Aza-BODIPY **1.32** could be used *in vivo* to image and localize subcutaneous tumours using the cyclic RGD peptide to target cancer cells (Scheme **1.26**, **b**).¹⁰⁵



Scheme 1.26 a, lysosome pH activated Off/On fluorescence for tumour imaging. **b**, BODIPY-RGD conjugate for *in vivo* tumour imaging.

More recently, novel B-F₂ containing structures have been developed as NIRF imaging probes (Scheme **1.27**). Tong *et al.* reported the synthesis of a merocyanine-based probe incorporating a tertiary amine and B-F₂ moiety as electron donor and acceptor motifs, respectively, to create a Donor- π -Acceptor construct along the main molecular axis; resulting in absorption and emission bands far into the NIR (Scheme **1.27**, **MCY-BF₂**).¹⁰⁶ They also found that this construct was ultrasensitive towards changes in polarity and

could be used *in vivo* to differentiate between normal and tumorous tissue in mice. Ulrich and Massue *et al.* described the design and synthesis of an increasingly π -conjugated boranil probe that emits in the NIR.¹⁰⁷ Extension of π -conjugation was achieved using a *N,N*-dibutylaniline stilbene motif, which also achieves a Donor- π -Acceptor construct with the B-F₂ moiety (Scheme 1.27, **PEB**). With promising photophysical properties the authors could further extend the use of **PEB** *in vitro* and monitored the distribution of the probe in live HeLa cells using two-photon absorption; like **MCY-BF₂**, **PEB** was found to be sensitive to the polarity of its surroundings.



Scheme 1.27 Molecular structures of NIR B-F₂ complexes **MCY-BF₂** and **PEB**.

1.3 Objectives of this Work

The objectives of this work are centred around novel uses of the B-F bond, particularly organotrifluoroborates, for fluorination and the synthesis of novel fluorophores with potential use as bi-modal imaging agents. Inspired by the seminal work of Frohn *et al.* on the use of organotrifluoroborates in the Balz-Schiemann reaction,³⁹ we wanted to further investigate the potential of these readily available reagents as sources of F⁻. Chapter 2 will focus on applying organotrifluoroborates, in solution, as F⁻ sources for a Balz-

Schiemann type reaction for the synthesis of aryl fluorides; the extension of this transformation to a one-pot two-step process will be described. Chapter 3 will present preliminary work on the use of organotrifluoroborates as an F^- source for the fluorination of unsymmetrical diaryliodonium salts. Chapter 4 will describe our attempts to extend the use of the trifluoroborate moiety as an F^- source in the intramolecular fluorination of various functionalities. Chapter 5 will focus on the synthesis of novel fluorophores incorporating a $B-F_n$ complex based on the benzothiazole core, within the context of developing potential bi-modal imaging agents for Alzheimer's disease.

2 Organotrifluoroborates as nucleophilic fluorine sources in the Balz-Schiemann reaction

Aryl fluorides are in heavy demand in multiple chemical domains. Despite significant advances in fluorination methodologies, the classical Balz-Schiemann reaction continues to be a popular process to introduce fluorine into aromatic scaffolds. While intense research has been dedicated to this reaction, the investigation of organotrifluoroborates as fluoride ion sources has been underutilized and is limited to one report. This chapter will introduce the major aspects of the Balz-Schiemann reaction investigated in the literature. The use of organotrifluoroborates, in solution, for the fluorination of aryl diazonium salts will be presented. Translation of this proof of concept towards a one-pot two-step methodology for the fluorination of anilines using organotrifluoroborates will be described.

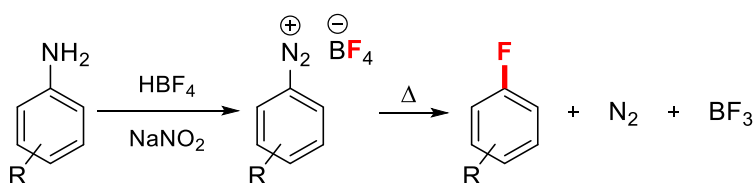
2.1 Introduction

There is an ever-increasing demand for fluorinated aromatic compounds given their importance in pharmaceuticals, agrochemicals and materials.^{7,108–112} Particularly for drugs, the incorporation of fluorine into a molecular scaffold can have advantageous effects on neighbouring proton acidities (pK_a), conformation, lipophilicity, bioavailability and, perhaps most importantly, metabolic stability.^{6,8–11,113} The inherent difficulty of forming C-F bonds has historically presented a considerable obstacle in the synthesis of fluorinated building blocks and advanced intermediates. To this end, significant advances have been made in the formation of aryl C-F bonds.¹¹⁴ These include improvements to traditional fluorination methods such as the Balz-Schiemann reaction²³ and Halex (halogen exchange) process.¹¹⁵ Important contributions include various transition metal

mediated processes starting from aryl(pseudo)halides, di-aryl iodonium salts and aryl boron(ate) species.^{40–46,116–119} While these methods have expanded the repertoire of fluorination processes, the Balz-Schiemann reaction continues to be a favourable method for the synthesis of aryl fluorides.^{120–127}

2.1.1 The Balz-Schiemann Reaction

This venerable reaction, first reported in 1927, represents one of the earliest and hence most frequently used methodologies for the synthesis of fluoroaromatic compounds.²³ The procedure is operationally simple; it requires diazotization of an aniline substrate, isolation and drying of the consequent aryl diazonium tetrafluoroborate salt after which, fluorodediazotiation is thermally induced (typically > 100 °C) to produce the desired aryl fluoride along with extrusion of molecular nitrogen and boron trifluoride (Scheme 2.1).



Scheme 2.1 Balz-Schiemann reaction.

2.1.1.1 Mechanism

The mechanism of the Balz-Schiemann reaction has been an area of intense study over the past 30 years. While a definite mechanism is yet to be described,¹²⁸ the weight of excellent experimental work, at present, implicates the formation of an aryl cation (I) as the first and rate-limiting step of the transformation (Figure 2.1, a).^{128–137} The dediazotiation process was determined to be first-order with respect to the aryl diazonium, providing evidence for an S_N1 process rather than a bimolecular reaction (S_NAr, II).^{131,132,136} Further evidence of an aryl cation intermediate is the observed isotopic

N_{α} – N_{β} rearrangement, up to 37%, of β - ^{15}N labelled aryl diazonium salts; in reactions conducted under an atmosphere of unlabelled nitrogen incorporation of “external” nitrogen, up to 17%, into the aryl diazonium salt was observed (Figure 2.1, b).^{133,134,137} Importantly, the ability of these intermediates to react with nitrogen highlights the highly reactive nature of aryl cations. A homolytic pathway, which has been invoked, has been regarded as non-productive, as it leads to the formation of unwanted side products and tars. Indeed, the radical pathway has been shown to be dependent on the solvent and reaction additives.^{131,132,135,136,138} Given a preponderance of evidence that suggests that the productive intermediate is **I**, the question arises as to the origin of the fluorine nucleophile, does BF_4^- react directly or does it first dissociate to provide F^- ? Evidence for direct fluorine transfer from BF_4^- was provided by Swain *et al.*, who demonstrated that rates of fluorodediazotation were independent of excess BF_3 .¹³¹ Therefore, a tight ion pair, **I**, is considered to be necessary for efficient fluorination. More recently, Singleton *et al.* have reported that a mechanism at the “boundary between $\text{S}_{\text{N}}\text{Ar}$ and $\text{S}_{\text{N}}1$ ” is probably operative wherein they do suggest that the mechanism involves dynamic transition structures where solvent reorganizes around the aryl cation.¹²⁸

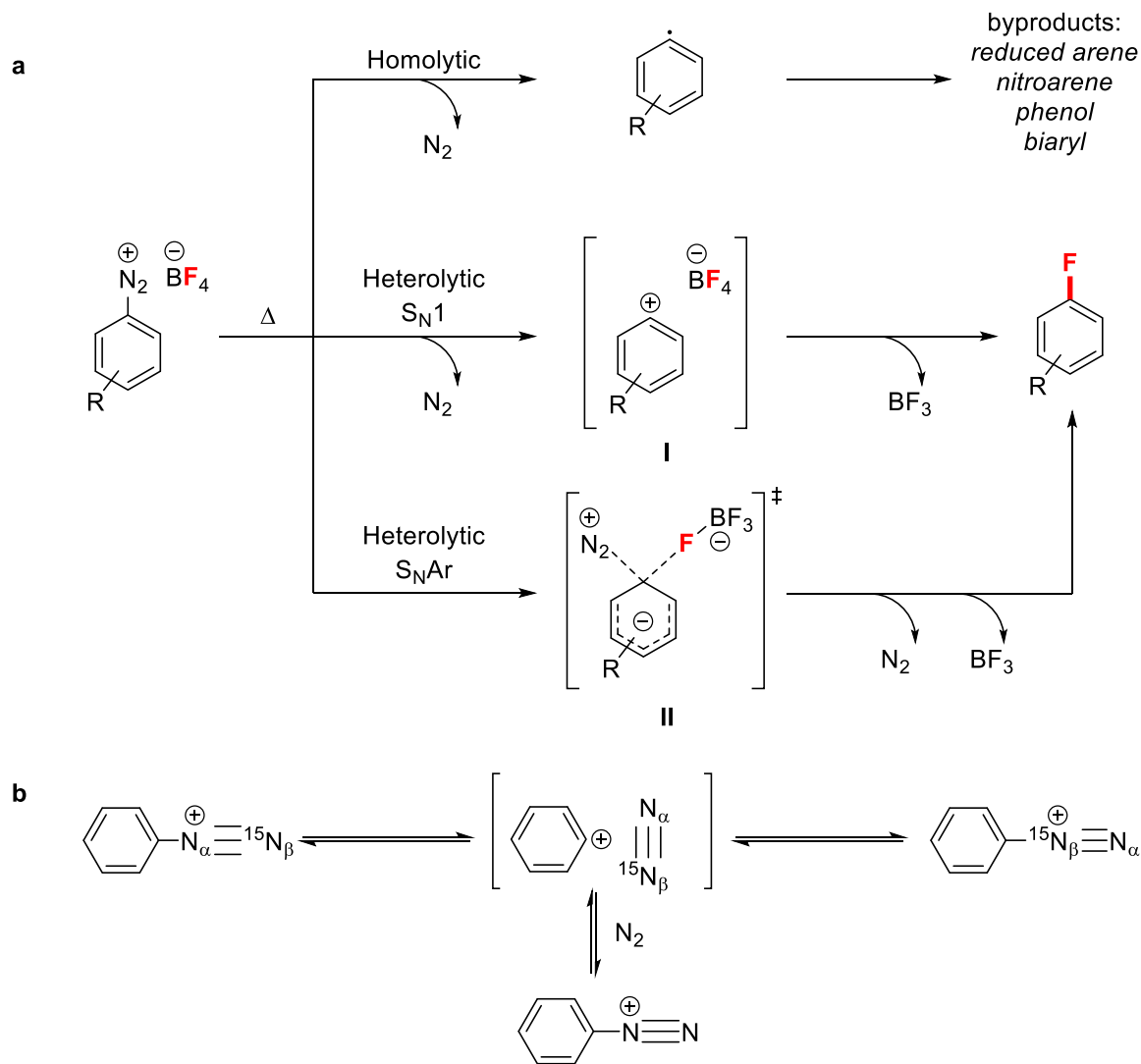


Figure 2.1 a, implicated mechanisms in the dediazonation of aryl diazonium tetrafluoroborates. **b**, isotopic rearrangement of ¹⁵N-labelled aryl diazonium salts.

2.1.1.2 Decomposition in the solid state

Despite its simplicity, the classical Balz-Schiemann reaction has been plagued by many limitations. The classical transformation suffers from reproducibility issues where it has been documented that yields of fluorobenzene can range from 51-100%.¹³⁹ This is primarily due to difficulties encountered in the precipitation, isolation, and drying of aryl diazonium tetrafluoroborates from aqueous solutions.^{139,140} Such is possibly the biggest limitation of the Balz-Schiemann reaction as the isolation step presents two considerable

disadvantages. Firstly, (hetero)aryl diazonium salts with polar substituents become increasingly difficult to precipitate¹⁴⁰ leading to an overall decrease in reaction efficiency and severely limiting the substrate scope. Secondly, and more importantly, the isolation of aryl diazonium salts poses a serious safety concern as they can be explosive even at low temperatures.^{139–141}

Since 1927, intense research has been dedicated towards improving on harsh reaction conditions and limited substrate scope. Fluorodediazoniatio n traditionally occurs by thermal decomposition, at high temperatures (> 100 °C), in the solid state. Usually, initial heating is required until decomposition begins which can spontaneously continue due to the highly exothermic nature of the transformation. Decompositions of this kind can quickly become uncontrollable leading to both product degradation and additional safety concerns.¹⁴⁰ Several conditions have been investigated to mitigate this issue including dilution of diazonium salts in inert solids (sand, kieselguhr or Na₂CO₃) thereby allowing for safer conditions.¹⁴⁰ While decomposition in inert solids is safer than that run with pure diazonium salts, heat exchange through large quantities of these solids becomes difficult limiting applications on larger scales.

2.1.1.3 Decomposition in inert solvents

The suspension and decomposition of diazonium salts in inert solvents was sought as an alternative. Aryl diazonium tetrafluoroborates could be efficiently decomposed in high boiling solvents such as toluene, xylenes and dichlorobenzenes. By contrast, the use of nucleophilic (alcohols and MeCN) or hygroscopic solvents resulted in low aryl fluoride yields due to increased by-products.^{136,138,140} Perfluorinated solvents have also proved efficient in Balz-Schiemann reactions where they have been observed to increase product

purity and suppress the formation of unwanted by-products.^{140,142} More recently, the use of ionic liquids in mediating the fluorodediazoniatio process has been demonstrated; a series of substrates, both electron poor and rich, could be fluorinated in quantitative NMR spectroscopy yields.¹⁴³ Interestingly, the use of ionic liquids with non-fluorinated anions resulted in anion metathesis under reaction conditions leading to products from aryl diazonium-solvent combination, affirming the importance of a tight ion pair for efficient fluorination.¹⁴³

2.1.1.4 Development of one-pot and continuous flow processes

Thus far, advances discussed have addressed the issue of poor reproducibility and substrate scope, however many of these methods require isolation of the aryl diazonium salt prior to decomposition. Given the risk associated with the isolation of diazonium salts, *vide supra*, efforts in recent years have focused on developing a safer and more generally applicable methodology via one-pot two-step (diazotization-fluorodediazoniatio) procedures as well as continuous flow processes.^{120,140,144–146} One-pot procedures have largely focused on the use of hydrogen fluoride (HF), whether in its anhydrous form or as an adduct with ammonium salts or pyridine (Olah's reagent).^{121,124,127,147} The use of "HF" allows for decreased decomposition temperatures and increased yields,¹⁴⁰ however the requirement of handling "HF" limits its general applicability due to added safety concerns. Flow processes have been developed that are able, through careful selection of (co)solvents, to allow the continuous generation and decomposition of aryl diazonium tetrafluoroborates but require high decomposition temperatures (> 125 °C).^{120,144,145}

2.1.1.5 Importance of the fluoro-ate anion

The effect of various “fluoro-ate” anions were investigated including hexafluorosilicates (SiF_6^{2-}), hexafluorophosphates (PF_6^-), hexafluorantimonates (SbF_6^-) and hexafluoroarsenates (AsF_6^-).^{148–151} PF_6^- and SiF_6^{2-} , were of initial interest due to their high insolubility in aqueous solutions, facilitating the aryl diazonium salt isolation process. These anions (X) afford a potentially higher effective fluoride concentration over BF_4^- by simply increasing the number of fluorine atoms around the aryl diazonium cation. An additional advantage is the weaker X-F bond when compared to B-F. Yet this has not always translated into higher yields and more efficient transformations as strong Lewis acids can be formed during the reaction (AsF_5 or SbF_5) which go on to catalyse the formation of by-products. Generally, reaction efficiencies with alternative fluoro-ate salts were highly dependent on substrate; no single anion proved more advantageous than the rest (Table 2.1).^{140,148–151}

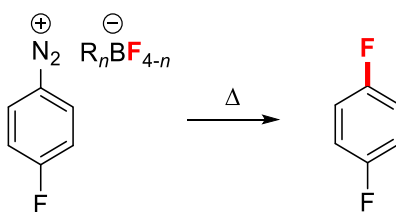
Table 2.1 Selected yields of aryl fluorides using different “fluoro-ate” anions

Aromatic Amine	Yield (%)				
	$\text{ArN}_2^+\text{BF}_4^-$	$\text{ArN}_2^+\text{SiF}_6^-$	$\text{ArN}_2^+\text{PF}_6^-$	$\text{ArN}_2^+\text{SbF}_6^-$	$\text{ArN}_2^+\text{AsF}_6^-$
Aniline	51-90	30	-	50	0
<i>o</i> -toluidine	45-65	69	58	21	0
<i>m</i> -toluidine	69-87	60	57	30	trace
<i>p</i> -toluidine	70	64	71	47	2
2-aminobenzoic acid	9	-	60	62	0
4-aminophenol	0	6.5	10-20	trace	-
2-aminopyridine	34	0	34	50	-
2-nitroaniline	9-17	-	10-20	40	31
3-nitroaniline	43-54	22	10-20	60	51

4-nitroaniline	40-58	34-43	63	60	0
----------------	-------	-------	----	----	---

2.1.1.6 Organotrifluoroborates as anions in Balz-Schiemann reaction

Despite the rich history of organofluoroborates,¹ in particular their application in metal mediated cross-coupling reactions with aryl diazonium salts, their use for fluorodediazotiation has not been extensively studied. To the best of our knowledge their application in Balz-Schiemann transformations is limited to but one report; Frohn *et al.* described the synthesis and subsequent thermolysis of a series 4-fluorobenzenediazonium perfluoroorganofluoroborates to produce 1,4-difluorobenzene (Table 2.2).³⁹ While this seminal report indeed proves the feasibility of using organotrifluoroborates as anions in the Balz-Schiemann reaction the investigation was quite limited. Only one aryl diazonium substrate was investigated, the authors did not explore other non-perfluorinated organofluoroborates and perhaps the biggest limitation was the necessity of isolating and drying the salts prior to decomposition. Nevertheless, inspired by this work, we sought to further investigate the potential of organotrifluoroborates to serve as F⁻ sources in the Balz-Schiemann reaction.

Table 2.2 Effect of perfluoroorganotrifluoroborates on the yield of 1,4-difluorobenzene

Entry	$R_nBF_{4-n}^-$	Yield (%) ^a
1		54
2		65
3		80
4		90

^a Yield determined by ¹⁹F NMR spectroscopy using C₆F₆ as internal standard

In contrast to the aforementioned fluoro-ate salts, organotrifluoroborates do not present the hypothetical advantage in terms of an increased number of fluorine atoms compared to BF_4^- (in fact the contrary would be the case). Nevertheless, the presence of an organic moiety was hypothesised to present two interesting advantages. Firstly, given the access to a diverse array of organotrifluoroborates the organic fragment can be used to tune solubility of the organotrifluoroborate into solvents compatible with fluorodediazotiation; allowing the development of one-pot two-step procedures and obviating the need for aryl

diazonium organotrifluoroborate salt isolation. Secondly, the organic moiety of organotrifluoroborates has been demonstrated, by Perrin *et al.*, to affect the rate at which aryl trifluoroborates undergo solvolysis.⁶⁵ Electron withdrawing-groups were found to retard solvolysis while electron-donating groups were found to accelerate the process. The ability to modulate, through stereoelectronic considerations of the organic fragment, the lability of fluorine on the organotrifluoroborate has potential for ameliorating reaction conditions and increasing fluorination efficiencies by facilitating fluorine transfer within the tight ion pair intermediate (I, Figure 2.1).

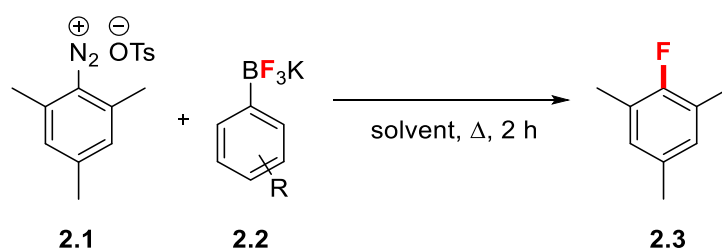
2.2 Results and Discussion

2.2.1 Initial optimization

We began the investigation by determining the viability of employing organotrifluoroborates as F⁻ sources for the fluorodediazoniaction of preformed aryl diazonium salts in solution. We started by reacting potassium aryl trifluoroborates (**2.2**) with 2,4,6-trimethylphenyldiazonium *p*-toluenesulphonate (**2.1**) in various solvents (Table 2.3); aryl diazonium *p*-toluenesulphonates are known to be safely isolable and bench-stable.¹⁵² Gratifyingly, decomposition of **2.1** in the presence of potassium phenyltrifluoroborate in *t*-BuOH provided 2-fluoro-1,3,5-trimethylbenzene (**2.3**) in moderate yield (Table 2.3, entry 1). Changing the substituent on **2.2** resulted in a decrease in yield for both electron withdrawing and donating groups (Table 2.3, entries 2 and 3), although the decrease was more marked using an electron-rich aryl trifluoroborate. Moderate yields were also observed in low-boiling halogenated solvents (Table 2.3, entries 4 and 5), most notably the 34% yield obtained in CH₂Cl₂ at 50 °C. These results are surprising as generally, aliphatic chlorinated solvents are incompatible

with the Balz-Schiemann reaction as they react with the diazonium salt to generate chloroaromatics.¹⁴⁰ A significant improvement in yields, 57% (Table 2.3, entry 6), was observed with THF as the solvent. Similar to results in *t*-BuOH, the use of electron-poor **2.2** resulted in diminished yields (Table 2.3, entries 7-10). Lowering of the reaction temperature (Table 2.3, entry 11) and decreasing or increasing equivalents of **2.2** (Table 2.3, entries 12 and 13) resulted in decreased yields.

Table 2.3 Initial optimization of Balz-Schiemann reaction using organotrifluoroborates



Entry	R	Solvent	Temperature (°C)	Yield (%) ^a
1	H	<i>t</i> -BuOH	95	39
2	4-methoxy	<i>t</i> -BuOH	95	10
3	4-formyl	<i>t</i> -BuOH	95	25
4	H	CHCl ₃	71	38
5	H	CH ₂ Cl ₂	50	34
6	H	THF	75	57
7	4-formyl	THF	75	35
8	3,4,5-trifluoro	THF	75	35
9	4-trifluoromethyl	THF	75	34
10	2-nitro	THF	75	29
11	H	THF	50	39
12 ^b	H	THF	75	39
13 ^c	H	THF	75	38

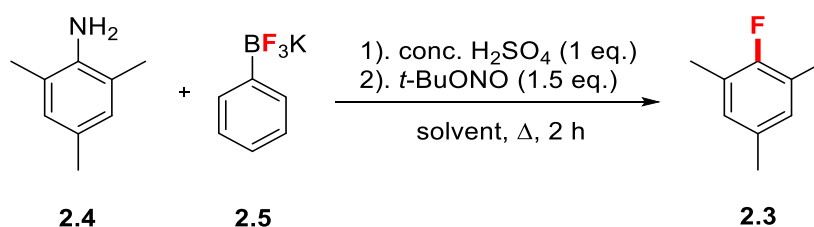
Reaction conditions: **2.1** (0.25 mmol), **2.2** (0.38 mmol), solvent (1.3 mL) in pressure vial with Teflon lined cap, heated at indicated temperature for 2 h. ^aYield determined by ¹⁹F NMR spectroscopy using 2,4-dinitrofluorobenzene as internal standard. ^b 1 eq. (0.25 mmol) of potassium phenyltrifluoroborate used. ^c 2 eq. (0.5 mmol) of potassium phenyltrifluoroborate used.

2.2.2 Extension to one-pot Balz-Schiemann reaction

Having proven organotrifluoroborates to in fact be capable of mediating fluorodediazoniations in solution with preformed aryl diazonium salts, we focused our attention on extending our methodology towards a one-pot two-step reaction, avoiding the need to isolate the aryl diazonium salt. We argued that the reaction would benefit from a one-pot process due the diazotization step occurring in the presence of the organotrifluoroborate, this may facilitate anion exchange towards the productive [aryl diazonium organotrifluoroborate] ion pair. We began exploring reactions starting from 2,4,6-trimethylaniline (**2.4**) under diazotization conditions (concentrated sulphuric acid and *t*-BuONO), in the presence of potassium phenyltrifluoroborate (**2.5**). We observed that *t*-BuOH provided the best yield, 55%, for the one-pot diazotization/fluorodediazonation reaction (Table **2.4**, entry 2). Other alcohols examined produced lower yields (Table **2.4**, entries 3-5), especially MeOH and EtOH. This can be expected due to the propensity of alcohols to promote the radical decomposition of aryl diazonium salts into the corresponding phenols, aryl ethers and arenes.¹³⁸ Chlorinated solvents provided diminished, but moderate yields as previously observed (Table **2.4**, entries 6-8). Using a nucleophilic solvent like MeCN resulted in expectedly low yields, probably due to the formation of the corresponding aryl acetamide after hydrolysis.¹⁴⁵ Ether solvents, THF and 1,4-dioxane, provided moderate yields as well (Table **2.4**, entries 1 and 15). All other solvents examined resulted in poor yields (Table **2.4**, entries 10-17);

predictably for non-polar solvents, such as toluene, cyclohexane and Et₂O, a result of poor solubility of starting materials in these solvents. Not unexpectedly, reactions in DMSO resulted in poor yields, likely due to the reduction of the formed aryl diazonium by DMSO into the corresponding arene, phenol and other reduction by-products (Table 2.4, entry 15).¹⁵³

Table 2.4 Optimization of one-pot Balz-Schiemann reaction solvent



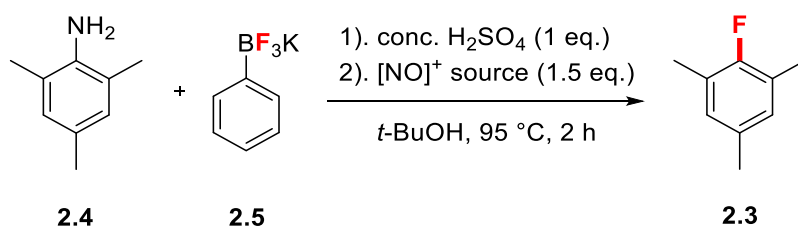
Entry	Solvent	Temperature (°C)	Yield (%) ^a
1	THF	75	41
2	<i>t</i> -BuOH	95	55
3	MeOH	75	10
4	EtOH	89	9
5	2-propanol	93	29
6	1,2-dichloroethane	94	34
7	CH ₂ Cl ₂	50	39
8	CHCl ₃	71	26
9	MeCN	92	6
10	1,4-dioxane	110	42
11	Acetone	66	15
12	DMF	153	6
13	Toluene	121	6
14	Cyclohexane	91	4
15	DMSO	189	12

16	Et ₂ O	45	9
17	HFIP	68	0

Reaction conditions: **2.4** (0.25 mmol), 95% H₂SO₄ (0.25 mmol), **2.5** (0.38 mmol), solvent (1.3 mL) in pressure vial with Teflon lined cap, Ar purge, then *t*-BuONO (0.38 mmol), rt for 20 min, then heated at indicated temperature for 2 h. ^aYield determined by ¹⁹F NMR spectroscopy using 2,4-dinitrofluorobenzene as an internal standard.

Having determined *t*-BuOH to be the most suitable solvent, we focused on optimizing remaining reaction parameters. We first examined the effect of other diazotizing agents on the reaction, *t*-Butyl and *n*-Butyl nitrite provided similar yields (Table 2.5, entries 1 and 2), while yields with *iso*-Amyl nitrite were significantly reduced (Table 2.5, entry 3). Continuing with *t*-Butyl nitrite as the [NO]⁺ source, we explored the effect of varying concentrations of **2.5** on reaction outcomes. As expected decreasing equivalents of **2.5** in the reaction mixture reduced yields significantly (Table 2.5, entries 4 and 5). A significant increase in yields was achieved when 3 equivalents of **2.5** were used however, moving to 5 equivalents did not result in further improvements in yield (Table 2.5, entry 8).

Table 2.5 Effect of diazotizing agent on reaction yields



Entry	[NO] ⁺ source	2.5 (eq.)	Yield (%) ^a
1	<i>t</i> -Butyl nitrite	1.5	55
2	<i>n</i> -Butyl nitrite	1.5	52
3	<i>iso</i> -Amyl nitrite	1.5	30

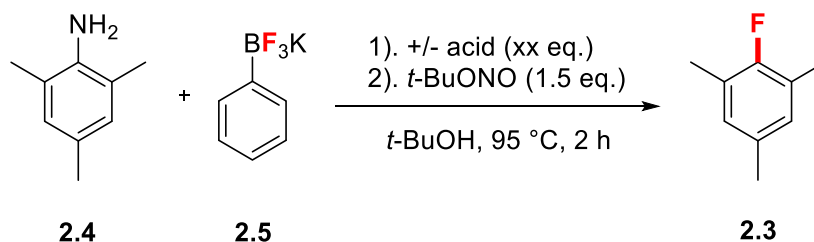
4	<i>t</i> -Butyl nitrite	1.0	26
5	<i>t</i> -Butyl nitrite	0.5	22
6	<i>t</i> -Butyl nitrite	2	50
7	<i>t</i> -Butyl nitrite	3	71
8	<i>t</i> -Butyl nitrite	5	66

Reaction conditions: **2.4** (0.25 mmol), 95% H₂SO₄ (0.25 mmol), **2.5** (xx eq.), *t*-BuOH (1.3 mL) in pressure vial with Teflon lined cap, Ar purge, then [NO]⁺ source (0.38 mmol), rt for 20 min, then heated at 95 °C for 2 h. ^aYield determined by ¹⁹F NMR spectroscopy using 2,4-dinitrofluorobenzene as an internal standard.

Some groups have reported that Brønsted or Lewis acids are not required for the diazotization step.^{143,145,146,154,155} It was clear that the transformation required the presence of an acid to facilitate the diazotization step, as in its absence poor yields were obtained (Table **2.6**, entry 1). Surprisingly, efficient transformations were observed when aqueous acids, namely HCl and HNO₃, were used (Table **2.6**, entries 4, 5 and 7). The presence of water is usually detrimental to fluorodediazotiation as it can act as a nucleophile attacking the intermediate aryl cation and producing phenol by-products.¹⁴⁰ The use of *p*-toluenesulfonic (Table **2.6**, entry 6) acid lowered yields to 40%, identical to the reactivity observed using **2.1**, the preformed salt, previously described (Table **2.3**, entry 1). Weak acids resulted in poor yields (Table **2.6**, entries 9 and 10), however H₃PO₄ significantly increased yields to 76% (Table **2.6**, entry 11). These results strongly suggest that both pK_a and nature of the acid are important for efficient transformations; the ion pair [aryl diazonium dihydrogen phosphate] may undergo a more facile anion metathesis to the productive [aryl diazonium organotrifluoroborate] when compared to other [aryl diazonium conjugate base] ion pairs. Gratifyingly, equivalents of **2.5** could be decreased, as similar yields were obtained using 1.5 or 3 equivalents (Table **2.6**, entries 11 and 12).

Equivalents of acid could be decreased to 0.5 before reaction yields diminished (Table 2.6, entries 14 and 15).

Table 2.6 Acid optimization for the one-pot reaction

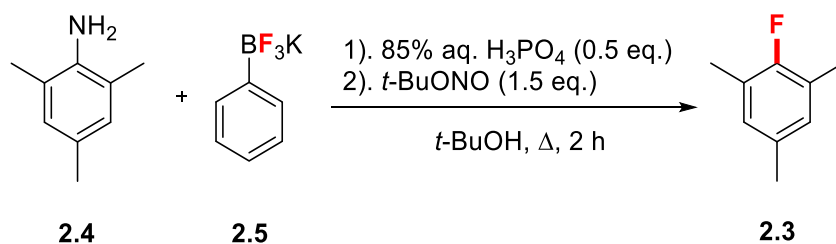


Entry	Acid (eq.)	Yield (%) ^a
1	-	26
2	95% H ₂ SO ₄ (1.0)	55
3	55-58% aq. HI (1.0)	9
4	48% aq. HBr (1.0)	34
5	37% aq. HCl (1.0)	57
6	<i>p</i> -Toluenesulfonic acid·H ₂ O (1.0)	40
7	65-70% aq. HNO ₃ (1.0)	64
8	Trifluoroacetic acid (1.0)	23
9	97% Formic acid (1.0)	6
10	Glacial acetic acid (1.0)	13
11	85% aq. H ₃ PO ₄ (1.0)	76
12 ^b	85% aq. H ₃ PO ₄ (1.0)	79
13	85% aq. H ₃ PO ₄ (2.0)	52
14	85% aq. H ₃ PO ₄ (0.5)	72
15	85% aq. H ₃ PO ₄ (0.25)	53

Reaction conditions: **2.4** (0.25 mmol), acid (xx eq.), **2.5** (0.38 mmol), *t*-BuOH (1.3 mL) in pressure vial with Teflon lined cap, Ar purge, then *t*-BuONO (0.38 mmol), rt for 20 min, then heated at 95 °C for 2 h. ^aYield determined by ¹⁹F NMR spectroscopy using 2,4-dinitrofluorobenzene as an internal standard. ^b 3 equivalents of potassium phenyltrifluoroborate used.

Finally, the effect of temperature on reaction efficiencies was studied. While most Balz-Schiemann reactions require high decomposition temperatures (except reactions run in anhydrous HF or HF solvents), see sections 2.1.1.2-4, identical yields could be obtained by running the reaction at 45-50 °C (Table 2.7, entry 73). While examining these conditions a decrease in reaction yields was observed when reaction vessels were not purged with Ar (Table 2.7, entry 7). However, upon degassing the solvent, yields could be increased to 81% (Table 2.7, entry 8). Interestingly, reactions run under N₂ atmosphere (Table 2.7, entry 9) were not significantly affected, given reports that homolytic decomposition of the diazonium can occur under these conditions.^{132,138,156} Reactions run under O₂ atmosphere (Table 2.7, entry 10) were also not affected; O₂ can act as a radical scavenger and shutdown radical pathways suppressing homolytic decomposition.¹⁵⁶

Table 2.7 Effect of temperature on reaction yields



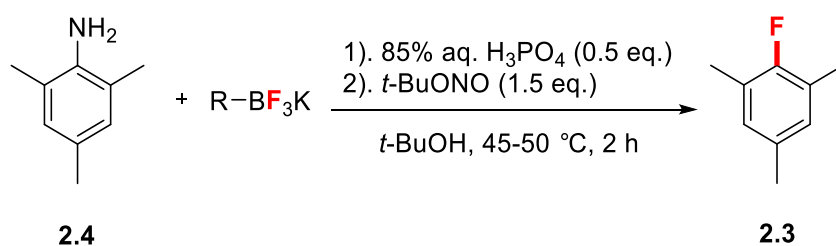
Entry	Temperature (°C) ^a	Yield (%) ^b
1	rt	33
2	45-50	73
3	55-60	70
4	75-80	66
5	95-100	72
6	105-110	68

7 ^c	45-50	58
8 ^d	45-50	81
9 ^e	45-50	68
10 ^f	45-50	66

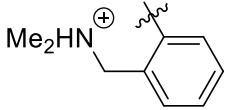
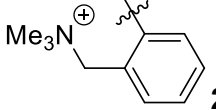
Reaction conditions: **2.4** (0.25 mmol), 85% aq. H₃PO₄ (0.5 eq.), **2.5** (0.38 mmol), *t*-BuOH (1.3 mL) in pressure vial with Teflon lined cap, Ar purge, then *t*-BuONO (0.38 mmol), rt for 20 min, then heated at indicated temperature for 2 h. ^a Oil bath temperature. ^b Yield determined by ¹⁹F NMR spectroscopy using 2,4-dinitrofluorobenzene as an internal standard. ^c No Ar purge of reaction vessel. ^d Degassed *t*-BuOH used. ^e N₂ atmosphere. ^f O₂ atmosphere.

With optimal conditions in hand, a vast array of organotrifluoroborates was explored to observe whether the reaction is modulated by the organic fragment. All other organotrifluoroborates examined provided lower reaction yields. Both electron withdrawing and donating substituents on the phenyl ring of the trifluoroborate provided similar yields (Table 2.8, entries 1-13). Zwitterionic trifluoroborates are known to have longer solvolytic half-lives due to stabilizing Coulombic interactions;⁷⁵ however, using zwitterions **2.6** and **2.7** resulted in diminished to trace yields, respectively (Table 2.8, entries 14 and 15). Alkyl trifluoroborates could mediate fluorination as well, albeit at lower yields (Table 2.8, entries 17-19).

Table 2.8 Effect of organotrifluoroborate on reaction yields



Entry	R	Yield (%) ^a
1	4-methoxyphenyl	34

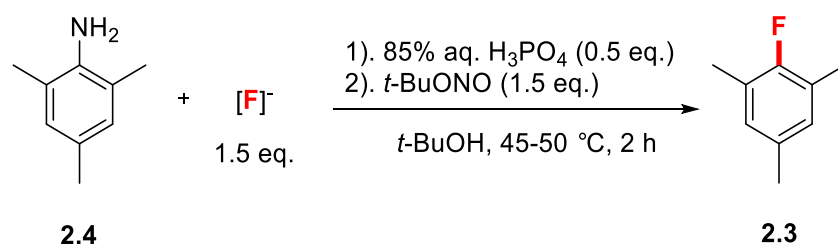
2	4-formylphenyl	44
3	4-benzoic acid	2
4	4-fluorophenyl	34
5	4-trifluoromethylphenyl	29
6	2-nitrophenyl	35
7	3-nitrophenyl	36
8	4-nitrophenyl	40
9	3-acetamidephenyl	56
10	2-hydroxyphenyl	46
11	3,5-bistrifluoromethylphenyl	42
12	Perfluorophenyl	50
13	2,4,6-trimethylphenyl	44
14	 2.6	46
15	 2.7	trace
16	vinyl	42
17	sec-butyl	44
18	cyclopropyl	33
19	n-butyl	41

Reaction conditions: **2.4** (0.25 mmol), 85% aq. H₃PO₄ (0.5 eq.), **RBF₃K** (0.75 mmol), *t*-BuOH (1.3 mL) in pressure vial with Teflon lined cap, Ar purge, then *t*-BuONO (0.38 mmol), rt for 20 min, then heated at indicated temperature for 2 h. ^aYield determined by ¹⁹F NMR spectroscopy using 2,4-dinitrofluorobenzene as an internal standard.

To support the specific value of organotrifluoroborates for this transformation, traditional sources of fluorine were explored to determine whether they could mediate fluorodediazotiation under established reaction conditions. Of all fluorine salts tested,

only KBF_4 gave trace amounts of the aryl fluoride, while no product formation was observed for others (Table 2.9). These results clearly support our hypothesis that organotrifluoroborates are better fluoride donors than the tetrafluoroborate anion. Moreover, these results demonstrate that under these mild conditions, a standard Balz-Schiemann reaction is not feasible. Finally, this result serves to exclude the possibility that BF_4^- , which may form adventitiously following C-B bond fission, is not functioning as a source of F^- under reaction conditions.

Table 2.9 Control fluorination experiments with various 'fluoride' salts

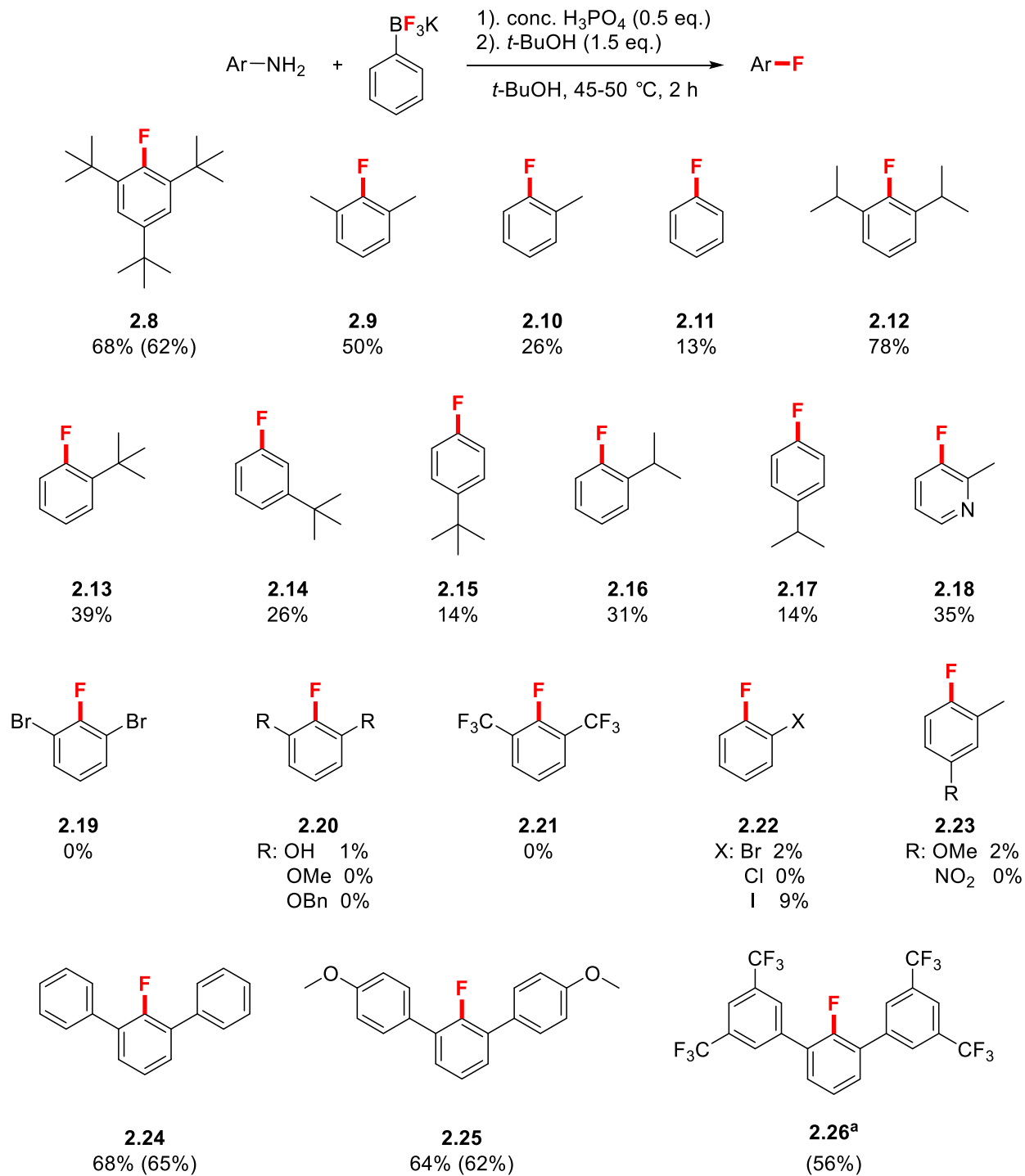


Entry	$[\text{F}]^-$	Yield (%) ^a
1	KBF_4	6
2	KF	0
3	TBAF (1M in THF)	0
4	CsF	0
5	KHF_2	0

Reaction conditions: **2.4** (0.25 mmol), 85% aq. H_3PO_4 (0.5 eq.), $[\text{F}]^-$ (0.38 mmol), $t\text{-BuOH}$ (1.3 mL) in pressure vial with Teflon lined cap, Ar purge, then $t\text{-BuONO}$ (0.38 mmol), rt for 20 min, then heated at 45-50 °C for 2 h. ^aYield determined by ^{19}F NMR spectroscopy using 2,4-dinitrofluorobenzene as an internal standard.

Having established an effective protocol, we turned to exploring the substrate scope of the transformation. Sterically hindered anilines were successfully fluorinated in good to high yields (Scheme 2.2, products **2.8**, **2.9**, **2.12** and **2.13**). Interestingly, removing steric

bulk from the *ortho* positions of the starting aniline was observed to correlate with decreasing yields of the corresponding aryl fluoride. While **2.8** was produced in 62% isolated yield, *ortho tert*-butyl substituted aniline decreased yields to 39% (**2.13**), progressively moving the substituent to the *meta* and *para* positions further diminished yields to 26% (**2.14**) and 14% (**2.15**), respectively. The same trend is observed for isopropyl substituents with decreasing yields observed in the series **2.12** (78%), **2.16** (31%), and **2.17** (14%). The sensitivity of the transformation towards steric bulk at both *ortho* positions is highlighted by the differences in reaction efficiencies observed between di and mono-*ortho* substituted anilines; yields are halved when comparing **2.9** (50%) to **2.10** (26%). Even more drastic is the yield obtained with **2.12** (78%) compared to **2.16** (31%). To support the hypothesis of required steric bulk at both *ortho* positions of the starting aniline, three substituted anilines were synthesized and efficiently fluorinated in good yields (Scheme **2.2**, products **2.24**, **2.25** and **2.26**), additionally showing that the transformation could tolerate the presence of heteroelements at auxiliary sites on the parent phenyl ring. The reaction conditions also allowed the fluorination of heterocycle **2.18** in moderate yield. Attempts to introduce heteroelement-containing steric bulk at *ortho* positions of the aniline resulted in only trace yields of the fluorinated product (Scheme **2.2**, products **2.19**, **2.20**, **2.21**, **2.22** and **2.23**).

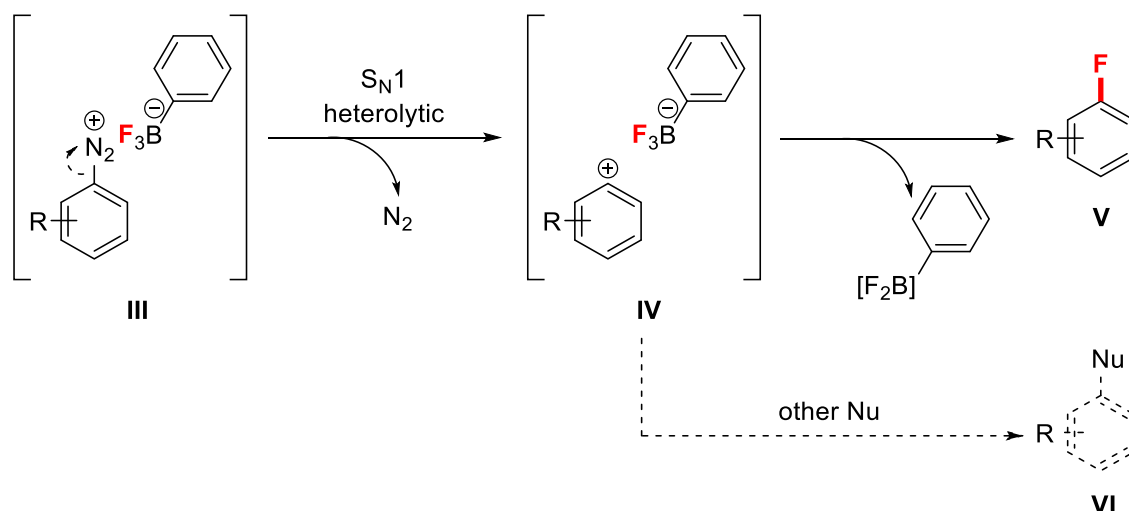


Scheme 2.2 Substrate scope of the one-pot Balz-Schiemann reaction with potassium phenyltrifluoroborate. Reaction conditions: aniline (0.25 mmol), 85% aq. H₃PO₄ (0.5 eq.), potassium phenyltrifluoroborate (0.38 mmol), *t*-BuOH (1.3 mL) in pressure vial with Teflon lined cap, Ar purge, then *t*-BuONO (0.38 mmol), rt for 20 min, then heated at 45-50 °C for 2 h. Yield determined by ¹⁹F NMR spectroscopy using 2,4-dinitrofluorobenzene as an internal standard. Isolated yield in parentheses. ^a 98% H₂SO₄ used instead of 85% aq. H₃PO₄ in *t*-BuOH at 95 °C.

2.2.3 Mechanism

The reactivity trend observed, especially the requirement for steric bulk at *ortho* positions, is not easy to rationalize. Balz-Schiemann reactions are known to tolerate both the presence and lack of steric hindrance.^{139,140} However, it has been reported that difficulties arise when diazonium salts are substituted with polar or p-electron-containing moieties, especially at the *ortho* position; *ortho*-fluoro and nitro phenyl diazonium tetrafluoroborates are known to undergo poor fluorodediazoniatio.^{139,140} For example, 1-fluoro-2,4-dimethoxybenzene can only be obtained in 10% yield from decomposition of the parent diazonium tetrafluoroborate.¹⁵⁷ These reports corroborate our experimental observations for **2.20**. On the other hand *ortho*-halogenated, except fluorine substitution, aryl diazonium salts undergo efficient fluorodediazoniatio.¹⁴⁰ The substituent-dependent reactivity has been suggested to relate to the stabilization of the aryl cation.¹⁴⁰ The enhanced reactivity and higher yields for certain di-*ortho*-substituted diazonium ions is consistent with the well-known effects of alkyl substituents that stabilize the intermediate aryl cation complex **IV** (Scheme **2.3**).^{128,129,131–137,158,159} Indeed, a single *ortho* methyl substitution on the benzenediazonium cation has been shown to be rate enhancing, with regards to trapping the aryl cation with a nucleophile, a second *ortho* methyl further enhances rates and yields due to further stabilization of intermediate **IV**.¹⁶⁰ My results with mono- and di-*ortho*-substituted anilines (Scheme **2.2**, products **2.10** vs. **2.9** and **2.16** vs. **2.12**) corroborate past findings to suggest that the mechanism for organotrifluoroborate engagement is likely consistent with a heterolytic reaction mechanism proceeding by a solvated ion pair.

We hypothesise that the reaction outcome is determined by the delicate balance between the kinetic and thermodynamic stability of the generated aryl cation. We therefore propose that under reaction conditions, tight ion pair **III** is formed in solution, S_N1 heterolytic decomposition produces intermediate **IV**. Intermediate **IV** can then either undergo fluorodediazoniatioin with the phenyltrifluoroborate anion or react with other nucleophiles in solution (Scheme **2.3**). Aryl cations of appropriate stability could persist long enough within the tight ion pair, **IV**, to be fluorinated producing **V**. Destabilized aryl cations may react more readily with other nucleophiles present in solution, namely water to produce unwanted by-products **VI**. The main side product observed was the corresponding phenol; however, in some cases biaryls from homocoupling of the substrate were observed (detected by GC-MS). The use of radical scavengers was investigated to suppress the formation of these wanted side-products and increase yields. Employing 2,2,6,6-tetramethyl-1-piperidinyloxy (TEMPO) had no effect on yields. Results using sodium ascorbate were inconsistent with yields either being unaffected or completely diminished; the ascorbate can behave as a single electron donor and therefore promote the homolytic decomposition of the aryl diazonium salt.



Scheme 2.3 Proposed reaction mechanism.

2.3 Conclusion and Perspectives

The Balz-Schiemann continues to be a relevant method for the synthesis of aryl fluorides due to its operational simplicity. However, the transformation remains limited by harsh reaction conditions, low yields and requirement for the isolation of potentially explosive intermediates. While several improvements have been made over the years and multiple sources of fluorine investigated, the use of organotrifluoroborates to mediate this reaction has been limited to but one report. To unveil the full potential of organotrifluoroborates to serve as F^- sources, we demonstrated that they could mediate fluorodediazotiation in solution with preformed aryl diazonium salts. This could be successfully extended to a one-pot two-step process avoiding the isolation of diazonium salts. The reaction conditions allowed the fluorination of various aniline substrates in moderate to good yield, and allows access to 2,6-disubstitued fluorobenzenes whose corresponding diazonium salts are known to be unstable.^{141,154} In stark contrast to typical Balz-Schiemann reactions that usually demand stringently dry decomposition; the described conditions employ an aqueous acid and can tolerate the presence of added equivalents of water without

diminishing yields. Furthermore, the low temperature (45 °C) at which diazonium decomposition and successful fluorination occur is unprecedented in Balz-Schiemann type transformations, excluding the use of HF reagents, presenting a mild route to aryl fluorides. Neither BF_4^- , KHF_2/HF , nor other fluoride ion sources afford more than trace quantities of aryl fluoride under conditions where the organotrifluoroborate does, thus demonstrating the critical role of these reagents in expanding the reaction manifold of the Balz-Schiemann reaction.

A short-term perspective involves further mechanistic studies and theoretical calculations to try to rationalize the substrate scope observed and the role of the organotrifluoroborate. With a firm understanding of the underlying selectivity and reactivity, reaction conditions can be tuned towards developing a generally applicable methodology for the fluorination of aromatic amines under operationally simple and mild experimental conditions. We foresee extending this methodology towards cartridge-based and continuous flow systems. Solid-supported boronic acids are commercially available, they can be converted to the corresponding trifluoroborate through standard methods and applied to our developed methodology. Solid-supported systems of this type would represent a recyclable fluorination reagent that can be easily collected from reaction mixtures by simple filtration. A more long-term perspective is to translate this methodology towards monofluoroborate systems. Monofluoroborates would be a more atom-economical fluorinating agent and have potential applications in radiofluorination. Work is currently underway towards expanding the application of organofluoroborates towards these two aims.

2.4 Experimental

General Information

Solvents and Reagents

Solvents (*t*-BuOH, Et₂O, MeOH, THF and acetone) used were all commercial grade and used as received with no drying. However, *t*-BuOH was degassed prior to its use and all reactions were performed under argon atmosphere unless otherwise stated. Commercially available compounds were used without further purification. Deuterated solvents for NMR spectroscopic analysis were purchased from Cambridge Isotopes Limited.

Analysis

NMR spectroscopy experiments were performed in deuterated solvents. ¹H NMR, ¹³C NMR, ¹¹B NMR and ¹⁹F spectra were recorded on 300 and 400 MHz Bruker spectrometers. Chemical shifts are reported in parts per million (ppm) relative to the residual protium in the solvents (¹H) or the solvent carbon (¹³C) as internal standards. ¹⁹F spectra of aryl fluorides were referenced to 2,4-dinitrofluorobenzene or 2,2,2-trifluoroethanol as internal standards (0.5 equivalents). ¹H NMR spectral data features are tabulated in the following order: chemical shift in ppm (δ) (multiplicity, coupling constant (*J*), integration, type of H). The following abbreviations were used to label the multiplicities in the NMR spectral data: s (singlet), b (broad), app (apparent), d (doublet), t (triplet), q (quartet), q_B (1:1:1:1 of peaks arising from coupling to ¹¹B with S=3/2, midpoint of signal reported), dd (doublet of doublets), dt (doublet of triplet), td (triplet of doublet), hept (heptet) and m (multiplet). Assignment of signals in ¹H and ¹³C NMR spectra were performed using ¹H-¹H COSY, HMQC, HSQC, HMBC, TOCSY and DEPT135 (dept polarization transfer with 135 degree read pulse to give XH, XH₃ positive and XH₂ negative with decoupling during acquisition) experiments where appropriate. Reactions were

monitored on silica gel 60F₂₅₄ pre-coated aluminium TLC plates purchased from EM Science.

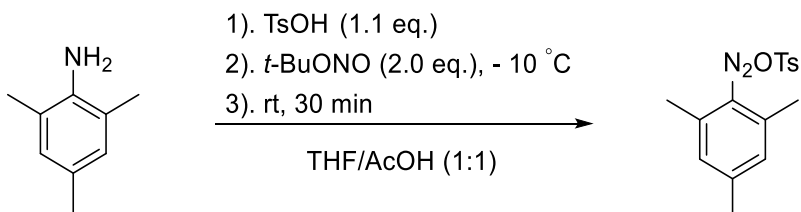
A significant background signal was observed, depending on the concentration of the sample, in the ¹¹B NMR spectra of some products as the utilized NMR tubes were constructed from borosilicate glass. Because of their low intensity (resulting from quadruple coupling), ¹³C signals arising from the quaternary carbon bearing the trifluoroborate group were not always observed and therefore were not always listed. We note that there are discrepancies between ¹J_{B-F} in the ¹⁹F and ¹¹B NMR spectra; possibly arising from asymmetry in the ¹⁹F multiplets. On this basis, the ¹¹B value is probably the most reliable, and therefore only this value is reported. In addition, ¹⁹F and ¹¹B chemical shifts were sometimes observed to be slightly different (0.1-2.0 ppm) from those reported in the literature.

Detection was accomplished by irradiation with a UV lamp ($\lambda = 254$ nm) or staining reagents (KMnO₄, HBQ) followed by heating. HBQ was particularly used to detect boron compounds on plates. Chromatographic separations were achieved on silica gel columns (Kieselgel 60, 40-63 μm).

IR spectra were recorded on a PerkinElmer Frontier FT-IR spectrometer with frequencies expressed in cm^{-1} .

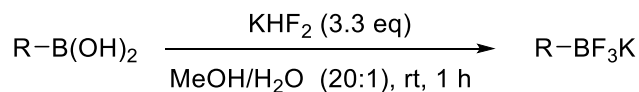
Low resolution mass spectra were obtained on Waters LC-MS and Agilent GC-MS. High-resolution mass spectra (HRMS) were recorded using either electron impact (EI) and desorption chemical ionization (DCI) using Kratos MS-50/Kraton Concept IIHQ spectrometers or electrospray ionization (ESI^{+/-} - TOF) using Waters/Micromass LCT spectrometer. Agilent GC-MS (7890B GC and 5977A MAD) was used to detect the formation of volatile by-products and confirm some NMR spectroscopy yields *via* the ALS-Split method.

Molecular sieves (pellets or powder) and magnesium sulphate were flame dried under high vacuum (<1 mbar) for 30 minutes. Degassing (sparging) of *t*-BuOH was performed by bubbling argon gas for 1 hour.

2,4,6-trimethylphenyldiazonium tosylate (2.1)

In a 100 mL round-bottom flask, 2,4,6-trimethylaniline (1.0 eq., 5.0 mmol, 0.702 mL) was dissolved in a 1:1 mixture of THF and glacial acetic acid (50 mL), followed by the addition of *para*-toluene sulfonic acid (1.1 eq., 5.5 mmol, 1.046 g). The solution was then cooled to -10 °C in an ice-brine bath and *t*-BuONO (2.0 eq., 10.0 mmol, 1.19 mL) was added dropwise. The reaction mixture was stirred for 30 min at -10 °C and further allowed to warm to room temperature for another 30 min. The resulting clear solution was poured into diethyl ether (add until precipitation) and the diazonium tosylate salt immediately precipitated. After careful filtration, the product was collected, washed three times with cold THF to remove the undesired organic compounds and then dried under high vacuum overnight. The title compound was isolated as a colourless powder (1.500 g, 95%). IR $\nu_{\text{max}}/\text{cm}^{-1}$ (neat film): 3032, 2261, 1589, 1406, 1311, 1193, 1120, 1032, 1010, 813, 678. ^1H NMR (300 MHz, DMSO- d_6) δ 7.48 (s, 2H), 7.45 (d, J = 8.1 Hz, 2H), 7.09 (d, J = 8.1 Hz, 2H), 2.67 (s, 6H), 2.47 (s, 3H), 2.28 (s, 3H). ^{13}C NMR (75 MHz, DMSO- d_6): δ = 153.3 (C_q), 145.7 (C_q), 143.7 (C_q), 137.6 (C_q), 130.7 (CH), 128.0 (CH), 125.5 (CH), 22.1 (CH₃), 20.8 (CH₃), 18.2 (CH₃). HRMS-ESI-TOF (m/z): found [M-OTs]⁺ 147.0918, calc'd C₉H₁₁N₂⁺ requires 147.0922.

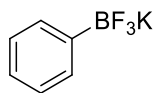
General Procedure B for the Synthesis of Potassium Aryltrifluoroborates



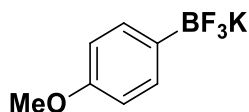
To a 25 mL round-bottom flask was added the aryl boronic acid (1.0 eq.), KHF₂ (3.3 eq.) and a 20:1 mixture of MeOH/distilled water (for every 2.0 mmol of the starting boronic acid, 4 mL of methanol and 0.2 mL of H₂O were required). The colourless reaction mixture was stirred for 30 min at room temperature where the solution became turbid (white). After complete conversion, solvents were removed by rotary evaporation and the remaining traces of water were dried under high vacuum overnight. Next, acetone was added to the point where most of the precipitate was dissolved and the solution was further dried using anhydrous magnesium sulphate. Following Buchner filtration, the filtrate was concentrated by rotary evaporation to a saturation point where Et₂O was added until the product precipitated out. The desired product was then collected by filtration, washed with cold Et₂O (3 times) and dried overnight on a high vacuum pump.

2.4.1 Characterization Data of the Synthesized Aryltrifluoroborates

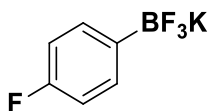
Potassium phenyltrifluoroborate (2a)



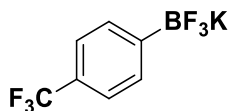
The title compound was prepared from phenylboronic acid (10.0 mmol) according to the general procedure **B** and isolated as a crystalline white solid (1.740 g, 95%). ¹H and ¹³C NMR data are in accordance with those previously reported in literature. ¹H NMR (300 MHz, DMSO-*d*₆) δ 7.32 (d, *J* = 7.3 Hz, 2H), 7.10 – 6.98 (m, 3H). ¹³C NMR (75 MHz, DMSO-*d*₆) δ 131.3 (CH), 126.2 (CH), 124.9 (CH). ¹¹B NMR (77 MHz, DMSO-*d*₆) δ 3.6 (bs). ¹⁹F NMR (282 MHz, DMSO-*d*₆) δ -139.7 (m). Spectroscopic data matches those previously reported.¹⁶¹

Potassium 4-methoxyphenyltrifluoroborate (2b)

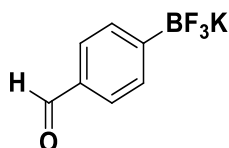
The title compound was prepared from 4-methoxyphenylboronic acid (2.0 mmol) according to the general procedure **B** and isolated as a crystalline white solid (0.419 g, 98%). ^1H and ^{13}C NMR data are in accordance with those previously reported in literature. ^1H NMR (300 MHz, $\text{DMSO-}d_6$) δ 7.67 (d, $J = 8.4$ Hz, 2H), 7.67 (d, $J = 8.4$ Hz, 2H), 3.67 (s, 3H). ^{13}C NMR (75 MHz, $\text{DMSO-}d_6$) δ 157.2 (C_q), 132.3 (CH), 111.9 (CH), 54.5 (CH_3). ^{11}B NMR (77 MHz, $\text{DMSO-}d_6$) δ 3.4 (bs). ^{19}F NMR (282 MHz, $\text{DMSO-}d_6$) δ -138.6 (bs). Spectroscopic data matches those previously reported.¹⁶²

Potassium 4-fluorophenyltrifluoroborate (2c)

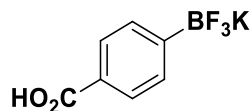
The title compound was prepared from 4-fluorophenylboronic acid (2.0 mmol) according to the general procedure **B** and isolated as a colourless solid (0.402 g, 84%). ^1H and ^{13}C NMR data are in accordance with those previously reported in literature. ^1H NMR (300 MHz, $\text{DMSO-}d_6$) δ 7.33 (t, $J = 7.3$ Hz, 2H), 6.88 (t, $J = 6.9$ Hz, 2H). ^{13}C NMR (75 MHz, $\text{DMSO-}d_6$) δ 160.9 (d, $^1J_{\text{C-F}} = 237.1$ Hz, C_q), 131.3 (d, $^3J_{\text{C-F}} = 6.6$ Hz, CH), 112.7 (d, $^2J_{\text{C-F}} = 18.3$ Hz, CH). ^{11}B NMR (77 MHz, $\text{DMSO-}d_6$) δ 4.4 (bs). ^{19}F NMR (282 MHz, $\text{DMSO-}d_6$) δ -118.9 – -119.1 (m, 1F), -139.1 – -139.4 (m, 3F). Spectroscopic data matches those previously reported.¹⁶³

Potassium 4-trifluoromethylphenyltrifluoroborate (2d)

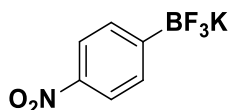
The title compound was prepared from 4-trifluoromethylphenylboronic acid (6.0 mmol) according to the general procedure **B** and isolated as a white crystalline solid (1.480 g, 98%). ^1H and ^{13}C NMR data are in accordance with those previously reported in literature. ^1H NMR (300 MHz, $\text{DMSO-}d_6$) δ 7.54 (d, $J = 7.5$ Hz, 2H), 7.53 (d, $J = 7.5$ Hz, 2H). ^{13}C NMR (75 MHz, $\text{DMSO-}d_6$) δ 131.7 (q, $^3J_{\text{C-F}} = 18.0$ Hz, CH), 126.4 (q, $^2J_{\text{C-F}} = 30.7$ Hz, C_q), 125.4 (q, $^1J_{\text{C-F}} = 271.4$ Hz, C_q), 122.8 (q, $^4J_{\text{C-F}} = 3.8$ Hz, CH). ^{11}B NMR (77 MHz, $\text{DMSO-}d_6$) δ 2.9 (bs). ^{19}F NMR (282 MHz, $\text{DMSO-}d_6$) δ -61.5 (bs, 3F), -140.5 (bs, 3F). Spectroscopic data matches those previously reported.¹⁶³

Potassium 4-formylphenyltrifluoroborate (2e)

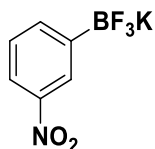
The title compound was prepared from 4-formylphenylboronic acid (2.0 mmol) according to the general procedure **B** and isolated as a white crystalline solid (0.331 g, 78%). ^1H and ^{13}C NMR data are in accordance with those previously reported in literature. ^1H NMR (300 MHz, $\text{DMSO-}d_6$) δ 9.91 (s, 1H), 7.66 (d, $J = 7.6$ Hz, 2H), 7.56 (d, $J = 7.8$ Hz, 2H). ^{13}C NMR (75 MHz, $\text{DMSO-}d_6$) δ 193.4 (C_q), 134.1 (C_q), 131.8 (CH), 127.9 (CH). ^{11}B NMR (77 MHz, $\text{DMSO-}d_6$) δ 2.9 (bs). ^{19}F NMR (282 MHz, $\text{DMSO-}d_6$) δ -139.9 (bs). Spectroscopic data matches those previously reported.¹⁶⁴

Potassium 4-carboxyphenyltrifluoroborate (2f)

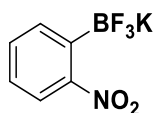
The title compound was prepared from 4-carboxyphenylboronic acid (6.0 mmol) according to the general procedure **B** and isolated as an off-white solid (1.310 g, 96%). IR $\nu_{\max}/\text{cm}^{-1}$ (neat film): 3034, 2659, 2536, 1713, 1685, 1561, 1514, 1425, 1368, 1318, 1289, 1220, 1188, 1125, 959, 851, 801, 708. ^1H NMR (300 MHz, DMSO- d_6) δ 12.40 (bs, 1H, OH), 7.71 (d, J = 8.1 Hz, 2H), 6.87 (d, J = 8.1 Hz, 2H). ^{13}C NMR (75 MHz, DMSO- d_6) δ 168.3 (C_q), 131.3 (CH), 127.5 (C_q), 127.4 (CH). ^{11}B NMR (77 MHz, DMSO- d_6) δ 3.7 (bs). ^{19}F NMR (282 MHz, DMSO- d_6) δ -140.3 (bs). HRMS-ESI-TOF (m/z): found [M-K]⁻ 188.0379, calc'd $\text{C}_7\text{H}_5^{10}\text{BF}_3\text{O}_2$ requires 188.0371.

Potassium 4-nitrophenyltrifluoroborate (2g)

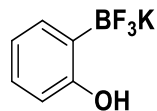
The title compound was prepared from 4-nitrophenylboronic acid (2.0 mmol) according to the general procedure **B** and isolated as a pale brown solid (0.332 g, 73%). ^1H and ^{13}C NMR data are in accordance with those previously reported in literature. ^1H NMR (300 MHz, Acetone- d_6) δ 7.98 (dd, J = 8.4, 1.0 Hz, 2H), 7.59 (dd, J = 8.4, 1.0 Hz, 2H). ^{13}C NMR (75 MHz, Acetone- d_6) δ 147.2 (C_q), 133.2 (CH), 121.8 (CH). ^{11}B NMR (77 MHz, Acetone- d_6) δ 2.7 (q, $J_{\text{B-F}}$ = 40.1 Hz). ^{19}F NMR (282 MHz, Acetone- d_6) δ -144.3 (q_B). Spectroscopic data matches those previously reported.¹⁶³

Potassium 3-nitrophenyltrifluoroborate (2h)

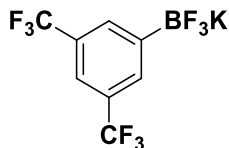
The title compound was prepared from 3-nitrophenylboronic acid (2.0 mmol) according to the general procedure **B** and isolated as a cream solid (0.350 mg, 80%). ^1H and ^{13}C NMR data are in accordance with those previously reported in literature. ^1H NMR (300 MHz, $\text{DMSO-}d_6$) δ 8.11 (s, 1H), 7.93 (dd, $J = 8.1, 2.7$ Hz, 1H), 7.75 (d, $J = 7.2$ Hz, 1H), 7.40 (dd, $J = 8.1, 7.2$ Hz, 1H). ^{13}C NMR (75 MHz, $\text{DMSO-}d_6$) δ 146.9 (C_q), 138.2 (CH), 127.8 (CH), 125.2 (CH), 120.2 (CH). ^{11}B NMR (77 MHz, $\text{DMSO-}d_6$) δ 2.6 (bs). ^{19}F NMR (282 MHz, $\text{DMSO-}d_6$) δ -140.5 – -140.8 (m). Spectroscopic data matches those previously reported.¹⁶⁵

Potassium 2-nitrophenyltrifluoroborate (2i)

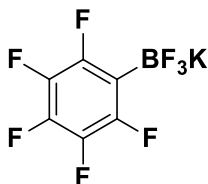
The title compound was prepared from 2-nitrophenylboronic acid (2.0 mmol) according to the general procedure **B** and isolated as a light beige solid (0.404 g, 88%). IR $\nu_{\text{max}}/\text{cm}^{-1}$ (neat film): 3672, 3067, 2863, 1610, 1569, 1520, 470, 1433, 1344, 1300, 1167, 1141, 1051, 999, 979, 965, 861, 880, 701. ^1H NMR (300 MHz, $\text{DMSO-}d_6$) 7.54 (d, $J_{\text{H-H}} = 7.1$ Hz, 1 H_{Ar}), 7.37 (appt, $J_{\text{H-H}} = 6.4$ Hz, 2 H_{Ar}), 7.30 – 7.19 (m, 1 H_{Ar}). ^{13}C NMR (75 MHz, $\text{DMSO-}d_6$) δ 155.0 (C_q), 134.1 (CH), 129.8 (CH), 126.3 (CH), 125.5 (C_q), 120.8 (CH). ^{11}B NMR (77 MHz, $\text{DMSO-}d_6$) δ 2.1 (q, $J_{\text{B-F}} = 47.7$). ^{19}F NMR (282 MHz, $\text{DMSO-}d_6$) δ -138.8 (q_B). HRMS (ESI-TOF) (m/z): found $[\text{M-K}]^-$ 189.0320, calc'd $\text{C}_6\text{H}_4^{10}\text{BF}_3\text{NO}_2$ requires 189.0324.

Potassium 2-hydroxyphenyltrifluoroborate (2j)

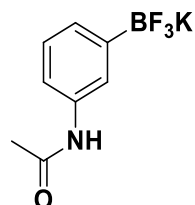
The title compound was prepared from 2-hydroxyphenylboronic acid (2.0 mmol) according to the general procedure **B** and isolated as a colourless solid (0.380 g, 95%). ^1H and ^{13}C NMR data are in accordance with those previously reported in literature. ^1H NMR (300 MHz, $\text{DMSO-}d_6$) δ 7.40 – 7.29 (bm, 1H, OH), 7.13 (d, J = 6.8 Hz, 1H), 6.92 (td, J = 7.6, 1.9 Hz, 1H), 6.61 (t, J = 7.2 Hz, 1H), 6.50 (d, J = 8.0 Hz, 1H). ^{13}C NMR (75 MHz, $\text{DMSO-}d_6$) δ 159.4 (C_q), 132.7 (CH), 126.9 (CH), 118.3 (CH), 113.2 (CH). ^{11}B NMR (77 MHz, $\text{DMSO-}d_6$) δ 4.0 (q, $J_{\text{B-F}}$ = 45.7 Hz). ^{19}F NMR (282 MHz, $\text{DMSO-}d_6$) δ -135.0 (q_B). Spectroscopic data matches those previously reported.¹⁶⁶

Potassium 3,5-bis(trifluoromethyl)phenyltrifluoroborate (2k)

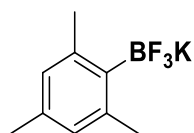
The title compound was prepared from 3, 5-bis(trifluoromethyl)phenylboronic acid (4.0 mmol) according to the general procedure **B** and isolated as an off-white solid (1.280 g, 99%). ^1H and ^{13}C NMR data are in accordance with those previously reported in literature. ^1H NMR (300 MHz, $\text{DMSO-}d_6$) δ 7.86 (s, 2H), 7.72 (s, 1H). ^{13}C NMR (75 MHz, $\text{DMSO-}d_6$) δ 131.8 (s, CH), 129.0 (q, $^2J_{\text{C-F}}$ = 31.5 Hz, C_q), 124.7 (q, $^1J_{\text{C-F}}$ = 270.7 Hz, C_q), 119.6-119.4 (m, CH). ^{11}B NMR (77 MHz, $\text{DMSO-}d_6$) δ 2.0 (bs). ^{19}F NMR (282 MHz, $\text{DMSO-}d_6$) δ -61.7 (s, 6F), -141.4 (bs, 3F). Spectroscopic data matches those previously reported.¹⁶⁷

Potassium 2,3,4,5,6-pentafluorophenyltrifluoroborate (2l)

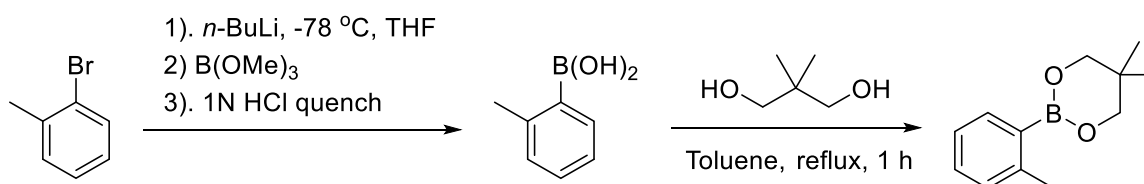
The title compound was prepared from 2, 3, 4, 5, 6-pentafluorophenylboronic acid (2.0 mmol) according to the general procedure **B** and isolated as a colourless solid (0.218 g, 40%). ^1H and ^{13}C NMR data are in accordance with those previously reported in literature. ^{13}C NMR (75 MHz, $\text{DMSO-}d_6$) δ 147.5 (d, $^1J_{\text{C-F}} = 239.1$ Hz, C_q), 138.3 (d, $^1J_{\text{C-F}} = 241.4$ Hz, C_q), 136.1 (d, $^1J_{\text{C-F}} = 244.1$ Hz, C_q). ^{11}B NMR (77 MHz, $\text{DMSO-}d_6$) δ 1.4 (q, $J = 33.7$ Hz). ^{19}F NMR (282 MHz, $\text{DMSO-}d_6$) δ -132.9 (q_B, 3F), -134.9 (bs, 2F), -161.3 (t, $J_{\text{F-F}} = 21.4$ Hz, 1F), -165.7 (bs, 2F). Spectroscopic data matches those previously reported.¹⁶⁶

Potassium 3-nitrophenyltrifluoroborate (2m)

The title compound was prepared from 3-nitrophenylboronic acid (2.0 mmol) according to the general procedure **B** and isolated as a colourless solid (0.383 g, 80%). IR $\nu_{\text{max}}/\text{cm}^{-1}$ (neat film): 3389, 3252, 1684, 1648, 1613, 1582, 1548, 1485, 1414, 1317, 1299, 1248, 1173, 995, 977, 944, 886, 872, 783. ^1H NMR (300 MHz, $\text{DMSO-}d_6$) δ 9.54 (bs, 1H), 7.49 – 7.45 (m, 1H), 7.28 (d, $J = 2.4$ Hz, 1H), 6.97 (m, 2H), 1.98 (s, 3H). ^{13}C NMR (75 MHz, $\text{DMSO-}d_6$) δ 167.5 (C_q), 137.6 (C_q), 126.6 (CH), 126.0 (CH), 122.6 (CH), 116.3 (CH), 23.7 (CH_3). ^{11}B NMR (77 MHz, $\text{DMSO-}d_6$) δ 3.5 (bs). ^{19}F NMR (282 MHz, $\text{DMSO-}d_6$) δ -139.5 (bs). HRMS-ESI-TOF (m/z): found $[\text{M-K}]^-$ 202.0647, calc'd $\text{C}_8\text{H}_8^{11}\text{BF}_3\text{NO}$ requires 202.0651.

Potassium 2,4,6-trimethylphenyltrifluoroborate (2n)

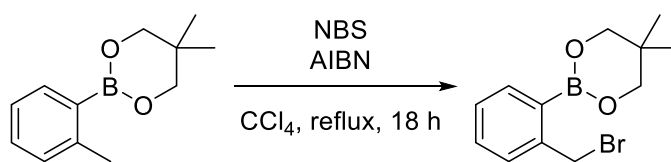
The title compound was prepared from 2, 4, 6-trimethylphenylboronic acid (2.0 mmol) according to the general procedure **B** and isolated as an off-white solid (0.384 g, 85%). IR $\nu_{\text{max}}/\text{cm}^{-1}$ (neat film): 3025, 2977, 2941, 2867, 1605, 1547, 1446, 1420, 1382, 1239, 1212, 1152, 1145, 1200, 1056, 1037, 938, 915, 886. ^1H NMR (300 MHz, $\text{DMSO-}d_6$) δ 6.74 (s, 2H), 2.20 (s, 3H), 2.16 (s, 6H). ^{13}C NMR (75 MHz, $\text{DMSO-}d_6$): δ 140.2 (C_q), 137.2 (C_q), 127.8 (CH). ^{11}B NMR (77 MHz, $\text{DMSO-}d_6$) δ 3.9 (bs). ^{19}F NMR (282 MHz, $\text{DMSO-}d_6$) δ -148.8 (s). HRMS-ESI-TOF (m/z): found $[\text{M-K}]^-$ 186.0936, calc'd $\text{C}_9\text{H}_{11}^{10}\text{BF}_3$ requires 187.0942.

Procedure for the synthesis of zwitterionic trifluoroborates 2.6 and 2.7**5,5-dimethyl-2-(*o*-tolyl)-1,3,2-dioxaborinane**

A 250 mL round-bottom flask was charged with a stir bar then flame dried, and purged with an Ar balloon. Under Ar, the flask was then charged with 2-bromotoluene (2.41 mL, 20 mmol) and THF (100 mL); the flask was then cooled to $-78\text{ }^\circ\text{C}$ in an acetone-dry ice bath. $n\text{-BuLi}$ (23.1 mL, 30 mmol) was added dropwise, via syringe, to the stirring reaction mixture over 2 minutes; the reaction mixture was stirred at $-78\text{ }^\circ\text{C}$ for 1 h. $\text{B}(\text{OMe})_3$ (4.46 mL, 40 mmol) was then added via syringe and the mixture stirred for an additional 30 min at $-78\text{ }^\circ\text{C}$ then allowed to stir for 3 h at rt. The crude reaction mixture was then

concentrated to dryness onto Celite and the residue purified by flash column chromatography on silica gel using an eluent of 100% hexane to 1:9 hexane/EtOAc. Identity of boronic acid was confirmed by crude NMR and mass spectrometry, boronic acid was used for next step without further purification. A 100 mL round-bottom flask was charged with a stir bar, condenser, Dean-Stark adapter, crude boronic acid (1.5996 g, 11.77 mmol), 2,2-dimethyl-1,3-propanediol (1.2414 g, 11.77 mmol) and toluene (75 mL). The reaction mixture was heated at reflux for 1 h then allowed to cool to rt. The reaction mixture was then concentrated under reduced pressure to an approximate volume of 50 mL after which it was filtered, and the filtrate concentrated to dryness under reduced pressure, and further dried under high vacuum overnight, to provide the desired boronic ester as a clear yellow oil (2.1421 g, 52% over two steps, GCMS purity: >97%). IR $\nu_{\text{max}}/\text{cm}^{-1}$ (neat film): 2961, 2932, 2888, 1599, 1476, 1302, 1275, 1135, 1106. ^1H NMR (300 MHz, Chloroform-*d*) δ 7.96 – 7.73 (m, 1H), 7.55 – 7.28 (m, 1H), 7.27 – 7.20 (m, 2H), 3.84 (s, 4H), 2.62 (s, 3H), 1.10 (s, 6H). ^{13}C NMR (75 MHz, Chloroform-*d*) δ 144.0 (C_q), 135.0 (CH), 130.1 (CH), 130.0 (CH), 124.7 (CH), 72.3 (CH₂), 31.7 (C_q), 22.5 (CH₃), 21.9 (CH₃). ^{11}B NMR (96 MHz, Chloroform-*d*) δ 27.53 (bs). GCMS-EI (*m/z*): 204 [M]⁺. Spectroscopic data matches those previously reported.¹⁶⁸

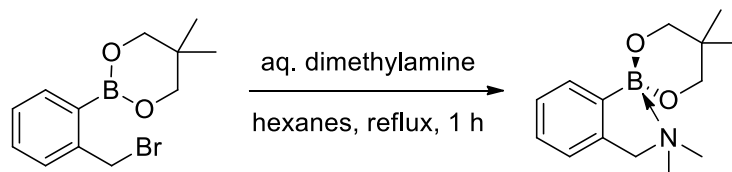
2-(2-(bromomethyl)phenyl)-5,5-dimethyl-1,3,2-dioxaborinane



A 50 mL round-bottom flask was charged with a stir bar and condenser and flame dried then purged with an Ar balloon. Under Ar, the flask was charged with 5,5-dimethyl-2-(o-tolyl)-1,3,2-dioxaborinane (2.1421 g, 10.5 mmol), N-bromosuccinimide (2.0524 g, 11.5 mmol), 2,2'-azobisisobutyronitrile (54.2 mg, 0.33 mmol) and degassed (freeze-pump-thaw x 3, then Ar bubbling) CCl₄ (20 mL). The light yellow reaction mixture was heated at reflux in an oil bath for 18 h. A white precipitate develops during the course of the reaction, after

allowing to cool to rt the reaction mixture is filtered and the precipitate washed with CCl_4 , the filtrate is concentrated under reduced pressure, and further dried under high vacuum overnight, to furnish the desired product as a clear dark brown oil (2.8049 g, 94%, GCMS purity: >90%). IR $\nu_{\text{max}}/\text{cm}^{-1}$ (neat film): 3065, 2962, 2935, 2891, 1719, 1476, 1286, 1245, 1127, 765. ^1H NMR (300 MHz, Chloroform-*d*) δ 7.88 – 7.80 (m, 1H), 7.37 (dt, $J = 4.4, 2.1$ Hz, 2H), 7.33 – 7.23 (m, 1H), 4.95 (s, 2H), 3.81 (s, 4H), 1.06 (s, 6H). ^{13}C NMR (75 MHz, Chloroform-*d*) δ 143.6 (C_q), 135.6 (CH), 130.6 (CH), 130.2 (CH), 127.6 (CH), 72.4 (CH_2), 34.6 (CH_2), 31.8 (C_q), 22.0 (CH_3). ^{11}B NMR (96 MHz, Chloroform-*d*) δ 27.07 (bs). GCMS-EI (m/z): 282 [Br^{79}M] $^+$, 284 [Br^{81}M] $^+$. Spectroscopic data matches those previously reported.¹⁶⁹

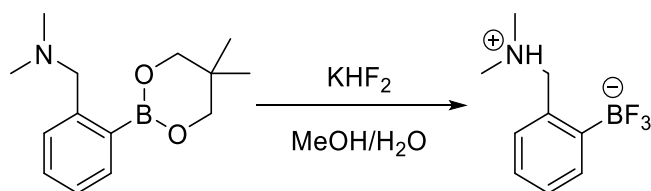
1-(2-(5,5-dimethyl-1,3,2-dioxaborinan-2-yl)phenyl)-*N,N*-dimethylmethanamine



A 100 mL round-bottom flask was charged with a stir bar, dimethylamine (6.0 mL, 40% aq. Solution) and Et_2O (50 mL). The flask was placed in an ice-bath and NaOH (10 g) was added; the solution was stirred for 30 min. The reaction mixture was then transferred to a separatory funnel and the organic layer collected in a 50 mL round-bottom flask charged with a stir bar. To this flask 2-bromomethylphenylboronic acid neopentyl ester (2.2 g, 7.8 mmol) followed by Et_2O (20 mL). This mixture was stirred at rt for 30 min and the developed precipitate filtered off, the filtrate was concentrated to ~10 mL and transferred to a 50 mL round-bottom flask charged with a stir bar. To this flask hexanes (15 mL) were added and the reaction mixture heated at reflux, in an oil bath, for 1 h. The reaction mixture was then cooled to rt and all solvent removed under reduced pressure, then further dried under high vacuum overnight, to yield the desired product as a clear dark brown oil (2.0988 g, 99%, GCMS purity: >91%). IR $\nu_{\text{max}}/\text{cm}^{-1}$ (neat film): 2952, 2891, 2869, 1717 1473, 1448, 1221, 1119, 747. ^1H NMR (300 MHz, Chloroform-*d*) δ 7.52 (dd,

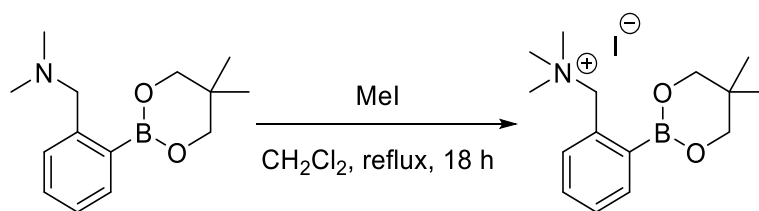
$J = 6.5, 1.8 \text{ Hz}, 1\text{H}$), $7.17 \text{ (pd, } J = 7.4, 1.5 \text{ Hz}, 2\text{H})$, $6.98 \text{ (d, } J = 7.0 \text{ Hz}, 1\text{H})$, $3.78 \text{ (s, } 2\text{H})$, $3.63 \text{ (s, } 4\text{H})$, $2.55 \text{ (s, } 6\text{H})$, $1.03 \text{ (s, } 6\text{H})$. $^{13}\text{C NMR}$ (75 MHz, Chloroform- d) δ 139.9 (C_q), 130.7 (CH), 127.44 (CH), 127.39 (CH), 123.2 (CH), 72.3 (CH_2), 64.6 (CH_2), 45.9 (CH_3), 32.2 (C_q), 22.3 (CH_3). $^{11}\text{B NMR}$ (96 MHz, Chloroform- d) δ 11.95 (bs). GCMS-EI (m/z): 246 $[\text{M-H}]^+$, 247 $[\text{M}]^+$. Spectroscopic data matches those previously reported.¹⁷⁰

(2-((dimethylammonio)methyl)phenyl)trifluoroborate (2.6)



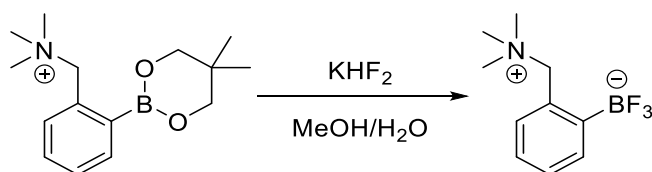
The title compound was prepared from 1-(2-(5,5-dimethyl-1,3,2-dioxaborinan-2-yl)phenyl)-N,N-dimethylmethanamine (2.0 mmol) according to the general procedure **B** and isolated as a beige powder (250.5 mg, 61%). IR $\nu_{\text{max}}/\text{cm}^{-1}$ (neat film): 3201, 3178, 2950, 1464, 1181, 1024, 973, 937 765. $^1\text{H NMR}$ (300 MHz, Acetonitrile- d_3) δ 7.63 (d, $J = 7.2 \text{ Hz}, 1\text{H}$), 7.35 – 7.27 (m, 1H), 7.27 – 7.18 (m, 2H), 4.27 (s, 2H), 2.75 (s, 6H). $^{13}\text{C NMR}$ (75 MHz, Acetonitrile- d_3) δ 133.88 (q, $^3J_{\text{C-F}} = 2.9 \text{ Hz}$) (CH), 133.86 (C_q), 131.8 (CH), 129.5 (CH), 127.6 (CH), 64.5 (CH_2), 43.5 (CH_3). $^{19}\text{F NMR}$ (282 MHz, Acetonitrile- d_3) δ -139.17. $^{11}\text{B NMR}$ (96 MHz, Acetonitrile- d_3) δ 3.17 (q, $J = 54.8, 54.4 \text{ Hz}$). HRMS-ESI (m/z): found $[\text{M-H}]^-$ 201.1049, calc'd $\text{C}_9\text{H}_{12}^{10}\text{BF}_3\text{N}^-$ requires 201.1049.

1-(2-(5,5-dimethyl-1,3,2-dioxaborinan-2-yl)phenyl)-*N,N,N*-trimethylmethanaminium iodide



A 10 mL flask, stir bar and attached condenser were flame dried then purged with Ar. The flask was then charged with 1-(2-(5,5-dimethyl-1,3,2-dioxaborinan-2-yl)phenyl)-*N,N*-dimethylmethanamine (250.4 mg, 1 mmol) and dry CH_2Cl_2 (5 mL). To this stirring reaction at rt, MeI (623 μL , 10 mmol) was added and left stirring at rt for 6 h; the reaction mixture was then heated at reflux overnight. After allowing to cool to rt the reaction mixture was dropped onto Et_2O to precipitate the product. The precipitate was collected by filtration and washed with Et_2O ; the product, a yellow powder, was collected and dried under high vacuum overnight (293.4 mg, 74%). IR $\nu_{\text{max}}/\text{cm}^{-1}$ (neat film): 3060, 3001, 2955, 2900, 2871, 1477, 1414, 1298, 1253, 881, 657. ^1H NMR (300 MHz, Acetonitrile- d_3) δ 8.02 – 7.95 (m, 1H), 7.62 – 7.46 (m, 3H), 4.89 (s, 2H), 3.85 (s, 4H), 3.05 (s, 9H), 1.00 (s, 6H). ^{13}C NMR (75 MHz, Acetonitrile- d_3) δ 136.5 (CH), 134.2 (CH), 132.9 (C_q), 131.0 (CH), 129.9 (CH), 72.1 (CH_2), 67.7 – 67.6 (m) (CH_2), 53.5 – 52.52 (m) (CH_3), 31.4 (C_q), 21.0 (C_q). ^{11}B NMR (96 MHz, Acetonitrile- d_3) δ 26.70 (bs). HRMS-ESI (m/z): found $[\text{M}-\text{I}]^+$ 261.2005, calc'd $\text{C}_{15}\text{H}_{25}^{10}\text{BNO}_2^+$ 261.2015.

trifluoro(2-((trimethylammonio)methyl)phenyl)borate (2.7)

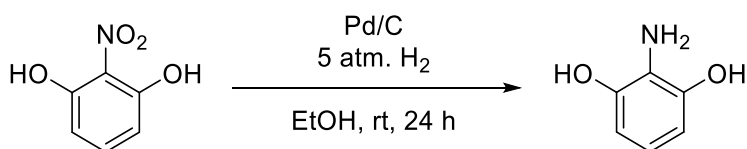


The title compound was prepared from 1-(2-(5,5-dimethyl-1,3,2-dioxaborinan-2-yl)phenyl)-*N,N*-dimethylmethanamine (0.72 mmol) according to the general procedure **B**

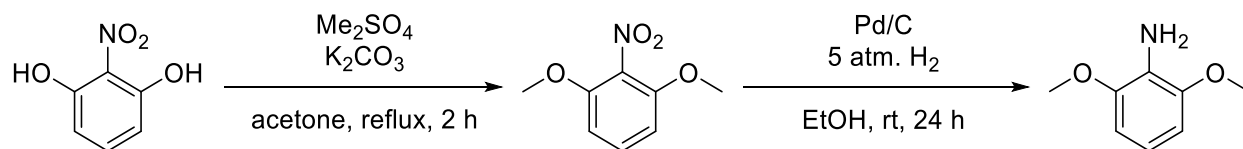
and isolated as a very hygroscopic resin (270.5 mg, >99%). Residual 2,2-dimethyl-1,3-propanediol could not be separated from the product, the crude was used as is. ^1H NMR (300 MHz, Acetonitrile- d_3) δ 7.68 (d, J = 7.4 Hz, 1H), 7.46 – 7.13 (m, 3H), 4.70 (s, 2H), 3.01 (s, 9H). ^{13}C NMR (75 MHz, Acetonitrile- d_3) δ 134.84, 132.87, 131.09, 129.74, 127.01, 70.16, 53.75. ^{19}F NMR (282 MHz, Acetonitrile- d_3) δ -135.39 – -136.91 (m). ^{11}B NMR (96 MHz, Acetonitrile- d_3) δ 3.00 (q, J = 53.2 Hz). LRMS-ESI (m/z): $[\text{M}+\text{K}]^+$ 256.

Synthesis of Anilines

2,6-dihydroxyaniline

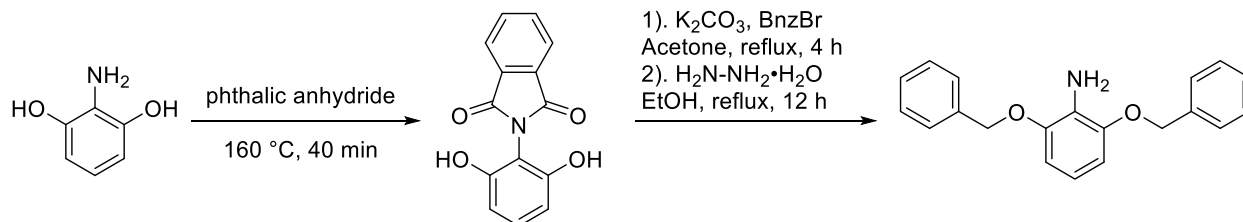


A glass reaction vessel is charged with a stir bar, 2-nitroresorcinol (7.7599 g, 50 mmol), palladium on carbon (10% loading, 532.1 mg, 0.5 mmol, 1 mol%) and 125 mL of EtOH. The glass vessel was loaded into a metal pressure reactor and the system evacuated and purged with Argon three times, then evacuated and charged with 5 atm. of H_2 . The reactor was sealed, and the reaction mixture stirred at room temperature for 24 h. After which the reaction mixture was filtered over Celite and the residue washed (2x10 mL EtOH). The filtrate was concentrated by rotary evaporation furnishing a white powder (6.0431 g, 97%). ^1H NMR (400 MHz, DMSO- d_6) δ 8.82 (bs, 2H), 6.33-6.23 (m, 4H). ^{13}C NMR (101 MHz, DMSO- d_6) δ 145.3 (C_q), 124.2 (C_q), 116.4 (CH), 107.1 (CH). MS-DCI(NH_3) (m/z): 126 $[\text{M}+\text{H}]^+$, 143 $[\text{M}+\text{NH}_4]^+$. Spectroscopic data matches those previously reported.¹⁷¹

2,6-bis(methoxy)aniline

A 250 mL round bottom flask was charged with a stir bar, 2-nitroresorcinol (15.5124 g, 100 mmol), K₂CO₃ (41 g, 300 mmol), Me₂SO₄ (28.39 mL, 300 mmol) and 100 mL acetone. The mixture was heated at reflux for 2 h then allowed to cool to room temperature. The solvent was then removed by rotary evaporation and further dried under high vacuum. The remaining residue was washed with H₂O and triethylamine to remove unreacted starting material, after which the remaining white powder was dried under high vacuum (14.7301 g, 80%) and used for the next step without further purification.

A glass reaction vessel is charged with a stir bar, 1,3-dimethoxy-2-nitrobenzene (3.66 g, 19.65 mmol), palladium on carbon (10% loading, 212.84 mg, 0.2 mmol, 1 mol%) and 50 mL of EtOH. The glass vessel was loaded into a metal pressure reactor and the system evacuated and purged with Argon three times, then evacuated and charged with 5 atm. of H₂. The reactor was sealed, and the reaction mixture stirred at rt for 24 h. After which the reaction mixture was filtered over Celite and the residue washed (2x10 mL EtOH). The filtrate was concentrated by rotary evaporation furnishing a white powder (2.8221 g, 92%). ¹H NMR (400 MHz, Chloroform-d) δ 6.70 (dd, J = 8.8, 7.7 Hz, 1H), 6.55 (d, J = 8.2 Hz, 2H), 3.86 (s, 7H). ¹³C NMR (101 MHz, Chloroform-d) δ 147.5 (C_q), 125.4 (C_q), 116.9 (CH), 104.1 (CH), 55.8 (CH₃). MS-DCI(NH₃) (*m/z*): 154 [M+H]⁺. Spectroscopic data matches those previously reported.¹⁷²

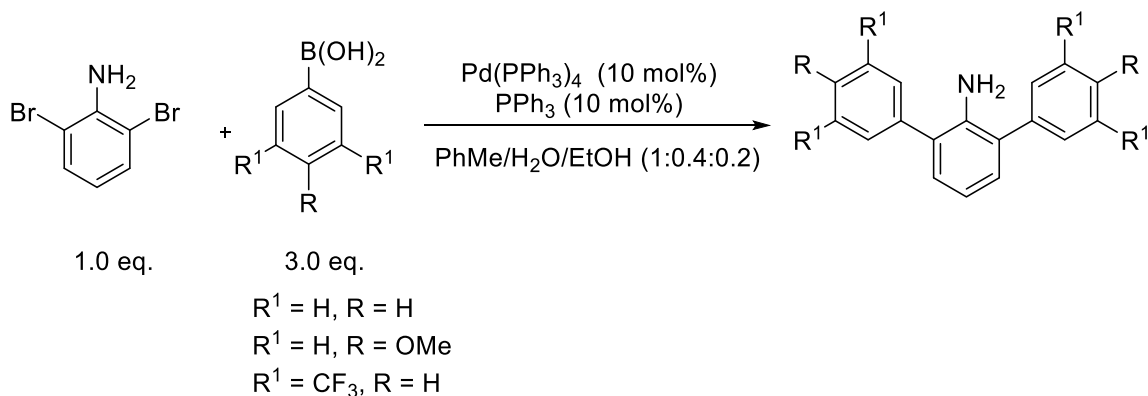
2,6-bis(benzyloxy)aniline

A 50 mL round bottom flask was charged with a stir bar, phthalic anhydride (1.4446 g, 9.75 mmol) and 2-aminoresorcinol (1.2521 g, 10 mmol). The flask was placed in a heat bath at 160 °C and stirred, as the anhydride began to melt the evolution of water vapour was observed along with a fluffy powder; stirring and temperature were maintained for 40 min. After allowing to cool to room temperature the residue was extracted with $CHCl_3$, CH_2Cl_2 and acetone. The CH_2Cl_2 and acetone fractions were combined and concentrated to furnish a black solid which was further triturated with Et_2O , the black solid was then dried over high vacuum (2.0979 g, 82%) and used for the next step without further purification.

A 100 mL round-bottom flask was charged with a stir bar, condenser, 2-(2,6-dihydroxyphenyl)isoindoline-1,3-dione (1.5 g, 5.9 mmol), benzyl bromide (1.75 mL, 14.7 mmol), K_2CO_3 (2.0458 g, 14.7 mmol) and acetone (30 mL). The flask was then placed in an oil bath and heated to reflux for 18 h, the reaction mixture was then allowed to cool to rt, then filtered to remove undissolved solids. The filtrate was concentrated to dryness then the residue dissolved in 100 mL EtOAc which was transferred into a separatory funnel. The organic phase was washed with aq. saturated $NaHCO_3$ (2 x 50 mL), then aq. NH_4OH (1 x 50 mL, pH ~10). The organic phase was then dried over Na_2SO_4 then filtered and concentrated to dryness, this residue was used for the next step without further purification. The dibenzylated product (1.555 g, 3.6 mmol) was loaded into a 120 mL pressure vial with EtOH (40 mL) and hydrazine monohydrate (535 μ L, 7.2 mmol). The vial was sealed and placed in an oil bath at 95 °C for 11h, after which it was allowed to cool to rt then filtered to remove undissolved solids. The filtrate was concentrated to dryness to furnish a purple viscous oil which was purified on silica gel using an eluent of 100%

hexane to 9:1 hexane/EtOAc. Desired fractions were collected and concentrated to furnish the desired aniline as a light pink crystalline powder (849.7 mg, 47%). IR $\nu_{\max}/\text{cm}^{-1}$ (neat film): 3474, 3378, 3063, 3032, 2867, 1602, 1501, 1477, 1466, 1453, 1135, 732. ^1H NMR (400 MHz, Chloroform-*d*) δ 7.48 (d, $J = 7.2$ Hz, 4H), 7.41 (t, $J = 7.3$ Hz, 4H), 7.35 (t, $J = 7.2$ Hz, 2H), 6.70 (dd, $J = 9.4, 6.8$ Hz, 1H), 6.65 – 6.61 (m, 2H), 5.12 (s, 4H), 4.20 (bs, 2H). ^{13}C NMR (75 MHz, DMSO-*d*₆) δ 146.9 (C_q), 137.4 (C_q), 128.7 (CH), 128.0 (CH), 127.6 (CH), 126.3 (C_q), 117.0 (CH), 106.1 (CH), 70.8 (CH₂). HRMS-EI (m/z): found $[\text{M}+\text{H}]^+$ 306.1498, calc'd C₂₀H₂₀NO₂ requires 306.1494.

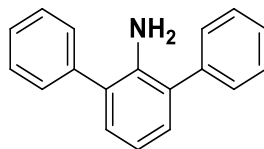
General Procedure C for the Synthesis of 2,6 Disubstituted Anilines



A 20 mL round bottom flask was charged with 2,6-dibromoaniline (1.0 eq, 1.0 mmol, 0.251 g), arylboronic acid (3.0 eq, 3.0 mmol, 0.367 g), Pd(PPh₃)₄ (0.1 eq., 10 mol%, 0.1 mmol, 0.116 g mg), PPh₃ (0.1 eq., 10 mol%, 0.1 mmol, 0.280 g), Na₂CO₃ (8.3 eq, 8.3 mmol, 0.881 mg), 10 mL toluene, 2 mL EtOH and 4 mL H₂O. The reaction mixture was partially degassed by bubbling with argon over an hour at room temperature and further refluxed for 12 h. After cooling to room temperature, 10 mL of H₂O were added and the aqueous phase was extracted with CH₂Cl₂ (3 x 10 mL). The combined organic phases were dried over anhydrous MgSO₄, filtered and concentrated by rotary evaporation. The crude residue was loaded onto Celite[®] and purified by silica gel flash column chromatography using 100% cyclohexane to an 80:20 mixture of cyclohexane/EtOAc. Desired fractions were collected, concentrated by rotary evaporation and further dried under high vacuum.

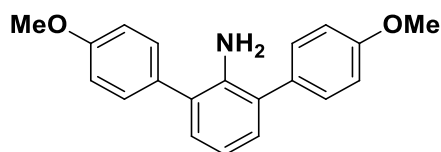
Characterization Data of the Synthesized Anilines

2,6-diphenylaniline

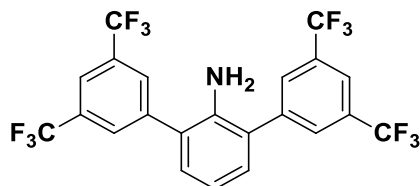


The title compound was prepared from 2, 6-dibromoaniline (1 mmol) and phenylboronic acid (3 mmol) according to the general procedure **C** and isolated as an off-white/yellow solid (0.209 g, 85%). IR $\nu_{\text{max}}/\text{cm}^{-1}$ (neat film): 2923, 1600, 1424, 1259, 1072, 1016, 798, 754, 703. ^1H NMR (300 MHz, Chloroform-*d*) δ 7.55-7.51 (m, 4H), 7.50-7.43 (m, 4H), 7.41-7.33 (m, 2H), 7.15 (d, $J = 7.5$ Hz, 2H), 6.90 (dd, $J = 7.9, 7.1$ Hz, 1H), 3.86 (bs, 2H). ^{13}C NMR (75 MHz, Chloroform-*d*) δ 140.9 (C_q), 139.9 (C_q), 129.9 (CH), 129.5 (CH), 128.1 (CH), 128.0 (C_q), 127.4 (CH), 118.2 (CH). HRMS-ESI-TOF (m/z): found $[\text{M}+\text{H}]^+$ 246.1277, calc'd C₁₈H₁₆N requires 246.1283.

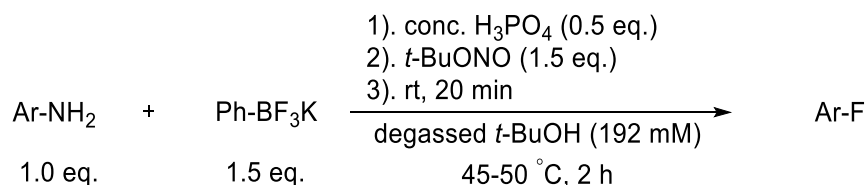
2,6-di-(4-methoxyphenyl)aniline



The title compound was prepared from 2, 6-dibromoaniline (1 mmol) and 4-methoxyphenylboronic acid (3 mmol) according to the general procedure **C** and isolated as a pale brown solid (0.284 g, 92%). IR $\nu_{\text{max}}/\text{cm}^{-1}$ (neat film): 3009, 2954, 2837, 1603, 1507, 1462, 1239, 1178, 1036, 838, 785, 732. ^1H NMR (300 MHz, Chloroform-*d*) δ 7.43(d, $J = 8.8$ Hz, 4H), 7.08 (d, $J = 7.5$ Hz, 2H), 7.01-6.97 (d, $J = 8.8$ Hz, 4H), 6.85 (dd, $J = 7.8, 7.2$ Hz, 1H), 3.85 (s, 6H). ^{13}C NMR (75 MHz, Chloroform-*d*) δ 158.9 (C_q), 141.0 (C_q), 132.1 (C_q), 130.5 (CH), 129.6 (CH), 127.8 (C_q), 118.3 (CH), 114.3 (CH), 55.4 (CH₃). HRMS-ESI-TOF (m/z): found $[\text{M}+\text{H}]^+$ 306.1480, calc'd C₂₀H₂₀NO₂ requires 306.1494.

2,6-di-(3,5-bis(trifluoromethyl)phenyl)aniline

The title compound was prepared from 2, 6-dibromoaniline (1 mmol) and 3,5-bis(trifluoromethyl)phenylboronic acid (3 mmol) according to the general procedure **C** but instead of refluxing, the vial was irradiated in a microwave reactor at maximum 200 W to maintain a temperature of 85°C for 1 h. It was isolated as a yellowish powder (0.505 g, 95%). IR $\nu_{\text{max}}/\text{cm}^{-1}$ (neat film): 3496, 3407, 3089, 3064, 1619, 1459, 1373, 1275, 1170, 1125, 1107, 900, 682. ^1H NMR (400 MHz, Chloroform-*d*) δ 7.99 (s, 4H), 7.91 (s, 2H), 7.18 (d, $J = 7.6$ Hz, 2H), 6.98 (dd, $J = 8.0, 7.2$ Hz, 1H), 3.70 (bs, 2H). ^{13}C NMR (101 MHz, Chloroform-*d*) δ 141.3 (C_q), 140.4 (2 x C_q), 132.4 (q, $^2J_{\text{C-F}} = 33.5$ Hz, CH), 131.1 (CH), 129.6 (CH), 125.4 (C_q), 123.2 (q, $^1J_{\text{C-F}} = 273.0$ Hz, C_q), 121.5 (hept, $^3J_{\text{C-F}} = 4.1$ Hz, CH), 119.2 (C_q). ^{19}F NMR (376 MHz, Chloroform-*d*) δ -62.84 (s). HRMS-DCI(CH_4) (m/z): found $[\text{M}]^+$ 517.0693, calc'd $\text{C}_{22}\text{H}_{11}\text{F}_{12}$ requires 517.0700.

General Procedure D for the Synthesis of Aryl Fluorides

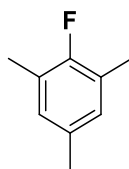
To a Pyrex tube charged with a stirring bar was added the aniline (1.0 eq., 0.25 mmol), phosphoric acid (0.5 eq., 0.125 mmol, 6.52 μL) and *t*-BuOH (1 mL). The mixture was stirred for few minutes to ensure the formation of the anilinium salt. Potassium phenyltrifluoroborate (1.5 eq., 0.375 mmol, 0.690 g) was added and the walls of the tube were washed using 0.3 mL of *t*-BuOH. The vial was purged with argon for 30 seconds prior to the dropwise addition of *t*-BuONO (1.5 eq., 0.375 mmol, 45.0

μL). The reaction mixture was allowed to diazotize for 20 min at room temperature before placing the tube in a silicon bath and heating to 50 °C for 2 h. After cooling to room temperature, 1-fluoro-2, 4-dinitrobenzene (0.5 eq.) was added to the crude mixture, followed by $\text{DMSO-}d_6$. Reaction yield was determined by ^{19}F NMR. Many aryl fluorides were not isolated due to their low boiling points and subsequent high volatility.

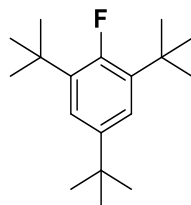
Regarding the isolated fluorinated compounds: 2,2,2-trifluoroethanol was used as the internal standard followed by Chloroform-*d*. For purification, the crude residue was loaded onto silica and purified by silica gel flash column chromatography using 100% pentane to a mixture of pentane/EtOAc as the eluent. Desired fractions were collected and concentrated to furnish a colourless solid which was further dried under high vacuum.

Characterization Data of the Synthesized Aryl Fluorides

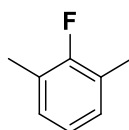
1-fluoro-2,4,6-trimethylbenzene (2.3)



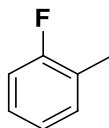
The title compound was obtained following the general procedure **D** in 81% NMR yield. ^{19}F NMR (282 MHz, $\text{DMSO-}d_6$) δ -128.1 (s), δ (*lit*) -128.0 (s). Spectroscopic data matches reports in the literature.¹⁷³

1,3,5-tri-*tert*-butyl-2-fluorobenzene (2.8)

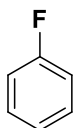
The title compound was obtained following general procedure **D** in 68% NMR yield, purified by silica gel flash column chromatography using 100% pentane and isolated as a colourless solid (0.410 g, 62%). IR $\nu_{\max}/\text{cm}^{-1}$ (neat film): 2960, 2906, 2871, 1607, 1574, 1512, 1455, 1436, 1363, 1284, 1247, 1236, 1220, 1204, 1160, 1115, 1039, 839. ^1H NMR (300 MHz, Chloroform-*d*) δ 7.20 (d, $J = 7.2$ Hz, 2H), 1.40 (s, 18H), 1.30 (s, 3H). ^{13}C NMR (75 MHz, Chloroform-*d*) δ 159.5 (d, $^1J_{\text{C-F}} = 249.2$ Hz, C_q), 144.9 (d, $^4J_{\text{C-F}} = 3.7$ Hz, C_q), 136.4 (d, $^2J_{\text{C-F}} = 13.8$ Hz, C_q), 122.1 (d, $^3J_{\text{C-F}} = 6.2$ Hz, CH), 34.9 (C_q), 34.8 (C_q), 31.8 (CH_3), 30.4 (d, $^5J_{\text{C-F}} = 4.1$ Hz, CH_3). ^{19}F NMR (282 MHz, Chloroform-*d*) δ -112.0 (s). HRMS-EI (m/z): found $[\text{M}]^+$ 264.22527, calc'd $\text{C}_{18}\text{H}_{29}\text{F}$ requires 264.22533.

1-fluoro-2,6-dimethylbenzene (2.9)

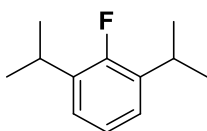
The title compound was obtained following general procedure **D** in 50% NMR yield. ^{19}F NMR (282 MHz, $\text{DMSO-}d_6$) δ -122.9 (s), δ (*lit*) -122.5 (s). Spectroscopic data matches reports in the literature.¹⁷⁴

1-fluoro-2-methylbenzene (2.10)

The title compound was obtained following general procedure **D** in 26% NMR yield. ^{19}F NMR (282 MHz, $\text{DMSO-}d_6$) δ -118.3 (s), δ (*lit*) -118.1 (s). Spectroscopic data matches reports in the literature.¹⁷⁵

1-fluorobenzene (2.11)

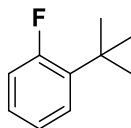
The title compound was obtained following general procedure **D** in 13% NMR yield. ^{19}F NMR (282 MHz, $\text{DMSO-}d_6$) δ -113.6 (s), δ (*lit*) -113.1 (s). Spectroscopic data matches reports in the literature.¹⁴⁴

1-fluoro-2,6-diisopropylbenzene (2.12)

The title compound was obtained following general procedure **D** in 78% NMR yield (73% GC-MS yield). The product was dissolved in acetone and analysed by GC-MS using ALS-SPLIT-L.M. method. Two peaks were observed with retention times (T_R) of 6.207 min and 8.030 min, respectively. The first peak (T_{R1} =6.207 min) had an m/z of 180.2 corresponding to the desired aryl fluoride which was obtained in 73% yield while the second peak (T_{R2} =8.030 min) had an m/z of 178.2 consistent with the phenol by-product. ^{19}F NMR (282

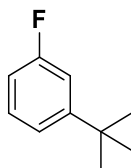
MHz, DMSO- d_6) δ -127.6 (s), δ (*lit*) -126.7 (t). Spectroscopic data matches reports in the literature.¹⁴⁵

1-*tert*-butyl-2-fluorobenzene (2.13)

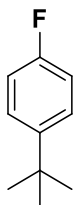


The title compound was obtained following general procedure **D** in 39% NMR yield. ^{19}F NMR (282 MHz, DMSO- d_6) δ -110.6 (s). Spectroscopic data matches reports in the literature.¹⁷⁶

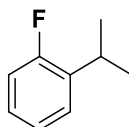
1-*tert*-butyl-3-fluorobenzene (2.14)



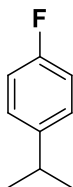
The title compound was obtained following general procedure **D** in 26% NMR yield. ^{19}F NMR (282 MHz, DMSO- d_6) δ -114.0 (s), δ (*lit*) -114.1 (s). Spectroscopic data matches reports in the literature.¹⁷⁷

1-tert-Butyl-4-fluorobenzene (2.15)

The title compound was obtained following general procedure **D** in 14% NMR yield. ^{19}F NMR (282 MHz, $\text{DMSO-}d_6$) δ -119.0 (s), δ (*lit*) -119.2 (s). Spectroscopic data matches reports in the literature.¹⁷⁴

1-Fluoro-2-isopropylbenzene (2.16)

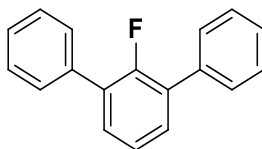
The title compound was obtained following general procedure **D** in 31% NMR yield. ^{19}F NMR (282 MHz, $\text{DMSO-}d_6$) δ -120.2 (s), δ (*lit*) -121.8 (s). Spectroscopic data matches reports in the literature.⁴⁶

1-fluoro-4-isopropylbenzene (2.17)

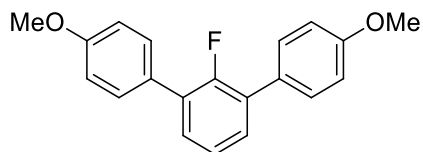
The title compound was obtained following general procedure **D** in 14% NMR yield. ^{19}F NMR (282 MHz, $\text{DMSO-}d_6$) δ -118.3 (s), δ (*lit*) -119.1 (s). Spectroscopic data matches reports in the literature.¹⁷⁷

3-fluoro-2-methylpyridine (2.18)

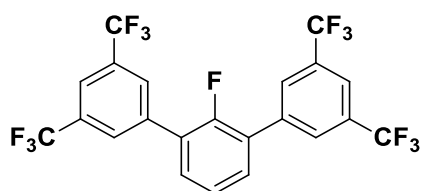
The title compound was obtained following general procedure **D** in 35% NMR yield. ^{19}F NMR (282 MHz, $\text{DMSO-}d_6$) δ -125.2 (s). Spectroscopic data matches reports in the literature.¹⁷⁸

1-fluoro-2,6-diphenylbenzene (2.24)

The title compound was obtained following general procedure **D** in 68% NMR yield, purified by silica gel flash column chromatography using 100% pentane and isolated as a colourless solid (0.403 g, 65%). IR $\nu_{\text{max}}/\text{cm}^{-1}$ (neat film): 3038, 2923, 1597, 1580, 1565, 1499, 1464, 1417, 1395, 1315, 1305, 1211, 1202, 1190, 1074, 1027, 977, 823. ^1H NMR (300 MHz, Chloroform-*d*) δ 7.62- 7.58 (m, 4H), 7.50-7.39 (m, 8H), 7.31-7.28 (m, 1H). ^{13}C NMR (75 MHz, Chloroform-*d*) δ 156.7 (d, $^1J_{\text{C-F}} = 249.7$ Hz, C_q), 136.1 (C_q), 130.2 (d, $^3J_{\text{C-F}} = 3.8$ Hz, CH), 129.36 (d, $^4J_{\text{C-F}} = 2.9$ Hz, CH), 128.6 (CH), 127.83 (CH), 124.5 (d, $J_{\text{C-F}} = 4.6$ Hz, CH). ^{19}F NMR (282 MHz, Chloroform-*d*) δ -123.7 (s, 1F). HRMS-EI (m/z): found $[\text{M}]^+$ 248.10034, calc'd $\text{C}_{18}\text{H}_{13}\text{F}$ requires 248.10013.

1-fluoro-2,6-bis(4-methoxyphenyl)benzene (2.25)

The title compound was obtained following general procedure **D** in 68% NMR yield, purified *via* reverse phase column chromatography using an eluent gradient of 100% H₂O to 100% MeCN over 1 hour and isolated as an off-white powder which was further dried under (0.478 g, 62%). IR $\nu_{\text{max}}/\text{cm}^{-1}$ (neat film): 2955, 2838, 1607, 1573, 1512, 1456, 1440, 1396, 1364, 1283, 1211, 1159, 1111, 1085, 1020, 1002, 889, 817. ¹H NMR (300 MHz, Chloroform-*d*) δ 7.53 (dd, $J = 8.8, 1.8$ Hz, 4H), 7.35 (t, $J = 7.4$ Hz, 2H), 7.23 (dd, $J = 8.2, 7.0$ Hz, 1H), 7.00 (d, $J = 8.8$ Hz, 4H). ¹³C NMR (75 MHz, Chloroform-*d*) δ 159.4 (C_q), 156.7 (d, $^1J_{\text{C-F}} = 248.4$ Hz, C_q), 130.5 (d, $^4J_{\text{C-F}} = 3.1$ Hz, CH), 129.4 (d, $^4J_{\text{C-F}} = 3.5$ Hz, CH), 128.6 (C_q), 124.4 (d, $^3J_{\text{C-F}} = 4.6$ Hz, CH), 114.0 (CH). ¹⁹F NMR (282 MHz, Chloroform-*d*) δ -123.6 (s, 1F). HRMS-DCI(CH₄) (m/z): found [M+H]⁺ 309.1291, calc'd C₂₀H₁₈FO₂ requires 309.1287.

1-fluoro-2,6-di-(3,5-bis(trifluoromethyl)phenyl)benzene (2.26)

The title compound was obtained following modified general procedure **D** (conc. H₂SO₄ 1 eq. and *t*-BuOH at 95 °C) and purified by silica gel flash column chromatography using an eluent gradient of 100% cyclohexane to 1:1 cyclohexane/EtOAc. Four fractions were collected during cyclohexane elution, two of which contained the desired product along with some undesired impurities. Further purification was achieved *via* reverse phase column chromatography using an eluent gradient of 100% H₂O to 100% MeCN over 1 hour. The desired fractions were concentrated to afford the desired product as an off-

white powder (0.074 g, 56%). ^1H NMR (300 MHz, Chloroform-*d*) δ 8.03 (s, 4H), 7.94 (s, 2H), 7.55 (t, $J = 7.1$ Hz, 2H), 7.43 (dd, $J = 8.5, 6.8$ Hz, 1H). ^{13}C NMR (75 MHz, Chloroform-*d*) δ 156.3 (d, $^1J_{\text{C-F}} = 251.8$ Hz, C_q), 137.3 (C_q), 132.1 (q, $^2J_{\text{C-F}} = 33.5$ Hz, C_q), 131.3 (d, $^2J_{\text{C-F}} = 3.0$ Hz, CH), 129.3 (CH), 127.4 (d, $^2J_{\text{C-F}} = 14.1$ Hz, C_q), 125.4 (d, $^2J_{\text{C-F}} = 4.7$ Hz, CH), 123.2 (q, $^1J_{\text{C-F}} = 272.8$ Hz, C_q), 121.9 (hept, $^3J_{\text{C-F}} = 3.6$ Hz, CH). ^{19}F NMR (282 MHz, Chloroform-*d*) δ -62.88 (s, 12F), -123.11 (s, 1F). HRMS-DCI(CH₄) (m/z): found [M]⁺ 520.0496, calc'd C₂₂H₉F₁₃ requires 520.0497.

3 Organotrifluoroborates as nucleophilic fluorine sources in the fluorination of diaryliodonium salts

In chapter 2, the development of a methodology for a one-pot two-step Balz-Schiemann reaction with organotrifluoroborates was described. Given the interesting reactivity observed, we were motivated to expand the fluorination reaction profile of organotrifluoroborates. Diaryliodonium salts presented the next logical substrate class to investigate as aryl cation equivalents. This chapter will briefly introduce the current literature on fluorinating diaryliodonium salts and our brief investigation of applying organotrifluoroborates towards the fluorination of these systems will be described.

3.1 Introduction

Hypervalent iodine compounds have become reagents of immense utility in organic synthesis. This special class of reagent has been found to be selective, mild and environmentally benign and as such they are considered to be competent alternatives to heavy-metal-based oxidants and organometallic catalysts.¹⁷⁹ Iodine(III) reagents, with two aryl ligands (diaryl- λ^3 -iodanes, more commonly known as diaryliodonium salts), have received considerable attention for the similar characteristics they share with their organometallic analogues. Owing to their favourable properties, these reagents allow efficient metal-free or catalysed transfer of aryl groups to a variety carbon and heteroatom (including nitrogen, chalcogen and halide) nucleophiles (Figure 3.1, a).^{180,181}

3.1.1 Diaryliodonium salt reactivity and selectivity

The reactivity of diaryliodonium salts has been rationalised through an λ^3 -iodane aryl cation equivalent (Figure 3.1, b); other intermediates (radical anions, aryl radicals and arynes) have also been proposed but will not be discussed in this chapter. Nu-I bond formation is the initial step due to the electrophilicity of the iodine atom, with release of the counter-ion. Consequent reductive elimination from this intermediate then generates the product and corresponding Ar-I (Figure 3.1, b). In metal mediated transformations, diaryliodonium salts are considered more reactive forms of aryl iodides which undergo oxidative addition to the metal centre, transferring an aryl moiety and ligand (Figure 3.1, b). The formed organometallic complex can then undergo further transformations with incoming nucleophiles leading to desired products.

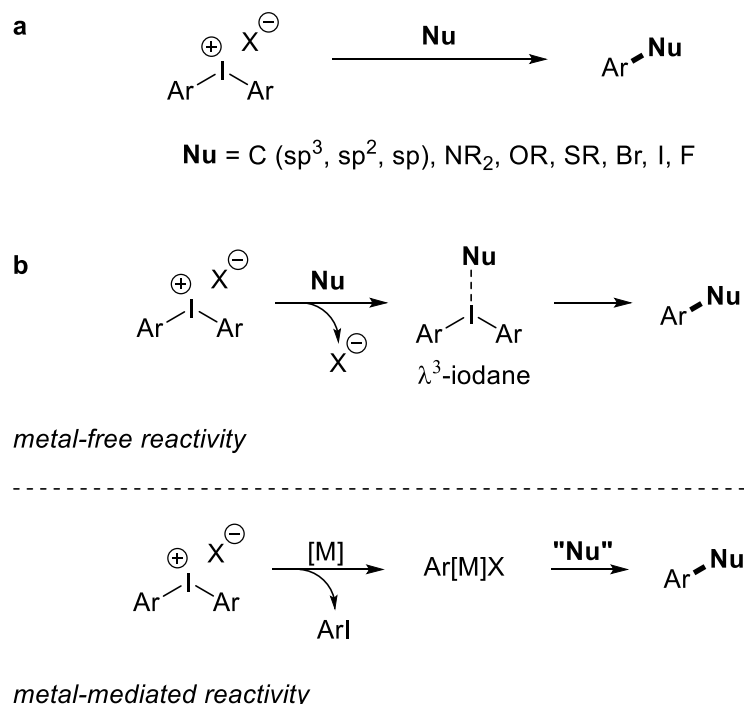


Figure 3.1 a, scope of nucleophiles arylated by diaryliodonium salts. b, intermediates implicated in the metal-free and metal-mediated arylation of nucleophiles with diaryliodonium salts.

For symmetrical diaryliodonium salts (Figure 3.1, a) there are no selectivity issues regarding which aryl fragment is transferred. As a result, symmetrical salts have generally been preferred in the synthesis of simple building blocks. However, with unsymmetrical diaryliodonium salts (Figure 3.2, $R_1 \neq R_2$) issues arise regarding the selectivity of aryl transfer. The geometry of the λ^3 -iodane intermediate is trigonal bipyramidal (T-shaped) and is in a rapidly exchanging equilibrium between two conformers where the aryl groups exchange the axial and equatorial positions, following the Berry mechanism. Arylated products are formed by the reductive elimination of the aryl group *syn* to the nucleophile. The energy barrier between both intermediates is low, and therefore product distribution is under Curtin-Hammett control where steric and electronic effects in the transition state are the dominant factors in the chemoselectivity of aryl group transfer.^{180,182} In the absence of steric factors, the equilibrium and therefore reaction outcome is entirely determined by electronic considerations. In such cases, the preferred intermediate places the most electron-deficient aryl ring in the equatorial position, co-planar with the lone pairs on the iodine atom, allowing the most efficient stabilization of the positive charges on iodine and the aryl ring in the transition state (Figure 3.2, a).¹⁸²⁻¹⁸⁴ When steric strain is present, the “*ortho*” effect along with electronic factors govern product distribution. The presence of steric bulk favours the intermediate where this aryl ring occupies the equatorial position, avoiding repulsive interactions with the lone pairs on iodine (Figure 3.2, b).^{182,183} It is important to note that the “*ortho*” effect is nucleophile dependant where the “*anti-ortho*” effect has been observed for boron and carbon nucleophiles with the least sterically hindered aryl ring functionalized.¹⁸⁰ While potentially problematic, unsymmetrical salts are highly desired in cases where the synthesis of starting aryl

moieties is expensive and laborious as these starting materials present a more atom economical functionalization approach.^{180,181,185} This has spurred the incorporation and development of “dummy ligands” that allow highly selective transfer of the desired aryl ring.

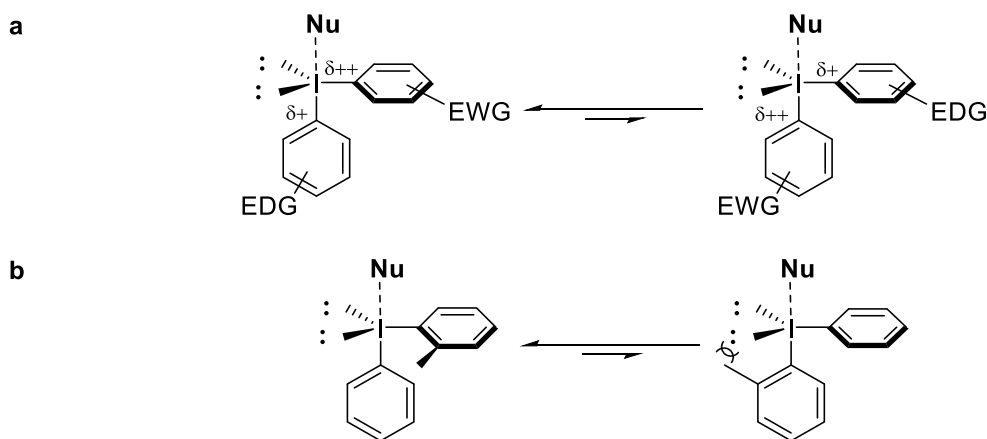
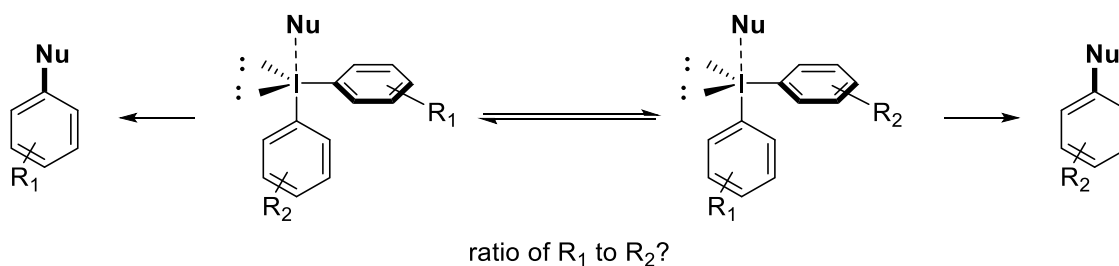


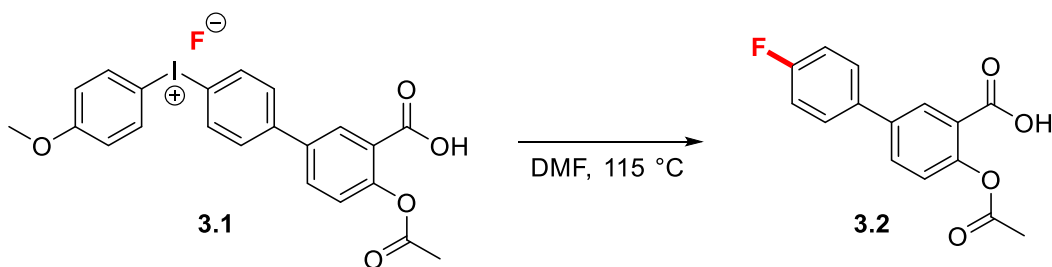
Figure 3.2 λ^3 -iodane equilibrium. **a**, electronic effect on equilibrium. **b**, steric "ortho" effect on equilibrium.

3.1.2 Fluorination of diaryliodonium salts

3.1.2.1 Metal-free fluorination of diaryliodonium salts

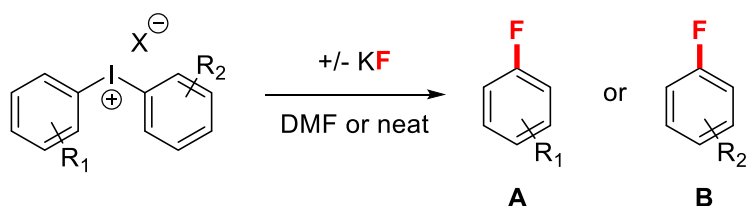
While diaryliodonium salts have been known since 1894 and are well known to react with a variety of nucleophiles, *vide supra*, their application towards the formation of aryl fluorides was first described in 1972. Schoenewaldt *et al.* described the synthesis and decomposition of 4'-(3-carboxy-4-acetoxy)-biphenyl-4-anisoyliodonium fluoride (**3.1**) to

provide *O*-acetyl-5-(4-fluorophenyl)salicylic acid (**3.2**) with no reported yield (Scheme 3.1).¹⁸⁶



Scheme 3.1 Fluorination of diaryliodonium salt **3.1**.

While this transformation was anecdotally reported, interest in the potential of this methodology increased, and, a decade later Van der Puy described the first systematic study of the conversion of diaryliodonium salts into aryl fluorides (Table 3.1).¹⁸⁷ The decomposition of these salts in solution provided the corresponding aryl fluoride in moderate yields (Table **3.1**, entries 1-4). For unsymmetrical salts complete selectivity was observed following the selectivity rules discussed above (Table **3.1**, entries 2 and 3). The presence of a nucleophilic anion, chlorine, competes with fluorine resulting in lower yields of the fluorinated product; instead chlorobenzene was the major product (65%) (Table **3.1**, entry 4). Aryl fluoride yields were improved by conducting the reaction in the melt (Table **3.1**, entries 5-10) and could be further increased in the presence of excess KF (Table **3.1**, entry 7). Furthermore, reactions conducted in the absence of solvent also avoided the formation of the reduced arene.

Table 3.1 Fluorination of diaryliodonium salts in solution and in the melt

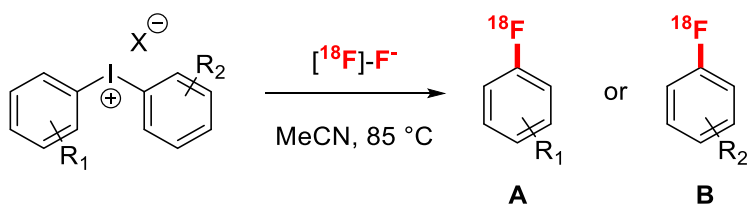
Entry	R ₁	R ₂	X	Product distribution (%) [*]	
				A	B
1 ^{a,b}	H	H	BF ₄		54
2 ^{a,b}	<i>p</i> -methoxy	H	CF ₃ COO	-	46
3 ^{a,b}	<i>p</i> -methoxy	H	<i>p</i> -toluenesulphonate	-	61
4 ^{a,b}	H	H	Cl		11
5 ^c	H	H	BF ₄		67
6 ^c	<i>m</i> -nitro	<i>m</i> -nitro	BF ₄		41
7 ^d	H	H	BF ₄		85
8 ^d	<i>m</i> -nitro	<i>m</i> -nitro	BF ₄		38
9 ^d	<i>p</i> -methoxy	<i>p</i> -methoxy	BF ₄		44
10 ^d	<i>p</i> -chloro	<i>p</i> -chloro	BF ₄		39

^a reaction in DMF (115-150 °C) with KF (2 eq.). ^b reduced product (benzene) observed (2-9%). ^c neat (211-233 °C) no KF. ^d neat (160-235 °C) with KF (3.5 eq.). * yields for symmetrical diaryliodonium salts are in the centre column.

Soon after, Grushin *et al.* described the near quantitative fluorination (96% yield) of diphenyliodonium tetrafluoroborate with KF and catalytic amounts of 18-crown-6 under mild conditions.¹⁸⁸ A decade later, Pike and Aigbirhio pioneered the application of this methodology towards the production of [¹⁸F]-fluoroarenes using both [¹⁸F]-KF/K₂₂₂ and [¹⁸F]-CsF.^{189,190} Moderate to good radiochemical yields (RCY) were obtained under mild reaction conditions (Table 3.2). For unsymmetrical salts, complete selectivity and high

yields of [^{18}F]-fluoroarenes were observed when electron-rich and sterically bulky aryl substituents were used (Table 3.2, entries 2, 3 and 5). Selectivity decreased when steric bulk was present on both aryl substituents and when the electronic character of both aryl rings was similar (Table 3.2, entries 6 and 4, respectively).

Table 3.2 Radiofluorination of diaryliodonium salts

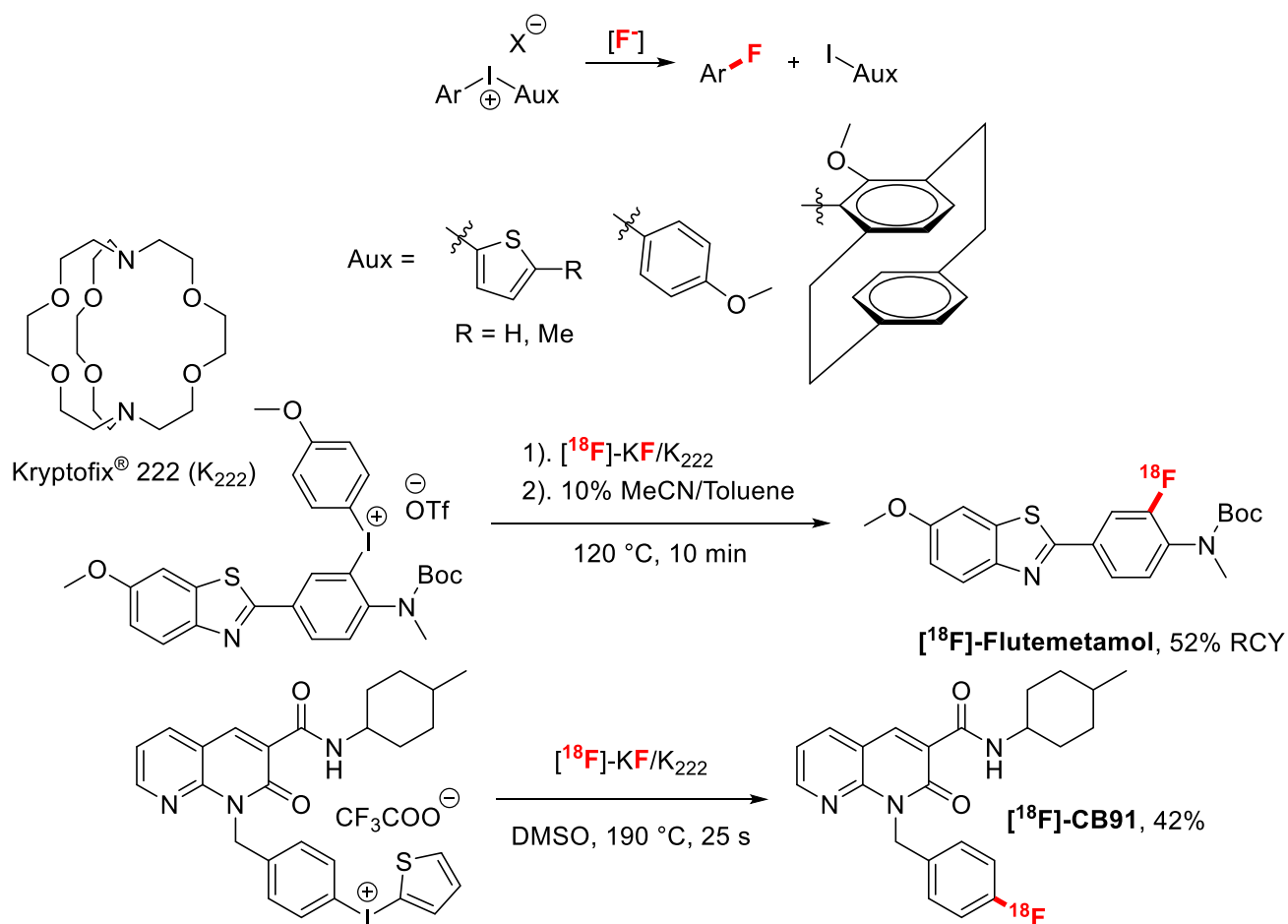


Entry	R ₁	R ₂	X	Product distribution/RCY (%) [*]	
				A	B
1 ^a	H	H	CF ₃ SO ₃	80	
2 ^a	4-OMe	H	CF ₃ SO ₃	-	96
3 ^a	2,4,6-(CH ₃) ₃	H	CF ₃ SO ₃	96	-
4 ^a	4-Br	H	CF ₃ SO ₃	66.5	28.5
5 ^a	4-OMe	H	Br	-	88
6 ^b	2,4,6-(CH ₃) ₃	2-CH ₃	CF ₃ SO ₃	52	13

^a [^{18}F]-KF/K₂₂₂. ^b [^{18}F]-CsF. * yields for symmetrical diaryliodonium salts are in the centre column.

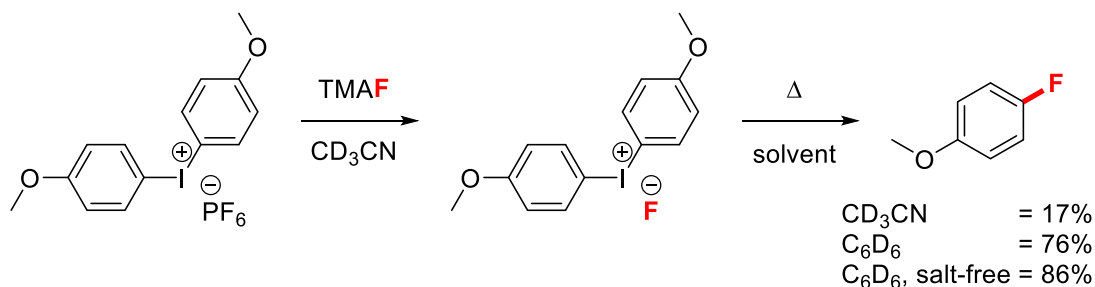
Given the potential applications in the production of [^{18}F]-radiotracers, research efforts have largely focused on the development of reaction conditions within the context of radiofluorination. Significant advances have been made in identifying and applying “dummy” ligands, or auxiliaries, allowing for increased chemoselectivity in the radiofluorination of unsymmetrical diaryliodonium salts (Figure 3.3). Electron-rich, 2-

thienyl and *p*-methoxyphenyl ligands proved to be efficient auxiliaries allowing the highly selective formation of [^{18}F]-fluoroarenes.^{191,192} DiMagno *et al.* developed a cyclophane auxiliary that allows the selective fluorination of highly electron rich aromatic rings through a combination of steric and electronic effects.¹⁹³ The cyclophane auxiliary allows the formation of 4-fluoroanisole in unprecedentedly high yields (81% yield), whereas only low yields could be obtained from the decomposition of the symmetrical diaryliodonium salt. These auxiliaries have been used in the production of clinically relevant PET tracers, specifically [^{18}F]-Flutemetamol and [^{18}F]-CB91 used in the diagnosis of Alzheimer's disease and imaging CB2 cannabinoid receptors, ® respectively (Scheme 3.2).^{194,195}



Scheme 3.2 Auxiliaries used for the selective fluorination of unsymmetrical diaryliodonium salts.

DiMagno *et al.* also showed that reaction efficiencies could be greatly improved through careful consideration of reaction solvent and the removal of salts prior to the thermal decomposition of (un)symmetrical diaryliodonium fluorides (Scheme 3.3).¹⁹⁶ They found that non-polar solvents (benzene and toluene) allowed for more efficient transformations due to the suppression of ligand exchange on the iodonium centre.¹⁹⁷ Additionally, the removal of spectator ions improved reaction yields by again suppressing ligand exchange processes and the dissociation of fluoride from the iodonium centre.

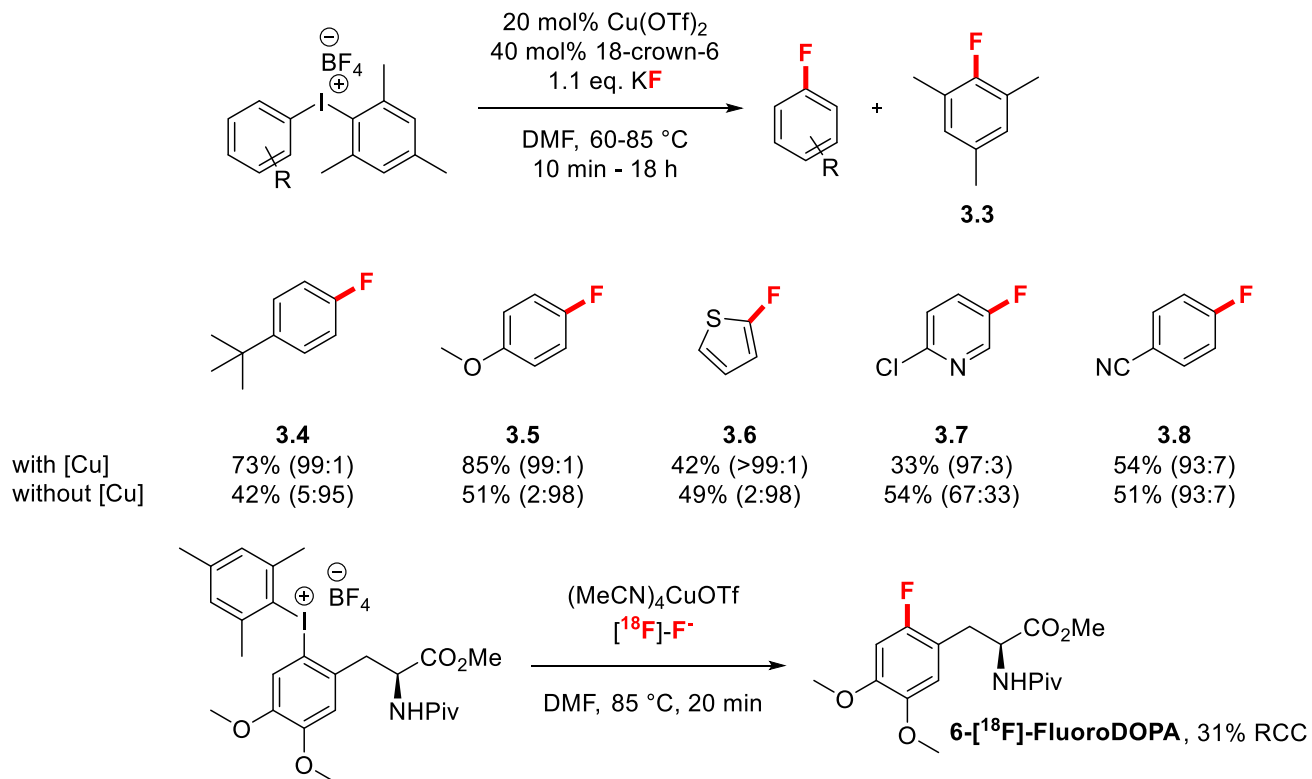


Scheme 3.3 Effect of solvent and salt removal on diaryliodonium fluorination.

Recent efforts have investigated the expansion of this methodology towards solid supported diaryliodonium salts for radiofluorination.^{198,199} Wirth *et al.* describe the synthesis of a series of unsymmetrical diaryliodonium salts supported on aminomethyl- and tris(aminoethyl)-functionalised resins. While the synthesis of the supported salts was successful, subsequent (radio)fluorination studies showed low transformation efficiencies where 4-(benzyloxy)fluorobenzene could only be obtained in 22% yield, and a maximum 3% radiochemical conversion (RCC) for [¹⁸F]-fluorobenzene.

3.1.2.2 Metal-mediated fluorination of diaryliodonium salts

Thus far reactions discussed have been metal-free, which underscores the ongoing interest in metal-free reactions in the literature regarding the fluorination of diaryliodonium salts. By contrast, it was only recently that Sanford *et al.* reported the Cu-catalysed fluorination of unsymmetrical diaryliodonium salts with KF (Scheme 3.4).¹¹⁷ This methodology takes advantage of the well documented rapid and sterically controlled oxidative addition of diaryliodonium salts to Cu^I, the less sterically hindered aryl group is transferred to the Cu^I centre. The Cu-based methodology allows a significant increase in reaction yields and selectivity for electron-rich aryl rings (Scheme 3.4, products 3.4, 3.5, 3.6 and 3.7); preferential oxidative addition onto Cu^I allows the reversal of the dominating “*ortho*” effect in the absence of Cu^I. The effect of Cu^I on selectivity and yield is negligible in the fluorination of electron-poor aromatic rings (Scheme 3.4, product 3.8) as the selectivity is determined electronically; the most electron-deficient aryl ring is typically fluorinated (Figure 3.2, a). Sanford *et al.* were able to successfully transfer this methodology towards radiofluorination, exemplified by the synthesis of protected 6-[¹⁸F]-fluorodopamine in 31% RCC (Scheme 3.4).²⁰⁰ The group recently showed that this could be further extended towards the one-pot Cu-mediated C-H [¹⁸F]-fluorination of electron-rich (hetero)aromatic systems, through the *in situ* formation of the diaryliodonium salt.²⁰¹

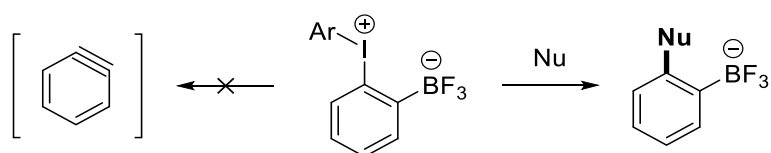


Scheme 3.4 Cu-catalysed fluorination of diaryliodonium salts. Values in brackets are the ratio of fluorinated product to **3.3**.

3.1.3 Organotrifluoroborates as an alternate source of fluorine

Unlike the Balz-Schiemann reaction, for which multiple sources of fluorine have been investigated (see Chapter 2, section 2.1.1.5), the fluorination of diaryliodonium salts has been limited to the use of alkali metal fluorides (KF and CsF), TMAF and BF₄⁻ as the source of F⁻. The interesting results we observed with organotrifluoroborates in the Balz-Schiemann reaction prompted us to ask whether these advantages could be extended towards diaryliodonium salts which, like aryl diazonium cations, are known aryl cation equivalents. Organotrifluoroborates and diaryliodonium salts have been used in concert for palladium-catalysed C-C bond formation.^{202,203} More recently, iodonium trifluoroborate

zwitterions have been synthesized and characterised, these interesting substrates have been applied as bifunctional arene reagents (Scheme 3.5).²⁰⁴ The authors report that these systems are not benzyne precursors, and no fluorinated by-products have been observed.



Scheme 3.5 Iodonium trifluoroborate zwitterion bifunctional reagents.

To the best of our knowledge the use of organotrifluoroborates for the fluorination of diaryliodonium salts is unprecedented. In addition to the facile modulation of solubility and reactivity of organotrifluoroborates (see Chapter 2, section 2.1.1.6), their use as an organic counter-ion to diaryliodonium salts is attractive. Diaryliodonium salt dissociation in solution is usually favoured (for all anions except BF_4^-), as this facilitates anion exchange between the counter-ion and incoming F^- .¹⁹¹ It would therefore be of interest to investigate the effect of an organotrifluoroborate counter-ion, that acts as a F^- source, on the fluorination of diaryliodonium salts.

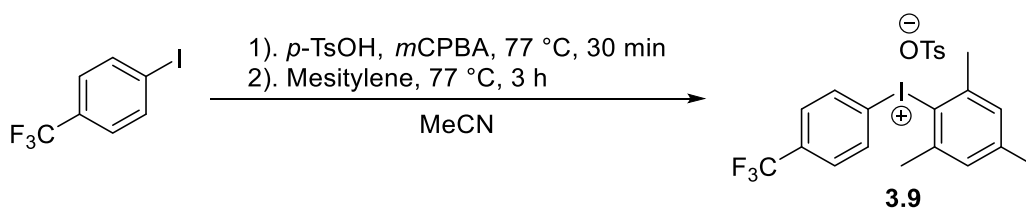
3.2 Results and Discussion

3.2.1 Synthesis of Unsymmetrical Diaryliodonium Phenyltrifluoroborates

We decided to begin the investigation with the synthesis of a series of unsymmetrical diaryliodonium salts to study the influence of the organotrifluoroborate anion on the selectivity of the reaction. With the increasing interest and application of unsymmetrical diaryliodonium salts in organic synthesis, many one-pot synthetic methodologies, largely

driven by Olofsson *et al.*, have been developed.^{205–208} These methods are attractive as they reduce reaction time and can increase the substrate scope especially when certain intermediates are not stable to isolation.¹⁸¹ The one-pot syntheses involve the *in situ* oxidation (usually with *m*CPBA) of an aryl iodide to an iodine(III) intermediate which can then undergo ligand exchange with the second aryl fragment to form the desired unsymmetrical salt.

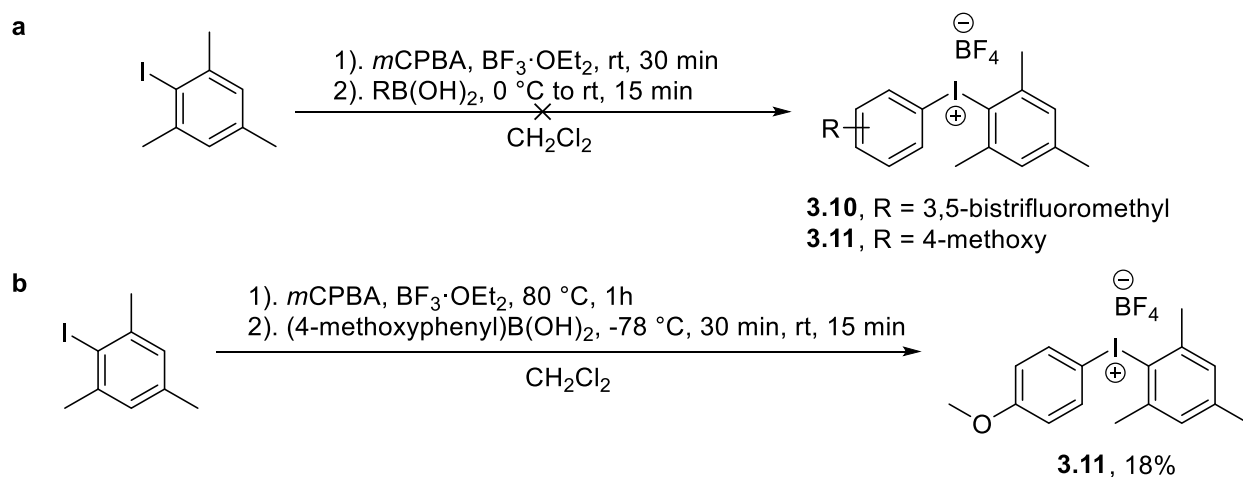
My first attempt involved exploiting a method developed by Stuart *et al.*, where 4-trifluoromethyliodobenzene is oxidized by *m*CPBA using *p*-TsOH as the activator in MeCN, ligand exchange with mesitylene is induced by its addition to the reaction mixture.²⁰⁷ Unfortunately in our hands, after reaction work-up, ¹H NMR spectroscopy showed that the intended product was formed (Scheme 3.6, product 3.9), but in poor yield and as an inseparable mixture with numerous impurities.



Scheme 3.6 Stuart *et al.* one-pot diaryliodonium salt synthesis conditions.

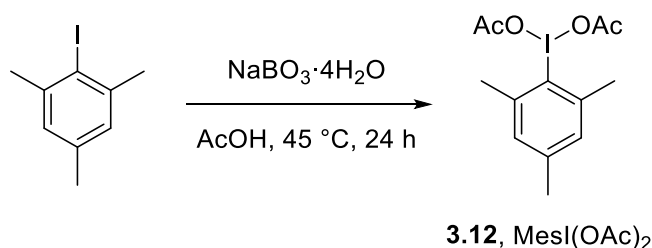
Prior to changing the synthetic method, we thought that the choice of counter-ion would be important in the anion exchange step following the synthesis of the diaryliodonium salt. Deciding that BF_4^- would be a suitable counter-ion for the subsequent exchange, due to its facile exchange with various anions, we tested a method described by Olofsson *et al.* This method still uses *m*CPBA as the oxidant, but it is activated by $\text{BF}_3 \cdot \text{OEt}_2$ as a Lewis

acid, ligand exchange is then promoted by the addition of the desired boronic acid into the reaction mixture (Scheme 3.7, a).²⁰⁵ Unfortunately, these conditions as described, did not work in our hands; after reaction work-up, several unidentifiable products were observed by TLC and NMR spectroscopy. However, by applying harsher conditions using an electron-rich arylboronic acid the desired salt **3.11** could be isolated pure but in poor yield (Scheme 3.7, b).



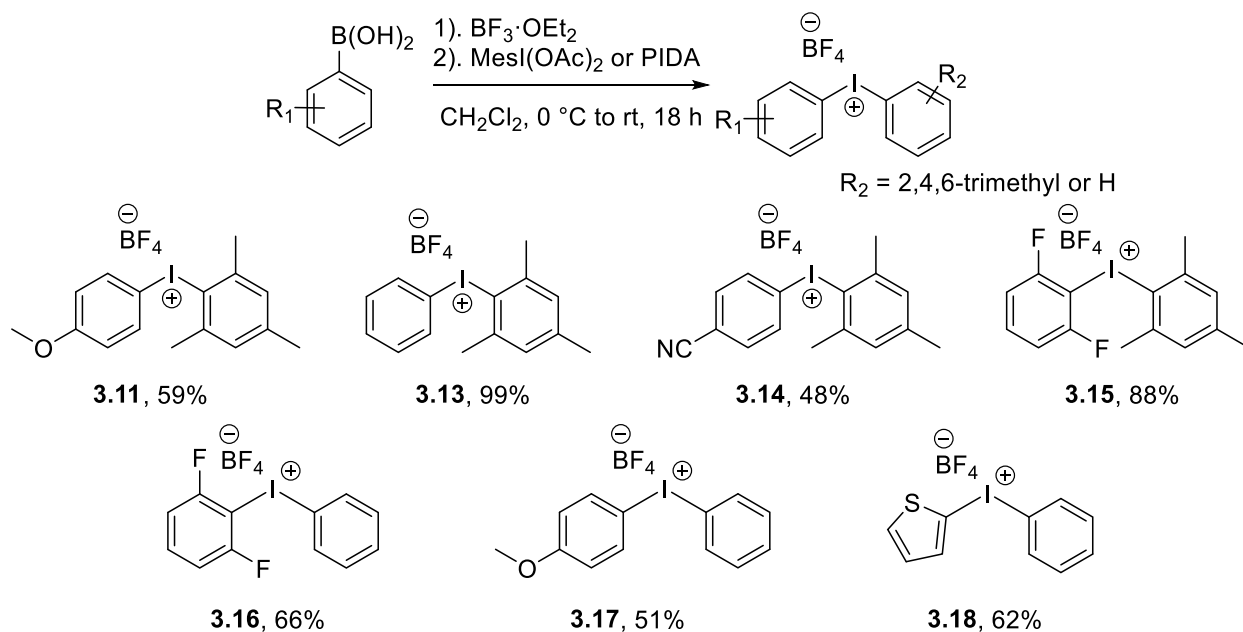
Scheme 3.7 Olofsson *et al.* one-pot diaryliodonium salt synthesis conditions. Isolated yields.

We attributed poor yields to the inefficient initial oxidation of iodomesitylene to iodomesitylene diacetate (**3.12**), the latter was therefore synthesized by oxidation of the former with sodium perborate in AcOH (Scheme 3.8).



Scheme 3.8 Synthesis of iodomesitylene diacetate.

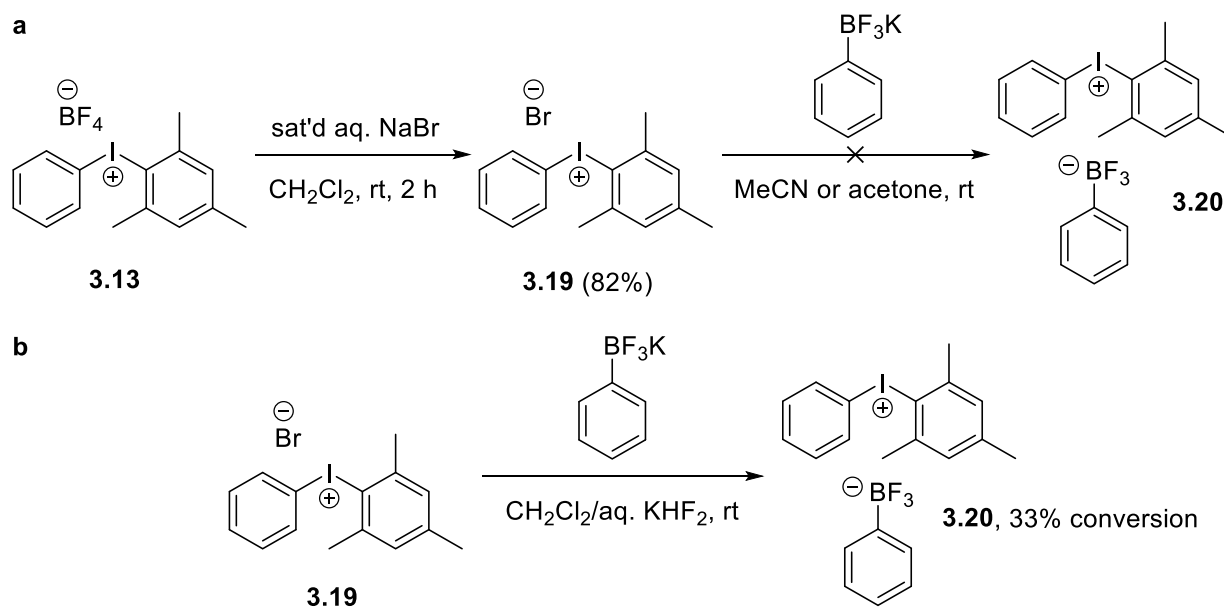
We applied **3.12** directly, bypassing *in situ* oxidation, with $\text{BF}_3 \cdot \text{OEt}_2$ in CH_2Cl_2 at 0°C for 10 min, after which the arylboronic acid was added (Scheme **3.9**). Gratifyingly, this modified protocol allowed the synthesis, in moderate to excellent yields, of a series of aryl(mesityl)iodonium tetrafluoroborate salts (Scheme **3.9**, products **3.11**, **3.13**, **3.14** and **3.15**). We could also synthesize a series of aryl(phenyl)iodonium salts by substituting $\text{MesI}(\text{OAc})_2$ for phenyliodine(III) diacetate (PIDA) (Scheme **3.9**, products **3.16**, **3.17** and **3.18**).



Scheme 3.9 Scope of unsymmetrical diaryliodonium tetrafluoroborate salts synthesized. Isolated yields.

With the tetrafluoroborate salts in hand, we focused our attention on developing efficient anion exchange conditions for the introduction of the organotrifluoroborate component. We argued that if we could initially displace BF_4^- with Br^- , anion exchange with potassium phenyltrifluoroborate (KPhBF_3) could be driven by KBr precipitation. Therefore, the bromide salt was synthesized by stirring a biphasic mixture of **3.13** in CH_2Cl_2 and a saturated aqueous NaBr solution, after simple extraction and Et_2O precipitation **3.19** was

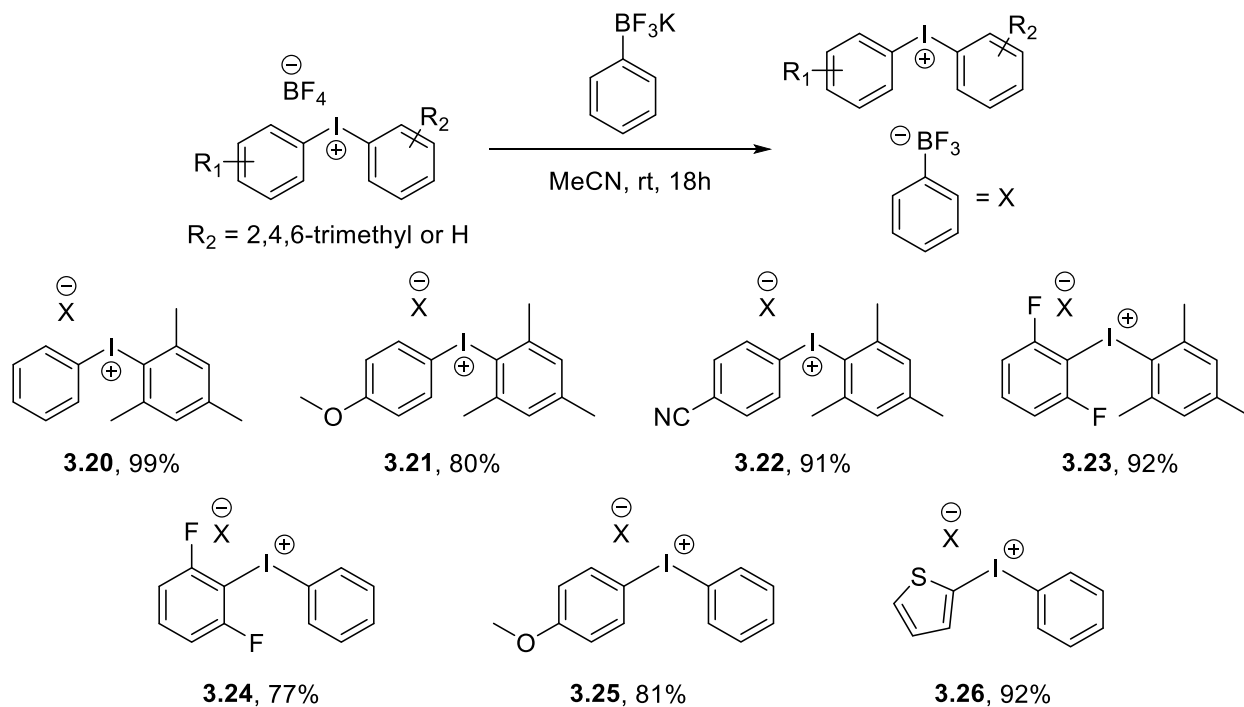
afforded in good yield and purity (Scheme 3.10, a). We then tested anion exchange in acetone and MeCN however, poor solubility of **3.19** in both solvents resulted in poor exchange after reaction work-up, as evidenced by ^1H , ^{19}F and ^{11}B NMR spectroscopy. The use of a biphasic mixture (CH_2Cl_2 /saturated aqueous KHF_2) incorporating the diaryliodonium salt and KPhBF_3 was attempted. This biphasic system did result in improved yields; however, the residue recovered after reaction work-up was an inseparable 2:1 mixture of **3.19** and **3.20** (Scheme 3.10, b).



Scheme 3.10 Attempts at anion exchange (isolated yields in parentheses). **a**, anion exchange in acetone or MeCN. **b**, anion exchange in biphasic CH_2Cl_2 /saturated aqueous KHF_2 .

Having encountered difficulties with bromide salt **3.19** we thought that perhaps we could take advantage of the increased solubility of the original tetrafluoroborate salt **3.13** and attempt anion exchange directly with KPhBF_3 . Gratifyingly, we found that both **3.13** and KPhBF_3 were soluble in MeCN. Work-up of the reaction mixture following overnight reaction, revealed that quantitative anion exchange had occurred, as evidenced by ^1H , ^{19}F and ^{11}B NMR spectroscopy; **3.20** was obtained in quantitative yield. These conditions

could be applied to all other tetrafluoroborate salts to provide the series of unsymmetrical diaryliodonium phenyltrifluoroborates, in good to excellent yields, in Scheme 3.11.



Scheme 3.11 Scope of unsymmetrical diaryliodonium phenyltrifluoroborates synthesized. Isolated yields.

Single crystals, suitable for X-ray analysis, of **3.20** were obtained to determine and compare its structure with those of similar diaryliodonium tetrafluoroborate or fluoride salts (Figure 3.3). Carbon-iodine bond lengths for **3.20** and **3.28** are almost identical, ranging from 2.114 – 2.122 Å; **3.27** displays the shortest C-I bond lengths (2.018 – 2.047 Å). As expected, **3.28** displays the shortest F-I distance, 2.544 Å, suggesting the existence of a F-I bond. However, **3.20** and **3.27** display significantly longer F-I distances 2.8560 and 2.9470 Å, respectively, as would be expected for counter-ions.

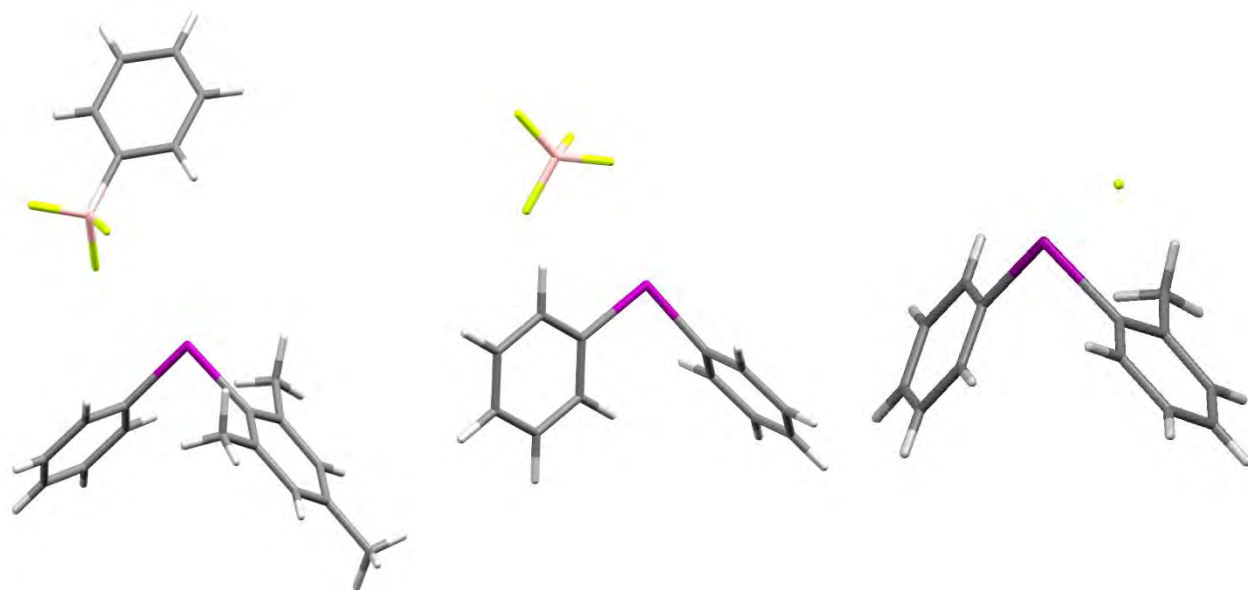


Figure 3.3 X-ray crystal structures of **3.20**, diphenyliodonium tetrafluoroborate (**3.27**),²⁰⁹ (2-methylphenyl)(phenyl)iodonium fluoride (**3.28**).²⁰⁹ Solvent molecules omitted for clarity. Hydrogen in white, carbon in grey, iodine in purple, boron in pink, fluorine in green/yellow.

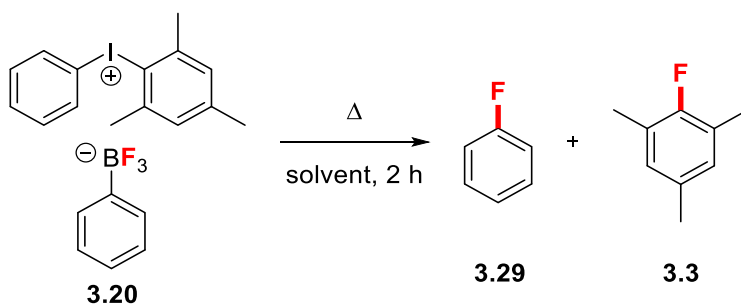
3.2.2 Fluorination studies of unsymmetrical diaryliodonium phenyltrifluoroborates

3.2.2.1 Solvent optimisation

we began the investigation by studying the decomposition of **3.20** in various solvents at different temperatures to determine if any fluorinated products could be detected (Table **3.3**). Based on selectivity rules (see section **3.1.1**) we expected the major product to be 2-fluoro-1,3,5-trimethylbenzene (**3.3**) due to electronic and steric effects, as the mesityl group is considered electron-rich and contains an *ortho* substituent. Generally, low boiling solvents resulted in no conversion of **3.20** (Table **3.3**, entries 1, 2 and 4); however, trace yields of **3.3** were observed in CDCl₃ and THF (Table **3.3**, entries 3 and 5). Otherwise, unreacted and/or deborylation of **3.20** was observed by ¹⁹F NMR spectroscopy. Higher

boiling solvents such as C₆D₆, CD₃CN and DMF which have been extensively used in the decomposition of diaryliodonium fluorides and tetrafluoroborates,^{187,210} did not result in any fluorinated products (Table 3.3, entries 7, 9 and 15, respectively). Yields could be increased by employing high boiling non-polar solvents such as toluene, xylenes and 1,2-dichlorobenzene which provided **3.3** in 22% yield (Table 3.3, entries 16-18). The use of non-polar, high boiling, solvents is consistent with previous reports of improved yields.^{187,196} Radical scavengers, such as TEMPO, have successfully been used in increasing the reproducibility and yields of diaryliodonium salt fluorinations by suppressing the propagation of *in situ* generated aryl radicals through the homolytic cleavage of the aryl-I bond.²¹¹ However, under our reaction conditions, the addition of 0.2 or 1.0 equivalents of TEMPO had no effect on reaction efficiencies (Table 3.3, entries 19 and 20, respectively).

Table 3.3 Solvent optimisation for the decomposition of **3.20**



Entry	Solvent	Temperature (°C)	Product distribution (%) ^a	
			3.29	3.3
1 ^b	Et ₂ O	80	-	-
2 ^b	CD ₂ Cl ₂	80	-	-
3 ^b	CDCl ₃	80	-	trace
4 ^b	Acetone- <i>d</i> ⁶	80	-	-
5 ^{b,c}	THF- <i>d</i> ⁸	80	-	trace

6 ^b	MTBE	80	-	-
7 ^b	C ₆ D ₆	100	-	-
8 ^b	Cyclohexane	100	-	trace
9 ^b	CD ₃ CN	100	-	-
10 ^b	<i>t</i> -BuOH	100	-	trace
11 ^b	1,2-dichloroethane	100	-	-
12 ^c	1,2-dimethoxyethane	100	-	-
13 ^{b,c}	1,4-dioxane	140	-	trace
14 ^c	DMSO- <i>d</i> ⁶	140	-	-
15 ^{b,c}	DMF- <i>d</i> ⁷	140	-	-
16 ^b	Toluene	140	-	8
17 ^{b,c}	Xylenes	140	trace	8
18 ^{b,c}	1,2-dichlorobenzene	140	trace	22
19 ^{c,d}	1,2-dichlorobenzene	140	-	15
20 ^{c,e}	1,2-dichlorobenzene	140	-	21

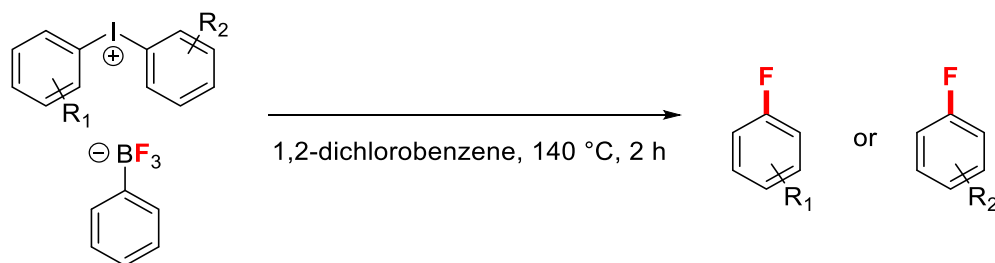
Reaction conditions: **3.20** (0.05 mmol), solvent (1.0 mL) in pressure vial with Teflon lined cap, heated at indicated temperature for 2 h. ^a Yields determined by ¹⁹F NMR spectroscopy using 2,2,2-trifluoroethanol as an internal standard. ^b unreacted **3.20** observed by ¹⁹F NMR. ^c deborylation observed by ¹⁹F NMR spectroscopy. ^d 0.2 eq. TEMPO added to reaction mixture. ^e 1.0 eq. TEMPO added to reaction mixture.

3.2.2.2 Reaction scope and selectivity

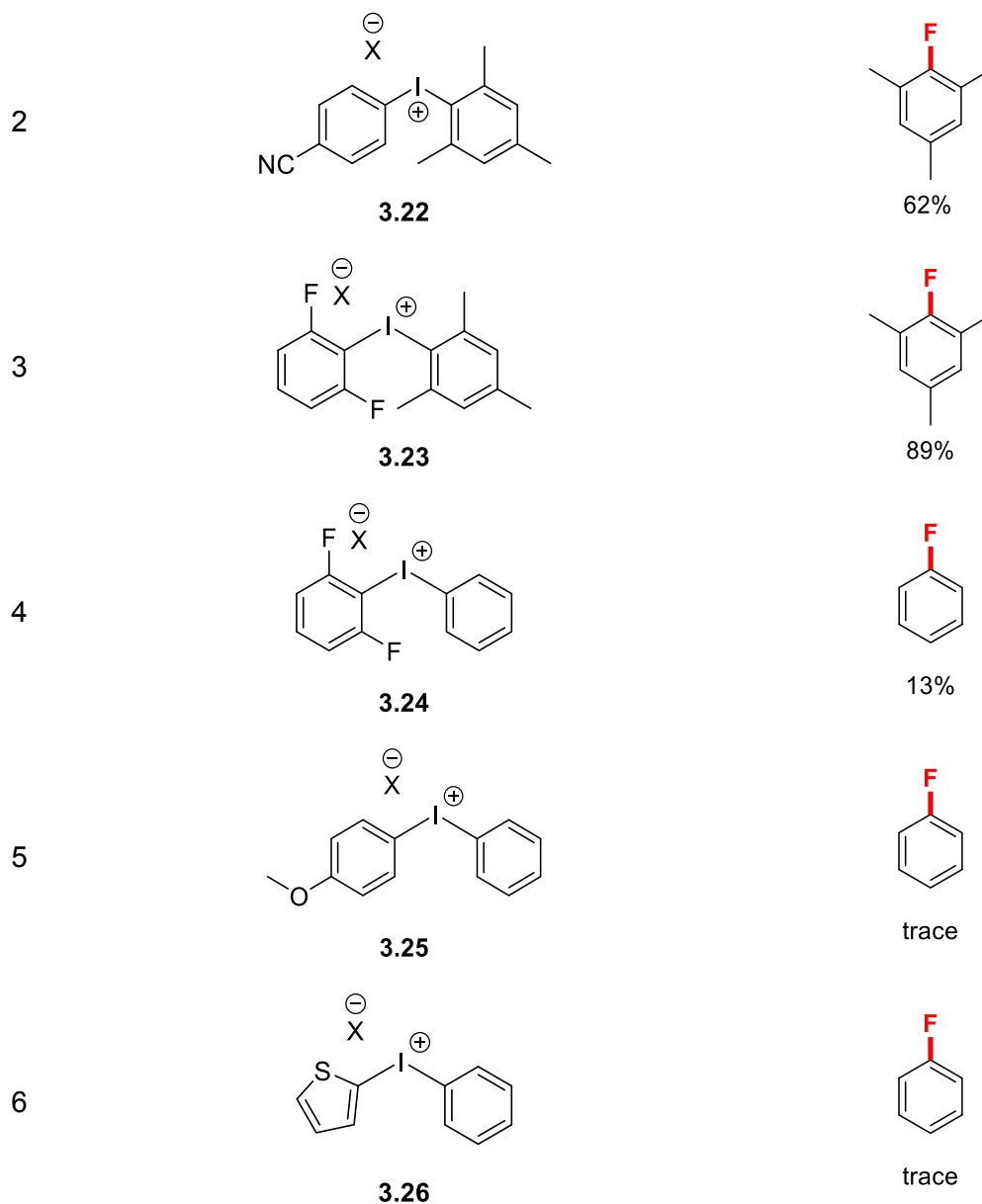
Having determined 1,2-dichlorobenzene as the optimal solvent we investigated the decomposition of salts **3.21-3.26** under reaction conditions (Table **3.4**). Decomposition of **3.21** selectively provided **3.3** in 16% yield (Table **3.4**, entry 1), no trace of 4-fluoroanisole (**3.5**) was detected, which was predicted to form to a certain extent given that both aryl rings are electron-rich. Salt **3.22** decomposed selectively to furnish **3.3** as the sole product in good yield (62%) (Table **3.4**, entry 2), this is surprising as the expected product should

be 4-fluorobenzonitrile (**3.8**) as it is the most electron-deficient and should therefore be preferentially fluorinated. Similarly, **3.23** provided **3.3** as the only product in excellent yields (89%) despite 1,2,3-trifluorobenzene being the expected product based on electronic and “*ortho*” effects (Table **3.4**, entry 3). More surprisingly, **3.24** which was expected to selectively decompose to 1,2,3-trifluorobenzene provided fluorobenzene as the sole product in 13% yield (Table **3.4**, entry 4). The decomposition of **3.25** and **3.26** delivered only trace (<2%) amounts of the expected product fluorobenzene; no traces 4-fluoroanisole or 2-fluorothiophene were detected (Table **3.4**, entries 5 and 6, respectively). Considering the decomposition of salts **3.20-3.23**, one appreciates an emergent trend of increasing yields of 2-fluoro-1,3,5-trimethylbenzene. The increase in yields is correlated with increasing electron-deficiency of the second aryl fragment in the order 4-OMe < H < 4-CN < 2,6-di-F.

Table 3.4 Product distribution from the decomposition of salts **3.21-3.26**



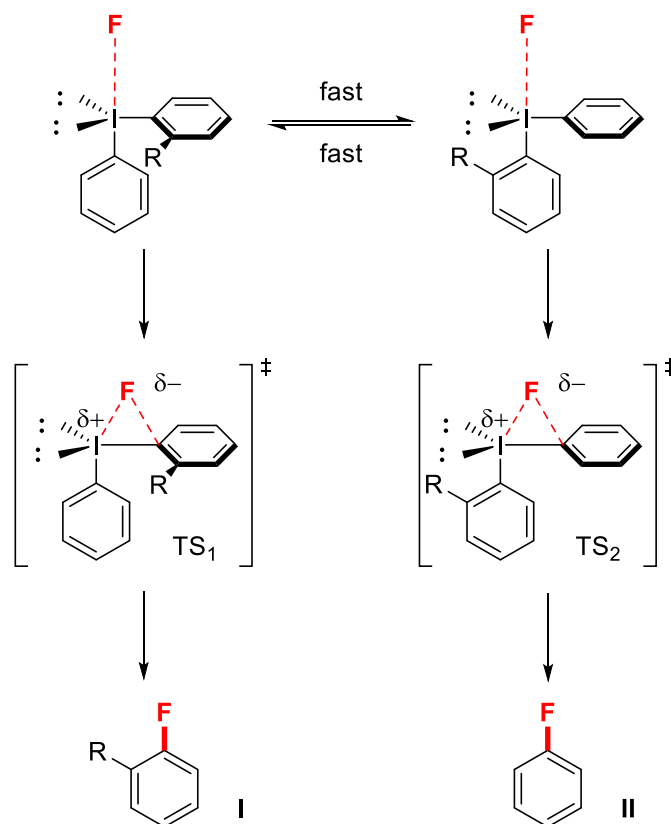
Entry	Precursor	Product distribution ^a
1	<p style="text-align: center;">3.21</p>	<p style="text-align: center;">16%</p>



Reaction conditions: precursor (0.05 mmol), 1,2-dichlorobenzene (1.0 mL) in pressure vial with Teflon lined cap, heated at 140 °C for 2 h, X = phenyltrifluoroborate.^a Yields determined by ¹⁹F NMR spectroscopy using 2,4-dinitrofluorobenzene as an internal standard.

3.2.2.3 Mechanism

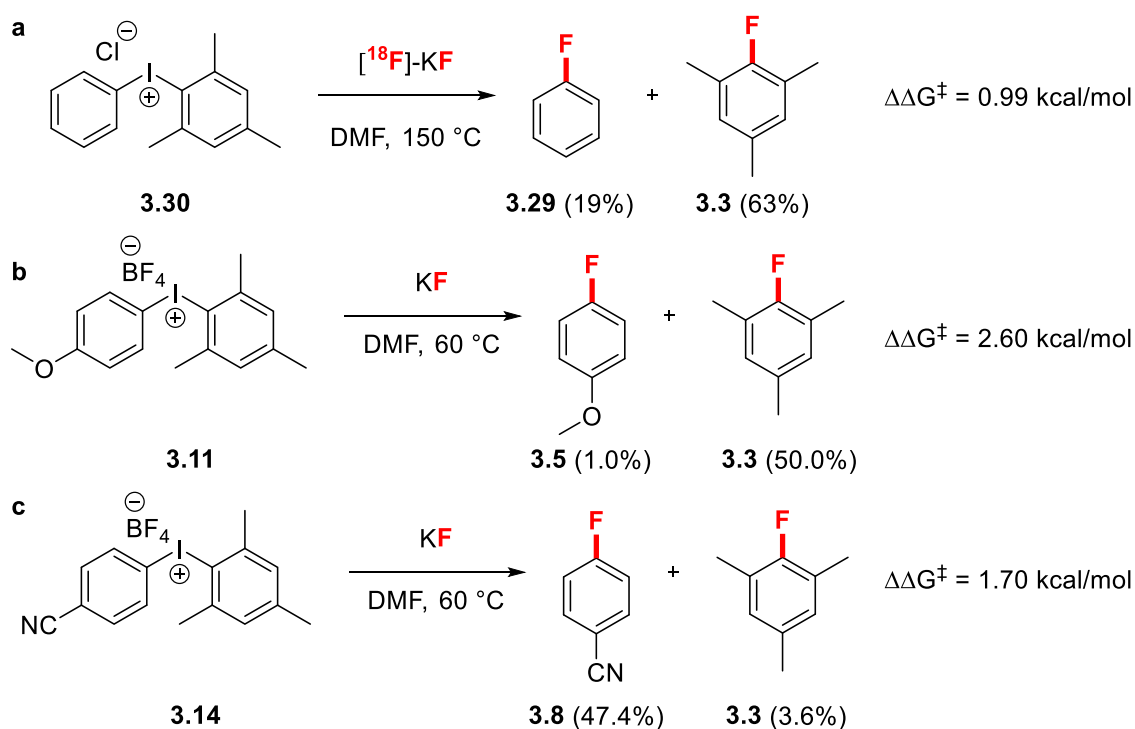
The reactivity and selectivity observed in the decomposition of diaryliodonium salts **3.20**-**3.26** seem to implicate a different mechanism than the one proposed in the decomposition of diaryliodonium fluorides (Scheme **3.12**).^{182,212}



Scheme 3.12 Accepted mechanism for the fluorination of unsymmetrical diaryliodonium salts.

As previously mentioned (see section 3.1.1, Figure 3.2), diaryliodonium salts are rapidly exchanging between two conformations in solution, where the ligands are interchanging between axial and equatorial positions relative to the lone pairs on I and F. F⁻ can attack either of the equally populated conformers to produce either TS₁ or TS₂. The fluorination of either transition state leads to the formation of a single fluorinated product (Scheme 3.12, I or II). The fluorination process has been suggested to be under Curtin-Hammett control and therefore the ratio of products observed is solely dependent on the difference in the free energies of TS₁ and TS₂ ($\Delta G_{\text{TS}_2} - \Delta G_{\text{TS}_1} = \Delta\Delta G^\ddagger$). For example, Pike *et al.* showed that radiofluorination of (2,4,6-trimethylphenyl)(phenyl)iodonium chloride (**3.30**)

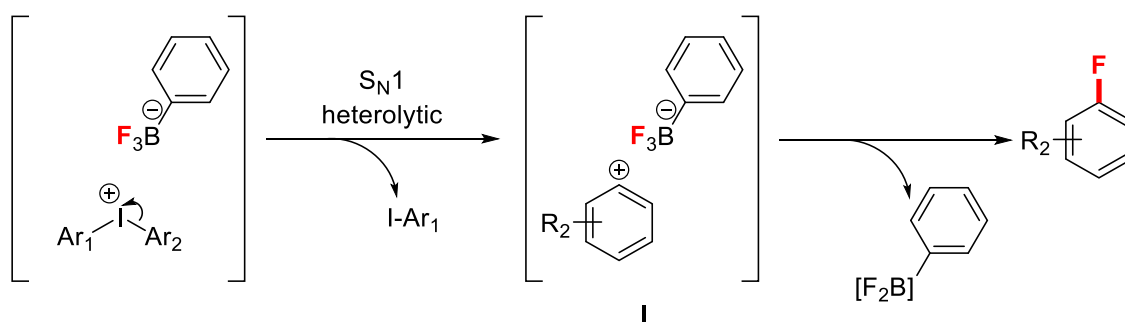
provided both **3.29** and **3.3** in 19 and 63% yield, respectively (Scheme **3.13**, **a**); this product distribution corresponded to a calculated $\Delta\Delta G^\ddagger$ of 0.99 kcal/mol (using $(I/II) = e^{-\frac{(\Delta G_{Ts1} - \Delta G_{Ts2})}{RT}}$).²¹² $\Delta\Delta G^\ddagger$ values could also be calculated given the product distributions reported for the fluorination of diaryliodonium tetrafluoroborates with KF by Sanford *et al.* (Scheme **3.13**, **b** and **c**).¹¹⁷ As predicted, larger values of $\Delta\Delta G^\ddagger$ correspond to more selective reactions.



Scheme 3.13 Product distribution and selectivity from the (radio)fluorination of **a**: **3.30**, **b**: **3.11** and **c**: **3.14**.

However, the results in Scheme **3.13** contradict, for the most part, experimental observations. The decomposition of **3.20** was completely selective (Table **3.3**, entry 13), as opposed to the fluorination of **3.30**. Similarly, **3.22** was fluorinated in the complete opposite selectivity to that observed for **3.14**. These findings, combined with the selectivity observed for the decomposition of **3.23** and **3.24**, suggest that product distributions are

not under Curtin-Hammett but simply kinetic control. If these salts all reacted according to the same mechanism, similar product distributions would be expected, as the transition states would be identical despite the source of F^- ($PhBF_3K$ vs. KF); phenyltrifluoroborates cannot be transferring F^- to either of the rapidly exchanging conformers to form TS_1 or TS_2 . We therefore propose the following mechanism, thermolysis of the diaryliodonium salt results in the heterolytic cleavage of the $I-Ar_1$ bond, forming an iodoarene and aryl cation. Fluorination of the aryl cation then occurs within the tight ion pair **I** with fluorine transfer directly from phenyltrifluoroborate (Scheme 3.14). This may account for the trend of increasing yields with more electron-deficient aryl ligands; $I-Ar_1$ becomes an increasingly activated leaving group leading to more efficient fluorination.

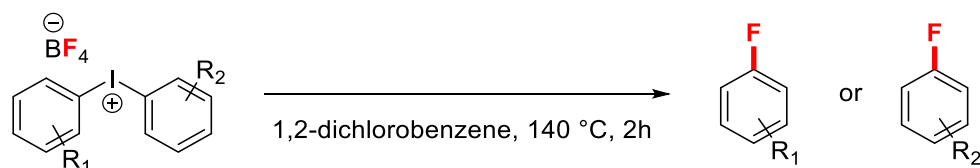


Scheme 3.14 Proposed mechanism for the fluorination of diaryliodonium salts with phenyltrifluoroborates.

This mechanism would also be consistent with the results observed for the decomposition of unsymmetrical diaryliodonium tetrafluoroborates **3.14** and **3.15** which displayed identical selectivity and yields as their corresponding phenyltrifluoroborate salts (Table 3.5, entries 1 and 2). Surprisingly, we did not observe any conversion of tetrafluoroborate salt **3.16** (Table 3.5, entry 3) in contrast to its corresponding phenyltrifluoroborate salt

3.24 (Table 3.4, entry 4). This result suggests that as observed in chapter 2, organotrifluoroborates may have a unique role as a fluorinating agent.

Table 3.5 Product distribution from the decomposition of salts 3.14-3.16



Entry	Precursor	Product distribution (%) ^a
1	<p style="text-align: center;">3.14</p>	<p style="text-align: center;">62</p>
2	<p style="text-align: center;">3.15</p>	<p style="text-align: center;">89</p>
3	<p style="text-align: center;">3.16</p>	no conversion

Reaction conditions: precursor (0.05 mmol), 1,2-dichlorobenzene (1.0 mL) in pressure vial with Teflon lined cap, heated at 140 °C for 2h. ^a Yields determined by ¹⁹F NMR spectroscopy using 2,4-dinitrofluorobenzene as an internal standard.

3.3 Conclusion and Perspectives

The fluorination of unsymmetrical diaryliodonium salts is a burgeoning area of research.

These substrates have found extensive applications in radiofluorination due to their ability

to provide both electron-poor and rich aryl fluorides. Most efforts have been directed towards unveiling underlying mechanisms of selectivity and improving reaction conditions within the context of radiochemistry. The fluorination of diaryliodonium salts has mostly been limited to alkali metal fluorides, and to the best of our knowledge the use of organotrifluoroborates for the fluorination of diaryliodonium salts is unprecedented. To this end a series of unsymmetrical diaryliodonium phenyltrifluoroborates were synthesized and fully characterised. The decomposition of these salts was investigated in various solvents and was found to be most efficient at high temperatures in non-polar solvents. All salts provided a single fluorinated product in complete selectivity in low to excellent yields. The selectivity observed seems to contrast with that observed in the decomposition of diaryliodonium fluorides; the experimental discrepancies suggest two different mechanisms. These studies are a proof of concept that organotrifluoroborates can be used in the fluorination of diaryliodonium salts. These preliminary results also expand the repertoire of organotrifluoroborates as a nucleophilic fluorine source.

Short-term perspectives for this work would involve further studies to confirm the proposed mechanism and explain the selectivity observed. Additionally, the use of alternative auxiliaries that would consistently provide high yields merit investigation. Electronic and steric properties on the organotrifluoroborates fragment could be investigated for effect on reaction efficiencies and selectivity. The counter-ion of diaryliodonium salts has been shown to have a significant effect on (radio)fluorination yields.¹⁹¹ It would therefore be of interest to investigate the solution phase fluorination of diaryliodonium salts of various counter-ions with organotrifluoroborates.

3.4 Experimental

General Information

Solvents and Reagents

All chemicals were purchased from commercial sources and used as received unless otherwise noted. Solvents used were all commercial grade and used as received with no drying, all reactions were performed in oven-dried glassware under argon atmosphere unless otherwise stated. Deuterated solvents for NMR spectroscopic analysis were purchased from Euriso-top.

Analysis

NMR experiments were performed in deuterated solvents. ^1H NMR, ^{13}C NMR, ^{11}B NMR and ^{19}F spectra were recorded on 300 Avance (300 MHz), 400 Avance (400 MHz) and Avancell 400 (400 MHz) Bruker spectrometers. All spectra were recorded at ambient temperature (298 K). Chemical shifts (δ) are reported in parts per million (ppm) relative to the residual protium in the solvents (^1H) or the solvent carbon (^{13}C) as internal standards. ^{19}F spectra of aryl fluorides were referenced to 2,4-dinitrofluorobenzene or 2,2,2-trifluoroethanol as internal standards (1 equivalent). Multiplicity of signals is indicated using the following abbreviations: s (singlet), b (broad), d (doublet), t (triplet), q (quartet), q_{B} (1:1:1:1 of peaks arising from coupling to ^{11}B with $S=3/2$, midpoint of signal reported), dd (doublet of doublets), dt (doublet of triplet), td (triplet of doublet), hept (heptet) and m (multiplet). ^{13}C signals arising from the quaternary carbon bearing the trifluoroborate group were not always observed and therefore were not always listed.

Reactions were monitored using Merck Silica gel 60 F₂₅₄ glass backed plates. TLC plates were visualized by UV fluorescence ($\lambda = 254$ nm) and one of the following stains: KMnO_4 or HBQ. Flash column chromatography was performed using VWR Chemicals Silica gel

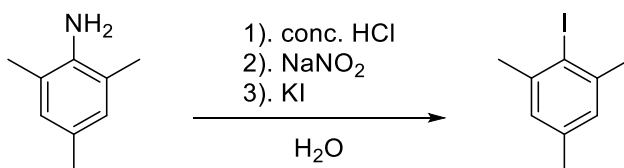
60 – 200 μm or using an automated Interchim Puriflash system using pre-packed Interchim 30 μm Silica gel cartridges.

IR spectra were recorded on a PerkinElmer Frontier FT-IR spectrometer with frequencies expressed in cm^{-1} .

Low resolution mass spectra were obtained on Waters LC-MS and Agilent GC-MS. High-resolution mass spectra (HRMS) were recorded using either electrospray ionization (ESI) or desorption chemical ionization (DCI) using Kratos MS-50 / Kratos Concept IISQ spectrometers.

3.4.1 Synthetic procedures and characterization data for 3.11 – 3.26

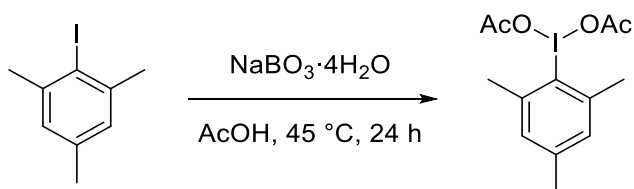
Iodomesitylene



A 250 mL round-bottom flask was charged with a stir bar and conc. HCl (50 mL), the flask was placed in an ice-water bath and cooled to 0 °C. 2,4,6-trimethylaniline (15.4 mL, 110 mmol) was added dropwise to the stirring HCl solution, after addition the reaction mixture was vigorously stirred for 20 minutes at 0 °C. NaNO₂ (7.9 g, 115 mmol) was dissolved in 35 mL of H₂O and the solution transferred to an addition funnel, this nitrite solution was added dropwise to the reaction mixture at 0 °C over 20 minutes; after addition was complete the brown reaction mixture was stirred at 0 °C for 1 hour. KI (24.9 g, 150 mmol) was dissolved in 35 mL H₂O and this solution transferred to an addition funnel, this solution was dropwise added to the reaction mixture over 30 minutes, maintaining the bath temperature at 0 °C. After addition was complete the reaction mixture was allowed to warm to rt and stirred overnight. The reaction mixture was transferred to a separatory funnel and the aqueous phase extracted with cyclohexane (3 x 150 mL). The organic phase was then washed with a 5% aqueous solution of Na₂S₂O₃ (100 mL), followed by

brine (150 mL). The organic phase was then dried over anhydrous MgSO_4 , filtered then concentrated under reduced pressure to furnish a viscous dark brown/red oil which slowly solidifies. The product was further purified by distilling at $85\text{ }^\circ\text{C}$ (10 mbar), followed by Silica gel chromatography using cyclohexane as the eluent to furnish the desired product as a light-yellow oil (10.39 g, 38%). ^1H NMR (400 MHz, Chloroform-*d*) δ 6.94 (s, 2H), 2.50 (s, 6H), 2.31 (s, 3H). ^{13}C NMR (101 MHz, Chloroform-*d*) δ 141.8 (C_q), 137.3 (C_q), 128.0 (CH), 104.4 (C_q), 29.6 (CH_3), 20.8 (CH_3). MS-DCI (m/z): 246 $[\text{M}]^+$, 245 $[\text{M}-\text{H}]^-$. Spectroscopic data consistent with those previously reported.²¹³

Iodomesitylene diacetate (3.12)



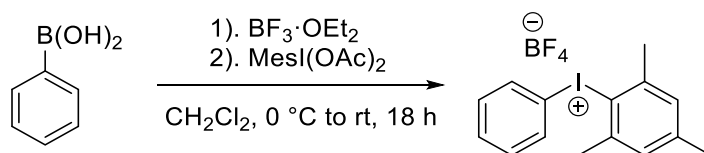
A 250 mL round-bottom flask was charged with a stir bar, iodomesitylene (4.9609 g, 20 mmol) and AcOH (182 mL), to which $\text{NaBO}_3 \cdot 4\text{H}_2\text{O}$ (30.8963 g, 200 mmol) was added in once portion. A condenser was attached to the flask and the homogenous mixture was stirred at $45\text{ }^\circ\text{C}$ for 24 h. After approximately 1 h of stirring and heating the reaction mixture became clear and pink in colour, this turned to colourless after 2h of heating and stirring, after 24 h the solution developed a white precipitate. The solution was then concentrated to about half its volume and H_2O (200 mL) was added and solution stirred vigorously for 20 min. The precipitate was then collected by filtration and washed with H_2O (3 x 25 mL); the precipitate was then transferred into a 50 mL flask and dissolved in 1:1 AcOH /acetic anhydride (16 mL) while heating at $80\text{ }^\circ\text{C}$. The mixture was then concentrated to dryness under reduced pressure to furnish a white crystalline precipitate which was triturated with Et_2O and collected by filtration and further washed with Et_2O , then dried under high vacuum overnight (4.7167 g, 64%). IR $\nu_{\text{max}}/\text{cm}^{-1}$ (neat film): 2989, 2973, 2901, 1645, 1368, 1267, 666. ^1H NMR (400 MHz, Chloroform-*d*) δ 7.09 (s, 2H), 2.70 (s, 6H), 2.35 (s, 3H), 1.96 (s, 6H). ^{13}C NMR (101 MHz, Chloroform-*d*) δ 176.6 (C_q), 143.3 (C_q), 141.5 (C_q),

129.7 (C_q), 129.1 (CH), 26.9 (CH₃), 21.3 (CH₃), 20.4 (CH₃). MS-DCI (*m/z*):304 [M-OAc]⁺. Spectroscopic data matches those previously described.²¹⁴

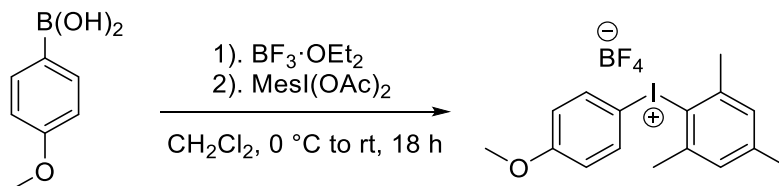
General procedure for the synthesis of unsymmetrical diaryliodonium tetrafluoroborates:^{117,205}

A round-bottom flask was charged with a stir bar, arylboronic acid (1 eq.) and CH₂Cl₂ (0.1 M), the reaction mixture was stirred and cooled to 0 °C in an ice-water bath and then BF₃·OEt₂ (3 eq.) was added, this solution was stirred at 0 °C for 10 minutes. In a separate flask iodomesitylene diacetate (MesI(OAc)₂) or phenyliodine(III) diacetate (PIDA) (1.1 eq) was dissolved in CH₂Cl₂ (0.37 M) and added dropwise to the reaction mixture at 0 °C. The resulting solution was allowed to warm to rt and stirred overnight. The reaction mixture was then transferred directly onto a plug of Silica gel and washed with CH₂Cl₂, the product was the eluted with 9.5:0.5 CH₂Cl₂/MeOH. Collected fractions were concentrated under reduced pressure then dropped on Et₂O to precipitate the product which was collected by filtration and further washed with Et₂O.

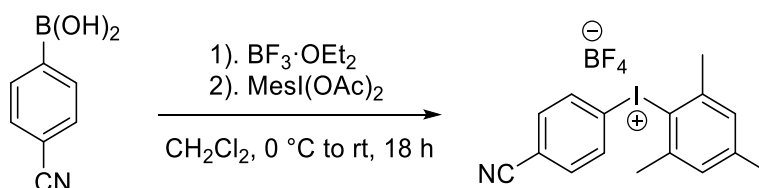
(2,4,6-trimethylphenyl)(phenyl)iodonium tetrafluoroborate (3.13)



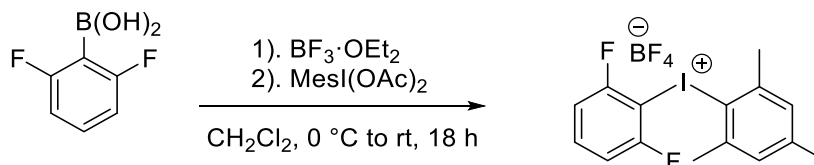
Isolated as a white fluffy powder (408.6 mg, 99%). IR $\nu_{\max}/\text{cm}^{-1}$ (neat film): 2989, 2970, 2901, 1473, 1445, 1057, 736. ¹H NMR (400 MHz, DMSO-*d*₆) δ 8.00 – 7.94 (m, 2H), 7.67 – 7.60 (m, 1H), 7.54 – 7.47 (m, 2H), 7.22 (s, 2H), 2.60 (s, 6H), 2.30 (s, 3H). ¹³C NMR (101 MHz, DMSO-*d*₆) δ 143.1 (C_q), 141.6 (C_q), 134.5 (CH), 131.9 (CH), 131.8 (CH), 129.8 (CH), 122.5 (C_q), 115.0 (C_q), 26.2 (CH₃), 20.5 (CH₃). ¹⁹F NMR (376 MHz, DMSO-*d*₆) δ -145.58 – -150.82 (m). ¹¹B NMR (128 MHz, DMSO-*d*₆) δ -1.29 (s). HRMS-ESI (*m/z*): found [M]⁺ 323.0295, calc'd C₁₅H₁₆I⁺ requires 323.0297.

(4-methoxyphenyl)(2,4,6-trimethylphenyl)iodonium tetrafluoroborate (3.11)

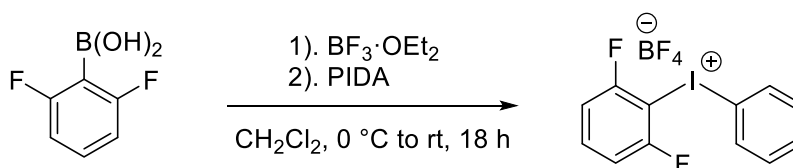
Isolated as a grey powder (262.8 mg, 59%). IR $\nu_{\text{max}}/\text{cm}^{-1}$ (neat film): 2989, 2973, 2901, 1582, 1569, 1486, 1302, 1259, 1051, 1027, 827. ^1H NMR (400 MHz, $\text{DMSO-}d_6$) δ 7.95 – 7.89 (m, 2H), 7.21 – 7.17 (m, 2H), 7.06 – 7.01 (m, 2H), 3.78 (s, 3H), 2.60 (s, 6H), 2.29 (s, 3H). ^{13}C NMR (101 MHz, $\text{DMSO-}d_6$) δ 161.7 (C_q), 142.9 (C_q), 141.3 (C_q), 136.6 (CH), 129.7 (CH), 123.0 (C_q), 117.50 (CH), 103.3 (C_q), 55.7 (CH_3), 26.2 (CH_3), 20.5 (CH_3). ^{19}F NMR (376 MHz, $\text{DMSO-}d_6$) δ -146.91 – -149.49 (m). ^{11}B NMR (128 MHz, $\text{DMSO-}d_6$) δ -1.30 (s). HRMS-ESI (m/z): found $[\text{M}]^+$ 353.0402, calc'd $\text{C}_{16}\text{H}_{18}\text{I}^+$ requires 353.0402.

(4-cyanophenyl)(2,4,6-trimethylphenyl)iodonium tetrafluoroborate (3.14)

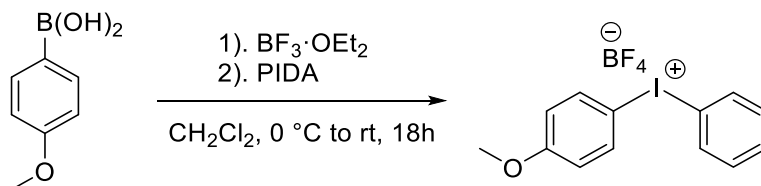
Isolated as a beige powder (208.9 mg, 48%). IR $\nu_{\text{max}}/\text{cm}^{-1}$ (neat film): 2989, 2970, 2901, 2237, 1482, 1066, 832. ^1H NMR (400 MHz, $\text{DMSO-}d_6$) δ 8.11 (d, $J = 8.7$ Hz, 2H), 7.96 (d, $J = 8.7$ Hz, 2H), 7.25 (s, 2H), 2.58 (s, 6H), 2.31 (s, 3H). ^{13}C NMR (101 MHz, $\text{DMSO-}d_6$) δ 143.5 (C_q), 141.8 (C_q), 135.1 (CH), 134.9 (CH), 130.0 (CH), 122.6 (C_q), 119.4 (C_q), 117.4 (C_q), 114.4 (C_q), 26.3 (CH_3), 20.6 (CH_3). ^{19}F NMR (376 MHz, $\text{DMSO-}d_6$) δ -146.91 – -149.84 (m). ^{11}B NMR (128 MHz, $\text{DMSO-}d_6$) δ -1.30 (s). HRMS-ESI (m/z): found $[\text{M}]^+$ 348.0254, calc'd $\text{C}_{16}\text{H}_{15}\text{I}^+$ requires 348.0249.

(2,6-difluorophenyl)(2,4,6-trimethylphenyl)iodonium tetrafluoroborate (3.15)

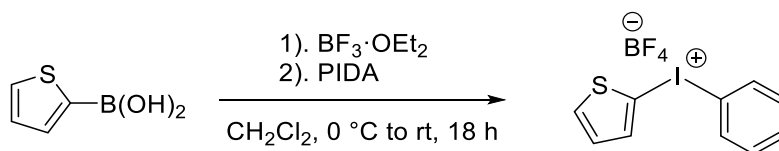
Isolated as a white powder (780.4 mg, 88%). IR $\nu_{\text{max}}/\text{cm}^{-1}$ (neat film): 3090, 3028, 2960, 2918, 1592, 1469, 1241, 1015, 994, 792. ^1H NMR (400 MHz, $\text{DMSO-}d_6$) δ 7.81 (tt, $J = 8.4, 6.7$ Hz, 1H), 7.45 (dd, $J = 8.3, 7.3$ Hz, 2H), 7.23 (s, 2H), 2.61 (s, 6H), 2.29 (s, 3H). ^{13}C NMR (101 MHz, $\text{DMSO-}d_6$) δ 160.6 (dd, $^1J_{\text{CF}} = 250.6, ^3J_{\text{CF}} = 5.9$ Hz) (C_q), 143.5 (C_q), 141.6 (C_q), 137.0 (t, $^3J_{\text{CF}} = 10.1$ Hz) (CH), 129.9 (CH), 122.8 (C_q), 113.48 – 113.1 (m) (CH), 91.7 (t, $^2J_{\text{CF}} = 28.1$ Hz) (C_q), 25.9 (t, $^6J_{\text{CF}} = 1.8$ Hz) (CH_3), 20.5 (CH_3). ^{19}F NMR (377 MHz, $\text{DMSO-}d_6$) δ -95.82 (t, $J = 7.0$ Hz, 2F), -147.71 – -149.04 (m, 4F). ^{11}B NMR (128 MHz, $\text{DMSO-}d_6$) δ -1.29 (s). HRMS-ESI (m/z): found $[\text{M}]^+$ 359.0110, calc'd $\text{C}_{15}\text{H}_{14}\text{F}_2\text{I}^+$ requires 359.0108.

(2,6-difluorophenyl)(phenyl)iodonium tetrafluoroborate (3.16)

Isolated as a white powder (267.4 mg, 66%). IR $\nu_{\text{max}}/\text{cm}^{-1}$ (neat film): 3096, 3058, 1591, 1467, 1447, 1241, 1054, 995, 987, 788, 744. ^1H NMR (400 MHz, $\text{DMSO-}d_6$) δ 8.20 (d, $J = 7.6$ Hz, 2H), 7.80 (tt, $^3J_{\text{HH}} = 8.4, ^4J_{\text{HF}} = 6.7$ Hz, 1H), 7.70 (t, $J = 7.4$ Hz, 1H), 7.55 (t, $J = 7.0$ Hz, 2H), 7.46 (dd, $^3J_{\text{HF}} = 8.5, ^3J_{\text{HF}} = 7.0$ Hz, 2H). ^{13}C NMR (101 MHz, $\text{DMSO-}d_6$) δ 160.1 (dd, $^1J_{\text{CF}} = 251.0, ^3J_{\text{CF}} = 5.5$ Hz) (C_q), 137.2 (t, $^3J_{\text{CF}} = 9.9$ Hz) (CH), 135.2 (CH), 132.5 (CH), 132.2 (CH), 117.1 (C_q), 113.3 – 112.9 (m) (CH), 94.3 (t, $^2J_{\text{CF}} = 28.2$ Hz) (C_q). ^{19}F NMR (377 MHz, $\text{DMSO-}d_6$) δ -96.40 (t, $J = 7.0$ Hz, 2F), -147.60 – -149.53 (m, 4F). ^{11}B NMR (128 MHz, $\text{DMSO-}d_6$) δ -1.29 (s). HRMS-ESI (m/z): found $[\text{M}]^+$ 316.9647, calc'd $\text{C}_{12}\text{H}_8\text{F}_2\text{I}^+$ requires 316.9639.

(4-methoxyphenyl)(phenyl)iodonium tetrafluoroborate (3.17)

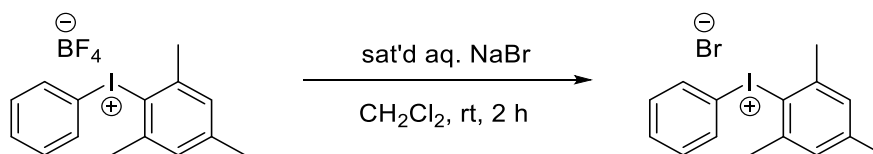
Isolated as a grey powder (199.3 mg, 51%). IR $\nu_{\text{max}}/\text{cm}^{-1}$ (neat film): 3196, 3097, 2951, 2846, 1573, 1489, 1302, 1260, 1181, 1047, 1013, 988, 830, 744. ^1H NMR (400 MHz, $\text{DMSO-}d_6$) δ 8.28 – 8.12 (m, 4H), 7.64 (t, $J = 7.4$ Hz, 1H), 7.52 (t, $J = 7.6$ Hz, 2H), 7.07 (d, $J = 8.5$ Hz, 2H). ^{13}C NMR (101 MHz, $\text{DMSO-}d_6$) δ 162.0 (C_q), 137.3 (CH), 134.8 (CH), 131.9 (CH), 131.7 (CH), 117.5 (CH), 117.0 (C_q), 105.4 (C_q), 55.7 (CH_3). ^{19}F NMR (376 MHz, $\text{DMSO-}d_6$) δ -148.05 – -148.35 (m). ^{11}B NMR (128 MHz, $\text{DMSO-}d_6$) δ -1.23 (s). HRMS-ESI (m/z): found $[\text{M}]^+$ 310.9935, calc'd $\text{C}_{13}\text{H}_{12}^{127}\text{IO}^+$ requires 310.9933.

(2-thienyl)(phenyl)iodonium tetrafluoroborate (3.18)

Isolated as a burgundy powder (467.5 mg, 62%). IR $\nu_{\text{max}}/\text{cm}^{-1}$ (neat film): 3092, 1559, 1470, 1443, 1386, 1227, 1049, 1031, 1007, 988, 846, 739, 726. ^1H NMR (400 MHz, $\text{DMSO-}d_6$) δ 8.25 (d, $J = 7.5$ Hz, 2H), 8.11 – 8.02 (m, 1H), 7.97 (d, $J = 5.3$ Hz, 1H), 7.66 (t, $J = 7.5$ Hz, 1H), 7.60 – 7.45 (m, 2H), 7.24 – 7.13 (m, 1H). ^{13}C NMR (101 MHz, $\text{DMSO-}d_6$) δ 140.4 (CH), 137.4 (CH), 134.6 (CH), 132.1 (CH), 131.7 (CH), 129.7 (CH), 119.3 (C_q), 100.7 (C_q). ^{19}F NMR (376 MHz, $\text{DMSO-}d_6$) δ -147.95 – -148.54 (m). ^{11}B NMR (128 MHz, $\text{DMSO-}d_6$) δ -1.27 (s). HRMS-ESI (m/z): found $[\text{M}]^+$ 286.9393, calc'd $\text{C}_{10}\text{H}_8^{127}\text{IS}^+$ requires 286.9391.

Synthesis of unsymmetrical diaryliodonium phenyltrifluoroborates

(2,4,6-trimethylphenyl)(phenyl)iodonium bromide (3.19)



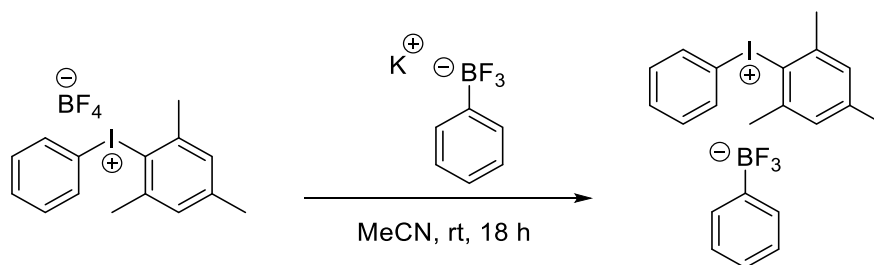
A 10 mL round-bottom flask was charged with a stir bar, mesityl(phenyl)iodonium tetrafluoroborate (98 mg, 0.24 mmol) and CH_2Cl_2 (1 mL). A saturated aqueous NaBr solution (1.3 mL) was then added and the biphasic reaction mixture stirred rapidly over 2 h. The phases were then allowed to separate, collecting the organic phase. The aqueous phase was extracted with CH_2Cl_2 (3 x 5 mL), the combined organic phases were dried over anhydrous MgSO_4 then filtered and concentrated to saturation. The remaining residue was dropped onto Et_2O to precipitate the desired salt as a fine white powder (78.5 mg, 82%). Complete substitution of tetrafluoroborate counter-ion was confirmed by ^{19}F NMR. IR $\nu_{\text{max}}/\text{cm}^{-1}$ (neat film): 3044, 3014, 2979, 2914, 1566, 1470, 1439, 997, 845, 736, 681. ^1H NMR (400 MHz, $\text{DMSO}-d_6$) δ 7.93 – 7.88 (m, 2H), 7.58 (t, $J = 7.4$ Hz, 1H), 7.46 (t, $J = 7.7$ Hz, 2H), 7.18 (s, 2H), 2.59 (s, 6H), 2.28 (s, 3H). ^{13}C NMR (101 MHz, $\text{DMSO}-d_6$) δ 142.6 (C_q), 141.2 (C_q), 134.1 (CH), 131.6 (CH), 131.3 (CH), 129.6 (CH), 124.4 (C_q), 116.9 (C_q), 26.3 (CH_3), 20.5 (CH_3). HRMS-ESI (m/z): found $[\text{M}]^+$ 323.0293, calc'd $\text{C}_{15}\text{H}_{16}^+$ requires 323.0297.

General procedure for the synthesis of unsymmetrical diaryliodonium aryltrifluoroborates:

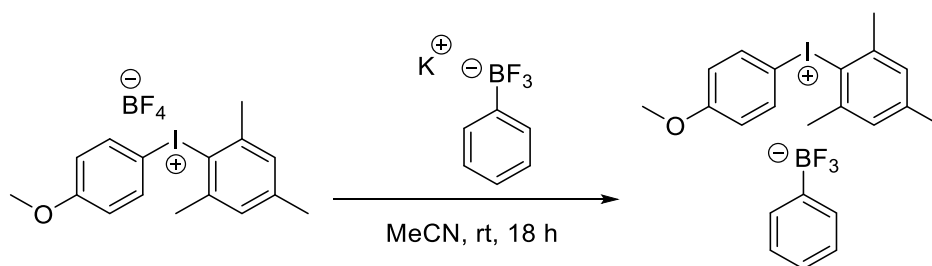
A round-bottom flask was charged with a stir bar, diaryliodonium tetrafluoroborate (1 eq.) and MeCN (0.1 M); to this stirring reaction mixture potassium phenyltrifluoroborate (1 eq.) was added in one portion and the mixture stirred at rt for 18 h. The reaction mixture was passed through a 0.2 μm PTFE filter to remove insoluble solids, and the filter washed with MeCN. The filtrate was then concentrated to dryness under reduced pressure, and then

left under high vacuum for 6h. The remaining residue was triturated with CH_2Cl_2 and the solution passed through 0.2 μm PTFE filter to remove insoluble solids. The filtrate was then concentrated to saturation and then dropped onto Et_2O to precipitate the product.

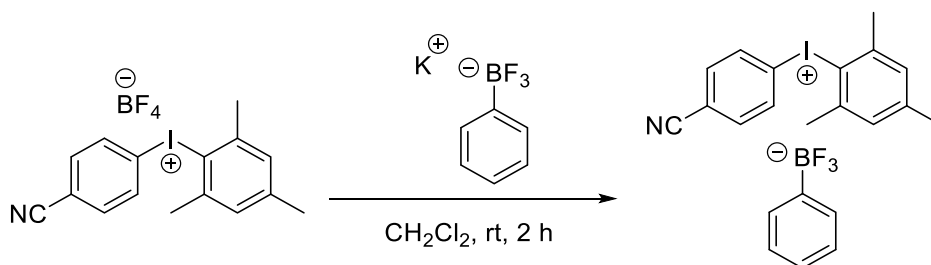
(2,4,6-trimethylphenyl)(phenyl)iodonium phenyltrifluoroborate (3.20)



Isolated as an off-white powder (54.7 mg, >99%). Colourless, single crystals suitable for X-ray analysis were grown by slow evaporation of a CHCl_3 solution. IR $\nu_{\text{max}}/\text{cm}^{-1}$ (neat film): 3071, 3049, 3009, 2984, 1441, 1200, 1005, 986, 937, 906, 752, 743, 707. ^1H NMR (400 MHz, $\text{DMSO}-d_6$) δ 7.99 – 7.95 (m, 2H), 7.65 – 7.60 (m, 1H), 7.53 – 7.46 (m, 2H), 7.32 (d, $J = 6.6$ Hz, 2H), 7.23 – 7.19 (m, 2H), 7.07 (dddt, $J = 7.3, 5.9, 1.4, 0.7$ Hz, 2H), 7.04 – 6.97 (m, 1H), 2.60 (s, 6H), 2.29 (s, 3H). ^{13}C NMR (101 MHz, $\text{DMSO}-d_6$) δ 143.1 (C_q), 141.6 (C_q), 134.5 (CH), 131.9 (CH), 131.8 (CH), 131.3 (q, $^3J_{\text{CF}} = 1.7$ Hz) (CH), 129.8 (CH), 126.2 (CH), 124.9 (CH), 122.6 (C_q), 114.5 (C_q), 26.3 (CH_3), 20.5 (CH_3). ^{19}F NMR (376 MHz, $\text{DMSO}-d_6$) δ -139.06 (q_B). ^{11}B NMR (128 MHz, $\text{DMSO}-d_6$) δ 3.15 (q, $J = 52.0$ Hz). HRMS-ESI (m/z): found $[\text{M}-\text{C}_6\text{H}_5\text{BF}_3]^+$ 323.0293, calc'd $\text{C}_{15}\text{H}_{16}^+$ requires 322.0297, found $[\text{M}-\text{C}_{15}\text{H}_{16}]^-$ 144.0474, calc'd $\text{C}_6\text{H}_5\text{BF}_3^-$ requires 144.0473. Anal. calc'd for $\text{C}_{21}\text{H}_{21}\text{BF}_3\text{I}$: C, 53.88; H, 4.52; N, 0.00. Found C, 52.85; H, 4.32; N, 0.02.

(4-methoxyphenyl)(2,4,6-trimethylphenyl)iodonium phenyltrifluoroborate (3.21)

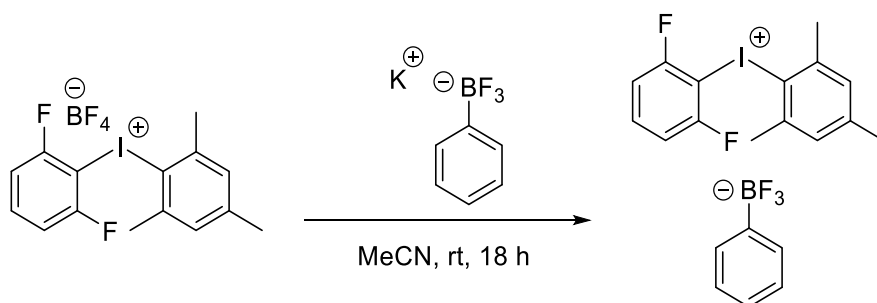
Isolated as a grey powder (234.1 mg, 80%). IR $\nu_{\text{max}}/\text{cm}^{-1}$ (neat film): 3085, 2970, 2845, 1571, 1486, 1253, 1195, 1020, 951, 941, 831, 754, 707. ^1H NMR (400 MHz, $\text{DMSO-}d_6$) δ 7.95 – 7.89 (m, 2H), 7.31 (d, $J = 6.8$ Hz, 2H), 7.19 (s, 2H), 7.10 – 6.97 (m, 5H), 3.78 (s, 3H), 2.60 (s, 6H), 2.28 (s, 3H). ^{13}C NMR (101 MHz, $\text{DMSO-}d_6$) δ 161.7 (C_q), 142.9 (C_q), 141.3 (C_q), 136.6 (CH), 131.3 (q, $^3J_{\text{CF}} = 1.9$ Hz) (CH), 129.7 (CH), 126.2 (CH), 124.8 (CH), 123.0 (C_q), 117.5 (CH), 103.3 (C_q), 55.7 (CH_3), 26.2 (CH_3), 20.5 (CH_3). ^{19}F NMR (376 MHz, $\text{DMSO-}d_6$) δ -139.13 (q_B). ^{11}B NMR (128 MHz, $\text{DMSO-}d_6$) δ 3.11 (q, $J = 53.1$ Hz). HRMS-ESI (m/z): found $[\text{M-C}_6\text{H}_5\text{BF}_3]^+$ 353.0397, calc'd $\text{C}_{16}\text{H}_{18}\text{I}^+$ requires 353.0402, found $[\text{M-C}_{16}\text{H}_{18}\text{I}]^-$ 144.0477, calc'd $\text{C}_6\text{H}_5\text{BF}_3^-$ requires 144.0473. Anal. calc'd for $\text{C}_{22}\text{H}_{23}\text{BF}_3\text{IO}$: C, 53.05; H, 4.65; N, 0.00. Found C, 53.21; H, 4.60; N, 0.03.

(4-cyanophenyl)(2,4,6-trimethylphenyl)iodonium phenyltrifluoroborate (3.22)

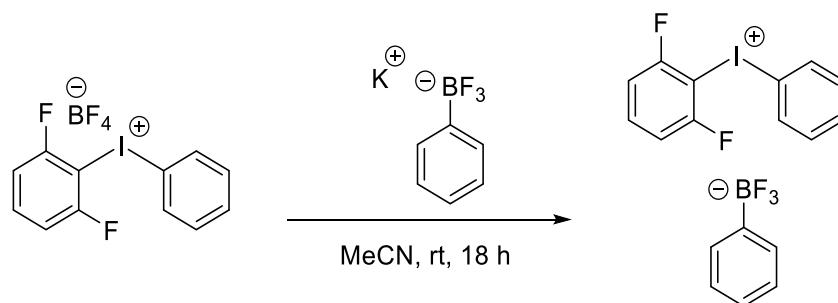
Isolated as a white powder (206.2 mg, 91%). IR $\nu_{\text{max}}/\text{cm}^{-1}$ (neat film): 3097, 3047, 3020, 3005, 2231, 1580, 1475, 1203, 948, 827, 751, 701. ^1H NMR (400 MHz, $\text{DMSO-}d_6$) δ 8.10 (d, $J = 8.7$ Hz, 2H), 7.95 (d, $J = 8.7$ Hz, 2H), 7.31 (d, $J = 6.7$ Hz, 2H), 7.25 (s, 2H), 7.07 (t, $J = 7.1$ Hz, 2H), 7.03 – 6.97 (m, 1H), 2.58 (s, 6H), 2.31 (s, 3H). ^{13}C NMR (101 MHz,

DMSO- d_6) δ 143.5 (C_q), 141.8 (C_q), 135.0 (CH), 134.9 (CH), 131.3 (q, $^3J_{CF}$ = 1.9 Hz) (CH), 130.0 (CH), 126.2 (CH), 124.8 (CH), 122.7 (C_q), 119.4 (C_q), 117.4 (C_q), 114.4 (C_q), 26.3 (CH₃), 20.5 (CH₃). ^{19}F NMR (376 MHz, DMSO- d_6) δ -139.12 (q_B). ^{11}B NMR (128 MHz, DMSO- d_6) δ 3.12 (q, J = 51.5 Hz). HRMS-ESI (m/z): found [M-C₆H₅BF₃]⁺ 348.0250, calc'd C₁₆H₁₅IN⁺ requires 348.0249, found [M-C₁₆H₁₅IN]⁻ 144.0477, calc'd C₆H₅BF₃⁻ requires 144.0473. Anal. calc'd for C₂₂H₂₀BF₃IN: C, 53.59; H, 4.09; N, 2.84. Found C, 53.30; H, 3.84; N, 2.82.

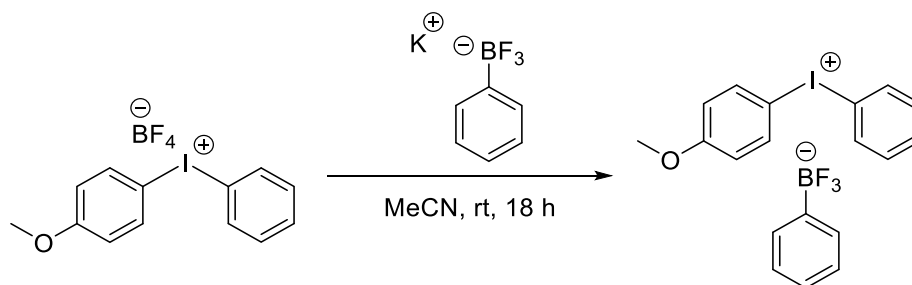
(2,6-difluorophenyl)(2,4,6-trimethylphenyl)iodonium phenyltrifluoroborate (3.23)



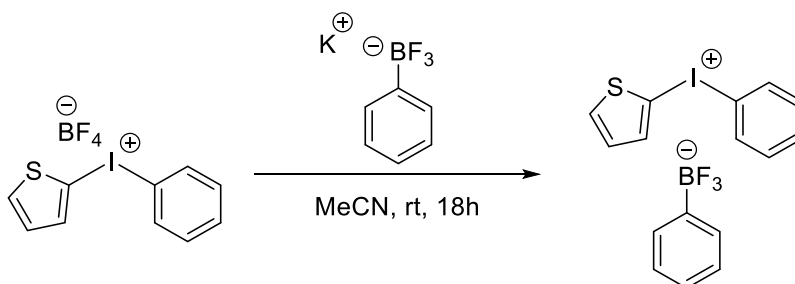
Isolated as a white powder (520 mg, 92%). IR $\nu_{\text{max}}/\text{cm}^{-1}$ (neat film): 3067, 3046, 3022, 3004, 2924, 1593, 1468, 1239, 1205, 1016, 995, 942, 925, 901, 892, 749. ^1H NMR (400 MHz, DMSO- d_6) δ 7.80 (tt, J = 8.5, 6.7 Hz, 1H), 7.44 (dd, J = 8.3, 7.3 Hz, 2H), 7.31 (d, J = 6.7 Hz, 2H), 7.22 (s, 2H), 7.07 (t, J = 7.3 Hz, 2H), 7.03 – 6.97 (m, 1H), 2.61 (s, 6H), 2.28 (s, 3H). ^{13}C NMR (101 MHz, DMSO- d_6) δ 160.6 (dd, $^1J_{CF}$ = 250.7, $^3J_{CF}$ = 6.0 Hz) (C_q), 143.5 (C_q), 141.6 (C_q), 137.0 (t, $^3J_{CF}$ = 10.1 Hz) (CH), 131.3 (q, $^3J_{CF}$ = 1.7 Hz) (CH), 129.9 (CH), 126.2 (CH), 124.9 (CH), 122.9 (C_q), 113.52 – 113.03 (m) (CH), 91.7 (t, $^2J_{CF}$ = 28.1 Hz) (C_q), 25.9 (t, $^6J_{CF}$ = 2.1 Hz) (CH₃), 20.5 (CH₃). ^{19}F NMR (376 MHz, DMSO- d_6) δ -95.84 (t, J = 7.0 Hz, 2F), -138.46 – -139.68 (q_B, 3F). ^{11}B NMR (128 MHz, DMSO- d_6) δ 3.13 (q, J = 52.8 Hz). HRMS-ESI (m/z): found [M-C₆H₅BF₃]⁺ 359.0112, calc'd C₁₅H₁₄F₂I⁺ requires 359.0108, found [M-C₁₅H₁₄F₂I]⁻ 144.0473, calc'd C₆H₅BF₃⁻ requires 144.0473. Anal. calc'd for C₂₁H₁₉BF₅I: C, 50.04; H, 3.80; N, 0.00. Found C, 49.97; H, 3.43; N, 0.04.

(2,6-difluorophenyl)(phenyl)iodonium phenyltrifluoroborate (3.24)

Isolated as a white powder (132.9 mg, 77%). IR $\nu_{\text{max}}/\text{cm}^{-1}$ (neat film): 3080, 3066, 3049, 3007, 1593, 1467, 1242, 1206, 998, 946, 898, 788, 753, 706. ^1H NMR (400 MHz, DMSO- d_6) δ 8.20 (d, $J = 7.7$ Hz, 2H), 7.80 (tt, $J = 8.5, 6.7$ Hz, 1H), 7.70 (t, $J = 7.4$ Hz, 1H), 7.55 (t, $J = 7.8$ Hz, 2H), 7.49 – 7.43 (m, 2H), 7.31 (d, $J = 6.9$ Hz, 2H), 7.07 (t, $J = 7.2$ Hz, 2H), 7.00 (t, $J = 7.1$ Hz, 1H). ^{13}C NMR (101 MHz, DMSO- d_6) δ 160.1 (dd, $^1J_{\text{CF}} = 251.0$, $^3J_{\text{CF}} = 5.5$ Hz) (C_q), 137.2 (t, $^3J_{\text{CF}} = 9.9$ Hz) (CH), 135.2 (CH), 132.5 (CH), 132.2 (CH), 131.3 (q, $^3J_{\text{CF}} = 1.8$ Hz) (CH), 126.2 (CH), 124.8 (CH), 117.1 (C_q), 113.1 (dd, $^2J_{\text{CF}} = 22.9$, $^4J_{\text{CF}} = 2.8$ Hz) (CH), 94.4 (t, $^2J_{\text{CF}} = 28.1$ Hz) (C_q). ^{19}F NMR (377 MHz, DMSO- d_6) δ -96.41 (t, $J = 7.0$ Hz, 2F), -137.87 – -140.92 (q_B , 3F). ^{11}B NMR (128 MHz, DMSO- d_6) δ 3.12 (q, $J = 50.6$ Hz). HRMS-ESI (m/z): found $[\text{M}-\text{C}_6\text{H}_5\text{BF}_3]^+$ 316.9644, calc'd $\text{C}_{12}\text{H}_8\text{F}_2^+$ requires 316.9639, found $[\text{M}-\text{C}_{12}\text{H}_8\text{F}_2]^-$ 144.0474, calc'd $\text{C}_6\text{H}_5\text{BF}_3^-$ requires 144.0473. Anal. calc'd for $\text{C}_{18}\text{H}_{13}\text{BF}_5\text{I}$: C, 46.80; H, 2.84; N, 0.00. Found C, 46.41; H, 2.25; N, 0.19.

(4-methoxyphenyl)(phenyl)iodonium phenyltrifluoroborate (3.25)

Isolated as a light grey powder (93.9 mg, 81%). IR $\nu_{\text{max}}/\text{cm}^{-1}$ (neat film): 3070, 3009, 2971, 2936, 2840, 1581, 1571, 1488, 1442, 1300, 1255, 1200, 1179, 1009, 990, 951, 904, 754. ¹H NMR (400 MHz, DMSO-*d*₆) δ 8.22 – 8.13 (m, 4H), 7.68 – 7.62 (m, 1H), 7.56 – 7.49 (m, 2H), 7.33 – 7.27 (m, 2H), 7.11 – 7.04 (m, 4H), 7.03 – 6.97 (m, 1H), 3.79 (s, 3H). ¹³C NMR (101 MHz, DMSO-*d*₆) δ 162.0 (C_q), 137.2 (CH), 134.8 (CH), 131.8 (CH), 131.6 (CH), 131.3 (q, ⁴J_{C-F} = 1.7 Hz) (CH), 126.1 (CH), 124.8 (CH), 117.5 (CH), 117.0 (C_q), 105.3 (C_q), 55.7 (CH₃). ¹⁹F NMR (376 MHz, DMSO-*d*₆) δ -139.14 (q_B). ¹¹B NMR (128 MHz, DMSO-*d*₆) δ 3.10 (q, *J* = 52.9 Hz). HRMS-ESI (*m/z*): found [M]⁺ 310.9929, calc'd C₁₃H₁₂¹²⁷IO⁺ requires 310.9933, found [M]⁻ 144.0456, calc'd C₆H₅¹⁰BF₃⁻ requires 144.0473. Anal. calc'd for C₁₉H₁₇BF₃IO: C, 50.04; H, 3.76; N, 0.00. Found C, 49.91; H, 3.18; N, 0.06.

(2-thienyl)(phenyl)iodonium tetrafluoroborate (3.26)

Isolated as a light pink powder (318.7 mg, 92%). IR $\nu_{\text{max}}/\text{cm}^{-1}$ (neat film): 3096, 3006, 1470, 1442, 1435, 1383, 1199, 1014, 1007, 988, 970, 890, 758, 736, 707. ¹H NMR (400 MHz, DMSO-*d*₆) δ 8.28 – 8.22 (m, 2H), 8.06 (dd, *J* = 3.8, 1.3 Hz, 1H), 7.97 (dd, *J* = 5.3,

1.3 Hz, 1H), 7.67 (ddt, $J = 8.5, 7.0, 1.1$ Hz, 1H), 7.54 (ddt, $J = 8.2, 7.3, 1.3$ Hz, 2H), 7.35 – 7.28 (m, 2H), 7.18 (dd, $J = 5.3, 3.8$ Hz, 1H), 7.07 (dddd, $J = 7.4, 5.9, 1.4, 0.7$ Hz, 2H), 7.04 – 6.98 (m, 1H). ^{13}C NMR (101 MHz, DMSO- d_6) δ 140.4 (CH), 137.4 (CH), 134.6 (CH), 132.1 (CH), 131.7 (CH), 131.3 (d, $^4J_{\text{C-F}} = 1.7$ Hz) (CH), 129.7 (CH), 126.2 (CH), 124.8 (CH), 119.3 (C_q), 100.7 (C_q). ^{19}F NMR (376 MHz, DMSO- d_6) δ -139.11 (q_B). ^{11}B NMR (128 MHz, DMSO- d_6) δ 3.09 (q, $J = 52.6$ Hz). HRMS-ESI (m/z): found $[\text{M}]^+$ 286.9396, calc'd C₁₀H₈¹²⁷I⁺ requires 286.9391, found $[\text{M}]^-$ 144.0475, calc'd C₆H₅¹⁰BF₃⁻ requires 144.0473. Anal. calc'd for C₁₆H₁₃BF₃IS: C, 44.48; H, 3.03; N, 0.00. Found C, 44.16; H, 2.32; N, 0.00.

Fluorination of unsymmetrical diaryliodonium phenyltrifluoroborates salts

General procedure for the fluorination of iodonium salts:

A 10 mL microwave vial was charged with iodonium salt (0.05 mmol) and solvent (1 mL), the vial was capped and sealed with a crimper. The vial was placed in an oil bath at the specified temperature and stirred at the designated temperature for 2 h. After allowing to cool to rt, an internal standard was added to the crude reaction mixture followed by d^6 -DMSO (0.5 mL) and the yield was determined by ^{19}F NMR spectroscopy.

4 Organotrifluoroborates applied towards intramolecular fluorination

Chapters 2 and 3 described the application of organotrifluoroborates in the context of intermolecular fluorination of aryl diazonium and diaryliodonium substrates, respectively. Having proven the ability of organotrifluoroborates to serve as fluoride ion sources in an intermolecular fashion, we were intrigued by the possibility of translating this technology towards fluorination in an intramolecular fashion. This chapter will briefly discuss previous efforts in the literature towards intramolecular fluorination.

4.1 Introduction

The fluorination of organic scaffolds has been the subject of intense effort, research and scrutiny for the better part of the last century. As a result, significant advances and developments have been made towards C(sp³, sp², sp)–F bond forming methodologies via nucleophilic, electrophilic and radical fluorination strategies.¹² Given the difficulties encountered in C–F formation, improvements in fluorination methodologies have largely been driven by the development of novel, stable and easy to handle fluorinating agents (Figure 4.1). These reagents function as exogenous sources of fluorine for intermolecular fluorination and their delivery of fluorine is facilitated by the nature of their environment and physicochemical properties. Given the particularities of synthesizing these reagents, with regards to reaction conditions and functional complexity, their application towards intramolecular fluorination is unreasonable and would be highly inefficient. It is therefore not surprising to find that there are only a few intramolecular fluorination strategies described in the literature.

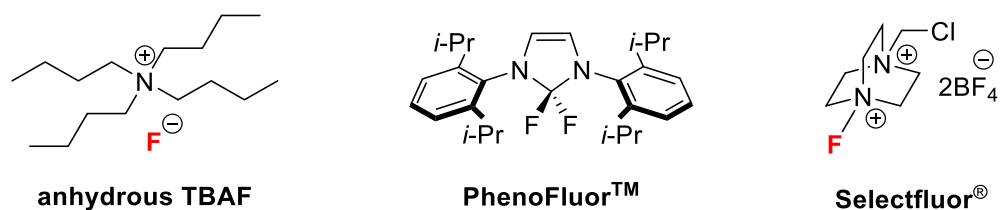
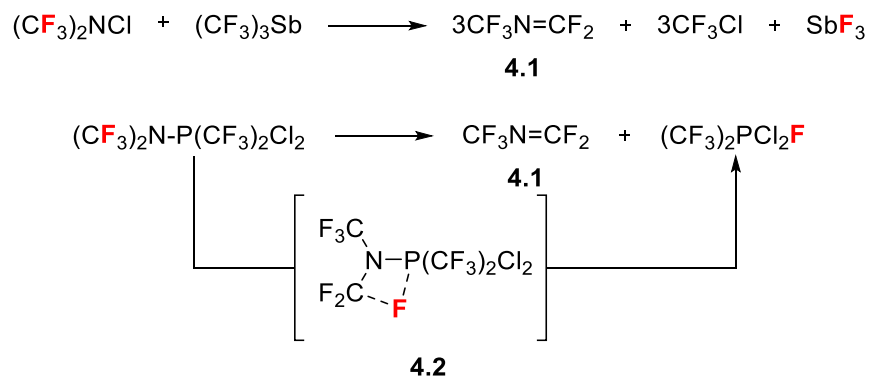


Figure 4.1 Selected fluorinating agents: anhydrous TBAF for nucleophilic fluorination, PhenoFluor™ for deoxyfluorination, Selectfluor® for electrophilic fluorination.

4.1.1 Intramolecular fluorination

The earliest reported examples of proposed, but unconfirmed, intramolecular fluorination appeared in the 1960s. Emeléus *et al.* observed that bis(trifluoromethyl)amino derivatives would react with sulphur, phosphorous and antimony compounds to produce perfluoro-2-azapropene (**4.1**) and other fluorinated derivatives (Scheme 4.1).²¹⁵ The formation of **4.1** was largely attributed to intramolecular fluorine transfer from an unstable intermediate, such as **4.2**, to yield the final product.

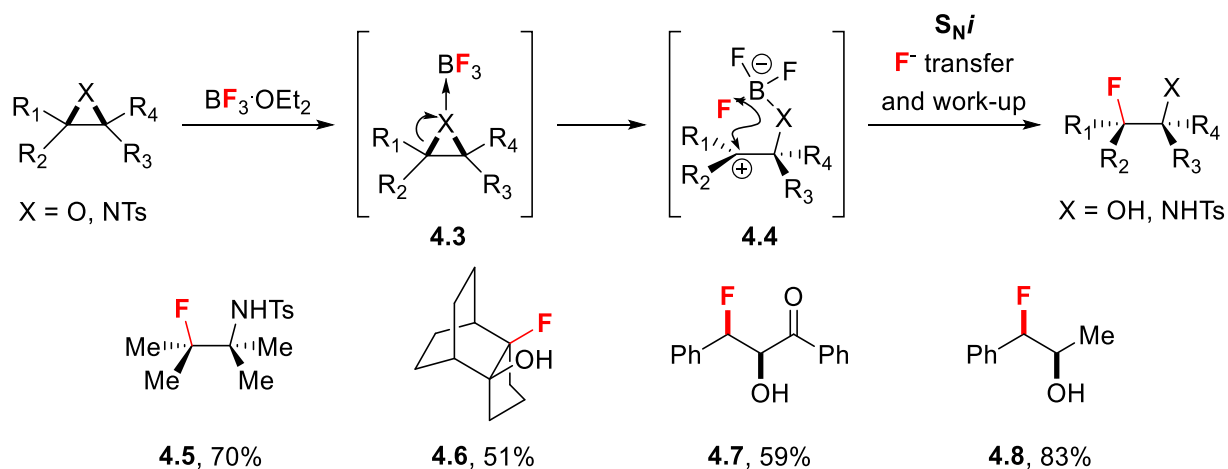


Scheme 4.1 Proposed intramolecular fluorination for the formation of fluorinated derivatives.

4.1.1.1 Intramolecular fluorine transfer to reaction intermediates

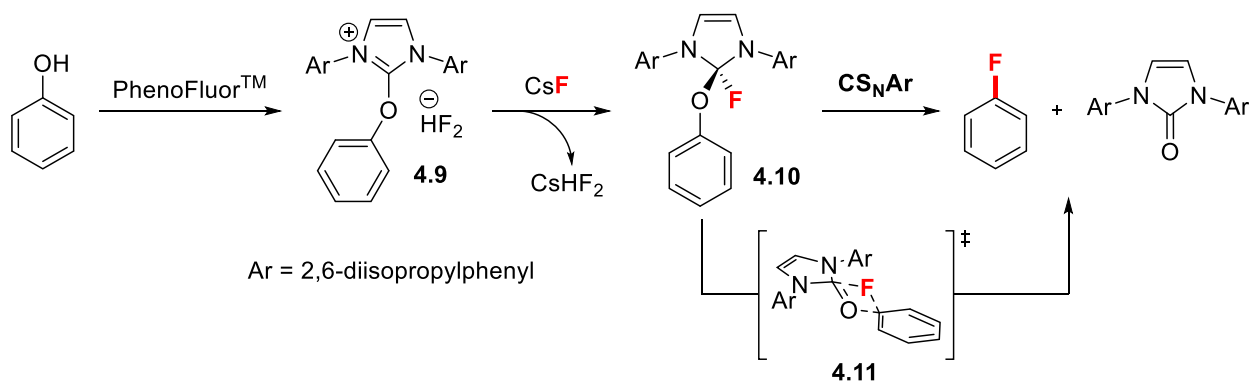
Using exogenous fluorine sources, there are several examples in the literature that strongly support the intramolecular transfer of fluorine to reaction intermediates. Most examples have been observed in the widespread use of $\text{BF}_3 \cdot \text{OEt}_2$ in the Lewis acid

catalysed ring-opening fluorination of strained rings such as epoxides and aziridines to produce *syn*-fluorohydrins and fluoroamines, respectively (Scheme 4.2); $\text{HBF}_4 \cdot \text{OEt}_2$ has also been used in the ring-opening of epoxides.^{3,216,217} The formation of *syn* or *anti* products is largely substrate dependent, where reaction outcomes are determined by the initial configuration of the starting epoxide (cis or trans) as well as the nature of the substituents α to the epoxide ($\text{R}_1\text{-R}_4$). Generally, trans-epoxides with p- or π -electron-donating groups in the α position result in *syn* products.^{3,217} The proposed mechanism implicates the activation of the epoxide or aziridine by lone pair donation into the vacant p-orbital of BF_3 to afford intermediate **4.3** resulting in heterolytic fission of a C-X bond to form carbocation intermediate **4.4**. To account for the formation of *syn*-fluorohydrins and fluoroamines, fluorine transfer is thought to occur via internal nucleophilic substitution ($\text{S}_{\text{N}}\text{i}$). This methodology has allowed access to *syn*-fluoroamine **4.5**,²¹⁸ as well as a wide array of *syn*-fluorohydrins in moderate to good yields (Scheme 4.2; products **4.6**, **4.7** and **4.8**).^{219–221}



Scheme 4.2 Intramolecular fluorine transfer in the synthesis of *syn*-fluorohydrins and fluoroamines.

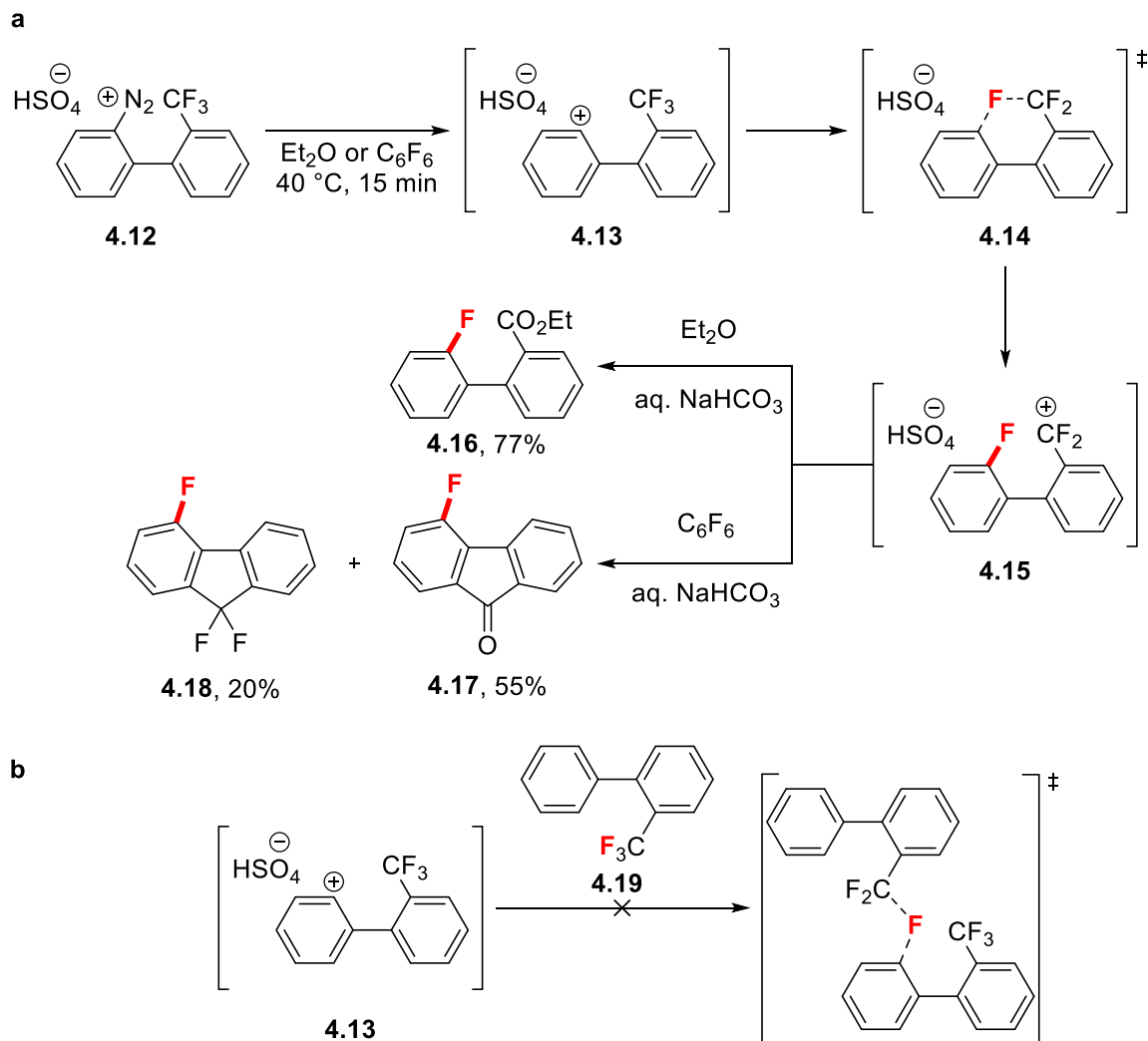
Intramolecular fluorination has also been implicated in the deoxyfluorination of phenols by PhenoFluor™ (Scheme 4.3).^{21,222} Ritter *et al.* propose that the mixture of phenol and PhenoFluor™ forms imidazolium salt **4.9** which, when attacked by fluoride forms tetrahedral intermediate **4.10**. Tetrahedral intermediate **4.10** then undergoes concerted nucleophilic aromatic substitution (CS_NAr) via transition state **4.11** to furnish the aryl fluoride. The structure of the transition state proposed has been supported by DFT calculations that identified a single maximum along the calculated reaction coordinate pathway from **4.10** to products as depicted in Scheme 4.3. These calculations were complemented by experimental verification, intermediate **4.10** was independently synthesized and characterised and could be converted to the aryl fluoride under reaction conditions. The concerted pathway fully accounts for the deoxyfluorination of both electron-rich and electron-poor arenes as opposed to typical nucleophilic aromatic substitution (S_NAr) proceeding via a Meisenheimer complex generally requiring electron-poor arenes.



Scheme 4.3 Proposed mechanism for deoxyfluorination of phenols by PhenoFluor™.

4.1.1.2 Formal intramolecular fluorination

To date, to the best of our knowledge, there is only one example of a formal intramolecular fluorine transfer where the source of fluoride is the starting substrate itself. Lectka *et al.*, in their seminal contribution, reported the first definitive intramolecular fluoride abstraction in solution via an intramolecular Balz-Schiemann type reaction (Scheme 4.4, a).²²³ The authors hypothesised that an aryl cation (**4.13**), generated from thermolysis and extrusion of N₂ from the preceding aryl diazonium salt **4.12**, would be sufficiently reactive that when positioned in close proximity to a C-F bond would allow F⁻ transfer through six-membered transition state **4.14**; intramolecular fluorine transfer generates intermediate benzylic cation **4.15**. In Et₂O, and following basic reaction work-up, ester **4.16** is formed in 77% when run under an O₂ atmosphere. The formation of **4.16** can be rationalized by the trapping of **4.15** by Et₂O forming an oxonium ion which is then hydrolysed upon work-up to the ester. However, reactions in C₆F₆ provided ketone **4.17** in 55% yield, after basic work-up of the reaction mixture; **4.17** is formed from the cyclization of intermediate **4.15** and subsequent hydrolysis. Additionally, trifluoro fluorene **4.18**, the product of cyclization of **4.15**, could be isolated, in 20% yield, along with **4.17** if the reaction mixture was purified directly on neutral alumina avoiding hydrolysis. The proposed mechanism is strongly supported by theoretical calculations that show **4.15** should be more stable than **4.13** by 45 kcal/mol, providing a substantial driving force for intramolecular fluorine transfer. When 2-(trifluoromethyl)biphenyl (**4.19**) was present as an additive during the thermolysis of **4.12** it could be recovered quantitatively indicating that fluorine abstraction does not occur intermolecularly (Scheme 4.4, b).

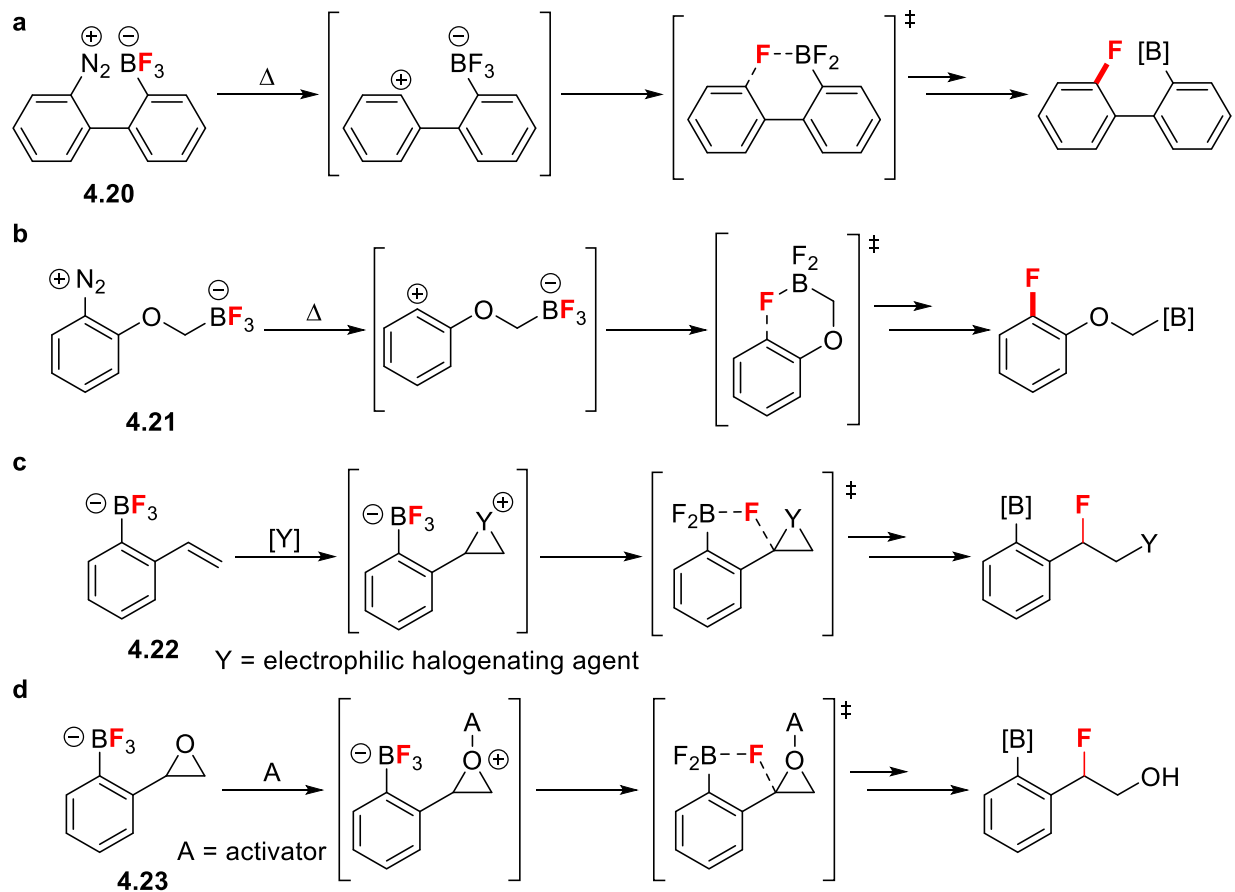


Scheme 4.4 a, proposed intramolecular fluorination mechanism. **b**, experimental evidence for absence of an intermolecular process.

4.1.2 Applying organotrifluoroborates as intramolecular sources of fluoride

The results presented in chapters 2 and 3 have identified organotrifluoroborates as viable fluoride ion sources for intermolecular fluorination. However, given the ability of incorporating trifluoroborate functionality into a diversity of organic scaffolds, we hypothesised that their integration into substrates containing an activated leaving group or functionalisable motif could allow an intramolecular fluorination process to ensue.

Therefore, we identified four substrate scaffolds that should be accessible and of interest to investigate within the context of intramolecular fluorination (Scheme 4.5).



Scheme 4.5 Proposed substrates for intramolecular fluorination with trifluoroborates. [B] = BF_3 , $\text{B}(\text{OR})_2$ (R = H, alkyl).

We thought that organotrifluoroborates would be well suited for intramolecular fluorination via a Balz-Schiemann type reaction. Therefore, we envisioned zwitterionic diazoniobiphenyltrifluoroborate (**4.20**), an analogue of diazonium salt **4.12**, to favour the intramolecular transfer of fluorine via a six-membered ring transition state (Scheme 4.5, **a**). Likewise, zwitterionic **4.21** bearing a methyltrifluoroborate moiety, tethered to the arene ring via either a methylene, ether or thioether linker could allow the intramolecular fluorination to occur in a similar fashion (Scheme 4.5, **b**).

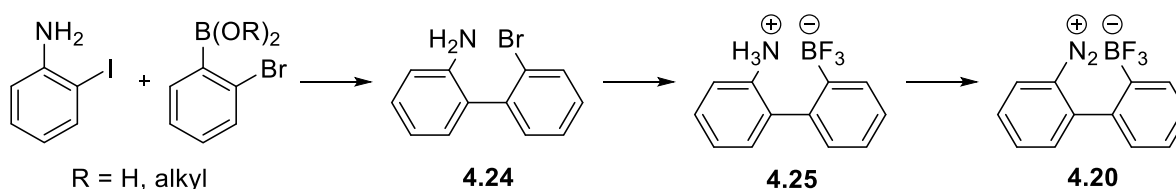
Additionally, on examination of reports utilizing BF_4^- and $\text{BF}_3 \cdot \text{OEt}_2$ as fluorinating agents, we found precedents for intermolecular halofluorination (chloro, bromo and iodo) of alkenes.^{224–228} Incorporating a trifluoroborate functionality in proximity to an alkene, as in scaffolds **4.22**, could allow intramolecular fluorination to occur on a halonium cation intermediate (Scheme **4.5, c**). Finally, **4.23** may allow the intramolecular ring-opening of the epoxide to produce fluorohydrins (Scheme **4.5, d**), analogous to reactivity observed with $\text{BF}_3 \cdot \text{OEt}_2$ (see section **4.1.1.1**). In all cases described above the C-B bond should still be available for further functionalisation via various methodologies.

4.2 Results and Discussion

4.2.1 Synthesis and fluorination studies of substrates for intramolecular Balz-Schiemann type reaction

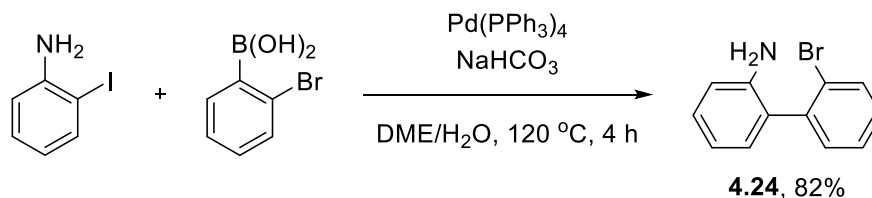
4.2.1.1 Synthesis of zwitterionic 2-diazonio-2-trifluoroboratebiphenyl **4.20**

We began the investigation by attempting to synthesize biphenyl substrate **4.20** (Scheme **4.6**). We envisioned accessing **4.20** over three synthetic steps (Scheme **4.6**), the initial biphenyl system (**4.24**) constructed through transition metal-catalysed cross-coupling of two appropriate aryl fragments. Borylation could then occur via metal-catalysis or lithium-halogen exchange, with subsequent conversion to the zwitterionic trifluoroborate (**4.25**). Finally, diazotization of **4.25** would furnish zwitterionic **4.20**.



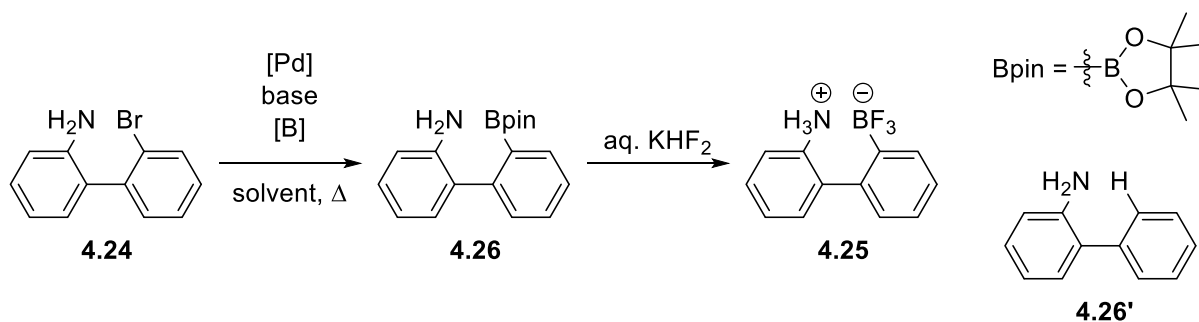
Scheme 4.6 Planned synthesis for substrate **4.20**.

The biphenyl system was easily obtained in good yield through Suzuki-Miyaura cross-coupling of 2-iodoaniline and 2-bromophenylboronic acid to produce 2'-bromo-[1,1'-biphenyl]-2-amine **4.24** (Scheme 4.7).



Scheme 4.7 Synthesis of **4.24** via Suzuki-Miyaura cross-coupling. Isolated yield.

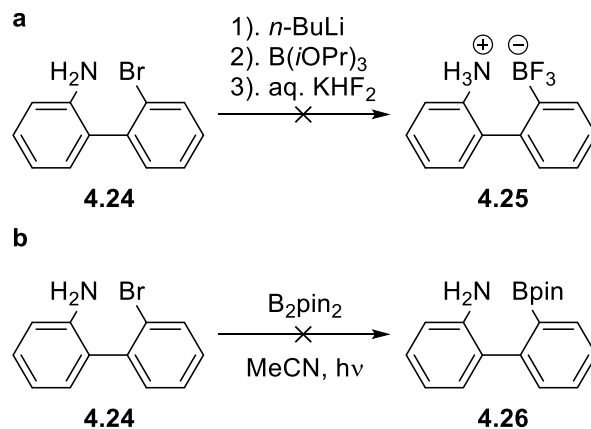
We next turned our attention towards the borylation step. When **4.24** was submitted to classical Miyaura borylation conditions we could not detect formation of the borylated product (**4.26** or **4.25**) by ¹¹B NMR spectroscopy or MS (Table 4.1, entries 1-3). We found only one instance in the literature for the borylation of substrate **4.24**, wherein the authors report the preparation of **4.26** in 74% using bis(pinacolato)diboron, catalysed by [PdCl₂(PPh₃)₂] in PEG 600 as the solvent.²²⁹ However, in our hands this protocol could not be reproduced; no trace of borylated product could be detected by ¹¹B NMR spectroscopy or MS (Table 4.1, entry 4). Additionally, microwave heating of the reaction mixture did not promote borylation (Table 4.1, entries 5 and 6). While quantitative conversion of starting material to a different product was verified by TLC for most reactions, ¹H NMR spectroscopic analysis of reaction crudes and isolated reaction products suggested that protodebrominated **4.26'** was the major reaction product. This is supported by the observation that only BF₄⁻ could be detected by ¹⁹F and ¹¹B NMR spectroscopy when crude borylation reaction mixtures were submitted to trifluoroborate forming conditions (aq. KHF₂).

Table 4.1 Borylation reaction conditions for the formation of **4.26** and **4.25**

Entry	Base	[Pd]	Solvent	Temperature (°C)	[B]	4.26 or 4.25 formation?
1	NaOAc	$[\text{PdCl}_2(\text{PPh}_3)_2]$	DMF	90	B_2pin_2	no
2	NEt_3	$[\text{PdCl}_2(\text{dppf})]\cdot\text{CH}_2\text{Cl}_2$	1,4-dioxane	100	HBpin	no
3	NaOAc	$[\text{PdCl}_2(\text{dppf})]\cdot\text{CH}_2\text{Cl}_2$	1,4-dioxane	110	B_2pin_2	no
4	NaOAc	$[\text{PdCl}_2(\text{PPh}_3)_2]$	PEG 600	90	B_2pin_2	no
5 ^a	NEt_3	$[\text{PdCl}_2(\text{dppf})]\cdot\text{CH}_2\text{Cl}_2$	1,4-dioxane	100	HBpin	no
6 ^a	NEt_3	$[\text{PdCl}_2(\text{dppf})]\cdot\text{CH}_2\text{Cl}_2$	Toluene	120	HBpin	no

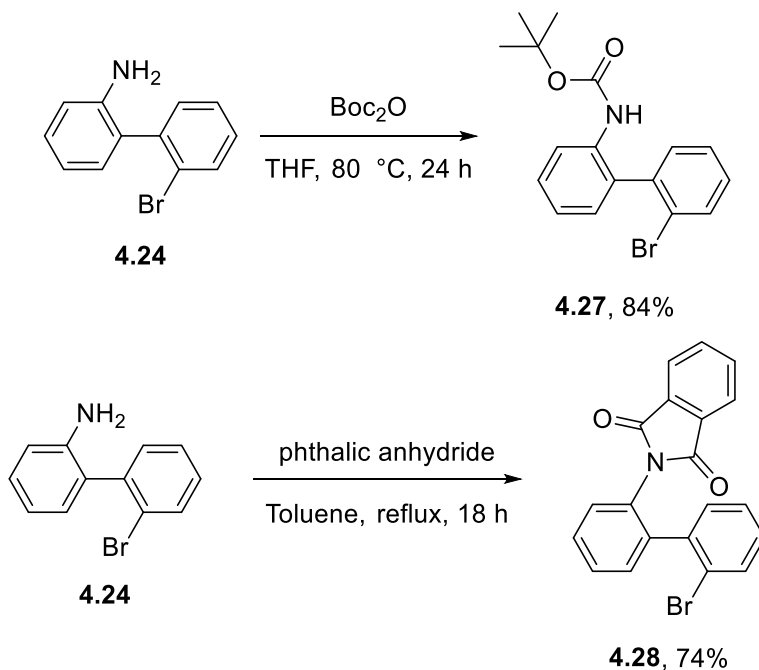
^a microwave heating

Attempts to borylate **4.24** via lithium-halogen exchange and trapping with $\text{B}(i\text{OPr})_3$ failed (Scheme **4.8, a**). Similarly, no borylated product could be detected via reported photoinduced borylation protocols (Scheme **4.8, b**).²³⁰



Scheme 4.8 Attempted borylation of **4.24** via **a**, lithium-halogen exchange. **b**, photolysis.

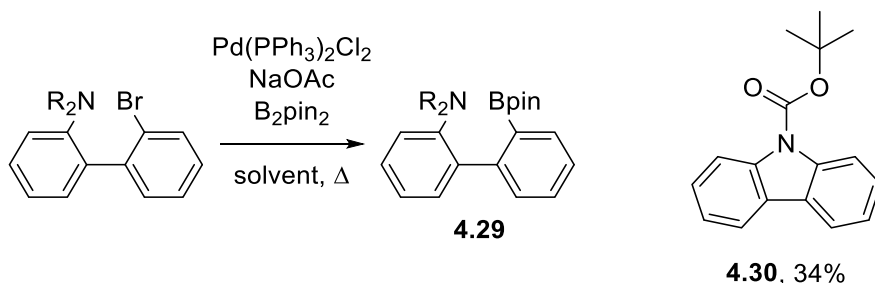
At this juncture we thought that perhaps issues in reactivity were due to the presence of an unprotected amine functionality, which may interfere in the catalytic cycle or participate in proton exchange processes with a lithiated species. Therefore, we proceeded to protect the amine functionality as *t*-butyl carbamate **4.27** or phthalimide **4.28** (Scheme **4.9**).



Scheme 4.9 Protection of **4.24** as carbamate **4.27** or phthalimide **4.28**. Isolated yields.

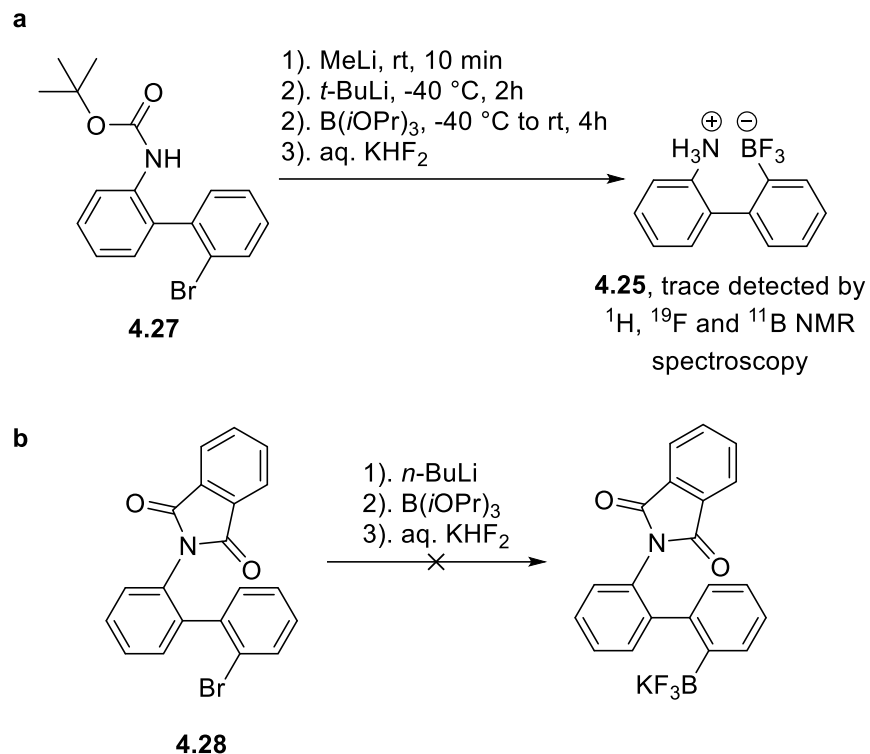
Subjecting **4.27** or **4.28** to classical Miyaura coupling conditions did not result in the formation of any borylated product as indicated by ^{11}B NMR spectroscopy and MS (Table **4.2**, entries 1 and 2). In fact, under reaction conditions **4.27** intramolecularly cyclised to produce *N*-Boc-carbazole **4.30** in 34% (Table **4.2**, entry 1).

Table 4.2 Attempted Pd-catalysed borylation of *N*-protected substrates **4.27** and **4.28**. Isolated yield of **4.30**



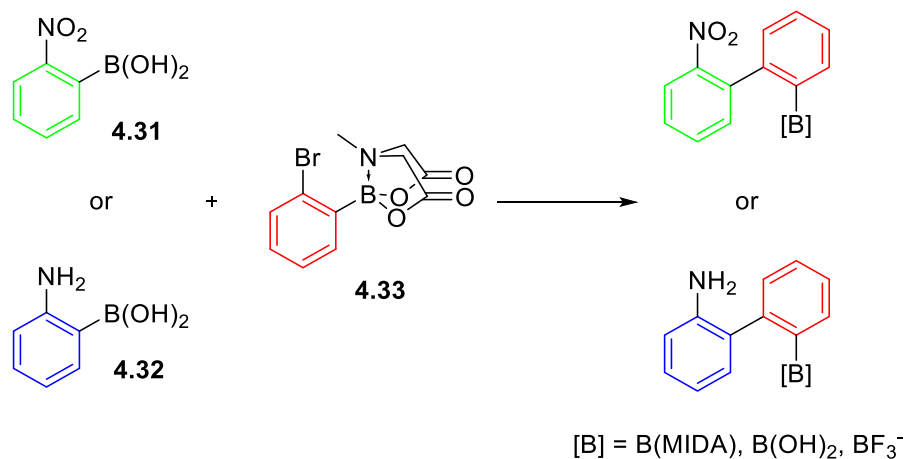
Entry	Substrate	[Pd]	Solvent	Temperature (°C)	4.29 formation?
1	4.27	$[\text{PdCl}_2(\text{PPh}_3)_2]$	1,4-dioxane	100	no, 4.30
2	4.28	$[\text{PdCl}_2(\text{PPh}_3)_2]$	DMF	90	no

N-Boc protected **4.27** did however allow borylation via lithium-halogen exchange as trace amounts of the desired zwitterion **4.25** could be observed after work-up of the crude reaction mixture (Scheme **4.10**, **a**). Efforts to borylate **4.28** under lithium-halogen exchange conditions did not result in any observable product formation (Scheme **4.10**, **b**).



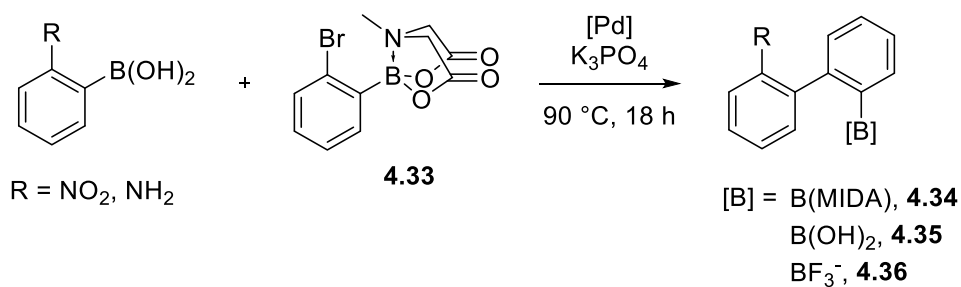
Scheme 4.10 Attempted borylation of **4.28** (a) and **4.29** (b) via lithium-halogen exchange.

Given our unsuccessful attempts to borylate the biphenyl system we sought to integrate the desired boron fragment in the first synthetic step. We hypothesised that this could be accomplished by re-examining the substitution of the coupling partners in the synthesis of the biphenyl fragment. Using the methodology developed by Burke *et al.*²³¹ a boronic acid can be effectively rendered unreactive towards Suzuki-Miyaura coupling conditions by rehybridizing the boron centre from sp^2 , the hybridization of boronic acids and esters, to sp^3 using methyliminodiacetic acid (MIDA) as a trivalent ligand for boron. We therefore proposed that the biphenyl fragment could be synthesized by the Suzuki-Miyaura cross-coupling of 2-nitrophenylboronic acid (**4.31**) or 2-aminophenylboronic acid (**4.32**) and 2-bromophenylboronic acid MIDA ester (**4.33**) (Scheme 4.11).



Scheme 4.11 Proposed synthesis of biphenyl scaffold using **4.33**.

We started by applying reaction conditions first developed by Burke *et al.*²³¹ which should allow formation of biphenyl **4.34** (Table **4.3**). However, in our hands the desired product could not be detected by TLC or NMR spectroscopy whether the nitro or amino boronic acid was used (Table **4.3**, entries 1-3). Coupling conditions described by Watson *et al.*²³²⁻²³⁵ which should have delivered boronic acid **4.35**, were then tested (Table **4.3**, entries 4-7). Unfortunately, no desired product could be detected by ¹¹B NMR spectroscopy or MS, microwave heating had no effect on the transformation (Table **4.3**, entries 5 and 7). When reaction crudes were treated with aq. KHF₂ trace amounts of desired trifluoroborate **4.36** could be detected only when 2-nitrophenylboronic acid was used (Table **4.3**, entry 8). The use of potassium 2-nitrophenyltrifluoroborate did not improve yields as only trace amounts of the desired product were observed; ¹H, ¹⁹F and ¹¹B NMR spectroscopy and MS indicated that the recovered residue was mostly unreacted trifluoroborate.

Table 4.3 Cross-coupling conditions for synthesis of biphenyl fragment using **4.33**

Entry	R	Catalyst	Solvent	Work-up	Coupling product formed?
1	NO ₂	Pd(OAc) ₂ , SPhos	THF	-	no
2	NO ₂	[Pd ₂ (dba) ₃]·CHCl ₃ , SPhos	THF	-	no
3	NH ₂	Pd(OAc) ₂ , SPhos	THF	-	no
4	NO ₂	[PdCl ₂ (dppf)]·CH ₂ Cl ₂	THF/H ₂ O	-	no
5 ^a	NO ₂	[PdCl ₂ (dppf)]·CH ₂ Cl ₂	THF/H ₂ O	-	no
6	NH ₂	[PdCl ₂ (dppf)]·CH ₂ Cl ₂	THF/H ₂ O	-	no
7 ^a	NH ₂	[PdCl ₂ (dppf)]·CH ₂ Cl ₂	THF/H ₂ O	-	no
8	NO ₂	[PdCl ₂ (dppf)]·CH ₂ Cl ₂	THF/H ₂ O	aq. KHF ₂	trace 4.36 detected by MS
9	NH ₂	[PdCl ₂ (dppf)]·CH ₂ Cl ₂	THF/H ₂ O	aq. KHF ₂	no
10 ^b	NO ₂	[PdCl ₂ (dppf)]·CH ₂ Cl ₂ , SPhos	THF/H ₂ O	aq. KHF ₂	trace 4.36 detected by MS

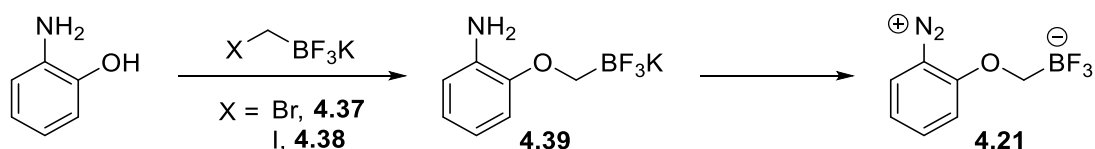
^a microwave heating. ^b potassium 2-nitrophenyltrifluoroborate used.

Having exhausted synthetic efforts and in the interest of time we decided to abandon the pursuit of further strategies towards obtaining biphenyl scaffold **4.20**.

4.2.1.2 Synthesis and fluorination studies of zwitterionic (2-diazoniophenoxy)methyltrifluoroborate 4.21

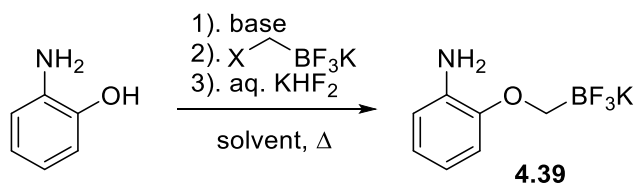
4.2.1.2.1 Synthesis of 4.21

We planned to prepare **4.21** over two synthetic steps, starting with the alkylation of 2-aminophenol with potassium halomethyltrifluoroborate (**4.37** or **4.38**) to provide **4.39** which can then be diazotized to afford zwitterion **4.21** (Scheme 4.12).



Scheme 4.12 Proposed synthesis of **4.21**.

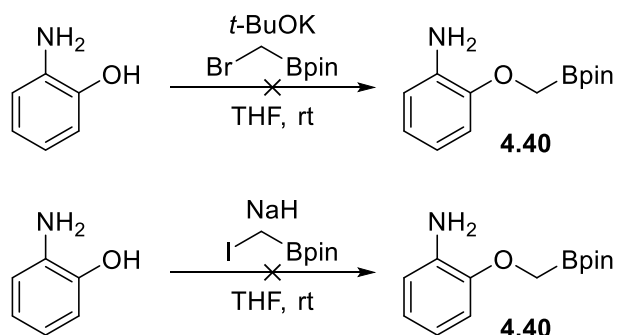
Molander *et al.* were the first to describe the alkylation of various substrates with **4.37**.²³⁶ However, under standard reported conditions we could not detect the formation of desired product **4.38** (Table 4.4, entry 1). Changing reaction conditions (i.e. solvent, base, temperature) generally had no effect on reaction transformations, at best trace amounts of **4.39** could be detected by MS. Attempts to drive the reaction forward by precipitation of halide salts (AgBr or KBr) were generally ineffective giving only trace yields of **4.39** (Table 4.4, entries 2-5). No improvements were observed using strong bases KH and *n*-BuLi (Table 4.4, entries 3 and 6). Using the more electrophilic potassium iodomethyltrifluoroborate (**4.38**) did not result in any improvement in conversions (Table 4.4, entries 12-19). Additives, such as TBAI and 15-crown-5 were explored in attempts to increase solvation and reactivity of the intermediate phenoxide ion however, these additives had no effect on reaction yields (Table 4.4, entries 3, 13 and 14).

Table 4.4 Conditions tested for the alkylation of 2-aminophenol

Entry	X	Solvent	Base	Temperature (°C)	Additive	4.39 formed?
1	Br	THF	NaH	rt	-	no
2	Br	THF	NaH	rt	AgOTf	no
3	Br	THF	KH	rt	TBAI	no
4	Br	THF	<i>t</i> -BuOK	50	AgOTf or AgOAc	trace
5	Br	DMF	<i>t</i> -BuOK	50	AgOTf or AgOAc	trace
6	Br	THF	<i>n</i> -BuLi	-78 to rt	-	no
7	Br	DMF	NaH	90	-	trace
8	Br	Acetone	K ₂ CO ₃	reflux	-	no
9	Br	THF	<i>t</i> -BuOK	rt	-	no
10	Br	THF	<i>t</i> -BuOK	reflux	-	trace
11	Br	DMF	<i>t</i> -BuOK	90	-	no
12	I	THF	<i>t</i> -BuOK	rt	-	no
13	I	THF	<i>t</i> -BuOK	rt	TBAI	no
14	I	THF	NaH	rt	15-crown-5	no
15	I	DMF	<i>t</i> -BuOK	rt	-	no
16	I	THF	<i>t</i> -BuOK	reflux	-	no
17	I	DMF	<i>t</i> -BuOK	50	-	no
18 ^a	I	THF	<i>t</i> -BuOK	110	-	no
19 ^a	I	DMF	<i>t</i> -BuOK	120	-	trace

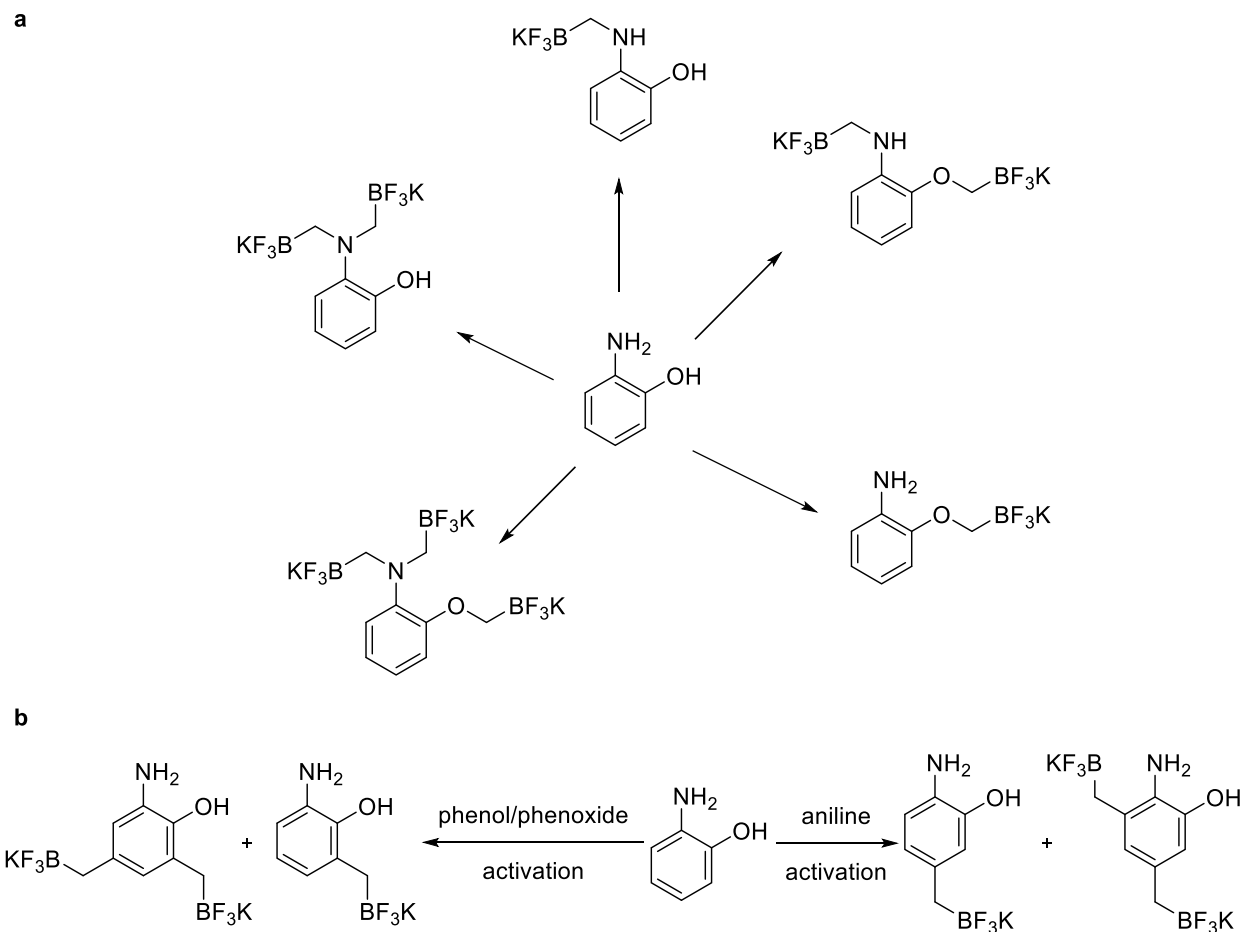
^a pressure vial used.

Similarly, attempts to alkylate 2-aminophenol with electrophilic bromo or iodomethylboronic acid pinacol ester did not work. The expected product **4.40** could not be detected by ^{11}B NMR spectroscopy or MS (Scheme **4.13**).



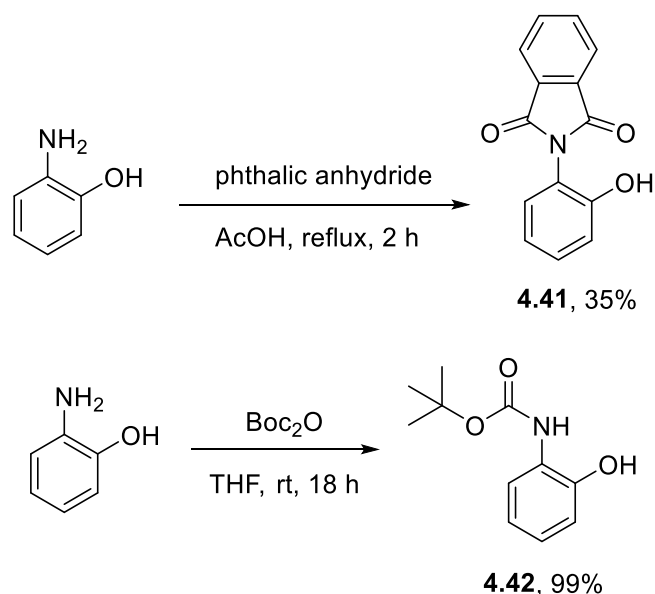
Scheme 4.13 Failed alkylation using boronic ester.

We hypothesised that poor reaction transformations were a result of the electron-rich nature of 2-aminophenol and the multiple alkylation sites available. Aminophenols are known to undergo, often unselective, *N*-, *O*- and *N,O*-dialkylation with alkyl halides under standard reaction conditions.²³⁷ The presence of multiply alkylated products under reaction conditions was confirmed by ^{19}F NMR spectroscopy of crude reaction mixtures in which we observed several peaks corresponding to B-F_n species (Scheme **4.14, a**). Additionally, given the presence of two strongly activating groups ($-\text{OH}$ or $-\text{O}^-$ and $-\text{NH}_2$) on the aromatic ring electrophilic aromatic substitution (EAS) processes may become viable in both the presence (BF_3 from heterolytic fission of C-B bond) and absence of a Lewis acid catalyst resulting in the single or multiple alkylation of the aromatic ring by methyltrifluoroborate (Scheme **4.14, b**).²³⁷



Scheme 4.14 Possible 2-aminophenol alkylation pathways. **a**, multiple *N*- and *O*-alkylation. **b**, EAS alkylation of aromatic ring.

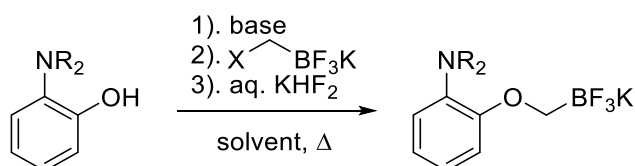
With the possibility of one or a combination of these pathways being responsible for the poor conversions observed we thought that masking both the nucleophilicity and activation ability of the amino functionality may lead to improved *O*-alkylation. Therefore, 2-aminophenol was *N*-protected as phthalimide (**4.41**) and *t*-butyl carbamate (**4.42**), which have been previously used in selective *O*-alkylation strategies.



Scheme 4.15 N-protection of 2-aminophenol as phthalimide **4.41** and carbamate **4.42**. Isolated yields.

However, attempted alkylations of both **4.41** and **4.42** only resulted in trace yields of the desired product detected by MS (Table **4.5**, entries 2, 3 and 7).

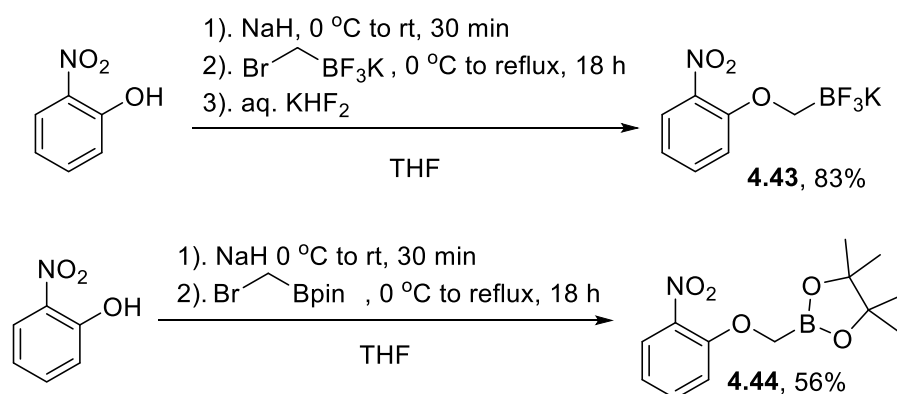
Table 4.5 Attempted alkylation of N-protected aminophenols **4.41** and **4.42**



Entry	Substrate	X	Solvent	Base	Temperature (°C)	Additive	O-alkylated product?
1	4.41	Br	THF	NaH	rt	-	no
2	4.41	Br	THF	<i>t</i> -BuOK	reflux	-	trace
3	4.41	I	Acetone	K ₂ CO ₃	reflux	-	trace
4	4.41	I	THF	NaH	reflux	-	no
5	4.41	I	THF	NaH	rt	15-crown-5	no

6	4.42	I	THF	NaH	rt	-	no
7	4.42	I	THF	NaH	reflux	-	trace

Given these results we sought to further deactivate the aromatic ring and chose to investigate the effect of substituting the amino group for nitro, which could be reduced back to the amine after alkylation. Gratifyingly, deprotonation of 2-nitrophenol with NaH in THF followed by the addition of trifluoroborate **4.37** and refluxing overnight allowed the recovery of mono O-alkylated trifluoroborate **4.43** in excellent yield (Scheme **4.16**). Alkylation could also be achieved using bromomethylboronic acid pinacol ester to produce nitrobenzene derivative **4.44** with albeit lower yields (Scheme **4.16**).

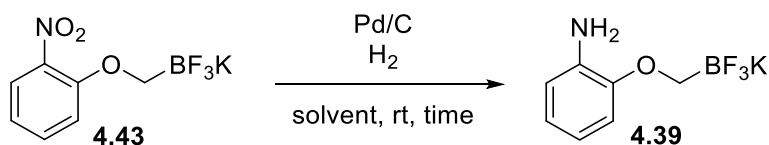


Scheme 4.16 Synthesis of **4.43** and **4.44** by alkylation of 2-nitrophenol. Isolated yields.

With **4.43** in hand, we turned towards optimising conditions for reduction of the nitrobenzene derivative into the corresponding aniline **4.39**. We thought that heterogenous reduction of the nitro group by Pd/C and H₂ would allow for a clean transformation and simplify reaction work-up. When MeOH was used as reaction solvent, complete conversion of **4.43** was observed by TLC after 30 min, work-up of the reaction crude yielded **4.39** in 67% as a mixture of inseparable impurities observed by ¹H, ¹⁹F and

^{11}B NMR spectroscopy (Table 4.6, entry 1). Degradation of 4.43 may arise from hydrolysis of the trifluoroborate to the boronic acid and eventual deborylation via transmetalation with Pd. We thought hydrolysis could be disfavoured in the presence of high concentrations of F^- in the reaction medium. Consequently, when a homogenous solution of MeOH and saturated aqueous KHF_2 (4.5 M) was used as the reaction solvent 4.39 could be cleanly isolated in quantitative yield (Table 4.6, entry 2). When reaction pH was decreased to ~ 1 using 1N HCl, yields decreased and inseparable impurities were observed by ^1H , ^{19}F and ^{11}B NMR spectroscopy (Table 4.6, entry 3). Reduction was equally efficient in EtOH, however slightly longer reaction times were required for complete conversion (Table 4.6, entry 4). Extended reaction times led to a decrease in yields, most probably due to Pd-mediated deborylation, therefore reaction mixtures need to be worked-up once complete conversion of starting material is determined.

Table 4.6 Optimisation of parameters for the reduction of 4.43



Entry	Solvent	Time (h)	Yield (%)
1 ^a	MeOH	0.5	67
2	MeOH/aq. KHF_2 (20:1)	1	99
3 ^a	MeOH/aq. KHF_2 + 1N HCl (10:1)	1	84
4	EtOH/aq. KHF_2 (10:1)	1.5	99

^a product isolated with inseparable impurities.

The retention of the trifluoroborate moiety after reduction was verified through ^1H - ^{19}F Heteronuclear Multiple Bond Correlation (HMBC) NMR spectroscopy, which showed a correlation between the ether methylene protons and the fluorine atoms on boron (Figure 4.2).

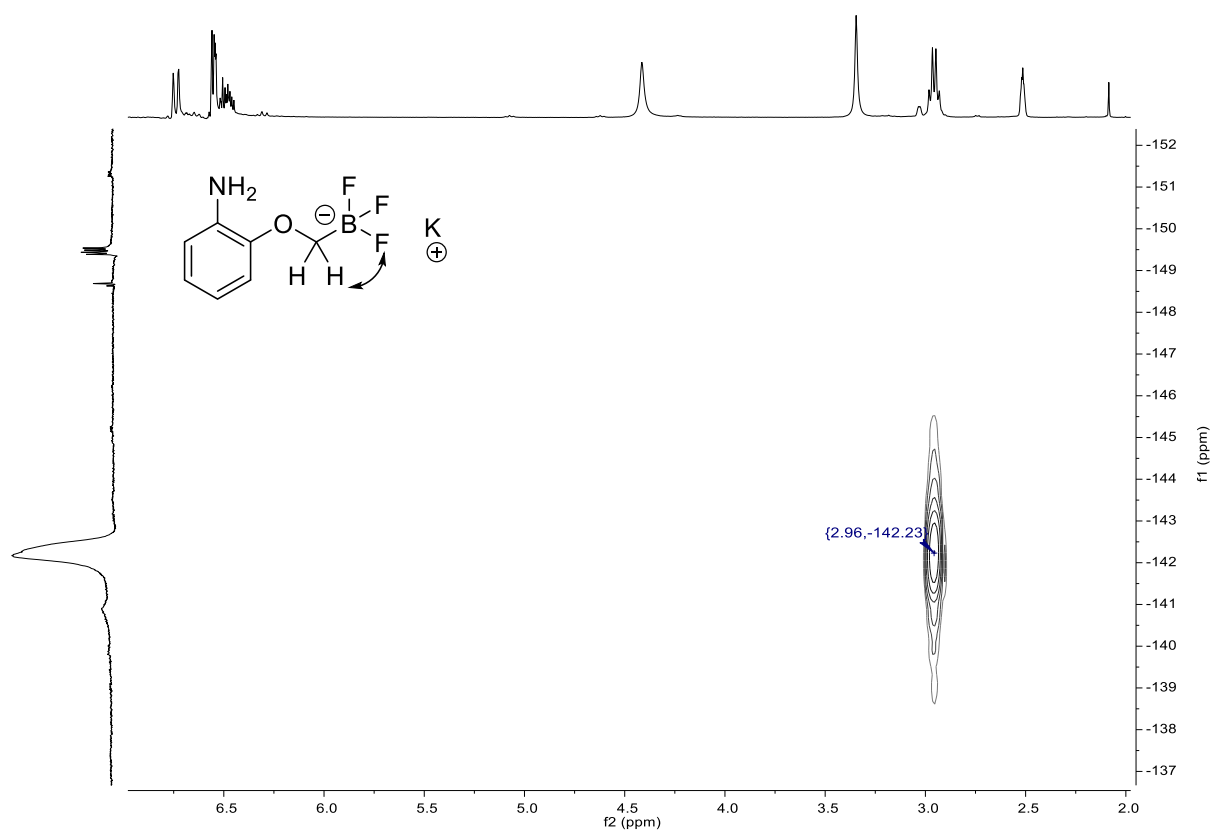
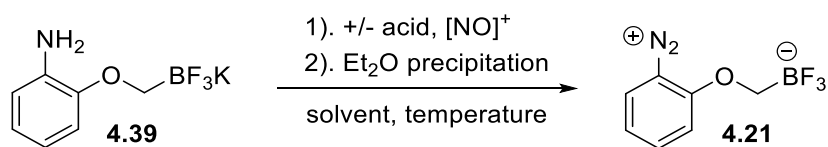


Figure 4.2 ^1H - ^{19}F HMBC NMR spectroscopy showing the correlation between methylene protons and fluorine atoms in **4.39**.

With this key starting material in hand, we could now turn our focus towards the last synthetic step, the diazotization of aniline **4.39** to the zwitterionic diazoniotrifluoroborate **4.21**. We initially attempted diazotization in acidic water using aqueous KHF_2 to disfavor hydrolysis of the trifluoroborate, the addition of NaNO_2 caused immediate gas evolution (N_2) which subsided after 5 minutes. TLC of the reaction mixture showed a complex

mixture of products, the desired product could not be detected by ^{19}F and ^{11}B NMR spectroscopy and MS (Table 4.7, entry 1). Diazotization in organic solvents in the absence (Table 4.7, entries 2-5) and presence of acid (entry 6) did not yield 4.21. However, conducting the diazotization at low temperature ($-40\text{ }^\circ\text{C}$) in MeCN using *p*-TsOH as an acid was successful, although the desired product precipitated along with inseparable impurities (Table 4.7, entry 7). Similar impurities were observed when isolation of the product was attempted by cold precipitation, impurities could not be removed by Silica gel flash column chromatography; 4.21 was found to be stable under purification conditions (Table 4.7, entry 8). During experiments, we had observed that *t*-BuONO, synthesized or purchased, was acidic (pH \sim 4-5) likely due to its slow hydrolysis into nitrous acid (HONO) and *t*-BuOH.²³⁸ The presence of additional equivalents of acid (HONO) could be causing the observed impurities and degradation products. Gratifyingly, when *t*-BuONO was neutralized by basic aqueous wash then dried (anhydrous MgSO_4) prior to use, 4.21 could be obtained cleanly after cold precipitation, albeit in moderate yield (Table 4.7, entry 9).

Table 4.7 Optimisation of parameters for the diazotization of 4.39



Entry	Solvent	[NO] ⁺	Acid	Temperature (°C) ^a	Yield (%)
1	Water	NaNO_2	KHF_2/HCl	0	0
2	THF	<i>t</i> -BuONO	-	0	0
3	AcOH	<i>t</i> -BuONO	-	0	0
4	1,4-dioxane	<i>t</i> -BuONO	-	0	0

5	MeCN	<i>t</i> -BuONO	-	0	0
6	MeCN	<i>t</i> -BuONO	<i>p</i> -TsOH	0	0
7 ^b	MeCN	<i>t</i> -BuONO	-	-40	>99% (impure)
8 ^{b,c}	MeCN	<i>t</i> -BuONO	<i>p</i> -TsOH	-40, precipitation at -40	>99% (impure)
9 ^d	MeCN	<i>t</i> -BuONO	<i>p</i> -TsOH	-40, precipitation at -40	31

^a Et₂O precipitation was conducted at rt, unless otherwise indicated. ^b precipitate contained **4.21** along with inseparable impurities. ^c attempted purification of precipitated crude by Silica gel flash chromatography. ^d *t*-BuONO washed with saturated aqueous NaHCO₃ and dried over anhydrous MgSO₄ immediately prior to use.

The formation of **4.21** was characterised by ¹H, ¹⁹F and ¹¹B NMR and IR spectroscopy, and HRMS. Formation of the diazo moiety was apparent by IR as the amine N-H stretching and bending bands disappear and are replaced by a prominent peak at 2273 cm⁻¹ corresponding to N-N triple bond stretching (Figure 4.3).²³⁹

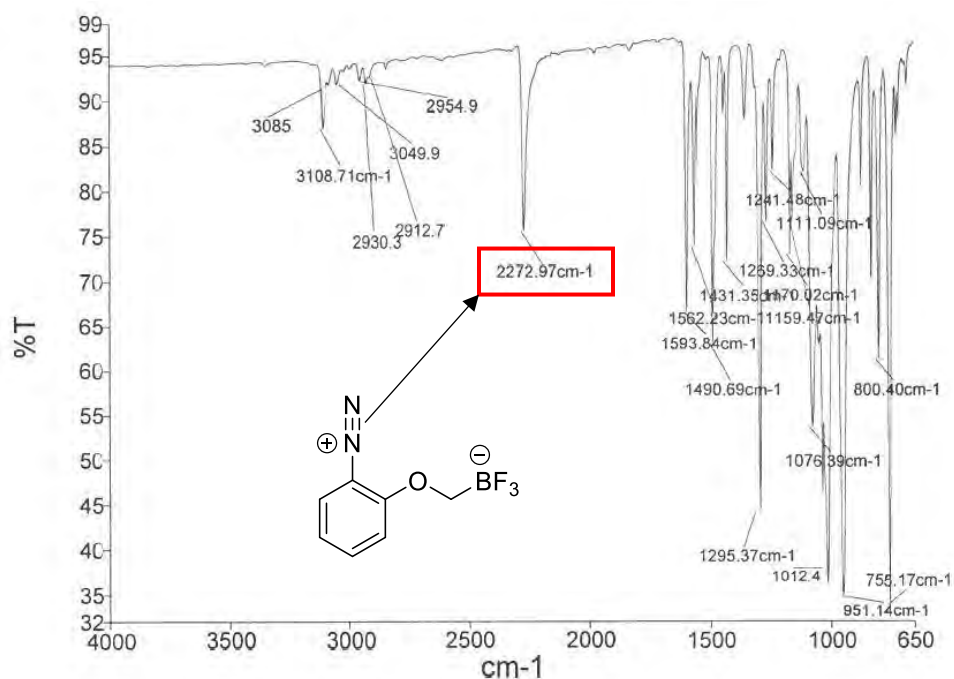


Figure 4.3 ATR IR spectrum of **4.21**.

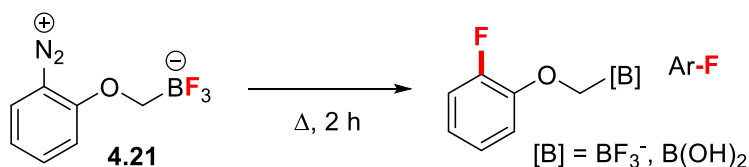
4.2.1.2.2 Fluorination studies of **4.21**

We studied the decomposition of **4.21** in a variety of solvents at low and elevated temperatures. We initially started by investigating the low temperature (45 °C) decomposition of **4.21** in a variety of solvents. Low conversions of **4.21** were observed in non-polar solvents hexane, cyclohexane and 1,2-dichlorobenzene (Table **4.8**, entries 1, 3 and 4); however, no fluorinated products could be observed by ^{19}F NMR spectroscopy. When toluene was used as the reaction solvent, no conversion of **4.21** was observed by ^{19}F NMR spectroscopy (Table **4.8**, entry 2). Similarly, low conversions with no fluorination products were also observed when more polar ethereal solvents were used (Table **4.8**, entries 5-8). Using HFIP resulted in 86% conversion of **4.21** without the formation of fluorinated products; significant deborylation producing BF_4^- was observed by ^{19}F NMR spectroscopy (Table **4.8**, entry 9). High stability was also observed in MeCN, where only 3% of **4.21** was converted (Table **4.8**, entry 11). Ethylene glycol resulted in complete degradation of **4.21** (Table **4.8**, entry 12).

Given the low conversions observed at 45 °C we thought that elevated decomposition temperatures may encourage the fluorodediazoniatio step to occur. Decomposition in toluene and 1,2-dichlorobenzene at 100 °C resulted in complete conversion of **4.21** accompanied by trace (~5%) yields of the desired 2-fluoroanisole derivative (Table **4.8**, entries 13 and 16). ^{19}F NMR spectroscopy revealed a multiplet at -136.7 ppm which corresponds well with literature reports for 2-fluoroanisole at -135 ppm.^{240,241} However, yields could not be improved by increasing reaction temperatures to 120 °C (entries 14 and 17). Conversely, in cyclohexane **4.21** displayed remarkable stability after 2h at 100 °C where only 24% conversion was observed (Table **4.8**, entry 15). All other solvents

tested resulted in complete degradation of the starting material (Table 4.8, entries 18-23). Heating 4.21 neat resulted in complete conversion with only trace yield of the 2-fluoroanisole derivative (Table 4.8, entry 24).

Table 4.8 Decomposition conditions for intramolecular fluorination of 4.21

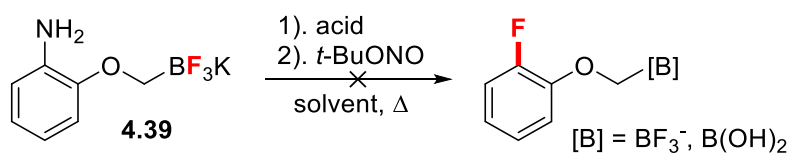


Entry	Solvent	Temperature (°C)	Conversion of 4.21 (%) ^a	Yield of Ar-F (%) ^a
1	Hexane	45	26	0
2	Toluene	45	<1	0
3	Cyclohexane	45	33	0
4	1,2-dichlorobenzene	45	19	0
5	Et ₂ O	45	50	0
6	THF	45	13	0
7	1,4-dioxane	45	10	0
8	1,2-dimethoxyethane	45	24	0
9	HFIP	45	86	0
10	<i>t</i> -BuOH	45	23	0
11	MeCN	45	3	0
12	Ethylene glycol	45	>99	0
13	Toluene	100	>99	5
14	Toluene	120	>99	5
15	Cyclohexane	100	24	0
16	1,2-dichlorobenzene	100	>99	5
17	1,2-dichlorobenzene	120	>99	4

18	1,4-dioxane	100	>99	0
19	1,2-dimethoxyethane	100	>99	0
20	<i>t</i> -BuOH	100	>99	0
21	<i>t</i> -BuOH	120	>99	0
22	MeCN	100	>99	0
23	Ethylene glycol	100	>99	0
24	-	100	>99	2

^a determined by ¹⁹F NMR spectroscopy using 2,4-dinitrofluorobenzene as an internal standard.

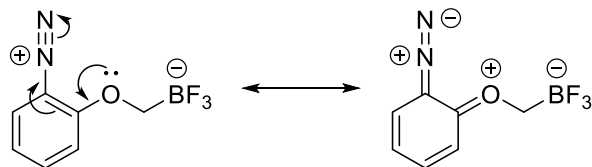
We also attempted to fluorinate aniline **4.39** in a one-pot two-step method, following conditions described in chapter 2; however, this only led to complete degradation of the starting material and no fluorinated products could be detected, as observed by ¹⁹F NMR spectroscopy (Scheme **4.17**).



Scheme 4.17 Attempted one-pot two step fluorination of **4.39**.

4.2.1.2.3 Discussion of results with **4.21**

Generally, reactions at low temperatures resulted in low conversions of **4.21**, decreased rates of dediazonation could be explained by resonance stabilization of the diazonium cation (Scheme **4.18**).^{140,242}



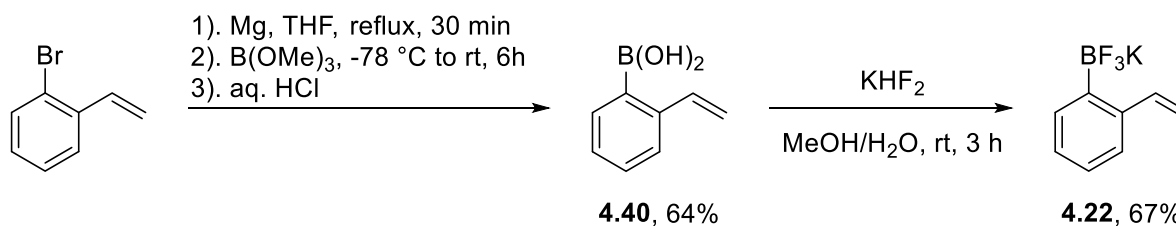
Scheme 4.18 Resonance stabilization of **4.21**.

When reaction temperatures were increased complete conversion of **4.21** was observed in all cases but one and, at best, trace yields of 2-fluoroanisole were detected in toluene and 1,2-dichlorobenzene as reaction solvents. ^{19}F NMR spectroscopic analysis of these reaction crudes revealed complete absence of signals that could be attributed to a trifluoroborate functionality and a prominent peak corresponding to BF_4^- indicating significant deborylation under reaction conditions. With this in mind, it is important to note that we cannot exclude the attribution of trace yields observed to fluorination by BF_4^- . Based on these results it can be concluded that **4.21** is not a suitable scaffold for the intramolecular transfer of fluorine to an aryl cation.

4.2.1.3 Synthesis and fluorination studies of styrene derivative **4.22**

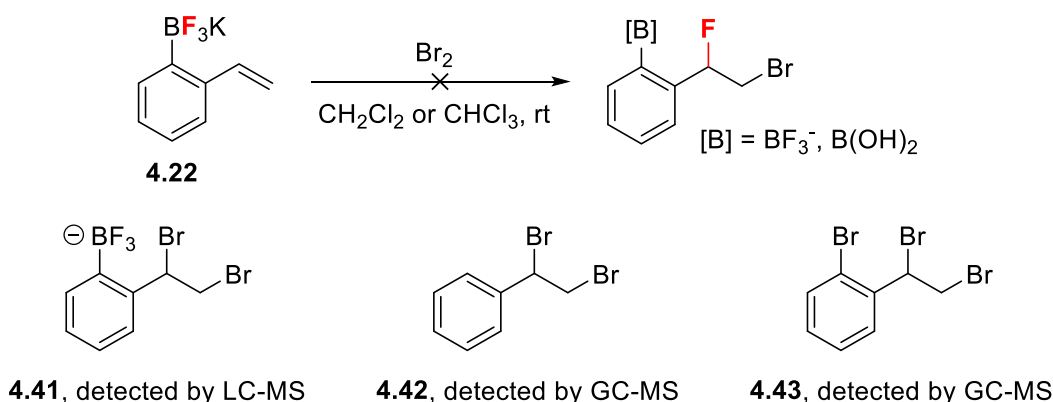
Experimental work using substrate **4.22** and NBS was performed by Samson Lai, an undergraduate student under my supervision.

Potassium 2-vinylphenyltrifluoroborate (**4.22**) was obtained over two steps in moderate yield (Scheme **4.19**).



Scheme 4.19 Synthesis of styrene derivative **4.22**.

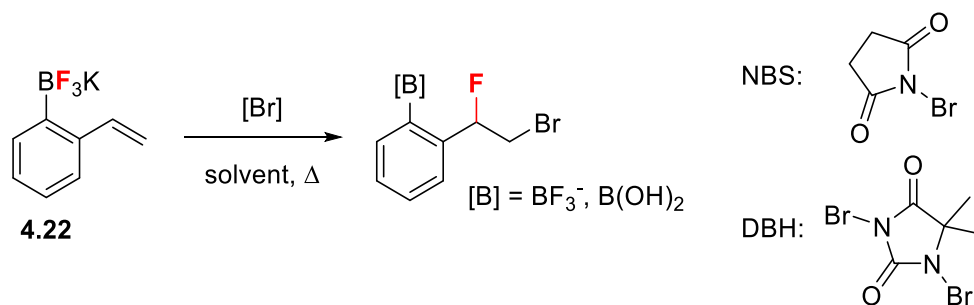
We decided to focus on the bromofluorination of **4.22** and began by investigating the effect of various electrophilic brominating agents on the transformation. Molecular bromine proved too reactive as reaction crudes revealed complete bromination of the alkene producing 2-(1,2-dibromoethyl)phenyltrifluoroborate (**4.41**) 1-bromo-2-(1,2-dibromoethyl)benzene (**4.42**) and 1-bromo-2-(1,2-dibromoethyl)benzene (**4.43**) (Scheme 4.20).



Scheme 4.20 Over-brominated products observed during attempted bromofluorination of **4.22** using Br_2 . We thought that using *N*-bromine agents would be advantageous by virtue of the fact that these are known to slowly release Br_2 into the reaction medium which may obviate the over-bromination previously observed. Unfortunately, use of *N*-bromosuccinimide (NBS) in various solvents at ambient temperatures did not result in any fluorinated products however, **4.42** was observed as the main product by GC-MS; ^{19}F and ^{11}B NMR spectroscopy evidenced significant deborylation (Table 4.9, entries 1-6). Similar results were observed when reaction temperatures were increased (Table 4.9, entries 7-11). However, in THF at 45°C trace yields of a fluorinated product were observed. ^{19}F NMR spectroscopy revealed a signal at -181 ppm with a ddd splitting pattern which corresponds well with the chemical shift and coupling constants reported for (2-bromo-1-

fluoroethyl)benzene ($\delta = -174$, ddd).²⁴⁰ Fluorination yields could not be increased by changing equivalents of NBS used (Table 4.9, entries 13-15) and when reaction temperatures were increased only deborylation was observed in the absence of any fluorinated products (Table 4.9, entries 16 and 17). 1,3-dibromo-5,5-dimethylhydantoin (DBH) allowed the formation of trace fluorinated product at ambient temperatures in CCl_4 and in both CH_2Cl_2 and CCl_4 with heating (Table 4.9, entries 19, 21 and 22, respectively).

Table 4.9 Effect of *N*-bromine reagents on bromofluorination of 4.22

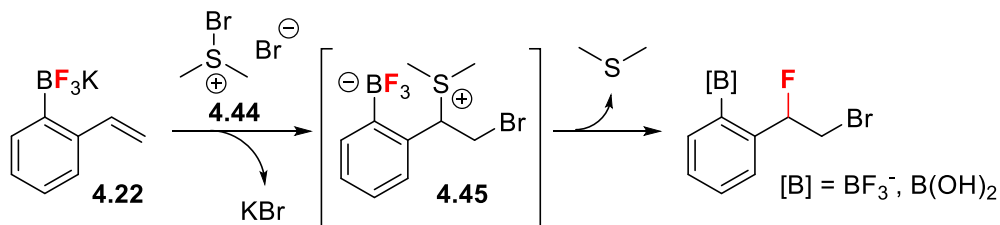


Entry	Solvent	$[\text{Br}]$ (eq.)	Temperature ($^\circ\text{C}$)	Yield (%) ^a
1	CH_2Cl_2	NBS (1.0)	rt	0
2	CHCl_3	NBS (1.0)	rt	0
3	CCl_4	NBS (1.0)	rt	0
4	MeCN	NBS (1.0)	rt	0
5	Acetone	NBS (1.0)	rt	0
6	THF	NBS (1.0)	rt	0
7	CH_2Cl_2	NBS (1.0)	45	0
8	CHCl_3	NBS (1.0)	45	0
9	CCl_4	NBS (1.0)	45	0
10	MeCN	NBS (1.0)	45	0
11	Acetone	NBS (1.0)	45	0
12	THF	NBS (1.0)	45	trace

13	THF	NBS (0.5)	45	trace
14	THF	NBS (2.0)	45	trace
15	THF	NBS (3.0)	45	trace
16	THF	NBS (1.0)	90	0
17	THF	NBS (1.0)	120	0
18	CH ₂ Cl ₂	DBH (0.5)	rt	0
19	CCl ₄	DBH (0.5)	rt	trace
20	THF	DBH (0.5)	rt	0
21	CH ₂ Cl ₂	DBH (0.5)	45	4
22	CCl ₄	DBH (0.5)	45	4
23	THF	DBH (0.5)	45	0

^a determined by ¹⁹F NMR spectroscopy using 2,4-dinitrofluorobenzene as an internal standard.

As a final approach we identified bromodimethylsulphonium bromide (**4.44**) as a brominating agent of potential advantages. Initial KBr precipitation should favour formation of zwitterionic 2-(2-bromo-1-dimethylsulphonioethyl)phenyltrifluoroborate (**4.45**) which, can then be fluorinated intramolecularly with concomitant release of dimethyl sulphide (Scheme **4.20**).

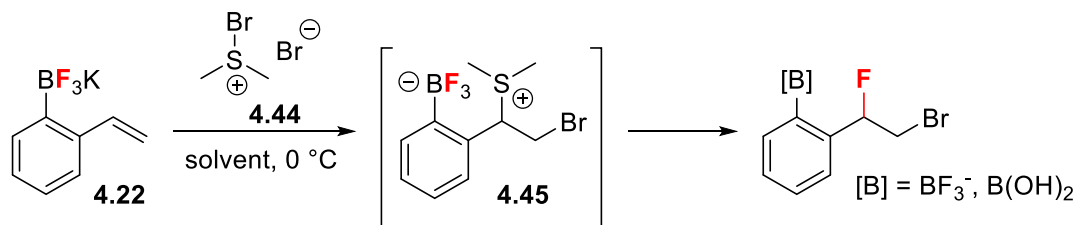


Scheme 4.21 Possible intramolecular fluorination via **4.45**.

We found that the slow addition of a solution of **4.44** into cold reaction mixtures did allow the formation of **4.45** as observed by MS (Table **4.10**, entries 1-4). However, no

fluorinated products were detected after extended stirring at 0 °C, ambient temperatures and eventually heating. Additionally, all attempts to isolate and characterize **4.45** failed.

Table 4.10 Effect of bromodimethylsulphonium bromide on bromofluorination of **4.22**



Entry	Solvent	4.45 formation? ^a	Yield of fluorinated product (%) ^b
1	CH ₂ Cl ₂	yes	0
2	CHCl ₃	yes	0
3	CCl ₄	yes	0
4	MeCN	yes	0

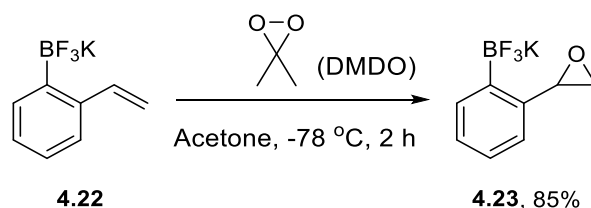
^a detected by LC-MS as [M⁷⁹Br+K]⁺ 351 and [M⁸¹Br+K]⁺ 353. ^b determined by ¹⁹F NMR spectroscopy using 2,4-dinitrofluorobenzene as an internal standard.

4.2.1.3.1 Discussion of results with styrene derivative **4.22**

In all conditions tested only trace yields of fluorinated product could be observed in the bromofluorination of **4.22**. Fluorination is occurring at the benzylic position as evidenced by the chemical shift, ~ -180 ppm, and coupling pattern observed by ¹⁹F NMR spectroscopy of crude reaction mixtures. In most cases, the major products detected were results of complete bromination of the alkene and deborylation. As stated above for studies with **4.21**, we cannot exclude BF₄⁻ as the fluorine source for trace yields observed. With these observations we conclude that **4.22** is not a suitable substrate for intramolecular halofluorination.

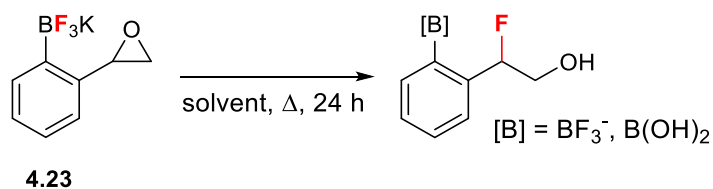
4.2.1.4 Synthesis and fluorination studies of styrene oxide derivative **4.23**

As alkene activation, via a halonium ion failed, efforts were focused towards the more stable epoxide derivative. Potassium 2-(oxiranyl)phenyltrifluoroborate (**4.23**) was obtained in excellent yield via epoxidation of styrene derivative **4.22** using dimethyldioxirane (DMDO), applying reaction conditions reported by Molander *et al.* (Scheme **4.22**).²⁴³



Scheme 4.22 Epoxidation of **4.22** to **4.23** using DMDO.

We began by investigating the ability of **4.23** towards intramolecular fluorination in the absence of epoxide activators. As expected, reactions at ambient temperatures did not result in the detection of any fluorinated product (Table **4.11**, entries 1-10). Elevated reaction temperatures were not found to improve the transformation (Table **4.11**, entries 11-15 and 17-22), except in MeCN where trace yield of the desired fluorohydrin was observed as a multiplet at -184 ppm in the ^{19}F NMR spectrum (Table **4.11**, entry 16), consistent with literature values for 2-fluoro-2-phenylethanol (-187 ppm).²²¹ Thermolysis in high-boiling solvents resulted in significant starting material degradation, evidenced by deborylation to BF_4^- , without the formation of fluorinated products (Table **4.11**, entries 23-27).

Table 4.11 Conditions tested for activator-free intramolecular fluorination of **4.23**

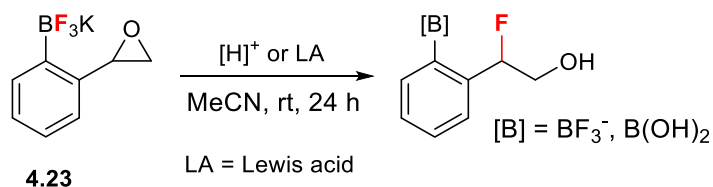
Entry	Solvent	Temperature (°C)	Fluorinated product? ^a
1	CH ₂ Cl ₂	rt	no
2	CHCl ₃	rt	no
3	CCl ₄	rt	no
4	Et ₂ O	rt	no
5	THF	rt	no
6	MeCN	rt	no
7	HFIP	rt	no
8	Acetone	rt	no
9	1,4-dioxane	rt	no
10	H ₂ O	rt	no
11	CH ₂ Cl ₂	50	no
12	CHCl ₃	50	no
13	CCl ₄	50	no
14	Et ₂ O	50	no
15	THF	50	no
16	MeCN	50	trace
17	HFIP	50	no
18	Acetone	50	no
19	<i>t</i> -BuOH	50	no
20	1,4-dioxane	50	no
21	H ₂ O	50	no
22	<i>t</i> -BuOH	50	no

23	DMSO	120	no
24	DMF	120	no
25	DMA	120	no
26	1,2-dichlorobenzene	120	no
27	Toluene	120	no

^a determined by ¹⁹F NMR spectroscopy.

Next, we thought that fluorination may be facilitated via epoxide activation by Brønsted or Lewis acids. We found however, under these reaction conditions no fluorinated product could be detected by ¹⁹F NMR spectroscopy (Table 4.12, entries 1-9). Significant starting material deborylation was observed, especially for reactions using Lewis acids. Given the fluorophilicity of most Lewis acids it is likely that degradation is initiated via initial fluorine abstraction from the trifluoroborate by the Lewis acid.

Table 4.12 Effect of epoxide activators on the intramolecular fluorination of **4.23**



Entry	Activator	Fluorinated product? ^a
1	TFA	no
2	conc. H ₂ SO ₄	no
3	<i>p</i> -TsOH	no
4	B(C ₆ F ₅) ₃	no
5	B(<i>i</i> OPr) ₃	no
6	MgCl ₂	no
7	LiCl	no

8	ZnCl ₂	no
9	CeCl ₃	no

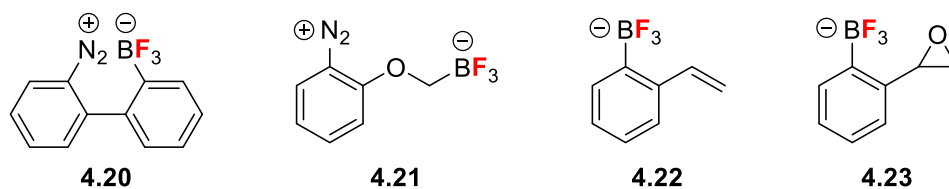
^a determined by ¹⁹F NMR spectroscopy.

4.2.1.4.1 Discussion of results with styrene oxide derivative 4.23

Fluorination of **4.23** to the corresponding fluorohydrin was only observed in one instance out of all conditions tested (Table **4.11**, entry 16). In most reactions conducted at ambient temperatures, **4.23** was found to be stable, while elevated temperatures resulted in deborylation to BF₄⁻ as observed by ¹⁹F NMR spectroscopy. The use of Brønsted and Lewis acids for epoxide activation led to starting material degradation via deborylation. With these observations, we conclude that **4.23** is not a suitable substrate for intramolecular fluorination of epoxides.

4.3 Conclusion and Perspectives

In our effort to widen the array of intramolecular fluorine delivery methodologies we synthesised a range of organotrifluoroborate containing scaffolds that position F⁻ near an electrophilic centre. We identified organotrifluoroborates as potential candidates for this type of transformation given their proven ability to transfer fluorine intermolecularly (see chapters 2 and 3). Within this context, we attempted the synthesis of four different trifluoroborate-containing scaffolds and their subsequent investigation for intramolecular fluorination (Scheme **4.34**).



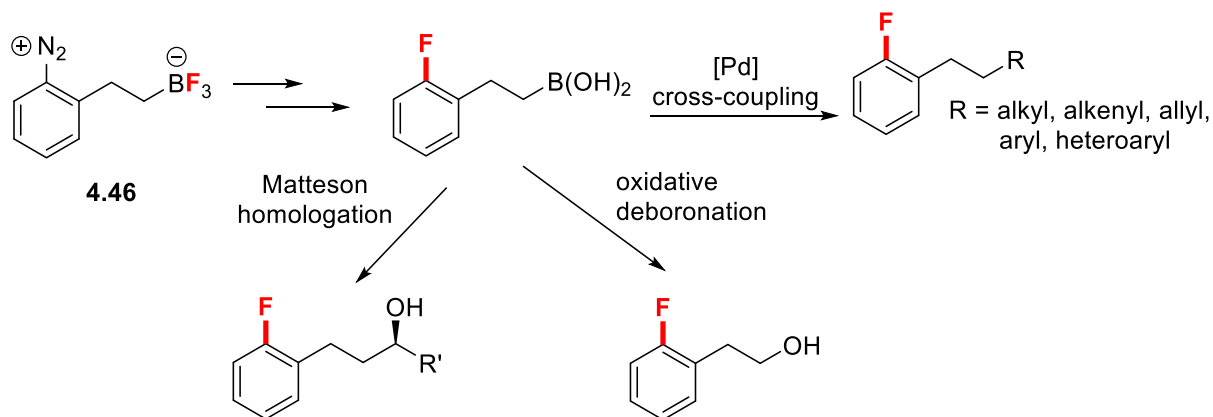
Scheme 4.23 Trifluoroborate-containing scaffolds for intramolecular fluorination.

Despite our efforts, **4.20** could not be synthesized due to difficulties in accessing a borylated biphenyl system (see section **4.2.1**). Due to time constraints we could not continue optimization of reaction conditions towards **4.20**. We do however continue to recognize the potential of **4.20** for intramolecular fluorine transfer, and therefore suggest that as perspective of this investigation further optimization towards synthesizing **4.20** continue.

We was able to successfully synthesize, isolate and characterize zwitterionic diazoniotrifluoroborate **4.21**. However, attempted fluorination of this substrate only resulted in the observation of trace yields of corresponding aryl fluoride. The substrate was generally found to be stable at low temperatures (45 °C). At higher temperatures (≥ 100 °C), trace yields of the corresponding aryl fluoride could be observed accompanied by significant degradation of the starting material.

A perspective for this substrate class would be synthesis and study of the corresponding all carbon derivative (**4.46**). This derivative will not be hampered by potential stabilization of the diazonium cation, as is possible for **4.21** (see Scheme **4.18**), and may therefore undergo dediazonation in milder conditions, avoiding the degradation observed at higher temperatures. If this strategy is successful, a long-term perspective would be applying

this methodology towards the synthesis of functionalisable aryl fluorides via the remaining boronic acid handle (Scheme 4.24).



Scheme 4.24 Further functionalization of aryl fluoride via boronic acid.

Styrene derivatives **4.22** and **4.23** were easily obtained in moderate to excellent yields respectively. Efficient bromofluorination failed using **4.22** and various electrophilic bromine sources. Major products were over-brominated and deborylated products, at best trace yields of (2-bromo-1-fluoroethyl)benzene could be observed. Similarly, **4.23** failed in intramolecular epoxide ring-opening by fluorine, the desired fluorohydrin was only observed in one case, whereas the majority of reaction conditions examined led to starting material degradation.

As a perspective for this substrate class one could imagine the introduction of the trifluoroborate moiety into scaffolds with increased conformational flexibility, compared to the styrene derivatives, which, may facilitate the fluorine transfer process (Scheme 4.25).



Scheme 4.25 Conformationally flexible alkene and epoxide containing trifluoroborate scaffolds

4.4 Experimental

General Information

Solvents and Reagents

All chemicals were purchased from commercial sources and used as received unless otherwise noted. Solvents used were all commercial grade and used as received with no drying, all reactions were performed in oven-dried glassware under argon atmosphere unless otherwise stated. Deuterated solvents for NMR spectroscopic analysis were purchased from Euriso-top.

Analysis

NMR experiments were performed in deuterated solvents. ^1H NMR, ^{13}C NMR, ^{11}B NMR and ^{19}F spectra were recorded on 300 Avance (300 MHz), 400 Avance (400 MHz) and Avance III 400 (400 MHz) Bruker spectrometers. All spectra were recorded at ambient temperature (298 K). Chemical shifts (δ) are reported in parts per million (ppm) relative to the residual protium in the solvents (^1H) or the solvent carbon (^{13}C) as internal standards. ^{19}F spectra of aryl fluorides were referenced to 2,4-dinitrofluorobenzene. Multiplicity of signals is indicated using the following abbreviations: s (singlet), b (broad), d (doublet), t (triplet), q (quartet), q_{B} (1:1:1:1 of peaks arising from coupling to ^{11}B with $S=3/2$, midpoint of signal reported), dd (doublet of doublets), dt (doublet of triplet), td (triplet of doublet), hept (heptet) and m (multiplet).

Reactions were monitored using Merck Silica gel 60 F₂₅₄ glass backed plates. TLC plates were visualized by UV fluorescence ($\lambda = 254$ nm) and one of the following stains: KMnO_4 or HBQ. Flash column chromatography was performed using VWR Chemicals Silica gel 60 – 200 μm or using an automated Interchim Puriflash system using pre-packed Interchim 30 μm Silica gel cartridges.

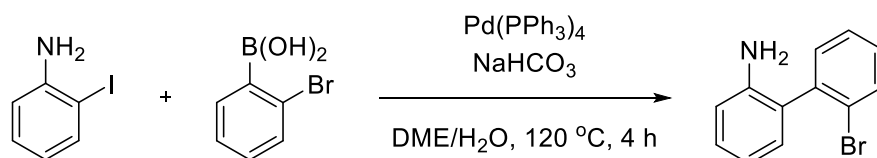
IR spectra were recorded on a PerkinElmer Frontier FT-IR spectrometer with frequencies expressed in cm^{-1} .

Low resolution mass spectra were obtained on Waters LC-MS and Agilent GC-MS. High-resolution mass spectra (HRMS) were recorded using either electrospray ionization (ESI)

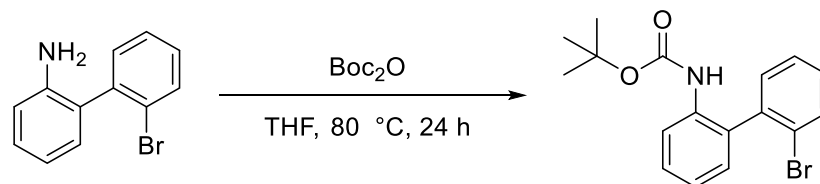
or desorption chemical ionization (DCI) using Kratos MS-50 / Kratos Concept I/HQ spectrometers.

4.4.1 Synthetic procedures and characterization data for 4.21 – 4.44

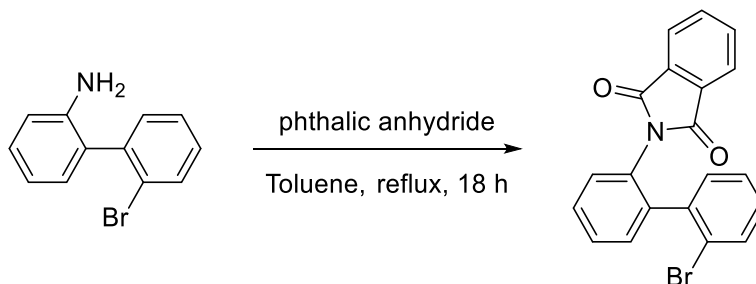
2'-bromo-[1,1'-biphenyl]-2-amine (4.24)



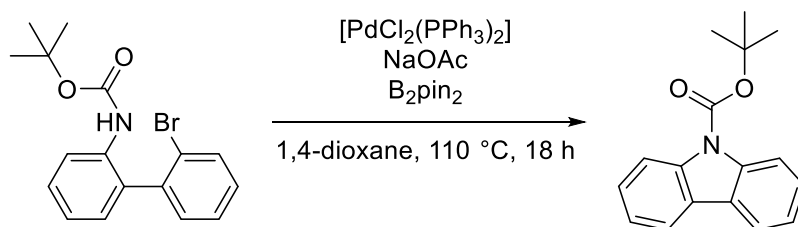
A 35 mL pressure vial was charged with a stir bar, 2-iodoaniline (442.6 mg, 2 mmol), 2-bromophenylboronic acid (482.8 mg, 2.4 mmol), NaHCO₃ (532.5 mg, 6 mmol), Pd(PPh₃)₄ (231 mg, 0.2 mmol, 10 mol%), DME (5.7 mL) and water (2.9 mL). The reaction mixture was stirred at rt for 5 mins, then degassed (three cycles of freeze-pump-thaw), the vial sealed and placed in an oil bath at 120 °C for 4 h. After to cooling to rt the reaction mixture was dropped onto water and extracted with Et₂O (3 x 25 mL). The combined organic phases were dried over anhydrous MgSO₄, filtered and concentrated onto Celite. The crude was purified by Silica gel flash column chromatography using 100% cyclohexane to cyclohexane/EtOAc (9:1). Desired fractions were collected and concentrated under reduced pressure to furnish the desired product as a clear oil that solidified upon standing (413.2 mg, 82%). ¹H NMR (300 MHz, Chloroform-*d*) δ 7.70 (dd, *J* = 7.9, 1.1 Hz, 1H), 7.43 – 7.31 (m, 2H), 7.24 (dddd, *J* = 9.1, 7.5, 4.8, 2.3 Hz, 2H), 7.07 (dd, *J* = 7.5, 1.6 Hz, 1H), 6.97 – 6.83 (m, 2H), 4.25 (bs, 2H). ¹³C NMR (75 MHz, Chloroform-*d*) δ 141.8 (C_q), 139.6 (C_q), 133.3 (CH), 132.0 (CH), 130.5 (CH), 129.5 (CH), 129.2 (CH), 128.3 (C_q), 127.9 (CH), 124.4 (CH), 119.7 (CH), 116.7 (CH). LRMS-ESI (*m/z*): [M⁷⁹Br+H]⁺ 248, [M⁸¹Br+H]⁺ 250. Spectroscopic data consistent with those previously reported.²⁴⁴

***N*-Boc-2'-bromo-[1,1'-biphenyl]-2-amine (4.27)**

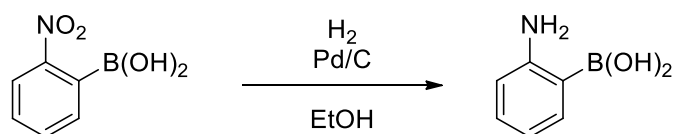
An oven dried 10 mL pressure vial was charged with, under Ar, 2'-bromo-[1,1'-biphenyl]-2-amine (298.3 mg, 1.2 mmol), Boc_2O (262.5 mg, 1.2 mmol) and THF (2.8 mL); the vial was placed in an oil bath at $80\text{ }^\circ\text{C}$ and stirred for 24h. TLC showed remaining starting material after 24 h, therefore NEt_3 (0.5 mL, 3.6 mmol) was added and the reaction mixture stirred for an additional 2h. After allowing to cool to rt, the reaction mixture was dropped sat'd NaHCO_3 and the aqueous phase was extracted with CH_2Cl_2 (3 x 10 mL). The combined organic phases were washed with brine then dried over anhydrous MgSO_4 , filtered and concentrated under reduced pressure to yield the product as a colourless viscous oil (352.2 mg, 84%). ^1H NMR (300 MHz, Chloroform-*d*) δ 8.07 (d, $J = 8.3$ Hz, 1H), 7.75 – 7.69 (m, 1H), 7.46 – 7.35 (m, 2H), 7.34 – 7.24 (m, 2H), 7.15 – 7.09 (m, 2H), 6.06 (s, 1H), 1.46 (s, 9H). ^{13}C NMR (75 MHz, Chloroform-*d*) δ 153.0 (C_q), 139.0 (C_q), 135.7 (C_q), 133.4 (CH), 132.0 (CH), 130.1 (C_q), 129.9 (CH), 129.1 (CH), 128.5 (CH), 128.0 (CH), 124.3 (C_q), 123.1 (CH), 120.3 (CH), 80.7 (C_q), 28.4 (CH_3). DCI- NH_3 -MS (m/z): $[\text{M}^{79}\text{Br}+\text{NH}_4]^+$ 365, $[\text{M}^{81}\text{Br}+\text{NH}_4]^+$ 367. Spectroscopic data consistent with those previously reported.²⁴⁵

***N*-Phthaloyl-2'-bromo-[1,1'-biphenyl]-2-amine (4.28)**

A 10 mL round-bottom flask was charged with a stir bar, 2'-bromo-[1,1'-biphenyl]-2-amine (308.5 mg, 1.21 mmol), phthalic anhydride (184.4 mg, 1.21 mmol) and toluene (3 mL); the flask was fixed with a condenser and the mixture heated at reflux for 18 h. After allowing to cool to rt, the crude reaction mixture was concentrated onto Celite under reduced pressure and then purified by silica gel column chromatography using an eluent of cyclohexane (100%) to cyclohexane/EtOAc (4:1); the desired product was isolated as an off-white crystalline powder (347.4 mg, 74%). IR $\nu_{\text{max}}/\text{cm}^{-1}$ (neat film): 3471, 3057, 2924, 2853, 1708, 1464, 1378, 1113, 765, 716. ^1H NMR (400 MHz, Chloroform-*d*) δ 7.83 – 7.76 (m, 2H), 7.72 – 7.65 (m, 2H), 7.58 – 7.51 (m, 3H), 7.51 – 7.45 (m, 1H), 7.42 – 7.36 (m, 1H), 7.29 – 7.23 (m, 1H), 7.19 (td, $J = 7.5, 1.2$ Hz, 1H), 7.07 (ddd, $J = 8.1, 7.3, 1.8$ Hz, 1H). ^{13}C NMR (101 MHz, Chloroform-*d*) δ 167.5 (C_q), 166.7 (C_q), 140.2 (C_q), 139.2 (C_q), 134.3 (CH), 134.2 (CH), 133.0 (CH), 132.0 (C_q), 131.8 (CH), 131.6 (C_q), 131.2 (CH), 130.0 (C_q), 129.24 (CH), 129.19 (CH), 129.14 (CH), 129.08 (CH), 127.0 (CH), 123.8 (CH), 123.7 (CH), 123.3 (C_q). MS-ESI (m/z): [M⁷⁹Br+H]⁺ 378, [M⁸¹Br+H]⁺ 380.

***N*-Boc-carbazole (4.30)**

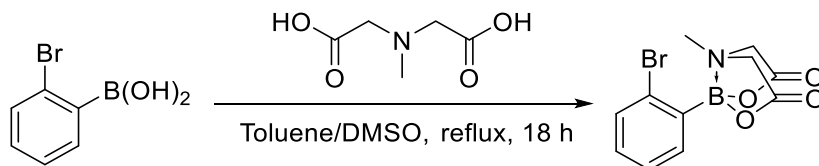
A 10 mL pressure vial was charged with a stir bar, *N*-Boc-2'-bromo-[1,1'-biphenyl]-2-amine (71 mg, 0.2 mmol), bis(pinacolato)diboron (76 mg, 0.3 mmol), NaOAc (74 mg, 0.9 mmol), Pd(PPh₃)Cl₂ (14 mg, 0.02 mmol, 10 mol%) and 1,4-dioxane (2 mL). The reaction mixture was stirred at rt for 5 mins, then degassed (three cycles of freeze-pump-thaw), the vial sealed and placed in an oil bath at 110 °C for 18 h. After to cooling to rt the reaction mixture was dropped onto water and extracted with EtOAc (3 x 10 mL). The combined organic phases were dried over anhydrous MgSO₄, filtered and concentrated onto Celite. The crude was purified by Silica gel flash column chromatography using 100% cyclohexane to cyclohexane/EtOAc (9:1). Desired fractions were collected and concentrated under reduced pressure to furnish the desired product as a clear oil (18.5 mg, 34%). ¹H NMR (300 MHz, Chloroform-*d*) δ 8.32 (d, *J* = 8.4 Hz, 2H), 7.99 (ddd, *J* = 7.7, 1.4, 0.7 Hz, 2H), 7.47 (ddd, *J* = 8.5, 7.3, 1.4 Hz, 2H), 7.36 (td, *J* = 7.5, 1.1 Hz, 2H), 1.77 (s, 9H). ¹³C NMR (101 MHz, Chloroform-*d*) δ 151.3 (C_q), 138.7 (C_q), 127.2 (CH), 125.9 (C_q), 123.1 (CH), 119.7 (CH), 116.4 (CH), 84.0 (C_q), 28.6 (CH₃). Spectroscopic data consistent with those previously reported.¹¹⁹

2-aminophenylboronic acid (4.32)

A 10 mL flask was charged with a stir bar and flame dried, after cooling to rt the flask was purged with Ar, and left under an Ar atmosphere. The flask was then charged with 2-

nitrophenylboronic acid (112.3 mg, 0.6 mmol), Pd/C (10 mg, 10% loading) and EtOH (5.5 mL). Under vigorous stirring the reaction flask was purged with H₂ using a balloon three times, then left under a H₂ balloon. The reaction mixture was stirred for 30 min at rt until complete consumption of starting material was determined by TLC (CH₂Cl₂/MeOH 9:1). The reaction mixture was filtered through a fine glass frit, and the insoluble residue was washed with EtOH (3 x 5 mL). The filtrate was concentrated under reduced pressure to furnish the product as an off-white powder which was further dried under high vacuum (59.9 mg, 65%). IR $\nu_{\text{max}}/\text{cm}^{-1}$ (neat film): 3440, 3397, 3317, 3022, 1611, 1463, 1417, 1271, 756. ¹H NMR (300 MHz, D₂O/DMSO-*d*₆) δ 7.42 (dd, *J* = 7.4, 1.7 Hz, 1H), 7.12 – 7.02 (m, 1H), 6.51 (t, *J* = 7.9 Hz, 2H). ¹³C NMR (75 MHz, D₂O/DMSO-*d*₆) δ 154.9 (C_q), 136.9 (CH), 132.8 (CH), 117.1 (CH), 116.1 (CH). No ¹¹B signal could be observed. MS-ESI (*m/z*): [M₂+H]⁺ 239. Spectroscopic information matches those found in the literature.²⁴⁶

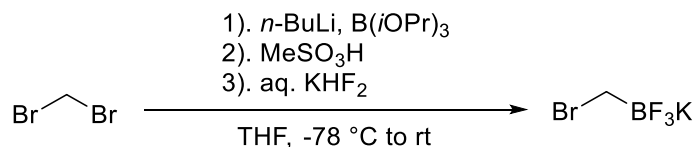
2-bromophenylboronic acid MIDA ester (4.33)



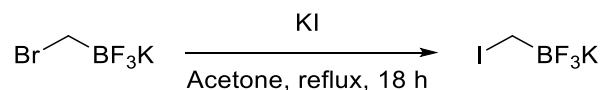
A 250 mL round-bottom flask, affixed with a condenser and Dean-Stark adapter, was charged with a stir bar, 2-bromophenylboronic acid (1.0199 g, 5 mmol), methyliminodiacetic acid (748.4 mg, 5 mmol), toluene (50 mL) and DMSO (20 mL). The reaction mixture was stirred and heated at reflux for 18h. After cooling to rt, all solvent was removed under reduced pressure and the residue concentrated onto Celite. The crude residue was purified by Silica gel flash column chromatography using an eluent gradient of 100% Et₂O to Et₂O/MeCN (1:1). Desired fractions were collected and concentrated to furnish the desired product as a white crystalline powder (1.5291 g, 97%). ¹H NMR (300 MHz, Acetonitrile-*d*₃) δ 7.67 (dd, *J* = 7.5, 1.9 Hz, 1H), 7.62 (dd, *J* = 7.9, 1.2 Hz, 1H), 7.39 (td, *J* = 7.4, 1.3 Hz, 1H), 7.30 (ddd, *J* = 7.8, 7.3, 2.0 Hz, 1H), 4.14 (d, *J* = 17.3 Hz, 2H), 4.03 (d, *J* = 17.3 Hz, 2H), 2.71 (s, 3H). ¹³C NMR (75 MHz, Acetonitrile-*d*₃) δ 169.5 (C_q), 137.4 (CH), 134.6 (CH), 132.4 (CH), 128.7 (C_q), 128.0 (CH), 65.3 (CH₂),

49.6 (CH₃). ¹¹B NMR (96 MHz, Acetonitrile-*d*₃) δ 11.5 (bs). Spectroscopic data consistent with those previously reported.²³¹

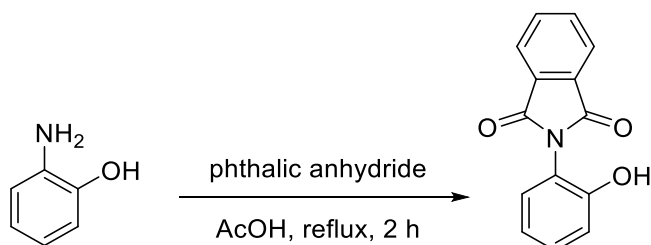
Potassium bromomethyltrifluoroborate (4.37)



A 500 mL flame-dried round-bottom flask equipped with an Ar balloon was charged with a stir bar, dibromomethane (9.82 mL, 0.14 mol), triisopropylborate (31.02 mL, 0.135 mol) and dry THF (200 mL); the flask was then cooled to -78 °C in a dry ice-acetone bath. To the stirring solution, a 1.47 M *n*-BuLi solution in hexanes (86.39 mL, 0.127 mol), was added dropwise to ensure that the internal temperature did not rise above -70 °C. After *n*-BuLi addition was completed the reaction mixture was stirred at -78 °C for 2.5 h. Methanesulphonic acid (4.12 mL, 0.064 mol) was then added to the reaction mixture slowly at -78 °C, then the flask was removed from the dry ice-acetone bath and allowed to warm to 0 °C. At this point KHF₂ (32.8595 g, 0.42 mol) was added in one portion followed by deionized water (43 mL). The reaction mixture was then stirred for an additional 30 min before all solvent was removed under reduced pressure and the remaining residue dried under high vacuum overnight. The dry white solid was then triturated with acetone (4 x 100 mL) and filtered to remove insoluble salts. The filtrate was concentrated under reduced pressure to the point of saturation after which Et₂O was added leading to the precipitation of the product as a fine white crystalline powder, which was collected by filtration further washed with Et₂O and dried under high vacuum (15.8322g, 62%). ¹H[¹¹B] NMR (400 MHz, Acetone-*d*₆) δ 2.21 (q, *J* = 5.7 Hz). ¹⁹F NMR (377 MHz, Acetone-*d*₆) δ -145.25 (q_B). ¹¹B NMR (128 MHz, Acetone-*d*₆) δ 2.61 (q, *J* = 50.4 Hz). MS-ESI (*m/z*): [M⁷⁹Br-K]⁻ 161, [M⁸¹Br-K]⁻ 163. Spectroscopic data consistent with those previously reported.²³⁶

Potassium iodomethyltrifluoroborate (4.38)

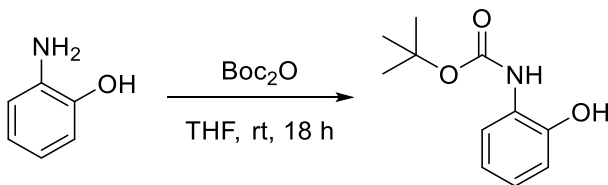
A 250 mL round-bottom flask was charged with a stir bar, potassium bromomethyltrifluoroborate (3.9970 g, 20 mmol), potassium iodide (3.3856 g, 20.5 mmol) and acetone (140 ml). The flask was fitted with a condenser and the flask heated to reflux in an oil bath; the reaction mixture was stirred at reflux overnight until the reaction was determined completed by ^{19}F NMR spectroscopy. The reaction had developed a white precipitate (KBr) which was filtered out, and the filtrate concentrated to saturation under reduced pressure. Et_2O (~150 mL) was added to induce precipitation of the desired product as a white crystalline powder. This was collected by filtration and further washed with Et_2O then dried under high vacuum overnight (4.8052 g, 97%). IR $\nu_{\text{max}}/\text{cm}^{-1}$ (neat film): 1398, 1163, 1073, 1056, 951, 930, 721. ^1H NMR (300 MHz, Acetone- d_6) δ 1.87 – 1.72 (m). ^{19}F NMR (282 MHz, Acetone- d_6) δ -144.14 (q_B). ^{11}B NMR (96 MHz, Acetone- d_6) δ 2.66 (q, $J = 50.7$ Hz). MS-ESI (m/z): $[\text{M-K}]^-$ 209. Spectroscopic data consistent with those previously reported.²³⁶

N-Phthaloyl-2-aminophenol (4.41)

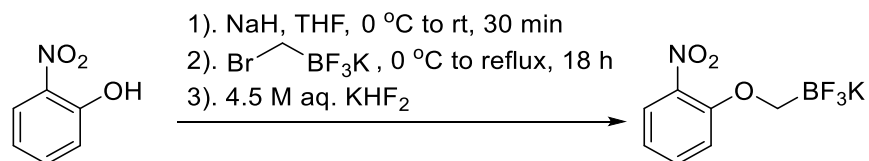
A 250 mL round-bottom flask was charged with a stir bar, 2-aminophenol (2.1831 g, 20 mmol), phthalic anhydride (2.9622 g, 20 mmol), AcOH (100 ml) and a condenser. The reaction mixture was vigorously stirred at reflux for 2 h after which it was allowed to cool to rt. The homogenous yellow solution was then dropped on cold water and extracted with CHCl_3 (3 x 50 mL). The combined organic phases were then washed with water (1 x 100

mL) followed by brine (3 x 100 mL). The organic solution was then dried over anhydrous Na_2SO_4 , then filtered and concentrated under reduced pressure to furnish a light pink solid (1.6717 g, 35%). IR $\nu_{\text{max}}/\text{cm}^{-1}$ (neat film): 3377, 1698, 1684, 1223, 1192, 719. ^1H NMR (300 MHz, $\text{DMSO}-d_6$) δ 9.85 (s, 1H), 7.99 - 7.88 (m, 4H), 7.31 (ddd, $J = 8.1, 7.3, 1.7$ Hz, 1H), 7.26 (dd, $J = 7.8, 1.7$ Hz, 1H), 6.99 (dd, $J = 8.2, 1.3$ Hz, 1H), 6.92 (td, $J = 7.6, 1.3$ Hz, 1H). ^{13}C NMR (75 MHz, $\text{DMSO}-d_6$) δ 167.2 (C_q), 154.0 (C_q), 134.6 (CH), 131.9 (C_q), 130.4 (CH), 130.4 (CH), 123.3 (CH), 119.1 (CH), 118.9 (C_q), 116.6 (CH). HRMS-ESI (m/z): found $[\text{M}-\text{H}]^-$ 238.0506, calc'd $\text{C}_{14}\text{H}_8\text{NO}_3^-$ requires 238.0504.

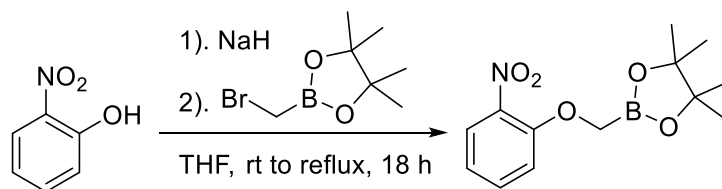
***N*-Boc-2-aminophenol (4.42)**



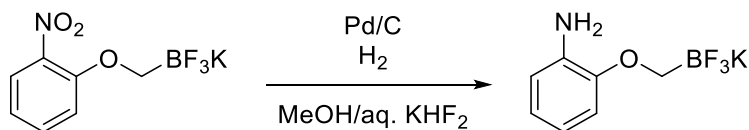
A 50 mL round-bottom flask was charged with a stir bar, 2-aminophenol (1 g, 10 mmol), Boc_2O (2.4 mL, 10.5 mmol) and dry THF (10 mL); the flask was purged with Ar and left to stir at rt for 18h. All solvent was removed under reduced pressure and the residue re-dissolved in EtOAc (50 mL) and dropped onto sat'd aq. NH_4Cl (50 mL). The phases were separated and the aqueous phase was extracted with EtOAc (3 x 50 mL). The combined organic phases were dried over anhydrous Na_2SO_4 , then filtered and concentrated under reduced pressure to furnish the desired product as a brown powder (2.2029 g, >99%). ^1H NMR (300 MHz, Chloroform-*d*) δ 8.14 (bs, 1H), 7.11 (dd, $J = 7.8, 1.5$ Hz, 1H), 7.03 (td, $J = 7.5, 7.1, 1.5$ Hz, 1H), 6.96 (dd, $J = 8.1, 1.6$ Hz, 1H), 6.85 (td, $J = 7.5, 1.7$ Hz, 1H), 6.70 (bs, 1H), 1.53 (s, 9H). ^{13}C NMR (75 MHz, Chloroform-*d*) δ 155.2 (C_q), 147.6 (C_q), 125.7 (CH), 121.5 (CH), 120.9 (CH), 118.9 (C_q), 82.2 (C_q), 28.4 (CH_3). Spectroscopic data consistent with those previously reported.²⁴⁷

Potassium (2-nitrophenoxy)methyltrifluoroborate (4.43)

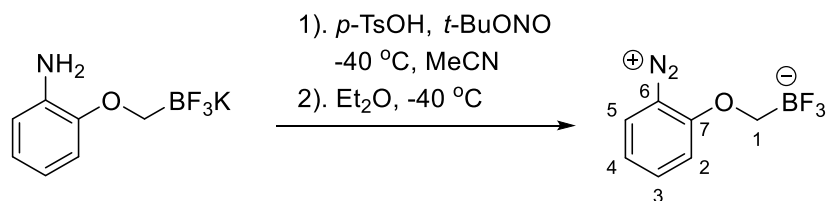
A 25 mL round-bottom flask was charged with a stir bar and condenser then flame dried and left under Ar atmosphere. The flask was cooled to 0 °C in an ice-water bath, then charged with NaH (80 mg, 2 mmol), 2-nitrophenol (301.4 mg, 2 mmol) and dry THF (10 mL); the flask was stirred at 0 °C for 15 min then at rt for 30 min. The reaction mixture was cooled back to 0 °C and potassium bromomethyltrifluoroborate (304.2 mg, 1.5 mmol) was added in one portion then the flask was placed in an oil bath and heated at reflux for 18 h. The reaction mixture was allowed to cool to rt and then quenched with 4.5 M aq. KHF₂ (1 mL); all solvent was then removed under reduced pressure and the residue further dried under high vacuum overnight. The dry residue was triturated with acetone and filtered through a 0.2 μm PTFE filter to remove insoluble impurities, the filtrate was then concentrated to the point of saturation and dropped onto Et₂O to precipitate the desired the product as an off-white powder which was collected by filtration and further washed with Et₂O then dried under high vacuum overnight (324 mg, 83%). IR $\nu_{\text{max}}/\text{cm}^{-1}$ (neat film): 3132, 3060, 2947, 2909, 2854, 1616, 1524, 1345, 1269, 1104, 1002, 968, 735. ¹H NMR (300 MHz, Acetone-*d*₆) δ 7.80 (dd, *J* = 8.1, 1.8 Hz, 1H), 7.59 (ddd, *J* = 8.9, 7.3, 1.8 Hz, 1H), 7.42 (dd, *J* = 8.6, 1.2 Hz, 1H), 6.96 (ddd, *J* = 8.2, 7.3, 1.2 Hz, 1H), 3.37 (q, *J* = 5.1 Hz, 2H). ¹³C NMR (75 MHz, Acetone-*d*₆) δ 157.0 (C_q), 140.3 (C_q), 135.4 (CH), 125.9 (CH), 119.2 (CH), 116.0 (CH). ¹⁹F NMR (282 MHz, Acetone-*d*₆) δ -146.18 (m). ¹¹B NMR (96 MHz, Acetone-*d*₆) δ 2.40 (m). HRMS-ESI (*m/z*): found [M-K]⁻ 220.0392, calc'd C₇H₆BF₃NO₃⁻ requires 220.0393.

4,4,5,5-tetramethyl-2-((2-nitrophenoxy)methyl)-1,3,2-dioxaborolane (4.44)

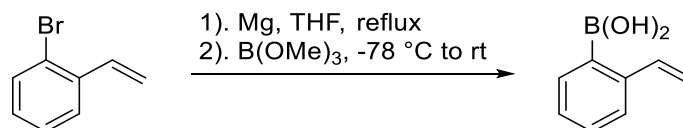
A 10 mL round-bottom flask was charged with a stir bar, condenser and flame-dried, once cooled the apparatus was purged with Ar and left under Ar atmosphere. The flask was then charged with NaH (47.1 mg, 1.2 mmol) and THF (5 mL), then cooled in ice-bath, after which 2-nitrophenol (161.7 mg, 1.2 mmol) was added in one portion causing the evolution of gas and the formation of a red heterogeneous mixture. The reaction mixture was then stirred at rt for 30 minutes after which 2-(bromomethyl)-4,4,5,5-tetramethyl-1,3,2-dioxaborolane (255 mg, 1.2 mmol) was added, the mixture was then stirred at rt for 5 h, then heated to reflux for 18 h. The reaction mixture was then cooled to rt and quenched with saturated aq. NH₄Cl (1mL), the aqueous phase was extracted with Et₂O (3 x 20 mL). The organic phase was dried over Na₂SO₄, then filtered and concentrated under reduced pressure onto Celite. The crude was purified by Silica gel flash column chromatography using a gradient of 100% CH₂Cl₂ to 95:5 CH₂Cl₂/MeOH. Desired fractions were collected and concentrated under reduced pressure, and under high vacuum overnight to furnish the product as a brown crystalline solid (181.6 mg, 56%). IR $\nu_{\text{max}}/\text{cm}^{-1}$ (neat film): 2981, 1931, 1607, 1525, 1350, 1237, 1223, 1140, 955, 844, 709. ¹H NMR (400 MHz, Methylene Chloride-*d*₂) δ 7.79 (dd, *J* = 8.0, 1.7 Hz, 1H), 7.53 (ddd, *J* = 8.6, 7.4, 1.7 Hz, 1H), 7.10 (dd, *J* = 8.5, 1.1 Hz, 1H), 7.00 (ddd, *J* = 8.3, 7.4, 1.2 Hz, 1H), 3.99 (s, 2H), 1.28 (s, 12H). ¹³C NMR (75 MHz, Methylene Chloride-*d*₂) δ 154.1 (C_q), 140.5 (C_q), 134.6 (CH), 125.9 (CH), 120.5 (CH), 114.6 (CH), 85.1 (C_q), 25.1 (CH₃). ¹¹B NMR (128 MHz, Methylene Chloride-*d*₂) δ 31.74. HRMS-EI (*m/z*): found [M]⁺ 278.12128, calc'd C₁₃H₁₈BNO₅⁺ requires 278.13144.

(2-aminophenoxy)methyltrifluoroborate (4.39)

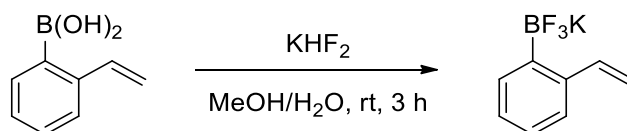
A 100 mL flask was charged with a stir bar then purged with Ar, and left under an Ar atmosphere. The flask was then charged with potassium (2-nitrophenoxy)methyltrifluoroborate (268 mg, 1.00 mmol), Pd/C (28 mg, 10% loading), MeOH (20 mL) and 4.5 M aq. KHF₂ (1 mL). Under vigorous stirring, the reaction flask was purged with a H₂ balloon three times, then left under a H₂ atmosphere. The reaction mixture was stirred at rt for 1.5 h until TLC (CH₂Cl₂/MeOH 9:1) determined all starting material was consumed, the mixture was then filtered through a fine glass frit and the insoluble residue washed with MeOH (3 x 5 mL). The filtrate was concentrated under reduced pressure to furnish the crude product as a brown powder. The residue was triturated with CHCl₃ (20 mL) and then MeCN (20 mL); the remaining residue was dissolved in MeOH and filtered through a 0.2 μm PTFE filter and concentrated under reduced pressure, then further dried under high vacuum overnight to furnish the product as a brown powder (226.3 mg, >99%). IR $\nu_{\text{max}}/\text{cm}^{-1}$ (neat film): 3403, 3205, 2921, 2851, 1618, 1600, 1503, 1097, 988, 808, 741. ¹H NMR (400 MHz, DMSO-*d*₆) δ 6.76 – 6.69 (m, 1H), 6.57 – 6.50 (m, 2H), 6.51 – 6.44 (m, 1H), 4.45 (bs, 2H), 2.94 (q, ³J_{H-F} = 5.1 Hz, 2H). ¹³C NMR (75 MHz, DMSO-*d*₆) δ 149.3 (C_q), 137.3 (C_q), 118.9 (CH), 116.4 (CH), 113.0 (CH), 110.2 (CH). ¹⁹F NMR (282 MHz, DMSO-*d*₆) δ -142.27 (m). ¹¹B NMR (96 MHz, DMSO-*d*₆) δ 3.00 (bs). HRMS-ESI (*m/z*): found [M-H]⁻ 190.0656, calc'd C₇H₈BF₃NO⁻ requires 190.0651.

(2-diazoniophenoxy)methyltrifluoroborate (4.21)

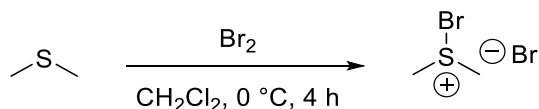
Two 25 mL flask was charged with a stir bar then flame dried and left under an Ar atmosphere with a balloon. The first flask was charged with *p*-TsOH (77.9 mg, 0.41 mmol) and dry MeCN (6 mL), *t*-BuONO (69.8 μ L, 0.58 mmol) was added to this stirring solution; the flask was then cooled to -40 °C in an acetonitrile/dry ice bath. The second flask was charged with potassium (2-aminophenoxy)methyltrifluoroborate (94 mg, 0.41mmol) and dry MeCN (6 mL); this flask was also cooled to -40 °C. Using a cannula and under Ar pressure the trifluoroborate solution was dropwise added to the *p*-TsOH/*t*-BuONO solution at -40 °C, after the first transfer the trifluoroborate flask was rinsed with ~5 mL dry MeCN to ensure quantitative transfer. The reaction mixture was allowed to stir at -40 °C for 1h, the reaction was then stopped by cannula transfer of the reaction mixture onto ~100 mL dry Et₂O cooled to -40 °C. The precipitate, a purple/brown powder, was collected by filtration at rt and washed with Et₂O. The precipitate was allowed to air dry then triturated with CHCl₃, the filtrate discarded. The remaining residue was then triturated with MeCN and filtered to removed insoluble impurities. The filtrate was concentrated to saturation then dropped on Et₂O producing a fine off-white precipitate which was collected by filtration and further washed with Et₂O then dried under high vacuum overnight (25.8 mg, 31%). IR $\nu_{\text{max}}/\text{cm}^{-1}$ (neat film): 3109, 3085, 3050, 2955, 2930, 2912, 2273, 1594, 1562, 1491, 1431, 1295, 1170, 1076, 1012, 951. ¹H NMR (400 MHz, DMSO-*d*₆) δ 8.37 (dd, *J* = 8.4, 1.7 Hz, 1H, H₅), 8.11 (ddd, *J* = 9.0, 7.3, 1.8 Hz, 1H, H₃), 7.60 (d, *J* = 9.0 Hz, 1H, H₂), 7.26 (t, *J* = 7.8 Hz, 1H, H₄), 3.63 (q, ³*J*_{H-F} = 4.9 Hz, 2H, H₁). ¹³C NMR (75 MHz, DMSO-*d*₆) δ 165.6 (C₇), 143.5 (C₃), 131.6 (C₅), 121.2 (C₄), 115.5 (C₂), 100.5 (C₆). ¹⁹F NMR (282 MHz, DMSO-*d*₆) δ -141.70 – -142.89 (m). ¹¹B NMR (96 MHz, DMSO-*d*₆) δ 2.35 (bs). HRMS-ESI (*m/z*): found [M+K]⁺ 241.0160, calc'd C₇H₆BF₃N₂OK⁺ requires 241.0162.

2-vinylphenylboronic acid (4.40)

A 5 mL round-bottom flask was charged with a stir bar and condenser and flame dried, the vessel was then purged with Ar and left under Ar atmosphere. The flask was then charged with Mg turnings (80.7 mg, 3.2 mmol) and one crystal of I₂, the solids were vigorously stirred until the Mg were coated with I₂ and had a purple brown colour. In a separate flame dried 5 mL round-bottom flask, under Ar atmosphere, 2-bromostyrene (342.5 μ L, 2.73 mmol) was dissolved in 2.4 mL THF. The 2-bromostyrene solution was added dropwise to the flask containing the Mg turnings as to maintain constant reflux, after addition was complete the reaction mixture was heated at reflux in an oil bath for 30 min, then allowed to cool to rt. Meanwhile, a flame dried 5 mL round-bottom flask, under Ar, was charged with B(OMe)₃ (353.5 μ L, 3.2 mmol) and THF (2.5 mL) and cooled to -78 °C. The Grignard solution was added dropwise to the borate solution and the resulting solution was stirred at -78 °C for 1 h, then allowed to warm to rt over 5h. The reaction mixture was quenched with 1 M aq. HCl (1 mL) then transferred into a separatory funnel and extracted with Et₂O (3 x 50 mL). The organic layer was dried over anhydrous Na₂SO₄ then filtered and concentrated to furnish the desired boronic acid as a white powder (254.7 mg, 63%). ¹H NMR (300 MHz, Methanol-*d*₄) δ 7.53 (d, *J* = 7.7 Hz, 1H), 7.28 (tt, *J* = 14.2, 7.1, 1.6 Hz, 3H), 6.76 (dd, *J* = 17.5, 11.0 Hz, 1H), 5.66 (dd, *J* = 17.5, 1.0 Hz, 1H), 5.24 (dd, *J* = 11.0, 1.0 Hz, 1H). ¹³C NMR (75 MHz, Methanol-*d*₄) δ 141.4 (C_q), 139.0 (CH), 132.6 (CH), 129.9 (CH), 128.2 (CH), 126.1 (CH), 115.1 (CH₂). ¹¹B NMR (96 MHz, Chloroform-*d*) δ 27.08 (bs). Spectroscopic data is consistent with those previously reported.^{248,249}

Potassium 2-vinylphenyltrifluoroborate (4.22)

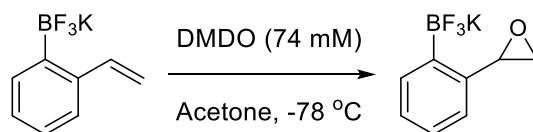
A 50 mL round-bottom flask was charged with a stir bar, 2-vinylphenylboronic acid (254.7 mg, 1.72 mmol), KHF_2 (444.6 mg, 5.7 mmol), MeOH (20 mL) and water (1.27 mL). The reaction mixture was sonicated for 1 min, then stirred at rt for 3 h at which point complete conversion of the boronic acid was confirmed by ^{11}B NMR. The reaction mixture was then concentrated to dryness under reduced pressure, then further dried under high vacuum. The residue was triturated with acetone (3 x 5 mL), which was filtered to remove insoluble impurities, the filtrate was then concentrated to saturation and dropped onto Et_2O to precipitate the product. The precipitate was collected by filtration and washed with Et_2O to furnish the desired product as a white powder (241.4 mg, 67%). IR $\nu_{\text{max}}/\text{cm}^{-1}$ (neat film): 3082, 3057, 3021, 3000, 1624, 1441, 1209, 1188, 911, 743. ^1H NMR (300 MHz, Methanol- d_4) δ 7.55 (dd, $J = 6.7, 2.1$ Hz, 1H), 7.55 – 7.46 (m, 1H), 7.41 (ddd, $J = 17.8, 11.0, 1.5$ Hz, 1H), 7.09 (tt, $J = 6.8, 3.5$ Hz, 2H), 5.61 – 5.47 (m, 1H), 5.03 (dd, $J = 11.0, 1.9$ Hz, 1H). ^{13}C NMR (75 MHz, Methanol- d_4) δ 142.2 (C_q), 141.2 (CH), 133.34 (q, $^3J_{\text{C-F}} = 3.2$ Hz), 127.4 (CH), 127.1 (CH), 124.4 (CH), 111.2 (CH_2). ^{19}F NMR (282 MHz, Methanol- d_4) δ -139.04 – -140.53 (m). ^{11}B NMR (96 MHz, Methanol- d_4) δ 3.76 (q, $J = 58.0$ Hz). HRMS-ESI (m/z): found $[\text{M-K}]^-$ 170.0624, calc'd $\text{C}_8\text{H}_7\text{BF}_3^-$ requires 170.0629.

Bromodimethylsulphonium bromide (4.44)

A 100 mL round-bottom flask was charged with a stir bar and addition funnel then flame dried under high vacuum and then allowed to cool to rt, the system was then purged with Ar. The round-bottom flask was then charged with dimethyl sulphide (3.7 mL, 50 mmol)

and dry CH_2Cl_2 (10 mL). The addition funnel was charged with Br_2 (2.56 mL, 50 mmol) and dry CH_2Cl_2 (10 mL). The reaction flask was cooled to $0\text{ }^\circ\text{C}$ in an ice bath and stirred rapidly to which, the bromine solution was added dropwise over a period of 30 min. With the addition of Br_2 an orange precipitate was observed developing. After 4 h the orange precipitate was collected by filtration and washed with Et_2O (4 x 20 mL) then left to dry under high vacuum to furnish a light orange powder (76%, 8.4860 g). IR $\nu_{\text{max}}/\text{cm}^{-1}$ (neat film): 2983, 2902, 1417, 1308, 1035, 983. ^1H NMR (300 MHz, Chloroform-*d*) δ 2.63 (s). ^{13}C NMR (75 MHz, Chloroform-*d*) δ 26.5 (CH_3). MS-ESI (*m/z*): $[\text{M}^{79}\text{Br}]^+$ 141, $[\text{M}^{81}\text{Br}]^+$ 143.

Potassium 2-(oxiranyl)phenyltrifluoroborate (4.23)



A 25 round-bottom flask was charged with a stir bar, potassium 2-vinylphenyltrifluoroborate (704 mg, 3.4 mmol) and acetone (3.5 mL); the flask was then cooled to $-78\text{ }^\circ\text{C}$. While stirring, a solution of DMDO in acetone (74 mM) (55.9 mL, 4.1 mmol) was added dropwise at $-78\text{ }^\circ\text{C}$; the yellow colour of the DMDO solution quickly disappeared. The reaction mixture was stirred at $-78\text{ }^\circ\text{C}$ for 2h then allowed to warm to rt after which half of the solvent was removed under reduced pressure and the product was precipitated, with the addition of Et_2O , as a white fluffy powder. The product was collected by filtration and further washed with Et_2O , then dried under high vacuum overnight (646.1 mg, 85%). IR $\nu_{\text{max}}/\text{cm}^{-1}$ (neat film): 3061, 3018, 1389, 1207, 1192, 958, 939, 746. ^1H NMR (300 MHz, DMSO-*d*₆) δ 7.44 – 7.31 (m, 1H), 7.08 – 6.95 (m, 2H), 6.90 – 6.79 (m, 1H), 4.35 – 4.27 (m, 1H), 2.99 (dd, $J = 5.7, 4.3$ Hz, 1H), 2.54 (dd, $J = 5.7, 2.7$ Hz, 1H). ^{13}C NMR (75 MHz, DMSO-*d*₆) δ 140.3 (C_q), 131.4 (q, $^3J_{\text{C-F}} = 2.8$ Hz, CH), 125.49 (CH), 125.45 (CH), 121.0 (CH), 51.43 – 51.28 (m) (CH), 51.1 (CH_2). ^{19}F NMR (282 MHz, DMSO-*d*₆) δ -135.10 – -136.33 (m). ^{11}B NMR (96 MHz, DMSO-*d*₆) δ 4.18 – 2.01 (m). HRMS-ESI (*m/z*): found $[\text{M-K}]^-$ 187.0545, calc'd $\text{C}_8\text{H}_7\text{BF}_3\text{O}^-$ requires 187.0542.

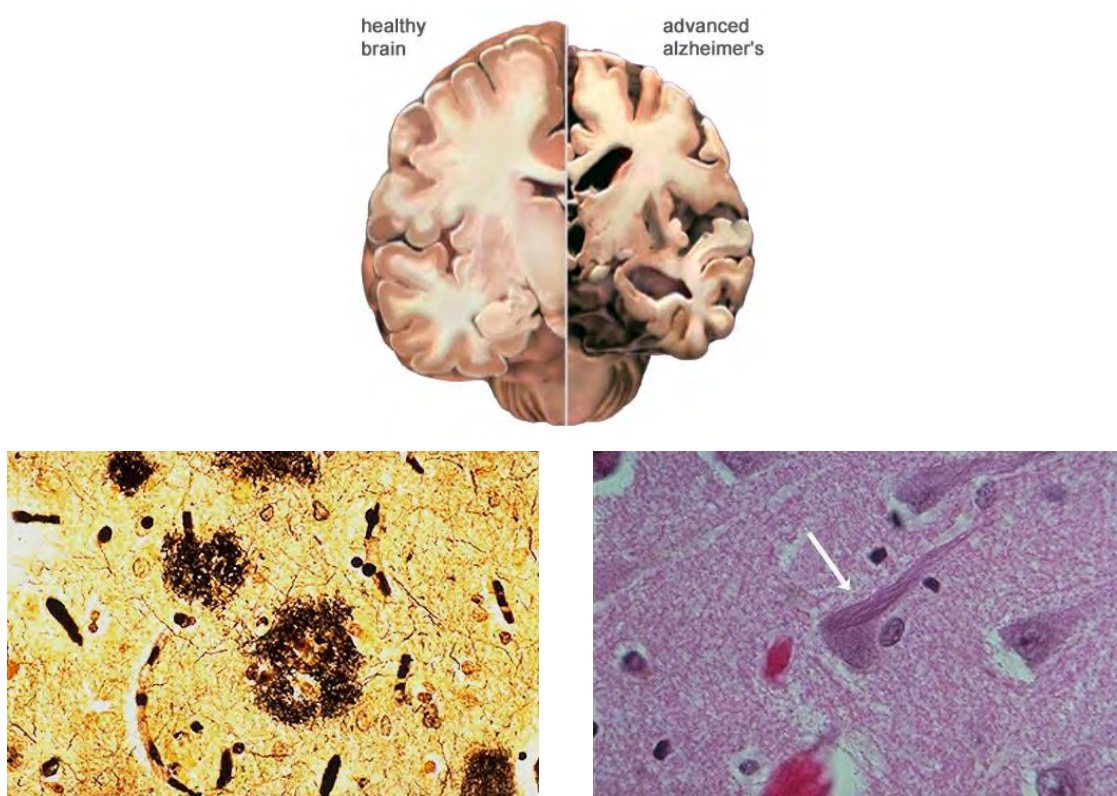
5 Benzothiazole B-F_n Complexes as Potential Bi-modal Imaging Agents for Alzheimer's Disease

Alzheimer's Disease (AD), the leading cause of dementia, is of increasing concern in a rapidly growing and ageing world population. To date, no validated biomarkers have been identified for the diagnosis of AD, definitive proof is only available via histopathologic evidence at autopsy. A domain of intense research resides in the development of non-invasive imaging tools for early-detection of disease features. Most strategies have focused on PET and NIRF imaging tracers targeting the amyloid- β (A β) peptide. To date, the development of bi-modal imaging tools has remained somewhat limited and is of considerable interest. This chapter will briefly introduce AD, its main molecular features and current developments in the imaging of such hallmarks. The design and synthesis of a series benzothiazole based B-F_n complexes, as potential bi-modal imaging agents, will then be described. The characterization of these complexes by various methods will be presented.

5.1 Introduction

The global incidence rate of dementia is projected to almost double in twenty years, reaching over 131 million cases by 2050.²⁵⁰ With aging global populations, the costs of dementia care are staggeringly increasing (\$818 million USD worldwide in 2015) and are estimated to reach \$2 trillion USD by 2030.²⁵⁰ Alzheimer's disease is the leading cause of dementia, accounting for approximately 56% of all cases,²⁵¹ and its worldwide prevalence is expected to quadruple in the next 40 years.²⁵²

AD is characterised by progressive cognitive decline accompanied by deficiencies in memory, learning ability, reason and communication. In later stages of the disease, symptom severity increases to include mood and behavioural changes, confusion, loss of judgement and a decline in motor function. Post-mortem hallmarks of AD are gross cerebral atrophy and neuro-histological evidence of extracellular A β peptide plaques and intracellular neurofibrillary tangles of hyperphosphorylated Tau protein (Figure 5.1).²⁵²



The aetiology of AD has been associated with aggregation of the A β peptide, forming insoluble plaques that are extracellularly deposited, while soluble peptide monomers are found in healthy brains.^{253,254} A β peptide aggregation is a consequence of the amyloid cascade in which metal ions (copper and zinc) are considered as triggering agents of the aggregation process (Figure 5.2). A β peptides are rich in β -sheets which are insoluble

and resistant to proteolytic digestion. While the plaques are a hallmark of AD, it is actually the soluble oligomeric forms of A β peptides that are considered the most toxic and have been implicated in the disruption of synaptic function and the production of Reactive Oxygen Species (ROS) leading to neuronal cell death.^{254,255}

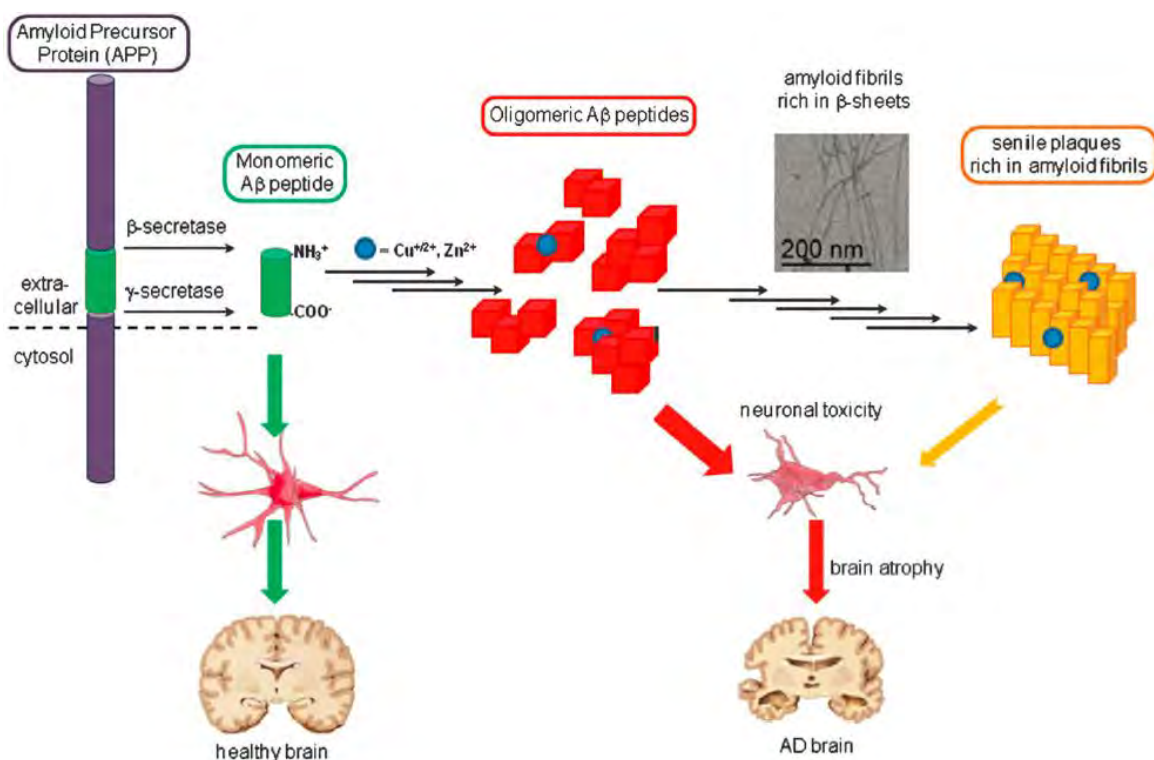
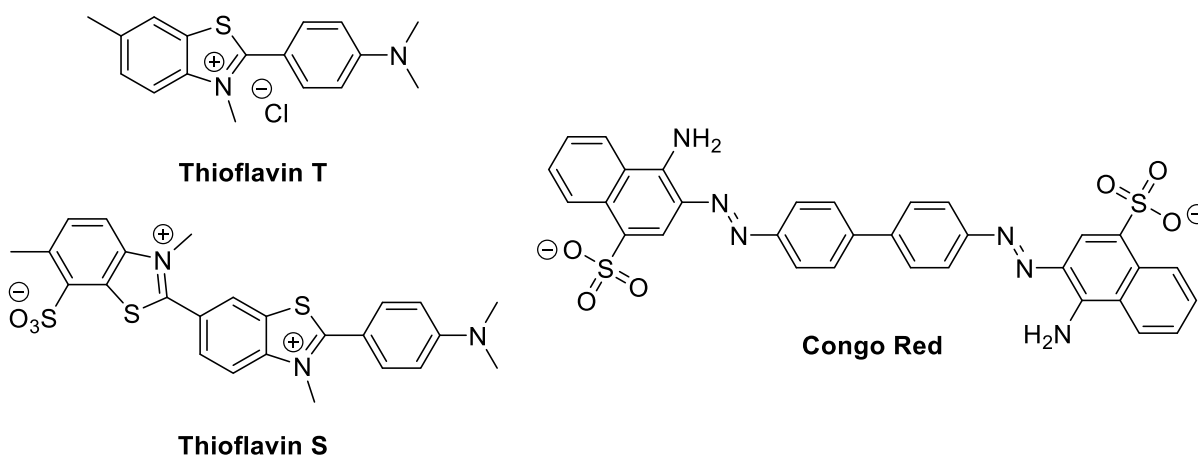


Figure 5.1 The amyloid cascade hypothesis (adapted with permission from Noël *et al.*, *Chem. Soc. Rev.*, **2013**, 42, 7747-7762, copyright Royal Society of Chemistry)

To date, there is no cure for AD. As such, disease management relies on managing symptoms arising from the underlying neurodegenerative process. The development of curative drugs is hampered by an incomplete understanding of disease origin and lack of physiological markers for early detection and diagnosis. The importance of early detection is highlighted by the presence of A β deposits several years prior to the appearance of clinical symptoms,²⁵⁶ and clinical diagnosis of AD is preceded by 3-6 years of mild cognitive impairment.^{257,258} Many drug candidates have failed due to their administration

at late stages of the disease when the pathology is already too advanced. Therefore, a complete picture of the amyloid cascade process, including the characterisation of intermediate species and A β aggregation phenomena, would aid in the design and development of diagnostic and curative tools for AD. In this context, the development of tools for the *in vivo* detection of early disease markers is of great importance.

Currently, definitive AD diagnosis is obtained by post-mortem histological staining of A β fibrils (with Thioflavin T (**ThT**), Thioflavin S (**ThS**) and Congo Red (**CR**), Scheme 5.1).^{259,260} Given the implication of A β oligomers and aggregates in disease origin and progression, A β has become the main target for non-invasive *in vivo* molecular imaging by various techniques. As such, the efficacy of prospective tracers for AD is evaluated based on their specificity for interaction with A β aggregates. Generally, MRI, PET, SPECT and more recently NIRF are predominant modalities employed in clinical settings. While MRI provides valuable structural information (cerebral atrophy), its sensitivity is too low for molecular imaging of A β aggregates. The following sections will describe current developments and requirements for tracers in the fields of PET and NIRF imaging for AD.



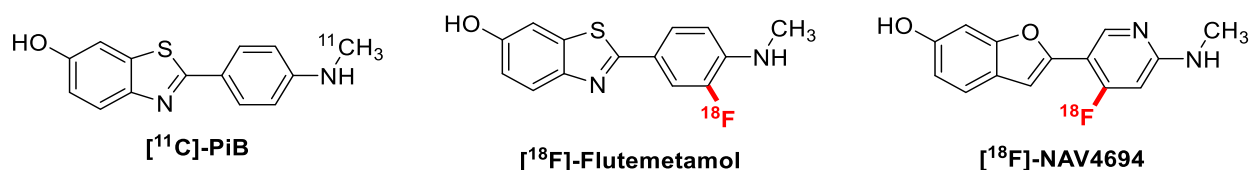
Scheme 5.1 Chemical structures of Thioflavin T (**ThT**), Thioflavin S (**ThS**) and Congo Red (**CR**)

5.1.1 PET Imaging for AD

Generally, the design of the most widely used PET tracers for AD have been inspired by the structures of **ThT** and **CR**. While the exact site of interaction of **ThT** and **CR** with fibrils is still unknown, the molecules are thought to insert into hydrophobic grooves in the folded peptide, assisted by π -stacking interactions with aromatic peptide residues. Generally, PET probes for A β aggregates must meet these requirements: 1) appropriate lipophilicity to allow Blood-Brain Barrier (BBB) permeability, 2) selectivity and affinity for amyloid plaques, 3) appropriate brain clearance/washout to allow determination of nonspecific and specific binding, 4) appropriate radioisotope half-life to allow time for synthesis, injection and image collection, and finally 5) stable to physiological conditions.

5.1.1.1 PET Ligands Derived from ThT/ThS

Due to ThT's affinity for A β fibrils, this dye has become the "Gold Standard" for the *in vitro* and *in vivo* detection of amyloid fibrils. It is therefore not surprising that a wide range of molecular probes developed for AD are 2-arylbenzothiazole derivatives of ThT (Scheme 5.2).^{260–267}



Scheme 5.2 Chemical structures of the most widely used **ThT** derived tracers selective for A β [¹¹C]-Pittsburgh Compound B, developed by Klunk *et al.* (Scheme 5.2, [¹¹C]-**PiB**) was the first, and currently most extensively used, PET tracer for A β plaques.^{262,268,269} As a neutral, lipophilic derivative of **ThT**, [¹¹C]-**PiB** shows excellent BBB permeability and binds to A β plaques with high affinity and specificity. Studies with [¹¹C]-**PiB** in human

patients showed increased localisation and retention of the tracer in frontotemporal and hippocampal areas of the brain in AD patients compared to healthy controls (Figure 5.3).^{269–272} Tracer uptake in brain regions known for higher A β deposits was confirmed via post-mortem histological staining.

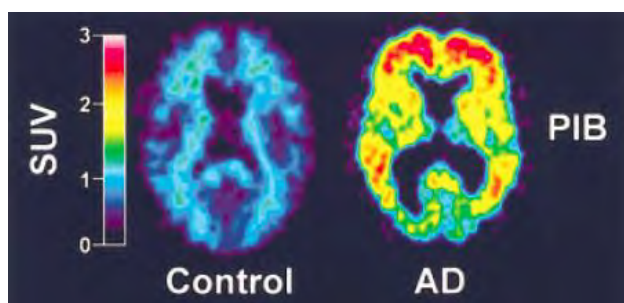


Figure 5.2 [^{11}C]-PiB standardized uptake value (SUV) in healthy (left) and AD (right) patients (adapted with permission from Klunk *et al.*, *Ann. Neurol.*, **2004**, 55, 306-319, copyright John Wiley and Sons)

However, routine clinical use of [^{11}C]-PiB is hampered by the short-lived nature of its ^{11}C radioisotope. The short half-life ($t_{1/2} = 20$ minutes) limits applications to centres equipped with onsite cyclotrons and radiosynthetic facilities capable of delivering ^{11}C -radiotracers. Therefore, the use of ^{18}F with a more appropriate half-life ($t_{1/2} = 110$ minutes) has been sought as a viable and necessary alternative, where centralized production and regional distribution is common practice as with [^{18}F]-FDG.

This led to the development of [^{18}F]-Flutemetamol (Scheme 5.2) which is identical in structure to [^{11}C]-PiB except for the inclusion of ^{18}F in the 2-aryl system.^{263,273} Studies with [^{18}F]-Flutemetamol have shown that it can effectively differentiate between AD patients and healthy controls.²⁷⁴ It was also not surprising given the extent of chemical structural similarity between [^{18}F]-Flutemetamol and [^{11}C]-PiB, that both these tracers were found to have similar retention characteristics and brain region distributions.²⁷⁵

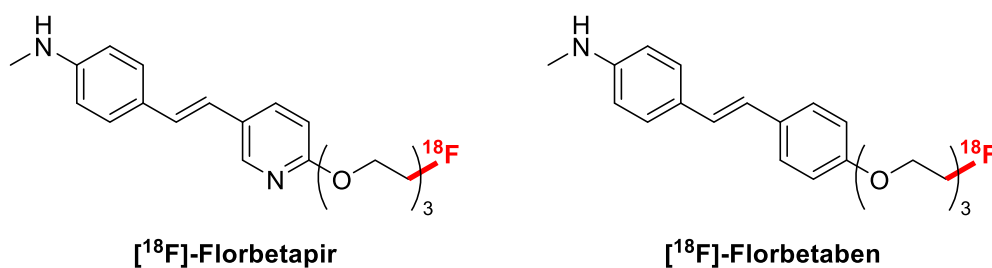
Interestingly, [^{18}F]-**Flutemetamol** has also shown the ability to differentiate AD from other neurodegenerative disorders.²⁷⁴ [^{18}F]-**Flutemetamol** successfully completed Phase III clinical trials and received Food and Drug Administration (FDA) and European Medicines Agency (EMA) approval for clinical use; manufactured and distributed by GE Healthcare as VizamyliTM. One drawback of [^{18}F]-**Flutemetamol** is its documented nonspecific retention in white matter, which can hamper visual assessments.²⁷⁵

Nonspecific binding to white matter was overcome by workers at AstraZeneca who developed [^{18}F]-**NAV4694** which incorporated a benzofuran ring that is structurally similar to benzothiazoles. [^{18}F]-**NAV4694** was shown to be capable of robustly distinguishing between AD patients and healthy controls, while showing less retention in white matter compared to other amyloid PET tracers, possibly allowing increased accuracy in clinical image interpretation.²⁷⁶ [^{18}F]-**NAV4694** was reported to have near identical imaging characteristics to that of [^{11}C]-**PiB**, specifically similar tracer retention and brain region distribution as well as low nonspecific binding to white matter.²⁷⁷

5.1.1.2 PET Ligands Derived from CR

Kung *et al.* simplified the chemical structure of **CR** leading to the development of stilbene derivatives [^{18}F]-**Florbetapir** and [^{18}F]-**Florbetaben** (Scheme 5.3).^{278–280} The structures of these two tracers are identical except for the replacement of the pyridine ring in [^{18}F]-**Florbetapir** with a phenyl ring in [^{18}F]-**Florbetaben**. Both tracers were shown to be successful in distinguishing AD patients from healthy controls, as well as showing similar retention and distribution characteristics compared to [^{11}C]-**PiB**.^{281–283} [^{18}F]-**Florbetapir** is notably known for its rapid reversible binding characteristics which allow image collection at 45–50 minutes post injection, compared to 90 minutes for [^{18}F]-

Florbetaben.²⁷² Both these tracers have successfully completed Phase III clinical trials and received FDA and EMA approval for clinical use; [¹⁸F]-Florbetapir is manufactured and distributed by Eli Lilly as Amyvid™ and [¹⁸F]-Florbetaben is manufactured and distributed by Piramal Imaging as NeuraCeq™.



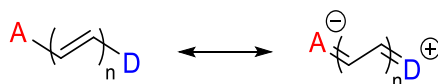
Scheme 5.3 Chemical structures of stilbene derivatives [¹⁸F]-Florbetapir and [¹⁸F]-Florbetaben

5.1.2 NIRF Imaging for AD

Fluorescence spectroscopy is emerging as an alternative and complementary non-invasive imaging modality for the *in vivo* detection of A β . Fluorescence allows rapid, highly sensitive, inexpensive, non-radiative and real-time visualization of biomolecules both *in vitro* and *in vivo*. For *in vivo* use it is important to note that fluorescent probes need to emit fluorescence in the so called therapeutic window (far-red or near-infrared region (NIR), 600-900 nm). NIR light is suitable for *in vivo* imaging due to appropriate tissue penetration depth, minimal biological matter auto-fluorescence and minimal photo-damage to biological samples.²⁸⁴ Additionally, absorption of NIR light by body tissues is minimal within this spectral range.

The design of NIRF probes for A β has largely exploited the incorporation of Donor(D)- π -Acceptor(A) motifs within the molecular scaffold. These molecular architectures allow for bathochromic shifts in absorption and emission by effectively lowering the energy difference between the Frontier Molecular Orbitals (FMOs), specifically between the

Highest Occupied Molecular Orbital (HOMO) and Lowest Unoccupied Molecular Orbital (LUMO), called the HOMO-LUMO gap. The HOMO-LUMO gap is lowered through the combined effect of a conjugated π system and D- π -A motif which generates a “push-pull” system. D- π -A molecules can be described by two resonance forms, one neutral and the other zwitterionic; the zwitterionic resonance form is a closer representation of the excited state (Scheme 5.4). This renders the entire molecular increasingly polarizable, and therefore the ground state is closer in energy to the excited state hence a lower HOMO-LUMO gap.²⁸⁵ NIRF probes normally display a change in emission properties once bound to A β aggregates, this aids in the differentiation between nonspecific and specific binding. Binding is usually accompanied by bathochromic shifts in emissions wavelength as well as increased quantum yield (QY).

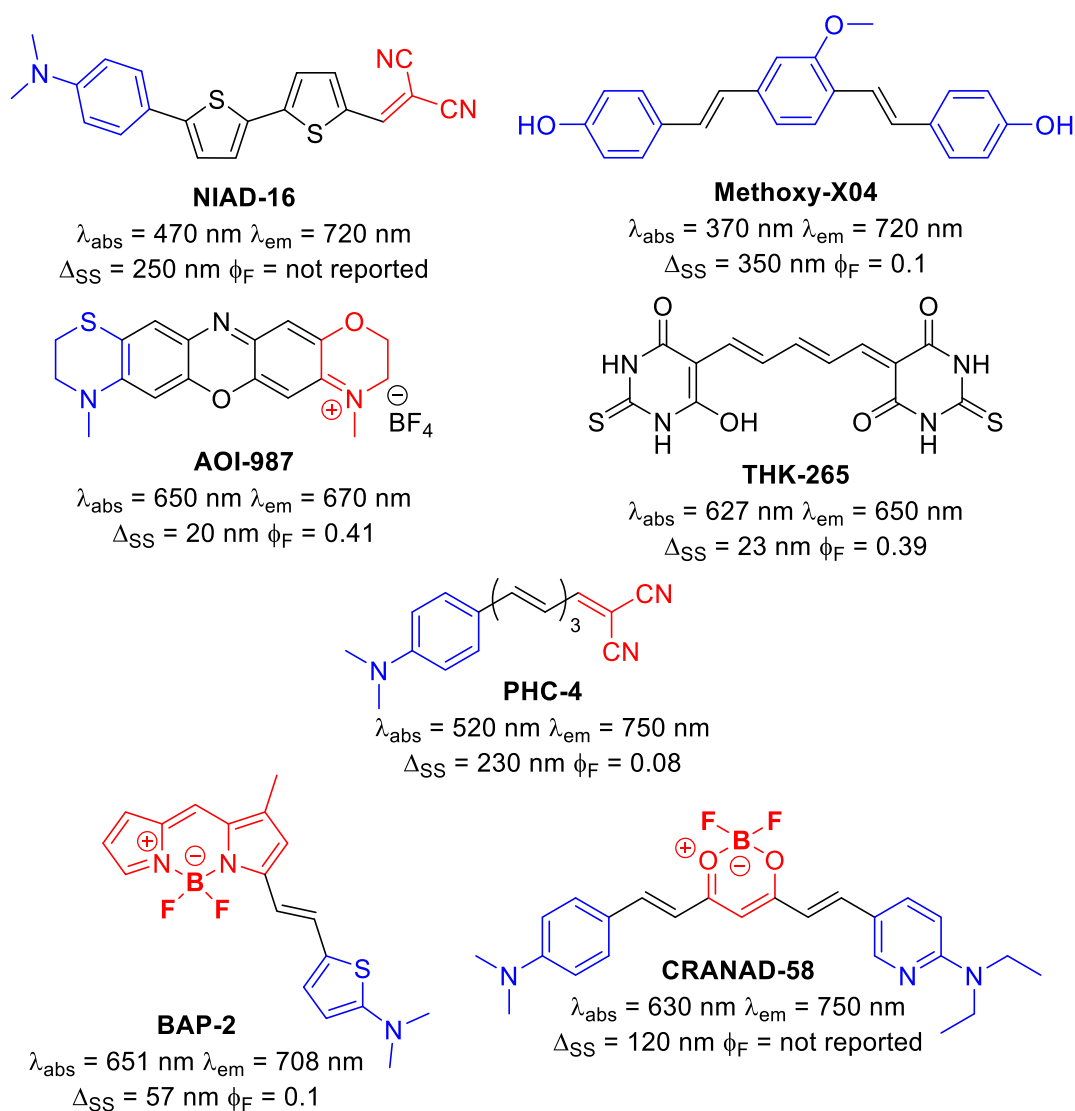


Scheme 5.4 D- π -A design of NIR fluorescent probes. Acceptor (A) in red, Donor (D) in blue

To date, no NIRF probe has been approved for clinical use. However, significant research is focused on the development of probes possessing favourable photophysical properties and affinity for A β aggregates for *in vivo* applications.^{285–287} The following section will discuss the most relevant probe from each family of reported probes and their current developments. As described for PET probes above, NIRF probes for A β aggregates must meet some of the same basic requirements as well as additional ones: 1) appropriate lipophilicity to allow BBB permeability, 2) selectivity and affinity for amyloid plaques, 3) appropriate brain clearance/washout to allow determination of nonspecific and specific binding, 4) stable to physiological conditions, 5) emission in the NIR, 6) large Stokes shift

and finally 7) some change in emission properties upon binding/interacting with A β aggregates.

Following design choices for PET probes for A β (see section 5.1.1), fluorescent probe structures have been inspired by dyes used for *in vitro* detection of amyloid aggregates. As such, they are generally planar and incorporate aromatic rings into their structure for favourable π -stacking interactions with aromatic residues of the A β peptide (Scheme 5.5).



Scheme 5.5 Selected structures and properties (Stokes shift = Δ_{SS} , Quantum Yield (QY) = Φ_{F}) of NIRF probes for A β . Acceptor motif in red, Donor motif in blue

Developed by Swager *et al.*, **NIAD-16** was a result of rational design and improvement based on its predecessor **NIAD-4**, this class of probe was designed by merging chemical features of **ThT**, **ThS** and **CR**.^{288–290} While possessing appropriate photophysical properties and the ability to detect A β plaques *in vitro*, no *in vivo* imaging has been reported using **NIAD-16**.

Klunk *et al.* reported the synthesis and photophysical properties of **CR** derivative **Methoxy-X04**.²⁹¹ The probe displayed emission well into the NIR, and was shown bind to A β aggregates selectively and with high affinity *in vitro*. Due to these favourable properties, the probe was investigated *in vivo* by injection into transgenic mice overexpressing amyloid lesions; **Methoxy-X04** was able to detect amyloid deposits at high resolution.²⁹¹

The development of **AOI-987** was considered a milestone in the development of NIRF probes, as it was the first to be used for the non-invasive *in vivo* detection of A β in AD animal models.²⁹² Although the molecule is charged it was able to sufficiently penetrate the BBB and bind to A β aggregates (with lower affinity compared to other probes). **AOI-987** was shown to be able to distinguish between transgenic mice (overexpressing amyloid deposits) and wild type by detecting A β aggregates *in vivo* in the former. The probe could also quantify amyloid plaque load in mice at different stages of the disease. Despite these favourable properties, **AOI-987** had a few drawbacks namely the small Stokes shift ($\Delta_{SS} = 20$ nm) and minor fluorescence changed upon interaction with A β aggregates. Additionally, the probe required extended washout times to clear the brain in order to differentiate between nonspecific and specific binding to A β aggregates.

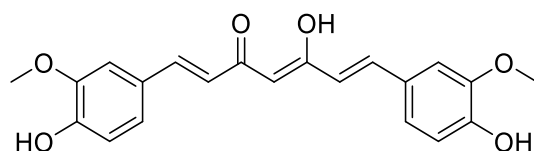
THK-265 represents another breakthrough in the development of NIRF probes for *in vivo* A β aggregate detection. The probe was developed by Okamura *et al.* through the virtual screening of various NIRF probes.²⁹³ In addition to displaying suitable photophysical properties, this probe binds A β aggregates with higher affinity than both **ThT** and **AOI-987**, the probe also displays a 6-fold increase in fluorescence intensity upon binding A β aggregates. **THK-265** successfully differentiated between wild type and transgenic mice (overexpression of amyloid plaques) by *in vivo* detection of aggregates. This probe was also shown to have faster clearance than **AOI-987**, allowing for faster determination of nonspecific and specific binding. As demonstrated with **AOI-987**, **THK-256** could be used to determine amyloid plaque loading in mice at different stages of the disease.²⁹⁴ While possessing many favourable properties, this probe still requires higher sensitivity for the *in vivo* real-time monitoring of brain amyloid plaques in a clinical context.

The synthesis of a family of simple conjugated probes was pioneered by Ono and Cui *et al.*, of which **PHC-4** displayed the most promising properties.^{295,296} **PHC-4** was shown to bind A β aggregates with higher affinity compared to previous generation probes. The probe also demonstrated favourable photophysical properties upon binding to A β aggregates, including a 62-fold increase in fluorescence and a bathochromic shift (80 nm) in emission wavelength. **PHC-4** was investigated in an *in vivo* AD animal model and was shown to be capable of differentiating between wild type and transgenic mice due to its faster clearance from brains of the former, highlighting specific binding to A β .

Notwithstanding the development of the aforementioned novel fluorescent compounds, BODIPY containing molecules have garnered considerable interest as NIRF probes for A β detection given their biocompatibility, lipophilicity and applications in

bioimaging.^{99,297,298} In this context, Ono *et al.* designed a series of BODIPY-based probes for the selective detection of A β aggregates.²⁹⁹ These probes were designed by incorporating features in the **NIAD** family of dyes, namely the conjugated thiophene moiety and from this series of probes, **BAP-2** emerged as the most promising. **BAP-2** was shown to selectively bind A β aggregates in high affinity in *in vitro* binding assays. However, the probe failed in *in vivo* experiments as differentiation between wild type and transgenic mice could not be observed due to the significant accumulation of the probe in the scalps of both. **BAP-2** also displayed other disadvantages, while emission was in the NIR (708 nm), the probe displayed a small Stokes shift (57 nm) which may cause potential interference via inner filter effects and Raman and Rayleigh scattering. Before potential clinical applications of BODIPY probes can be considered their downfalls of narrow Stokes shifts and nonspecific binding in lipophilic tissues need to be addressed.

The final class of probe is structurally derived from curcumin (Scheme 5.6). It is important to note that curcumin has been shown to reduce oxidative damage and amyloid plaque accumulation in *in vitro* rat models.³⁰⁰ The natural compound has also been studied as an *in vivo* probe for A β aggregates due to its fluorescent properties. However, due to its hydrophilic nature the compound exhibited poor BBB permeability, and emission was not in the NIR requiring invasive imaging techniques.³⁰⁰



Scheme 5.6 Chemical structure of the natural compound curcumin

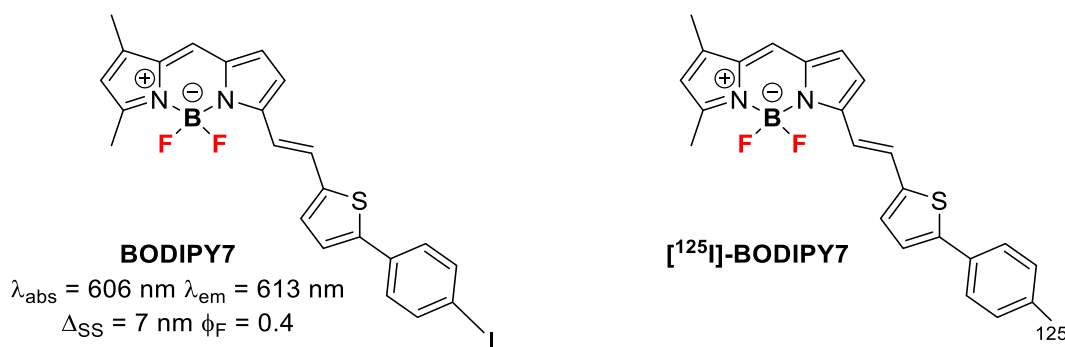
This however inspired Ran *et al.* to synthesize a series of curcumin analogues incorporating a difluoroborate moiety.³⁰¹ They rationalized that the difluoroborate motif would impart a bathochromic shift in emission by creating an acceptor motif within the molecular scaffold, as well as by rigidifying the molecular structure inducing increased planarity. These design considerations led to the development of **CRANAD-58** as the most promising candidate from this family of probes.³⁰¹ While possessing ideal NIR absorption and emission properties, this probe was shown to selectively bind A β aggregates in high affinity; binding was accompanied by significant increases in fluorescence intensity (up to 114-fold). Additionally, **CRANAD-58** demonstrated the ability to distinguish between soluble and insoluble forms of A β as observed by different emission peak shifts corresponding to the content of monomeric or aggregated A β . This is an important observation as it is the soluble forms of A β (dimers and oligomers) that are considered toxic, and precede the formation of plaques.^{252,255,302,303} **CRANAD-58** was also shown to be capable of differentiating between wild type and transgenic mice prior to formation of insoluble A β deposits; highlighting the ability of this probe to detect the presence of soluble A β plaques *in vivo*.

5.1.3 Bi-modal Imaging Probes for AD

Dual-mode imaging probes are of interest for their ability to provide complementary information. When the dual functionality comprises the coupling of non-radiative and radiative modalities, these can be used for cross-validation of each imaging technique.

There are only a few reports on the synthesis and evaluation of bi-modal imaging probes for amyloid plaques. The first of such probes was reported in 2010 by Ono *et al.* where they described the development of a dual functional SPECT/Fluorescent probe for the *in*

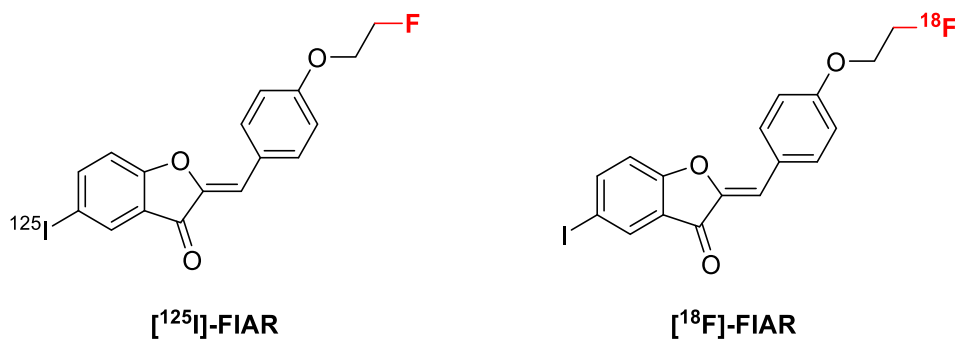
in vivo imaging of A β plaques. The probe was identical in chemical structure to a previous NIRF probe they had reported, **BODIPY7**, except where the molecule was labelled with ^{125}I (Scheme 5.7, [^{125}I]-**BODIPY7**).³⁰⁴ While **BODIPY7** was found to effectively distinguish between wild type and transgenic mice by the *in vitro* staining of brain slices, its optical properties were outside the NIR and therefore could not be translated to *in vivo* experiments. *In vivo* SPECT experiments showed that [^{125}I]-**BODIPY7** exhibited low brain uptake despite its lipophilic character, this was attributed to rapid trapping of the probe in the liver. As a result of these observations it was deemed that [^{125}I]-**BODIPY7** fell short on several criteria required for a potential SPECT/NIRF probe, namely photophysical properties outside the NIR, small Stokes shift, and low brain uptake of the radiolabelled probe.



Scheme 5.7 Chemical structures of **BODIPY7** and [^{125}I]-**BODIPY7**

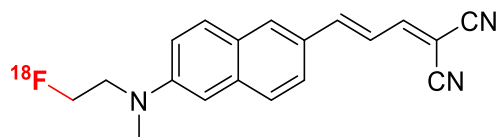
A year later Ono *et al.* developed **FIAR**, a bi-modal (PET/SPECT) radiotracer for *in vivo* imaging of A β plaques (Scheme 5.8).³⁰⁵ **FIAR** was demonstrated to bind A β aggregates in high affinity and could distinguish between the brain sections of wild type and transgenic mice. The radiolabelled analogues displayed good brain uptake values along with reasonable clearance, however continued distribution of the tracers in blood may hinder image interpretation due to background issues. Despite the promising

characteristics of **FIAR**, its largest drawback remains its synthesis. Sharing one common intermediate, four synthetic steps are required to reach [^{125}I]-**FIAR**, and three different synthetic steps are required for [^{18}F]-**FIAR**. The development of an advanced common intermediate that could be readily radiolabelled with the desired radioisotope would be a welcome advancement.



Scheme 5.8 Chemical structures of radiotracers [^{125}I]-**FIAR** and [^{18}F]-**FIAR**

More recently Cui *et al.* described the synthesis and evaluation of a dual mode probe for use in NIRF and Cerenkov Luminescence Imaging (CLI) (Scheme 5.9).³⁰⁶ [^{18}F]-**FDANIR-4c** was developed as a derivative of their previously reported NIRF probes, and its structure is similar to that of **PHC-4** (see section 5.1.2). Non-radiolabelled **FDANIR-4c** was used for *in vivo* NIRF imaging and was shown able to distinguish between wild type and transgenic mice. However, while possessing all the requisite photophysical and biodistribution properties for NIRF imaging, the radiolabelled probe failed to show any difference in wild type and transgenic mice by CLI. This failure in terms of differentiating was attributed to slow brain clearance of [^{18}F]-**FDANIR-4c**, the presence of radiometabolites of [^{18}F]-**FDANIR-4c** which may blur the desired observable signal and finally the Cerenkov luminescence emitted by the probe was in the ultraviolet and blue region (ultraviolet and blue light are significantly scattered and absorbed in tissue).

[¹⁸F]-FDANIR-4c

$$\lambda_{\text{abs}} = 506 \text{ nm } \lambda_{\text{em}} = 771 \text{ nm}$$

$$\Delta_{\text{SS}} = 265 \text{ nm } \phi_{\text{F}} = 0.3$$

Scheme 5.9 Chemical structure of [¹⁸F]-FDANIR-4c

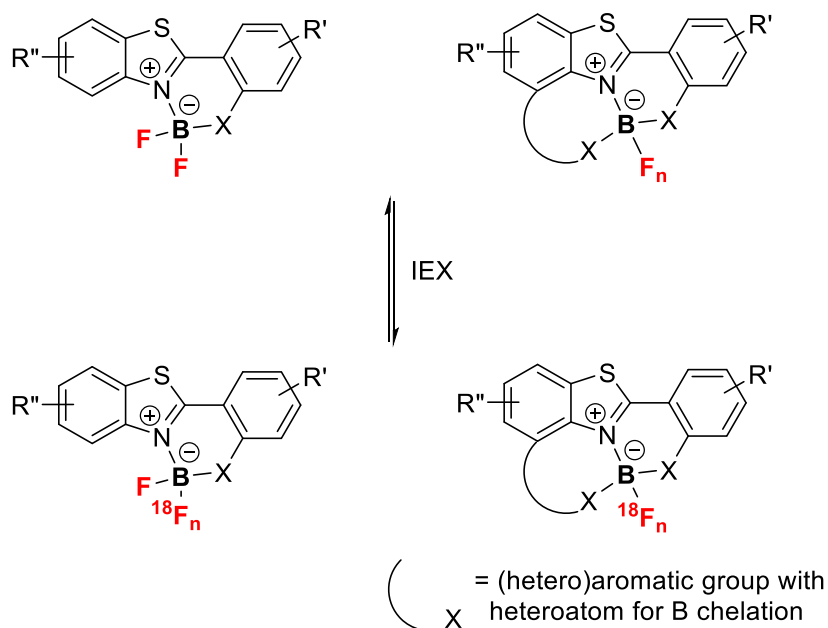
5.1.4 Benzothiazole-based B-F_n Complexes as Potential Bi-modal probes for A β

As discussed above, significant advances have been made towards *in vivo* imaging of A β aggregates in pursuit of the earlier detection of AD biomarkers. Thus far, three PET probes have been approved for clinical use in AD diagnosis, while no NIRF candidates have begun trials in humans. Additionally, advances in the development of bi-modal probes have been quite limited. There remains a clear demand for improved bi-modal probes specific for A β , in which the dual imaging modalities can be facilely accessed from the same compound. In this context we identified the benzothiazole core as an appropriate starting point given its documented affinity for A β aggregates, and its incorporation into clinically relevant PET probes. Inspired by **BAP-2** and **CRANAD-58**, we envisioned that fluoroborate chelation by the benzothiazole ligand would incur favourable photophysical properties due to increased structural rigidity, and the fluoroborate moiety acting as an acceptor according to D- π -A architecture (Scheme 5.10). The difluoroborate moiety should allow facile access to a PET probe via IEX, as has been successfully demonstrated with BODIPY probes.⁹⁰

Benzothiazole-based B-F₂ complexes are a recent development having been first reported in 2009 by Kim *et al.*³⁰⁷ The synthesis of other derivatives was reported in the

following years, with most complexes sharing similar photophysical properties and exhibiting emissions in the blue and green region, while mostly displaying narrow Stokes shifts similar to BODIPY probes.^{307–312} Only one reported benzothiazole B-F₂ complex, reported by Ahn *et al.*, emits just below the NIR cut-off.³¹³

In addition to synthesizing benzothiazole B-F₂ complexes we were interested in the possibility of further functionalizing the benzothiazole core into a tritopic (three heteroatoms for boron coordination) ligand for monofluoroborate chelation (Scheme 5.10). To the best of our knowledge, complexes of this nature have not been previously described, and their synthesis, characterization and investigation of photophysical properties and stability would be of interest. These monofluoroborate complexes would also be well-suited for IEX as there is only one fluoride to exchange, increasing the overall efficiency of the process.

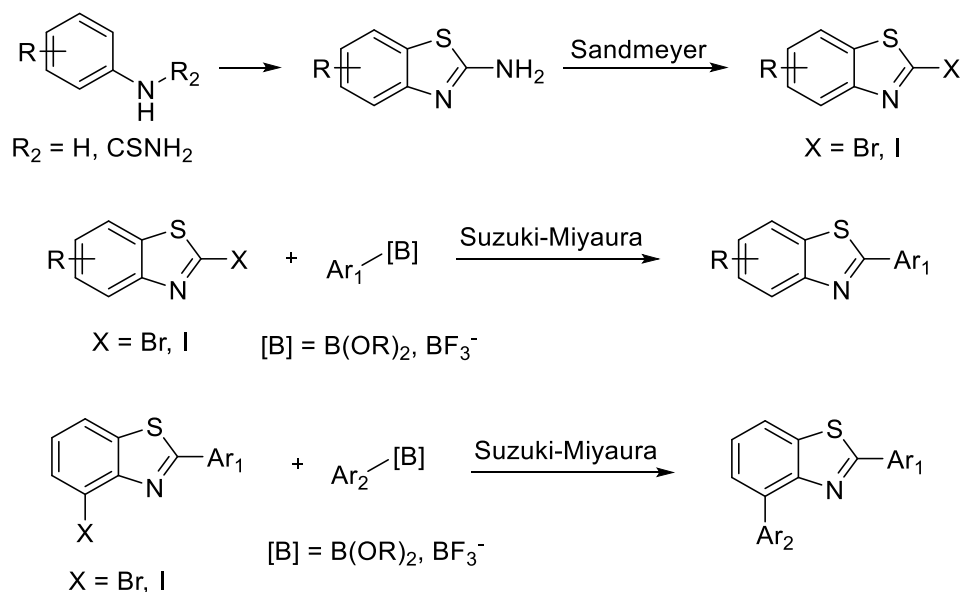


Scheme 5.10 Chemical structure of proposed benzothiazole B-F_n complexes and potential synthesis of PET probes by IEX

5.2 Results and Discussion

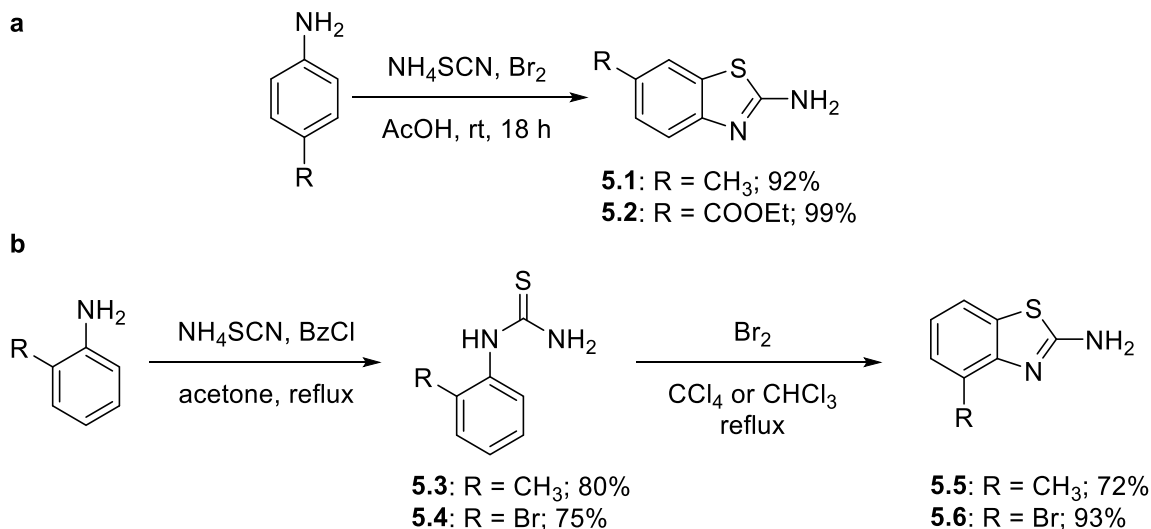
5.2.1 Synthesis of Benzothiazolyl B-F_n Complexes

The benzothiazole core is considered a privileged bicyclic heterocycle in light of its applications in pharmaceutical, agrochemical and materials chemistry.^{314–316} This has driven the development of increasingly efficient methodologies towards the synthesis of 2-aryl benzothiazole scaffolds^{252,317,318} A practical and convergent strategy involves initial generation of the 2-aminobenzothiazole scaffold from the aniline or arylthiourea, consequently, the 2- position is halogenated via a Sandmeyer reaction to provide 2-halobenzothiazole which can then be further elaborated via Suzuki-Miyaura cross-coupling with an arylboron derivative (Scheme 5.11). If R₁ is a halogen, further functionalization can be introduced through a second Suzuki-Miyaura cross-coupling to furnish 2,4-diarylbenzothiazoles (Scheme 5.11, Ar₁ = Ar₂ or Ar₁ ≠ Ar₂). Finally, B-F_n complexes can be formed using BF₃·OEt₂ in the presence of a base. This strategy is attractive as it is highly modular, allowing synthetic flexibility regarding the starting aniline as well as the availability of a large variety of arylboronic acids as coupling partners.



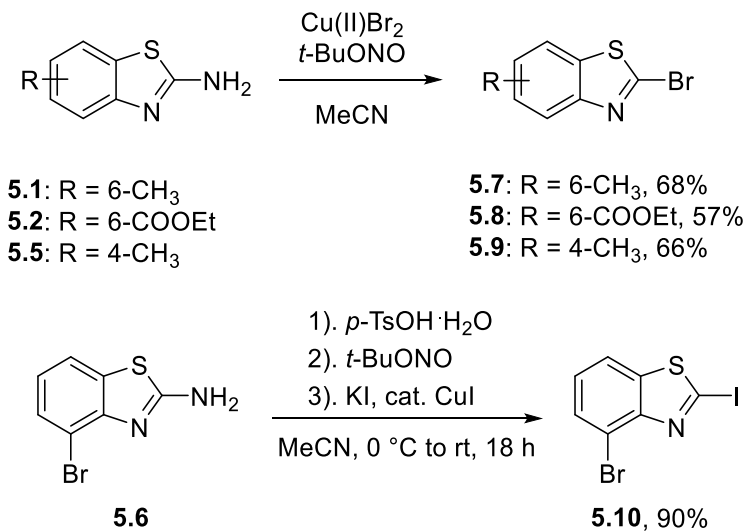
Scheme 5.11 Modular synthetic strategy towards functionalized 2-arylbenzothiazoles and 2,4-diarylbenzothiazoles

We began this investigation by synthesizing a series of 4- and 6-substituted 2-aminobenzothiazoles. 6-Substituted-2-aminobenzothiazoles could be directly obtained, in excellent yield, from the corresponding 4-substituted anilines via Brewster thiocyanation followed by Br₂ mediated oxidative cyclization in AcOH^{319,320} (Scheme 5.12, a, products 5.1 and 5.2). 4-Substituted-2-aminobenzothiazoles cannot be obtained in this manner due to preferential thiocyanation at the activated *para* position relative to the aniline.^{319,321} Therefore, the corresponding thioureas were first isolated according to conditions reported by Rasmussen and Jung (Scheme 5.12, b, products 5.3 and 5.4),^{322,323} subsequent Hegershoff cyclization^{324,325} with Br₂ yielded the corresponding 4-Substituted-2-aminobenzothiazoles in good to excellent yields (Scheme 5.12 b, products 5.5 and 5.6).



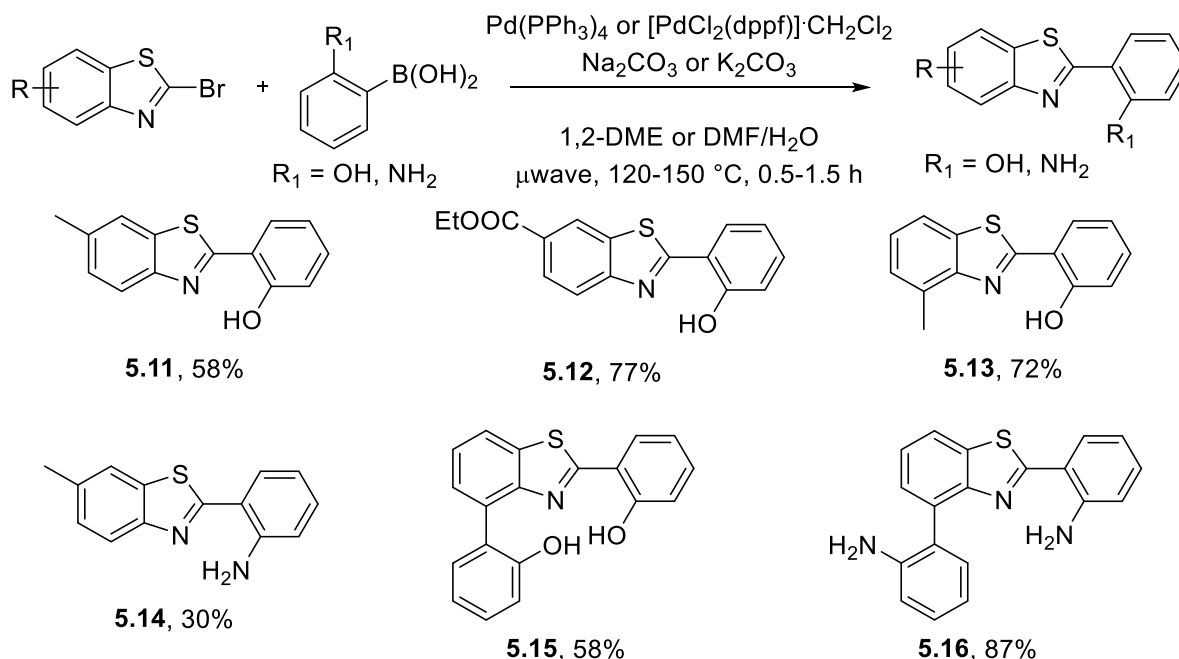
Scheme 5.12 a, Synthesis of 6-substituted-2-aminobenzothiazoles from anilines. **b**, Synthesis of 4-substituted-2-aminobenzothiazoles via arylthioureas. Isolated yields.

Sandmeyer bromination of 2-aminobenzothiazoles **5.1**, **5.2** and **5.5** was achieved in moderate yields via copper mediated bromination of the *in situ* formed diazonium cation (Scheme **5.13**, products **5.7**, **5.8** and **5.9**) using conditions as reported by Dehaen *et al.*³²⁶ Similarly, one-pot iodination of **5.6** to 2-iodo-4-bromobenzothiazole (**5.10**) was carried out in excellent yield using a modified procedure from Filimonov *et al.*¹⁵² Given the difference in reactivities of C(sp²)-I and C(sp²)-Br bonds with respect to oxidative addition to a metal centre, **5.10** will allow chemoselective and regioselective cross-coupling with various aryl boron derivatives.



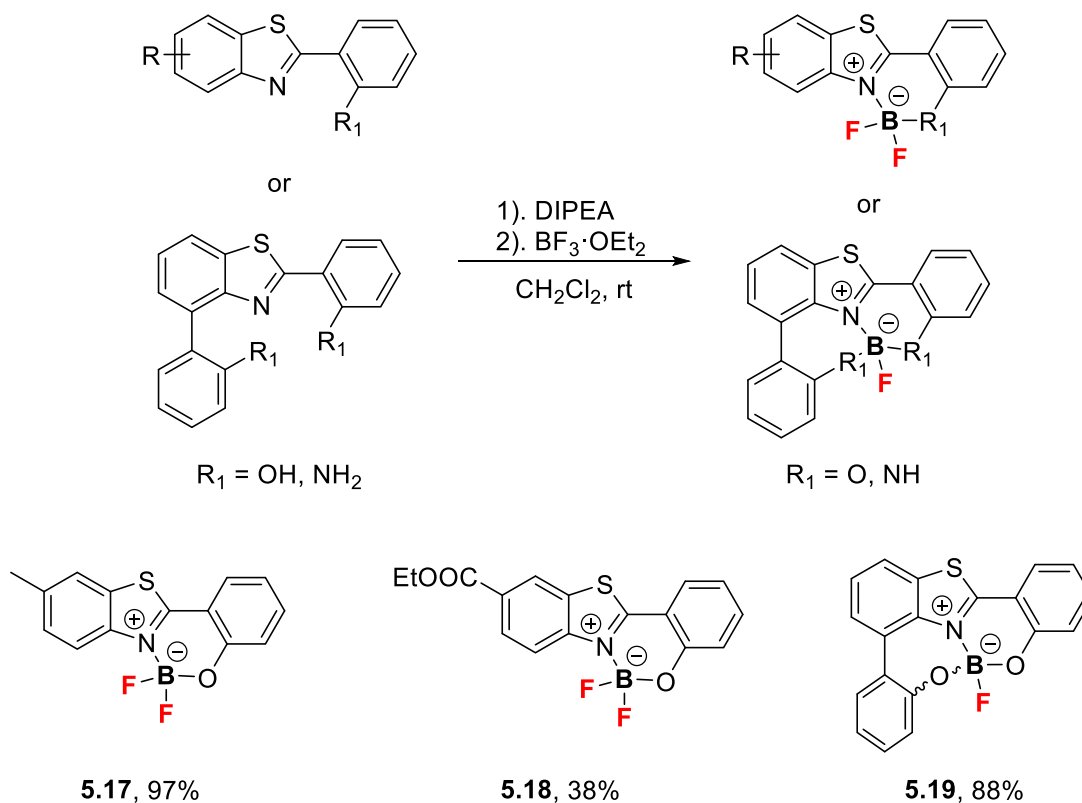
Scheme 5.13 Sandmeyer bromination and iodination of 2-aminobenzothiazoles. Isolated yields.

With 2-bromobenzothiazoles **5.7-5.9** in hand, we proceeded with microwave-assisted Suzuki-Miyaura cross-coupling with 2-hydroxyphenylboronic acid to provide the corresponding 2-arylbenzothiazoles in moderate yield (Scheme **5.14**, products **5.11**, **5.12** and **5.13**). Cross-coupling of **5.7** with 2-aminophenylboronic acid provided **5.14** in low yield. (Scheme **5.14**). Under similar reaction conditions one-pot di-arylation of **5.10** with 2-hydroxyphenylboronic acid or 2-aminophenylboronic acid could be achieved in moderate to good yields, respectively (Scheme **5.14**, products **5.15** and **5.16**).



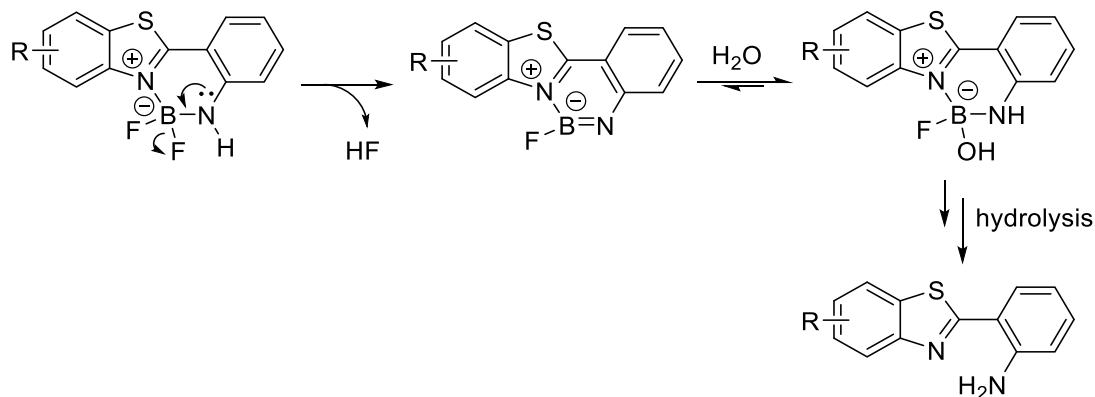
Scheme 5.14 2-arylbenzothiazole synthesis via Suzuki-Miyaura cross-coupling. Isolated yields.

With this first series of ligands in hand, we studied their ability to undergo formation of B-F_n complexes. Using standard conditions, the ligands were reacted with BF₃·OEt₂ in the presence of DIPEA as a base in CH₂Cl₂ (Scheme 5.15). Ligands **5.11**, **5.12** and **5.15** readily formed the corresponding B-F_n complexes **5.17**, **5.18** and **5.19** which could be isolated after chromatography in moderate to excellent yields. With ligands **5.13** and **5.14** the formation of new compounds in reaction mixtures was evident by TLC however, attempts to isolate these products resulted in hydrolysis of presumed B-F₂ complexes back to the starting ligands. No conversion of **5.16** could be observed when reactions were run at ambient temperature or upon heating (CH₂Cl₂ at 50 °C or toluene at 90 °C).

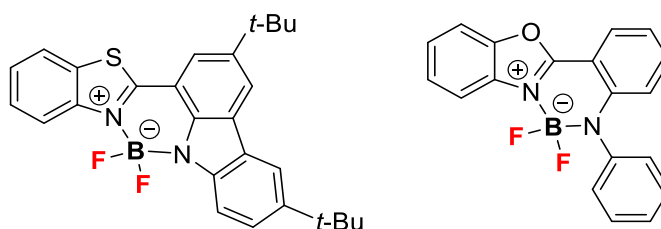


Scheme 5.15 Isolated benzothiazole B-F_n complexes. Isolated yields.

We postulated that the instability of a B-F₂ complex with **5.13** may be due to the steric hindrance imposed by the methyl group at position 4 on the benzothiazole scaffold. For aniline-containing ligands, **5.14** and **5.16**, we thought that if B-F_n complexation occurs, degradation via HF elimination followed by hydrolysis would restore the starting ligand (Scheme **5.16**). We could not find any literature precedent for 2-(benzo[*d*]thiazol-2-yl)aniline B-F₂ complexes; indeed, the only reported analogous family of compounds incorporated carbazoles or diarylamines at the 2 position of a benzothiazole or benzoxazole scaffold, respectively (Scheme **5.17**).^{310,327}

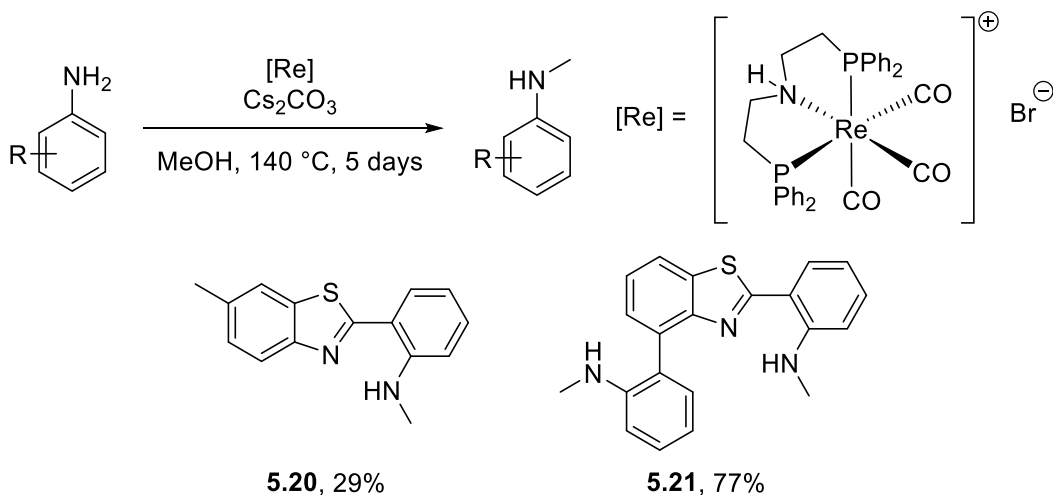


Scheme 5.16 Possible degradation pathway of 2-(benzo[d]thiazol-2-yl)aniline B-F_n complexes via HF elimination and hydrolysis



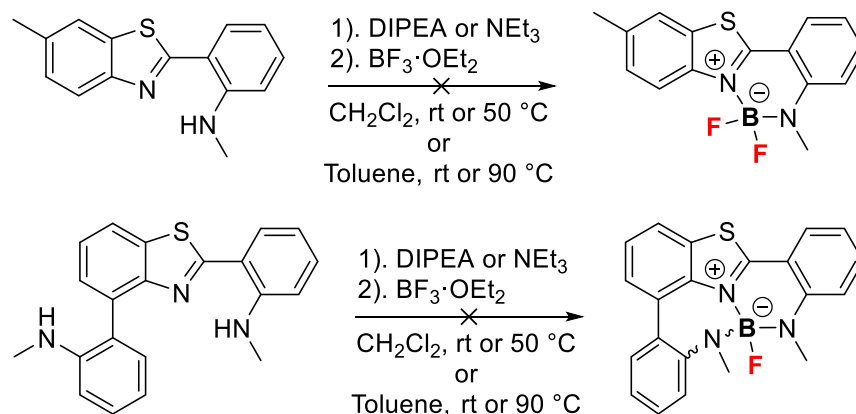
Scheme 5.17 Reported *N,N*-benzothiazole and *N,N*-benzoxazole B-F₂ complexes

With that in mind, we thought that *N*-functionalizing anilines **5.14** and **5.16** may facilitate B-F_n complex formation. Hence, we decided that addition of a methyl group would avoid presumed HF elimination degradation while not significantly affecting the electronics and steric environment of the aniline. Applying a rhenium catalysed *N*-mono methylation protocol,³²⁸ kindly provided by the group of Pr. Jean-Baptiste Sortais at the LCC, allowed the successful mono-methylation of **5.14** and the double mono-methylation of **5.16** in low to good yields, respectively (Scheme **5.18**).



Scheme 5.18 mono *N*-methylation of **5.14** and **5.16** to **5.20** and **5.21**, respectively. Isolated yields.

However, despite these modifications B-F_n complexes could not be obtained from **5.20** and **5.21** (Scheme 5.19).

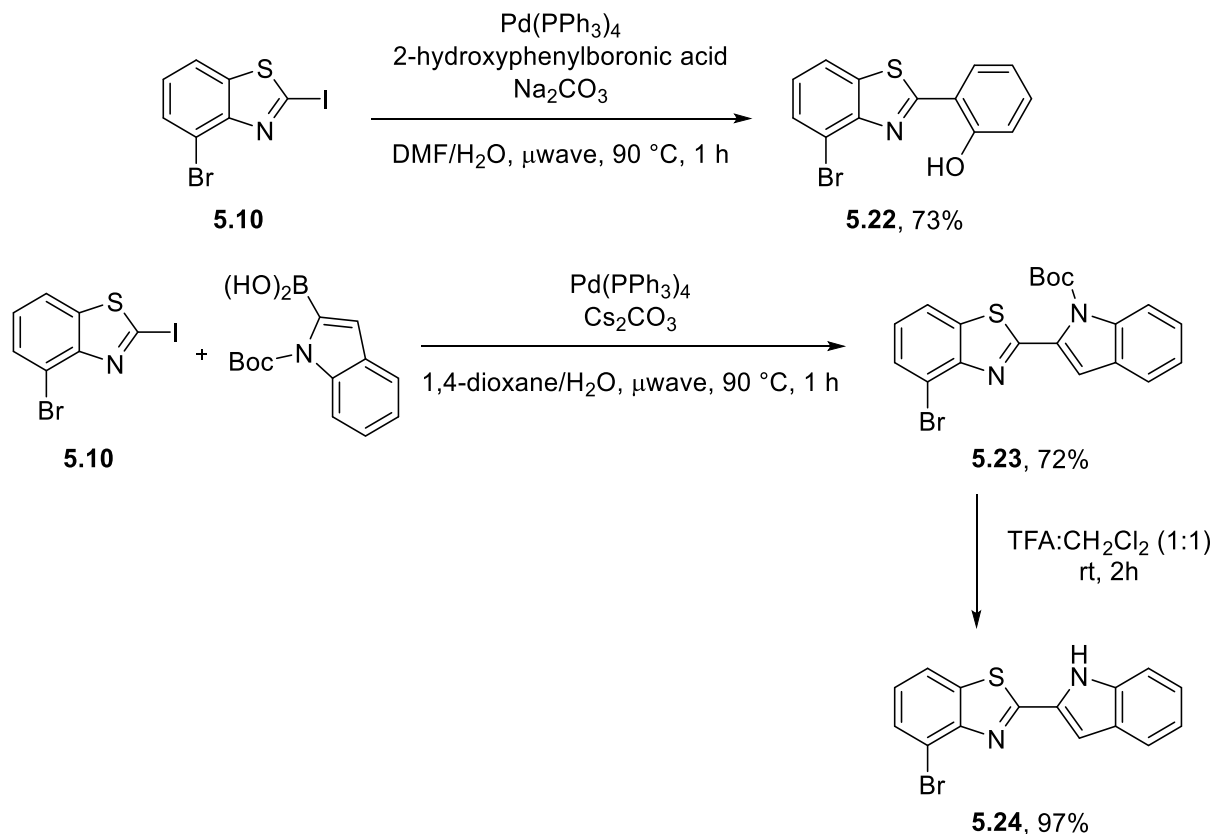


Scheme 5.19 Attempted formation of B-F_n complexes with **5.20** and **5.21**.

We continued by synthesizing products of selective mono-arylation of **5.10**, which was achieved by initial cross-coupling at the 2-position with concomitant release of iodide. We found that by lowering reaction temperatures to 90 °C selective arylation could be achieved while keeping the carbon-bromine bond at position-4 intact. As such, 2-hydroxyphenylboronic acid and *N*-Boc-indole-2-boronic acid could be coupled to **5.10** furnishing 2-aryl-4-bromobenzothiazoles **5.22** and **5.23**, respectively in good yields

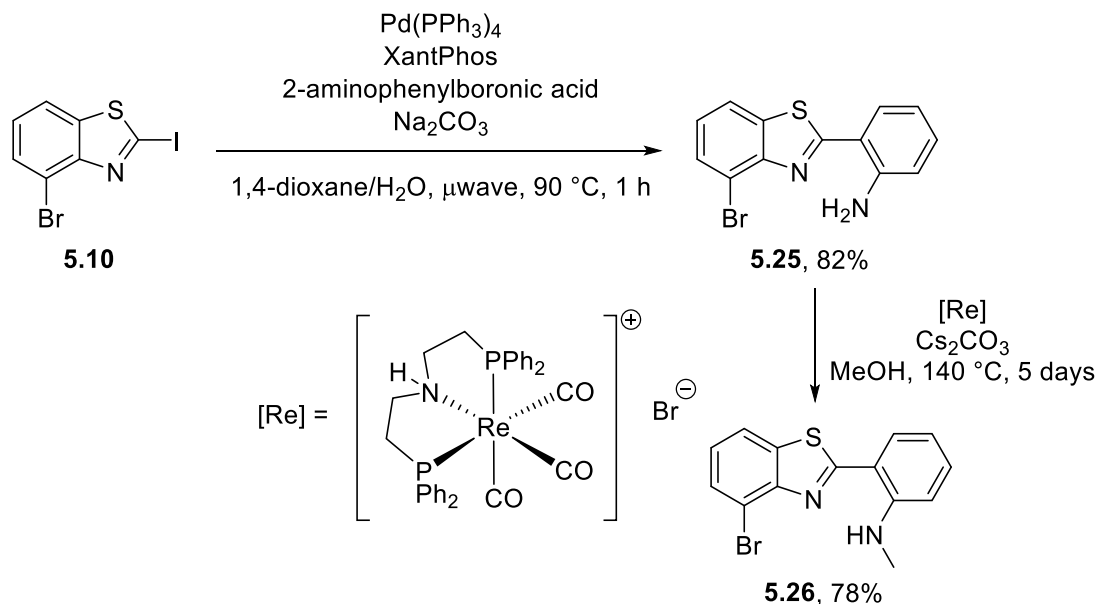
(Scheme 5.20). Subsequent Boc deprotection of **5.23** provided unprotected indole **5.24**

(Scheme 5.20).



Scheme 5.20 Selective mono-arylation of **5.10** via Suzuki-Miyaura cross-coupling. Isolated yields.

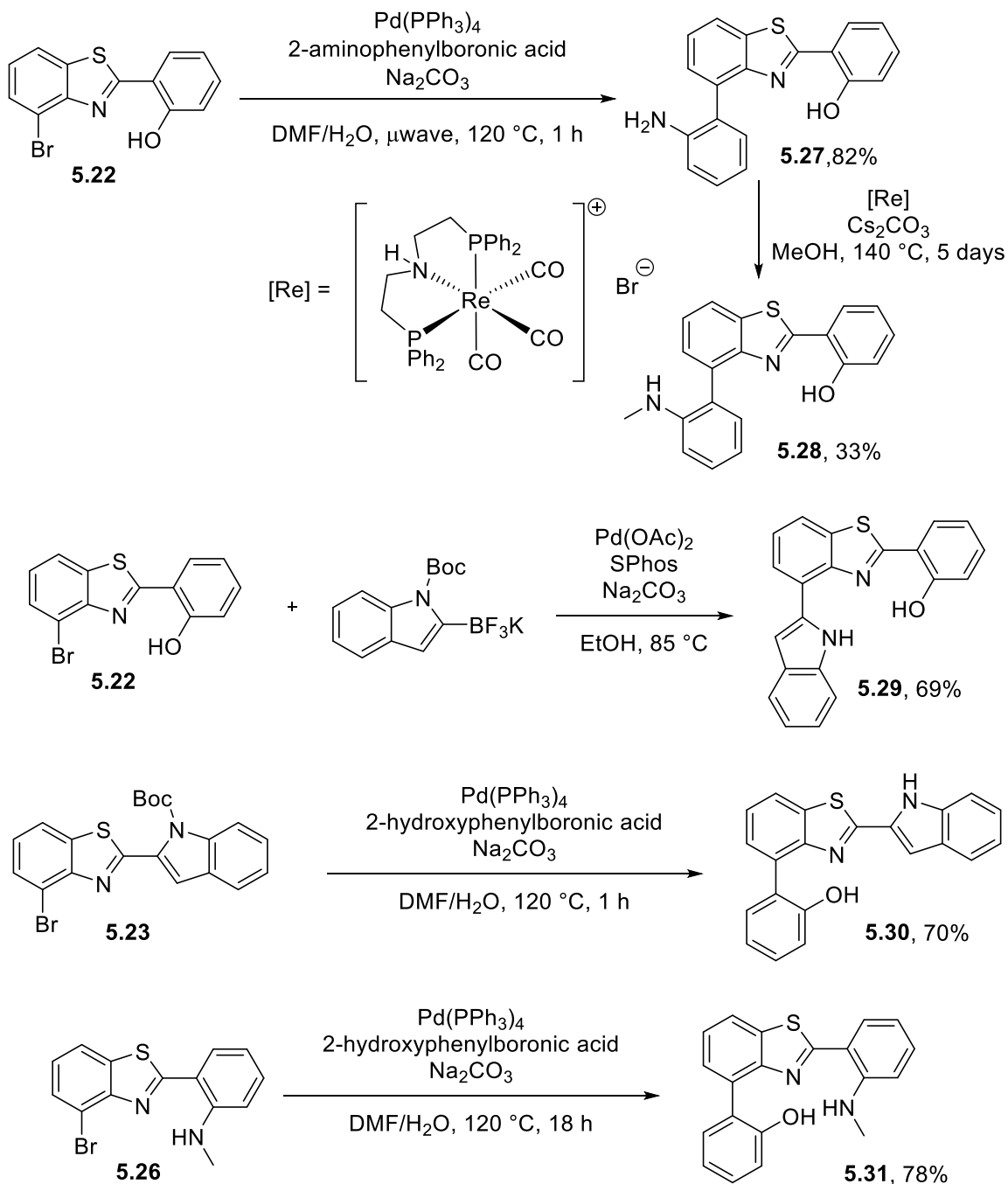
Coupling of 2-aminophenylboronic acid proved to be more challenging, as standard reaction conditions resulted in low yields (~50%) of the desired product, which unfortunately could not be separated from impurities. However, we found that employing XantPhos as a ligand allowed the clean isolation and high yield of **5.25**, which was subsequently *N*-methylated (**5.26**) (Scheme 6.21).



Scheme 5.21 Synthesis of **5.25**. Isolated yields.

We proceeded to study the ability of **5.22**, **5.24**, **5.25** and **5.26** towards the formation of their corresponding B-F₂ complexes. Unfortunately, under various reaction conditions (see Scheme **5.19**) no conversion of the starting materials could be observed by TLC, and NMR spectroscopic analysis of crude reaction mixtures did not indicate the formation of B-F₂ species. These results may provide additional evidence to the incompatibility of certain substituents at the 4-position of the benzothiazole scaffold.

The final series of ligands were synthesized by a second arylation through the 4-bromo site (Scheme **5.22**). Using standard coupling conditions, 2-aminophenylboronic acid was coupled to **5.22** to provide **5.27**, which was subsequently *N*-methylated to give **5.28**. Under conditions reported by Molander *et al.*³²⁹ potassium *N*-Boc-indole-2-trifluoroborate could be coupled to **5.22**, furnishing **5.29** after Boc deprotection. Finally, 2-hydroxyphenylboronic acid was coupled to **5.23** and **5.26** providing **5.30** (following Boc deprotection) and **5.31**, respectively.

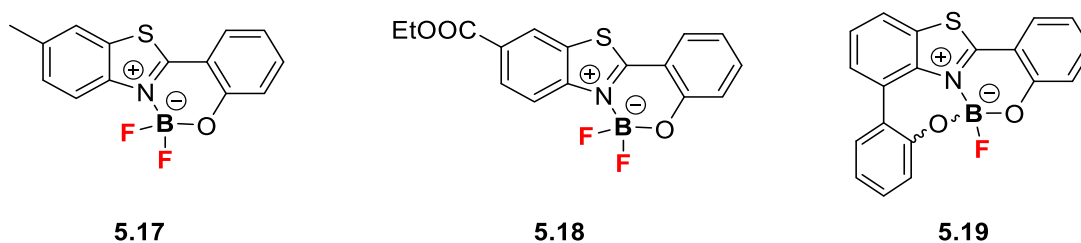


Scheme 5.22 Synthesis of 2,4-diarylbenzothiazoles. Isolated yields.

We then studied the formation of B-F complexes using **5.27-5.31**. Unfortunately, using several reaction conditions (see Scheme **5.19**) We could not observe the formation of any B-F complexes by TLC or NMR spectroscopy.

5.2.1.1 Summary of Ligand and B-F_n Complex Syntheses

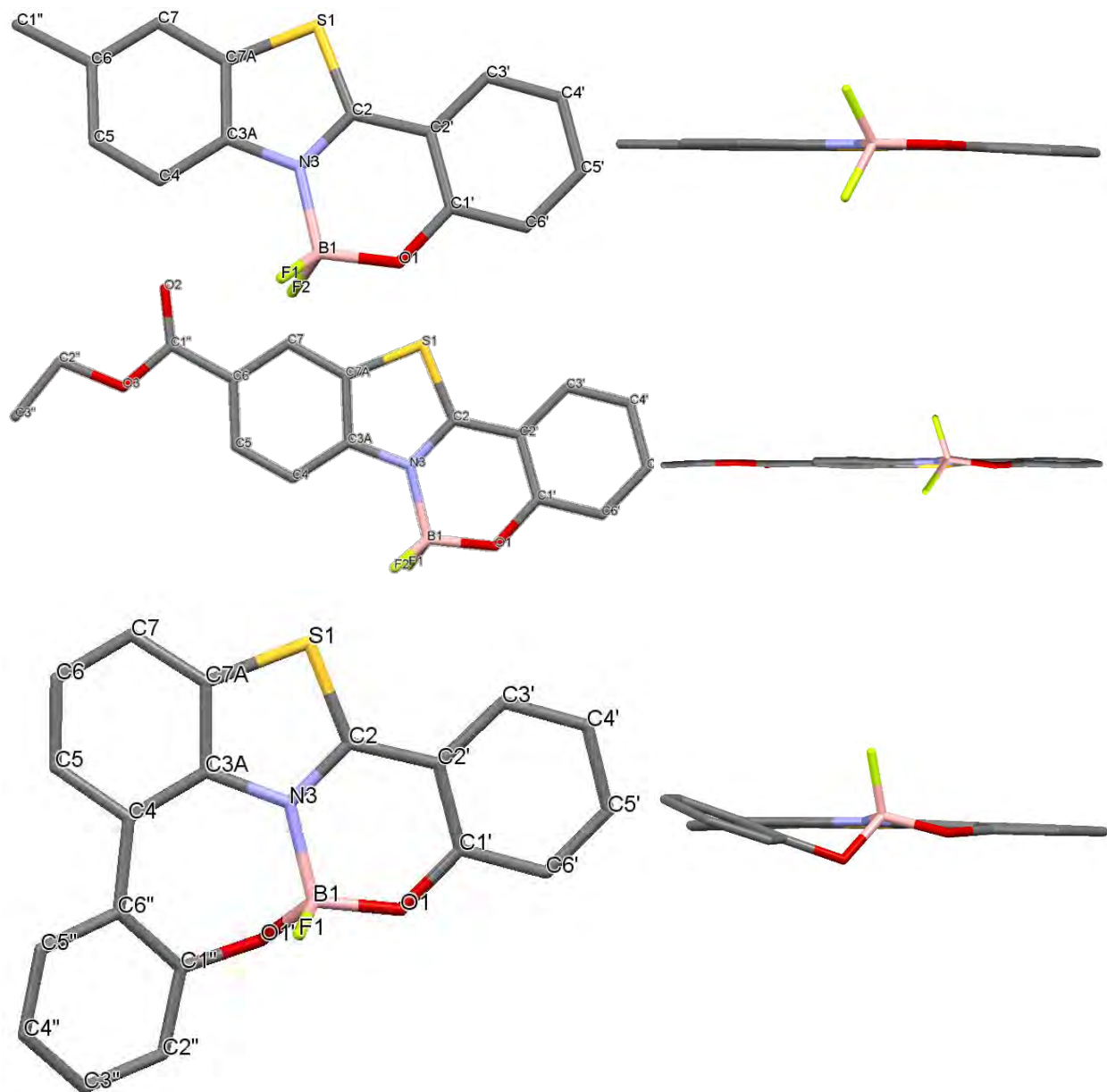
A series of variously substituted 2-aryl and 2,4-diaryl benzothiazole ligands, were synthesized. These ligands were then investigated regarding their ability to form isolable B-F_n complexes. From the family of ligands synthesized, three B-F_n complexes were amenable to isolation and complete characterization (Scheme 5.23). Attempted formation of B-F_n complexes with all other ligands failed. With **5.13** and **5.14**, we observed conversion of starting materials, which we attributed to the formation of transient B-F₂ complexes that could not be isolated (attempted isolation resulted in recovery of starting material). No conversion was observed for all 2-aryl-4-bromobenzothiazole ligands (**5.22-5.26**), lack of reactivity is tentatively attributed to the steric hindrance imposed by the substituent at position 4 on the benzothiazole core. Similarly, no B-F complexes could be formed with 2,4-diarylbenzothiazole ligands **5.27-5.31**. For indole substituted 2,4-diarylbenzothiazoles (**5.29** and **5.30**) geometry of the free ligands may not be optimal for boron complexation, inefficient chelating heteroatom orbital orientation may disfavor complexation and the resulting ring systems may be too strained to form stable complexes.



Scheme 5.23 Isolated B-F_n complexes

5.2.2 Structure of B-F_n Complexes

The molecular structure of all boron complexes was determined by X-ray crystallography; single crystals of **5.17-5.19** were obtained by slow vapour diffusion of cyclohexane into saturated solutions of complexes in CHCl₃ or acetone (Figure **5.4**).

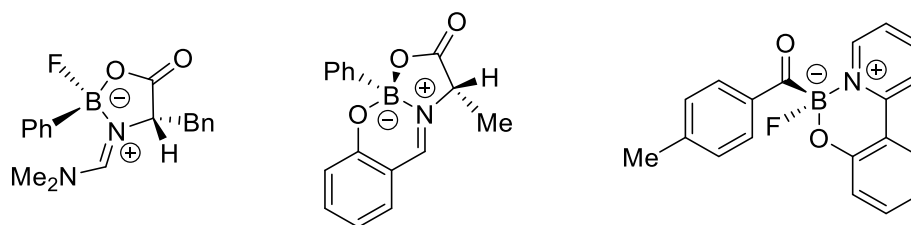


5.17 crystalized in the triclinic P_{-1} , while **5.18** and **5.19** in the monoclinic $P_{21/c}$ space groups. In **5.17** and **5.19**, atoms forming the six-membered chelate ring are almost all coplanar with angles between the benzothiazole and C2 attached phenol ring planes of 3.12 and 3.33°, respectively. However, **5.18** exhibited greater torsion between the two ring systems with the angle between both planes being 6.20°. All complexes display a slightly distorted tetrahedral geometry at boron with the F1 and F2 (for **5.17** and **5.18**) or F1 and O1' (for **5.19**) atoms above and below the main molecular plane. For both **5.17** and **5.18**, the F1-B1-F2 plane dissects the six-membered chelate plane almost perpendicularly (89.7 and 89.6°, respectively), while for **5.19** the F1-B1-O1' plane is at 88.3° relative to the six-membered chelating plane. The phenol at C4 in **5.19** displays considerable torsion from the remainder of the molecule with a dihedral angle between the benzothiazole and C4 attached phenol ring of 21.44°.

The B1-N1 bond distances are generally consistent in **5.17-5.19**, ranging from 1.580-1.589 Å. The B1-O1 bond distances are similar in **5.17** and **5.18** at 1.441 and 1.445 Å, respectively. However, in **5.19** the B1-O1 bond is slightly longer (1.450 Å) while the B1-O1' bond is the shortest of all B-O bonds (1.423 Å). This may be due to ring strain in the six-membered chelating system containing O1, while the seven-membered chelating system, containing O1', allows O1' to adopt a further optimized geometry leading to greater orbital overlap and therefore a shorter B-O bond distance. Structural characteristics for **5.17** and **5.18** are generally consistent with reported 2-arylbzothiazole B-F₂ complexes.³⁰⁷⁻³¹³ To the best of our knowledge, **5.19** is the first benzothiazole-based mono-fluoroborate complex and is a new addition to the few reported examples of boron chelation in a seven-membered ring.³³⁰⁻³³³

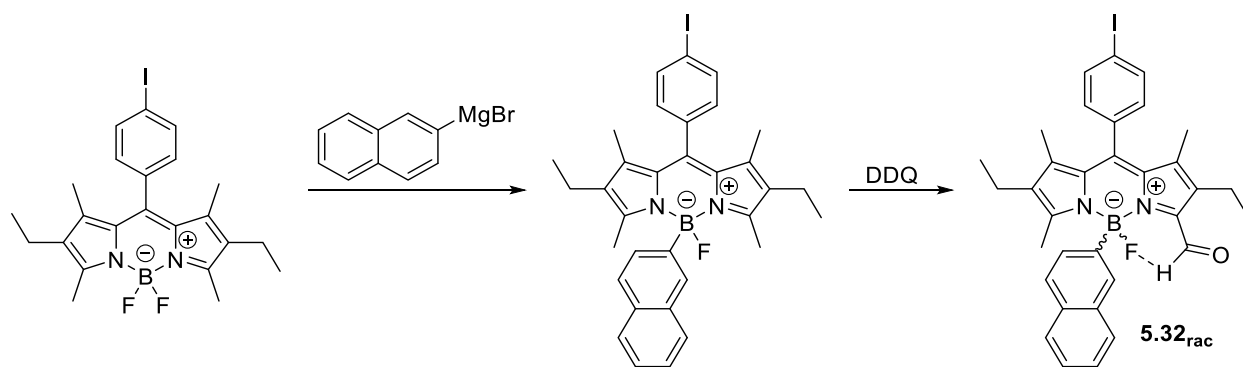
5.2.2.1 Asymmetry of B-F complex 5.19

Chiral boron complexes have been the subject of intense development and study due to their important applications as asymmetric catalysts in organic transformations.^{334,335} In most cases chirality is derived from an asymmetric carbon within the molecular scaffold and not by asymmetry at the boron centre. Asymmetric boron complexes that are stable and can be resolved are rare due to facile dissociation and inversion process which lead to racemization.^{336,337} There are however reported examples of stable chiral oxazaborolidinone and salicylaldehyde boronate complexes and more recently acylboronates (Scheme 5.24).^{338–341}



Scheme 5.24 Selected examples of chiral boron complexes

While there are examples of chiral boron-containing fluorophores, most examples that have been reported incorporate a chiral carbon or are axially chiral (using binaphthyl substituents for example) as opposed to an asymmetric centre at boron.^{342,343} In 2010 Ulrich *et al.* reported the first synthesis and resolution of a chiral BODIPY (Scheme 5.25, product 5.32).³⁴⁴ They achieved chirality through initial mono-substitution at boron followed by desymmetrization of the BODIPY core via oxidation of the 3-methyl group to an aldehyde. The aldehyde functionality is crucial for both asymmetry and configurational stability of the B-F complex via hydrogen bonding (H---F). The racemic mixture was successfully resolved by chiral HPLC and the enantiomers were found to be stable to inversion about the boron centre.



Scheme 5.25 Synthesis of racemic **5.32**

Similarly, complex **5.19** contains an asymmetric boron centre, and the crystal structure shows the complex crystallizes as a pair of enantiomers (Figure **5.5**).

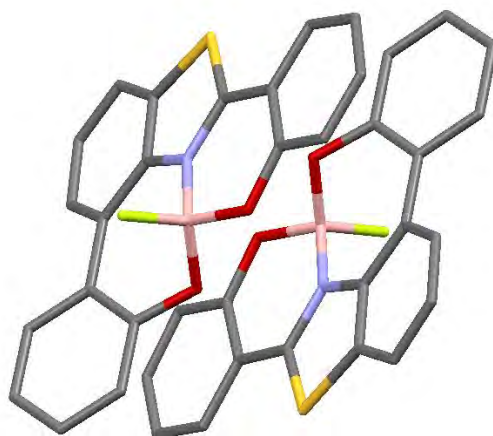


Figure 5.3 Enantiomers of **5.19** in the X-ray crystal structure. Hydrogen atoms omitted for clarity

The racemic mixture was successfully resolved by analytical HPLC using a ChiralPak IA column (25x250 mm, 5 μ m) with 100% MeOH as the eluent; the enantiomers were separated by ~4 min in elution sequence in a 1:1 ratio (Figure **5.6**, left). Resolution was then conducted on a preparative scale (ChiralPak IA column, 20x250 mm, 5 μ m) to allow the isolation of 39.8 and 40.9 mg of **5.19a** of **5.19b**, respectively. Repeated analytical HPLC injections of the separated enantiomers over several days (stored at ambient

temperatures, exposed to atmosphere and light) showed single peaks for both, highlighting their stability towards racemization via inversion (Figure 5.6, right, top and bottom). Additionally, the enantiomers were found to be stable to racemization in CDCl_3 at 50 °C for 3 hours. Analytical HPLC injections of the enantiomers stored in wet MeOH showed no evidence of inversion, although some hydrolysis to the free ligand was observed.

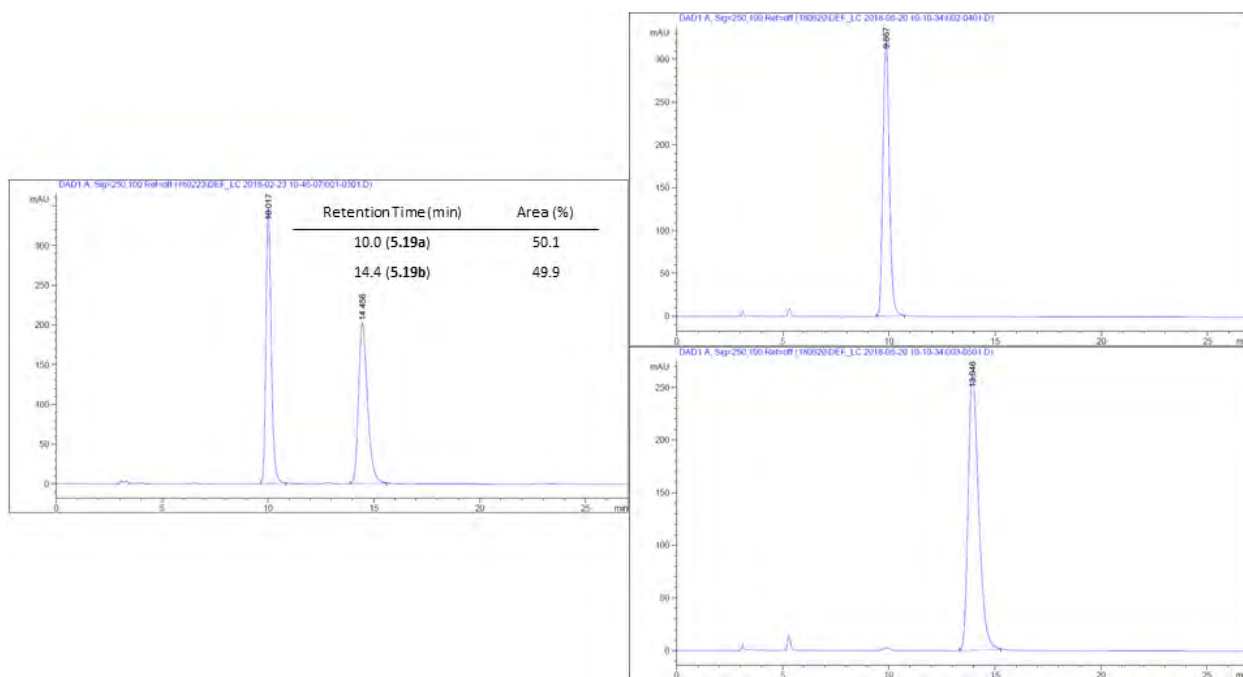


Figure 5.4 HPLC chromatogram of racemic **5.19** (left), **5.19a** (right, top) and **5.19b** (right, bottom) after 1 week

The enantiomeric nature of **5.19a** and **5.19b** was further confirmed by circular dichroism (CD) spectroscopy (Figure 5.7). The racemic mixture displays no interaction with circularly polarized light, while the spectra of the enantiomers are mirror images.

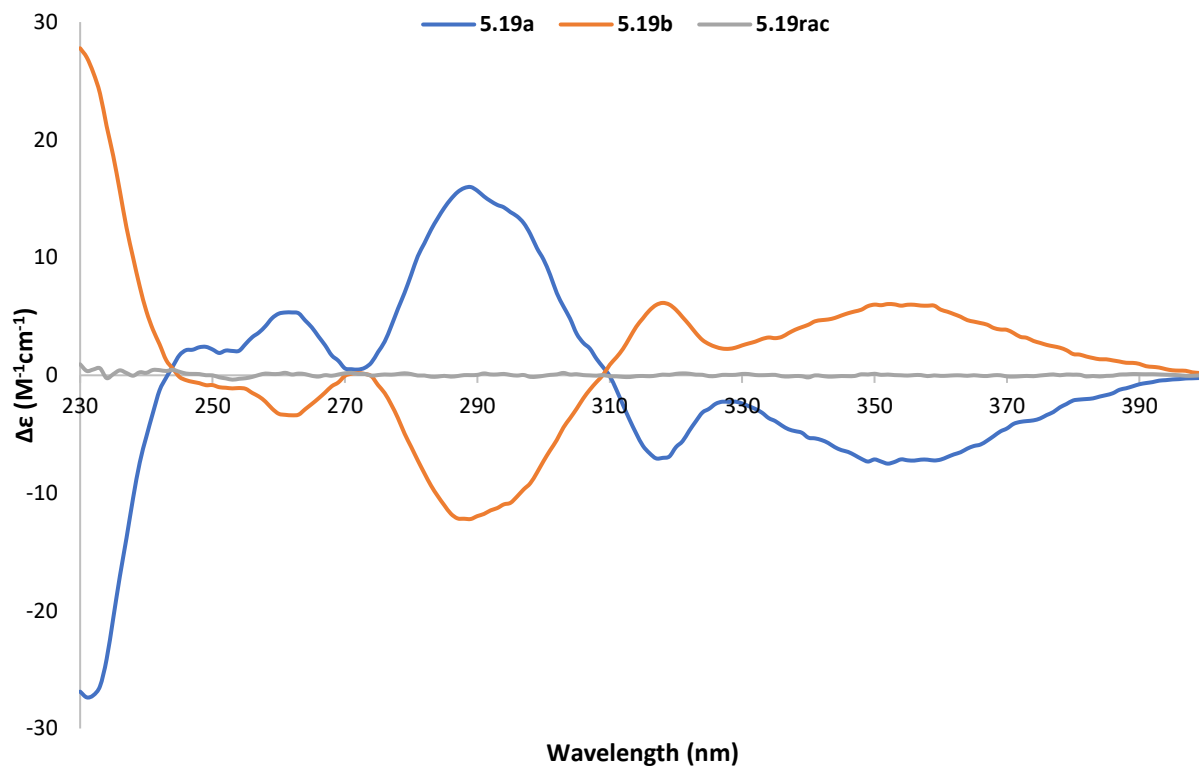
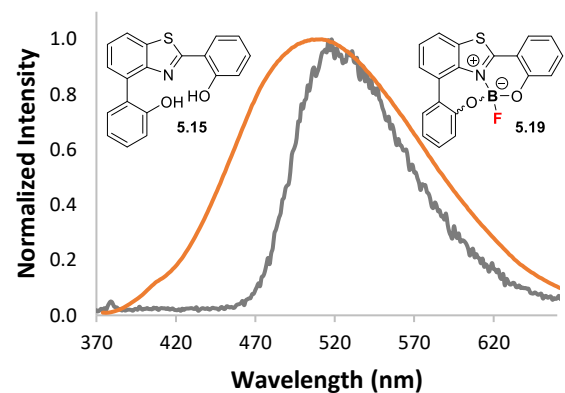
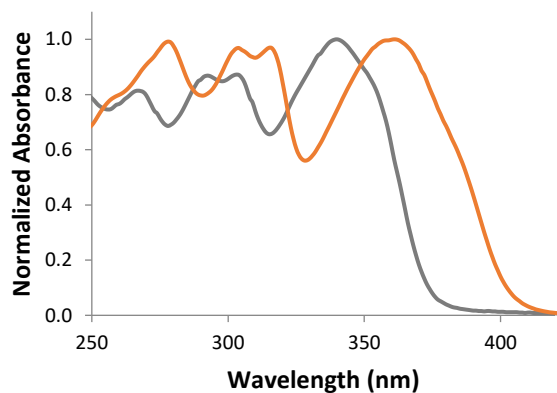
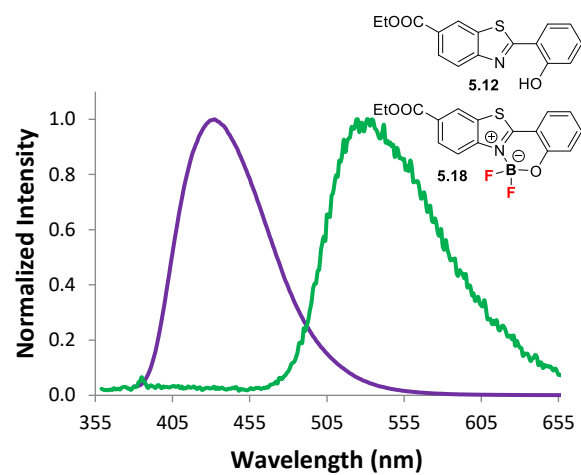
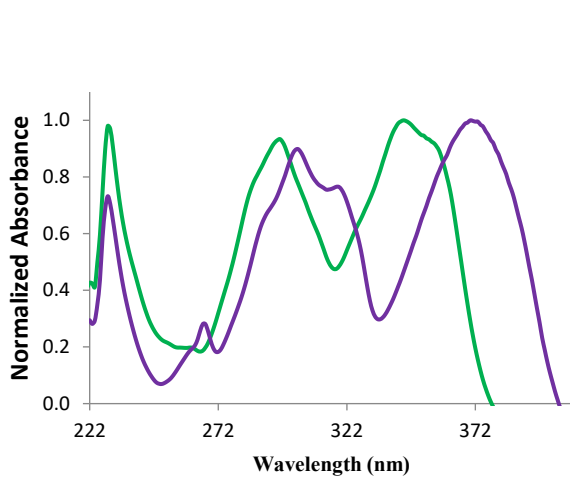
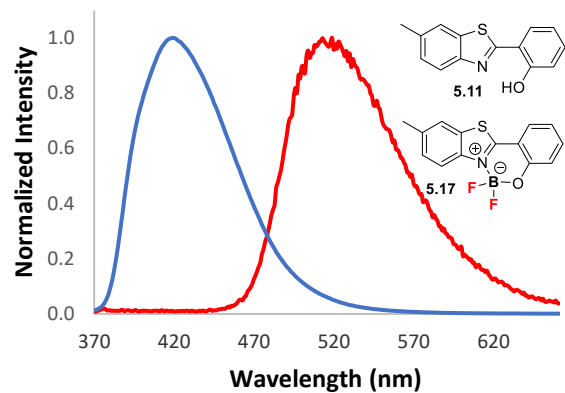
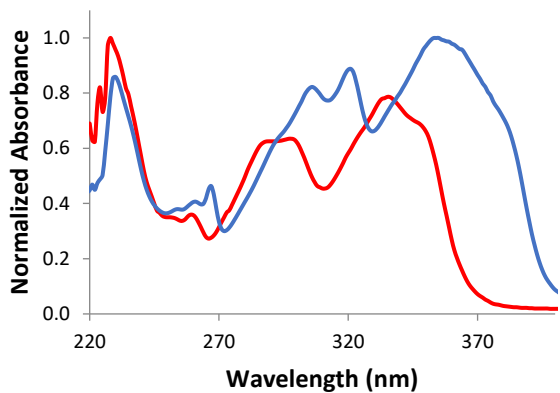


Figure 5.5 CD spectra of **5.19_{rac}**, **5.19a** and **5.19b** in CH_2Cl_2 at 25 °C

5.2.3 Photophysical Studies of B-F_n Complexes

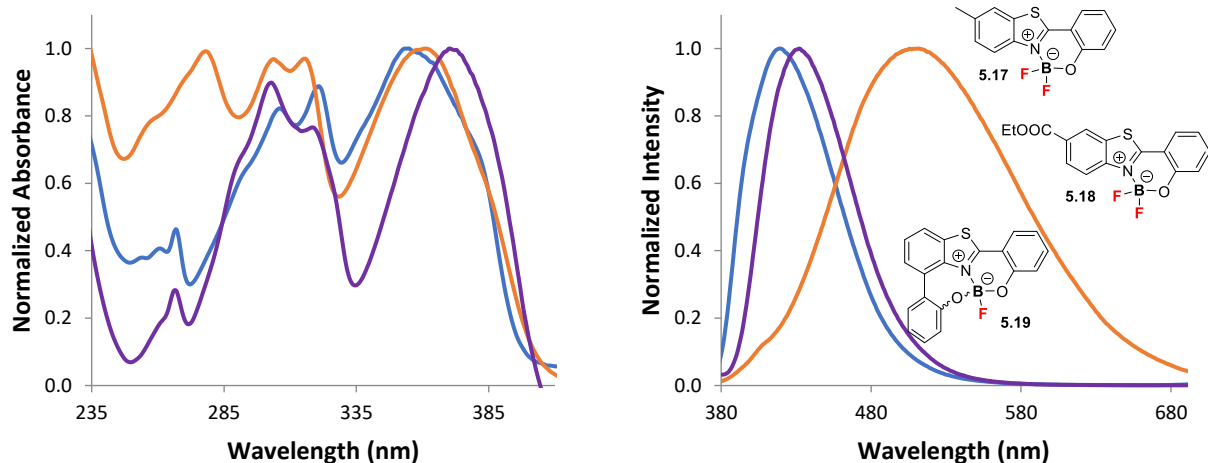
The absorption and emission spectra of compounds **5.11**, **5.12**, **5.15** and **5.17-5.19**, in CH_2Cl_2 , are displayed in Figure 5.7; the spectra are of the free ligand overlaid with its corresponding boron complex.



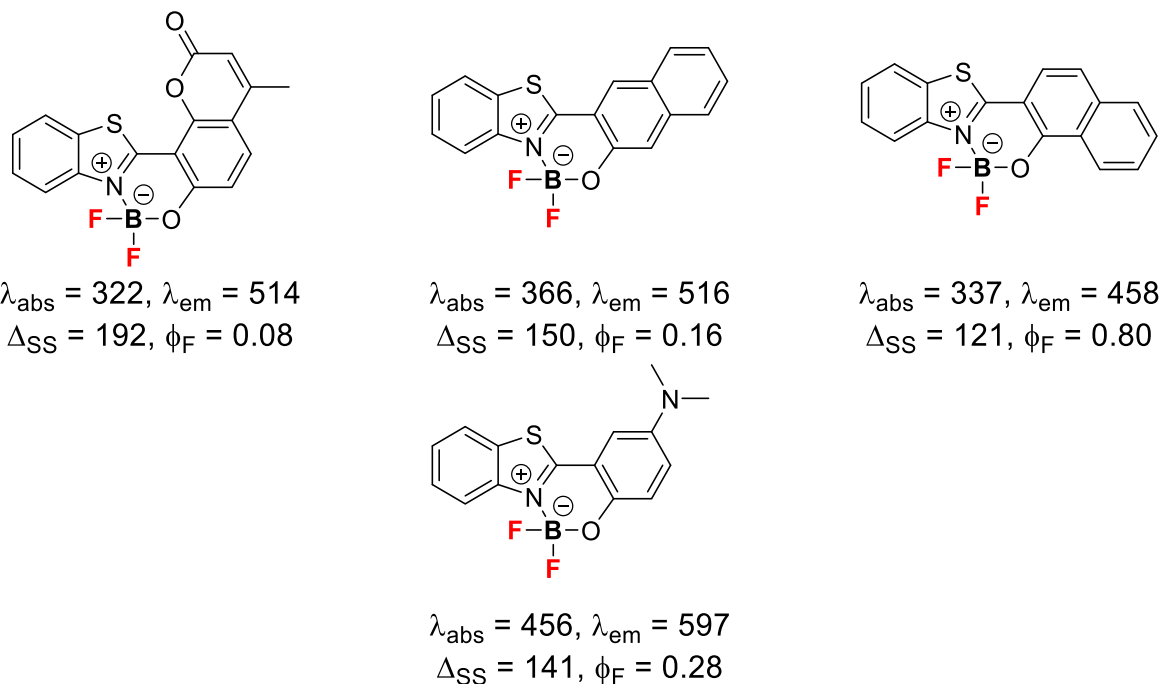
While the same absorption profile is maintained going from free ligand to complex, all B-F_n complexes display a significant red-shift in absorption maxima (λ_{\max}) when compared to their free ligand precursors (Table 5.1). The red-shifts observed (19, 26 and 22 nm for **5.17**, **5.18** and **5.19**, respectively) evidence increased rigidity in ring coplanarity induced by B-F_n complexation, allowing for a greater extent of π -conjugation throughout the molecular scaffold. The absorption and emission spectra of complexes **5.17-5.19**, in CH₂Cl₂, are represented in Figure 5.8. All three complexes exhibit quite similar absorption profiles, with λ_{\max} of 355, 370 and 361 nm for **5.17**, **5.18** and **5.19**, respectively. The λ_{\max} of **5.17** and **5.19** are almost identical which is expected considering their electronic similarity (see X-ray crystal structures Figure 5.4). The torsion between the phenol ring system at C4 and the benzothiazole core suggest poor π -conjugation between the two systems. The λ_{\max} of **5.17** is red shifted by ~15 nm compared to **5.18** and **5.19**, this is attributed to the electron-withdrawing effect of the ethyl ester substituent at position C6 (enhanced D- π -A electronics).

Despite the similarity in absorption spectra of **5.17-5.19**, their emission properties are markedly different (Figure 5.8). Complexes **5.17** and **5.18** are potent blue-emitters displaying emissions at 419 ($\Phi_F = 0.50$) and 432 nm ($\Phi_F = 0.58$), respectively, with **5.18** maintaining a similar red-shift of 13 nm compared to **5.17**; both compounds exhibit narrow Stokes shifts of 64 and 62 nm for **5.17** and **5.18**, respectively. Meanwhile, **5.19** is a green-emitter with a broader emission band, with a maximum at 512 nm ($\Phi_F = 0.10$), representing a significant Stokes shift of 151 nm, more than double those of **5.17** and

5.18 (Table 5.1). It is also worthy to note that all compounds **5.11**, **5.12**, **5.15** and **5.17-5.19** exhibit solid-state fluorescence when irradiated with a UV-lamp (365 nm).



Generally, complexes **5.17** and **5.18** display similar photophysical properties to previously reported 2-arylbenzothiazole B-F₂ complexes.^{307–310,312,313} Complex **5.19** is the notable exception: while possessing similar absorption properties to previously reported benzothiazole B-F₂ complexes, its emission properties resemble those of highly conjugated systems or systems with significant D- π -A architectures (Scheme 5.26).^{308,309,313} More importantly, the photophysical properties observed for **5.19** approach those for previously reported NIRF imaging probes for A β .^{285,286} The properties observed thus far with **5.19** are promising with regards to large Stokes shift and emission wavelength. Increasing conjugation and D- π -A characteristics are viable strategies to further red-shift emissions towards the NIR region. Interestingly, only **5.19** displays positive solvatochromism in polar solvents, evidenced by increased bathochromic shifts in emission as solvent polarity increases.



Scheme 5.26 Selected examples of highly conjugated (top) and enhanced D- π -A (bottom) 2-arylbenzothiazole B-F₂ complexes

Table 5.1 Photophysical properties of **5.11**, **5.12**, **5.15** and **5.17-5.19**

	Solvent	$\lambda_{\text{abs(max)}} \text{ (nm)}$	$\epsilon \text{ (} 10^3 \text{ M}^{-1} \text{ cm}^{-1}\text{)}$	$\lambda_{\text{em}} \text{ (nm)}$	$\Phi_{\text{F}}^{\text{a}}$	$\Delta_{\text{SS}} \text{ (nm)}^{\text{b}}$
5.11	CH ₂ Cl ₂	336	15.8	519	-	183
5.17	CH ₂ Cl ₂	355	12.6	419	0.50 ^c	64
5.17	THF	364	20.0	423	-	59
5.17	MeCN	359	15.8	422	-	63
5.12	CH ₂ Cl ₂	344	15.8	531	-	187
5.18	CH ₂ Cl ₂	370	15.8	432	0.58 ^d	62
5.18	THF	357	50.1	436	-	79
5.18	MeCN	363	25.1	436	-	73
5.15	CH ₂ Cl ₂	339	15.8	513	-	174
5.19	CH ₂ Cl ₂	361	31.6	512	0.10 ^e	151
5.19	THF	360	20.0	514	-	154
5.19	MeCN	356	20.0	527	-	171

^a Measured using 9,10-diphenylanthracene as a reference ($\Phi_F = 0.97$ in cyclohexane).

^b Stokes shift. ^c $\lambda_{exc} = 366$. ^d $\lambda_{exc} = 373$. ^e $\lambda_{exc} = 368$.

5.2.3.1 Theoretical Calculations

To further and better understand the absorption and emission properties of the complexes synthesized, we decided to carry out time-dependant density functional theory (TD-DFT) calculations. Ground state geometries (S_0) were optimized using the DFT/B3LYP method with 6-31G basis sets. TD-DFT calculations were carried out, in CH_2Cl_2 as the solvent according to the Polarizable Continuum Model (PCM), using the B3LYP method with 6-31G basis sets in Gaussian 09.³⁴⁵ HOMO and LUMO energies, representations, transitions, oscillator strengths (f) and calculated λ_{max} are displayed in Figure 5.9. Calculated excitation energies for **5.17** (353 nm) nicely match with those observed experimentally (355 nm), both the HOMO and HOMO-1 orbitals are implicated in the transition ($f=0.3624$), contributing 69.4 and 11.3%, respectively. Only one transition (366 nm, HOMO→LUMO, 69.8% contribution, $f=0.3785$) is implicated in the first excited state of **5.18** and supports the experimentally observed λ_{max} (370 nm). The calculated λ_{max} for **5.19** (380 nm, HOMO→LUMO, 70.2% contribution, $f=0.1464$) is in good agreement with experimental results (361 nm).

As seen in Figure 5.9, LUMO orbitals of **5.17** and **5.19** are very similar in energy (-2.31 and -2.30 eV, respectively), while **5.18** was calculated to have the lowest LUMO energy (-2.60 eV). Larger differences are observed in the HOMO, and more notably HOMO-1 energies of **5.17-5.19**. Similar electronic distribution in the HOMO orbitals of **5.17** and **5.18** are predicted, where electron density is delocalized over the entirety of the π -conjugated system. The LUMO orbitals of these two complexes shows redistribution of

electron density into orbitals that are still delocalized over the entire system. However, for **5.19** HOMO orbital electron density is concentrated on the benzothiazole core as well as the phenol ring at position C4. In the LUMO, there is a significant rearrangement of electron density from the C4 to C2 phenol ring. This considerable redistribution of electron density may be a plausible explanation for the larger Stokes shift of **5.19**, compared to that of **5.17** and **5.18**. This shift in electron density may also be a factor in the decreased quantum yield observed for **5.19**.³¹³ The polarized HOMO and LUMO orbitals of **5.19** may also explain the positive solvatochromism in emission observed in MeCN (Table **5.1**).

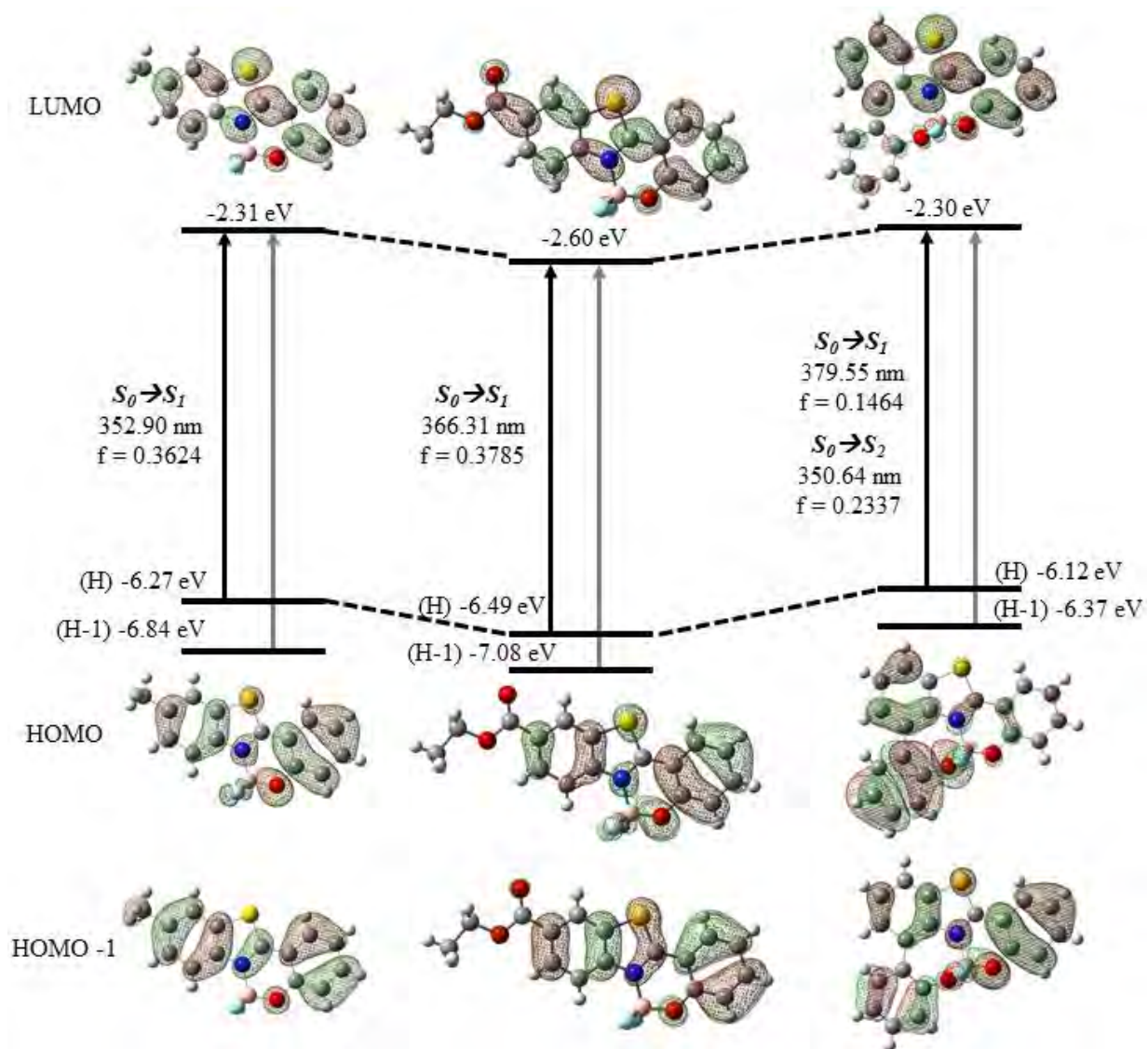


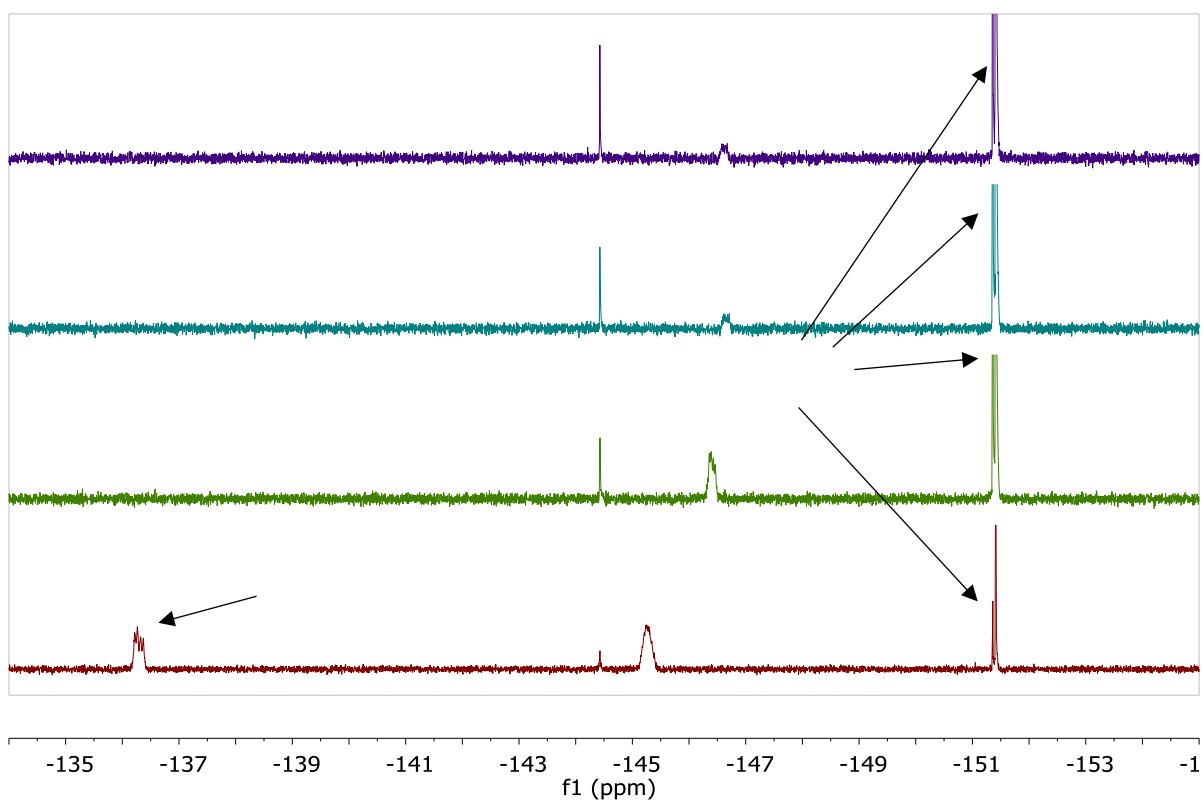
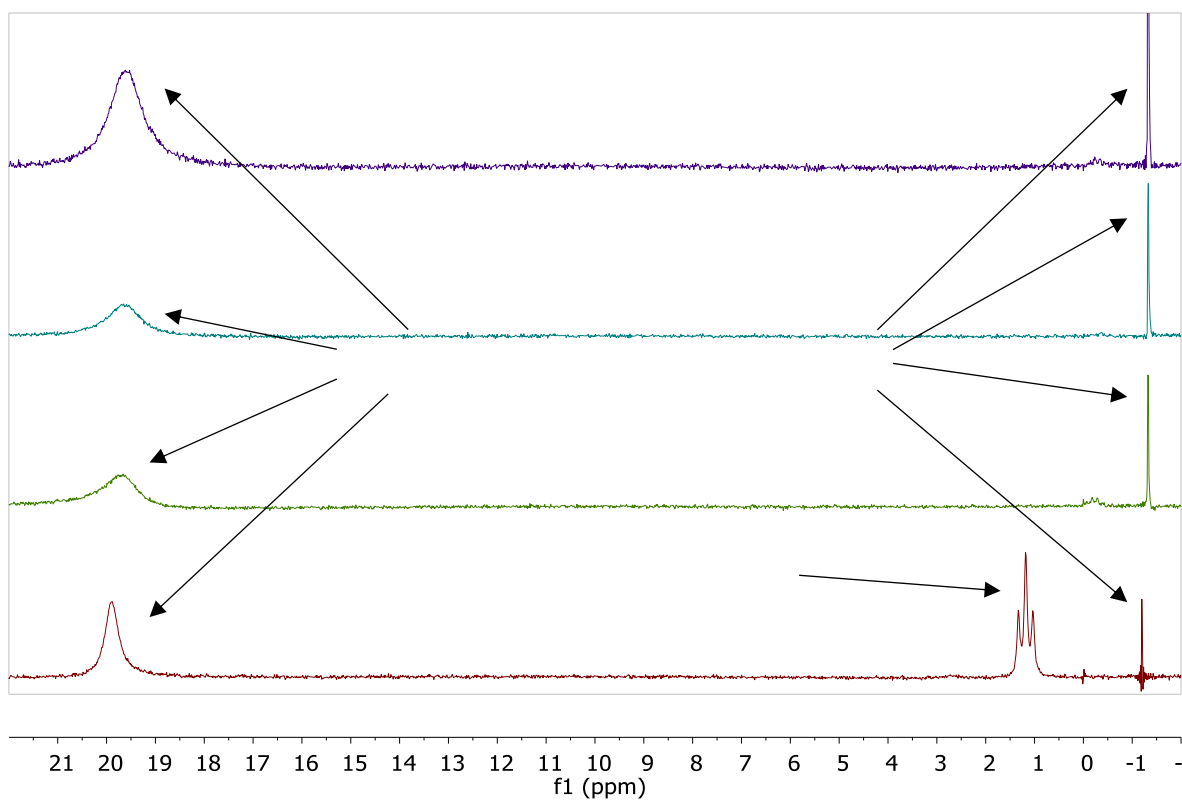
Figure 5.6 Calculated FMOs, excitation energies and corresponding oscillator strengths (f) for **5.17** (left), **5.18** (middle) and **5.19** (right)

5.2.4 Stability Studies of B-F_n Complexes

Given prospective applications of these complexes *in vivo*, we briefly examined the stability of **5.17-5.19** to the presence of water. We observed that **5.18** hydrolysed to the free ligand after extended periods of time in organic solvent, exposed to moisture and air. However, **5.17** and **5.19** were stable for months stored as solids in ambient conditions and in organic solvents (CH₃CN, CH₂Cl₂ and CHCl₃) exposed to moisture and air.

To further probe this, we investigated the stability of **5.17** and **5.19** to increasing amounts of water and monitored the hydrolysis of the B-F_n complex by NMR spectroscopy. Each complex was dissolved in 0.6 mL CD₃CN followed by 0.1 mL D₂O; stability was monitored via ¹⁹F and ¹¹B NMR spectroscopy (Figure **5.10**). Immediate hydrolysis of **5.17** is apparent at t=0, as degradation by-products are observed in ¹⁹F and ¹¹B NMR spectroscopy (BF₄⁻ and B(OH)₃); complete hydrolysis is apparent at t = 14 hours. However, **5.19** displayed exceptional stability for over 289 hours, as no hydrolysis of the B-F bond or degradation products were observed by ¹¹B and ¹⁹F NMR spectroscopy.

The enhanced hydrolytic stability of **5.19** can be tentatively attributed to two factors: 1) increased steric protection, 2) tridentate chelation of boron. The second phenol ring at position 4 on the benzothiazole core provides additional hydrophobic steric bulk which may disfavour water solvation and therefore retard hydrolysis. The benzothiazole core being a tritopic ligand may also disfavour ligand dissociation, as the boron centre would require rehybridization from sp³ to sp². Rehybridization, in turn would induce geometrical reorganization at boron from tetrahedral to trigonal planar, which may be disfavoured given the geometrical restrictions imposed by the non-planar tritopic benzothiazole ligand. These results importantly highlight that electronic factors are not a deciding factor in the stability of these complexes. The average B-F bond length in **5.19** (1.391 Å) is longer than that of **5.17** (1.381 Å) an indication that the boron centre in **5.19** is less electron deficient than in **5.17**, solely based on these properties one would have predicted increased stability for **5.17** compared to **5.19**.



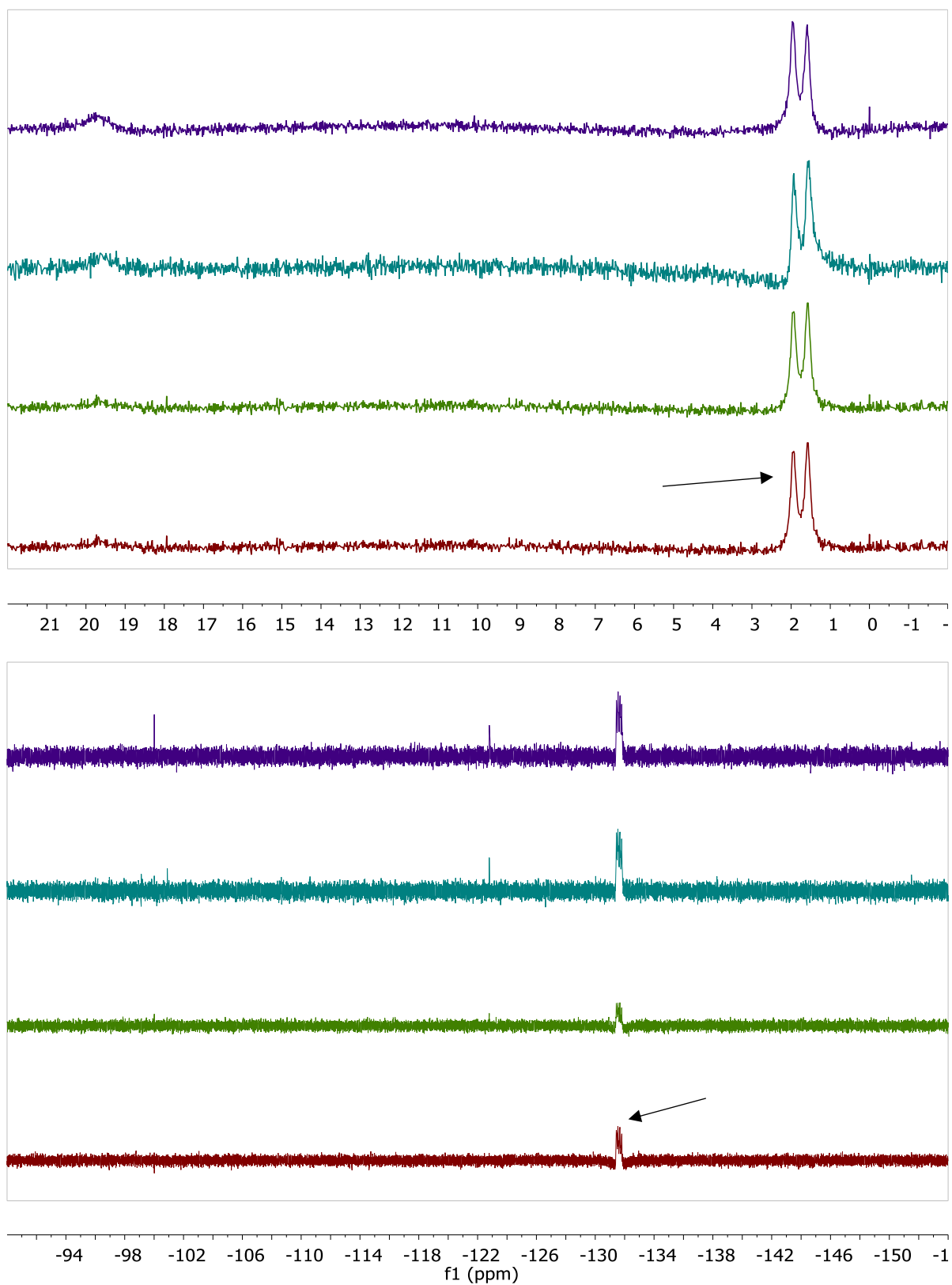
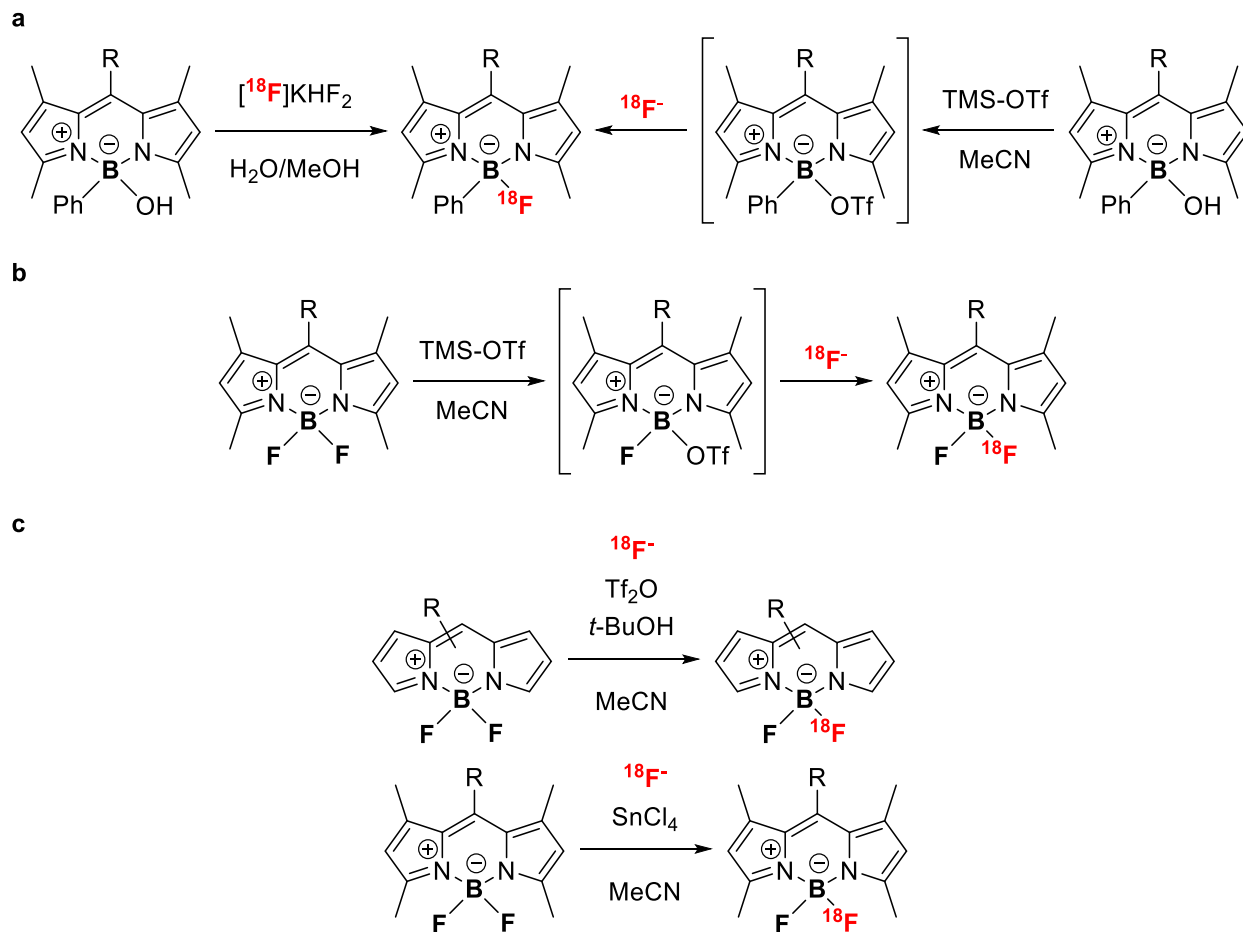


Figure 5.7 ^{19}F and ^{11}B NMR spectra evolution for **5.17** (top two spectra) and **5.19** (bottom two spectra) in $\text{CD}_3\text{CN}/\text{D}_2\text{O}$

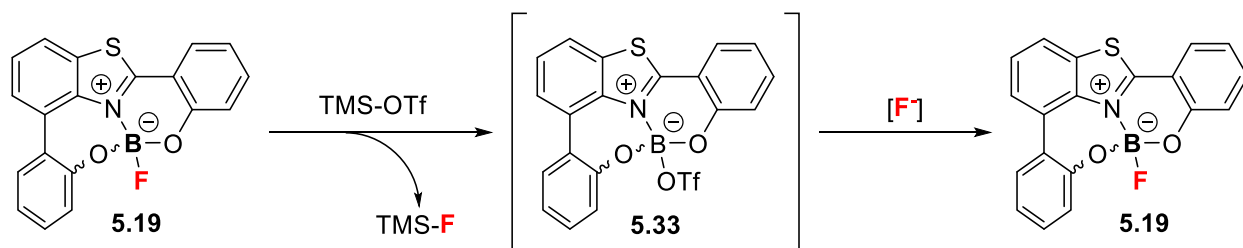
5.2.4.1 Fluorine exchange studies of **5.19**

With the favourable aqueous stability observed for **5.19** we continued by investigating the possibility of fluorine exchange at boron, in line with prospective applications in radiolabelling with ^{18}F for PET probe synthesis. Significant developments have been reported in the synthesis and ^{19}F - ^{18}F IEX of BODIPY dyes for the generation of bi-modal imaging agents. These efforts have largely been driven by Gabbaï, Weissleder and Mazitschek. These groups simultaneously demonstrated that BODIPY derivatives could be pre-activated by the abstraction of one fluorine atom at boron and replacement with labile hydroxide or trifluoromethanesulfonate (OTf, triflate). These pre-activated BODIPYs could then be facilely radiolabelled under mild aqueous or anhydrous conditions (Scheme **5.27**).^{87,346} Soon after, both Gabbaï and Weissleder demonstrated that pre-activation could be avoided via Brønsted or Lewis acid assisted IEX (Scheme **5.27, c**).^{88,90}



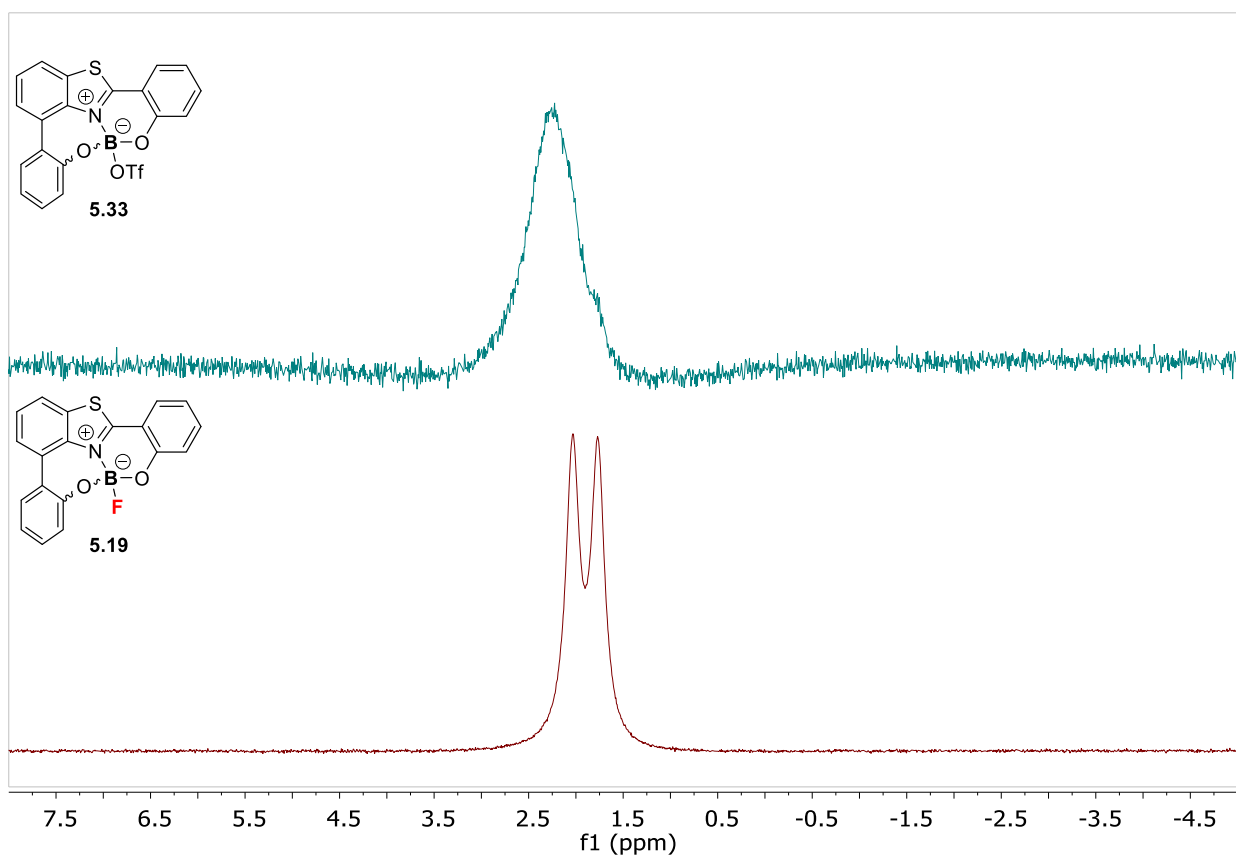
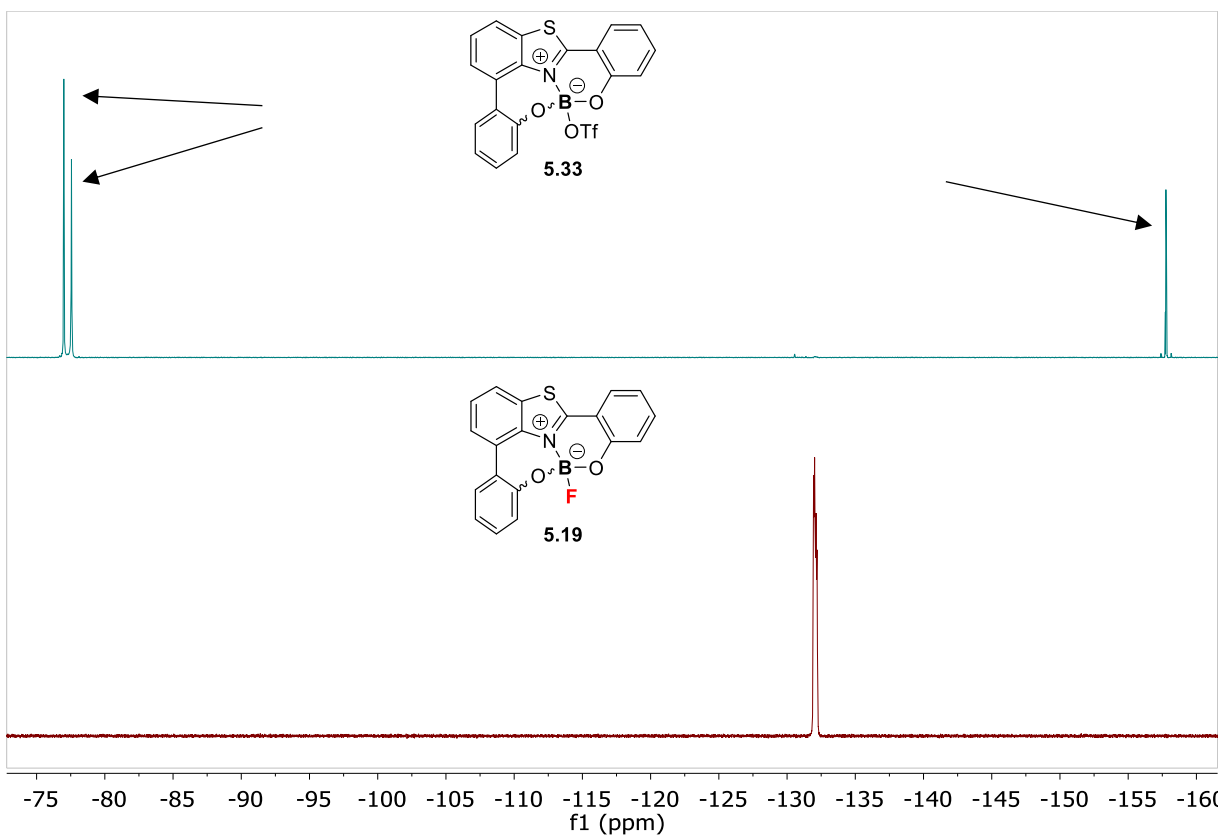
Scheme 5.27 BODIPY radiolabelling strategies via hydroxide (**a**) or triflate pre-activation (**b**) and Brønsted or Lewis acid-assisted IEX (**c**)

We thought that pre-activation with triflate would be the simplest methodology to test fluoride exchange on **5.19**, as fluoride abstraction and formation of the intermediate borenium species (**5.33**) should be observable by ^1H , ^{19}F and ^{11}B NMR spectroscopy (Scheme **5.28**).



Scheme 5.28 Fluoride abstraction from **5.19** to form **5.33** and proposed regeneration of **5.19** by addition of $[F^-]$ source

Treatment of **5.19** with TMS-OTf (2 eq.) resulted in quantitative fluoride abstraction to provide **5.33** in $CDCl_3$, as observed by 1H , ^{19}F and ^{11}B NMR spectroscopy (Figure **5.11**). The B-F signal in the ^{19}F NMR spectrum, (q_B , 1:1:1:1) centred at -132.07 ppm, completely disappears and a new peak attributed to TMS-F, centred at -157.77 (dh, $J_{F-Si} = 14.9$ Hz, $J_{F-H} = 7.4$ Hz) appears. ^{19}F NMR spectroscopy also shows two peaks for OTf (-76.99 and -77.57 ppm) one attributed to the remaining equivalent of TMS-OTf and the other to OTf. In the ^{11}B NMR spectrum, the doublet centred at 1.9 ppm ($J_{B-F} = 34.4$ Hz) evolves into a broad singlet centred at 2.20 ppm, confirming fluoride abstraction (loss of B-F coupling) while maintaining a quaternary boron centre. Complete conversion of **5.19** was also supported by 1H NMR spectroscopy, where all aromatic proton signals are shifted downfield with respect to **5.19** and the free ligand **5.15**. These studies present promising results regarding possible radiolabelling of **5.19** via IEX. Conditions under which **5.33** can be fluorinated back to **5.19** are currently being investigated.



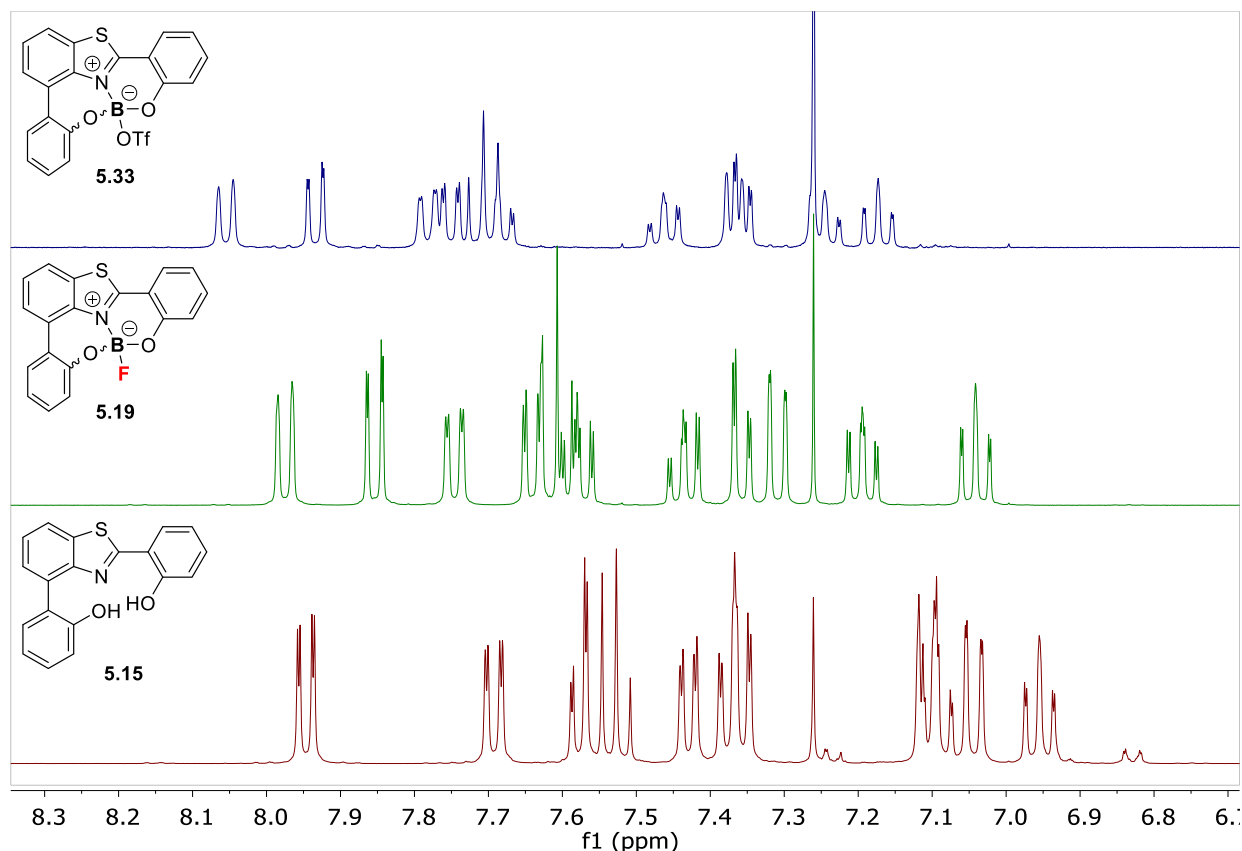
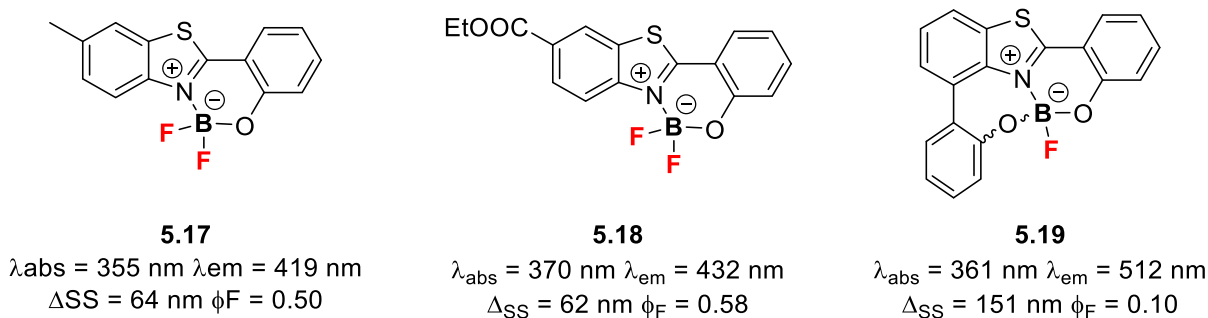


Figure 5.8 Evolution of ^{19}F (top), ^{11}B (middle) and ^1H (bottom) NMR spectra of **5.19** with TMS-OTf

5.3 Conclusion and Perspectives

Bi-modal imaging probes for $\text{A}\beta$ are of interest given their potential in cross-validation of imaging techniques and the complementary information they can provide. Within this context we investigated the synthesis of various novel benzothiazole-based B-F_n fluorophores. From the series of synthesized substituted 2-arylbenzothiazoles and 2,4-diarylbenzothiazoles three B-F_n complexes were isolated and fully characterised (Scheme **5.29**). The photophysical properties of these complexes were then studied. B-F_2 complexes **5.17** and **5.18** displayed similar absorption and emission properties to similar complexes previously reported, they were characterised as strong blue emitters with narrow Stokes shifts. Complex **5.19** displayed promising and interesting properties

and was found to be a green light emitter with a significantly large Stokes shift (151 nm), this complex was also found to display positive solvatochromism in polar solvents. Theoretical calculations were conducted in order to support and better understand the experimentally observed photophysical properties.



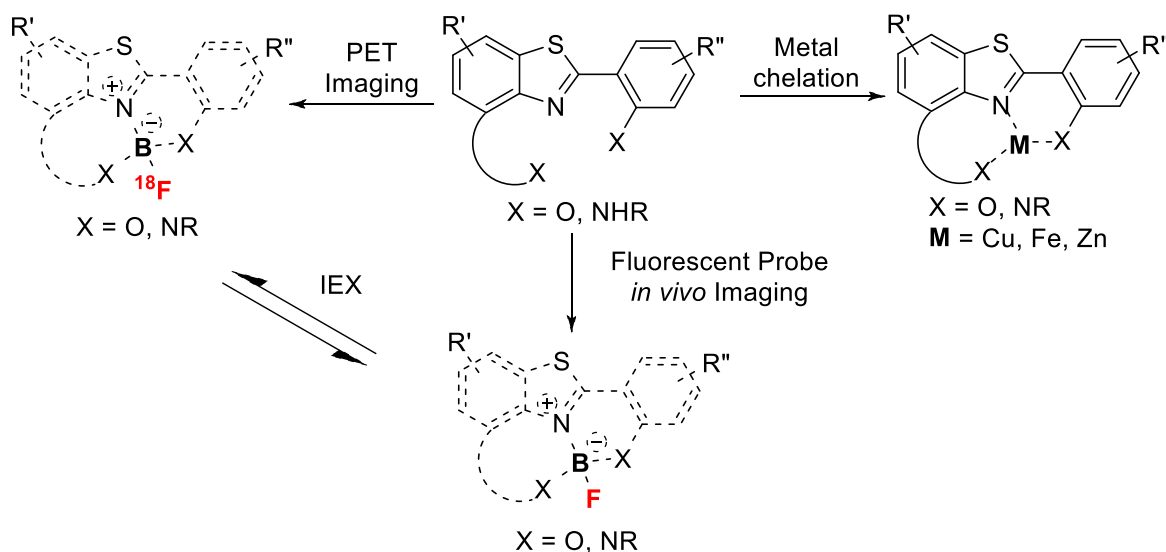
Scheme 5.29 Isolated and characterised B-F_n complexes

Complex **5.19**, synthesized as a racemic pair of enantiomers, was chirally resolved and characterised by CD. The separated enantiomers were shown to be stable to racemization via inversion.

The stability of complexes **5.17-5.19** were studied. **5.18** was found to degrade, via deborylation, to the starting ligand upon extended exposure to moisture and ambient conditions. Complex **5.17** was found to be more resilient, however exposure to increasing aqueous conditions resulted in rapid degradation. Complex **5.19** was shown to be most stable, with exceptional stability without degradation in CD₃CN/D₂O solution for up to 289h. Additionally, fluoride abstraction from **5.19** was demonstrated. These studies highlight **5.19** as a promising candidate for further studies and structural elaboration with regards to the development of a bi-modal probe. In the short-term the stability of **5.19** needs to be investigated in more physiologically relevant conditions (aqueous buffered solutions). It would also be important to study the affinity of **5.19** for A β aggregates via *in*

vitro assays. The further functionalization of **5.19** with electron-donating moieties or increasing conjugation would help in further red-shifting absorption and emission into the NIR.

Long-term perspectives for complexes of this architecture would be to develop a theranostic platform based on the starting ligand (Scheme **5.30**). Facile interchange between both imaging modalities is envisioned via IEX, and the benzothiazole ligand itself can be used a potential metal chelator for therapeutic use, give the implication of metal ions in the aetiology of AD.^{255,302,303,347}



Scheme 5.30 Prospective theranostic platform based on benzothiazole ligand

5.4 Experimental

General Information

Solvents and Reagents

All chemicals were purchased from commercial sources and used as received unless otherwise noted. Solvents used were all commercial grade and used as received with no drying, all reactions were performed in oven-dried glassware under argon atmosphere unless otherwise stated. Deuterated solvents for NMR spectroscopic analysis were purchased from Euriso-top.

Analysis

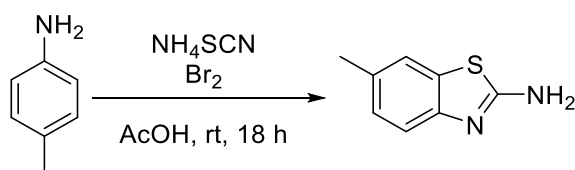
NMR experiments were performed in deuterated solvents. ^1H NMR, ^{13}C NMR, ^{11}B NMR and ^{19}F spectra were recorded on 300 Avance (300 MHz), 400 Avance (400 MHz) and AvanceIII 400 (400 MHz) Bruker spectrometers. All spectra were recorded at ambient temperature (298 K). Chemical shifts (δ) are reported in parts per million (ppm) relative to the residual protium in the solvents (^1H) or the solvent carbon (^{13}C) as internal standards. Multiplicity of signals is indicated using the following abbreviations: s (singlet), b (broad), d (doublet), t (triplet), q (quartet), q_{B} (1:1:1:1 set of peaks arising from coupling to ^{11}B with $S=3/2$, midpoint of signal reported), dd (doublet of doublets), dt (doublet of triplet), td (triplet of doublet), hept (heptet) and m (multiplet).

Reactions were monitored using Merck Silica gel 60 F₂₅₄ or Aluminium Oxide (Basic) 60 F₂₅₄ glass backed plates. TLC plates were visualized by UV fluorescence ($\lambda = 254, 365$ nm) and one of the following stains: KMnO_4 or HBQ. Flash column chromatography was performed using VWR Chemicals Silica gel 60 – 200 μm or on an automated Interchim puriFlash system using pre-packed Interchim 30 μm Silica gel cartridges or Acros Aluminium Oxide (Basic) Brockmann I 50-200 μm .

IR spectra were recorded on a PerkinElmer Spectrum One or Frontier FT-IR spectrometer with frequencies expressed in cm^{-1} . UV/Vis spectra were recorded on an Agilent 8453 Spectroscopy System using a 10 mm Quartz cuvette. Fluorescence spectra were recorded on a HORIBA Jobin Yvon FluoroMax-4 Spectrofluorometer. Quantum yield measurements were done using 9,10-diphenylanthracene as a reference ($\Phi=0.97$ in cyclohexane, $\lambda_{\text{exc}} = 355$). Circular Dichroism spectra were recorded on a Jasco J-815 CD Spectropolarimeter using a 10 mm Quartz cuvette, with D.I.T = 0.5 sec, Scanning Speed = 100 nm/min, Band width = 1.00 nm at 25 °C. High-resolution mass spectra (HRMS) were recorded using either electrospray ionization (ESI) or desorption chemical ionization (DCI) using a Waters GCT Premier or Sciex QTRAP 4500 AB or Thermo Fisher Scientific DSQ II spectrometers. X-ray crystallography was performed on single crystal diffractometers: Agilent Gemini, Bruker Nonius and Bruker Kappa Apex II.

5.4.1 Synthetic procedures and characterization data for 5.1 – 5.31

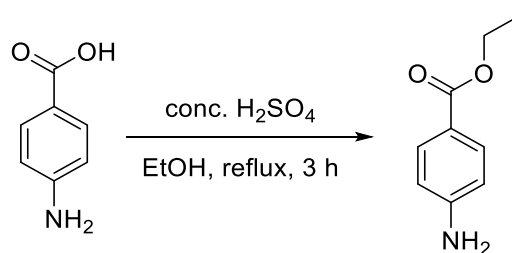
2-amino-6-methylbenzothiazole (5.1)



A 250 mL round-bottom flask was charged with a stir bar, *p*-toluidine (9.995 g, 93.27 mmol), NH₄SCN (35.00 g, 459.8 mmol) and AcOH (100 mL). An addition funnel was then charged with Br₂ (5.2 mL, 101.5 mmol), which was diluted with AcOH (20 mL). The resulting Br₂ solution was then added to the reaction mixture dropwise over 10 minutes. With the addition of Br₂ a pink slurry forms. After Br₂ addition is complete, the slurry is allowed to react for 18 h at rt. The reaction mixture had then formed a thick non-stirrable slurry. To this slurry a solution of NaOH was added as to adjust the pH to 7-8. The mixture was then washed with a 5% aq. Na₂S₂O₃ solution resulting in a fine precipitate. The yellow precipitate was collected, washed with 5% aq. Na₂S₂O₃ and water then placed in a

desiccator under high vacuum to dry (14.0401 g, 92%). IR $\nu_{\text{max}}/\text{cm}^{-1}$ (neat film): 3394, 3273, 3257, 3124, 1622, 1532, 1463, 1278, 806, 603. ^1H NMR (400 MHz, Acetone- d_6) δ 7.43 (s, 1H), 7.28 (d, $J = 8.1$ Hz, 1H), 7.05 (dd, $J = 8.0, 1.5$ Hz, 1H), 6.67 (bs, 2H), 2.34 (s, 3H). ^{13}C NMR (101 MHz, Acetone- d_6) δ 166.4 (C_q), 151.9 (C_q), 132.7 (C_q), 131.6 (C_q), 127.4 (CH), 121.6 (CH), 119.0 (CH), 21.1 (CH₃). HRMS-ESI (m/z): found $[\text{M}+\text{H}]^+$ 165.0487, calc'd C₈H₉N₂S requires 165.0486.

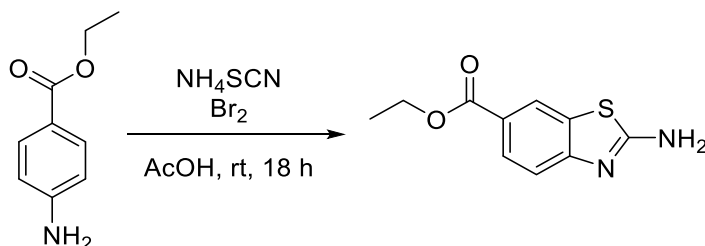
Ethyl 4-aminobenzoate



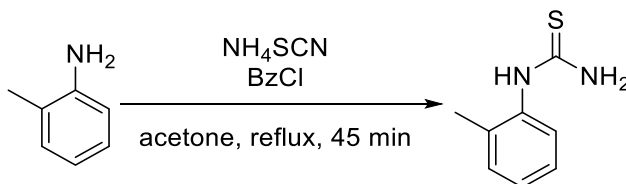
A 250 mL round-bottom flask was charged with a stir bar, condenser, 4-aminobenzoic acid (10.055 g, 73 mmol) and 50 mL of EtOH. The resulting slurry was stirred and the flask was placed in an ice-bath at 0°C. H₂SO₄ (98%, 7.8 mL, 140.4 mmol) was diluted into 20 mL of EtOH and the resulting solution was added dropwise to the stirring slurry over a period of 3 min. The solution formed a thick white precipitate and was then allowed to warm up to room temperature; the reaction mixture was then heated at reflux for 3 hours. It was observed that after refluxing for 5 minutes the white precipitate dissolved, resulting in a clear light orange solution. After reflux the mixture is allowed to cool to room temperature. The reaction mixture was then basified with a saturated aqueous solution of NaHCO₃ to a pH of 7-8. The aqueous phase was then extracted with Et₂O (3 x 100 mL). The combined organic phases were subsequently washed with saturated aqueous NaHCO₃ (100 mL) and brine (100 mL). The combined organic extracts were collected and dried over anhydrous Na₂SO₄. The solution was then filtered and concentrated by rotary evaporation under reduced pressure. The product, an off-white powder, was left to dry overnight on a high vacuum pump (11.180 g, 92%). IR $\nu_{\text{max}}/\text{cm}^{-1}$ (neat film): 3421, 3343, 3222, 2985, 2899, 1680, 1542, 1366, 1272, 845, 770, 700. ^1H NMR (400 MHz,

Chloroform-*d* δ 7.85 (d, J = 8.6 Hz, 2H), 6.63 (d, J = 8.6 Hz, 2H), 4.31 (q, J = 7.1 Hz, 2H), 4.03 (bs, 2H) 1.35 (t, J = 7.1 Hz, 3H). ^{13}C NMR (101 MHz, Chloroform-*d*) δ 166.8 (C_q), 150.9 (C_q), 131.6 (CH), 120.1 (C_q), 113.9 (CH), 60.4 (CH₂), 14.5 (CH₃). MS-DCI(NH₃) (m/z): 166 [M+H]⁺. Anal. calc'd for C₉H₁₁NO₂: C, 65.44; H, 6.71; N, 8.48. Found C, 65.51; H, 6.49; N, 8.47.

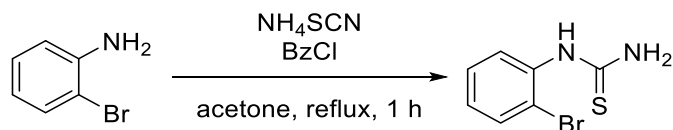
Ethyl 2-aminobenzothiazole-6-carboxylate (5.2)



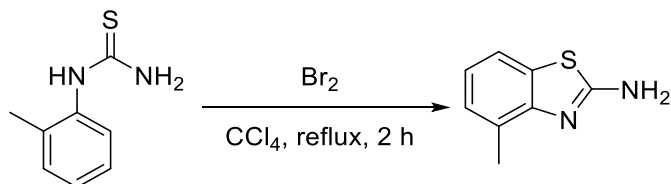
A 250 mL round-bottom flask was charged with a stir bar, ethyl 4-aminobenzoate (10.008 g, 60.6 mmol), NH₄SCN (18.560 g, 242.4 mmol) and 50 mL AcOH. An addition funnel was then charged with Br₂ (3.2 mL, 60.6 mmol), which was diluted with 20 mL of AcOH. The resulting Br₂ solution was then added to the reaction mixture dropwise over approximately 10 minutes; with the addition of Br₂ a pink slurry forms. After Br₂ addition is complete the reaction mixture is stirred overnight at rt. The next day the reaction mixture had formed a thick non-stirrable slurry. To this slurry a solution of NaOH was added to adjust the pH to 7-8. The mixture was then washed with a 5% aq. Na₂S₂O₃ solution resulting in a fine precipitate. The precipitate was collected, washed with 5% aq. Na₂S₂O₃ and water then placed in a desiccator under high vacuum to dry overnight (18.410 g, 99%). IR $\nu_{\text{max}}/\text{cm}^{-1}$ (neat film): 3345, 3310, 3076, 2971, 1685, 1524, 1462, 1277, 1112, 892, 825, 765. ^1H NMR (400 MHz, DMSO-*d*₆) δ 8.27 (d, J = 1.8 Hz, 1H), 7.89 (bs, 2H), 7.81 (dd, J = 8.4, 1.8 Hz, 1H), 7.37 (d, J = 8.4 Hz, 1H), 4.28 (q, J = 7.1 Hz, 2H), 1.31 (t, J = 7.1 Hz, 3H). ^{13}C NMR (101 MHz, DMSO-*d*₆) δ 169.8 (C_q), 165.7 (C_q), 156.9 (C_q), 131.2 (C_q), 127.1 (CH), 122.5 (CH), 122.0 (C_q), 117.1 (CH), 60.4 (CH₂), 14.3 (CH₃). HRMS-ESI (m/z): found [M+H]⁺ 223.0538, calc'd C₁₀H₁₁N₂O₂S requires 223.0541.

(*o*-tolyl)thiourea (5.3)

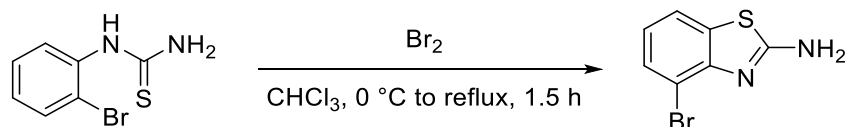
A 250 mL round-bottom flask was charged with a stir bar, condenser, NH_4SCN (19.809 g, 0.26 mol) and acetone (100 mL). Benzoyl chloride (27.9 mL, 0.24 mol) was then added over 5 min via syringe to the stirring solution producing a thick yellow precipitate, which was then heated to reflux for 15 min. The mixture was then allowed to cool to rt at which point *o*-Toluidine (21.43 mL, 0.20 mol) diluted with acetone (50 mL) was added via an addition funnel over 15 min. The reaction mixture was then heated to reflux until consumption of starting material by TLC (45 min). The reaction mixture was dropped onto cold water (300 mL); the light yellow precipitate was collected and washed with cold water (3 x 100 mL), and finally with cold $\text{H}_2\text{O}/\text{MeOH}$ (1:1) producing an off-white powder. 10% aq. NaOH solution (200 mL) was prepared and heated to 80°C in an Erlenmeyer flask into which the collected precipitate was dissolved, this was left to hydrolyze for 15 min. HCl (37%, aq. solution) was then added to the stirring mixture to adjust the pH to ~ 2 , then NaHCO_3 was then added slowly to increase the pH to ~ 8 . The precipitate formed was collected by filtration, washed with water until washes were neutral then dried under high vacuum (26.4761 g, 80%). IR $\nu_{\text{max}}/\text{cm}^{-1}$ (neat film): 3376, 3357, 3263, 3179, 1615, 1495, 1452, 1110, 824, 758, 697. ^1H NMR (400 MHz, Acetone- d_6) δ 8.66 (bs, 1H), 7.37 – 7.15 (m, 4H), 6.72 (bs, 2H), 2.29 (s, 3H). ^{13}C NMR (101 MHz, Acetone- d_6) δ 183.9 (C_q), 137.6 (C_q), 136.3 (C_q), 131.79 (CH), 128.5 (CH), 128.3 (CH), 127.6 (CH), 17.9 (CH_3). MS-ESI (m/z): 167 [$\text{M}+\text{H}$] $^+$. Anal. calc'd for $\text{C}_8\text{H}_{10}\text{N}_2\text{S}$: C, 57.80; H, 6.06; N, 16.85. Found C, 58.98; H, 5.58; N, 16.09.

2-bromophenylthiourea (5.4)

A two-necked 250 mL round-bottom flask was charged with a stir bar, condenser, NH_4SCN (10.9250 g, 0.13 mol) and acetone (50 mL). Benzoyl chloride (13.93 mL, 0.12 mol) was added dropwise via syringe to the rapidly stirring reaction mixture. The mixture was heated at reflux for 15 min, and then cooled back down to rt. In an addition funnel, 2-bromoaniline (22.63 mL, 0.1 mol) was diluted with acetone (25 mL), this solution was added dropwise to the vigorously stirring reaction mixture over 15 min. The reaction mixture was then heated at reflux for 1 h. The crude mixture was then dropped onto excess water and vigorously stirred. A yellow precipitate formed and was collected by filtration and washed with water until washes were colourless. The precipitate was then washed with cold MeOH/ H_2O solution (1:1). In a 1L Erlenmyer flask, 10% aq. NaOH solution (400 mL) was prepared and heated to 80 °C. The washed precipitate was then added to this base solution for hydrolysis. The precipitate dissolved into the base solution producing a clear yellow solution, this was stirred at 80 °C for 15 minutes. The solution was then acidified to pH 2 using concentrated HCl (37%, 12 M), producing a white precipitate. The solution was then basified to pH 9 using a 25% aq. NH_4OH solution. The formed white precipitate was collected and washed with water until washes were neutral; product was then dried under high vacuum (17.3748 g, 75%). IR $\nu_{\text{max}}/\text{cm}^{-1}$ (neat film): 3425, 3253, 3245, 3124, 3002, 1619, 1500, 1466, 1427, 1290, 1063, 1039, 1025, 818, 758, 706. ^1H NMR (400 MHz, Acetone- d_6) δ 8.66 (bs, 1H), 7.72 (dd, J = 8.0, 1.4 Hz, 1H), 7.66 (dd, J = 8.0, 1.4 Hz, 1H), 7.40 (td, J = 7.9, 1.4 Hz, 1H), 7.20 (td, J = 7.8, 1.6 Hz, 1H), 7.09 (bs, 2H). ^{13}C NMR (101 MHz, Acetone- d_6) δ 184.2 (C_q), 138.2 (C_q), 133.8 (CH), 130.1 (CH), 128.9 (CH), 128.9 (CH), 121.1 (C_q). HRMS-ESI (m/z): found $[\text{M}^{79}\text{Br}+\text{H}]^+$ 230.9595, calc'd $\text{C}_7\text{H}_8\text{N}_2\text{S}^{79}\text{Br}$ requires 230.9592, found $[\text{M}^{81}\text{Br}+\text{H}]^+$ 232.9574, calc'd $\text{C}_7\text{H}_8\text{N}_2\text{S}^{81}\text{Br}$ requires 232.9572.

2-amino-4-methylbenzothiazole (5.5)

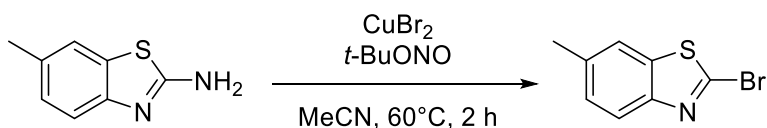
A two-necked 500 mL round-bottom flask was charged with a stir bar, condenser (with a NaOH trap to neutralize HBr fumes), *o*-tolylthiourea (16.617 g, 0.10 mol) and CCl₄ (80 mL). An addition funnel was charged with Br₂ (6.15 mL, 0.12 mol) and dissolved in CCl₄ (36 mL). This bromine solution was added dropwise to the stirring solution over 1.5 h. The solution was then heated at reflux for 2 hours until starting material was consumed by TLC. The reaction mixture was then cooled to rt and the solvent removed by rotary evaporation. The remaining residue was then suspended in water and washed with a 5% aq. Na₂S₂O₃ solution to remove excess traces of bromine, then filtered and washed with water. The residue was then suspended in water and 25% NH₄OH aq. solution was added to basify the solution to pH 10. The fine white precipitate was collected and washed with water until washes were neutral; the precipitate was dried under high vacuum (11.8534 g, 72%). IR $\nu_{\text{max}}/\text{cm}^{-1}$ (neat film): 3448, 3287, 3062, 2941, 1642, 1537, 1409, 871, 733, 692. ¹H NMR (400 MHz, Acetone-*d*₆) δ 7.57 (d, *J* = 7.8 Hz, 1H), 7.20 (d, *J* = 7.3 Hz, 1H), 7.09 (t, *J* = 7.6 Hz, 1H), 6.07 (bs, 2H), 2.58 (s, 3H). ¹³C NMR (101 MHz, Acetone-*d*₆) δ 166.3 (C_q), 152.9 (C_q), 132.2 (C_q), 128.9 (C_q), 127.1 (CH), 122.1 (CH), 119.0 (CH), 18.5 (CH₃). HRMS-ESI (*m/z*): found [M+H]⁺ 165.0487, calc'd C₈H₉N₂S requires 165.0486.

2-amino-4-bromobenzothiazole (5.6)

A 50 mL two-necked round-bottom flask was charged with a stir bar, 2-bromophenylthiourea (2.3204 g, 10 mmol) and CHCl₃ (10 mL). Bromine (0.51 mL, 10

mmol) was dissolved in CHCl_3 (5 mL) in an addition funnel and affixed to the main neck of the round-bottom flask, the second neck was connected to a base trap to neutralize HBr fumes developed during the course of the reaction. The flask was cooled to 0°C in an ice-bath and the bromine solution was added dropwise to the vigorously stirring reaction mixture (note: often the sides needed to be scraped down as the bromine solution would coagulate on the bottom and sides of the flask). The addition funnel was then replaced with a condenser and the reaction mixture heated at reflux for 1.5 h until complete conversion of starting material was determined by TLC; with external heat HBr gas evolution became consistently rapid. During the course of the reaction a fine yellow precipitate evolved in a clear red/brown solution. After cooling to rt, solvent removed under reduced pressure. The remaining residue was dissolved in EtOAc (100 mL) and washed with sat'd aq. NaHCO_3 (2 x 100 mL), 5% aq. $\text{Na}_2\text{S}_2\text{O}_3$ (2 x 50 mL) and finally brine (2 x 50 mL). The organic phase was dried over anhydrous MgSO_4 the filtered and concentrated under reduced pressure and further dried under high vacuum overnight to furnish the product as a yellow powder (2.1296 g, 93%). IR $\nu_{\text{max}}/\text{cm}^{-1}$ (neat film): 3446, 3277, 3073, 2926, 1635, 1531, 1415, 1269, 882, 750, 725. ^1H NMR (400 MHz, Acetone- d_6) δ 7.64 (d, $J = 7.7$ Hz, 1H), 7.51 (bs, 2H), 7.45 (d, $J = 7.8$ Hz, 1H), 6.96 (t, $J = 7.8$ Hz, 1H). ^{13}C NMR (101 MHz, Acetone- d_6) δ 168.2 (C_q), 151.8 (C_q), 132.9 (C_q), 129.7 (CH), 123.1 (CH), 121.0 (CH), 111.9 (CH). HRMS-ESI (m/z): found $[\text{M}^{79}\text{Br}+\text{H}]^+$ 228.9440, calc'd $\text{C}_7\text{H}_6\text{N}_2\text{S}^{79}\text{Br}$ requires 228.9435, $[\text{M}^{81}\text{Br}+\text{H}]^+$ 230.9418, calc'd $\text{C}_7\text{H}_6\text{N}_2\text{S}^{81}\text{Br}$ requires 230.9419.

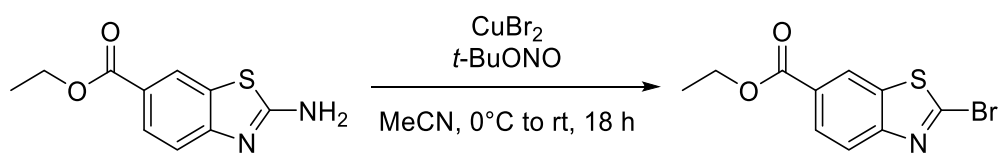
2-bromo-6-methylbenzothiazole (5.7)



A 250 mL round-bottom flask was charged with a stir bar and CuBr_2 (12.915 g, 58.00 mmol). The flask was placed under high vacuum for 15 min, then purged with Ar. Under positive Ar pressure, $t\text{-BuONO}$ (8.6 mL, 72 mmol) and MeCN (120 mL) were added to the flask. The reaction mixture heated to 55°C for 15 min under stirring. 2-amino-6-

methylbenzothiazole (7.8858 g, 48.00 mmol) was then added portion-wise to the stirring reaction mixture over 5 minutes; rapid gas evolution was observed. The reaction mixture was then heated at 60°C for 1.5 h under positive Ar pressure. The reaction mixture was then allowed to cool to rt and 2 N HCl (120 mL) was added to quench the reaction mixture, with the notable evolution of gas. The mixture was then transferred into a separatory funnel and additional 2N HCl was added along with brine. The aqueous phase was extracted with EtOAc (4 x 200 mL). The combined organic extracts were dried over anhydrous Na₂SO₄, then filtered and concentrated under reduced pressure to produce a black/brown oil. This residue was further purified through a silica plug using EtOAc as the eluent, it was observed that a black residue was trapped by the silica and the desired product eluted out as an orange/red solution. Solvent was removed under reduced pressure to afford the desired compound as a brown crystalline material (7.4388 g, 68%). ¹H NMR (400 MHz, Chloroform-*d*) δ 7.87 – 7.79 (m, 1H), 7.59 – 7.54 (m, 1H), 7.30 – 7.27 (m, 1H), 2.47 (s, 3H). ¹³C NMR (101 MHz, Chloroform-*d*) δ 151.8 (C_q), 137.5 (C_q), 137.3 (C_q), 133.0 (C_q), 130.6 (CH), 127.3 (CH), 125.7 (CH), 118.3 (CH), 18.4 (CH₃). MS-DCI(NH₃) (*m/z*): 228 [M⁷⁹Br+H]⁺, 230 [M⁸¹Br+H]⁺. Spectroscopic data matches that found in the literature.³⁴⁸

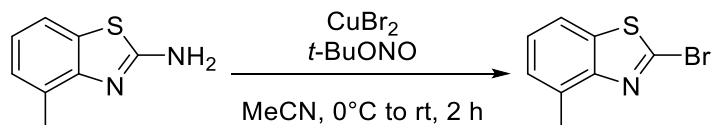
Ethyl 2-bromobenzothiazole-6-carboxylate (5.8)



A 250 mL round-bottom flask was charged with a stir bar, ethyl 2-aminobenzothiazole-6-carboxylate (14.086 g, 63.38 mmol), CuBr₂ (24.676 g, 126.8 mmol) and 50 mL MeCN. The flask was placed in an ice-bath at 0°C and stirred. To the reaction mixture, under vigorous stirring, *t*-BuONO (14.2 mL, 126.8 mmol) was added dropwise; evolution of gas was observed. The ice-bath was then removed and the solution was allowed to warm up to rt, and stirred overnight. The mixture was concentrated to dryness by rotary evaporation under reduced pressure. The solid residue was then dissolved in CH₂Cl₂ (50

mL), to which sat'd aq. NH_4Cl (50 mL) was added. The aqueous phase was further extracted with CH_2Cl_2 (4 x 50 mL). The combined organic extracts were then washed with 5% aq. $\text{Na}_2\text{S}_2\text{O}_3$ solution (100 mL). The organic phase was then filtered through a plug of Celite and silica, and further eluted with EtOAc/cyclohexane (1:1), to remove traces of Cu and Br. The organic phase was dried over anhydrous Na_2SO_4 , then concentrated to dryness by rotary evaporation. The product, a yellow powder, was left to dry overnight on a high vacuum pump (10.330 g, 57%). IR $\nu_{\text{max}}/\text{cm}^{-1}$ (neat film): 2987, 1715, 1467, 1400, 1256, 987, 834, 766, 721. ^1H NMR (400 MHz, Chloroform-*d*) δ 8.52 (s, 1H), 8.14 (d, J = 8.3 Hz, 1H), 8.00 (d, J = 8.5 Hz, 1H), 4.41 (q, J = 7.2 Hz, 2H), 1.41 (t, J = 7.1 Hz, 3H). ^{13}C NMR (101 MHz, Chloroform-*d*) δ 165.8 (C_q), 155.2 (C_q), 142.5 (C_q), 133.2 (C_q), 128.0 (C_q), 127.9 (CH), 123.0 (CH), 122.6 (CH), 61.6 (CH₂), 14.5 (CH₃). MS-DCI(NH_3) (m/z): 286 [$\text{M}^{79}\text{Br}+\text{H}$]⁺, 288 [$\text{M}^{81}\text{Br}+\text{H}$]⁺. Anal. calc'd for $\text{C}_{10}\text{H}_8\text{BrNO}_2\text{S}$: C, 41.97; H, 2.82; N, 4.89. Found C, 41.67; H, 2.36; N, 4.83.

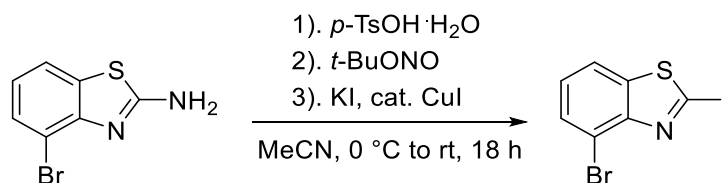
2-bromo-4-methylbenzothiazole (5.9)



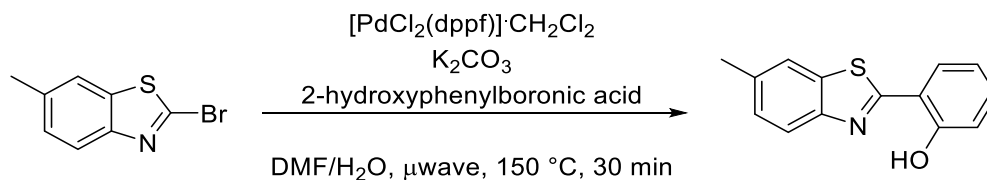
A 500 mL round-bottom flask was charged with a stir bar, CuBr_2 (15.979 g, 73 mmol), $t\text{-BuONO}$ (11.8 mL, 99 mmol) and MeCN (200 mL). 2-amino-4-methylbenzothiazole (9.9936 g, 61 mmol) was added portionwise to this stirring solution and evolution of gas was observed. The solution was stirred under positive Ar pressure for 2 h until all starting material was consumed by TLC. The reaction was quenched with 1 N aq. HCl (200 mL), after cessation of gas evolution, the mixture was transferred into a separatory funnel and additional 1 N HCl and brine were added. The aqueous phase was extracted with EtOAc (3 x 500 mL), the combined organic extracts were washed with additional 1 N HCl , then dried over anhydrous MgSO_4 . The solution was then filtered and concentrated under reduced pressure yielding a brown viscous oil. This residue was purified through a silica plug using EtOAc-pentane (1:1) as the eluent, the solvent was removed under reduced pressure to furnish a brown solid (9.3832 g, 68%). IR $\nu_{\text{max}}/\text{cm}^{-1}$ (neat film): 2918, 1571,

1465, 1008, 980, 839, 768, 738. ^1H NMR (400 MHz, Chloroform-*d*) δ 7.60 (d, J = 7.7 Hz, 1H), 7.31 – 7.26 (m, 1H), 7.24 (d, J = 7.1 Hz, 1H), 2.70 (s, 3H). ^{13}C NMR (75 MHz, Chloroform-*d*) δ 151.8 (C_q), 137.6 (C_q), 137.4 (C_q), 133.0 (C_q), 127.3 (CH), 125.8 (CH), 118.4 (CH), 18.4 (CH₃). MS-DCI(NH₃) m/z : 228 [$\text{M}^{79}\text{Br}+\text{H}$]⁺, 230 [$\text{M}^{81}\text{Br}+\text{H}$]⁺. Anal. calc'd for C₈H₆BrNS: C, 42.12; H, 2.65; N, 6.14. Found C, 39.69; H, 1.96; N, 5.75.

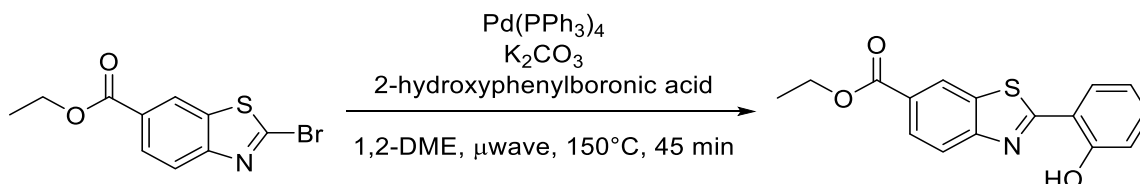
2-iodo-4-bromobenzothiazole (5.10)



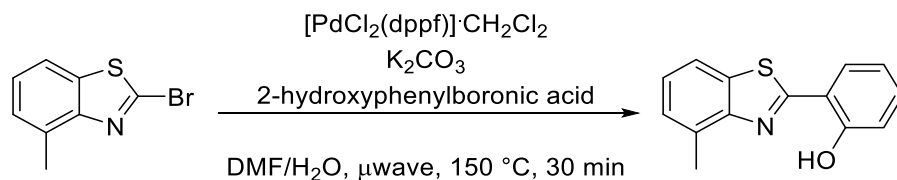
A 500 mL round-bottom flask was charged with a stir bar, 2-amino-4-bromobenzothiazole (9.85 g, 42 mmol), *p*-TsOH·H₂O (24.9 g, 129 mmol) and MeCN (172 mL). The heterogenous reaction mixture was stirred and cooled in an ice-brine bath to 0 °C, at which point *t*-BuONO (15.3 mL, 129 mmol) was added dropwise, over 10 min, via an addition funnel; after the addition was complete the reaction mixture was stirred at 0 °C for 30 min. An additional funnel was then charged with a water (43 mL) solution of KI (21.4 g, 129 mmol) and CuI (819 mg, 4.3 mmol). The KI solution was added dropwise to the vigorously stirred reaction mixture at 0 °C over 20 minutes; the reaction mixture was then allowed to warm to rt overnight. The crude reaction mixture was concentrated under reduced pressure to ~70 mL and then dropped on sat'd aq. NaHCO₃ (150 mL) and the aqueous phase extracted with EtOAc (4 x 150 mL), the combined organic phases were then washed with a 5% aqueous Na₂S₂O₃ solution (4 x 150 mL). The organic phase was dried over anhydrous MgSO₄, filtered and concentrated under reduced pressure to furnish the product as a brown powder (13.1607 g, 90%). IR $\nu_{\text{max}}/\text{cm}^{-1}$ (neat film): 3089, 3064, 2931, 2851, 1442, 1391, 1203, 952, 842, 764, 732. ^1H NMR (400 MHz, DMSO-*d*₆) δ 8.12 (dd, J = 8.1, 1.0 Hz, 1H), 7.72 (dd, J = 7.8, 1.0 Hz, 1H), 7.37 (t, J = 7.9 Hz, 1H). ^{13}C NMR (101 MHz, DMSO-*d*₆) δ 152.0 (C_q), 139.8 (C_q), 129.7 (CH), 126.9 (CH), 121.1 (CH), 114.6 (C_q), 112.8 (C_q). HRMS-ESI (m/z): found [$\text{M}^{79}\text{Br}+\text{H}$]⁺ 339.8298, calc'd C₇H₄NS⁷⁹BrI requires 339.8293, [$\text{M}^{81}\text{Br}+\text{H}$]⁺ 341.8279, calc'd C₇H₄NS⁸¹BrI requires 341.8272.

2-(2-hydroxyphenyl)-6-methylbenzothiazole (5.11)

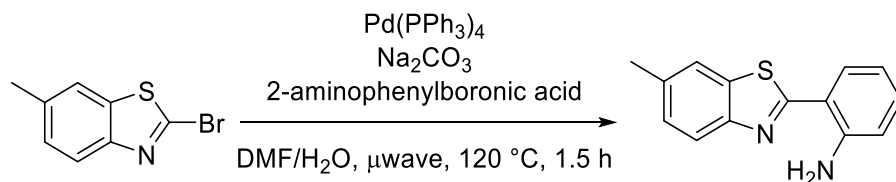
A 20 mL microwave vial was charged with a stir bar, 2-bromo-6-methylbenzothiazole (421.7 mg, 1.85 mmol), 2-hydroxyphenylboronic acid (317.2 mg, 2.3 mmol), PdCl₂(dppf)·CH₂Cl₂ (141.5 mg, 0.2 mmol, 10 mol%), K₂CO₃ solution (2 M, 3 mL) and DMF (5 mL). The vial was heated at 150 °C under microwave irradiated for 30 minutes. The vial was allowed to cool to rt; the reaction mixture was then dropped on water and saturated aq. NH₄Cl. The aqueous phase was extracted with CH₂Cl₂ (3 x 50 mL); the combined organic extracts were dried over anhydrous MgSO₄, filtered and concentrated under reduced pressure. The concentrated solution was then loaded onto Celite. The crude mixture was purified by silica flash chromatography using pentane/CH₂Cl₂ (100:0 to 80:20). Fractions were collected and concentrated yielding a fluffy white powder (236.3 mg, 58%). IR $\nu_{\text{max}}/\text{cm}^{-1}$ (neat film): 3044, 2981, 2916, 1584, 1482, 1223, 977, 833, 816, 741, 712. ¹H NMR (400 MHz, Acetone-*d*₆) δ 12.27 (bs, 1H), 7.96 (d, *J* = 8.4 Hz, 1H), 7.92 (dt, *J* = 1.7, 0.8 Hz, 1H), 7.80 (dd, *J* = 7.9, 1.6 Hz, 1H), 7.47 – 7.39 (m, 2H), 7.06 (dd, *J* = 8.4, 1.1 Hz, 1H), 7.02 (ddd, *J* = 7.9, 7.3, 1.2 Hz, 1H), 2.51 (s, 3H). ¹³C NMR (75 MHz, Chloroform-*d*) δ 168.5 (C_q), 158.0 (C_q), 150.0 (C_q), 136.0 (C_q), 132.9 (C_q), 132.6 (CH), 128.39 (CH), 128.37 (CH), 121.8 (CH), 121.4 (CH), 119.6 (CH), 117.9 (CH), 117.1 (C_q), 21.7 (CH₃). HRMS-ESI (*m/z*): found [M+H]⁺ 242.0640, calc'd C₁₄H₁₂NOS requires 242.0640.

Ethyl 2-(2-hydroxyphenyl)benzothiazole-6-carboxylate (5.12)

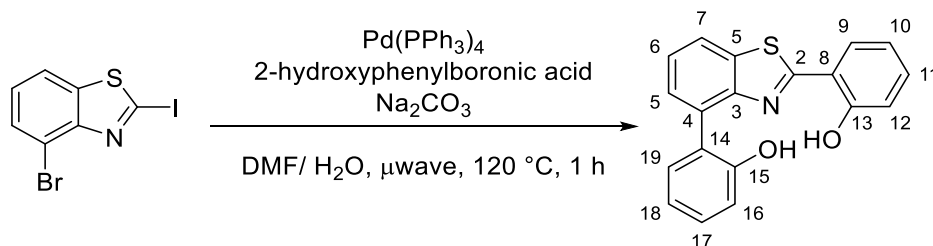
A 10 mL microwave vial was loaded with a stir bar, ethyl 2-bromobenzothiazole-6-carboxylate (285.0 mg, 1 mmol), 2-hydroxyphenylboronic acid (180.3 mg, 1.3 mmol), K_2CO_3 (138.7 mg, 1 mmol), $Pd(PPh_3)_4$ (64.2 mg, 0.05 mmol, 5 mol%), 0.5 mL H_2O and 4 mL 1,2-dimethoxyethane. The vial was placed in a microwave reactor, the reactor was programmed to maintain $150^\circ C$ for 30 minutes. The reaction mixture was allowed to cool to rt; it was noticeable that a yellow fluorescent precipitate was deposited in the microwave vial. The reaction mixture was dissolved into EtOAc (~30 mL), then filtered through Celite. The solution was then dry-loaded onto Celite for purification by flash column chromatography using CH_2Cl_2 /EtOAc/hexane (1:1:8) as the eluent. The product was isolated as a light yellow powder, which fluoresces yellow under 365 nm light (229.4 mg, 77% yield). IR ν_{max}/cm^{-1} (neat film): 3390, 2985, 2908, 2920, 1708, 1593, 1480, 1268, 1213, 971, 904, 816, 767, 741, 718, 702. 1H NMR (400 MHz, Chloroform-*d*) δ 8.63 (d, J = 1.6 Hz, 1H), 8.19 (dd, J = 8.6, 1.7 Hz, 1H), 8.02 (d, J = 8.6 Hz, 1H), 7.72 (dd, J = 7.9, 1.6 Hz, 1H), 7.42 (ddd, J = 8.6, 7.2, 1.6 Hz, 1H), 7.12 (dd, J = 8.4, 1.1 Hz, 1H), 7.01 – 6.96 (m, 1H), 4.44 (q, J = 7.1 Hz, 2H), 1.45 (t, J = 7.1 Hz, 3H). ^{13}C NMR (101 MHz, Chloroform-*d*) δ 172.7 (C_q), 166.1 (C_q), 158.3 (C_q), 154.9 (C_q), 133.6 (CH), 132.7 (C_q), 128.8 (CH), 128.1 (CH), 127.8 (C_q), 123.8 (CH), 121.9 (CH), 119.9 (CH), 118.2 (CH), 116.7 (C_q), 61.6 (CH_2), 14.5 (CH_3). MS-DCI(NH_3) (m/z): 300 $[M+H]^+$. Anal. calc'd for $C_{16}H_{13}NO_3S$: C, 64.20; H, 4.38; N, 4.68. Found C, 64.97; H, 4.13; N, 4.17.

2-(2-hydroxyphenyl)-4-methylbenzothiazole (5.13)

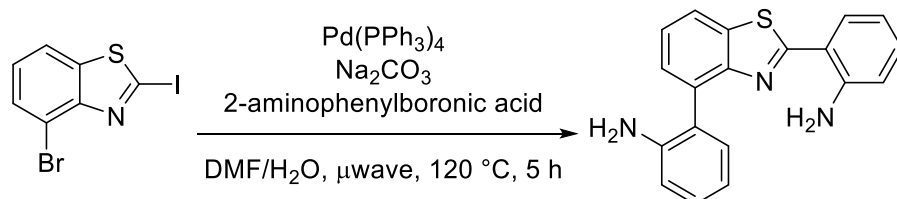
A 10 mL microwave vial was charged with a stir bar, 2-bromo-4-methylbenzothiazole (447.4 mg, 2 mmol), 2-hydroxyphenylboronic acid (334.3 mg, 2.4 mmol), Pd(dppf)Cl₂·CH₂Cl₂ (148.5 mg, 0.2 mmol, 10 mol%), aq. K₂CO₃ solution (2 M, 3 mL) and DMF (5 mL). The vial was heated at 150 °C under microwave irradiation for 30 min. The vial was allowed to cool to rt; the reaction mixture was then dropped onto water and saturated aq. NH₄Cl. The aqueous phase was extracted with CH₂Cl₂ (3 x 50 mL); the combined organic extracts were dried over anhydrous MgSO₄, filtered and concentrated under reduced pressure. The concentrated solution is then loaded onto Celite. The crude mixture was purified by silica flash chromatography using a pentane/CH₂Cl₂ (100:0 to 80:20). Fractions were collected and concentrated yielding a fluffy white powder (340.0 mg, 72%). IR $\nu_{\text{max}}/\text{cm}^{-1}$ (neat film): 2928, 2858, 2846, 1620, 1579, 1479, 1217, 975, 815, 773, 743, 712. ¹H NMR (400 MHz, Chloroform-*d*) δ 7.73 (t, *J* = 4.6 Hz, 1H), 7.70 (dd, *J* = 7.8, 1.6 Hz, 1H), 7.39 (ddd, *J* = 8.7, 7.3, 1.6 Hz, 1H), 7.34 – 7.28 (m, 2H), 7.11 (dd, *J* = 8.4, 1.1 Hz, 1H), 6.99 – 6.94 (m, 1H), 2.75 (s, 3H). ¹³C NMR (101 MHz, Chloroform-*d*) δ 168.5 (C_q), 158.1 (C_q), 151.3 (C_q), 132.7 (CH), 132.5 (C_q), 132.1 (C_q), 128.4 (CH), 127.4 (CH), 125.7 (CH), 119.6 (CH), 119.1 (CH), 117.9 (CH), 117.1 (C_q), 18.5 (CH₃). MS-DCI(NH₃) (*m/z*): 242 [M+H]⁺. Anal. calc'd for C₁₄H₁₁NOS: C, 69.68; H, 4.59; N, 5.80. Found C, 69.33; H, 4.22; N, 5.64.

2-(6-methylbenzo[d]thiazol-2-yl)aniline (5.14)

A 35 mL microwave vial was charged with a stir bar, 2-bromo-6-methylbenzothiazole (268.4 mg, 1.2 mmol), 2-aminophenylboronic acid (187.3 mg, 1.4 mmol), Na₂CO₃ (318 mg, 3 mmol), Pd(PPh₃)₄ (18 mg, 0.02 mmol), DMF (8 mL) and water (2 mL). The crude mixture was then degassed (3 x freeze-pump-thaw method) and purged with Ar. The vial was loaded into a microwave reactor and heated at 120 °C for 1.5h. The reaction mixture was cooled to rt before being transferred to a separatory funnel with sat'd aq. NaHCO₃ (100 mL), the aqueous phase was extracted with EtOAc (3 x 50 mL). The combined aqueous phases were washed with brine (3 x 50 mL), then dried over anhydrous MgSO₄, filtered and the filtrate concentrated onto Celite under reduced pressure. The crude material was purified using Si gel flash chromatography using an eluent of 100% cyclohexane to cyclohexane/CH₂Cl₂ (7:3). Desired fractions were collected and concentrated under reduced pressure, and further under high vacuum overnight to furnish the desired compound as a yellow powder (85.4 mg, 30%). IR $\nu_{\text{max}}/\text{cm}^{-1}$ (neat film): 3461, 3291, 3070, 3022, 2917, 2857, 1613, 1588, 1559, 1493, 1458, 1443, 1227, 1157, 965, 816, 746, 738. ¹H NMR (400 MHz, Chloroform-*d*) δ 7.85 (d, *J* = 8.3 Hz, 1H), 7.69 (dd, *J* = 7.9, 1.4 Hz, 1H), 7.67 (s, 1H), 7.26 (dd, *J* = 8.1, 1.4 Hz, 2H), 7.21 (ddd, *J* = 8.4, 7.2, 1.4 Hz, 1H), 6.78 (dd, *J* = 8.2, 0.9 Hz, 1H), 6.74 (ddd, *J* = 8.1, 7.2, 1.2 Hz, 1H), 6.37 (bs, 2H), 2.49 (s, 3H). ¹³C NMR (101 MHz, Chloroform-*d*) δ 168.3 (C_q), 152.0 (C_q), 146.8 (C_q), 135.1 (C_q), 133.6 (C_q), 131.5 (CH), 130.3 (CH), 127.7 (CH), 122.1 (CH), 121.1 (CH), 117.0 (CH), 116.9 (CH), 115.6 (C_q), 21.7 (CH₃). HRMS-ESI (*m/z*): found [M+H]⁺ 241.0801, calc'd C₁₄H₁₃N₂S⁺ requires 214.0799.

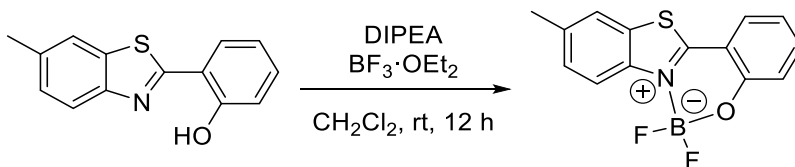
2,4-di(2-hydroxyphenyl)benzothiazole (5.15)

A 35 mL microwave vial was charged with a stir bar, 2-iodo-4-bromobenzothiazole (368.5 mg, 1.1 mmol), 2-hydroxyphenylboronic acid (383 mg, 2.8 mmol), $\text{Pd(PPh}_3)_4$ (132 mg, 10 mol%), Na_2CO_3 (1.07 g, 10 mmol), DMF (9 mL) and water (3 mL). The reaction mixture was degassed the freeze-pump-thaw method three times and then purged with Ar. The vial was loaded into a microwave reactor and programmed to be heated at $120\text{ }^\circ\text{C}$ for 1h, after which the crude was dropped onto water (50 mL) and the phases separated. The aqueous phase was extracted with EtOAc (3 x 25 mL), the combined organic phases were dried over anhydrous MgSO_4 , filtered and concentrated onto Celite. The crude residue was purified by Silica gel flash column chromatography using cyclohexane/EtOAc (4:2 to 1:1). Desired fractions were collected and concentrated to furnish the desired product as a tan foam which was further dried under vacuum overnight (189.5 mg, 55%). IR $\nu_{\text{max}}/\text{cm}^{-1}$ (neat film): 3377, 2926, 2855, 1613, 1583, 1489, 1470, 1450, 1350, 977, 743, 716. $^1\text{H NMR}$ (400 MHz, Chloroform-*d*) δ 7.95 (dd, $J = 7.8, 1.4$ Hz, 1H, H₇), 7.69 (dd, $J = 7.9, 1.6$ Hz, 1H, H₉), 7.58 (dd, $J = 7.5, 1.4$ Hz, 1H, H₅), 7.53 (t, $J = 7.6$ Hz, 1H, H₆), 7.43 (dd, $J = 7.5, 1.7$ Hz, 1H, H₁₉), 7.37 (ddd, $J = 8.7, 7.3, 1.6$ Hz, 2H, H₁₁, H₁₇), 7.14 – 7.07 (m, 2H, H₁₆, H₁₈), 7.04 (dd, $J = 8.4, 1.1$ Hz, 1H, H₁₂), 6.95 (ddd, $J = 8.2, 7.3, 1.2$ Hz, 1H, H₁₀), 5.53 (bs, 1H, -OH). $^{13}\text{C NMR}$ (101 MHz, Chloroform-*d*) δ 169.9 (C₂), 157.9 (C₁₃), 153.0 (C₁₅), 150.0 (C₃), 133.5 (C₁), 133.3 (C₁₁), 131.6 (C₄), 131.3 (C₁₉), 130.2 (C₁₇), 128.6 (C₉), 128.4 (C₅), 126.3 (C₆), 125.4 (C₁₄), 121.4 (C₇), 121.1 (C₁₈), 119.8 (C₁₀), 118.1 (C₁₂), 116.9 (C₁₆), 116.8 (C₈). HRMS-ESI (m/z): found $[\text{M}+\text{H}]^+$ 320.0753, calc'd $\text{C}_{19}\text{H}_{14}\text{NO}_2\text{S}$ requires 320.0745.

2,2'-(benzo[d]thiazole-2,4-diyl)dianiline (5.16)

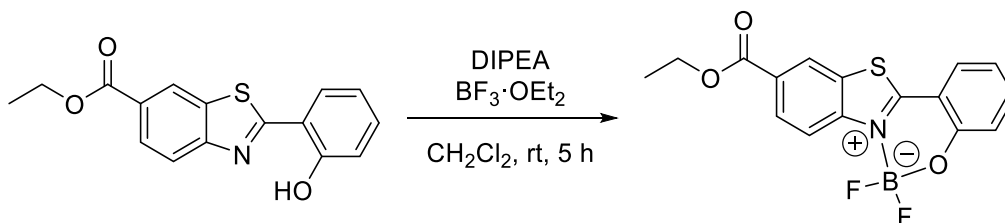
A 10 mL microwave vial was charged with a stir bar, 2-iodo-4-bromobenzothiazole (34 mg, 0.1 mmol), 2-aminophenylboronic acid (41.1 mg, 0.3 mmol), Na₂CO₃ (106 mg, 1 mmol), Pd(PPh₃)₄ (12 mg, 0.01 mmol), DMF (0.6 mL) and water (0.2 mL). The crude mixture was then degassed (3 x freeze-pump-thaw method) and purged with Ar. The vial was loaded into a microwave reactor and heated at 120 °C for 5h. The reaction mixture was cooled to rt before being transferred to a separatory funnel with sat'd aq. NaHCO₃ (10 mL), the aqueous phase was extracted with EtOAc (3 x 15 mL). The combined aqueous phases were washed with brine (3 x 20 mL), then dried over anhydrous MgSO₄, filtered and the filtrate concentrated onto Celite under reduced pressure. The crude material was purified using Silica gel flash chromatography using an eluent of 100% cyclohexane to 70:30 cyclohexane/EtOAc. Desired fractions were collected and concentrated under reduced pressure, and further under high vacuum overnight to furnish the desired compound as a red powder (27.6 mg, 87%). IR $\nu_{\text{max}}/\text{cm}^{-1}$ (neat film): 3457, 3372, 3305, 3055, 3024, 2924, 2853, 1698, 1614, 1593, 1494, 1223, 963, 748. ¹H NMR (300 MHz, Acetone-*d*₆) δ 8.03 (dq, *J* = 5.8, 3.6 Hz, 1H), 7.68 (dd, *J* = 8.0, 1.5 Hz, 1H), 7.50 (dd, *J* = 4.6, 0.8 Hz, 2H), 7.28 – 7.10 (m, 3H), 6.95 (bs, 2H), 6.91 – 6.83 (m, 2H), 6.74 (td, *J* = 7.4, 1.2 Hz, 1H), 6.66 (ddd, *J* = 8.1, 7.1, 1.2 Hz, 1H), 4.46 (bs, 2H). ¹³C NMR (75 MHz, Acetone-*d*₆) δ 156.5 (C_q), 152.6 (C_q), 148.8 (C_q), 146.4 (C_q), 134.9 (C_q), 134.6 (C_q), 132.5 (CH), 131.9 (CH), 130.7 (CH), 129.5 (CH), 128.4 (CH), 126.2 (CH), 125.4 (C_q), 121.6 (CH), 117.8 (CH), 117.5 (CH), 116.9 (CH), 116.4 (CH), 114.9 (C_q). HRMS-ESI (*m/z*): found [M+H]⁺ 318.1062, calc'd C₁₉H₁₆N₃S⁺ requires 318.1065.

6,6-difluoro-10-methyl-6*H*-benzo[*e*]benzo[4,5]thiazolo[3,2-*c*][1,3,2]oxazaborinin-7-ium-6-uide (5.17)



A 10 mL round bottom flask was charged with a stir bar, 2-(2-hydroxyphenyl)-6-methylbenzothiazole (239.2 mg, 1 mmol), dry CH₂Cl₂ (10 mL) and DIPEA (216.5 μ L, 1.5 mmol). The mixture was allowed to stir at rt for 10 minutes at which point BF₃·OEt₂ (502.4 μ L, 4 mmol) was added; evolving a white precipitate. The mixture was allowed to stir at rt for 12 hours. The mixture was then dropped onto excess pentane, causing further evolution of a white precipitate. The precipitate was collected by filtration, washed with pentane and finally triturated with CHCl₃; the filtrate was collected and concentrated under reduced pressure to furnish a light yellow powder (>99%). NMR analysis indicated the formation of the desired product accompanied with undesired DIPEA salts. The residue was dry loaded onto Celite and further loaded onto a plug of basic alumina. The product was eluted using dry CH₂Cl₂, until no fluorescence was observed in the eluent. Solvent was removed under reduced pressure and further dried under high vacuum, yielding a yellow powder (277.6 mg, 97%). IR $\nu_{\text{max}}/\text{cm}^{-1}$ (neat film): 2917, 2849, 1615, 1570, 1509, 1488, 1468, 1276, 1057, 1011, 951, 914, 819, 804, 768. ¹H NMR (300 MHz, Acetone-*d*₆) δ 8.17 (dt, *J* = 8.7, 1.6 Hz, 1H), 8.09 (dp, *J* = 1.5, 0.7 Hz, 1H), 7.91 (ddd, *J* = 7.9, 1.6, 0.5 Hz, 1H), 7.67 (ddd, *J* = 8.7, 7.3, 1.7 Hz, 1H), 7.62 (ddt, *J* = 8.6, 1.1, 0.5 Hz, 1H), 7.17 – 7.08 (m, 2H), 2.56 (s, 3H). ¹³C NMR (101 MHz, Acetone-*d*₆) δ 169.5 (C_q), 156.9 (t, ³*J*_{C-F} = 2.0 Hz, C_q), 142.4 (C_q), 139.1 (C_q), 137.7 (CH), 131.0 (CH), 128.3 (CH), 123.6 (CH), 121.4 (CH), 120.5 (CH), 120.2 (t, ⁴*J*_{C-F} = 3.6 Hz, CH), 118.4 (C_q), 114.3 (C_q), 21.5 (CH₃). ¹⁹F NMR (282 MHz, Acetone-*d*₆) δ -136.42 (q_B). ¹¹B NMR (96 MHz, Acetone-*d*₆) δ 1.24 (t, *J*_{B-F} = 14.0 Hz). HRMS-ESI (*m/z*): found [M-F]⁻ 270.0569, calc'd C₁₄H₁₁BFNOS requires 270.0675, [M-BF₂+H]⁺ 242.0646, calc'd C₁₄H₁₂NOS requires 242.0634. Anal. calc'd for C₁₄H₁₀BF₂NOS: C, 58.16; H, 3.49; N, 4.84. Found C, 59.00; H, 3.48; N, 4.48.

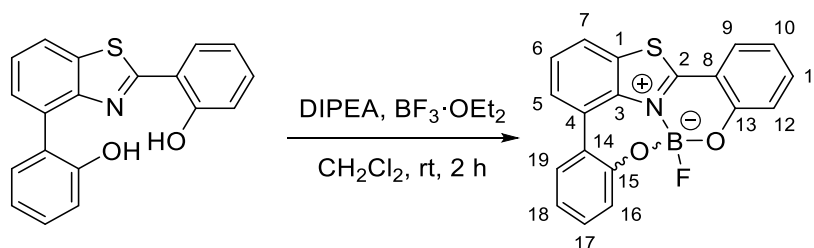
10-(ethoxycarbonyl)-6,6-difluoro-6*H*-benzo[*e*]benzo[4,5]thiazolo[3,2-*c*][1,3,2]oxazaborinin-7-ium-6-uide (5.18)



A 50 mL round bottom flask was charged with a stir bar, ethyl 2-(2-hydroxyphenyl)benzothiazole-6-carboxylate (233.5 mg, 0.78 mmol), 2 mL CH₂Cl₂ and DIPEA (204 mL, 1.17 mmol). The mixture was stirred under Ar atmosphere for 10 minutes after which BF₃·OEt₂ (400 mL, 3.2 mmol) was added dropwise to the stirring solution. The mixture was left to react overnight at room temperature until starting material was consumed (Basic Alumina TLC). The reaction mixture was then diluted with dry pentane, which resulted in the formation of a white precipitate. The reaction mixture was filtered through a frit collecting the precipitate which was washed several times with pentane; the filtrate was discarded. The solid precipitate was then dissolved in CHCl₃ and concentrated to dryness onto Celite. The crude reaction mixture was then purified on a basic alumina column, eluting with CH₂Cl₂/pentane (1:1) until the eluent was no longer fluorescent. The solvent was then removed by rotary evaporation to afford a light yellow powder, which was further dried under high vacuum (103.4 mg, 38%). IR $\nu_{\text{max}}/\text{cm}^{-1}$ (neat film): 3000, 1714, 1506, 1484, 1405, 1273, 1238, 1138, 1099, 1072, 901, 826, 757, 629, 619. ¹H NMR (300 MHz, Chloroform-*d*) δ 8.62 (dd, *J* = 1.6, 0.6 Hz, 1H), 8.42 (d, *J* = 8.8 Hz, 1H), 8.31 (dd, *J* = 8.8, 1.6 Hz, 1H), 7.67 (ddd, *J* = 7.9, 1.6, 0.5 Hz, 1H), 7.61 (ddd, *J* = 8.7, 7.3, 1.6 Hz, 1H), 7.22 (ddd, *J* = 8.5, 1.1, 0.5 Hz, 1H), 7.04 (ddd, *J* = 8.1, 7.3, 1.1 Hz, 1H), 4.46 (q, *J* = 7.1 Hz, 2H), 1.45 (t, *J* = 7.1 Hz, 3H). ¹³C NMR (75 MHz, Chloroform-*d*) δ 171.6 (t, ³*J*_{C-F} = 2.0 Hz, C_q), 165.0 (C_q), 156.8 (t, ³*J*_{C-F} = 1.9 Hz, C_q), 146.4 (C_q), 138.0 (CH), 130.0 (CH), 129.7 (C_q), 129.3 (C_q), 127.3 (CH), 124.1 (CH), 120.9 (CH), 120.7 (CH), 120.4 (t, ⁴*J*_{C-F} = 3.7 Hz, CH), 113.2 (C_q), 62.1 (CH₂), 14.5 (CH₃). ¹⁹F NMR (282 MHz, Chloroform-*d*) δ -135.63 (m). ¹¹B NMR (96 MHz, Chloroform-*d*) δ 1.28 (t, *J* = 12.1 Hz). HRMS-ESI

(*m/z*): found $[M+H]^+$ 300.0696, calc'd $C_{16}H_{14}NO_3S$ requires 300.0694. Anal. calc'd for $C_{16}H_{12}BF_2NO_3S$: C, 55.36; H, 3.48; N, 4.03. Found C, 55.42; H, 3.46; N, 3.95.

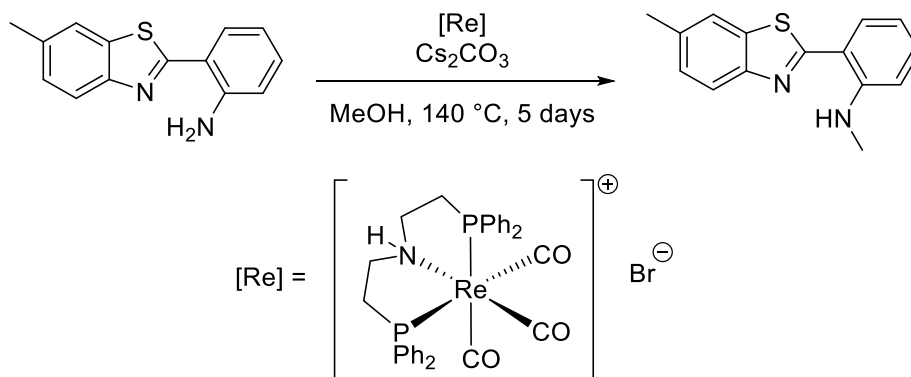
6a-fluoro-6a*H*-6,7-dioxa-1-thia-1a¹-aza-6a-borabenz[*a*]benzo[5,6]cyclohepta[1,2,3,4-*def*]fluoren-1a¹-ium-7-uide (5.19)



A 10 mL Wheaton vial was charged with a stir bar, 2,4-di(2-hydroxyphenyl)benzothiazole (33.8 mg, 0.1 mmol), dry CH_2Cl_2 (2 mL) and DIPEA (53 μ L, 0.3 mmol). The mixture was allowed to stir at rt for 10 minutes at which point $BF_3 \cdot OEt_2$ (100 μ L, 4.8 mmol) was added. The clear brown reaction mixture was allowed to stir at rt for 2h, at which point complete consumption of starting material was determined by TLC (basic Alumina, cyclohexane/ CH_2Cl_2 1:1). The mixture was then dropped onto excess pentane, causing precipitation of a white solid. The precipitate was collected by filtration, washed with pentane and finally dissolved into $CHCl_3$; the filtrate was collected and concentrated onto Celite and purified by basic Alumina flash column chromatography using cyclohexane/ CH_2Cl_2 (1:1) as the eluent. Desired fractions were collected and concentrated to furnish the desired product as a light-yellow powder which was further dried under high vacuum (32.4 mg, 88%). IR ν_{max}/cm^{-1} (neat film): 1611, 1509, 1480, 1468, 1291, 1275, 1076, 1009, 846, 823, 747. 1H NMR (400 MHz, Chloroform-*d*) δ 7.98 (dt, $J = 7.8, 0.9$ Hz, 1H, H₅), 7.86 (dd, $J = 8.0, 1.1$ Hz, 1H, H₇), 7.75 (dd, $J = 8.0, 1.6$ Hz, 1H, H₁₉), 7.68 – 7.54 (m, 3H, H₆, H₉, H₁₁), 7.44 (ddd, $J = 8.1, 7.1, 1.6$ Hz, 1H, H₁₇), 7.36 (dd, $J = 8.0, 1.5$ Hz, 1H, H₁₆), 7.31 (dd, $J = 8.5, 1.0$ Hz, 1H, H₁₂), 7.20 (ddd, $J = 7.9, 7.1, 1.5$ Hz, 1H, H₁₈), 7.04 (ddd, $J = 8.0, 7.3, 1.1$ Hz, 1H, H₁₀). ^{13}C NMR (101 MHz, Chloroform-*d*) δ 166.2 (C₂), 156.3 (C₁₅), 156.1 (C₁₃), 140.7 (C₃), 136.8 (C₁₁), 131.4 (C₄), 131.2 (C₁), 131.0 (C₁₇), 129.6 (C₁₉), 129.3 (C₅), 127.6 (C₆), 126.9 (C₉), 126.8 (C₁₄), 124.1 (C₁₆), 123.2 (C₁₈), 121.1 (C₇), 120.9 (C₁₀), 120.7 (C₁₂), 114.4 (C₈). ^{19}F NMR (377 MHz, Chloroform-*d*)

δ -132.09 (q_B). ¹¹B NMR (128 MHz, Chloroform-*d*) δ 1.90 (d, *J* = 34.5 Hz). HRMS-ESI (*m/z*): found [M+Na]⁺ 370.0491, calc'd C₁₉H₁₁BFNNaO₂S requires 370.0480.

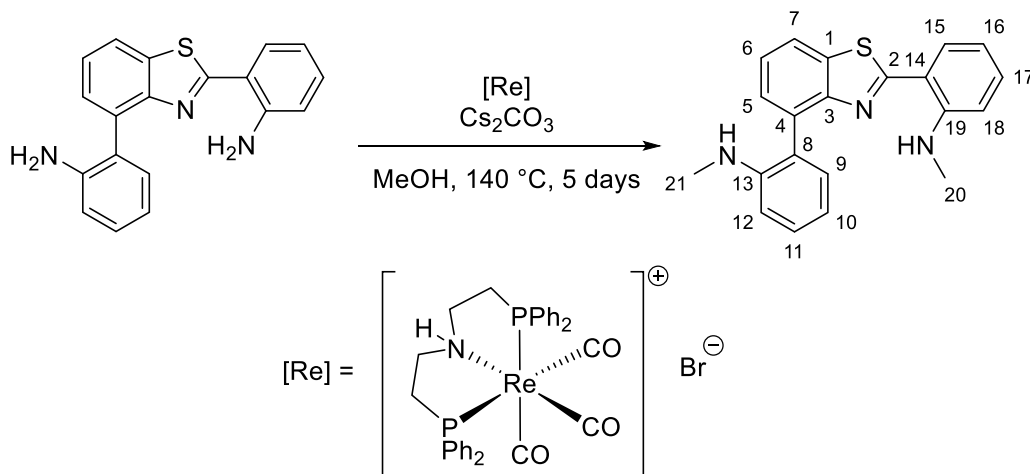
***N*-methyl-2-(6-methylbenzo[*d*]thiazol-2-yl)aniline (5.20)**



An oven dried 10 mL Pyrex Wheaton vial was charged with a stir bar, [Re] (16 mg, 0.025 mmol, 5 mol%), Cs₂CO₃ (118 mg, 0.036 mmol, 100 mol%), 2-(6-methylbenzo[*d*]thiazol-2-yl)aniline (85.4 mg, 0.36 mmol) and dry MeOH (1.5 mL). The vial was purged with Ar, then the reaction mixture degassed (3 cycles of freeze-pump-thaw) and left under an atmosphere of Ar before being sealed with a Teflon lined cap. The vial was placed in an oil bath at 140 °C for 5 days; reaction progress monitored by LCMS and TLC (9:1 cyclohexane/EtOAc). The reaction mixture was cooled to rt, and diluted with EtOAc (10 mL) and passed through a Silica plug, and the Silica washed with EtOAc. The organic phase was washed with saturated aqueous NaHCO₃ (1 x 50 mL) and brine (1 x 100 mL). The organic phase was dried over anhydrous MgSO₄, then filtered and concentrated onto Celite and purified by Silica flash column chromatography (eluent: 100% cyclohexane to 9:1 cyclohexane/EtOAc). Desired fractions were combined and concentrated under reduced pressure to provide the product as a yellow powder (26 mg, 29%). Starting material could be recovered from purification (55.4 mg, 65% recovery). IR ν_{max} /cm⁻¹ (neat film): 3282, 2923, 2860, 2820, 1610, 1581, 1524, 1499, 1450, 1309, 1217, 1174, 960, 814, 734. ¹H NMR (300 MHz, Chloroform-*d*) δ 8.77 (bs, 1H), 7.85 (d, *J* = 8.3 Hz, 1H), 7.72 (dd, *J* = 7.9, 1.4 Hz, 1H), 7.66 (s, 1H), 7.37 – 7.29 (m, 1H), 7.26 (dd, *J* = 8.3, 1.2 Hz, 1H), 6.77 (d, *J* = 8.2 Hz, 1H), 6.73 – 6.65 (m, 1H), 3.04 (d, *J* = 5.0 Hz, 3H), 2.49 (s, 3H).

^{13}C NMR (75 MHz, Chloroform-*d*) δ 168.7 (C_q), 151.9 (C_q), 148.4 (C_q), 135.0 (C_q), 133.5 (C_q), 132.0 (CH), 130.6 (CH), 127.6 (CH), 121.9 (CH) 121.1 (CH), 115.2 (CH), 115.1 (C_q), 110.9 (CH), 29.9 (CH₃), 21.7 (CH₃). HRMS-ESI (*m/z*): found [M+H]⁺ 255.0963, calc'd C₁₅H₁₅N₂S⁺ requires 255.0956.

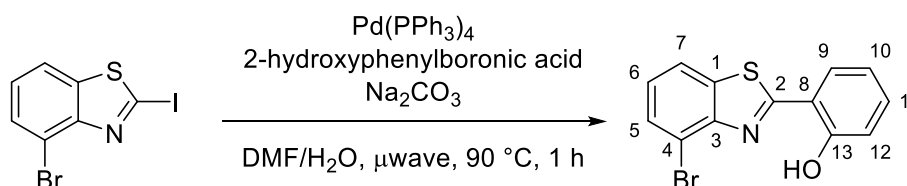
2,2'-(benzo[*d*]thiazole-2,4-diyl)bis(*N*-methylaniline) (5.21)



Two oven dried 10 mL Pyrex Wheaton vials were each charged with a stir bar, [Re] (20 mg, 0.025 mmol, 5 mol%), Cs₂CO₃ (190 mg, 0.6 mmol, 100 mol%), 2,2'-(benzo[*d*]thiazole-2,4-diyl)dianiline (180 mg, 0.6 mmol) and dry MeOH (2 mL). The vials were purged with Ar, then the reaction mixtures degassed (3 cycles of freeze-pump-thaw) and left under an atmosphere of Ar before being sealed with a Teflon lined cap. The vials were placed in an oil bath at 140 °C for 5 days; reaction progress monitored by LCMS and TLC (4:1 cyclohexane/EtOAc). The reaction mixtures were cooled to rt, the content of both vials combined and the mixture diluted with EtOAc (10 mL) and passed through a Silica plug, and the Silica washed with EtOAc. The organic phase was washed with saturated aqueous NaHCO₃ (1 x 50 mL) and brine (1 x 100 mL). The organic phase was dried over anhydrous MgSO₄, then filtered and concentrated onto Celite and purified by Silica flash column chromatography (eluent: 100% cyclohexane to 9:1 cyclohexane/EtOAc). Desired fractions were combined and concentrated under reduced pressure to provide the product as a yellow foam (301.2 mg, 77%). IR ν_{max} /cm⁻¹ (neat film): 3430, 3271, 2919, 2814, 1608,

1578, 1523, 1508, 1501, 1313, 1219, 1171, 959, 746. ^1H NMR (400 MHz, Chloroform-*d*) δ 7.88 (dd, $J = 7.8, 1.3$ Hz, 1H, H₅), 7.71 (dd, $J = 7.9, 1.5$ Hz, 1H, H₁₅), 7.50 (dd, $J = 7.4, 1.3$ Hz, 1H, H₇), 7.44 (t, $J = 7.6$ Hz, 1H, H₆), 7.39 (td, $J = 8.0, 1.6$ Hz, 1H, H₁₁), 7.35 – 7.29 (m, 2H, H₉, H₁₇), 6.90 (t, $J = 6.8$ Hz, 2H, H₁₀, H₁₂), 6.74 – 6.64 (m, 2H, H₁₆, H₁₈), 2.83 (s, 3H, H₂₀), 2.81 (s, 3H, H₂₁). ^{13}C NMR (101 MHz, Chloroform-*d*) δ 169.3 (C₂), 151.5 (C₃), 148.6 (C₁₉), 146.2 (C₁₃), 133.8 (C₁), 133.1 (C₈), 132.4 (C₁₇), 131.3 (C₉), 130.4 (C₁₅), 129.4 (C₁₁), 127.6 (C₇), 125.7 (C₄), 125.5 (C₆), 120.6 (C₅), 117.5 (C₁₀), 115.0 (C₁₆), 114.5 (C₁₄), 111.1 (C₁₈), 110.8 (C₁₂), 31.3 (C₂₁), 29.8 (C₂₀). HRMS-ESI (m/z): found $[\text{M}+\text{H}]^+$ 346.1387, calc'd C₂₁H₂₀N₃S requires 346.1378.

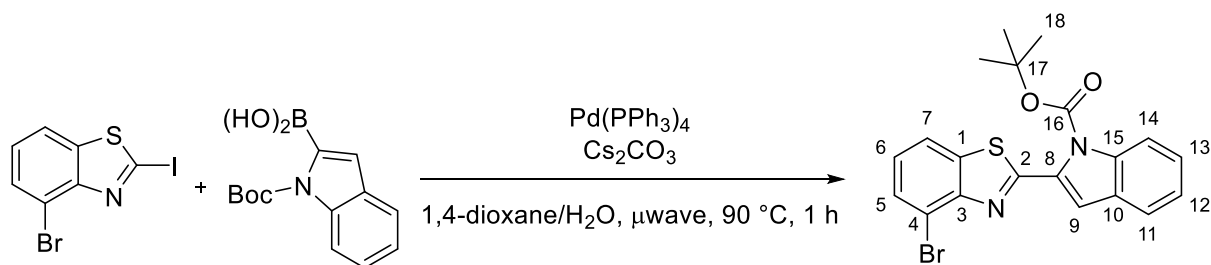
2-(2-hydroxyphenyl)-4-bromobenzothiazole (5.22)



A 10 mL μ wave vial was charged with a stir bar, 2-iodo-4-bromobenzothiazole (35 mg, 0.1 mmol), 2-hydroxyphenylboronic acid (20.5 mg, 0.15 mmol), Pd(PPh₃)₄ (12 mg, 10 mol%), Na₂CO₃ (74 mg, 0.7 mmol), DMF (0.8 mL) and water (0.2 mL). The reaction mixture was stirred at rt for 5 minutes, while purging with Ar. The vial was then loaded into a microwave reactor and heated at 90 °C for 1h, after which TLC (cyclohexane/CH₂Cl₂, 3:2) showed complete conversion of starting material. The crude was dropped onto brine (10 mL) and the phases separated, the aqueous phase was extracted with EtOAc (3 x 15 mL) and the combined organic phases washed with brine (2 x 10 mL). The organic phase was dried over anhydrous MgSO₄, then filtered and concentrated on Celite. The crude was purified on Si gel flash column chromatography using 100% cyclohexane to 4:1 cyclohexane/CH₂Cl₂ as the eluent. Fractions were collected and concentrated to furnish the product as an off-white powder which was further dried under high vacuum (23 mg, 73%). IR $\nu_{\text{max}}/\text{cm}^{-1}$ (neat film): 3045, 2922, 2851, 1586, 1482, 1266, 1218, 1091, 977, 743. ^1H NMR (400 MHz, Chloroform-*d*) δ 7.79 (dd, $J = 8.0, 1.0$ Hz, 1H, H₅), 7.66 (dd, $J = 7.8, 1.0$ Hz, 1H, H₇), 7.63 (dd, $J = 7.9, 1.6$ Hz, 1H,

H₉), 7.39 (ddd, $J = 8.6, 7.2, 1.6$ Hz, 1H, H₁₁), 7.23 (t, $J = 7.9$ Hz, 1H, H₆), 7.11 (dd, $J = 8.4, 1.2$ Hz, 1H, H₁₂), 6.94 (ddd, $J = 8.2, 7.3, 1.2$ Hz, 1H, H₁₀). ¹³C NMR (101 MHz, Chloroform-*d*) δ 169.8 (C₂), 158.2 (C₁₃), 150.3 (C₃), 133.4 (C₁₁, C₁), 130.1 (C₇), 128.5 (C₉), 126.5 (C₆), 120.7 (C₅), 119.7 (C₁₀), 118.2 (C₁₂), 116.5 (C₈), 115.8 (C₄). HRMS-DCI-CH₄ (m/z): found $[M]^+$ 305.9602, calc'd C₁₃H₉NOS⁷⁹Br⁺ requires 305.9588.

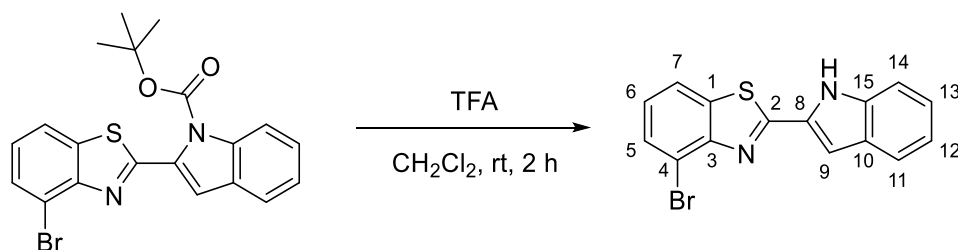
***tert*-butyl 2-(4-bromobenzo[*d*]thiazol-2-yl)-1*H*-indole-1-carboxylate (5.23)**



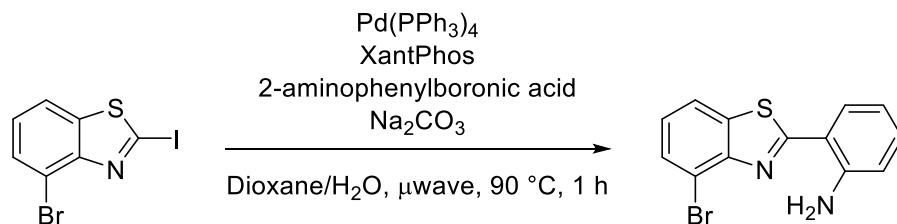
A 35 mL microwave vial was charged with a stir bar, 2-iodo-4-bromobenzothiazole (34.3 mg, 0.1 mmol), *N*-Boc-indole-2-boronic acid (32 mg, 0.12 mmol), Pd(PPh₃)₄ (65 mg, 50 mol%), Cs₂CO₃ (84.7 mg, 0.26 mmol), 1,4-dioxane (7.7 mL) and water (0.3 mL). The reaction mixture was degassed the freeze-pump-thaw method three times and then purged with Ar. The vial was loaded into a microwave reactor and programmed to be heated at 90 °C for 1h, after which the crude was dropped onto water (10 mL) and the phases separated. The aqueous phase was extracted with EtOAc (3 x 10 mL), the combined organic phases were dried over anhydrous MgSO₄, filtered and concentrated onto Celite. The crude residue was purified by Silica gel flash column chromatography using 100% cyclohexane to cyclohexane/EtOAc (9.5:0.5). Desired fractions were collected and concentrated to furnish the desired product as a yellow oil which was further dried under vacuum overnight (31 mg, 72%). IR $\nu_{\max}/\text{cm}^{-1}$ (neat film): 3066, 2978, 2930, 1735, 1442, 1368, 1321, 1221, 1157, 1132, 1006, 739. ¹H NMR (400 MHz, Chloroform-*d*) δ 8.22 (dd, $J = 8.3, 0.9$ Hz, 1H, H₁₁), 7.84 (dd, $J = 8.0, 1.1$ Hz, 1H, H₇), 7.71 (dd, $J = 7.8, 1.1$ Hz, 1H, H₅), 7.59 (dt, $J = 7.8, 1.0$ Hz, 1H, H₁₄), 7.40 (ddd, $J = 8.5, 7.2, 1.3$ Hz, 1H, H₁₂), 7.30 – 7.22 (m, 2H, H₆, H₁₃), 7.03 (s, 1H, H₉), 1.34 (s, 9H, H₁₈). ¹³C NMR (101 MHz, Chloroform-*d*) δ 161.0 (C₂), 151.8 (C₃), 149.5 (C₁₆), 138.3 (C₁₅), 136.3 (C₁), 131.4

(C₈), 130.1 (C₅), 128.3 (C₁₀), 126.5 (C₁₂), 126.3 (C₆), 123.5 (C₁₃), 121.6 (C₁₄), 120.8 (C₇), 117.1 (C₄), 115.5 (C₁₁), 115.1 (C₉), 84.5 (C₁₇), 27.8 (C₁₈). HRMS-DCI(CH₄) (*m/z*): found [M]⁺ 428.0194, calc'd C₂₀H₁₇⁷⁹BrN₂O₂S requires 428.0194.

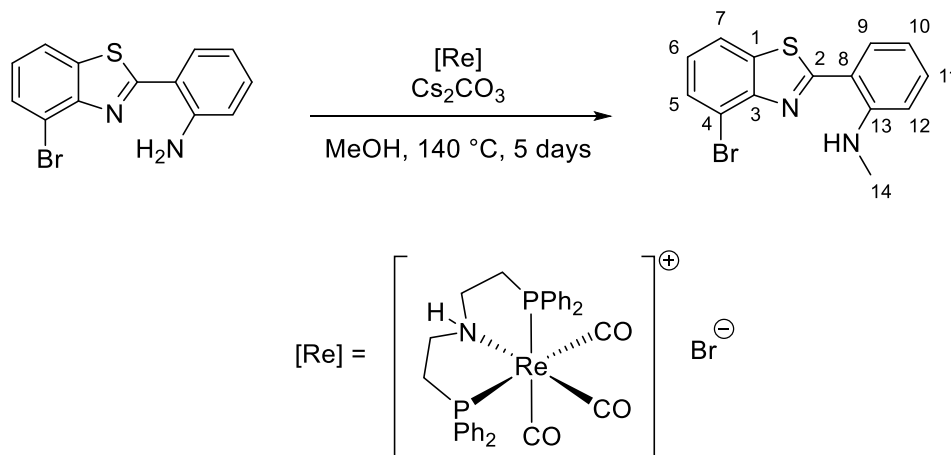
4-bromo-2-(1*H*-indol-2-yl)benzo[*d*]thiazole (5.24)



A 10 mL round-bottom flask was charged with a stir bar, tert-butyl 2-(4-bromobenzo[*d*]thiazol-2-yl)-1*H*-indole-1-carboxylate (150 mg, 0.35 mmol) and CH₂Cl₂ (1 mL). TFA (1 mL) was added via syringe dropwise and the reaction mixture stirred at rt for 2h. All solvent was removed under reduced pressure and the residue dissolved in CH₂Cl₂ (10 mL) and dropped onto saturated aq. NaHCO₃. The phases were separated and the aqueous phase extracted with CH₂Cl₂ (3 x 10 mL). The combined organic phases were dried over anhydrous MgSO₄, filtered and concentrated onto Celite. The crude residue was purified by Silica gel flash column chromatography using 100% cyclohexane to cyclohexane/EtOAc (9:1). Desired fractions were collected and concentrated to furnish the desired product as a yellow powder which was further dried under vacuum overnight (111.3 mg, 97%). IR $\nu_{\text{max}}/\text{cm}^{-1}$ (neat film): 3398, 3380, 3058, 2960, 2921, 2852, 1588, 1557, 1459, 1439, 1397, 1339, 1302, 1142, 1035, 917, 788, 766, 747, 733, 668. ¹H NMR (400 MHz, Chloroform-*d*) δ 9.54 (bs, 1H, NH), 7.81 (dd, *J* = 8.0, 1.1 Hz, 1H, H₇), 7.68 (ddd, *J* = 8.0, 2.2, 1.0, 2H, H₅, H₁₁), 7.45 (dq, *J* = 8.3, 0.9 Hz, 1H, H₁₄), 7.31 (ddd, *J* = 8.2, 7.0, 1.2 Hz, 1H, H₁₃), 7.23 (t, *J* = 7.9 Hz, 1H, H₆), 7.19 – 7.13 (m, 2H, H₉, H₁₂). ¹³C NMR (101 MHz, Chloroform-*d*) δ 160.5 (C₂), 151.9 (C₃), 137.2 (C₁₅), 135.6 (C₁), 131.0 (C₈), 130.1 (C₅), 128.5 (C₁₀), 126.2 (C₆), 125.1 (C₁₃), 121.9 (C₁₁), 121.01 (C₇), 120.95 (C₁₂), 116.5 (C₄), 111.8 (C₁₄), 106.2 (C₉). HRMS-DCI(CH₄) (*m/z*): found [M+H]⁺ 328.9749, calc'd C₁₅H₉⁷⁹BrN₂S requires 328.9748.

2-(2-aminophenyl)-4-bromobenzothiazole (5.25)

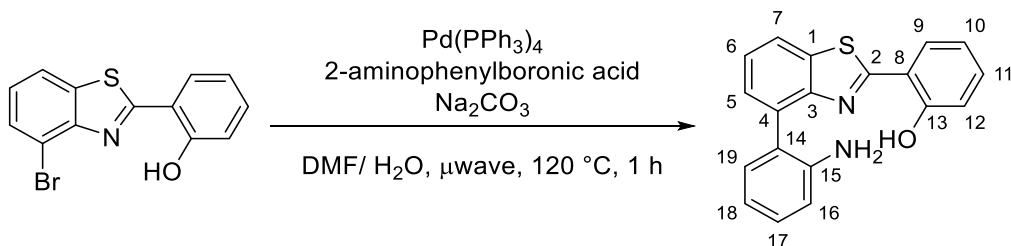
A 10 mL microwave vial was charged with a stir bar, 2-iodo-4-bromobenzothiazole (34.1 mg, 0.1 mmol), 2-aminophenylboronic acid (21.8 mg, 0.15 mmol), Na_2CO_3 (48 mg, 0.45 mmol), $\text{Pd(PPh}_3)_4$ (12 mg, 10 mol%), 1,4-dioxane (0.8 mL) and water (0.2 mL). The vial was purged with Ar and loaded into a microwave reactor and heated at $90\text{ }^\circ\text{C}$ for 1h. The reaction mixture was cooled to rt before being transferred to a separatory funnel with sat'd aq. NaHCO_3 (10 mL), the aqueous phase was extracted with EtOAc (3 x 10 mL). The combined aqueous phases were washed with brine (3 x 20 mL), then dried over anhydrous MgSO_4 , filtered and the filtrate concentrated onto Celite under reduced pressure. The crude material was purified by Silica gel flash column chromatography using an eluent of 100% cyclohexane to cyclohexane/EtOAc (4:1). Desired fractions were collected and concentrated under reduced pressure, and further under high vacuum overnight to furnish the desired compound as a yellow powder (25 mg, 82%). IR $\nu_{\text{max}}/\text{cm}^{-1}$ (neat film): 3460, 3295, 3063, 2924, 1615, 1594, 1494, 1449, 1227, 964, 735. $^1\text{H NMR}$ (300 MHz, Chloroform-*d*) δ 7.79 (dd, $J = 8.0, 1.0$ Hz, 1H), 7.66 (dd, $J = 8.0, 1.4$ Hz, 1H), 7.64 (dd, $J = 7.8, 1.0$ Hz, 1H), 7.24 (ddd, $J = 8.5, 7.1, 1.5$ Hz, 1H), 7.20 (t, $J = 7.9$ Hz, 1H), 6.82 (dd, $J = 8.3, 0.8$ Hz, 1H), 6.74 (ddd, $J = 8.2, 7.2, 1.1$ Hz, 1H). $^{13}\text{C NMR}$ (75 MHz, Chloroform-*d*) δ 169.7 (C_q), 152.0 (C_q), 147.0 (C_q), 134.1 (C_q), 132.2 (CH), 130.3 (CH), 129.5 (CH), 125.8 (CH), 120.4 (CH), 117.3 (CH), 117.1 (CH), 116.1 (C_q), 114.9 (C_q). HRMS-ESI (m/z): found $[\text{M}^{79}\text{Br}+\text{H}]^+$ 304.9752, calc'd $\text{C}_{13}\text{H}_{10}\text{N}_2\text{SBr}^+$ requires 304.9748.

2-(2-methylaminophenyl)-4-bromobenzothiazole (5.26)

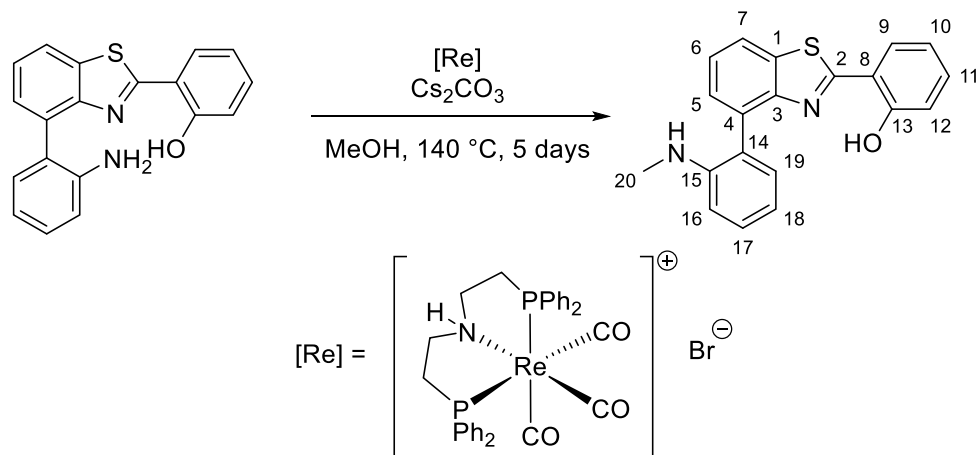
An oven dried 10 mL Pyrex Wheaton vial was charged with a stir bar, [Re] (23 mg, 0.025 mmol, 5 mol%), Cs₂CO₃ (188.9 mg, 0.6 mmol, 100 mol%), 2-(2-aminophenyl)-4-bromobenzothiazole (174.5 mg, 0.6 mmol) and dry MeOH (2 mL). The vial was purged with Ar, then the reaction mixture degassed (3 cycles of freeze-pump-thaw) and left under an atmosphere of Ar before being sealed with a Teflon lined cap. The vial was then placed in an oil bath at 140 °C and reaction progress monitored by TLC (9:1 cyclohexane/EtOAc). After 5 days, the reaction mixture was cooled to rt, diluted with EtOAc and passed through a Silica plug in a Pasteur pipette and eluted with EtOAc. The residue was concentrated onto Celite and purified using Silica gel flash column chromatography using 100% cyclohexane to cyclohexane/CH₂Cl₂ (7:3). Desired fractions were collected and concentrated under reduced pressure to furnish the desired product as a yellow powder, which was further dried under high vacuum overnight (142.3 mg, 78%). IR $\nu_{\text{max}}/\text{cm}^{-1}$ (neat film): 3275, 3098, 3056, 2924, 2890, 2859, 2820, 1612, 1575, 1525, 1499, 1454, 1305, 1218, 1173, 954, 732. ¹H NMR (400 MHz, Chloroform-*d*) δ 9.05 (bs, 1H, -NH), 7.78 (dd, *J* = 7.9, 1.0 Hz, 1H, H₇), 7.69 (dd, *J* = 7.9, 1.5 Hz, 1H, H₉), 7.63 (dd, *J* = 7.8, 1.0 Hz, 1H, H₅), 7.36 (ddd, *J* = 8.6, 7.1, 1.5 Hz, 1H, H₁₁), 7.19 (t, *J* = 7.9 Hz, 1H, H₆), 6.80 (dd, *J* = 8.5, 1.1 Hz, 1H, H₁₂), 6.69 (ddd, *J* = 8.1, 7.1, 1.1 Hz, 1H, H₁₀), 3.08 (d, *J* = 3.9 Hz, 3H, H₁₄). ¹³C NMR (101 MHz, Chloroform-*d*) δ 170.0 (C₂), 151.8 (C₃), 148.9 (C₁₃), 134.0 (C₁), 132.8 (C₁₁), 130.6 (C₉), 129.4 (C₅), 125.7 (C₆), 120.4 (C₇), 115.8 (C₄), 115.1 (C₁₀), 114.2

(C₈), 111.2 (C₁₂), 30.0 (C₁₄). HRMS-ESI (*m/z*): found [M⁷⁹Br+H]⁺ 318.9892, calc'd C₁₄H₁₂N₂S⁷⁹Br requires 318.9905.

2-(2-hydroxyphenyl)-4-(2-aminophenyl)benzothiazole (5.27)



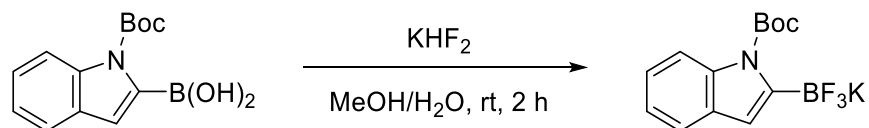
A 10 mL microwave vial was charged with a stir bar, 2-(2-hydroxyphenyl)-4-bromobenzothiazole (33.6 mg, 0.1 mmol), 2-aminophenylboronic acid (28.7 mg, 0.21 mmol), Pd(PPh₃)₄ (12 mg, 10 mol%), Na₂CO₃ (78 mg, 0.7 mmol), DMF (0.8 mL) and water (0.2 mL). The reaction mixture was degassed the freeze-pump-thaw method three times and then purged with Ar. The vial was loaded into a microwave reactor and programmed to be heated at 120 °C for 1h, after which the crude was dropped onto water (10 mL) and the phases separated. The aqueous phase was extracted with EtOAc (3 x 10 mL), the combined organic phases were dried over anhydrous MgSO₄, filtered and concentrated onto Celite. The crude residue was purified by Silica gel flash column chromatography using cyclohexane/EtOAc (4:2 to 1:1). Desired fractions were collected and concentrated to furnish the desired product as a yellow powder which was further dried under vacuum overnight (28.7 mg, 82%). IR $\nu_{\text{max}}/\text{cm}^{-1}$ (neat film): 3466, 3371, 3211, 3057, 3021, 2920, 2250, 1936, 1612, 1577, 1482, 1467, 1219, 1151, 977, 726. ¹H NMR (400 MHz, Chloroform-*d*) δ 12.27 (bs, 1H, -OH), 7.91 (dd, *J* = 7.9, 1.4 Hz, 1H, H₇), 7.68 (dd, *J* = 7.8, 1.6 Hz, 1H, H₉), 7.56 (dd, *J* = 7.4, 1.4 Hz, 1H, H₅), 7.50 (t, *J* = 7.6 Hz, 1H, H₆), 7.36 (ddd, *J* = 8.6, 7.2, 1.6 Hz, 1H, H₁₁), 7.31 – 7.20 (m, 2H, H₁₇, H₁₉), 7.04 (dd, *J* = 8.3, 1.2 Hz, 1H, H₁₂), 6.98 – 6.84 (m, 3H, H₁₀, H₁₆, H₁₈), 3.76 (bs, 1H, -NH₂). ¹³C NMR (101 MHz, Chloroform-*d*) δ 169.2 (C₂), 158.0 (C₁₃), 150.0 (C₃), 144.0 (C₁₅), 133.6 (C₄), 133.4 (C₁), 133.0 (C₁₁), 131.3 (C₁₉), 129.5 (C₁₇), 128.4 (C₉), 128.2 (C₅), 126.1 (C₆), 124.4 (C₁₄), 120.9 (C₇), 119.6 (C₁₀), 118.7 (C₁₈), 118.0 (C₁₂), 116.9 (C₈), 116.2 (C₁₆). HRMS-ESI (*m/z*): found [M+H]⁺ 319.0905, calc'd C₁₉H₁₅N₂OS requires 319.0905.

2-(2-hydroxyphenyl)-4-(2-methylaminophenyl)benzothiazole (5.28)

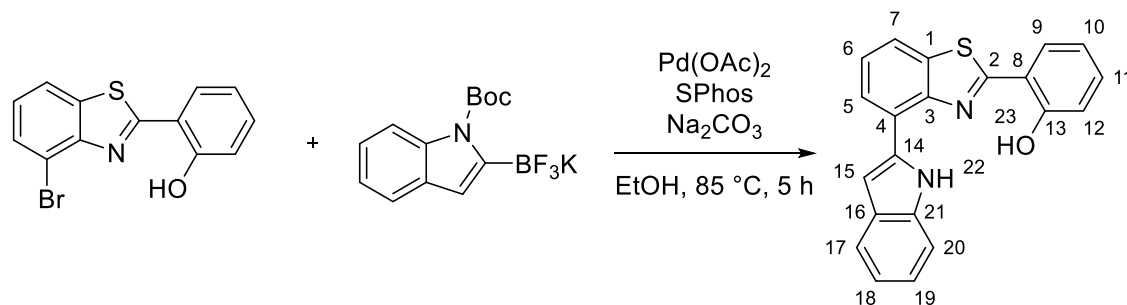
An oven dried 10 mL Pyrex Wheaton vial was charged with a stir bar, [Re] (21 mg, 0.025 mmol, 5 mol%), Cs₂CO₃ (170 mg, 0.5 mmol, 100 mol%), 2-(2-hydroxyphenyl)-4-(2-aminophenyl)benzothiazole (156.7 mg, 0.5 mmol) and dry MeOH (2 mL). The vial was purged with Ar, then the reaction mixture degassed (3 cycles of freeze-pump-thaw) and left under an atmosphere of Ar before being sealed with a Teflon lined cap. The vial was then placed in an oil bath at 140 °C and reaction progress monitored by TLC (9:1 cyclohexane/EtOAc). After 5 days, the reaction mixture was cooled to rt, diluted with EtOAc and passed through a Silica plug in a Pasteur pipette and eluted with EtOAc. The residue was concentrated onto Celite and purified using Silica gel flash column chromatography using 100% cyclohexane to cyclohexane/EtOAc (9:1). Desired fractions were collected and concentrated under reduced pressure to furnish the desired product as a yellow powder, which was further dried under high vacuum overnight (54.7 mg, 33%). Starting material could be recovered from purification (75 mg, 48% recovery). IR $\nu_{\text{max}}/\text{cm}^{-1}$ (neat film): 3434, 3048, 2922, 2814, 1620, 1603, 1580, 1510, 1481, 1313, 1218, 1155, 975, 745. ¹H NMR (400 MHz, Chloroform-*d*) δ 7.92 (dd, J = 7.7, 1.5 Hz, 1H, H₇), 7.68 (dd, J = 7.9, 1.6 Hz, 1H, H₉), 7.55 (dd, J = 7.4, 1.5 Hz, 1H, H₅), 7.50 (t, J = 7.6 Hz, 1H, H₆), 7.36 (dddd, J = 8.2, 7.2, 6.3, 1.6 Hz, 2H, H₁₁, H₁₇), 7.24 (dd, J = 7.5, 1.7 Hz, 1H, H₁₉), 7.03 (dd, J = 8.4, 1.1 Hz, 1H, H₁₆), 6.97 – 6.90 (m, 1H, H₁₀), 6.86 (td, J = 7.5, 1.2 Hz, 1H, H₁₈), 6.82 (d, J = 8.2 Hz, 1H, H₁₂), 3.84 (bs, 1H, -NH), 2.82 (s, 3H, H₂₀). ¹³C NMR (101 MHz, Chloroform-*d*) δ 169.1 (C₂), 158.1 (C₁₃), 150.3 (C₃), 146.5 (C₁₅), 133.6 (C₁), 133.5

(C₄), 133.0 (C₁₁), 130.9 (C₁₉), 129.7 (C₁₇), 128.42 (C₉), 128.39 (C₅), 126.2 (C₆), 124.2 (C₁₄), 120.9 (C₇), 119.5 (C₁₀), 118.1 (C₁₆), 117.0 (C₁₈), 116.9 (C₈), 110.4 (C₁₂), 30.9 (C₂₀). HRMS-ESI (*m/z*): found [M+H]⁺ 333.1062, calc'd C₂₀H₁₇N₂OS requires 333.1062.

Potassium *N*-Boc-indole-2-trifluoroborate



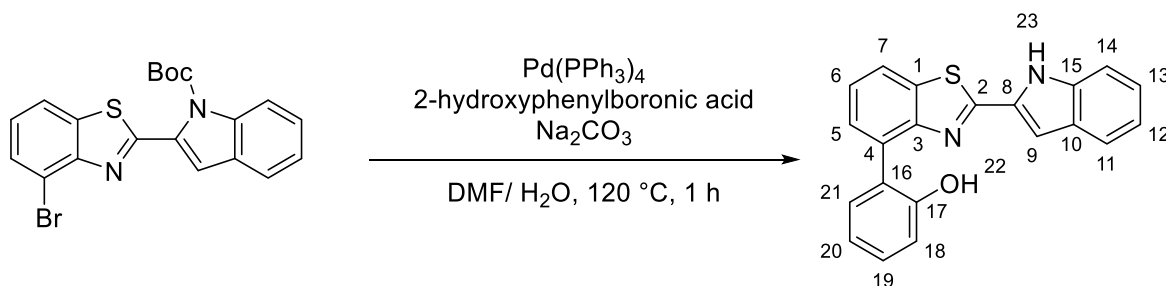
A 25 mL round-bottom flask was charged with a stir bar, *N*-(tert-butoxycarbonyl)indole-2-boronic acid (1.1653 g, 4.5 mmol) and MeOH (1.3 mL). The reaction mixture was stirred until all boronic acid had dissolved then aq. KHF₂ (4.5 M, 3.3 mL, 14.9 mmol) was added dropwise; the reaction became a pink slurry, additional MeOH was added to ensure efficient stirring. The reaction mixture was stirred at rt for 2h after which complete conversion was determined by ¹¹B NMR. All solvent was removed under reduced pressure and the white residue left to dry under high vacuum for 6h. The crude was triturated with acetone (3 x 20 mL) and filtered to remove insoluble solids. The acetone filtrate was concentrated to saturation then dropped onto pentane to precipitate the desired salt as a white powder which was collected by filtration, washed with pentane then dried under high vacuum overnight (1.4246 g, >99%). ¹H NMR (400 MHz, DMSO-*d*₆) δ 8.07 – 7.95 (m, 1H), 7.42 – 7.35 (m, 1H), 7.05 (pd, *J* = 7.1, 1.5 Hz, 2H), 6.40 (d, *J* = 0.8 Hz, 1H), 1.57 (s, 9H). ¹⁹F NMR (376 MHz, DMSO-*d*₆) δ -135.84 – -136.78 (m). ¹¹B NMR (128 MHz, DMSO-*d*₆) δ 1.46 (bs). LRMS-ESI (*m/z*): [M-K]⁻ 284. Characterization data matches previous literature reports.³²⁹

2-(4-(1*H*-indol-2-yl)benzo[*d*]thiazol-2-yl)phenol (5.29)

A 10 mL microwave vial was charged with a stir bar, 2-(4-bromobenzo[*d*]thiazol-2-yl)phenol (31.4 mg, 0.1 mmol), potassium *N*-(tert-butoxycarbonyl)indole-2-trifluoroborate (41.3 mg, 0.12 mmol), Pd(OAc)₂ (2.6 mg, 10 mol%) and SPhos (10.3 mg, 25 mol%). The vial was placed under vacuum and purged with Ar (x 3) before EtOH (1 mL) was added. The vial was loaded into a microwave reactor and heated at 85 °C for 5 h. The crude was dropped onto brine (10 mL) and extracted with EtOAc (3 x 10 mL). The combined organic phases were dried over anhydrous MgSO₄, filtered and all solvent removed under reduced pressure. The residue was dissolved in CH₂Cl₂ (1 mL) and TFA (1 mL) and stirred at rt for 2h. Solvent was removed under reduced pressure and the residue dissolved in CH₂Cl₂ (10 mL) and washed with saturated aq. NaHCO₃ (2 x 10 mL) until pH was basic (~8) then brine (10 mL). The organic phase was dried over anhydrous MgSO₄, filtered and concentrated onto Celite. The crude residue was purified on Si gel flash column chromatography using an eluent of 100% cyclohexane to 8.5:1.5 cyclohexane/EtOAc. Desired fractions were collected and concentrated to furnish the desired product as an orange powder which was further dried under high vacuum overnight (23.6 mg, 69%). IR $\nu_{\max}/\text{cm}^{-1}$ (neat film): 3441, 3357, 3054, 2956, 2919, 2846, 1621, 1583, 1481, 1450, 1418, 1301, 1222, 747. ¹H NMR (400 MHz, Chloroform-*d*) δ 11.91 (s, 1H, H₂₃), 9.32 (s, 1H, H₂₂), 7.83 (dd, *J* = 7.6, 1.1 Hz, 1H, H₅), 7.80 (dd, *J* = 8.0, 1.1 Hz, 1H, H₇), 7.70 (td, *J* = 7.8, 7.4, 1.3 Hz, 2H, H₉, H₁₇), 7.51 (dq, *J* = 8.1, 0.9 Hz, 1H, H₂₀), 7.45 (t, *J* = 7.8 Hz, 1H, H₆), 7.40 (ddd, *J* = 8.6, 7.2, 1.6 Hz, 1H, H₁₁), 7.29 – 7.22 (m, 1H, H₁₉), 7.17 (ddd, *J* = 8.0, 7.0, 1.0 Hz, 1H, H₁₈), 7.12 (dd, *J* = 8.4, 1.1 Hz, 1H, H₁₂), 7.09 (dd, *J* = 2.2, 0.9 Hz, 1H, H₁₅), 6.98 (ddd, *J* = 8.2, 7.3, 1.2 Hz, 1H, H₁₀). ¹³C NMR (101 MHz, Chloroform-*d*) δ 169.6 (C₂), 157.5

(C₁₃), 148.1 (C₃), 137.0 (C₂₁), 135.4 (C₁₄), 134.2 (C₁), 133.3 (C₁₁), 128.76 (C₉), 128.7 (C₁₆), 126.3 (C₄), 126.0 (C₆), 125.1 (C₅), 123.0 (C₁₉), 121.0 (C₁₇), 120.47 (C₇), 120.43 (C₁₈), 120.1 (C₁₀), 118.0 (C₁₂), 117.0 (C₈), 111.5 (C₂₀), 102.4 (C₁₅). HRMS-ESI (*m/z*): found [M+H]⁺ 343.0902, calc'd C₂₁H₁₅N₂OS requires 343.0905.

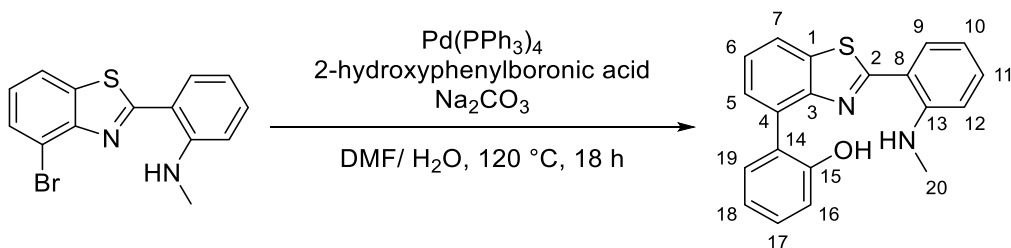
2-(2-(1*H*-indol-2-yl)benzo[*d*]thiazol-4-yl)phenol (5.30)



A 10 mL microwave vial was charged with a stir bar, *tert*-butyl 2-(4-bromobenzo[*d*]thiazol-2-yl)-1*H*-indole-1-carboxylate (33.1 mg, 0.077 mmol), 2-hydroxyphenylboronic acid (23.3 mg, 0.15 mmol), Pd(PPh₃)₄ (12 mg, 10 mol%), Na₂CO₃ (64 mg, 0.6 mmol), DMF (0.8 mL) and water (0.2 mL). The reaction mixture was degassed the freeze-pump-thaw method three times and then purged with Ar. The vial was loaded into a microwave reactor and heated at 120 °C for 1 h. The crude was dropped onto water (10 mL) and the phases separated. The aqueous phase was extracted with EtOAc (3 x 10 mL), the combined organic phases were dried over anhydrous MgSO₄, filtered and concentrated. The crude was dissolved in CH₂Cl₂ (1 mL) and TFA (1 mL) and stirred at rt for 2h. Solvent was removed under reduced pressure and the crude dissolved in CH₂Cl₂ (10 mL). The organic phase was washed with saturated aq. NaHCO₃ (2 x 10 mL) until pH was basic (~ 8) and finally with brine (10 mL). The organic phase was dried over anhydrous MgSO₄, then filtered and concentrated onto Celite. The crude residue was purified by Silica gel flash column chromatography using 100% cyclohexane to cyclohexane/EtOAc (4:1). Desired fractions were collected and concentrated to furnish the desired product as a yellow powder which was further dried under vacuum overnight (18.4 mg, 70%). IR ν_{max} /cm⁻¹ (neat film): 3348, 3061, 2927, 2846, 2248, 1584, 1549, 1458, 1340, 1230, 1141, 1024, 905, 728. ¹H NMR (400 MHz, Chloroform-*d*) δ 9.27 (s, 1H, NH), 7.90 (dd, *J* = 7.9, 1.2 Hz,

1H, H₇), 7.67 (dq, $J = 8.1, 1.0$ Hz, 1H, H₁₁), 7.61 (dd, $J = 7.6, 1.2$ Hz, 1H, H₅), 7.56 – 7.47 (m, 2H, H₆, H₂₁), 7.45 – 7.36 (m, 2H, H₁₄, H₁₉), 7.31 (ddd, $J = 8.3, 7.0, 1.2$ Hz, 1H, H₁₃), 7.25 – 7.19 (m, 2H, H₉, H₁₈), 7.19 – 7.08 (m, 2H, H₁₂, H₂₀). ¹³C NMR (101 MHz, Chloroform-*d*) δ 161.3 (C₂), 154.3 (C₁₇), 149.8 (C₃), 137.5 (C₁₅), 134.4 (C₄), 133.4 (C₁), 131.6 (C₂₁), 130.2 (C₈), 130.1 (C₁₉), 129.2 (C₅), 128.4 (C₁₀), 127.1 (C₁₆), 126.4 (C₆), 125.5 (C₁₃), 121.9 (C₁₁), 121.6 (C₂₀), 121.2 (C₁₂), 121.0 (C₇), 119.7 (C₁₈), 112.0 (C₁₄), 107.2 (C₉). HRMS-ESI (m/z): found $[M+H]^+$ 343.0904, calc'd C₂₁H₁₅N₂OS requires 343.0905.

2-(2-methylaminophenyl)-4-(2-hydroxyphenyl)benzothiazole (5.31)



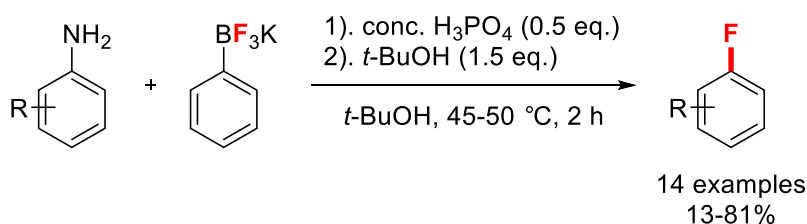
A 10 mL round-bottom flask with condenser was charged with a stir bar, 2-(4-bromobenzo[*d*]thiazol-2-yl)-*N*-methylaniline (101.9 mg, 0.32 mmol), 2-hydroxyphenylboronic acid (71 mg, 0.5 mmol), Pd(PPh₃)₄ (36 mg, 10 mol%), Na₂CO₃ (212 mg, 2 mmol), DMF (2.4 mL) and water (0.6 mL). The reaction mixture was degassed the freeze-pump-thaw method three times and then purged with Ar. The flask was placed in an oil bath at 120 °C for 18h. The crude was dropped onto water (10 mL) and the phases separated. The aqueous phase was extracted with EtOAc (3 x 10 mL), the combined organic phases were dried over anhydrous MgSO₄, filtered and concentrated onto Celite. The crude residue was purified by Silica gel flash column chromatography using 100% cyclohexane to cyclohexane/EtOAc (4:1). Desired fractions were collected and concentrated to furnish the desired product as a yellow foam which was further dried under vacuum overnight (82.7 mg, 78%). IR $\nu_{\max}/\text{cm}^{-1}$ (neat film): 3343, 3060, 2922, 2817, 1608, 1575, 1492, 1448, 1312, 1216, 1172, 961, 748. ¹H NMR (400 MHz, Chloroform-*d*) δ 8.27 (bs, 1H, -NH), 7.91 (dd, $J = 7.8, 1.3$ Hz, 1H, H₇), 7.74 (dd, $J = 7.9, 1.5$ Hz, 1H, H₉), 7.56 (dd, $J = 7.5, 1.3$ Hz, 1H, H₅), 7.52 – 7.45 (m, 2H, H₆, H₁₉), 7.43 – 7.32 (m, 2H, H₁₁,

H₁₇), 7.18 (dd, $J = 8.1, 1.2$ Hz, 1H, H₁₆), 7.11 (td, $J = 7.5, 1.3$ Hz, 1H, H₁₈), 6.92 (bs, 1H, -OH), 6.75 (d, $J = 8.5$ Hz, 1H, H₁₂), 6.70 (ddd, $J = 8.1, 7.1, 1.1$ Hz, 1H, H₁₀), 2.92 (s, 3H, H₂₀). ¹³C NMR (101 MHz, Chloroform-*d*) δ 171.1 (C₂), 153.8 (C₁₅), 150.5 (C₃), 148.5 (C₁₃), 133.4 (C₁), 133.0 (C₁₁), 131.8 (C₄), 131.6 (C₁₉), 130.8 (C₉), 129.9 (C₁₇), 128.2 (C₅), 126.7 (C₁₄), 125.8 (C₆), 121.2 (C₁₈), 120.7 (C₇), 118.0 (C₁₆), 115.4 (C₁₀), 114.1 (C₈), 111.4 (C₁₂), 29.8 (C₂₀). HRMS-DCI(CH₄) (m/z): found [M+H]⁺ 333.1048, calc'd C₂₀H₁₇N₂OS requires 333.1062.

6 Conclusion

The work presented in this thesis has mainly focused on the use of B-F bonds, particularly organotrifluoroborates, as F⁻ sources in the inter- and intramolecular fluorination of various substrates. This work has also applied B-F bonds in the synthesis of novel fluorophores as potential bi-modal imaging agents.

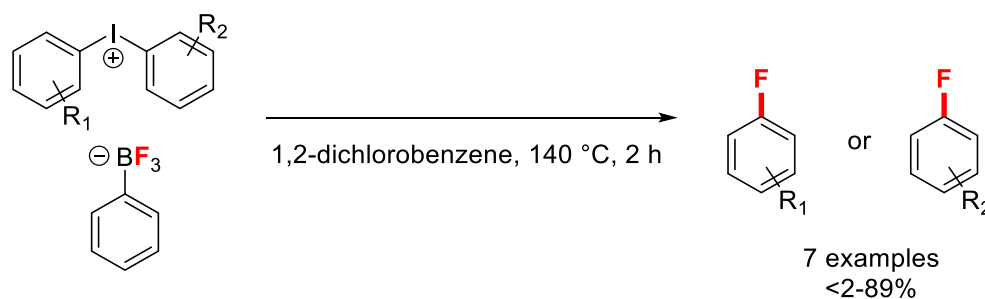
Chapter 2 described the application of organotrifluoroborates as a source of F⁻ in the fluorodediazotization of aryl diazonium salts. Preliminary results demonstrated that aryl diazonium salts could be fluorinated using organotrifluoroborates salts in the solution-phase. This methodology was then extended to a one-pot two-step diazotization/fluorodediazotiation protocol, avoiding the isolation of aryl diazonium salts (Scheme 6.1). This protocol allows the fluorination of anilines under unprecedentedly mild conditions in low to excellent yields. The transformation was particularly efficient for highly sterically hindered anilines, yields decreased as steric hindrance was removed from one or both *ortho* positions.



Scheme 6.1 Reaction summary for one-pot two-step Balz-Schiemann reaction with organotrifluoroborates.

Chapter 3 reports preliminary results from the investigation of organotrifluoroborates as F⁻ sources in the fluorination of unsymmetrical diaryliodonium salts. The work mainly focused on the synthesis, isolation and characterisation of unsymmetrical diaryliodonium phenyltrifluoroborate salts, which have not been previously described (7 examples).

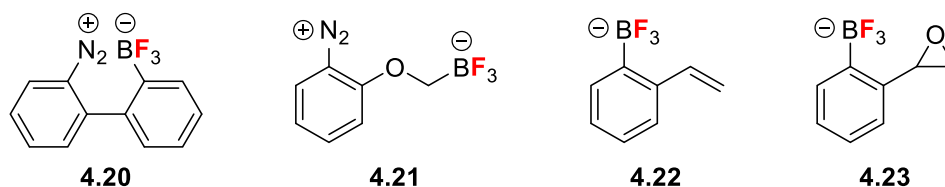
Fluorination of these salts, in the solution-phase, was then investigated (Scheme 6.2). These salts were fluorinated in trace to excellent yields, with absolute selectivity in the aryl ring fluorinated. The fluorination selectivity observed was in contrast to product distribution predicted by the accepted mechanism of unsymmetrical diaryliodonium salt fluorination with F^- , which is under Curtin-Hammett control. These findings suggest that fluorination using organotrifluoroborates is under simple kinetic control and fluorination results from direct F^- transfer from phenyltrifluoroborate and not from release of F^- into the reaction medium.



Scheme 6.2 Reaction summary for thermolysis of unsymmetrical diaryliodonium phenyltrifluoroborate salts.

Following results observed in chapters 2 and 3 with the application of organotrifluoroborates as sources of F^- for intermolecular fluorination, chapter 4 explores our attempts to translate this towards intramolecular fluorination. To this end, four different molecular scaffolds were identified, and their synthesis attempted (Scheme 6.3). We attempted to synthesize **4.20**, however all methods failed to produce more than trace yields of the aniline precursor. Zwitterion **4.21** was synthesized and fully characterised, and fluorination via an intramolecular Balz-Schiemann type reaction investigated; the corresponding aryl fluoride could only be detected in trace amounts. Styrene derivative **4.22** was synthesized, fully characterised and studied with respect to bromofluorination

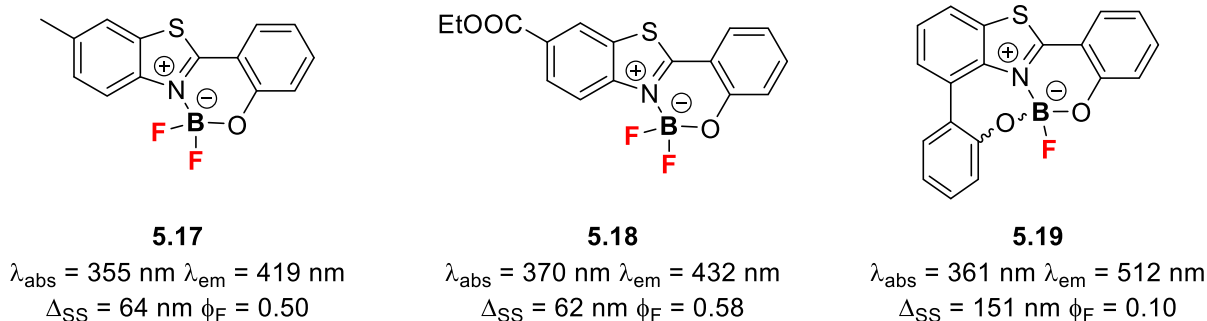
reactions using various electrophilic brominating agents; only trace yields of the desired product could be detected. Styrene oxide derivative **4.23** was also synthesized and fully characterised, however fluorination by intramolecular epoxide ring-opening could only be detected in trace amounts.



Scheme 6.3 Molecular scaffolds for intramolecular fluorination using trifluoroborate moiety.

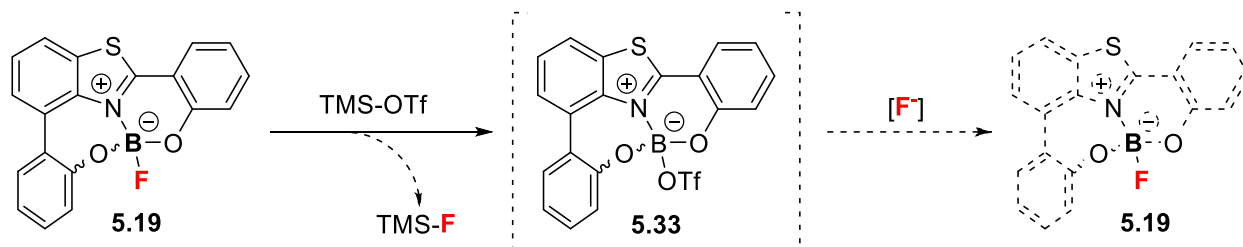
Chapters 2-4 have demonstrated the utility of using organotrifluoroborates as competent F^- sources, which is a departure from classical and traditional applications of organotrifluoroborates. This work has also shown that novel reactivity and applications can be found in well-established reagents.

Finally, chapter 5 describes the synthesis of novel fluorophores, incorporating a $B-F_n$ complex, based on the benzothiazole scaffold. A series of variously substituted 2-arylbenzothiazoles and 2,4-diarylbenzothiazoles were synthesized from which three $B-F_n$ complexes could be isolated and fully characterised (Scheme 6.4). Complex **5.19** was found to have the most promising photophysical properties: NIR-approaching emission and large Stokes shift. The aqueous stability of these complexes was investigated, from which **5.19** emerged as the most stable.



Scheme 6.4 Isolated and characterised B-F_n complexes.

Additionally, **5.19** containing an asymmetric boron centre was synthesized as a racemic mixture of enantiomers, could be chirally resolved and the enantiomers characterised by CD spectroscopy; the enantiomers were found to be stable to racemization via inversion. Finally, F⁻ abstraction from **5.19** was demonstrated, with the formation of the corresponding borenium ion (Scheme **6.5**), highlighting the possibility to perform ¹⁹F-¹⁸F isotope exchange on this substrate.



Scheme 6.5 Fluoride abstraction from **5.19**.

This work serves to confirm the advantages, in structure and properties, conferred by incorporation of a B-F moiety into a molecular scaffold. This work has also possibly inspired the opening of new avenues towards the production of bi-modal imaging tracers for clinical applications.

7 Résumé Français

7.1 Introduction

Cette thèse s'articule autour d'un thème central, la liaison Bore-Fluor (B-F). La liaison B-F a une longue et riche histoire dans les transformations chimiques ainsi que dans les études de matériaux et de liaisons fondamentales, tout en trouvant des applications utiles dans les processus de couplage, de capture et de détection des ions fluorure et de fluoration dans des contextes chimiques et radiochimiques pour n'en citer que quelques unes. La polyvalence de la liaison B-F a également montré une immense utilité dans des domaines aussi vastes que la tomographie par émission de positrons (TEP) et l'imagerie par fluorescence. Nous nous intéressons particulièrement à l'utilisation de la liaison B-F pour la formation de liaisons nucléophiles carbone-fluor (C-F) et au développement de nouveaux fluorophores ayant des applications potentielles comme agents d'imagerie bi-modale TEP / fluorescence.

Contrairement à l'utilisation abondante de BF_4^- et $\text{BF}_3 \cdot \text{OEt}_2$ comme sources de fluor nucléophile (F^-) en chimie de synthèse, il existe peu de rapports décrivant l'utilisation d'organofluoroborates comme sources F^- . Les organotrifluoroborates sont des outils de synthèse attrayants pour l'élaboration de molécules organiques. Cependant, la fonctionnalité trifluoroborate est généralement considérée comme un groupe auxiliaire, et son potentiel en tant que source F^- est demeuré inexploré. Dans ce contexte, nous nous sommes intéressés à la capacité des organotrifluoroborates à servir de sources compétentes de F^- . Dans une mise à jour de la réaction historique de Balz-Schiemann, qui utilise traditionnellement le BF_4^- comme source de F^- , il a été démontré que les organotrifluoroborates interviennent dans la fluorodediazotation des sels d'aryle

diazonium générés *in situ* dans des conditions de réaction exceptionnellement douces (chapitre 2).

Dans les réactions avec une classe de substrat analogue, des sels de diaryliodonium asymétriques pourraient également être fluorés en utilisant du phényltrifluoroborate par décomposition thermique de la paire d'ions (chapitre 3). Enfin, la capacité du groupement trifluoroborate à médier les réactions de transfert de fluor intramoléculaires a été étudiée par la synthèse de divers motifs moléculaires contenant un fragment trifluoroborate (chapitre 4).

De nouveaux complexes fluoroborate ($B-F_n$) du motif 2-aryl-benzothiazole ont été étudiés en tant que fluorophores. Trois complexes ont été isolés, caractérisés et leurs propriétés photophysiques ont été explorées. Un complexe de monofluoroborate de 2,4-diarylbenzothiazole présentant les propriétés photophysiques les plus prometteuses s'est révélé stable aux conditions aqueuses. L'abstraction du fluorure de ce complexe a également été démontrée, fournissant des résultats préliminaires prometteurs pour la viabilité du radiomarquage via l'échange d'isotopes ^{19}F - ^{18}F . Le complexe de monofluoroborate a également montré des propriétés structurales intéressantes étant donné le centre asymétrique du bore. Les énantiomères du complexe ont été résolus par chromatographie chirale à partir du mélange racémique, caractérisé par le dichroïsme circulaire et leur stabilité vis à vis de la racémisation étudiée (chapitre 5).

7.2 Résumé Chapitre 2

La réaction Balz-Schiemann continue d'être une méthode pertinente pour la synthèse des fluorures d'aryle en raison de sa simplicité de mise en œuvre (Schéma 7.1). Cependant,

la transformation reste limitée par les conditions de réaction dures, de faibles rendements et la nécessité d'isoler les intermédiaires potentiellement explosifs. Bien que plusieurs améliorations aient été apportées au fil des ans et que de multiples sources de fluor aient été étudiées, l'utilisation des organotrifluoroborates comme médiateurs de cette réaction s'est limitée à un seul rapport.

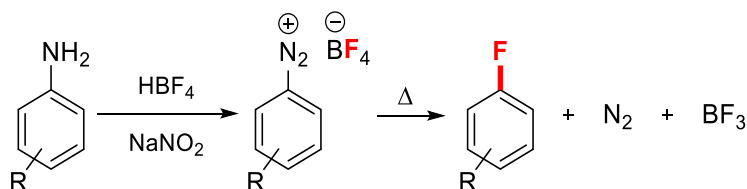


Schéma 7.1 La réaction Balz-Schiemann.

Afin de révéler le potentiel des organotrifluoroborates en tant que sources F^- , nous avons démontré qu'ils pouvaient médier la fluorodiazonation en solution avec des sels d'aryle diazonium préformés (Schéma 7.2).

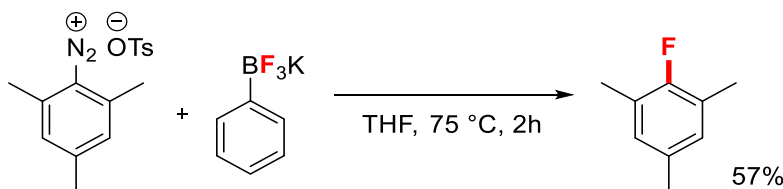
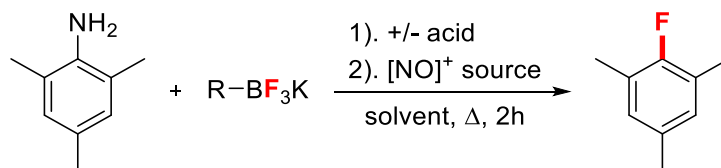


Schéma 7.2 Fluoruration du sel d'aryle diazonium avec du phényltrifluoroborate.

Cela a pu être étendu avec succès à un procédé en deux étapes évitant l'isolement des sels de diazonium potentiellement explosifs. Pour cela, plusieurs paramètres de réaction ont été étudiés.



- Effet de solvant

En général, les alcools protiques (MeOH et EtOH) donnent des rendements médiocres, très probablement en raison de la promotion de la décomposition radicalaire de l'aryle diazonium. Les solvants chlorés peuvent être utilisés mais conduisant à des rendements modérés. Les solvants non polaires à point d'ébullition élevé ont donné des rendements médiocres, en raison de l'insolubilité du réactif dans ces solvants. Le *t*-BuOH s'est révélé être le meilleur solvant de réaction (rendement de 55%).

- Effet de la source de $[\text{NO}]^+$, acide et des équivalents d'organotrifluoroborate

Trois sources $[\text{NO}]^+$ différentes ont été testées, le *t*-BuONO s'est avéré offrir les meilleurs rendements (55%). Un acide est requis pour que la réaction ait lieu. L'acide sulfurique, l'acide chlorhydrique et l'acide nitrique se sont avérés efficaces dans la réaction. Cependant, l'utilisation d'acide phosphorique a permis d'augmenter les rendements à 76% et les équivalents d'acide utilisés ont pu être abaissés à 0,5. L'augmentation du nombre d'équivalents d'organotrifluoroborate utilisé n'a pas amélioré les rendements de réaction.

- Effet de la température

Avec ces premiers paramètres de réaction optimisés, l'effet de la température sur les rendements de réaction a été étudié. Les températures de réaction peuvent être abaissées de 105-110 à 45-50 °C tout en maintenant des rendements de réaction similaires. Enfin, une légère amélioration des rendements a été observée lors de l'utilisation de solvant dégazé (81%).

- Effet de l'organotrifluoroborate

Plusieurs organotrifluoroborates ont été employés dans la réaction pour étudier l'effet du fragment organique sur l'efficacité de la réaction. Les organotrifluoroborates aromatiques enrichis et appauvris en électrons (par rapport au PhBF_3K) fonctionnaient cependant avec des rendements inférieurs. Les trifluoroborates d'alkyle ont également pu être utilisés, mais là encore avec des rendements inférieurs. Le phényltrifluoroborate de potassium s'est révélé fournir les meilleurs rendements.

Les conditions de réaction ont permis la fluoration de divers substrats d'aniline avec un rendement modéré à bon, et ont permis l'accès à des fluorobenzènes 2,6-disubstitués dont les sels de diazonium correspondants sont connus pour être instables (Schéma 7.3). Contrairement aux conditions classiques de la réaction de Balz-Schiemann qui exigent habituellement une décomposition sèche stricte, les conditions décrites utilisent un acide aqueux et peuvent tolérer la présence d'équivalents d'eau ajoutés sans diminution des rendements. Ce point apparaît particulièrement important du fait de la forte propension des ions fluorures à être hydratés, et semble indiquer une non implication des fluorures libres mais plus un transfert direct du fluorure depuis l'organotrifluoroborate. De plus, la faible température (45 °C) à laquelle se produit la décomposition du diazonium et la fluoration réussie est sans précédent dans les transformations de type Balz-Schieman (à l'exception de l'utilisation de réactifs HF) faisant de cette approche une voie d'accès douce aux fluorures d'aryle. Le schéma 7.3 illustre l'étendue de la méthode développée au cours de nos travaux.

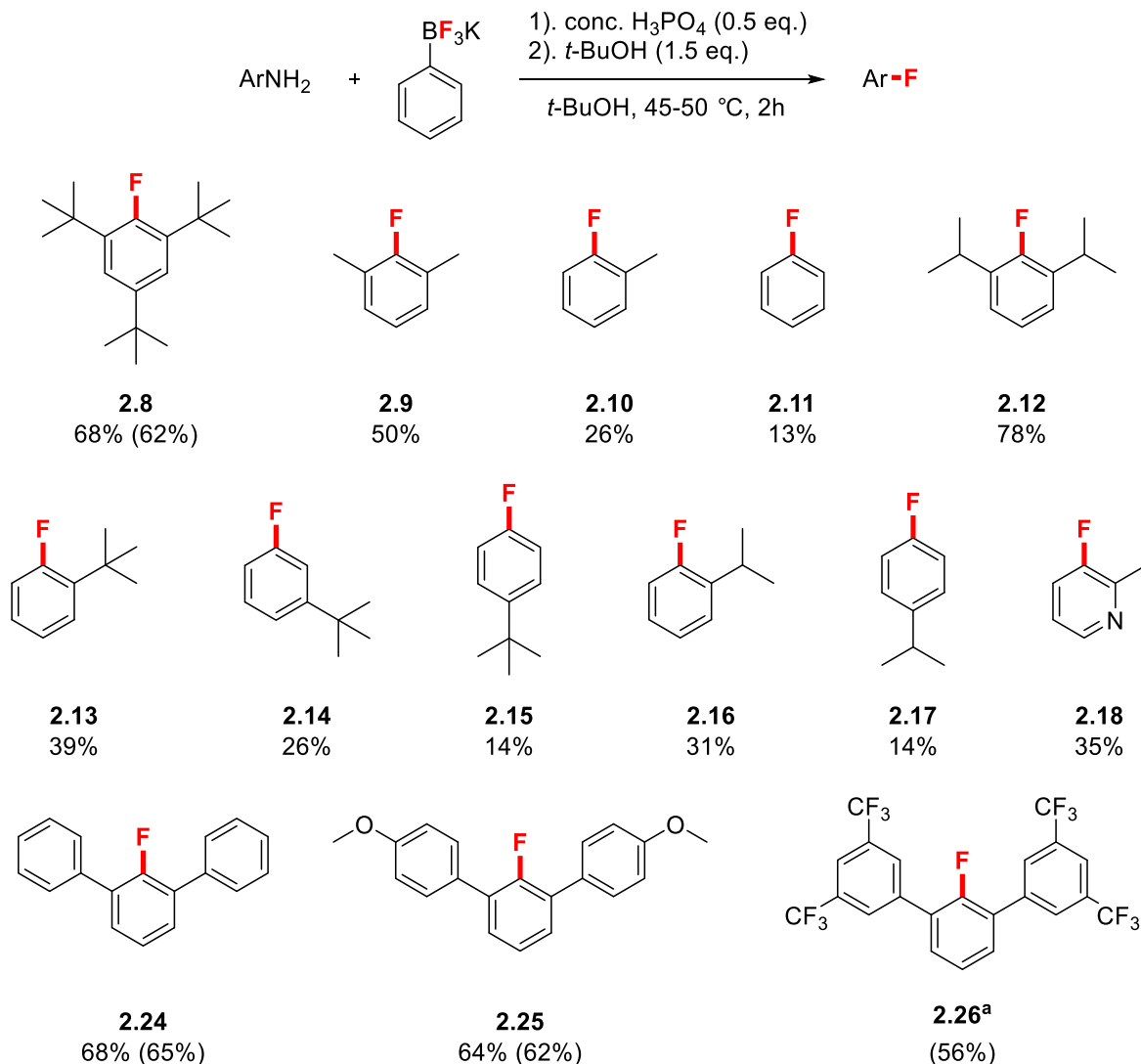


Schéma 7.3 Substrat de la réaction de Balz-Schiemann en un pot avec le phényltrifluoroborate de potassium. Conditions de réaction : aniline (0,25 mmol), 85% H₃PO₄ aq. (0,5 éq.), Phényltrifluoroborate de potassium (0,38 mmol), *t*-BuOH (1,3 ml) dans un flacon de pression avec capuchon doublé de téflon, purge Ar, puis *t*-BuONO (0,38 mmol), t.a. pendant 20 min, puis chauffé à 45-50 °C pendant 2h. Rendement déterminé par RMN ¹⁹F en utilisant le 2,4-dinitrofluorobenzène comme étalon interne. Rendement isolé entre parenthèses. ^a 98% H₂SO₄ utilisé comme acide dans du *t*-BuOH à 95 °C.

Enfin, les sources traditionnelles de fluorures comme BF₄⁻, et d'autres sources telles que TBAF, CsF et KF ne conduisent au plus qu'à des traces de fluorure d'aryle dans des conditions établies avec l'organotrifluoroborate, démontrant ainsi le rôle critique de ces réactifs dans l'expansion des réactions de Balz-Schiemann.

7.3 Résumé Chapitre 3

Dans le chapitre 2, nous avons décrit le développement d'une méthodologie pour une réaction de Balz-Schiemann en deux étapes en un pot avec des organotrifluoroborates. Compte tenu de la réactivité intéressante observée, nous avons été motivés pour élargir le profil de réaction de fluoration des organotrifluoroborates. Les sels de diaryliodonium ont présenté la classe de substrat logique suivante à étudier en tant qu'équivalents de cation aryle.

La fluoration des sels de diaryliodonium dissymétriques est un domaine de recherche croissant. Ces substrats ont trouvé de nombreuses applications en radiofluoration en raison de leur capacité à fournir des fluorures d'aryle riches et pauvres en électrons. La plupart des efforts ont été orientés vers l'exploration des mécanismes sous-jacents de la sélectivité et l'amélioration des conditions de réaction dans le contexte de la radiochimie du fluor. La fluoration des sels de diaryliodonium se limite principalement aux fluorures de métaux alcalins et, à notre connaissance, l'utilisation d'organotrifluoroborates pour la fluoration de sels de diaryliodonium est sans précédent.

Une série de phényltrifluoroborates de diaryliodonium dissymétriques ont été synthétisés et entièrement caractérisés. La synthèse de ces sels a commencé en utilisant un protocole modifié décrit par Olofsson *et al.* En utilisant cette méthodologie, sept sels de tétrafluoroborate de diaryliodonium dissymétriques ont pu être obtenus avec des rendements modérés à excellents (Schéma 7.4).

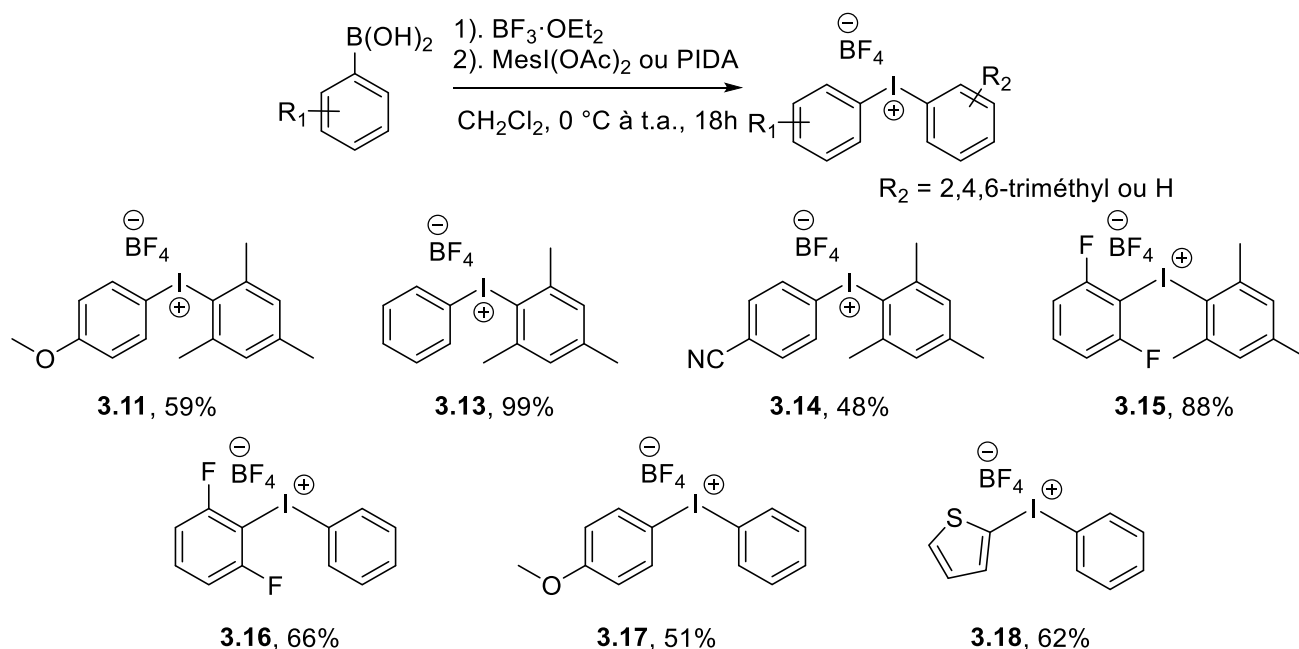


Schéma 7.4 Sels de tétrafluoroborate de diaryliodonium dissymétriques synthésisés.

L'utilisation du phényltrifluoroborate de potassium, dans MeCN, a permis un échange quantitatif d'anions mis en évidence par RMN ¹H, ¹⁹F et ¹¹B pour fournir les sels souhaités avec un rendement bon à excellent (Schéma 7.5).

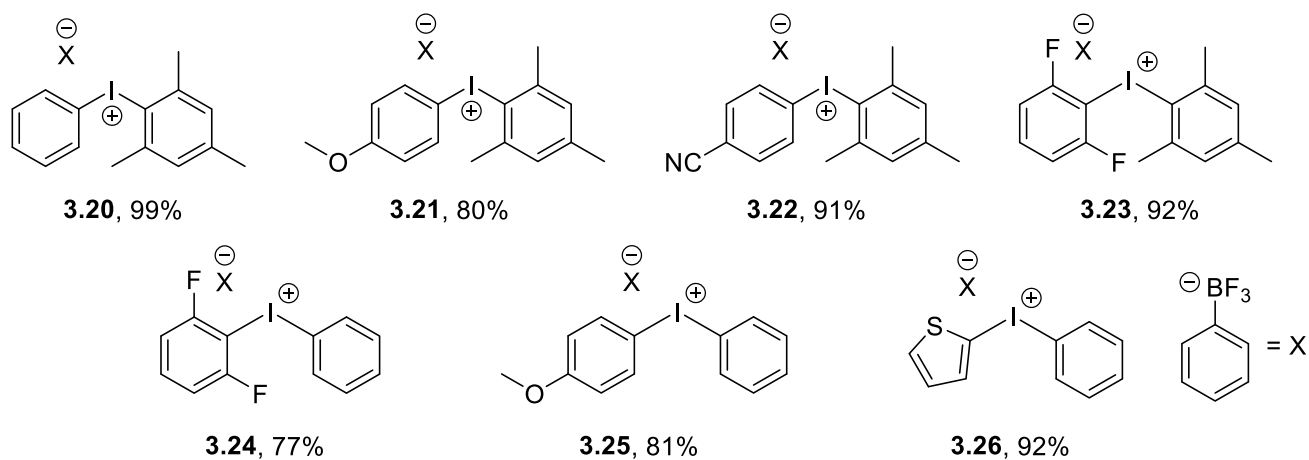
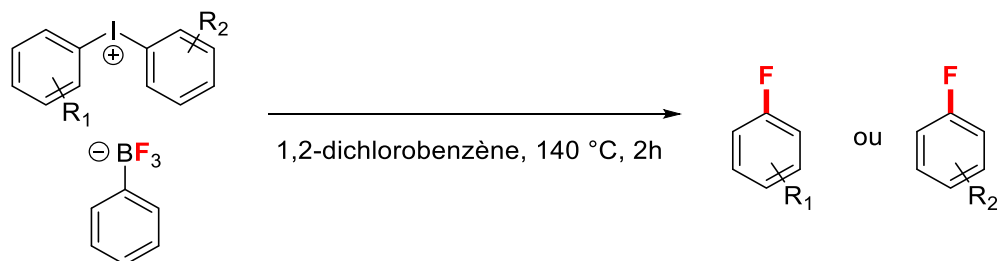


Schéma 7.5 Sels de phényltrifluoroborate de diaryliodonium dissymétriques synthésisés.

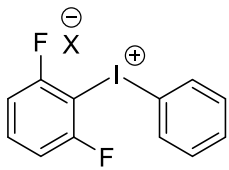
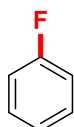
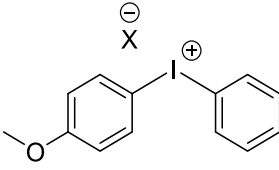
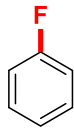
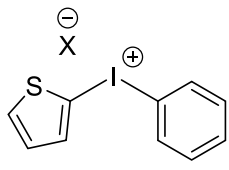
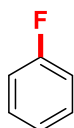
La décomposition de ces sels a été étudiée dans divers solvants et s'est avérée la plus efficace dans le 1,2-dichlorobenzène à 120 ° C. Tous les sels ont fourni un seul produit

fluoré en une sélectivité complète avec des rendements variant de faibles à excellents (Tableau 7.1).

Tableau 7.1 Distribution du produit à partir de la décomposition des sels 3.20-3.26.



Numéro	Composé	Distribution du produit (%) ^a
1	<p style="text-align: center;">3.20</p>	<p style="text-align: center;">22</p>
1	<p style="text-align: center;">3.21</p>	<p style="text-align: center;">16</p>
2	<p style="text-align: center;">3.22</p>	<p style="text-align: center;">62</p>
3	<p style="text-align: center;">3.23</p>	

4	 3.24	89 
5	 3.25	13 
6	 3.26	trace 

Conditions de réaction : précurseur (0,05 mmol), 1,2-dichlorobenzène (1,0 ml) dans un flacon de pression avec un capuchon doublé de téflon, chauffé à 140 °C pendant 2 heures, X = phényltrifluoroborate. ^a Rendements déterminés par RMN ¹⁹F en utilisant le 2,4-dinitrofluorobenzène comme étalon interne.

La sélectivité observée semble contraster avec celle observée dans la décomposition des fluorures de diaryliodonium ; les écarts expérimentaux suggèrent deux mécanismes différents. Ces études prouvent que les organotrifluoroborates peuvent être utilisés dans la fluoration des sels de diaryliodonium. Ces résultats préliminaires élargissent également le répertoire des organotrifluoroborates en tant que source de fluor nucléophile.

7.4 Résumé Chapitre 4

Dans notre effort d'élargir la gamme des méthodologies de transfert intramoléculaire de fluor, nous avons synthétisé une gamme de motifs contenant des organotrifluoroborates qui positionnent F⁻ près d'un centre électrophile. Nous avons identifié les

organotrifluoroborates comme candidats potentiels pour ce type de transformation, compte tenu de leur capacité avérée à transférer le fluor de façon intermoléculaire (voir les chapitres 2 et 3). Dans ce contexte, nous avons tenté de synthétiser quatre substrats différents contenant du trifluoroborate et d'enquêter ensuite sur la fluoration intramoléculaire (Schéma 7.6). Ces substrats seraient intéressants, car dans tous les cas, le C-B devrait être maintenu et permettre une fonctionnalisation ultérieure après la fluoration.

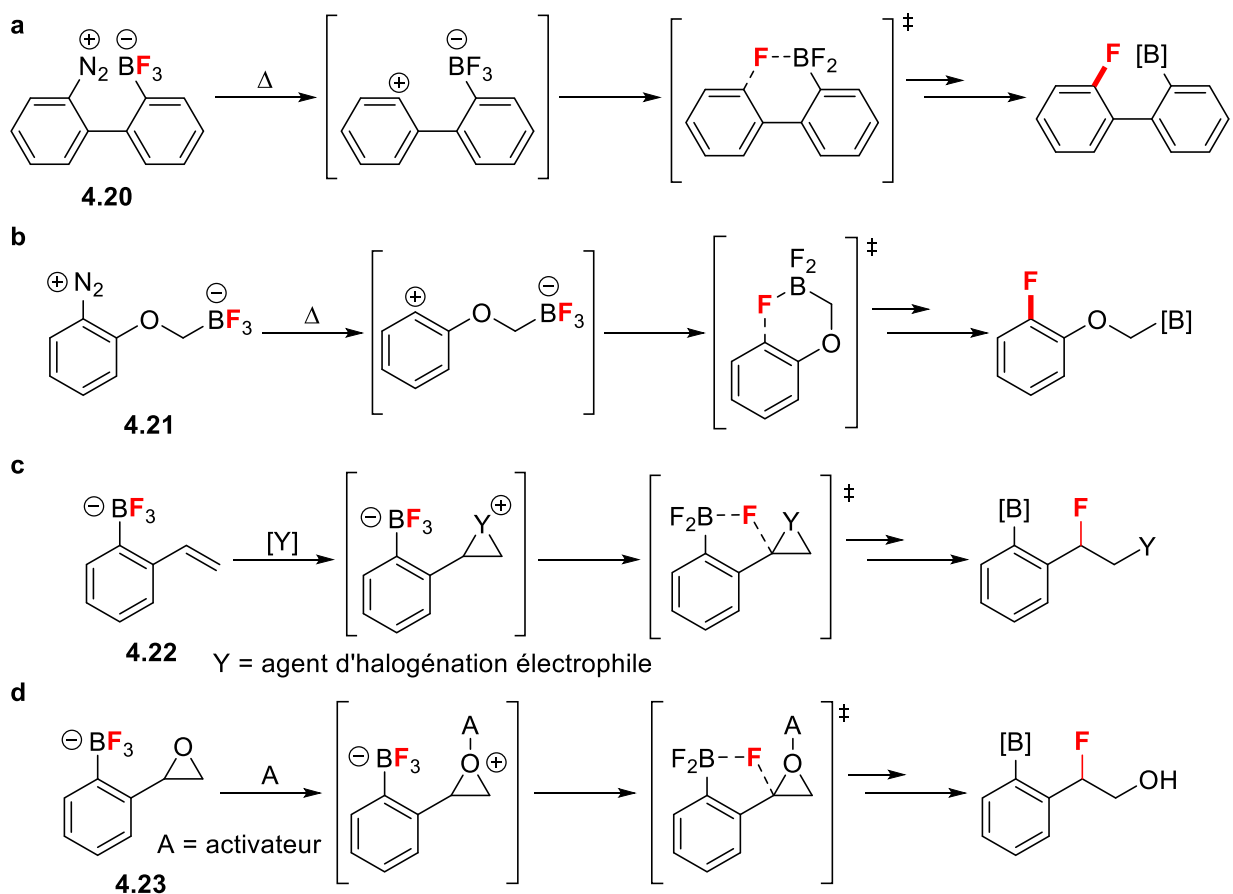


Schéma 7.6 Substrats proposés pour la fluoration intramoléculaire avec des trifluoroborates. [B] = BF_3^- , $\text{B}(\text{OR})_2^-$ (R = H, alkyle).

Malgré des efforts synthétiques conséquents, **4.20** n'a pas pu être obtenu en raison des difficultés d'accès à un système biphenyle borylé (voir section **4.2.1**). En raison des

contraintes de temps, nous n'avons pas poursuivi nos tentatives d'accéder de manière efficace à **4.20**. Cependant nous percevons un grand potentiel de **4.20** pour le transfert intramoléculaire de fluor et conservons des perspectives quant à l'optimisation de la synthèse **4.20**.

Nous avons pu synthétiser, isoler et caractériser le diazoniotrifluoroborate zwitterionique **4.21**. Ce substrat a été synthétisé par alkylation du 2-nitrophénol avec du bromométhyltrifluoroborate de potassium, suivi par la réduction du groupe nitro en amine. L'étape finale consistait en une diazotation et une précipitation du produit à basse température (Schéma 7.7).

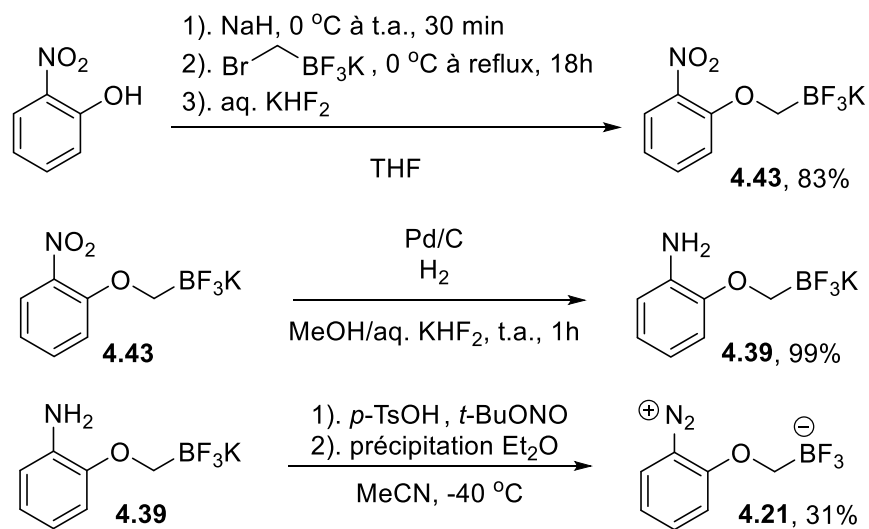


Schéma 7.7 Synthèse du diazoniotrifluoroborate **4.21**.

Cependant, fluoration de **4.21** n'a conduit qu'à l'observation de rendements en traces de fluorure d'aryle correspondant. Le substrat s'est révélé généralement stable à basse température (45 °C). A des températures plus élevées (≥ 100 °C), des traces de fluorure d'aryle correspondant ont pu être observées, accompagnées d'une dégradation significative du produit de départ.

Les dérivés de styrène **4.22** et **4.23** ont été facilement obtenus avec des rendements modérés à excellents, respectivement. La bromofluoruration efficace a échoué en utilisant **4.22** et diverses sources de brome électrophiles. Les principaux produits étaient des produits de polybromation et de deborylation, seules des traces de (2-bromo-1-fluoroéthyl)benzène ont été observés. De manière similaire, **4.23** ont échoué dans l'ouverture du cycle époxyde intramoléculaire par le fluor, la fluorohydrine désirée n'a été observée que dans un cas, alors que la majorité des conditions de réaction examinées ont conduit à la dégradation du produit de départ.

7.5 Résumé Chapitre 5

La maladie d'Alzheimer (MA), la principale cause de démence, est de plus en plus préoccupante dans une population mondiale vieillissante et en croissance rapide. À ce jour, aucun biomarqueur validé n'a été identifié pour le diagnostic de la MA. La preuve définitive n'est disponible que par des preuves histopathologiques à l'autopsie. Un domaine de recherche intense est le développement d'outils d'imagerie non invasifs pour la détection précoce des caractéristiques de la maladie. La plupart des stratégies se sont concentrées sur les traceurs d'imagerie TEP et fluorescence proche infrarouge (NIRF) ciblant le peptide amyloïde- β ($A\beta$). À ce jour, le développement d'outils d'imagerie bi-modale est resté quelque peu limité et présente un intérêt considérable. Les sondes d'imagerie bi-modales pour $A\beta$ présentent un intérêt compte tenu de leur potentiel de validation croisée des techniques d'imagerie et des informations complémentaires qu'elles peuvent fournir.

Alors que les sondes fluorescentes ont été couramment utilisées en biologie comme colorants sélectifs, la translation de ces sondes en applications *in vivo* a nécessité le

développement de sondes émettrices proches infrarouge (NIR). Les longueurs d'onde d'émission peuvent être déplacées vers le NIR en augmentant le degré de conjugaison π au sein de la structure moléculaire de la sonde. Une autre stratégie réussie implique la rigidification des échafaudages moléculaires par la complexation B-F₂, ce qui rend la structure entière de plus en plus plane et augmente l'étendue de la conjugaison π . Une rigidité structurelle accrue et une conjugaison π induisent généralement des profils d'absorption et d'émission nets, des rendements quantiques élevés et augmentent la durée de vie de la fluorescence. De plus, le complexe cyclique B-F₂ peut fonctionner comme un accepteur dans les architectures électroniques Donneur- π -Accepteur. Dans ce contexte, nous avons étudié la synthèse de divers nouveaux fluorophores B-F_n à base de motif benzothiazole.

Une série de 2-arylbzothiazoles et de 2,4-diarylbzothiazoles substitués ont été synthétisés en utilisant des couplages Suzuki-Miyaura. À partir de ces ligands, trois complexes B-F_n ont été isolés avec succès et complètement caractérisés par divers moyens spectroscopiques (Schéma 7.8).

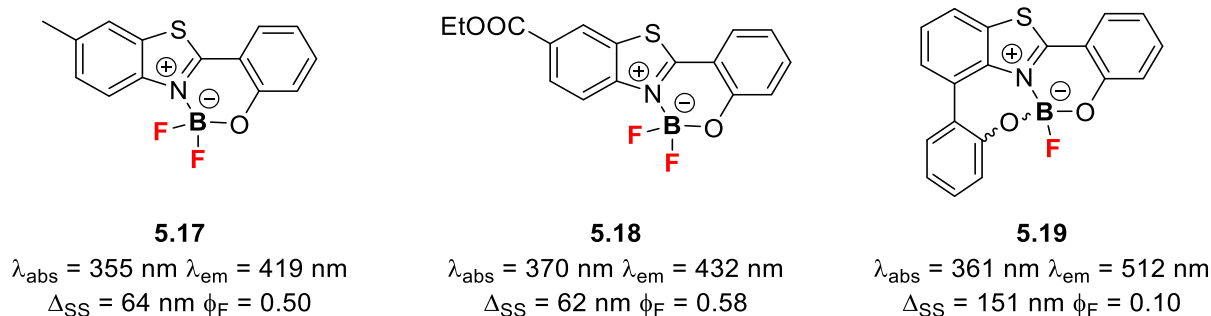
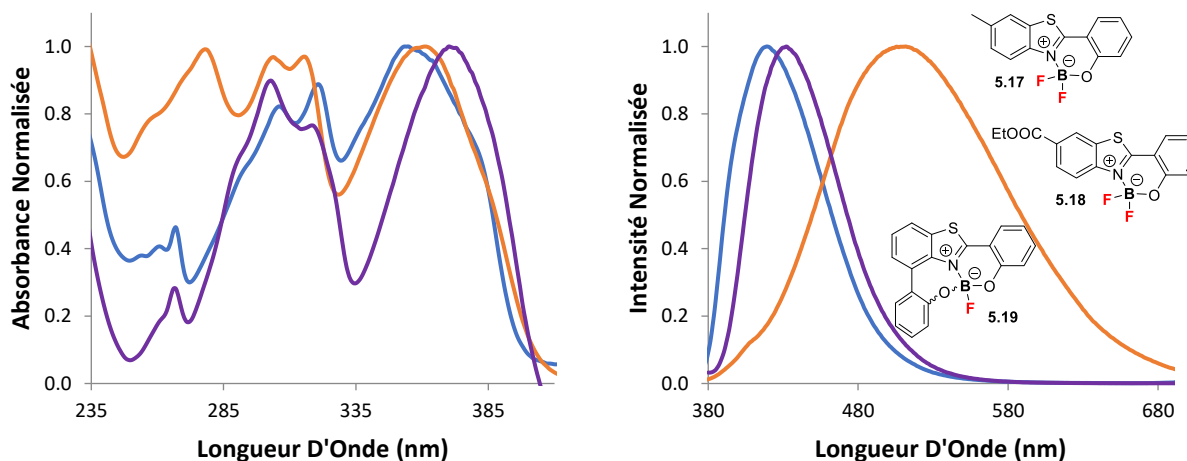


Schéma 7.8 Complexes B-F_n isolés et caractérisés.

Les propriétés photophysiques de ces complexes ont ensuite été étudiées (Figure 7.1).

Les complexes B-F₂ **5.17** et **5.18** ont présenté des propriétés d'absorption et d'émission

similaires à celles des complexes similaires précédemment rapportés, ils ont été caractérisés comme des émetteurs bleus puissants avec des déplacements de Stokes étroits. Le complexe **5.19** présentait des propriétés prometteuses et intéressantes et s'est avéré être un émetteur de lumière verte avec un décalage de Stokes significativement élevé (151 nm). Ce complexe s'est également avéré présenter un solvatochromisme positif dans les solvants polaires. Des calculs théoriques ont été effectués afin de soutenir et de mieux comprendre les propriétés photophysiques observées expérimentalement.



Le complexe **5.19** contient un centre de bore asymétrique et a été synthétisé sous la forme d'une paire d'énantiomères racémiques. Les énantiomères peuvent être résolus par HPLC chirale et caractérisés par un dichroïsme circulaire. Les énantiomères se sont révélés stables à la racémisation par inversion (Figure 7.2), même après avoir été chauffés à 50 °C dans du CHCl₃ pendant 3 heures.

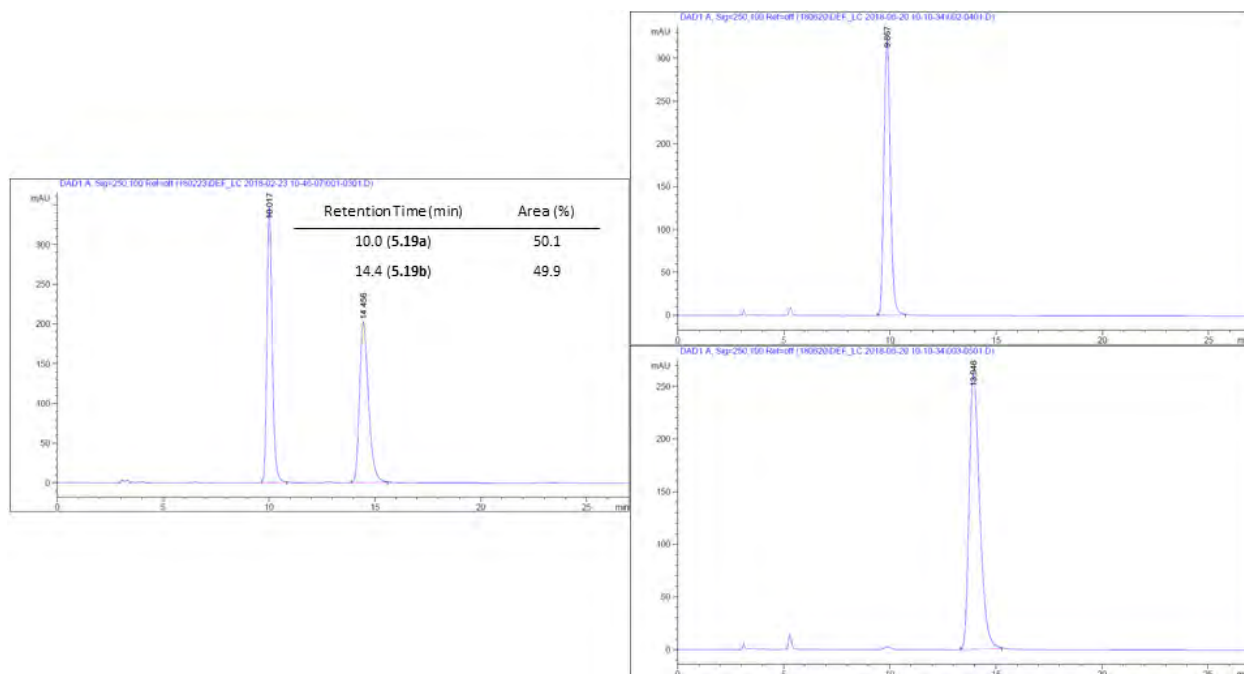


Figure 7.1 Chromatogramme HPLC de racémique **5.19** (à gauche), **5.19a** (à droite, en haut) et **5.19b** (à droite, en bas) après 1 semaine.

La stabilité des complexes **5.17-5.19** en présence d'eau a été étudiée. **5.18** s'est avéré se dégrader, par deborylation, en ligand de départ lors d'une exposition prolongée à l'humidité et aux conditions ambiantes. Le complexe **5.17** s'est révélé plus résistant, mais l'exposition à des équivalents d'eau a entraîné une dégradation rapide. Le complexe **5.19** s'est avéré le plus stable, avec une stabilité exceptionnelle sans dégradation de la solution $\text{CD}_3\text{CN} / \text{D}_2\text{O}$ jusqu'à 289 heures. De plus, une extraction de fluorure à partir de **5.19** a été démontrée (Schéma 7.9). Ces études mettent en évidence **5.19** en tant que candidat prometteur pour d'autres études et l'élaboration structurale en ce qui concerne le développement d'une sonde bi-modale.

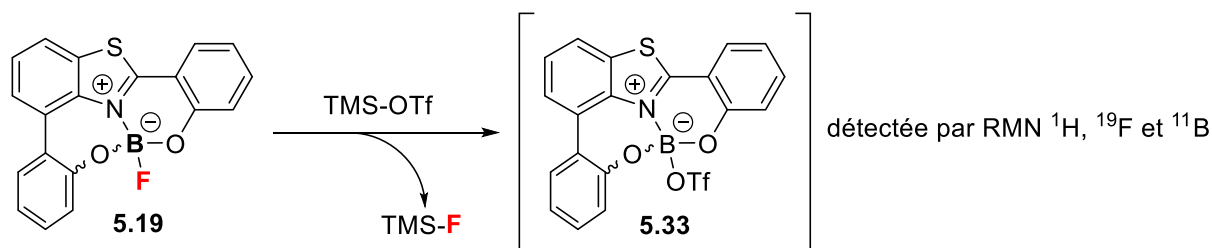


Schéma 7.9 Abstraction du fluorure de **5.19** à la forme **5.33**.

7.6 Conclusion

Les travaux présentés dans cette thèse ont principalement porté sur l'utilisation des liaisons B-F, en particulier des organotrifluoroborates, en tant que sources F^- dans la fluoration inter et intramoléculaire de divers substrats. Ces travaux ont également appliqué des liaisons B-F dans la synthèse de nouveaux fluorophores en tant qu'agents d'imagerie bimodale potentiels.

Le chapitre 2 décrit l'application des organotrifluoroborates comme source de F^- dans la fluorodediazotation des sels d'aryle diazonium. Les résultats préliminaires ont montré que les sels d'aryle diazonium pouvaient être fluorés en utilisant des sels d'organotrifluoroborates en solution. Cette méthodologie a ensuite été étendue à un protocole de diazotation / fluorodediazotation en deux étapes et un seul pot, en évitant l'isolement des sels d'aryle diazonium (Schéma **7.10**). Ce protocole permet la fluoration des anilines dans des conditions sans précédent, avec des rendements modérés à excellents. La transformation était particulièrement efficace pour les anilines fortement stériquement encombrées, les rendements diminuant lorsque l'encombrement stérique était diminué sur l'une ou les deux positions *ortho*.

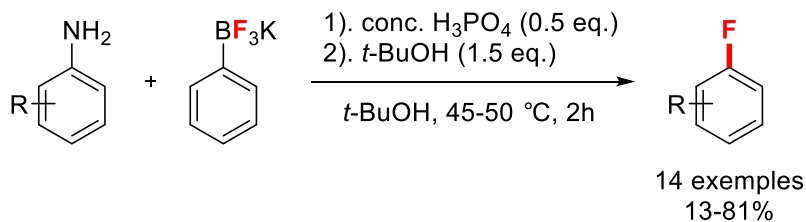


Schéma 7.10 Résumé de la réaction de Balz-Schiemann en deux étapes en un pot avec des organotrifluoroborates.

Le chapitre 3 présente les résultats préliminaires des recherches sur les organotrifluoroborates en tant que sources F⁻ dans la fluoration de sels de diaryliodonium dissymétriques. Les travaux ont principalement porté sur la synthèse, l'isolement et la caractérisation de sels de phényltrifluoroborate de diaryliodonium dissymétriques, qui n'ont pas été décrits précédemment (7 exemples). La fluoration de ces sels, en solution, a ensuite été étudiée (Schéma 7.11). Ces sels ont conduits à des fluorures d'aryles avec des rendements allant de faibles à excellent, et ce avec une sélectivité totale de l'introduction du fluor sur l'un des deux motifs aryles de l'iodonium. La sélectivité de la fluoration observée contrastait avec la distribution du produit prédite par le mécanisme accepté de fluoration asymétrique du sel de diaryliodonium avec F⁻, qui est sous le contrôle de Curtin-Hammett. Ces résultats suggèrent que la fluoration utilisant des organotrifluoroborates est soumise à un contrôle cinétique simple et que la fluoration résulte du transfert direct de F⁻ phényltrifluoroborate et non de la libération de F⁻ dans le milieu réactionnel.

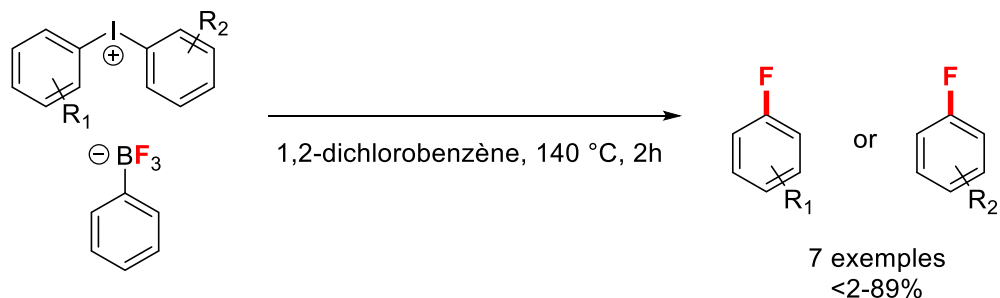
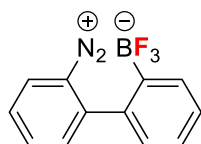
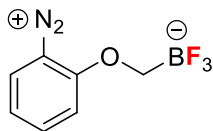


Schéma 7.11 Résumé de la réaction pour la thermolyse de sels de phényltrifluoroborate de diaryliodonium dissymétriques.

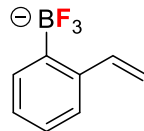
À la suite des résultats observés dans les chapitres 2 et 3 avec l'application de composés organotrifluoroborés en tant que sources de F^- pour la fluoration intermoléculaire, le chapitre 4 explore nos tentatives pour traduire cela en fluoration intramoléculaire. Quatre motifs moléculaires différents ont été identifiés et leur synthèse tentée (Schéma 7.12). Nous avons essayé de synthétiser **4.20**, cependant toutes les méthodes employées n'ont pas abouti à atteindre plus que des traces du précurseur de l'aniline. Le zwitterion **4.21** a été synthétisé et entièrement caractérisé, et la fluoration via une réaction intramoléculaire de type Balz-Schiemann a été étudiée ; le fluorure d'aryle correspondant ne peut être détecté qu'à l'état de traces. Le dérivé de styrène **4.22** a été synthétisé, entièrement caractérisé et étudié en ce qui concerne les réactions de bromofluoration en utilisant divers agents de bromation électrophiles ; seuls des rendements en trace du produit souhaité pouvaient être détectés. Le dérivé d'oxyde de styrène **4.23** a également été synthétisé et entièrement caractérisé, mais la fluoration par ouverture de cycle époxyde intramoléculaire n'a pu être détectée qu'à l'état de traces.



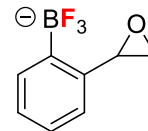
4.20



4.21



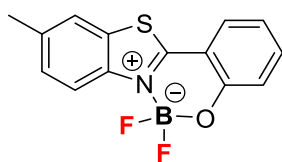
4.22



4.23

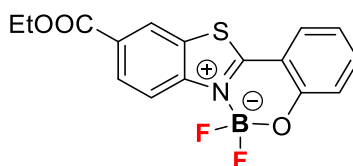
Schéma 7.12 Motifs moléculaires pour la fluoration intramoléculaire utilisant un groupement trifluoroborate.

Enfin, le chapitre 5 décrit la synthèse de nouveaux fluorophores, incorporant un complexe B-F_n, basé sur le motif benzothiazole. Une série de 2-arylbenzothiazoles et de 2,4-diarylbenzothiazoles diversement substitués a été synthétisée à partir de laquelle trois complexes B-F_n ont pu être isolés et complètement caractérisés (Schéma 7.13). Le complexe **5.19** s'est avéré avoir les propriétés photophysiques les plus prometteuses : émission proche du NIR et grand décalage de Stokes. La stabilité aqueuse de ces complexes a été étudiée, à partir de laquelle **5.19** est apparu comme le plus stable.



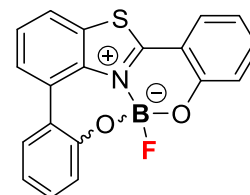
5.17

$\lambda_{\text{abs}} = 355 \text{ nm}$ $\lambda_{\text{em}} = 419 \text{ nm}$
 $\Delta_{\text{SS}} = 64 \text{ nm}$ $\phi_{\text{F}} = 0.50$



5.18

$\lambda_{\text{abs}} = 370 \text{ nm}$ $\lambda_{\text{em}} = 432 \text{ nm}$
 $\Delta_{\text{SS}} = 62 \text{ nm}$ $\phi_{\text{F}} = 0.58$



5.19

$\lambda_{\text{abs}} = 361 \text{ nm}$ $\lambda_{\text{em}} = 512 \text{ nm}$
 $\Delta_{\text{SS}} = 151 \text{ nm}$ $\phi_{\text{F}} = 0.10$

Schéma 7.13 Complexes B-F_n isolés et caractérisés.

De plus, **5.19** contenant un centre de bore asymétrique a été synthétisé sous forme d'un mélange racémique d'énantiomères, pouvant être dédoublé par HPLC chirale et les énantiomères caractérisés par spectroscopie CD ; les énantiomères se sont révélés stables à la racémisation par inversion. Finalement, abstraction de F⁻ de **5.19** a été démontrée, avec la formation de l'ion borénium correspondant (Schéma 7.14), mettant en évidence la possibilité d'effectuer un échange d'isotopes ¹⁹F-¹⁸F sur ce substrat.

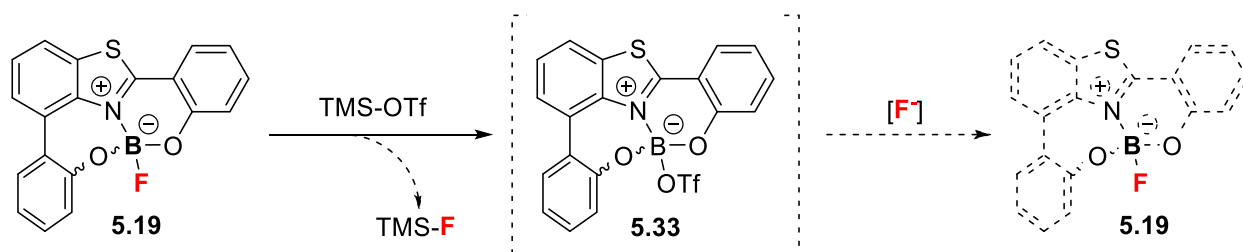


Schéma 7.14 Abstraction du fluorure de **5.19**.

References

- (1) Molander, G. A. *J. Org. Chem.* **2015**, *80* (16), 7837–7848.
- (2) Wade, C. R.; Broomsgrove, A. E. J.; Aldridge, S.; Gabbaï, F. P. *Chem. Rev.* **2010**, *110* (7), 3958–3984.
- (3) Cresswell, A. J.; Davies, S. G.; Roberts, P. M.; Thomson, J. E. *Chem. Rev.* **2015**, *115* (2), 566–611.
- (4) Perrin, D. M. *Acc. Chem. Res.* **2016**, *49* (7), 1333–1343.
- (5) Kowada, T.; Kikuchi, K.; Maeda, H.; Kikuchi, K. *Chem. Soc. Rev.* **2015**, *44* (14), 4953–4972.
- (6) Rowley, M.; Hallett, D. J.; Goodacre, S.; Moyes, C.; Crawforth, J.; Sparey, T. J.; Patel, S.; Marwood, R.; Patel, S.; Thomas, S.; Hitzel, L.; O'Connor, D.; Szeto, N.; Castro, J. L.; Hutson, P. H.; Macleod, A. M. *J. Med. Chem.* **2001**, *44* (10), 1603–1614.
- (7) Dollé, F.; Roeda, D.; Kuhnast, B.; Lasne, M. In *Fluorine and Health*; Elsevier, 2008; pp 3–65.
- (8) Swallow, S. *Prog. Med. Chem.* **2015**, *54* (2), 65–133.
- (9) Smart, B. E. *J. Fluor. Chem.* **2001**, *109* (1), 3–11.
- (10) Bott, G.; Field, L. D.; Sternhell, S. *J. Am. Chem. Soc.* **1980**, *102* (17), 5618–5626.
- (11) Rosenblum, S. B.; Huynh, T.; Afonso, A.; Davis, H. R.; Yumibe, N.; Clader, J. W.; Burnett, D. A. *J. Med. Chem.* **1998**, *41* (Sch 58235), 973–980.
- (12) Champagne, P. A.; Desroches, J.; Hamel, J.-D.; Vandamme, M.; Paquin, J.-F. *Chem. Rev.* **2015**, *115* (17), 9073–9174.
- (13) Wilkinson, J. A. *Chem. Rev.* **1992**, *92* (4), 505–519.
- (14) Czarnowski, J.; Castellano, E.; Schumacher, H. J. *Chem. Commun. (London)* **1968**, No. 20, 1255–1255.
- (15) Yang, J.-D.; Wang, Y.; Xue, X.-S.; Cheng, J.-P. *J. Org. Chem.* **2017**, *82* (8), 4129–4135.
- (16) Zhan, C.-G.; Dixon, D. A. *J. Phys. Chem. A* **2004**, *108* (11), 2020–2029.
- (17) Sun, H.; DiMagno, S. G. *J. Am. Chem. Soc.* **2005**, *127* (7), 2050–2051.
- (18) Sun, H.; DiMagno, S. G. *Chem. Commun.* **2007**, No. 5, 528–529.
- (19) Olah, G. A.; Shih, J. G.; Prakash, G. K. S. *J. Fluor. Chem.* **1986**, *33* (1–4), 377–396.
- (20) Olah, G. A.; Vankar, Y. D.; Nojima, M.; Kerekes, I.; Olah, J. A. *J. Org. Chem.* **1979**, *44* (22), 3872–3881.

- (21) Neumann, C. N.; Ritter, T. *Acc. Chem. Res.* **2017**, *50* (11), 2822–2833.
- (22) Ni, C.; Jiang, F.; Zeng, Y.; Hu, J. *J. Fluor. Chem.* **2015**, *179*, 3–13.
- (23) Balz, G.; Schiemann, G. *Berichte der Dtsch. Chem. Gesellschaft (A B Ser.)* **1927**, *60* (5), 1186–1190.
- (24) De Meio, G.; Morgan, J.; Pinhey, J. T. *Tetrahedron* **1993**, *49* (36), 8129–8138.
- (25) De Meio, G. V.; Pinhey, J. T. *J. Chem. Soc. Chem. Commun.* **1990**, *8* (15), 1065.
- (26) Saito, M.; Miyamoto, K.; Ochiai, M. *Chem. Commun.* **2011**, *47* (12), 3410.
- (27) Bloodworth, A. J.; Bowyer, K. J.; Mitchell, J. C. *Tetrahedron Lett.* **1987**, *28* (44), 5347–5350.
- (28) Kunz, H.; Sager, W. *Helv. Chim. Acta* **1985**, *68* (1), 283–287.
- (29) Faller, J. W.; Linebarrier, D. L. *Organometallics* **1990**, *9* (12), 3182–3184.
- (30) Launay, G. G.; Slawin, A. M. Z.; O'Hagan, D. *Beilstein J. Org. Chem.* **2010**, *6* (Scheme 1), 4–9.
- (31) Jaber, J. J.; Mitsui, K.; Rychnovsky, S. D. *J. Org. Chem.* **2001**, *66* (13), 4679–4686.
- (32) Yoshida, J. ichi; Ishichi, Y.; Isoe, S. *J. Am. Chem. Soc.* **1992**, *114* (19), 7594–7595.
- (33) Yadav, J. S.; Reddy, B. V. S.; Ramesh, K.; Kumar, G. G. K. S. N.; Grée, R. *Tetrahedron Lett.* **2010**, *51* (12), 1578–1581.
- (34) Yadav, J. S.; Subba Reddy, B. V.; Anusha, B.; Subba Reddy, U. V.; Bhadra Reddy, V. V. *Tetrahedron Lett.* **2010**, *51* (21), 2872–2874.
- (35) Zhao, H.; Leamer, L. A.; Gabbaï, F. P. *Dalton Trans.* **2013**, *42* (23), 8164–8178.
- (36) Kim, Y.; Gabbaï, F. P. *J. Am. Chem. Soc.* **2009**, *131* (9), 3363–3369.
- (37) Zhao, H.; Gabbaï, F. P. *Org. Lett.* **2011**, *13* (6), 1444–1446.
- (38) Perrio, C.; Schmitt, S.; Pla, D.; Gabbaï, F. P.; Chansaenpak, K.; Mestre-Voegtle, B.; Gras, E. *Chem. Commun.* **2017**, *53* (2), 340–343.
- (39) Bardin, V. V.; Frohn, H.-J. *J. Fluor. Chem.* **2013**, *156*, 333–338.
- (40) Petasis, N.; Yudin, A.; Zavialov, I.; Prakash, G.; Olah, G. *Synlett* **1997**, *1997* (5), 606–608.
- (41) Cazorla, C.; Métay, E.; Andrioletti, B.; Lemaire, M. *Tetrahedron Lett.* **2009**, *50* (27), 3936–3938.
- (42) Ye, Y.; Sanford, M. S. *J. Am. Chem. Soc.* **2013**, *135* (12), 4648–4651.
- (43) Ye, Y.; Schimler, S. D.; Hanley, P. S.; Sanford, M. S. *J. Am. Chem. Soc.* **2013**, *135* (44), 16292–16295.
- (44) Mazzotti, A. R.; Campbell, M. G.; Tang, P.; Murphy, J. M.; Ritter, T. *J. Am. Chem.*

- Soc. **2013**, 135 (38), 14012–14015.
- (45) Dubbaka, S. R.; Narreddula, V. R.; Gadde, S.; Mathew, T. *Tetrahedron* **2014**, 70 (51), 9676–9681.
- (46) Dubbaka, S.; Gadde, S.; Narreddula, V. *Synthesis (Stuttg)*. **2015**, 47 (06), 854–860.
- (47) Pysz, M. A.; Gambhir, S. S.; Willmann, J. K. *Clin. Radiol.* **2010**, 65 (7), 500–516.
- (48) Herschman, H. R. *Science (80-)*. **2003**, 302 (5645), 605–608.
- (49) Le Bars, D. *J. Fluor. Chem.* **2006**, 127 (11), 1488–1493.
- (50) Varagnolo, L.; Stokkel, M. P. M.; Mazzi, U.; Pauwels, E. K. J. *Nucl. Med. Biol.* **2000**, 27 (2), 103–112.
- (51) Hamacher, K.; Coenen, H. H.; Stöcklin, G. *J. Nucl. Med.* **1986**, 27 (2), 235–238.
- (52) Dammacco, F.; Rubini, G.; Ferrari, C.; Vacca, A.; Racanelli, V. *Clin. Exp. Med.* **2014**, 15 (1), 1–18.
- (53) Studenov, A. R.; Adam, M. J.; Wilson, J. S.; Ruth, T. J. *J. Label. Compd. Radiopharm.* **2005**, 48 (7), 497–500.
- (54) Vabre, B.; Chansaenpak, K.; Wang, M.; Wang, H.; Li, Z.; Gabbaï, F. P. *Chem. Commun.* **2017**, 53 (62), 8657–8659.
- (55) Litau, S.; Niedermoser, S.; Vogler, N.; Roscher, M.; Schirmacher, R.; Fricker, G.; Wängler, B.; Wängler, C. *Bioconjug. Chem.* **2015**, 26 (12), 2350–2359.
- (56) Niedermoser, S.; Chin, J.; Wangler, C.; Kostikov, A.; Bernard-Gauthier, V.; Vogler, N.; Soucy, J.-P.; McEwan, A. J.; Schirmacher, R.; Wangler, B. *J. Nucl. Med.* **2015**, 56 (7), 1100–1105.
- (57) Wängler, C.; Waser, B.; Alke, A.; Iovkova, L.; Buchholz, H. G.; Niedermoser, S.; Jurkschat, K.; Fottner, C.; Bartenstein, P.; Schirmacher, R.; Reubi, J. C.; Wester, H. J.; Wängler, B. *Bioconjug. Chem.* **2010**, 21 (12), 2289–2296.
- (58) Dialer, L. O.; Selivanova, S. V.; Müller, C. J.; Müller, A.; Stellfeld, T.; Graham, K.; Dinkelborg, L. M.; Krämer, S. D.; Schibli, R.; Reiher, M.; Ametamey, S. M. *J. Med. Chem.* **2013**, 56 (19), 7552–7563.
- (59) Scheinberg, D.; Strand, M.; Gansow, O. *Science (80-)*. **1982**, 215 (4539), 1511–1513.
- (60) D'Souza, C. A.; McBride, W. J.; Sharkey, R. M.; Todaro, L. J.; Goldenberg, D. M. *Bioconjug. Chem.* **2011**, 22 (9), 1793–1803.
- (61) Shetty, D.; Choi, S. Y.; Jeong, J. M.; Lee, J. Y.; Hoigebazar, L.; Lee, Y.-S.; Lee, D. S.; Chung, J.-K.; Lee, M. C.; Chung, Y. K. *Chem. Commun.* **2011**, 47 (34), 9732.
- (62) Bhalla, R.; Darby, C.; Levason, W.; Luthra, S. K.; McRobbie, G.; Reid, G.; Sanderson, G.; Zhang, W. *Chem. Sci.* **2014**, 5 (1), 381–391.

- (63) Bhalla, R.; Levason, W.; Luthra, S. K.; McRobbie, G.; Sanderson, G.; Reid, G. *Chem. - A Eur. J.* **2015**, *21* (12), 4688–4694.
- (64) Ting, R.; Adam, M. J.; Ruth, T. J.; Perrin, D. M. *J. Am. Chem. Soc.* **2005**, *127* (38), 13094–13095.
- (65) Ting, R.; Harwig, C. W.; Lo, J.; Li, Y.; Adam, M. J.; Ruth, T. J.; Perrin, D. M. *J. Org. Chem.* **2008**, *73* (12), 4662–4670.
- (66) Ting, R.; Harwig, C.; auf dem Keller, U.; McCormick, S.; Austin, P.; Overall, C. M.; Adam, M. J.; Ruth, T. J.; Perrin, D. M. *J. Am. Chem. Soc.* **2008**, *130* (36), 12045–12055.
- (67) Li, Y.; Ting, R.; Harwig, C. W.; Auf Dem Keller, U.; Bellac, C. L.; Lange, P. F.; Inkster, J. A. H.; Schaffer, P.; Adam, M. J.; Ruth, T. J.; Overall, C. M.; Perrin, D. M. *Medchemcomm* **2011**, *2* (10), 942–949.
- (68) auf dem Keller, U.; Bellac, C. L.; Li, Y.; Lou, Y.; Lange, P. F.; Ting, R.; Harwig, C.; Kappelhoff, R.; Dedhar, S.; Adam, M. J.; Ruth, T. J.; Benard, F.; Perrin, D. M.; Overall, C. M. *Cancer Res.* **2010**, *70* (19), 7562–7569.
- (69) Schirmacher, R.; Bradtmöller, G.; Schirmacher, E.; Thews, O.; Tillmanns, J.; Siessmeier, T.; Buchholz, H. G.; Bartenstein, P.; Wängler, B.; Niemeyer, C. M.; Jurkschat, K. *Angew. Chemie - Int. Ed.* **2006**, *45* (36), 6047–6050.
- (70) Liu, Z.; Li, Y.; Lozada, J.; Pan, J.; Lin, K.-S.; Schaffer, P.; Perrin, D. M. *J. Label. Compd. Radiopharm.* **2012**, *55* (14), 491–496.
- (71) Liu, Z.; Li, Y.; Lozada, J.; Wong, M. Q.; Greene, J.; Lin, K.-S.; Yapp, D.; Perrin, D. M. *Nucl. Med. Biol.* **2013**, *40* (6), 841–849.
- (72) Liu, Z.; Li, Y.; Lozada, J.; Schaffer, P.; Adam, M. J.; Ruth, T. J.; Perrin, D. M. *Angew. Chemie - Int. Ed.* **2013**, *52* (8), 2303–2307.
- (73) Li, Y.; Guo, J.; Tang, S.; Lang, L.; Chen, X.; Perrin, D. M. *Am. J. Nucl. Med. Mol. Imaging* **2013**, *3* (1), 44–56.
- (74) Li, Y.; Liu, Z.; Harwig, C. W.; Pourghiasian, M.; Lau, J.; Lin, K.-S.; Schaffer, P.; Benard, F.; Perrin, D. M. *Am. J. Nucl. Med. Mol. Imaging* **2013**, *3* (1), 57–70.
- (75) Wade, C. R.; Zhao, H.; Gabbaï, F. P. *Chem. Commun.* **2010**, *46* (34), 6380.
- (76) Lee, M. H.; Agou, T.; Kobayashi, J.; Kawashima, T.; Gabbaï, F. P. *Chem. Commun.* **2007**, No. 11, 1133–1135.
- (77) Chiu, C. W.; Gabbaï, F. P. *J. Am. Chem. Soc.* **2006**, *128* (44), 14248–14249.
- (78) Hudnall, T. W.; Gabbaï, F. P. *J. Am. Chem. Soc.* **2007**, *129* (39), 11978–11986.
- (79) Liu, Z.; Chao, D.; Li, Y.; Ting, R.; Oh, J.; Perrin, D. M. *Chem. - A Eur. J.* **2015**, *21* (10), 3924–3928.
- (80) Liu, Z.; Amouroux, G.; Zhang, Z.; Pan, J.; Hundal-Jabal, N.; Colpo, N.; Lau, J.; Perrin, D. M.; Bénard, F.; Lin, K.-S. *Mol. Pharm.* **2015**, *12* (3), 974–982.

- (81) Pourghiasian, M.; Liu, Z.; Pan, J.; Zhang, Z.; Colpo, N.; Lin, K. S.; Perrin, D. M.; Bénard, F. *Bioorganic Med. Chem.* **2015**, *23* (7), 1500–1506.
- (82) Liu, Z.; Pourghiasian, M.; Benard, F.; Pan, J.; Lin, K.-S.; Perrin, D. M. *J. Nucl. Med.* **2014**, *55* (9), 1499–1505.
- (83) Chansaenpak, K.; Wang, M.; Wu, Z.; Zaman, R.; Li, Z.; Gabbaï, F. P. *Chem. Commun.* **2015**, *51* (62), 12439–12442.
- (84) Chansaenpak, K.; Wang, M.; Wang, H.; Giglio, B. C.; Gabbaï, F. P.; Wu, Z.; Li, Z. *RSC Adv.* **2017**, *7* (29), 17748–17751.
- (85) Chansaenpak, K.; Wang, M.; Liu, S.; Wu, Z.; Yuan, H.; Conti, P. S.; Li, Z.; Gabbaï, F. P. *RSC Adv.* **2016**, *6* (28), 23126–23133.
- (86) Chansaenpak, K.; Vabre, B.; Gabbaï, F. P. *Chem. Soc. Rev.* **2016**, *45* (4), 954–971.
- (87) Hendricks, J. A.; Keliher, E. J.; Wan, D.; Hilderbrand, S. A.; Weissleder, R.; Mazitschek, R. *Angew. Chemie - Int. Ed.* **2012**, *51* (19), 4603–4606.
- (88) Liu, S.; Lin, T.-P.; Li, D.; Leamer, L.; Shan, H.; Li, Z.; Gabbaï, F. P.; Conti, P. S. *Theranostics* **2013**, *3* (3), 181–189.
- (89) Liu, S.; Li, D.; Zhang, Z.; Surya Prakash, G. K.; Conti, P. S.; Li, Z. *Chem. Commun.* **2014**, *50* (55), 7371.
- (90) Keliher, E. J.; Klubnick, J. a; Reiner, T.; Mazitschek, R.; Weissleder, R. *ChemMedChem* **2014**, 1368–1373.
- (91) Owens, E. A.; Henary, M.; El Fakhri, G.; Choi, H. S. *Acc. Chem. Res.* **2016**, *49* (9), 1731–1740.
- (92) Hilderbrand, S. A.; Weissleder, R. *Curr. Opin. Chem. Biol.* **2010**, *14* (1), 71–79.
- (93) Zhang, X.; Bloch, S.; Akers, W.; Achilefu, S. In *Current Protocols in Cytometry*; John Wiley & Sons, Inc.: Hoboken, NJ, USA, 2012; pp 1–20.
- (94) Fischer, G. W.; Silvay, G. *HSR Proc. Intensive Care Cardiovasc. Anesth.* **2010**, *2* (4), 249–256.
- (95) Lutzweiler, C.; Razansky, D. *Sensors* **2013**, *13* (6), 7345–7384.
- (96) Frath, D.; Massue, J.; Ulrich, G.; Ziessel, R. *Angew. Chemie - Int. Ed.* **2014**, *53* (9), 2290–2310.
- (97) Berezin, M. Y.; Akers, W. J.; Guo, K.; Fischer, G. M.; Daltrozzo, E.; Zumbusch, A.; Achilefu, S. *Biophys. J.* **2009**, *97* (9), L22–L24.
- (98) Fischer, G. M.; Jüngst, C.; Isomäki-Kron Dahl, M.; Gauss, D.; Möller, H. M.; Daltrozzo, E.; Zumbusch, A. *Chem. Commun.* **2010**, *46* (29), 5289–5291.
- (99) Ni, Y.; Wu, J. *Org. Biomol. Chem.* **2014**, *12* (23), 3774.

- (100) Ziesel, R.; Ulrich, G.; Harriman, A. *New J. Chem.* **2007**, 31 (4), 496.
- (101) Ulrich, G.; Ziesel, R.; Harriman, A. *Angew. Chemie - Int. Ed.* **2008**, 47 (7), 1184–1201.
- (102) Kowada, T.; Kikuta, J.; Kubo, A.; Ishii, M.; Maeda, H.; Mizukami, S.; Kikuchi, K. *J. Am. Chem. Soc.* **2011**, 133 (44), 17772–17776.
- (103) Rodríguez, G.; Nargoli, J.; López, A.; Moyna, G.; Álvarez, G.; Fernández, M.; Osorio-Martínez, C. A.; González, M.; Cerecetto, H. *RSC Adv.* **2017**, 7 (13), 7983–7989.
- (104) Grossi, M.; Morgunova, M.; Cheung, S.; Scholz, D.; Conroy, E.; Terrile, M.; Panarella, A.; Simpson, J. C.; Gallagher, W. M.; O’Shea, D. F. *Nat. Commun.* **2016**, 7.
- (105) Wu, D.; Cheung, S.; O’Sullivan, C. J.; Gao, Y.; Chen, Z. L.; O’Shea, D. F. *RSC Adv.* **2016**, 6 (90), 87373–87379.
- (106) Xiao, H.; Li, P.; Zhang, W.; Tang, B. *Chem. Sci.* **2016**, 7 (2), 1588–1593.
- (107) Frath, D.; Didier, P.; Mély, Y.; Massue, J.; Ulrich, G. *ChemPhotoChem* **2017**, 1 (4), 108–108.
- (108) Gillis, E. P.; Eastman, K. J.; Hill, M. D.; Donnelly, D. J.; Meanwell, N. a. *J. Med. Chem.* **2015**, 58 (21), 8315–8359.
- (109) Orsi, D. L.; Altman, R. A. *Chem. Commun.* **2017**, 53 (53), 7168–7181.
- (110) Zhou, Y.; Wang, J.; Gu, Z.; Wang, S.; Zhu, W.; Aceña, J. L.; Soloshonok, V. A.; Izawa, K.; Liu, H. *Chem. Rev.* **2016**, 116 (2), 422–518.
- (111) Fujiwara, T.; O’Hagan, D. *J. Fluor. Chem.* **2014**, 167, 16–29.
- (112) Grainger, D. W.; Stewart, C. W. 2001; pp 1–14.
- (113) Tressaud, A.; Haufe, G. *Fluorine and Health, Molecular Imaging, Biomedical Materials and Pharmaceuticals*; 2012.
- (114) Campbell, M. G.; Ritter, T. *Chem. Rev.* **2015**, 115 (2), 612–633.
- (115) Fulmer, G. R.; Miller, A. J. M.; Sherden, N. H.; Gottlieb, H. E.; Nudelman, A.; Stoltz, B. M.; Bercaw, J. E.; Goldberg, K. I. *Organometallics* **2010**, 29 (9), 2176–2179.
- (116) Sather, A. C.; Buchwald, S. L. *Acc. Chem. Res.* **2016**, 49 (10), 2146–2157.
- (117) Ichiishi, N.; Canty, A. J.; Yates, B. F.; Sanford, M. S. *Org. Lett.* **2013**, 15 (19), 5134–5137.
- (118) Lee, H.; Börgel, J.; Ritter, T. *Angew. Chemie - Int. Ed.* **2017**, 56 (24), 6966–6969.
- (119) Sather, A. C.; Lee, H. G.; De La Rosa, V. Y.; Yang, Y.; Müller, P.; Buchwald, S. L. *J. Am. Chem. Soc.* **2015**, 137 (41), 13433–13438.
- (120) Yu, Z.; Lv, Y.; Yu, C. *Org. Process Res. Dev.* **2012**, 16 (10), 1669–1672.

- (121) Abele, S.; Schmidt, G.; Fleming, M. J.; Steiner, H. *Org. Process Res. Dev.* **2014**, *18* (8), 993–1001.
- (122) Thibault, C.; L'Heureux, A.; Bhide, R. S.; Ruel, R. *Org. Lett.* **2003**, *5* (26), 5023–5025.
- (123) Kiryanov, A. A.; Seed, A. J.; Sampson, P. *Tetrahedron Lett.* **2001**, *42* (50), 8797–8800.
- (124) Fukuhara, T.; Yoneda, N.; Suzuki, A. *J. Fluor. Chem.* **1988**, *38* (3), 435–438.
- (125) Argentini, M.; Wiese, C.; Weinrecht, R. *J. Fluor. Chem.* **1994**, *68* (2), 141–144.
- (126) Søndergaard, K.; Kristensen, J. L.; Gillings, N.; Begtrup, M. *European J. Org. Chem.* **2005**, No. 20, 4428–4433.
- (127) Fukuhara, T.; Yoneda, N.; Takamura, K.; Suzuki, A. *J. Fluor. Chem.* **1991**, *51* (2), 299–304.
- (128) Ussing, B. R.; Singleton, D. A. *J. Am. Chem. Soc.* **2005**, *127* (9), 2888–2899.
- (129) Laali, K.; Szele, I.; Yoshida, K. *Helv. Chim. Acta* **1983**, *66* (6), 1710–1720.
- (130) Becker, H. G. O.; Israel, G. *J. für Prakt. Chemie* **1979**, *321* (4), 579–586.
- (131) Swain, C. G.; Rogers, R. J. *J. Am. Chem. Soc.* **1975**, *97* (4), 799–800.
- (132) Burri, P.; Loewenschuss, H.; Zollinger, H.; Zwolinski, G. K. *Helv. Chim. Acta* **1974**, *57* (2), 395–402.
- (133) Bergstrom, R. G.; Landells, R. G. M. M.; Wahl, G. H.; Zollinger, H. *J. Am. Chem. Soc.* **1976**, *98* (11), 3301–3305.
- (134) Laali, K.; Szele, I.; Zollinger, H. *Helv. Chim. Acta* **1983**, *66* (6), 1737–1747.
- (135) Nakazumi, H.; Kitao, T.; Zollinger, H. *J. Org. Chem.* **1987**, *52* (13), 2825–2830.
- (136) Swain, C. G.; Sheats, J. E.; Harbison, K. G. *J. Am. Chem. Soc.* **1975**, *97* (4), 783–790.
- (137) Szele, I.; Zollinger, H. *J. Am. Chem. Soc.* **1978**, *100* (9), 2811–2815.
- (138) Fernández-Alonso, A.; Bravo-Díaz, C. *Org. Biomol. Chem.* **2008**, *6* (21), 4004.
- (139) Roe, A. In *Organic Reactions*; John Wiley & Sons, Inc.: Hoboken, NJ, USA, 2011; pp 193–228.
- (140) Langlois, B. In *Houben-Weyl Methods in Organic Chemistry, Volume E10 - Organofluorine Compounds*; Baasner, B., Hagemann, H., Tatlow, J. C., Eds.; Thieme Medical Publishers Inc., 2000; pp 686–740.
- (141) Myhre, P. C.; Edmonds, J. W.; Kruger, J. D. *J. Am. Chem. Soc.* **1966**, *88* (11), 2459–2466.
- (142) Döbele, M.; Vanderheiden, S.; Jung, N.; Bräse, S. *Angew. Chemie - Int. Ed.* **2010**,

- 49 (34), 5986–5988.
- (143) Laali, K. K.; Gettewert, V. J. *J. Fluor. Chem.* **2001**, *107* (1), 31–34.
- (144) Yu, Z.; Lv, Y.; Yu, C.; Su, W. *Tetrahedron Lett.* **2013**, *54* (10), 1261–1263.
- (145) Park, N. H.; Senter, T. J.; Buchwald, S. L. *Angew. Chemie - Int. Ed.* **2016**, *55* (39), 11907–11911.
- (146) Milner, D. J. *Synth. Commun.* **1992**, *22* (1), 73–82.
- (147) Sasaki, K.; Oishi, M.; Imaki, N. *J. Fluor. Chem.* **1996**, *76* (1), 59–62.
- (148) Rutherford, K. G.; Redmond, W.; Rigamonti, J. *J. Org. Chem.* **1961**, *26* (12), 5149–5152.
- (149) Cheek, P. H.; Wiley, R. H.; Roe, A. *J. Am. Chem. Soc.* **1949**, *71* (5), 1863–1863.
- (150) Tamura, M.; Shibakami, M.; Sekiya, A. *European J. Org. Chem.* **1998**, *1998* (4), 725–727.
- (151) Sellers, C.; Suschitzky, H. *J. Chem. Soc. C Org.* **1968**, 2317.
- (152) Filimonov, V. D.; Trusova, M.; Postnikov, P.; Krasnokutskaya, E. a.; Lee, Y. M.; Hwang, H. Y.; Kim, H.; Chi, K. W. *Org. Lett.* **2008**, *10* (18), 3961–3964.
- (153) Zollinger, H. *Angew. Chemie Int. Ed. English* **1978**, *17* (3), 141–150.
- (154) Park, N. H. Development of New Transition Metal Catalysts for C-N Bond Formation and Continuous Flow Processes for C-F Bond Formation, 2015.
- (155) Garel, L.; Saint-Jalmes, L. *Tetrahedron Lett.* **2006**, *47* (32), 5705–5708.
- (156) Broxton, T. J.; Bunnett, J. F.; Paik, C. H. *J. Chem. Soc. D Chem. Commun.* **1970**, No. 20, 1363.
- (157) Bélanger, P. C.; Lau, C. K.; Williams, H. W. R.; Dufresne, C.; Scheigetz, J. *Can. J. Chem.* **1988**, *66* (6), 1479–1482.
- (158) Szele, I.; Zollinger, H. *Helv. Chim. Acta* **1978**, *61* (5), 1721–1729.
- (159) Fujimoto, T.; Becker, F.; Ritter, T. *Org. Process Res. Dev.* **2014**, *18* (8), 1041–1044.
- (160) Maskill, H.; McCrudden, K. *Croat. Chem. Acta* **1992**, *65* (3), 567–574.
- (161) Zhang, L.; Meng, T.; Wu, J. *J. Org. Chem.* **2007**, *72* (24), 9346–9349.
- (162) Molander, G. A.; Trice, S. L. J.; Dreher, S. D. *J. Am. Chem. Soc.* **2010**, *132* (50), 17701–17703.
- (163) Li, W.; Nelson, D. P.; Jensen, M. S.; Hoerrner, R. S.; Cai, D.; Larsen, R. D.; Reider, P. J. *J. Org. Chem.* **2002**, *67* (15), 5394–5397.
- (164) Molander, G. A.; Fumagalli, T. *J. Org. Chem.* **2006**, *71* (15), 5743–5747.
- (165) Oliveira, R. A.; Silva, R. O.; Molander, G. A.; Menezes, P. H. *Magn. Reson. Chem.*

- 2009**, 47 (10), 873–878.
- (166) Cazorla, C.; De Vries, T. S.; Vedejs, E. *Org. Lett.* **2013**, 15 (5), 984–987.
- (167) Lennox, A. J. J.; Lloyd-Jones, G. C. *Angew. Chemie - Int. Ed.* **2012**, 51 (37), 9385–9388.
- (168) Moldoveanu, C.; Wilson, D. A.; Wilson, C. J.; Leowanawat, P.; Resmerita, A.-M.; Liu, C.; Rosen, B. M.; Percec, V. *J. Org. Chem.* **2010**, 75 (16), 5438–5452.
- (169) Stones, D.; Manku, S.; Lu, X.; Hall, D. G. *Chem. - A Eur. J.* **2004**, 10 (1), 92–100.
- (170) Cromwell, O. R.; Chung, J.; Guan, Z. *J. Am. Chem. Soc.* **2015**, 137 (20), 6492–6495.
- (171) Pasceri, R.; Siegel, D.; Ross, D.; Moody, C. J. *J. Med. Chem.* **2013**, 56 (8), 3310–3317.
- (172) Hoshino, Y.; Okuno, M.; Kawamura, E.; Honda, K.; Inoue, S. *Chem. Commun.* **2009**, No. 17, 2281.
- (173) Laali, K. K.; Okazaki, T.; Bunge, S. D. *J. Org. Chem.* **2007**, 72 (18), 6758–6762.
- (174) Vints, I.; Gateno, J.; Rozen, S. *J. Org. Chem.* **2013**, 78 (23), 11794–11797.
- (175) Purrington, S. T.; Woodard, D. L.; Cale, N. C. *J. Fluor. Chem.* **1990**, 48 (3), 345–352.
- (176) Lohre, C.; Dröge, T.; Wang, C.; Glorius, F. *Chem. - A Eur. J.* **2011**, 17 (22), 6052–6055.
- (177) Milner, P. J.; Kinzel, T.; Zhang, Y.; Buchwald, S. L. *J. Am. Chem. Soc.* **2014**, 136 (44), 15757–15766.
- (178) Timperley, C. M.; Banks, R. E.; Young, I. M.; Haszeldine, R. N. *J. Fluor. Chem.* **2011**, 132 (8), 541–547.
- (179) Yoshimura, A.; Zhdankin, V. V. *Chem. Rev.* **2016**, 116 (5), 3328–3435.
- (180) Stuart, D. R. *Chem. - A Eur. J.* **2017**, 23 (63), 15852–15863.
- (181) Merritt, E. A.; Olofsson, B. *Angew. Chemie - Int. Ed.* **2009**, 48 (48), 9052–9070.
- (182) Pinto de Magalhães, H.; Lüthi, H. P.; Togni, A. *Org. Lett.* **2012**, 14 (15), 3830–3833.
- (183) Yusubov, M. S.; Svitich, D. Y.; Larkina, M. S.; Zhdankin, V. V. *Arkivoc* **2013**, 2013 (1), 364–395.
- (184) Martín-Santamaría, S.; Carroll, M. A.; Carroll, C. M.; Carter, C. D.; Pike, V. W.; Rzepa, H. S.; Widdowson, D. A. *Chem. Commun.* **2000**, No. 8, 649–650.
- (185) Olofsson, B. In *Hypervalent Iodine Chemistry*; Wirth, T., Ed.; Springer International Publishing: Cham, 2016; Vol. 373, pp 135–166.
- (186) Schoenewaldt, E. F.; Hazen, G. G.; Shuman, R. F. Biphenyl Containing Diazonium

- Fluoride Compounds. US3660372A, 1972.
- (187) Der Puy, M. Van. *J. Fluor. Chem.* **1982**, 21 (3), 385–392.
- (188) Grushin, V. V.; Kantor, M. M.; Tolstaya, T. P.; Shcherbina, T. M. *Bull. Acad. Sci. USSR Div. Chem. Sci.* **1984**, 33 (10), 2130–2135.
- (189) Pike, V. W.; Aigbirhio, F. I. *J. Chem. Soc., Chem. Commun.* **1995**, No. 21, 2215–2216.
- (190) Shah, A.; Pike, V. W.; Widdowson, D. a. *J. Chem. Soc. Perkin Trans. 1* **1998**, 1 (13), 2043–2046.
- (191) Ross, T. L.; Ermert, J.; Hocke, C.; Coenen, H. H. *J. Am. Chem. Soc.* **2007**, 129 (25), 8018–8025.
- (192) Chun, J.-H.; Lu, S.; Pike, V. W. *European J. Org. Chem.* **2011**, 2011 (23), 4439–4447.
- (193) Graskemper, J. W.; Wang, B.; Qin, L.; Neumann, K. D.; DiMagno, S. G. *Org. Lett.* **2011**, 13 (12), 3158–3161.
- (194) Linstad, E. J.; Vāvere, A. L.; Hu, B.; Kempinger, J. J.; Snyder, S. E.; DiMagno, S. G. *Org. Biomol. Chem.* **2017**, 15 (10), 2246–2252.
- (195) Saccomanni, G.; Pascali, G.; Carlo, S. Del; Panetta, D.; De Simone, M.; Bertini, S.; Burchielli, S.; Digiacomo, M.; Macchia, M.; Manera, C.; Salvadori, P. A. *Bioorganic Med. Chem. Lett.* **2015**, 25 (12), 2532–2535.
- (196) Wang, B.; Qin, L.; Neumann, K. D.; Uppaluri, S.; Cerny, R. L.; DiMagno, S. G. *Org. Lett.* **2010**, 12 (15), 3352–3355.
- (197) Wang, B.; Cerny, R. L.; Uppaluri, S.; Kempinger, J. J.; DiMagno, S. G. *J. Fluor. Chem.* **2010**, 131 (11), 1113–1121.
- (198) Wadsworth, H. J.; Widdowson, D. A.; Wilson, E.; Carroll, M. A. Radical Trap In Fluoridation Of Iodonium Salt. WO2005061415 A1, 2005.
- (199) Edwards, R.; de Vries, W.; Westwell, A. D.; Daniels, S.; Wirth, T. *European J. Org. Chem.* **2015**, 2015 (31), 6909–6916.
- (200) Ichiishi, N.; Brooks, A. F.; Topczewski, J. J.; Rodnick, M. E.; Sanford, M. S.; Scott, P. J. H. *Org. Lett.* **2014**, 16 (12), 3224–3227.
- (201) McCammant, M. S.; Thompson, S.; Brooks, A. F.; Krska, S. W.; Scott, P. J. H.; Sanford, M. S. *Org. Lett.* **2017**, 19 (14), 3939–3942.
- (202) Kang, S. K.; Lee, H. W.; Jang, S. B.; Ho, P. S. *J. Org. Chem.* **1996**, 61 (14), 4720–4724.
- (203) Xia, M.; Chen, Z.-C. C. *Synth. Commun.* **1999**, 29 (14), 2457–2465.
- (204) Robidas, R.; Guérin, V.; Provençal, L.; Echeverria, M.; Legault, C. Y. *Org. Lett.* **2017**, acs.orglett.7b03307.

- (205) Bielawski, M.; Aili, D.; Olofsson, B. *J. Org. Chem.* **2008**, *73* (12), 4602–4607.
- (206) Bielawski, M.; Olofsson, B. *Chem. Commun.* **2007**, *2* (24), 2521.
- (207) Seidl, T. L.; Sundalam, S. K.; McCullough, B.; Stuart, D. R. *J. Org. Chem.* **2016**, *81* (5), 1998–2009.
- (208) Merritt, E.; Malmgren, J.; Klinke, F.; Olofsson, B. *Synlett* **2009**, *2009* (14), 2277–2280.
- (209) Groom, C. R.; Bruno, I. J.; Lightfoot, M. P.; Ward, S. C. *Acta Crystallogr. Sect. B Struct. Sci. Cryst. Eng. Mater.* **2016**, *72* (2), 171–179.
- (210) Tredwell, M.; Gouverneur, V. *Angew. Chemie - Int. Ed.* **2012**, *51* (46), 11426–11437.
- (211) Carroll, M. A.; Nairne, J.; Smith, G.; Widdowson, D. A. *J. Fluor. Chem.* **2007**, *128* (2), 127–132.
- (212) Chun, J.-H.; Lu, S.; Lee, Y.-S.; Pike, V. W. *J. Org. Chem.* **2010**, *75* (10), 3332–3338.
- (213) Mo, F.; Yan, J. M.; Qiu, D.; Li, F.; Zhang, Y.; Wang, J. *Angew. Chemie - Int. Ed.* **2010**, *49* (11), 2028–2032.
- (214) Cresswell, A. J.; Lloyd-Jones, G. C. *Chem. - A Eur. J.* **2016**, *22* (36), 12641–12645.
- (215) Ang, H. G.; Syn, Y. C. In *Polymer*, 1974; Vol. M, pp 1–64.
- (216) Parker, R. E.; Isaacs, N. S. *Chem. Rev.* **1959**, *59* (4), 737–799.
- (217) Dobrynin, A. A.; Akhrem, Aiexsander, M. M.; N, V.; Akhrem, A. A.; Moiseenkov, A. M.; Dobrynin, V. N. *Russ. Chem. Rev.* **1968**, *37* (6), 448.
- (218) Sugihara, Y.; Iimura, S.; Nakayama, J. *Chem. Commun.* **2002**, *2* (2), 134–135.
- (219) House, H. O. *J. Am. Chem. Soc.* **1956**, *78* (10), 2298–2302.
- (220) Weber, F. G.; Giese, H.; Köppel, H.; Reinhold, M.; Strobel, R.; Radeaglia, R.; Storek, W. *J. für Prakt. Chemie* **1985**, *327* (1), 133–143.
- (221) Cresswell, A. J.; Davies, S. G.; Lee, J. A.; Roberts, P. M.; Russell, A. J.; Thomson, J. E.; Tyte, M. J. *Org. Lett.* **2010**, *12* (13), 2936–2939.
- (222) Neumann, C. N.; Hooker, J. M.; Ritter, T. *Nature* **2016**, *534* (7607), 369–373.
- (223) Ferraris, D.; Cox, C.; Anand, R.; Lectka, T. *J. Am. Chem. Soc.* **1997**, *119* (18), 4319–4320.
- (224) Heasley, G. E.; Mark Janes, J.; Stark, S. R.; Robinson, B. L.; Heasley, V. L.; Shellhamer, D. F. *Tetrahedron Lett.* **1985**, *26* (15), 1811–1814.
- (225) Heasley, V. L.; Shellhamer, D. F.; Gipe, R. K.; Wiese, H. C.; Oakes, M. L.; Heasley, G. E. *Tetrahedron Lett.* **1980**, *21* (43), 4133–4136.

- (226) Barluenga, J.; Campos, P. J.; González, J. M.; Suárez, J. L.; Asensio, G. *J. Org. Chem.* **1991**, *56* (6), 2234–2237.
- (227) Heasley, V. L.; Gipe, R. K.; Martin, J. L.; Wiese, H. C.; Oakes, M. L.; Shellhamer, D. F.; Heasley, G. E.; Robinson, B. L. *J. Org. Chem.* **1983**, *48* (19), 3195–3199.
- (228) Evans, R. D.; Schauble, J. H. *Synthesis (Stuttg)*. **1987**, *1987* (06), 551–554.
- (229) Jiang, Q.; Duan-Mu, D.; Zhong, W.; Chen, H.; Yan, H. *Chem. - A Eur. J.* **2013**, *19* (6), 1903–1907.
- (230) Mfuh, A. M.; Doyle, J. D.; Chhetri, B.; Arman, H. D.; Larionov, O. V. *J. Am. Chem. Soc.* **2016**, *138* (9), 2985–2988.
- (231) Gillis, E. P.; Burke, M. D. *J. Am. Chem. Soc.* **2007**, *129* (21), 6716–6717.
- (232) Fyfe, J. W. B.; Seath, C. P.; Watson, A. J. B. *Angew. Chemie - Int. Ed.* **2014**, *53* (45), 12077–12080.
- (233) Fyfe, J. W. B.; Valverde, E.; Seath, C. P.; Kennedy, A. R.; Redmond, J. M.; Anderson, N. A.; Watson, A. J. B. *Chem. - A Eur. J.* **2015**, *21* (24), 8951–8964.
- (234) Muir, C. W.; Vantourout, J. C.; Isidro-Llobet, A.; Macdonald, S. J. F.; Watson, A. J. B. *Org. Lett.* **2015**, *17* (24), 6030–6033.
- (235) Molloy, J. J.; Law, R. P.; Fyfe, J. W. B.; Seath, C. P.; Hirst, D. J.; Watson, A. J. B. *Org. Biomol. Chem.* **2015**, *13* (10), 3093–3102.
- (236) Molander, G. A.; Ham, J. *Org. Lett.* **2006**, *8* (10), 2031–2034.
- (237) Wang, R.; Xu, J. *Arkivoc* **2010**, *2010* (9), 293–299.
- (238) Doyle, M. P.; Terpstra, J. W.; Pickering, R. A.; LePoire, D. M. *J. Org. Chem.* **1983**, *48* (20), 3379–3382.
- (239) Whetsel, K. B.; Hawkins, G. F.; Johnson, F. E. *J. Am. Chem. Soc.* **1956**, *78* (14), 3360–3363.
- (240) Singh, S.; DesMarteau, D. D.; Zuberi, S. S.; Witz, M.; Huang, H. N. *J. Am. Chem. Soc.* **1987**, *109* (23), 7194–7196.
- (241) Stavber, S.; Zupan, M. *J. Org. Chem.* **1985**, *50* (19), 3609–3612.
- (242) Canning, P. S. J.; McCrudden, K.; Maskill, H.; Sexton, B. *J. Chem. Soc. Perkin Trans. 2* **1999**, No. 12, 2735–2740.
- (243) Molander, G. A.; Ribagorda, M. *J. Am. Chem. Soc.* **2003**, *125* (37), 11148–11149.
- (244) Pan, X.; Wilcox, C. S. *J. Org. Chem.* **2010**, *75* (19), 6445–6451.
- (245) Kim, B. S.; Lee, S. Y.; Youn, S. W. *Chem. - An Asian J.* **2011**, *6* (8), 1952–1957.
- (246) Groziak, M.; Ganguly, A.; Robinson, P. *J. Am. Chem. Soc.* **1994**, No. c, 3124–3130.
- (247) Jackl, M. K.; Legnani, L.; Morandi, B.; Bode, J. W. *Org. Lett.* **2017**, *19* (17), 4696–

4699.

- (248) Schlicht, C. Model studies toward six-membered ring formation with oxy-ene reactions, ETH Zürich, 2005.
- (249) Schmid, G. A. Modellstudien zur thermisch oder anionisch induzierten Oxy-En-Reaktion, ETH Zürich, 2000.
- (250) Prince, M.; Wimo, A.; Guerchet, M.; Ali, G.-C.; Wu, Y.-T.; Prina, M. *World Alzheimer Report 2015 The Global Impact of Dementia*; London, 2015.
- (251) Querfurth, H. W.; LaFerla, F. M. *N. Engl. J. Med.* **2010**, *362* (4), 329–344.
- (252) Noël, S.; Cadet, S.; Gras, E.; Hureau, C. *Chem. Soc. Rev.* **2013**, *42* (19), 7747.
- (253) Viles, J. H. *Coord. Chem. Rev.* **2012**, *256* (19–20), 2271–2284.
- (254) Valensin, D.; Gabbiani, C.; Messori, L. *Coord. Chem. Rev.* **2012**, *256* (19–20), 2357–2366.
- (255) Cheignon, C.; Jones, M.; Atrián-Blasco, E.; Kieffer, I.; Faller, P.; Collin, F.; Hureau, C. *Chem. Sci.* **2017**, *8* (7), 5107–5118.
- (256) Bolognesi, M. L. In *Medicinal Chemistry Approaches to Personalized Medicine*; Lackey, K., Roth, B. D., Eds.; Methods and Principles in Medicinal Chemistry; Wiley-VCH Verlag GmbH & Co. KGaA: Weinheim, Germany, 2013; pp 211–226.
- (257) Winblad, B.; Palmer, K.; Kivipelto, M.; Jelic, V.; Fratiglioni, L.; Wahlund, L.-O.; Nordberg, A.; Backman, L.; Albert, M.; Almkvist, O.; Arai, H.; Basun, H.; Blennow, K.; de Leon, M.; DeCarli, C.; Erkinjuntti, T.; Giacobini, E.; Graff, C.; Hardy, J.; Jack, C.; Jorm, A.; Ritchie, K.; van Duijn, C.; Visser, P.; Petersen, R. C. *J. Intern. Med.* **2004**, *256* (3), 240–246.
- (258) Petersen, R. C.; Smith, G. E.; Waring, S. C.; Ivnik, R. J.; Tangalos, E. G.; Kokmen, E. *Arch. Neurol.* **1999**, *56* (3), 303–308.
- (259) Biancalana, M.; Koide, S. *Biochim. Biophys. Acta - Proteins Proteomics* **2010**, *1804* (7), 1405–1412.
- (260) Ribeiro Morais, G.; Paulo, A.; Santos, I. *European J. Org. Chem.* **2012**, No. 7, 1279–1293.
- (261) Wang, Y.; Mathis, C. A.; Huang, G. F.; Debnath, M. L.; Holt, D. P.; Shao, L.; Klunk, W. E. *J. Mol. Neurosci.* **2003**, *20* (3), 255–260.
- (262) Mathis, C. A.; Wang, Y.; Holt, D. P.; Huang, G. F.; Debnath, M. L.; Klunk, W. E. *J. Med. Chem.* **2003**, *46* (13), 2740–2754.
- (263) Serdons, K.; Terwinghe, C.; Vermaelen, P.; Laere, K. Van; Kung, H.; Mortelmans, L.; Bormans, G. *J. Med. Chem.* **2009**, *52*, 1428–1437.
- (264) Henriksen, G.; Hauser, A. I.; Westwell, A. D.; Yousefi, B. H.; Schwaiger, M.; Drzezga, A.; Wester, H. J. *J. Med. Chem.* **2007**, *50* (6), 1087–1089.

- (265) Neumaier, B.; Deisenhofer, S.; Sommer, C.; Solbach, C.; Reske, S. N.; Mottaghy, F. *Appl. Radiat. Isot.* **2010**, *68* (6), 1066–1072.
- (266) Serdons, K.; Verduyckt, T.; Vanderghinste, D.; Borghgraef, P.; Cleynhens, J.; Van Leuven, F.; Kung, H.; Bormans, G.; Verbruggen, A. *Eur. J. Med. Chem.* **2009**, *44* (4), 1415–1426.
- (267) Lee, B. C.; Kim, J. S.; Kim, B. S.; Son, J. Y.; Hong, S. K.; Park, H. S.; Moon, B. S.; Jung, J. H.; Jeong, J. M.; Kim, S. E. *Bioorganic Med. Chem.* **2011**, *19* (9), 2980–2990.
- (268) Price, J. C.; Klunk, W. E.; Lopresti, B. J.; Lu, X.; Hoge, J. a; Ziolkko, S. K.; Holt, D. P.; Meltzer, C. C.; DeKosky, S. T.; Mathis, C. a. *J. Cereb. Blood Flow Metab.* **2005**, *25* (11), 1528–1547.
- (269) Klunk, W. E.; Engler, H.; Nordberg, A.; Wang, Y.; Blomqvist, G.; Holt, D. P.; Bergström, M.; Savitcheva, I.; Huang, G. F.; Estrada, S.; Ausén, B.; Debnath, M. L.; Barletta, J.; Price, J. C.; Sandell, J.; Lopresti, B. J.; Wall, A.; Koivisto, P.; Antoni, G.; Mathis, C. A.; Långström, B. *Ann. Neurol.* **2004**, *55* (3), 306–319.
- (270) Rowe, C. C.; Ellis, K. A.; Rimajova, M.; Bourgeat, P.; Pike, K. E.; Jones, G.; Fripp, J.; Tochon-Danguy, H.; Morandea, L.; O’Keefe, G.; Price, R.; Raniga, P.; Robins, P.; Acosta, O.; Lenzo, N.; Szoeki, C.; Salvado, O.; Head, R.; Martins, R.; Masters, C. L.; Ames, D.; Villemagne, V. L. *Neurobiol. Aging* **2010**, *31* (8), 1275–1283.
- (271) Rowe, C. C.; Ng, S.; Ackermann, U.; Gong, S. J.; Pike, K.; Savage, G.; Cowie, T. F.; Dickinson, K. L.; Maruff, P.; Darby, D.; Smith, C.; Woodward, M.; Merory, J.; Tochon-Danguy, H.; O’Keefe, G.; Klunk, W. E.; Mathis, C. A.; Price, J. C.; Masters, C. L.; Villemagne, V. L. *Neurology* **2007**, *68* (20), 1718–1725.
- (272) Villemagne, V. L.; Rowe, C. C. *PET Clin.* **2010**, *5* (1), 33–53.
- (273) Serdons, K.; Verduyckt, T.; Vanderghinste, D.; Cleynhens, J.; Borghgraef, P.; Vermaelen, P.; Terwinghe, C.; Leuven, F. Van; Laere, K. Van; Kung, H.; Bormans, G.; Verbruggen, A. *Bioorganic Med. Chem. Lett.* **2009**, *19* (3), 602–605.
- (274) Heurling, K.; Leuzy, A.; Zimmer, E. R.; Lubberink, M.; Nordberg, A. *Eur. J. Nucl. Med. Mol. Imaging* **2016**, *43* (S1), 362–373.
- (275) Mountz, J. M.; Laymon, C. M.; Cohen, A. D.; Zhang, Z.; Price, J. C.; Boudhar, S.; McDade, E.; Aizenstein, H. J.; Klunk, W. E.; Mathis, C. A. *NeuroImage Clin.* **2015**, *9*, 592–598.
- (276) Cselenyi, Z.; Jonhagen, M. E.; Forsberg, A.; Halldin, C.; Julin, P.; Schou, M.; Johnstrom, P.; Varnas, K.; Svensson, S.; Farde, L. *J. Nucl. Med.* **2012**, *53* (3), 415–424.
- (277) Rowe, C. C.; Pejoska, S.; Mulligan, R. S.; Jones, G.; Chan, J. G.; Svensson, S.; Cselenyi, Z.; Masters, C. L.; Villemagne, V. L. *J. Nucl. Med.* **2013**, *54* (6), 880–886.
- (278) Zhang, W.; Kung, M.-P.; Oya, S.; Hou, C.; Kung, H. F. *Nucl. Med. Biol.* **2007**, *34* (1), 89–97.

- (279) Zhang, W.; Oya, S.; Kung, M.-P.; Hou, C.; Maier, D. L.; Kung, H. F. *J. Med. Chem.* **2005**, *48* (19), 5980–5988.
- (280) Zhang, W.; Oya, S.; Kung, M.-P.; Hou, C.; Maier, D. L.; Kung, H. F. *Nucl. Med. Biol.* **2005**, *32* (8), 799–809.
- (281) Villemagne, V. L.; Ong, K.; Mulligan, R. S.; Holl, G.; Pejoska, S.; Jones, G.; O'Keefe, G.; Ackerman, U.; Tochon-Danguy, H.; Chan, J. G.; Reiningger, C. B.; Fels, L.; Putz, B.; Rohde, B.; Masters, C. L.; Rowe, C. C. *J. Nucl. Med.* **2011**, *52* (8), 1210–1217.
- (282) Wong, D. F.; Rosenberg, P. B.; Zhou, Y.; Kumar, A.; Raymont, V.; Ravert, H. T.; Dannals, R. F.; Nandi, A.; Brasic, J. R.; Ye, W.; Hilton, J.; Lyketsos, C.; Kung, H. F.; Joshi, A. D.; Skovronsky, D. M.; Pontecorvo, M. J. *J. Nucl. Med.* **2010**, *51* (6), 913–920.
- (283) *Imaging in Neurodegenerative Disorders*; Saba, L., Ed.; Oxford University Press, 2015.
- (284) Raymond, S. B.; Kumar, A. T. N.; Boas, D. A.; Bacskai, B. J. *Phys. Med. Biol.* **2009**, *54* (20), 6201–6216.
- (285) Staderini, M.; Martín, M. A.; Bolognesi, M. L.; Menéndez, J. C. *Chem. Soc. Rev.* **2015**, *44* (7), 1807–1819.
- (286) Tong, H.; Lou, K.; Wang, W. *Acta Pharm. Sin. B* **2015**, *5* (1), 25–33.
- (287) Fu, H.; Cui, M. *Curr. Med. Chem.* **2018**, *25*, 1–24.
- (288) Nesterov, E. E.; Skoch, J.; Hyman, B. T.; Klunk, W. E.; Bacskai, B. J.; Swager, T. M. *Angew. Chemie - Int. Ed.* **2005**, *44* (34), 5452–5456.
- (289) Meek, S. T.; Nesterov, E. E.; Swager, T. M. *Org. Lett.* **2008**, *10* (14), 2991–2993.
- (290) Raymond, S. B.; Skoch, J.; Hills, I. D.; Nesterov, E. E.; Swager, T. M.; Bacskai, B. J. *Eur. J. Nucl. Med. Mol. Imaging* **2008**, *35* (SUPPL. 1), 93–98.
- (291) Klunk, W. E.; Bacskai, B. J.; Mathis, C. A.; Kajdasz, S. T.; McLellan, M. E.; Frosch, M. P.; Debnath, M. L.; Holt, D. P.; Wang, Y.; Hyman, B. T. *J. Neuropathol. Exp. Neurol.* **2002**, *61* (9), 797–805.
- (292) Hintersteiner, M.; Enz, A.; Frey, P.; Jatón, A.-L.; Kinzy, W.; Kneuer, R.; Neumann, U.; Rudin, M.; Staufenbiel, M.; Stoeckli, M.; Wiederhold, K.-H.; Gremlich, H.-U. *Nat. Biotechnol.* **2005**, *23*, 577.
- (293) Okamura, N.; Mori, M.; Furumoto, S.; Yoshikawa, T.; Harada, R.; Ito, S.; Fujikawa, Y.; Arai, H.; Yanai, K.; Kudo, Y. *J. Alzheimer's Dis.* **2011**, *23* (1), 37–48.
- (294) Schmidt, A.; Pahnke, J. *J. Alzheimer's Dis.* **2012**, *30* (3), 651–664.
- (295) Zhou, K.; Bai, H.; Feng, L.; Dai, J.; Cui, M. *Anal. Chem.* **2017**, *89* (17), 9432–9437.
- (296) Cui, M.; Ono, M.; Watanabe, H.; Kimura, H.; Liu, B.; Saji, H. *J. Am. Chem. Soc.* **2014**, *136* (9), 3388–3394.

- (297) Liu, Y.; Song, N.; Chen, L.; Liu, S.; Xie, Z. *Chem. - An Asian J.* **2018**, *13* (8), 989–995.
- (298) Courtis, A. M.; Santos, S. A.; Guan, Y.; Hendricks, J. A.; Ghosh, B.; Szantai-Kis, D. M.; Reis, S. A.; Shah, J. V.; Mazitschek, R. *Bioconjug. Chem.* **2014**, *25* (6), 1043–1051.
- (299) Watanabe, H.; Ono, M.; Matsumura, K.; Yoshimura, M.; Kimura, H.; Saji, H. *Mol. Imaging* **2013**, *12* (5), 7290.2013.00049.
- (300) Garcia-Alloza, M.; Borrelli, L. A.; Rozkalne, A.; Hyman, B. T.; Bacskai, B. J. *J. Neurochem.* **2007**, *102* (4), 1095–1104.
- (301) Zhang, X.; Tian, Y.; Li, Z.; Tian, X.; Sun, H.; Liu, H.; Moore, A.; Ran, C. *J. Am. Chem. Soc.* **2013**, *135* (44), 16397–16409.
- (302) Alies, B.; Hureau, C.; Faller, P. *Metallomics* **2013**, *5* (3), 183–192.
- (303) Cassagnes, L. E.; Hervé, V.; Nepveu, F.; Hureau, C.; Faller, P.; Collin, F. *Angew. Chemie - Int. Ed.* **2013**, *52* (42), 11110–11113.
- (304) Ono, M.; Ishikawa, M.; Kimura, H.; Hayashi, S.; Matsumura, K.; Watanabe, H.; Shimizu, Y.; Cheng, Y.; Cui, M.; Kawashima, H.; Saji, H. *Bioorganic Med. Chem. Lett.* **2010**, *20* (13), 3885–3888.
- (305) Watanabe, H.; Ono, M.; Kimura, H.; Kagawa, S.; Nishii, R.; Fuchigami, T.; Haratake, M.; Nakayama, M.; Saji, H. *Bioorganic Med. Chem. Lett.* **2011**, *21* (21), 6519–6522.
- (306) Fu, H.; Peng, C.; Liang, Z.; Dai, J.; Liu, B.; Cui, M. *Chem. Commun.* **2016**, *52* (86), 12745–12748.
- (307) Kwak, M. J.; Kim, Y. *Bull. Korean Chem. Soc.* **2009**, *30* (12), 2865–2866.
- (308) Xie, L.; Chen, Y.; Wu, W.; Guo, H.; Zhao, J.; Yu, X. *Dye. Pigment.* **2012**, *92* (3), 1361–1369.
- (309) Li, X.; Son, Y.-A. *Dye. Pigment.* **2014**, *107*, 182–187.
- (310) Maeda, C.; Todaka, T.; Ueda, T.; Ema, T. *Chem. - A Eur. J.* **2016**, *22* (22), 7508–7513.
- (311) Maeda, C.; Todaka, T.; Ueda, T.; Ema, T. *Org. Biomol. Chem.* **2017**, *15* (44), 9283–9287.
- (312) Maeda, C.; Nagahata, K.; Ema, T. *Org. Biomol. Chem.* **2017**, *15* (37), 7783–7788.
- (313) Santra, M.; Moon, H.; Park, M.-H. H.; Lee, T.-W. W.; Kim, Y. K.; Ahn, K. H. *Chemistry* **2012**, *18* (32), 9886–9893.
- (314) Keri, R. S.; Patil, M. R.; Patil, S. A.; Budagumpi, S. *Eur. J. Med. Chem.* **2015**, *89*, 207–251.
- (315) Gill, R. K.; Rawal, R. K.; Bariwal, J. *Arch. Pharm. (Weinheim)*. **2015**, *348* (3), 155–

178.

- (316) Le Bozec, L.; Moody, C. J. *Aust. J. Chem.* **2009**, *62* (7), 639–647.
- (317) Prajapati, N. P.; Vekariya, R. H.; Borad, M. A.; Patel, H. D. *RSC Adv.* **2014**, *4* (104), 60176–60208.
- (318) Dadmal, T. L.; Katre, S. D.; Mandewale, M. C.; Kumbhare, R. M. *New J. Chem.* **2018**, *42* (2), 776–797.
- (319) Brewster, R. Q.; Dains, F. B. *J. Am. Chem. Soc.* **1936**, *58* (8), 1364–1366.
- (320) Jimonet, P.; Audiau, F.; Barreau, M.; Blanchard, J.-C.; Boireau, A.; Bour, Y.; Coléno, M.-A.; Doble, A.; Doerflinger, G.; Do Huu, C.; Donat, M.-H.; Duchesne, J. M.; Ganil, P.; Guérémy, C.; Honoré, E.; Just, B.; Kerphirique, R.; Gontier, S.; Hubert, P.; Laduron, P. M.; Le Blevec, J.; Meunier, M.; Miquet, J.-M.; Nemecek, C.; Pasquet, M.; Piot, O.; Pratt, J.; Rataud, J.; Reibaud, M.; Stutzmann, J.-M.; Mignani, S. *J. Med. Chem.* **1999**, *42* (15), 2828–2843.
- (321) Panizzi, J.-C.; Davidovics, G.; Guglielmetti, R.; Mille, G.; Metzger, J.; Chouteau, J. *Can. J. Chem.* **1971**, *49* (6), 956–964.
- (322) Rasmussen, C. R.; Villani Jr, F. J.; Weaner, L. E.; Reynolds, B. E.; Hood, A. R.; Hecker, L. R.; Nortey, S. O.; Hanslin, A.; Costanzo, M. J.; Powell, E. T.; Molinari, A. J.; Villani, Jr., F. J.; Weaner, L. E.; Reynolds, B. E.; Hood, A. R.; Hecker, L. R.; Nortey, S. O.; Hanslin, A.; Costanzo, M. J.; Powell, E. T.; Molinari, A. J. *Synthesis (Stuttg)*. **1988**, *1988* (06), 456–459.
- (323) Thanigaimalai, P.; Le Hoang, T. A.; Lee, K. C.; Bang, S. C.; Sharma, V. K.; Yun, C. Y.; Roh, E.; Hwang, B. Y.; Kim, Y.; Jung, S. H. *Bioorganic Med. Chem. Lett.* **2010**, *20* (9), 2991–2993.
- (324) Hugershoff, A. *Berichte der Dtsch. Chem. Gesellschaft* **1903**, *36* (3), 3121–3134.
- (325) Hugershoff, A. *Berichte der Dtsch. Chem. Gesellschaft* **1901**, *34* (2), 3130–3135.
- (326) Metten, B.; Smet, M.; Boens, N.; Dehaen, W. *Synthesis (Stuttg)*. **2005**, *2005* (11), 1838–1844.
- (327) Meesala, Y.; Kavala, V.; Chang, H.-C.; Kuo, T.-S.; Yao, C.-F.; Lee, W.-Z. *Dalt. Trans.* **2015**, *44* (3), 1120–1129.
- (328) Wei, D.; Sadek, O.; Dorcet, V.; Roisnel, T.; Darcel, C.; Gras, E.; Clot, E.; Sortais, J. *J. Catal.* **2018**, *366*, 300–309.
- (329) Molander, G. A.; Canturk, B.; Kennedy, L. E. *J. Org. Chem.* **2009**, *74* (3), 973–980.
- (330) Singh, R. S.; Yadav, M.; Gupta, R. K.; Pandey, R.; Pandey, D. S. *Dalt. Trans.* **2013**, *42* (5), 1696–1707.
- (331) Wu, L.; Burgess, K. *J. Am. Chem. Soc.* **2008**, *130* (12), 4089–4096.
- (332) Murale, D. P.; Lee, K. M.; Kim, K.; Churchill, D. G. *Chem. Commun.* **2011**, *47* (46), 12512.

- (333) Chen, Y.; Qi, D.; Zhao, L.; Cao, W.; Huang, C.; Jiang, J. *Chem. - A Eur. J.* **2013**, *19* (23), 7342–7347.
- (334) Deloux, L.; Srebnik, M. *Chem. Rev.* **1993**, *93* (2), 763–784.
- (335) De Vries, T. S.; Prokofjevs, A.; Vedejs, E. *Chem. Rev.* **2012**, *112* (7), 4246–4282.
- (336) Toyota, S.; Ito, F.; Yamamoto, T.; Akashi, H.; Iwanaga, T. *Bull. Chem. Soc. Jpn.* **2006**, *79* (5), 796–798.
- (337) Toyota, S.; Ito, F.; Nitta, N.; Hakamata, T. *Bull. Chem. Soc. Jpn.* **2004**, *77* (11), 2081–2088.
- (338) Vedejs, E.; Fields, S. C.; Hayashi, R.; Hitchcock, S. R.; Powell, D. R.; Schrimpf, M. R. *J. Am. Chem. Soc.* **1999**, *121* (11), 2460–2470.
- (339) Vedejs, E.; Chapman, R. W.; Lin, S.; Müller, M.; Powell, D. R. *J. Am. Chem. Soc.* **2000**, *122* (13), 3047–3052.
- (340) Vedejs, E.; Fields, S. C.; Lin, S.; Schrimpf, M. R. *J. Org. Chem.* **1995**, *60* (10), 3028–3034.
- (341) Noda, H.; Bode, J. W. *J. Am. Chem. Soc.* **2015**, *137* (11), 3958–3966.
- (342) Pu, L. *Chem. Rev.* **2004**, *104* (3), 1687–1716.
- (343) Lu, H.; Mack, J.; Nyokong, T.; Kobayashi, N.; Shen, Z. *Coord. Chem. Rev.* **2016**, *318*, 1–15.
- (344) Haefele, A.; Zedde, C.; Retaillieu, P.; Ulrich, G.; Ziesel, R. *Org. Lett.* **2010**, *12* (8), 1672–1675.
- (345) Frisch, M. J.; Trucks, G. W.; Schlegel, H. B.; Scuseria, G. E.; Robb, M. A.; Cheeseman, J. R.; Scalmani, G.; Barone, V.; Mennucci, B.; Petersson, G. A.; Nakatsuji, H.; Caricato, M.; Li, X.; Hratchian, H. P.; Izmaylov, A. F.; Bloino, J.; Zheng, G.; Sonnenberg, J. L.; Hada, M.; Ehara, M.; Toyota, K.; Fukuda, R.; Hasegawa, J.; Ishida, M.; Nakajima, T.; Honda, Y.; Kitao, O.; Nakai, H.; Vreven, T.; Montgomery, J. A. J.; Peralta, J. E.; Ogliaro, F.; Bearpark, M.; Heyd, J. J.; Brothers, E.; Kudin, K. N.; Staroverov, V. N.; Kobayashi, R.; Normand, J.; Raghavachari, K.; Rendell, A.; Burant, J. C.; Iyengar, S. S.; Tomasi, J.; Cossi, M.; Rega, N.; Millam, J. M.; Klene, M.; Knox, J. E.; Cross, J. B.; Bakken, V.; Adamo, C.; Jaramillo, J.; Gomperts, R.; Stratmann, R. E.; Yazyev, O.; Austin, A. J.; Cammi, R.; Pomelli, C.; Ochterski, J. W.; Martin, R. L.; Morokuma, K.; Zakrzewski, V. G.; Voth, G. A.; Salvador, P.; Dannenberg, J. J.; Dapprich, S.; Daniels, A. D.; Farkas, O.; Foresman, J. B.; Ortiz, J. V.; Cioslowski, J.; Fox, D. J. Gaussian, Inc.: Wallingford CT 2009.
- (346) Li, Z.; Lin, T. P.; Liu, S.; Huang, C. W.; Hudnall, T. W.; Gabbaï, F. P.; Conti, P. S. *Chem. Commun.* **2011**, *47* (33), 9324–9326.
- (347) Faller, P.; Hureau, C.; Berthoumieu, O. *Inorg. Chem.* **2013**, *52* (21), 12193–12206.
- (348) Hrobárik, P.; Hrobáriková, V.; Sigmundová, I.; Zahradník, P.; Fakis, M.; Polyzos, I.;

Persephonis, P. *J. Org. Chem.* **2011**, 76 (21), 8726–8736.

Exploiting Boron-Fluorine Bonds for Fluorination and Synthesis of Potential Bi-modal Imaging Agents

The B-F bond has an expansive and rich history in chemical transformations and the versatility of the B-F bond has also shown immense utility in fields as far reaching as Positron Emission Tomography (PET) and fluorescence imaging.

The application of B-F bonds for nucleophilic Carbon-Fluorine (C-F) bond formation and the development of novel fluorophores with potential applications in PET/fluorescence bi-modal imaging is reported in this document.

Organotrifluoroborates are well known as indispensable synthetic tools for the elaboration of organic molecules. However, the trifluoroborate functionality is generally regarded as an auxiliary group, and its potential as a nucleophilic fluoride (F^-) source has remained untested. In this context, the ability of organotrifluoroborates to serve as competent sources of F^- was investigated. In an update to the historic Balz-Schiemann reaction, that traditionally uses BF_4^- as a source of F^- , organotrifluoroborates were shown to mediate the fluorodediazotiation of *in situ* generated aryl diazonium salts under mild reaction conditions. In reactions with an analogous substrate class, unsymmetrical diaryliodonium salts could also be fluorinated using phenyltrifluoroborate via thermal decomposition of the ion pair. Finally, the ability of the trifluoroborate moiety to mediate intramolecular fluorination reactions was investigated through the synthesis of various trifluoroborate-containing molecular scaffolds.

We also investigated novel fluoroborate ($B-F_n$) complexes of the 2-aryl-benzothiazole scaffold, known for its interaction with $A\beta$ aggregates, as fluorescent probes. Three complexes were isolated, characterized and their photophysical properties are reported. A 2,4-diaryl-benzothiazole monofluoroborate complex displaying the most promising photophysical properties, was shown to be stable to aqueous conditions. Fluoride abstraction from this complex was also demonstrated, providing promising preliminary results towards the viability of radiolabelling via ^{19}F - ^{18}F isotope exchange. The monofluoroborate complex also showed interesting structural properties given the asymmetric boron centre. Enantiomers of the complex were successfully resolved by chiral chromatography from the racemic mixture, characterized by Circular Dichroism and their stability to inversion investigated.

Exploitation du Couple Bore-Fluor pour la Fluoration et la Synthèse d'Agent d'Imagerie Bimodaux Potentiels

La liaison Bore-Fluor (B-F) a une longue et riche histoire dans le domaine des transformations chimiques. De plus, cette liaison B-F est utilisée dans une grande diversité de domaines tel que la médecine nucléaire avec l'imagerie de Tomographie par Émission de Positrons (TEP) ou l'imagerie de fluorescence.

Dans le cadre de cette thèse, nous nous intéressons à l'utilisation de la liaison B-F pour la formation nucléophile de liaison Carbone-Fluor (C-F) et le développement de nouveaux fluorophores ayant des applications potentielles dans les domaines de l'imagerie bimodale TEP et l'imagerie de fluorescence.

Les organotrifluoroborates sont connus pour être des outils de synthèse d'importance majeure pour la conception de molécules organiques. Cependant, le groupement trifluoroborate n'est généralement utilisé qu'en tant que groupement partant, c'est à dire par rupture de la liaison C-B. Ainsi, son potentiel en tant que source de fluorure nucléophile (F^-) n'est pas étudié. C'est pourquoi, nous nous sommes intéressé à l'aptitude des organotrifluoroborates à servir de source de fluorure. En effet, si historiquement la réaction de Balz-Schiemann, utilise le BF_4^- comme source de F^- , nous avons démontré que les organotrifluoroborates sont capables de réaliser la réaction de fluoro-dédiazotation de sels d'aryldiazonium générés *in situ* dans des conditions réactionnelles douces. De plus, dans des réactions avec une classe de substrats analogues, des sels dissymétriques de diaryliodonium pourraient être fluorés par des phényltrifluoroborates par décomposition thermique de la paire d'ion. Finalement, l'aptitude du groupement trifluoroborate à promouvoir des réactions de fluoration intramoléculaires a été étudiée par la synthèse de divers motifs contenant ce groupement.

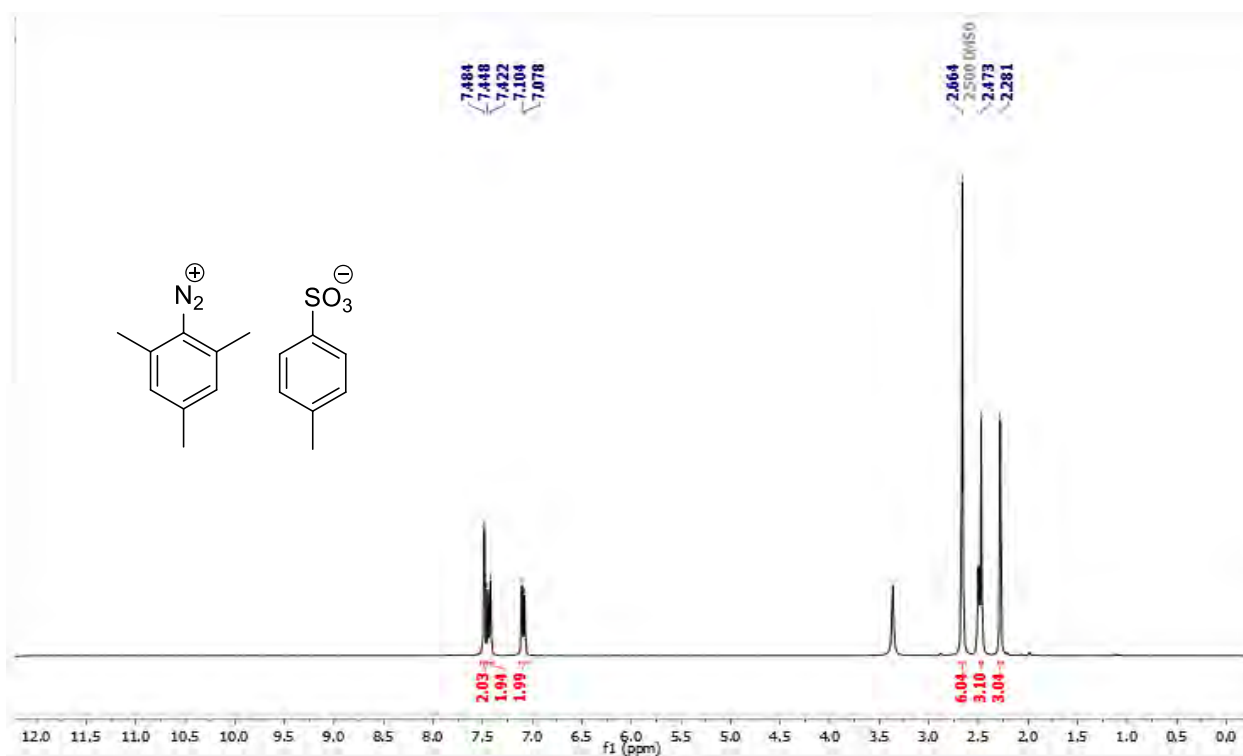
Nous avons également étudié de nouveaux complexes fluoroborates ($B-F_n$) dérivés du motif 2-aryl-benzothiazole comme sondes fluorescentes. Trois complexes ont été isolés, caractérisés, et leurs propriétés photo-physiques rapportées. Un complexe monofluoroborate de 2,4-diaryl-benzothiazole présentant les propriétés photo-physiques les plus prometteuses s'est révélé stable en conditions aqueuses. De plus, l'abstraction de fluorure de ce complexe a été démontrée, fournissant ainsi des résultats préliminaires prometteurs vers la viabilité du radiomarquage par échange isotopiques ^{19}F - ^{18}F . Ce complexe monofluoroborate a également montré des propriétés structurales intéressantes par la présence d'un bore stéréogène. Les énantiomères de ce complexe ont été dédoublés par chromatographie chirale à partir du mélange racémique puis caractérisés par dichroïsme circulaire. Enfin, la stabilité configurationnelle du bore a été étudiée.

Annex A: Chapter 2

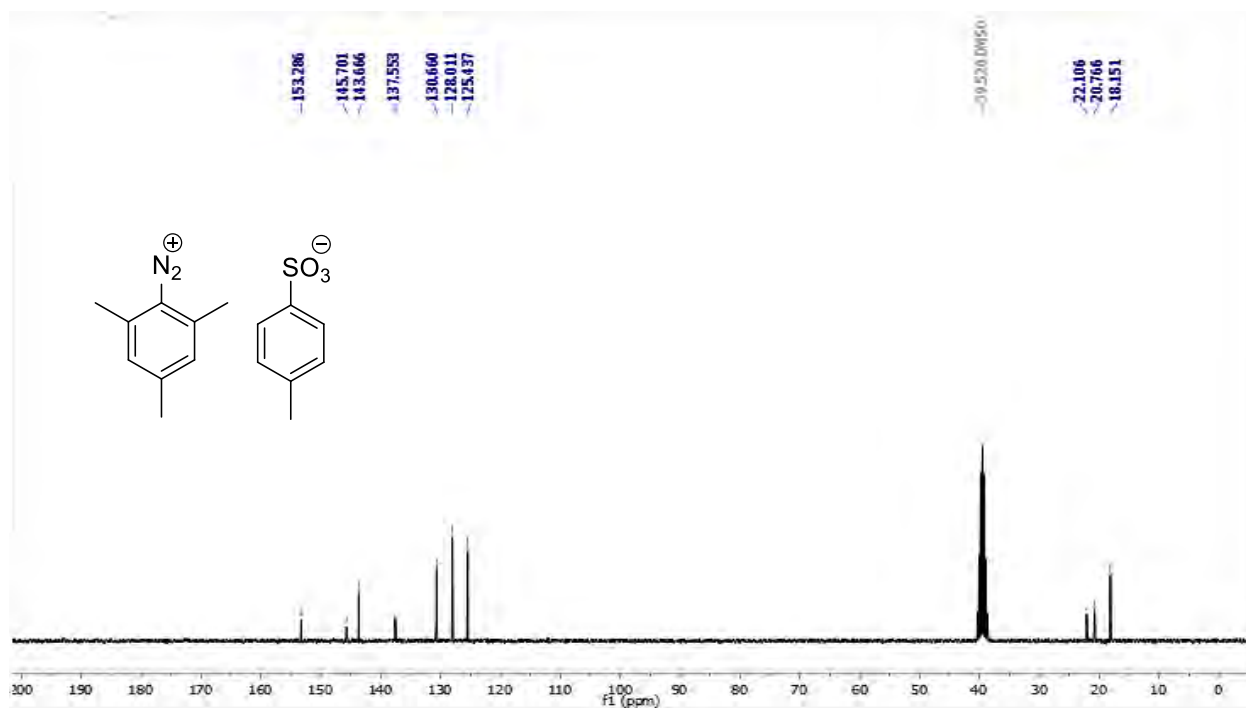
NMR Spectra of selected compounds

2,4,6-trimethylphenyldiazonium Tosylate (1)

^1H NMR

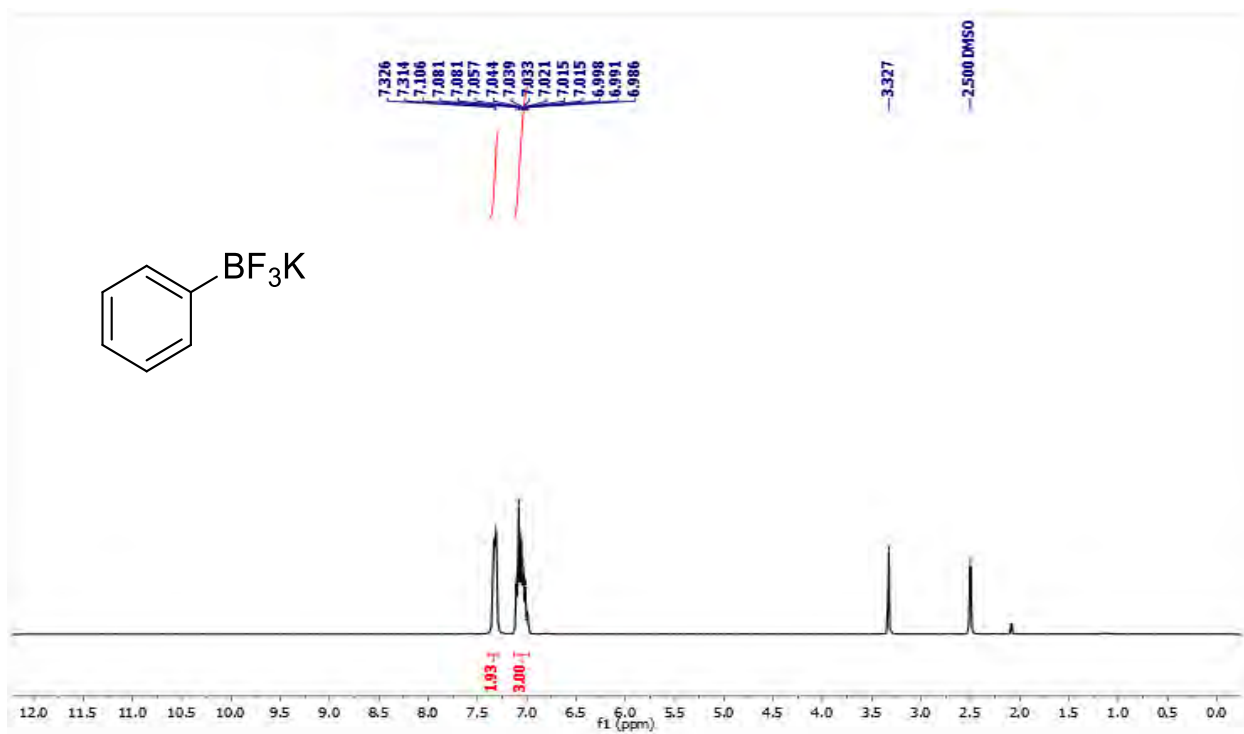


^{13}C NMR

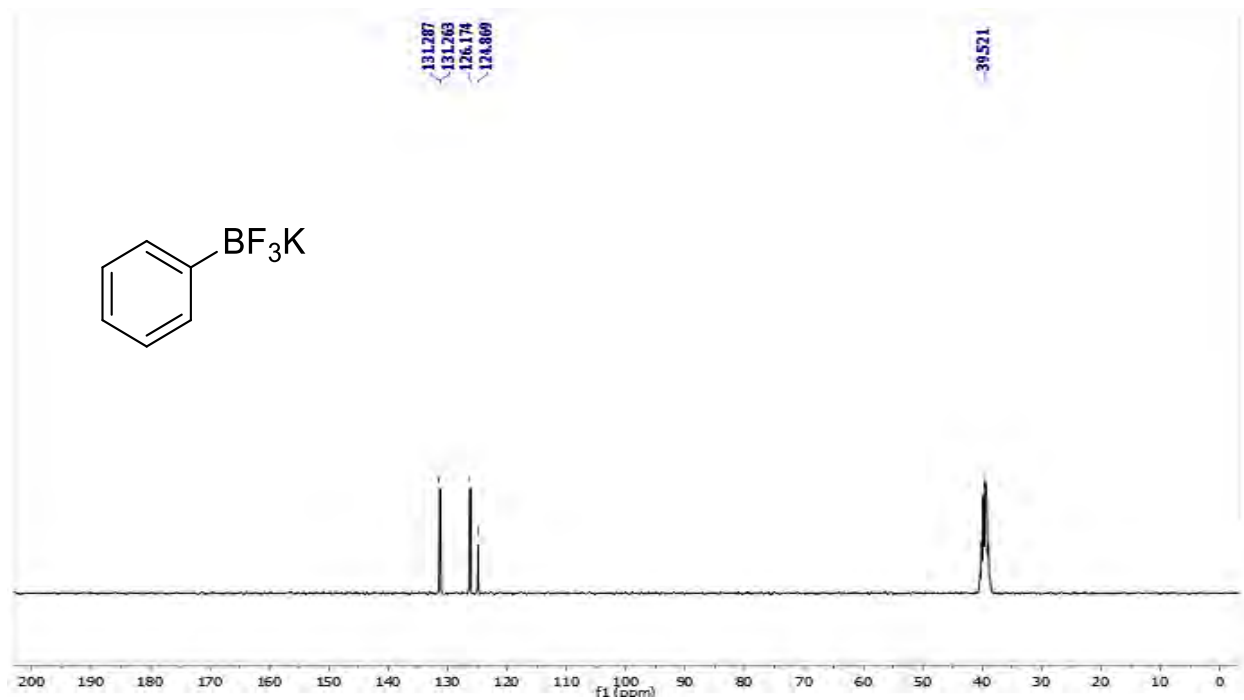


Potassium phenyltrifluoroborate (**2a**)

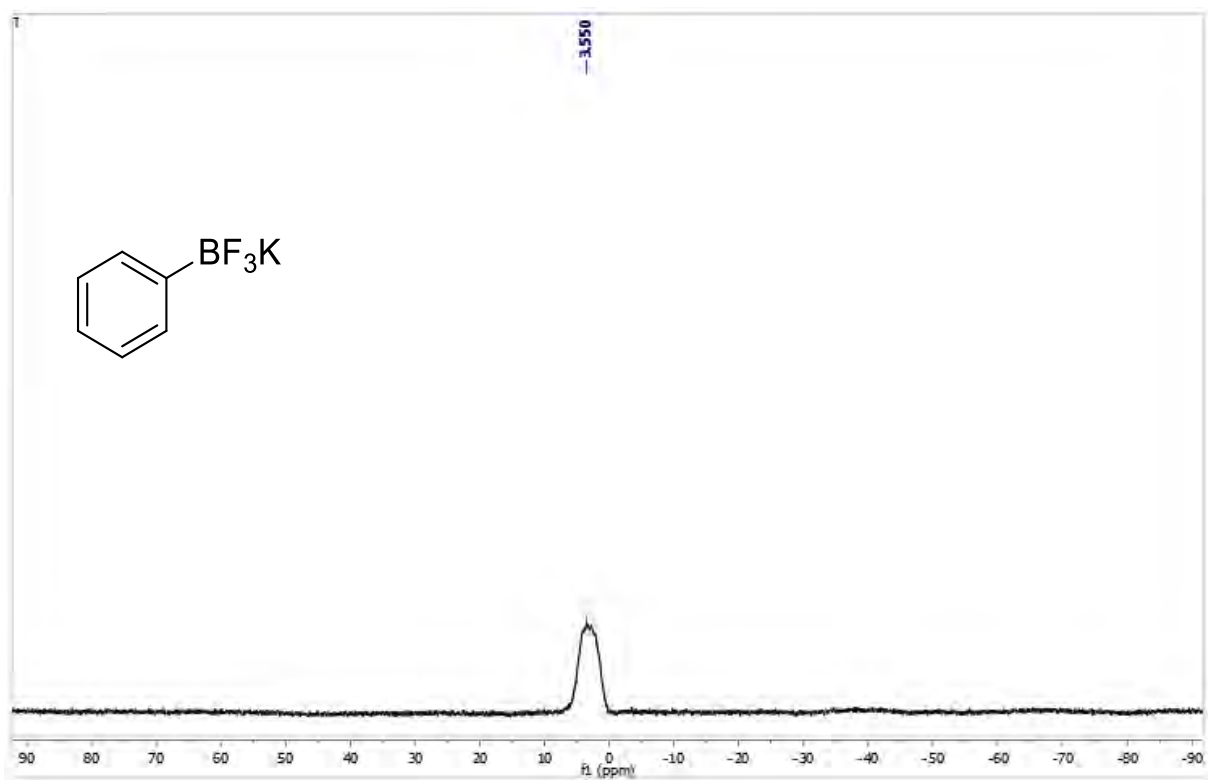
^1H NMR



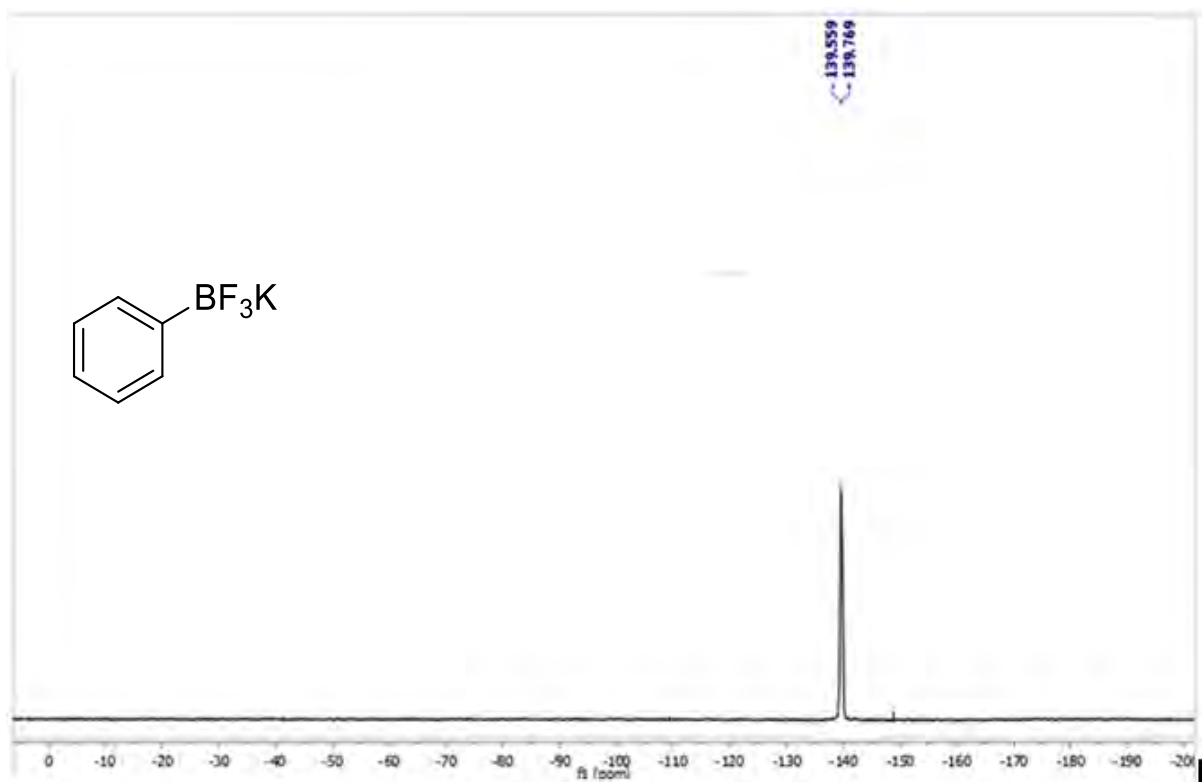
^{13}C NMR



^{11}B NMR

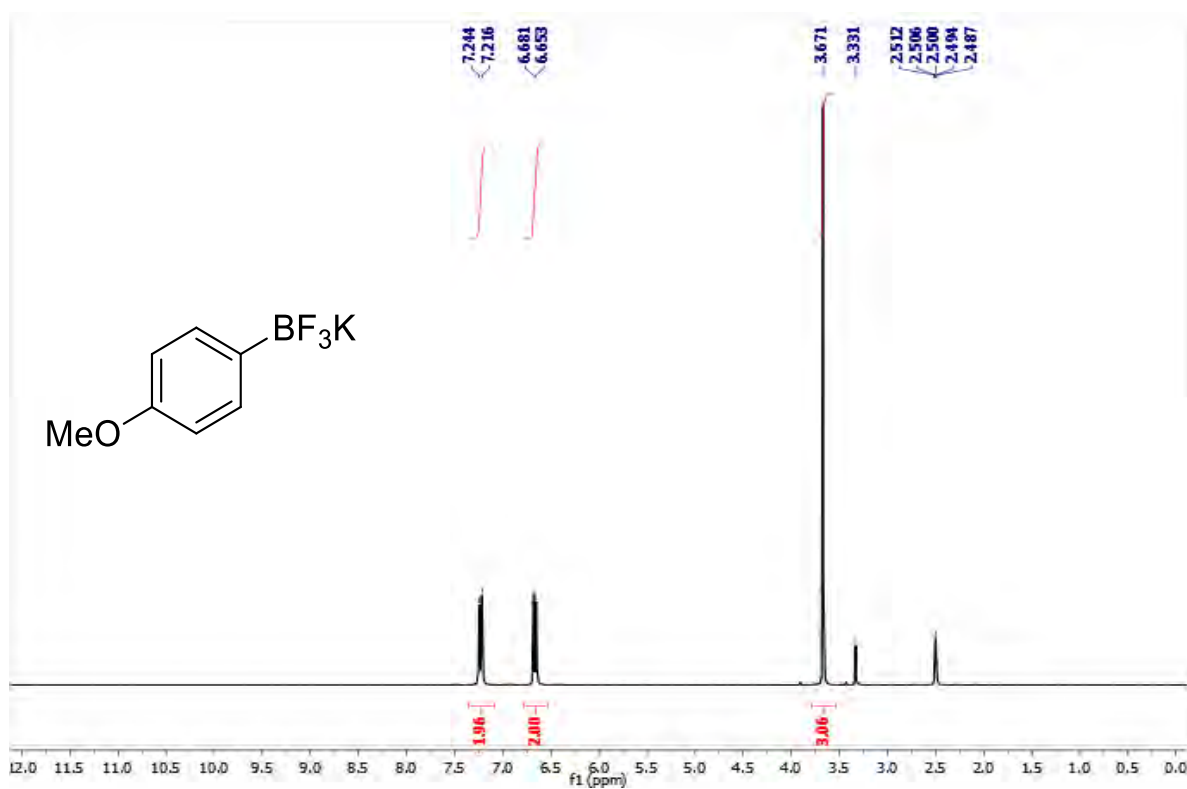


^{19}F NMR

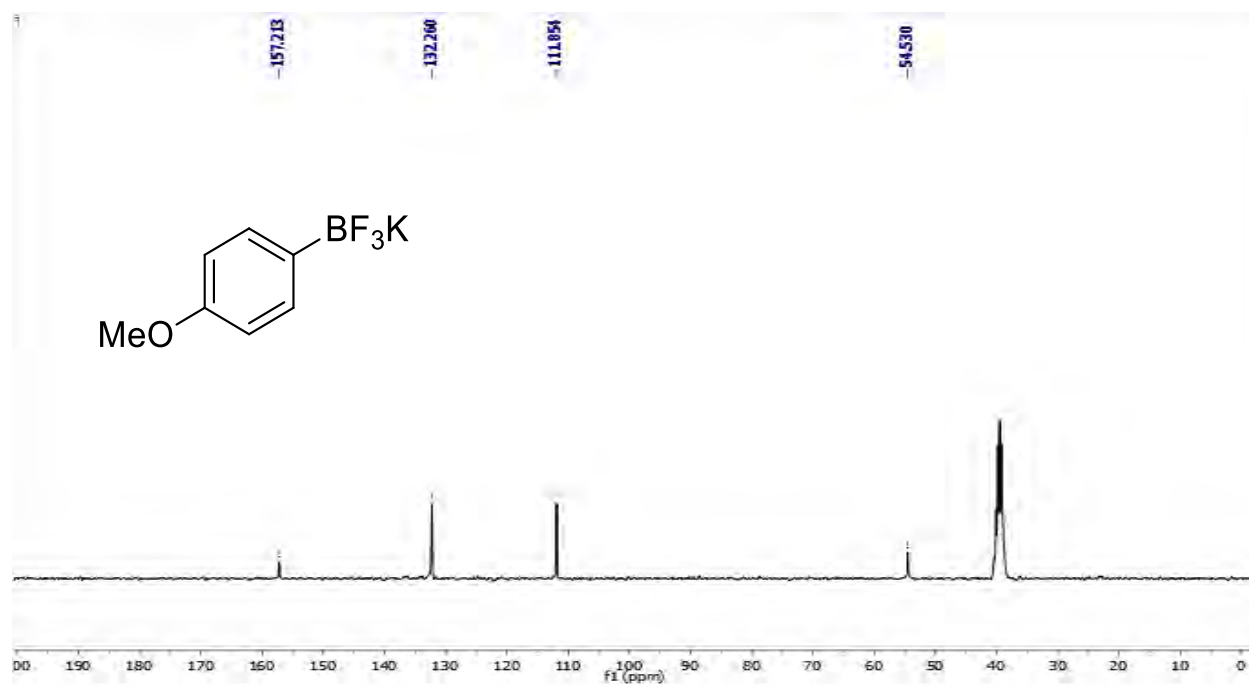


Potassium 4-methoxyphenyltrifluoroborate (**2b**)

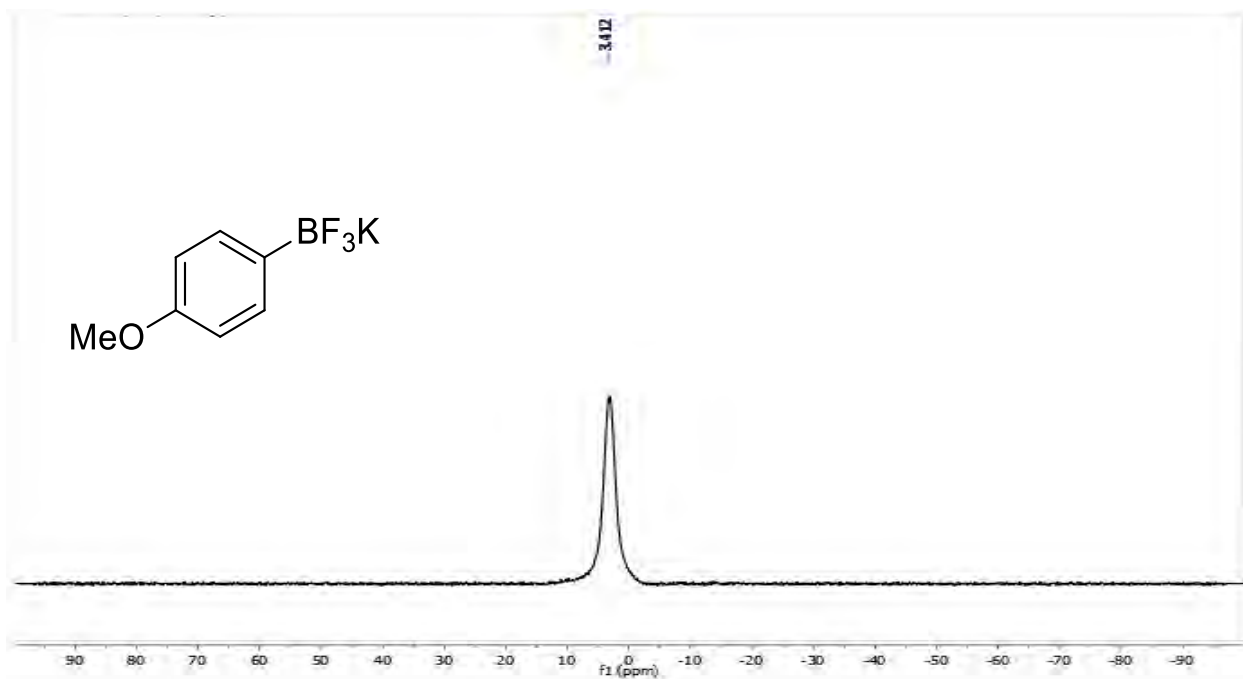
¹H NMR



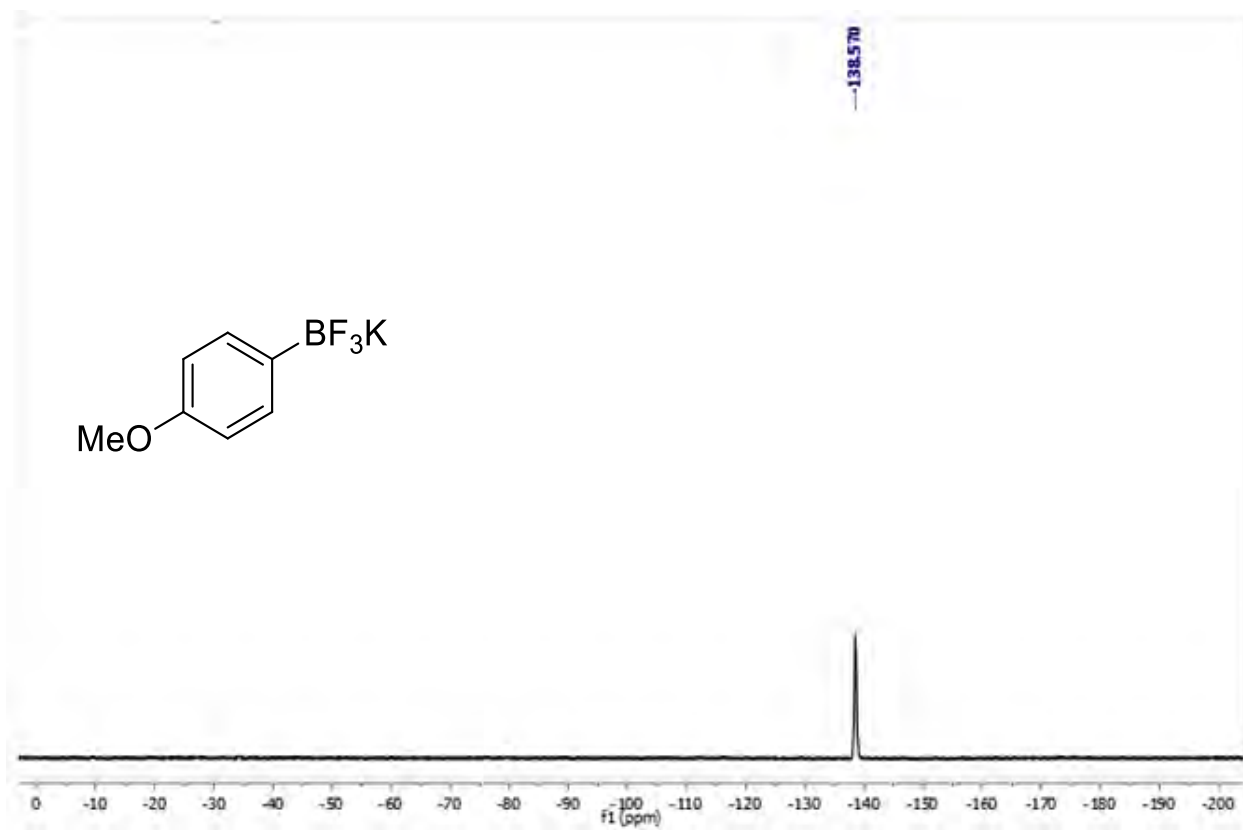
¹³C NMR



^{11}B NMR

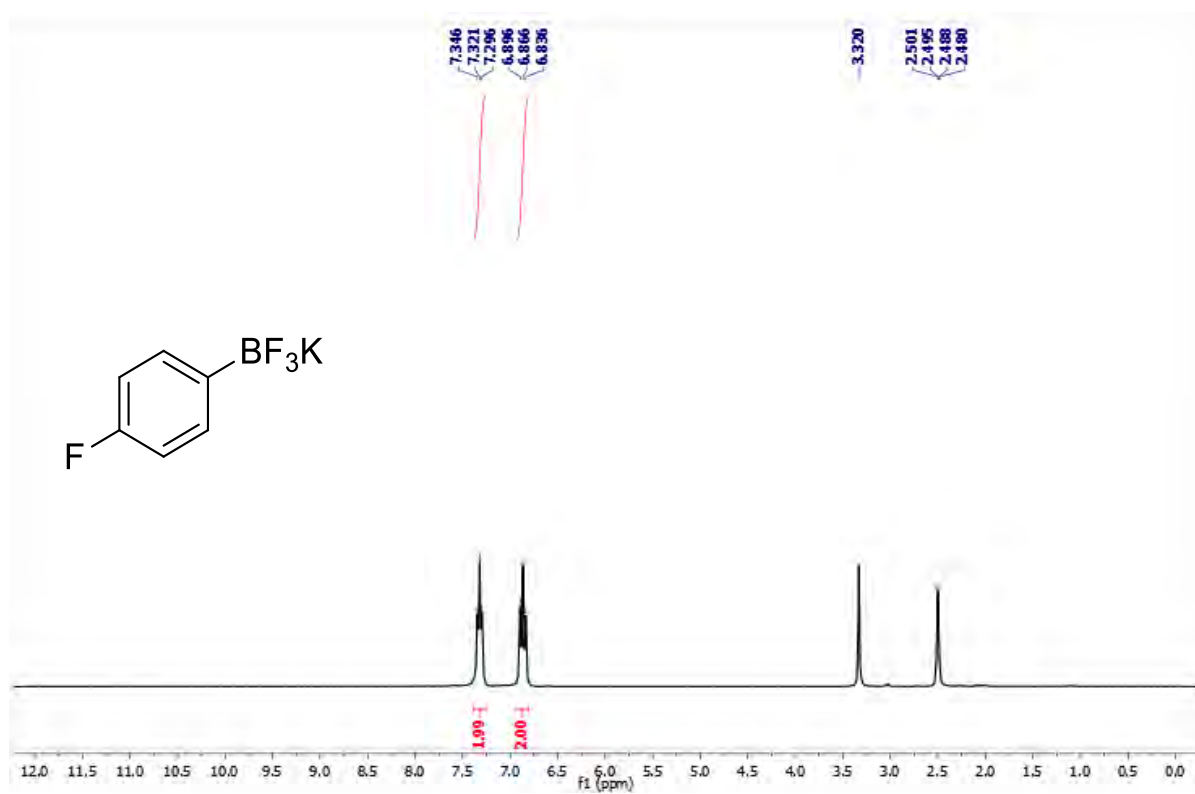


^{19}F NMR

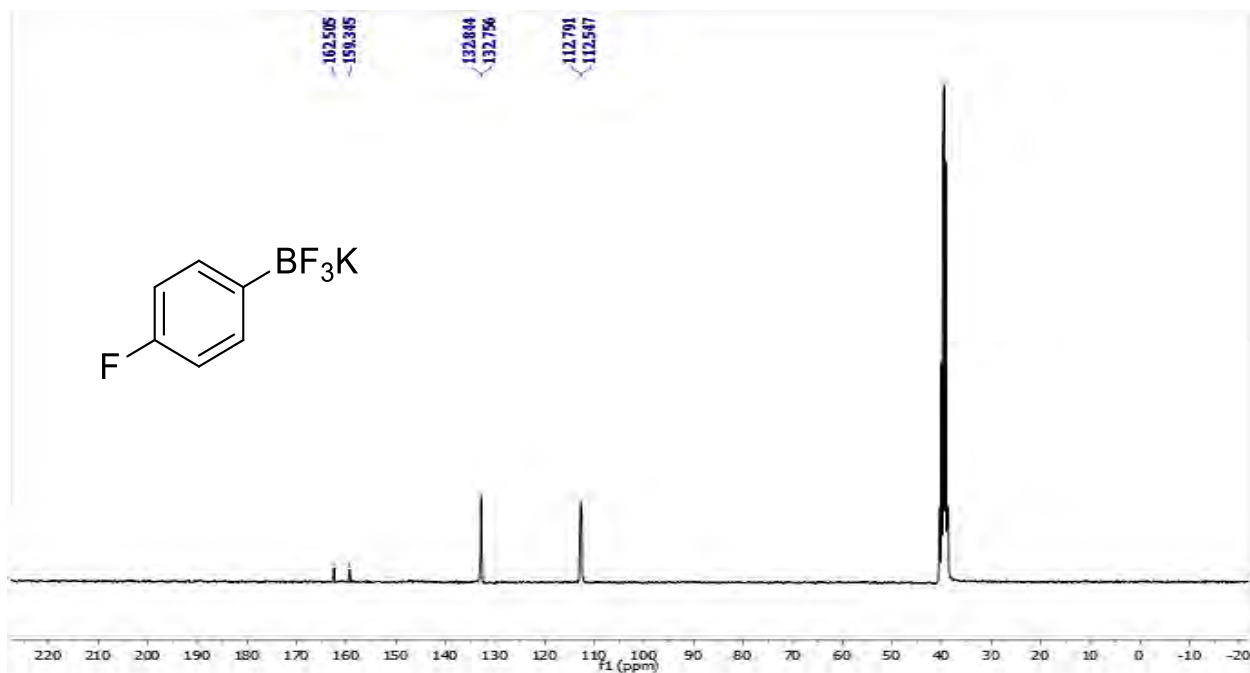


Potassium 4-fluorophenyltrifluoroborate (**2c**)

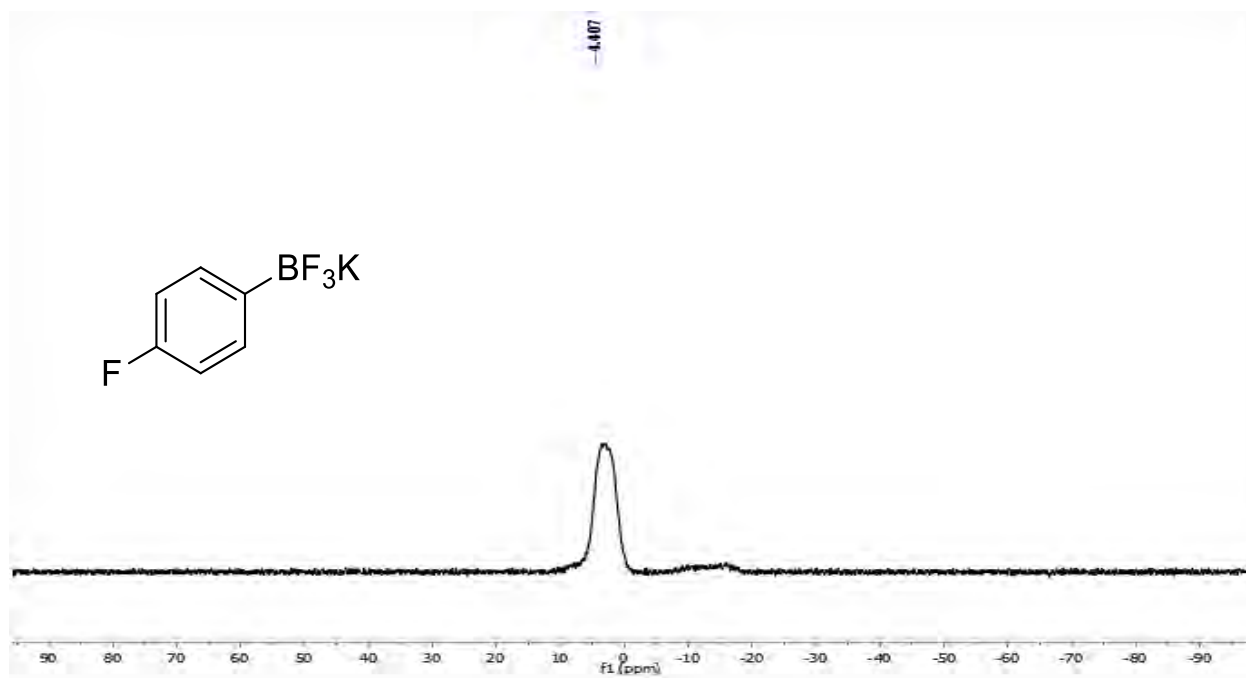
¹H NMR



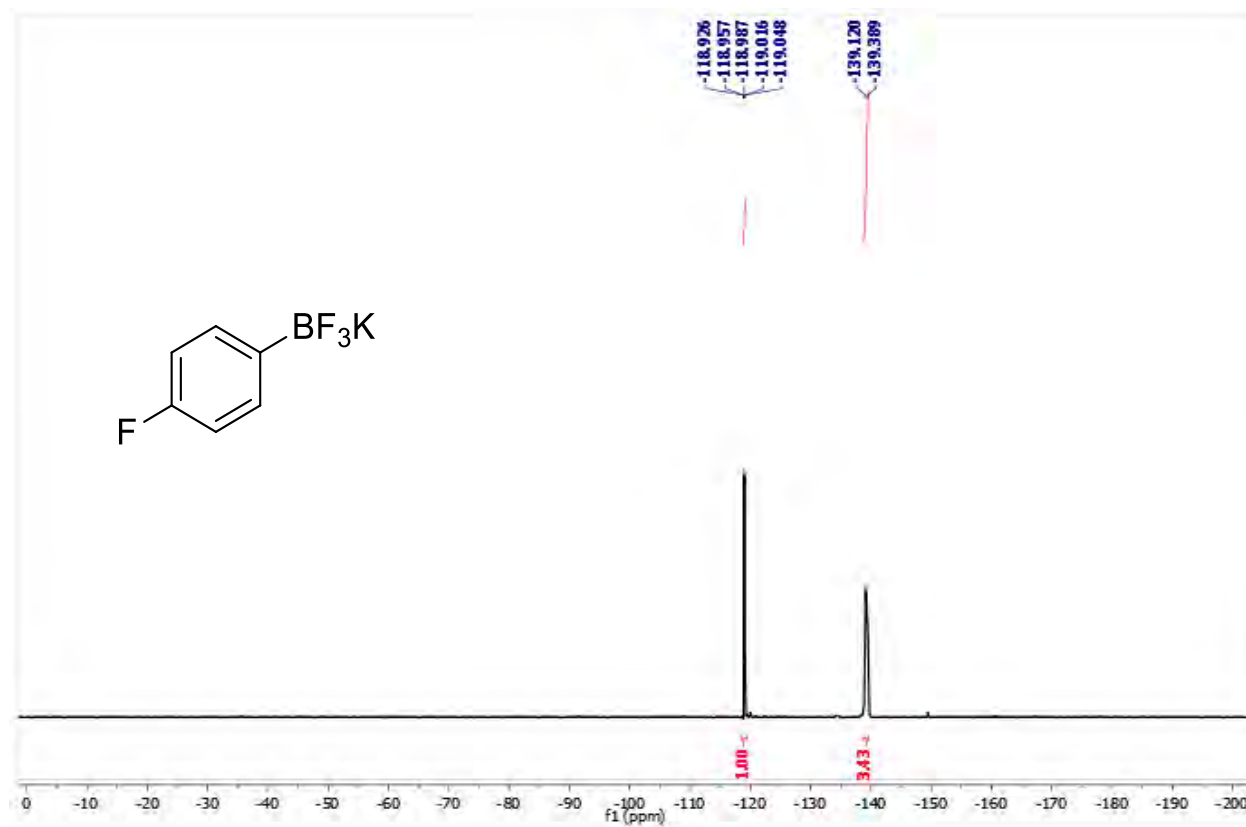
¹³C NMR



^{11}B NMR

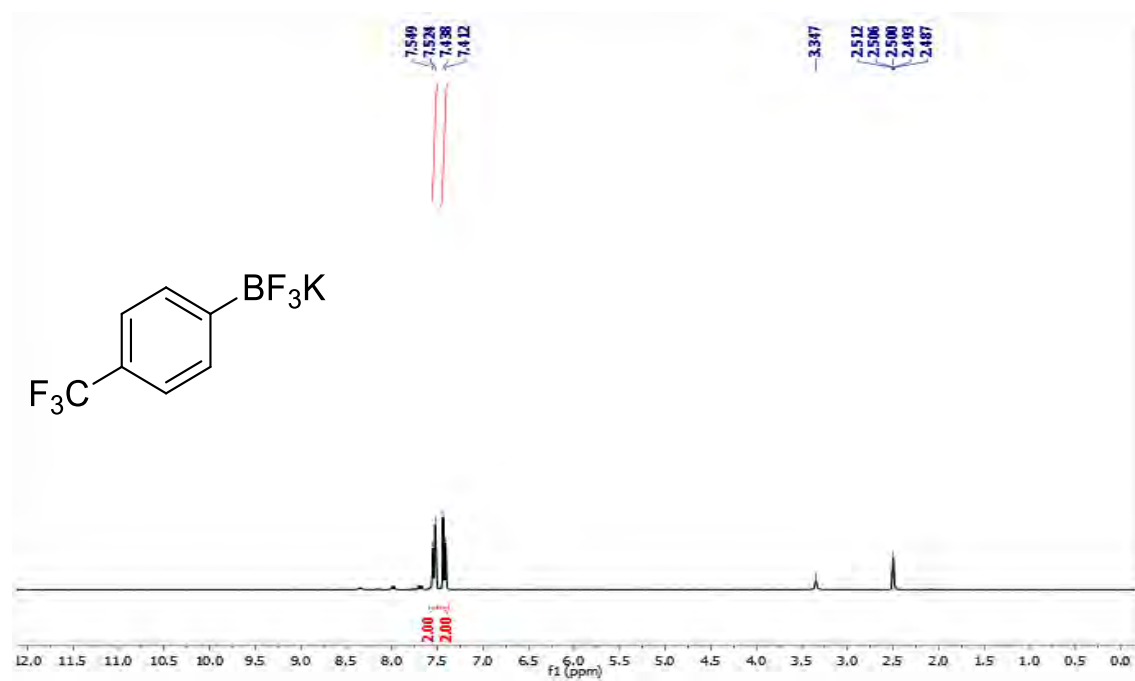


^{19}F NMR

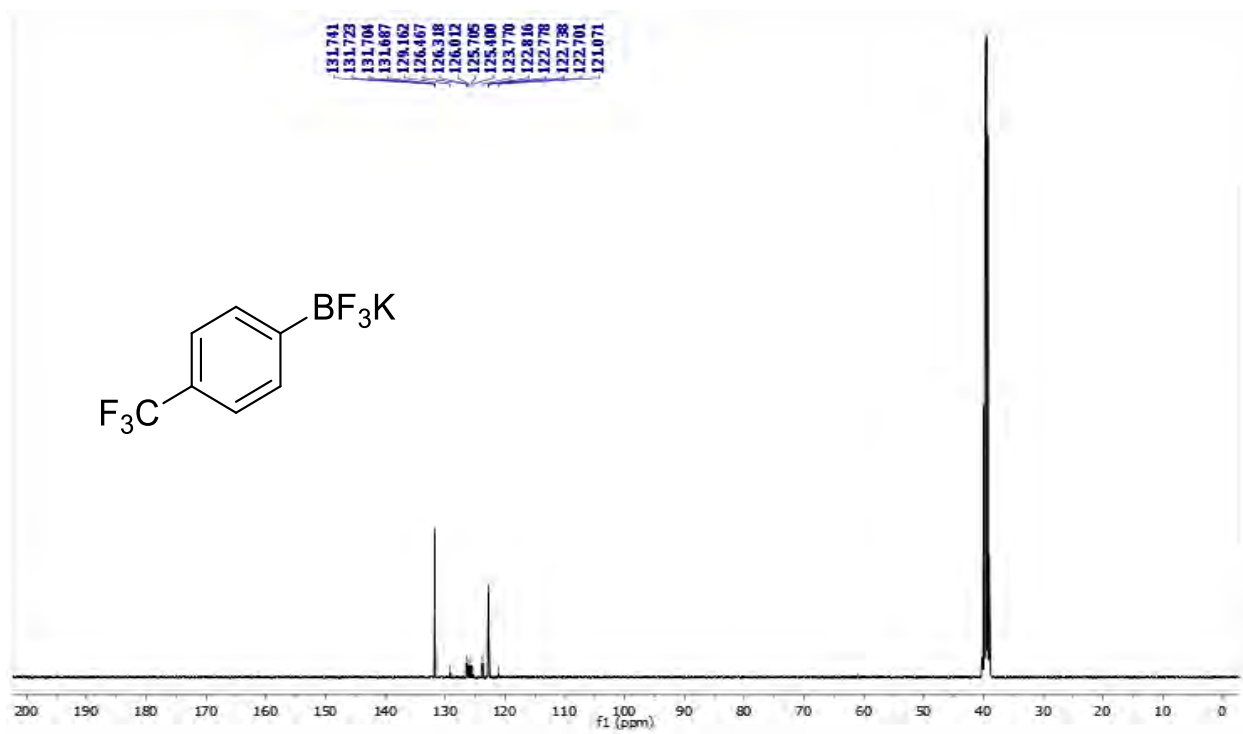


Potassium 4-trifluoromethylphenyltrifluoroborate (**2d**)

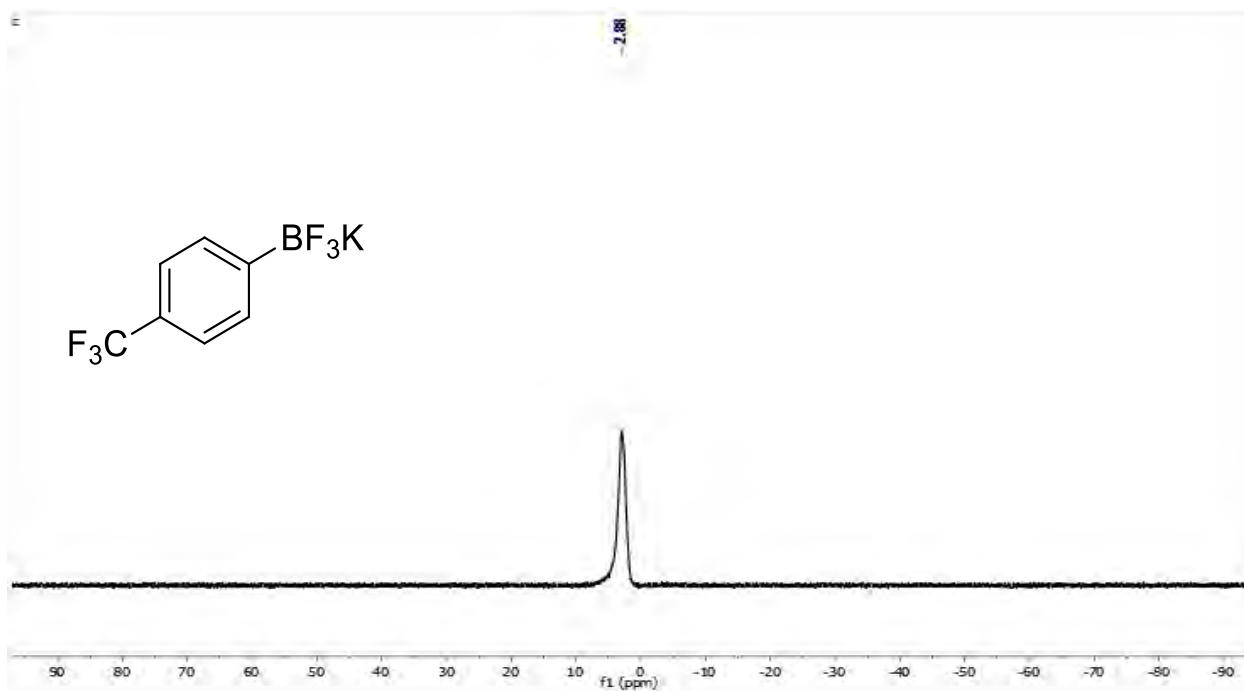
^1H NMR



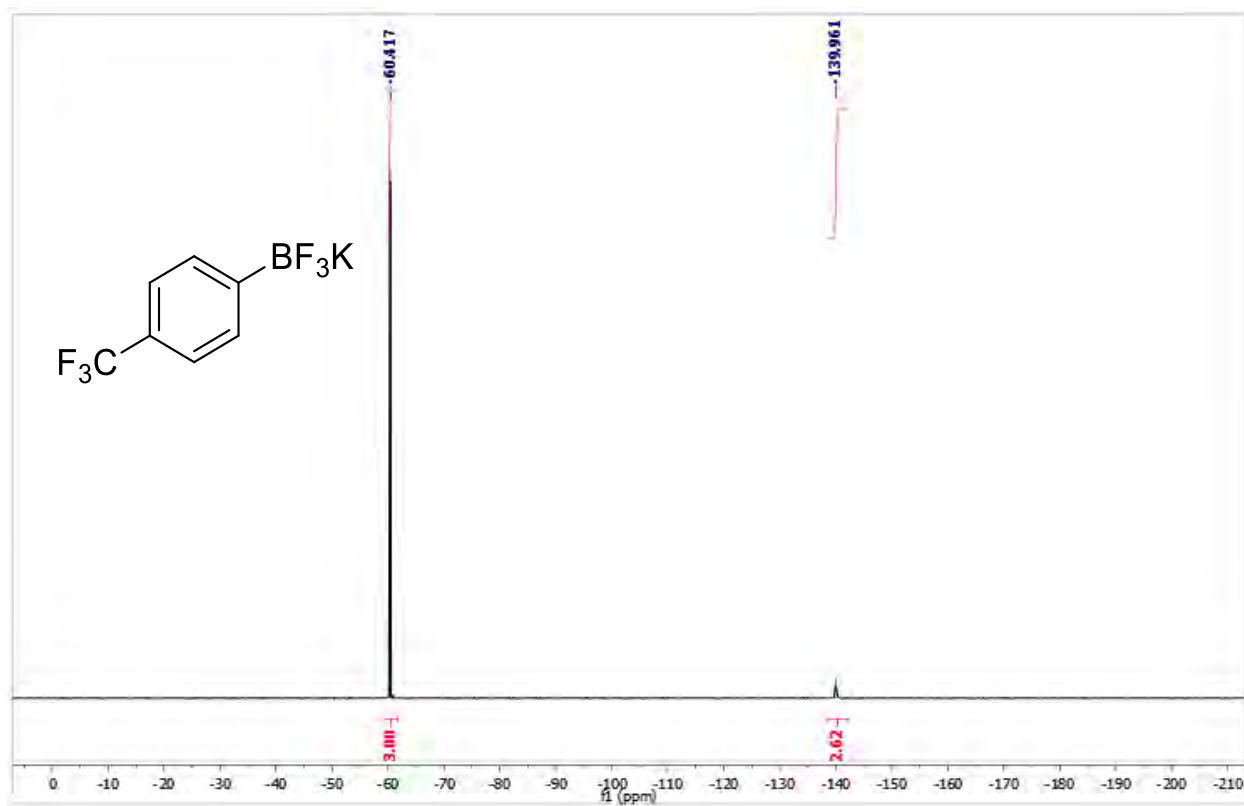
^{13}C NMR



^{11}B NMR

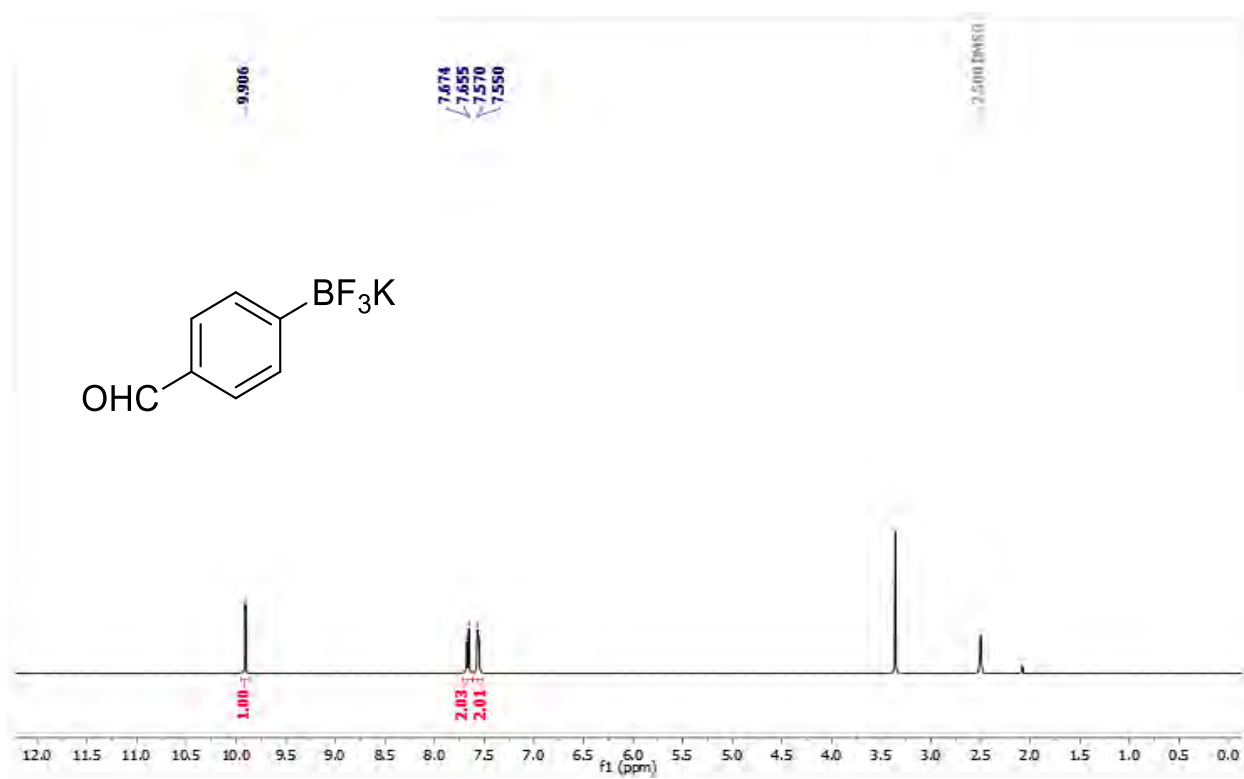


^{19}F NMR

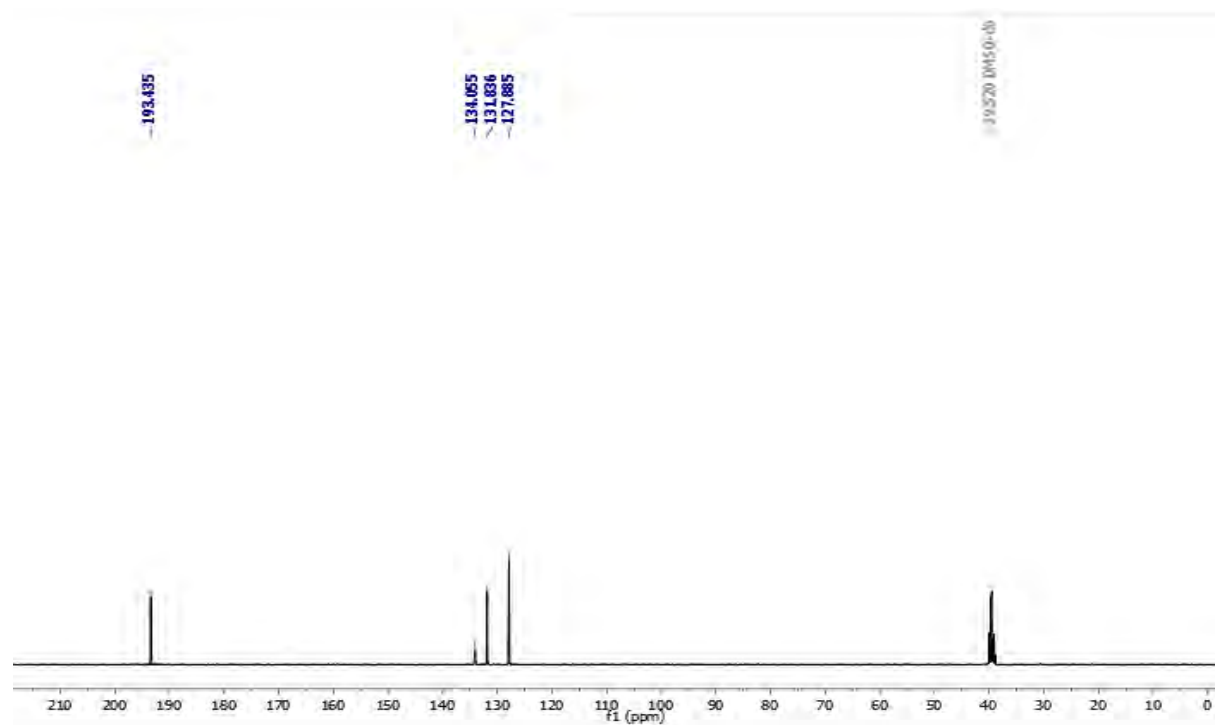


Potassium 4-formylphenyltrifluoroborate (**2e**)

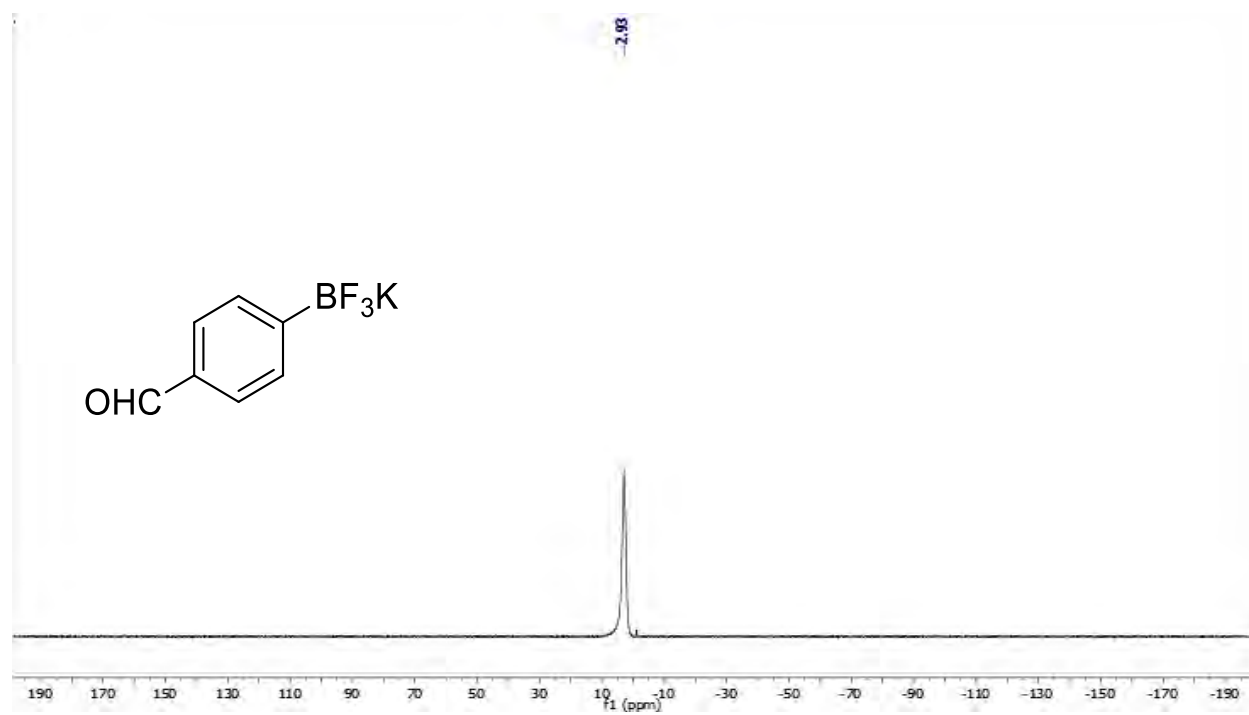
¹H NMR



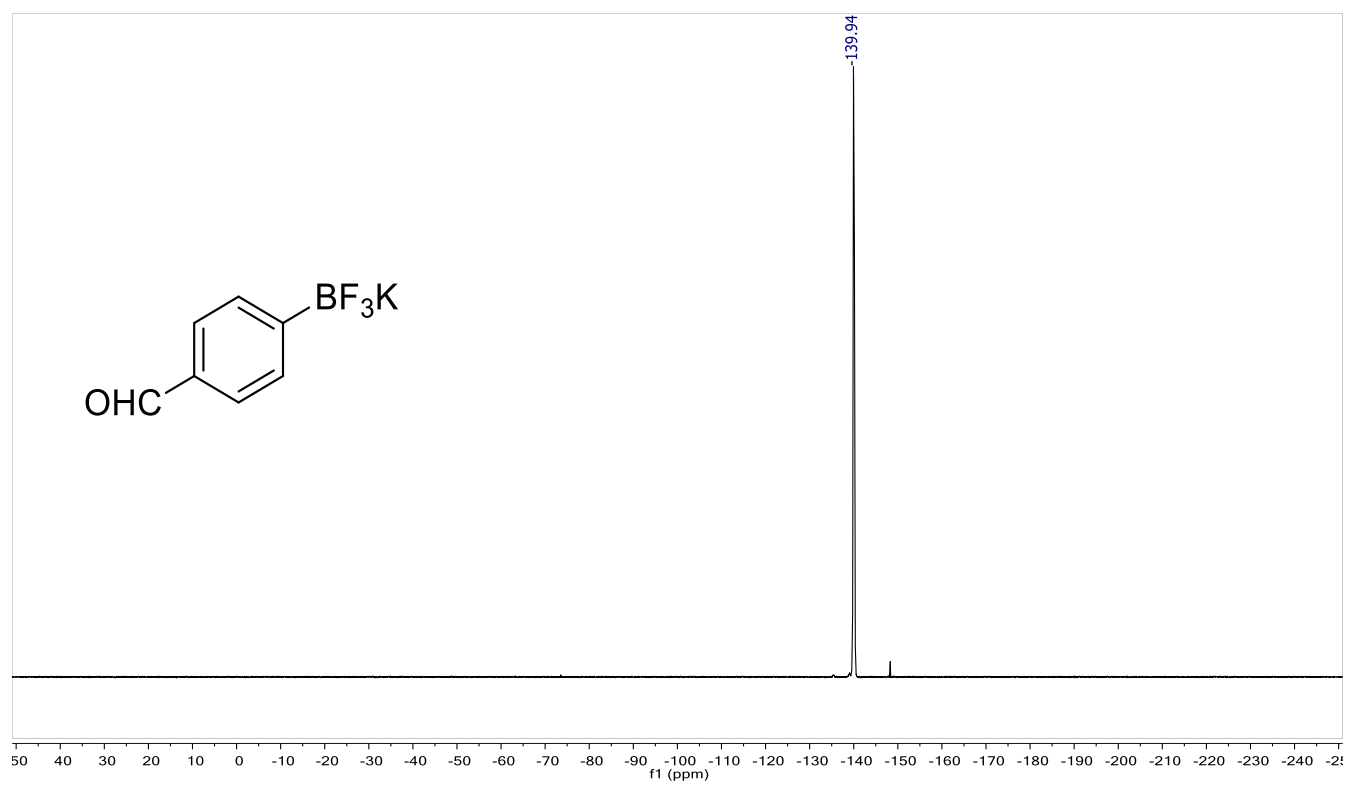
¹³C NMR



^{11}B NMR



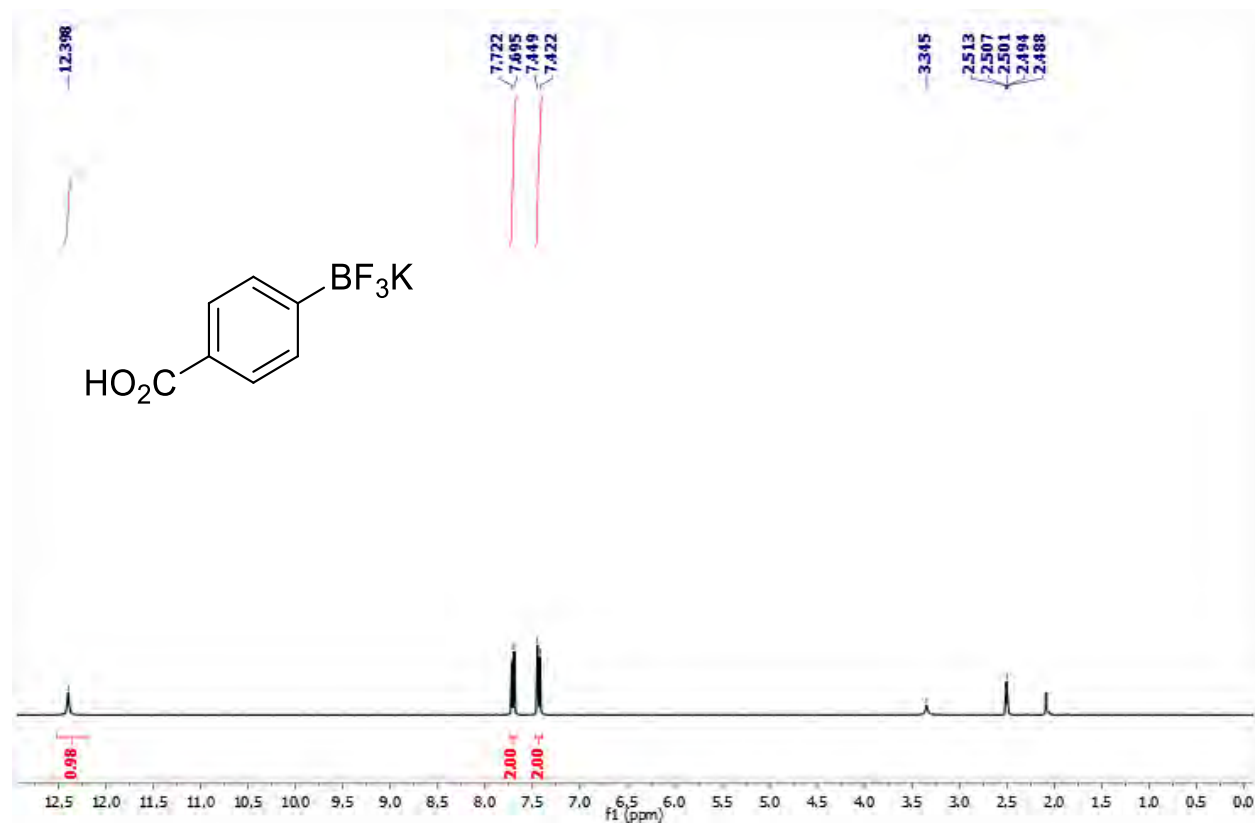
^{19}F NMR



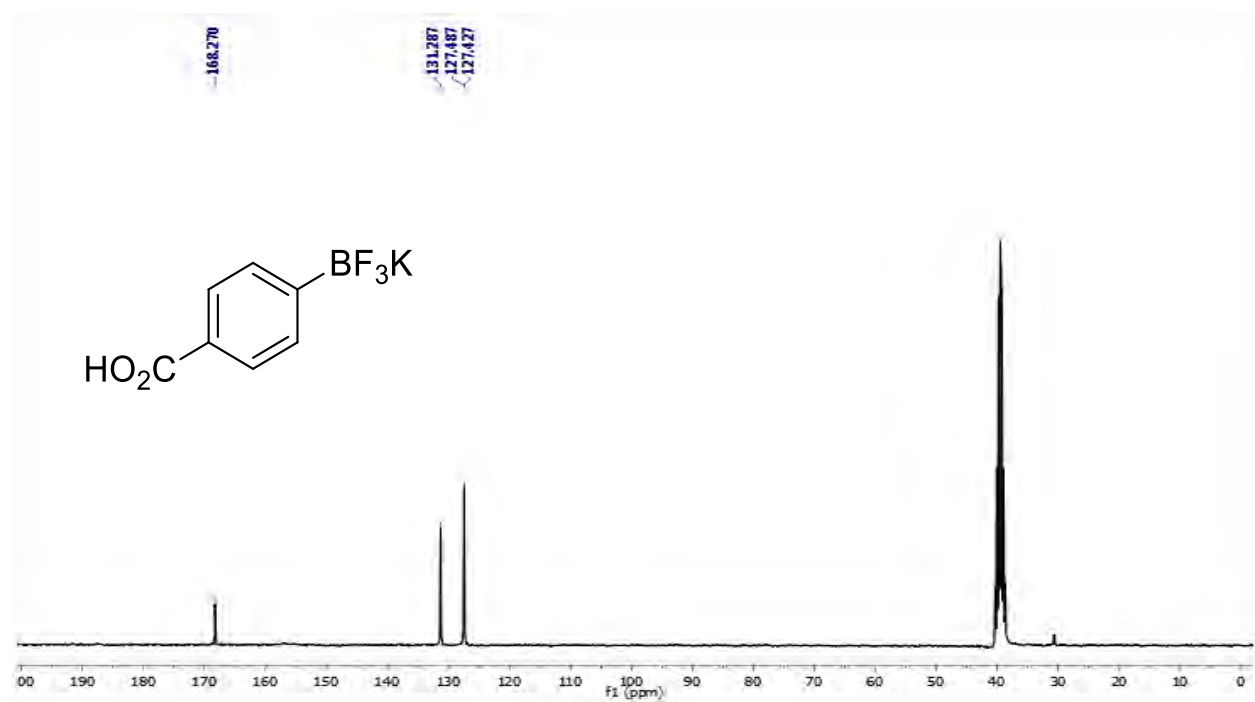
Potassium 4-carboxyphenyltrifluoroborate (**2f**)

^1H

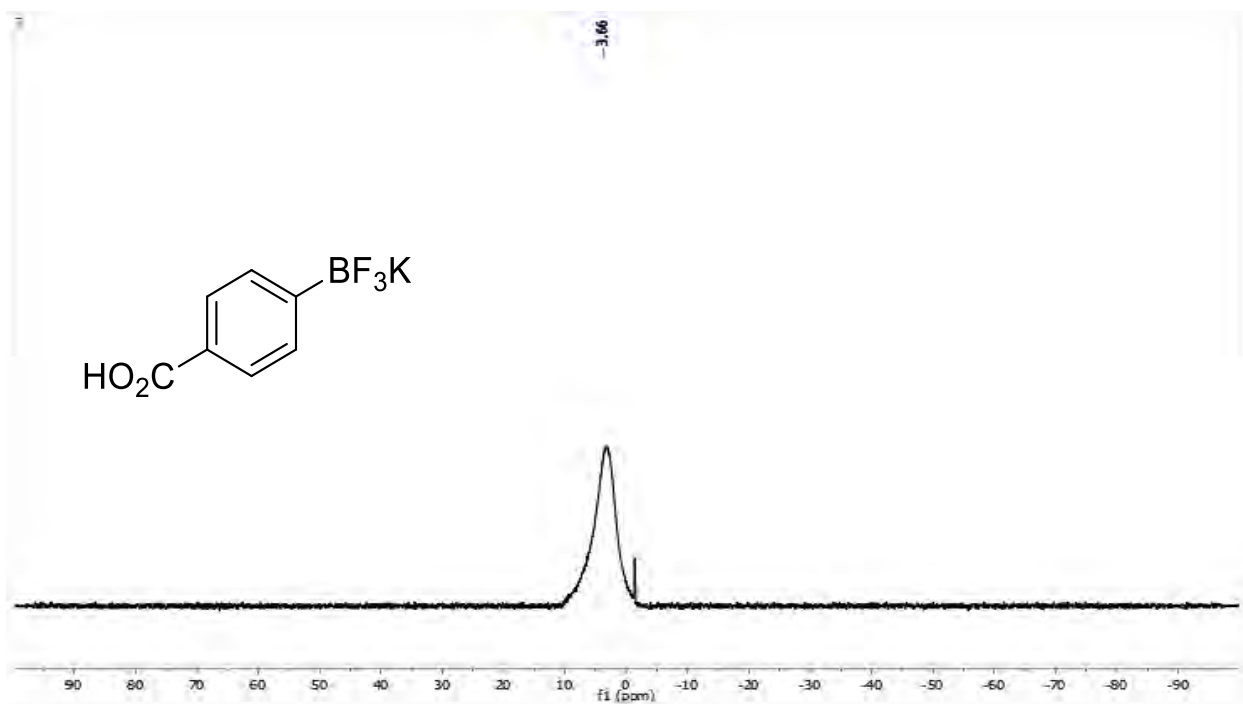
NMR



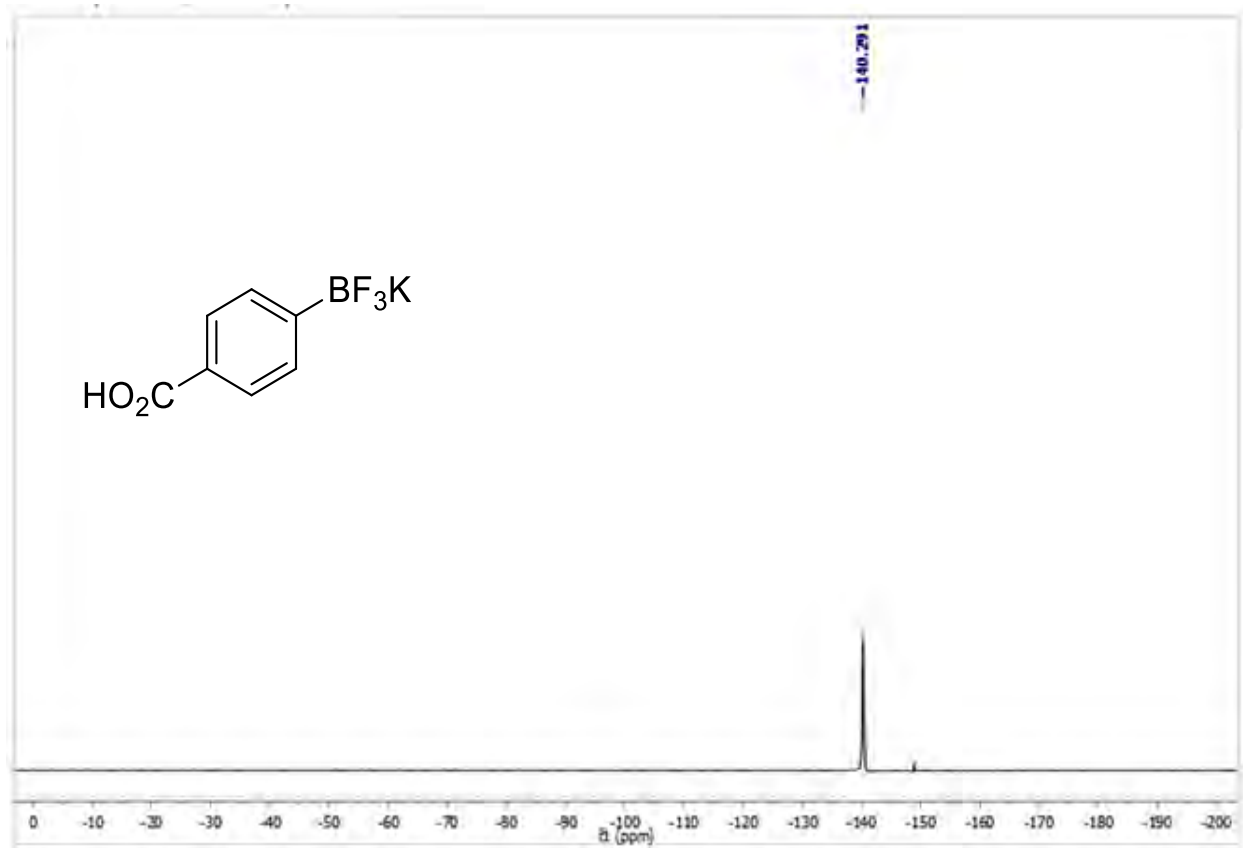
^{13}C NMR



^{11}B NMR

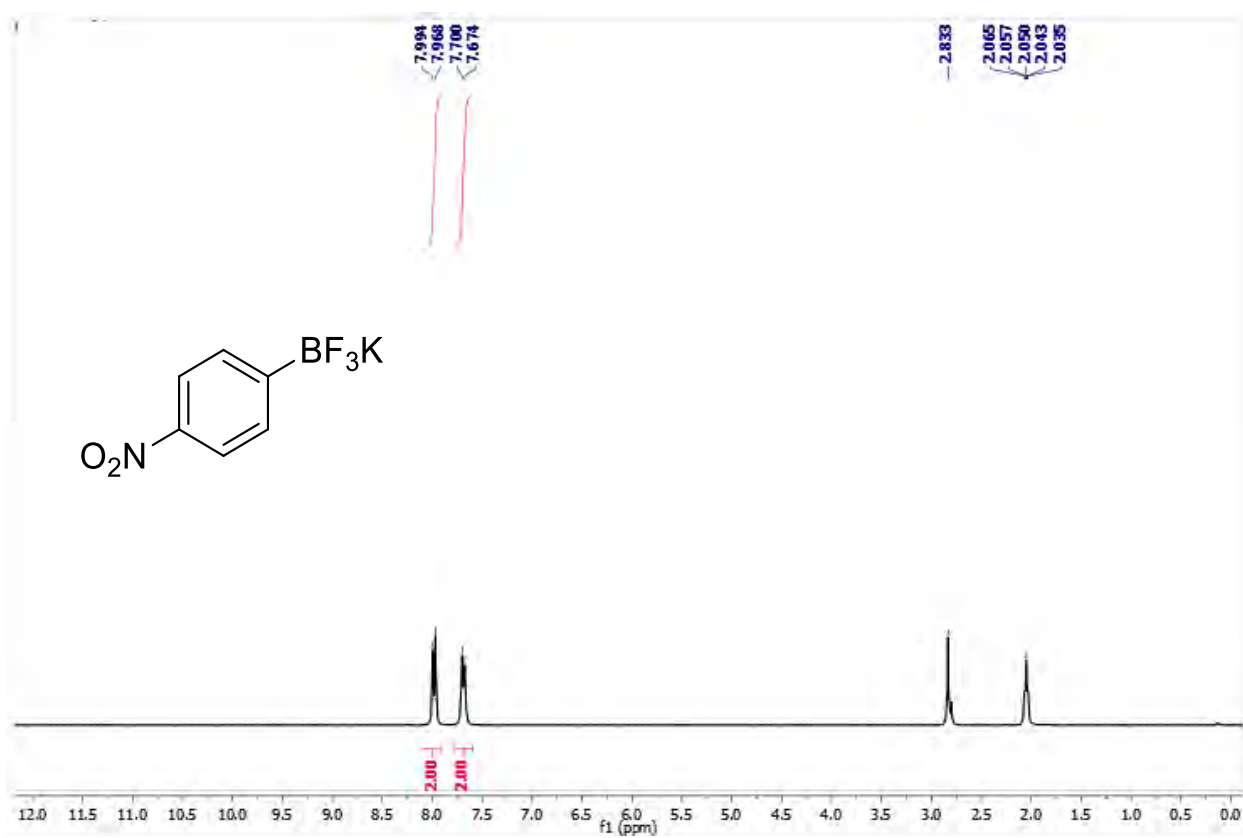


^{19}F NMR

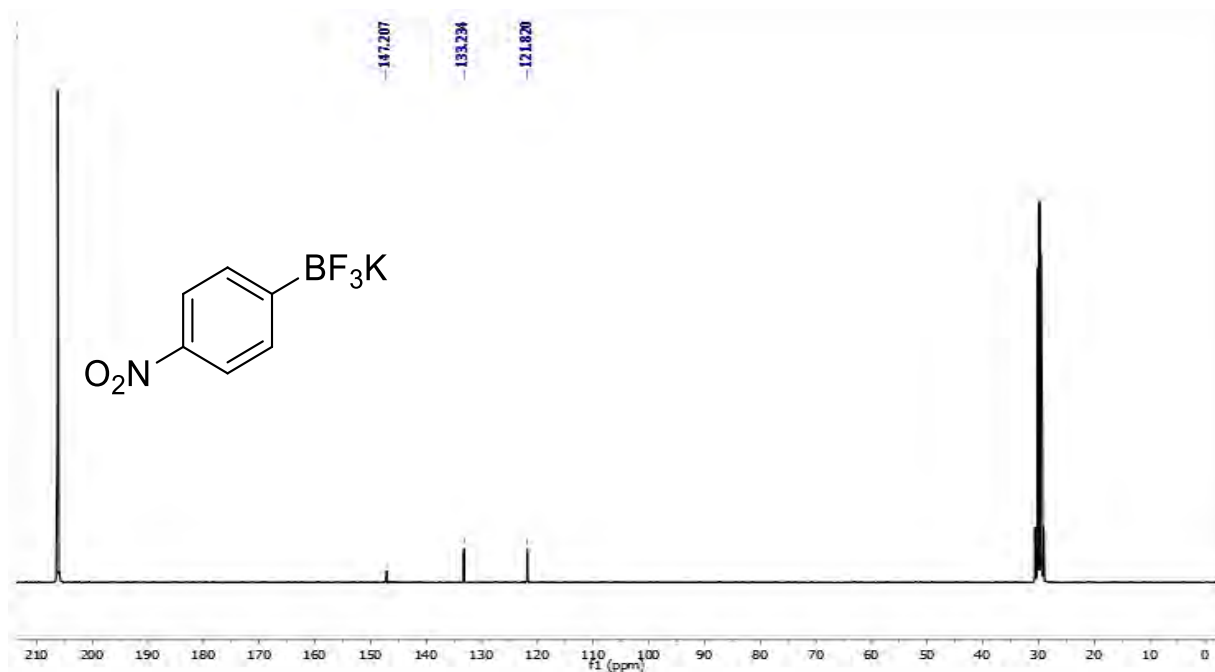


Potassium 4-nitrophenyltrifluoroborate (**2g**)

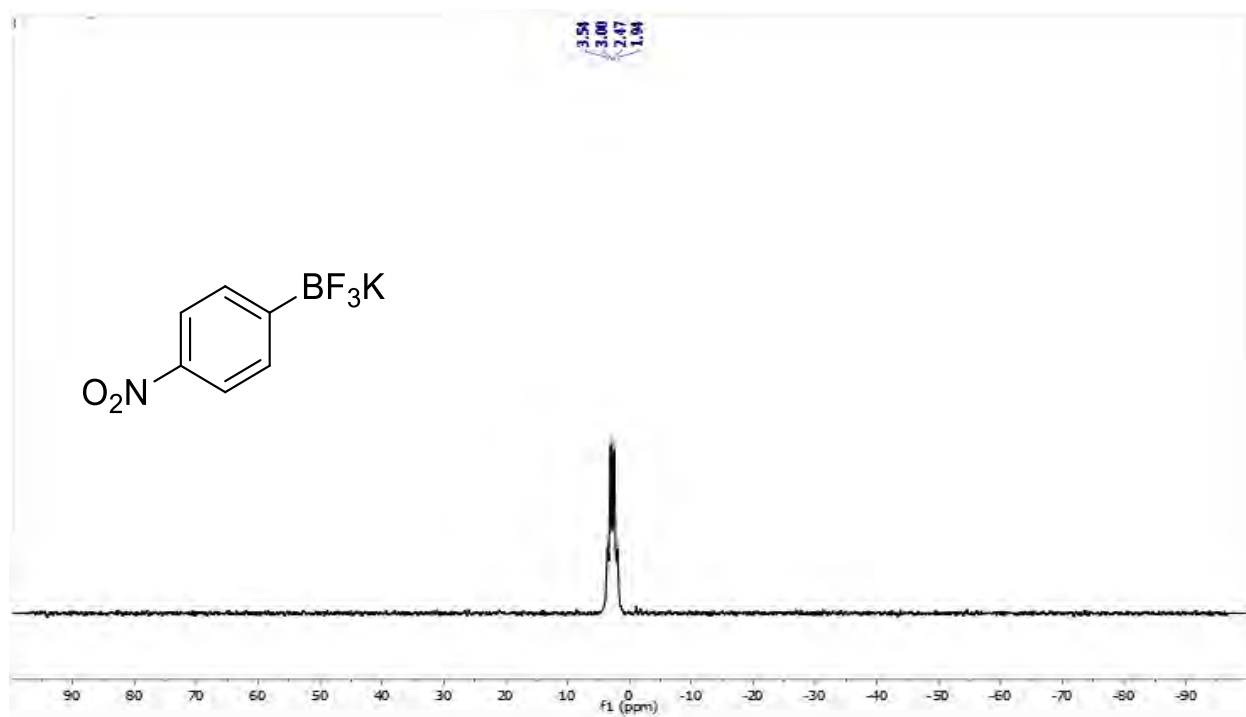
^1H NMR



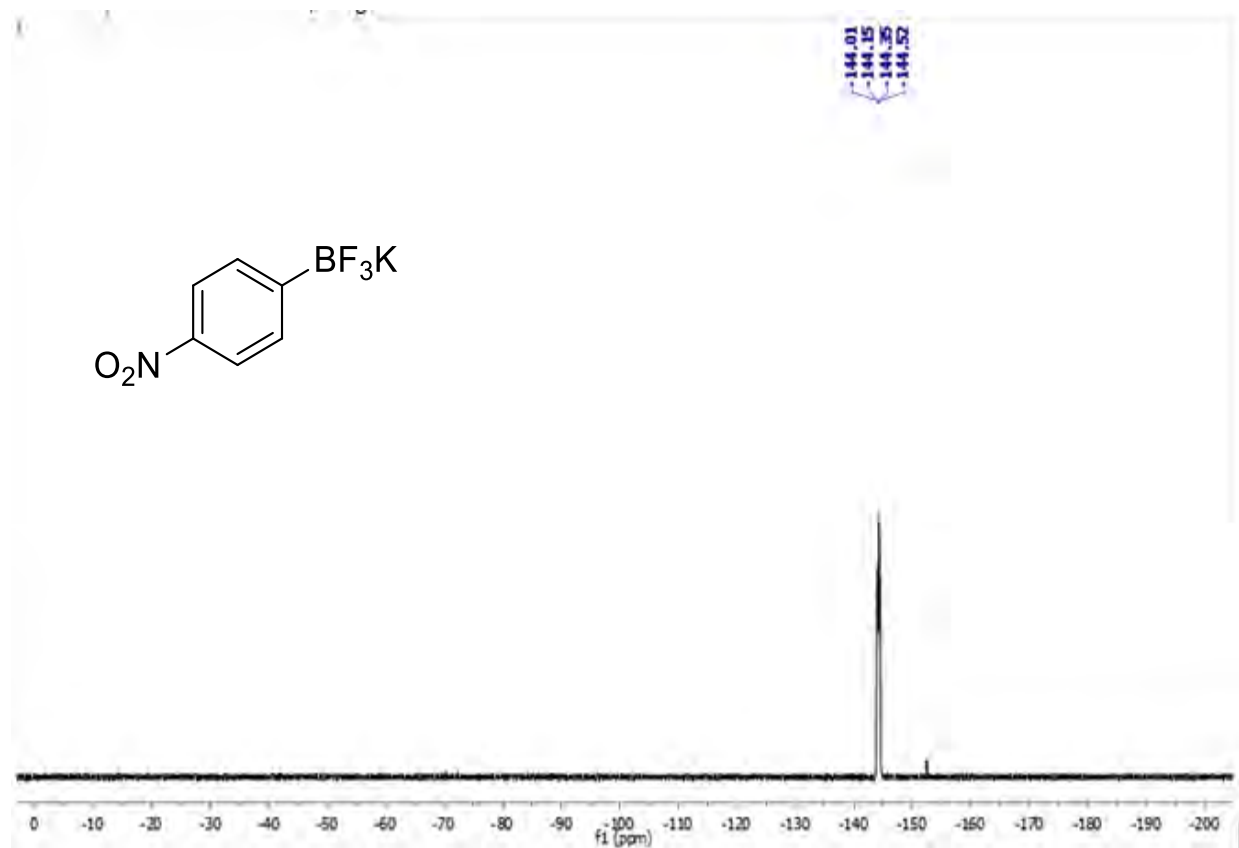
^{13}C NMR



^{11}B NMR

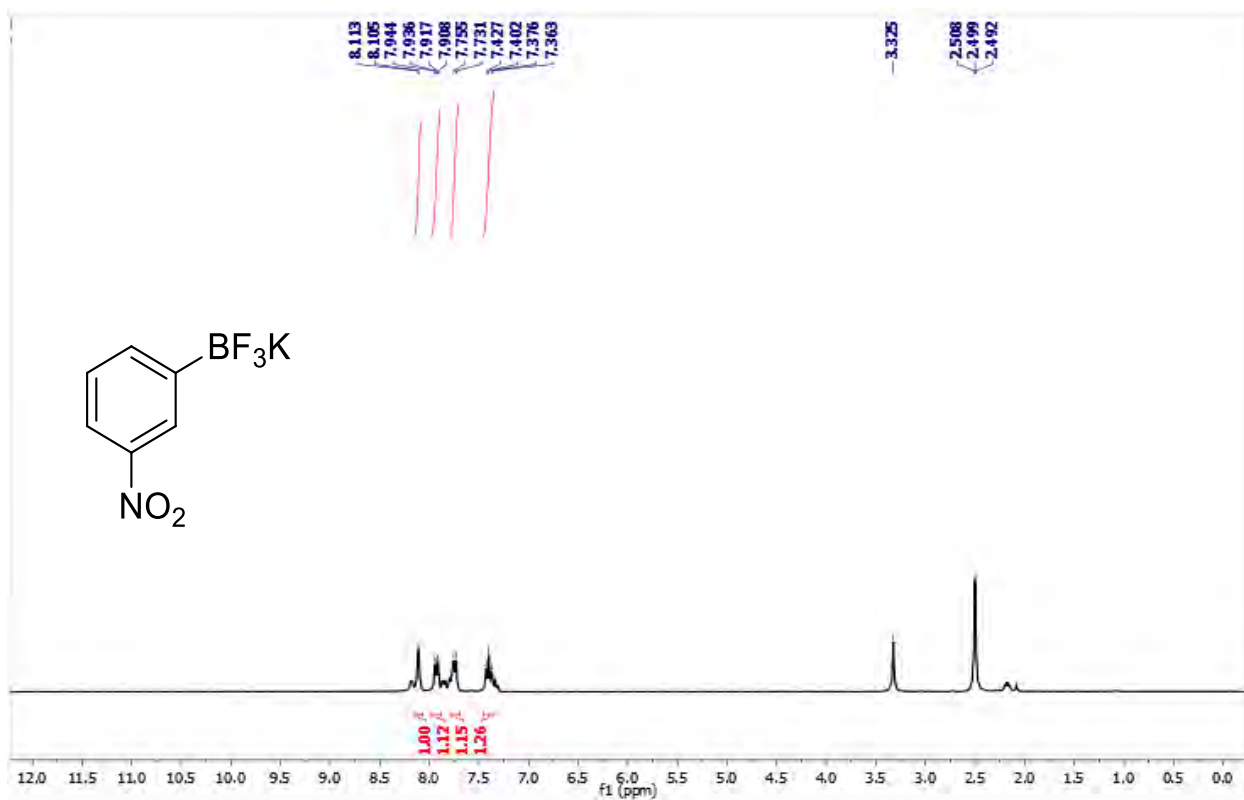


^{19}F NMR

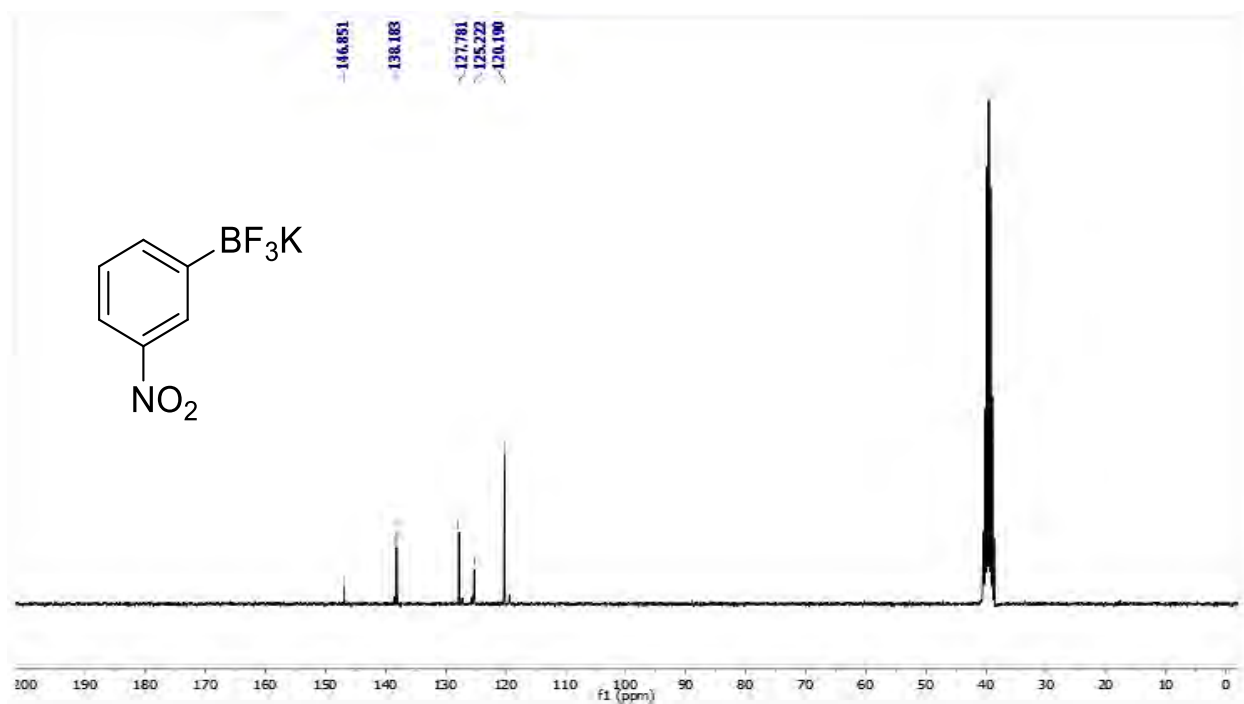


Potassium 3-nitrophenyltrifluoroborate (**2h**)

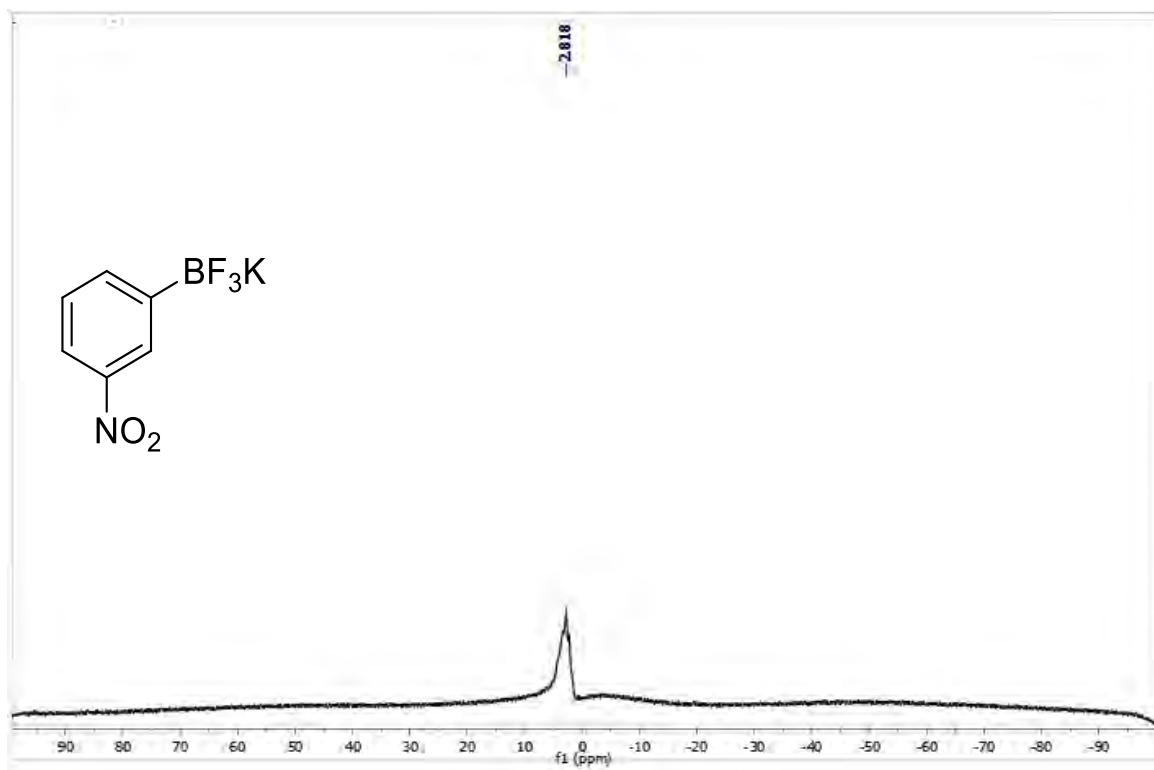
¹H NMR



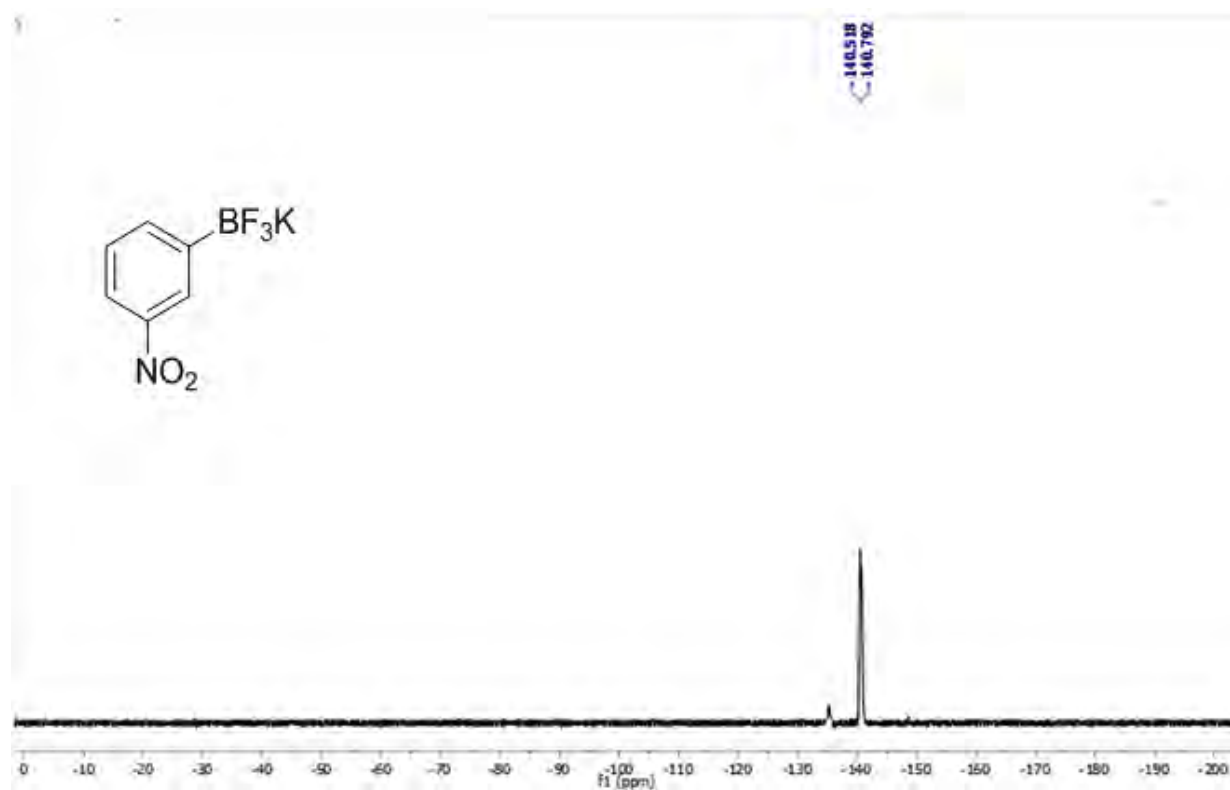
¹³C NMR



^{11}B NMR

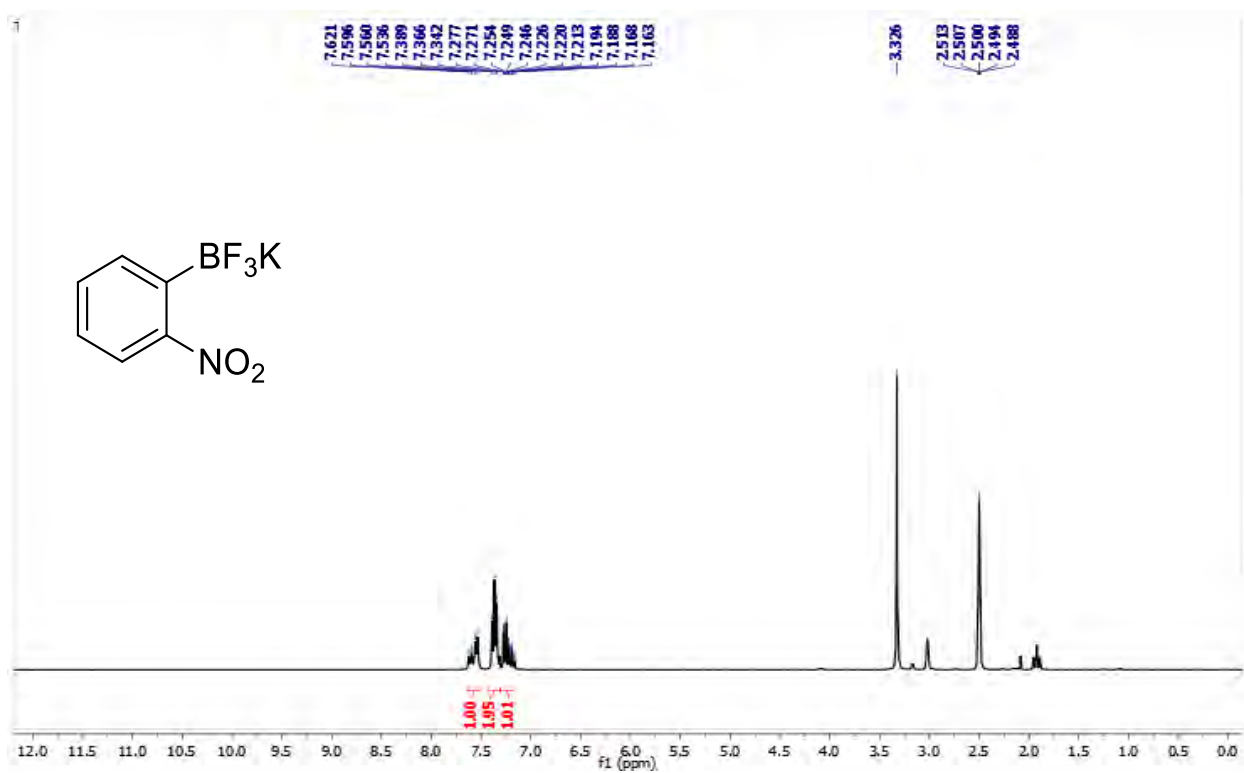


^{19}F NMR

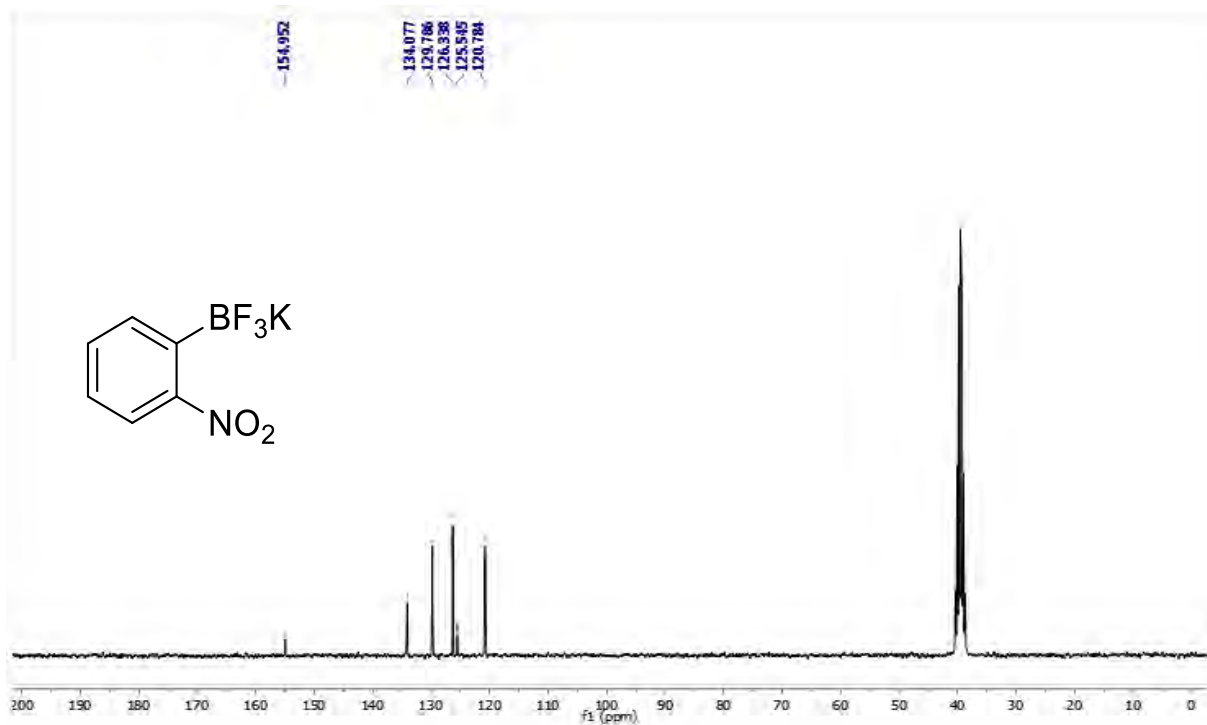


Potassium 2-nitrophenyltrifluoroborate (**2i**)

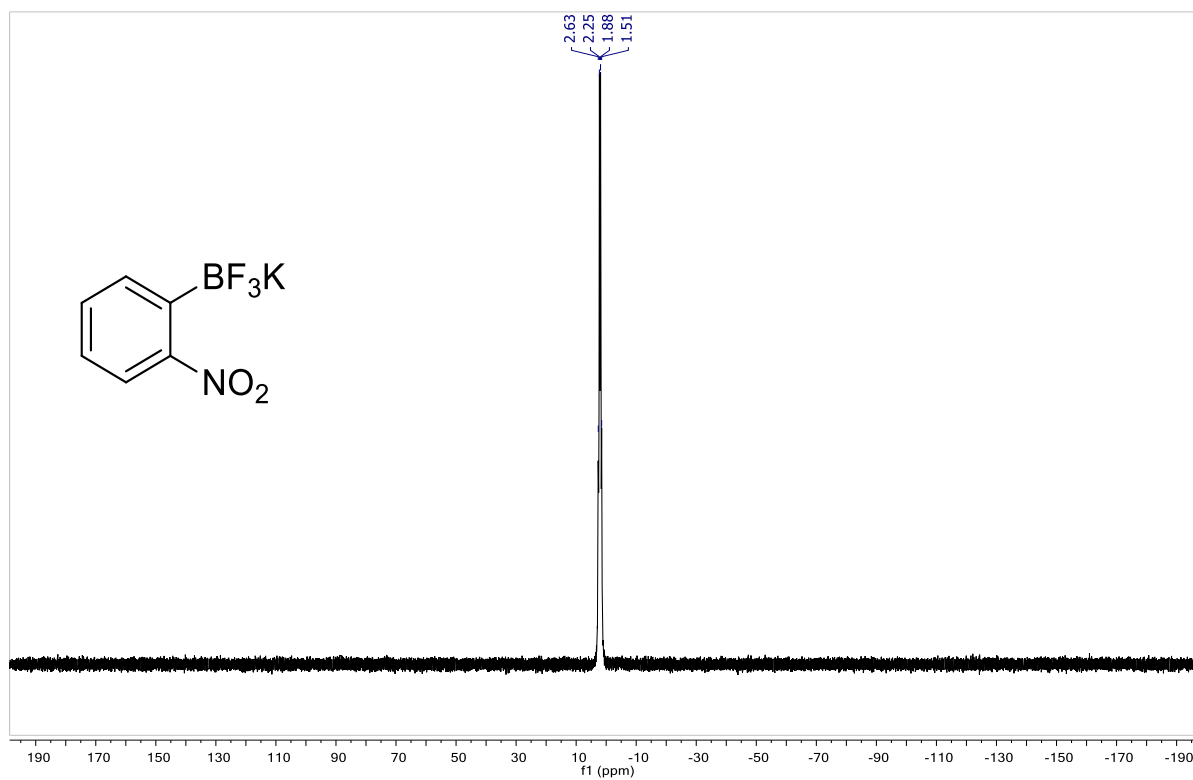
^1H NMR



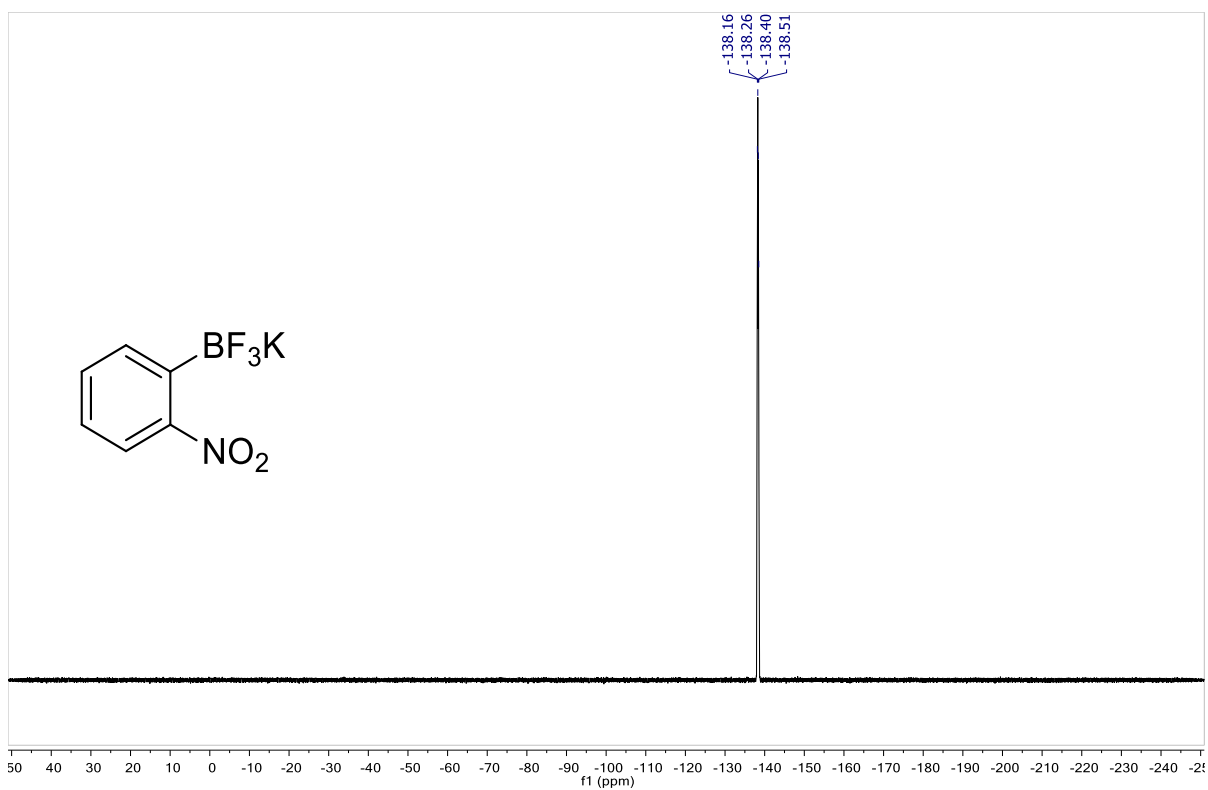
^{13}C NMR



^{11}B NMR

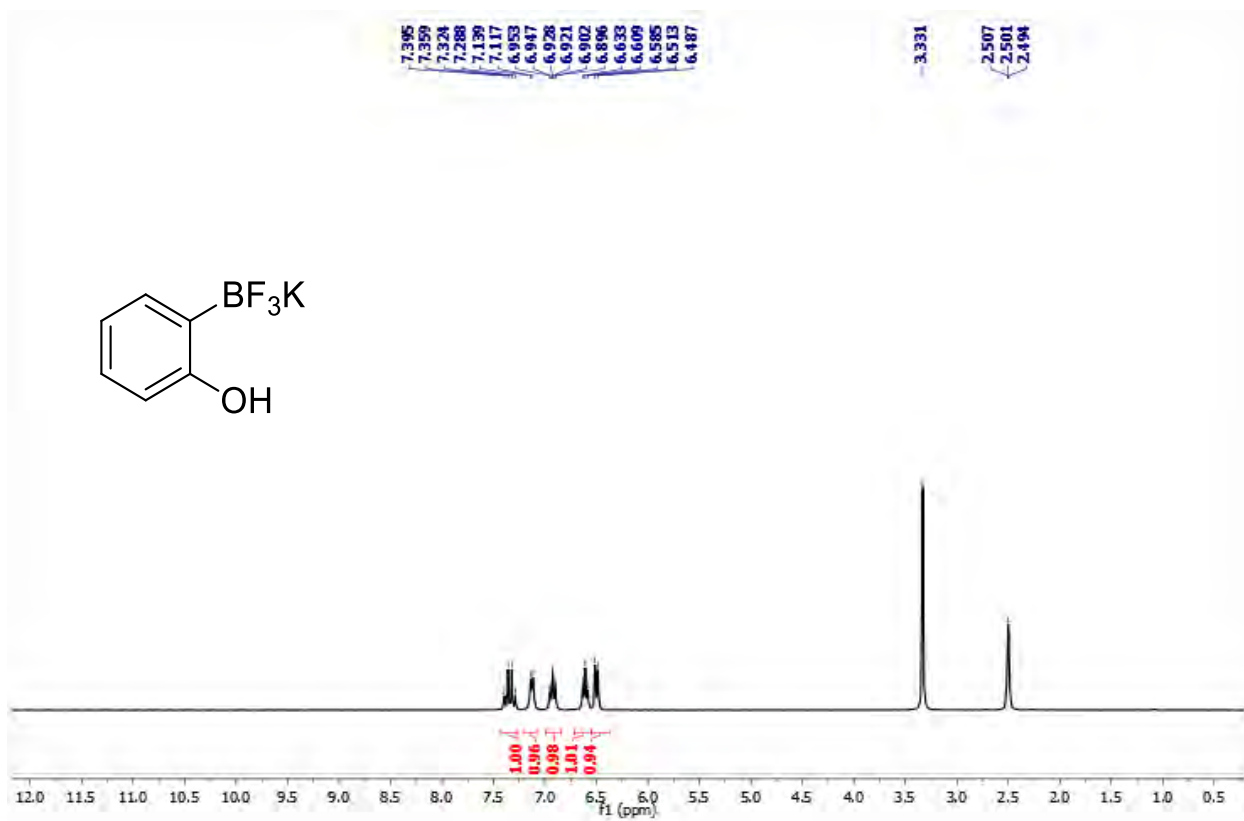


^{19}F NMR

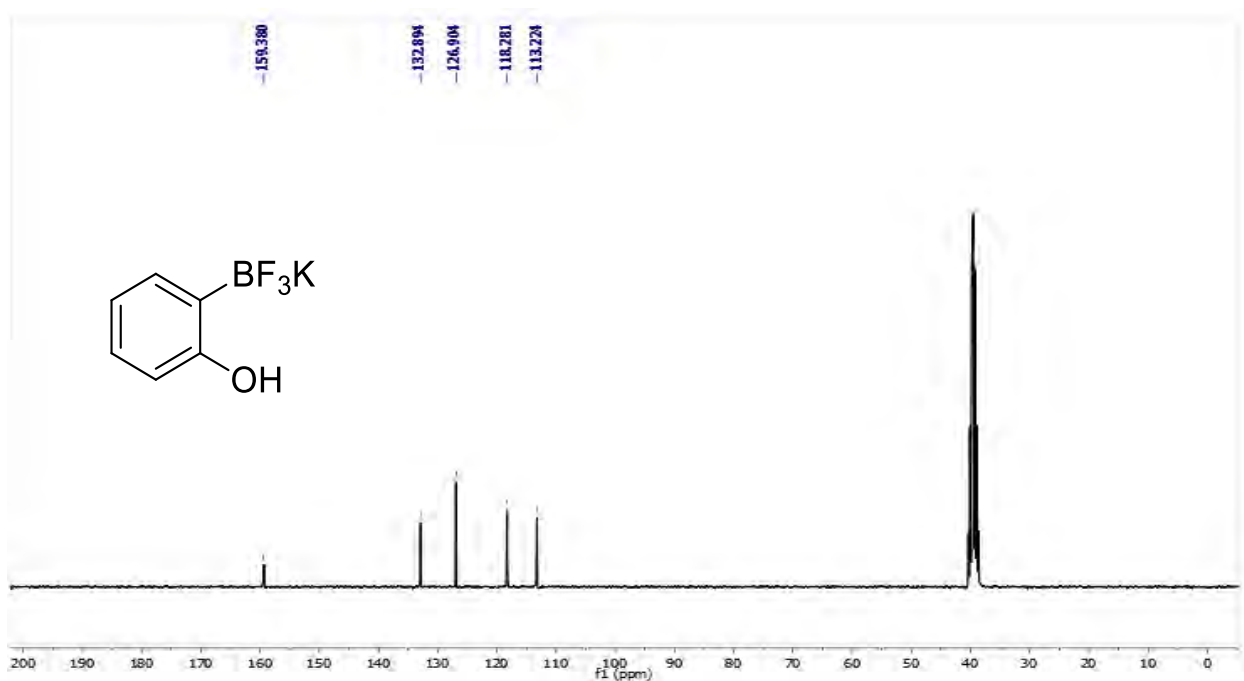


Potassium 2-hydroxyphenyltrifluoroborate (**2j**)

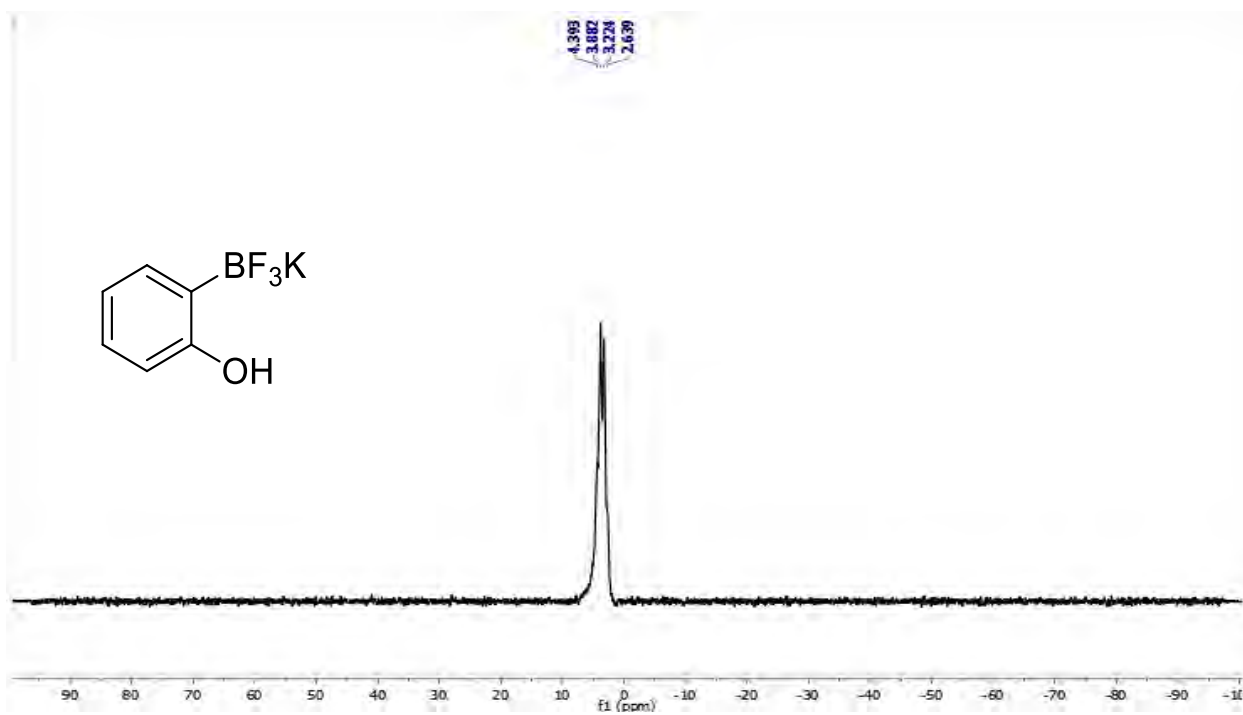
¹H NMR



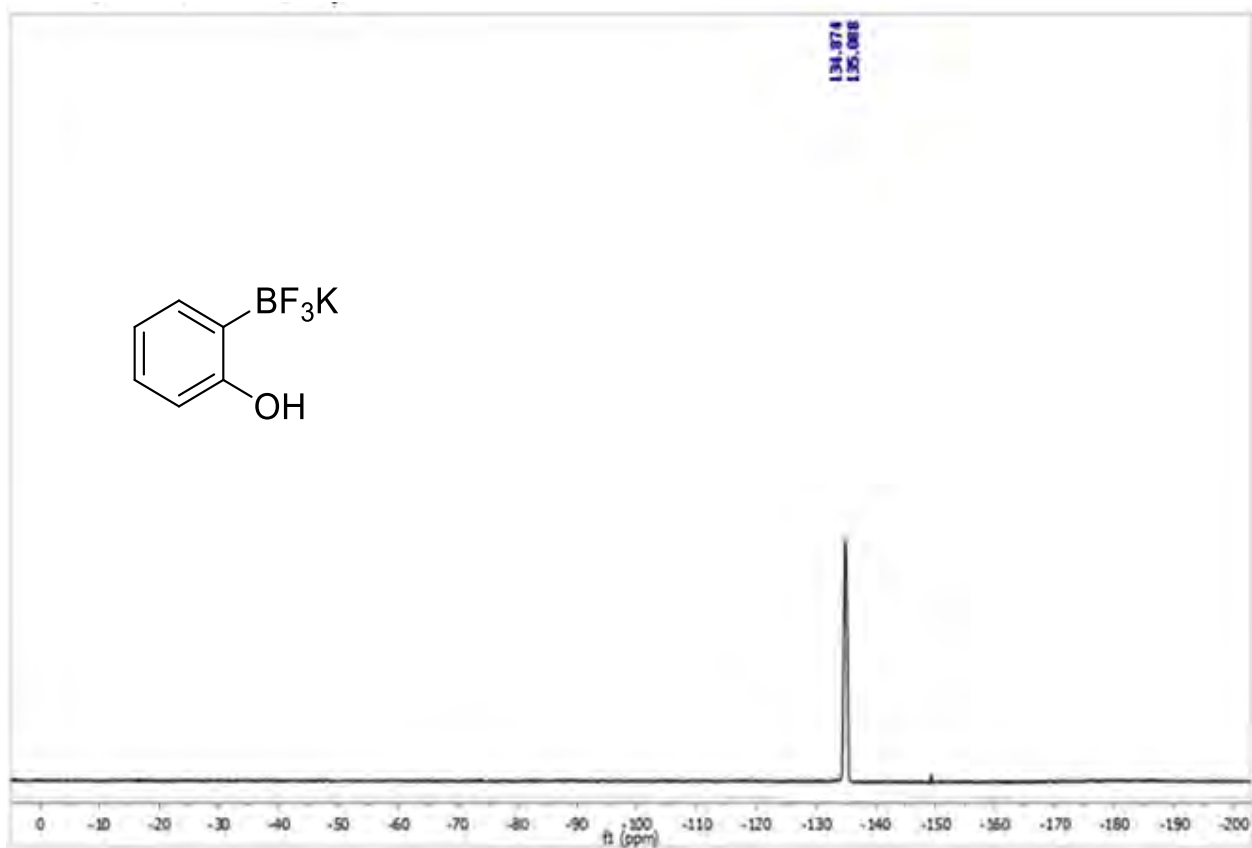
¹³C NMR



^{11}B NMR

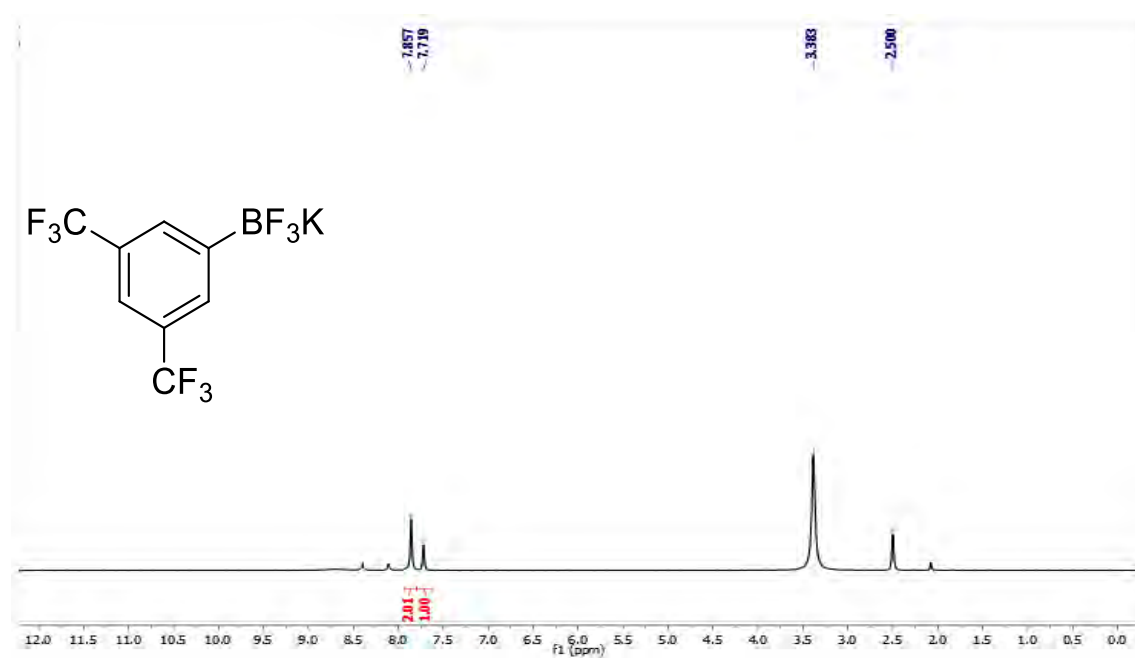


^{19}F NMR

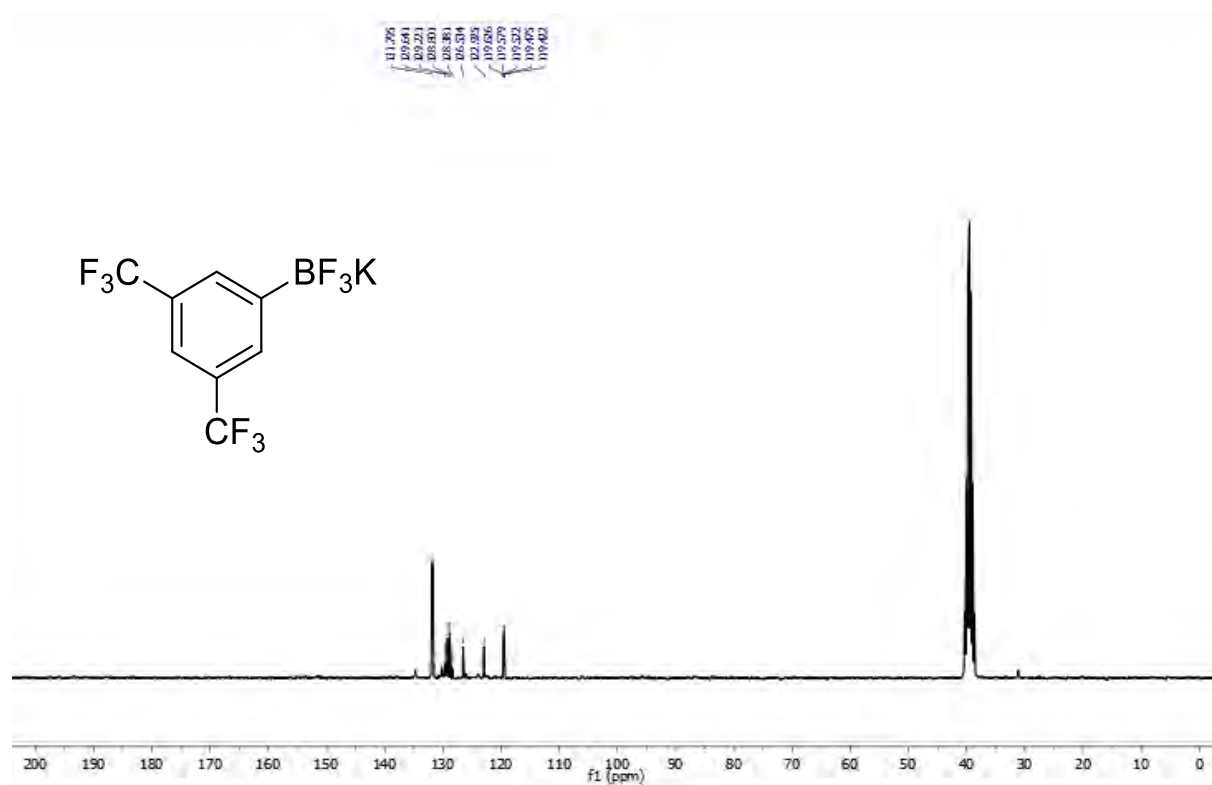


Potassium 3,5-bis(trifluoromethyl)phenyltrifluoroborate (**2k**)

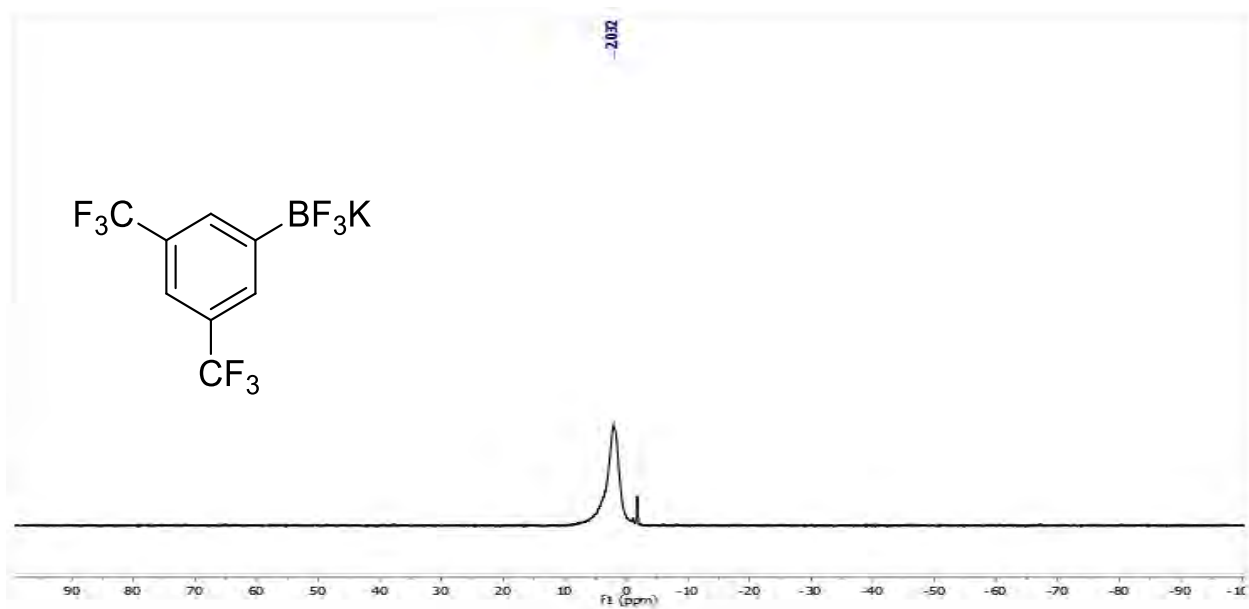
^1H NMR



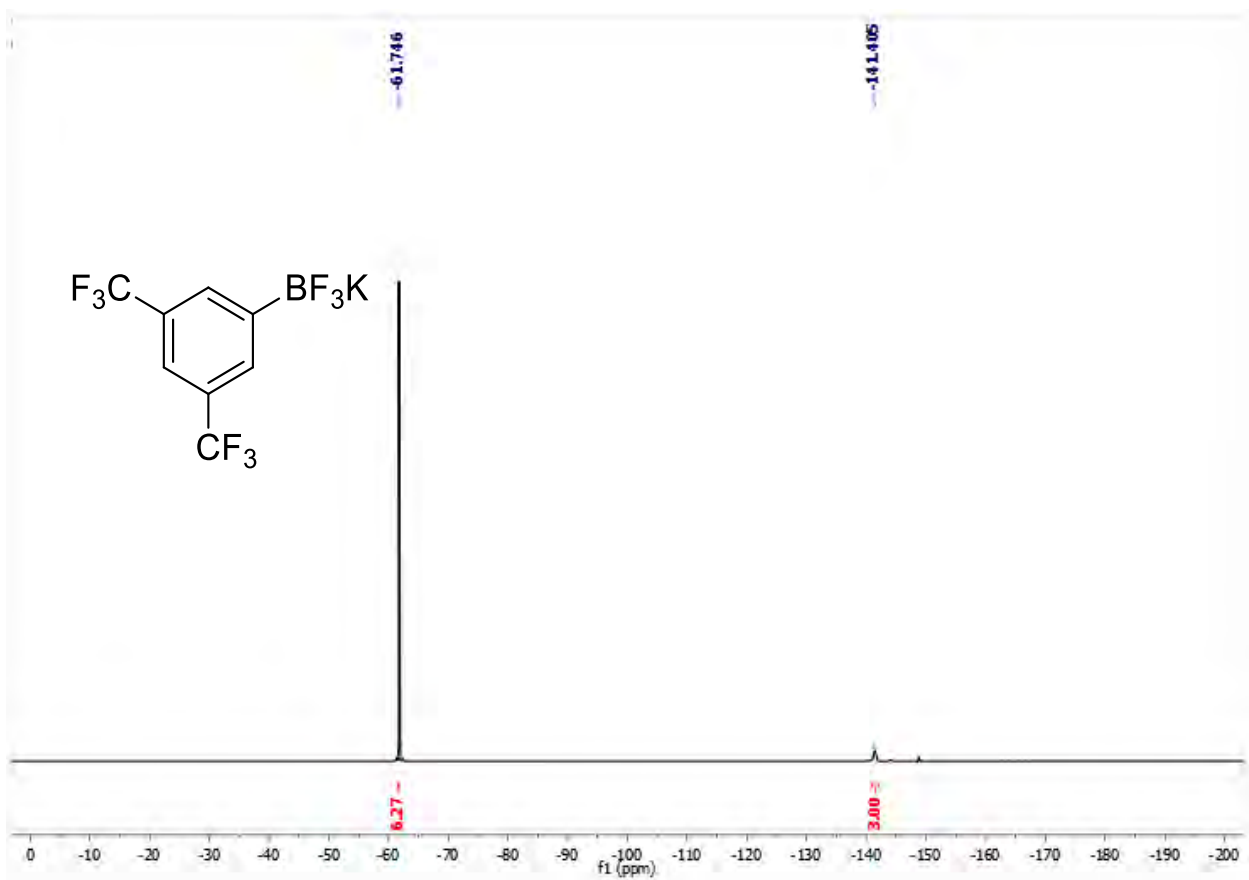
^{13}C NMR



^{11}B NMR

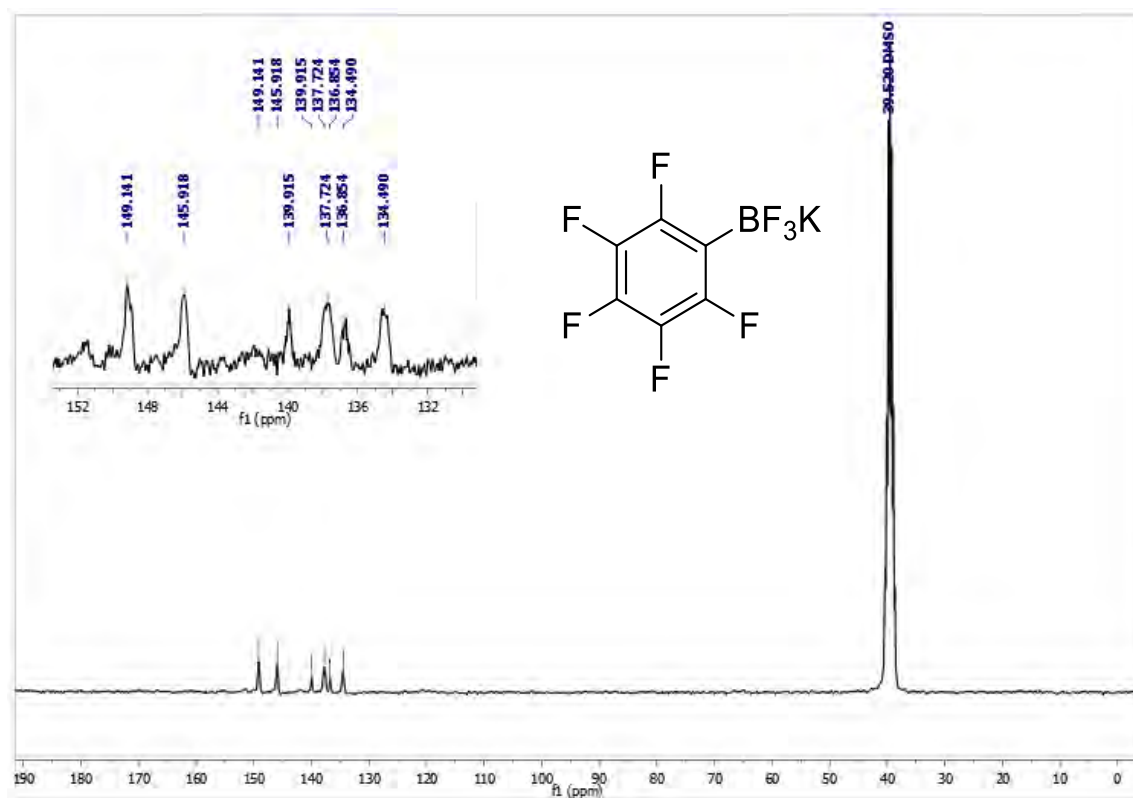


^{19}F NMR

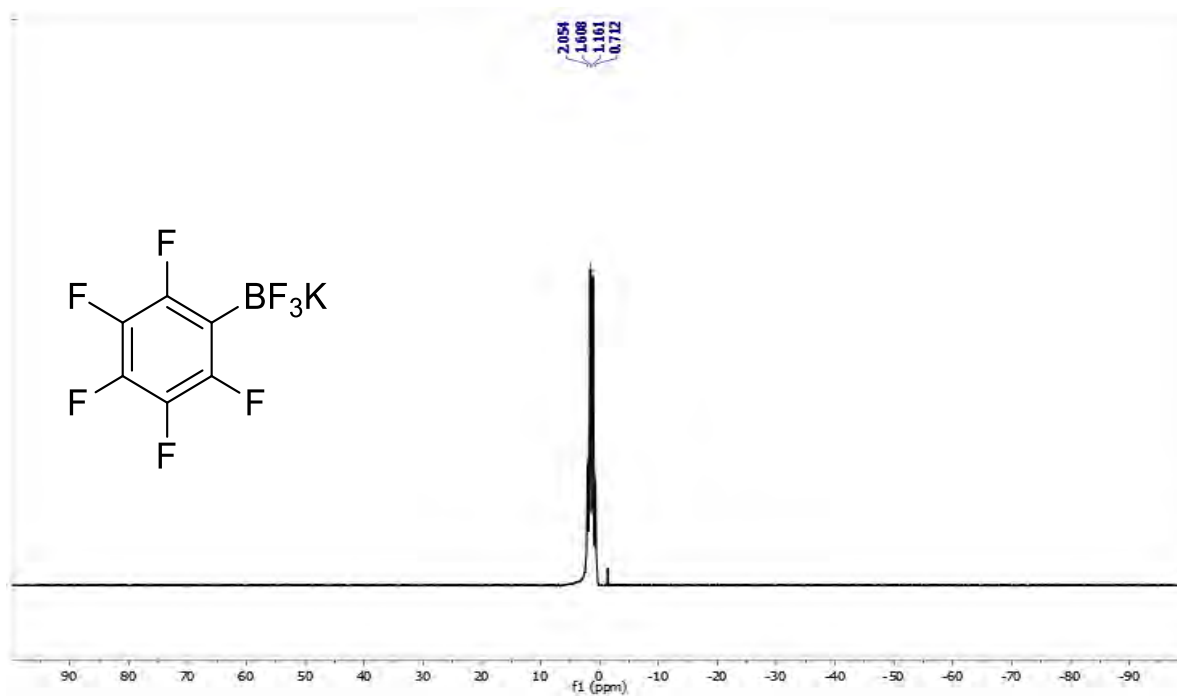


Potassium 2,3,4,5,6-pentafluorophenyltrifluoroborate (2I)

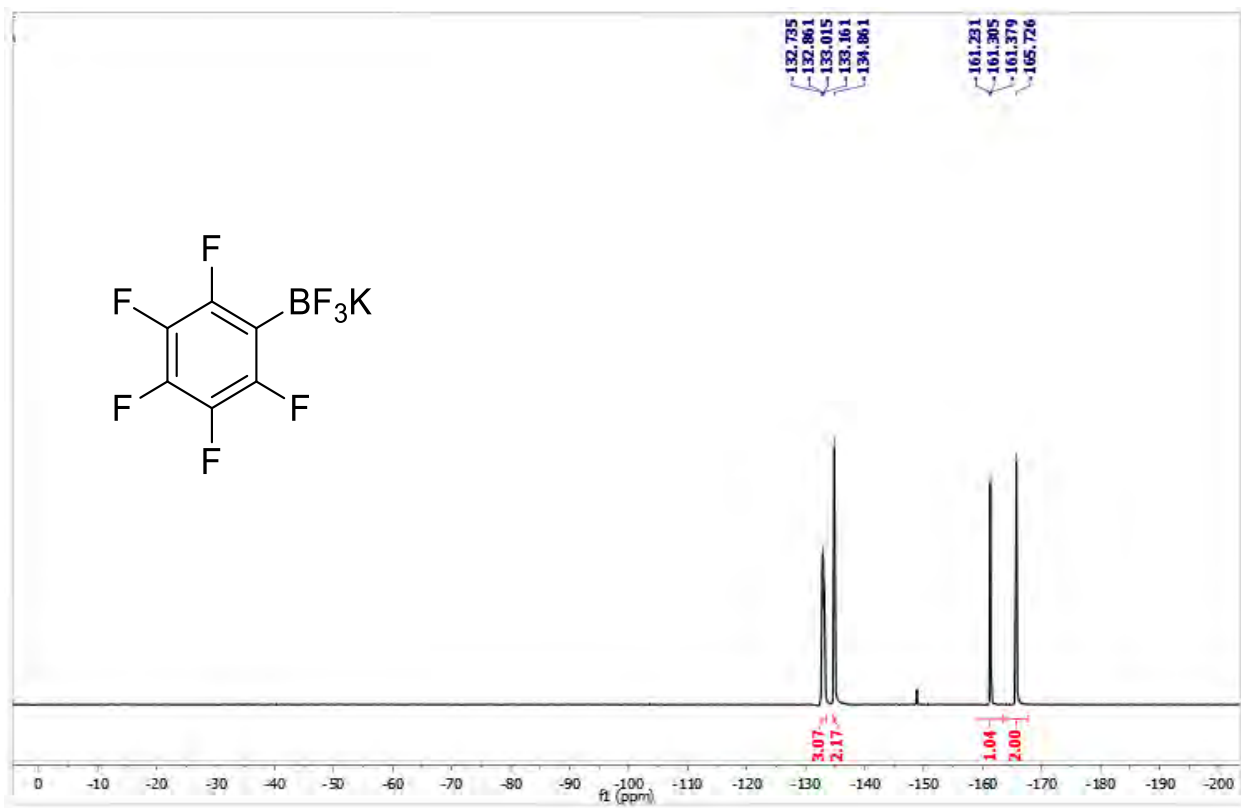
^{13}C NMR



^{11}B NMR

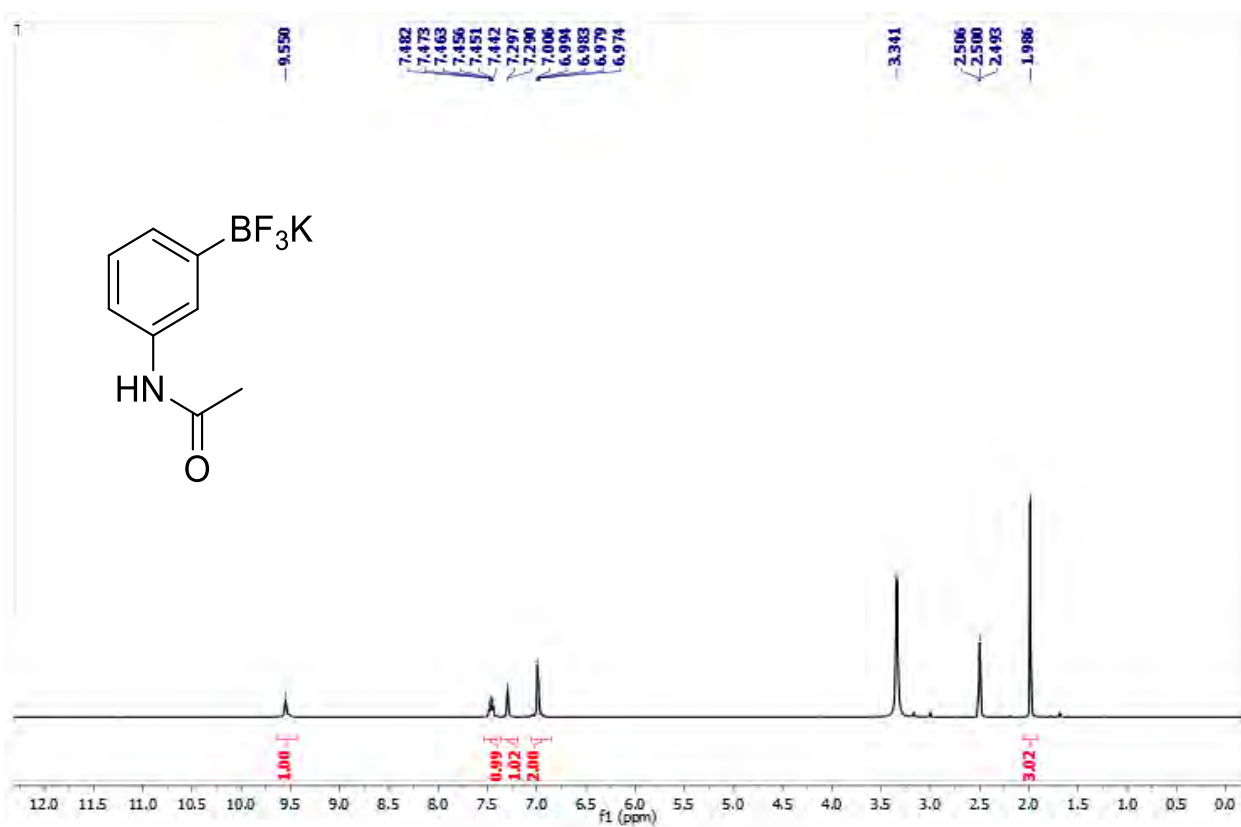


^{19}F NMR

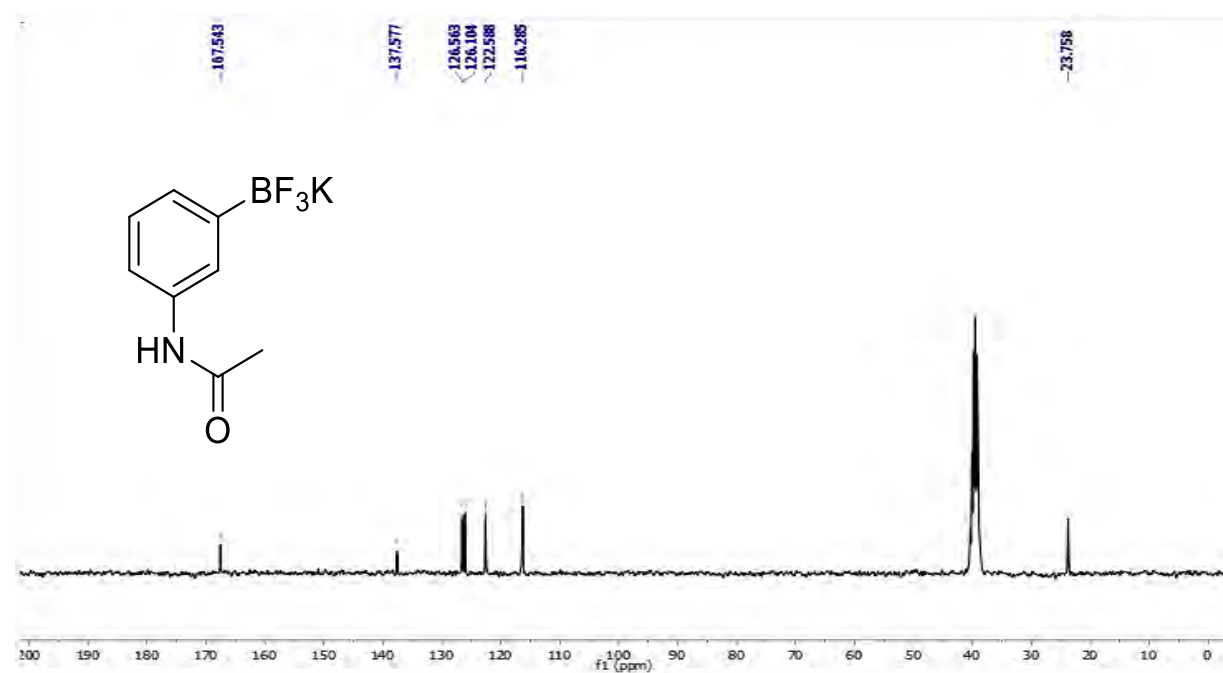


Potassium 3-nitrophenyltrifluoroborate (**2m**)

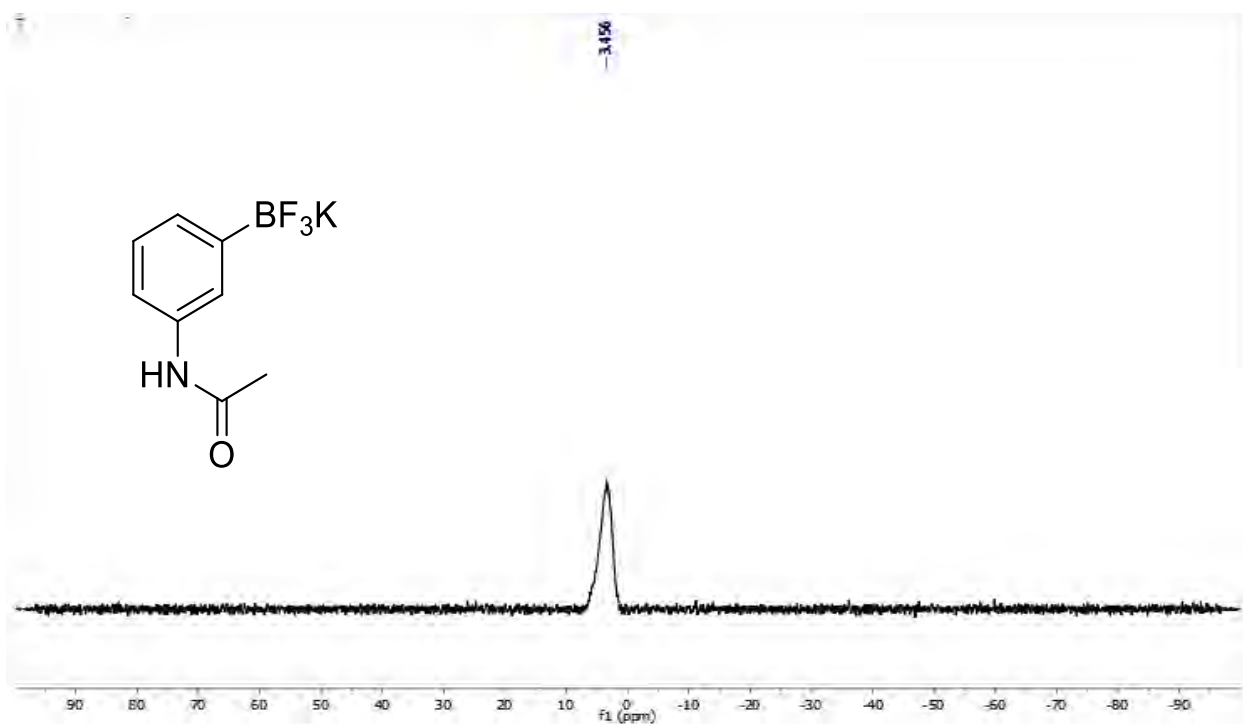
^1H NMR



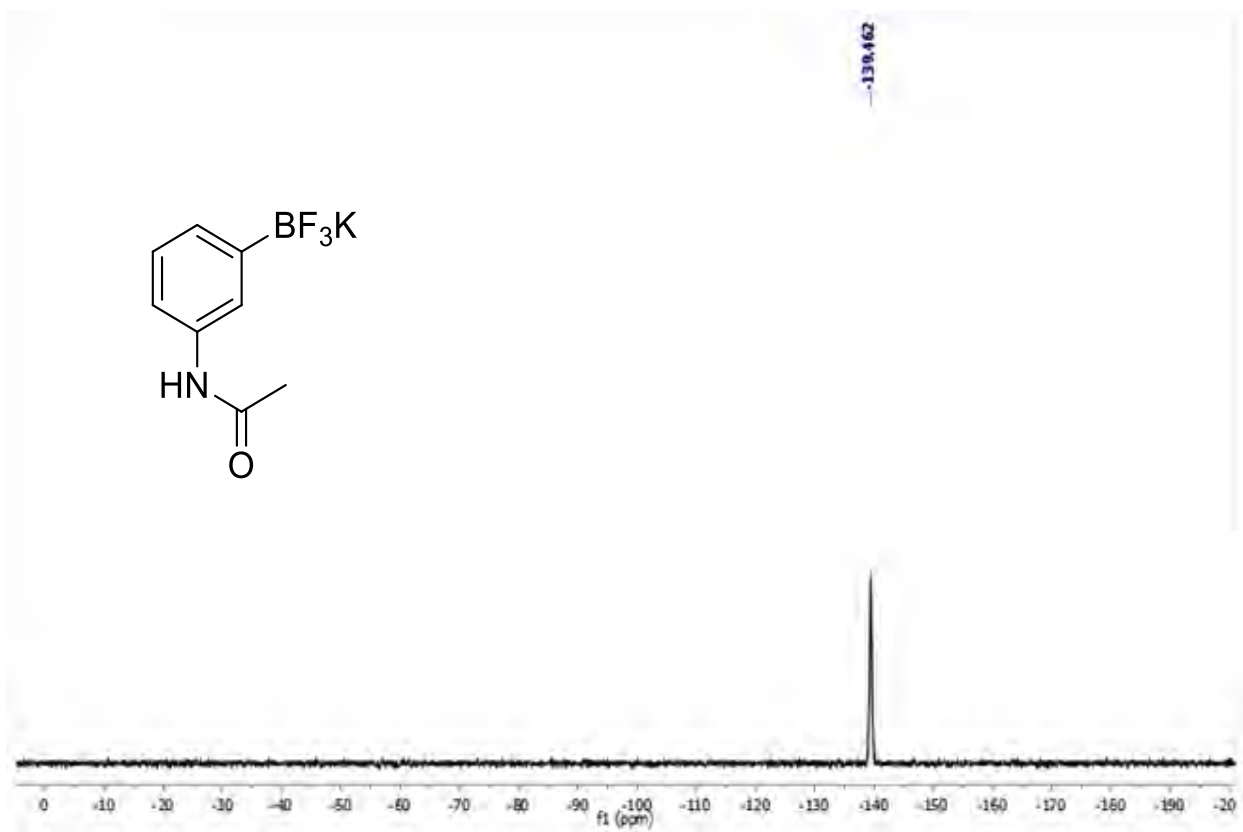
^{13}C NMR



^{11}B NMR

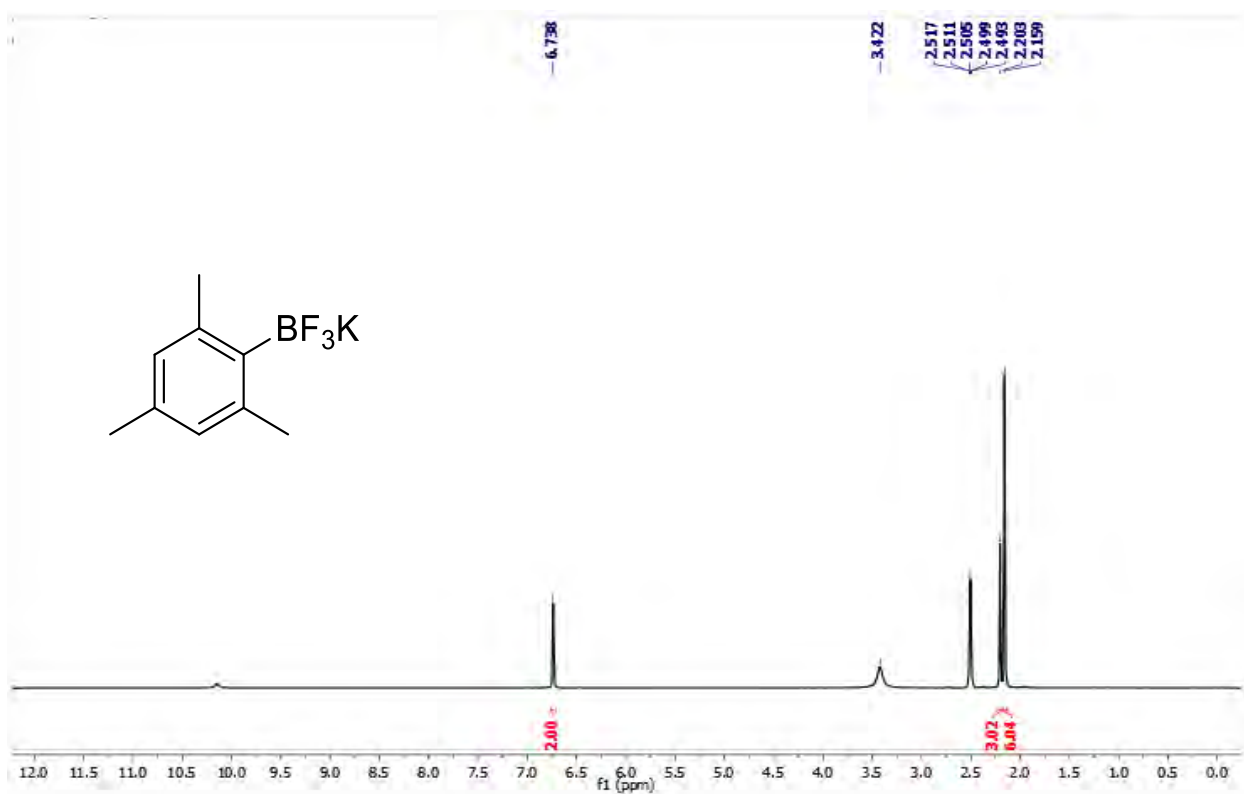


^{19}F NMR

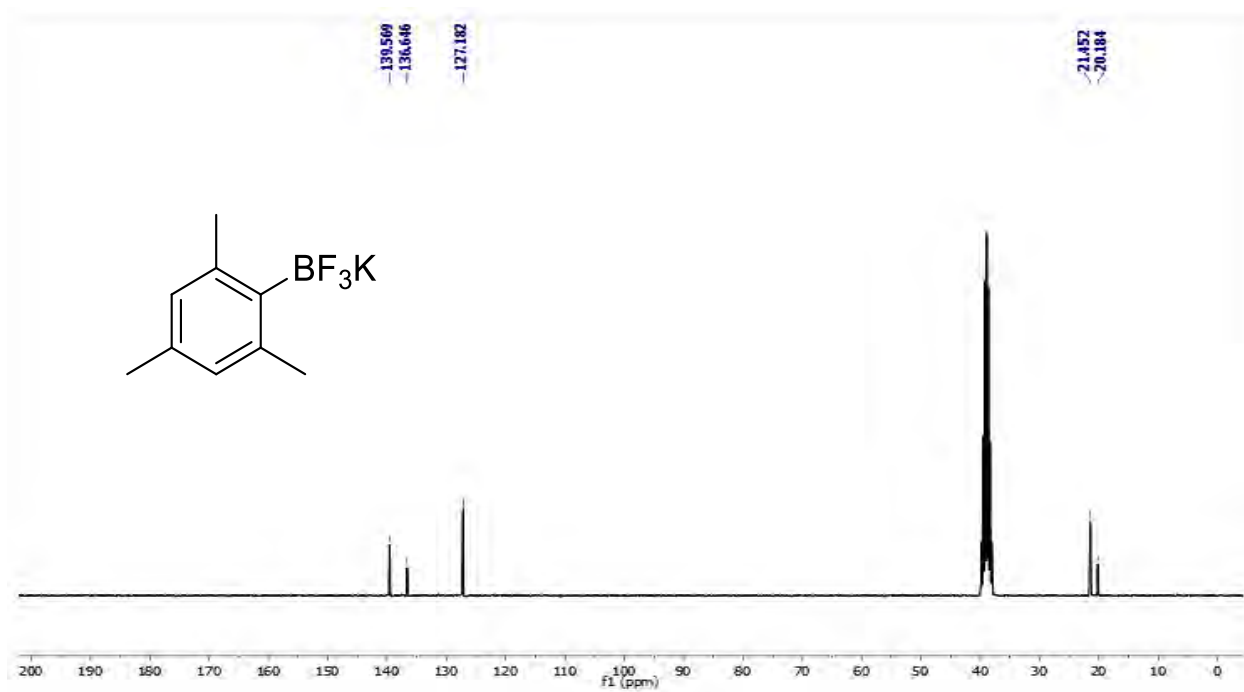


Potassium 2,4,6-trimethylphenyltrifluoroborate (**2n**)

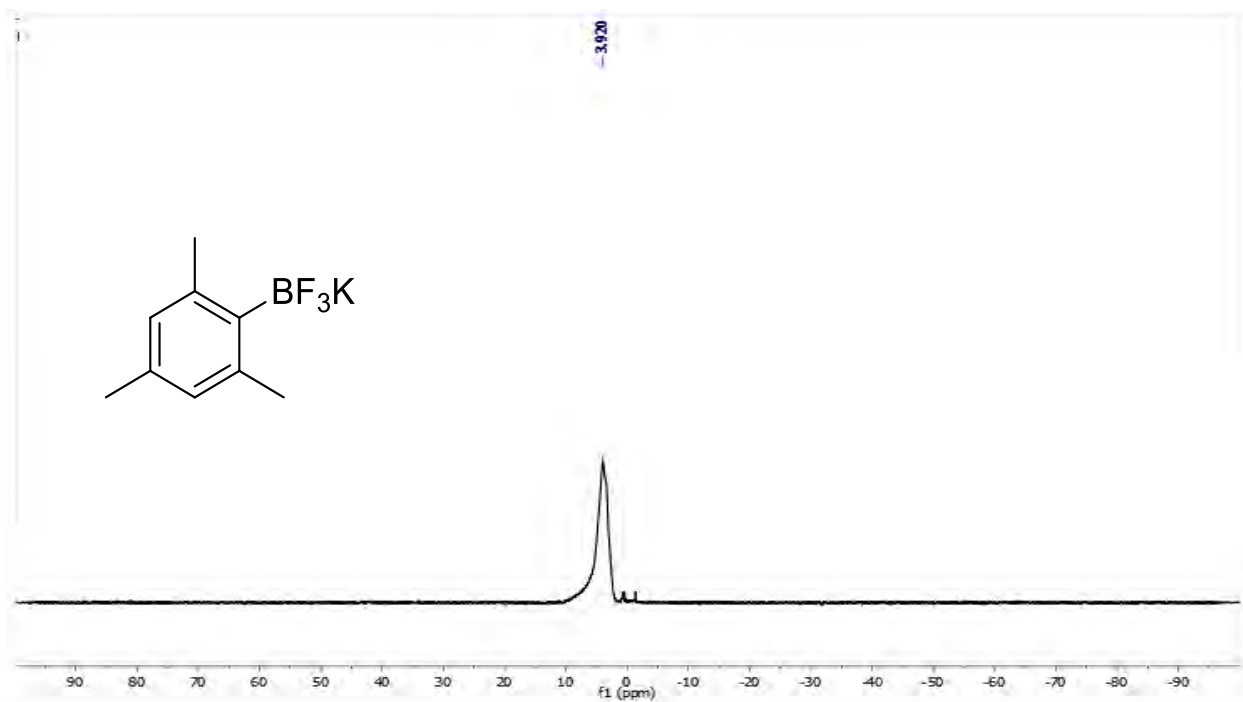
^1H NMR



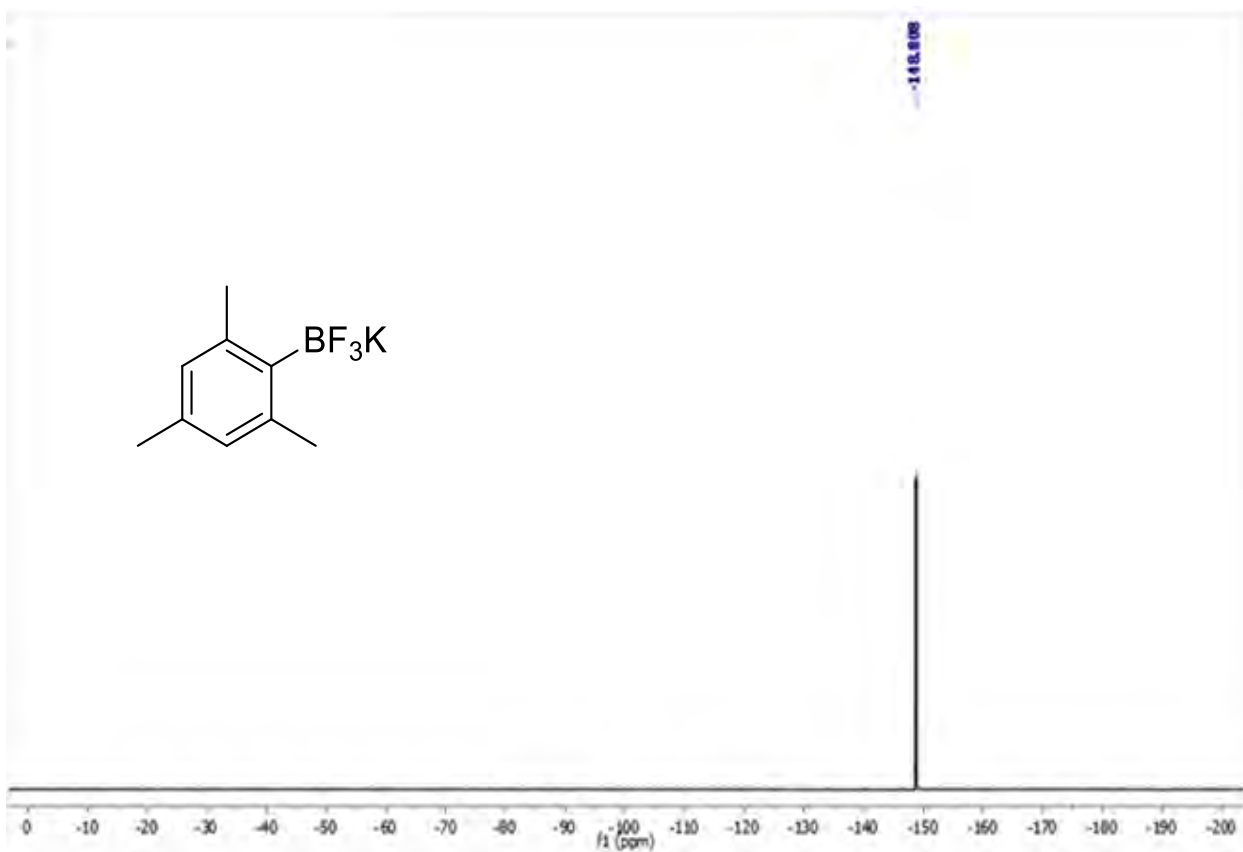
^{13}C NMR



^{11}B NMR

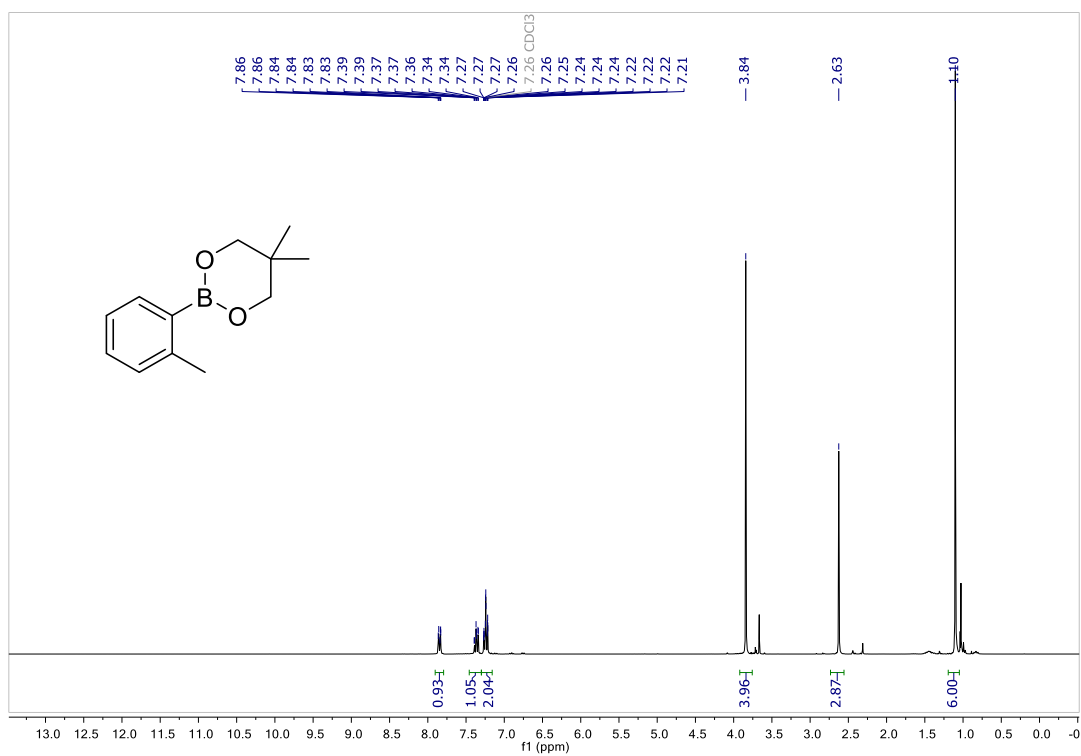


^{19}F NMR

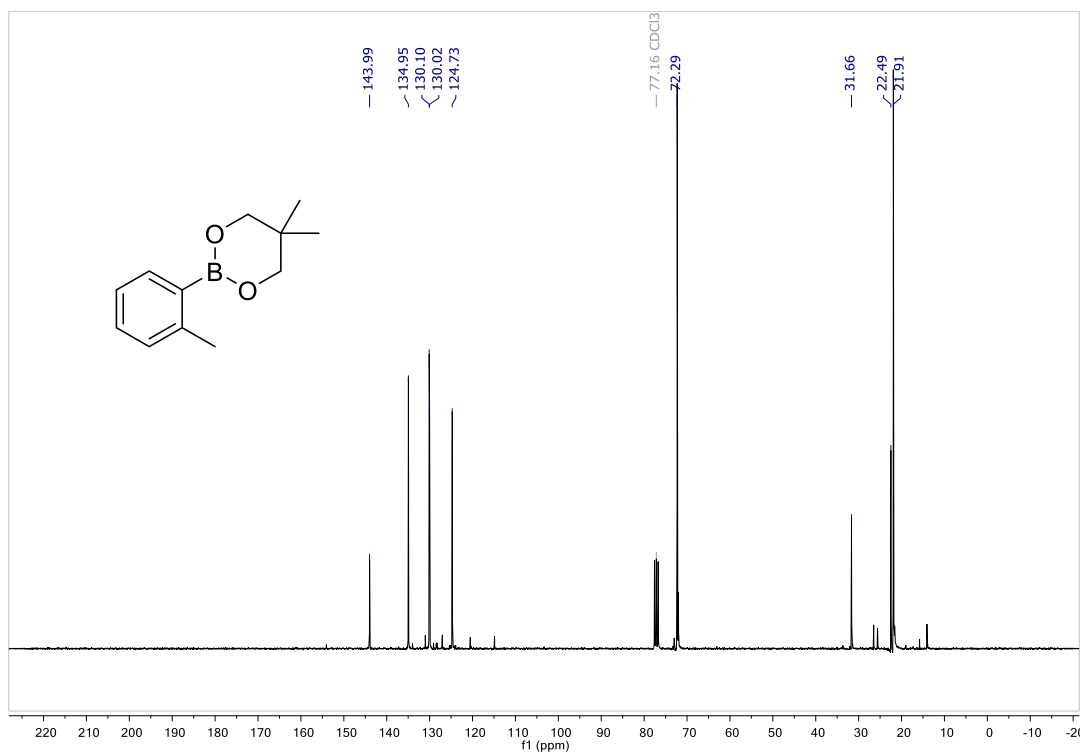


5,5-dimethyl-2-(o-tolyl)-1,3,2-dioxaborinane

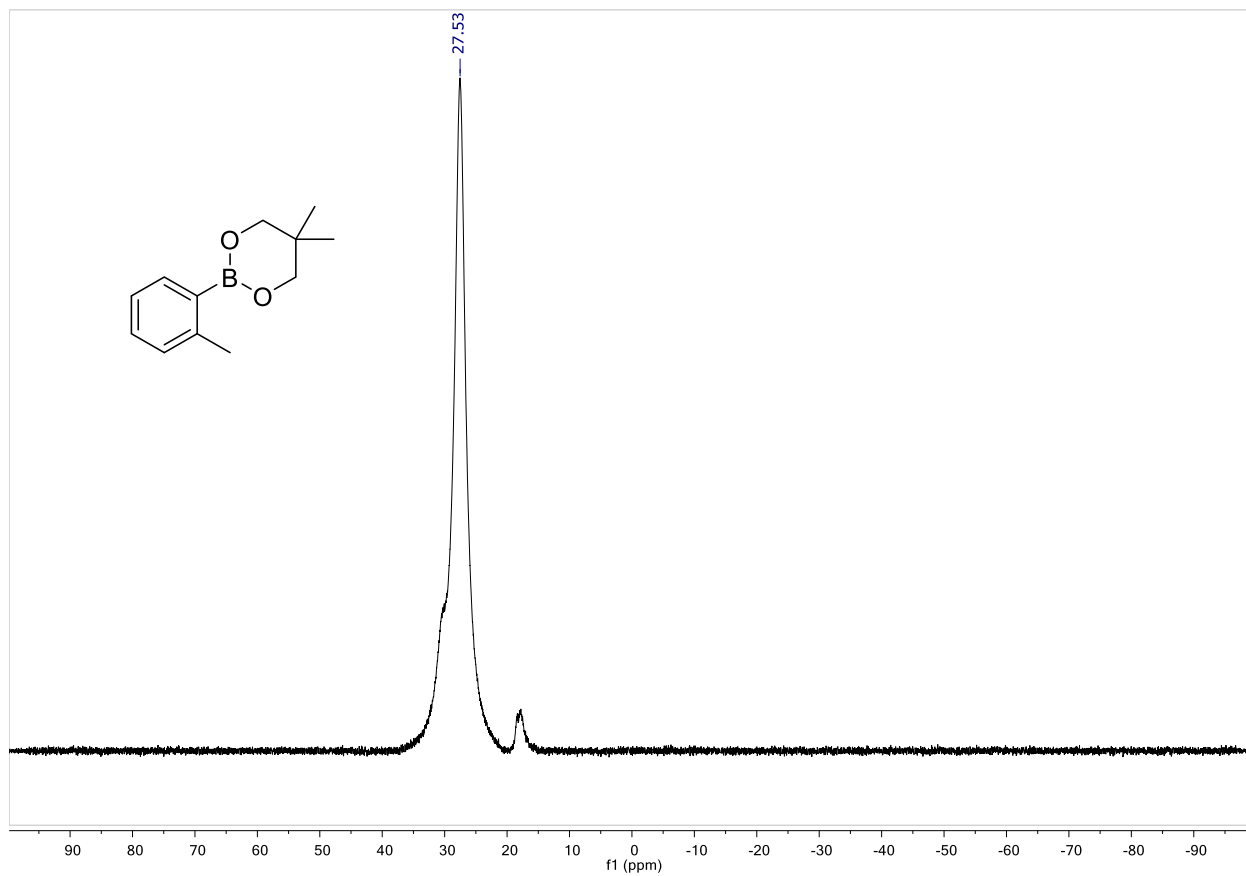
^1H NMR



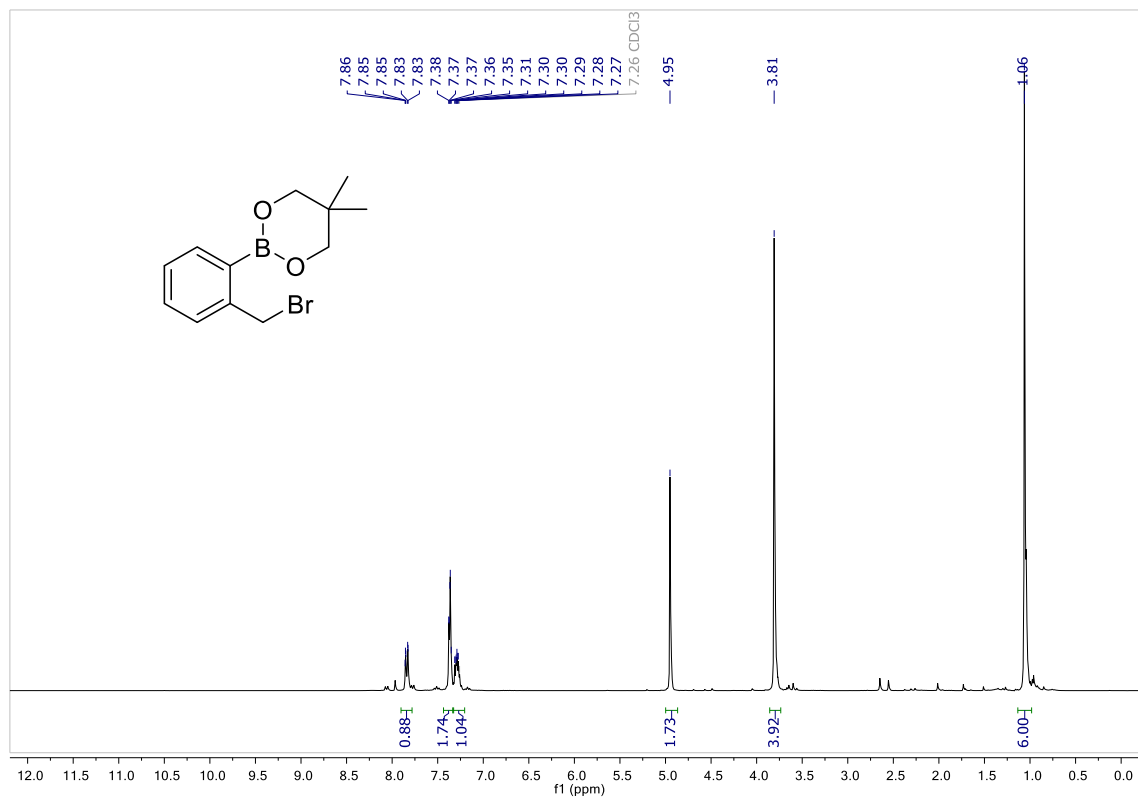
^{13}C NMR



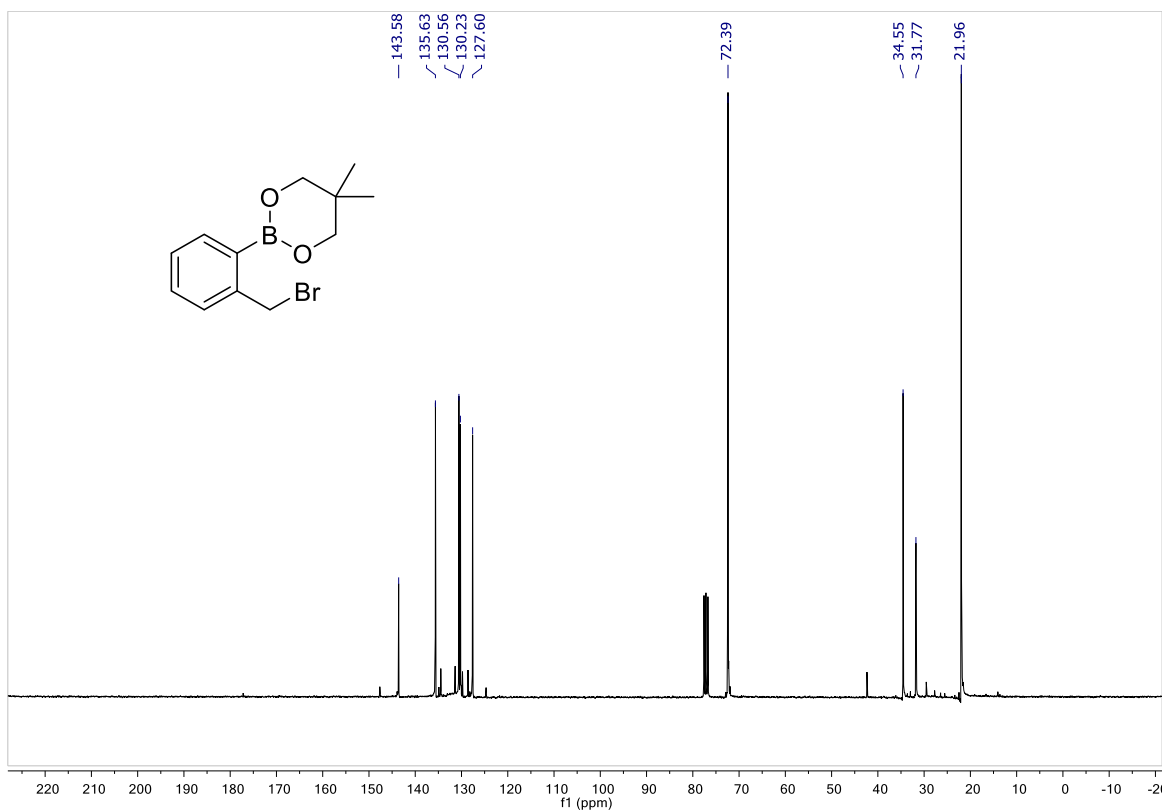
^{11}B NMR



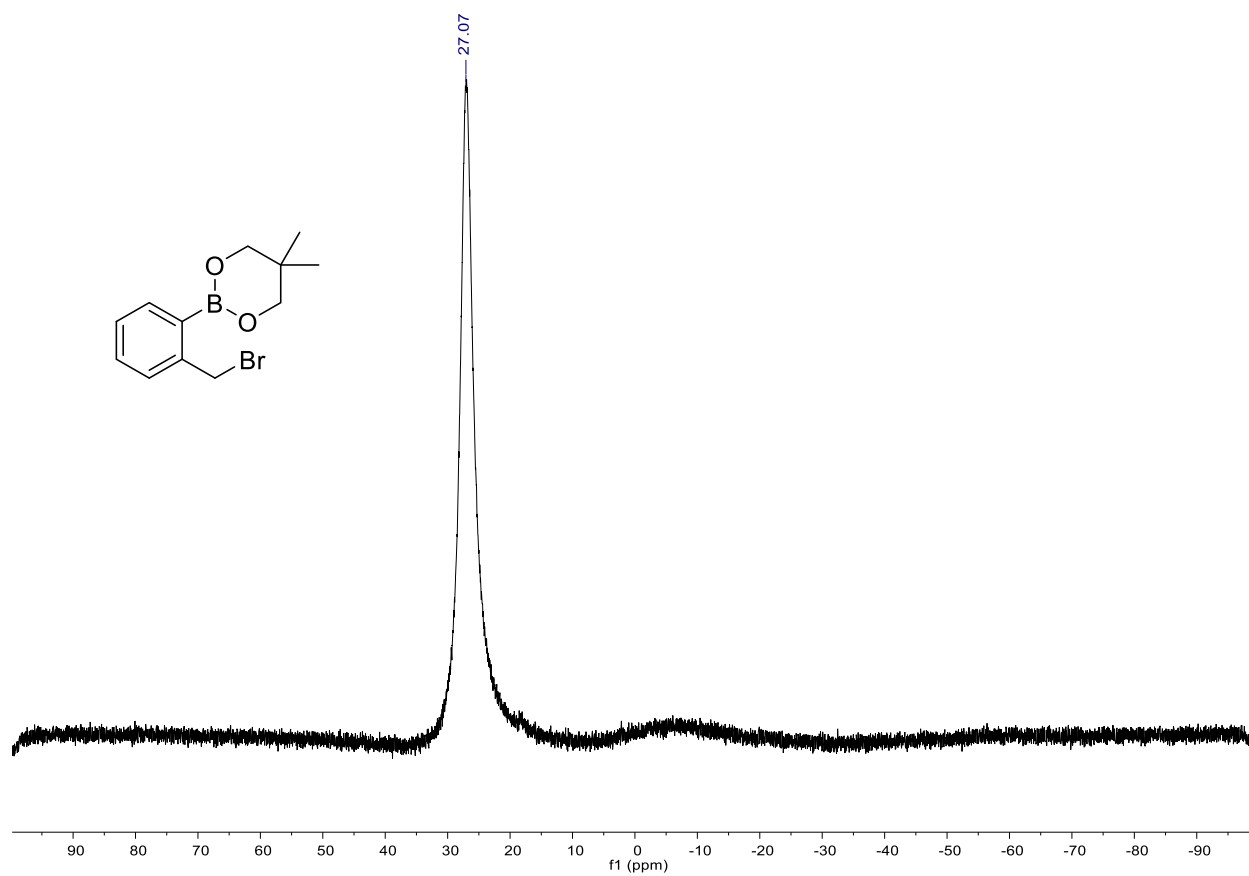
2-(2-(bromomethyl)phenyl)-5,5-dimethyl-1,3,2-dioxaborinane
¹H NMR



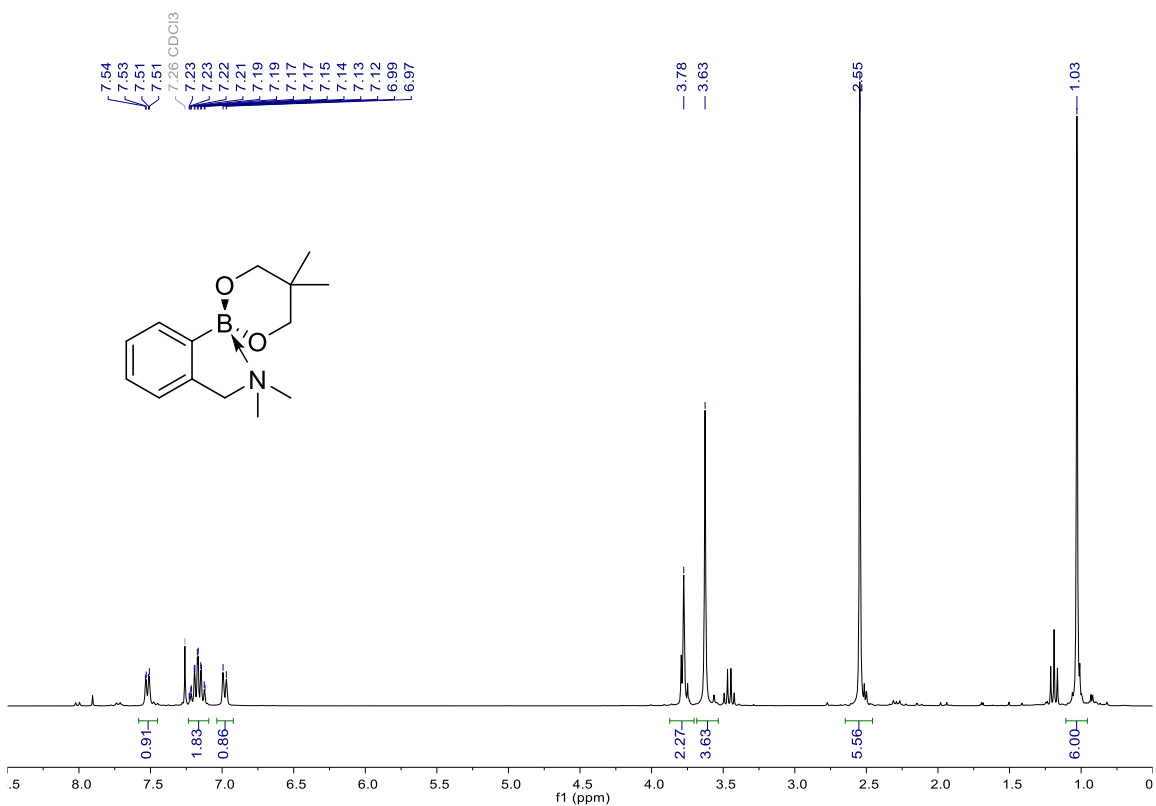
¹³C NMR



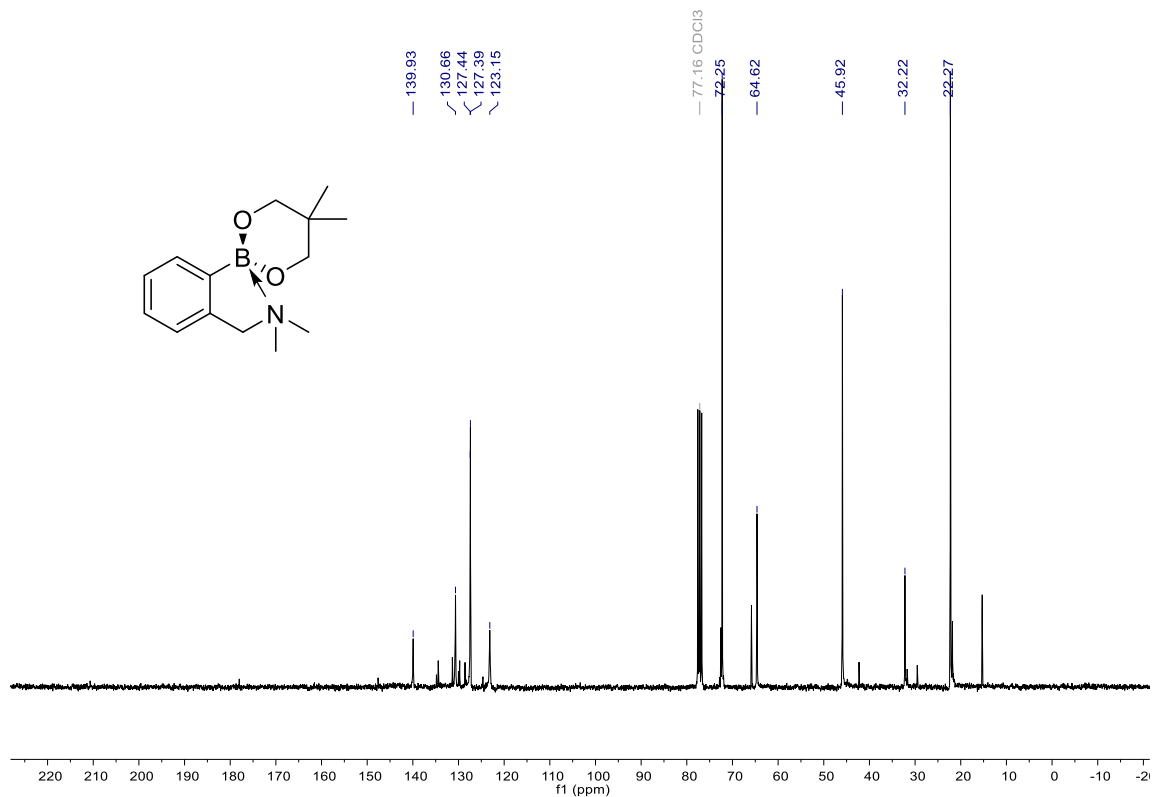
^{11}B NMR



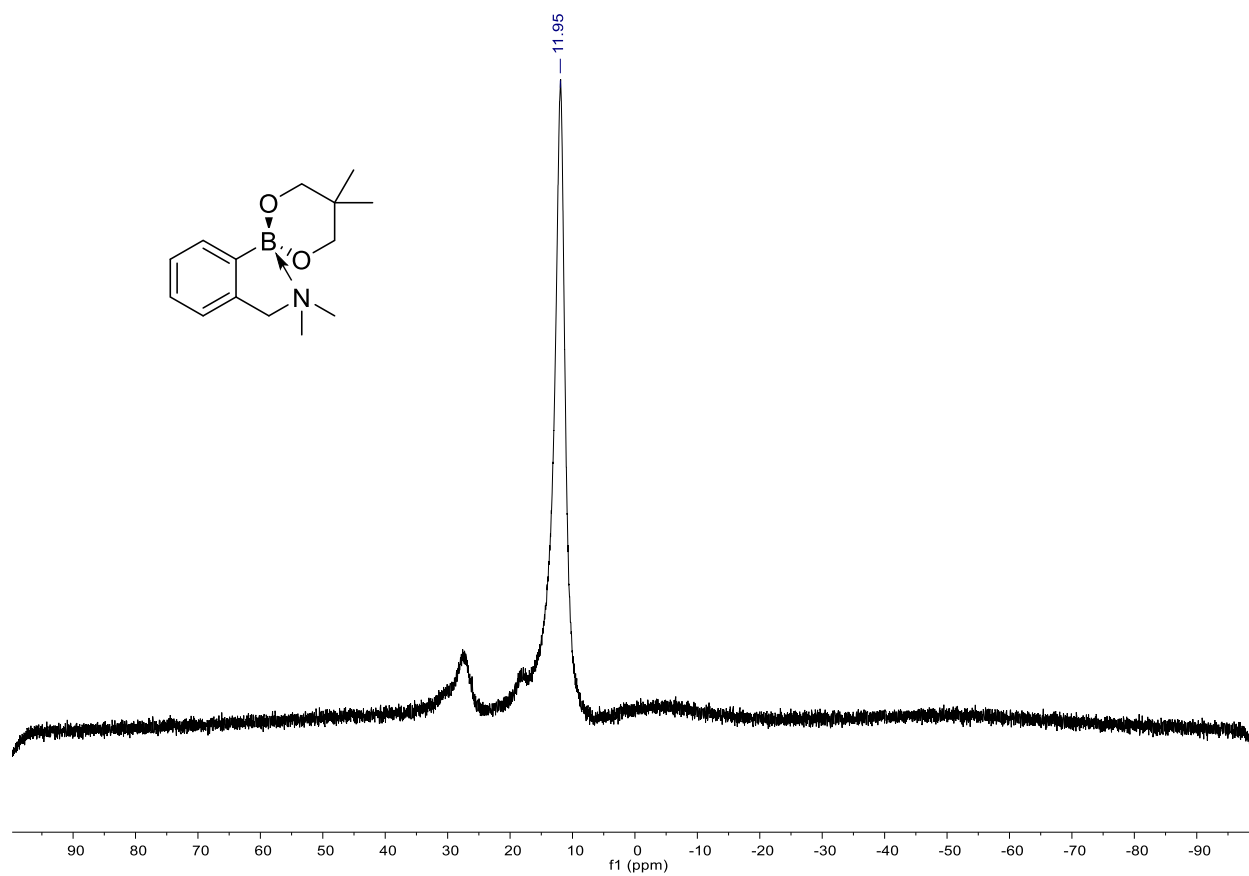
1-(2-(5,5-dimethyl-1,3,2-dioxaborinan-2-yl)phenyl)-N,N-dimethylmethanamine
¹H NMR



¹³C NMR

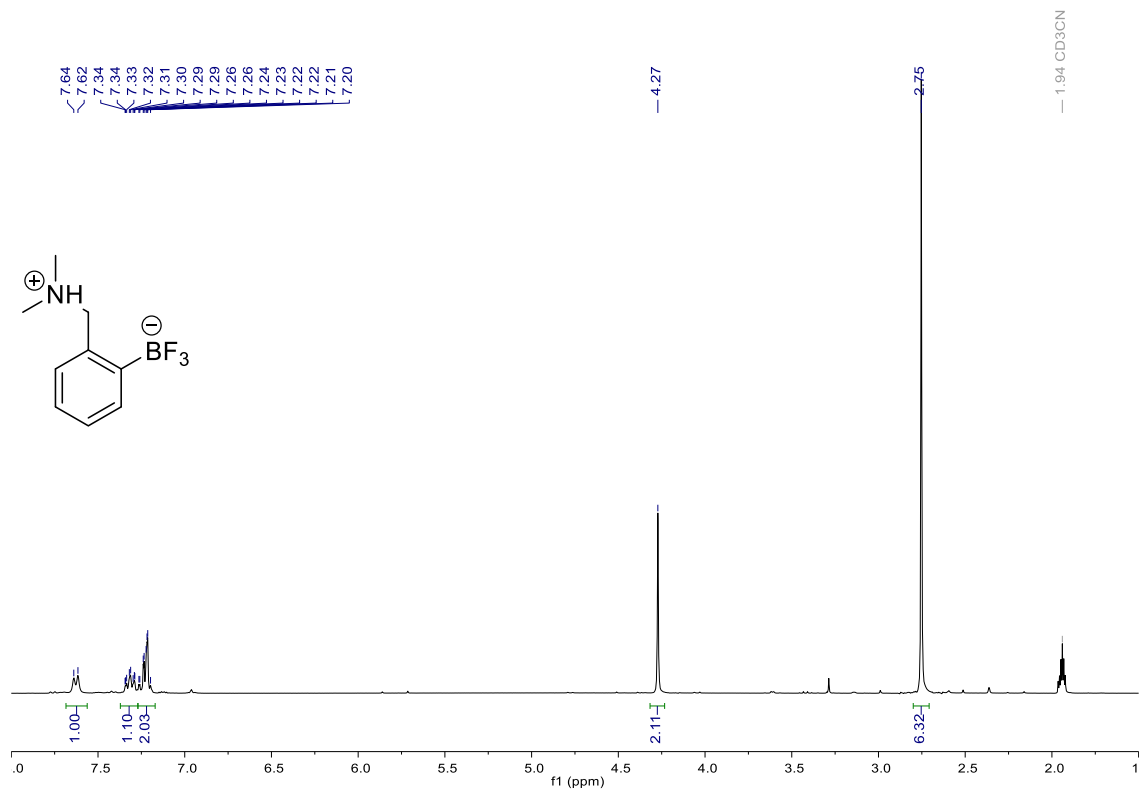


^{11}B NMR

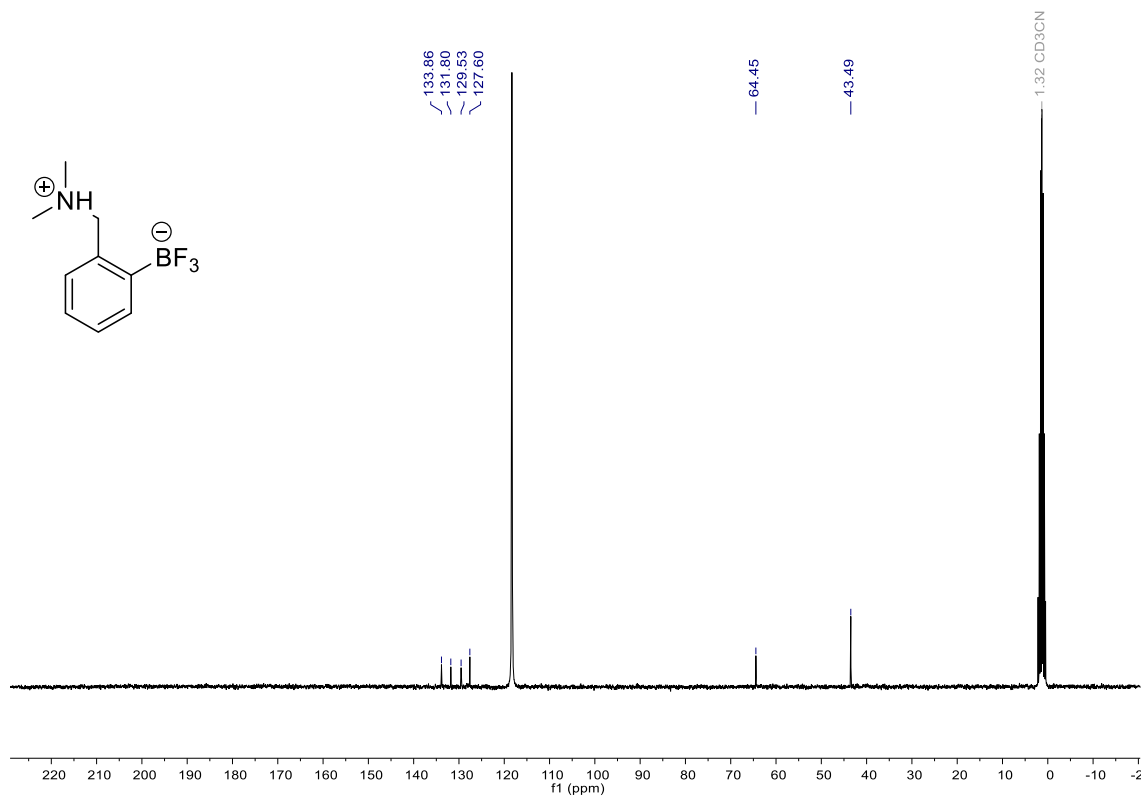


(2-((dimethylammonio)methyl)phenyl)trifluoroborate (2.6)

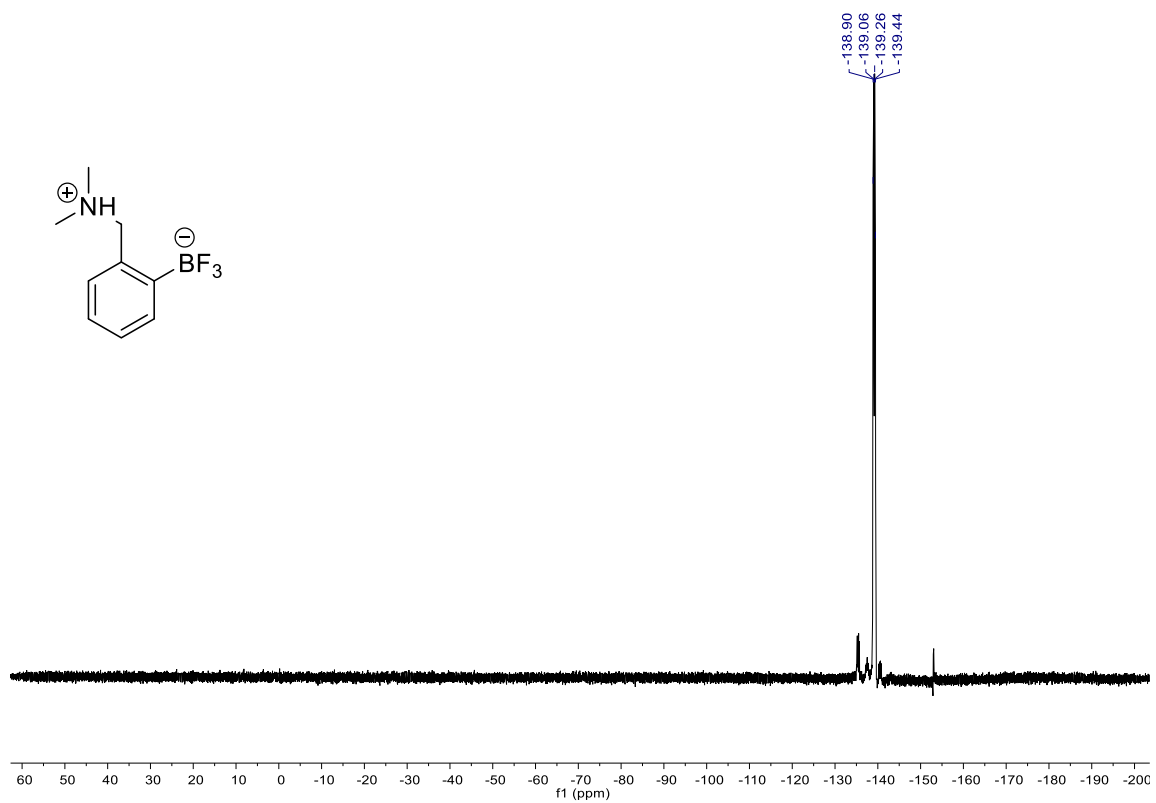
^1H NMR



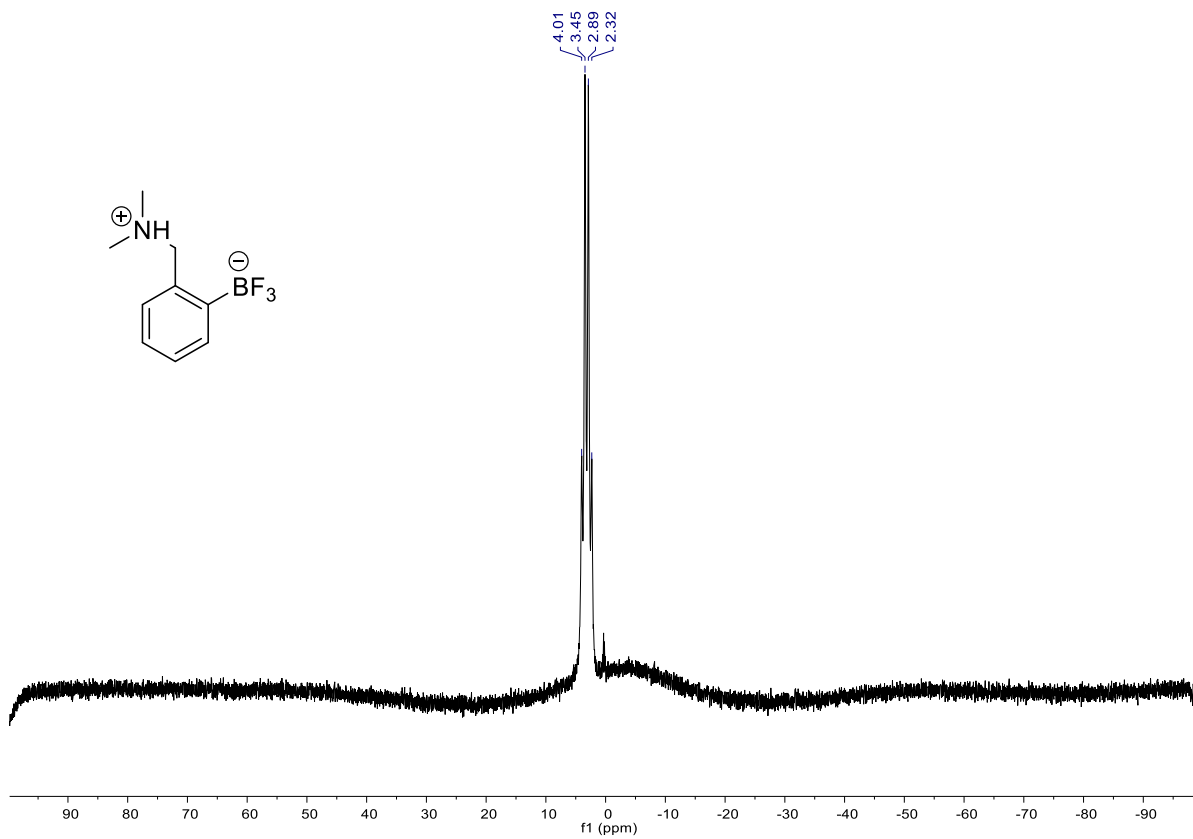
^{13}C NMR



¹⁹F NMR

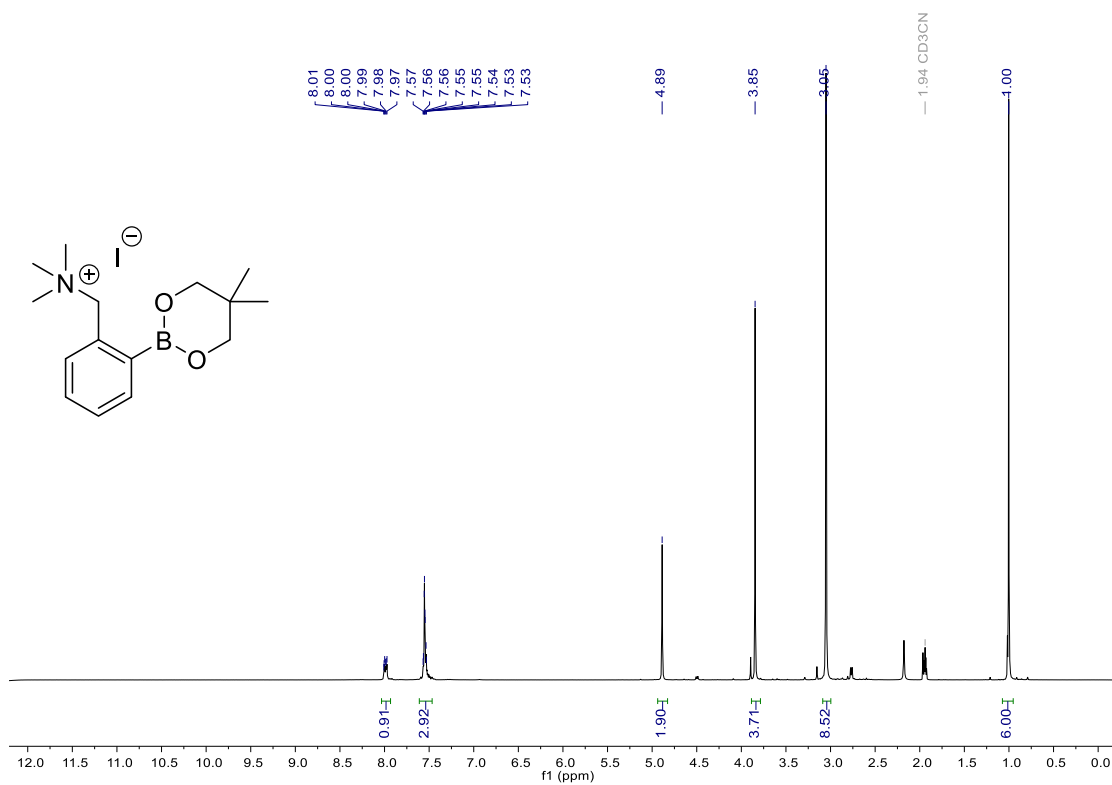


¹¹B NMR

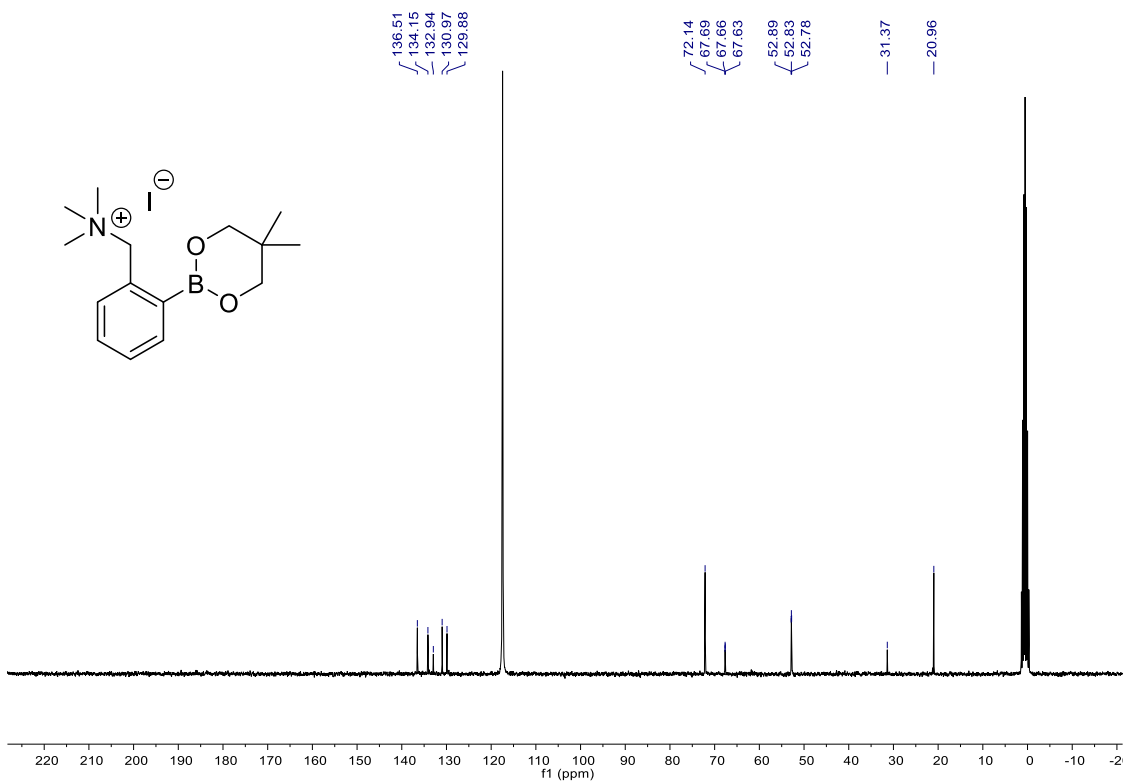


1-(2-(5,5-dimethyl-1,3,2-dioxaborinan-2-yl)phenyl)-N,N,N-trimethylmethanaminium iodide

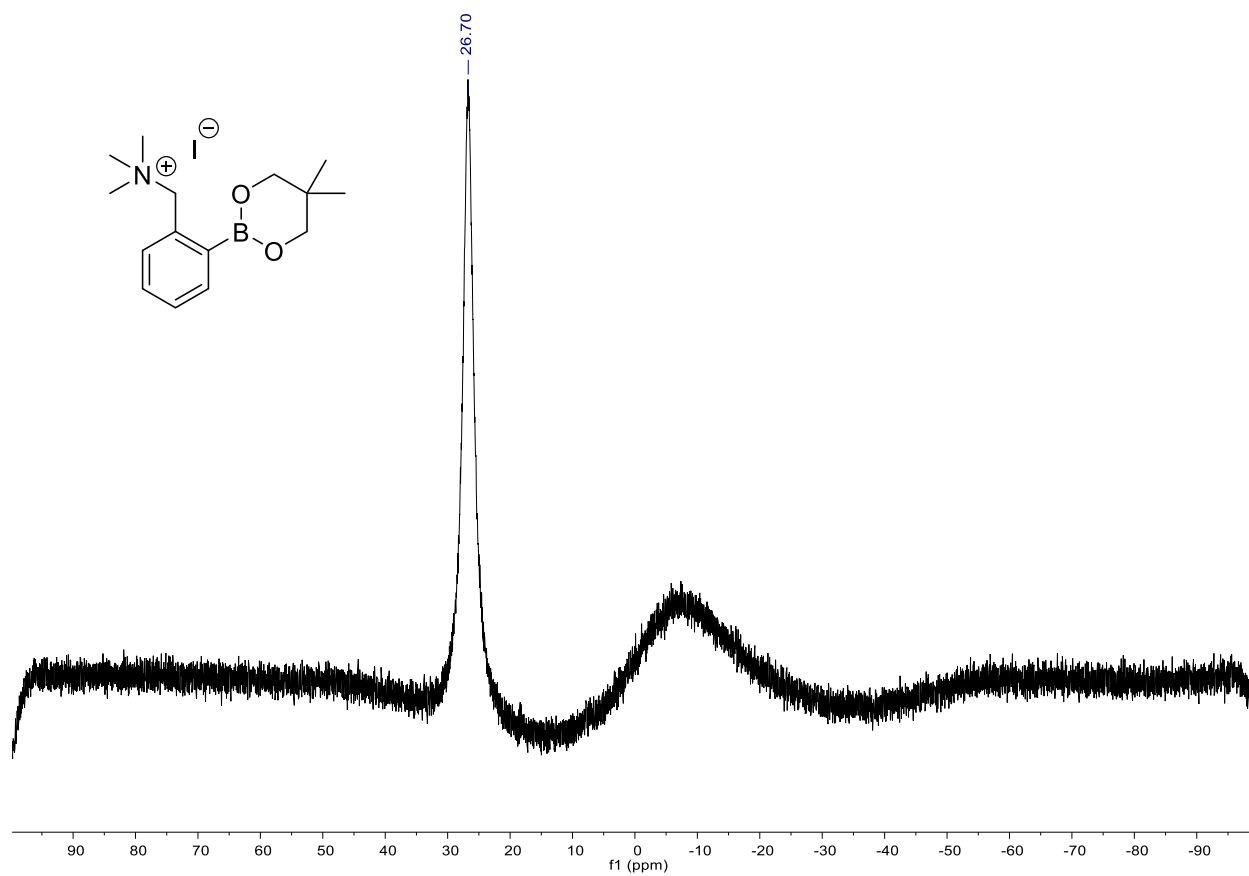
^1H NMR



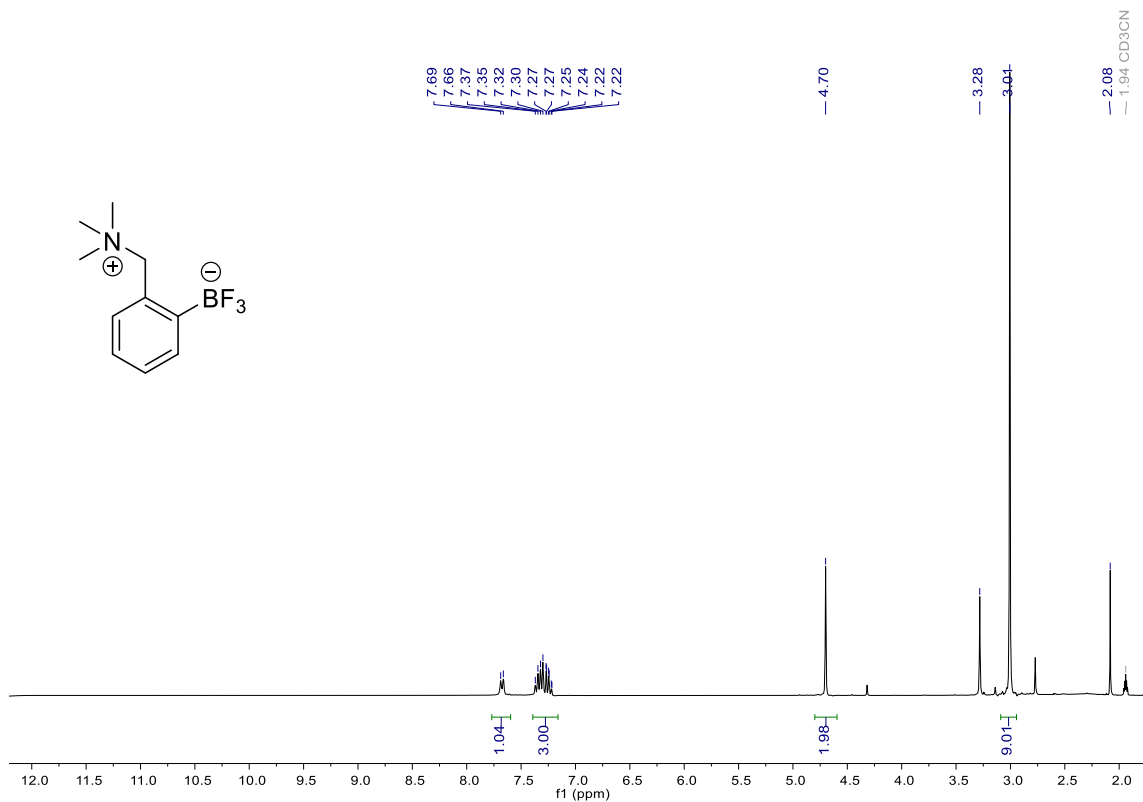
^{13}C NMR



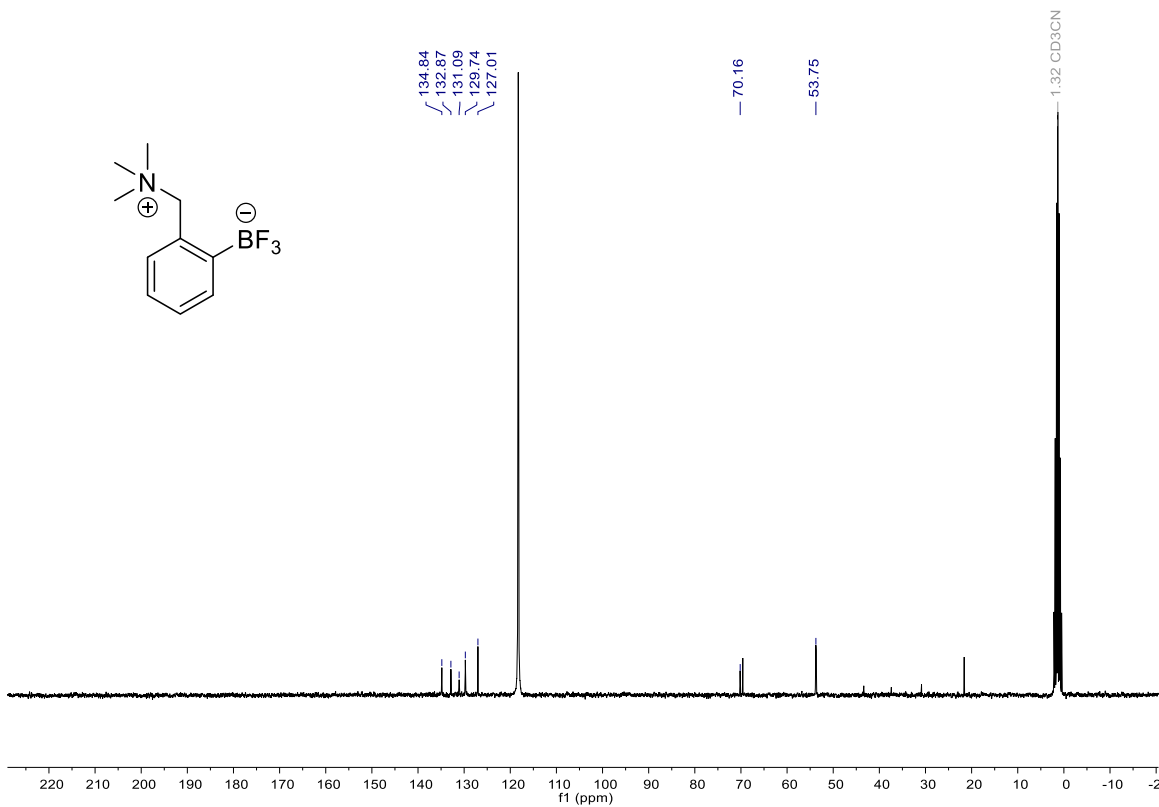
^{11}B NMR



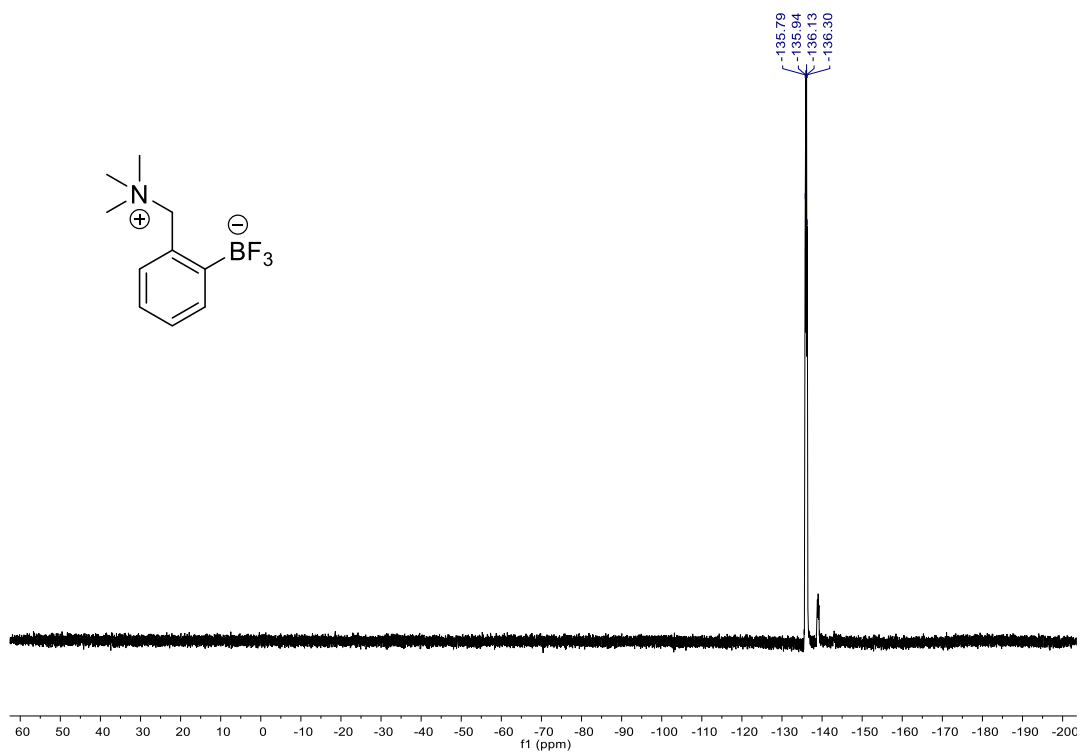
trifluoro(2-((trimethylammonio)methyl)phenyl)borate (2.7)
¹H NMR



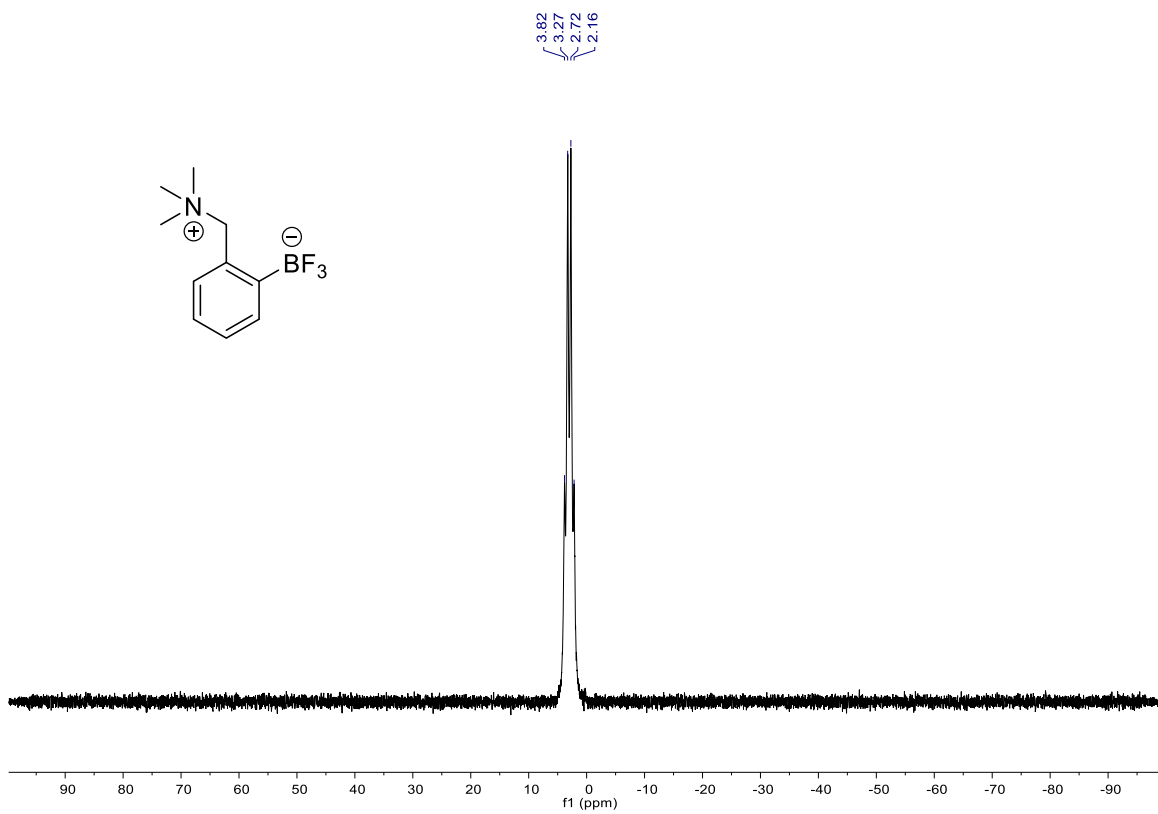
¹³C NMR



^{19}F NMR

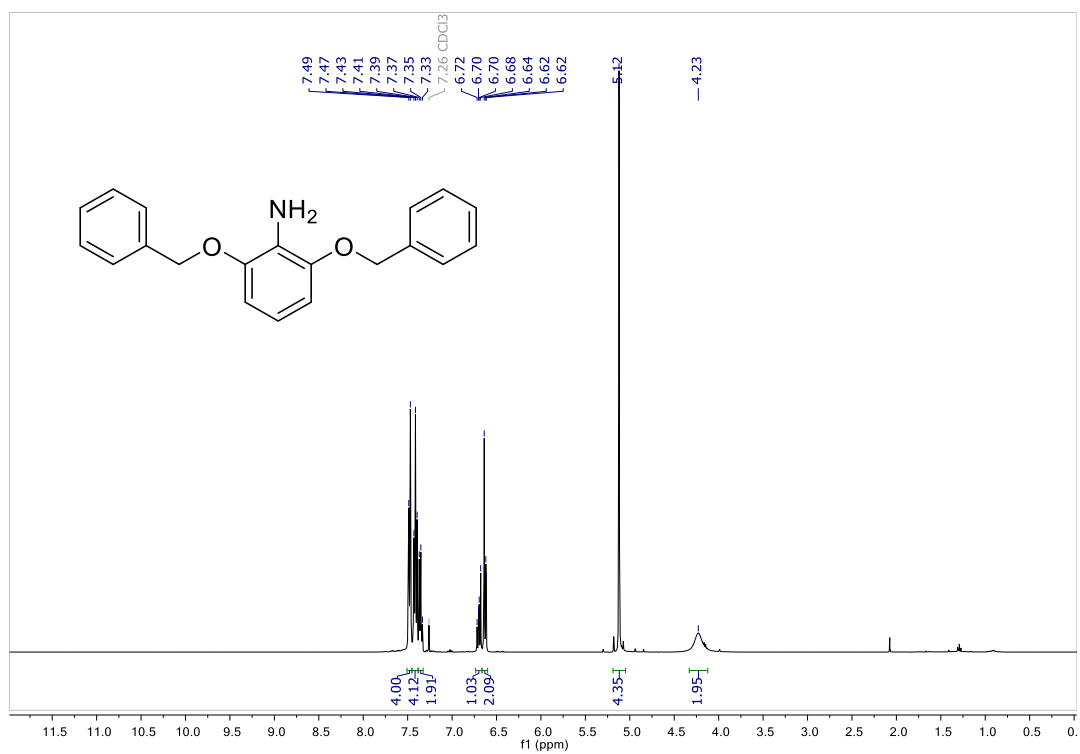


^{11}B NMR

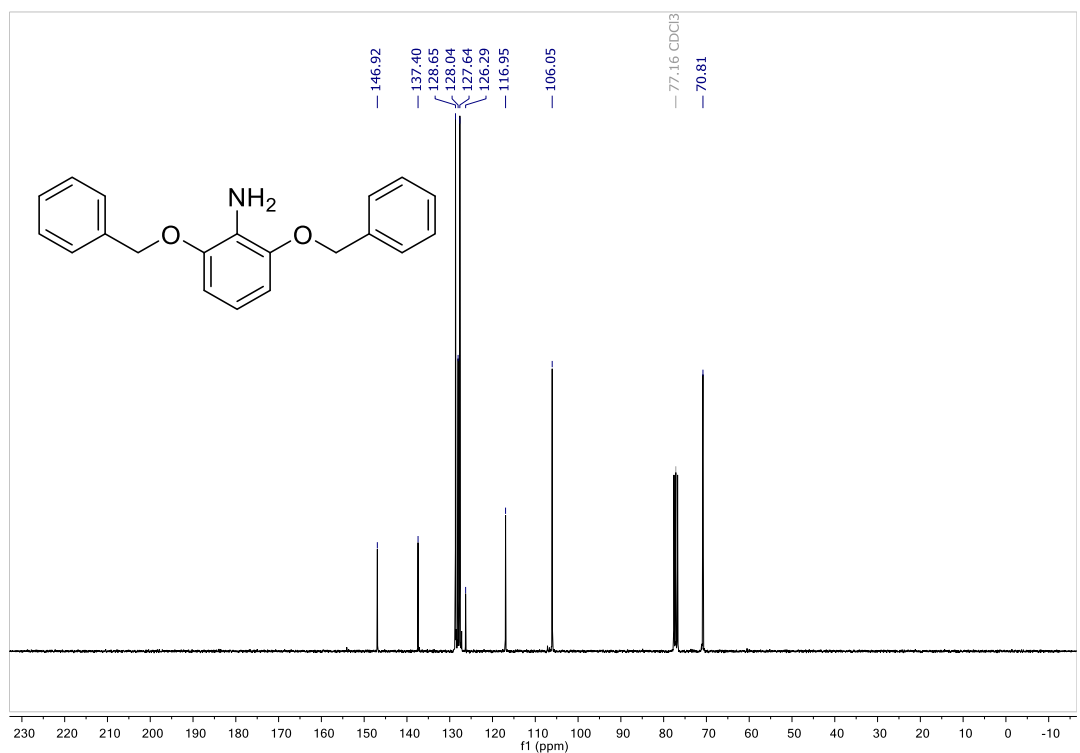


2,6-bis(benzyloxy)aniline

¹H NMR

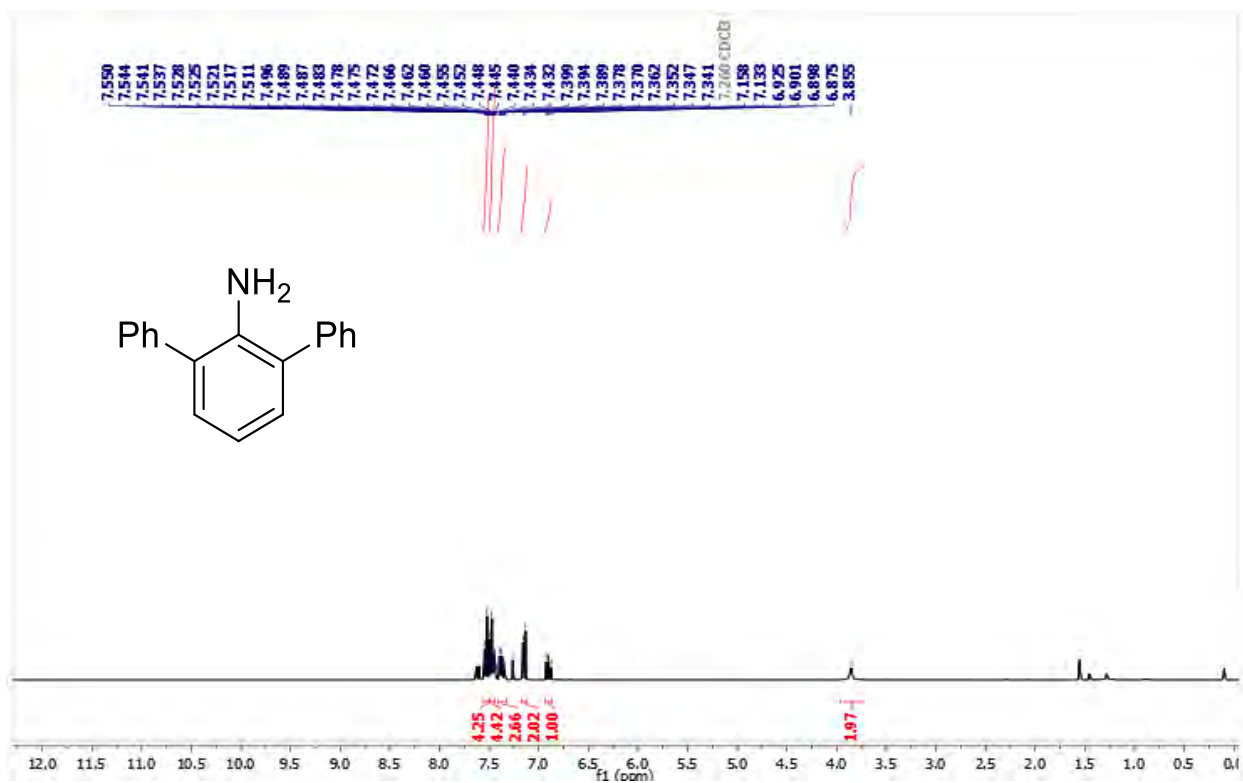


¹³C NMR

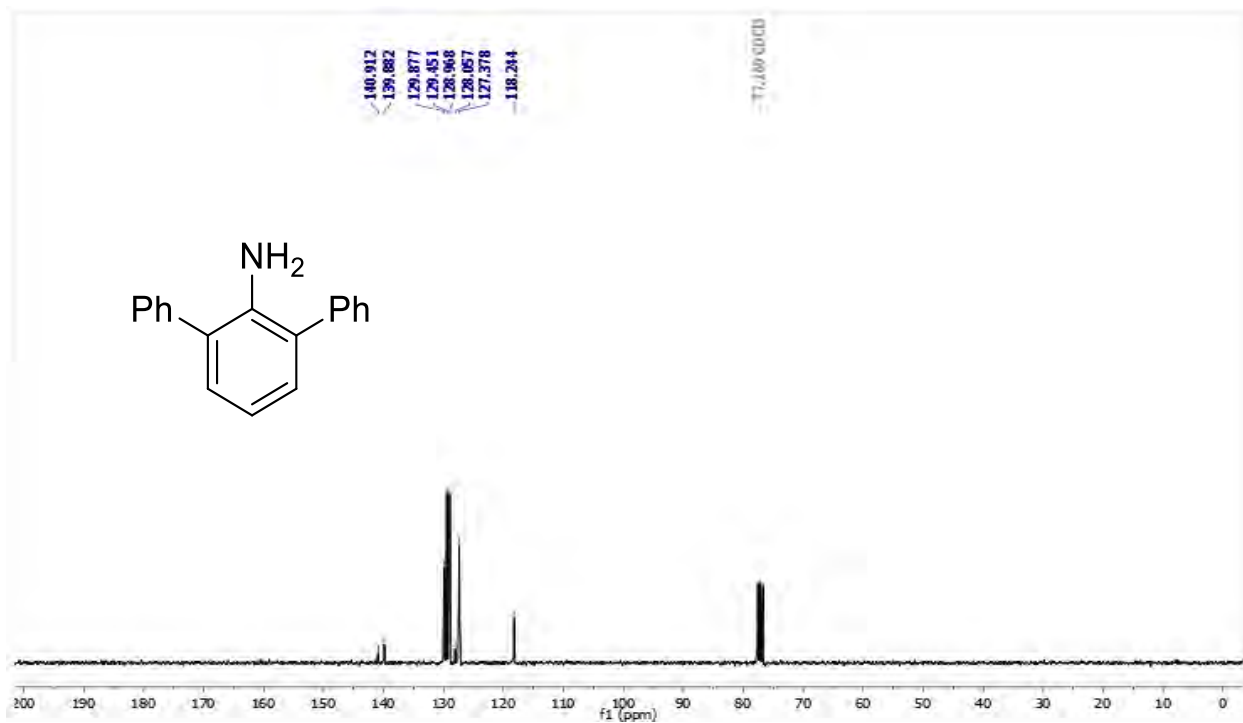


2,6-diphenylaniline

¹H NMR

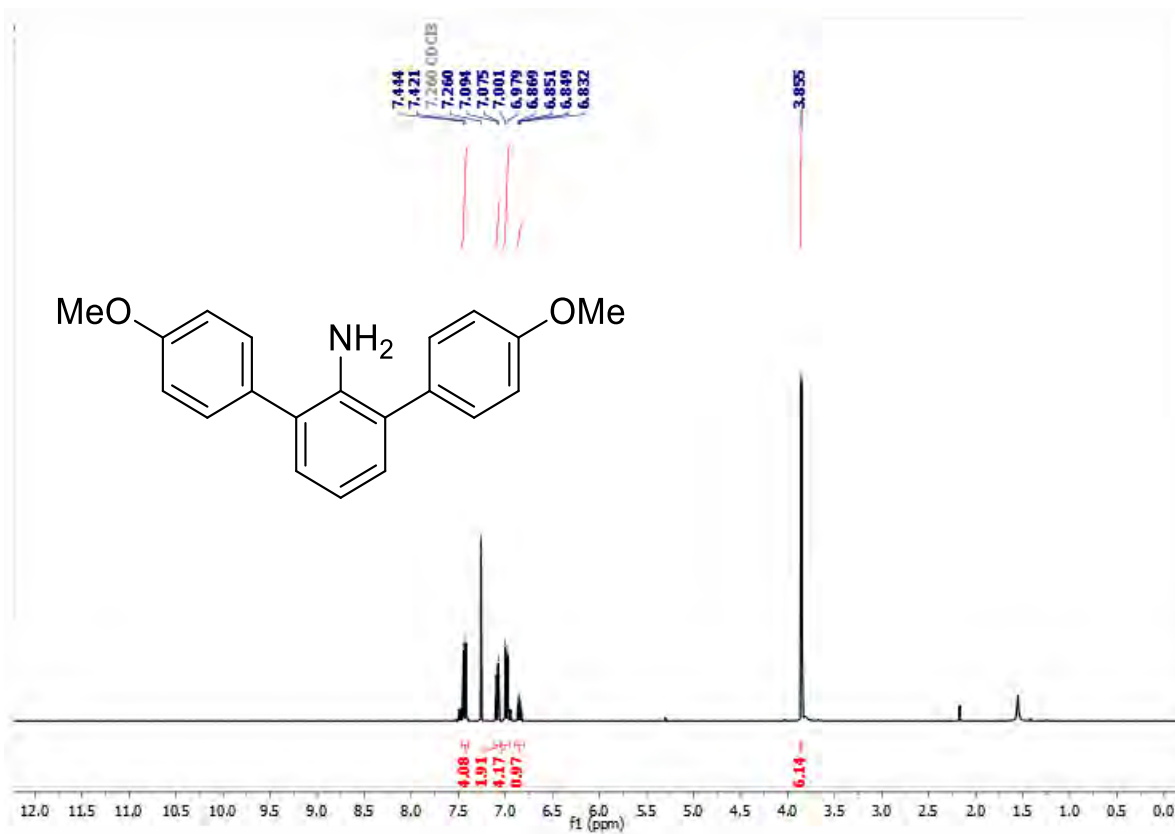


¹³C NMR

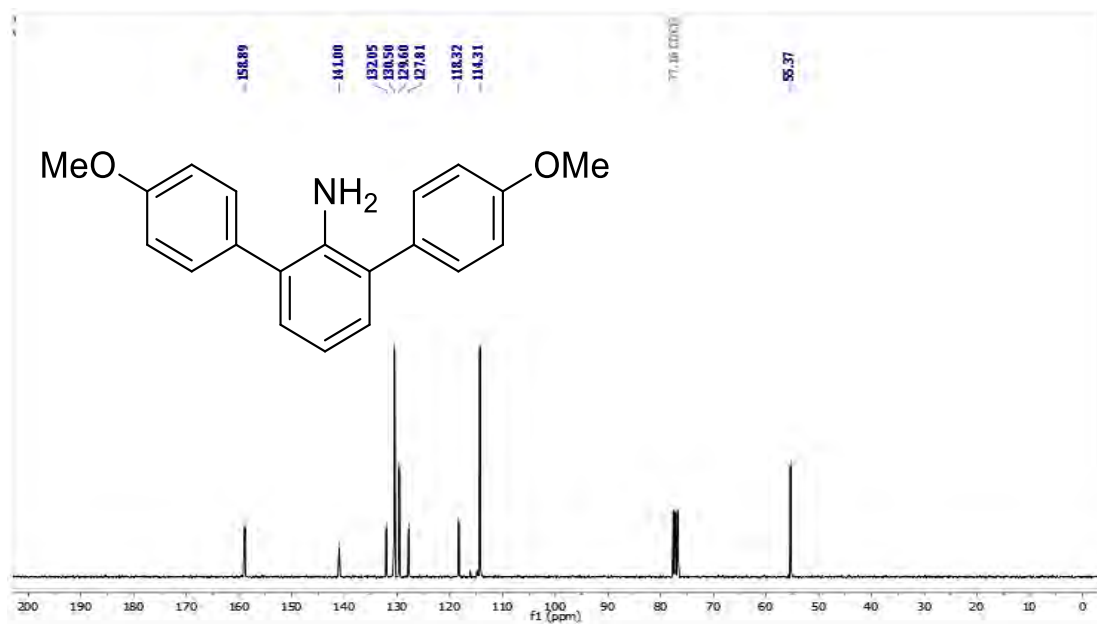


2,6-di-(4-methoxyphenyl)aniline

¹H NMR

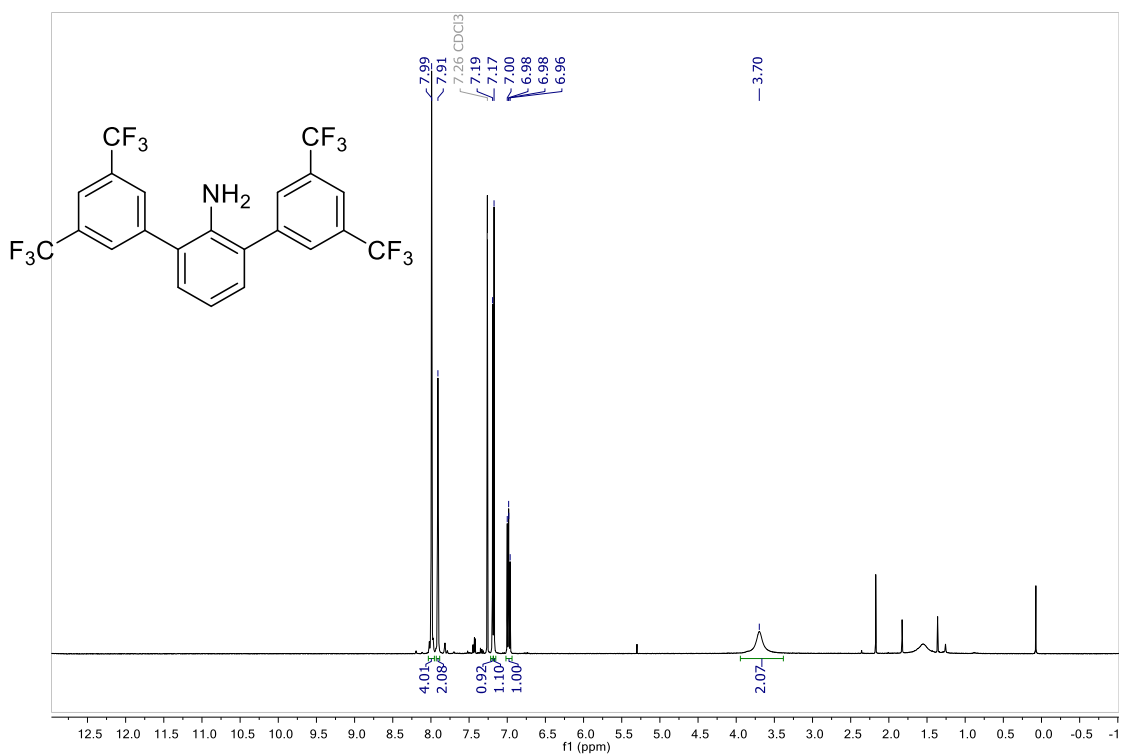


¹³C NMR

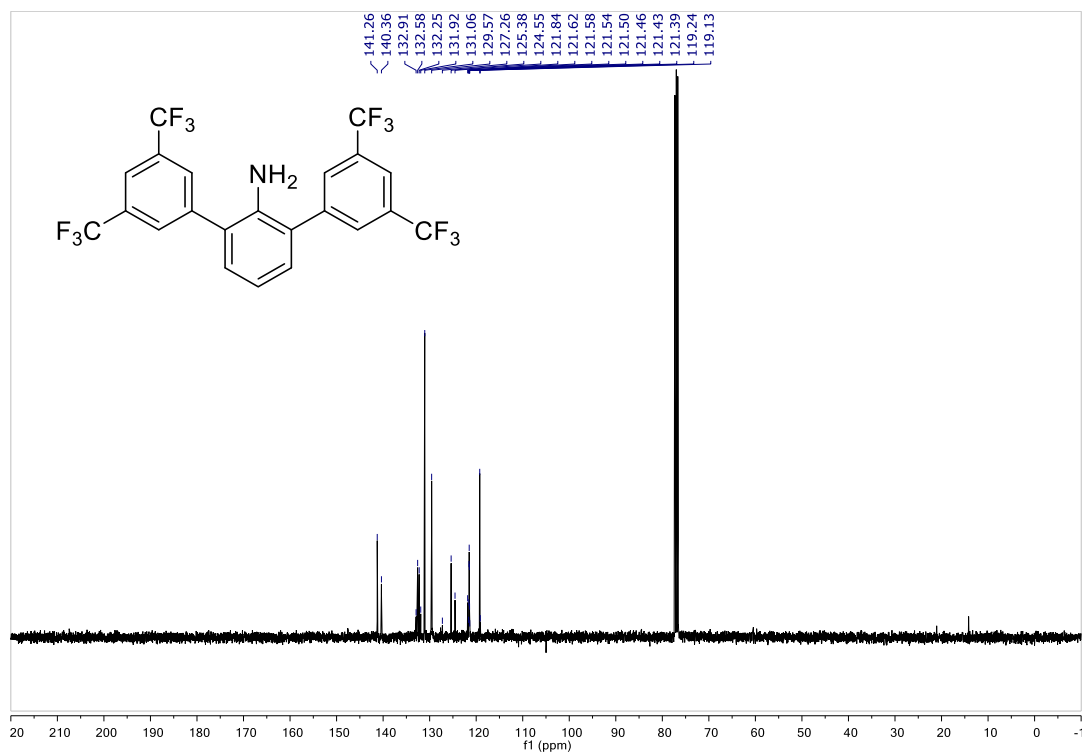


2,6-di-((3,5-bis(trifluoromethyl)methoxyphenyl)amino)aniline

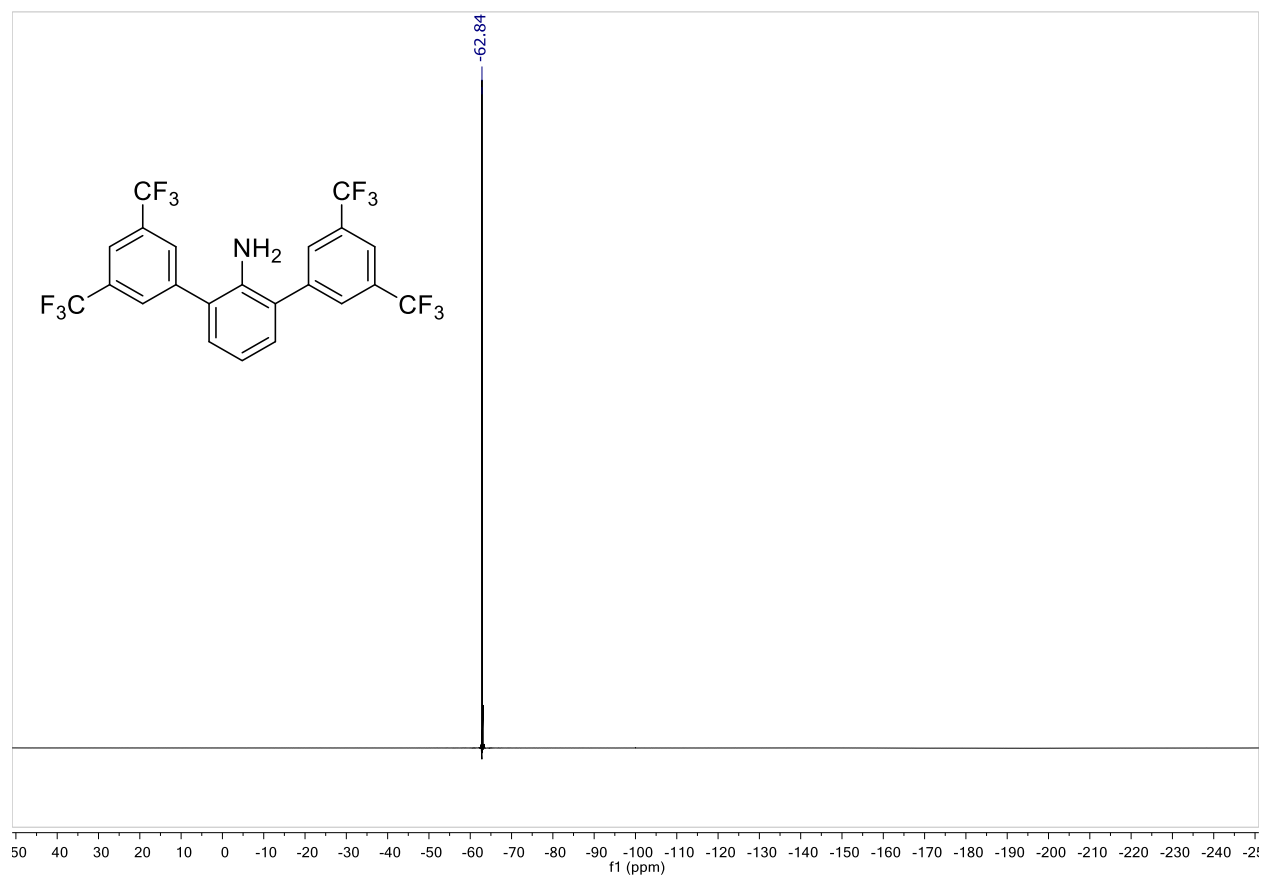
^1H NMR



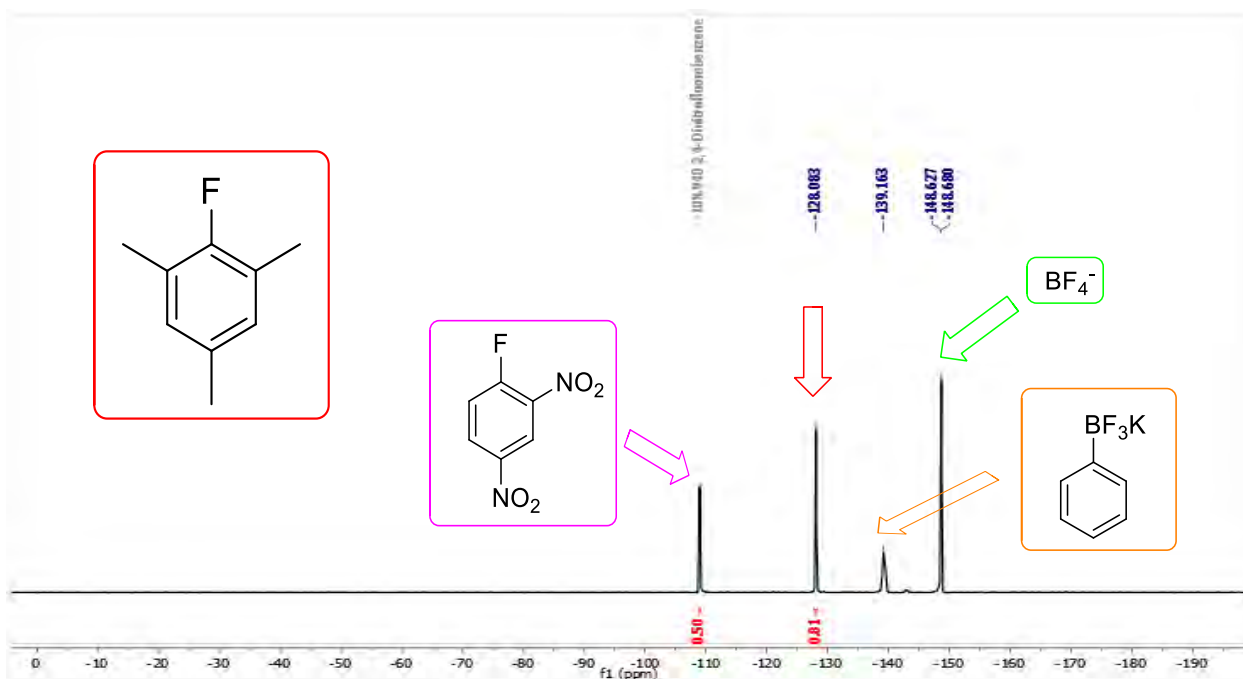
^{13}C NMR



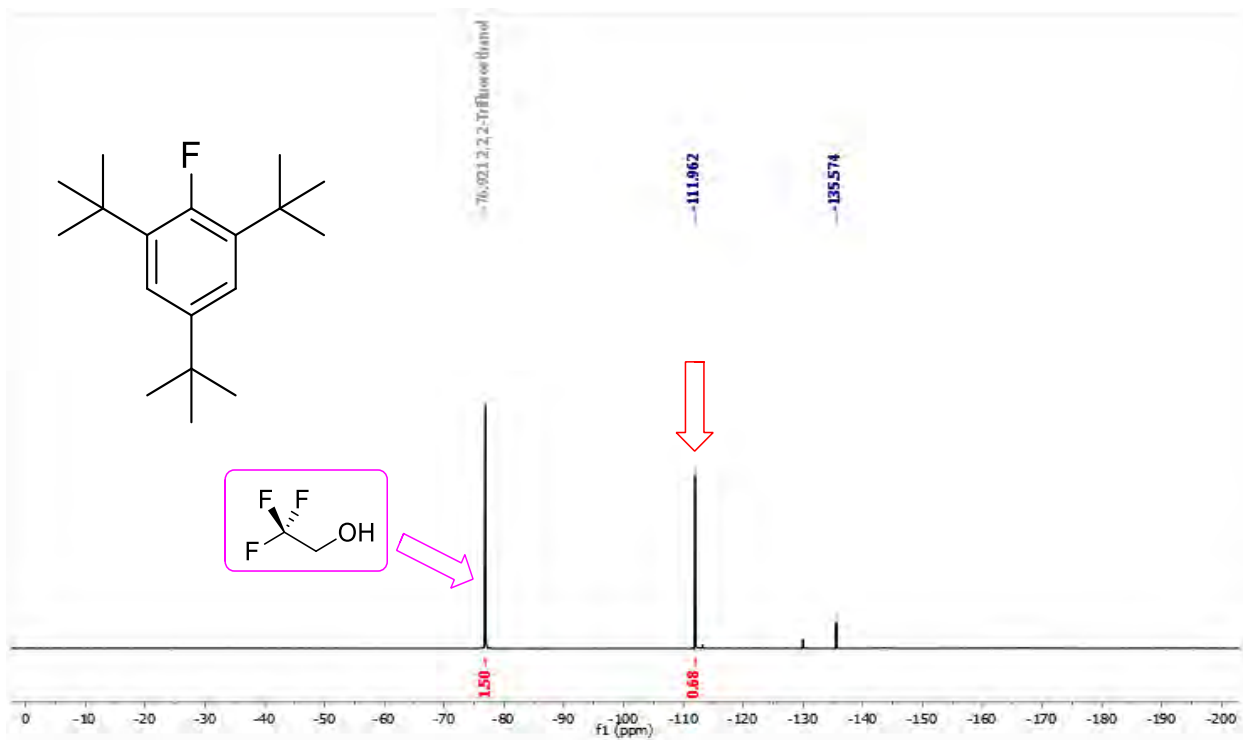
^{19}F NMR



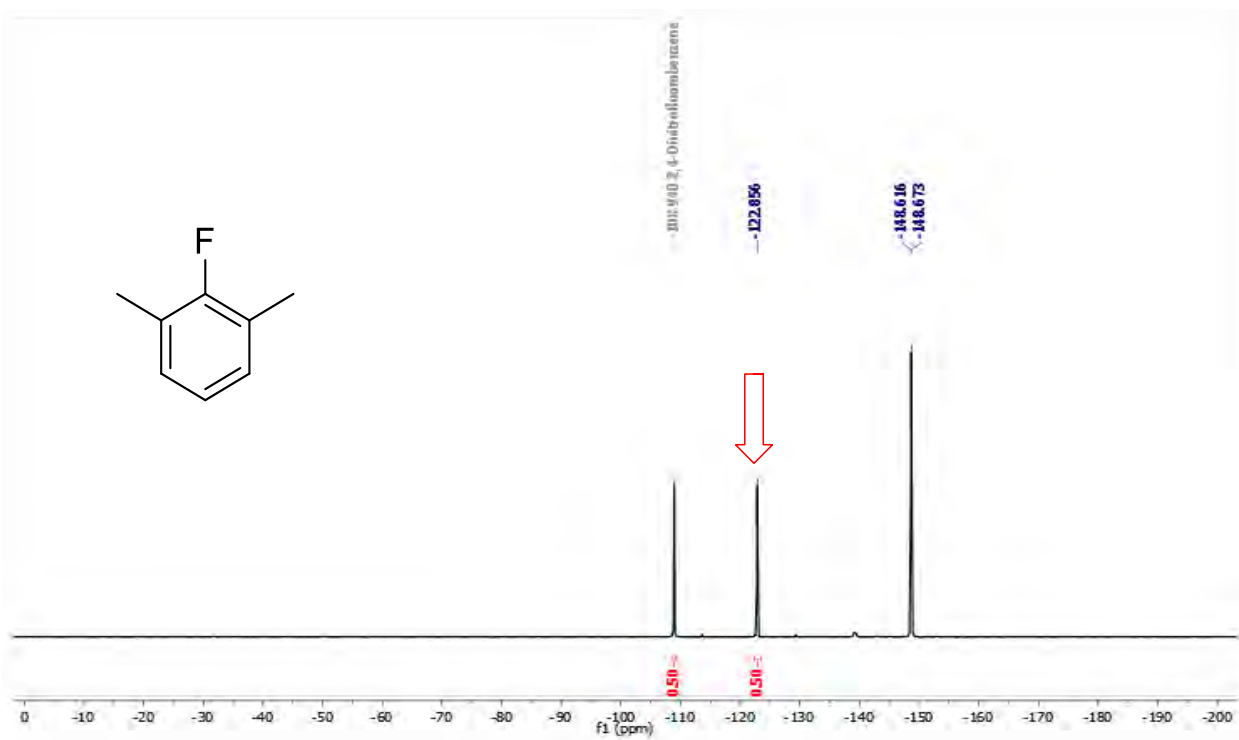
^{19}F NMR 1-fluoro-2,4,6-trimethylbenzene, **2.3**, using 2,4-dinitrofluorobenzene as the I.S.



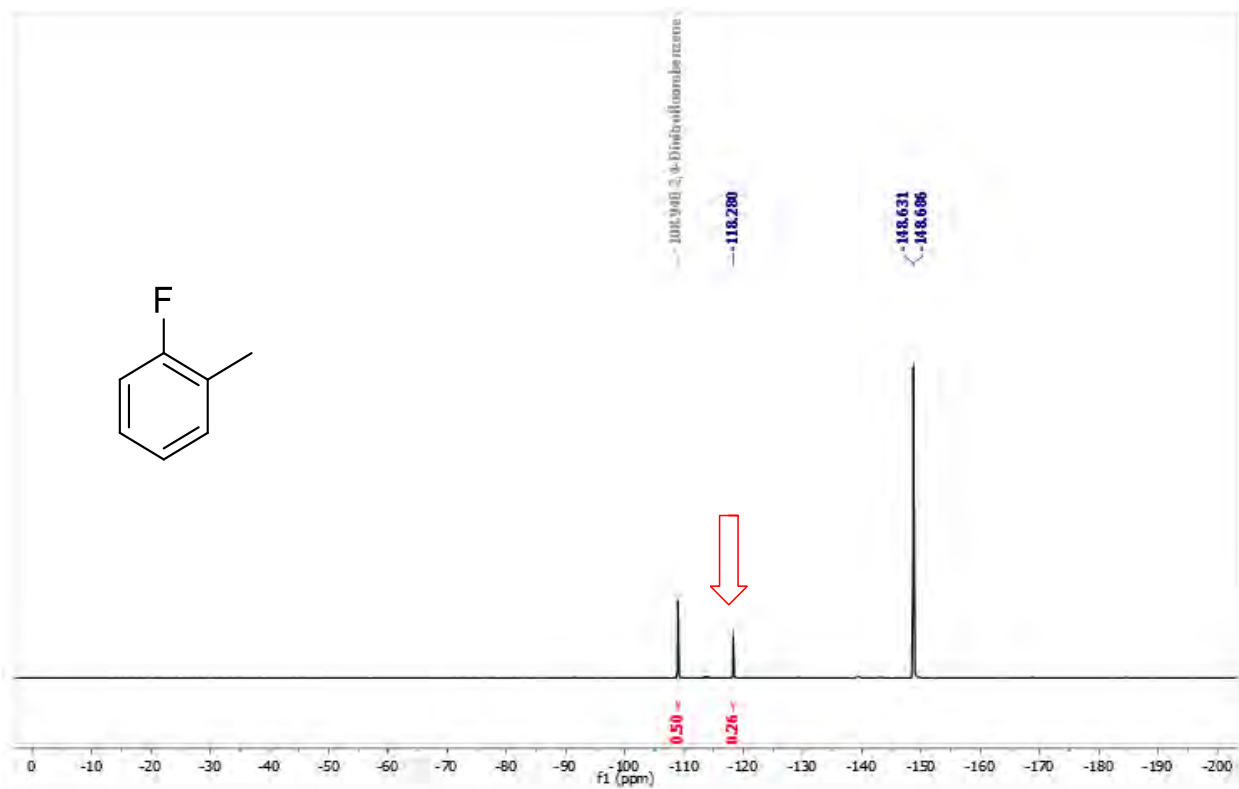
^{19}F NMR 1,3,5-tri-*tert*-butyl-2-fluorobenzene, **2.8**, using 2,2,2-trifluoroethanol as the I.S.



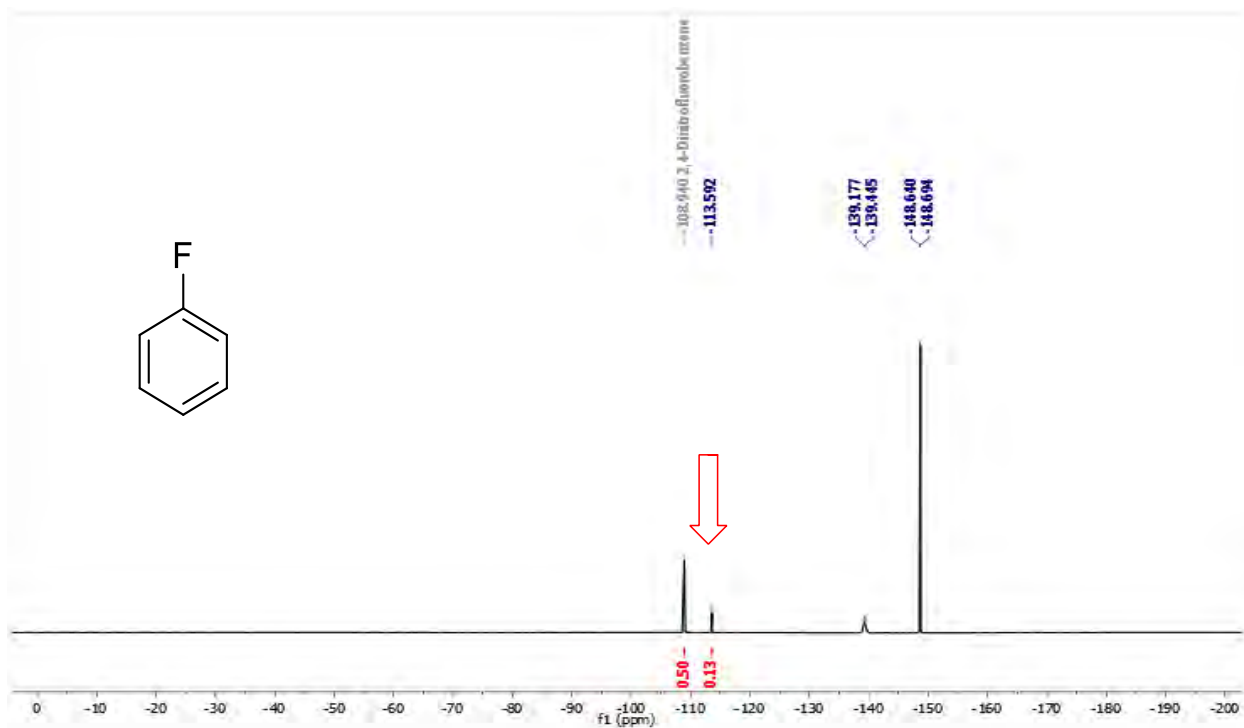
^{19}F NMR 1-fluoro-2,6-dimethylbenzene, **2.9**, using 2,4-dinitrofluorobenzene as the I.S.



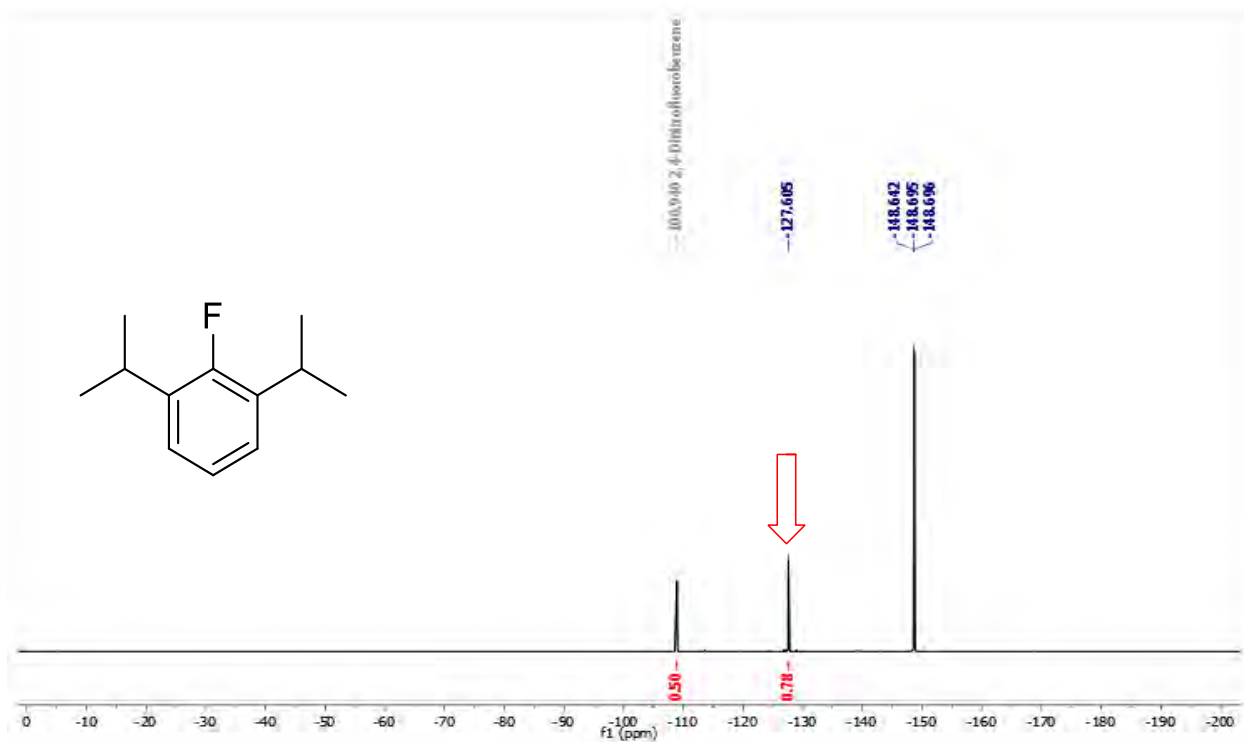
^{19}F NMR 1-fluoro-2-methylbenzene, **2.10**, using 2,4-dinitrofluorobenzene as the I.S.



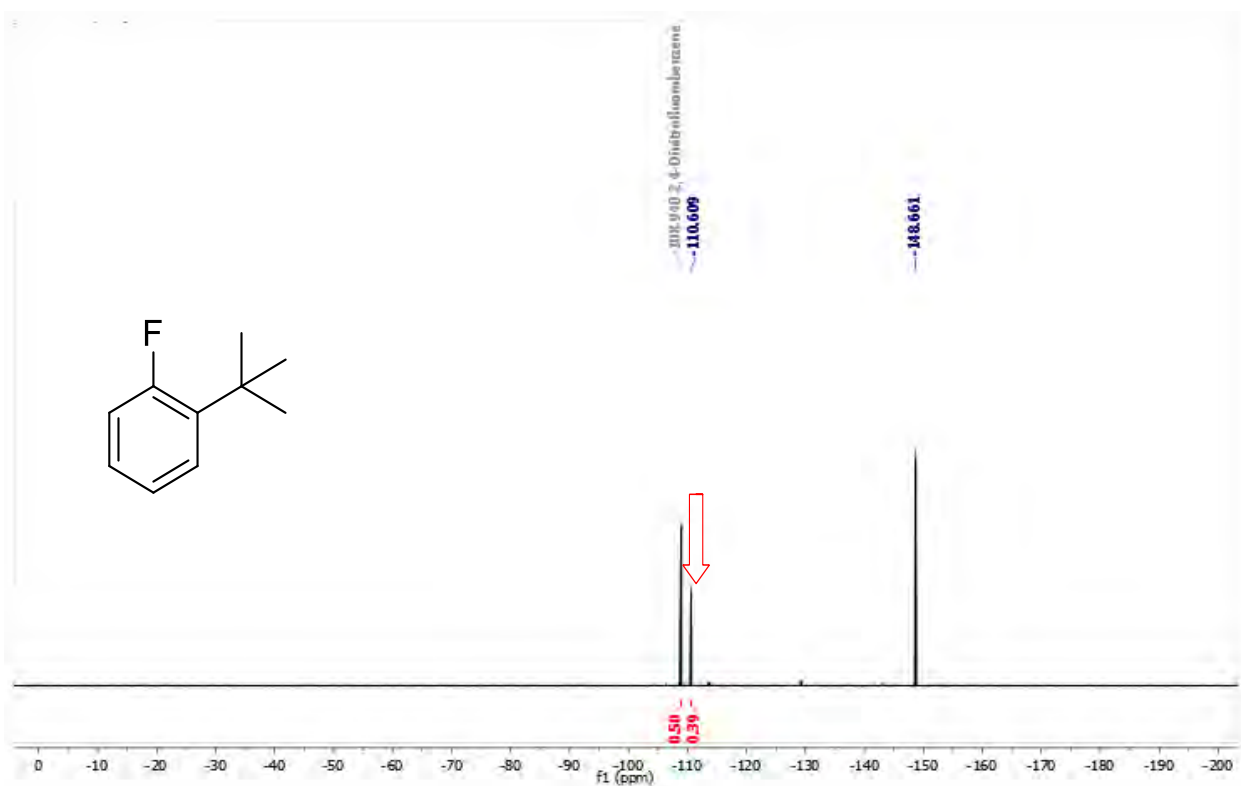
^{19}F NMR 1-fluorobenzene, **2.11**, using 2,4-dinitrofluorobenzene as the I.S.



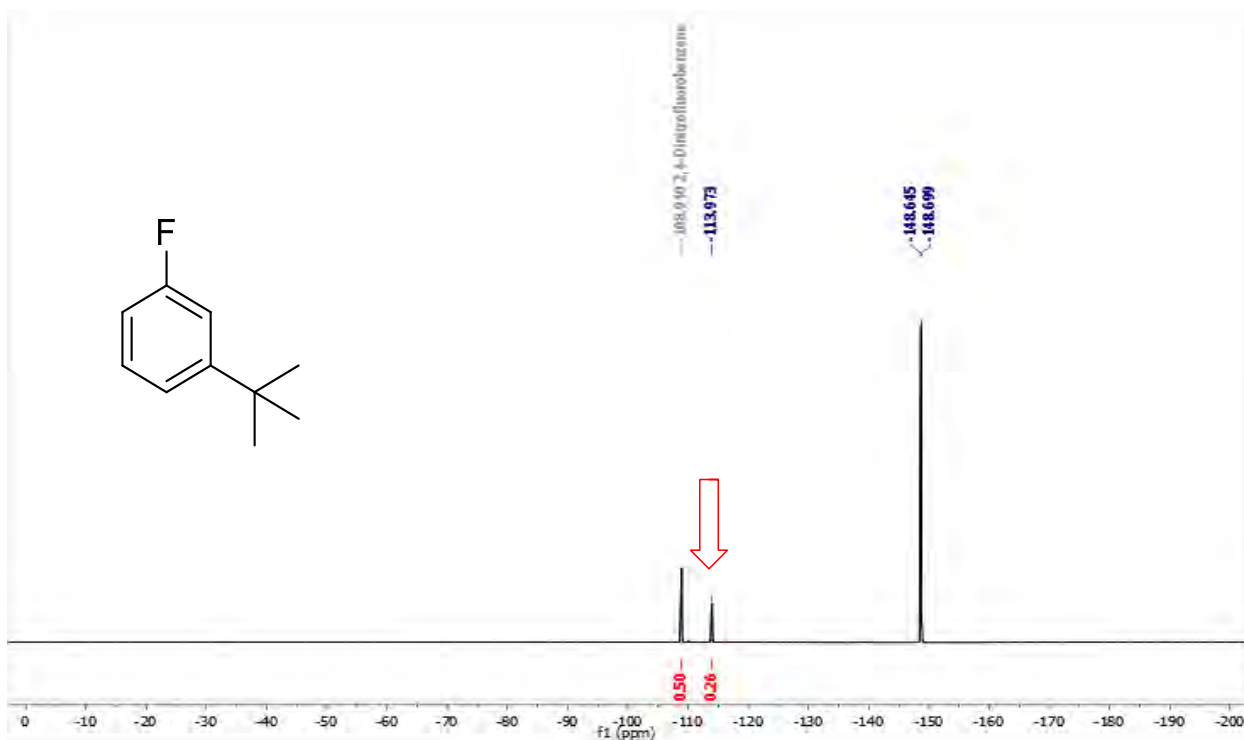
^{19}F NMR 1-fluoro-2,6-diisopropylbenzene, **2.12**, using 2,4-dinitrofluorobenzene as the I.S.



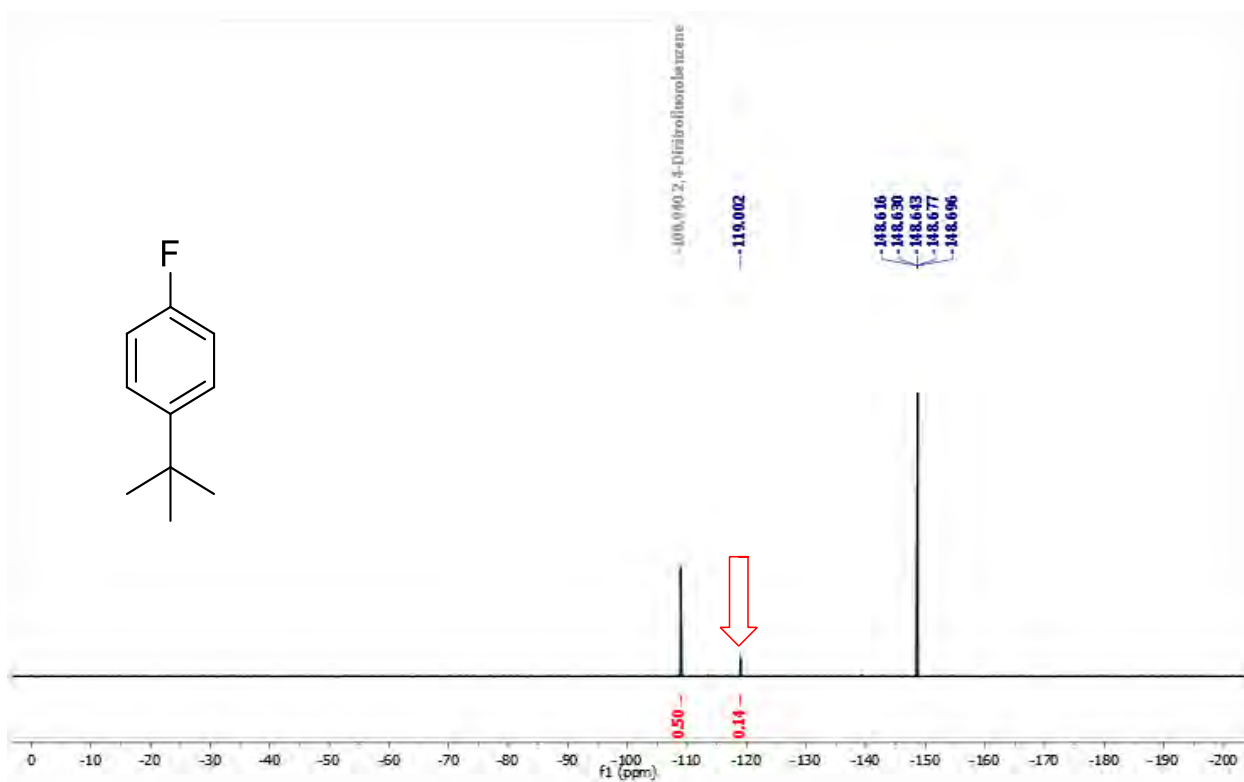
^{19}F NMR 1-*tert*-butyl-2-fluorobenzene, **2.13**, using 2,4-dinitrofluorobenzene as the I.S.



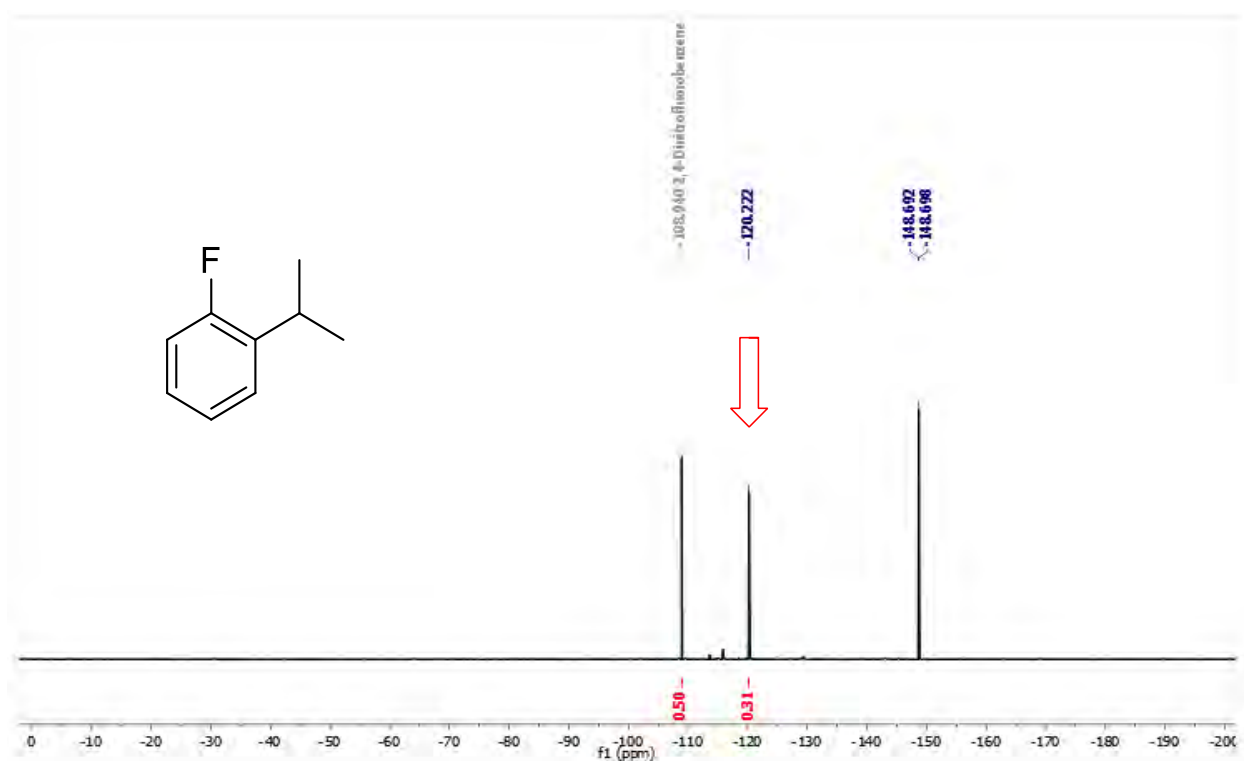
^{19}F NMR 1-*tert*-butyl-3-fluorobenzene, **2.14**, using 2,4-dinitrofluorobenzene as the I.S.



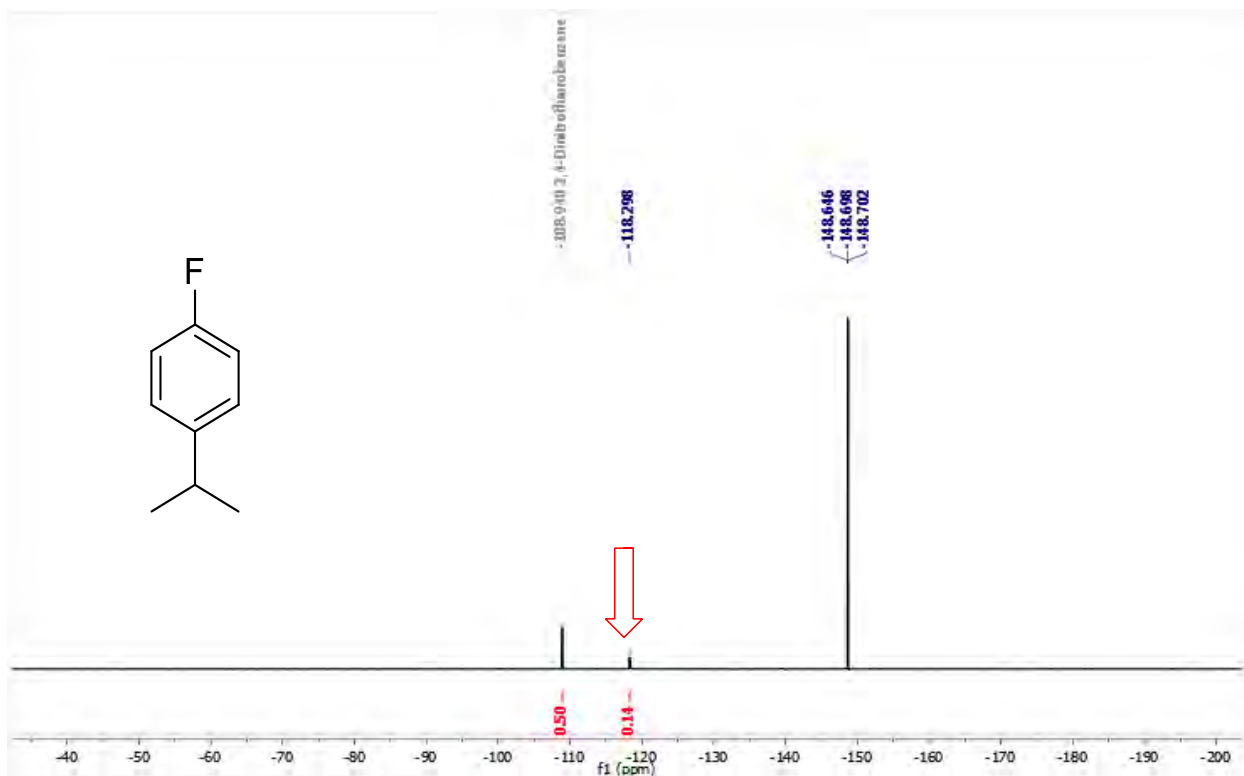
^{19}F NMR 1-tert-Butyl-4-fluorobenzene, **2.15**, using 2,4-dinitrofluorobenzene as the I.S.



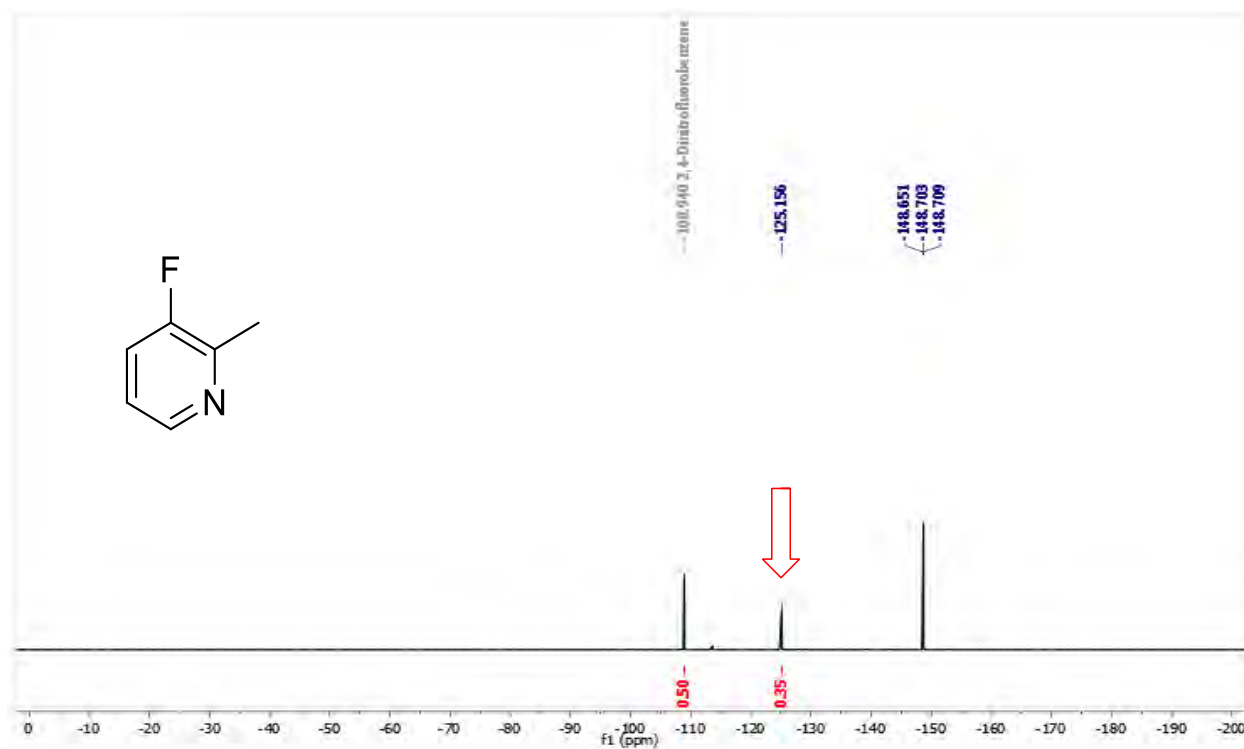
^{19}F NMR 1-fluoro-4-isopropylbenzene, **2.16**, using 2,4-dinitrofluorobenzene as the I.S.



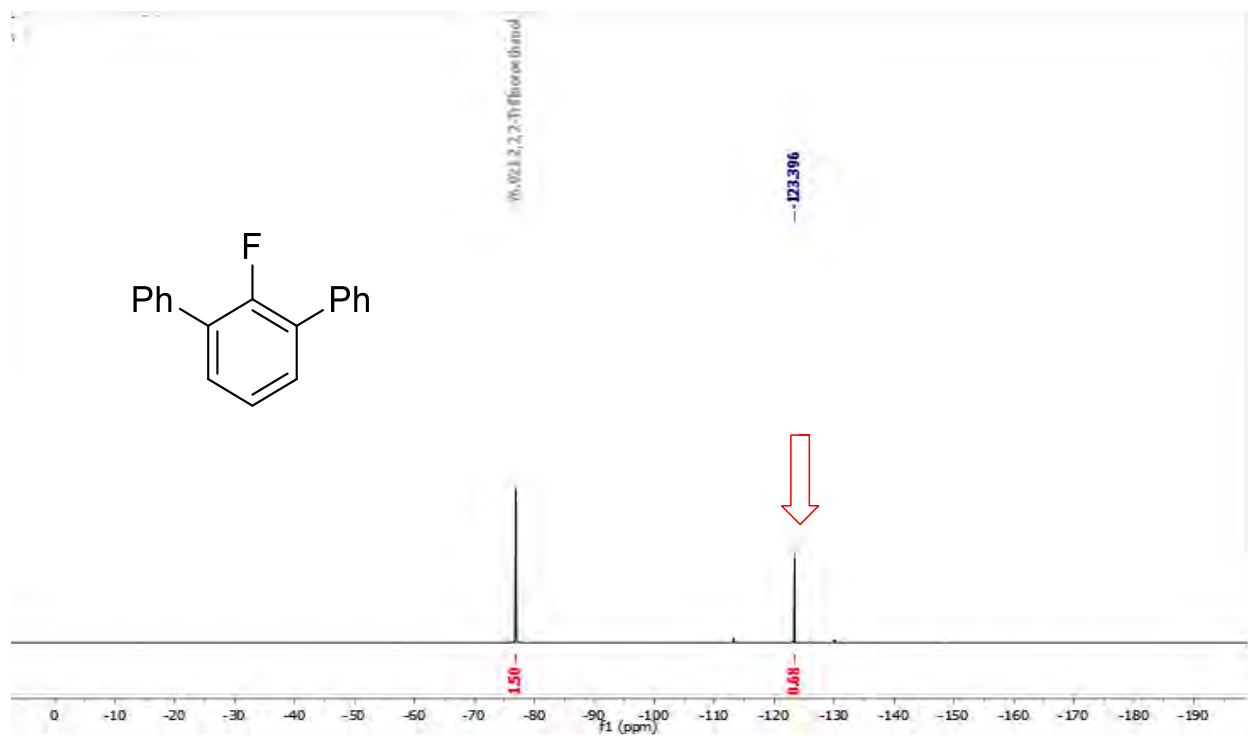
^{19}F NMR 1-fluoro-4-isopropylbenzene, **2.17**, using 2,4-dinitrofluorobenzene as the I.S.



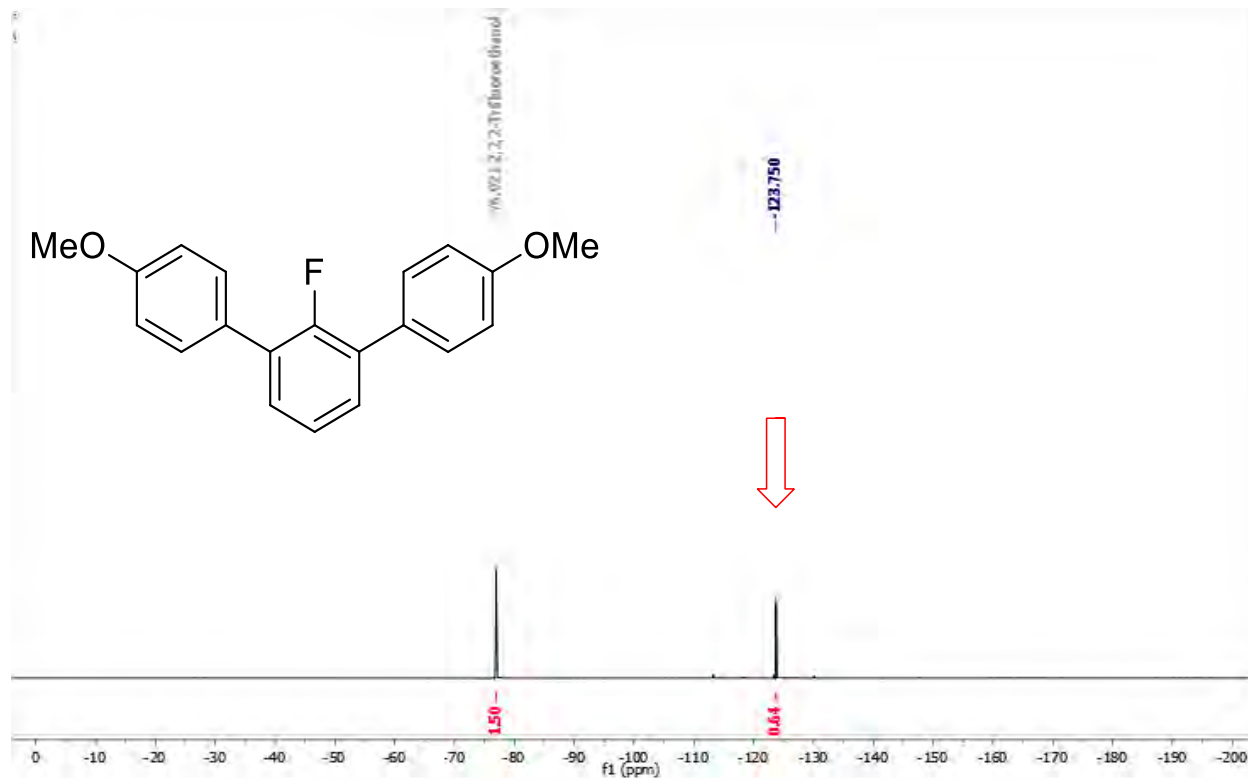
^{19}F NMR 3-fluoro-2-methylpyridine, **2.18**, using 2,4-dinitrofluorobenzene as the I.S.



^{19}F NMR 1-fluoro-2,6-diphenylbenzene, **2.24**, using 2,2,2-trifluoroethanol as the I.S.



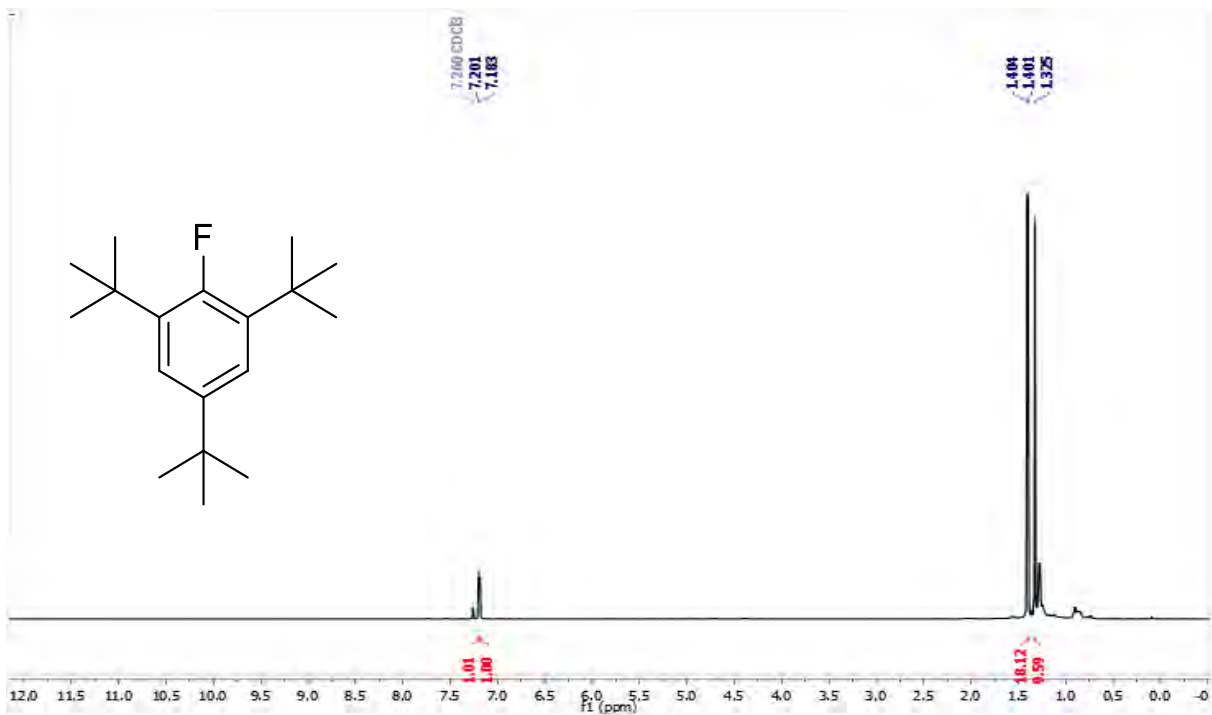
^{19}F NMR 1-fluoro-2,6-bis(4-methoxyphenyl)benzene, **2.25**, using 2,2,2-trifluoroethanol as the I.S.



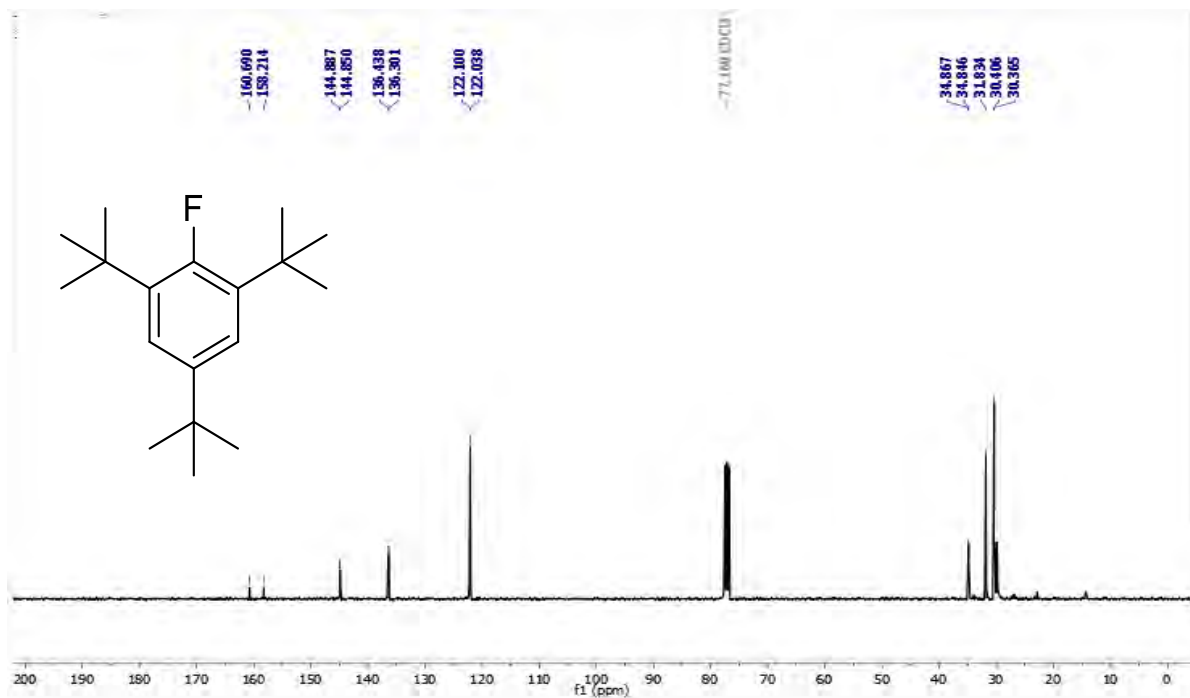
^1H , ^{13}C and ^{19}F NMR Spectra of Isolated Aryl Fluorides

1,3,5-tri-*tert*-butyl-2-fluorobenzene (**2.8**)

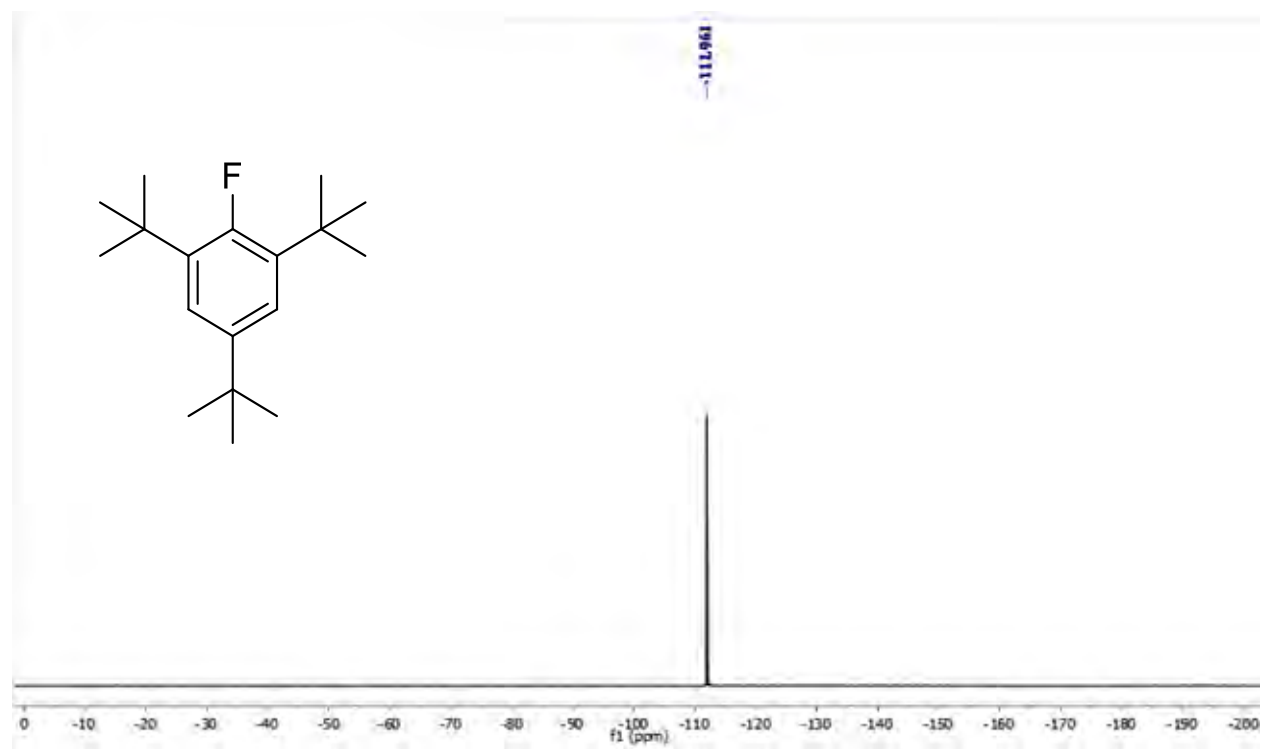
^1H NMR



^{13}C NMR

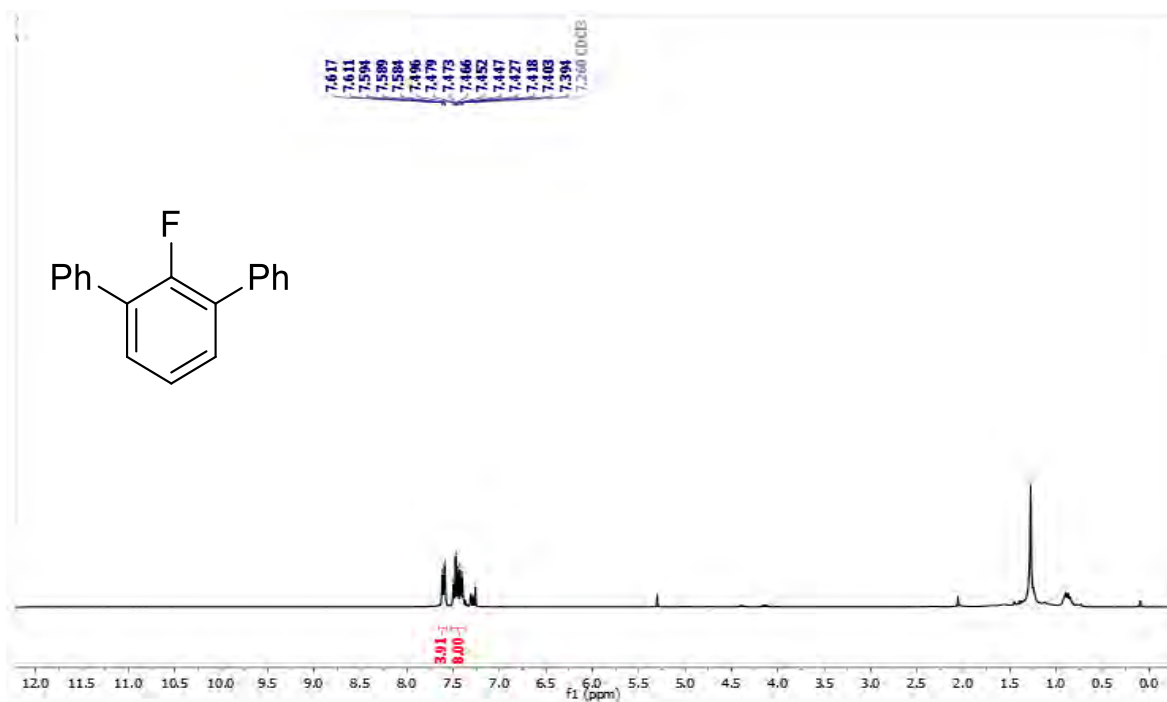


^{19}F NMR

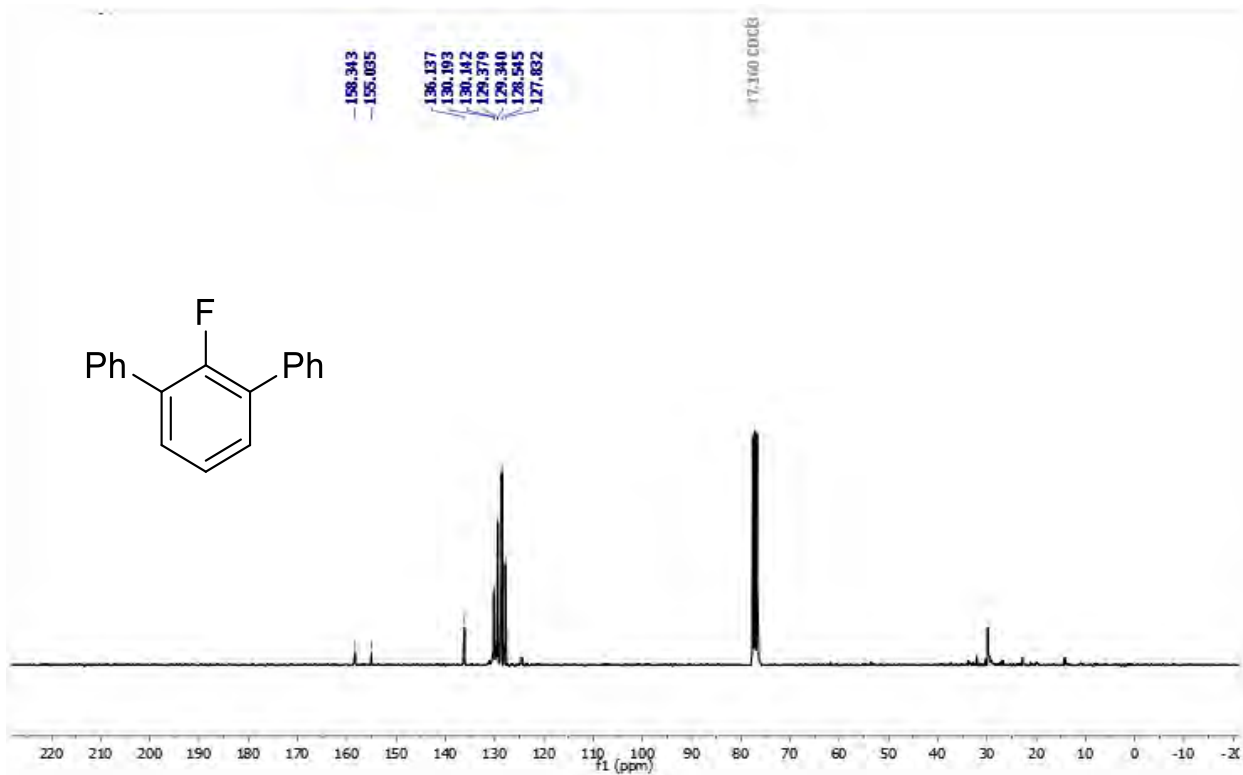


1-fluoro-2,6-diphenylbenzene (2.24)

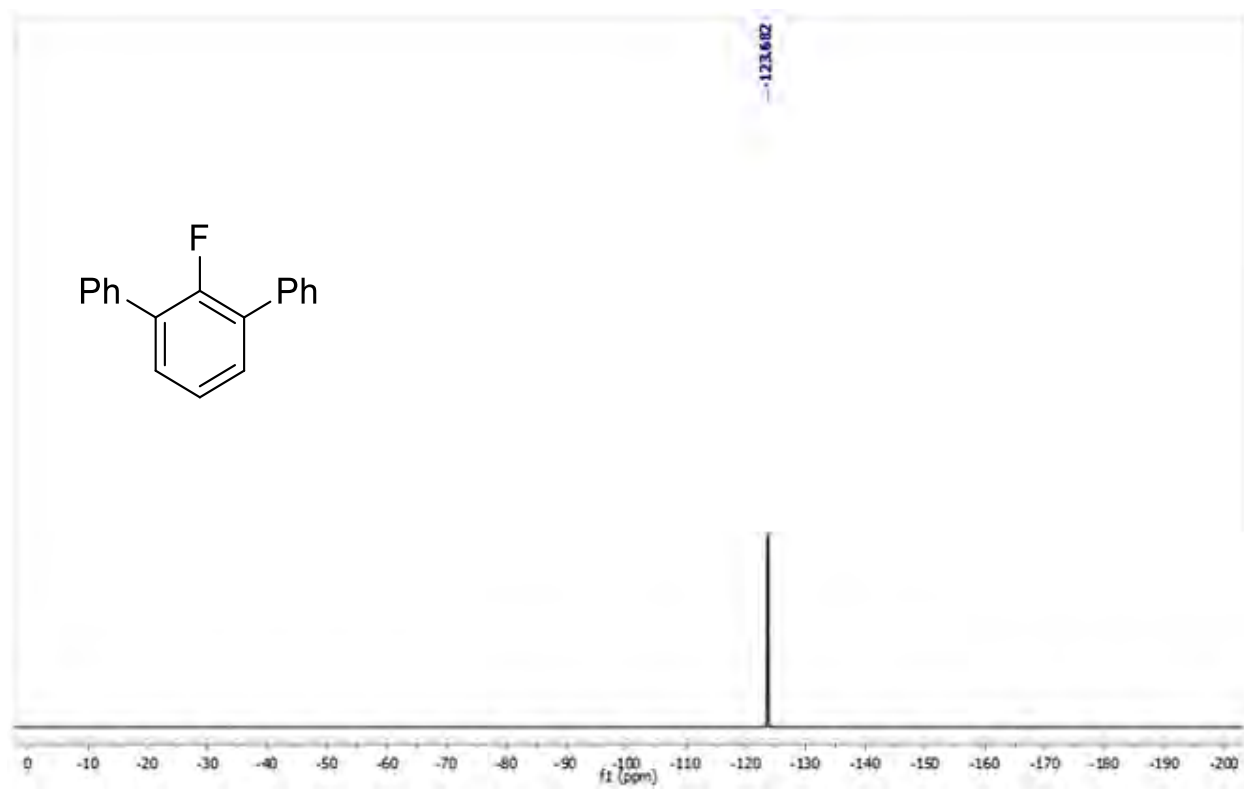
¹H NMR



¹³C NMR

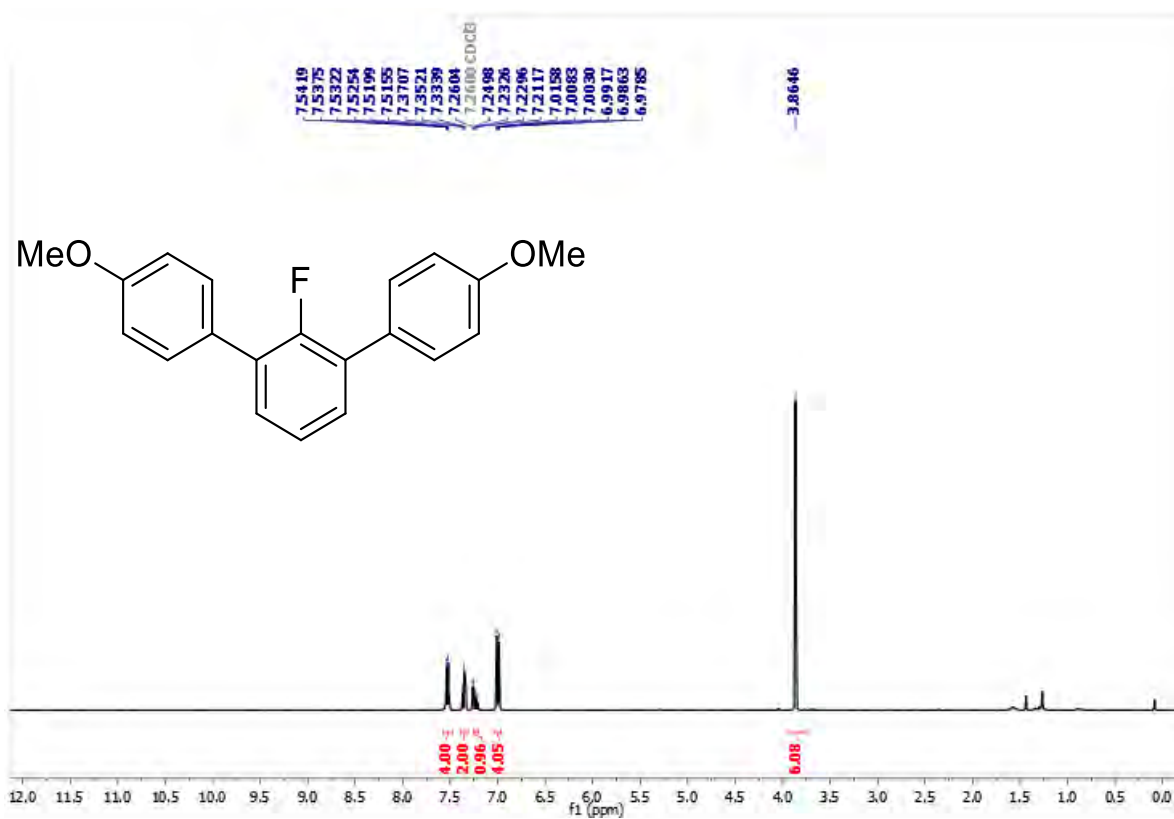


^{19}F NMR

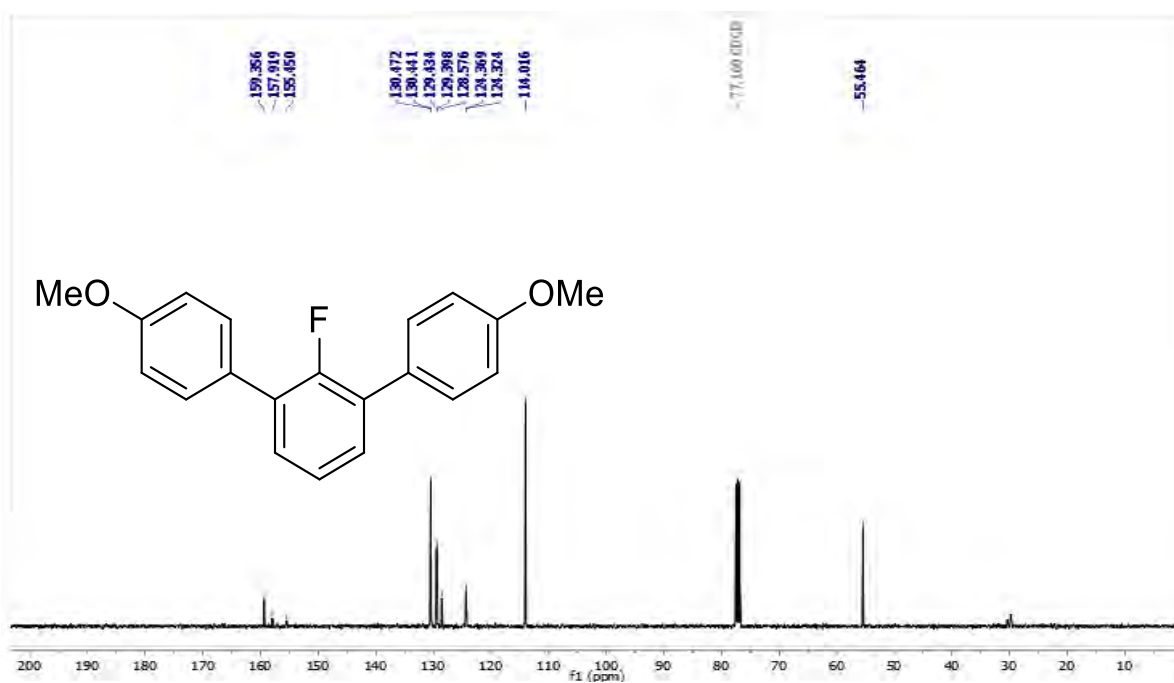


1-fluoro-2,6-bis(4-methoxyphenyl)benzene (2.25)

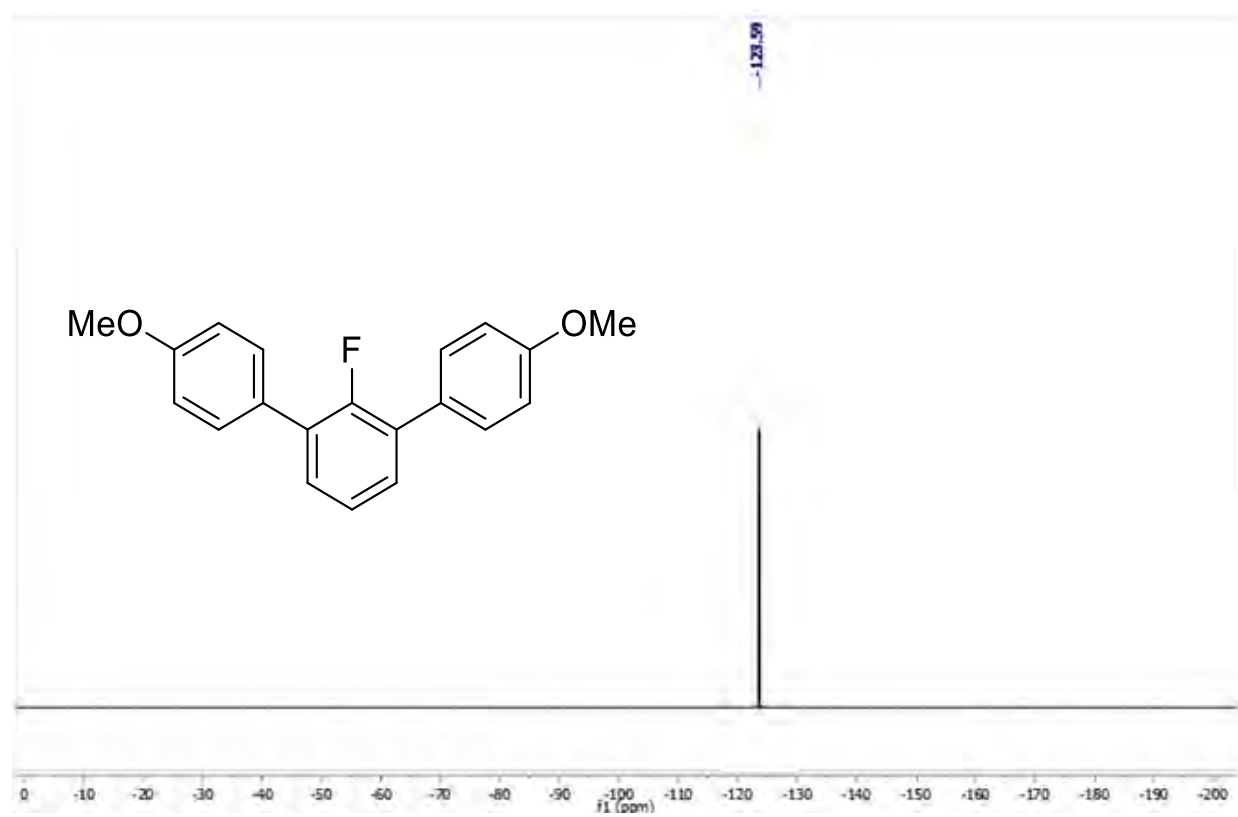
¹H NMR



¹³C NMR

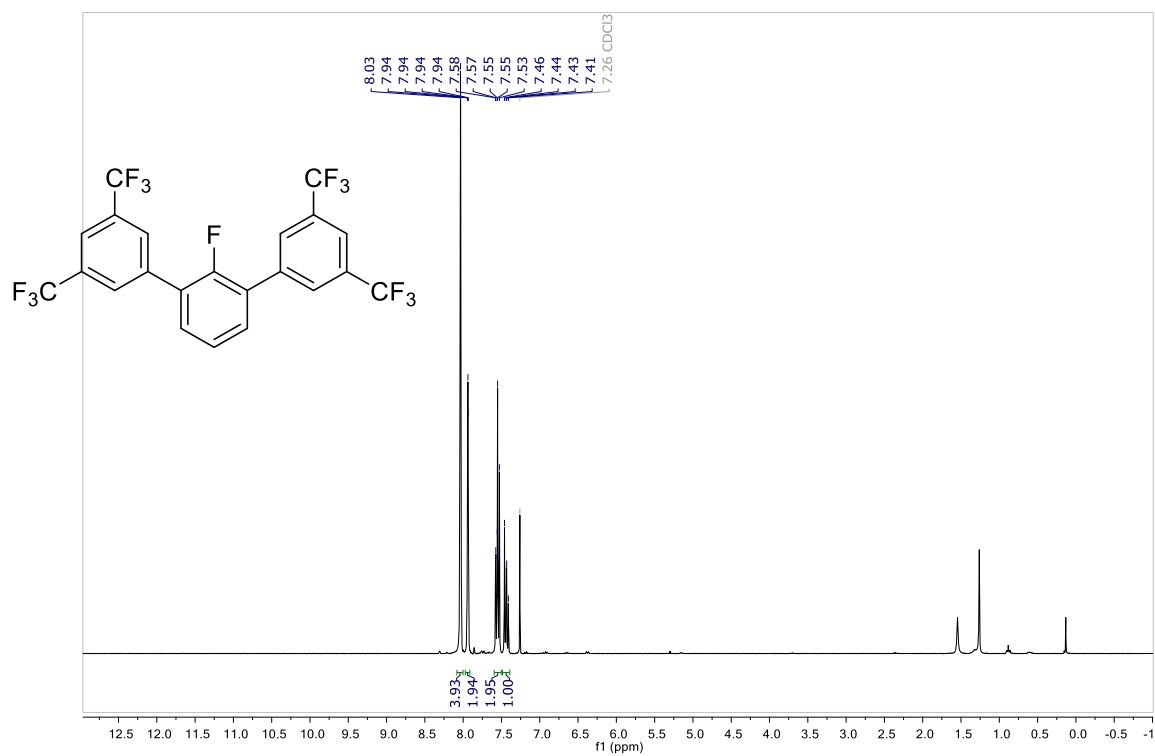


^{19}F NMR

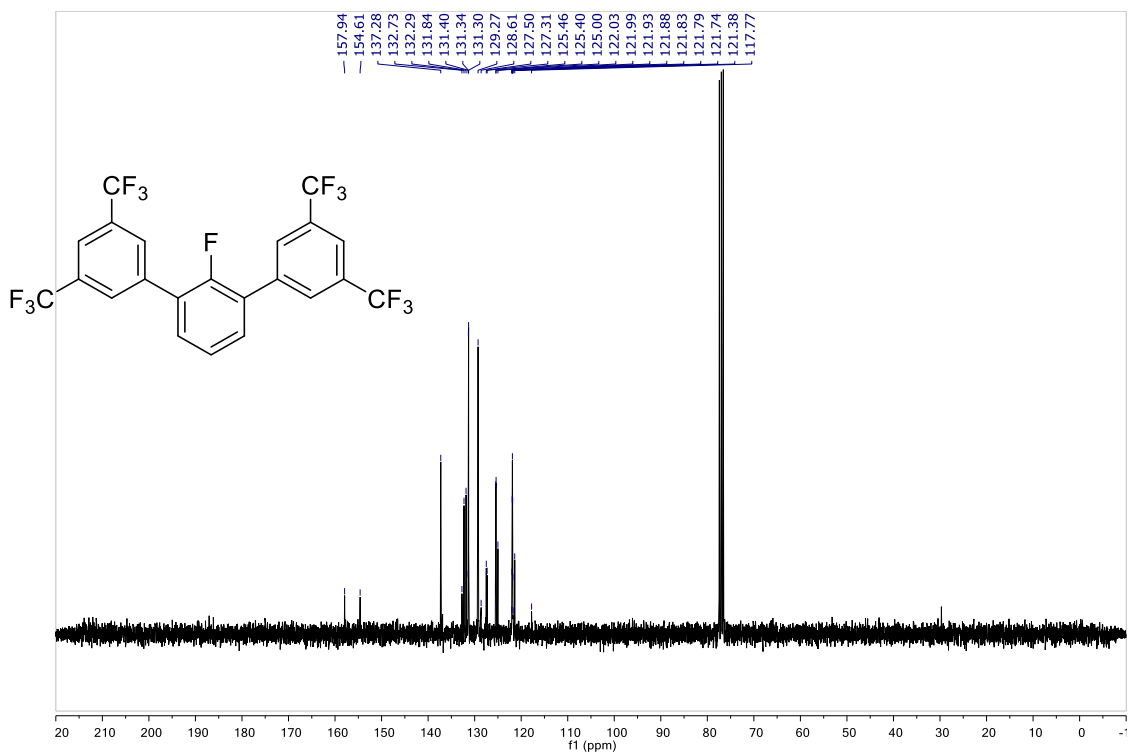


1-fluoro-2,6-di-[3,5-bis(trifluoromethyl)phenyl]benzene (2.26)

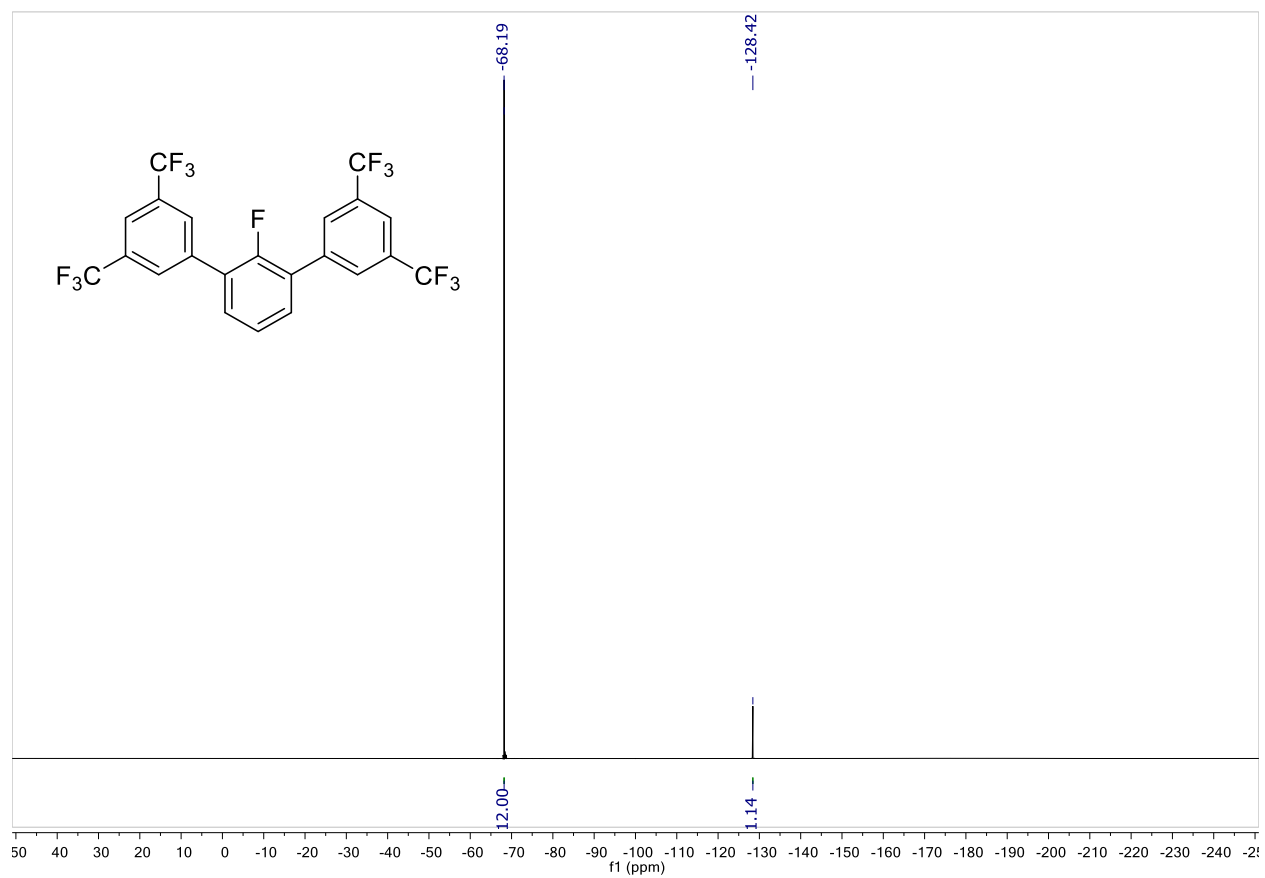
¹H NMR



¹³C NMR



^{19}F NMR

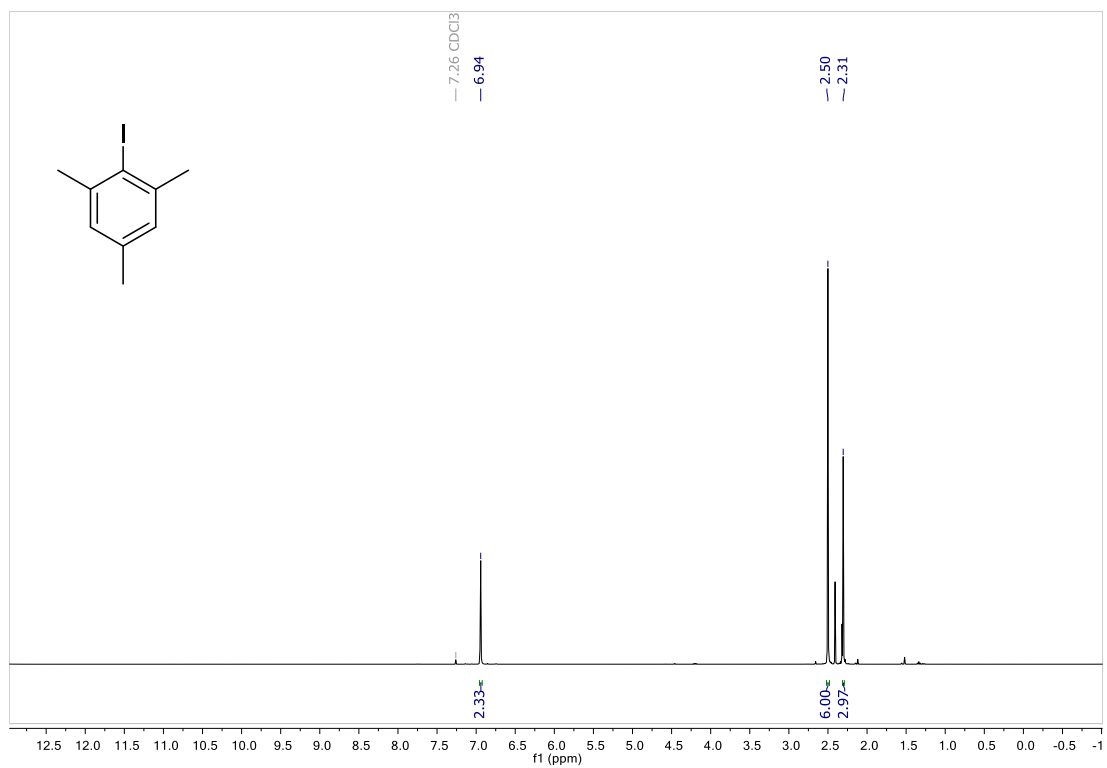


Annex B: Chapter 3

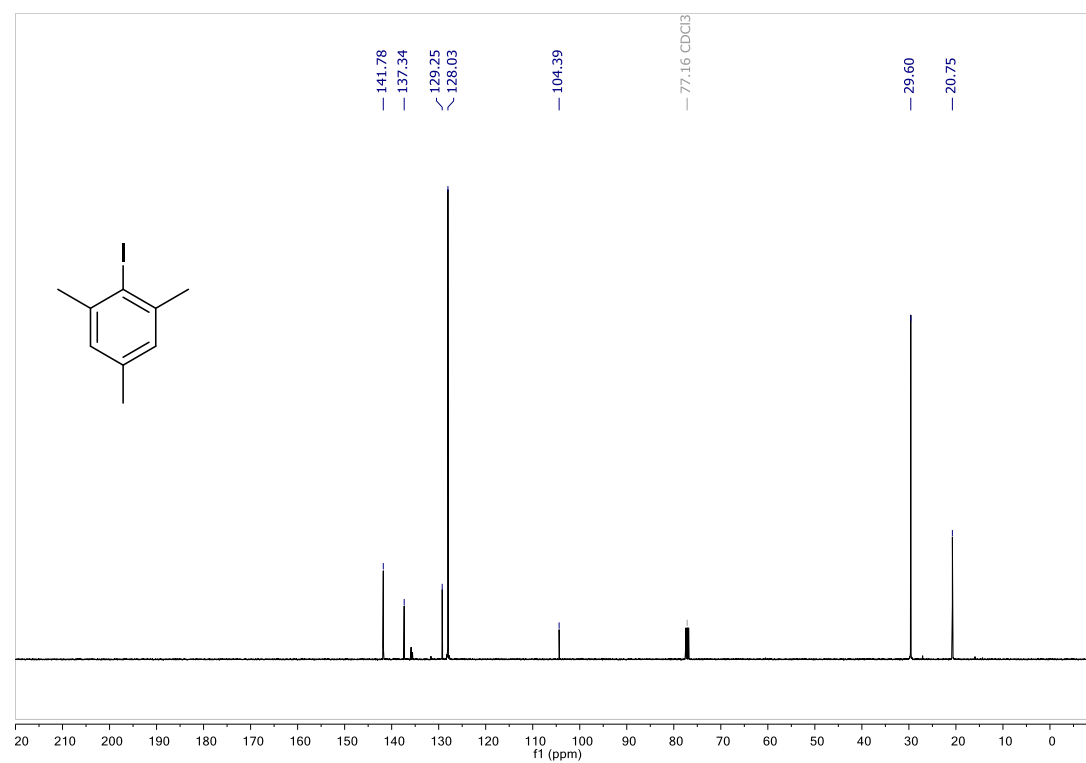
NMR Spectra of selected compounds

Iodomesitylene

^1H NMR

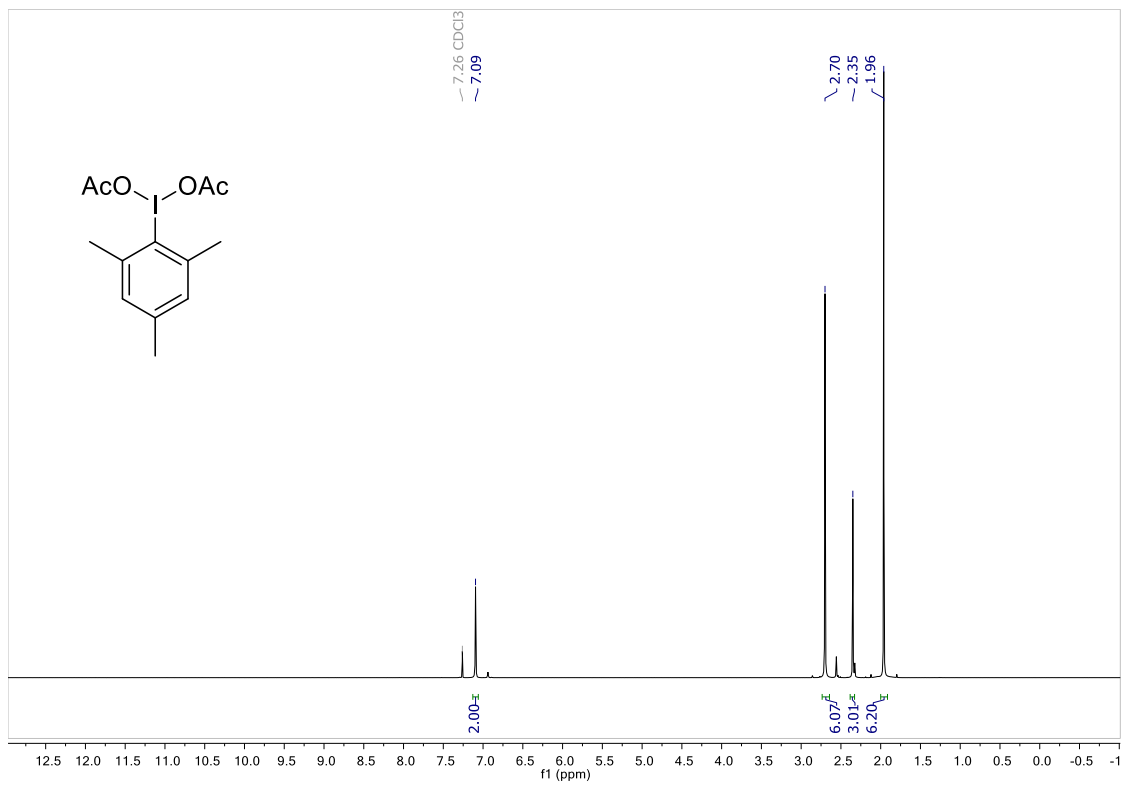


^{13}C NMR

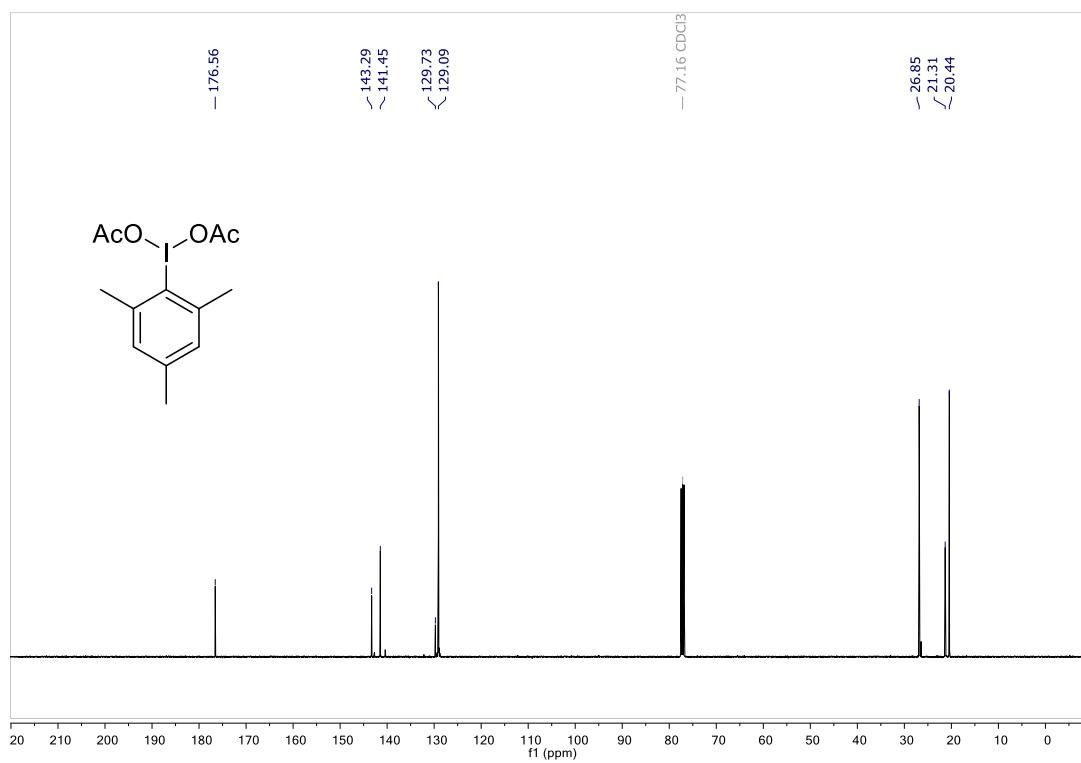


Iodomesitylene diacetate (3.12)

¹H NMR

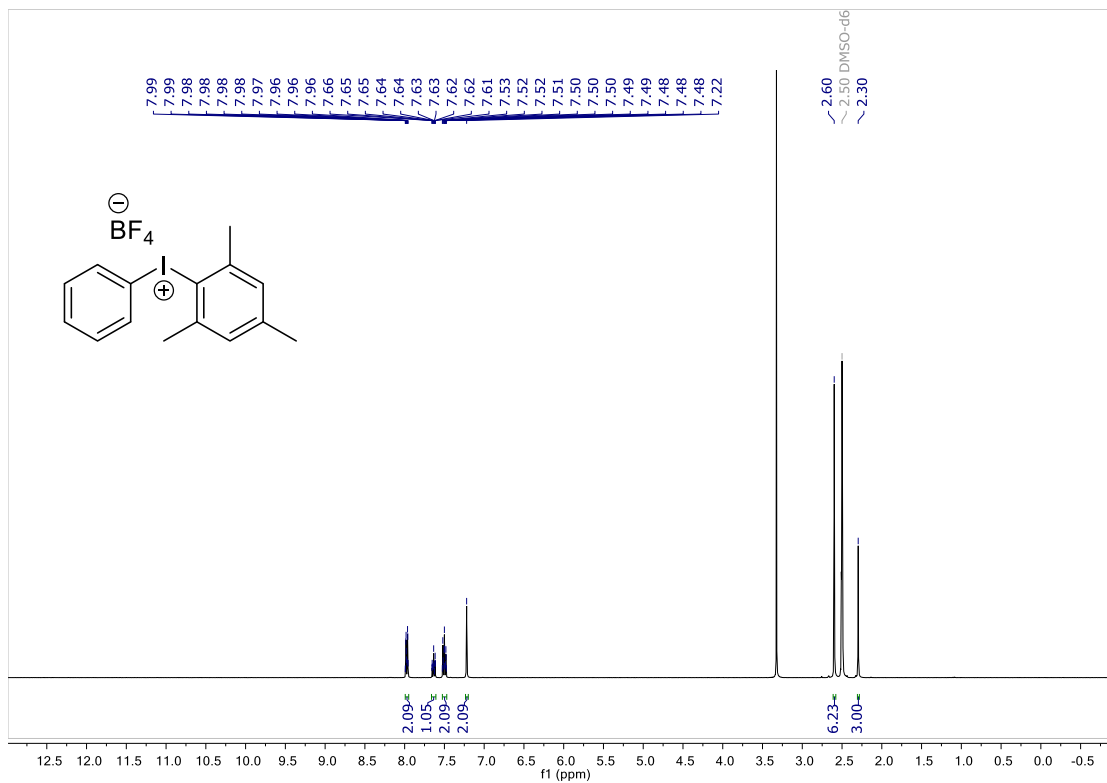


¹³C NMR

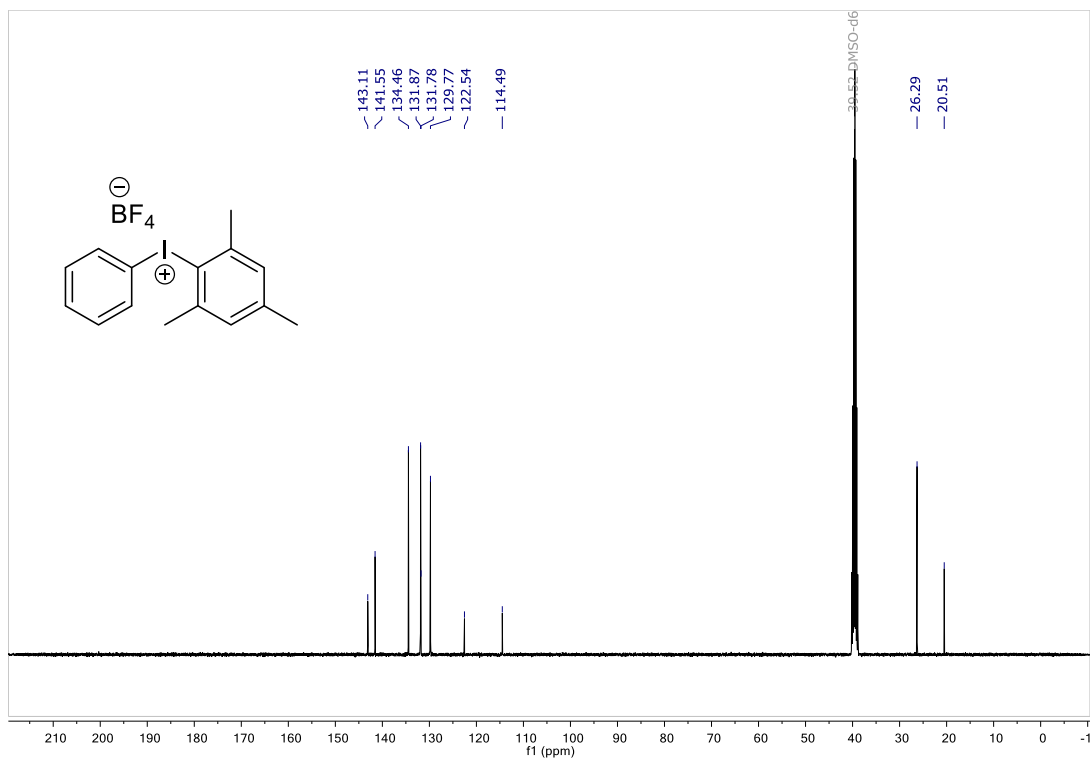


(2,4,6-trimethylphenyl)(phenyl)iodonium tetrafluoroborate (**3.13**)

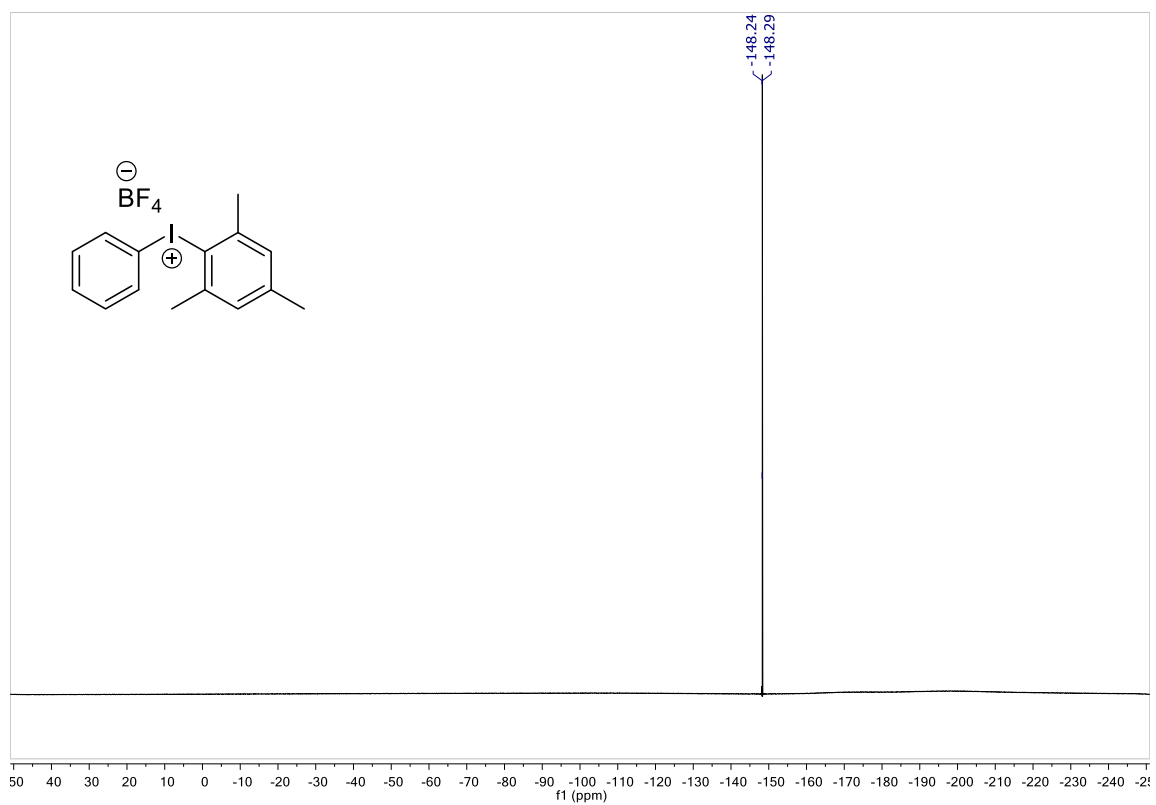
^1H NMR



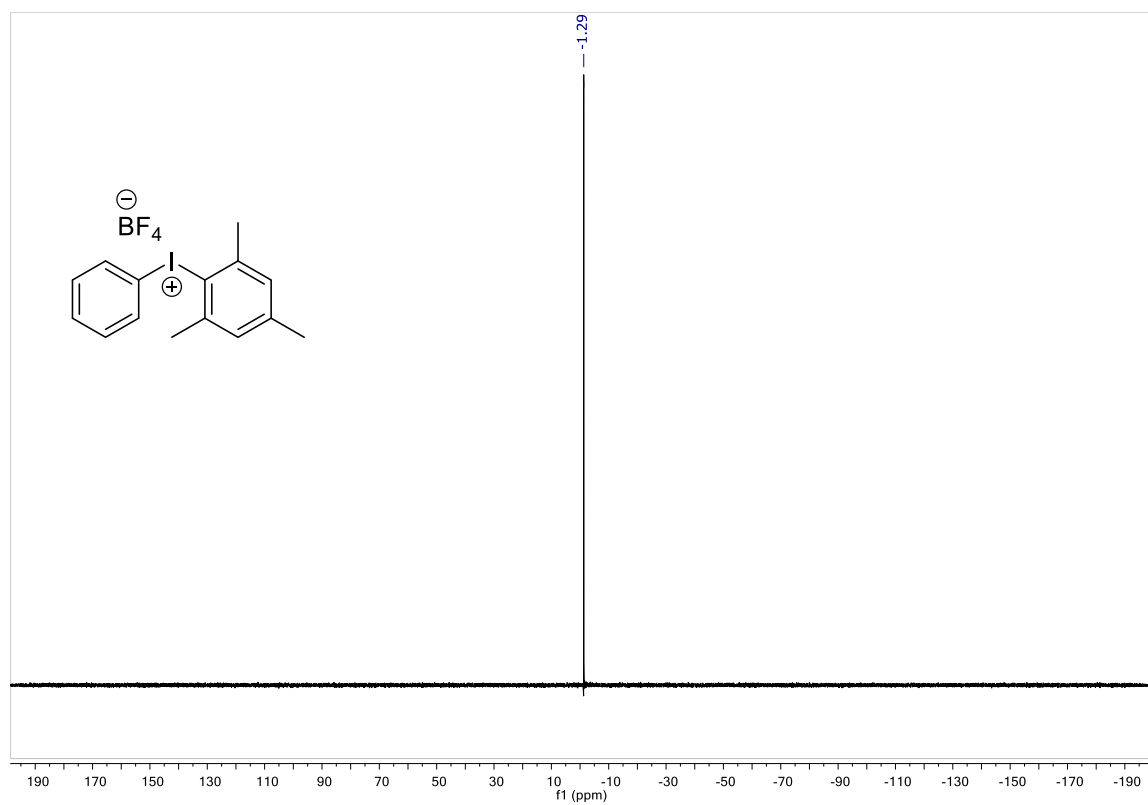
^{13}C NMR



^{19}F NMR

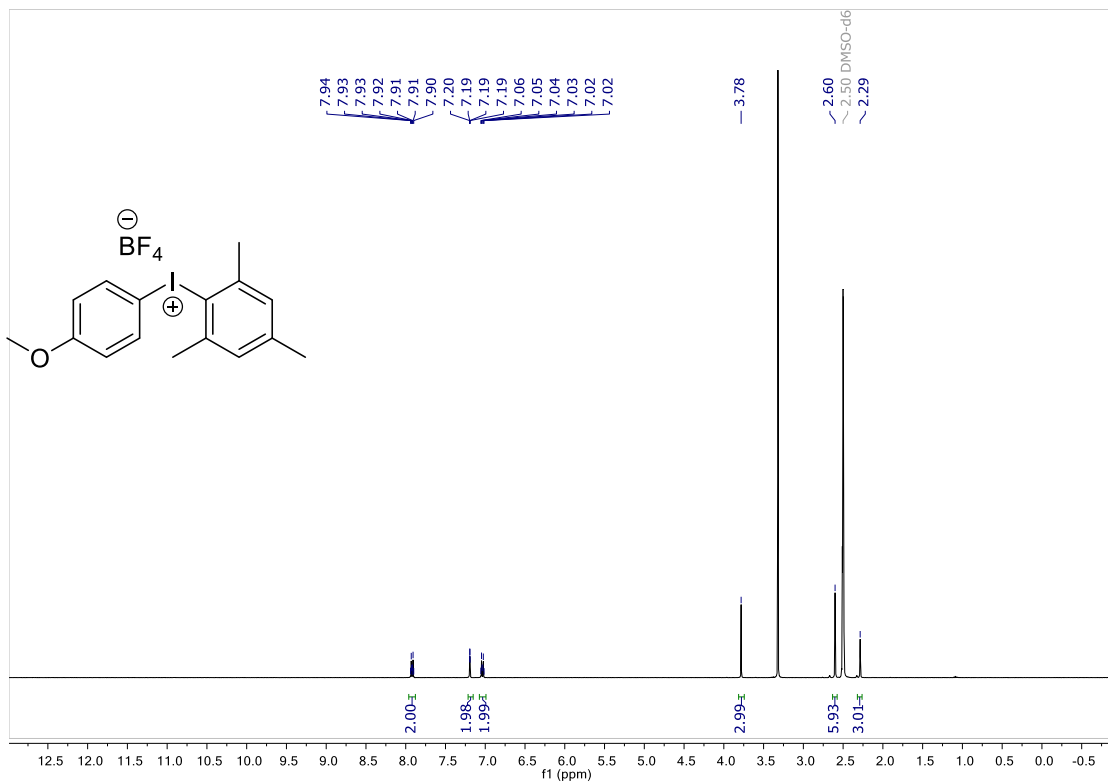


^{11}B NMR

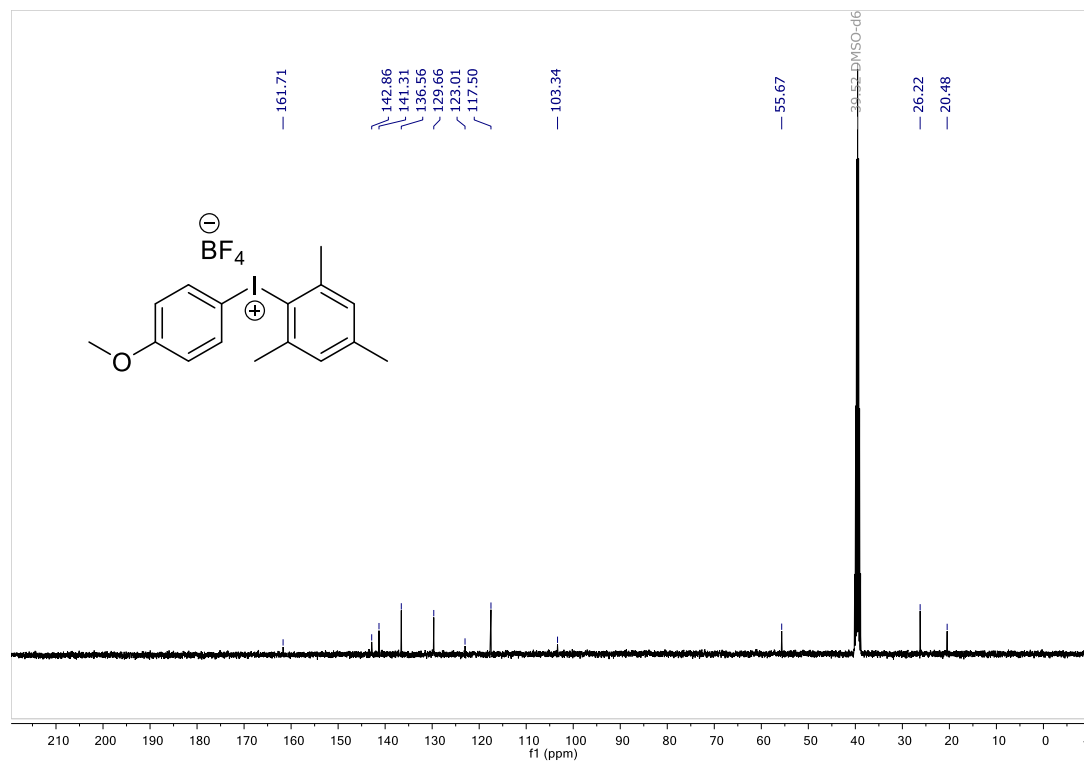


(4-methoxyphenyl)(2,4,6-trimethylphenyl)iodonium tetrafluoroborate (**3.11**)

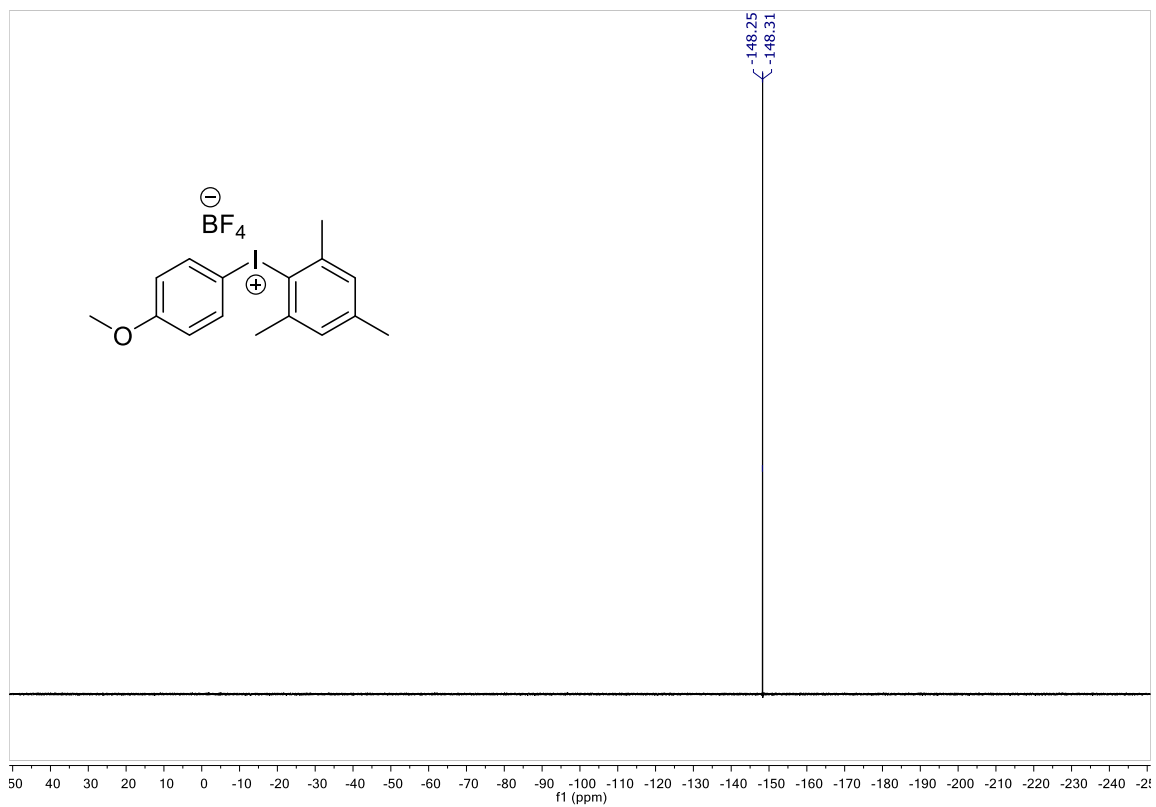
^1H NMR



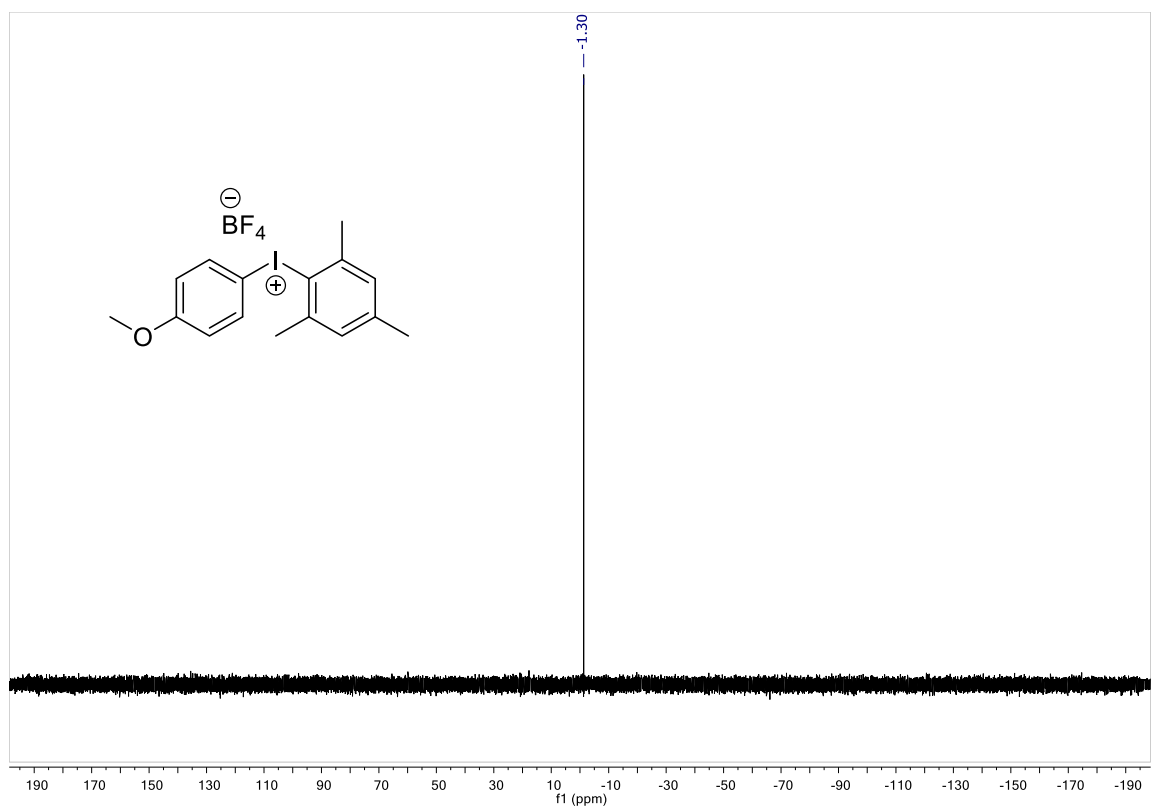
^{13}C NMR



^{19}F NMR

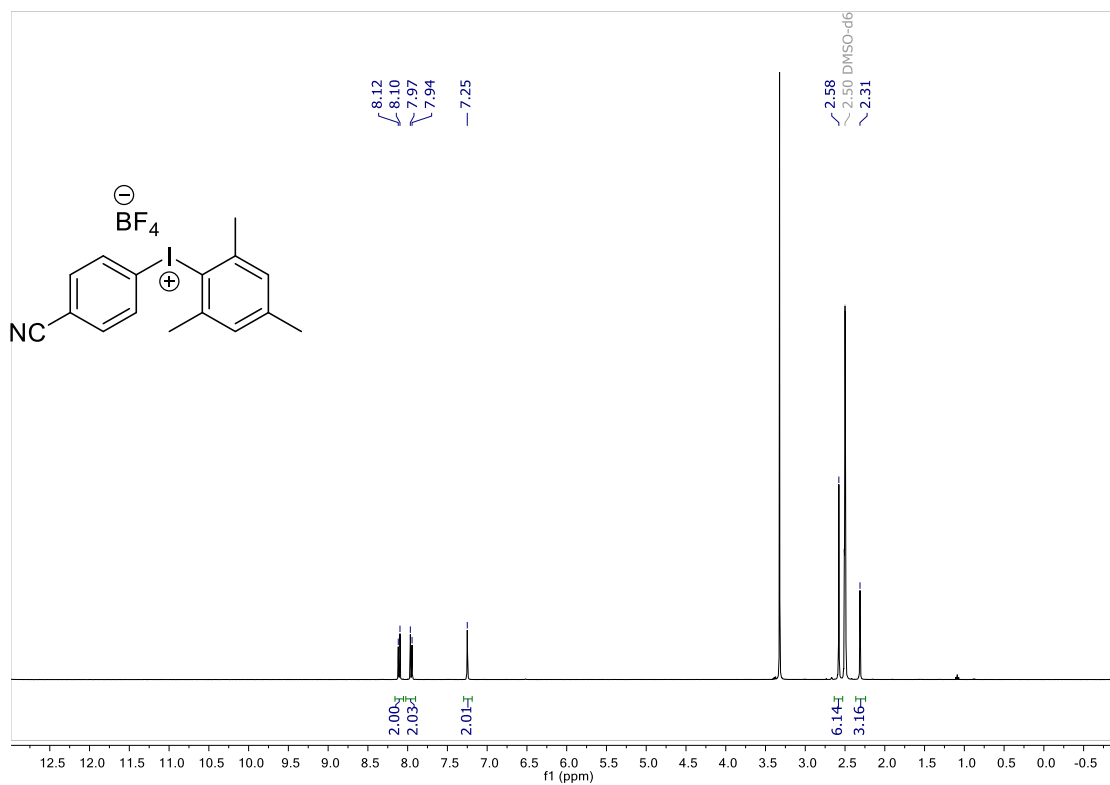


^{11}B NMR

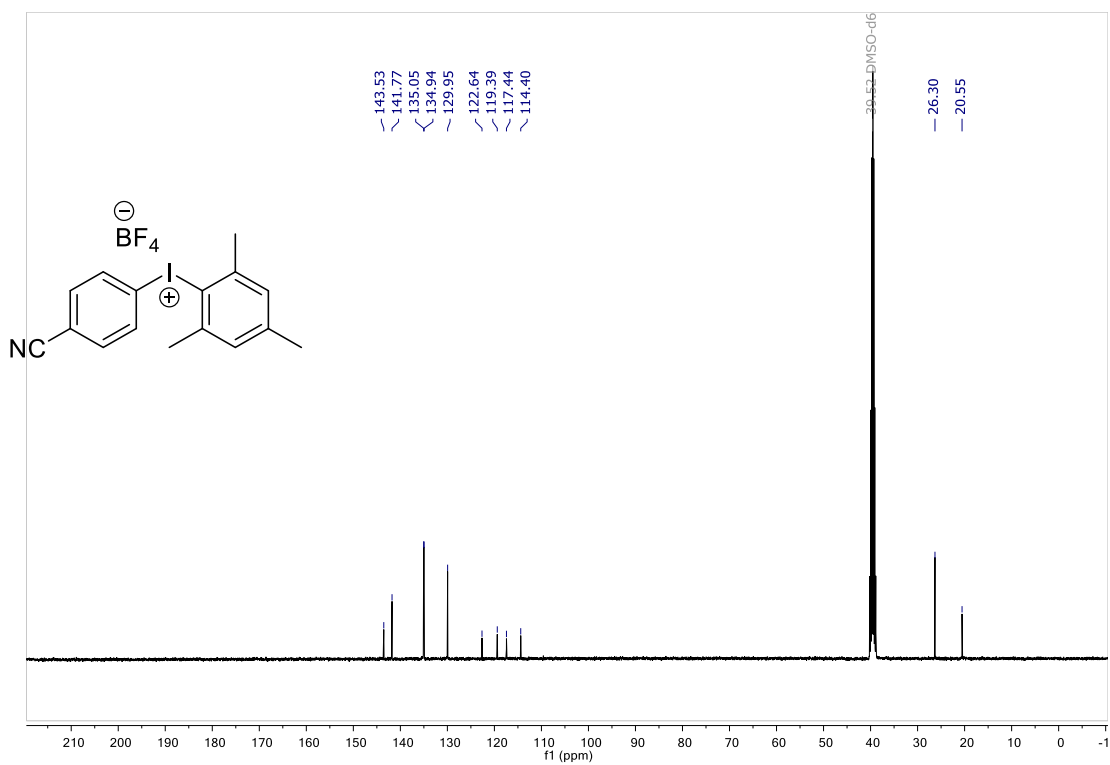


(4-cyanophenyl)(2,4,6-trimethylphenyl)iodonium tetrafluoroborate (**3.14**)

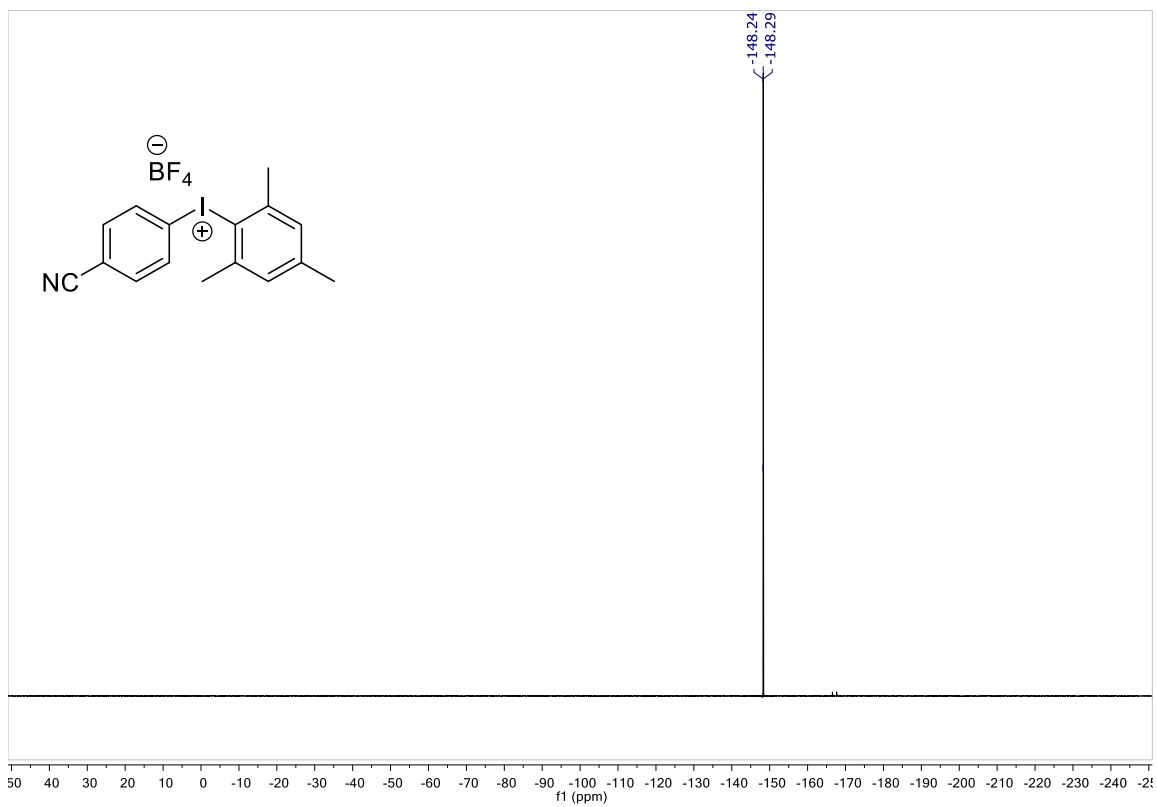
^1H NMR



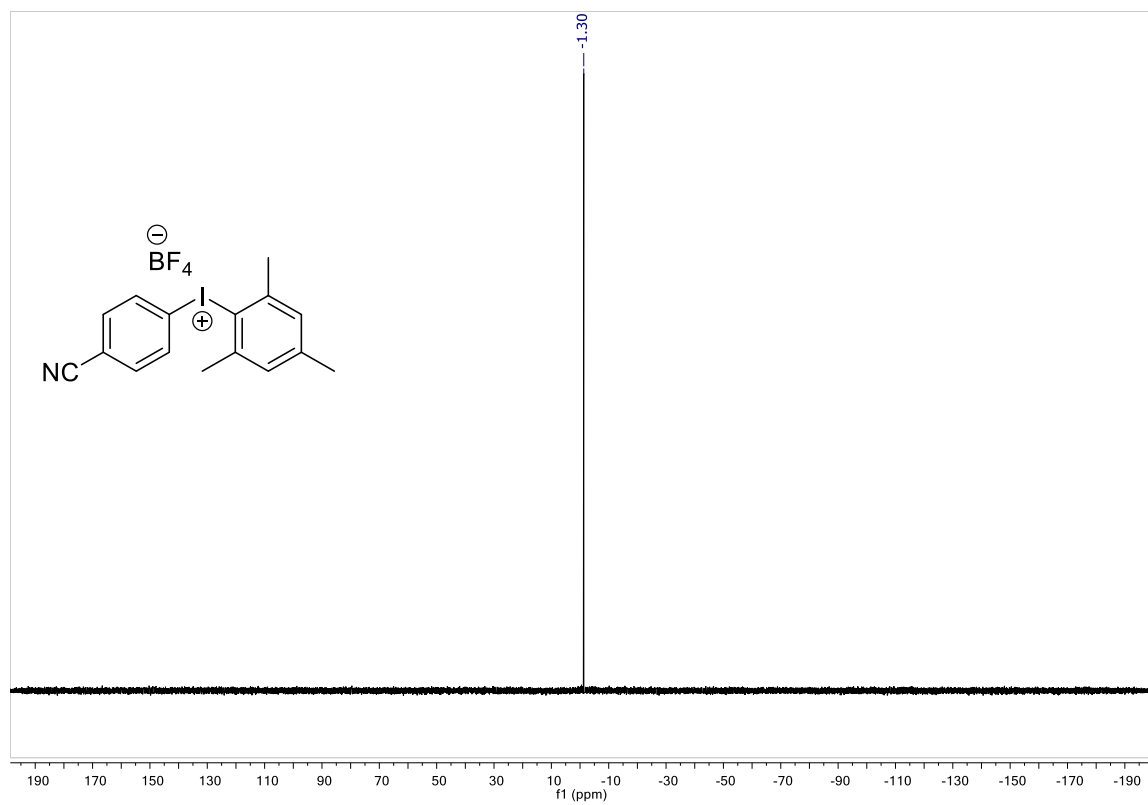
^{13}C NMR



¹⁹F NMR

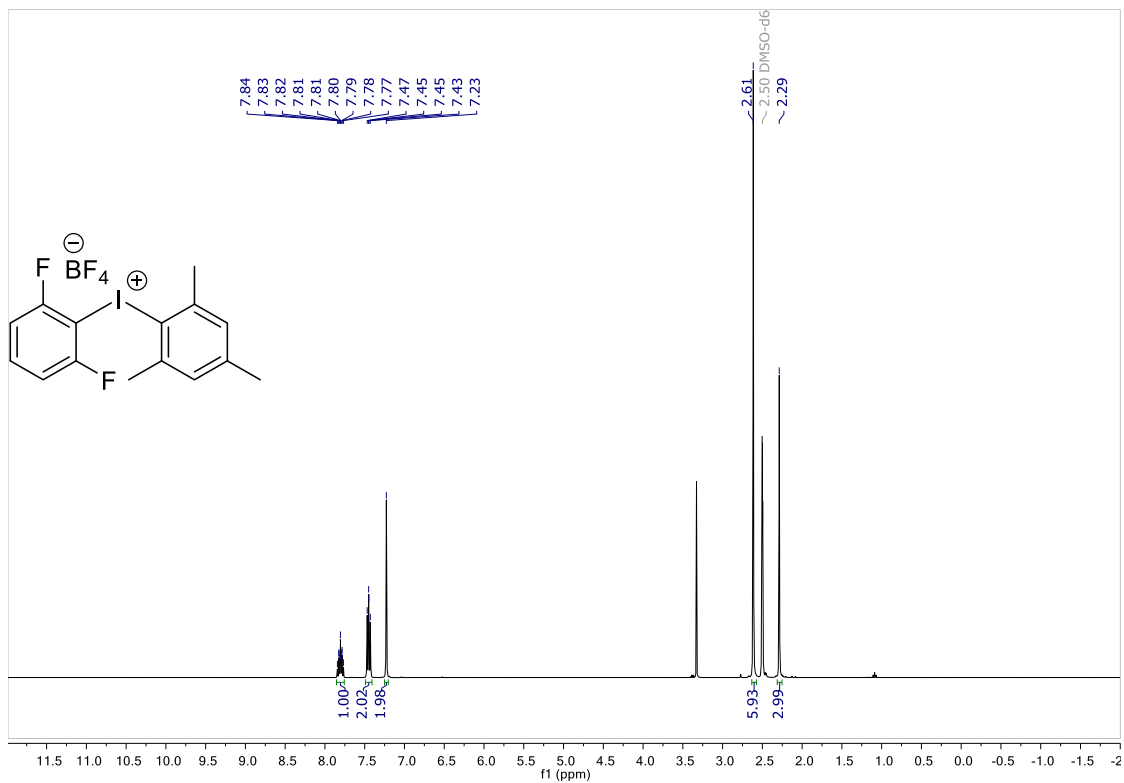


¹¹B NMR

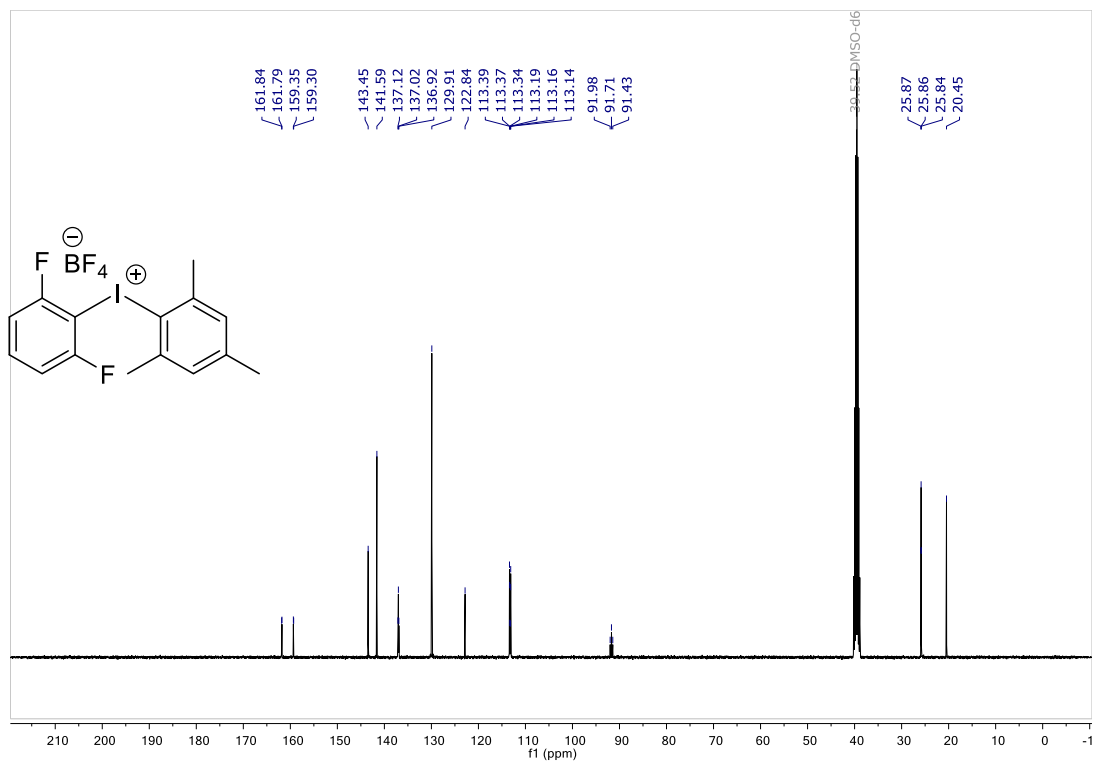


(2,6-difluorophenyl)(2,4,6-trimethylphenyl)iodonium tetrafluoroborate (**3.15**)

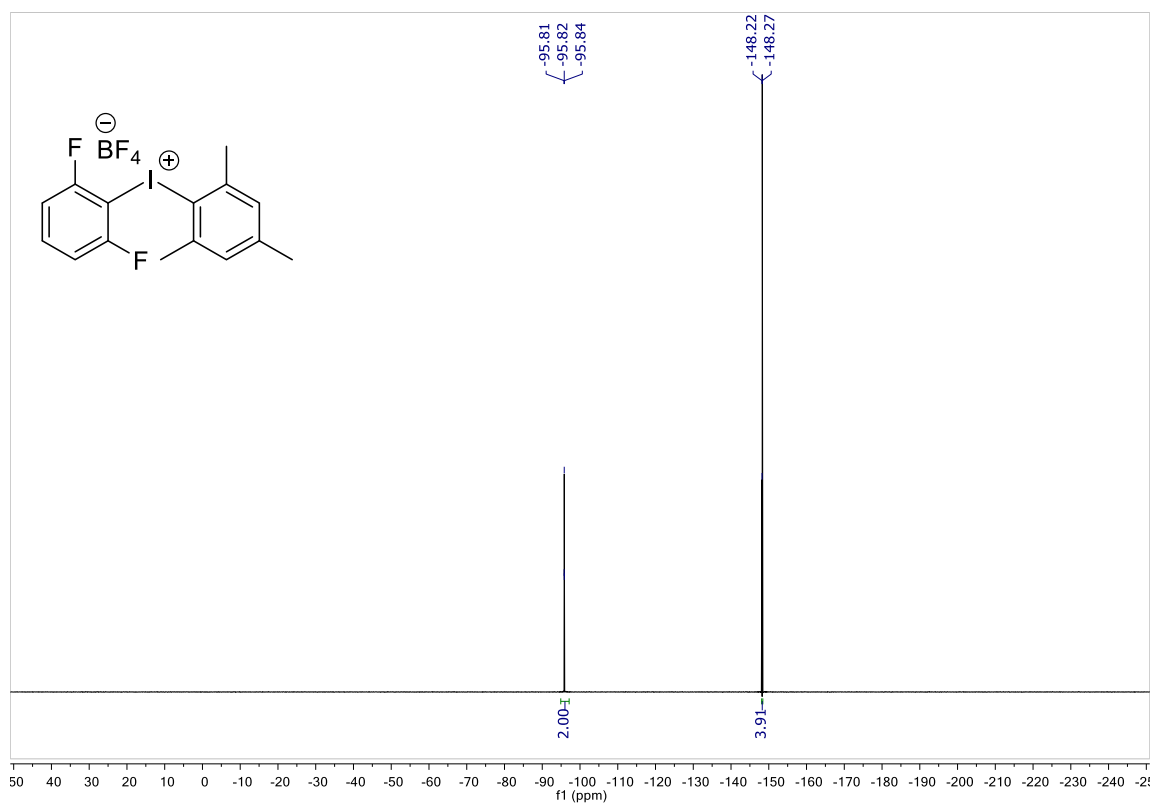
^1H NMR



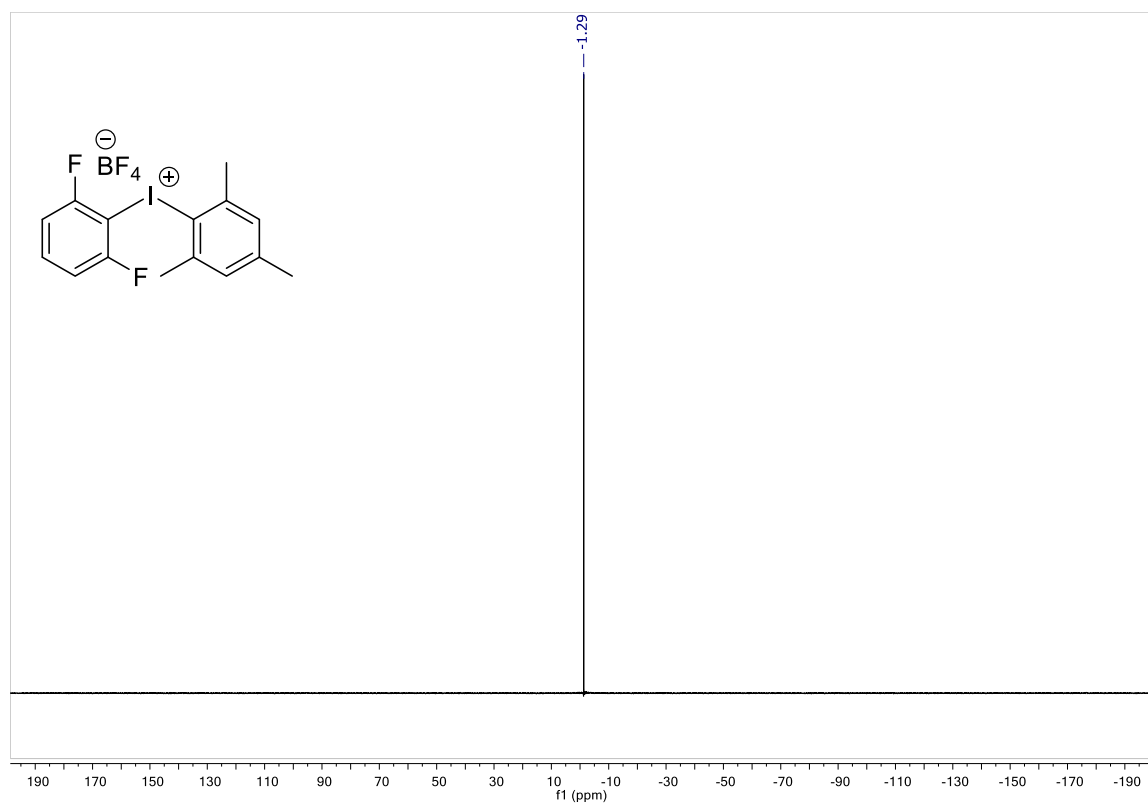
^{13}C NMR



^{19}F NMR

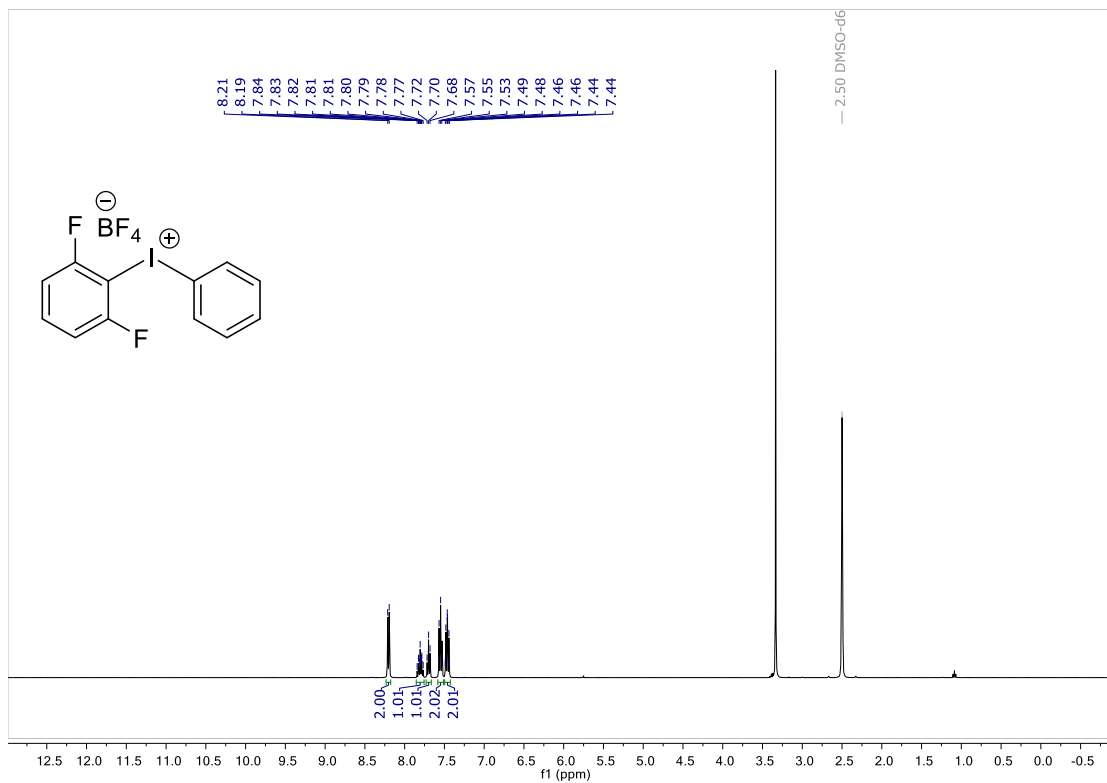


^{11}B NMR

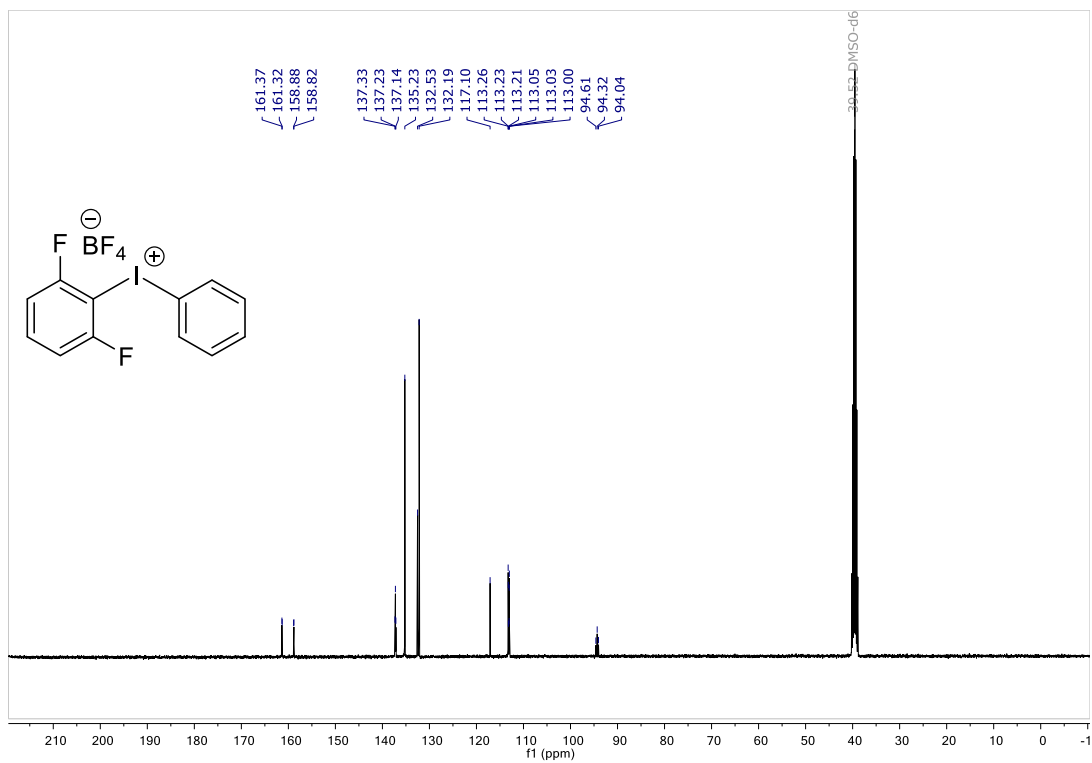


(2,6-difluorophenyl)(phenyl)iodonium tetrafluoroborate (**3.16**)

^1H NMR



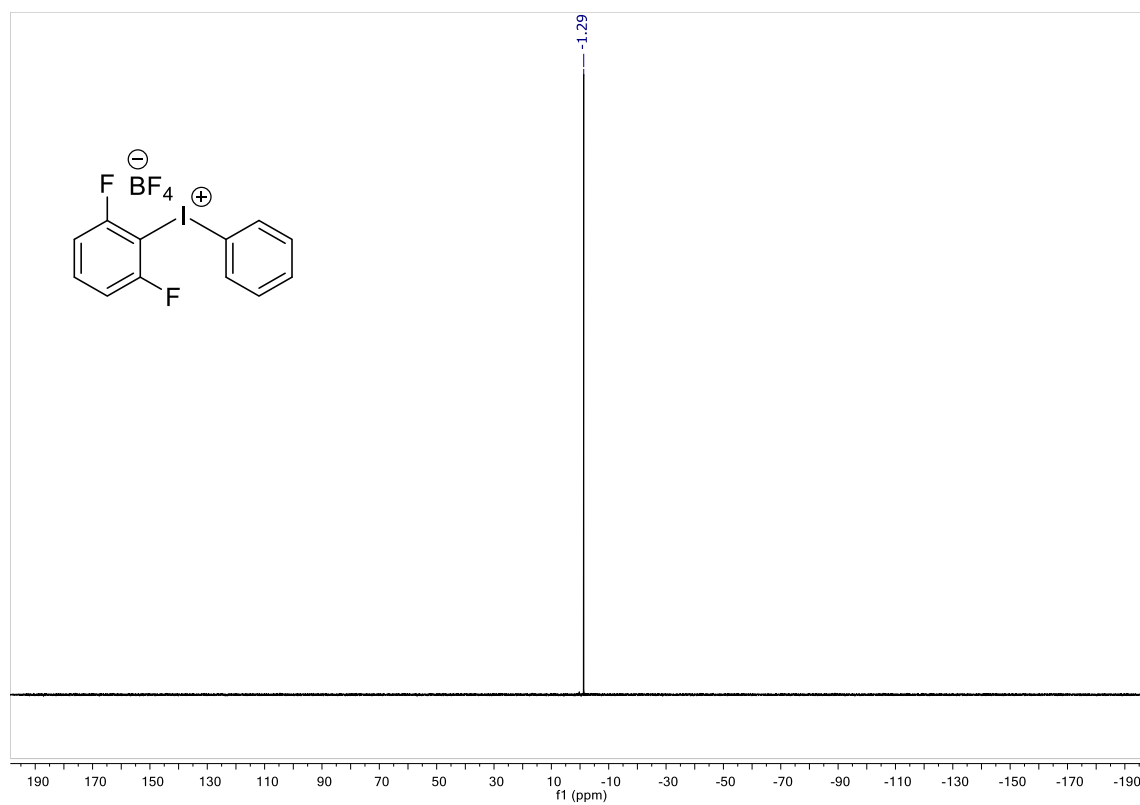
^{13}C NMR



^{19}F NMR

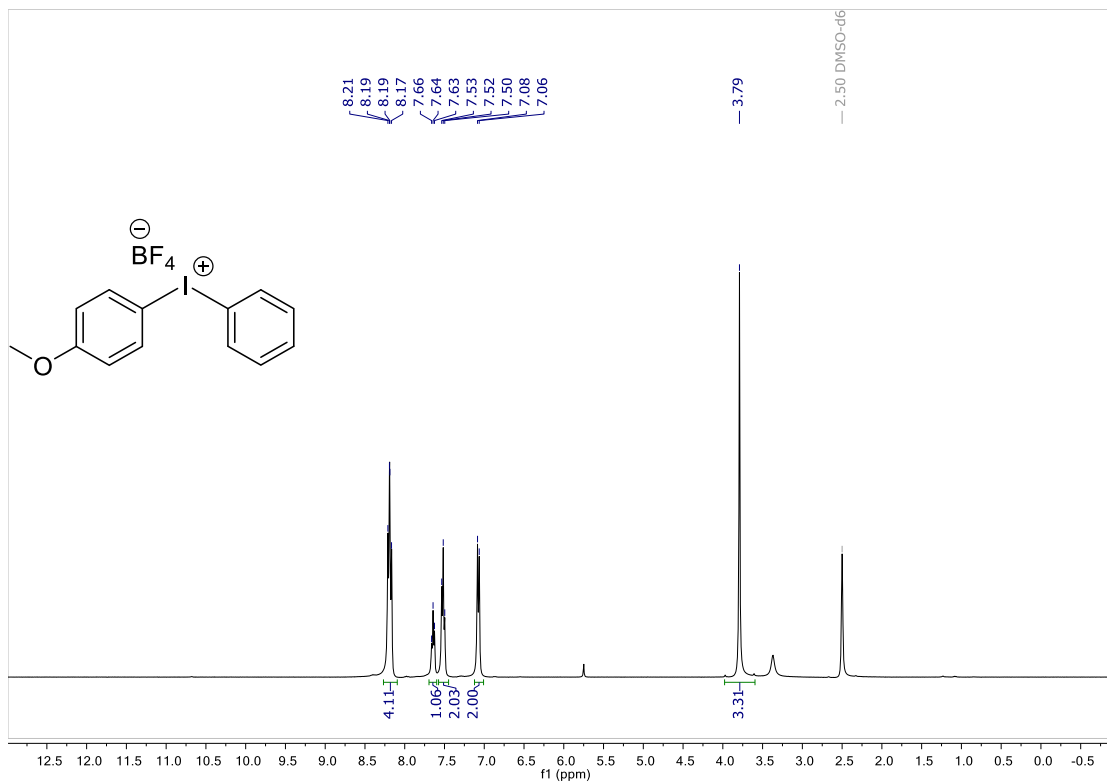


^{11}B NMR

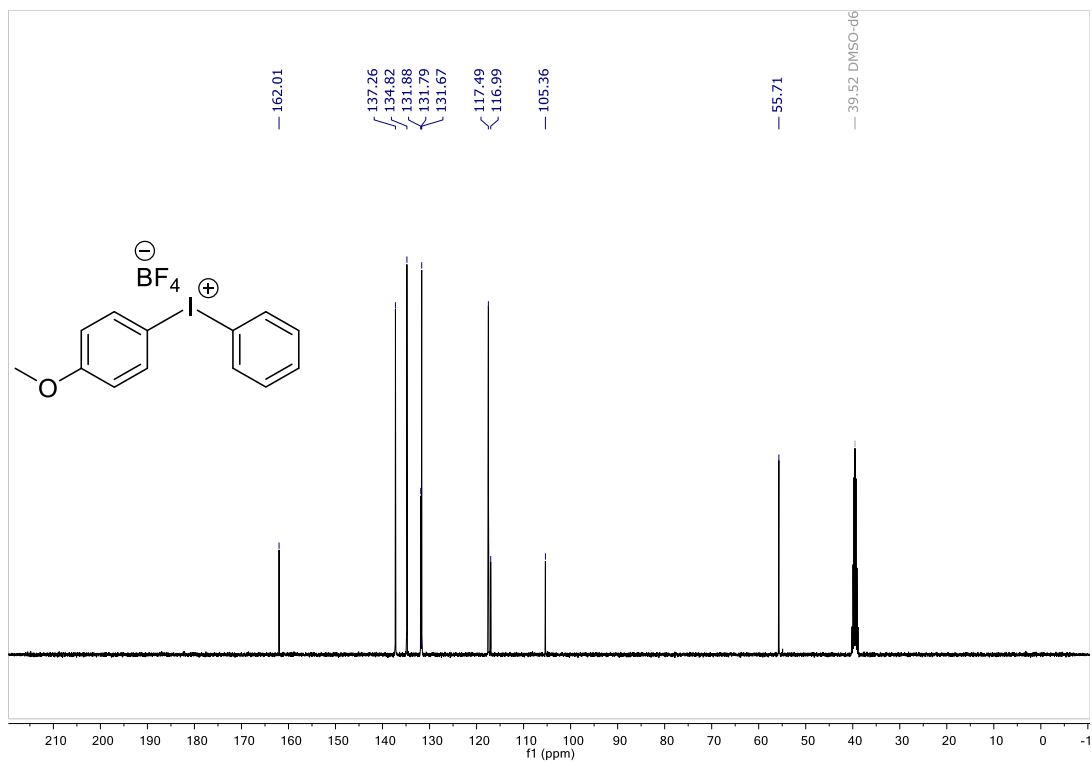


(4-methoxyphenyl)(phenyl)iodonium tetrafluoroborate (**3.17**)

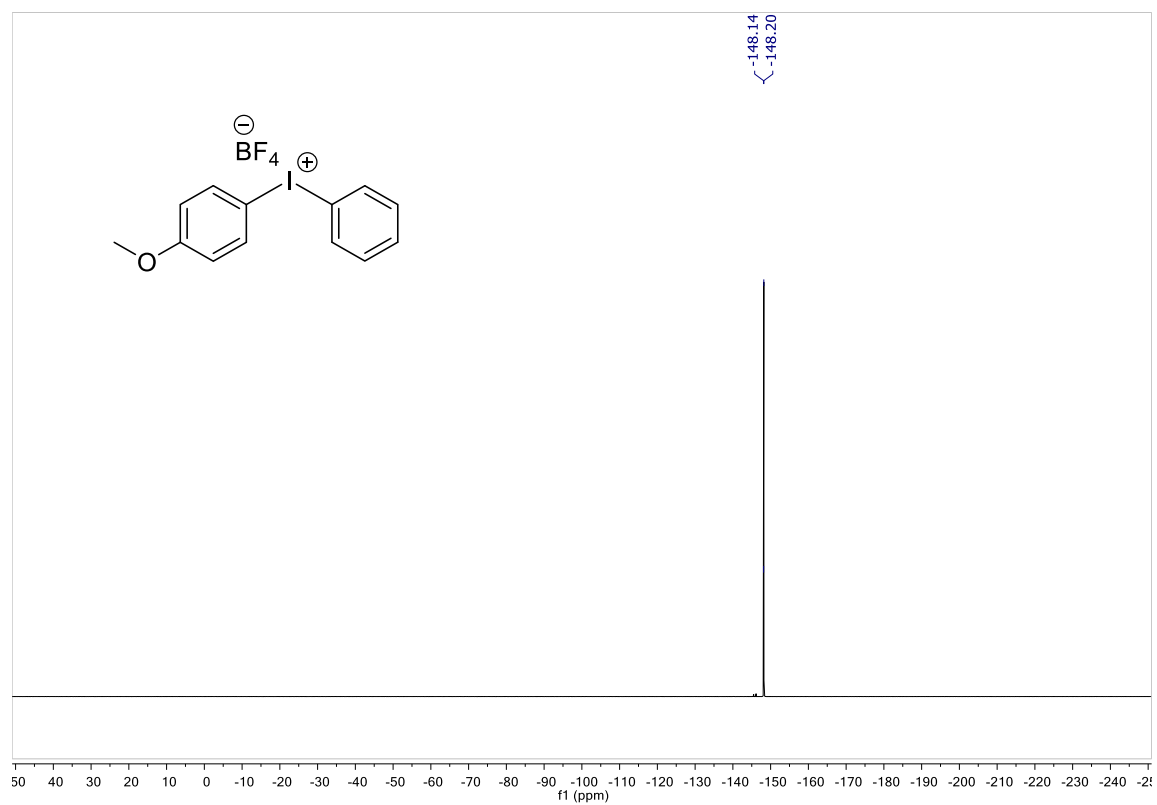
^1H NMR



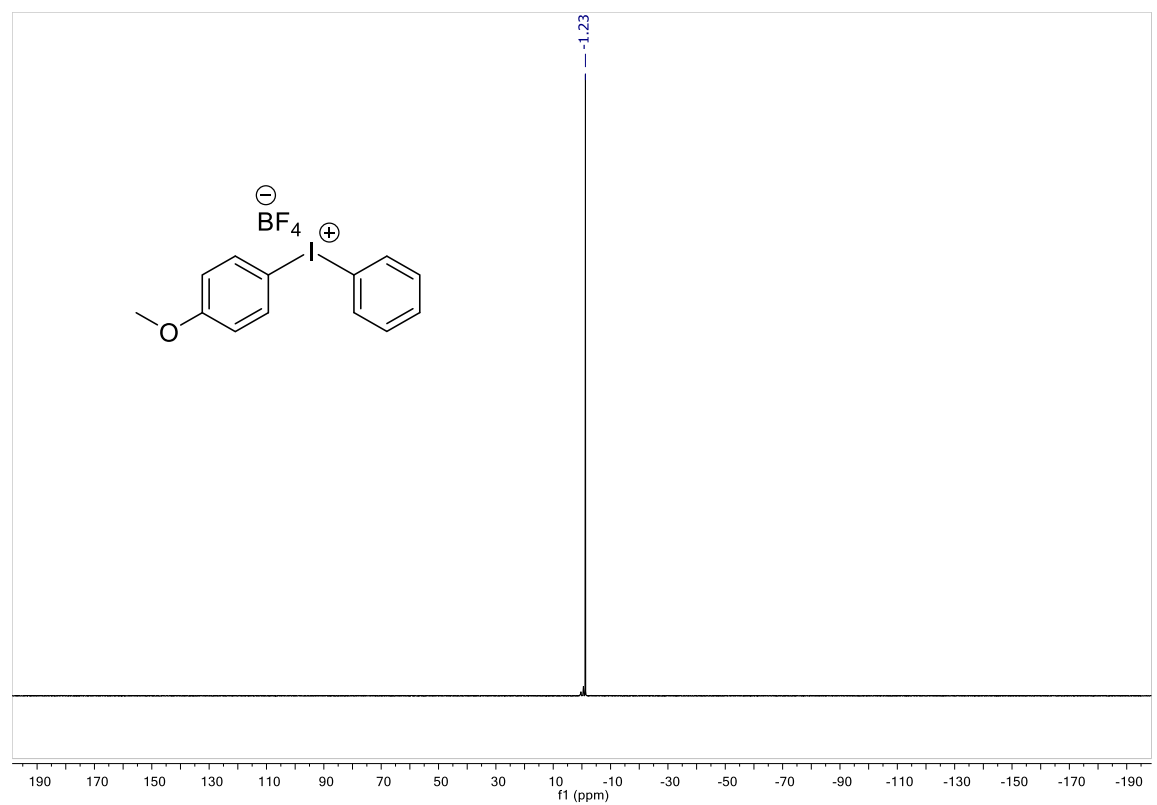
^{13}C NMR



^{19}F NMR

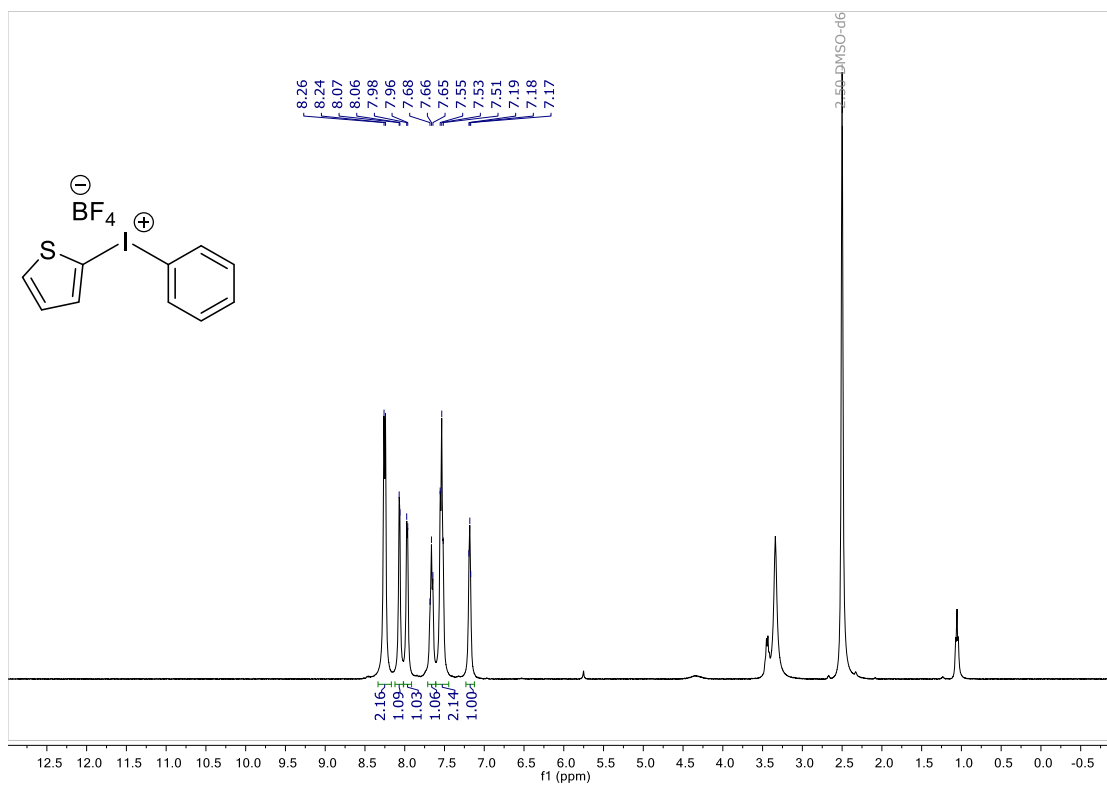


^{11}B NMR

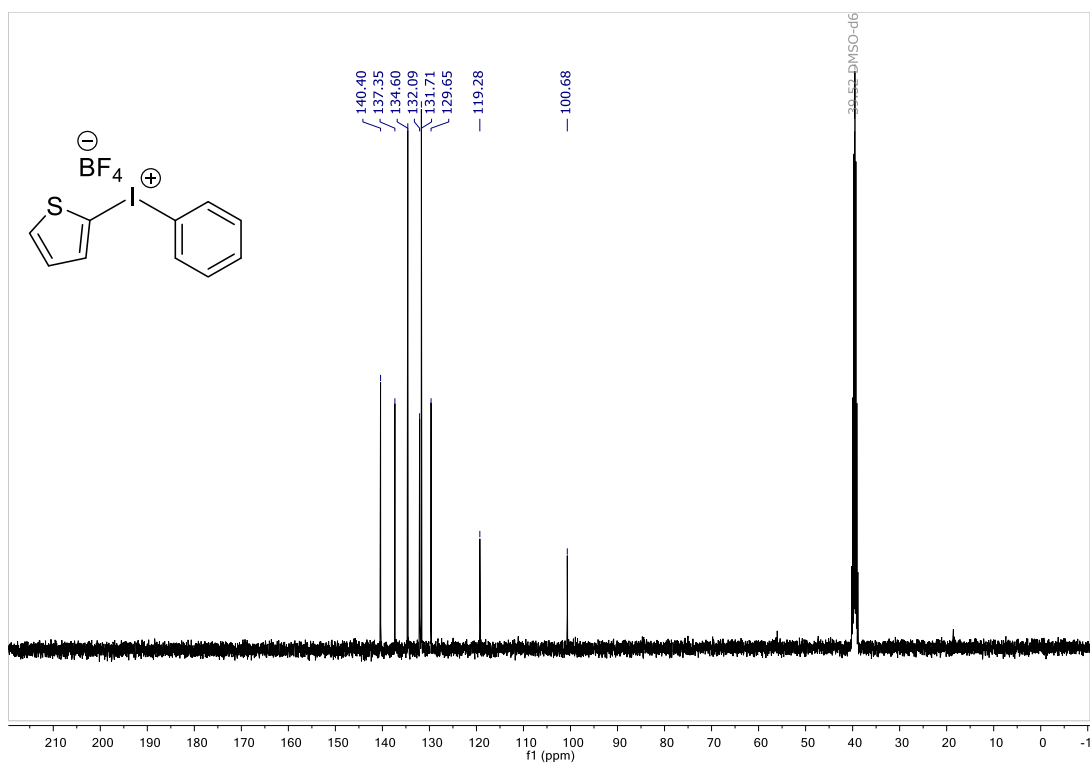


(2-thienyl)(phenyl)iodonium tetrafluoroborate (**3.18**)

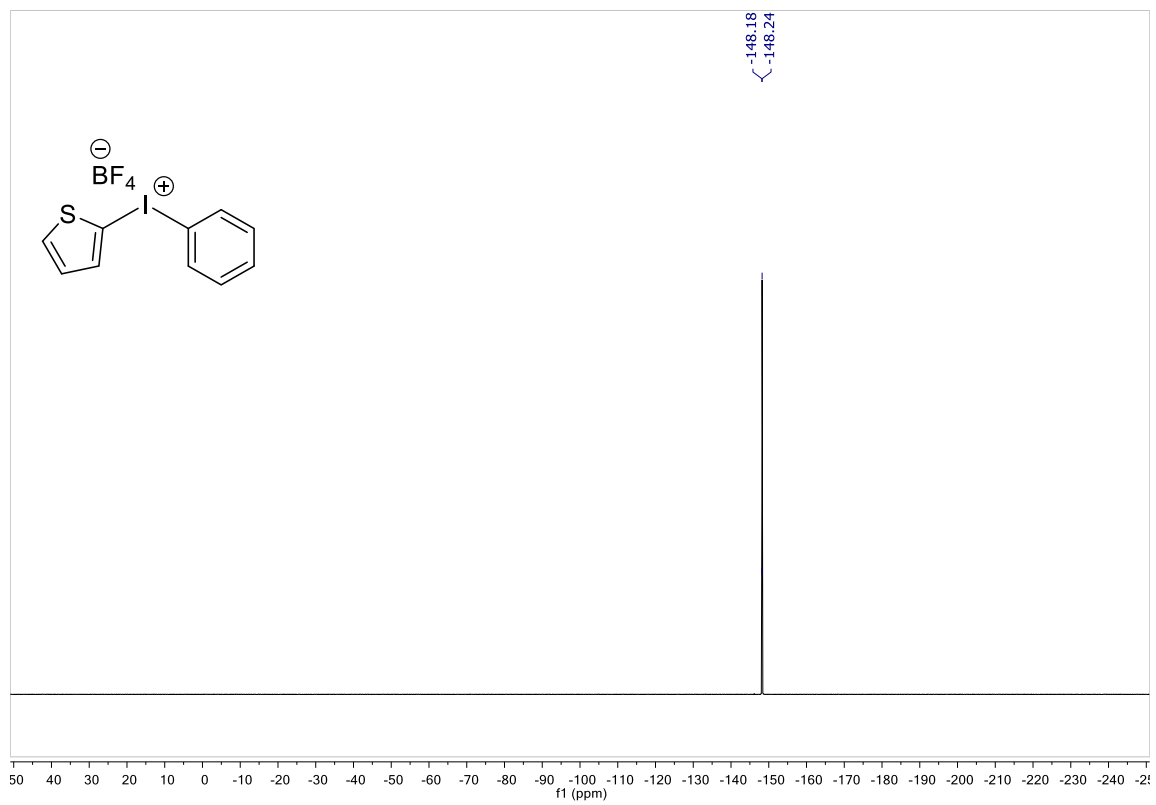
^1H NMR



^{13}C NMR



^{19}F NMR

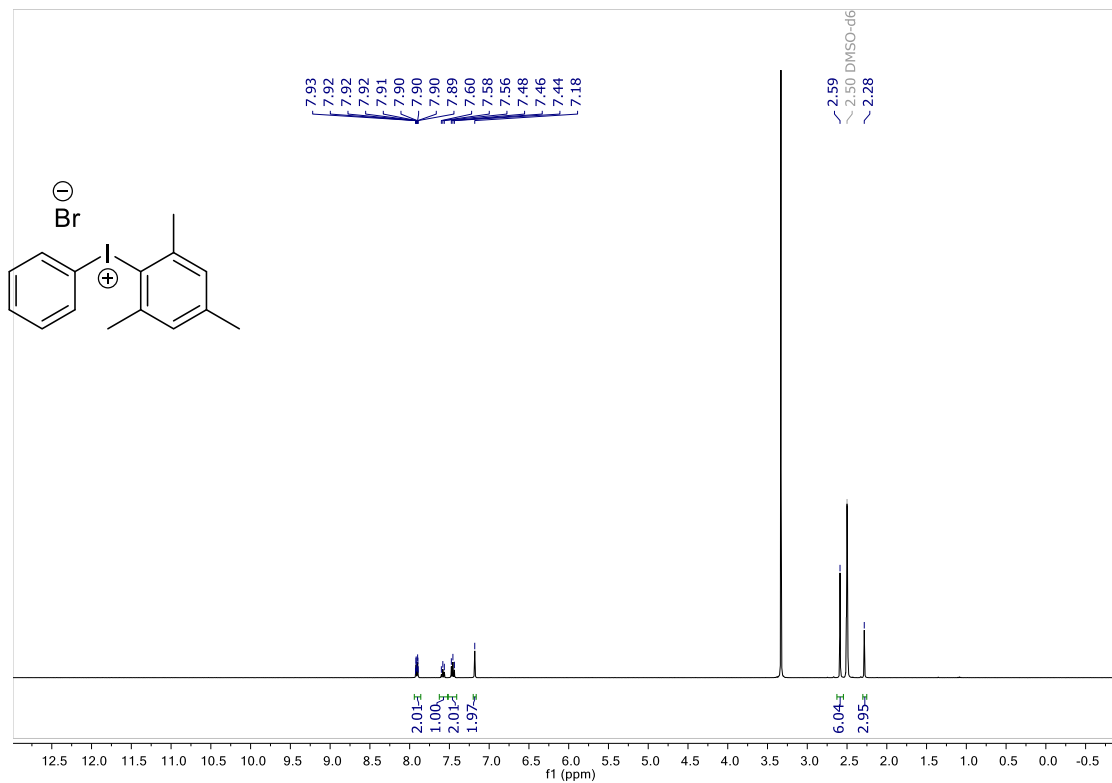


^{11}B NMR

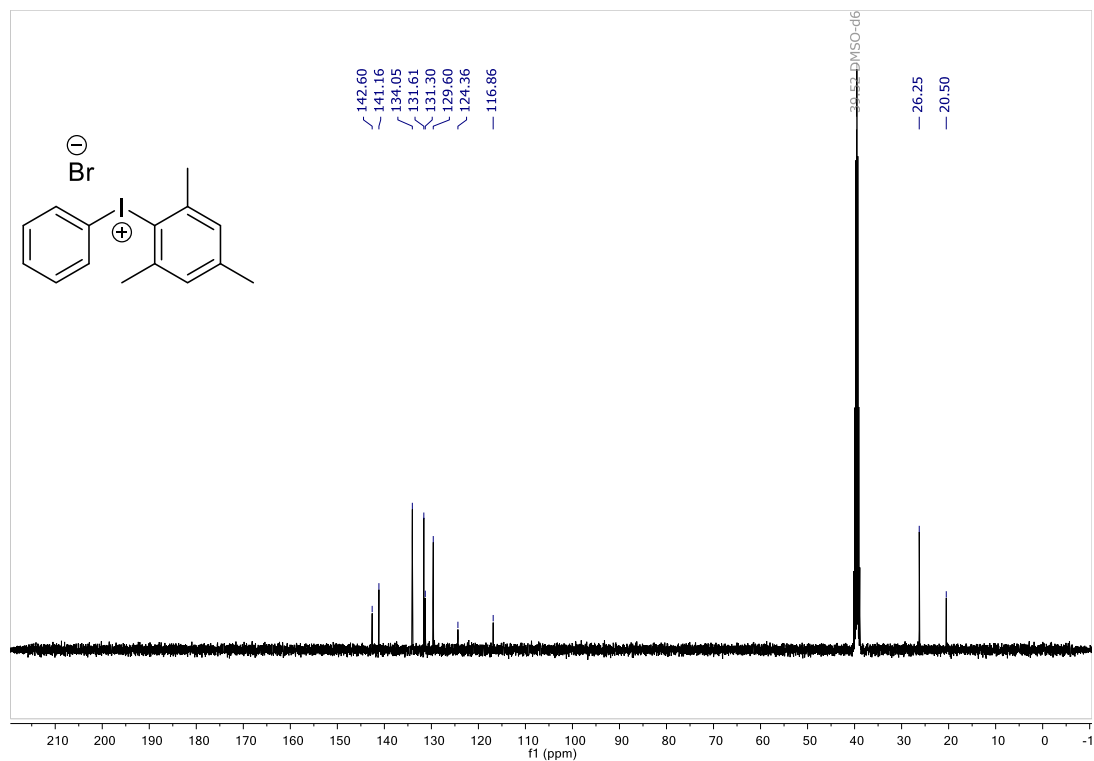


(2,4,6-trimethylphenyl)(phenyl)iodonium bromide (**3.19**)

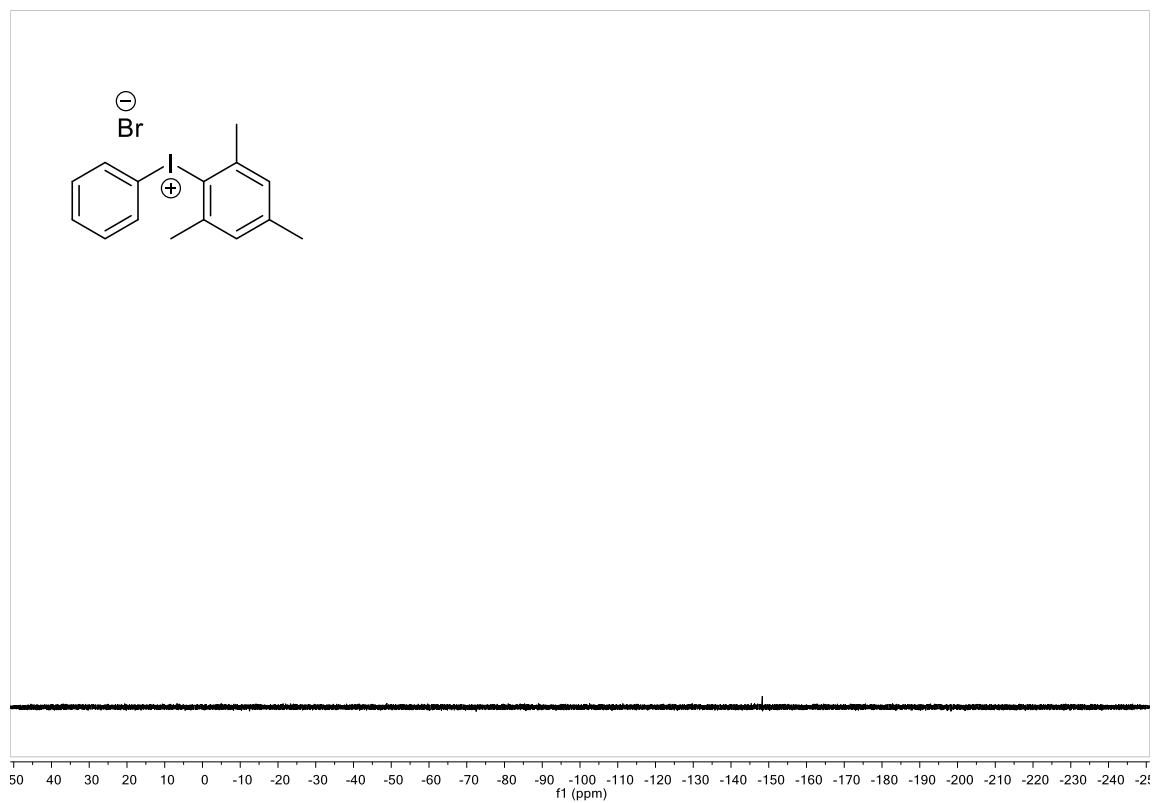
^1H NMR



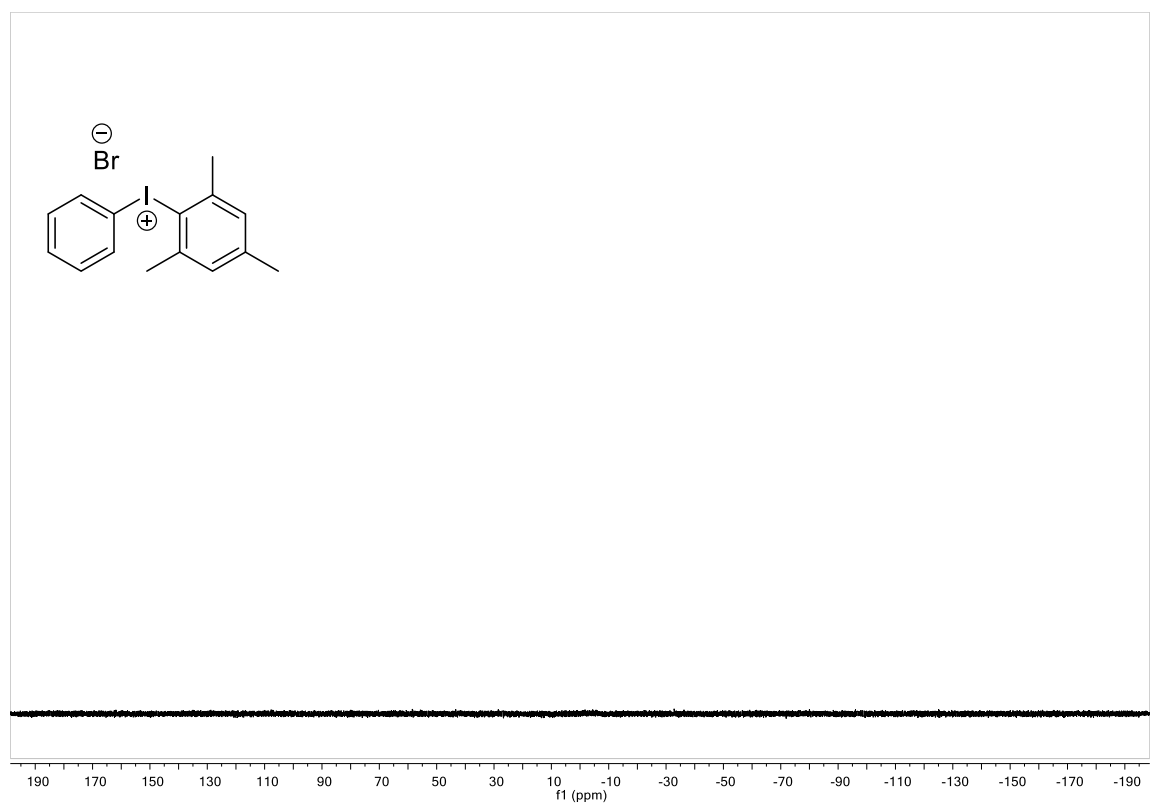
^{13}C NMR



^{19}F NMR

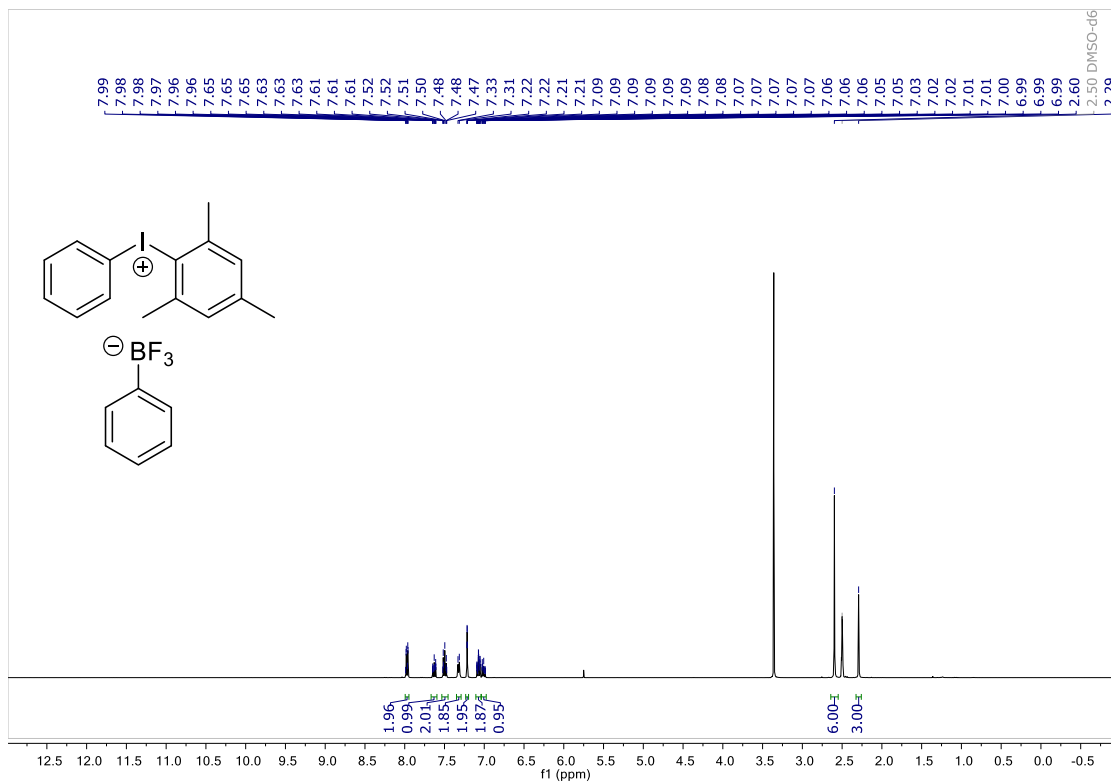


^{11}B NMR

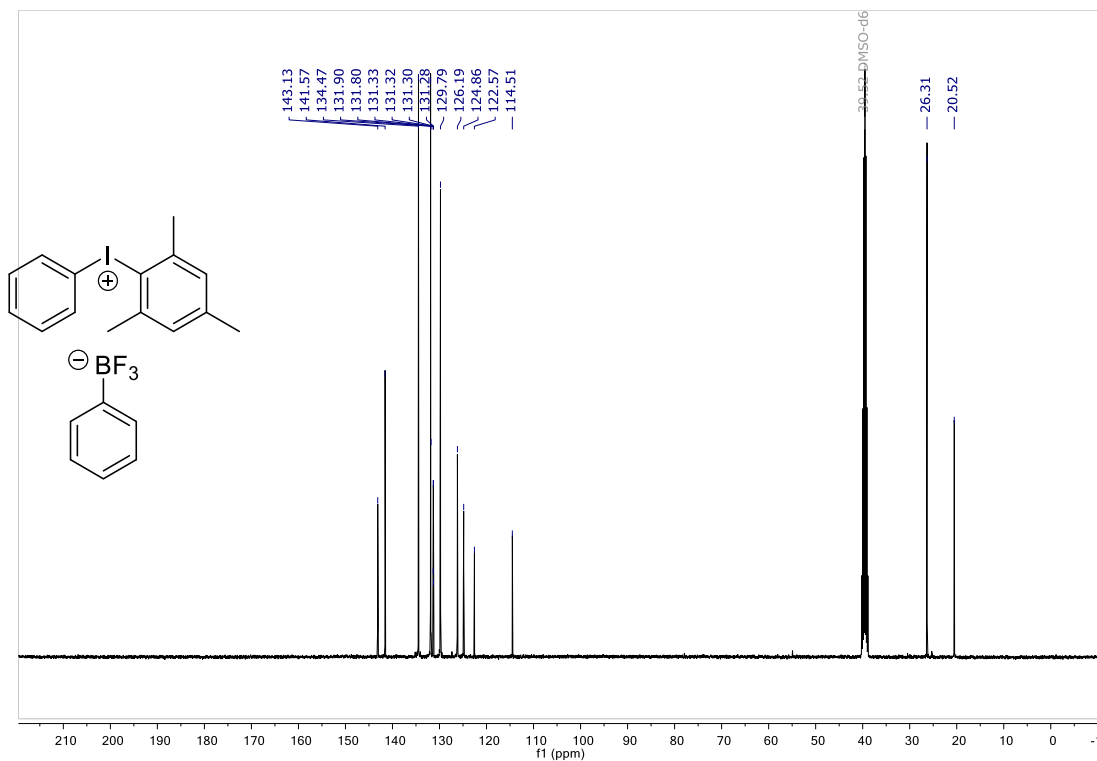


(2,4,6-trimethylphenyl)(phenyl)iodonium phenyltrifluoroborate (**3.20**)

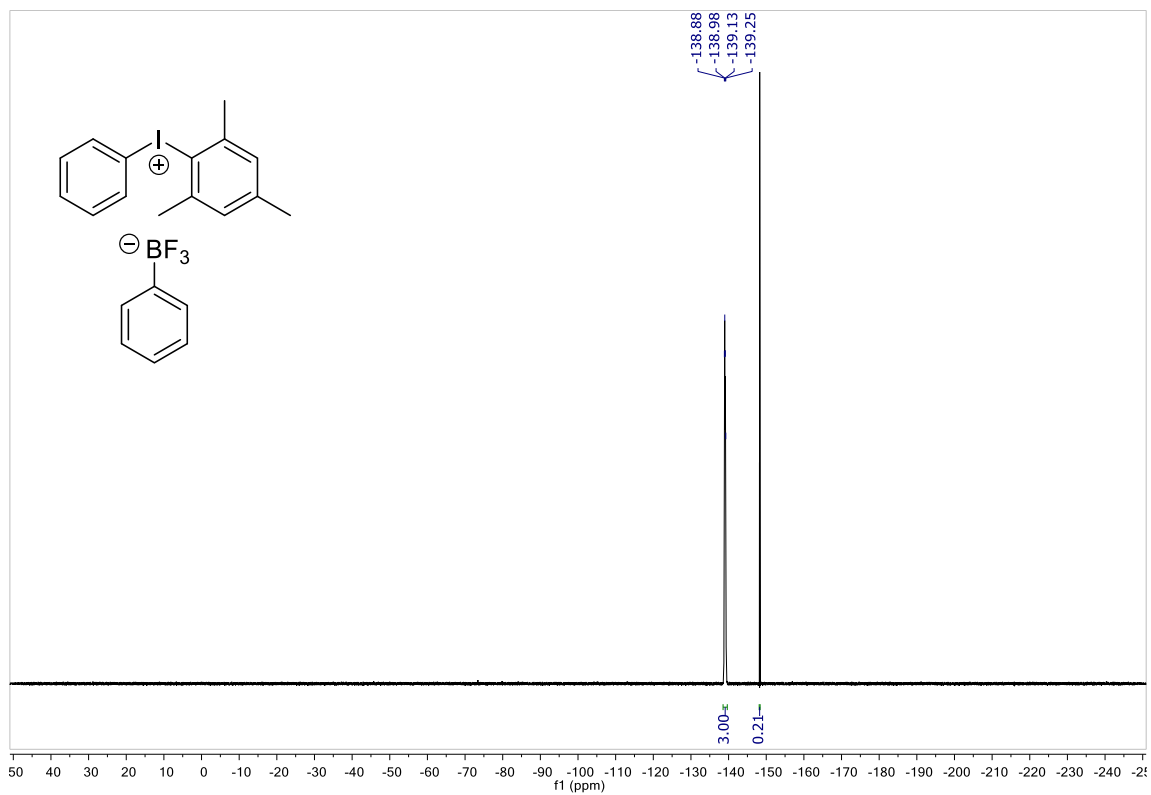
^1H NMR



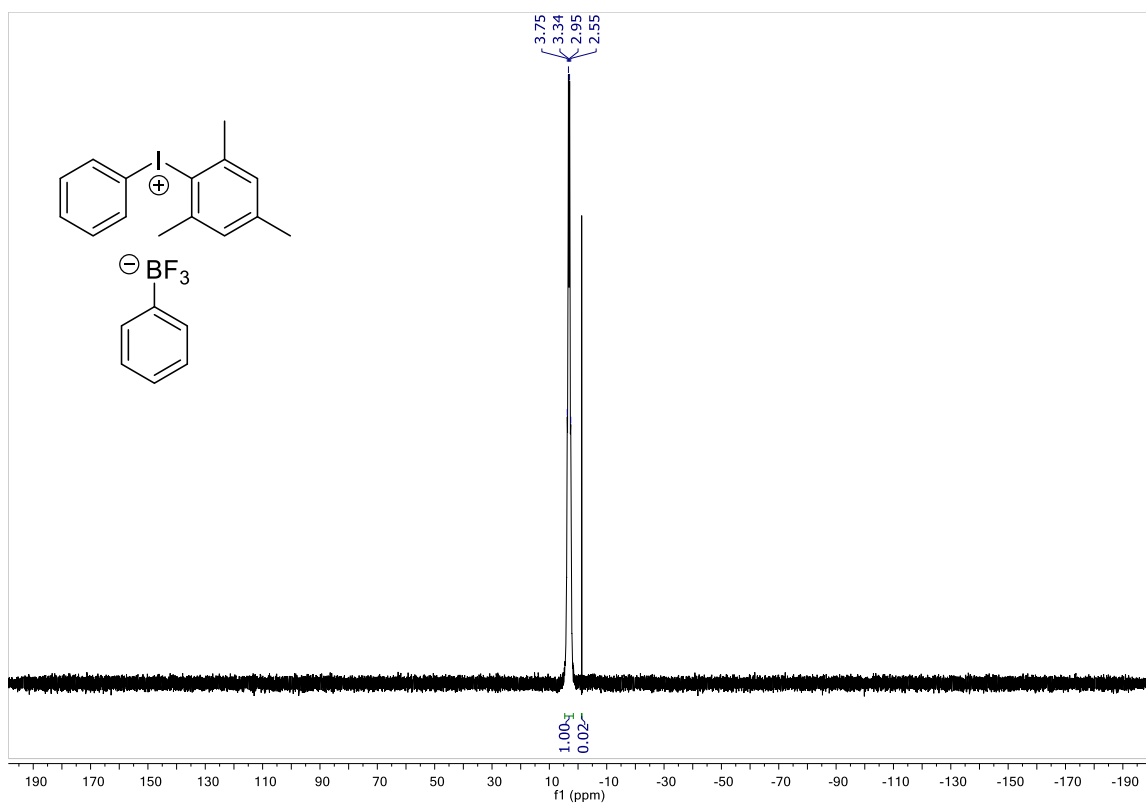
^{13}C NMR



¹⁹F NMR

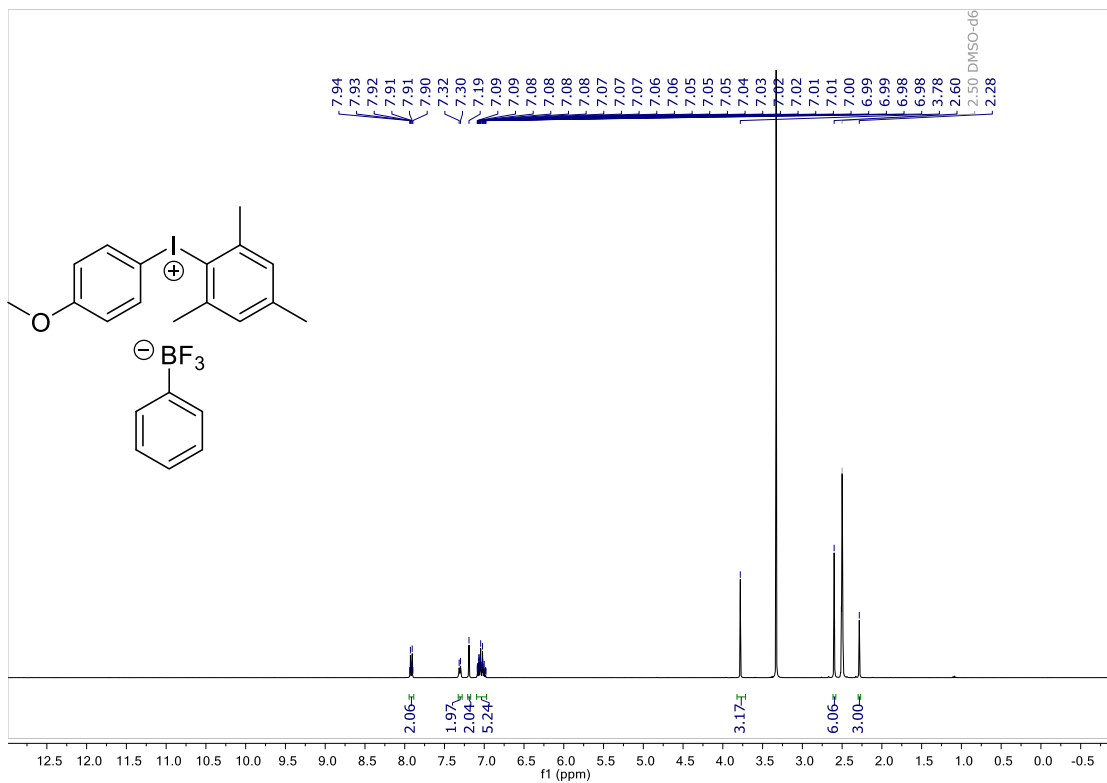


¹¹B NMR

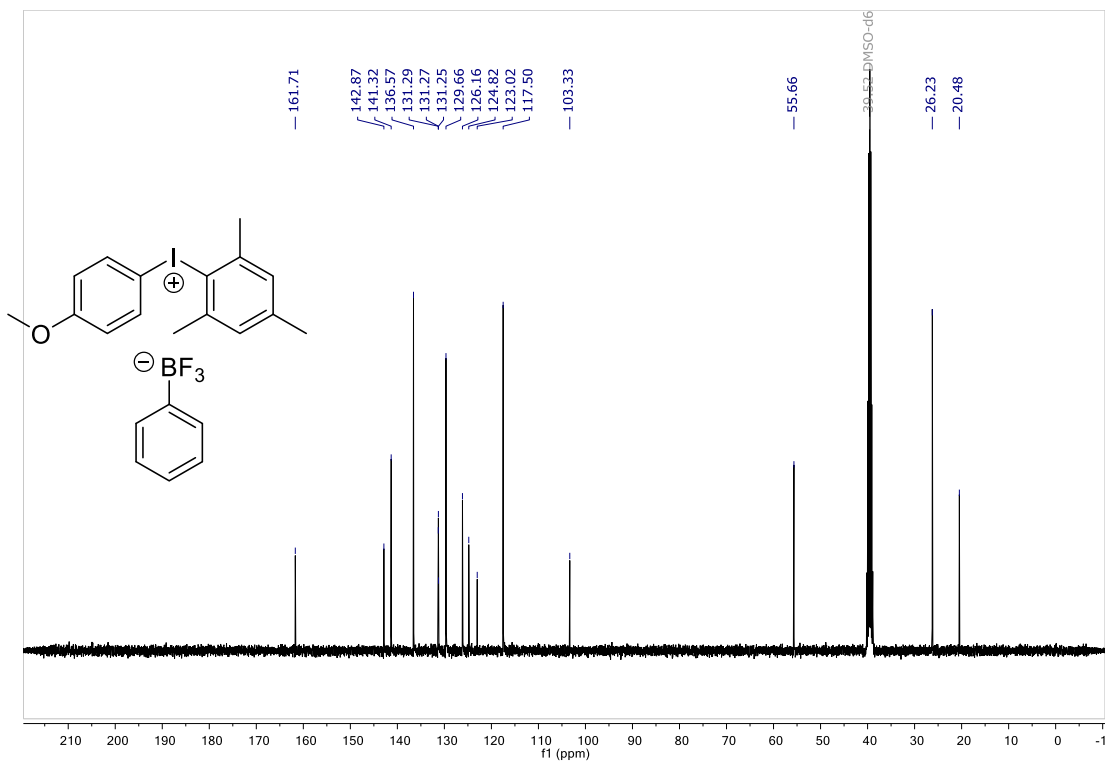


(4-methoxyphenyl)(2,4,6-trimethylphenyl)iodonium phenyltrifluoroborate (**3.21**)

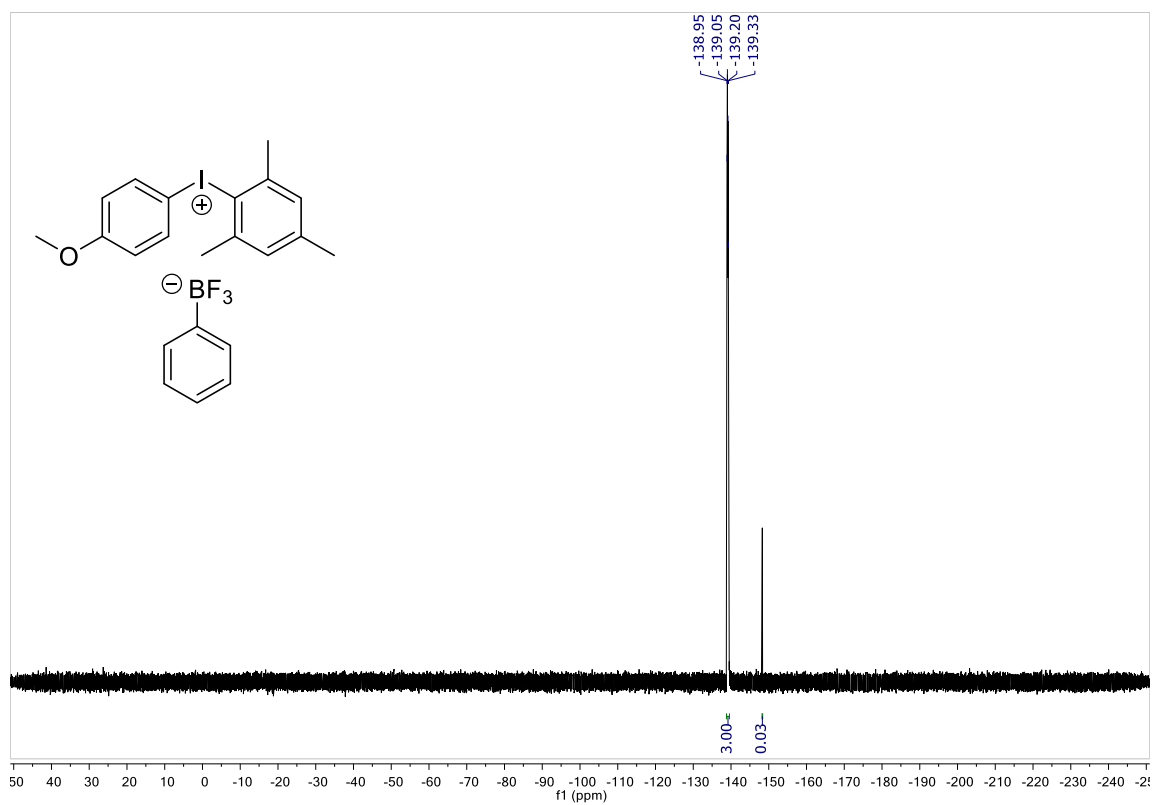
^1H NMR



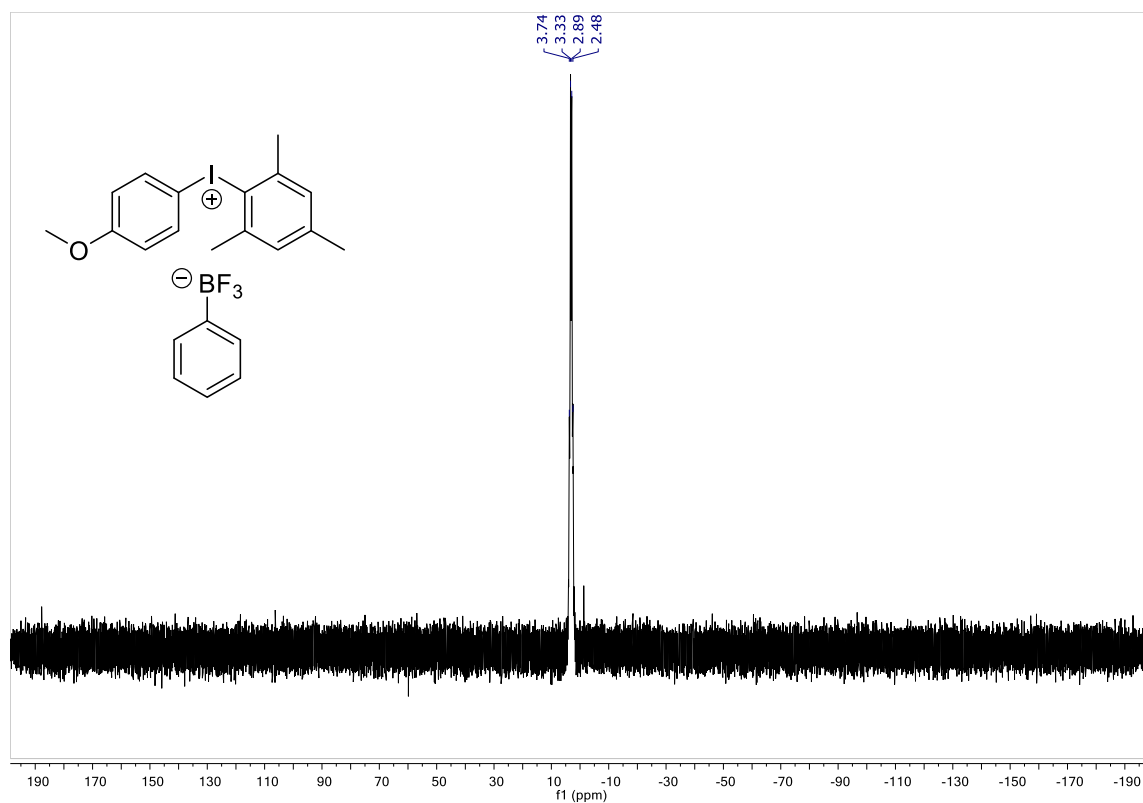
^{13}C NMR



^{19}F NMR

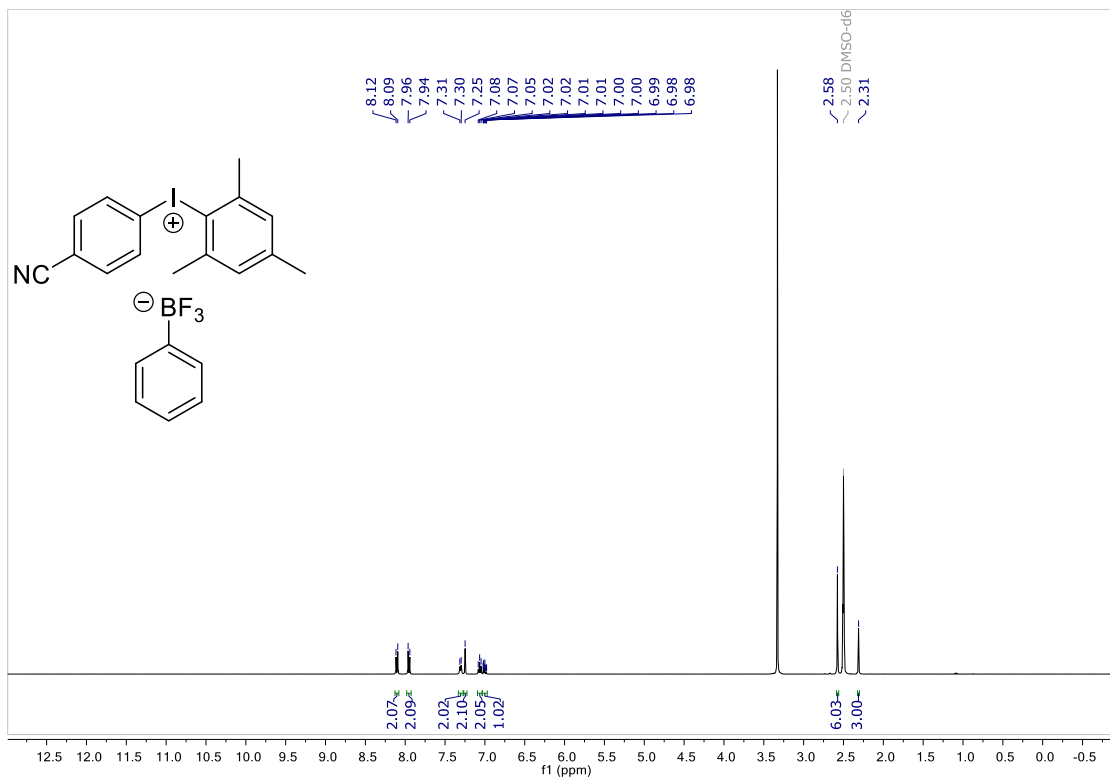


^{11}B NMR

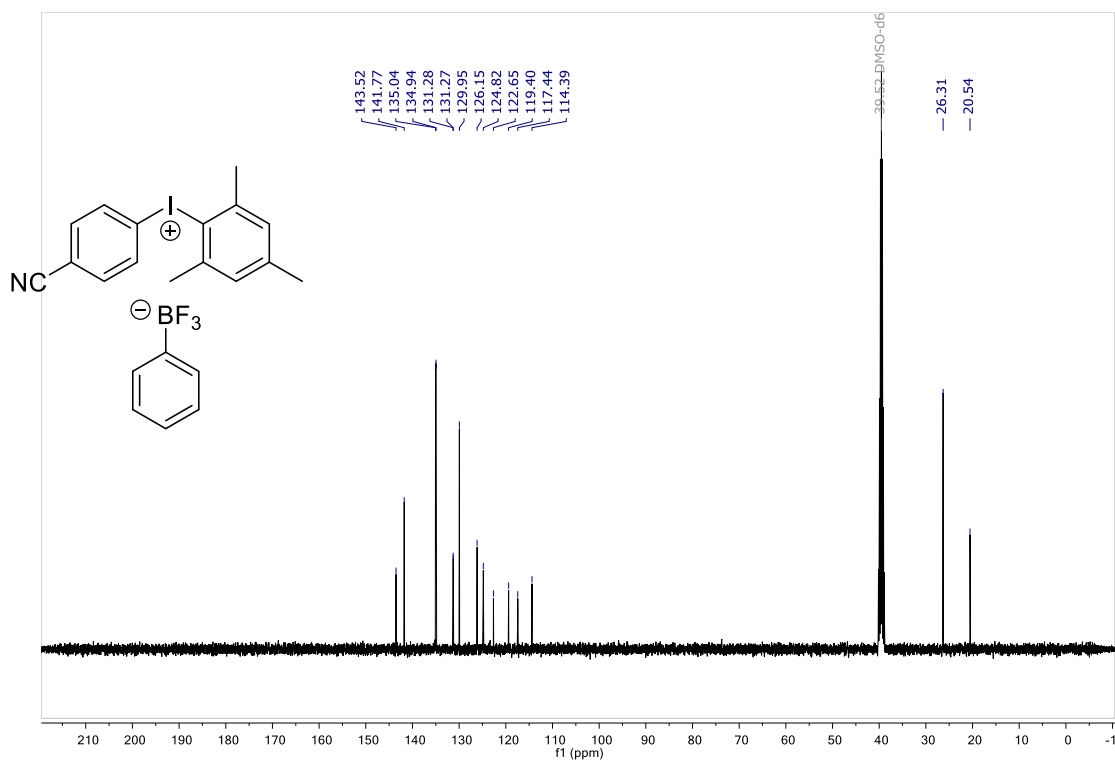


(4-cyanophenyl)(2,4,6-trimethylphenyl)iodonium phenyltrifluoroborate (**3.22**)

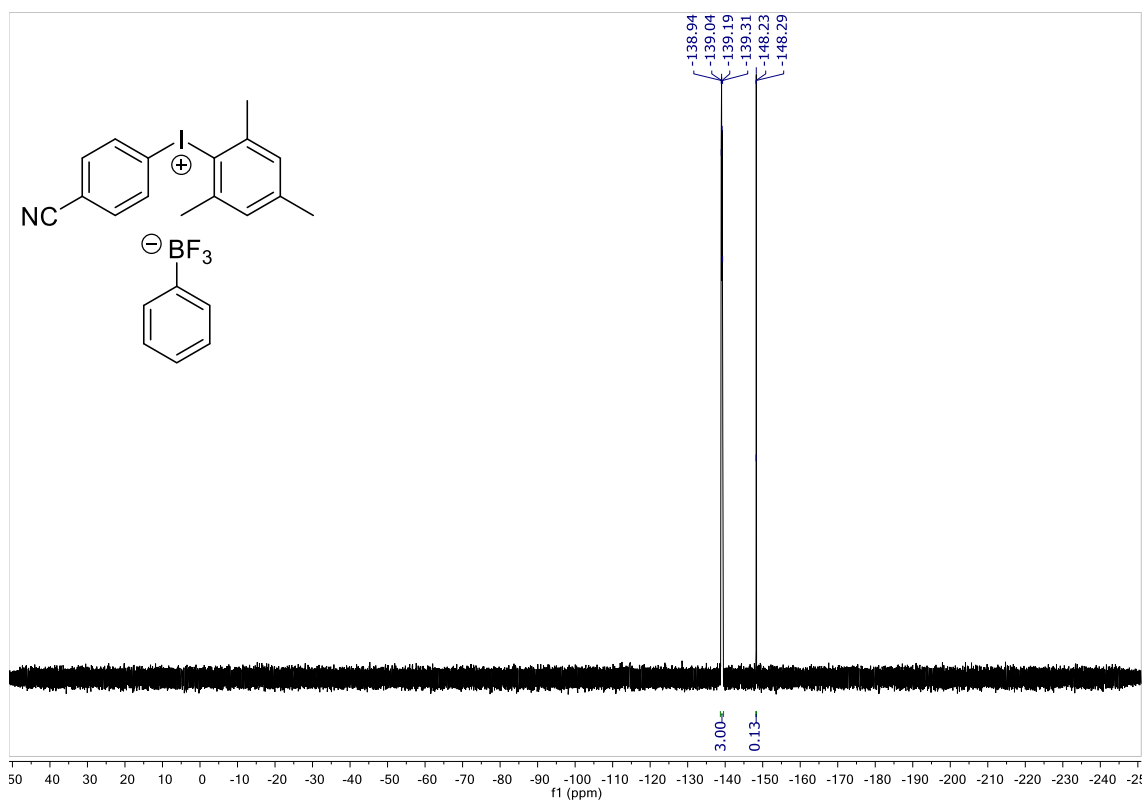
^1H NMR



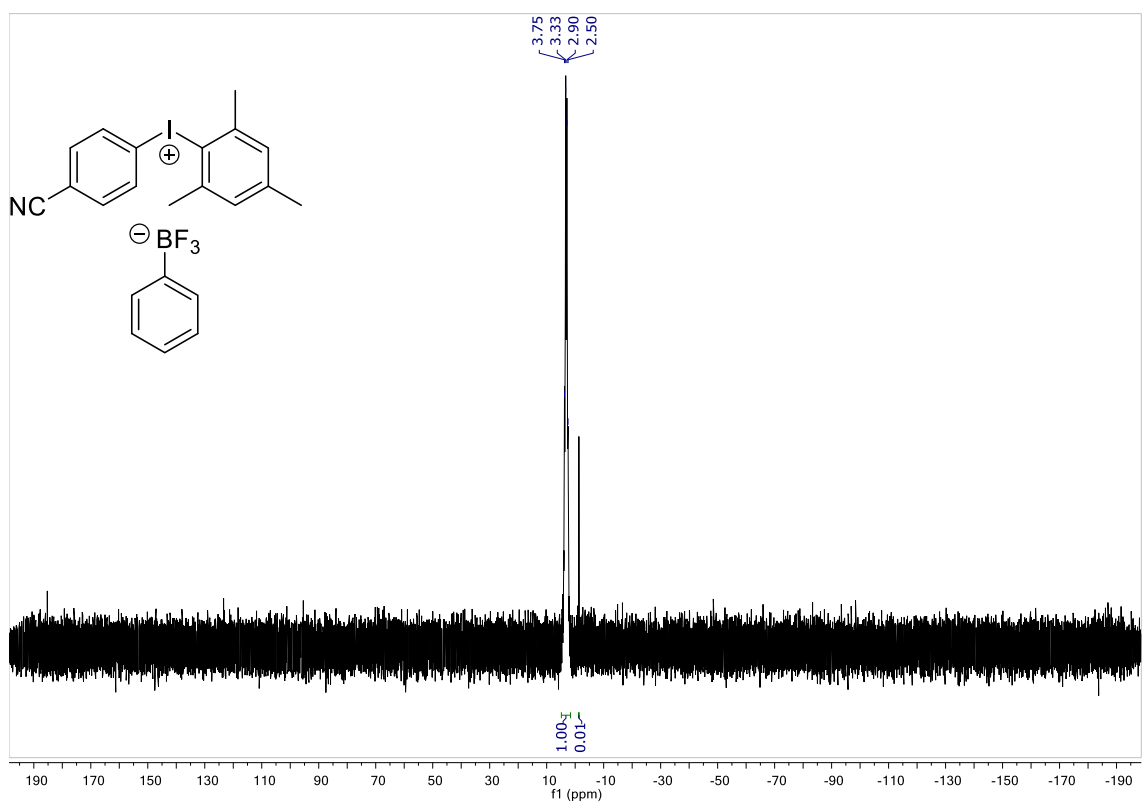
^{13}C NMR



^{19}F NMR

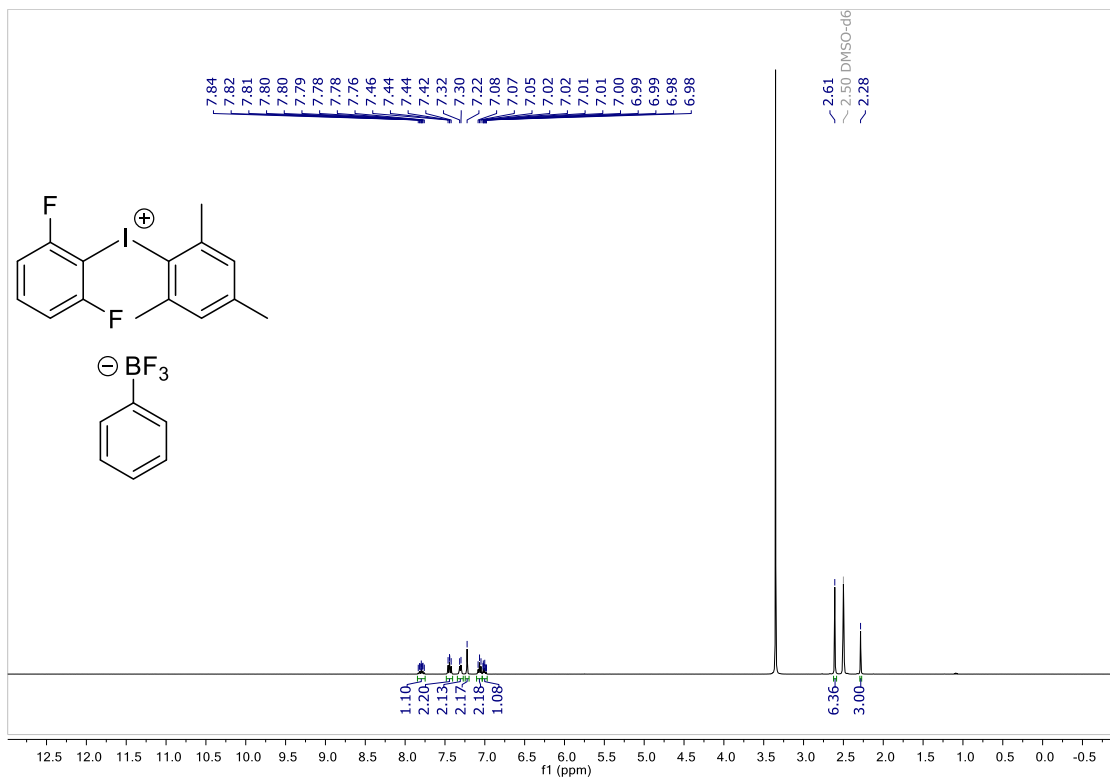


^{11}B NMR

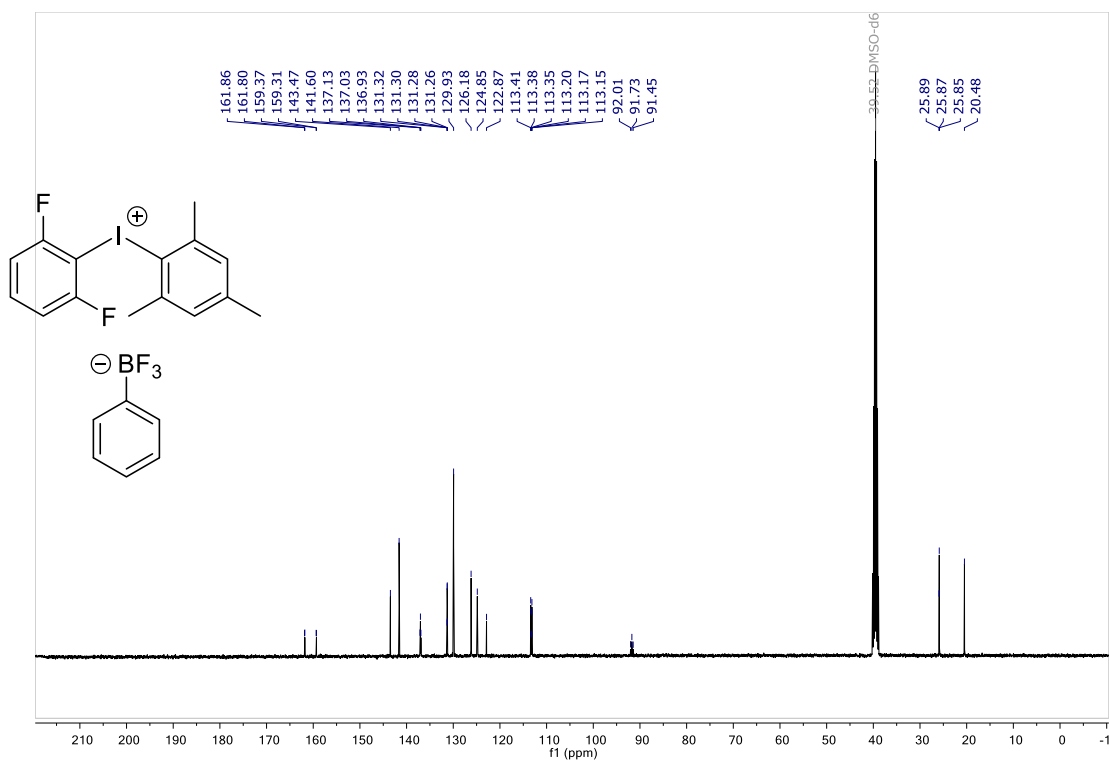


(2,6-difluorophenyl)(2,4,6-trimethylphenyl)iodonium phenyltrifluoroborate (**3.23**)

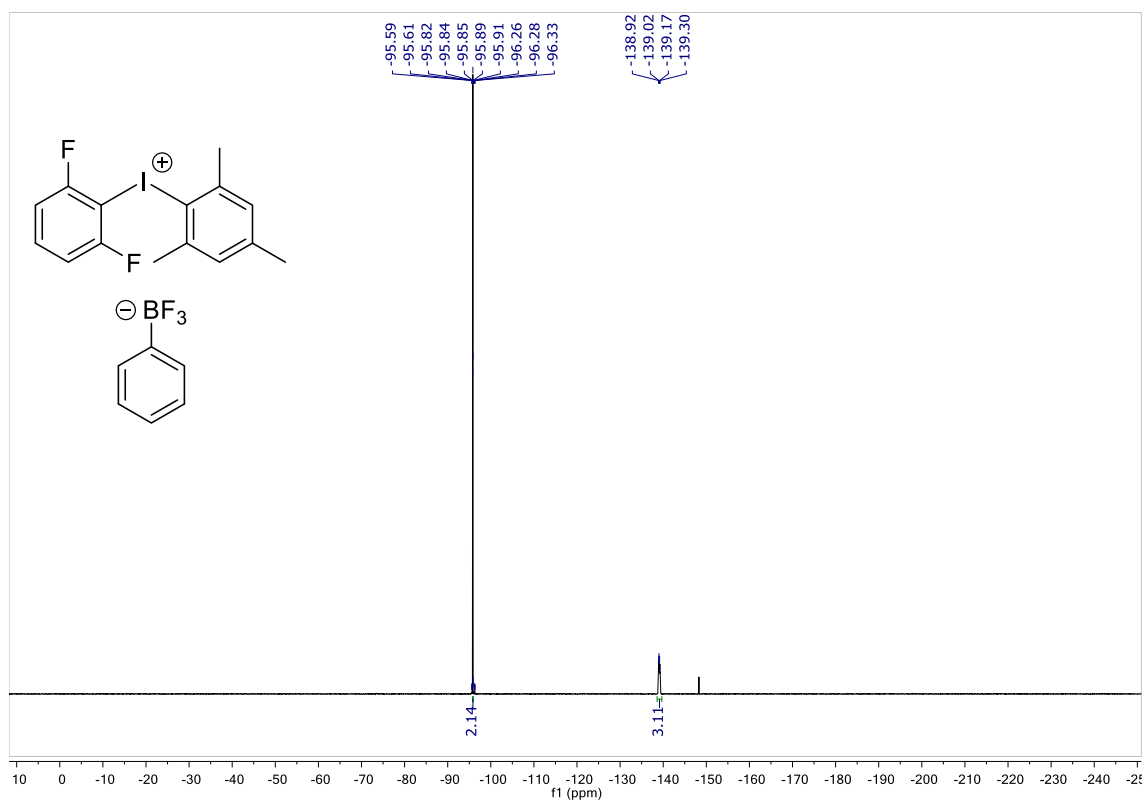
^1H NMR



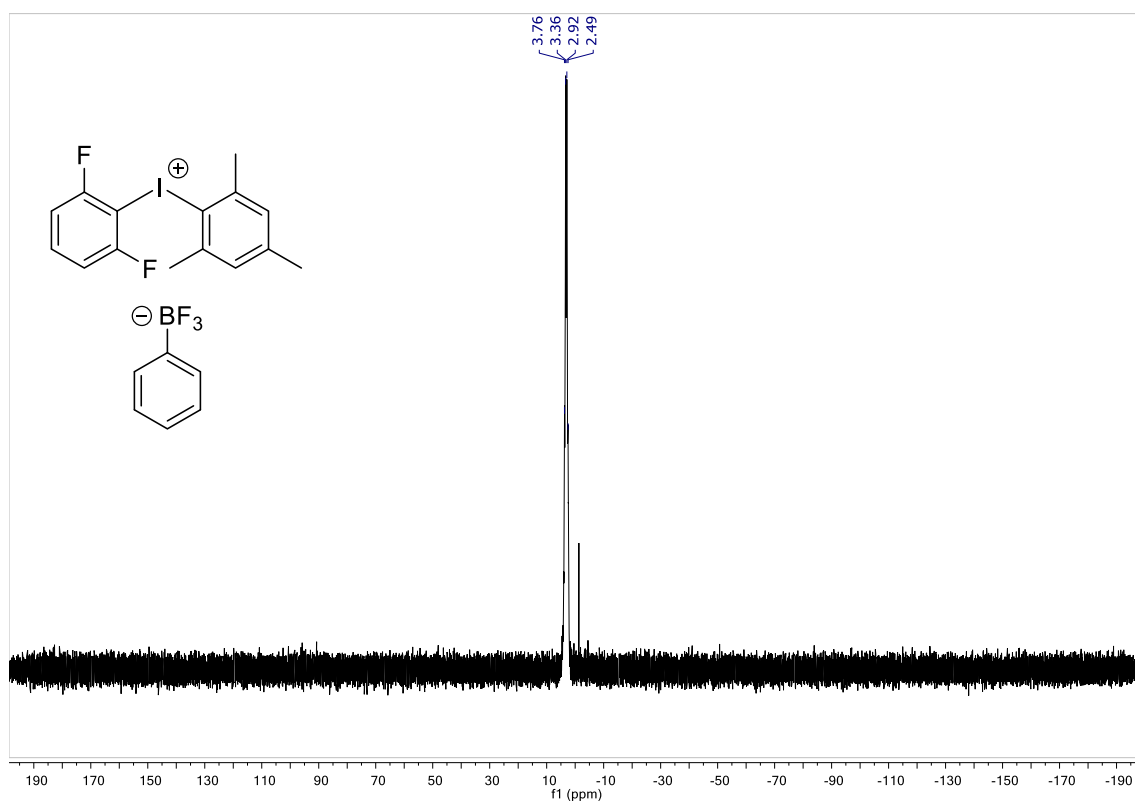
^{13}C NMR



^{19}F NMR

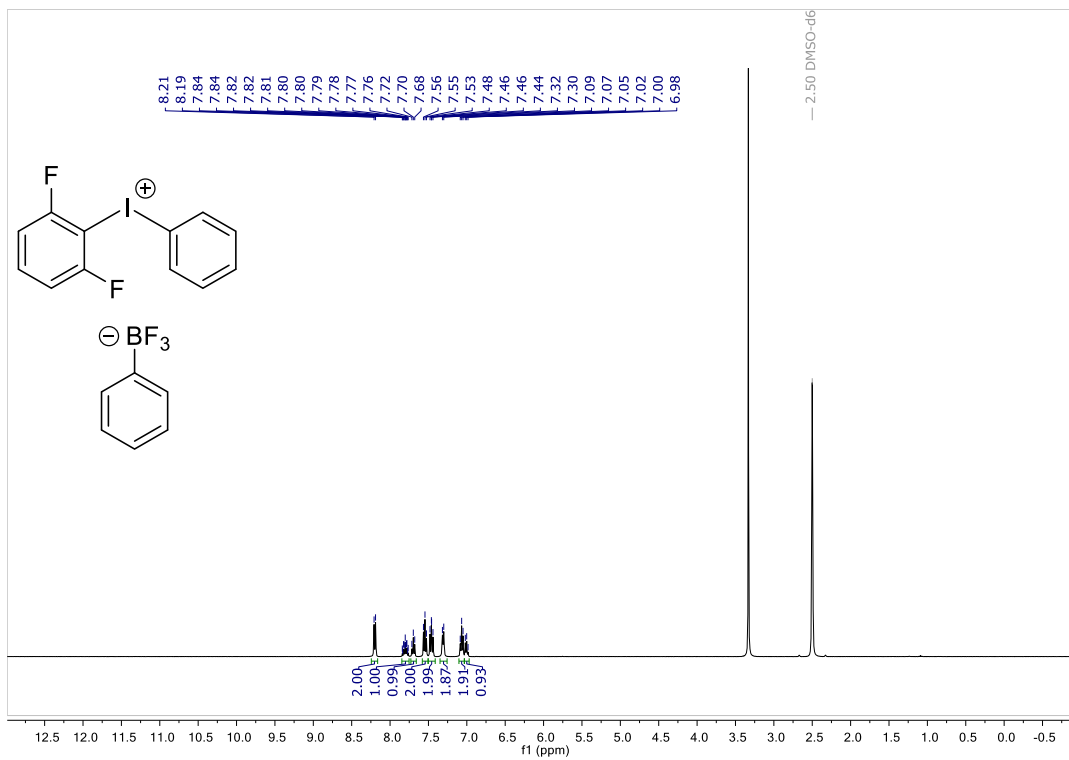


^{11}B NMR

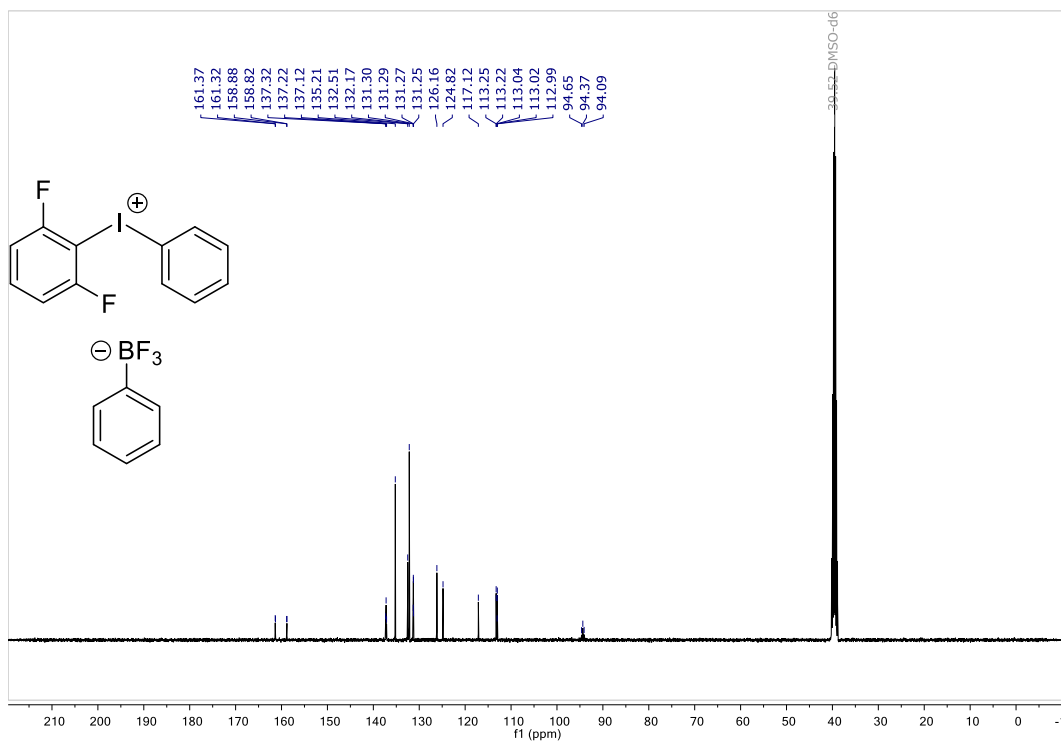


(2,6-difluorophenyl)(phenyl)iodonium phenyltrifluoroborate (**3.24**)

^1H NMR



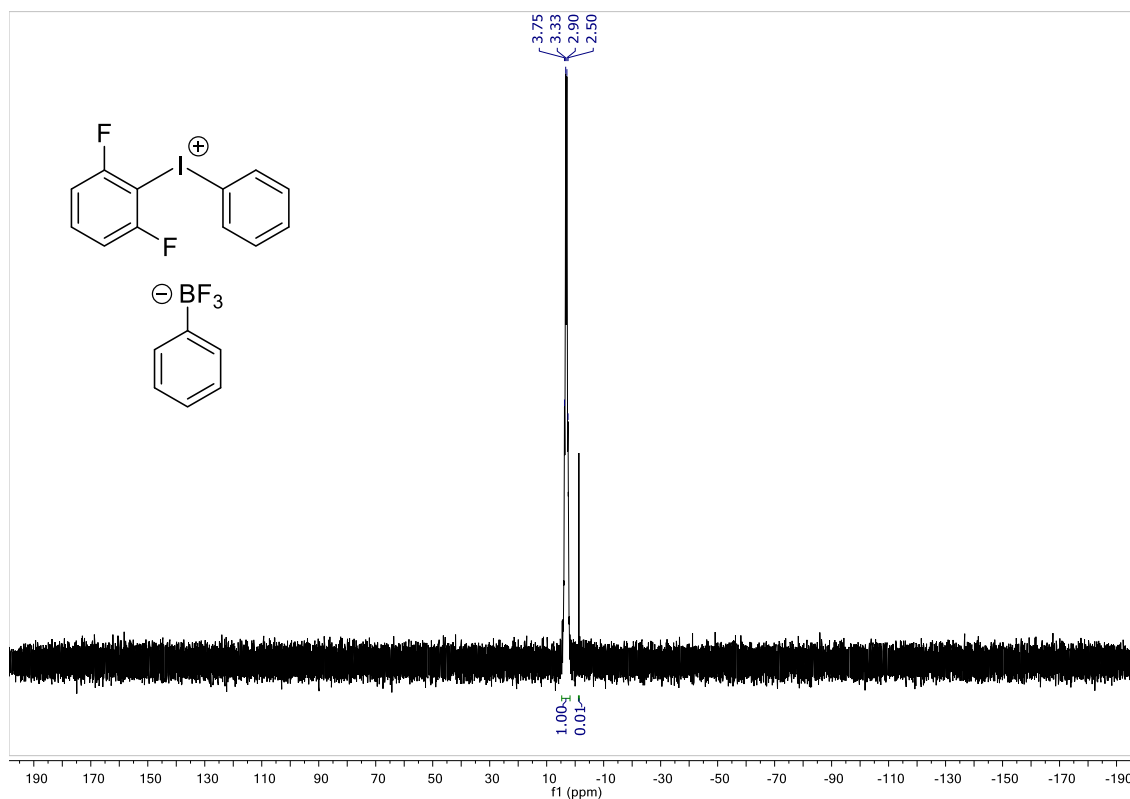
^{13}C NMR



^{19}F NMR

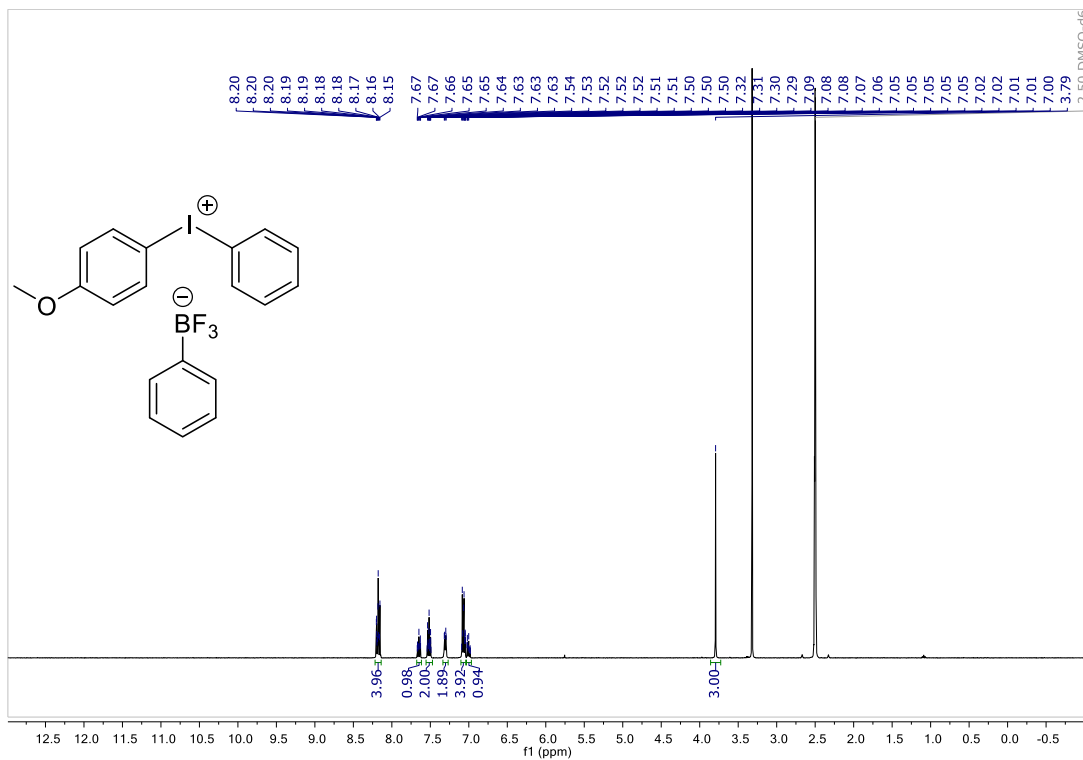


^{11}B NMR

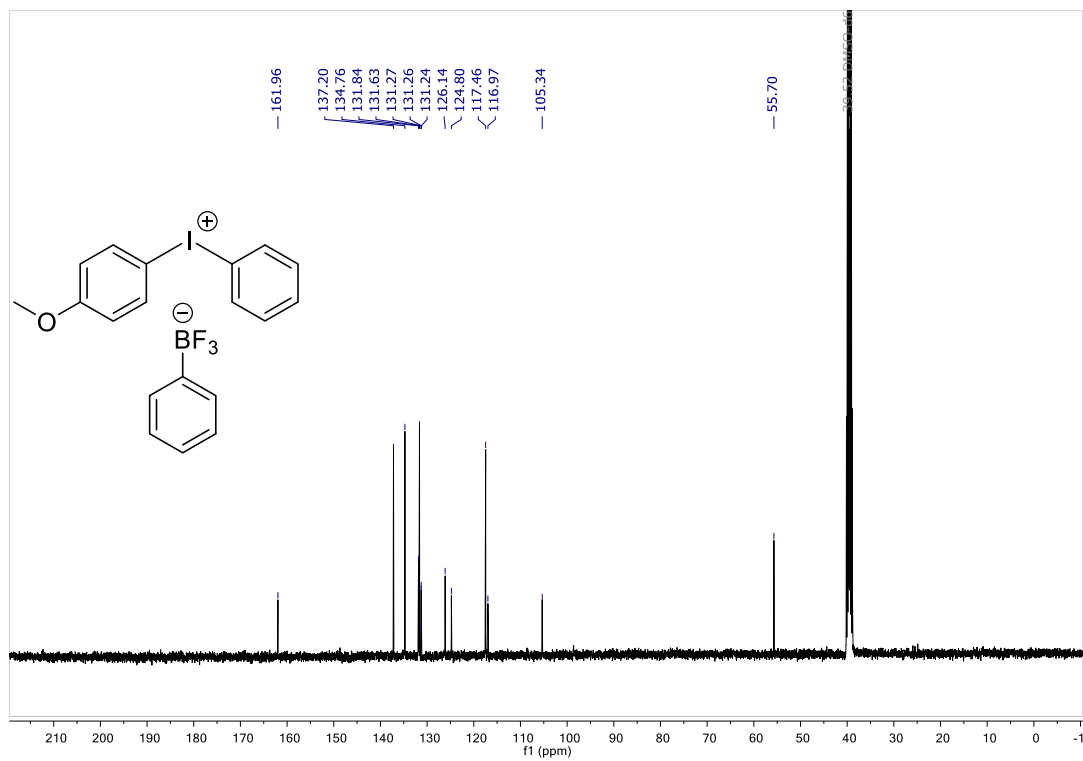


(4-methoxyphenyl)(phenyl)iodonium phenyltrifluoroborate (**3.25**)

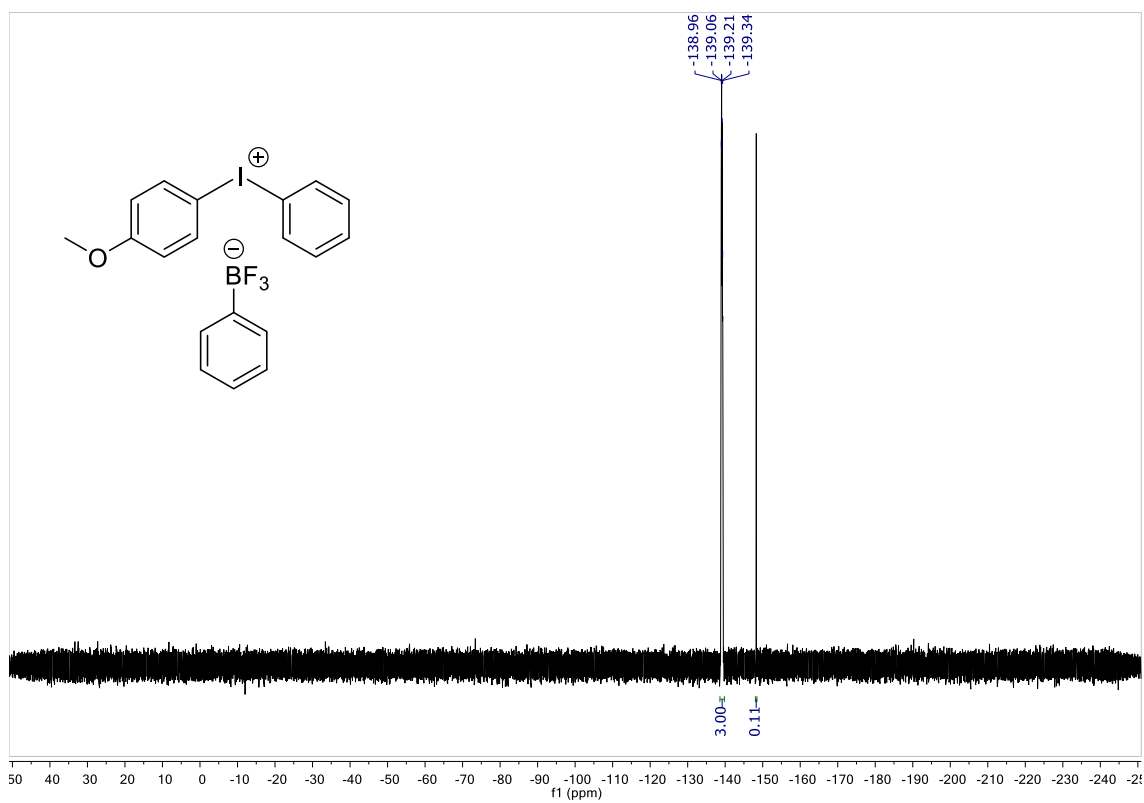
^1H NMR



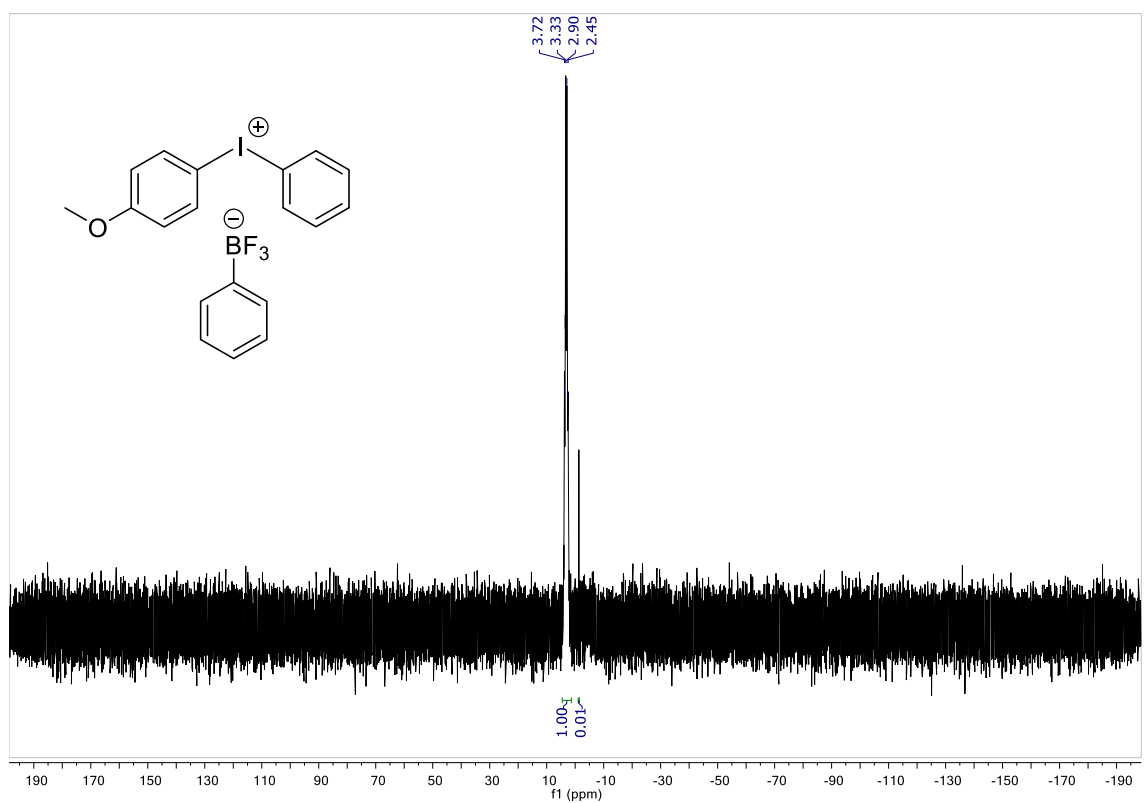
^{13}C NMR



^{19}F NMR

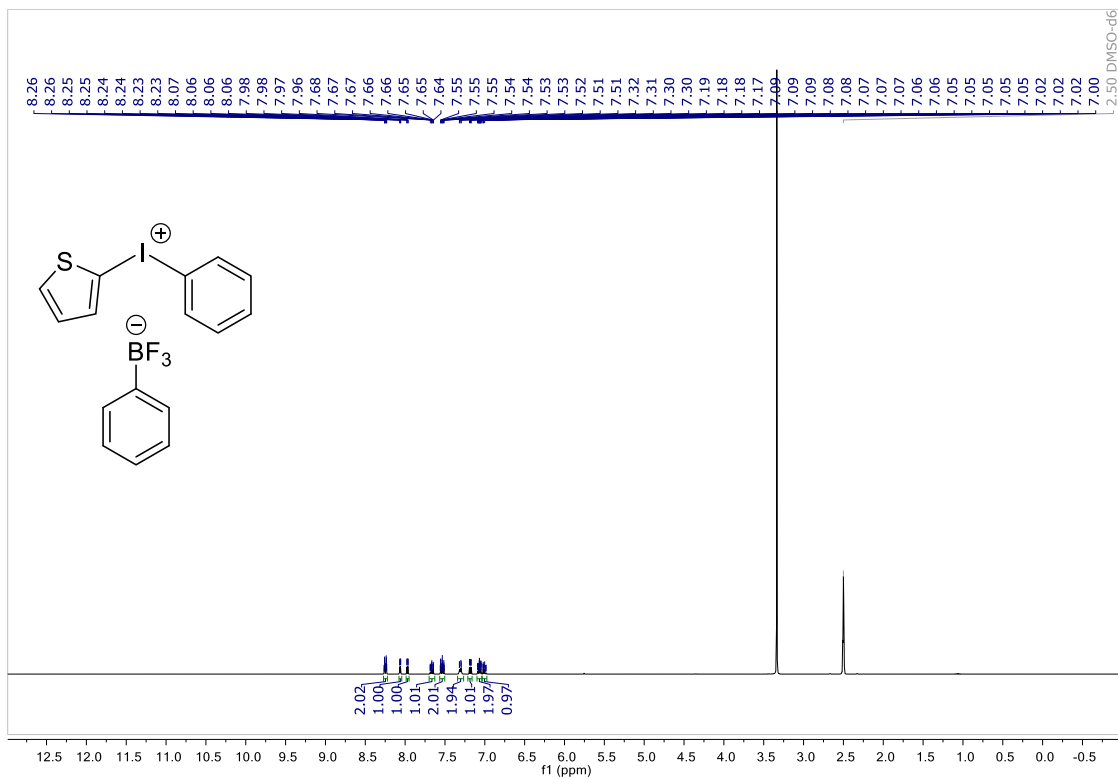


^{11}B NMR

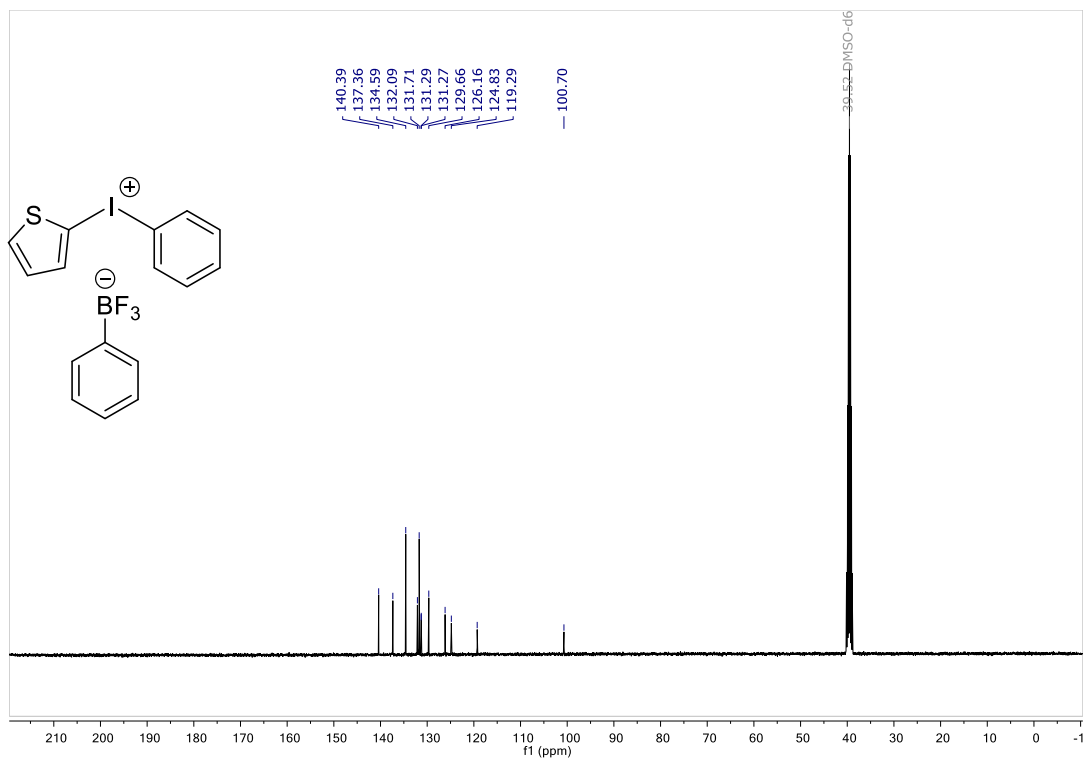


(2-thienyl)(phenyl)iodonium tetrafluoroborate (**3.26**)

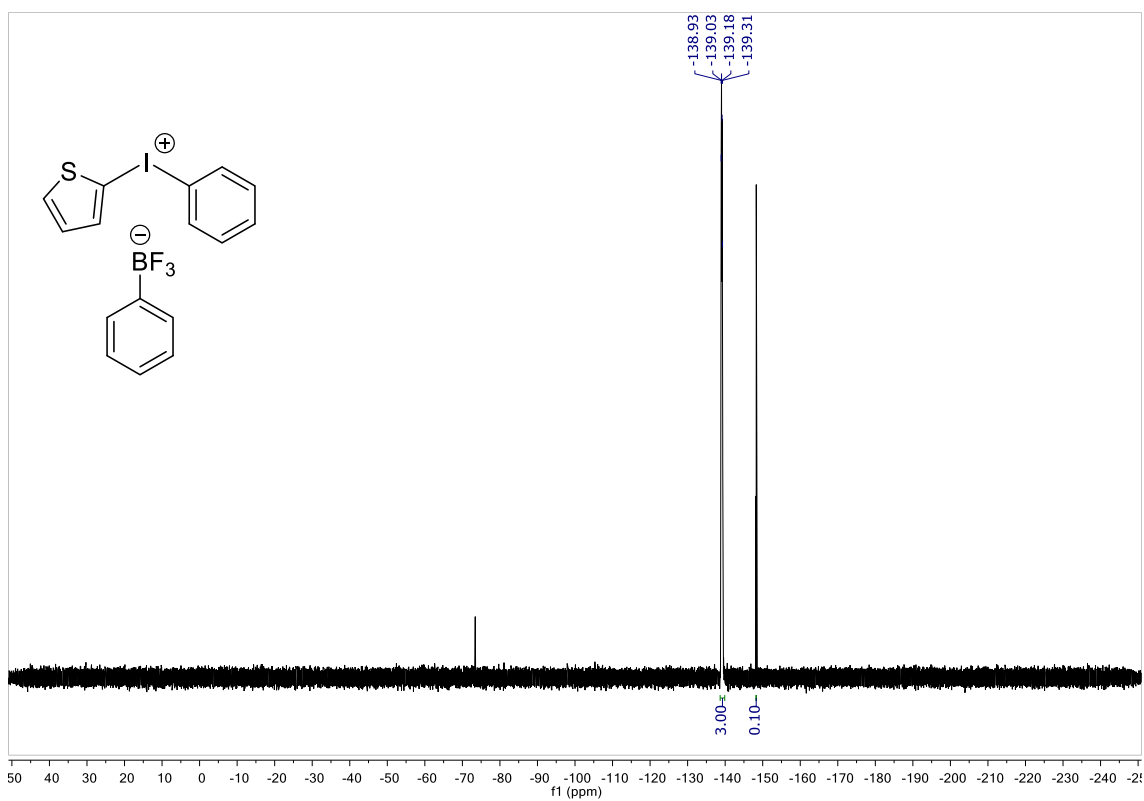
^1H NMR



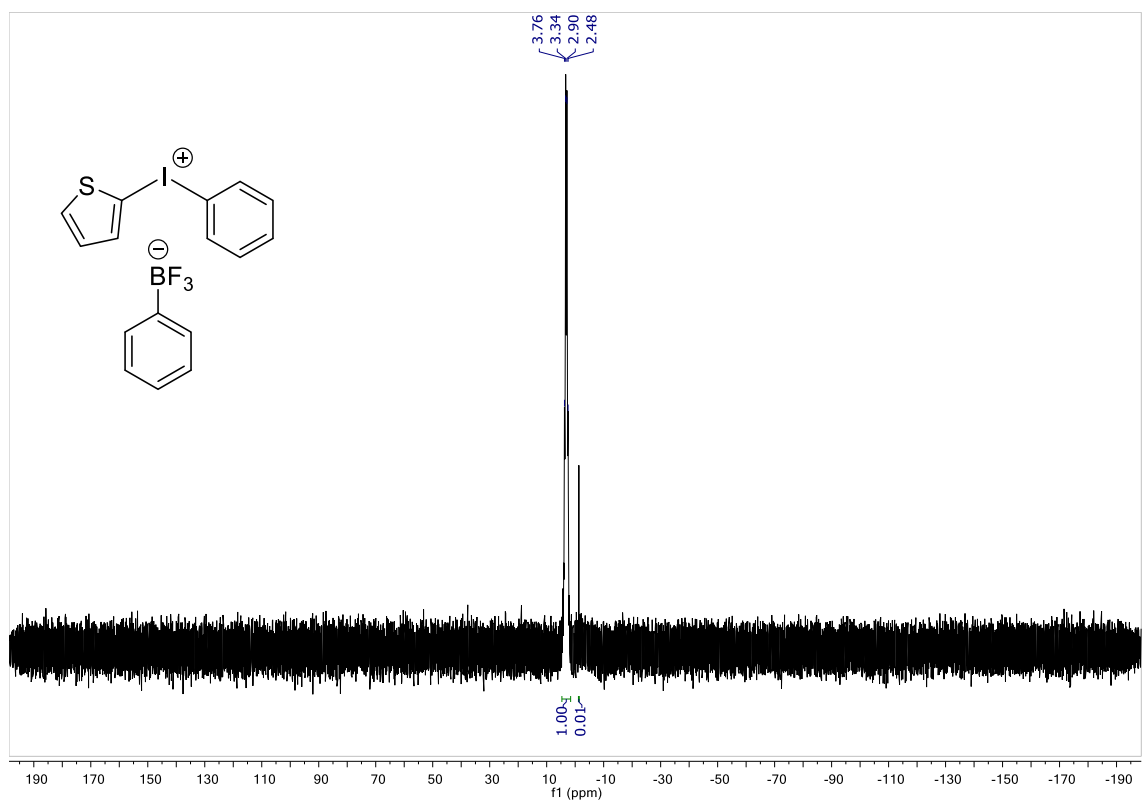
^{13}C NMR



^{19}F NMR



^{11}B NMR



X-ray Data Tables

(2,4,6-trimethylphenyl)(phenyl)iodonium phenyltrifluoroborate (3.20)

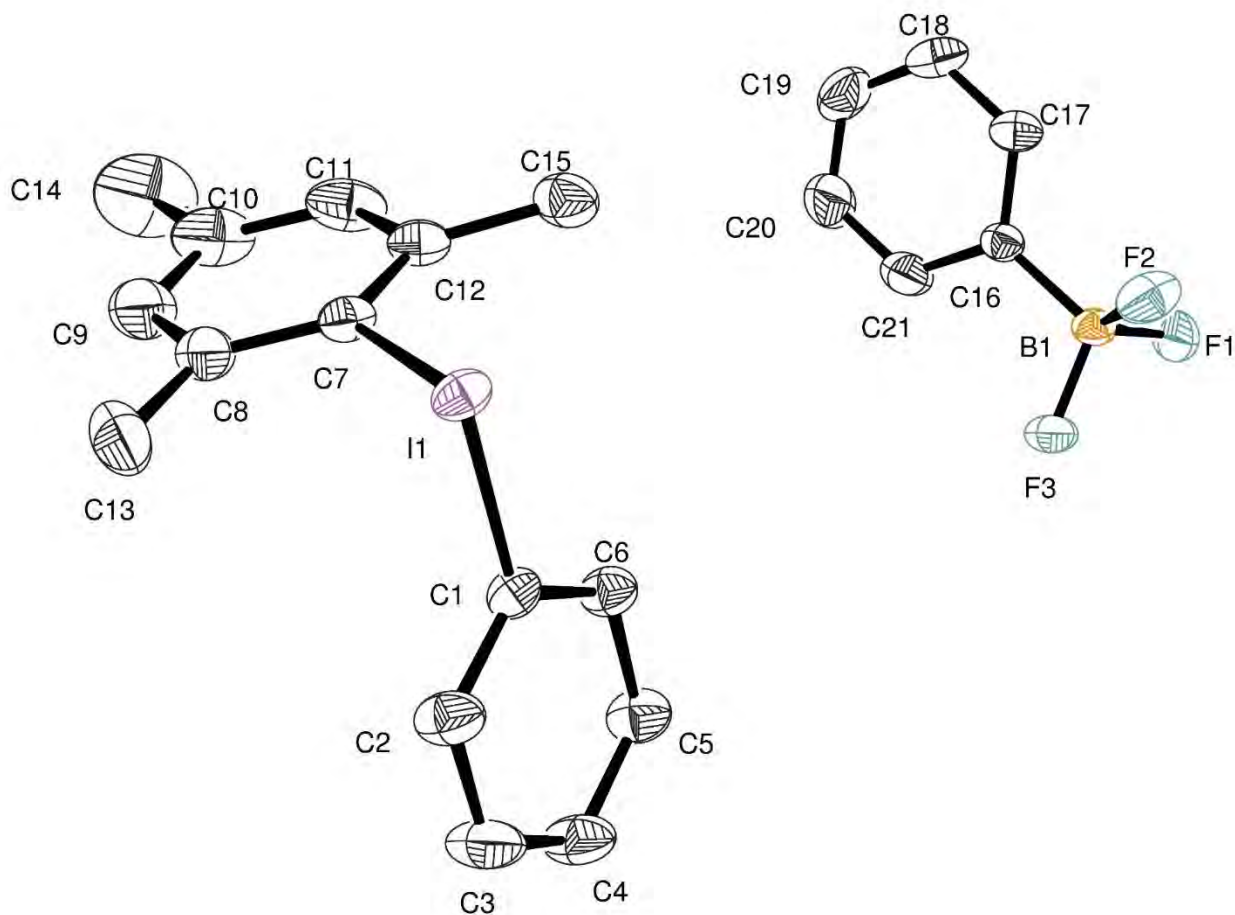


Table 1. Crystal data and structure refinement for OS-6-058.

Identification code	OS-6-058
Empirical formula	C ₁₅ H ₁₆ I, C ₆ H ₅ B F ₃
Formula weight	468.09
Temperature	180(2) K
Wavelength	0.71073 Å
Crystal system, space group	Orthorhombic, P b c a
Unit cell dimensions	a = 9.8952(9) Å alpha = 90 deg. b = 16.6269(15) Å beta = 90 deg.

$c = 24.170(2) \text{ \AA}$ $\gamma = 90 \text{ deg.}$
 Volume $3976.6(6) \text{ \AA}^3$
 Z, Calculated density 8, 1.564 Mg/m^3
 Absorption coefficient 1.639 mm^{-1}
 F(000) 1856
 Crystal size $0.600 \times 0.300 \times 0.040 \text{ mm}$
 Theta range for data collection $2.450 \text{ to } 32.028 \text{ deg.}$
 Limiting indices $-14 \leq h \leq 14$, $-24 \leq k \leq 24$,
 $-36 \leq l \leq 36$
 Reflections collected / unique $101023 / 6921$ [R(int) = 0.0350]
 Completeness to theta = 25.242 100.0%
 Refinement method Full-matrix least-squares on F^2
 Data / restraints / parameters $6921 / 0 / 238$
 Goodness-of-fit on F^2 1.264
 Final R indices [$>2\sigma(I)$] $R1 = 0.0320$, $wR2 = 0.0719$
 R indices (all data) $R1 = 0.0395$, $wR2 = 0.0748$
 Largest diff. peak and hole 0.670 and $-1.516 \text{ e.\AA}^{-3}$

Table 2. Atomic coordinates ($\times 10^4$) and equivalent isotropic displacement parameters ($\text{\AA}^2 \times 10^3$) for OS-6-058. $U(\text{eq})$ is defined as one third of the trace of the orthogonalized U_{ij} tensor.

	x	y	z	$U(\text{eq})$
C(1)	2041(2)	1790(1)	3232(1)	24(1)
C(2)	831(2)	1457(2)	3395(1)	36(1)
C(3)	-274(2)	1965(2)	3453(1)	45(1)
C(4)	-149(2)	2781(2)	3356(1)	39(1)
C(5)	1078(2)	3100(1)	3189(1)	33(1)
C(6)	2199(2)	2603(1)	3124(1)	28(1)
C(7)	4787(2)	1438(1)	3827(1)	26(1)
C(8)	4503(2)	1093(2)	4339(1)	35(1)
C(9)	5191(3)	1411(2)	4793(1)	47(1)
C(10)	6118(3)	2031(2)	4740(1)	51(1)
C(11)	6375(2)	2341(2)	4219(1)	43(1)
C(12)	5723(2)	2054(1)	3748(1)	29(1)
C(13)	3514(3)	409(2)	4411(1)	52(1)
C(14)	6845(4)	2365(3)	5241(2)	86(1)
C(15)	6076(2)	2395(2)	3192(1)	37(1)
C(16)	8168(2)	9671(1)	3457(1)	28(1)
C(17)	9462(2)	9448(1)	3285(1)	33(1)
C(18)	10502(2)	9286(2)	3659(1)	40(1)
C(19)	10263(3)	9351(2)	4214(1)	54(1)
C(20)	9010(3)	9588(3)	4401(1)	70(1)
C(21)	7979(3)	9747(2)	4027(1)	52(1)
B(1)	6987(2)	9827(2)	3019(1)	28(1)
F(1)	7042(2)	10623(1)	2795(1)	45(1)
F(2)	7054(2)	9295(1)	2573(1)	51(1)
F(3)	5688(1)	9761(1)	3264(1)	37(1)
I(1)	3712(1)	1011(1)	3130(1)	26(1)

Table 3. Bond lengths [\AA] and angles [deg] for OS-6-058.

C(1)-C(2)	1.377(3)
C(1)-C(6)	1.385(3)
C(1)-I(1)	2.115(2)
C(2)-C(3)	1.389(3)
C(2)-H(2)	0.9500
C(3)-C(4)	1.383(4)
C(3)-H(3)	0.9500
C(4)-C(5)	1.384(3)
C(4)-H(4)	0.9500
C(5)-C(6)	1.392(3)
C(5)-H(5)	0.9500
C(6)-H(6)	0.9500
C(7)-C(8)	1.392(3)
C(7)-C(12)	1.394(3)
C(7)-I(1)	2.114(2)
C(8)-C(9)	1.397(4)
C(8)-C(13)	1.511(4)
C(9)-C(10)	1.386(5)
C(9)-H(9)	0.9500
C(10)-C(11)	1.385(5)
C(10)-C(14)	1.515(4)
C(11)-C(12)	1.393(3)

C(11)-H(11)	0.9500
C(12)-C(15)	1.498(3)
C(13)-H(13A)	0.9800
C(13)-H(13B)	0.9800
C(13)-H(13C)	0.9800
C(14)-H(14A)	0.9800
C(14)-H(14B)	0.9800
C(14)-H(14C)	0.9800
C(15)-H(15A)	0.9800
C(15)-H(15B)	0.9800
C(15)-H(15C)	0.9800
C(16)-C(17)	1.395(3)
C(16)-C(21)	1.396(4)
C(16)-B(1)	1.598(3)
C(17)-C(18)	1.395(4)
C(17)-H(17)	0.9500
C(18)-C(19)	1.368(5)
C(18)-H(18)	0.9500
C(19)-C(20)	1.377(5)
C(19)-H(19)	0.9500
C(20)-C(21)	1.389(4)
C(20)-H(20)	0.9500
C(21)-H(21)	0.9500
B(1)-F(2)	1.396(3)
B(1)-F(3)	1.419(3)
B(1)-F(1)	1.431(3)
C(2)-C(1)-C(6)	123.0(2)
C(2)-C(1)-I(1)	117.80(16)
C(6)-C(1)-I(1)	119.15(16)
C(1)-C(2)-C(3)	117.9(2)
C(1)-C(2)-H(2)	121.0
C(3)-C(2)-H(2)	121.0
C(4)-C(3)-C(2)	120.6(2)
C(4)-C(3)-H(3)	119.7
C(2)-C(3)-H(3)	119.7
C(3)-C(4)-C(5)	120.3(2)
C(3)-C(4)-H(4)	119.9
C(5)-C(4)-H(4)	119.9
C(4)-C(5)-C(6)	120.3(2)
C(4)-C(5)-H(5)	119.8
C(6)-C(5)-H(5)	119.8
C(1)-C(6)-C(5)	117.8(2)
C(1)-C(6)-H(6)	121.1
C(5)-C(6)-H(6)	121.1
C(8)-C(7)-C(12)	124.0(2)
C(8)-C(7)-I(1)	117.88(17)
C(12)-C(7)-I(1)	118.10(16)
C(7)-C(8)-C(9)	116.4(2)
C(7)-C(8)-C(13)	123.0(2)
C(9)-C(8)-C(13)	120.6(2)
C(10)-C(9)-C(8)	122.1(3)
C(10)-C(9)-H(9)	119.0
C(8)-C(9)-H(9)	119.0
C(11)-C(10)-C(9)	118.9(2)
C(11)-C(10)-C(14)	120.3(3)
C(9)-C(10)-C(14)	120.8(3)
C(10)-C(11)-C(12)	122.0(3)
C(10)-C(11)-H(11)	119.0
C(12)-C(11)-H(11)	119.0
C(11)-C(12)-C(7)	116.6(2)
C(11)-C(12)-C(15)	119.6(2)

C(7)-C(12)-C(15)	123.8(2)
C(8)-C(13)-H(13A)	109.5
C(8)-C(13)-H(13B)	109.5
H(13A)-C(13)-H(13B)	109.5
C(8)-C(13)-H(13C)	109.5
H(13A)-C(13)-H(13C)	109.5
H(13B)-C(13)-H(13C)	109.5
C(10)-C(14)-H(14A)	109.5
C(10)-C(14)-H(14B)	109.5
H(14A)-C(14)-H(14B)	109.5
C(10)-C(14)-H(14C)	109.5
H(14A)-C(14)-H(14C)	109.5
H(14B)-C(14)-H(14C)	109.5
C(12)-C(15)-H(15A)	109.5
C(12)-C(15)-H(15B)	109.5
H(15A)-C(15)-H(15B)	109.5
C(12)-C(15)-H(15C)	109.5
H(15A)-C(15)-H(15C)	109.5
H(15B)-C(15)-H(15C)	109.5
C(17)-C(16)-C(21)	116.1(2)
C(17)-C(16)-B(1)	121.2(2)
C(21)-C(16)-B(1)	122.7(2)
C(16)-C(17)-C(18)	122.4(2)
C(16)-C(17)-H(17)	118.8
C(18)-C(17)-H(17)	118.8
C(19)-C(18)-C(17)	119.5(2)
C(19)-C(18)-H(18)	120.3
C(17)-C(18)-H(18)	120.3
C(18)-C(19)-C(20)	120.0(3)
C(18)-C(19)-H(19)	120.0
C(20)-C(19)-H(19)	120.0
C(19)-C(20)-C(21)	120.1(3)
C(19)-C(20)-H(20)	119.9
C(21)-C(20)-H(20)	119.9
C(20)-C(21)-C(16)	121.8(3)
C(20)-C(21)-H(21)	119.1
C(16)-C(21)-H(21)	119.1
F(2)-B(1)-F(3)	108.5(2)
F(2)-B(1)-F(1)	107.0(2)
F(3)-B(1)-F(1)	105.28(17)
F(2)-B(1)-C(16)	111.89(18)
F(3)-B(1)-C(16)	111.97(19)
F(1)-B(1)-C(16)	111.9(2)
C(7)-I(1)-C(1)	95.46(8)

Symmetry transformations used to generate equivalent atoms:

Table 4. Anisotropic displacement parameters ($\text{Å}^2 \times 10^3$) for OS-6-058.
The anisotropic displacement factor exponent takes the form:
 $-2 \pi^2 [h^2 a^{*2} U_{11} + \dots + 2 h k a^* b^* U_{12}]$

	U11	U22	U33	U23	U13	U12
C(1)	25(1)	20(1)	28(1)	-2(1)	-3(1)	2(1)
C(2)	26(1)	26(1)	56(2)	2(1)	-2(1)	-1(1)
C(3)	22(1)	37(1)	76(2)	6(1)	5(1)	0(1)
C(4)	25(1)	32(1)	59(2)	-1(1)	2(1)	7(1)
C(5)	30(1)	23(1)	46(1)	-2(1)	-1(1)	3(1)
C(6)	25(1)	24(1)	35(1)	-1(1)	-1(1)	2(1)

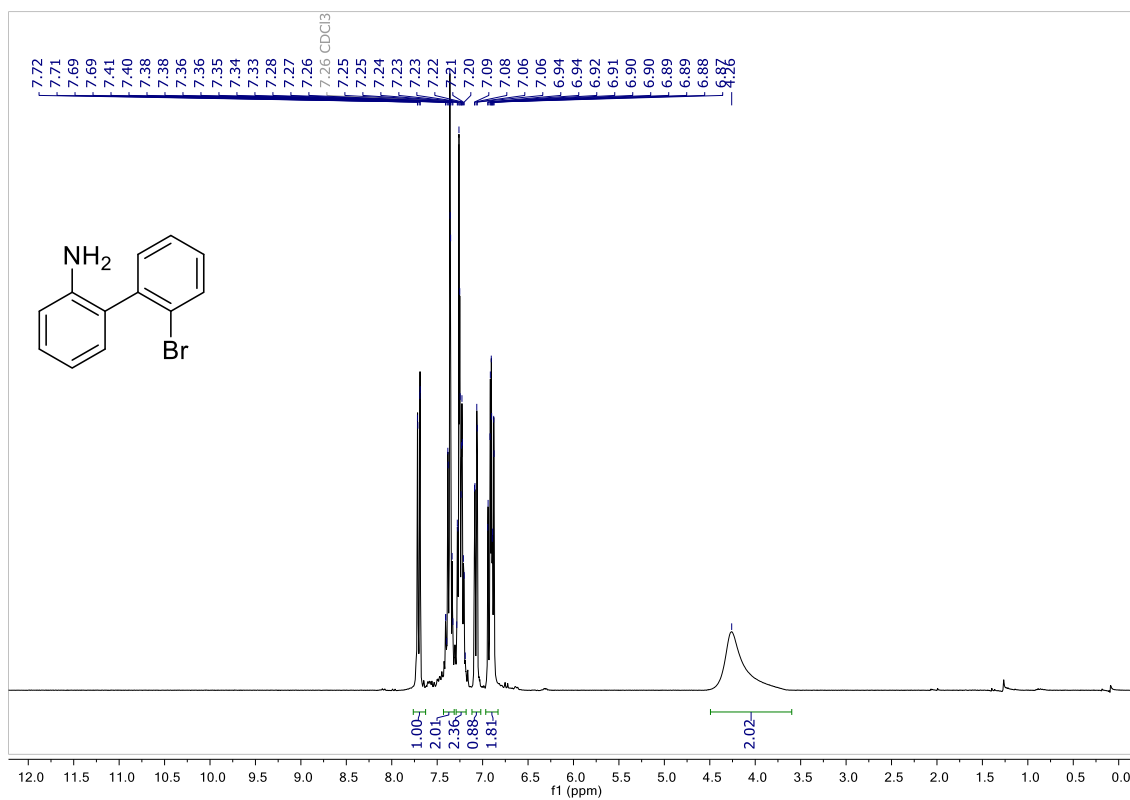
C(7)	21(1)	29(1)	27(1)	-5(1)	-2(1)	4(1)
C(8)	28(1)	47(1)	30(1)	1(1)	0(1)	3(1)
C(9)	39(1)	74(2)	27(1)	-4(1)	0(1)	6(1)
C(10)	36(1)	75(2)	41(1)	-25(1)	-5(1)	2(1)
C(11)	28(1)	51(2)	50(2)	-22(1)	1(1)	-5(1)
C(12)	23(1)	29(1)	36(1)	-7(1)	2(1)	3(1)
C(13)	48(2)	65(2)	44(2)	18(1)	4(1)	-11(1)
C(14)	69(2)	135(4)	53(2)	-43(2)	-16(2)	-13(3)
C(15)	30(1)	31(1)	51(2)	3(1)	5(1)	-3(1)
C(16)	24(1)	26(1)	33(1)	1(1)	3(1)	-1(1)
C(17)	28(1)	27(1)	43(1)	-7(1)	3(1)	0(1)
C(18)	26(1)	29(1)	66(2)	-7(1)	-4(1)	3(1)
C(19)	38(1)	64(2)	59(2)	13(2)	-17(1)	-7(1)
C(20)	44(2)	132(4)	36(2)	12(2)	-4(1)	-4(2)
C(21)	32(1)	91(2)	35(1)	-1(2)	5(1)	3(1)
B(1)	25(1)	26(1)	33(1)	0(1)	5(1)	7(1)
F(1)	48(1)	38(1)	51(1)	18(1)	9(1)	6(1)
F(2)	46(1)	63(1)	46(1)	-25(1)	-11(1)	21(1)
F(3)	23(1)	35(1)	51(1)	4(1)	4(1)	2(1)
I(1)	25(1)	24(1)	29(1)	-6(1)	-4(1)	5(1)

Annex C: Chapter 4

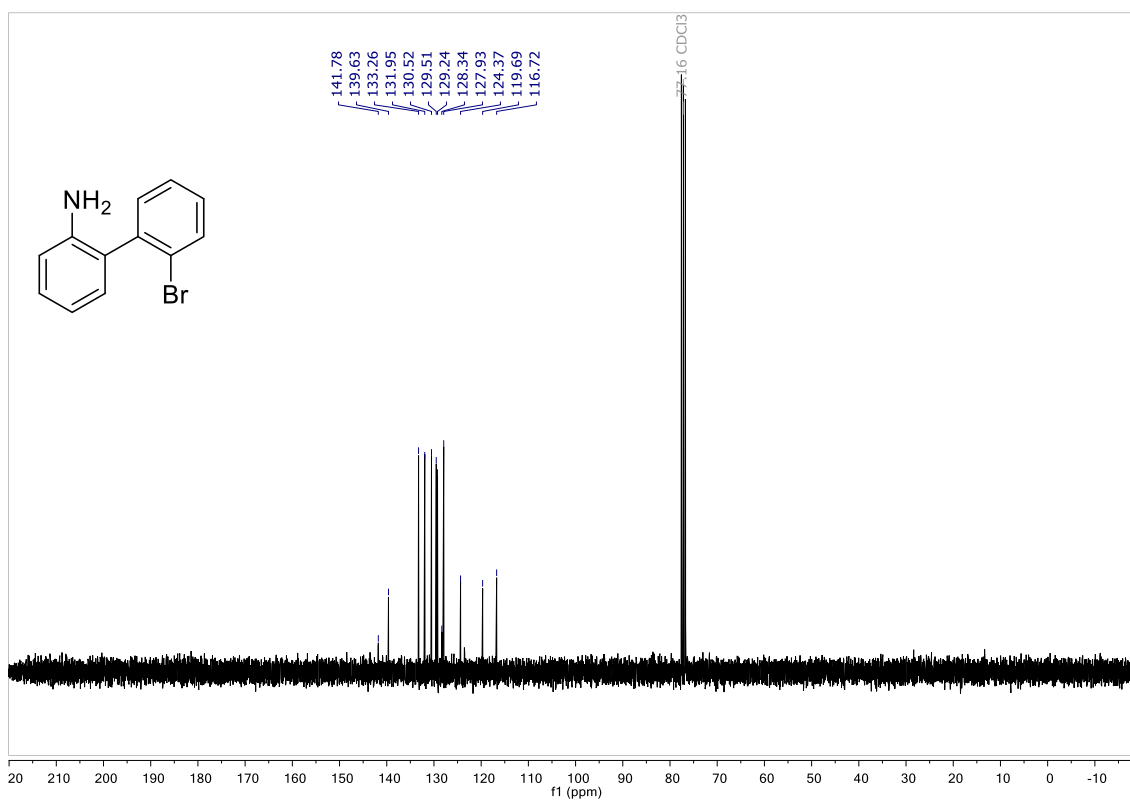
NMR Spectra of selected compounds

2'-bromo-[1,1'-biphenyl]-2-amine (4.24)

¹H NMR

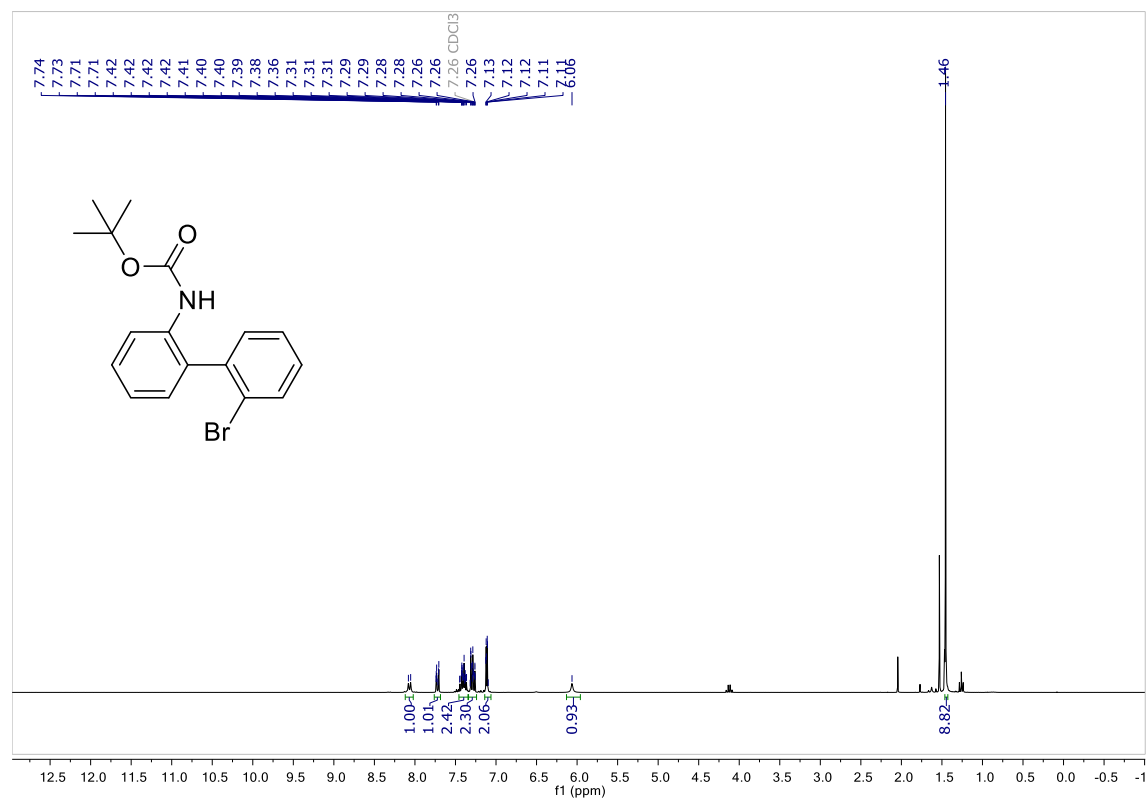


¹³C NMR

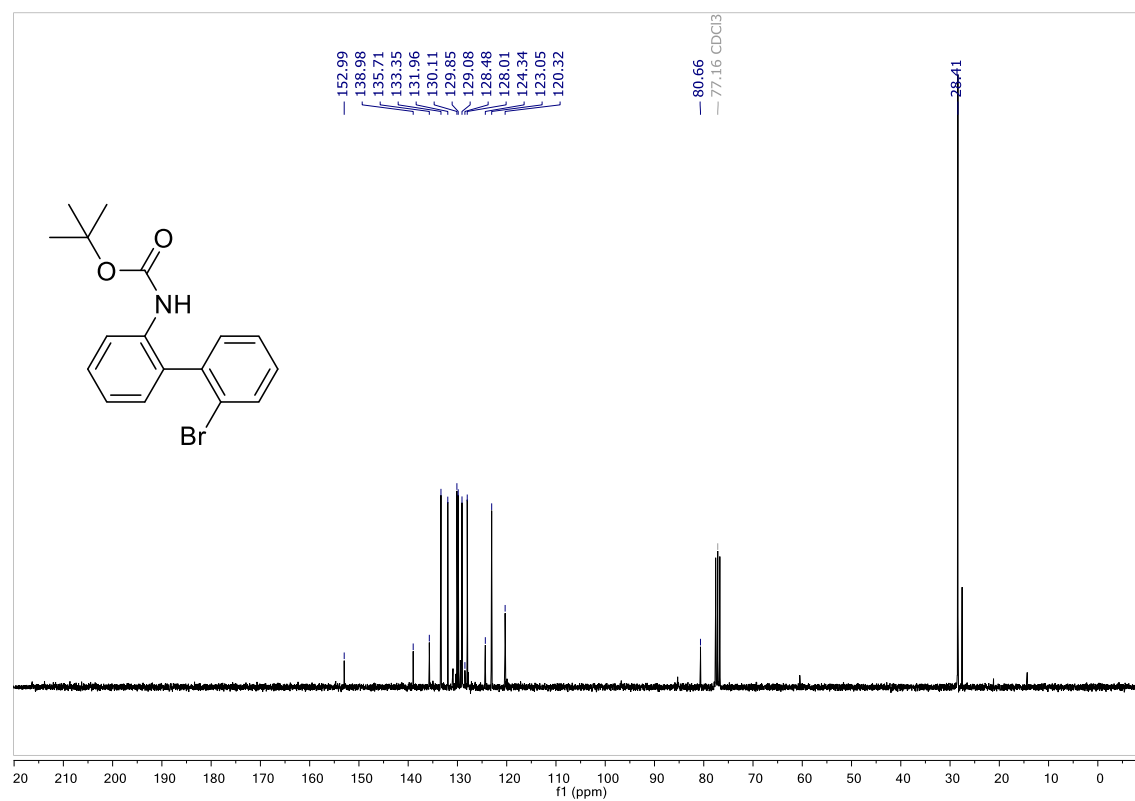


N-Boc-2'-bromo-[1,1'-biphenyl]-2-amine (4.27)

¹H NMR

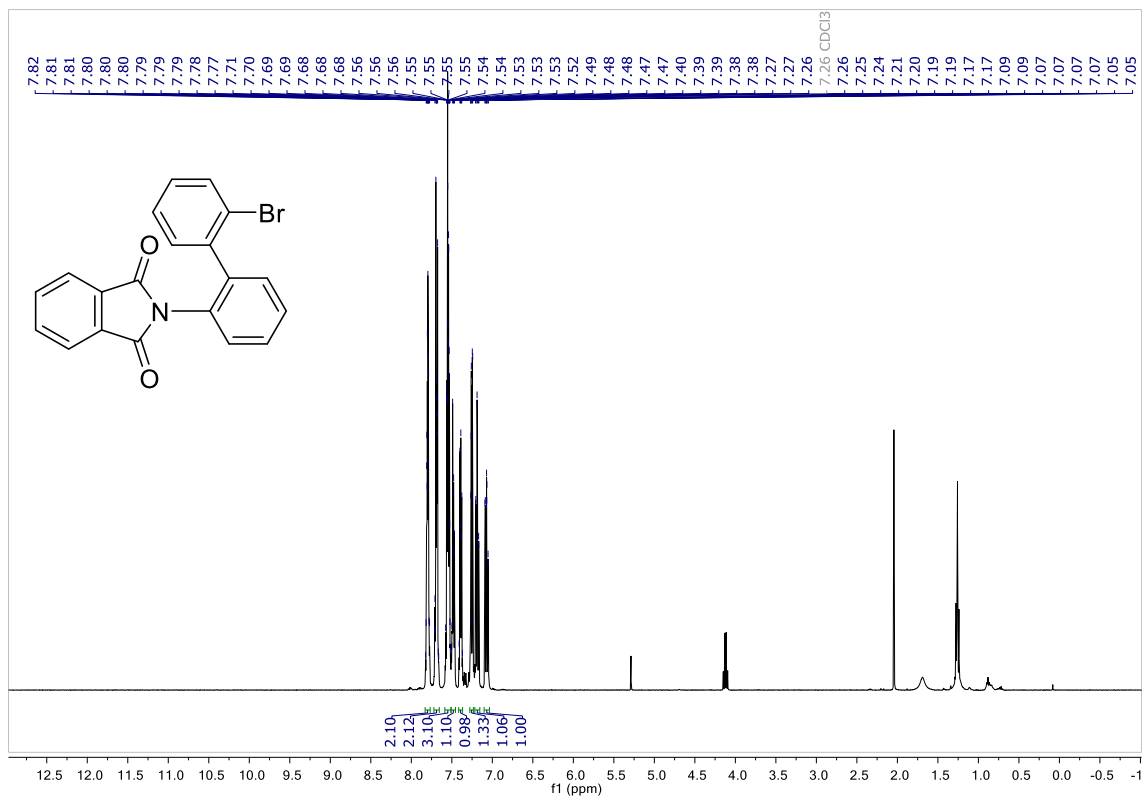


¹³C NMR

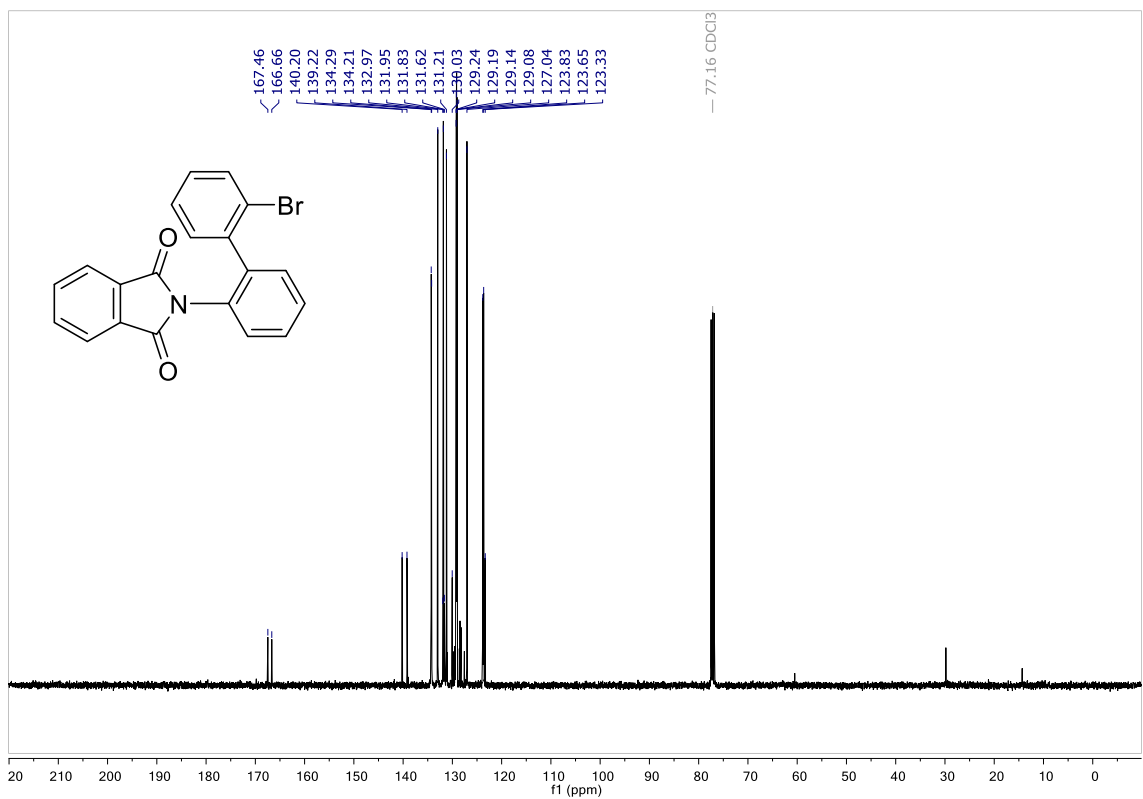


N-Phthaloyl-2'-bromo-[1,1'-biphenyl]-2-amine (**4.28**)

¹H NMR

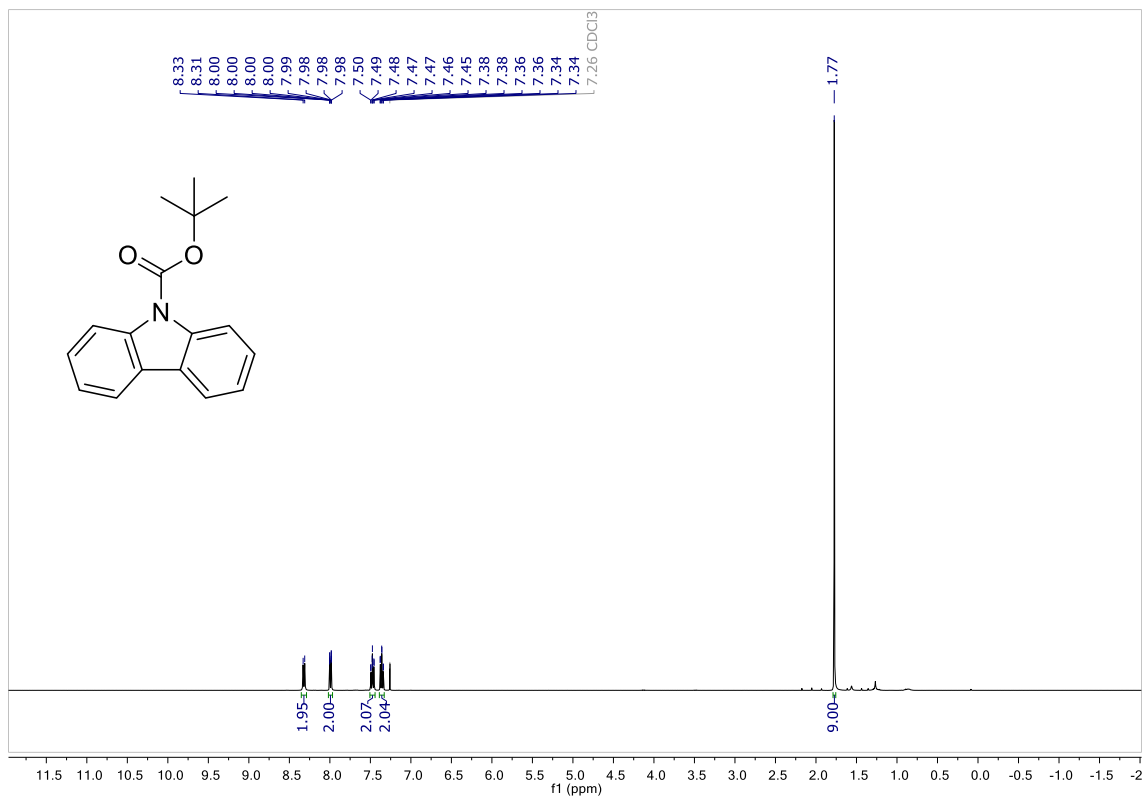


¹³C NMR

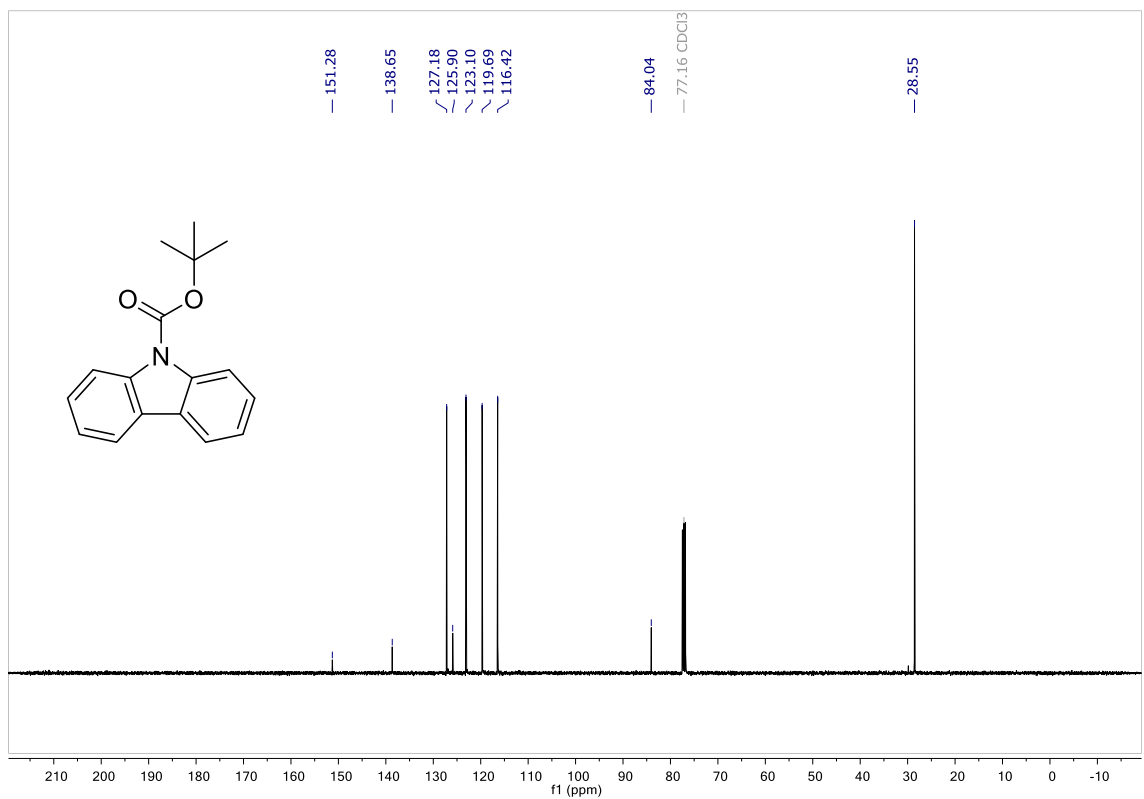


N-Boc-carbazole (4.30)

¹H NMR

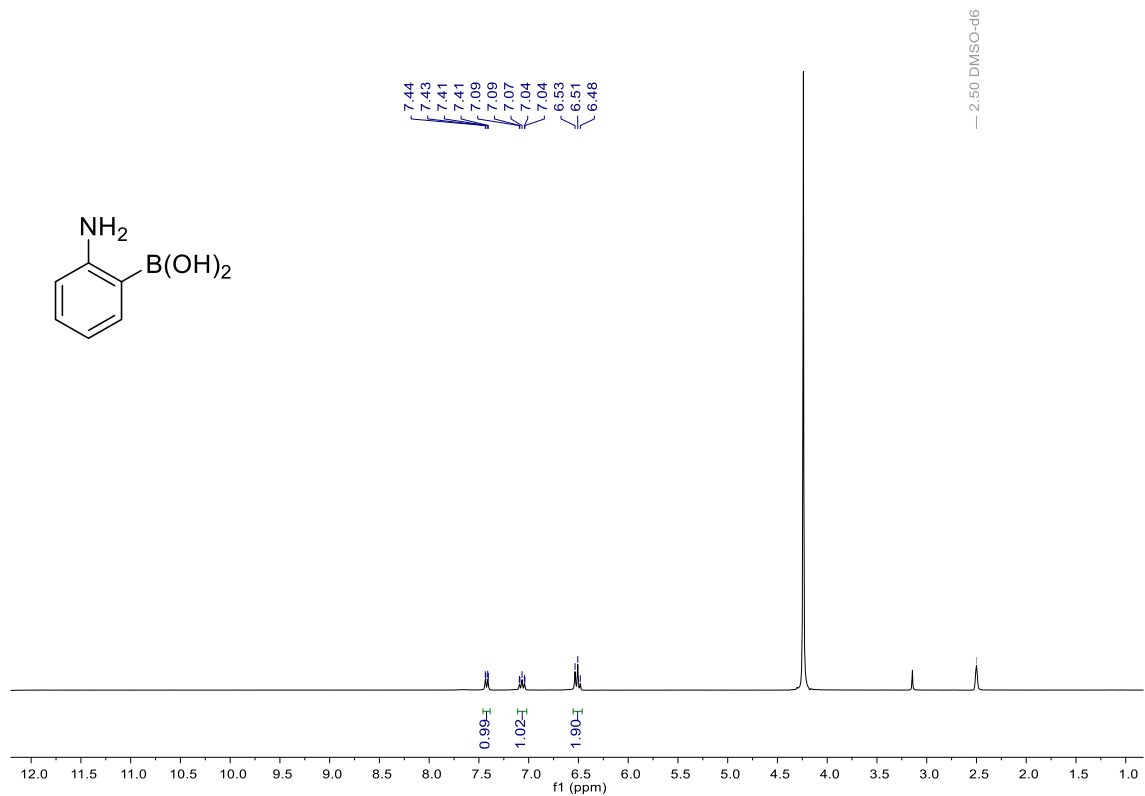


¹³C NMR

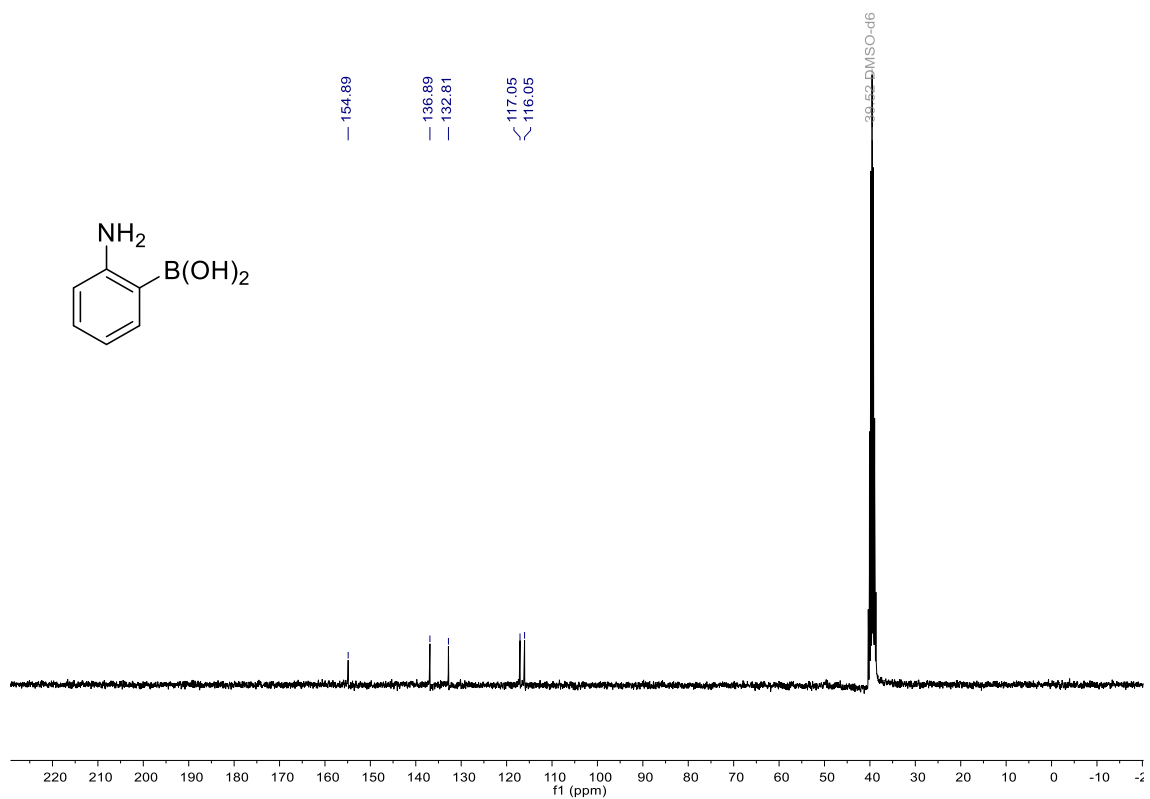


2-aminophenylboronic acid (4.32)

^1H NMR

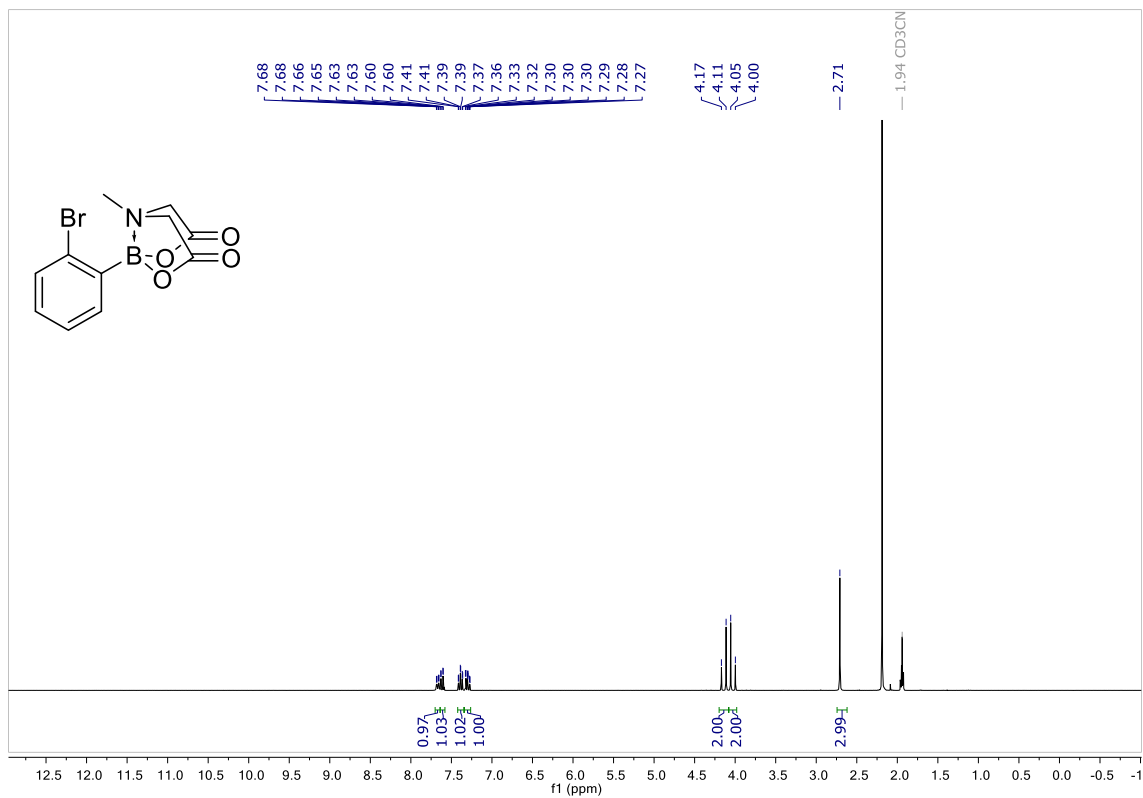


^{13}C NMR

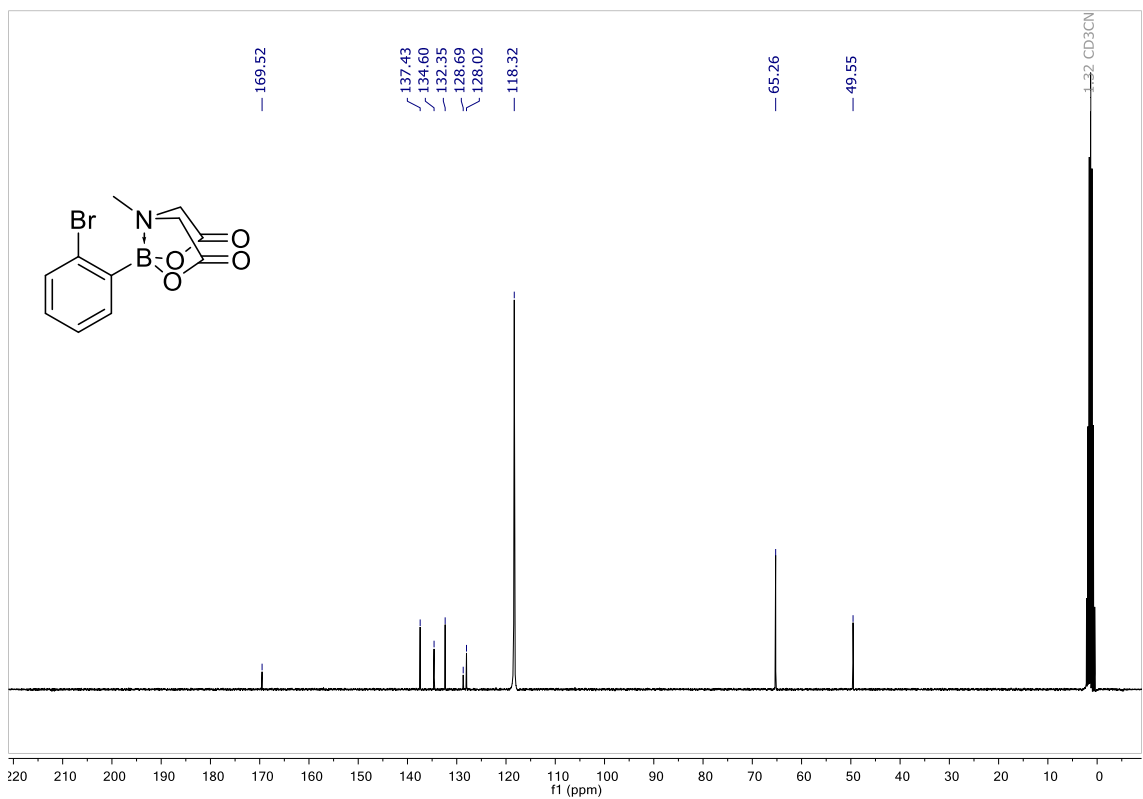


2-bromophenylboronic acid MIDA ester (**4.33**)

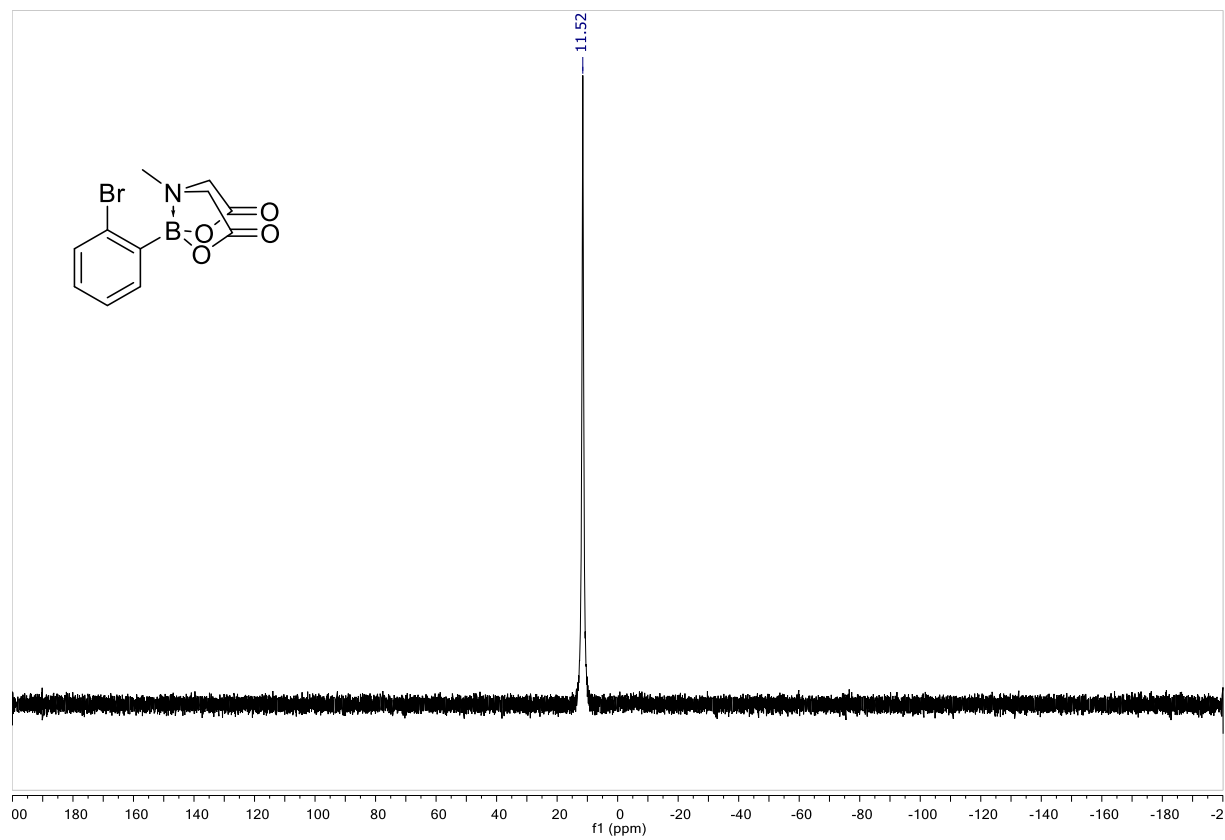
¹H NMR



¹³C NMR

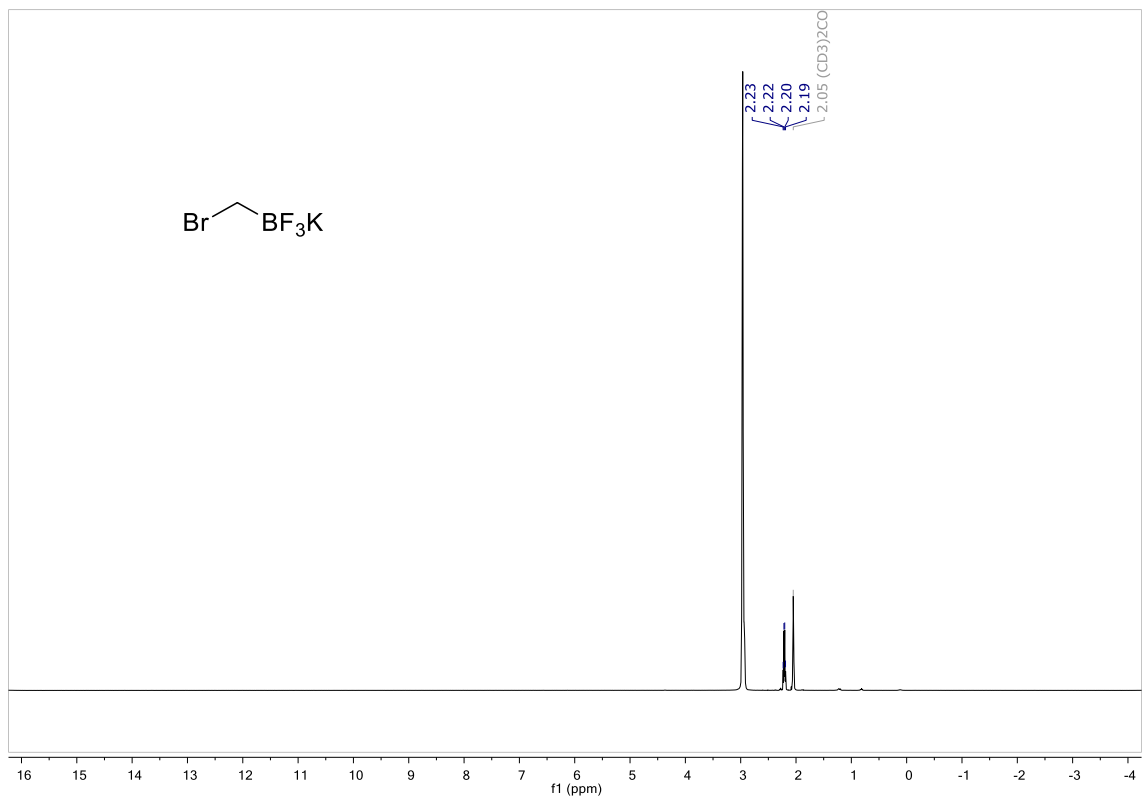


¹¹B NMR

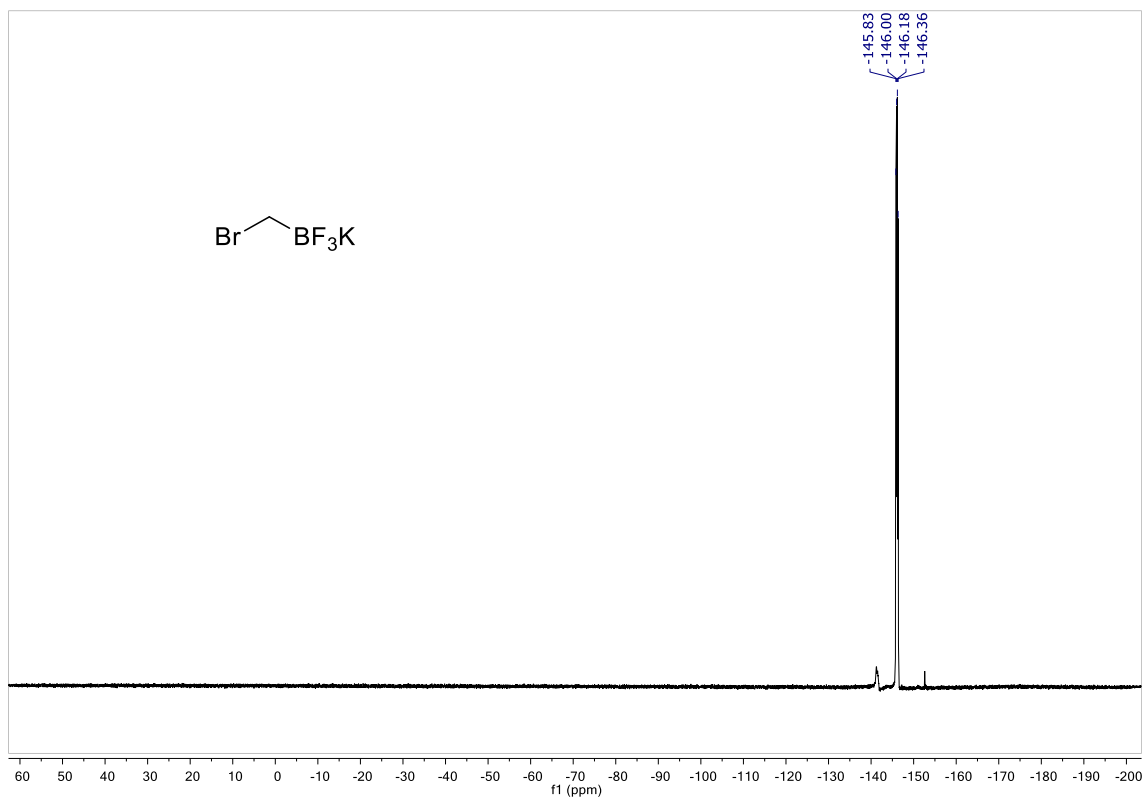


Potassium bromomethyltrifluoroborate (**4.37**)

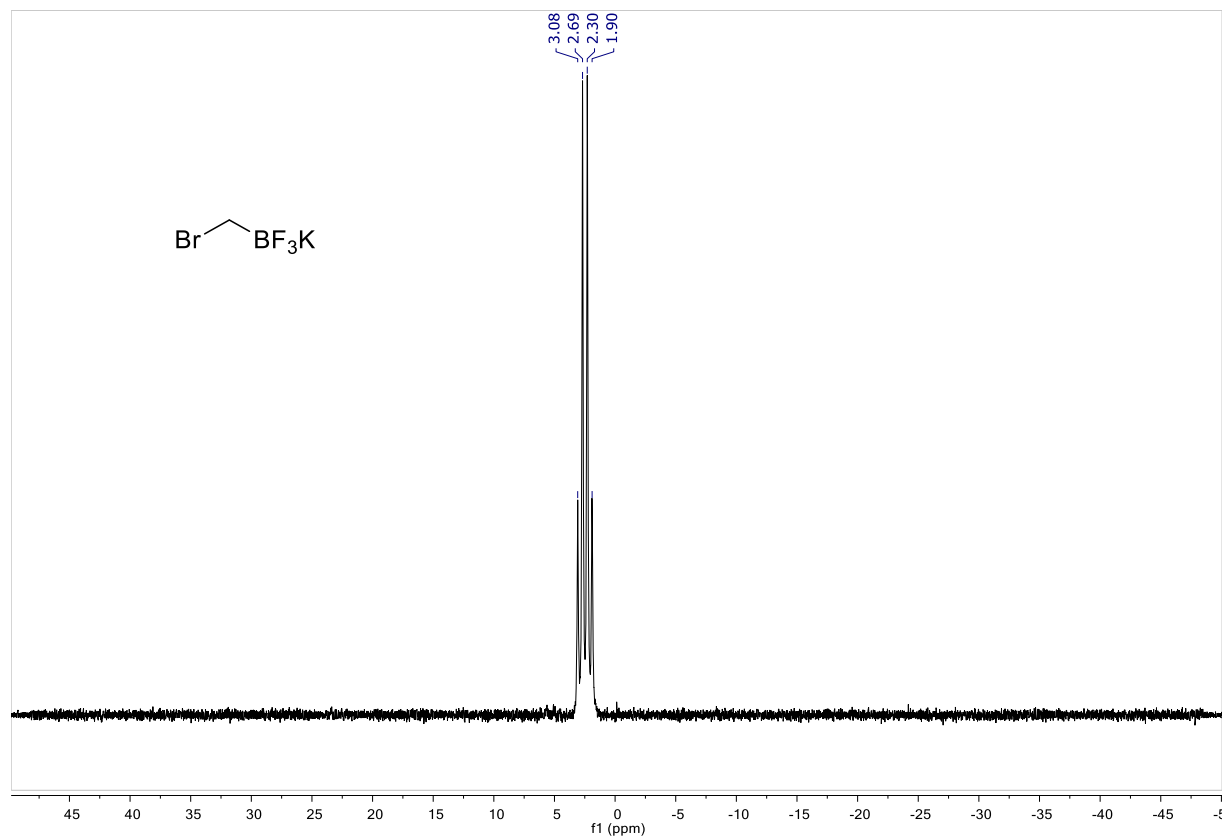
^1H NMR



^{19}F NMR

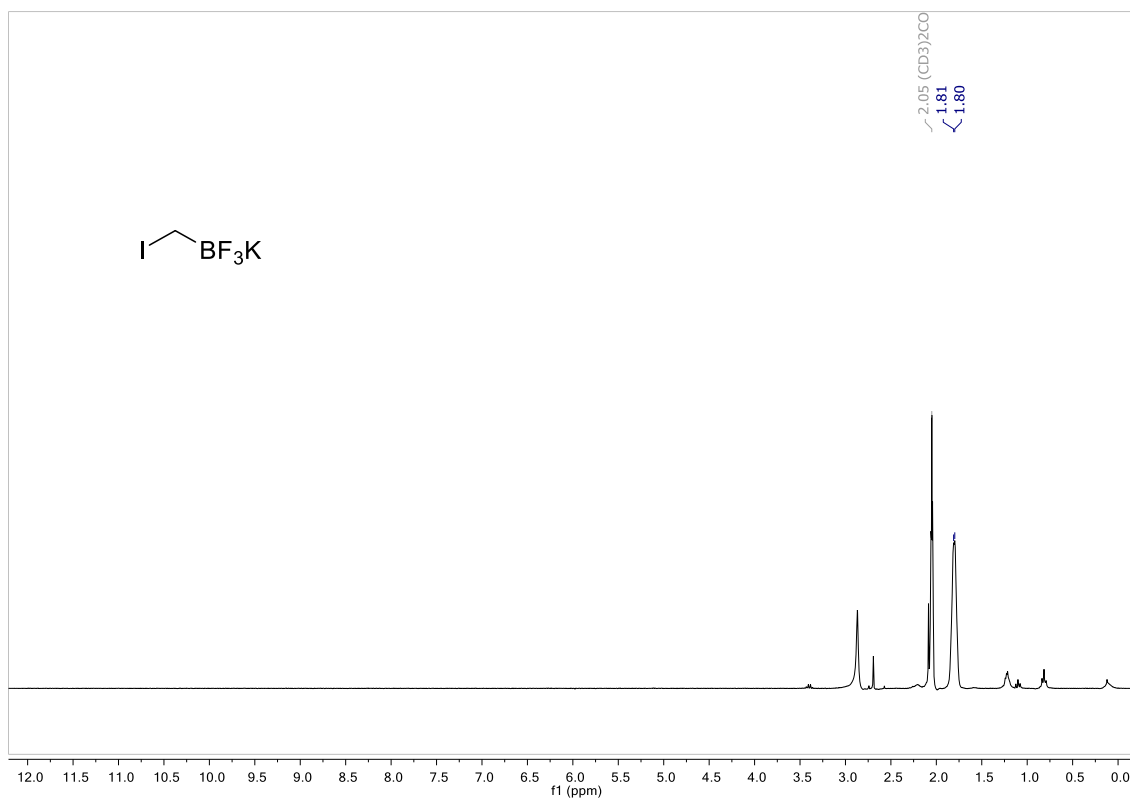


^{11}B NMR

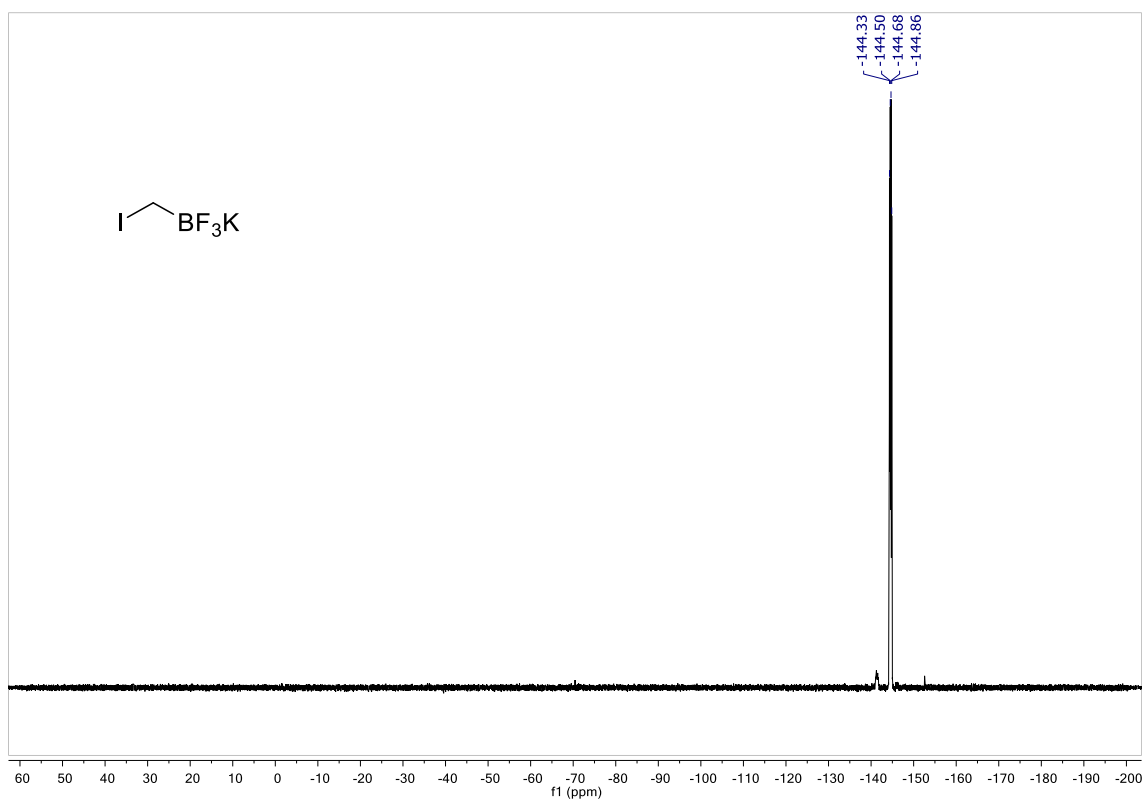


Potassium iodomethyltrifluoroborate (**4.38**)

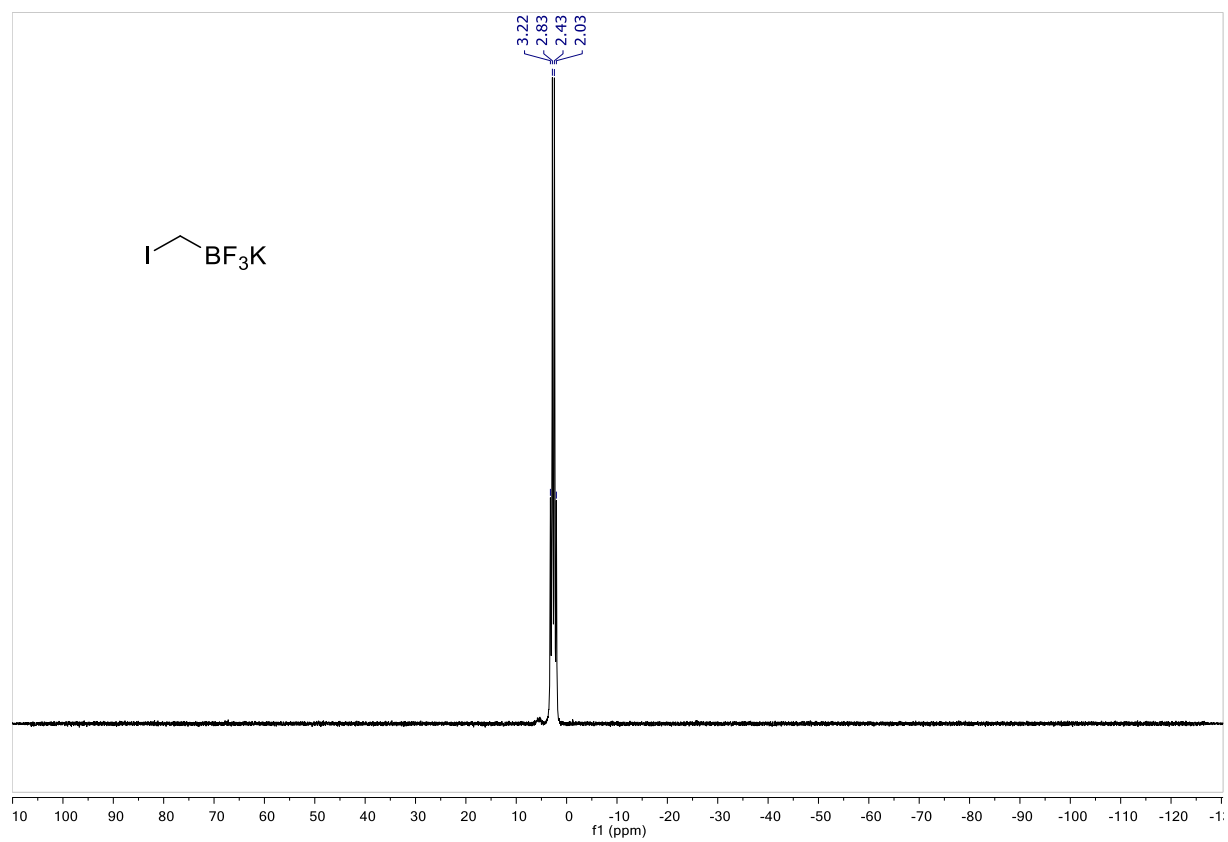
^1H NMR



^{19}F NMR

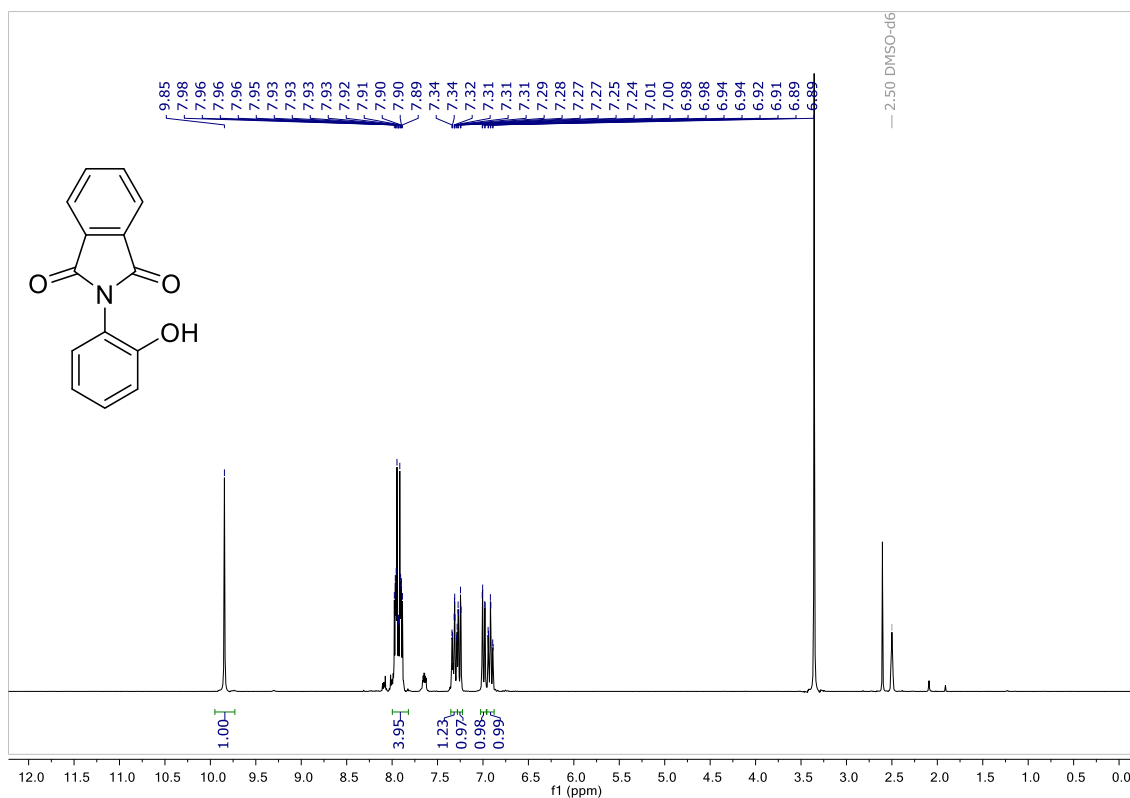


^{11}B NMR

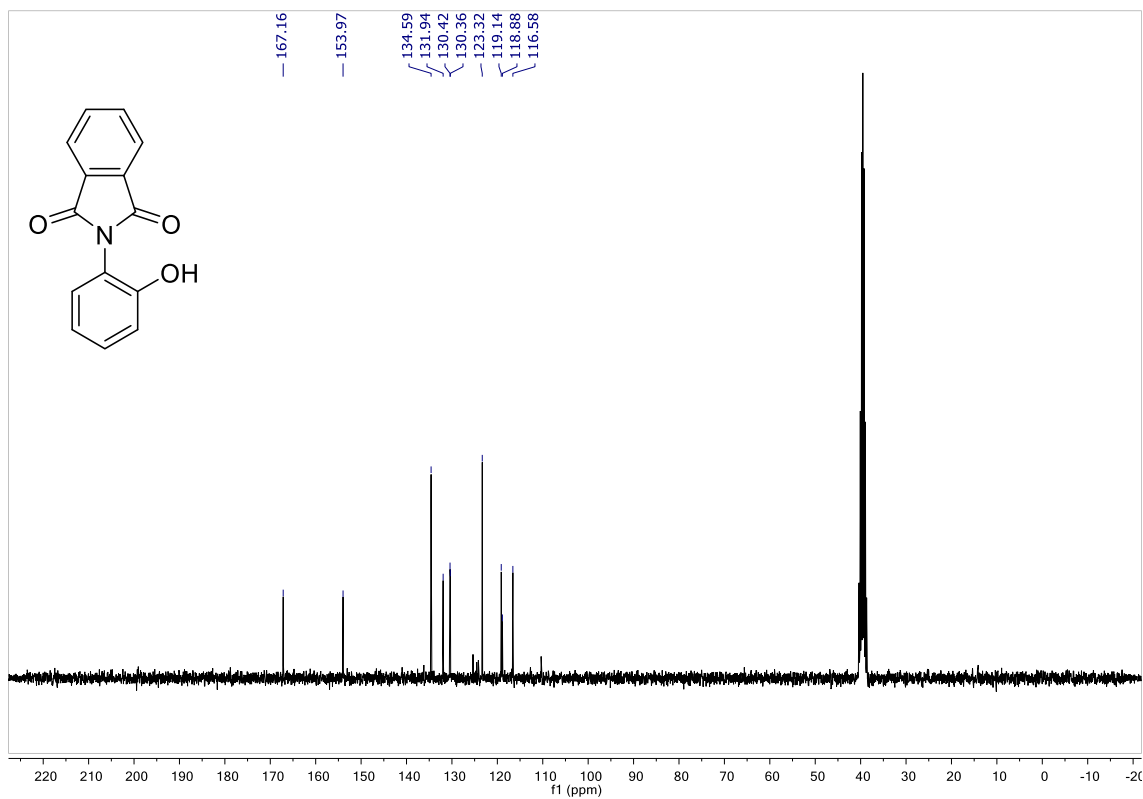


N-Phthaloyl-2-aminophenol (4.41)

¹H NMR

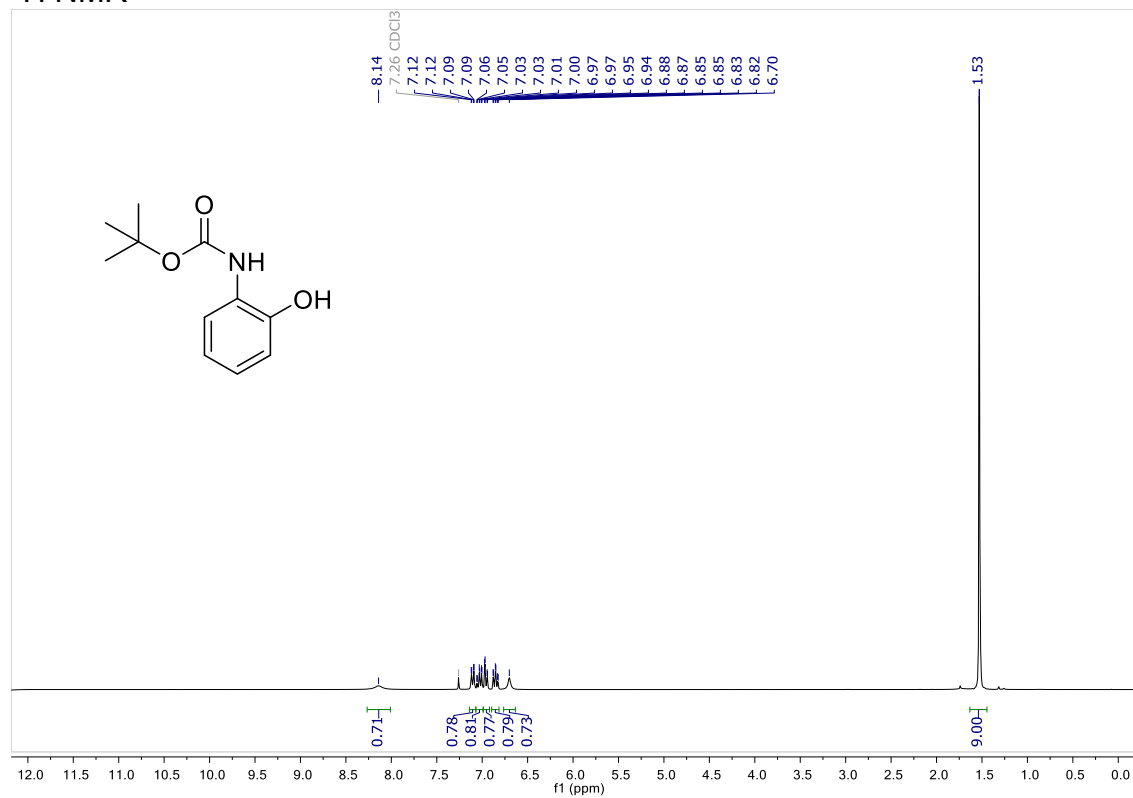


¹³C NMR

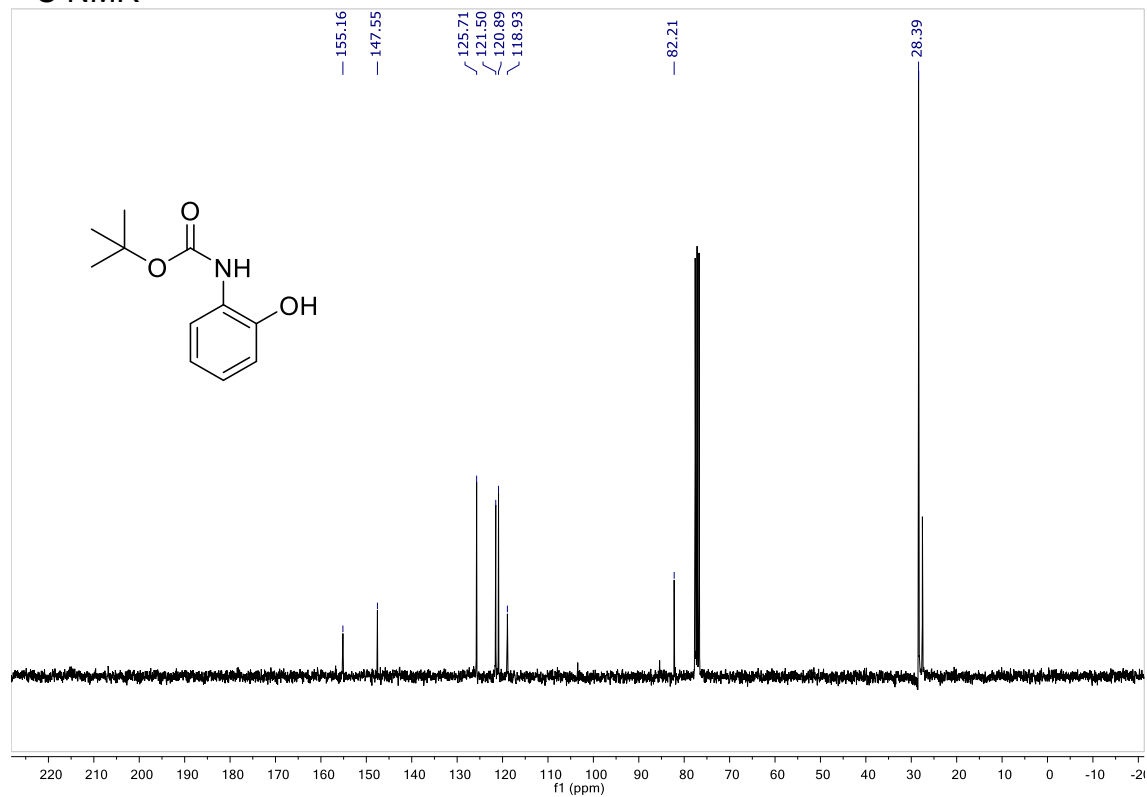


N-Boc-2-aminophenol (4.42)

¹H NMR

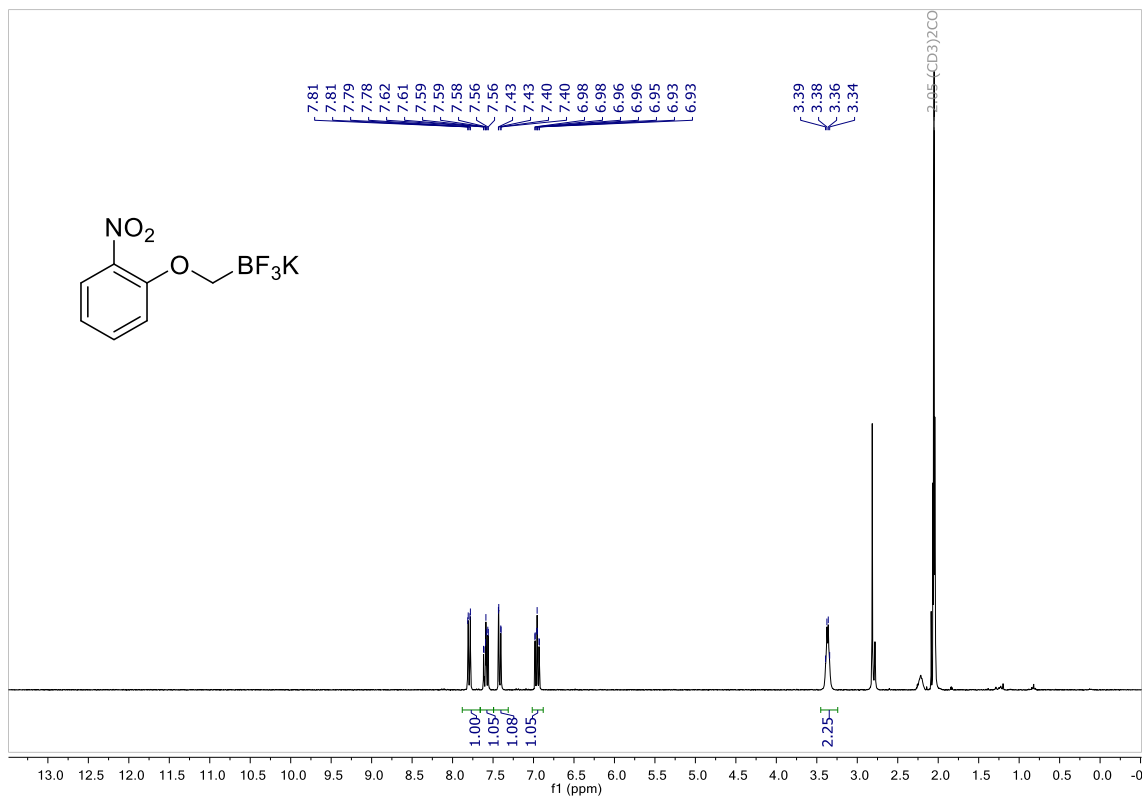


¹³C NMR

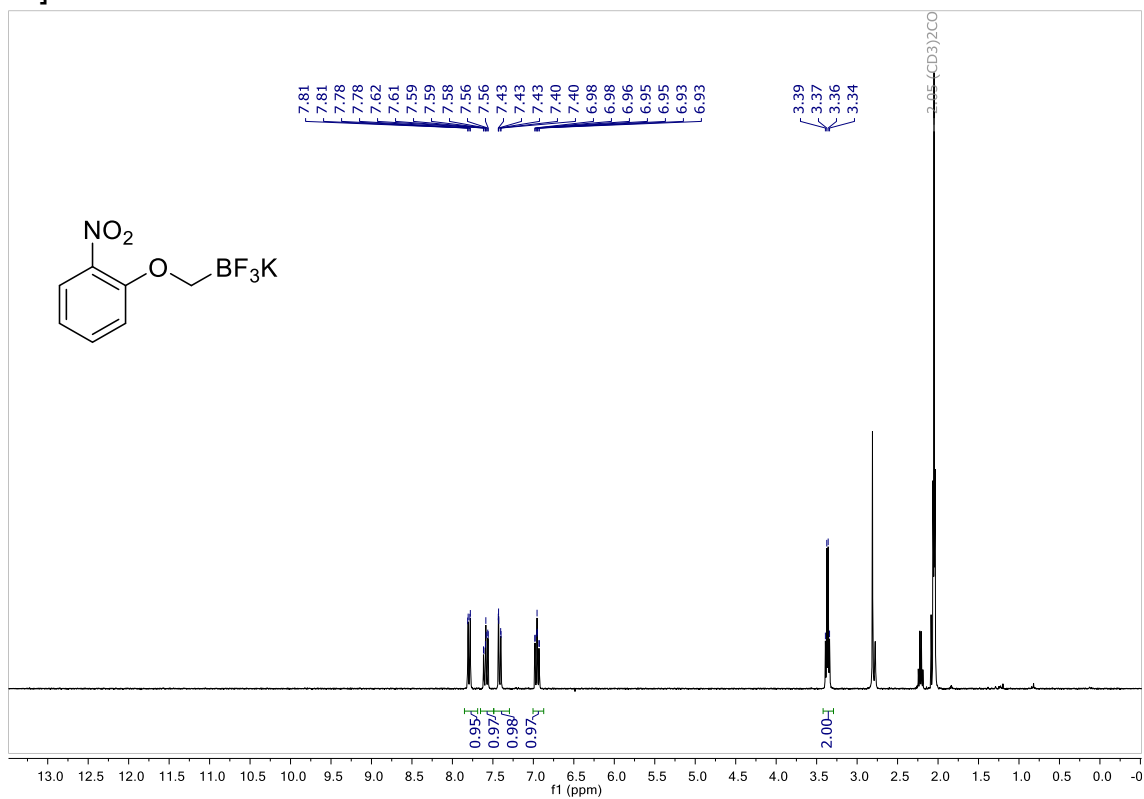


Potassium (2-nitrophenoxy)methyltrifluoroborate (**4.43**)

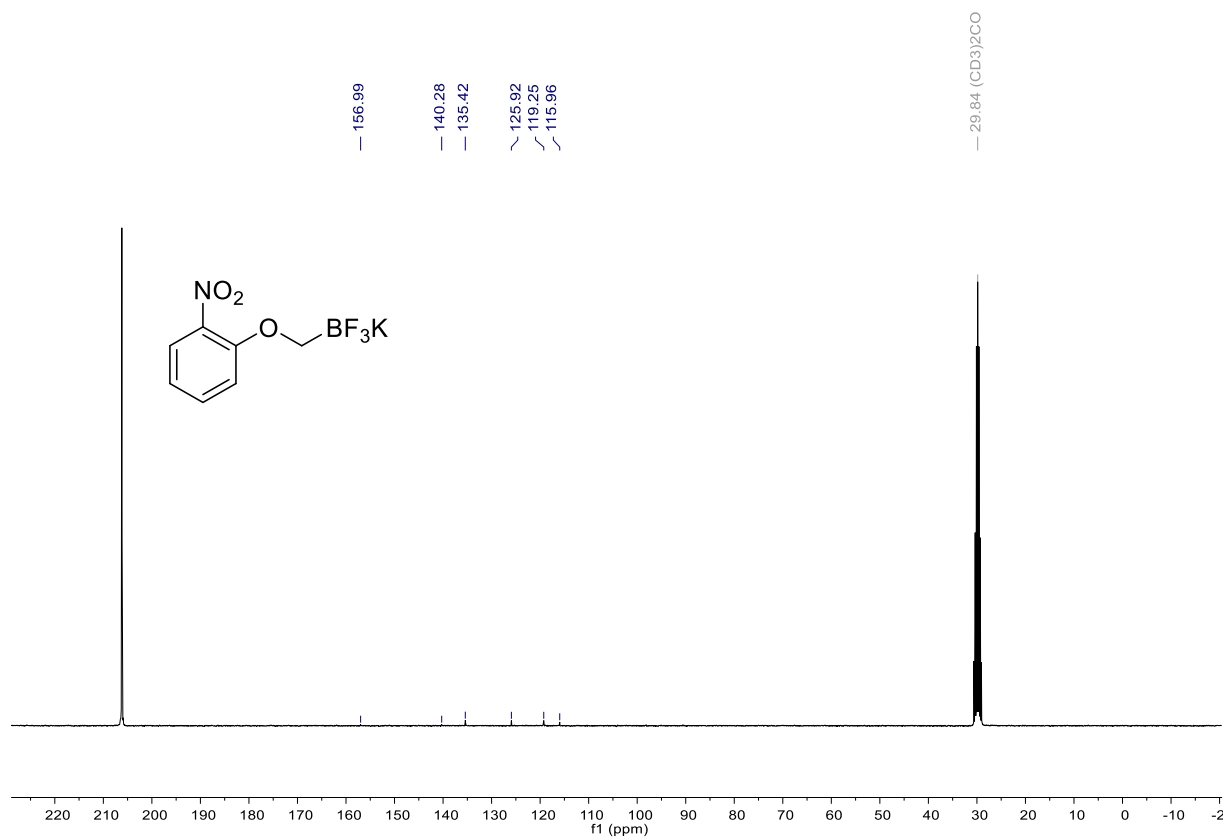
^1H NMR



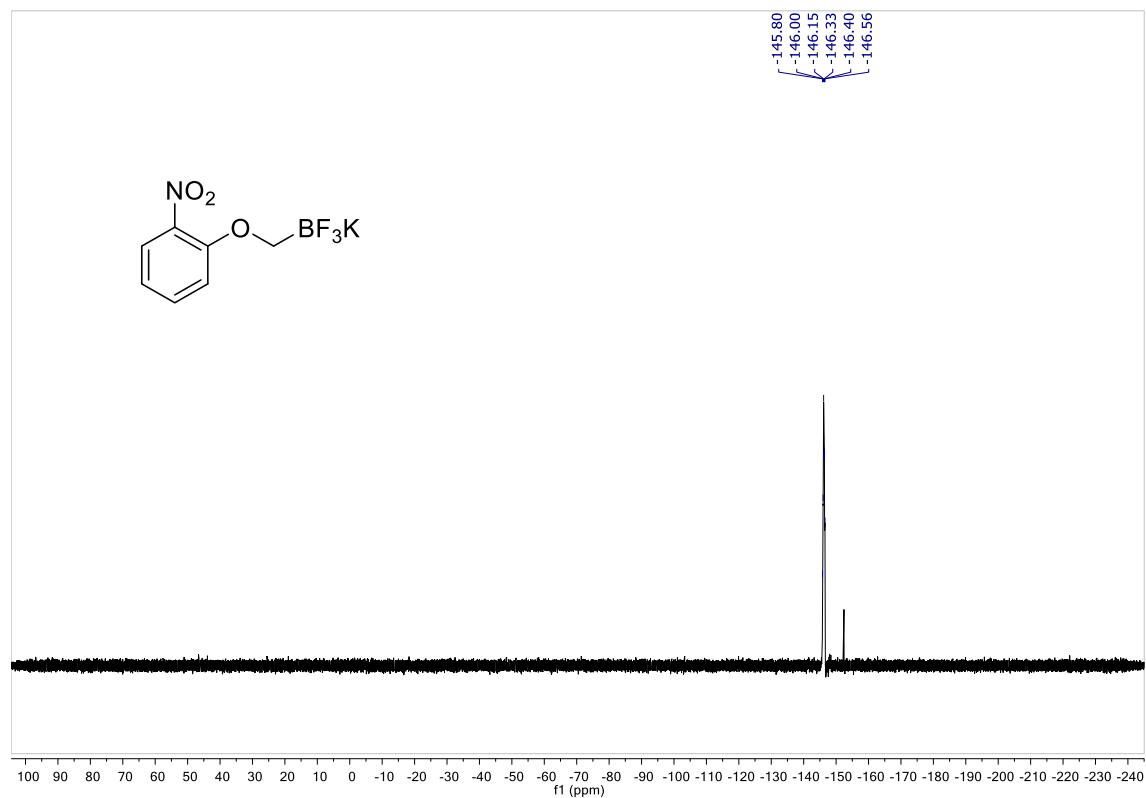
$^1\text{H}[^{11}\text{B}]$ NMR



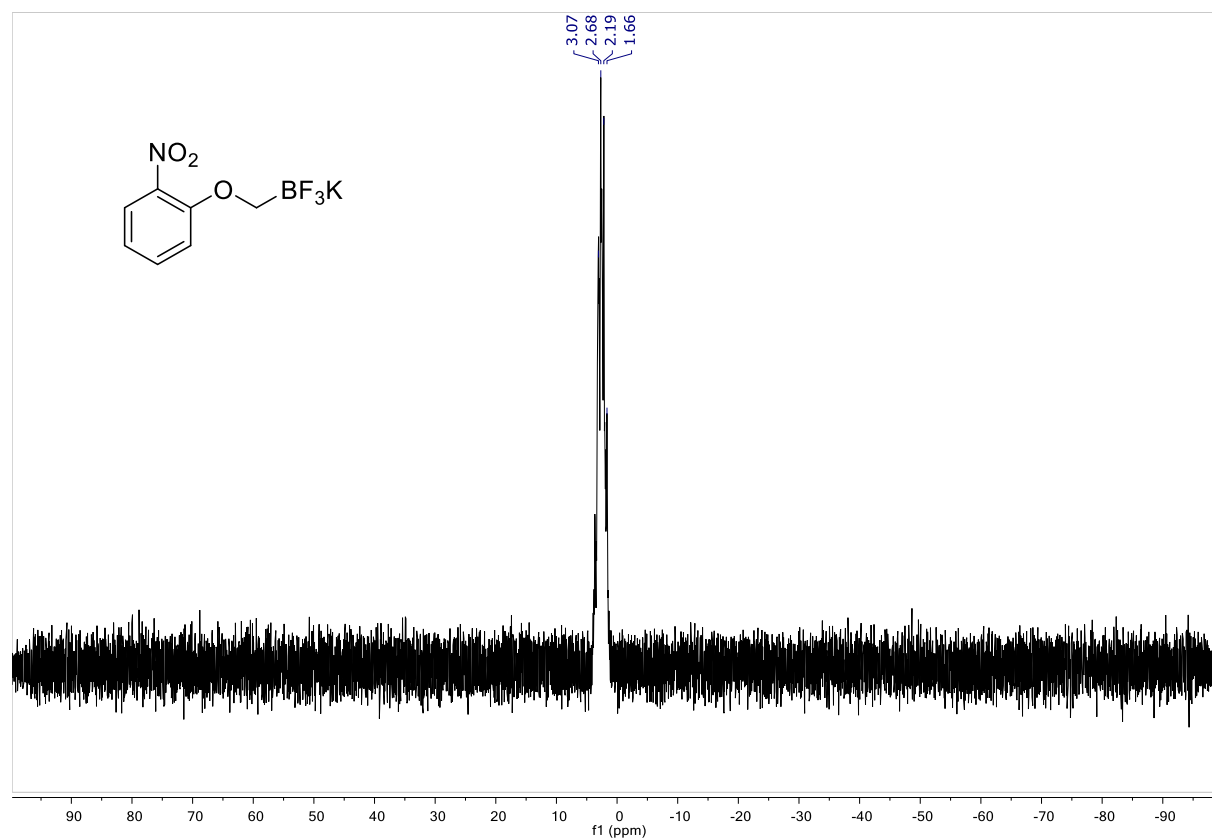
¹³C NMR



¹⁹F NMR

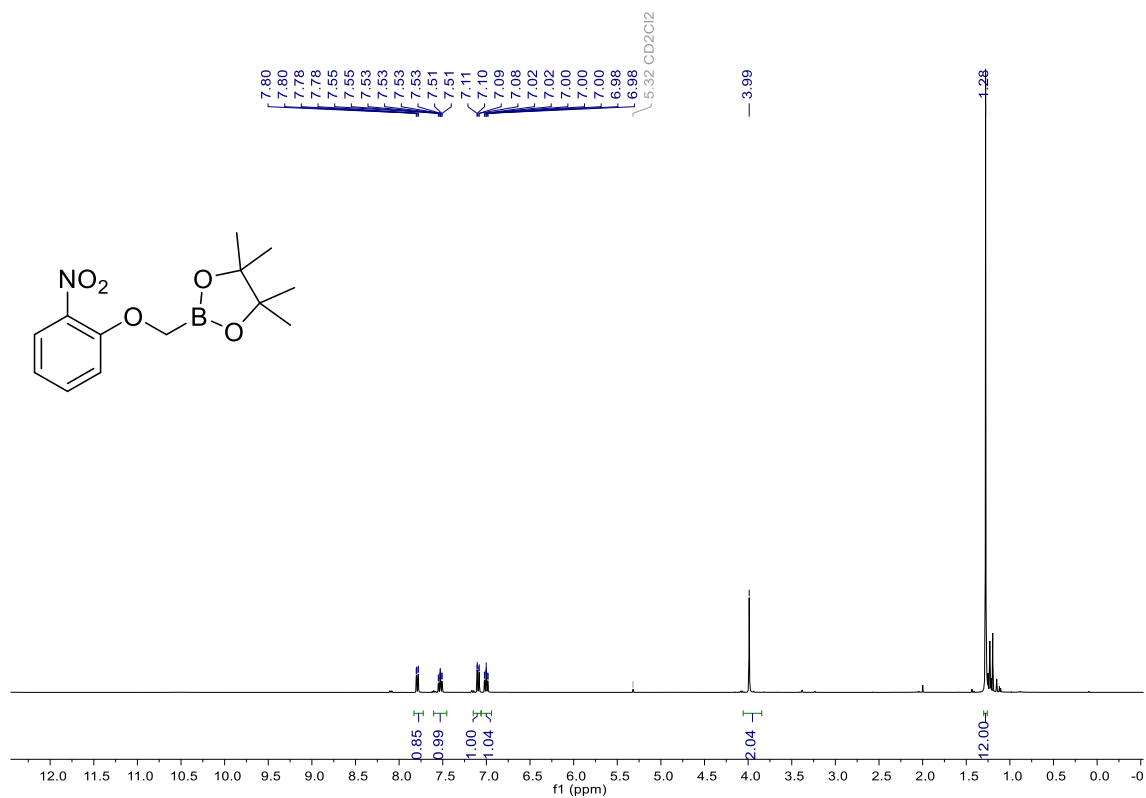


^{11}B NMR

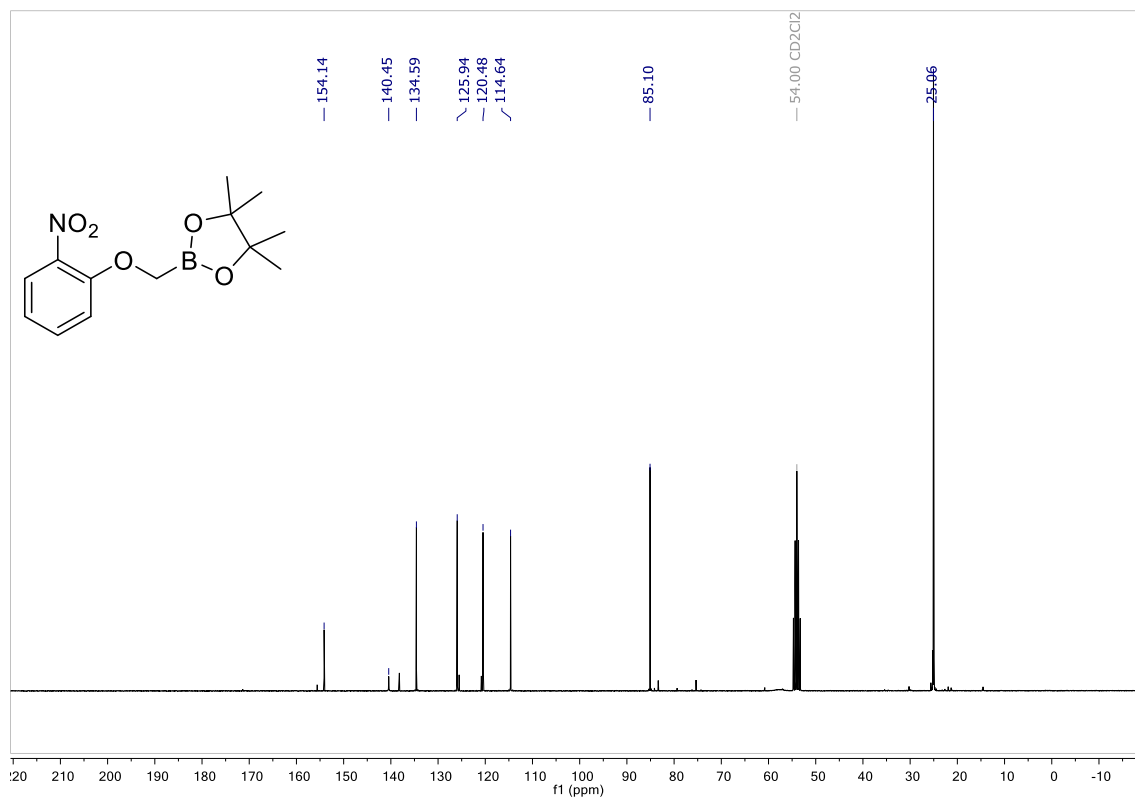


4,4,5,5-tetramethyl-2-((2-nitrophenoxy)methyl)-1,3,2-dioxaborolane (**4.44**)

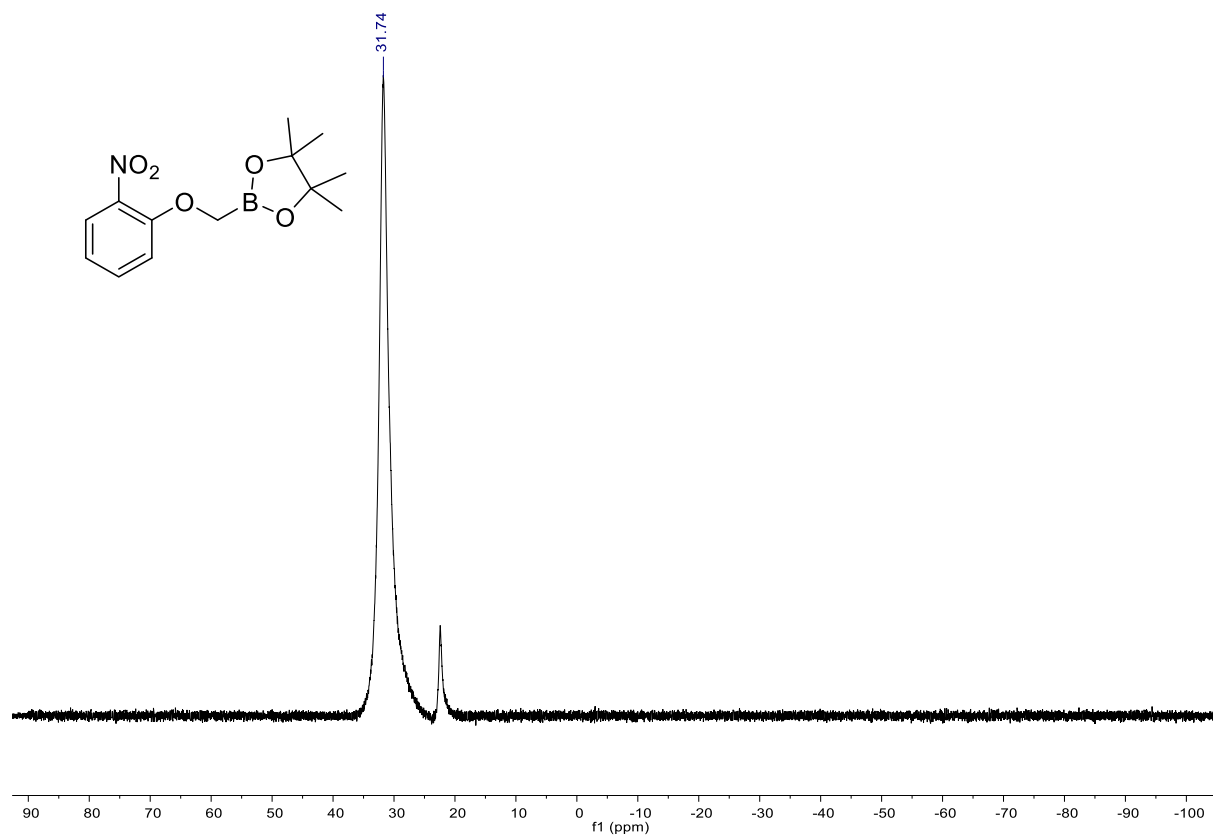
¹H NMR



¹³C NMR

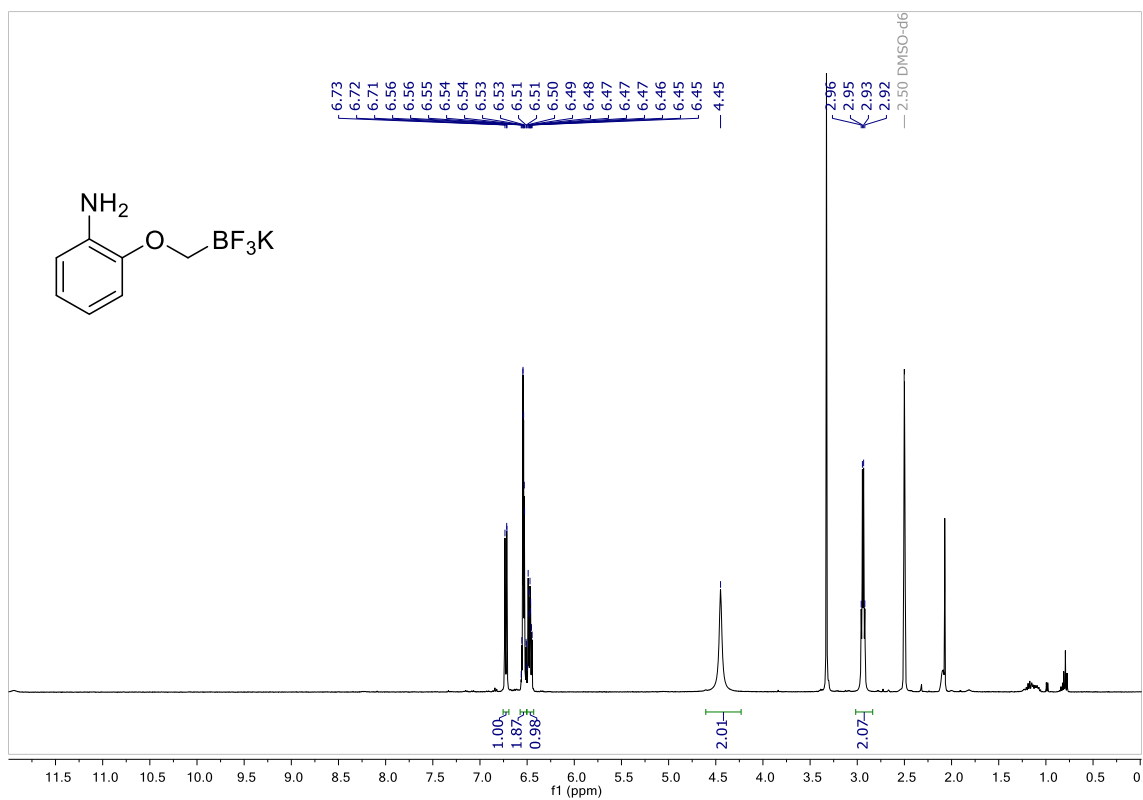


^{11}B NMR

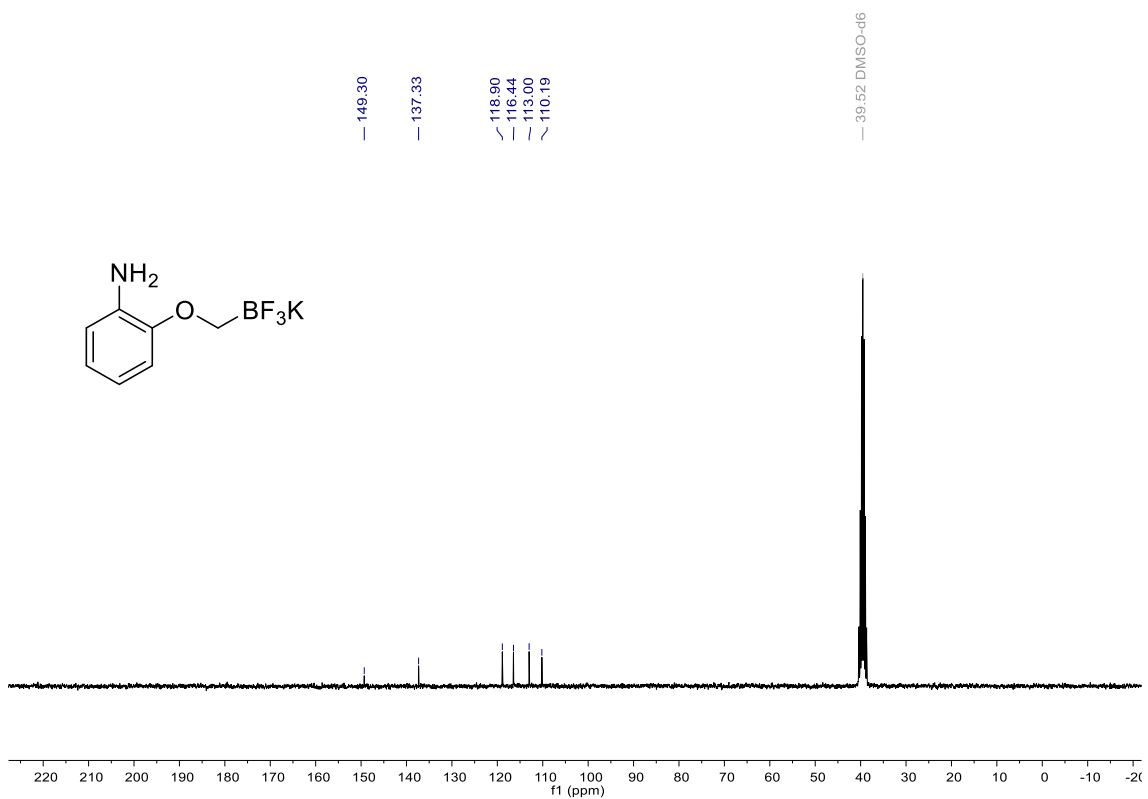


(2-aminophenoxy)methyltrifluoroborate (4.39)

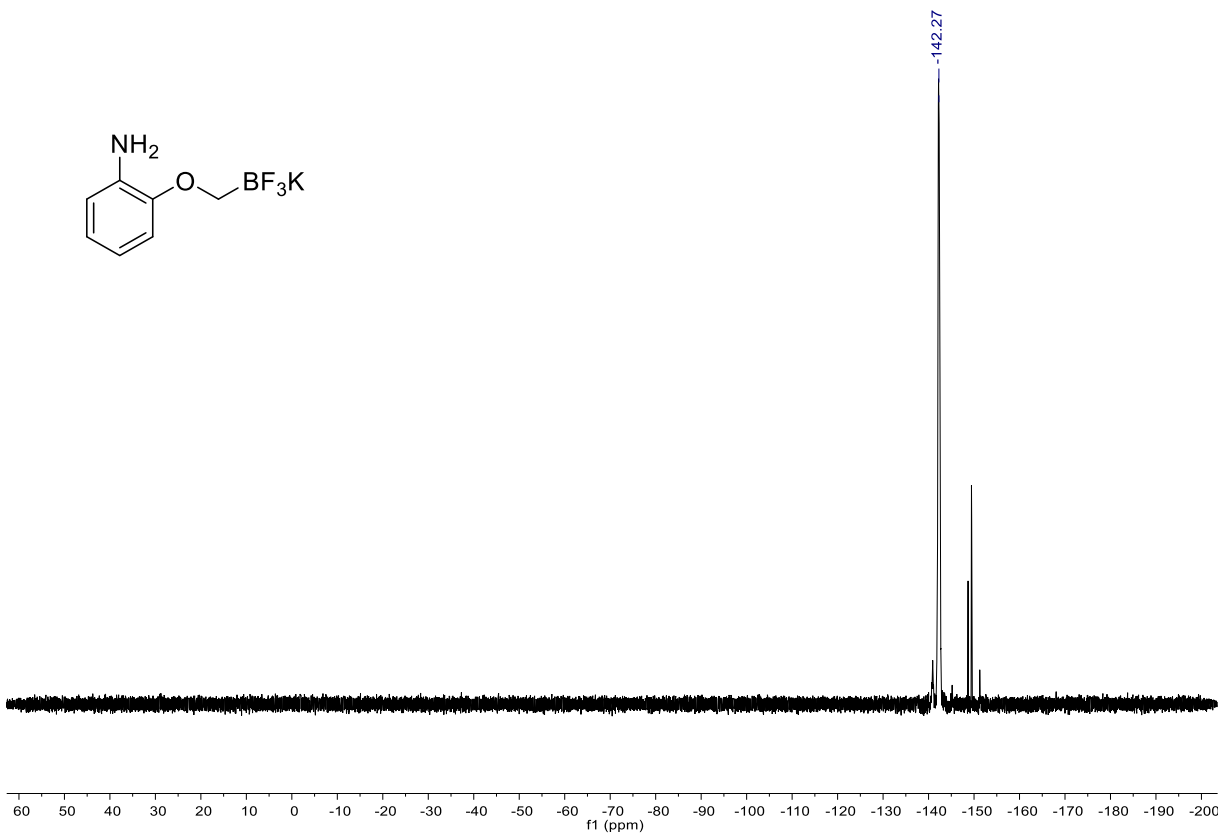
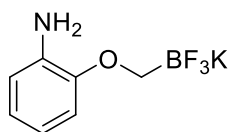
^1H NMR



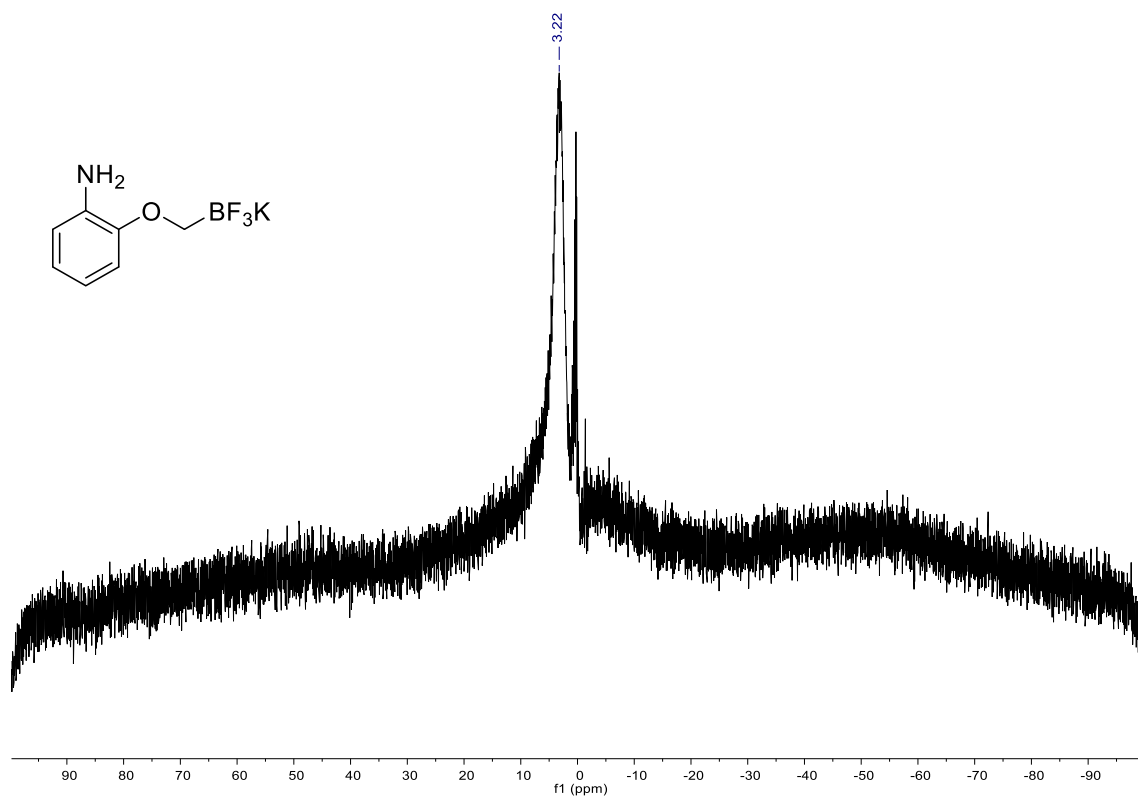
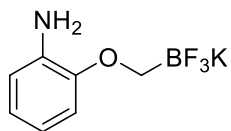
^{13}C NMR



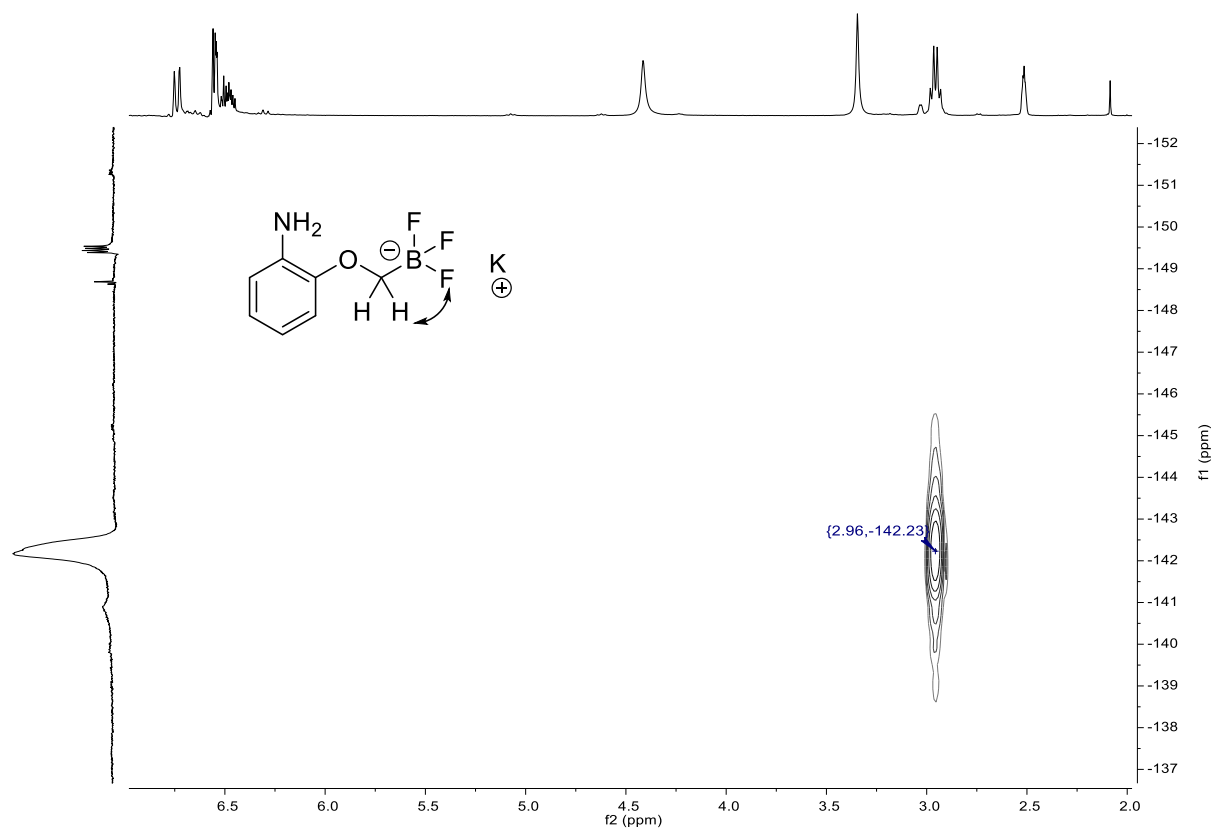
¹⁹F NMR



¹¹B NMR

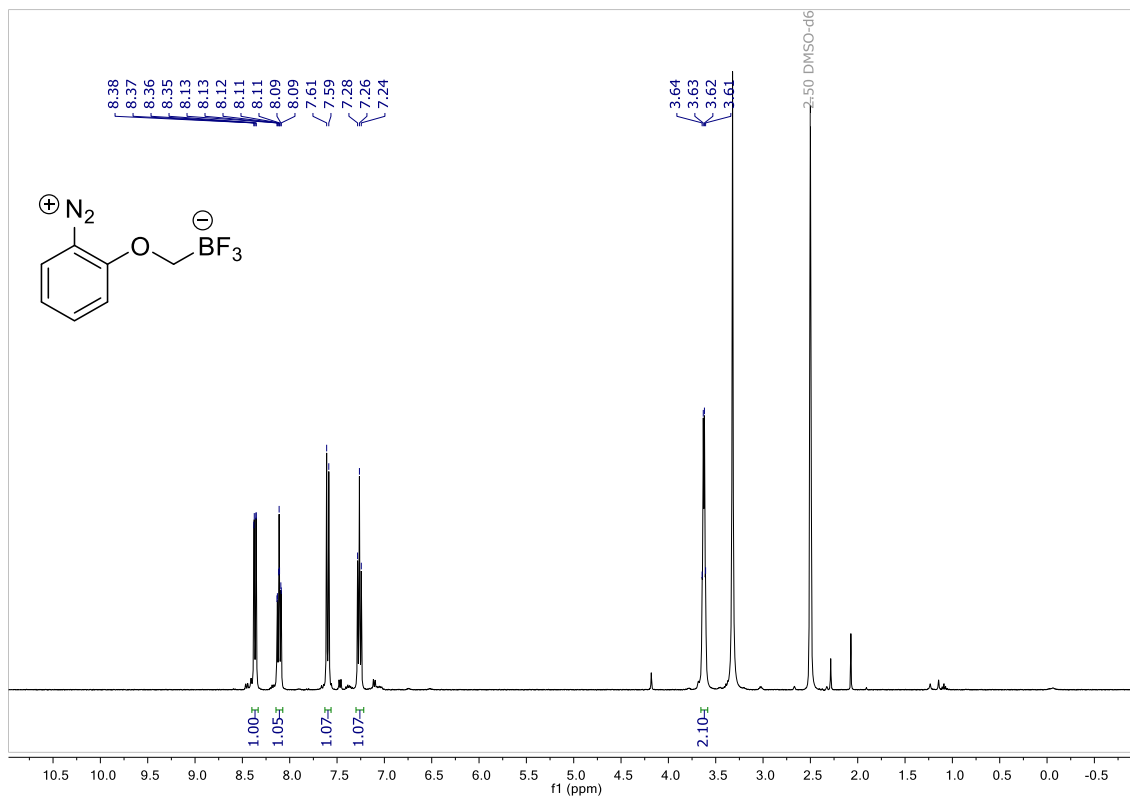


^1H - ^{19}F HMBC NMR

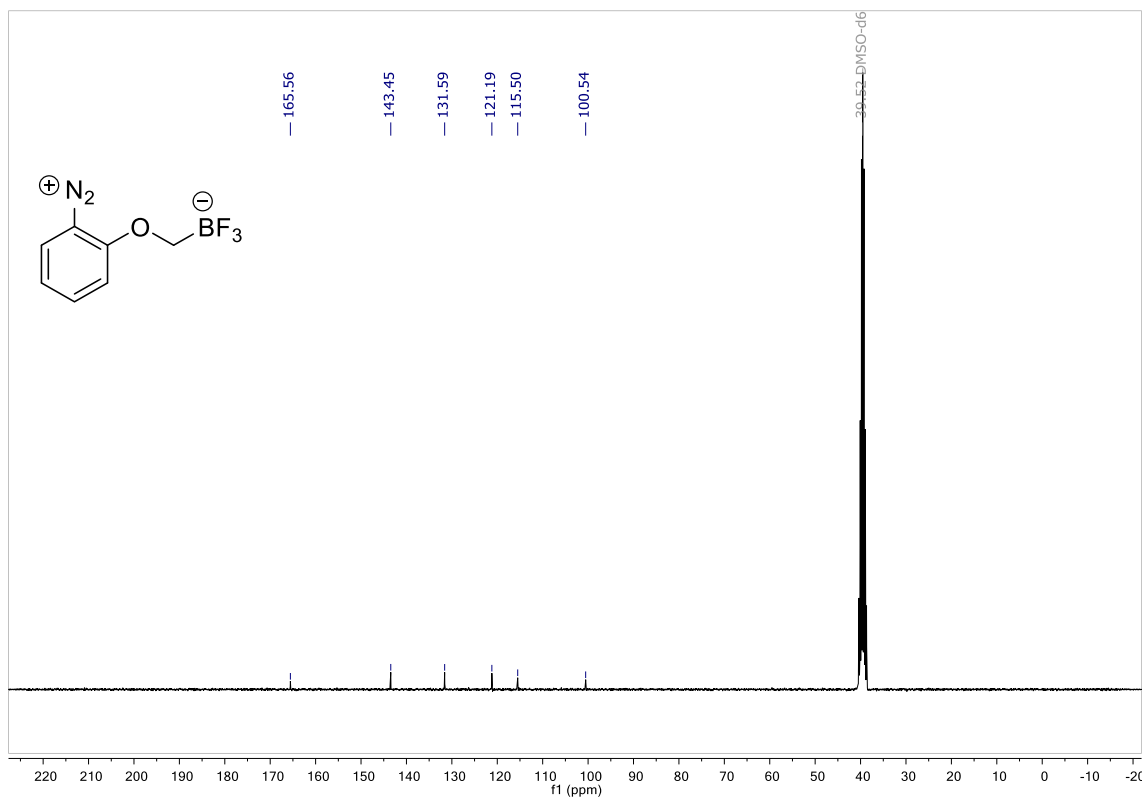


(2-diazoniophenoxy)methyltrifluoroborate (4.21)

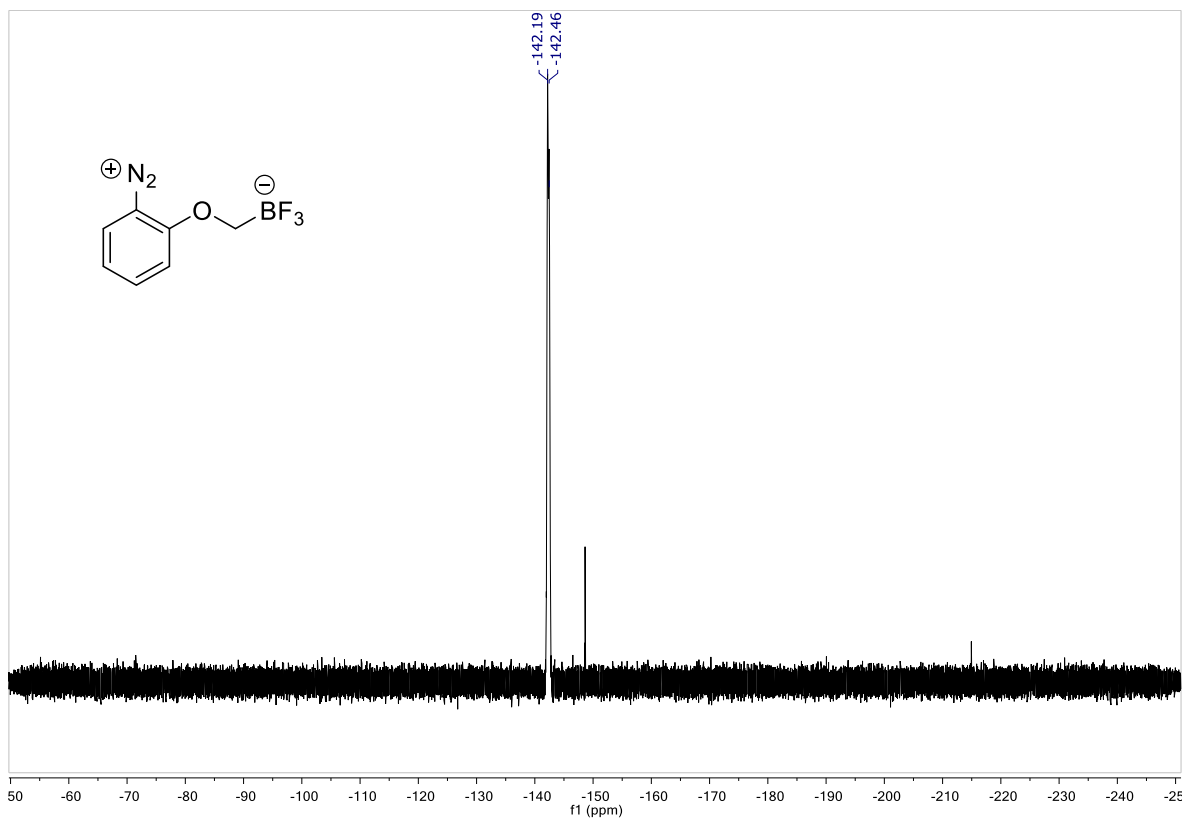
^1H NMR



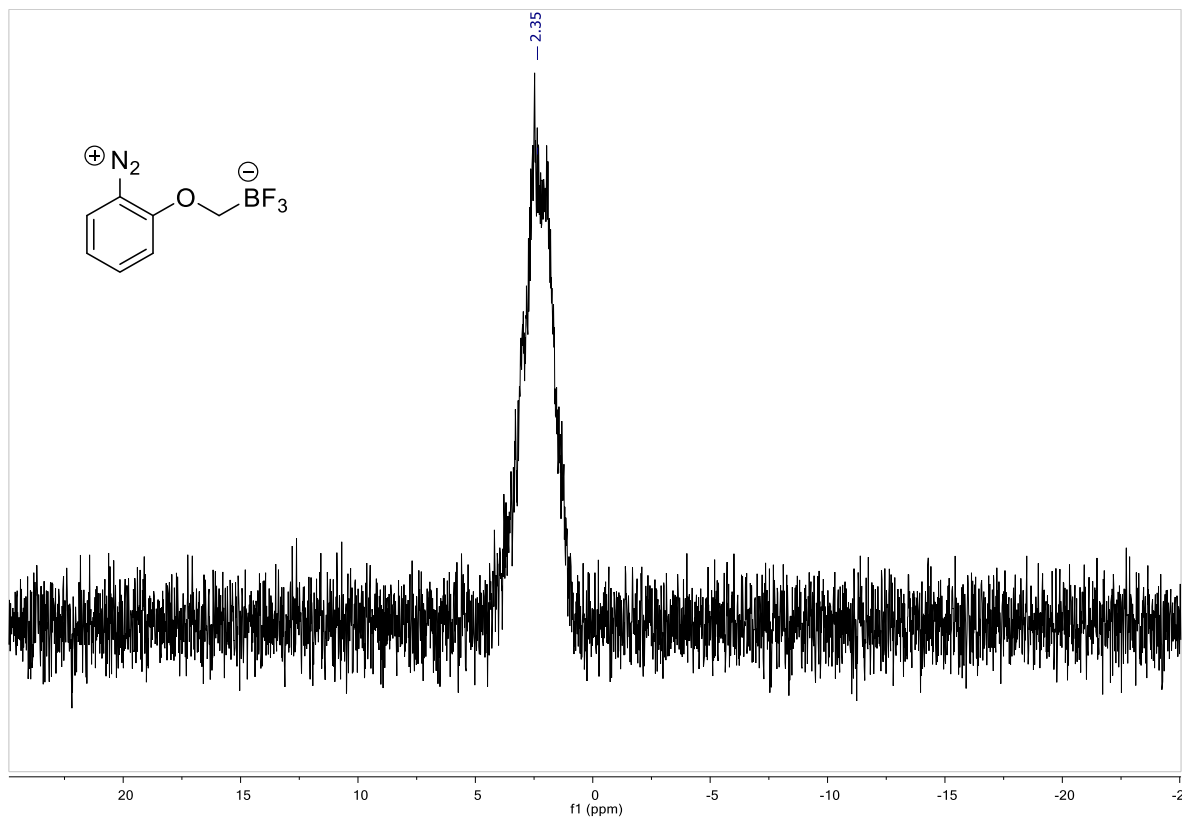
^{13}C NMR



^{19}F NMR

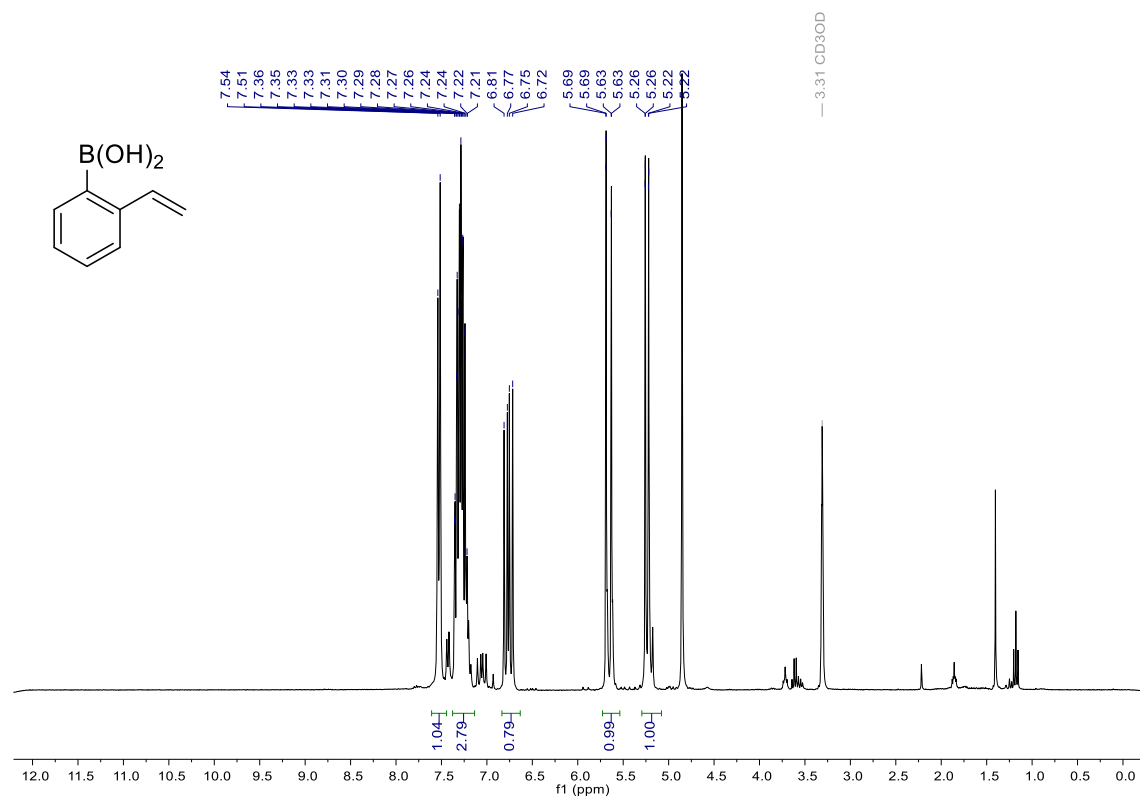


^{11}B NMR

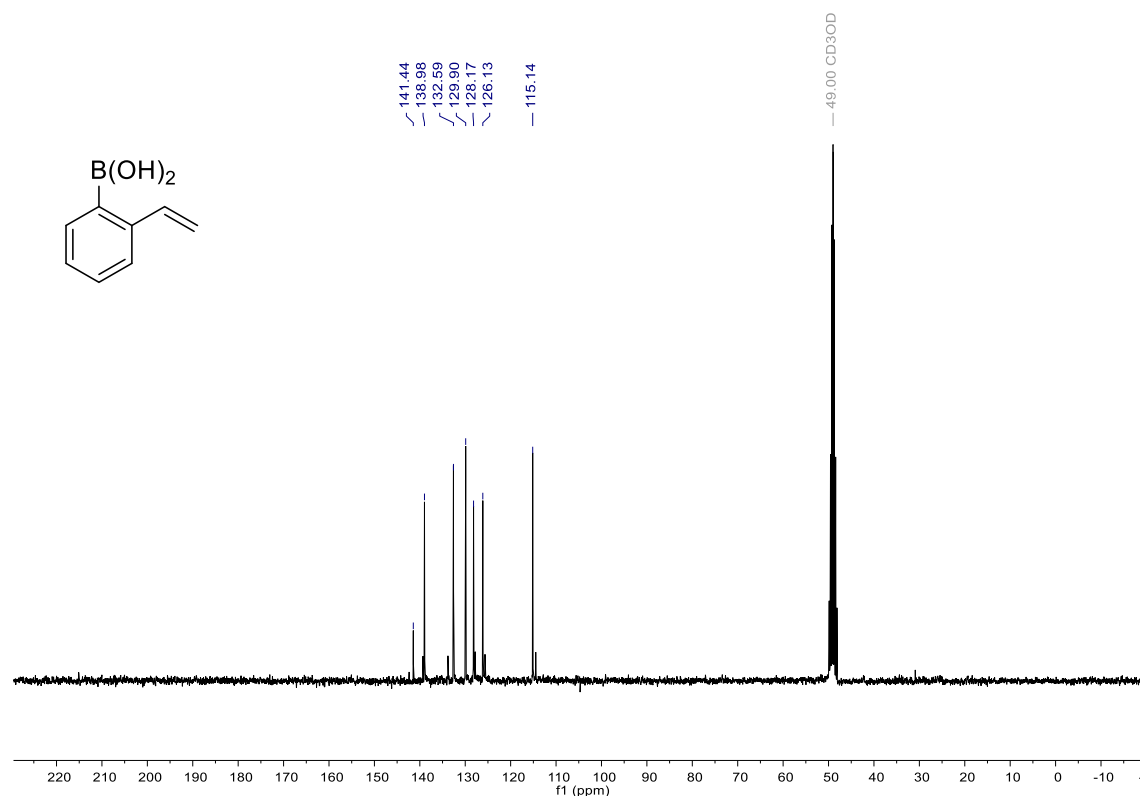


2-vinylphenylboronic acid (**4.40**)

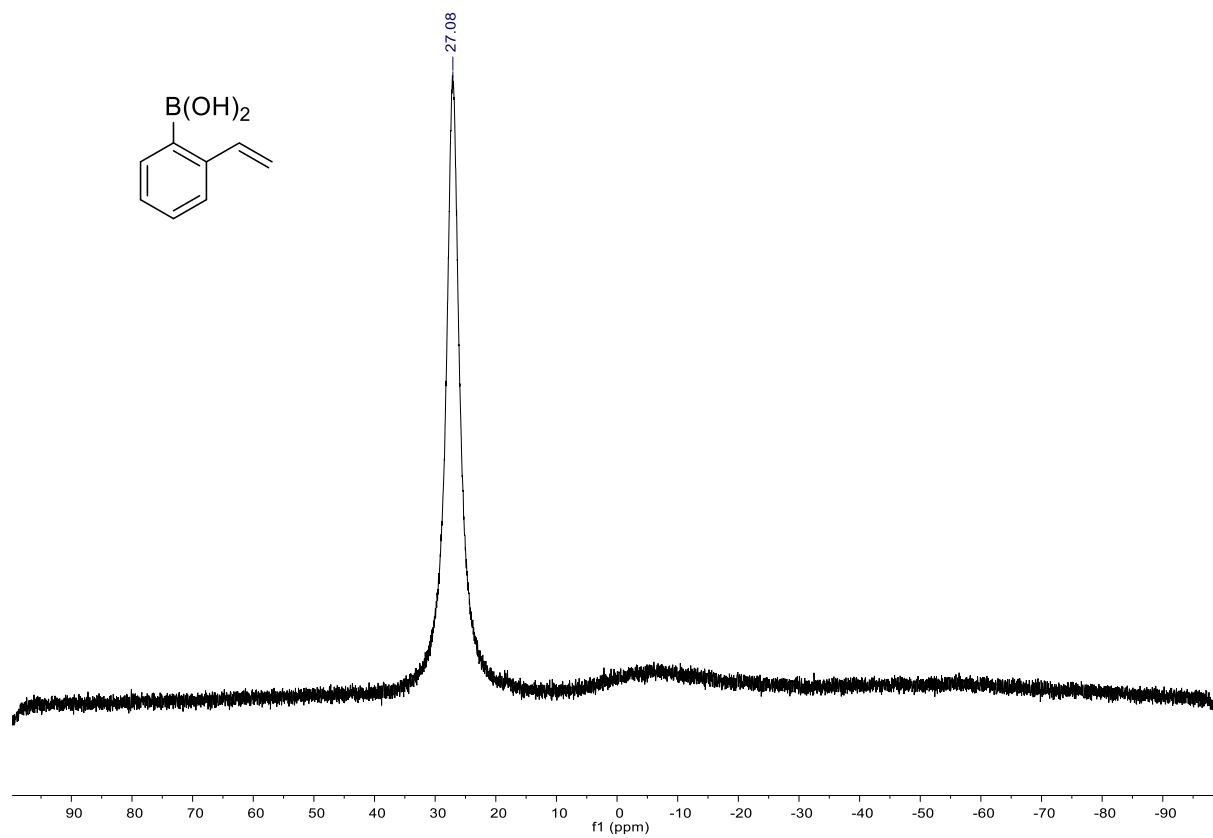
¹H NMR



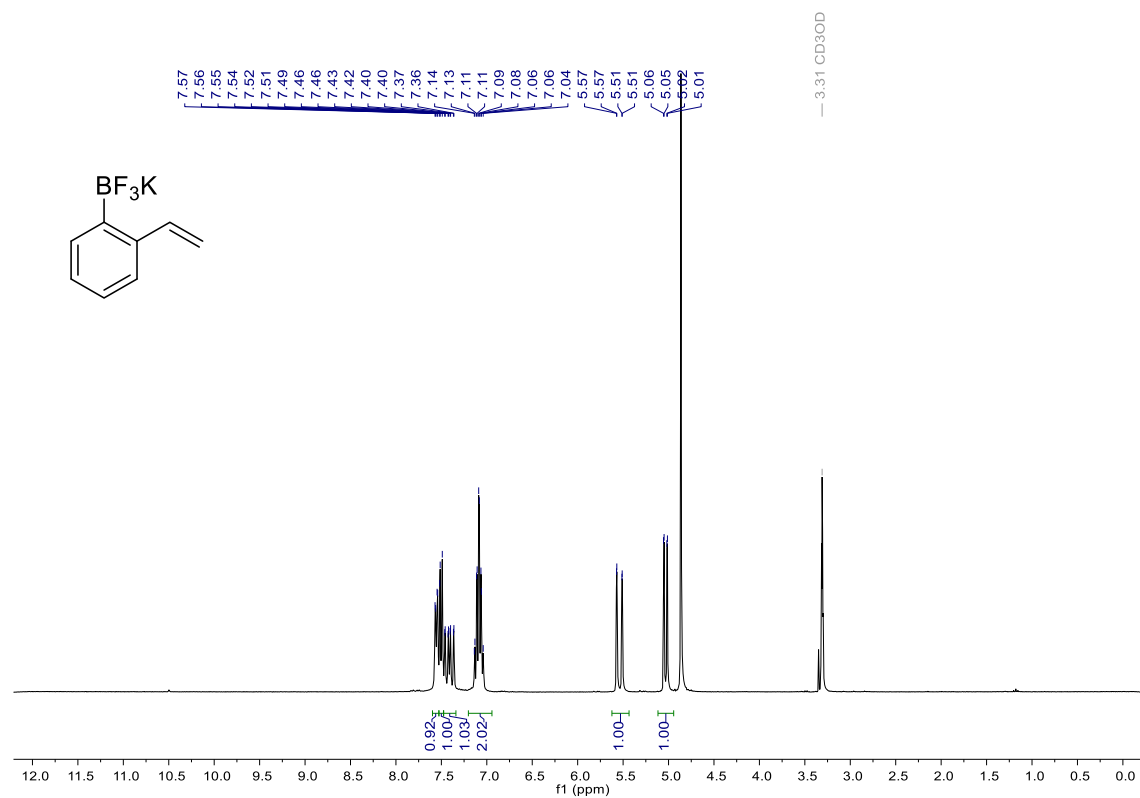
¹³C NMR



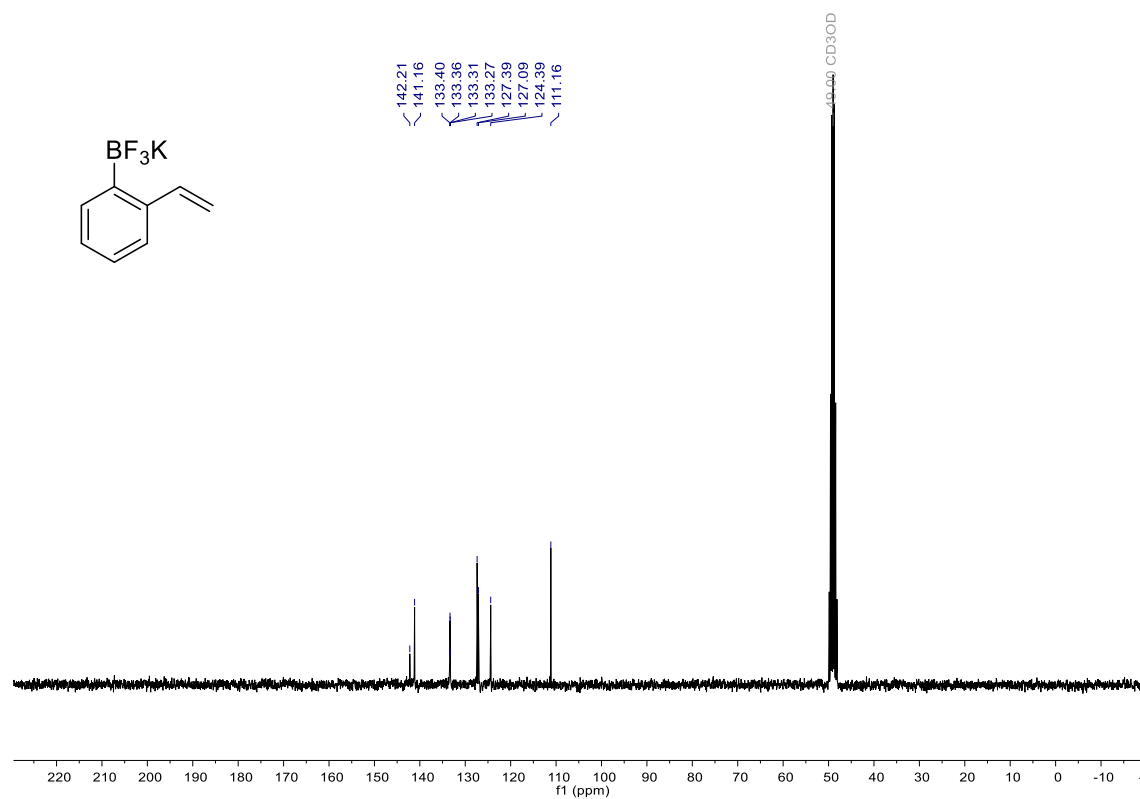
^{11}B NMR



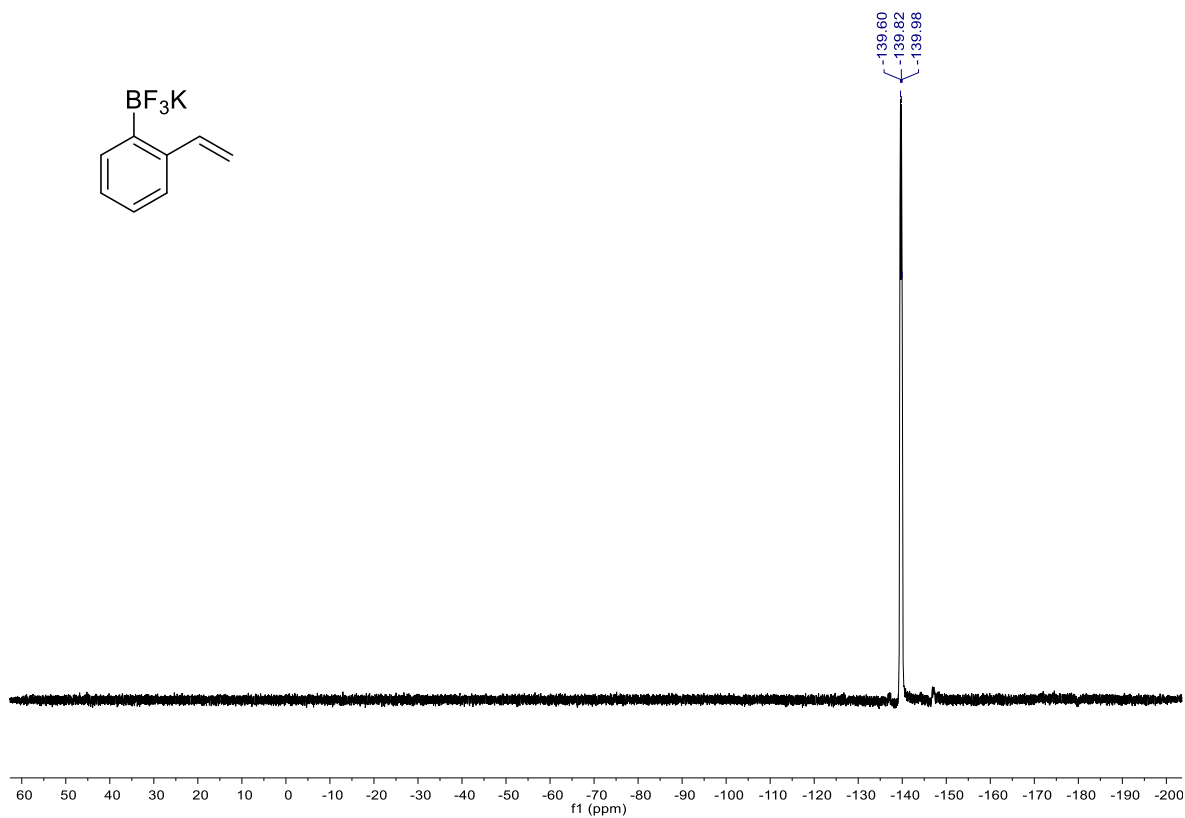
Potassium 2-vinylphenyltrifluoroborate (**4.22**)
¹H NMR



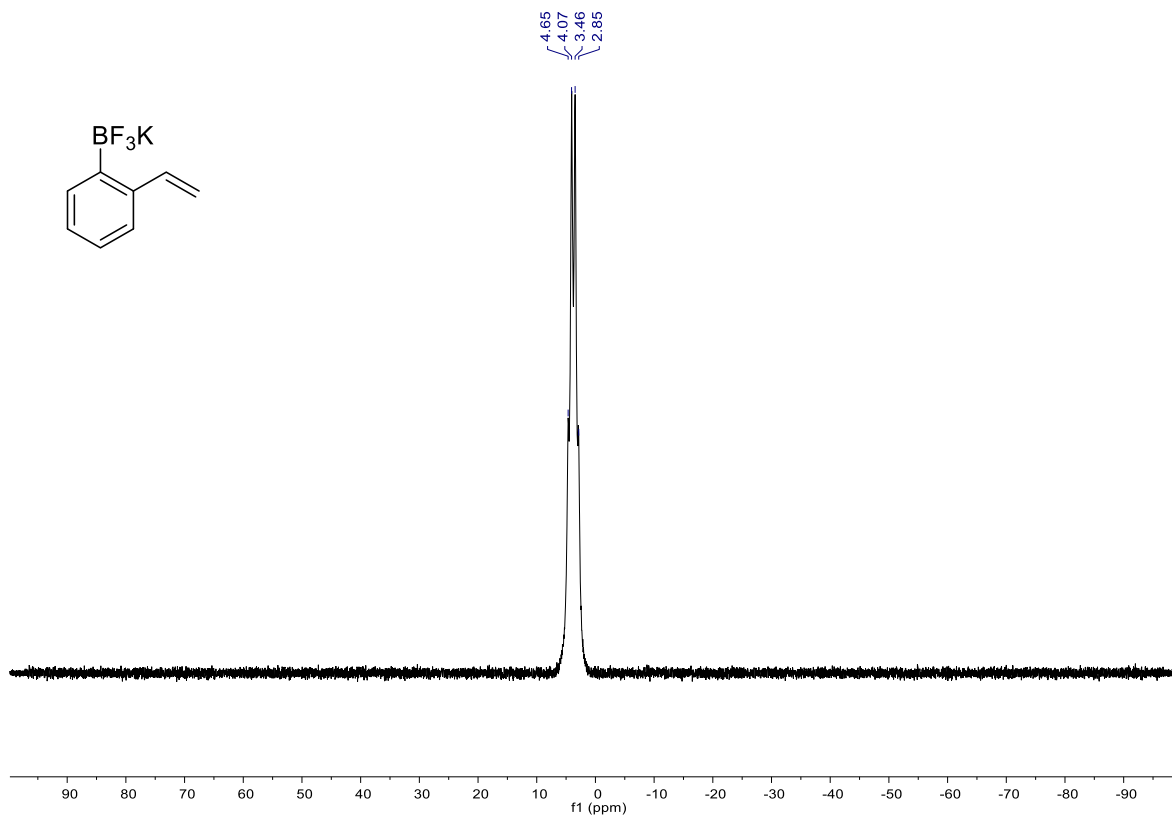
¹³C NMR



^{19}F NMR

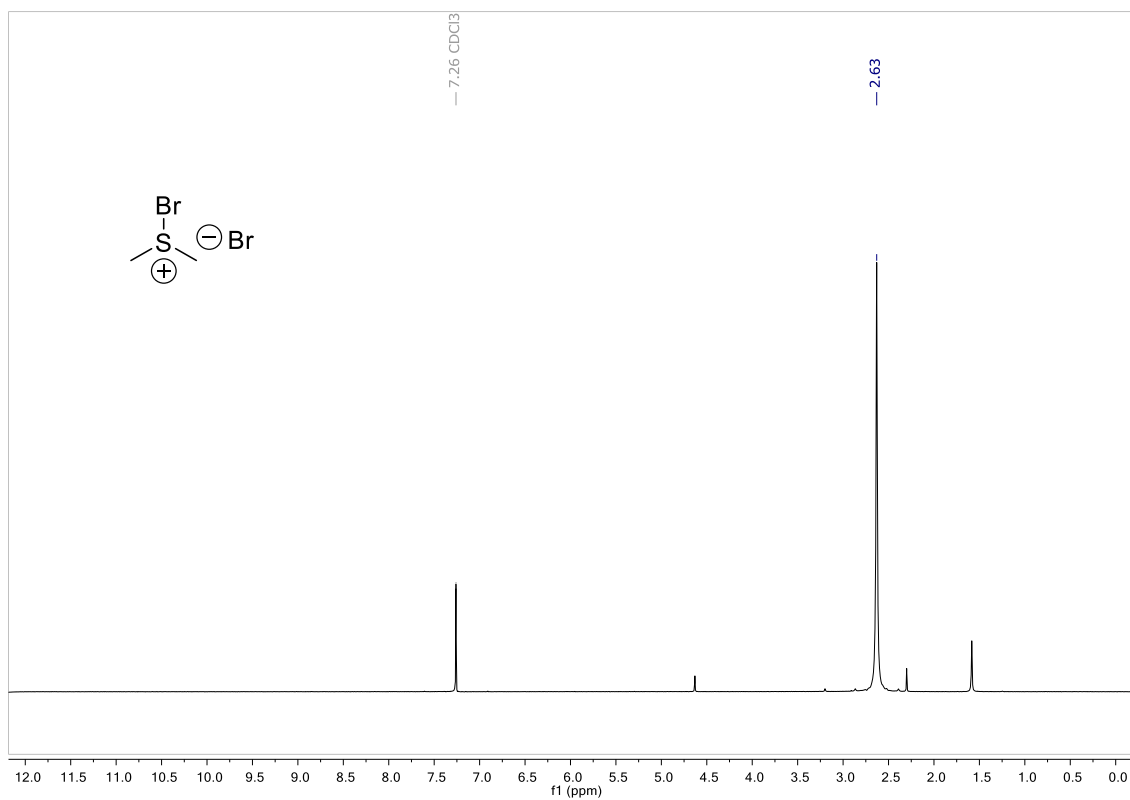


^{11}B NMR

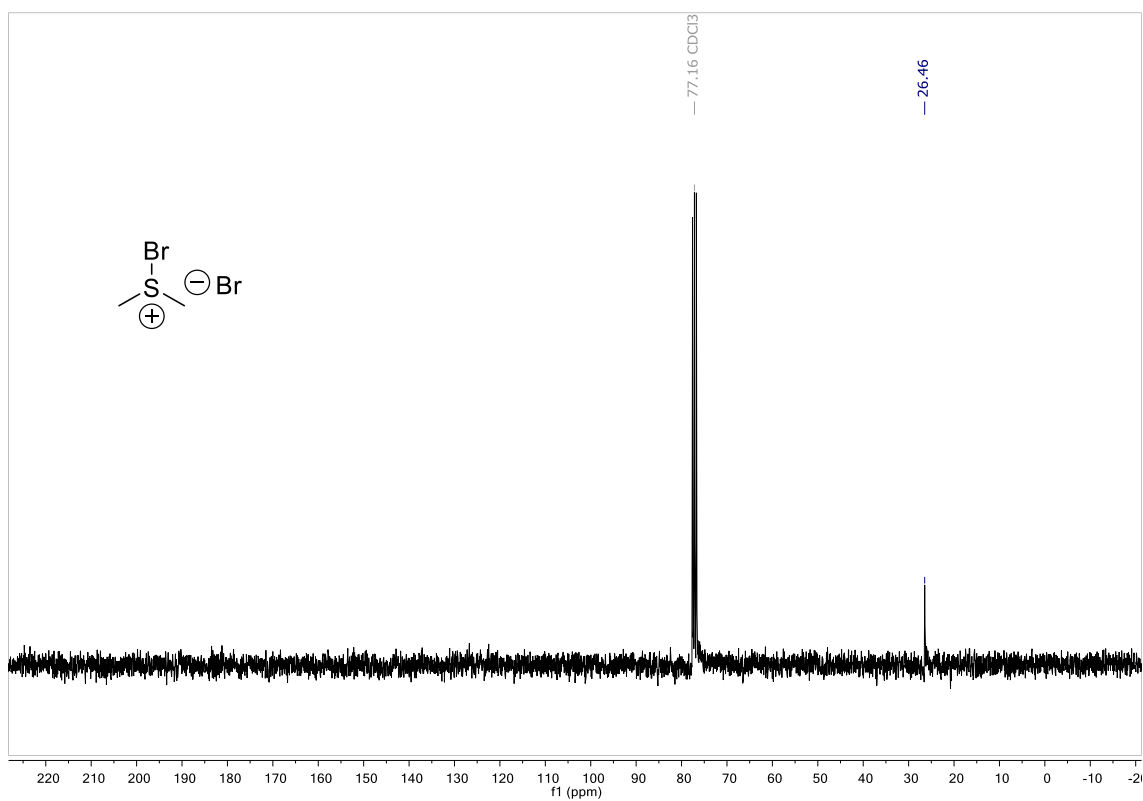


Bromodimethylsulfonium bromide (4.44)

^1H NMR

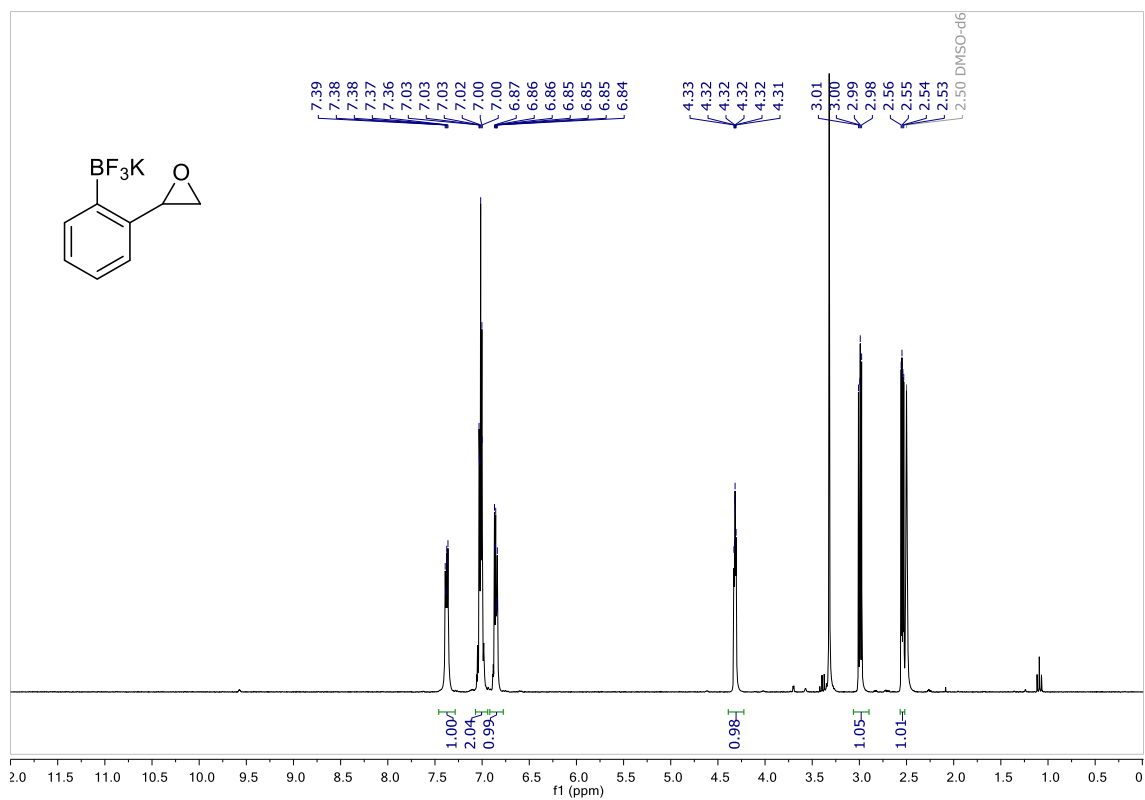


^{13}C NMR

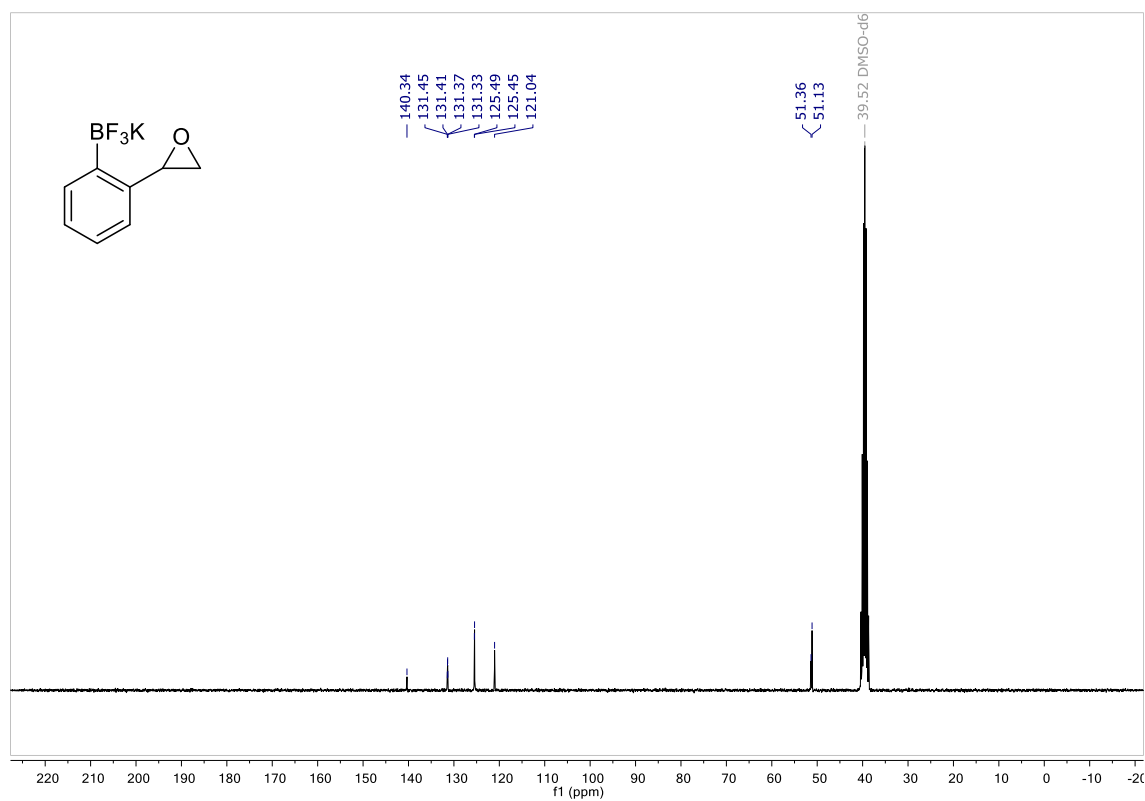


Potassium 2-oxiranylphenyltrifluoroborates (4.23)

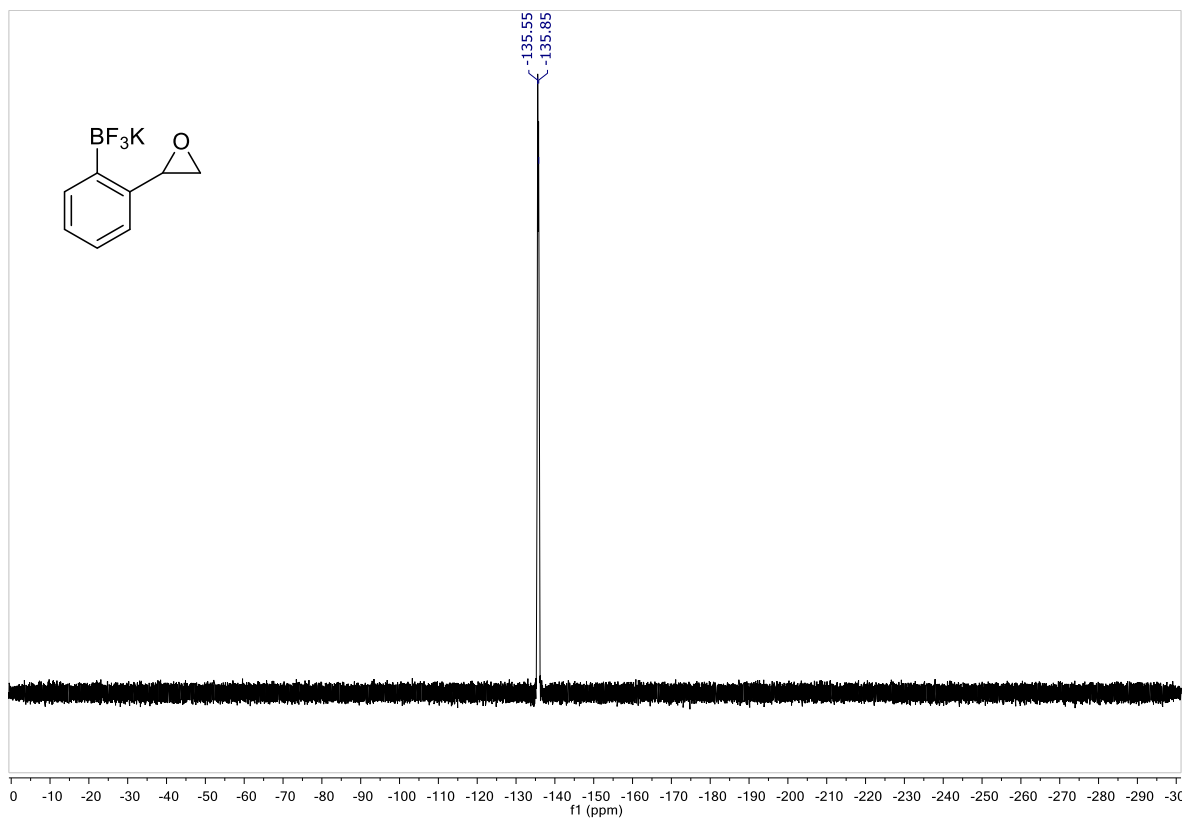
^1H NMR



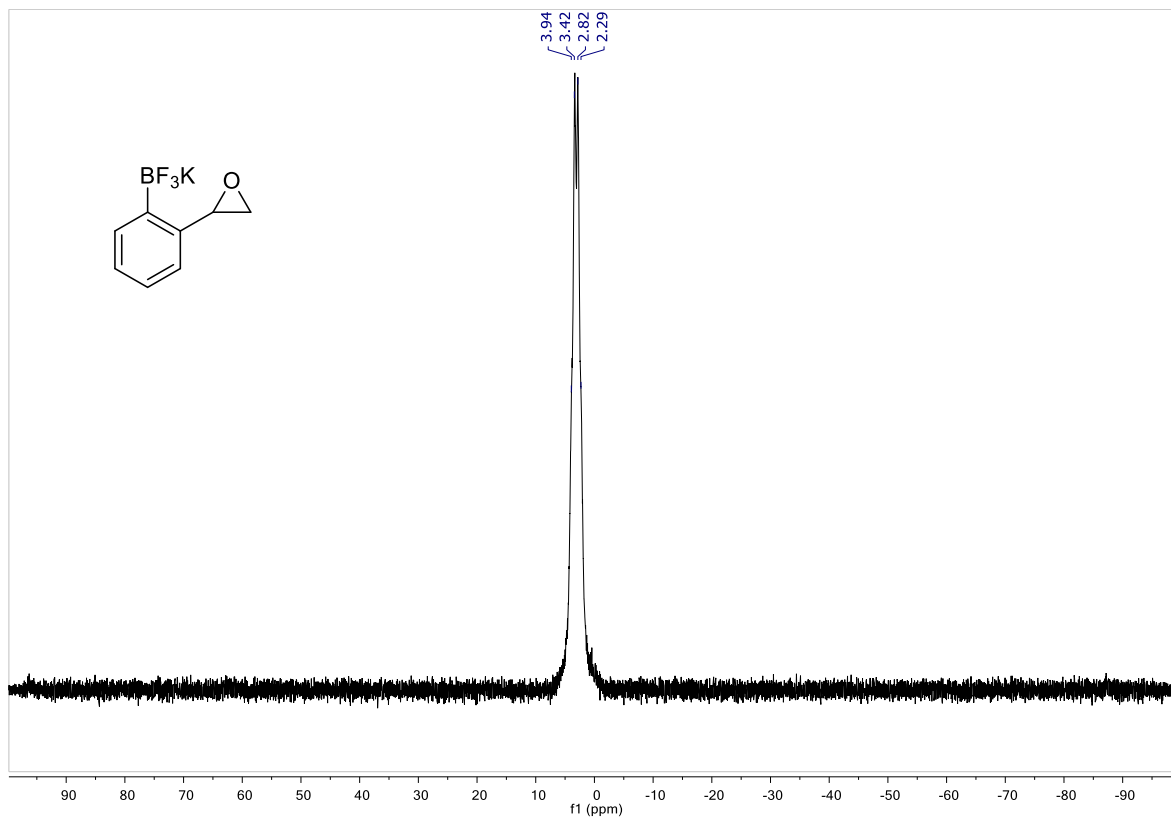
^{13}C NMR



^{19}F NMR



^{11}B NMR

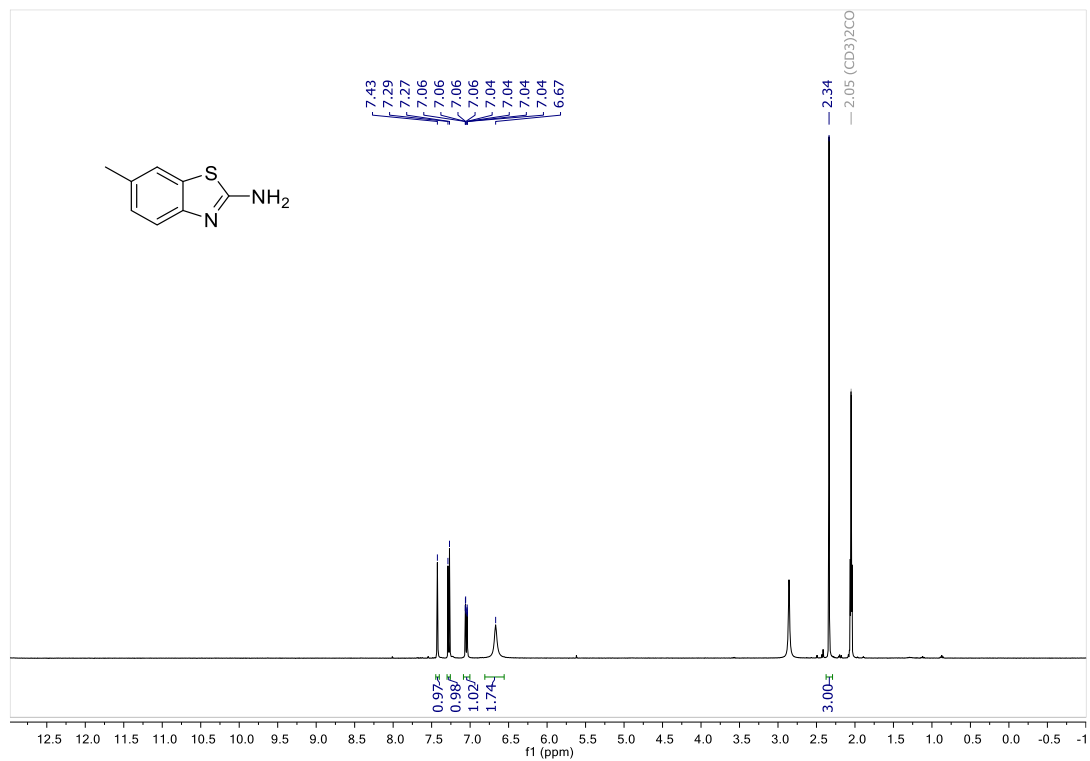


Annex D: Chapter 5

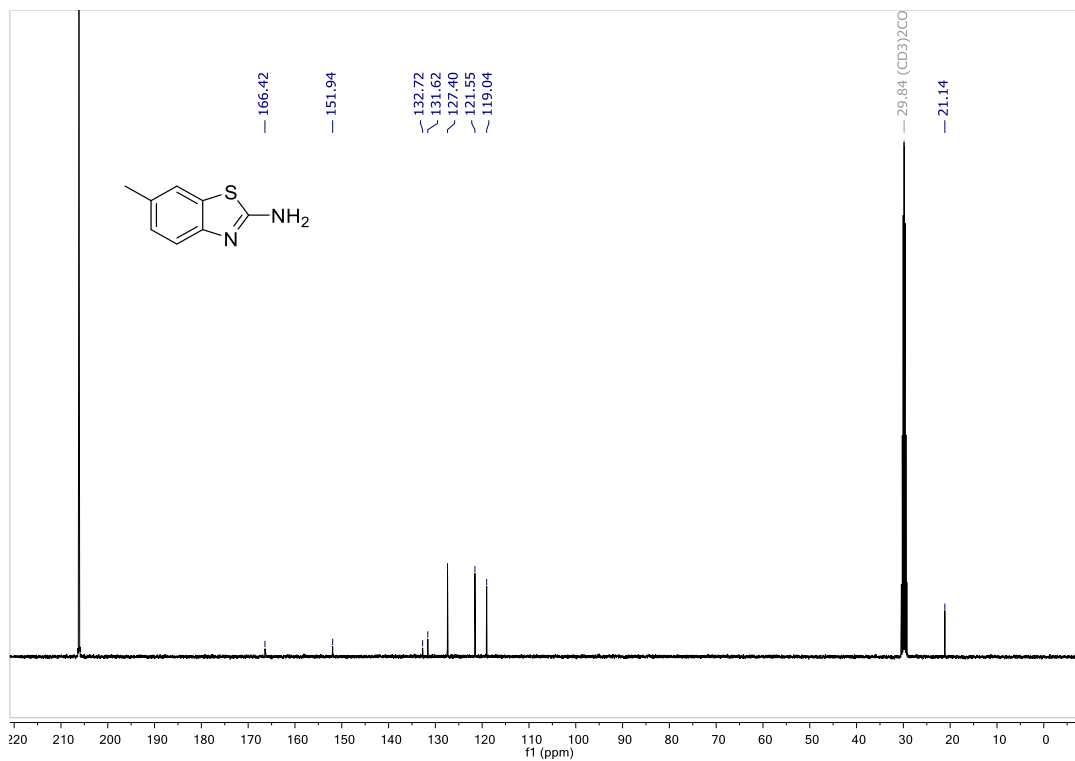
NMR Spectra of selected compounds

2-amino-6-methylbenzothiazole (5.1)

^1H NMR

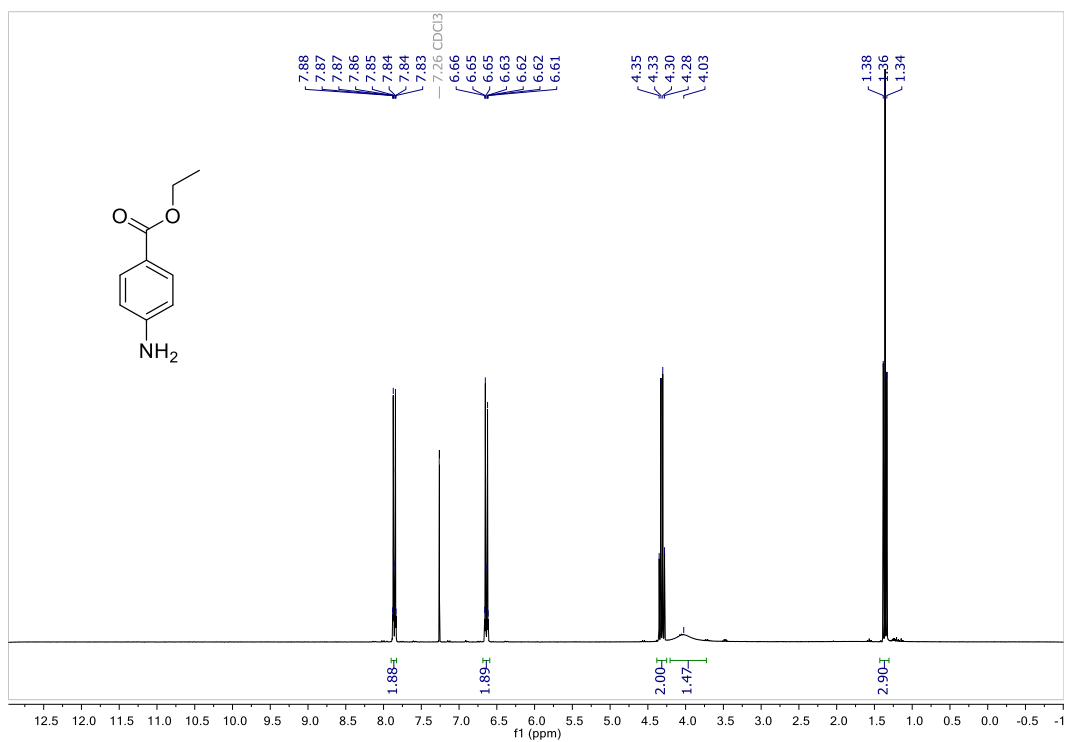


^{13}C NMR

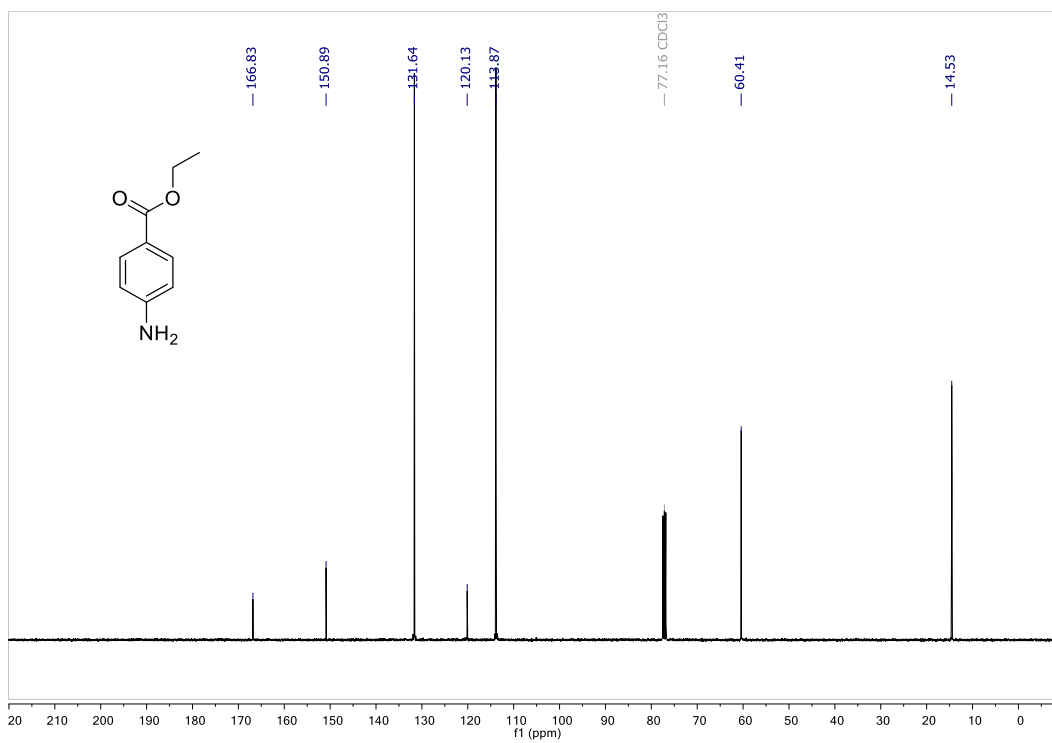


Ethyl 4-aminobenzoate

¹H NMR

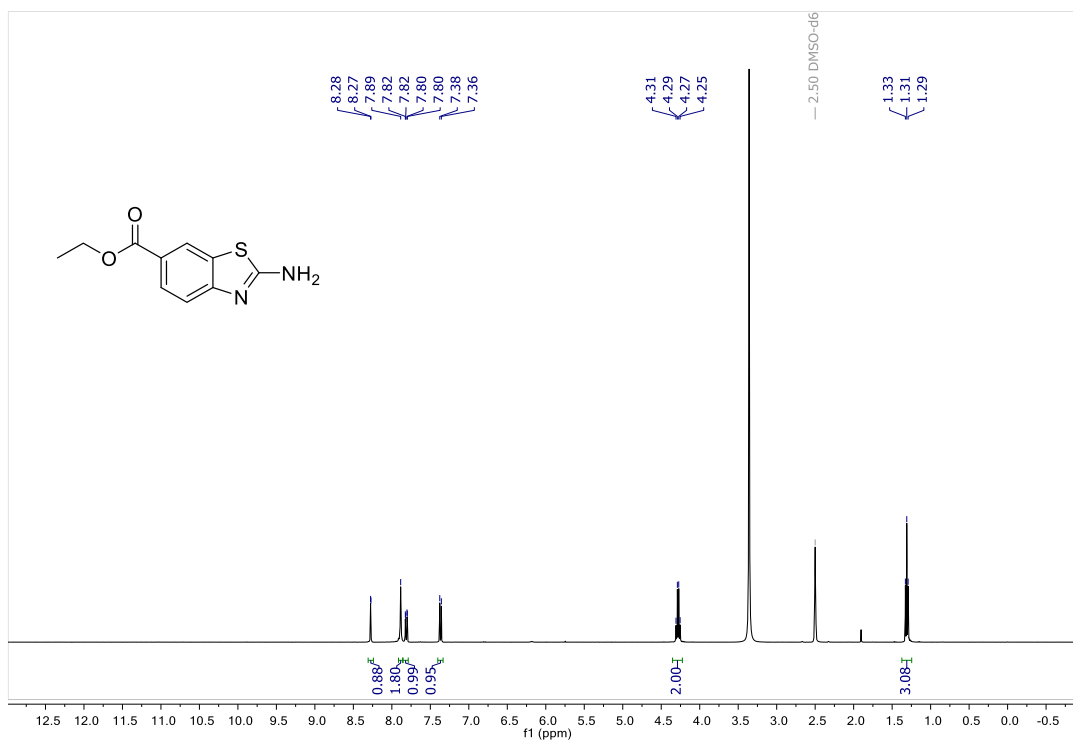


¹³C NMR

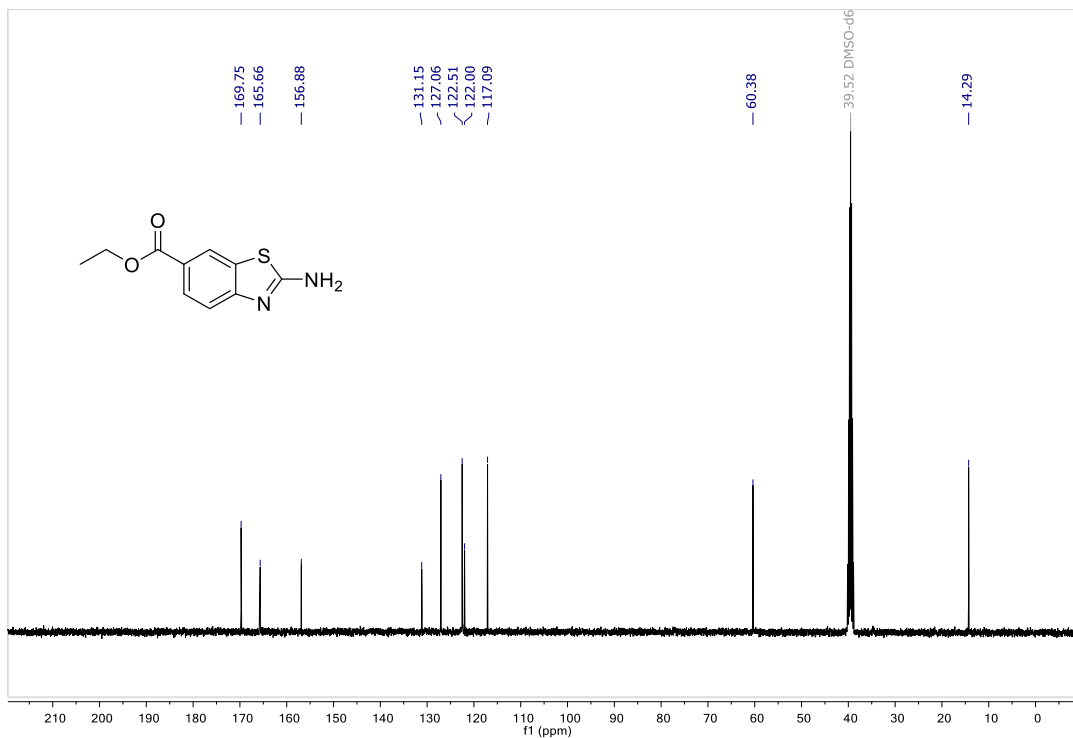


Ethyl 2-aminobenzothiazole-6-carboxylate (5.2)

¹H NMR

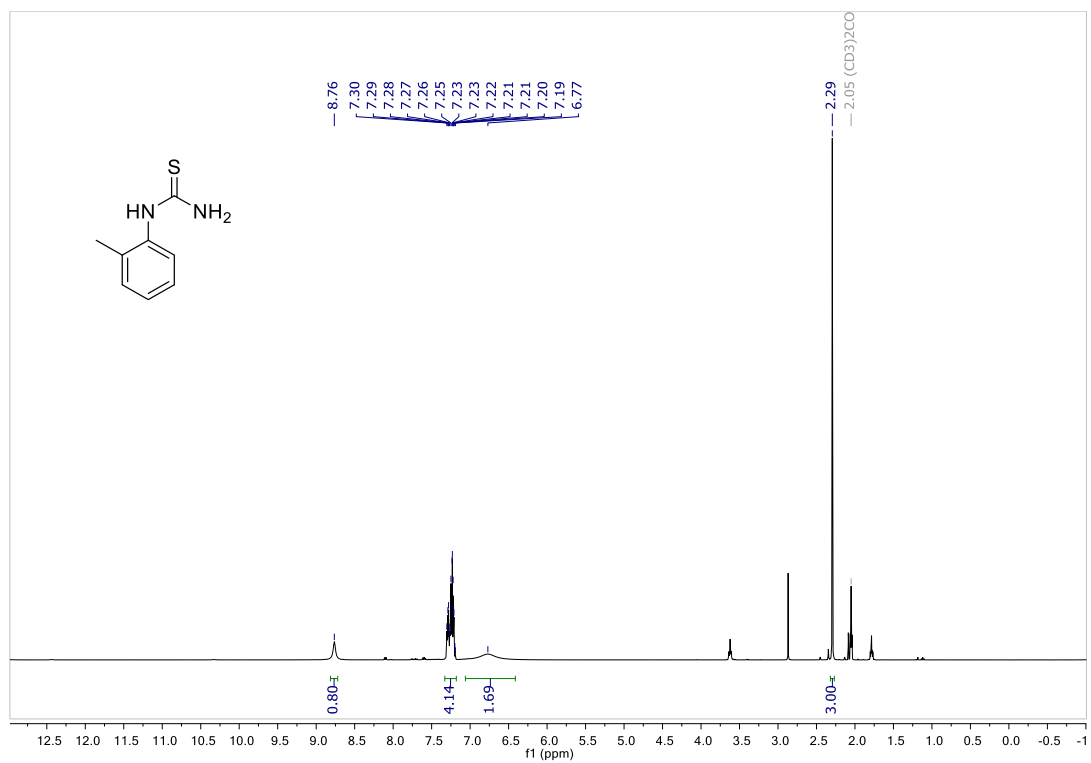


¹³C NMR

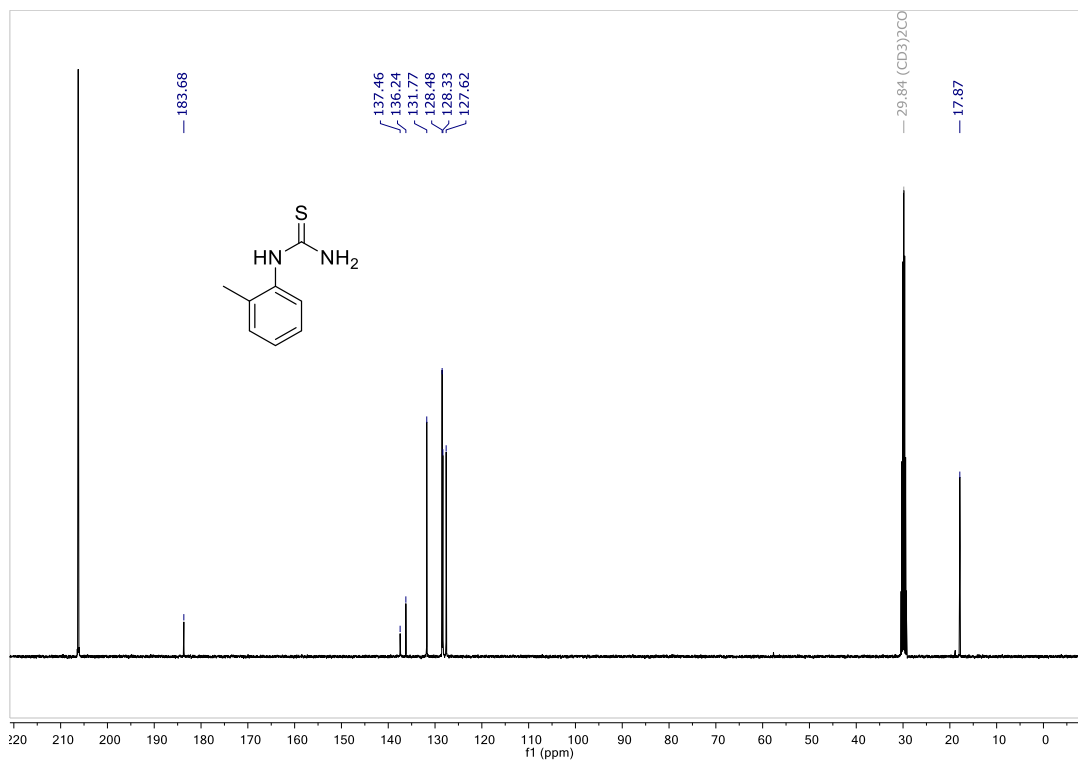


(o-tolyl)thiourea (5.3)

¹H NMR

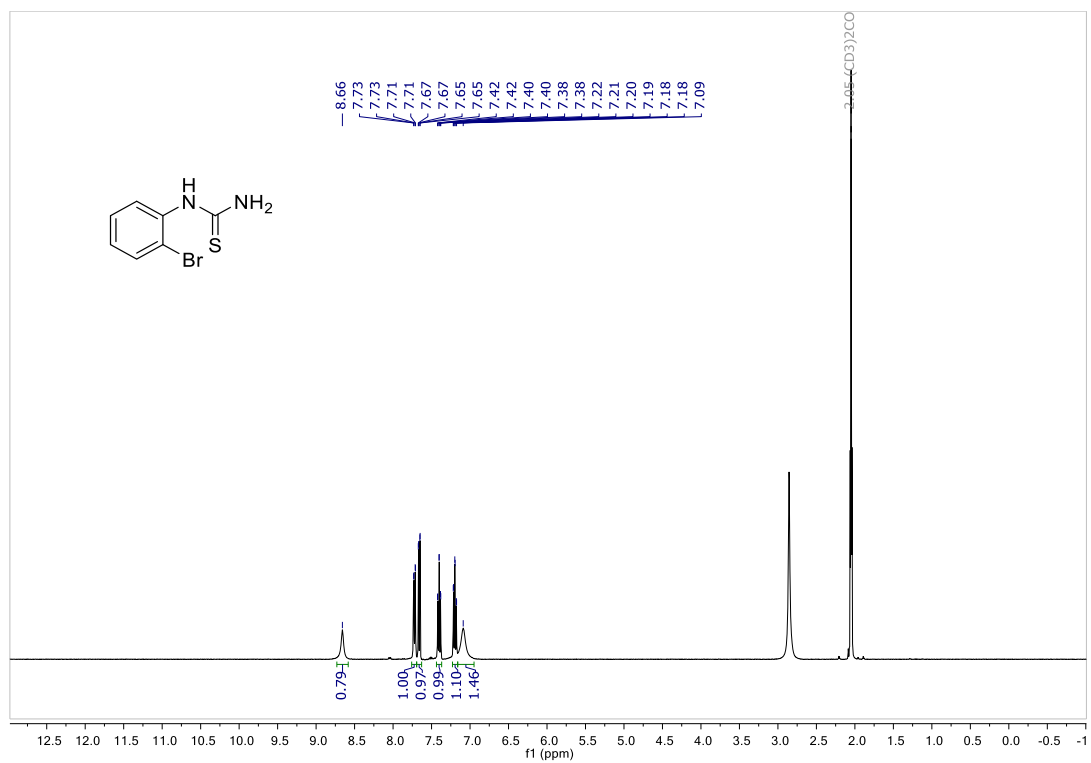


¹³C NMR

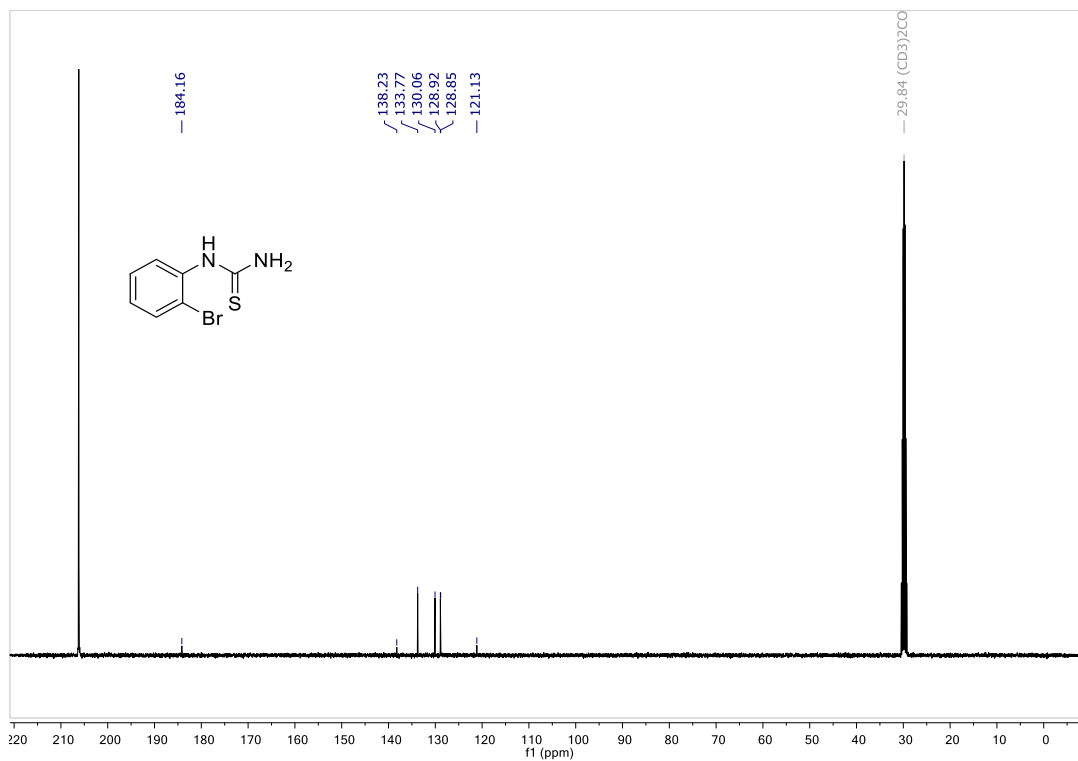


2-bromophenylthiourea (5.4)

¹H NMR

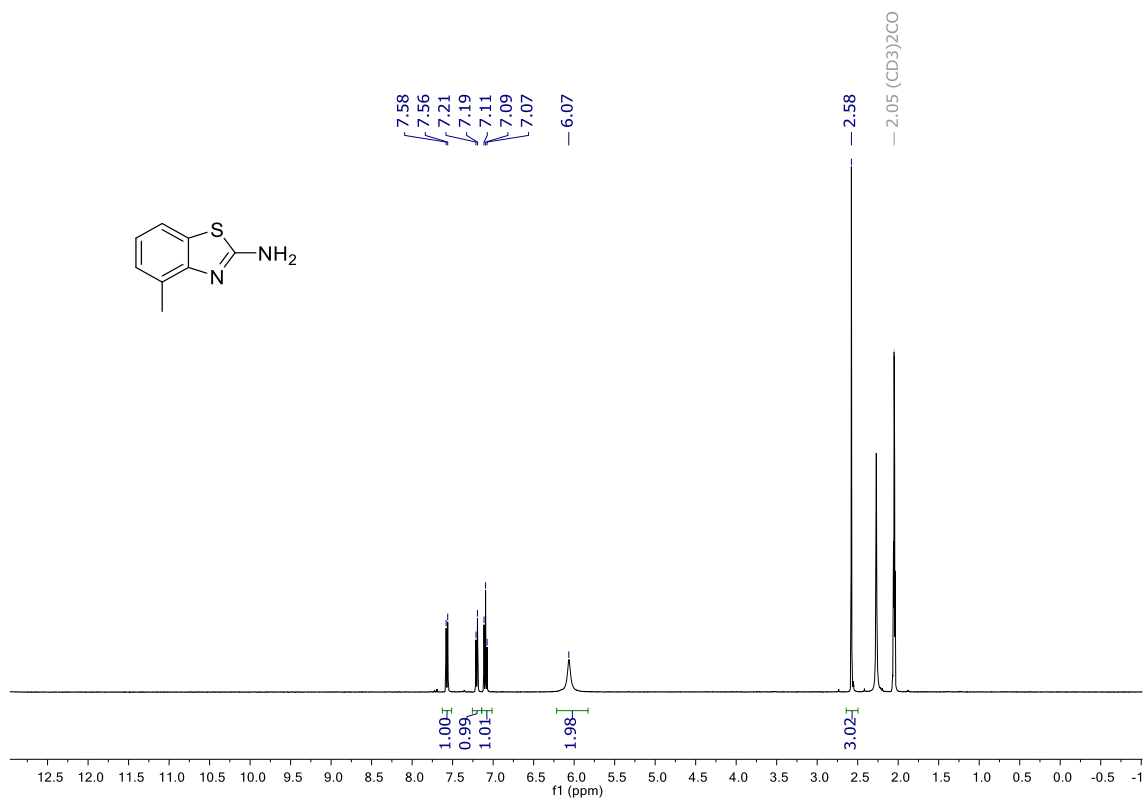


¹³C NMR

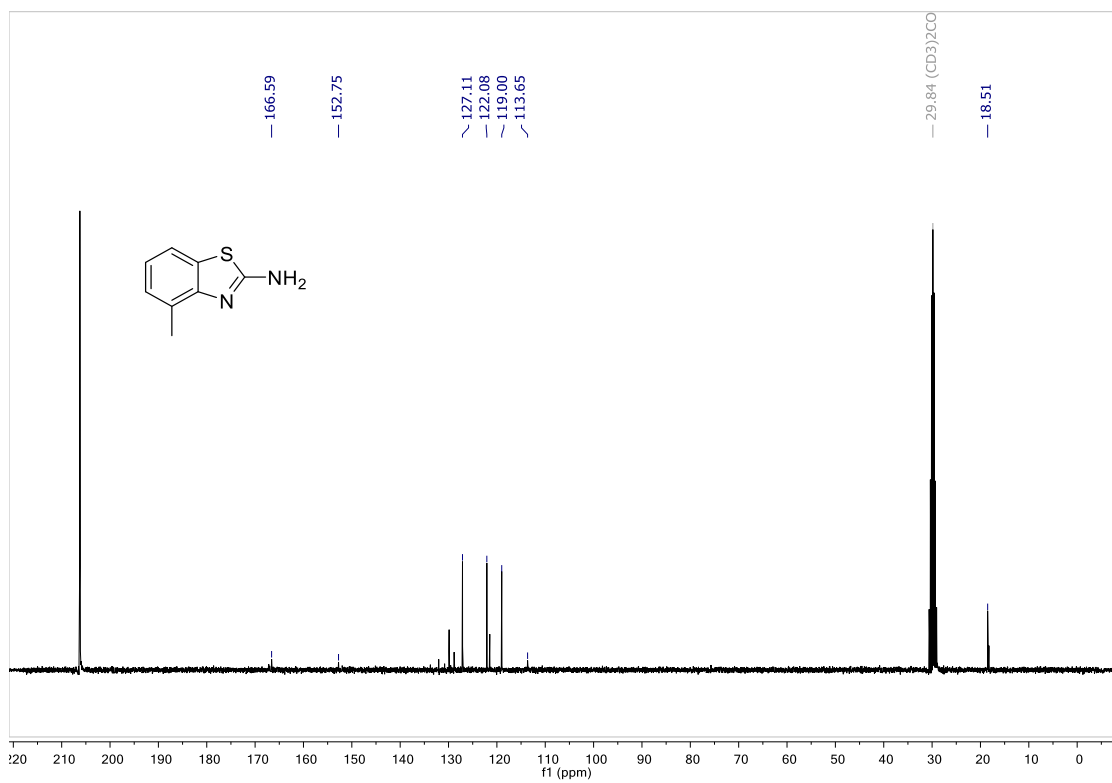


2-amino-4-methylbenzothiazole (5.5)

¹H NMR

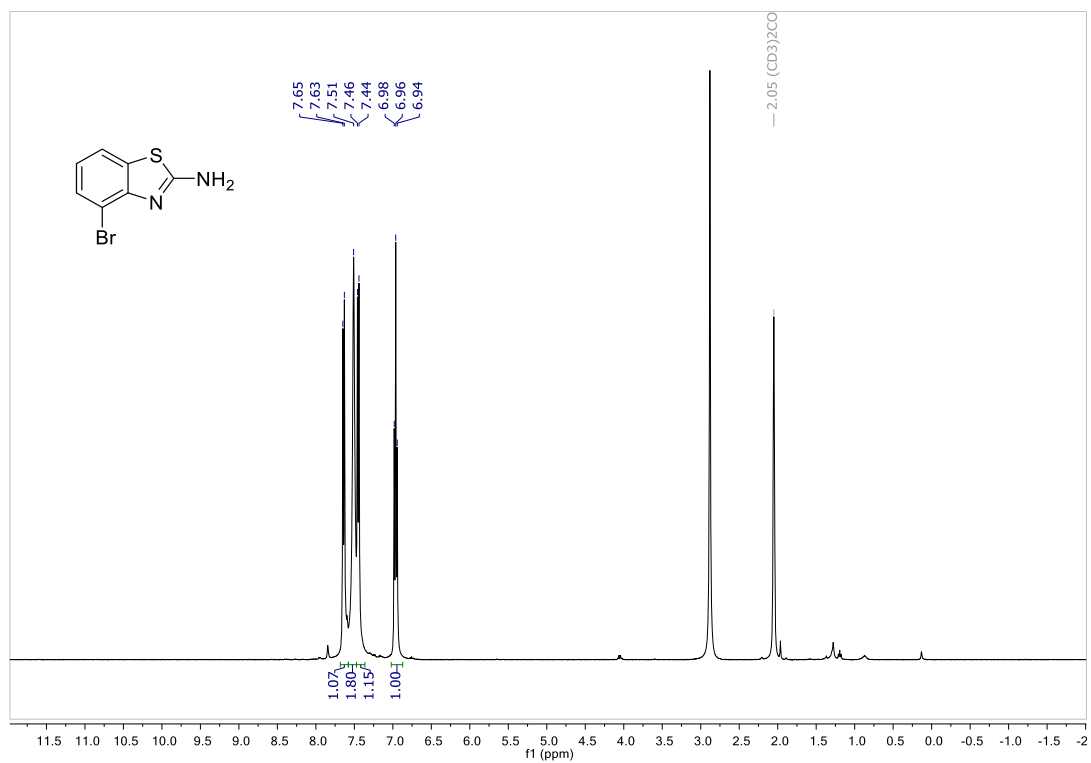


¹³C NMR

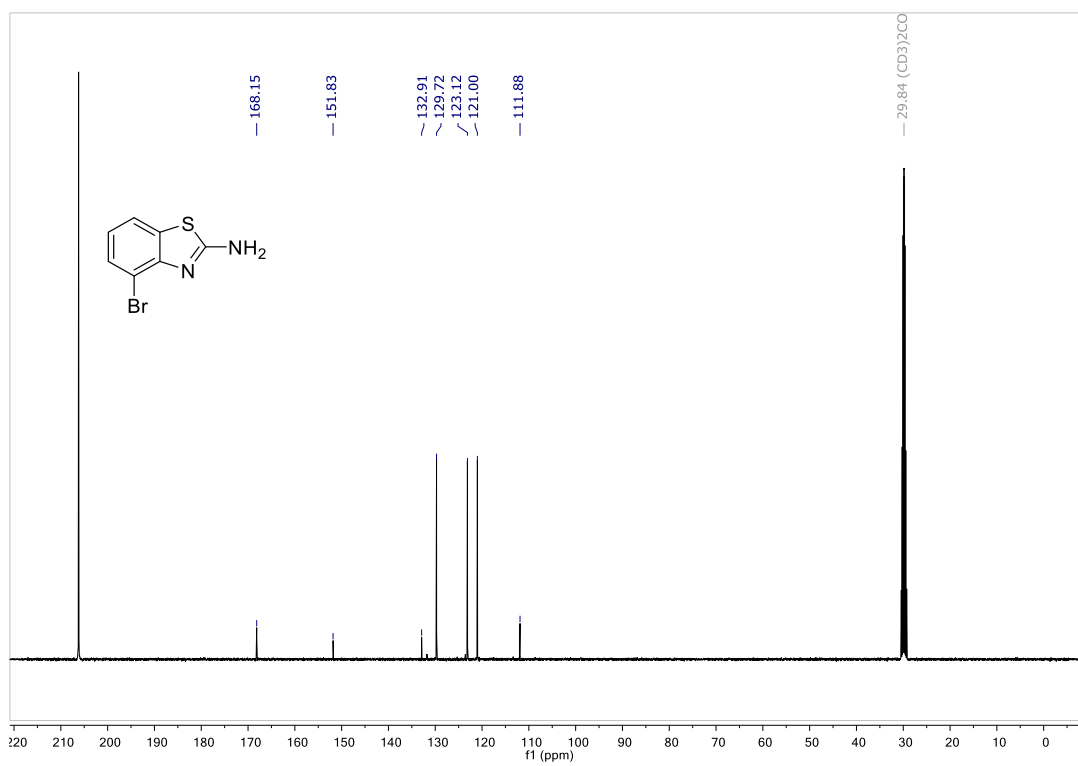


2-amino-4-bromobenzothiazole (5.6)

¹H NMR

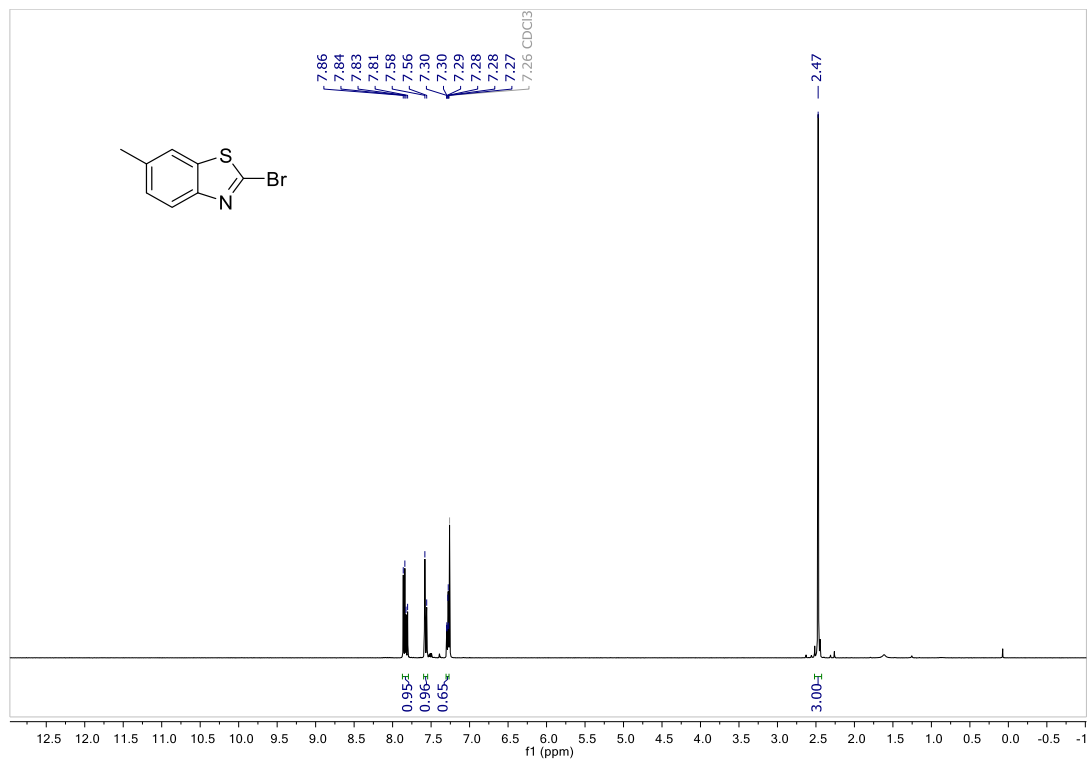


¹³C NMR

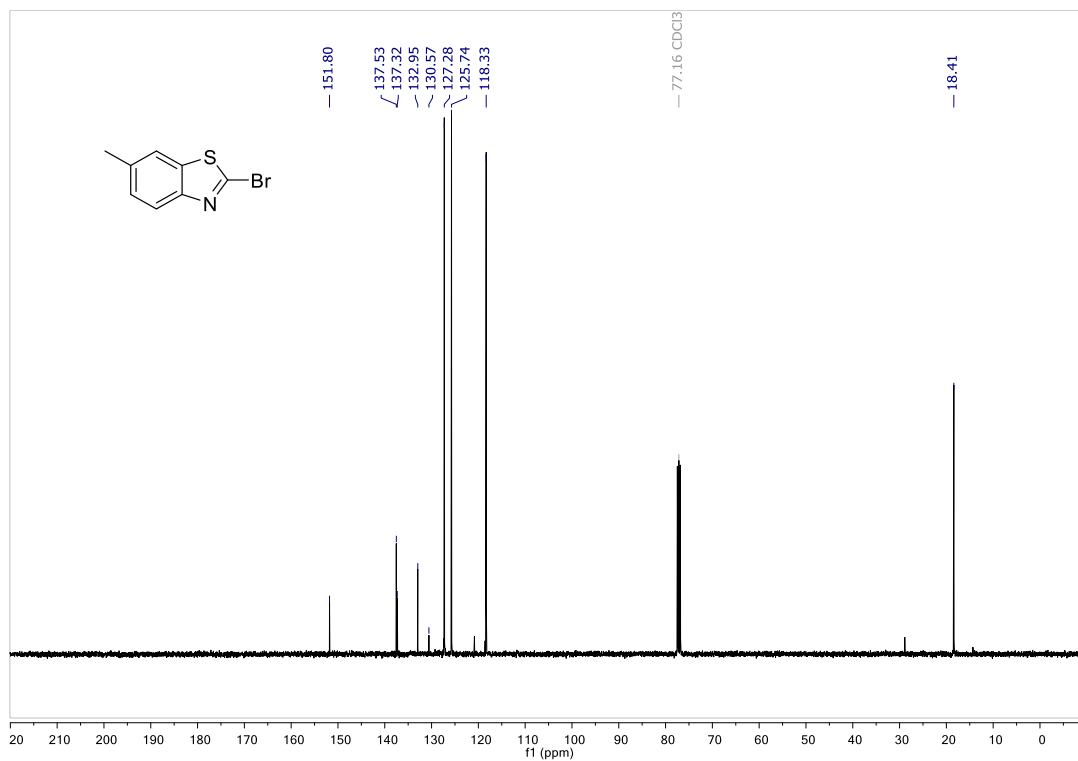


2-bromo-6-methylbenzothiazole (5.7)

¹H NMR

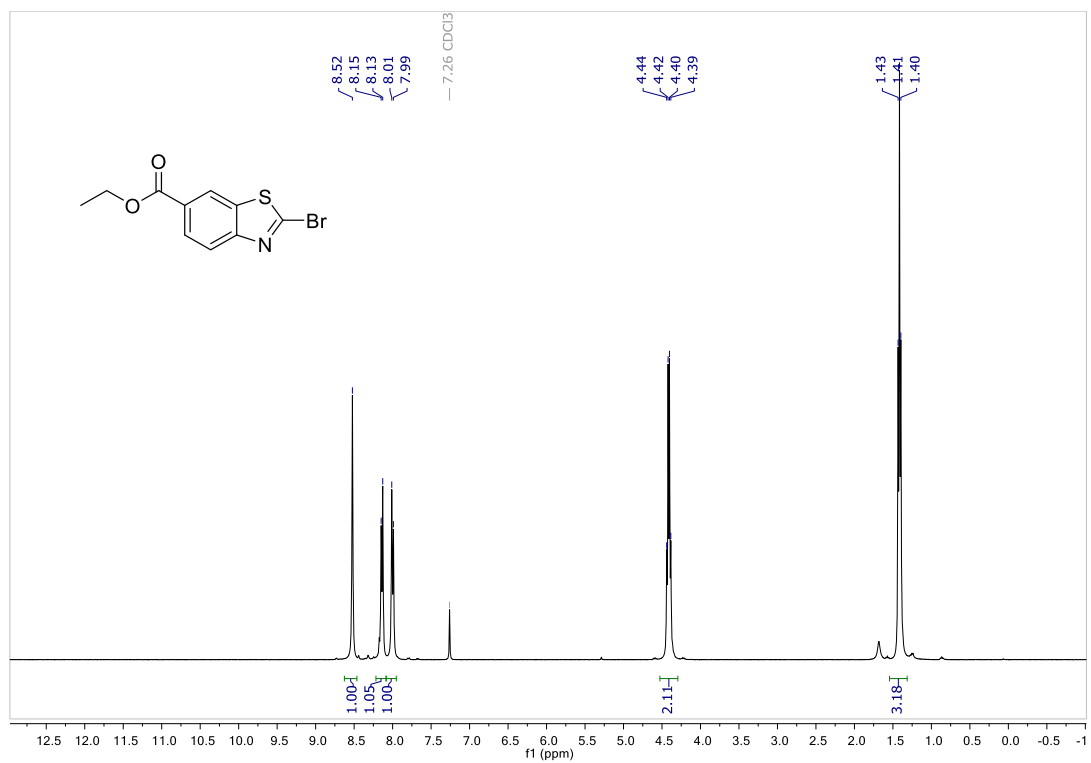


¹³C NMR

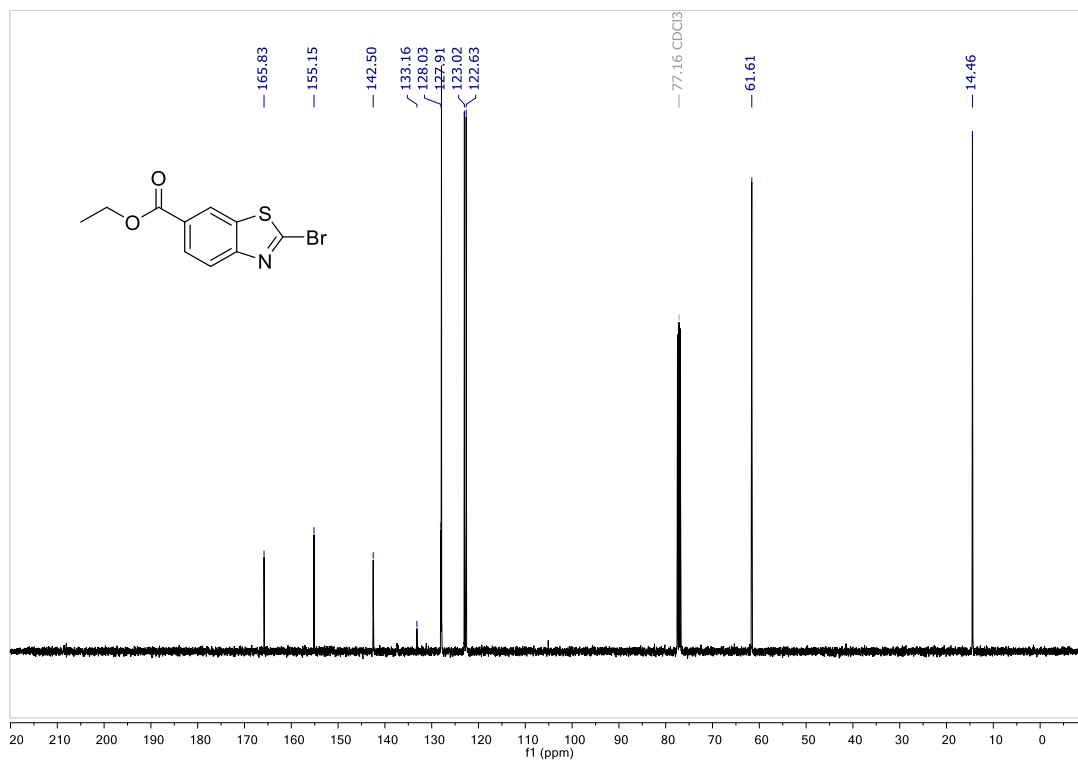


Ethyl 2-bromobenzothiazole-6-carboxylate (5.8)

¹H NMR

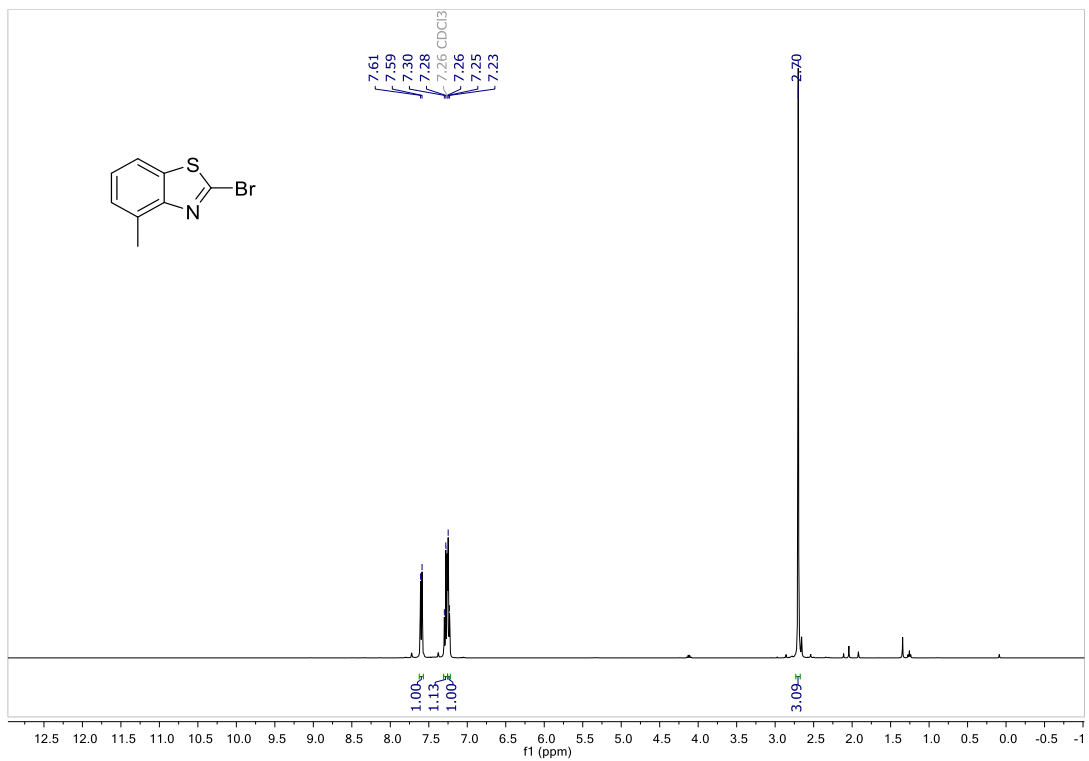


¹³C NMR

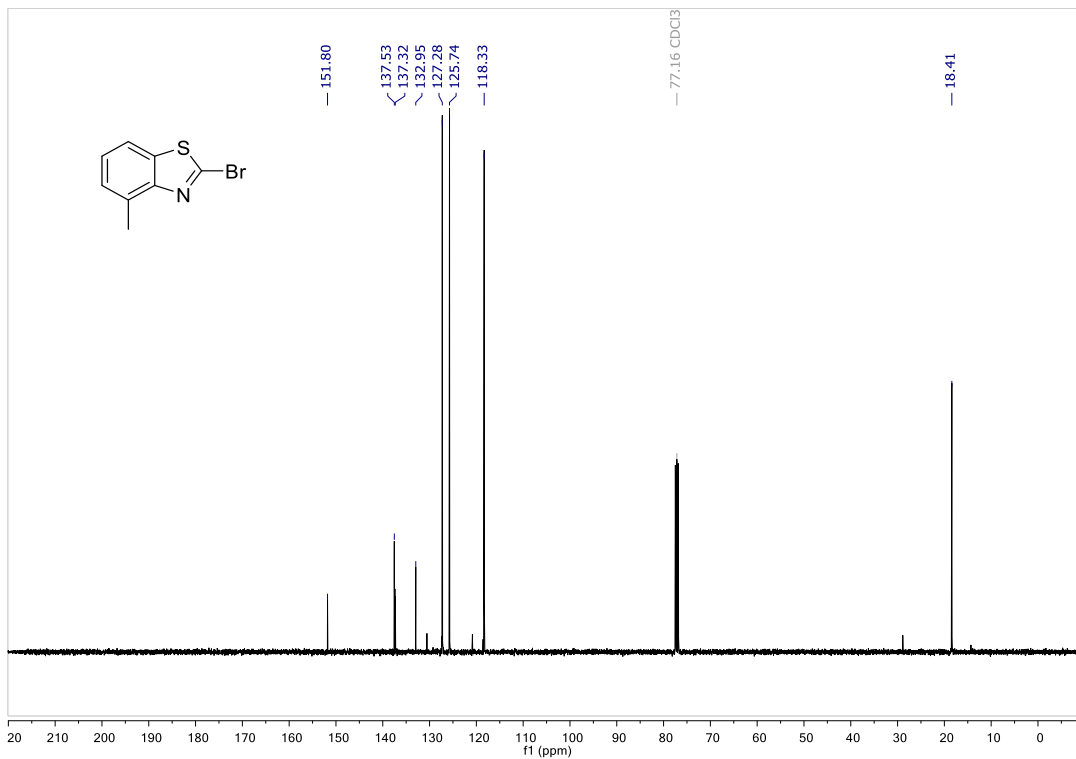


2-bromo-4-methylbenzothiazole (5.9)

¹H NMR

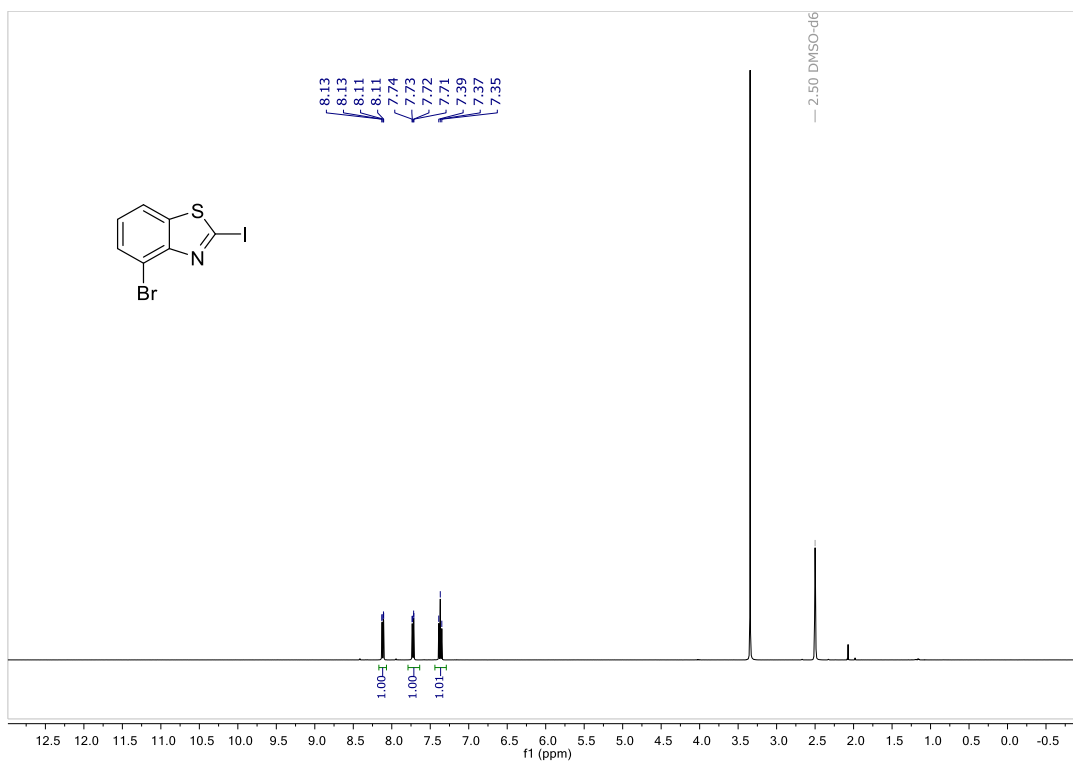


¹³C NMR

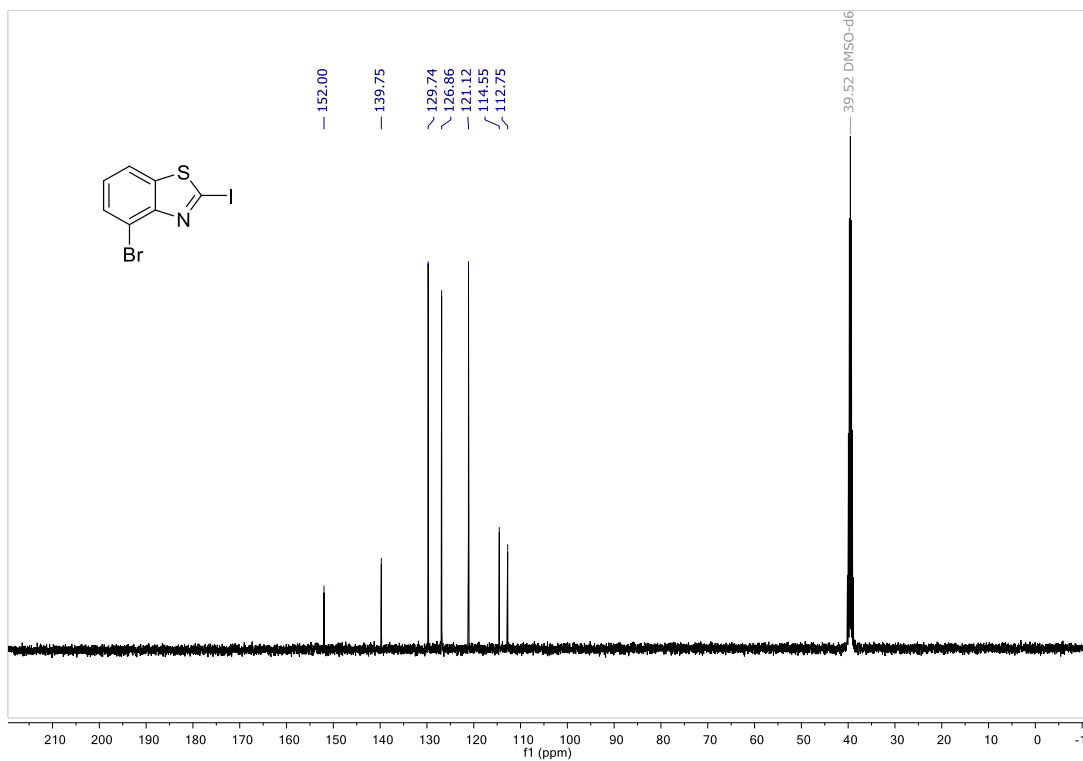


2-iodo-4-bromobenzothiazole (5.10)

¹H NMR

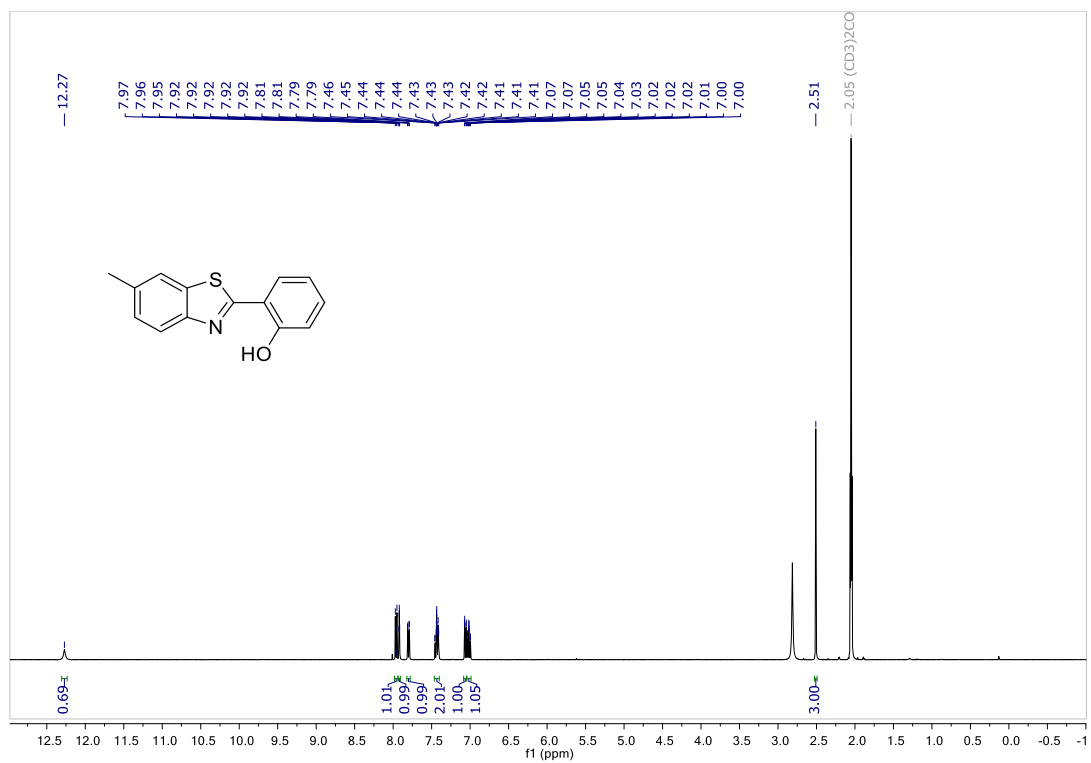


¹³C NMR

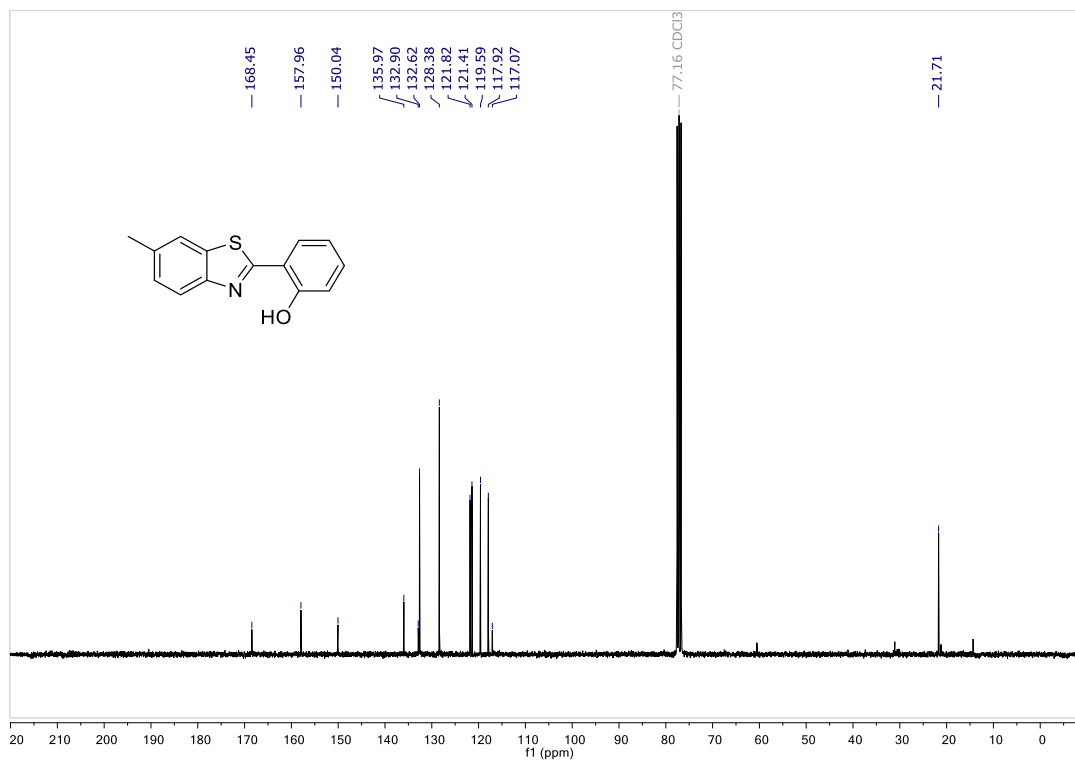


2-(2-hydroxyphenyl)-6-methylbenzothiazole (5.11)

¹H NMR

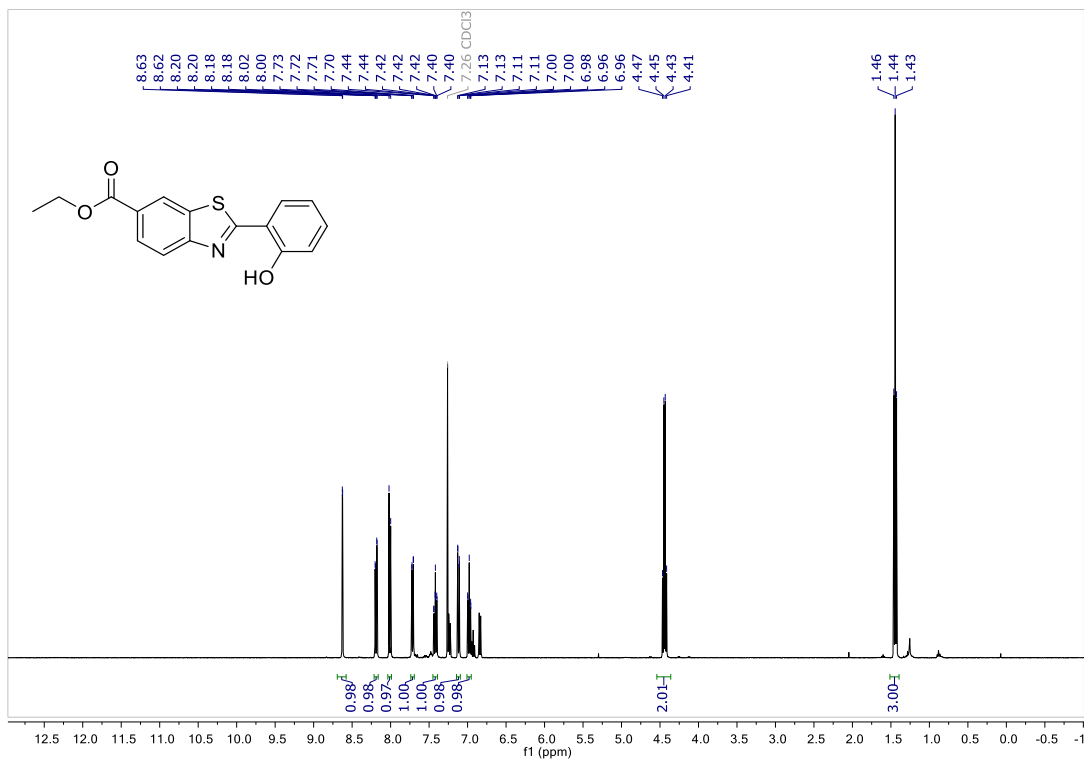


¹³C NMR

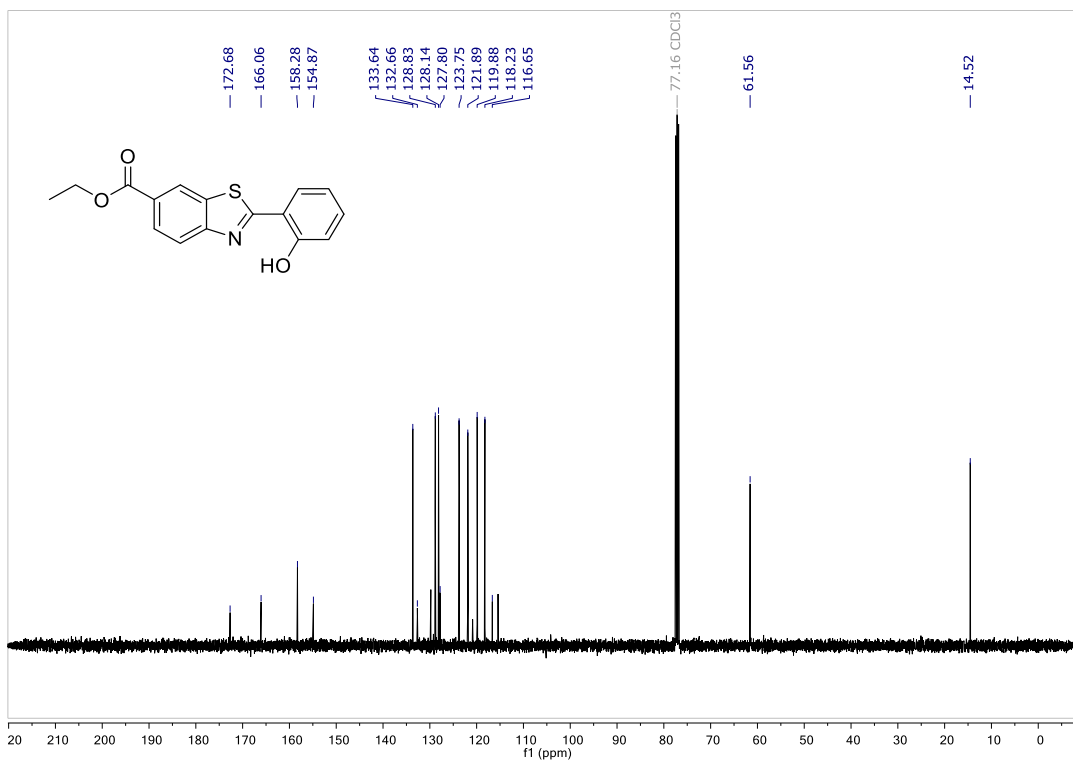


Ethyl 2-(2-hydroxyphenyl)benzothiazole-6-carboxylate (5.12)

¹H NMR

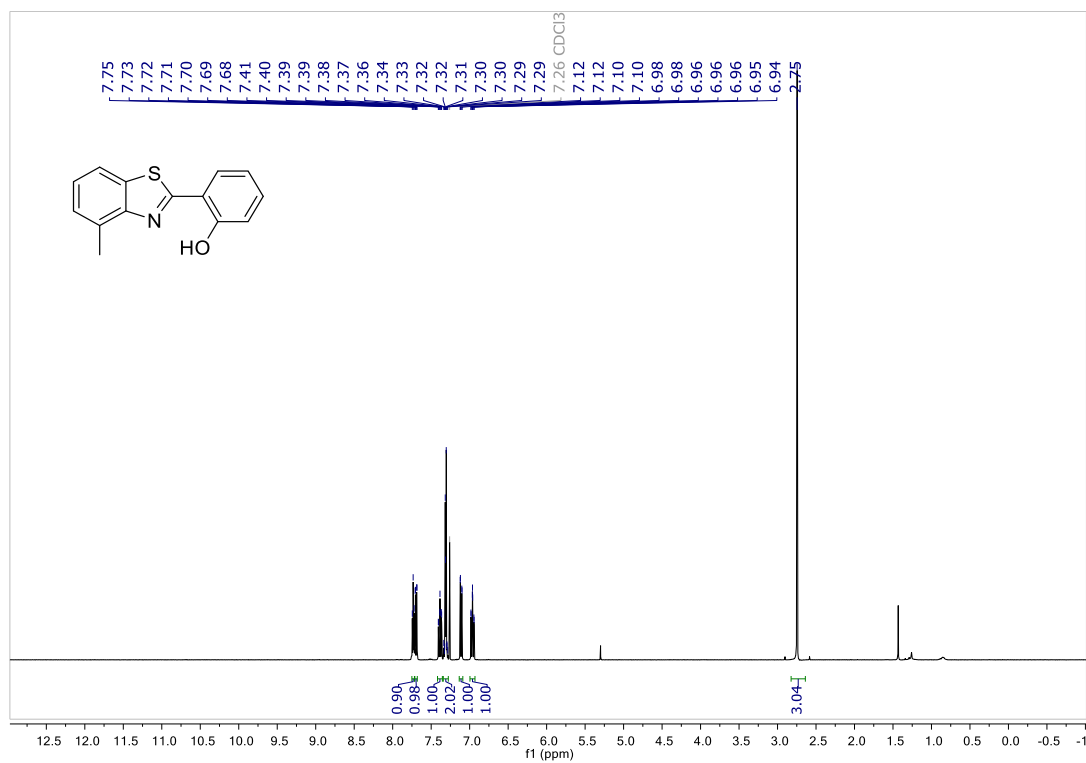


¹³C NMR

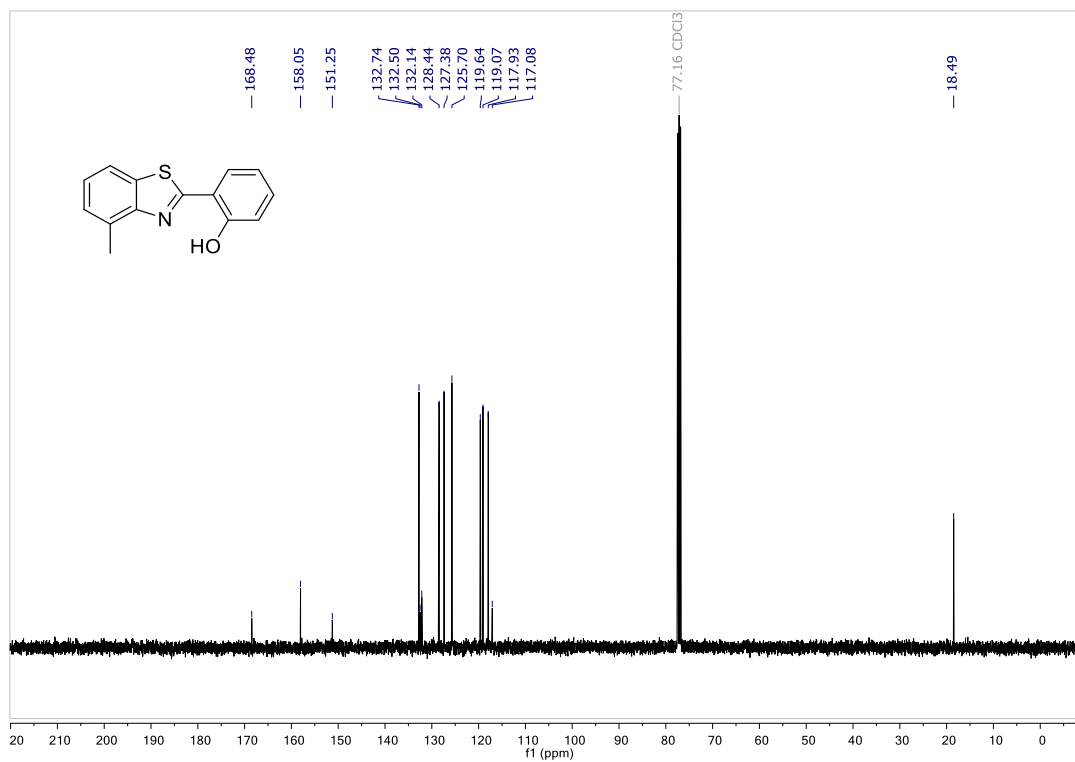


2-(2-hydroxyphenyl)-4-methylbenzothiazole (5.13)

¹H NMR

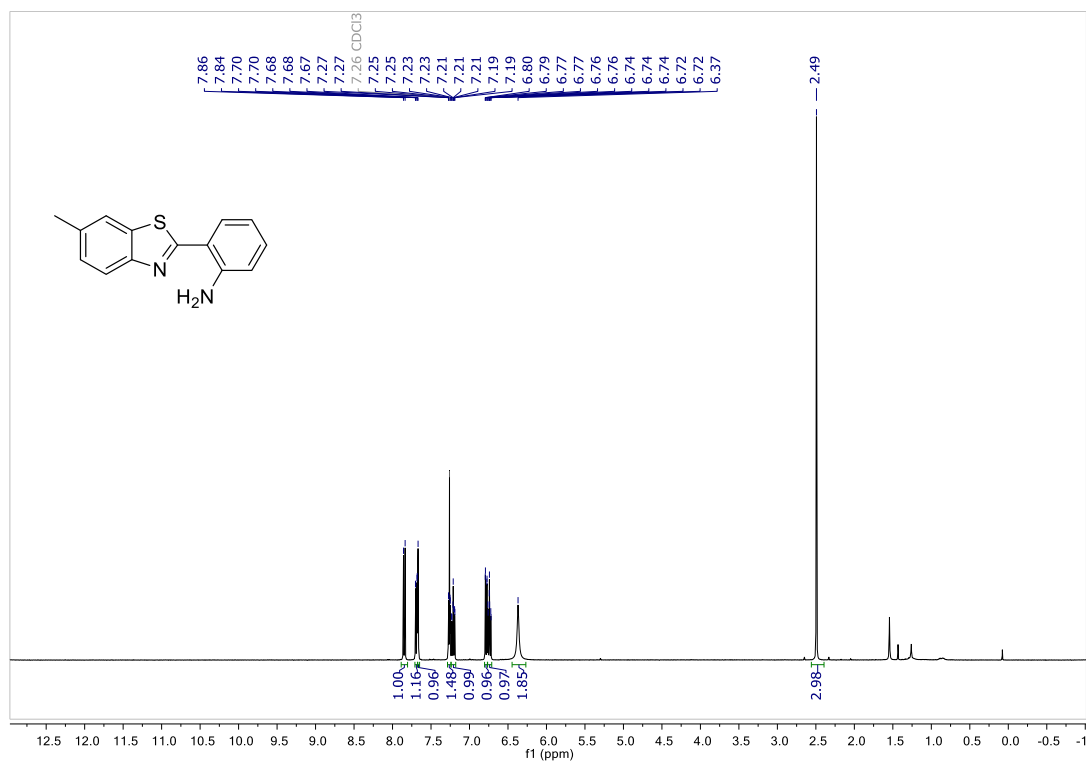


¹³C NMR

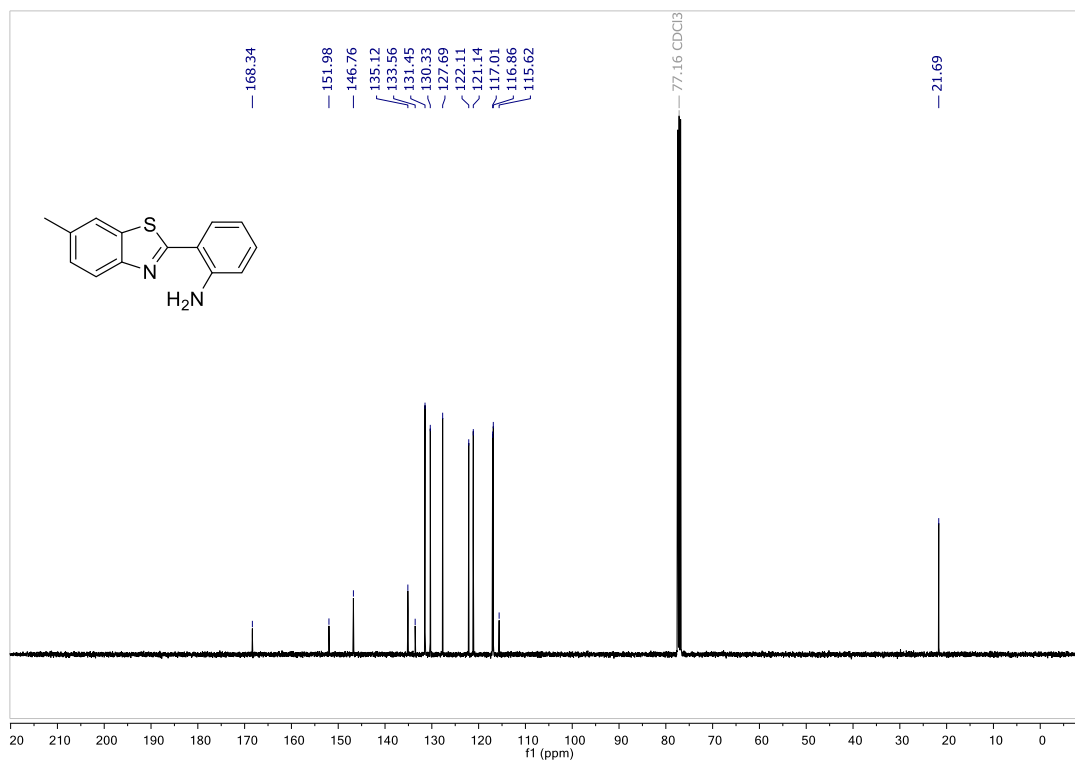


2-(6-methylbenzo[d]thiazol-2-yl)aniline (5.14)

¹H NMR

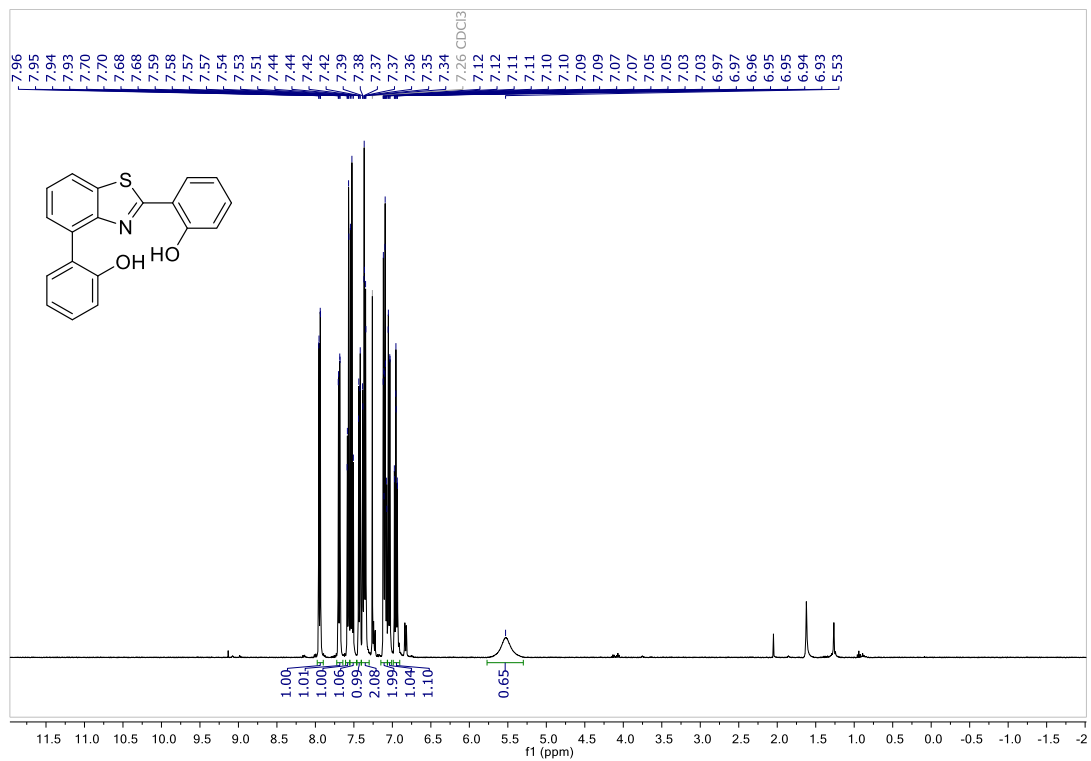


¹³C NMR

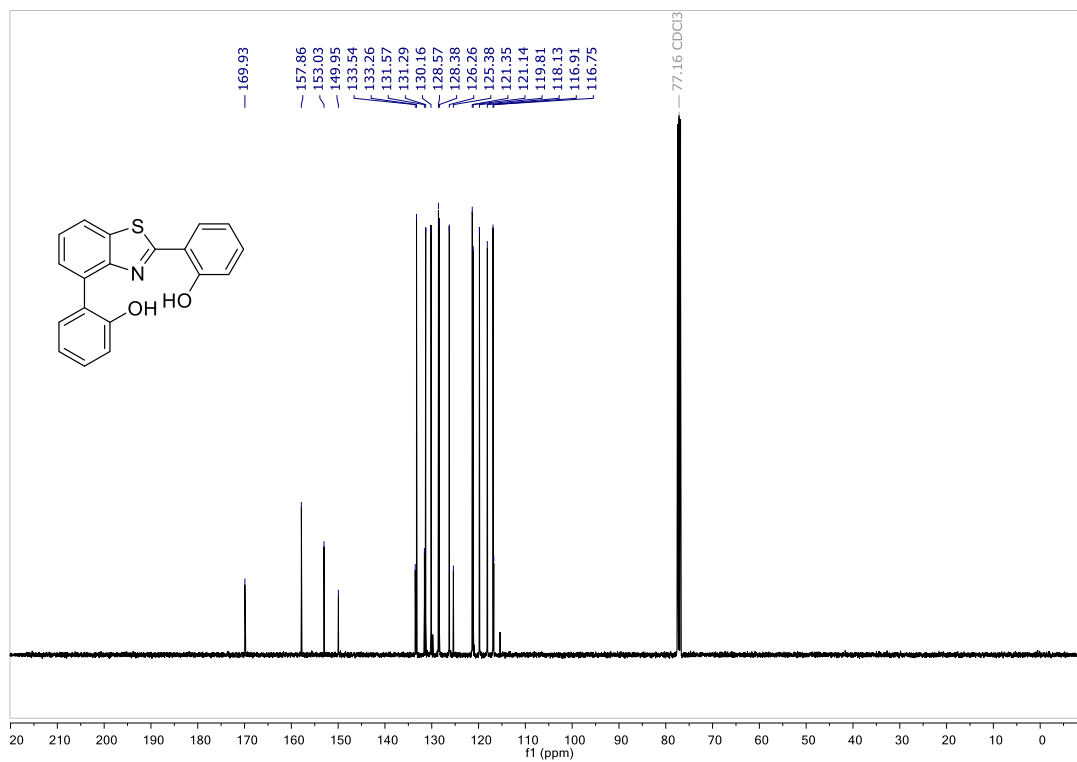


2,2'-(benzo[d]thiazole-2,4-diyl)diphenol (5.15)

¹H NMR

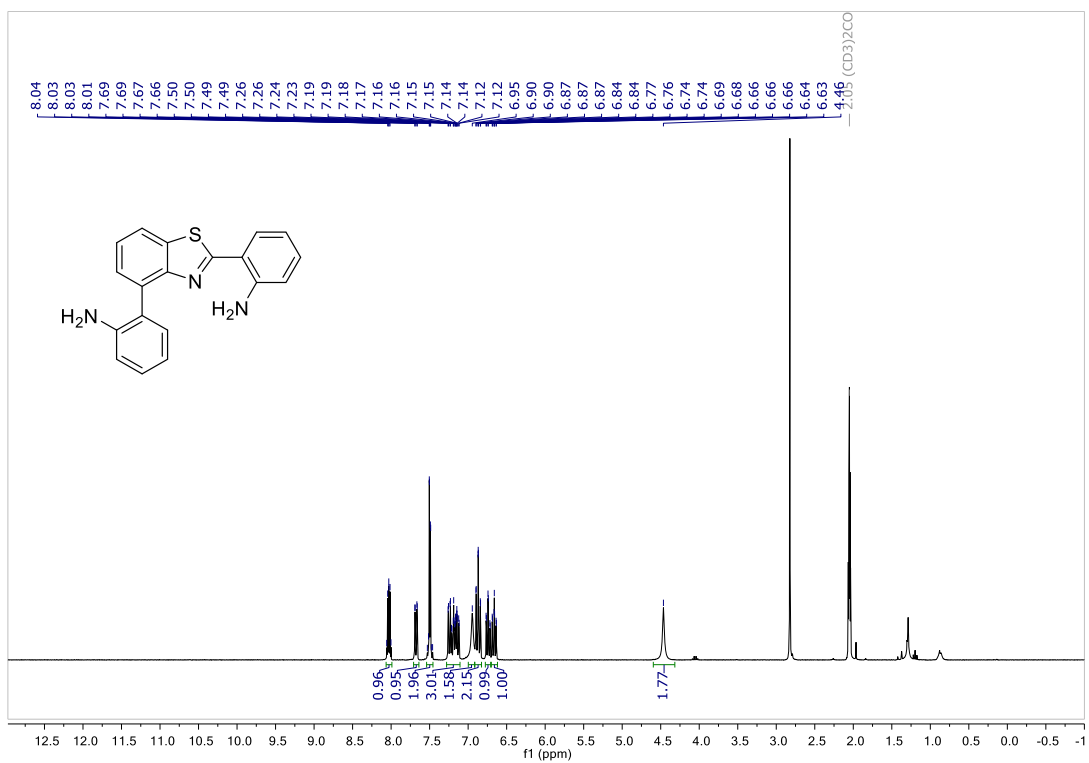


¹³C NMR

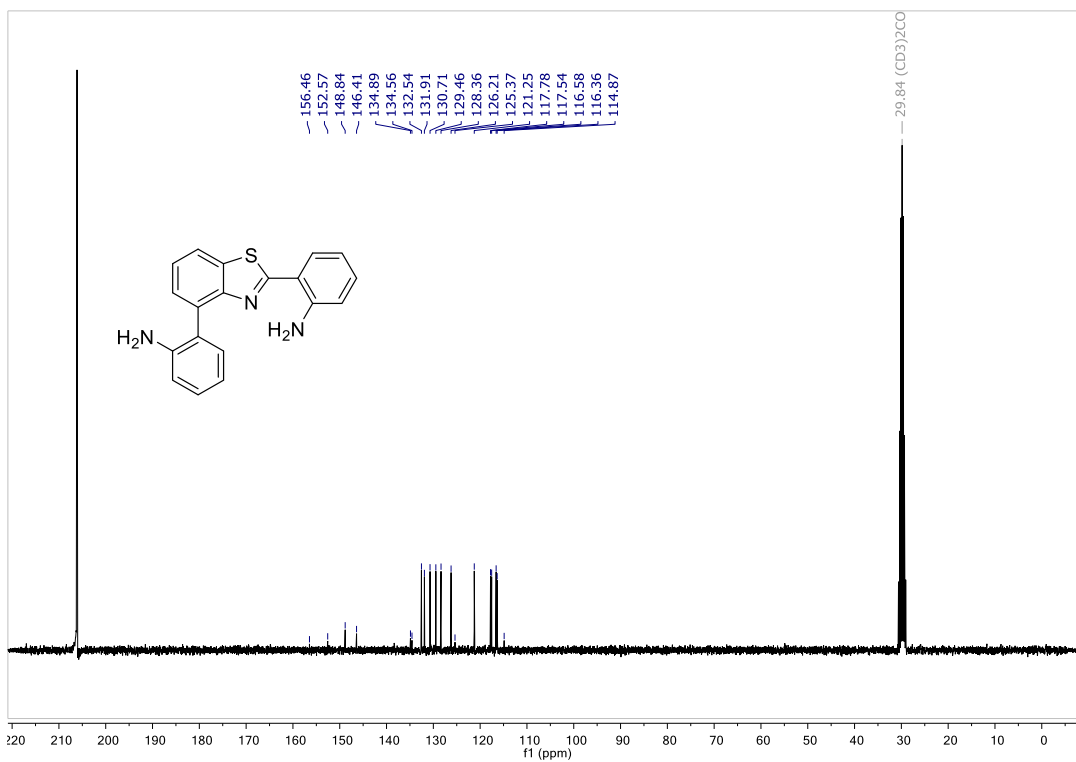


2,2'-(benzo[d]thiazole-2,4-diyl)dianiline (5.16)

¹H NMR

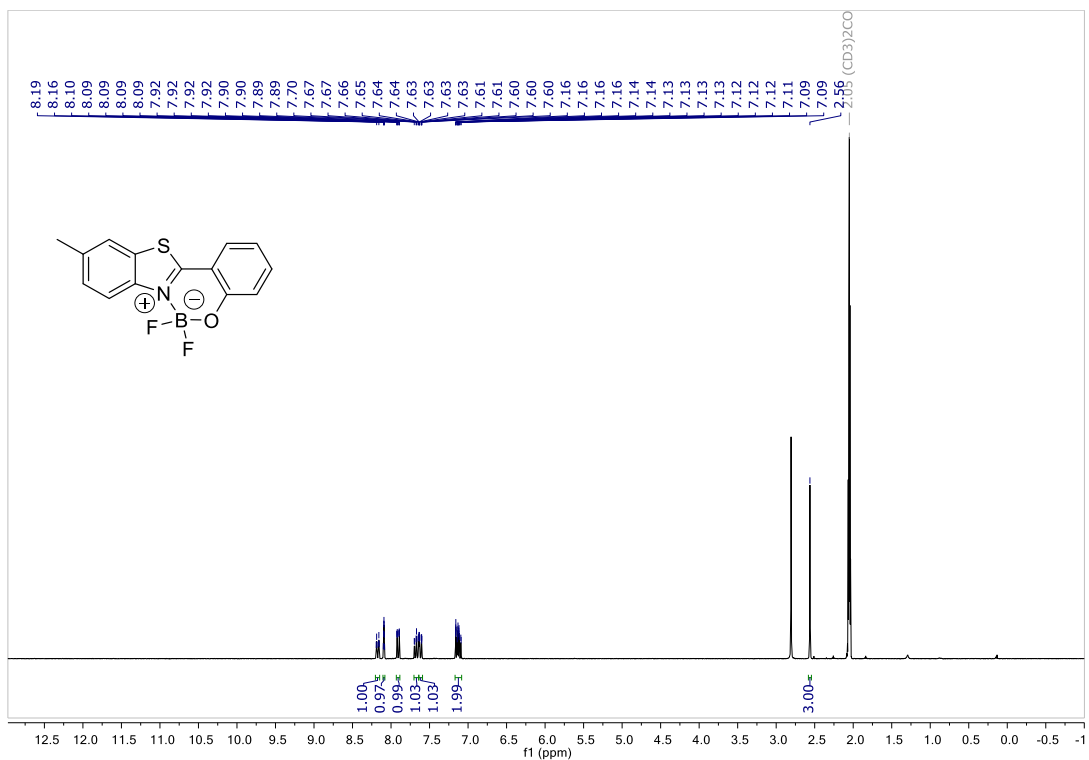


¹³C NMR

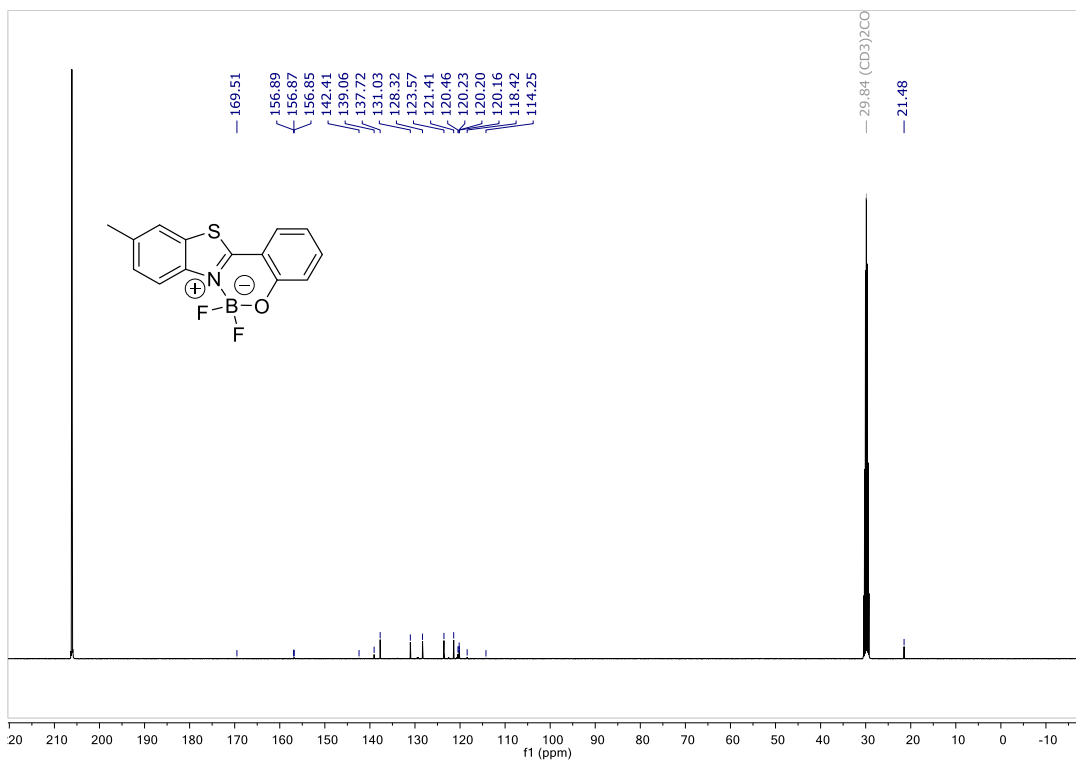


6,6-difluoro-10-methyl-6H-benzo[e]benzo[4,5]thiazolo[3,2-c][1,3,2]oxazaborinin-7-ium-6-uide (5.17)

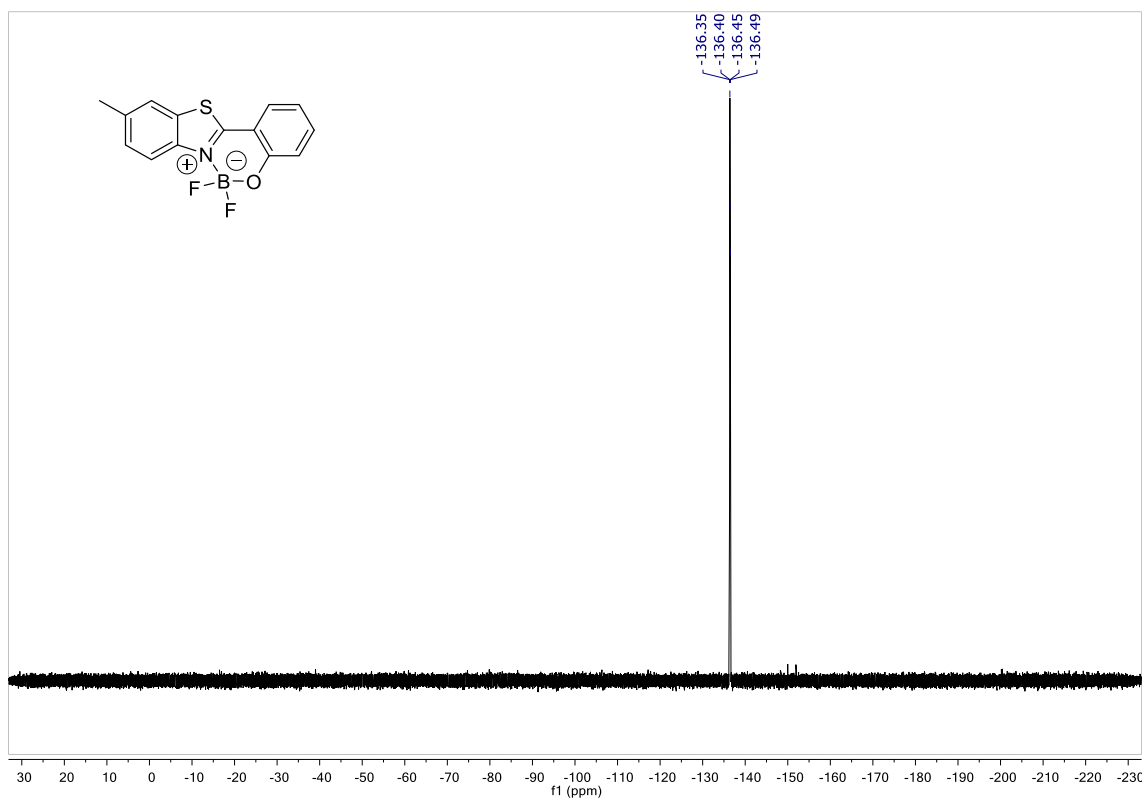
¹H NMR



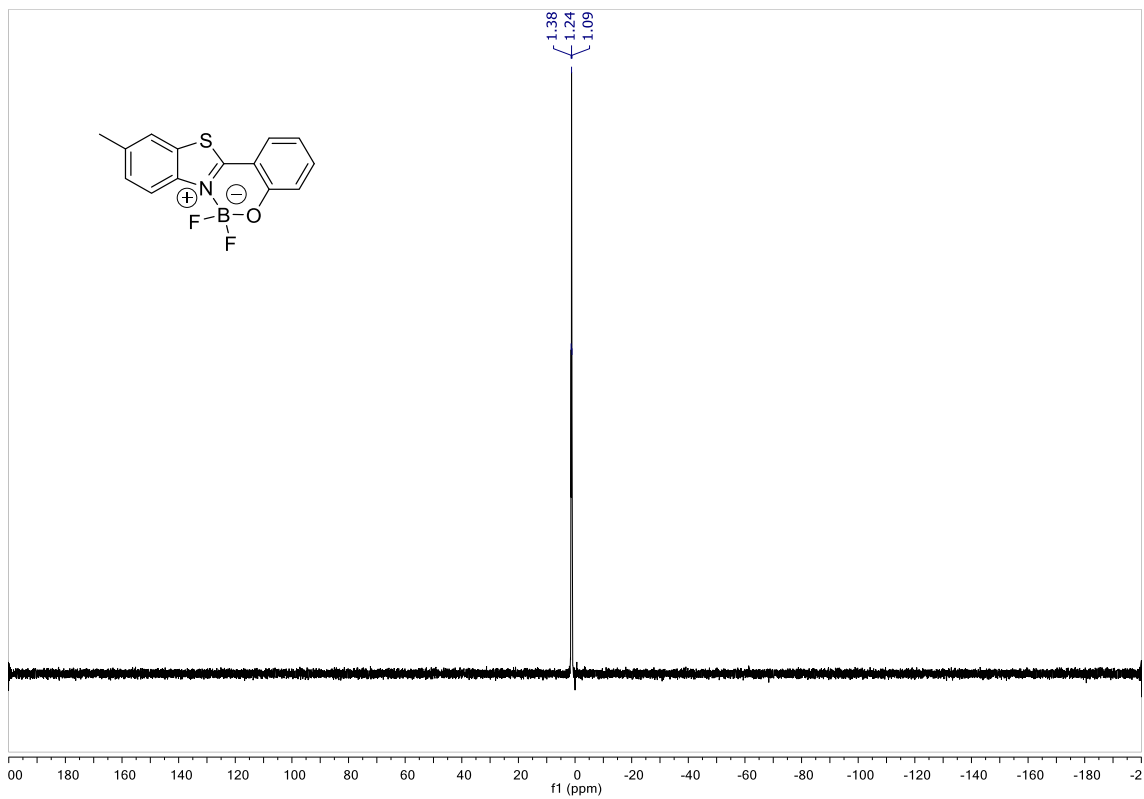
¹³C NMR



¹⁹F NMR

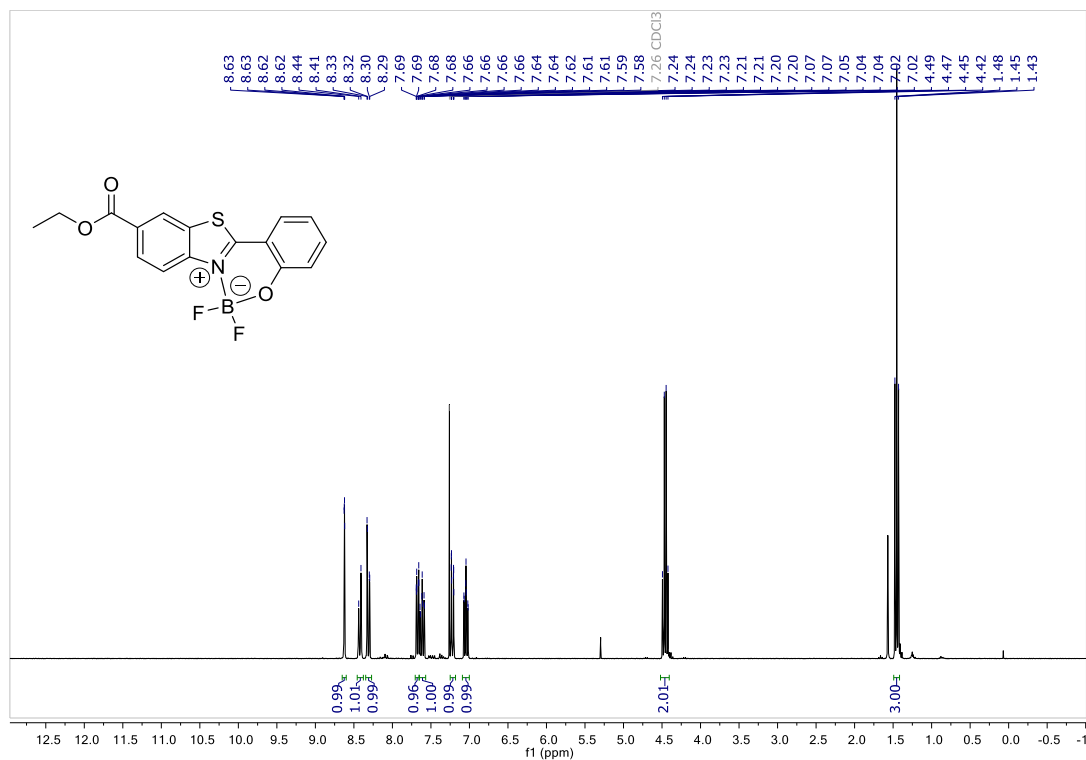


¹¹B NMR

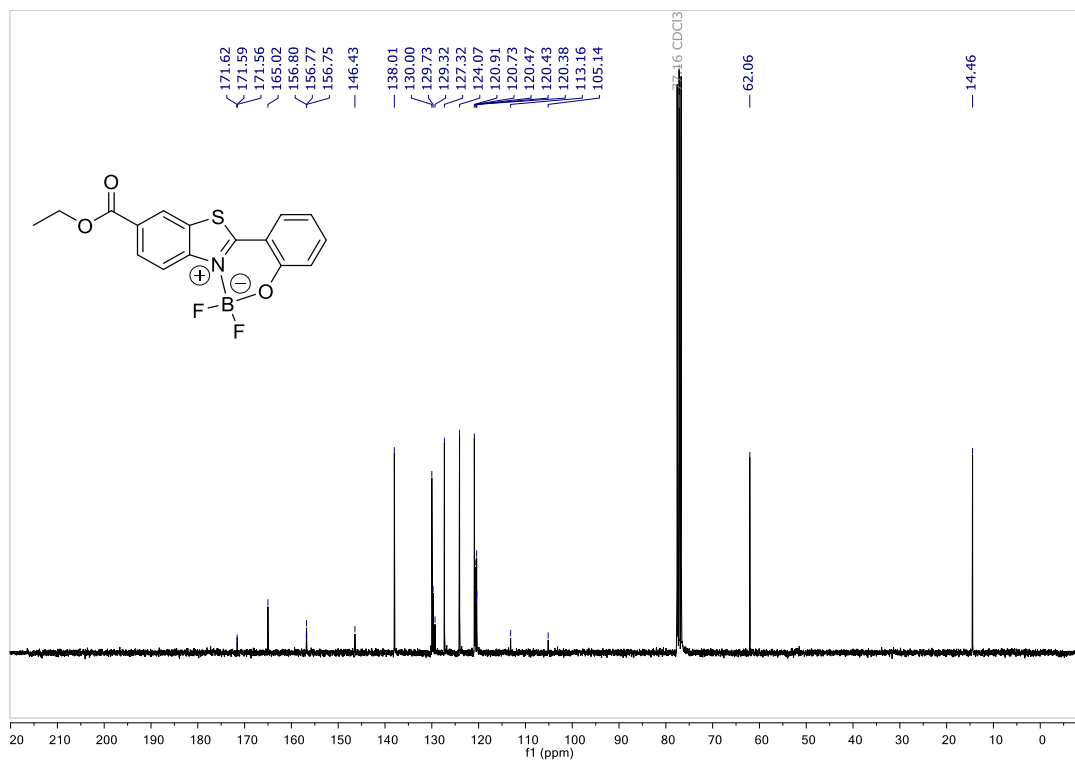


10-(ethoxycarbonyl)-6,6-difluoro-6*H*-benzo[*e*]benzo[4,5]thiazolo[3,2-*c*][1,3,2]oxazaborinin-7-ium-6-uide (5.18)

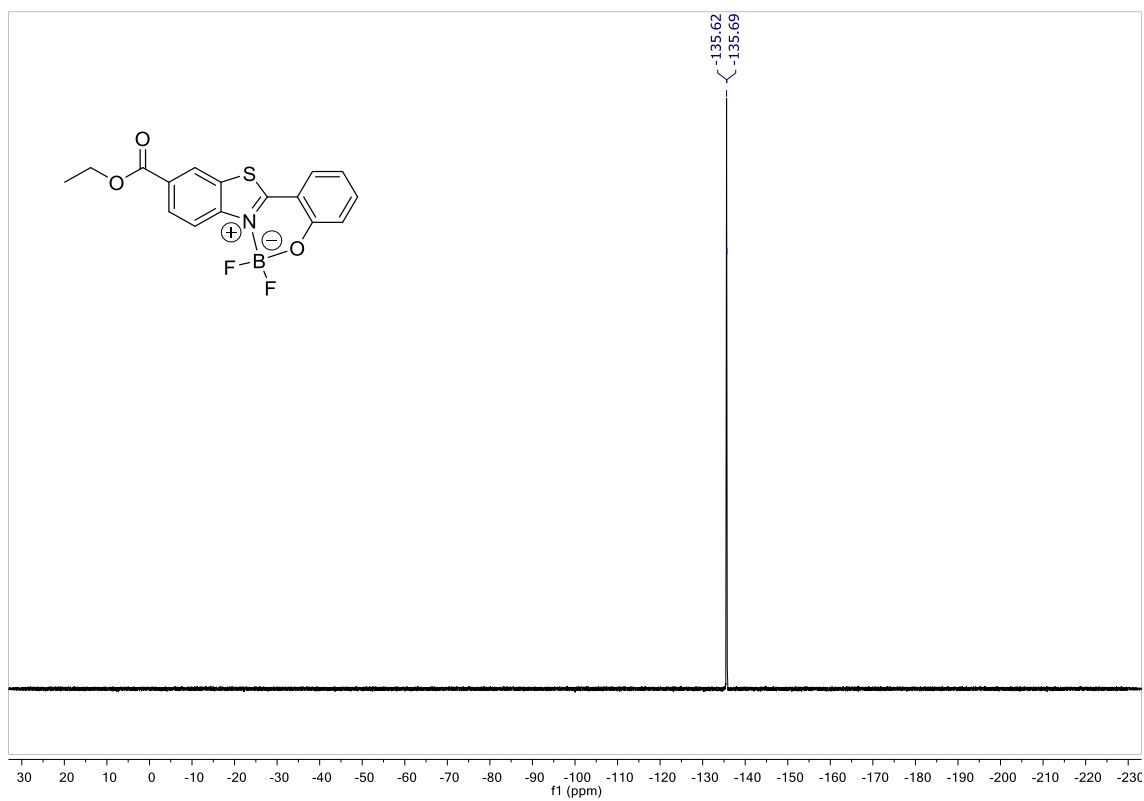
¹H NMR



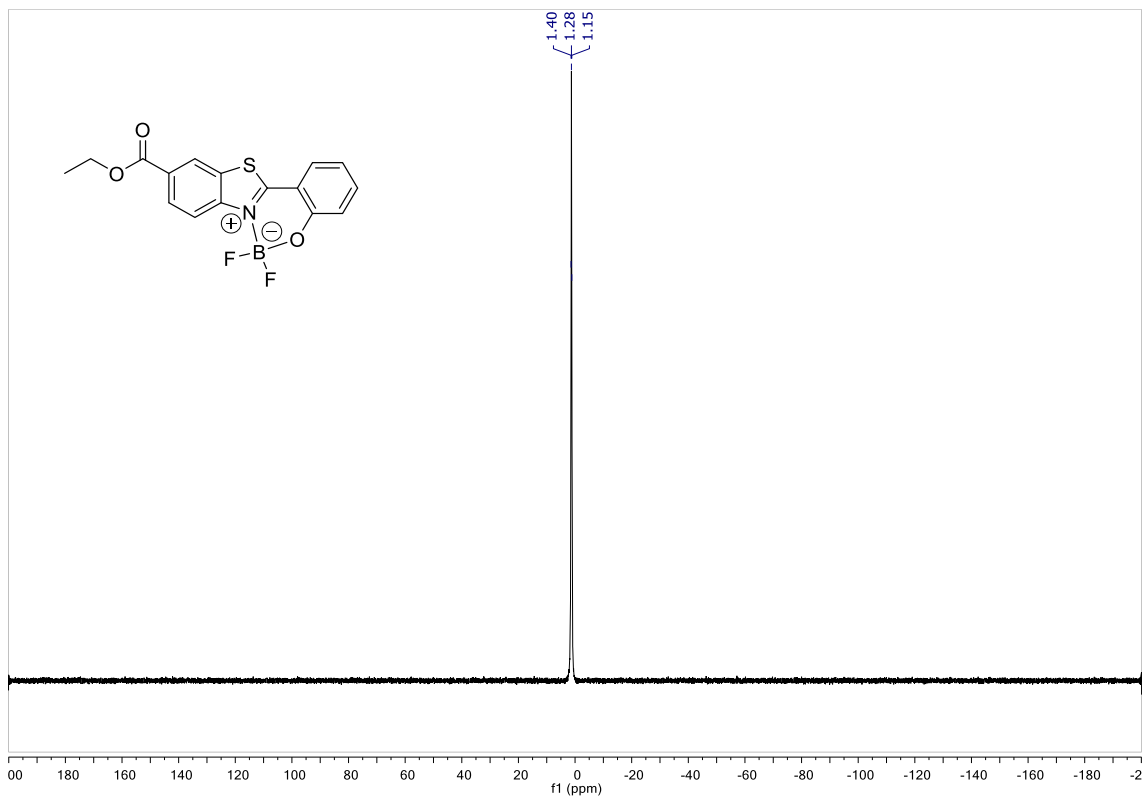
¹³C NMR



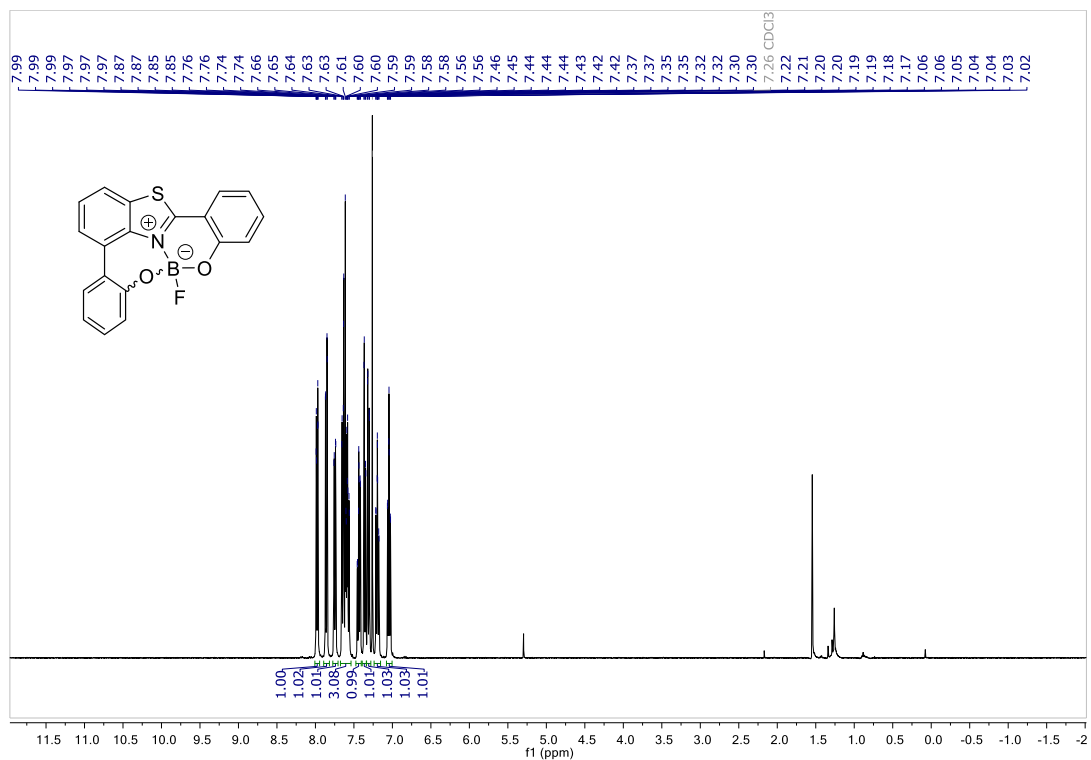
^{19}F NMR



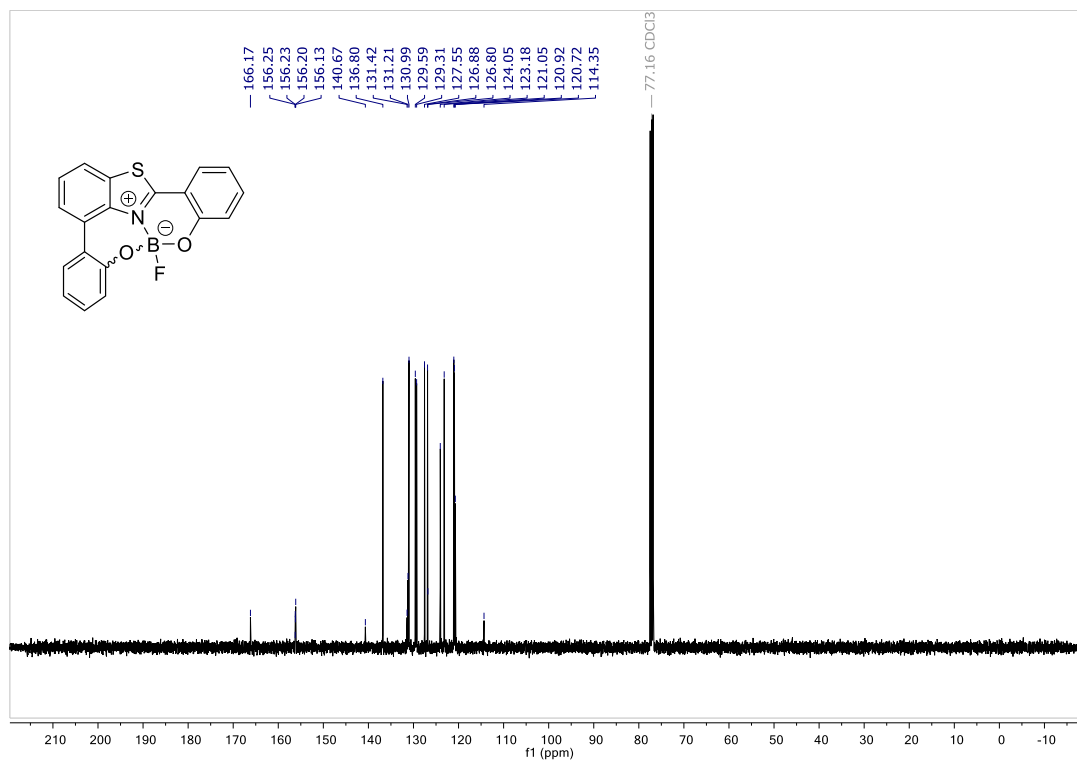
^{11}B NMR



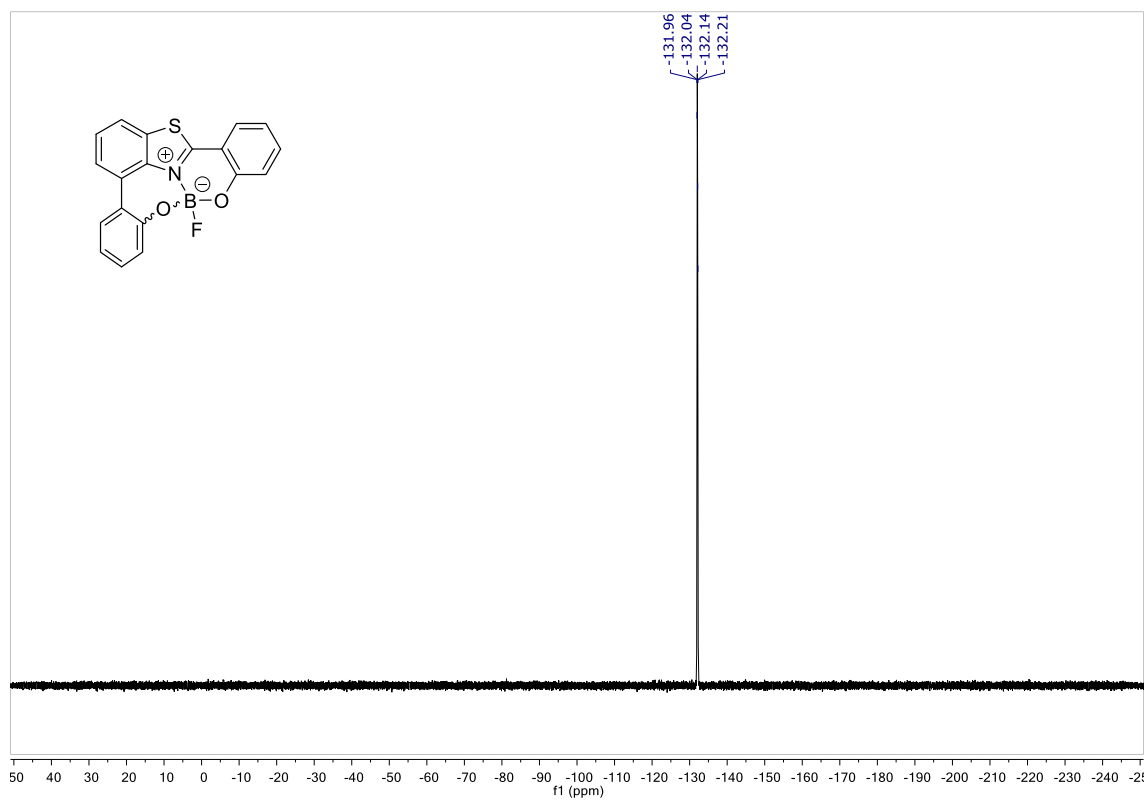
6a-fluoro-6a*H*-6,7-dioxa-1-thia-1a¹-aza-6a-borabenz[*a*]benzo[5,6]cyclohepta[1,2,3,4-*def*]fluoren-1a¹-ium-7-uide (5.19)
¹H NMR



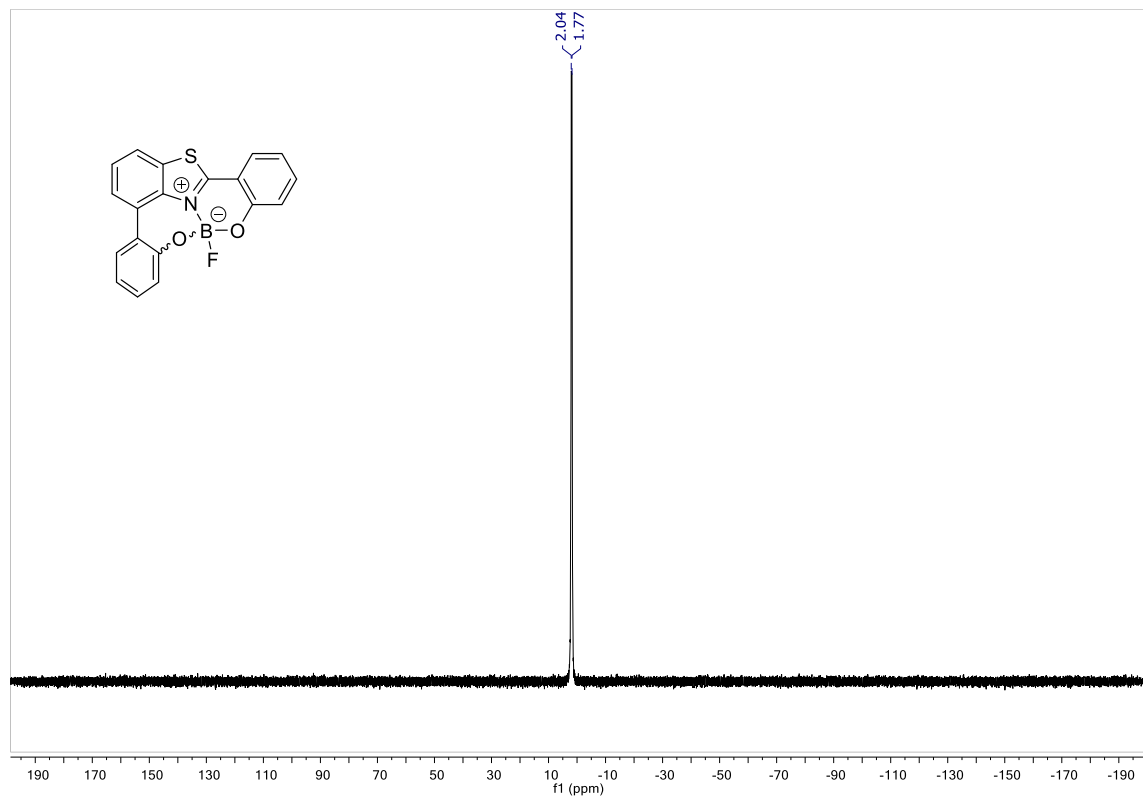
¹³C NMR



¹⁹F NMR

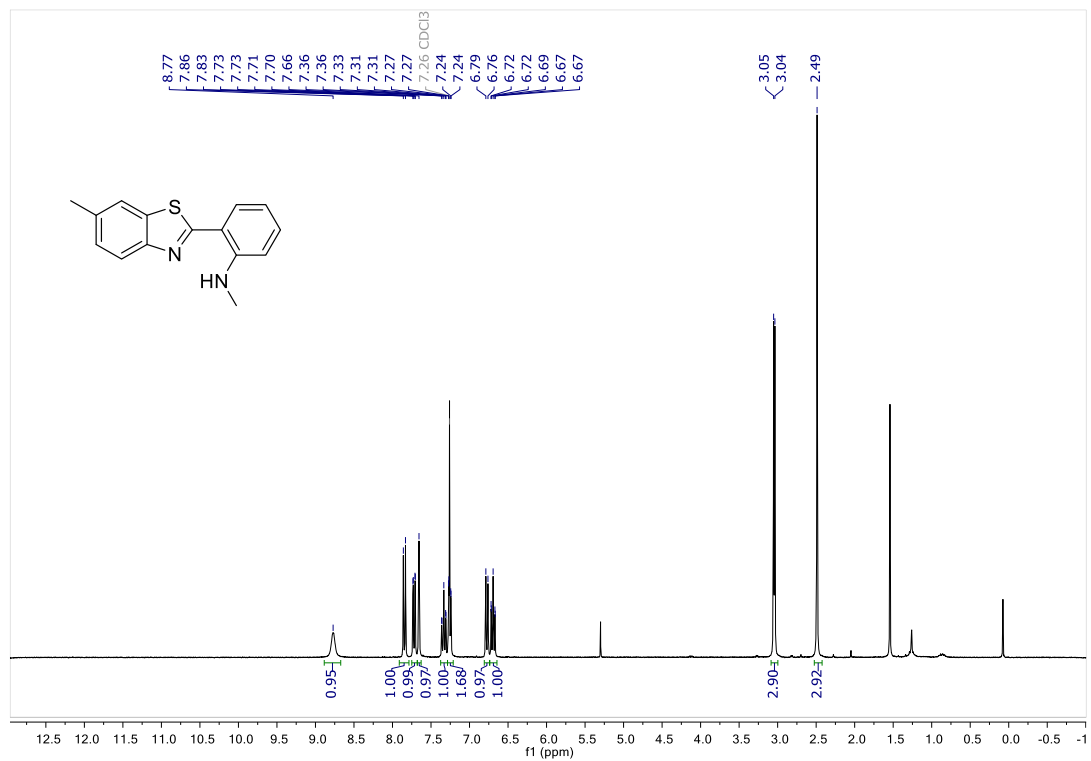


¹¹B NMR

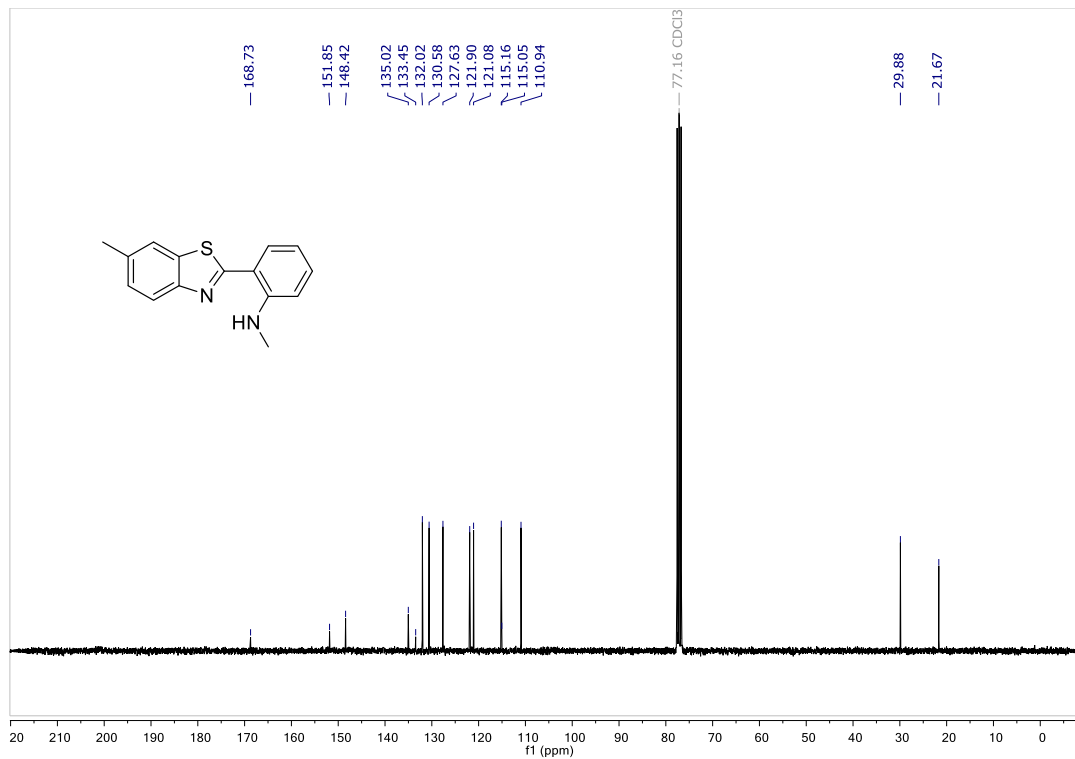


***N*-methyl-2-(6-methylbenzo[*c*]thiazol-2-yl)aniline (5.20)**

¹H NMR

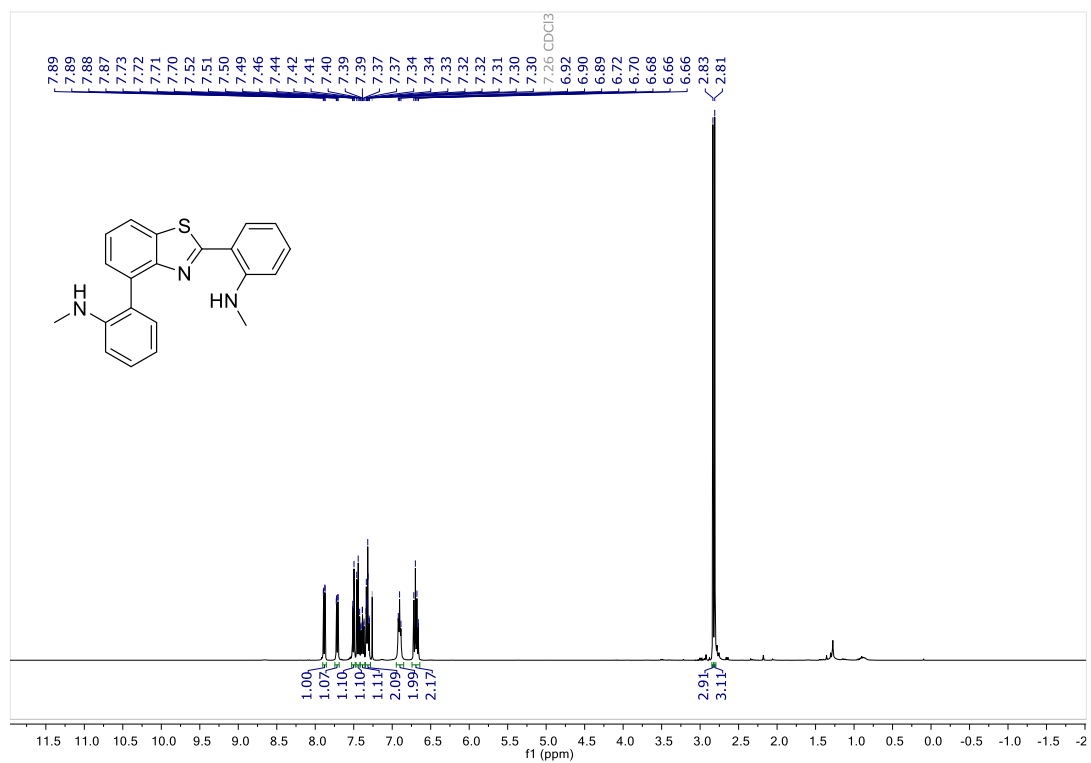


¹³C NMR

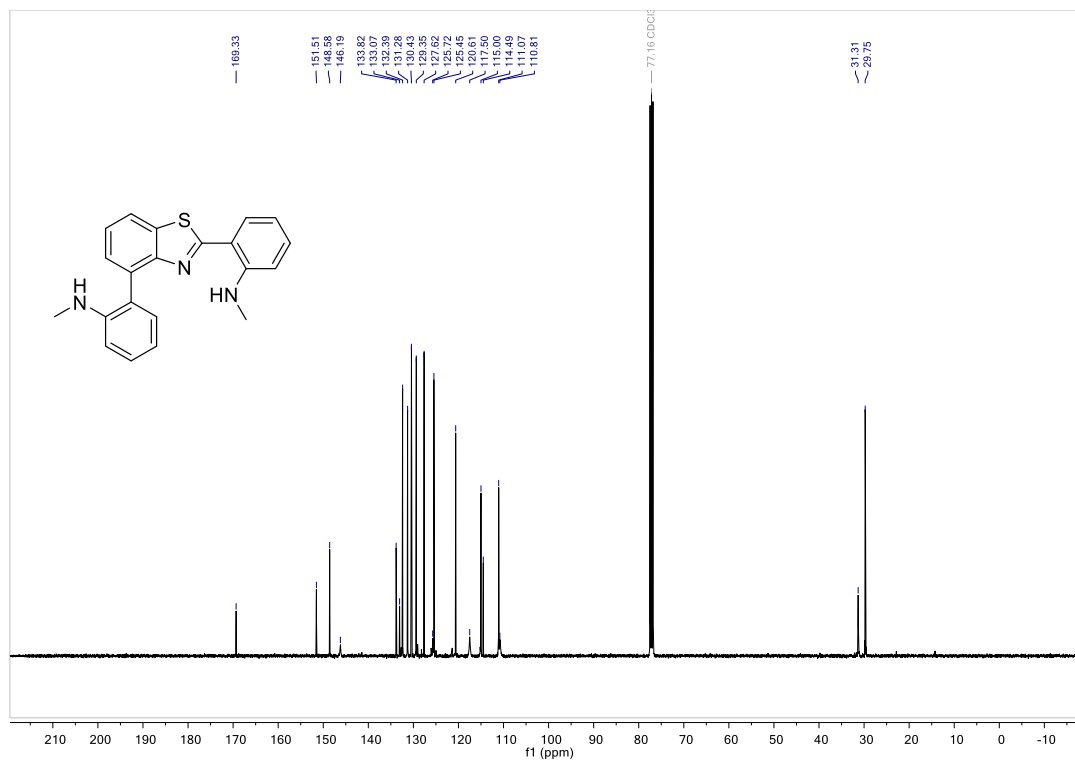


2,2'-(benzo[d]thiazole-2,4-diyl)bis(N-methylaniline) (5.21)

¹H NMR

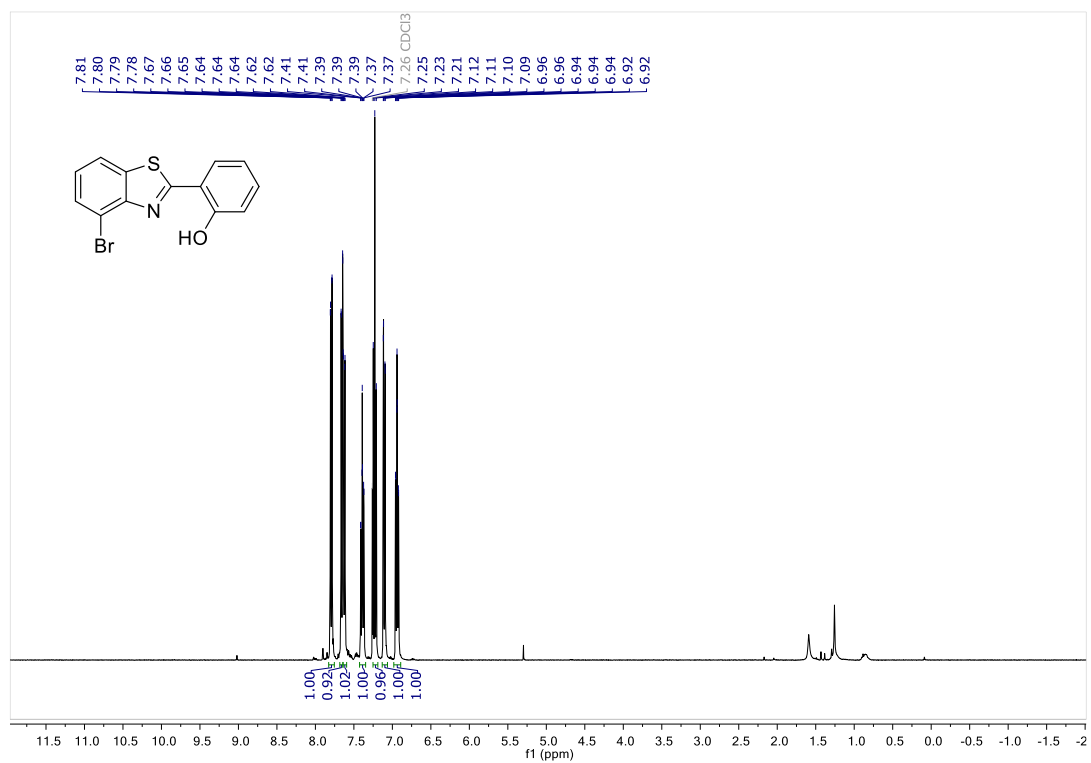


¹³C NMR

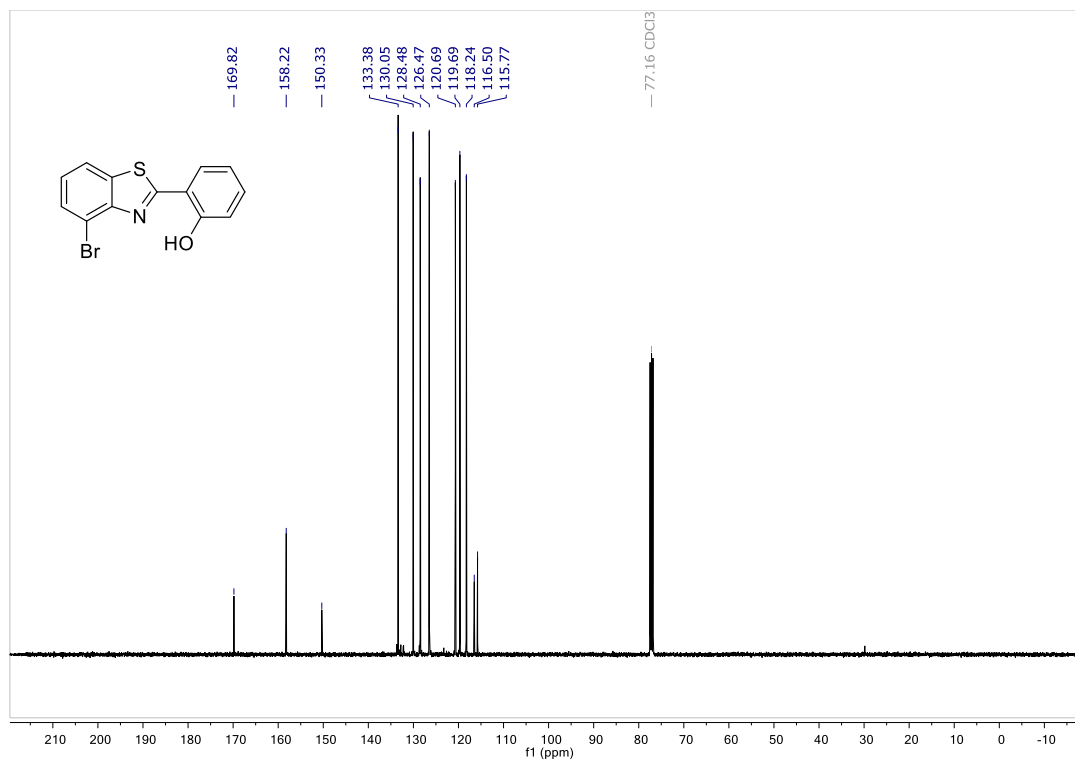


2-(2-hydroxyphenyl)-4-bromo-benzothiazole (5.22)

¹H NMR

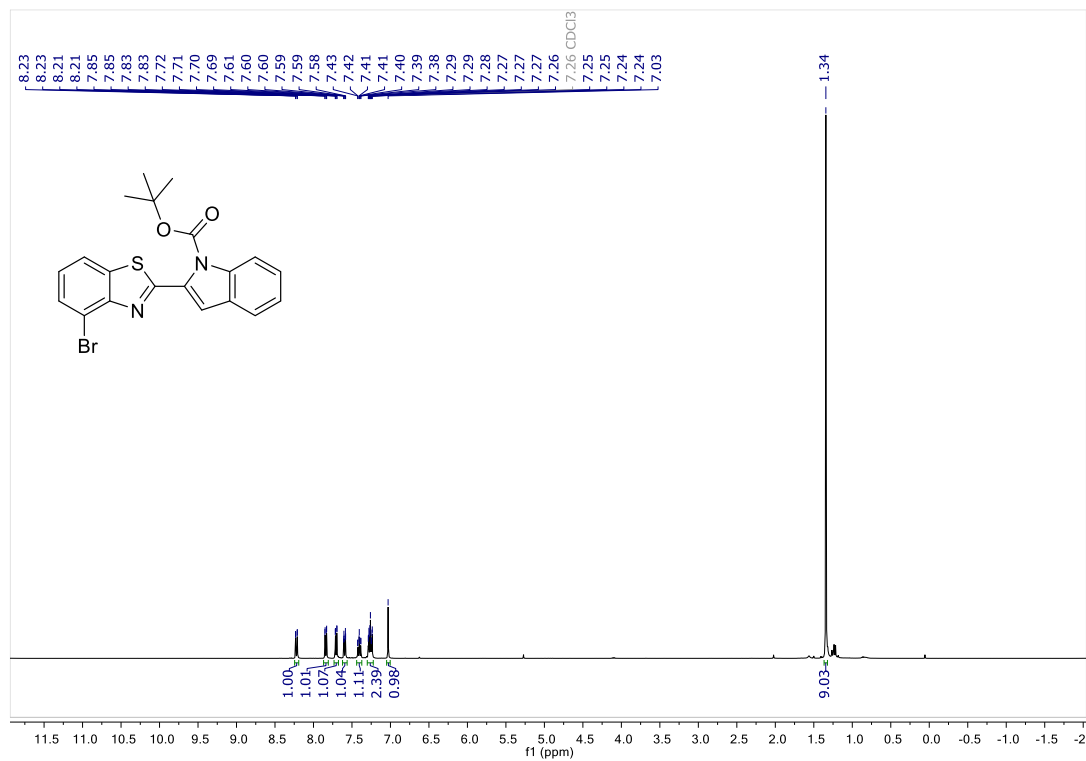


¹³C NMR

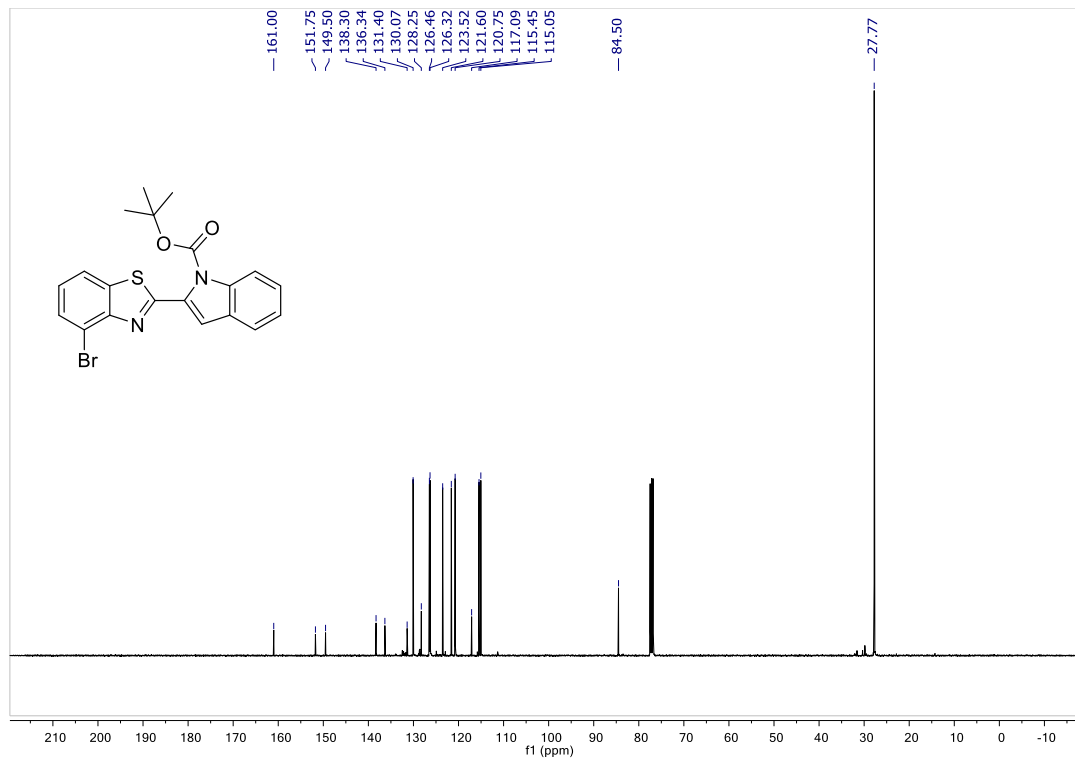


***tert*-butyl 2-(4-bromobenzo[d]thiazol-2-yl)-1H-indole-1-carboxylate (5.23)**

¹H NMR

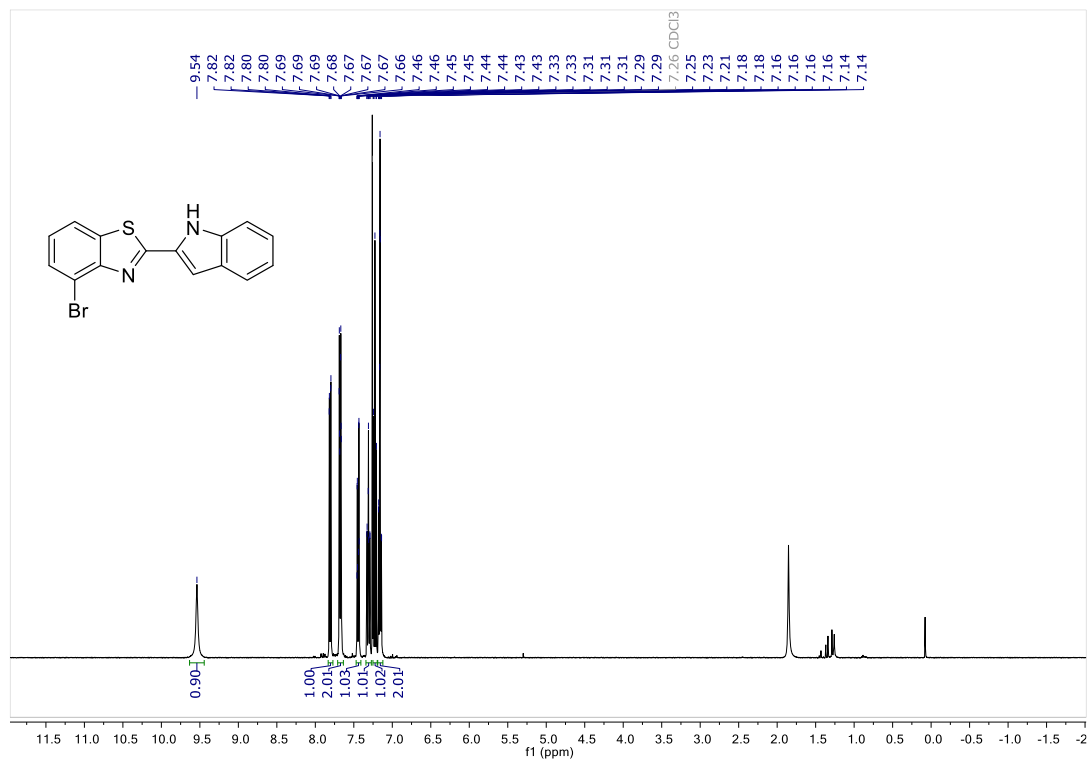


¹³C NMR

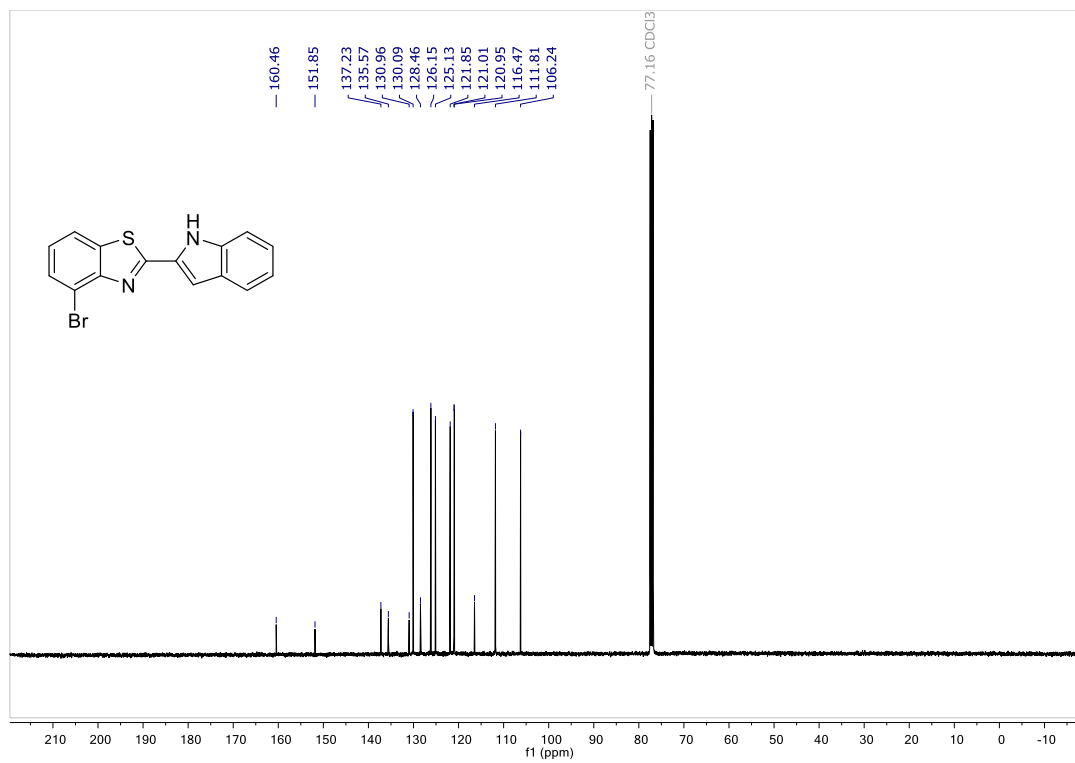


4-bromo-2-(1H-indol-2-yl)benzo[d]thiazole (5.24)

¹H NMR

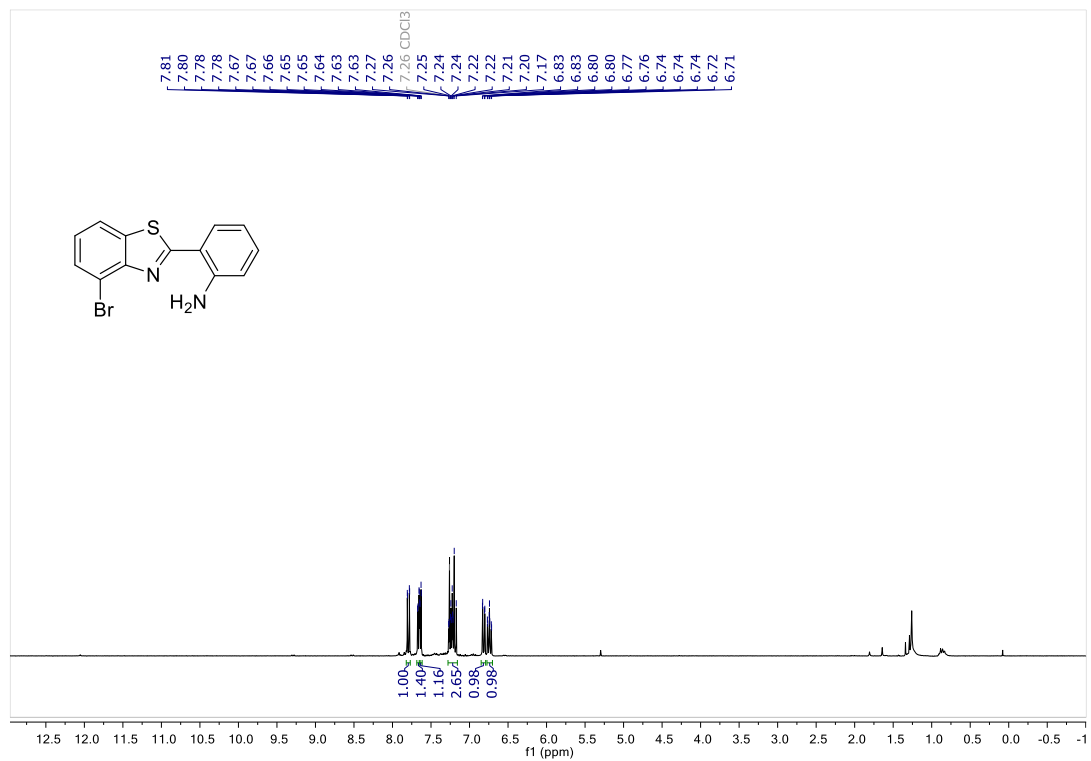


¹³C NMR

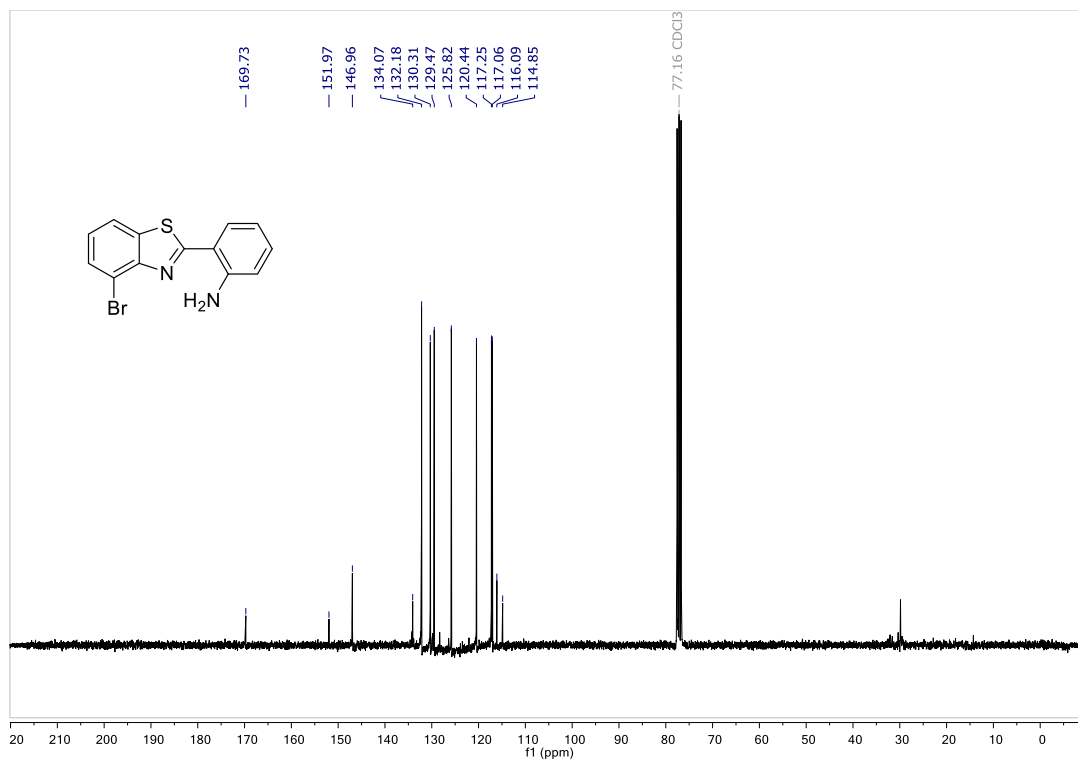


2-(2-aminophenyl)-4-bromobenzothiazole (5.25)

¹H NMR

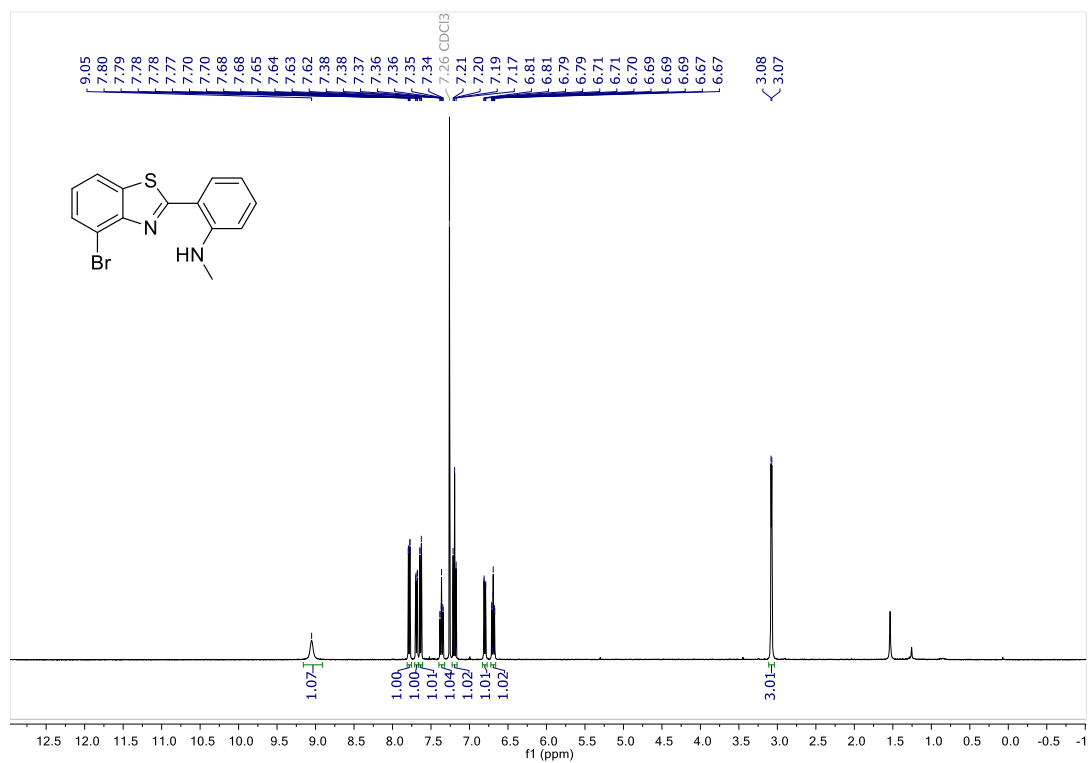


¹³C NMR

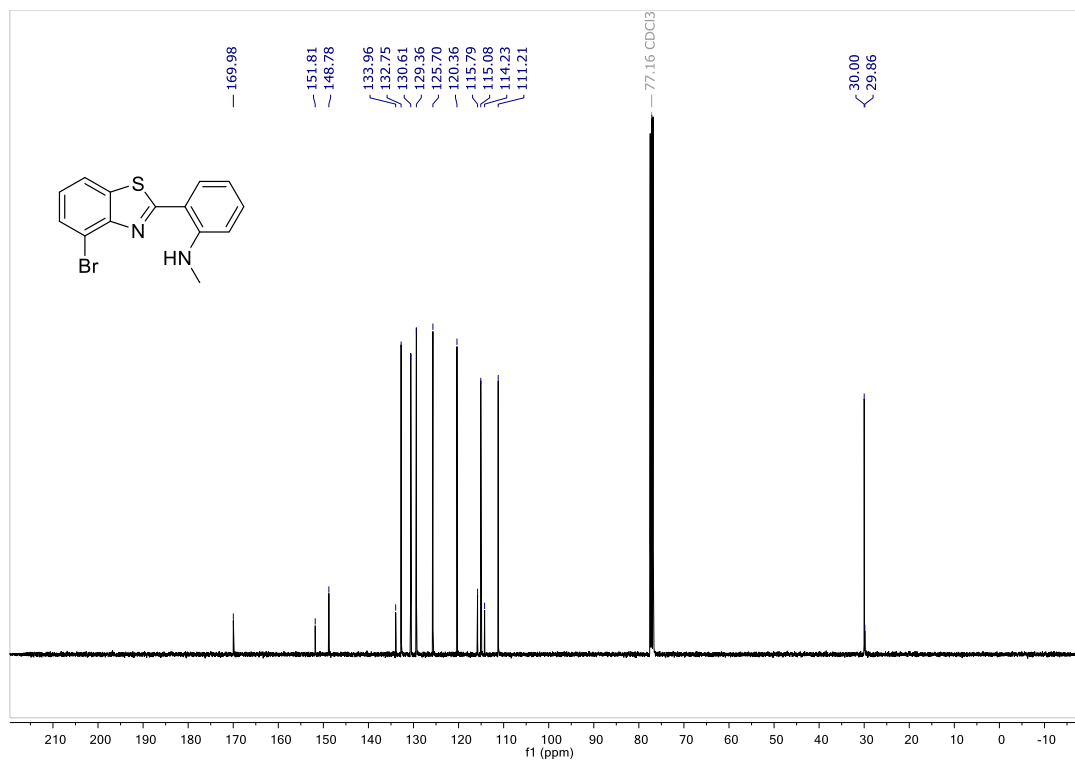


2-(2-methylaminophenyl)-4-bromobenzothiazole (5.26)

¹H NMR

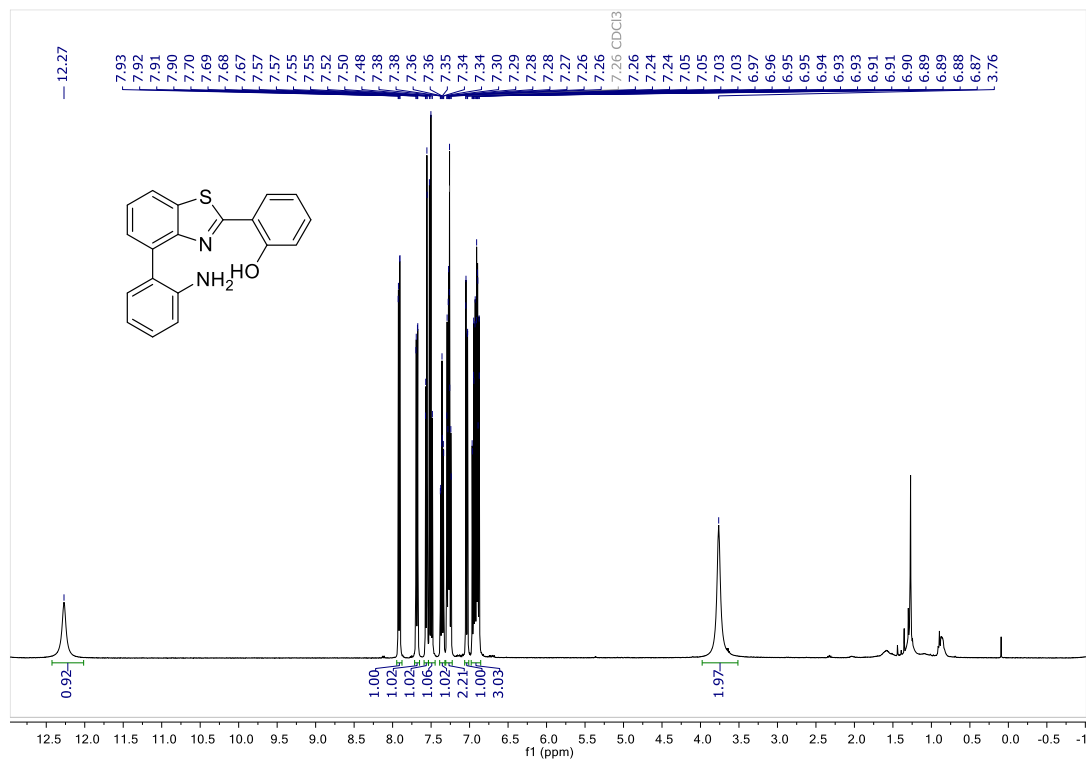


¹³C NMR

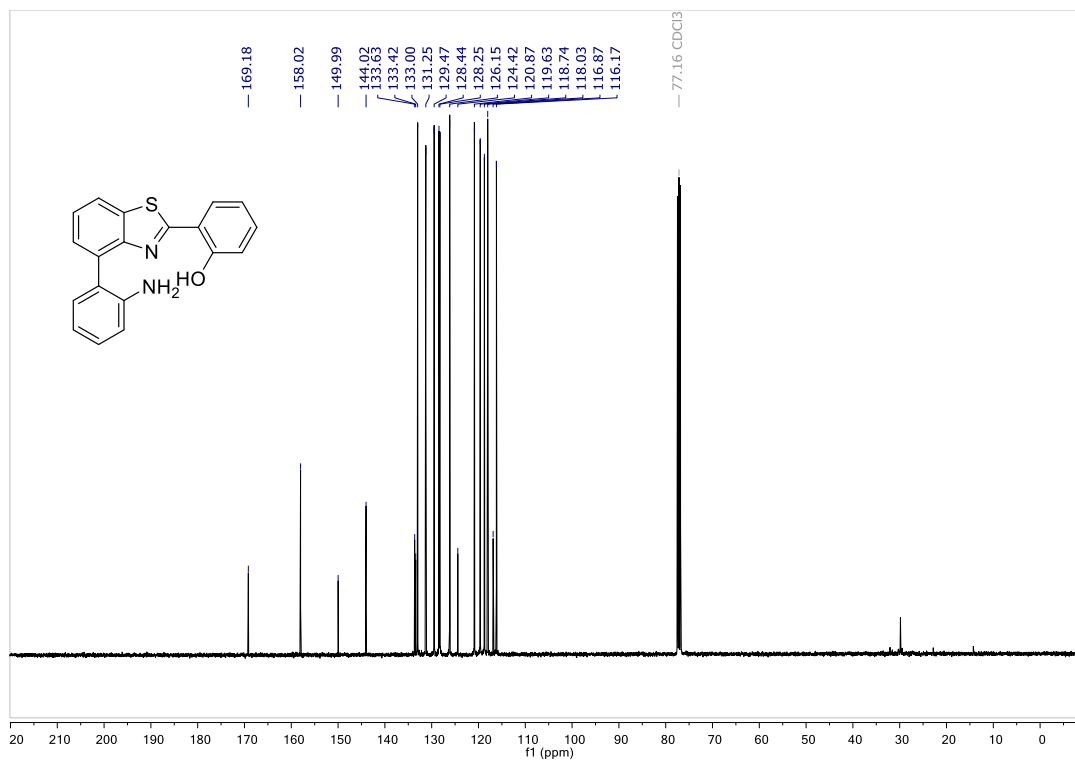


2-(2-hydroxyphenyl)-4-(2-aminophenyl)benzothiazole (5.27)

¹H NMR

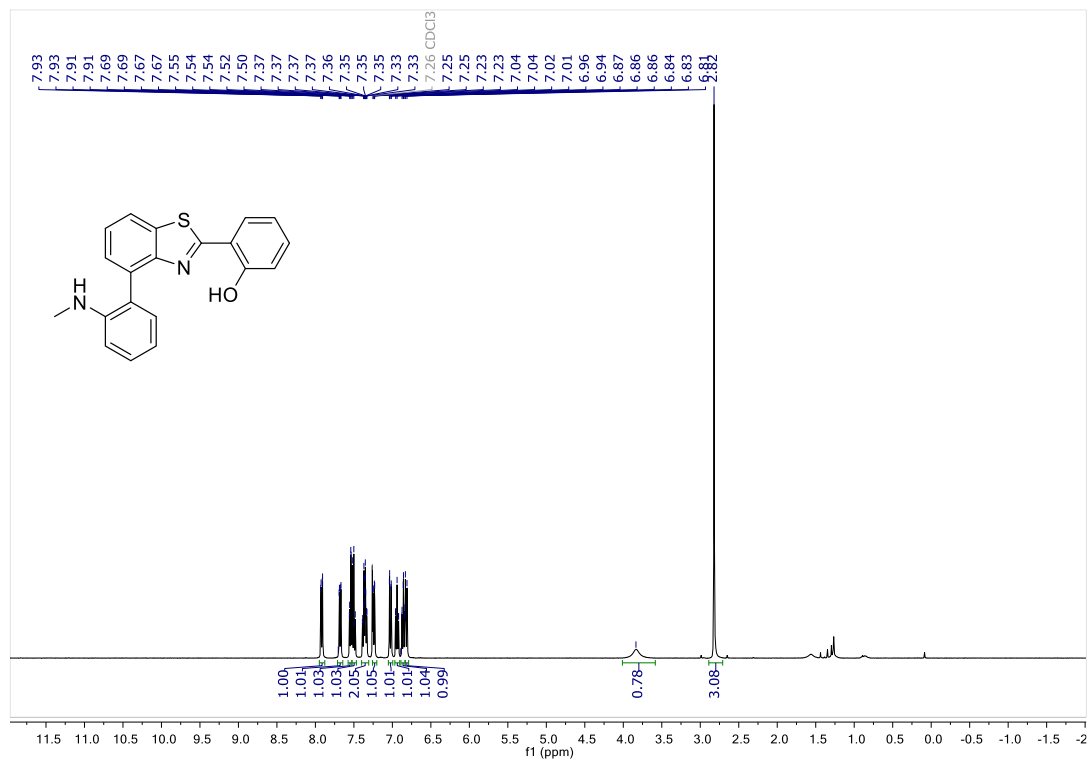


¹³C NMR

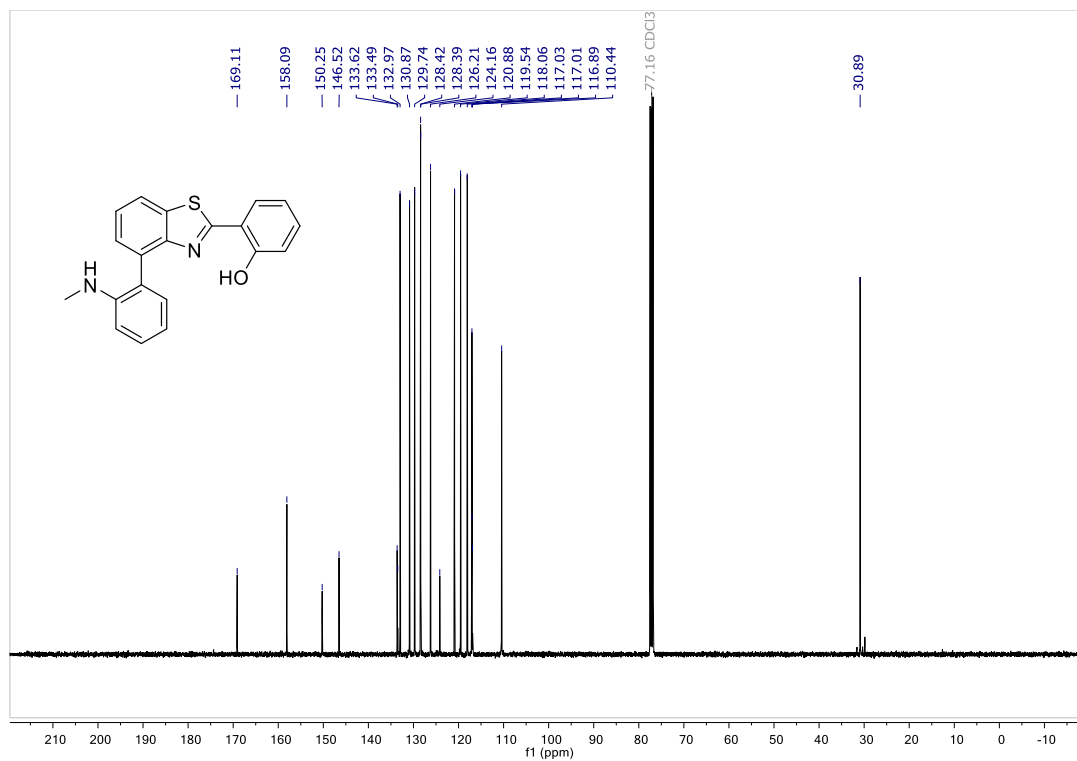


2-(2-hydroxyphenyl)-4-(2-methylaminophenyl)benzothiazole (5.28)

¹H NMR

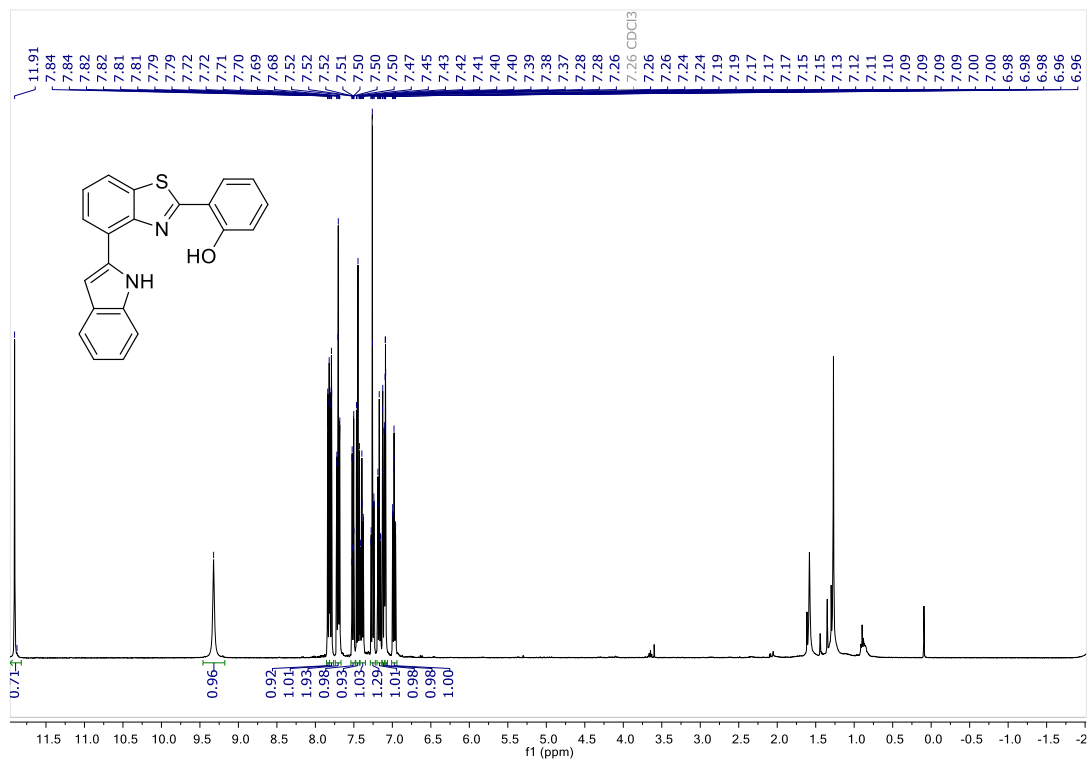


¹³C NMR

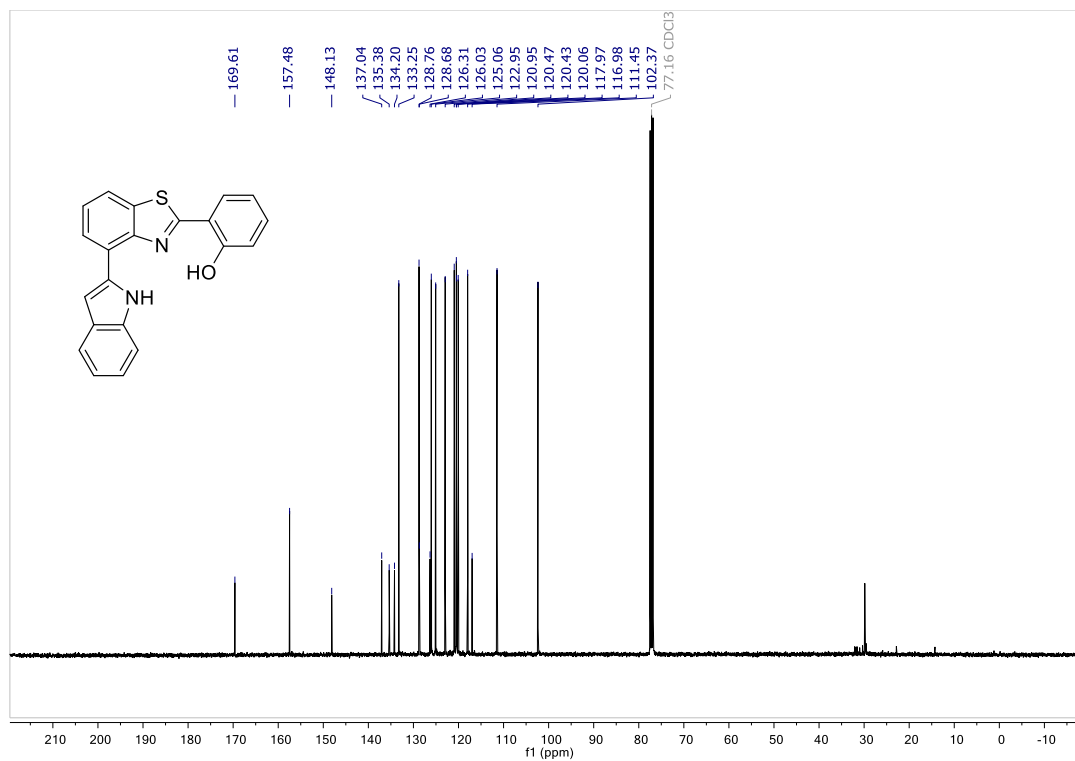


2-(4-(1H-indol-2-yl)benzo[d]thiazol-2-yl)phenol (5.29)

¹H NMR

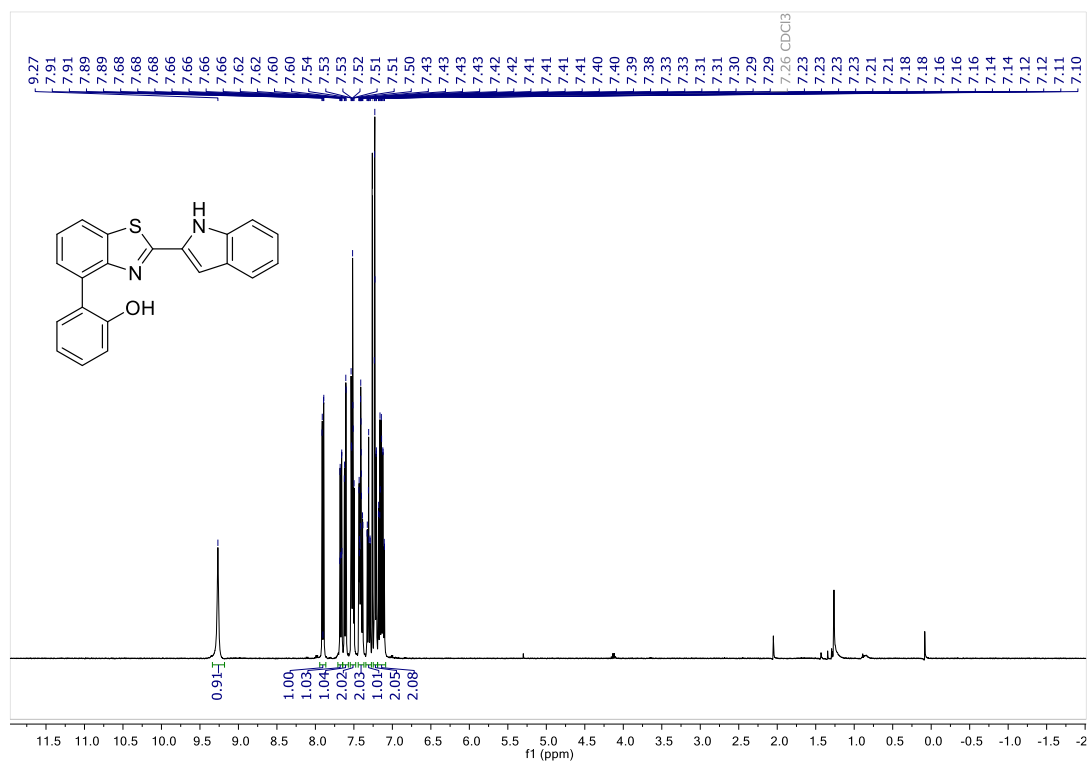


¹³C NMR

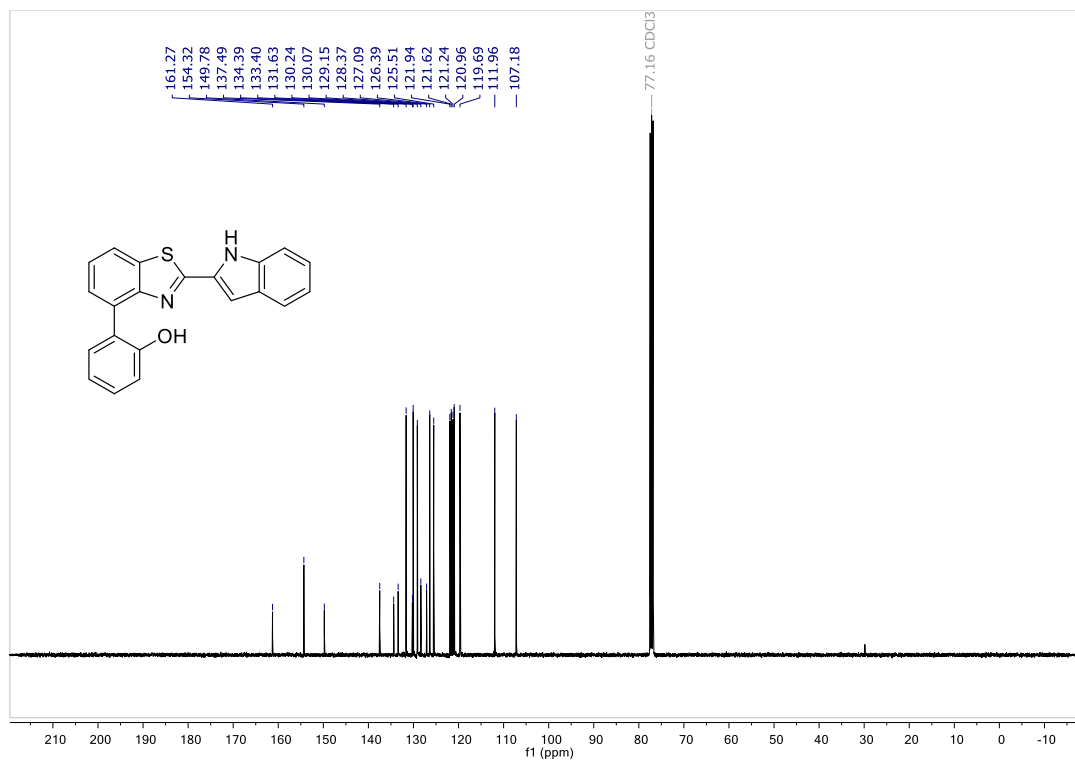


2-(2-(1H-indol-2-yl)benzo[d]thiazol-4-yl)phenol (5.30)

¹H NMR

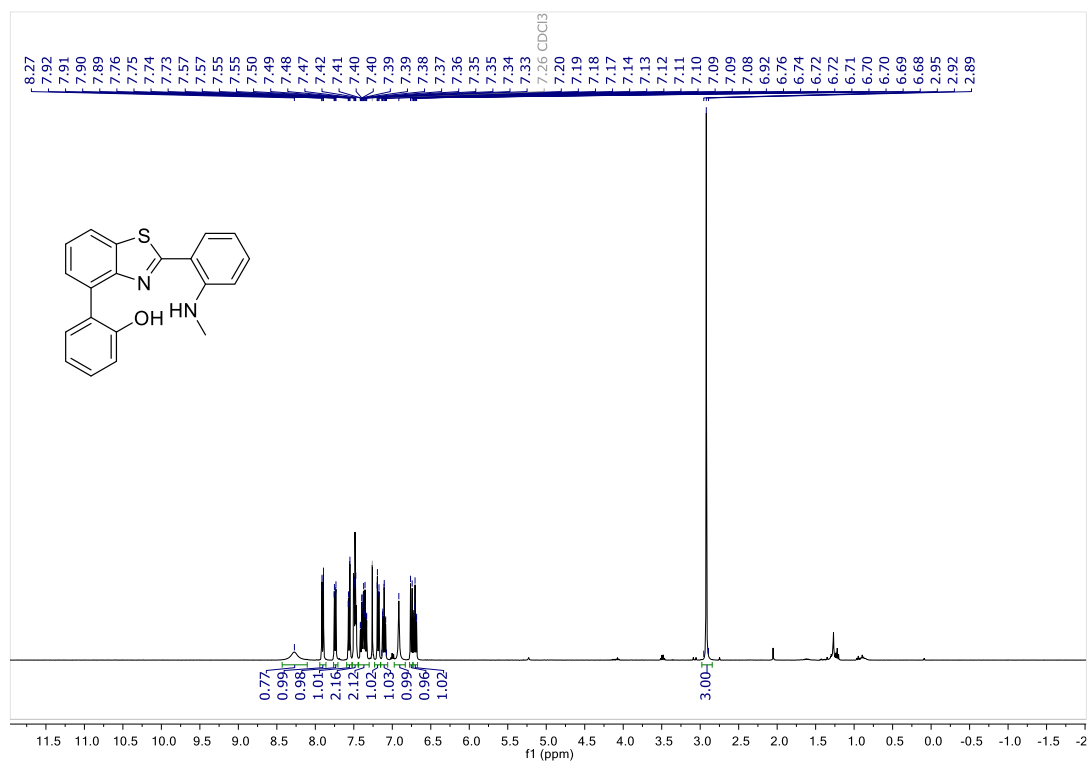


¹³C NMR

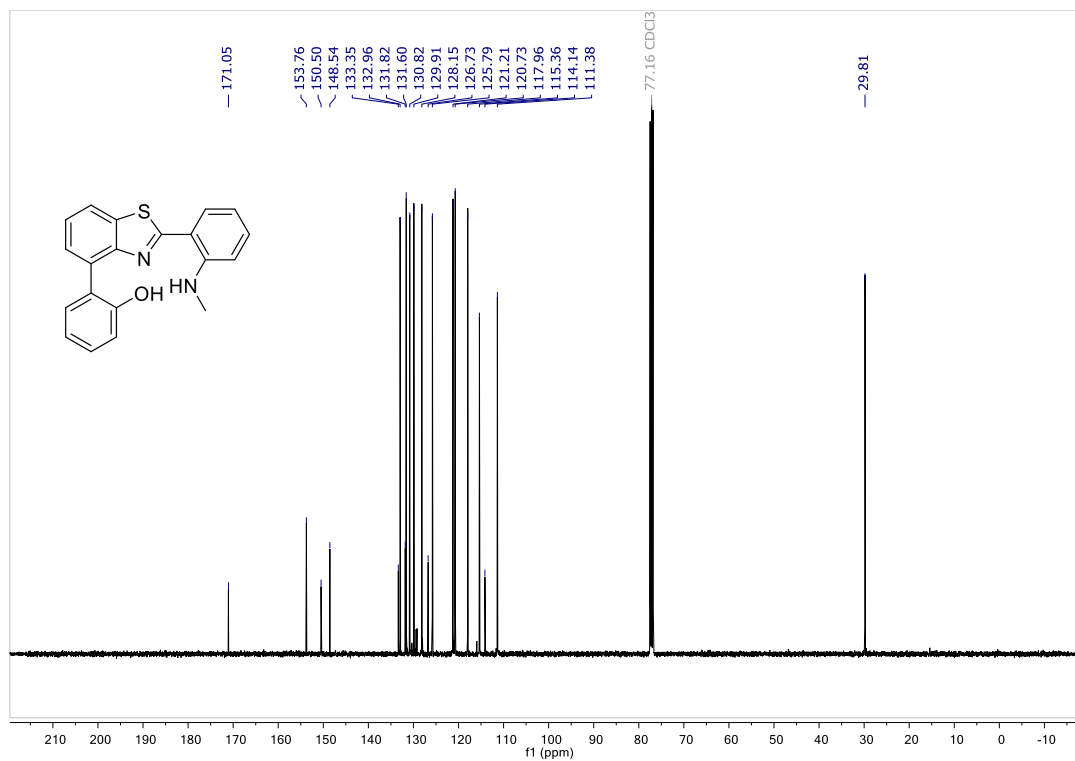


2-(2-methylaminophenyl)-4-(2-hydroxyphenyl)benzothiazole (5.31)

¹H NMR



¹³C NMR



X-ray Data Tables

2-(2-hydroxyphenyl)-6-methylbenzothiazole (5.11)

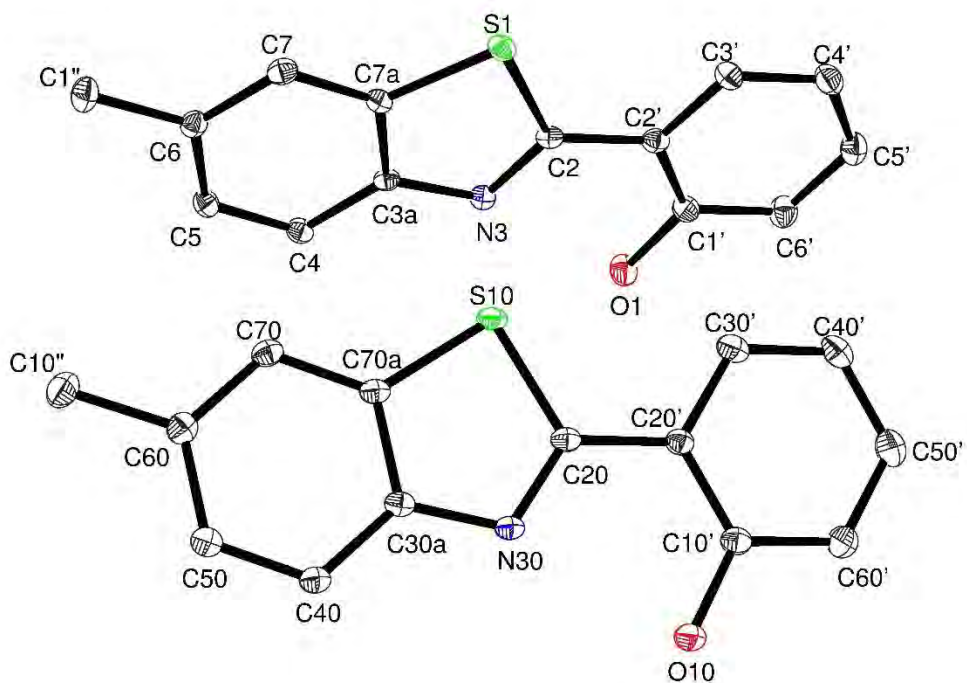


Table 1. Crystal data and structure refinement for MA-1-042.

Identification code	MA-1-042
Empirical formula	C ₁₄ H ₁₁ N O S
Formula weight	241.30
Temperature	100(2) K
Wavelength	0.71073 Å
Crystal system, space group	orthorhombic, P c a 21
Unit cell dimensions	a = 26.0273(18) Å alpha = 90 deg. b = 5.8320(4) Å beta = 90 deg. c = 14.5701(10) Å gamma = 90 deg.
Volume	2211.6(3) Å ³
Z, Calculated density	8, 1.449 Mg/m ³
Absorption coefficient	0.272 mm ⁻¹
F(000)	1008

Crystal size	0.22 x 0.08 x 0.06 mm
Theta range for data collection	1.56 to 30.50 deg.
Limiting indices	-37<=h<=37, -8<=k<=8, -20<=l<=20
Reflections collected / unique	65690 / 6772 [R(int) = 0.0390]
Completeness to theta = 30.50	99.9 %
Refinement method	Full-matrix least-squares on F ²
Data / restraints / parameters	6772 / 2 / 318
Goodness-of-fit on F ²	1.126
Final R indices [I>2sigma(I)]	R1 = 0.0297, wR2 = 0.0829
R indices (all data)	R1 = 0.0330, wR2 = 0.0886
Largest diff. peak and hole	0.497 and -0.307 e.A ⁻³

Table 2. Atomic coordinates ($\times 10^4$) and equivalent isotropic displacement parameters ($\text{\AA}^2 \times 10^3$) for map. U(eq) is defined as one third of the trace of the orthogonalized Uij tensor.

	x	y	z	U(eq)
C(1')	8311(1)	4907(3)	6315(1)	13(1)
C(1'')	11457(1)	1360(3)	7076(1)	18(1)
C(2)	9105(1)	2805(2)	6751(1)	11(1)
C(2')	8546(1)	2971(2)	6722(1)	12(1)
C(3')	8231(1)	1258(3)	7096(1)	15(1)
C(3A)	9922(1)	3830(2)	6556(1)	11(1)
C(4)	10346(1)	5162(3)	6289(1)	12(1)
C(4')	7699(1)	1424(3)	7061(1)	17(1)
C(5)	10836(1)	4330(2)	6457(1)	13(1)
C(5')	7473(1)	3336(3)	6651(1)	17(1)
C(6)	10919(1)	2198(2)	6898(1)	13(1)
C(6')	7775(1)	5073(3)	6286(1)	18(1)
C(7)	10499(1)	890(2)	7171(1)	13(1)
C(7A)	10005(1)	1716(2)	6992(1)	11(1)
C(10')	8487(1)	9868(3)	9663(1)	14(1)
C(10'')	11645(1)	6464(3)	8951(1)	19(1)
C(20')	8731(1)	7914(2)	9287(1)	12(1)
C(20)	9290(1)	7737(2)	9295(1)	11(1)
C(30')	8426(1)	6196(3)	8889(1)	16(1)
C(30A)	10104(1)	8818(2)	9491(1)	11(1)
C(40')	7894(1)	6393(3)	8858(1)	18(1)
C(40)	10522(1)	10170(3)	9744(1)	13(1)
C(50')	7662(1)	8326(3)	9237(1)	19(1)
C(50)	11016(1)	9383(3)	9561(1)	14(1)
C(60')	7950(1)	10045(3)	9636(1)	17(1)
C(60)	11103(1)	7256(2)	9131(1)	14(1)
C(70)	10687(1)	5900(2)	8876(1)	13(1)
C(70A)	10191(1)	6688(2)	9059(1)	12(1)
N(3)	9409(1)	4404(2)	6428(1)	12(1)
N(30)	9590(1)	9353(2)	9618(1)	11(1)
O(1)	8585(1)	6644(2)	5945(1)	18(1)
O(10)	8754(1)	11596(2)	10059(1)	18(1)
S(1)	9417(1)	435(1)	7234(1)	12(1)
S(10)	9609(1)	5385(1)	8815(1)	13(1)

Table 3. Bond lengths [Å] and angles [deg] for map.

C(1')-O(1)	1.3513(18)
C(1')-C(6')	1.400(2)
C(1')-C(2')	1.414(2)
C(1'')-C(6)	1.506(2)
C(1'')-H(1A)	0.9800
C(1'')-H(1B)	0.9800
C(1'')-H(1C)	0.9800
C(2)-N(3)	1.3112(18)
C(2)-C(2')	1.458(2)
C(2)-S(1)	1.7514(14)
C(2')-C(3')	1.4028(19)
C(3')-C(4')	1.387(2)
C(3')-H(3')	0.9500
C(3A)-N(3)	1.3885(18)
C(3A)-C(4)	1.404(2)
C(3A)-C(7A)	1.4037(19)
C(4)-C(5)	1.387(2)
C(4)-H(4)	0.9500
C(4')-C(5')	1.396(2)
C(4')-H(4')	0.9500
C(5)-C(6)	1.416(2)
C(5)-H(5)	0.9500
C(5')-C(6')	1.388(2)
C(5')-H(5')	0.9500
C(6)-C(7)	1.392(2)
C(6')-H(6')	0.9500
C(7)-C(7A)	1.3972(19)
C(7)-H(7)	0.9500
C(7A)-S(1)	1.7380(14)
C(10')-O(10)	1.3531(18)
C(10')-C(60')	1.400(2)
C(10')-C(20')	1.4156(19)
C(10'')-C(60)	1.509(2)
C(10'')-H(10A)	0.9800
C(10'')-H(10B)	0.9800
C(10'')-H(10C)	0.9800
C(20')-C(30')	1.4035(19)
C(20')-C(20)	1.460(2)
C(20)-N(30)	1.3109(18)
C(20)-S(10)	1.7487(14)
C(30')-C(40')	1.388(2)
C(30')-H(30A)	0.9500
C(30A)-N(30)	1.3870(19)
C(30A)-C(40)	1.394(2)
C(30A)-C(70A)	1.4110(19)
C(40')-C(50')	1.394(2)
C(40')-H(40A)	0.9500
C(40)-C(50)	1.389(2)
C(40)-H(40)	0.9500
C(50')-C(60')	1.381(2)
C(50')-H(50A)	0.9500
C(50)-C(60)	1.408(2)
C(50)-H(50)	0.9500
C(60')-H(60A)	0.9500
C(60)-C(70)	1.391(2)
C(70)-C(70A)	1.396(2)
C(70)-H(70)	0.9500
C(70A)-S(10)	1.7314(15)
O(1)-H(1)	0.867(19)
O(10)-H(10)	0.856(19)

O(1)-C(1')-C(6')	117.53(14)
O(1)-C(1')-C(2')	122.55(13)
C(6')-C(1')-C(2')	119.92(14)
C(6)-C(1")-H(1A)	109.5
C(6)-C(1")-H(1B)	109.5
H(1A)-C(1")-H(1B)	109.5
C(6)-C(1")-H(1C)	109.5
H(1A)-C(1")-H(1C)	109.5
H(1B)-C(1")-H(1C)	109.5
N(3)-C(2)-C(2')	123.06(12)
N(3)-C(2)-S(1)	115.11(11)
C(2')-C(2)-S(1)	121.82(10)
C(3')-C(2')-C(1')	118.59(13)
C(3')-C(2')-C(2)	121.65(12)
C(1')-C(2')-C(2)	119.75(12)
C(4')-C(3')-C(2')	121.28(14)
C(4')-C(3')-H(3')	119.4
C(2')-C(3')-H(3')	119.4
N(3)-C(3A)-C(4)	125.76(13)
N(3)-C(3A)-C(7A)	114.81(12)
C(4)-C(3A)-C(7A)	119.43(13)
C(5)-C(4)-C(3A)	118.67(14)
C(5)-C(4)-H(4)	120.7
C(3A)-C(4)-H(4)	120.7
C(3')-C(4')-C(5')	119.53(14)
C(3')-C(4')-H(4')	120.2
C(5')-C(4')-H(4')	120.2
C(4)-C(5)-C(6)	121.89(13)
C(4)-C(5)-H(5)	119.1
C(6)-C(5)-H(5)	119.1
C(6')-C(5')-C(4')	120.48(14)
C(6')-C(5')-H(5')	119.8
C(4')-C(5')-H(5')	119.8
C(7)-C(6)-C(5)	119.37(13)
C(7)-C(6)-C(1")	120.25(13)
C(5)-C(6)-C(1")	120.38(13)
C(5')-C(6')-C(1')	120.18(14)
C(5')-C(6')-H(6')	119.9
C(1')-C(6')-H(6')	119.9
C(6)-C(7)-C(7A)	118.77(14)
C(6)-C(7)-H(7)	120.6
C(7A)-C(7)-H(7)	120.6
C(7)-C(7A)-C(3A)	121.86(13)
C(7)-C(7A)-S(1)	128.59(11)
C(3A)-C(7A)-S(1)	109.55(10)
O(10)-C(10')-C(60')	118.01(13)
O(10)-C(10')-C(20')	122.27(13)
C(60')-C(10')-C(20')	119.71(13)
C(60)-C(10")-H(10A)	109.5
C(60)-C(10")-H(10B)	109.5
H(10A)-C(10")-H(10B)	109.5
C(60)-C(10")-H(10C)	109.5
H(10A)-C(10")-H(10C)	109.5
H(10B)-C(10")-H(10C)	109.5
C(30')-C(20')-C(10')	118.76(13)
C(30')-C(20')-C(20)	121.12(13)
C(10')-C(20')-C(20)	120.10(12)
N(30)-C(20)-C(20')	123.04(12)
N(30)-C(20)-S(10)	115.21(11)
C(20')-C(20)-S(10)	121.68(10)
C(40')-C(30')-C(20')	121.17(14)
C(40')-C(30')-H(30A)	119.4

C(20')-C(30')-H(30A)	119.4
N(30)-C(30A)-C(40)	126.25(13)
N(30)-C(30A)-C(70A)	114.32(12)
C(40)-C(30A)-C(70A)	119.42(14)
C(30')-C(40')-C(50')	119.14(14)
C(30')-C(40')-H(40A)	120.4
C(50')-C(40')-H(40A)	120.4
C(50)-C(40)-C(30A)	118.99(14)
C(50)-C(40)-H(40)	120.5
C(30A)-C(40)-H(40)	120.5
C(60')-C(50')-C(40')	121.18(15)
C(60')-C(50')-H(50A)	119.4
C(40')-C(50')-H(50A)	119.4
C(40)-C(50)-C(60)	121.67(14)
C(40)-C(50)-H(50)	119.2
C(60)-C(50)-H(50)	119.2
C(50')-C(60')-C(10')	120.04(14)
C(50')-C(60')-H(60A)	120.0
C(10')-C(60')-H(60A)	120.0
C(70)-C(60)-C(50)	119.60(14)
C(70)-C(60)-C(10")	120.55(13)
C(50)-C(60)-C(10")	119.85(14)
C(60)-C(70)-C(70A)	118.83(13)
C(60)-C(70)-H(70)	120.6
C(70A)-C(70)-H(70)	120.6
C(70)-C(70A)-C(30A)	121.49(13)
C(70)-C(70A)-S(10)	128.72(11)
C(30A)-C(70A)-S(10)	109.78(11)
C(2)-N(3)-C(3A)	111.21(12)
C(20)-N(30)-C(30A)	111.36(12)
C(1')-O(1)-H(1)	104.3(18)
C(10')-O(10)-H(10)	102.1(16)
C(7A)-S(1)-C(2)	89.31(7)
C(70A)-S(10)-C(20)	89.33(7)

Symmetry transformations used to generate equivalent atoms:

Table 4. Anisotropic displacement parameters ($\text{Å}^2 \times 10^3$) for map.
The anisotropic displacement factor exponent takes the form:
 $-2 \pi^2 [h^2 a^{*2} U_{11} + \dots + 2 h k a^* b^* U_{12}]$

	U11	U22	U33	U23	U13	U12
C(1')	14(1)	13(1)	13(1)	2(1)	0(1)	-1(1)
C(1")	12(1)	21(1)	20(1)	0(1)	-2(1)	3(1)
C(2)	14(1)	9(1)	9(1)	0(1)	-2(1)	0(1)
C(2')	15(1)	12(1)	10(1)	-2(1)	0(1)	-1(1)
C(3')	15(1)	14(1)	16(1)	1(1)	1(1)	-2(1)
C(3A)	13(1)	9(1)	9(1)	-1(1)	-1(1)	1(1)
C(4)	14(1)	11(1)	12(1)	1(1)	1(1)	-1(1)
C(4')	16(1)	17(1)	19(1)	1(1)	2(1)	-4(1)
C(5)	12(1)	14(1)	13(1)	1(1)	1(1)	-2(1)
C(5')	13(1)	22(1)	18(1)	-1(1)	0(1)	0(1)
C(6)	13(1)	14(1)	11(1)	-2(1)	0(1)	1(1)
C(6')	15(1)	19(1)	18(1)	2(1)	-1(1)	2(1)
C(7)	16(1)	12(1)	12(1)	0(1)	-1(1)	2(1)
C(7A)	13(1)	10(1)	10(1)	0(1)	0(1)	-2(1)
C(10')	16(1)	13(1)	12(1)	-1(1)	-1(1)	-1(1)
C(10")	17(1)	19(1)	21(1)	0(1)	3(1)	3(1)

C(20')	13(1)	11(1)	11(1)	-1(1)	0(1)	-1(1)
C(20)	15(1)	9(1)	9(1)	0(1)	0(1)	0(1)
C(30')	18(1)	14(1)	16(1)	-1(1)	0(1)	-3(1)
C(30A)	15(1)	10(1)	8(1)	0(1)	0(1)	-1(1)
C(40')	16(1)	19(1)	20(1)	-1(1)	-2(1)	-5(1)
C(40)	16(1)	11(1)	13(1)	-2(1)	0(1)	0(1)
C(50')	15(1)	23(1)	20(1)	2(1)	-2(1)	-2(1)
C(50)	16(1)	14(1)	14(1)	0(1)	0(1)	-1(1)
C(60')	15(1)	16(1)	19(1)	0(1)	-1(1)	2(1)
C(60)	16(1)	15(1)	12(1)	2(1)	2(1)	0(1)
C(70)	16(1)	11(1)	11(1)	0(1)	2(1)	1(1)
C(70A)	16(1)	10(1)	11(1)	-1(1)	1(1)	0(1)
N(3)	12(1)	11(1)	11(1)	0(1)	0(1)	0(1)
N(30)	15(1)	9(1)	9(1)	-1(1)	0(1)	0(1)
O(1)	16(1)	15(1)	24(1)	8(1)	2(1)	0(1)
O(10)	15(1)	15(1)	25(1)	-7(1)	-2(1)	0(1)
S(1)	14(1)	10(1)	13(1)	3(1)	0(1)	-1(1)
S(10)	16(1)	10(1)	13(1)	-3(1)	0(1)	-1(1)

2,2'-(benzo[d]thiazole-2,4-diyl)diphenol (5.15)

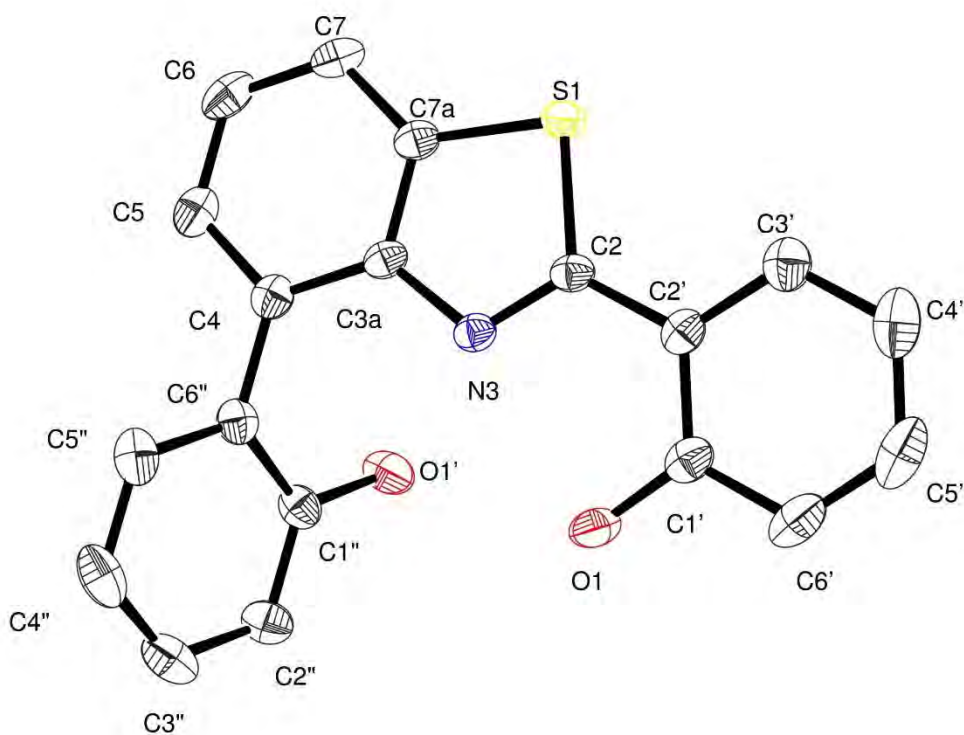


Table 1. Crystal data and structure refinement for OS-1-125-2.

Identification code	OS-1-125-2	
Empirical formula	C ₁₉ H ₁₃ N O ₂ S	
Formula weight	319.36	
Temperature	180(2) K	
Wavelength	0.71073 Å	
Crystal system, space group	monoclinic, C 2/c	
Unit cell dimensions	a = 10.6417(2) Å	alpha = 90 deg.
	b = 13.8292(3) Å	beta = 93.887(2) deg.
	c = 20.4893(4) Å	gamma = 90 deg.
Volume	3008.40(10) Å ³	
Z, Calculated density	8, 1.410 Mg/m ³	
Absorption coefficient	0.224 mm ⁻¹	
F(000)	1328	
Crystal size	0.38 x 0.24 x 0.2 mm	

Theta range for data collection	3.05 to 26.36 deg.
Limiting indices	-13<=h<=13, -17<=k<=17, -25<=l<=25
Reflections collected / unique	29848 / 3072 [R(int) = 0.0298]
Completeness to theta = 26.36	99.8 %
Refinement method	Full-matrix least-squares on F ²
Data / restraints / parameters	3072 / 2 / 216
Goodness-of-fit on F ²	1.057
Final R indices [I>2sigma(I)]	R1 = 0.0312, wR2 = 0.0760
R indices (all data)	R1 = 0.0351, wR2 = 0.0787
Largest diff. peak and hole	0.220 and -0.290 e.A ⁻³

Table 2. Atomic coordinates ($\times 10^4$) and equivalent isotropic displacement parameters ($\text{\AA}^2 \times 10^3$) for omar2. U(eq) is defined as one third of the trace of the orthogonalized Uij tensor.

	x	y	z	U(eq)
C(1")	2468(1)	-1016(1)	2319(1)	26(1)
C(2")	2230(2)	-1937(1)	2552(1)	32(1)
C(3")	2916(2)	-2720(1)	2353(1)	36(1)
C(4")	3851(2)	-2588(1)	1926(1)	37(1)
C(5")	4086(1)	-1673(1)	1693(1)	31(1)
C(6")	3396(1)	-871(1)	1875(1)	24(1)
C(4)	3652(1)	99(1)	1604(1)	24(1)
C(5)	4851(1)	502(1)	1646(1)	30(1)
C(6)	5094(1)	1409(1)	1381(1)	33(1)
C(7)	4154(1)	1942(1)	1054(1)	29(1)
C(7A)	2951(1)	1541(1)	993(1)	23(1)
C(3A)	2694(1)	636(1)	1266(1)	21(1)
C(2)	789(1)	952(1)	798(1)	21(1)
C(2')	-532(1)	780(1)	598(1)	23(1)
C(3')	-1200(1)	1369(1)	142(1)	30(1)
C(4')	-2446(2)	1189(1)	-49(1)	38(1)
C(5')	-3048(1)	415(1)	222(1)	42(1)
C(6')	-2420(1)	-177(1)	677(1)	37(1)
C(1')	-1160(1)	-3(1)	869(1)	26(1)
N(3)	1461(1)	331(1)	1148(1)	21(1)
O(1')	1828(1)	-227(1)	2520(1)	35(1)
O(1)	-577(1)	-599(1)	1324(1)	32(1)
S(1)	1591(1)	2002(1)	590(1)	25(1)

Table 3. Bond lengths [Å] and angles [deg] for omar2.

C(1")-O(1')	1.3656(16)
C(1")-C(2")	1.3897(19)
C(1")-C(6")	1.4002(19)
C(2")-C(3")	1.383(2)
C(2")-H(2B)	0.9500
C(3")-C(4")	1.381(2)
C(3")-H(3B)	0.9500
C(4")-C(5")	1.382(2)
C(4")-H(4B)	0.9500
C(5")-C(6")	1.3942(19)
C(5")-H(5B)	0.9500
C(6")-C(4)	1.4840(19)
C(4)-C(5)	1.3899(19)
C(4)-C(3A)	1.4055(18)
C(5)-C(6)	1.399(2)
C(5)-H(5)	0.9500
C(6)-C(7)	1.378(2)
C(6)-H(6)	0.9500
C(7)-C(7A)	1.3929(18)
C(7)-H(7)	0.9500
C(7A)-C(3A)	1.4053(18)
C(7A)-S(1)	1.7380(14)
C(3A)-N(3)	1.3834(16)
C(2)-N(3)	1.3005(17)
C(2)-C(2')	1.4572(18)
C(2)-S(1)	1.7514(13)
C(2')-C(3')	1.398(2)
C(2')-C(1')	1.4061(19)
C(3')-C(4')	1.379(2)
C(3')-H(3A)	0.9500
C(4')-C(5')	1.383(2)
C(4')-H(4A)	0.9500
C(5')-C(6')	1.379(2)
C(5')-H(5A)	0.9500
C(6')-C(1')	1.393(2)
C(6')-H(6A)	0.9500
C(1')-O(1)	1.3619(18)
O(1')-H(1A)	0.843(9)
O(1)-H(1)	0.848(9)
O(1')-C(1")-C(2")	121.47(12)
O(1')-C(1")-C(6")	118.01(12)
C(2")-C(1")-C(6")	120.51(12)
C(3")-C(2")-C(1")	120.28(14)
C(3")-C(2")-H(2B)	119.9
C(1")-C(2")-H(2B)	119.9
C(4")-C(3")-C(2")	120.02(14)
C(4")-C(3")-H(3B)	120.0
C(2")-C(3")-H(3B)	120.0
C(3")-C(4")-C(5")	119.67(14)
C(3")-C(4")-H(4B)	120.2
C(5")-C(4")-H(4B)	120.2
C(4")-C(5")-C(6")	121.66(14)
C(4")-C(5")-H(5B)	119.2
C(6")-C(5")-H(5B)	119.2
C(5")-C(6")-C(1")	117.83(13)
C(5")-C(6")-C(4)	120.34(12)
C(1")-C(6")-C(4)	121.82(12)
C(5)-C(4)-C(3A)	116.80(12)
C(5)-C(4)-C(6")	122.01(12)

C(3A)-C(4)-C(6")	121.13(12)
C(4)-C(5)-C(6)	121.91(13)
C(4)-C(5)-H(5)	119.0
C(6)-C(5)-H(5)	119.0
C(7)-C(6)-C(5)	121.43(13)
C(7)-C(6)-H(6)	119.3
C(5)-C(6)-H(6)	119.3
C(6)-C(7)-C(7A)	117.56(13)
C(6)-C(7)-H(7)	121.2
C(7A)-C(7)-H(7)	121.2
C(7)-C(7A)-C(3A)	121.46(12)
C(7)-C(7A)-S(1)	128.86(11)
C(3A)-C(7A)-S(1)	109.68(9)
N(3)-C(3A)-C(7A)	114.19(11)
N(3)-C(3A)-C(4)	124.95(11)
C(7A)-C(3A)-C(4)	120.82(12)
N(3)-C(2)-C(2')	122.11(11)
N(3)-C(2)-S(1)	114.95(10)
C(2')-C(2)-S(1)	122.94(10)
C(3')-C(2')-C(1')	118.67(12)
C(3')-C(2')-C(2)	122.02(12)
C(1')-C(2')-C(2)	119.31(12)
C(4')-C(3')-C(2')	121.30(14)
C(4')-C(3')-H(3A)	119.3
C(2')-C(3')-H(3A)	119.3
C(3')-C(4')-C(5')	119.24(15)
C(3')-C(4')-H(4A)	120.4
C(5')-C(4')-H(4A)	120.4
C(6')-C(5')-C(4')	120.98(14)
C(6')-C(5')-H(5A)	119.5
C(4')-C(5')-H(5A)	119.5
C(5')-C(6')-C(1')	120.09(15)
C(5')-C(6')-H(6A)	120.0
C(1')-C(6')-H(6A)	120.0
O(1)-C(1')-C(6')	118.27(13)
O(1)-C(1')-C(2')	122.01(12)
C(6')-C(1')-C(2')	119.70(14)
C(2)-N(3)-C(3A)	112.03(11)
C(1")-O(1')-H(1A)	110.4(14)
C(1')-O(1)-H(1)	107.5(15)
C(7A)-S(1)-C(2)	89.12(6)

Symmetry transformations used to generate equivalent atoms:

Table 4. Anisotropic displacement parameters ($\text{\AA}^2 \times 10^3$) for omar2.
 The anisotropic displacement factor exponent takes the form:
 $-2 \pi^2 [h^2 a^{*2} U_{11} + \dots + 2 h k a^* b^* U_{12}]$

	U11	U22	U33	U23	U13	U12
C(1")	30(1)	24(1)	23(1)	-1(1)	2(1)	3(1)
C(2")	40(1)	28(1)	28(1)	3(1)	4(1)	-2(1)
C(3")	53(1)	23(1)	32(1)	1(1)	-6(1)	2(1)
C(4")	49(1)	32(1)	29(1)	-5(1)	-5(1)	15(1)
C(5")	32(1)	39(1)	23(1)	-2(1)	0(1)	9(1)
C(6")	26(1)	28(1)	19(1)	0(1)	-2(1)	2(1)
C(4)	25(1)	30(1)	18(1)	-2(1)	4(1)	1(1)
C(5)	24(1)	43(1)	23(1)	-2(1)	1(1)	0(1)
C(6)	24(1)	47(1)	27(1)	-6(1)	4(1)	-12(1)
C(7)	31(1)	32(1)	24(1)	-2(1)	7(1)	-11(1)
C(7A)	26(1)	25(1)	20(1)	-2(1)	5(1)	-3(1)
C(3A)	23(1)	24(1)	18(1)	-3(1)	6(1)	-3(1)
C(2)	24(1)	20(1)	20(1)	-1(1)	7(1)	-2(1)
C(2')	22(1)	25(1)	22(1)	-6(1)	5(1)	0(1)
C(3')	29(1)	35(1)	27(1)	-3(1)	3(1)	3(1)
C(4')	31(1)	50(1)	33(1)	-10(1)	-4(1)	10(1)
C(5')	23(1)	55(1)	47(1)	-22(1)	1(1)	-1(1)
C(6')	26(1)	38(1)	48(1)	-13(1)	10(1)	-9(1)
C(1')	25(1)	26(1)	30(1)	-7(1)	8(1)	-2(1)
N(3)	22(1)	21(1)	20(1)	-1(1)	5(1)	-2(1)
O(1')	46(1)	26(1)	35(1)	4(1)	21(1)	7(1)
O(1)	29(1)	29(1)	41(1)	4(1)	10(1)	-7(1)
S(1)	27(1)	22(1)	27(1)	4(1)	4(1)	-3(1)

6,6-difluoro-10-methyl-6*H*-benzo[*e*]benzo[4,5]thiazolo[3,2-*c*][1,3,2]oxazaborinin-7-ium-6-uide (5.17)

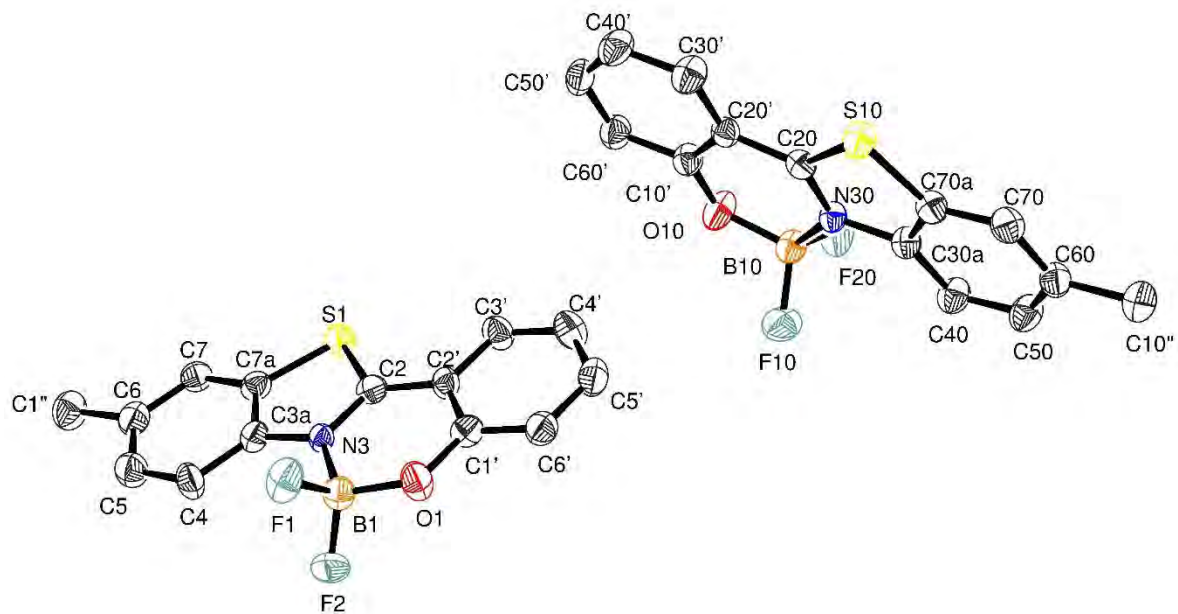


Figure 1 : Asymmetric Unit

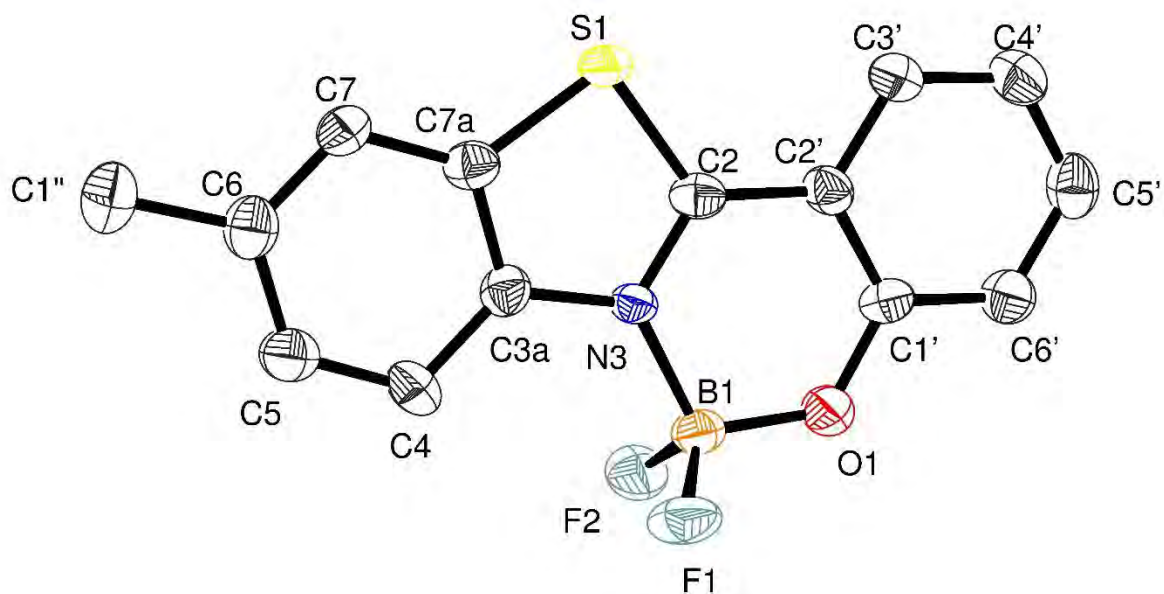


Figure 2 : Molecule

Table 1. Crystal data and structure refinement for OS-1-130-2.

Identification code	OS-1-130-2	
Empirical formula	C14 H10 B F2 N O S	
Formula weight	289.10	
Temperature	173(2) K	
Wavelength	0.71073 Å	
Crystal system, space group	triclinic, P -1	
Unit cell dimensions	a = 7.4543(3) Å	alpha = 82.933(2) deg.
	b = 7.5121(3) Å	beta = 81.709(2) deg.
	c = 23.0392(9) Å	gamma = 87.306(3) deg.
Volume	1266.39(9) Å ³	
Z, Calculated density	4, 1.516 Mg/m ³	
Absorption coefficient	0.272 mm ⁻¹	
F(000)	592	
Crystal size	0.20 x 0.05 x 0.05 mm	
Theta range for data collection	5.30 to 26.37 deg.	
Limiting indices	-9<=h<=9, -9<=k<=9, -28<=l<=28	
Reflections collected / unique	68259 / 5149 [R(int) = 0.0936]	
Completeness to theta = 26.37	99.2 %	
Max. and min. transmission	0.7461 and 0.7021	
Refinement method	Full-matrix least-squares on F ²	
Data / restraints / parameters	5149 / 0 / 363	
Goodness-of-fit on F ²	1.053	
Final R indices [I>2sigma(I)]	R1 = 0.0536, wR2 = 0.0982	
R indices (all data)	R1 = 0.0863, wR2 = 0.1103	
Largest diff. peak and hole	0.389 and -0.281 e.Å ⁻³	

Table 2. Atomic coordinates ($\times 10^4$) and equivalent isotropic displacement parameters ($\text{\AA}^2 \times 10^3$) for os1302_0m. U(eq) is defined as one third of the trace of the orthogonalized Uij tensor.

	x	y	z	U(eq)
S(1)	3298(1)	2891(1)	4585(1)	34(1)
S(10)	2223(1)	11701(1)	371(1)	33(1)
C(2)	5148(4)	3526(4)	4078(1)	30(1)
F(20)	-88(3)	5736(3)	852(1)	51(1)
N(3)	6692(3)	3353(3)	4304(1)	25(1)
F(10)	2824(3)	5436(2)	1024(1)	49(1)
C(3A)	6487(4)	2707(4)	4901(1)	30(1)
O(10)	709(3)	6832(3)	1669(1)	41(1)
N(30)	1726(3)	8354(3)	669(1)	25(1)
C(2')	5084(4)	4138(4)	3467(1)	30(1)
C(1')	6717(4)	4545(4)	3101(1)	32(1)
C(7A)	4701(4)	2365(4)	5131(1)	31(1)
C(6')	6707(4)	5075(4)	2505(1)	37(1)
C(7)	4207(4)	1712(4)	5725(1)	33(1)
C(6)	5558(5)	1408(4)	6084(1)	38(1)
C(5)	7361(4)	1763(5)	5841(2)	42(1)
C(4)	7864(5)	2398(4)	5260(1)	39(1)
C(1'')	5123(5)	731(5)	6727(1)	48(1)
C(20)	1602(4)	9906(4)	890(1)	26(1)
C(4')	3482(5)	4864(5)	2628(2)	44(1)
C(5')	5085(5)	5227(4)	2271(1)	40(1)
C(70A)	2677(4)	10274(4)	-175(1)	30(1)
C(3')	3460(4)	4313(4)	3223(1)	37(1)
C(30A)	2334(4)	8511(4)	63(1)	28(1)
O(1)	8304(3)	4439(3)	3313(1)	43(1)
C(40)	2581(4)	7128(4)	-300(1)	36(1)
B(1)	8570(5)	3848(5)	3916(2)	34(1)
C(50)	3174(5)	7576(4)	-891(1)	39(1)
F(2)	9675(2)	2298(3)	3939(1)	45(1)
C(60)	3539(4)	9343(4)	-1139(1)	35(1)
F(1)	9336(2)	5151(3)	4161(1)	48(1)
C(70)	3281(4)	10708(4)	-777(1)	34(1)
C(20')	1021(4)	10025(4)	1508(1)	27(1)
C(10')	621(4)	8429(4)	1877(1)	31(1)
C(60')	116(4)	8485(4)	2484(1)	36(1)
C(50')	-8(4)	10113(4)	2711(1)	37(1)
C(40')	361(5)	11684(4)	2344(1)	41(1)
C(30')	875(5)	11654(4)	1745(1)	38(1)
C(10'')	4164(5)	9738(5)	-1790(1)	45(1)
B(10)	1270(5)	6521(5)	1066(2)	32(1)

Table 3. Bond lengths [Å] and angles [deg] for os1302_0m.

S(1)-C(2)	1.720(3)
S(1)-C(7A)	1.747(3)
S(10)-C(20)	1.723(3)
S(10)-C(70A)	1.738(3)
C(2)-N(3)	1.325(4)
C(2)-C(2')	1.432(4)
F(20)-B(10)	1.375(4)
N(3)-C(3A)	1.391(4)
N(3)-B(1)	1.582(4)
F(10)-B(10)	1.383(4)
C(3A)-C(7A)	1.383(4)
C(3A)-C(4)	1.401(4)
O(10)-C(10')	1.341(3)
O(10)-B(10)	1.437(4)
N(30)-C(20)	1.323(3)
N(30)-C(30A)	1.397(4)
N(30)-B(10)	1.578(4)
C(2')-C(3')	1.400(4)
C(2')-C(1')	1.401(4)
C(1')-O(1)	1.340(4)
C(1')-C(6')	1.382(4)
C(7A)-C(7)	1.399(4)
C(6')-C(5')	1.389(4)
C(6')-H(6')	0.9500
C(7)-C(6)	1.387(4)
C(7)-H(7)	0.9500
C(6)-C(5)	1.404(4)
C(6)-C(1")	1.500(4)
C(5)-C(4)	1.370(5)
C(5)-H(5)	0.9500
C(4)-H(4)	0.9500
C(1")-H(1A)	0.9800
C(1")-H(1B)	0.9800
C(1")-H(1C)	0.9800
C(20)-C(20')	1.438(4)
C(4')-C(5')	1.368(5)
C(4')-C(3')	1.380(4)
C(4')-H(4')	0.9500
C(5')-H(5')	0.9500
C(70A)-C(30A)	1.391(4)
C(70A)-C(70)	1.397(4)
C(3')-H(3')	0.9500
C(30A)-C(40)	1.401(4)
O(1)-B(1)	1.442(4)
C(40)-C(50)	1.376(4)
C(40)-H(40)	0.9500
B(1)-F(1)	1.373(4)
B(1)-F(2)	1.394(4)
C(50)-C(60)	1.402(4)
C(50)-H(50)	0.9500
C(60)-C(70)	1.389(4)
C(60)-C(10")	1.503(4)
C(70)-H(70)	0.9500
C(20')-C(30')	1.395(4)
C(20')-C(10')	1.400(4)
C(10')-C(60')	1.401(4)
C(60')-C(50')	1.381(4)
C(60')-H(60')	0.9500
C(50')-C(40')	1.379(5)
C(50')-H(50')	0.9500

C(40')-C(30')	1.379(4)
C(40')-H(40')	0.9500
C(30')-H(30')	0.9500
C(10")-H(10D)	0.9800
C(10")-H(10E)	0.9800
C(10")-H(10F)	0.9800
C(2)-S(1)-C(7A)	90.26(14)
C(20)-S(10)-C(70A)	90.43(14)
N(3)-C(2)-C(2')	122.1(3)
N(3)-C(2)-S(1)	113.1(2)
C(2')-C(2)-S(1)	124.8(2)
C(2)-N(3)-C(3A)	113.8(2)
C(2)-N(3)-B(1)	121.7(2)
C(3A)-N(3)-B(1)	124.5(2)
C(7A)-C(3A)-N(3)	112.6(3)
C(7A)-C(3A)-C(4)	120.7(3)
N(3)-C(3A)-C(4)	126.8(3)
C(10')-O(10)-B(10)	125.7(2)
C(20)-N(30)-C(30A)	113.3(2)
C(20)-N(30)-B(10)	122.2(2)
C(30A)-N(30)-B(10)	124.4(2)
C(3')-C(2')-C(1')	119.2(3)
C(3')-C(2')-C(2)	122.5(3)
C(1')-C(2')-C(2)	118.3(3)
O(1)-C(1')-C(6')	118.7(3)
O(1)-C(1')-C(2')	121.6(3)
C(6')-C(1')-C(2')	119.7(3)
C(3A)-C(7A)-C(7)	121.5(3)
C(3A)-C(7A)-S(1)	110.3(2)
C(7)-C(7A)-S(1)	128.2(2)
C(1')-C(6')-C(5')	120.3(3)
C(1')-C(6')-H(6')	119.9
C(5')-C(6')-H(6')	119.9
C(6)-C(7)-C(7A)	118.3(3)
C(6)-C(7)-H(7)	120.8
C(7A)-C(7)-H(7)	120.8
C(7)-C(6)-C(5)	119.2(3)
C(7)-C(6)-C(1")	121.2(3)
C(5)-C(6)-C(1")	119.6(3)
C(4)-C(5)-C(6)	123.1(3)
C(4)-C(5)-H(5)	118.5
C(6)-C(5)-H(5)	118.5
C(5)-C(4)-C(3A)	117.3(3)
C(5)-C(4)-H(4)	121.4
C(3A)-C(4)-H(4)	121.4
C(6)-C(1")-H(1A)	109.5
C(6)-C(1")-H(1B)	109.5
H(1A)-C(1")-H(1B)	109.5
C(6)-C(1")-H(1C)	109.5
H(1A)-C(1")-H(1C)	109.5
H(1B)-C(1")-H(1C)	109.5
N(30)-C(20)-C(20')	121.8(3)
N(30)-C(20)-S(10)	113.3(2)
C(20')-C(20)-S(10)	124.8(2)
C(5')-C(4')-C(3')	120.6(3)
C(5')-C(4')-H(4')	119.7
C(3')-C(4')-H(4')	119.7
C(4')-C(5')-C(6')	120.2(3)
C(4')-C(5')-H(5')	119.9
C(6')-C(5')-H(5')	119.9
C(30A)-C(70A)-C(70)	121.2(3)
C(30A)-C(70A)-S(10)	110.3(2)

C(70)-C(70A)-S(10)	128.5(2)
C(4')-C(3')-C(2')	120.1(3)
C(4')-C(3')-H(3')	120.0
C(2')-C(3')-H(3')	120.0
C(70A)-C(30A)-N(30)	112.6(2)
C(70A)-C(30A)-C(40)	120.2(3)
N(30)-C(30A)-C(40)	127.1(3)
C(1')-O(1)-B(1)	125.9(2)
C(50)-C(40)-C(30A)	118.0(3)
C(50)-C(40)-H(40)	121.0
C(30A)-C(40)-H(40)	121.0
F(1)-B(1)-F(2)	109.4(3)
F(1)-B(1)-O(1)	111.5(3)
F(2)-B(1)-O(1)	110.2(3)
F(1)-B(1)-N(3)	108.5(3)
F(2)-B(1)-N(3)	107.0(3)
O(1)-B(1)-N(3)	110.2(3)
C(40)-C(50)-C(60)	122.6(3)
C(40)-C(50)-H(50)	118.7
C(60)-C(50)-H(50)	118.7
C(70)-C(60)-C(50)	119.1(3)
C(70)-C(60)-C(10")	121.1(3)
C(50)-C(60)-C(10")	119.7(3)
C(60)-C(70)-C(70A)	118.9(3)
C(60)-C(70)-H(70)	120.6
C(70A)-C(70)-H(70)	120.6
C(30')-C(20')-C(10')	119.8(3)
C(30')-C(20')-C(20)	122.4(3)
C(10')-C(20')-C(20)	117.8(3)
O(10)-C(10')-C(20')	122.1(3)
O(10)-C(10')-C(60')	118.4(3)
C(20')-C(10')-C(60')	119.4(3)
C(50')-C(60')-C(10')	119.8(3)
C(50')-C(60')-H(60')	120.1
C(10')-C(60')-H(60')	120.1
C(40')-C(50')-C(60')	120.5(3)
C(40')-C(50')-H(50')	119.7
C(60')-C(50')-H(50')	119.7
C(50')-C(40')-C(30')	120.6(3)
C(50')-C(40')-H(40')	119.7
C(30')-C(40')-H(40')	119.7
C(40')-C(30')-C(20')	119.9(3)
C(40')-C(30')-H(30')	120.1
C(20')-C(30')-H(30')	120.1
C(60)-C(10")-H(10D)	109.5
C(60)-C(10")-H(10E)	109.5
H(10D)-C(10")-H(10E)	109.5
C(60)-C(10")-H(10F)	109.5
H(10D)-C(10")-H(10F)	109.5
H(10E)-C(10")-H(10F)	109.5
F(20)-B(10)-F(10)	109.9(3)
F(20)-B(10)-O(10)	110.4(3)
F(10)-B(10)-O(10)	110.2(3)
F(20)-B(10)-N(30)	108.5(3)
F(10)-B(10)-N(30)	107.6(3)
O(10)-B(10)-N(30)	110.2(2)

Symmetry transformations used to generate equivalent atoms:

Table 4. Anisotropic displacement parameters ($\text{\AA}^2 \times 10^3$) for os1302_0m.

The anisotropic displacement factor exponent takes the form:

$$-2 \pi^2 [h^2 a^{*2} U_{11} + \dots + 2 h k a^* b^* U_{12}]$$

	U11	U22	U33	U23	U13	U12
S(1)	20(1)	50(1)	31(1)	-3(1)	-1(1)	-5(1)
S(10)	48(1)	21(1)	31(1)	-2(1)	-4(1)	-5(1)
C(2)	25(2)	31(2)	35(2)	-10(1)	-4(1)	-2(1)
F(20)	71(1)	42(1)	44(1)	0(1)	-17(1)	-31(1)
N(3)	20(1)	34(1)	23(1)	-6(1)	-4(1)	-4(1)
F(10)	65(1)	32(1)	45(1)	3(1)	2(1)	12(1)
C(3A)	32(2)	34(2)	26(2)	-6(1)	-2(1)	-4(1)
O(10)	67(2)	25(1)	29(1)	-4(1)	4(1)	-8(1)
N(30)	31(1)	21(1)	24(1)	-5(1)	-6(1)	-5(1)
C(2')	31(2)	32(2)	29(2)	-7(1)	-9(1)	-3(1)
C(1')	26(2)	34(2)	34(2)	-6(1)	-1(1)	-6(1)
C(7A)	28(2)	34(2)	33(2)	-9(1)	-2(1)	-2(1)
C(6')	35(2)	42(2)	33(2)	-7(1)	-3(1)	-1(2)
C(7)	28(2)	39(2)	31(2)	-3(1)	2(1)	-2(1)
C(6)	46(2)	37(2)	32(2)	-6(1)	-4(2)	0(2)
C(5)	33(2)	53(2)	39(2)	-6(2)	-5(2)	-4(2)
C(4)	37(2)	49(2)	34(2)	-5(2)	-15(1)	-3(2)
C(1")	57(2)	50(2)	34(2)	1(2)	-3(2)	-4(2)
C(20)	27(2)	23(1)	30(2)	-3(1)	-8(1)	-2(1)
C(4')	40(2)	49(2)	45(2)	-2(2)	-17(2)	-4(2)
C(5')	55(2)	38(2)	30(2)	-6(1)	-9(2)	-2(2)
C(70A)	33(2)	26(2)	32(2)	-4(1)	-8(1)	-4(1)
C(3')	29(2)	47(2)	36(2)	-2(2)	-8(1)	-3(2)
C(30A)	29(2)	27(2)	28(2)	-4(1)	-5(1)	-5(1)
O(1)	29(1)	69(2)	30(1)	3(1)	-3(1)	-6(1)
C(40)	45(2)	30(2)	34(2)	-9(1)	-5(1)	-5(1)
B(1)	26(2)	43(2)	32(2)	-4(2)	-1(2)	-7(2)
C(50)	48(2)	35(2)	33(2)	-10(1)	-3(2)	-4(2)
F(2)	28(1)	59(1)	46(1)	-8(1)	0(1)	8(1)
C(60)	34(2)	41(2)	29(2)	-4(1)	-6(1)	0(1)
F(1)	37(1)	65(1)	47(1)	-19(1)	-2(1)	-23(1)
C(70)	39(2)	29(2)	33(2)	3(1)	-5(1)	-4(1)
C(20')	28(2)	27(2)	28(2)	-5(1)	-8(1)	-1(1)
C(10')	35(2)	28(2)	30(2)	-5(1)	-6(1)	-3(1)
C(60')	42(2)	36(2)	30(2)	-3(1)	-4(1)	-1(2)
C(50')	37(2)	49(2)	28(2)	-11(2)	-6(1)	-2(2)
C(40')	51(2)	34(2)	39(2)	-14(2)	-5(2)	-2(2)
C(30')	50(2)	27(2)	37(2)	-6(1)	-3(2)	-8(2)
C(10")	50(2)	51(2)	31(2)	-4(2)	-2(2)	0(2)
B(10)	42(2)	24(2)	30(2)	-4(1)	-3(2)	-5(2)

10-(ethoxycarbonyl)-6,6-difluoro-6*H*-benzo[*e*]benzo[4,5]thiazolo[3,2-*c*][1,3,2]oxazaborinin-7-ium-6-uide (5.18)

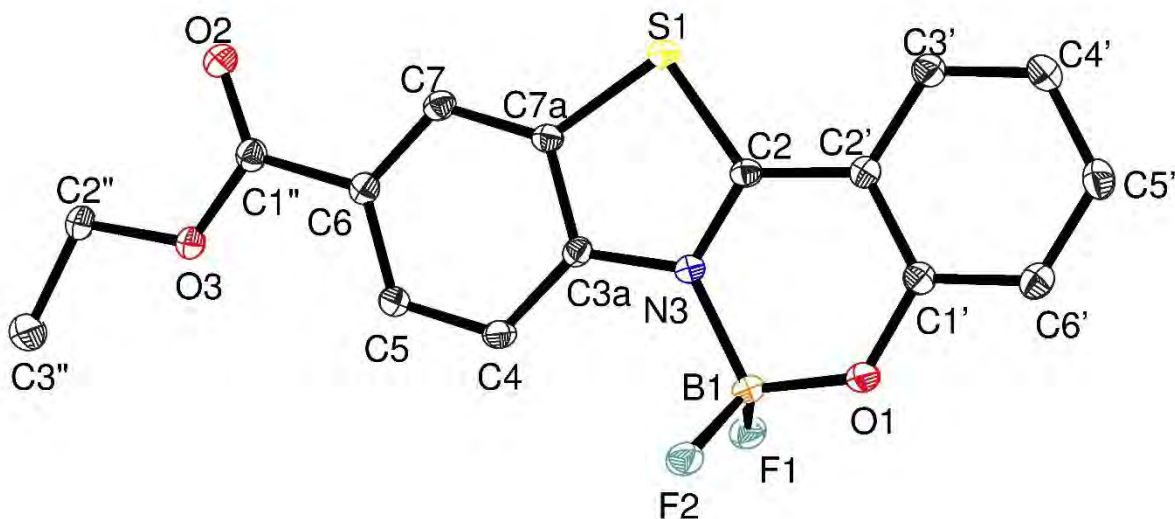


Table 1. Crystal data and structure refinement for OS-2-127.

Identification code	OS-2-127
Empirical formula	C ₁₆ H ₁₂ B F ₂ N O ₃ S
Formula weight	347.14
Temperature	100(2) K
Wavelength	0.71073 Å
Crystal system, space group	monoclinic, P 2 ₁ /c
Unit cell dimensions	a = 7.0017(5) Å alpha = 90 deg. b = 16.9701(11) Å beta = 102.567(2) deg. c = 12.5627(10) Å gamma = 90 deg.
Volume	1456.93(18) Å ³
Z, Calculated density	4, 1.583 Mg/m ³
Absorption coefficient	0.261 mm ⁻¹
F(000)	712
Crystal size	0.16 x 0.04 x 0.04 mm
Theta range for data collection	3.21 to 30.51 deg.
Limiting indices	-9<=h<=9, -24<=k<=24, -17<=l<=17
Reflections collected / unique	34049 / 4423 [R(int) = 0.0505]

Completeness to theta = 30.51	99.9 %
Max. and min. transmission	0.7461 and 0.6831
Refinement method	Full-matrix least-squares on F ²
Data / restraints / parameters	4423 / 0 / 218
Goodness-of-fit on F ²	1.042
Final R indices [I>2sigma(I)]	R1 = 0.0384, wR2 = 0.0922
R indices (all data)	R1 = 0.0548, wR2 = 0.1005
Largest diff. peak and hole	0.405 and -0.279 e.A ⁻³

Table 2. Atomic coordinates ($\times 10^4$) and equivalent isotropic displacement parameters ($\text{\AA}^2 \times 10^3$) for os-2-127_a. U(eq) is defined as one third of the trace of the orthogonalized Uij tensor.

	x	y	z	U(eq)
C(3")	7667(3)	9484(1)	5007(1)	33(1)
C(2")	8219(2)	8928(1)	5953(1)	21(1)
C(1")	8250(2)	7544(1)	6215(1)	16(1)
C(6)	7911(2)	6771(1)	5635(1)	14(1)
C(7)	8102(2)	6089(1)	6255(1)	15(1)
C(7A)	7814(2)	5371(1)	5700(1)	13(1)
C(3A)	7315(2)	5342(1)	4557(1)	13(1)
C(4)	7122(2)	6036(1)	3941(1)	16(1)
C(5)	7427(2)	6743(1)	4485(1)	15(1)
C(2)	7437(2)	4033(1)	4933(1)	13(1)
C(2')	7271(2)	3208(1)	4684(1)	14(1)
C(3')	7724(2)	2622(1)	5492(1)	17(1)
C(4')	7472(2)	1837(1)	5218(1)	20(1)
C(5')	6769(2)	1626(1)	4124(1)	19(1)
C(6')	6335(2)	2192(1)	3316(1)	18(1)
C(1')	6584(2)	2989(1)	3583(1)	15(1)
B(1)	6511(2)	4358(1)	2891(1)	16(1)
N(3)	7098(2)	4578(1)	4152(1)	13(1)
O(3)	7968(2)	8140(1)	5505(1)	19(1)
O(2)	8725(2)	7621(1)	7196(1)	21(1)
O(1)	6116(2)	3523(1)	2782(1)	21(1)
F(2)	4862(1)	4784(1)	2428(1)	21(1)
F(1)	8056(1)	4572(1)	2423(1)	19(1)
S(1)	8017(1)	4421(1)	6231(1)	15(1)

Table 3. Bond lengths [Å] and angles [deg] for os-2-127_a.

C(3")-C(2")	1.500(2)
C(3")-H(3B)	0.9800
C(3")-H(3C)	0.9800
C(3")-H(3D)	0.9800
C(2")-O(3)	1.4466(18)
C(2")-H(2A)	0.9900
C(2")-H(2B)	0.9900
C(1")-O(2)	1.2123(17)
C(1")-O(3)	1.3339(17)
C(1")-C(6)	1.494(2)
C(6)-C(7)	1.386(2)
C(6)-C(5)	1.4115(19)
C(7)-C(7A)	1.3957(19)
C(7)-H(7)	0.9500
C(7A)-C(3A)	1.4029(18)
C(7A)-S(1)	1.7401(14)
C(3A)-N(3)	1.3896(18)
C(3A)-C(4)	1.399(2)
C(4)-C(5)	1.374(2)
C(4)-H(4)	0.9500
C(5)-H(5)	0.9500
C(2)-N(3)	1.3310(18)
C(2)-C(2')	1.434(2)
C(2)-S(1)	1.7235(14)
C(2')-C(3')	1.408(2)
C(2')-C(1')	1.4108(19)
C(3')-C(4')	1.377(2)
C(3')-H(3A)	0.9500
C(4')-C(5')	1.402(2)
C(4')-H(4A)	0.9500
C(5')-C(6')	1.382(2)
C(5')-H(5A)	0.9500
C(6')-C(1')	1.395(2)
C(6')-H(6A)	0.9500
C(1')-O(1)	1.3403(17)
B(1)-F(2)	1.3798(18)
B(1)-F(1)	1.3872(18)
B(1)-O(1)	1.445(2)
B(1)-N(3)	1.5918(19)
C(2")-C(3")-H(3B)	109.5
C(2")-C(3")-H(3C)	109.5
H(3B)-C(3")-H(3C)	109.5
C(2")-C(3")-H(3D)	109.5
H(3B)-C(3")-H(3D)	109.5
H(3C)-C(3")-H(3D)	109.5
O(3)-C(2")-C(3")	106.52(12)
O(3)-C(2")-H(2A)	110.4
C(3")-C(2")-H(2A)	110.4
O(3)-C(2")-H(2B)	110.4
C(3")-C(2")-H(2B)	110.4
H(2A)-C(2")-H(2B)	108.6
O(2)-C(1")-O(3)	124.46(14)
O(2)-C(1")-C(6)	124.71(14)
O(3)-C(1")-C(6)	110.83(12)
C(7)-C(6)-C(5)	121.25(13)
C(7)-C(6)-C(1")	118.31(12)
C(5)-C(6)-C(1")	120.44(13)
C(6)-C(7)-C(7A)	117.54(12)
C(6)-C(7)-H(7)	121.2

C(7A)-C(7)-H(7)	121.2
C(7)-C(7A)-C(3A)	121.25(13)
C(7)-C(7A)-S(1)	128.77(11)
C(3A)-C(7A)-S(1)	109.97(10)
N(3)-C(3A)-C(4)	126.36(12)
N(3)-C(3A)-C(7A)	113.00(12)
C(4)-C(3A)-C(7A)	120.62(13)
C(5)-C(4)-C(3A)	118.28(13)
C(5)-C(4)-H(4)	120.9
C(3A)-C(4)-H(4)	120.9
C(4)-C(5)-C(6)	121.05(13)
C(4)-C(5)-H(5)	119.5
C(6)-C(5)-H(5)	119.5
N(3)-C(2)-C(2')	121.60(12)
N(3)-C(2)-S(1)	113.62(10)
C(2')-C(2)-S(1)	124.76(10)
C(3')-C(2')-C(1')	119.73(13)
C(3')-C(2')-C(2)	122.54(13)
C(1')-C(2')-C(2)	117.72(12)
C(4')-C(3')-C(2')	120.43(14)
C(4')-C(3')-H(3A)	119.8
C(2')-C(3')-H(3A)	119.8
C(3')-C(4')-C(5')	119.40(14)
C(3')-C(4')-H(4A)	120.3
C(5')-C(4')-H(4A)	120.3
C(6')-C(5')-C(4')	121.08(14)
C(6')-C(5')-H(5A)	119.5
C(4')-C(5')-H(5A)	119.5
C(5')-C(6')-C(1')	120.09(14)
C(5')-C(6')-H(6A)	120.0
C(1')-C(6')-H(6A)	120.0
O(1)-C(1')-C(6')	118.45(13)
O(1)-C(1')-C(2')	122.27(13)
C(6')-C(1')-C(2')	119.26(13)
F(2)-B(1)-F(1)	109.99(12)
F(2)-B(1)-O(1)	110.45(12)
F(1)-B(1)-O(1)	111.56(12)
F(2)-B(1)-N(3)	107.92(12)
F(1)-B(1)-N(3)	107.70(12)
O(1)-B(1)-N(3)	109.11(11)
C(2)-N(3)-C(3A)	112.97(11)
C(2)-N(3)-B(1)	122.45(12)
C(3A)-N(3)-B(1)	124.58(11)
C(1'')-O(3)-C(2'')	116.97(11)
C(1')-O(1)-B(1)	125.48(11)
C(2)-S(1)-C(7A)	90.42(7)

Symmetry transformations used to generate equivalent atoms:

Table 4. Anisotropic displacement parameters ($\text{Å}^2 \times 10^3$) for os-2-127_a.
The anisotropic displacement factor exponent takes the form:
 $-2 \pi^2 [h^2 a^{*2} U_{11} + \dots + 2 h k a^* b^* U_{12}]$

	U11	U22	U33	U23	U13	U12
C(3'')	58(1)	17(1)	22(1)	1(1)	4(1)	1(1)
C(2'')	30(1)	13(1)	17(1)	-3(1)	3(1)	0(1)
C(1'')	14(1)	16(1)	17(1)	-1(1)	3(1)	1(1)
C(6)	12(1)	16(1)	15(1)	-1(1)	2(1)	1(1)

C(7)	13(1)	18(1)	13(1)	-1(1)	2(1)	1(1)
C(7A)	13(1)	16(1)	12(1)	1(1)	2(1)	1(1)
C(3A)	12(1)	14(1)	13(1)	-2(1)	2(1)	1(1)
C(4)	17(1)	18(1)	12(1)	1(1)	2(1)	2(1)
C(5)	17(1)	15(1)	14(1)	1(1)	3(1)	1(1)
C(2)	12(1)	16(1)	11(1)	0(1)	2(1)	1(1)
C(2')	13(1)	14(1)	14(1)	-1(1)	4(1)	0(1)
C(3')	18(1)	17(1)	16(1)	0(1)	3(1)	2(1)
C(4')	24(1)	16(1)	21(1)	4(1)	4(1)	2(1)
C(5')	22(1)	14(1)	23(1)	0(1)	6(1)	-1(1)
C(6')	18(1)	18(1)	17(1)	-3(1)	4(1)	-2(1)
C(1')	14(1)	15(1)	16(1)	1(1)	4(1)	-1(1)
B(1)	18(1)	16(1)	12(1)	-1(1)	2(1)	0(1)
N(3)	14(1)	14(1)	11(1)	0(1)	2(1)	0(1)
O(3)	27(1)	13(1)	15(1)	-2(1)	3(1)	0(1)
O(2)	29(1)	17(1)	15(1)	-3(1)	1(1)	0(1)
O(1)	32(1)	16(1)	13(1)	0(1)	0(1)	-3(1)
F(2)	21(1)	24(1)	16(1)	-2(1)	-2(1)	6(1)
F(1)	23(1)	21(1)	16(1)	0(1)	7(1)	-1(1)
S(1)	18(1)	14(1)	11(1)	0(1)	2(1)	1(1)

6a-fluoro-6a*H*-6,7-dioxa-1-thia-1a¹-aza-6a-borabenz[*a*]benzo[5,6]cyclohepta[1,2,3,4-*def*]fluoren-1a¹-ium-7-uide (5.19)

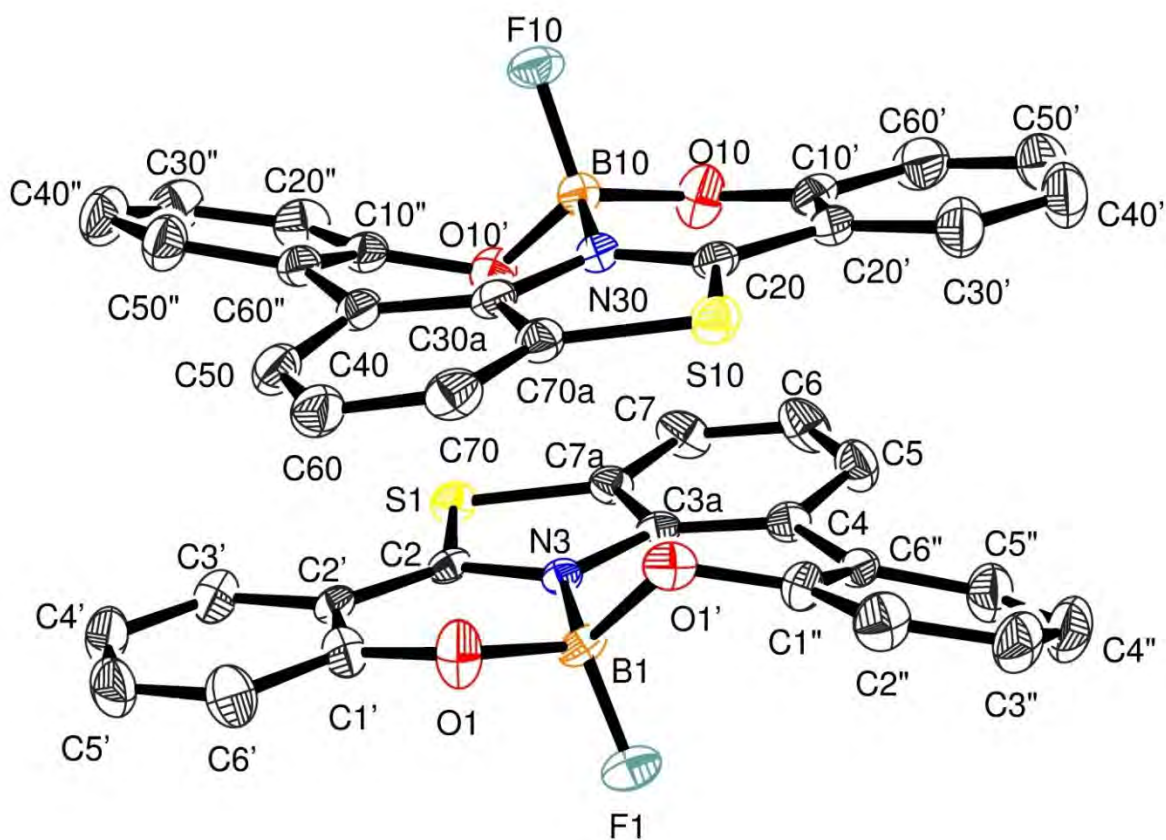


Figure 1 : Asymmetric Unit

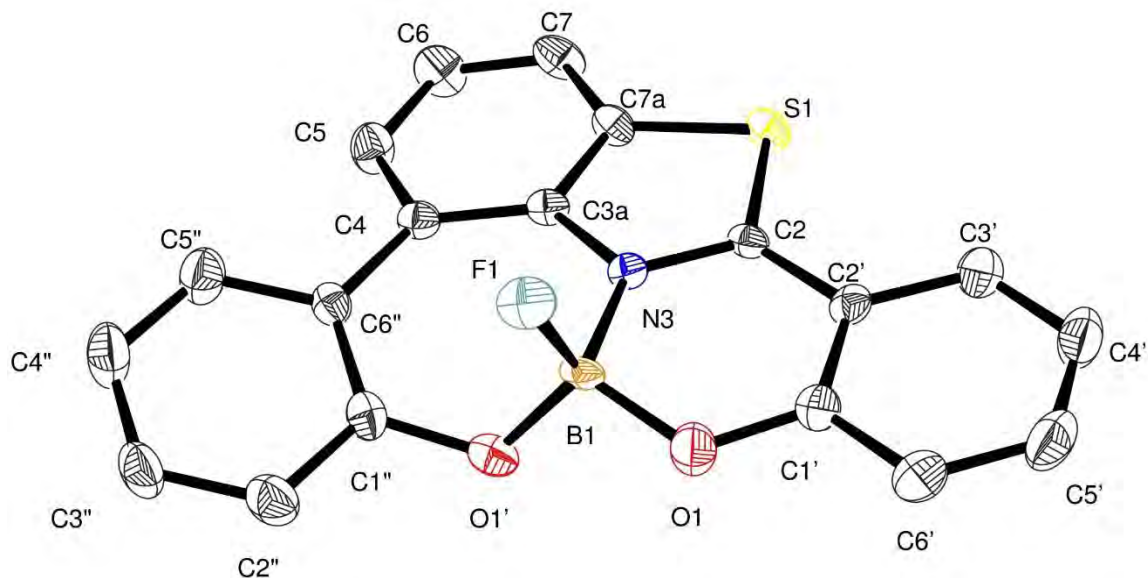


Figure 2 : Molecule

Table 1. Crystal data and structure refinement for OS-1-130-3.

Identification code	OS-1-130-3	
Empirical formula	C ₁₉ H ₁₁ B F N O ₂ S	
Formula weight	347.16	
Temperature	173(2) K	
Wavelength	0.71073 Å	
Crystal system, space group	monoclinic, P 2 ₁ /c	
Unit cell dimensions	a = 21.6889(15) Å	alpha = 90 deg.
	b = 8.3584(6) Å	beta = 108.741(3) deg.
	c = 17.3466(12) Å	gamma = 90 deg.
Volume	2977.9(4) Å ³	
Z, Calculated density	8, 1.549 Mg/m ³	
Absorption coefficient	0.242 mm ⁻¹	
F(000)	1424	
Crystal size	0.4 x 0.04 x 0.04 mm	
Theta range for data collection	5.11 to 26.37 deg.	
Limiting indices	-27<=h<=27, -10<=k<=10, -21<=l<=21	
Reflections collected / unique	138878 / 6038 [R(int) = 0.0983]	

Completeness to theta = 26.37	99.2 %
Refinement method	Full-matrix least-squares on F ²
Data / restraints / parameters	6038 / 0 / 451
Goodness-of-fit on F ²	1.059
Final R indices [I>2sigma(I)]	R1 = 0.0560, wR2 = 0.1321
R indices (all data)	R1 = 0.0896, wR2 = 0.1551
Largest diff. peak and hole	0.887 and -0.341 e.A ⁻³

Table 2. Atomic coordinates ($\times 10^4$) and equivalent isotropic displacement parameters ($\text{\AA}^2 \times 10^3$) for test2_a. U(eq) is defined as one third of the trace of the orthogonalized U_{ij} tensor.

	x	y	z	U(eq)
C(2)	2235(1)	9084(3)	2541(2)	17(1)
N(3)	2782(1)	8282(3)	2635(1)	16(1)
S(1)	2108(1)	9527(1)	3440(1)	21(1)
C(4)	3716(2)	7033(4)	3743(2)	20(1)
C(5)	3930(2)	6818(4)	4588(2)	28(1)
C(6)	3618(2)	7446(4)	5103(2)	32(1)
C(7)	3057(2)	8323(4)	4809(2)	28(1)
C(7A)	2818(2)	8534(4)	3974(2)	20(1)
C(3A)	3130(1)	7912(4)	3441(2)	17(1)
C(2')	1799(1)	9491(4)	1745(2)	20(1)
C(1')	1959(2)	8958(4)	1066(2)	25(1)
C(6')	1558(2)	9360(4)	286(2)	33(1)
C(5')	1002(2)	10229(5)	188(2)	37(1)
C(4')	828(2)	10726(5)	854(2)	36(1)
C(3')	1225(2)	10366(4)	1626(2)	30(1)
C(6'')	4106(1)	6324(4)	3260(2)	20(1)
C(1'')	3862(2)	5935(4)	2430(2)	24(1)
C(2'')	4252(2)	5148(4)	2050(2)	32(1)
C(3'')	4894(2)	4778(4)	2474(2)	33(1)
C(4'')	5150(2)	5221(5)	3275(2)	39(1)
C(5'')	4762(2)	5973(5)	3660(2)	33(1)
O(1)	2477(1)	8028(3)	1143(1)	32(1)
O(1')	3224(1)	6229(3)	1956(1)	25(1)
B(1)	3014(2)	7857(4)	1881(2)	19(1)
F(1)	3510(1)	8930(2)	1906(1)	30(1)
S(10)	2871(1)	2528(1)	1578(1)	24(1)
C(20)	2763(1)	2986(4)	2488(2)	21(1)
N(30)	2223(1)	3805(3)	2411(2)	20(1)
C(40)	1293(2)	5113(4)	1325(2)	22(1)
C(50)	1082(2)	5367(4)	487(2)	27(1)
C(60)	1370(2)	4726(4)	-50(2)	31(1)
C(70)	1914(2)	3766(4)	228(2)	28(1)
C(70A)	2165(2)	3561(4)	1067(2)	22(1)
C(30A)	1870(1)	4195(4)	1609(2)	21(1)
C(20')	3209(2)	2568(4)	3277(2)	23(1)
C(10')	3081(2)	3168(4)	3965(2)	27(1)
C(60')	3511(2)	2803(5)	4741(2)	36(1)
C(50')	4046(2)	1848(5)	4806(2)	40(1)
C(40')	4183(2)	1293(5)	4130(2)	41(1)
C(30')	3766(2)	1646(4)	3367(2)	34(1)
C(60'')	906(2)	5802(4)	1824(2)	23(1)
C(10'')	1148(2)	6153(4)	2649(2)	24(1)
C(20'')	762(2)	6927(4)	3040(2)	32(1)
C(30'')	126(2)	7349(4)	2621(2)	36(1)
C(40'')	-133(2)	6964(5)	1804(2)	35(1)
C(50'')	248(2)	6191(4)	1420(2)	30(1)
O(10)	2566(1)	4101(3)	3906(1)	33(1)
O(10')	1780(1)	5847(3)	3108(1)	26(1)
B(10)	2005(2)	4238(4)	3178(2)	22(1)
F(10)	1528(1)	3134(2)	3192(1)	29(1)

Table 3. Bond lengths [Å] and angles [deg] for test2_a.

C(2)-N(3)	1.325(4)
C(2)-C(2')	1.441(4)
C(2)-S(1)	1.708(3)
N(3)-C(3A)	1.395(4)
N(3)-B(1)	1.586(4)
S(1)-C(7A)	1.733(3)
C(4)-C(5)	1.401(4)
C(4)-C(3A)	1.414(4)
C(4)-C(6")	1.491(4)
C(5)-C(6)	1.387(5)
C(5)-H(5)	0.9500
C(6)-C(7)	1.369(5)
C(6)-H(6)	0.9500
C(7)-C(7A)	1.385(4)
C(7)-H(7)	0.9500
C(7A)-C(3A)	1.408(4)
C(2')-C(3')	1.401(4)
C(2')-C(1')	1.403(4)
C(1')-O(1)	1.337(4)
C(1')-C(6')	1.395(5)
C(6')-C(5')	1.371(5)
C(6')-H(6')	0.9500
C(5')-C(4')	1.389(5)
C(5')-H(5')	0.9500
C(4')-C(3')	1.373(5)
C(4')-H(4')	0.9500
C(3')-H(3')	0.9500
C(6")-C(5")	1.399(4)
C(6")-C(1")	1.403(4)
C(1")-O(1')	1.386(4)
C(1")-C(2")	1.395(4)
C(2")-C(3")	1.385(5)
C(2")-H(2")	0.9500
C(3")-C(4")	1.371(5)
C(3")-H(3")	0.9500
C(4")-C(5")	1.382(5)
C(4")-H(4")	0.9500
C(5")-H(5")	0.9500
O(1)-B(1)	1.434(4)
O(1')-B(1)	1.427(4)
B(1)-F(1)	1.389(4)
S(10)-C(20)	1.713(3)
S(10)-C(70A)	1.733(3)
C(20)-N(30)	1.326(4)
C(20)-C(20')	1.442(4)
N(30)-C(30A)	1.394(4)
N(30)-B(10)	1.589(4)
C(40)-C(50)	1.392(4)
C(40)-C(30A)	1.414(4)
C(40)-C(60")	1.502(4)
C(50)-C(60)	1.385(5)
C(50)-H(50)	0.9500
C(60)-C(70)	1.379(5)
C(60)-H(60)	0.9500
C(70)-C(70A)	1.390(4)
C(70)-H(70)	0.9500
C(70A)-C(30A)	1.401(4)
C(20')-C(30')	1.400(5)
C(20')-C(10')	1.403(5)
C(10')-O(10)	1.338(4)

C(10')-C(60')	1.403(5)
C(60')-C(50')	1.384(5)
C(60')-H(60')	0.9500
C(50')-C(40')	1.380(6)
C(50')-H(50')	0.9500
C(40')-C(30')	1.374(5)
C(40')-H(40')	0.9500
C(30')-H(30')	0.9500
C(60")-C(10")	1.388(4)
C(60")-C(50")	1.411(4)
C(10")-O(10')	1.371(4)
C(10")-C(20")	1.395(5)
C(20")-C(30")	1.381(5)
C(20")-H(20")	0.9500
C(30")-C(40")	1.384(5)
C(30")-H(30")	0.9500
C(40")-C(50")	1.378(5)
C(40")-H(40")	0.9500
C(50")-H(50")	0.9500
O(10)-B(10)	1.450(4)
O(10')-B(10)	1.423(4)
B(10)-F(10)	1.392(4)

N(3)-C(2)-C(2')	121.5(3)
N(3)-C(2)-S(1)	113.4(2)
C(2')-C(2)-S(1)	125.0(2)
C(2)-N(3)-C(3A)	114.2(2)
C(2)-N(3)-B(1)	121.4(2)
C(3A)-N(3)-B(1)	124.3(2)
C(2)-S(1)-C(7A)	90.45(14)
C(5)-C(4)-C(3A)	114.3(3)
C(5)-C(4)-C(6")	118.6(3)
C(3A)-C(4)-C(6")	127.1(3)
C(6)-C(5)-C(4)	124.0(3)
C(6)-C(5)-H(5)	118.0
C(4)-C(5)-H(5)	118.0
C(7)-C(6)-C(5)	121.5(3)
C(7)-C(6)-H(6)	119.3
C(5)-C(6)-H(6)	119.3
C(6)-C(7)-C(7A)	116.6(3)
C(6)-C(7)-H(7)	121.7
C(7A)-C(7)-H(7)	121.7
C(7)-C(7A)-C(3A)	122.8(3)
C(7)-C(7A)-S(1)	126.2(2)
C(3A)-C(7A)-S(1)	111.0(2)
N(3)-C(3A)-C(7A)	110.8(3)
N(3)-C(3A)-C(4)	128.3(3)
C(7A)-C(3A)-C(4)	120.9(3)
C(3')-C(2')-C(1')	119.3(3)
C(3')-C(2')-C(2)	122.9(3)
C(1')-C(2')-C(2)	117.8(3)
O(1)-C(1')-C(6')	118.6(3)
O(1)-C(1')-C(2')	121.8(3)
C(6')-C(1')-C(2')	119.6(3)
C(5')-C(6')-C(1')	119.8(3)
C(5')-C(6')-H(6')	120.1
C(1')-C(6')-H(6')	120.1
C(6')-C(5')-C(4')	121.3(3)
C(6')-C(5')-H(5')	119.3
C(4')-C(5')-H(5')	119.3
C(3')-C(4')-C(5')	119.5(3)
C(3')-C(4')-H(4')	120.2
C(5')-C(4')-H(4')	120.2

C(4')-C(3')-C(2')	120.5(3)
C(4')-C(3')-H(3')	119.8
C(2')-C(3')-H(3')	119.8
C(5")-C(6")-C(1")	116.7(3)
C(5")-C(6")-C(4)	118.4(3)
C(1")-C(6")-C(4)	124.9(3)
O(1')-C(1")-C(2")	116.4(3)
O(1')-C(1")-C(6")	123.0(3)
C(2")-C(1")-C(6")	120.6(3)
C(3")-C(2")-C(1")	120.9(3)
C(3")-C(2")-H(2")	119.6
C(1")-C(2")-H(2")	119.6
C(4")-C(3")-C(2")	119.2(3)
C(4")-C(3")-H(3")	120.4
C(2")-C(3")-H(3")	120.4
C(3")-C(4")-C(5")	120.1(3)
C(3")-C(4")-H(4")	119.9
C(5")-C(4")-H(4")	119.9
C(4")-C(5")-C(6")	122.4(3)
C(4")-C(5")-H(5")	118.8
C(6")-C(5")-H(5")	118.8
C(1')-O(1)-B(1)	124.3(2)
C(1")-O(1')-B(1)	116.8(2)
F(1)-B(1)-O(1')	113.1(3)
F(1)-B(1)-O(1)	111.3(3)
O(1')-B(1)-O(1)	108.6(3)
F(1)-B(1)-N(3)	106.1(2)
O(1')-B(1)-N(3)	108.3(3)
O(1)-B(1)-N(3)	109.3(2)
C(20)-S(10)-C(70A)	89.98(15)
N(30)-C(20)-C(20')	121.5(3)
N(30)-C(20)-S(10)	113.7(2)
C(20')-C(20)-S(10)	124.8(2)
C(20)-N(30)-C(30A)	113.9(3)
C(20)-N(30)-B(10)	121.6(3)
C(30A)-N(30)-B(10)	124.5(2)
C(50)-C(40)-C(30A)	113.8(3)
C(50)-C(40)-C(60")	119.1(3)
C(30A)-C(40)-C(60")	127.1(3)
C(60)-C(50)-C(40)	125.1(3)
C(60)-C(50)-H(50)	117.5
C(40)-C(50)-H(50)	117.5
C(70)-C(60)-C(50)	120.6(3)
C(70)-C(60)-H(60)	119.7
C(50)-C(60)-H(60)	119.7
C(60)-C(70)-C(70A)	116.2(3)
C(60)-C(70)-H(70)	121.9
C(70A)-C(70)-H(70)	121.9
C(70)-C(70A)-C(30A)	123.1(3)
C(70)-C(70A)-S(10)	125.5(2)
C(30A)-C(70A)-S(10)	111.4(2)
N(30)-C(30A)-C(70A)	111.0(3)
N(30)-C(30A)-C(40)	128.0(3)
C(70A)-C(30A)-C(40)	121.0(3)
C(30')-C(20')-C(10')	120.1(3)
C(30')-C(20')-C(20)	122.1(3)
C(10')-C(20')-C(20)	117.7(3)
O(10)-C(10')-C(60')	118.8(3)
O(10)-C(10')-C(20')	122.1(3)
C(60')-C(10')-C(20')	119.1(3)
C(50')-C(60')-C(10')	119.1(4)
C(50')-C(60')-H(60')	120.5
C(10')-C(60')-H(60')	120.5

C(40')-C(50')-C(60')	122.0(3)
C(40')-C(50')-H(50')	119.0
C(60')-C(50')-H(50')	119.0
C(30')-C(40')-C(50')	119.5(4)
C(30')-C(40')-H(40')	120.3
C(50')-C(40')-H(40')	120.3
C(40')-C(30')-C(20')	120.2(4)
C(40')-C(30')-H(30')	119.9
C(20')-C(30')-H(30')	119.9
C(10'')-C(60'')-C(50'')	116.8(3)
C(10'')-C(60'')-C(40'')	125.4(3)
C(50'')-C(60'')-C(40'')	117.8(3)
O(10')-C(10'')-C(60'')	122.4(3)
O(10')-C(10'')-C(20'')	116.7(3)
C(60'')-C(10'')-C(20'')	120.8(3)
C(30'')-C(20'')-C(10'')	121.1(3)
C(30'')-C(20'')-H(20'')	119.4
C(10'')-C(20'')-H(20'')	119.4
C(20'')-C(30'')-C(40'')	119.2(3)
C(20'')-C(30'')-H(30'')	120.4
C(40'')-C(30'')-H(30'')	120.4
C(50'')-C(40'')-C(30'')	119.6(3)
C(50'')-C(40'')-H(40'')	120.2
C(30'')-C(40'')-H(40'')	120.2
C(40'')-C(50'')-C(60'')	122.4(3)
C(40'')-C(50'')-H(50'')	118.8
C(60'')-C(50'')-H(50'')	118.8
C(10')-O(10)-B(10)	123.9(3)
C(10'')-O(10')-B(10)	118.5(2)
F(10)-B(10)-O(10')	113.0(3)
F(10)-B(10)-O(10)	110.7(3)
O(10')-B(10)-O(10)	108.5(3)
F(10)-B(10)-N(30)	106.6(3)
O(10')-B(10)-N(30)	109.3(3)
O(10)-B(10)-N(30)	108.7(3)

Symmetry transformations used to generate equivalent atoms:

Table 4. Anisotropic displacement parameters ($\text{Å}^2 \times 10^3$) for test2_a. The anisotropic displacement factor exponent takes the form: $-2 \pi^2 [h^2 a^{*2} U_{11} + \dots + 2 h k a^* b^* U_{12}]$

	U11	U22	U33	U23	U13	U12
C(2)	17(1)	16(2)	21(2)	-4(1)	11(1)	-3(1)
N(3)	17(1)	18(1)	15(1)	-1(1)	7(1)	-2(1)
S(1)	23(1)	23(1)	23(1)	-1(1)	14(1)	1(1)
C(4)	22(2)	20(2)	20(2)	-1(1)	9(1)	-2(1)
C(5)	29(2)	34(2)	22(2)	6(1)	8(1)	7(2)
C(6)	45(2)	37(2)	17(2)	7(1)	12(2)	9(2)
C(7)	42(2)	27(2)	21(2)	0(1)	19(2)	5(2)
C(7A)	24(2)	20(2)	22(2)	1(1)	13(1)	1(1)
C(3A)	21(2)	19(2)	15(1)	-1(1)	10(1)	-3(1)
C(2')	15(1)	19(2)	23(2)	-1(1)	5(1)	-5(1)
C(1')	25(2)	24(2)	23(2)	0(1)	5(1)	3(1)
C(6')	35(2)	38(2)	22(2)	-1(2)	4(2)	3(2)
C(5')	31(2)	38(2)	30(2)	7(2)	-5(2)	-1(2)
C(4')	22(2)	37(2)	42(2)	4(2)	1(2)	2(2)
C(3')	21(2)	33(2)	33(2)	-3(2)	7(1)	0(1)

C(6")	19(2)	18(2)	26(2)	1(1)	10(1)	-1(1)
C(1")	20(2)	26(2)	29(2)	1(1)	10(1)	3(1)
C(2")	34(2)	35(2)	31(2)	-4(2)	16(2)	3(2)
C(3")	27(2)	39(2)	38(2)	-2(2)	18(2)	8(2)
C(4")	24(2)	51(2)	45(2)	4(2)	13(2)	10(2)
C(5")	26(2)	43(2)	28(2)	4(2)	7(1)	6(2)
O(1)	29(1)	48(2)	20(1)	-3(1)	7(1)	12(1)
O(1')	31(1)	23(1)	26(1)	-4(1)	14(1)	-1(1)
B(1)	18(2)	22(2)	20(2)	-9(1)	13(1)	-4(1)
F(1)	30(1)	34(1)	31(1)	-3(1)	18(1)	-9(1)
S(10)	23(1)	25(1)	28(1)	-1(1)	12(1)	1(1)
C(20)	20(2)	19(2)	26(2)	1(1)	10(1)	-4(1)
N(30)	17(1)	19(1)	22(1)	1(1)	6(1)	-2(1)
C(40)	18(2)	20(2)	29(2)	0(1)	8(1)	-3(1)
C(50)	20(2)	34(2)	29(2)	1(2)	9(1)	-2(1)
C(60)	26(2)	41(2)	27(2)	6(2)	10(1)	-2(2)
C(70)	29(2)	35(2)	23(2)	-2(1)	14(1)	-4(2)
C(70A)	22(2)	20(2)	25(2)	-1(1)	8(1)	-3(1)
C(30A)	19(2)	23(2)	20(2)	0(1)	7(1)	-6(1)
C(20')	19(2)	19(2)	28(2)	1(1)	5(1)	-4(1)
C(10')	20(2)	29(2)	30(2)	3(1)	6(1)	-7(1)
C(60')	33(2)	44(2)	29(2)	4(2)	6(2)	-8(2)
C(50')	33(2)	43(2)	35(2)	11(2)	0(2)	-1(2)
C(40')	28(2)	38(2)	48(2)	5(2)	1(2)	7(2)
C(30')	28(2)	31(2)	37(2)	-1(2)	4(2)	3(2)
C(60")	20(2)	19(2)	30(2)	1(1)	10(1)	-1(1)
C(10")	22(2)	18(2)	31(2)	0(1)	7(1)	-3(1)
C(20")	36(2)	31(2)	33(2)	-4(2)	16(2)	-1(2)
C(30")	30(2)	36(2)	50(2)	-9(2)	23(2)	2(2)
C(40")	23(2)	42(2)	43(2)	0(2)	13(2)	5(2)
C(50")	21(2)	38(2)	30(2)	2(2)	9(1)	4(2)
O(10)	27(1)	49(2)	22(1)	-5(1)	7(1)	4(1)
O(10')	25(1)	24(1)	30(1)	-4(1)	7(1)	-1(1)
B(10)	21(2)	23(2)	22(2)	2(1)	7(1)	-1(1)
F(10)	28(1)	27(1)	40(1)	1(1)	20(1)	-5(1)
